THE POST-TRIASSIC UPLIFT AND EROSION HISTORY OF THE SOUTHWESTERN UK

By

JOHN EDWARD KELLY

A thesis submitted to the University of Birmingham for the degree of
DOCTOR OF PHILOSOPHY

School of Geography, Earth
& Environmental Sciences
The University of Birmingham
December 2010

ABSTRACT

The passive continental margins which surround the North Atlantic region have been subject to widespread post-Triassic exhumation, the timing, magnitude and causes of which are debated. Exhumation of up to 6km (but more generally ≤3km) has been shown to have affected the Western UK Continental Shelf. This region contains a series of intra-plate extensional basins which formed during Permian-Jurassic rifting. Using a combination of palaeothermal (apatite fission-track analysis and vitrinite reflectance data) seismic and compaction data, this study has revealed an exhumation history of far greater complexity than previously suspected across the Southwest UK, with regional kilometre-scale exhumation episodes beginning during the Upper Triassic-Lower Jurassic (215-195Ma), Lower Cretaceous (140-120Ma), early Paleogene (75-55Ma), Eocene-Oligocene (35-20Ma) and Neogene (20-10Ma). Upper Triassic-Lower Jurassic exhumation appears confined to the footwalls of major basin bounding faults, suggesting footwall uplift was the principal cause of this episode of exhumation. Lower Cretaceous exhumation corresponds with continental breakup SW of Britain, suggesting a causative link. Early Paleogene exhumation was coeval with the Laramide phase of Alpine orogeny suggesting a causative link and additionally, marked heterogeneities in the pattern of this exhumation have been identified, casting doubt on the previously invoked role of plume-related epeirogenesis. Eocene-Oligocene and Neogene exhumation coincides temporally with the Pyrenean and Late Alpine compressional episodes. Seismic data shows that early and late Cenozoic exhumation was probably caused by compressional deformation related to Alpine orogenesis and/or Atlantic ridge-push. These observations imply that events at plate margins have exerted the primary control upon intra-plate exhumation in the Southwest UK onshore and offshore basin system with local faults providing an important control on the distribution of this exhumation.

DEDICATION

This thesis is dedicated to the memory of Debbie and Hazel, friends who are sadly missed and to my family Mom, Dad, Nan, Juliette and Connor.

ACKNOWLEDGEMENTS

First and foremost my thanks must go to my principal supervisor Dr Jonathan Turner without whom this thesis would not exist. I am extremely grateful to have been given the opportunity to study for a PhD at the University of Birmingham under his tutelage. I thank him for his continual support, advice, discussions and encouragement during the course of my studies and especially for his time and dedication to reading through the script.

A substantial debt of gratitude is also owed to Dr Paul Green of Geotrack International Pty Ltd whose knowledge and expertise in all things fission-track have been invaluable to this research. I also thank his dedicated team of staff who were responsible for providing the palaeothermal data for this project.

Within Earth Sciences at the University of Birmingham I would like to thank Professor Graham Westbrook, Professor John Tellam, Professor Tim Reston and the late Dr Ken Thomson for invaluable help and advice during the course of my studies. My gratitude is also extended to Anne Ankcorn and Kevin Burkhill of the drawing office for their assistance in crafting my sketches into works of art. Additional thanks goes to all of the members of staff within the department for making it such a fun and lively place to study as well as all the support and secretarial staff who variously solved my computer issues, paid my expenses and provided sustenance in the form of biscuits and buffets. I would also like to thank the school for funding the PhD through the schools scholarship programme.

Outside of University of Birmingham I would like to thank Professor Graham Williams and Eva Palinicek of Keele University for help and advice early on in the project and Dr Chris Elders of Royal Holloway University of London.

Palaeothermal data for this project was primarily provided by Geotrack but additional thanks must go to the staff of Keiraville Consultants for the processing of VR data and to Ocean Grove for the provision of VR samples in the North Celtic Sea Basin. Compaction data was provided by the British Geological Survey and I would like to thank Chris Wheatley, Mary Cole, Mike Howe, Emma Jane, Scott Renshaw and Gareth Williams for variously providing access, data, permission and assistance with regards to core data and geophysical logs. My thanks also go to Fugro and Providence Resources Ltd for permission to use the seismic dataset of the North Celtic Sea Basin and St. George's Channel Basin.

Special thanks must go to the wide assortment of characters and personalities that make up the University of Birmingham Earth Science Postgraduate community; Tim, Beth, Leyla, Nick, Rob, Andy, Phil, Babangida, Kate, Rachel, Russell and Simon; who made these passing years both amusing and enjoyable as well as being forced to sit through my various rants/presentations (delete as appropriate). Additional thanks go to all my friends, the UoB Jitsu crew who provided a constructive outlet for my violent stresses as well as excuses for drink and merriment and to all my friends from GKR Karate and Yardley & District RFC.

Finally I would like to thank my family without whom I would not have got this far. My thanks and appreciation for all you have done for me and the support you have always given me. Thank You.

Contents

Abstract....ii

Dedication....iii

Acknowledgements....iv

Contents....v

List of Figures....xv

List of Tables....xxv

Chapter 1: Introduction....1

1.1: Introduction....1

1.2: Aims and Objectives....3

1.3: Database....4

1.4: Basins of the Western Approaches-Celtic Sea basin system....7

1.4.1: North Celtic Sea Basin (NCSB)....9

1.4.2: South Celtic Sea Basin (SCSB)....9

1.4.3: Bristol Channel Basin (BCB)....10

1.4.4: St. George's Channel Basin (SGCB)....12

1.4.5: South Wales Coalfield and Pre-Mesozoic basin evolution....13

1.5: Background to research and previous work....14

1.5.1: Early Cretaceous exhumation....23

1.5.2: Late Cretaceous-Cenozoic exhumation....25

1.5.2.1: Magmatic underplating and the role of the Iceland Plume 30

1.5.2.2: Localised hotspot-related uplift 37

1.5.2.3: Intra-plate shortening (tectonic inversion) 38

1.5.3: Neogene exhumation across the North Atlantic region 49

Chapter 2: Techniques used to estimate the magnitude and timing of exhumation 52

2.1: Introduction 52

2.1.1: Definitions 53

2.1.1.1: Uplift 53

2.1.1.2: Exhumation 55

2.2: Estimating exhumation using compaction data 60

2.2.1: Compaction 62

2.2.2: Calculation of exhumation magnitudes 69

2.2.3: Estimating porosities from sonic velocity data 71

2.2.4: Density derived porosity 76

2.2.5: Controls on Velocity-Depth trends 77

2.2.5.1: Dewatering, viscosity and critical porosity 78

2.2.5.2: Lithology and Clay content 80

2.2.5.3: Abnormal Pressure 82

2.2.5.4: Rebound, Exhumation and Micro-cracks 83

2.2.5.5: Additional controls 85

2.2.6: Limitations of compaction studies 87

2.3: Estimating exhumation using palaeothermal data 89

2.3.1: Apatite Fission Track Analysis (AFTA) 89

2.3.1.1: Basic Principles of Apatite Fission Track Analysis 90

2.3.1.2: Fission-track dating 92

2.3.1.2.1: The significance of track age 95

2.3.1.3: Quantitative understanding of Fission-Track Annealing in Apatite 95

2.3.1.3.1: Annealing Kinetics and modelling the development of AFTA parameters 96

2.3.1.3.2: Compositional effects 97

2.3.1.3.3: Distributions of Chlorine content in common AFTA samples 101

2.3.1.3.4: Effects from other elements 102

2.3.1.3.5: Pressure effects 104

2.3.1.3.6: Alternative kinetic models 105

2.3.1.4: Deriving thermal history information from fission-track data 107

2.3.1.4.1: Cooling History 110

2.3.1.4.2: Allowing for tracks inherited from source areas 114

2.3.1.5: Plots of fission track age and mean track length versus depth and temperature 116

2.3.2: Vitrinite Reflectance (VR) 119

2.3.3: Thermal History Reconstruction (THR) 119

2.3.3.1: Construction of geothermal gradients 121

2.3.4: Limitations of AFTA and VR 127

Chapter 3: Regional Geology and exhumation history of the Western Approaches-Celtic Sea basin system 132

3.1: Introduction 132

3.2: Regional crustal structure 139

3.3: Tectono-stratigraphy of the Western Approaches-Celtic Sea basin system 144

3.3.1: Permian 146

3.3.2: Triassic 152

3.3.3: Jurassic 155

3.3.4: Cretaceous 162

3.3.5: Cenozoic 172

3.4: The timing of maximum former deeper burial from seismic 181

Chapter 4: Using compactional data to estimate exhumation in the offshore basins of the SW UK 196

4.1: Introduction 196

4.2: Determination of former deeper burial from porosity 200

4.2.1: Porosity calculation 206

4.2.2: Density derived porosity 206

4.2.2.1: Calculation of a density derived porosity trend 208

4.3: Determination of former deeper burial using ITT 215

4.3.1: Statistical curve fitting technique 215

4.3.1.1: Statistical fitting technique 217

4.3.1.2: Error assessment of the statistical fit 218

4.3.2: The Supercurve Technique 219

4.3.2.1: Corrections 221

4.3.3: The Japsen Relationships 223

4.3.4: Exhumation magnitudes relative to interval transit time-depth trends derived for the offshore SW UK 226

4.4: Exhumation results from the porosity data of the offshore SW UK 235

4.4.1: Wyllie derived exhumation 236

4.4.2: Raymer derived exhumation 247

4.4.3: Porosity relationship derived exhumation 251

4.5: Burial anomaly results from the ITT data of the offshore SW UK 261

4.5.1: Burial anomaly derived from comparison with the statistical curve fitting technique 261

4.5.2: Interpretation of results from the supercurve 265

4.5.3: Japsen Relationships 271

4.5.4: Hillis trend 276

4.6: Discussion – Validity of compactionally derived exhumation and implications for the exhumation of the offshore SW UK 280

4.6.1: Robustness of the methods used 281

4.6.1.1: Porosity approach 281

4.6.1.2: Porosity relationships 283

4.6.1.2.1: Linear Relationship 284

4.6.1.2.2: Power Relationship 284

4.6.1.2.3: Exponential Relationship 285

4.6.1.2.4: Hybrid Relationship 285

4.6.1.3 The use of a 'normal' compaction trend 287

4.6.1.4: The use of ITT to estimate former deeper burial 288

4.6.1.4.1: The statistical curve fitting approach 289

4.6.1.4.2: The supercurve and Japsen approach 290

4.6.1.5: Choice of compactional technique relevant to estimating former deeper burial in the SW UK. 293

4.6.2: The magnitude and distribution of burial anomalies in the SW UK 295

4.6.3: Implications for the relative role of Inversion versus underplating as the cause of exhumation in the SW UK 298

4.7: Conclusions 301

Chapter 5: The thermal and exhumation history of the SW UK 303

5.1: Introduction 303

5.2: Methodology 304

5.3: Thermal history data results from the SW UK 313

5.3.1: Regional AFTA dataset analysis - 'Boomerang Plots' 313

5.3.2: Palaeothermal history of the SW UK 315

5.3.2.1: Results from SW Wales 315

5.3.2.2: Results from North Devon 318

5.3.2.3: Results from South Wales 320

5.3.2.4: Results from North Somerset 322

5.3.2.5: Results from South Devon 324

5.3.3: Estimating the magnitude of exhumation using palaeothermal profiles from boreholes 326

5.3.3.1: Burton Row borehole 330

5.3.3.2: Senghenydd borehole 334

5.3.3.3: Gwendraeth Valley 2 borehole 336

5.3.3.4: Offshore Exploration wells 338

5.3.3.4.1: Wells which show evidence of elevated palaeotemperature due to deeper burial 344

5.3.3.4.1.1: Exploration well 42/21-1 344

5.3.3.4.1.2: Exploration well 48/30-1 346

5.3.3.4.1.3: Exploration well 48/30-2 347

5.3.3.4.1.4: Exploration Well 49/26-1a 348

5.3.3.4.1.5: Exploration Well 103/02-1 349

5.3.3.4.1.6: Exploration Well 106/28-1 352

5.3.3.4.2: Wells which show evidence of the passage of hot fluids 354

5.3.3.4.2.1: Exploration well 42/17-1 354

5.3.3.4.2.2: Exploration Well 49/09-1 356

5.3.3.4.2.3: Exploration Well 57/09-1 358

5.3.3.4.2.4: Exploration Well 102/28-1 359

5.3.3.4.2.5: Exploration Well 103/21-1 361

5.3.3.4.2.6: Exploration Well 106/24-1 363

5.3.3.4.2.7: Exploration Well 106/24a-2b 367

5.3.3.4.2.8: Exploration Well 107/16-1 369
5.3.3.4.3: Wells in which VR data is unreliable 373
5.3.3.4.3.1: Exploration Well 103/18-1 373
5.3.4: Thermal history modelling of AFTA data 376
5.3.4.1: The timing of cooling episodes 376
5.3.4.2: The magnitude and distribution of exhumation episodes 384
5.4: Discussion – The Mesozoic-Cenozoic exhumation of the SW UK as inferred from AFTA and VR 395
5.4.1: Timing 395
5.4.2: Magnitude and distribution 397
5.4.3: driving mechanisms for Mesozoic-Cenozoic exhumation in the SW UK 403
5.4.3.1: The Upper Triassic-Lower Jurassic episode 406
5.4.3.2: The Lower Cretaceous episode 410
5.4.3.3: The Cenozoic episodes 411
5.5: Conclusions 418
Chapter 6: Discussion & Synthesis 420
6.1: Introduction 420
6.2: Upper Triassic-Lower Jurassic Exhumation 421
6.2.1: Timing of Upper Triassic-Lower Jurassic exhumation 421
6.2.2: Magnitude and distribution of Upper Triassic-Lower Jurassic exhumation 422
6.2.3: Causes of Upper Triassic-Lower Jurassic exhumation 424
6.3: Lower Cretaceous Exhumation 428

6.3.1: Timing of Lower Cretaceous exhumation 428

6.3.2: Magnitude and distribution of Lower Cretaceous exhumation 430

6.3.3: Potential driving mechanisms of Lower Cretaceous exhumation 431

6.4: Paleogene Exhumation 435

6.4.1: Timing of Paleogene exhumation 435

6.4.2: Magnitude and distribution of Paleogene exhumation 439

6.4.3: Potential driving mechanisms of early Paleogene exhumation 443

6.5: Neogene Exhumation 457

6.5.1: Timing of Neogene exhumation 457

6.5.2: Magnitude and distribution of Neogene exhumation 459

6.5.3: Potential driving mechanisms of Neogene exhumation 460

6.6: Implications 466

6.6.1: General comments on the nature of exhumation episodes 466

6.6.2: Implications for Petroleum prospectivity 470

6.6.3: General implications of the results of this study for understanding the 474

exhumation histories of passive margin and intraplate regions 474

Chapter 7: Conclusions 485

7.1: Conclusions 485

7.2: Recommendations for further work 491

References 496

APPENDIX A 546

APPENDIX B.....581

APPENDIX C.....614

LIST OF FIGURES

1.1	Location map of wells used in the study	6
1.2	Location map of seismic survey lines	7
1.3	Map of the sedimentary basins of the North Atlantic region	8
1.4	Seismic cross-section through the North Celtic Sea Basin and South Celtic Sea Basin	10
1.5	Structural section across the Bristol Channel Basin	12
1.6	Palaeotectonic reconstruction of the North Atlantic during the Jurassic and early Cretaceous	20
1.7	Palaeotectonic reconstruction of the North Atlantic during the late Cretaceous and Paleocene	21
1.8	Palaeotectonic reconstruction of the North Atlantic during the Oligocene and Miocene	22
1.9	Palaeogeographic reconstruction of NW Europe during the early Cretaceous	24
1.10	Palaeogeographic reconstruction of NW Europe during the late Cretaceous	27
1.11	Quaternary sub-crop map of the offshore SW UK	28
1.12	Palaeogeographic reconstruction of NW Europe during the Paleocene	29
1.13	Comparison of timing of onshore early Paleogene magmatic activity across the British Isles with periods of submarine fan deposition in North Sea Basin	31
1.14	Diagram illustrating the effect of magmatic underplating	33
1.15	Zones of thermal and dynamic uplift associated with a mantle plume	34
1.16	Gravity map of the UK illustrating predicted thickness of underplating	36
1.17	Cope's (1994) late Cretaceous erosion map for the Irish Sea	37
1.18	Effect of shortening column of crust by horizontal compression on surface uplift	40
1.19	Classical positive inversion structure	41
1.20	Palaeogeographic reconstruction of NW Europe during the Oligocene	42
1.21	Palaeogeographic reconstruction of NW Europe during the Miocene	43
1.22	Cenozoic event stratigraphy for the British Isles	44
1.23	Stress map of Europe and the North Atlantic	46
1.24	Correlation of Cenozoic tectonic events in southern Britain and the Alpine foreland	48
1.25	Areas of Neogene uplift and subsidence around the North Atlantic	51
2.1	Schematic cross sections illustrating the possible effects of erosion on the elevation of mountain belts and valleys	55
2.2	Some typical responses of the sonic log	61
2.3	Compaction in a shale sequence	63
2.4	Porosity evolution in a Chalk sequence during burial	63
2.5	Porosity-depth curves for shales	65
2.6	Porosity-depth curves for sandstones	66
2.7	Porosity-depth curves for limestones	67
2.8	Evolution of porosity vs. depth trends in exhumed sedimentary basins	70
2.9	Method used to calculate exhumation from compaction data for a well or borehole	71

2.10	Diagrammatic representation of the path of P-waves through a rock	72
2.11	Interval transit time compared to measured porosity in a dolomite	73
2.12	Porosity predictions from the Wyllie time average equation in sediments calcareous oozes and oceanic basalts	75
2.13	Empirical relationship between porosity and transit time of the shales of Cretaceous age in western Canada	79
2.14	Influence of clay content on the P-wave velocity-porosity relationship at a constant confining pressure	81
2.15	Calculated velocity and porosity using a sand/clay model at various pressures	82
2.16	A graph showing porosity rebound versus depth	85
2.17	Diagram showing the effects of gas saturation on the P-wave velocity of a rock	86
2.18	The maximum extent of the two major Pliestocene glaciations in the British terrestrial record	86
2.19	Diagram illustrating the general principles for calculating exhumation from thermal history data	91
2.20	Formation of fission-tracks in uranium bearing minerals	92
2.21	Application of external detector method in order to determine fission-track age of apatite sample	93
2.22	Results of Laslett et al. (1987) annealing model fitted to experimental Data	99
2.23	Mean track length in apatite's with four different Chlorine contents	100
2.24	Comparison of measured mean track length in samples from four Otway Basin reference wells and predicted mean track lengths from the new multi-compositional kinetic model of fission track annealing	101
2.25	Range of Cl content in apatite's from different sources	103
2.26	Comparison of predictions of Carlson's (1990) models with data from South Texas	106
2.27	Comparison of mean track length in samples from four Otway Basin reference wells and predicted mean track lengths from three kinetic models for fission track annealing	107
2.28	Forward modelling methodology of Green et al. (1989) for measured apatite fission track age and track length distributions	109
2.29	The thermal response of fission-tracks in apatite to geological thermal histories	110
2.30	Predicted fission-track length distributions for various thermal history Scenarios	113
2.31	Typical pattern of AFTA parameters in a well in which samples throughout the entire section are currently at their maximum temperatures since deposition and those in which they were hotter in the past	118
2.32	Constraining geothermal gradient	122
2.33	Palaeotemperature profiles produced by heating due to deeper burial, elevated basal heat flow and fluid flow	123
2.34	Estimation of amount of additional section by extrapolation of palaeotemperature profile to assumed palaeosurface temperature	124
2.35	Accuracy of geothermal gradient	126

2.36 Graphical construction of Dow (1977) for the estimation of removed section at an unconformity 127
2.37 Pitfalls in VR interpretation 131

3.1 Free-air gravity anomaly map of the offshore Western Shelves region 135
3.2 Chronostratigraphy of the St. George's Channel Basin 136
3.3 Chronostratigraphy of the Celtic Sea basins 137
3.4 Terranes of the Caledonian and Variscan orogens in Britain and Ireland 138
3.5 Variscan inversion tectonics and other structural elements of the British Isles and Ireland 140
3.6 Depth to seismic reflection Moho beneath the western UK region 141
3.7 Part of BIRPS SWAT2 seismic reflection profile through St. George's Channel Basin 142
3.8 Depth converted geological sections through the Western Approaches-Celtic Sea basin system 143
3.9 Late Carboniferous palaeogeography showing basement structural features 145
3.10 Early Permian framework of the Arctic-North Atlantic domain 147
3.11 Stratigraphic correlation chart of the Mesozoic-Cenozoic for the Western Shelves area 148
3.12 Decompaction of a sedimentary sequence by backstripping 151
3.13 Crustal subsidence history curve for Dorset Basin 151
3.14 Tectonic map of the Celtic Sea-Western Approaches area 155
3.15 Rhaetian-Hettangian palaeogeography 156
3.16 Late Jurassic framework of Arctic-North Atlantic domain 159
3.17 Generalised variation in global sea-level for the Jurassic and Cretaceous periods 163
3.18 Generalised palaeogeography during Early Cretaceous times 164
3.19 Plate reconstruction showing the opening of the North Atlantic 165
3.20 Generalised palaeogeography during Late Cretaceous times 171
3.21 Generalised palaeogeography during Paleocene times 174
3.22 Generalised palaeogeography during Oligocene times 175
3.23 Generalised palaeogeography during Miocene times 176
3.24 Schematic structural cross-section of the Channel area 178
3.25 Geological map of the Celtic Sea-Western Approaches area 178
3.26 Map highlighting the location of the seismic data used in this study 184
3.27 Example of the well data used to tie the seismic lines 185
3.28 Seismic line from the NCSB showing the two unconformities recognised in this study 186
3.29 Seismic line from the NCSB showing the two unconformities recognised in this study 187
3.30 Seismic section from the SGCB showing evidence of compressional reactivation of normal faults 188
3.31 Seismic section from the SGCB showing the onlapping of reflectors against the base Cenozoic unconformity 189
3.32 Seismic section from the SGCB showing evidence of compressional reactivation of normal faults 190
3.33 Seismic section from the SGCB showing evidence of the erosional nature of the 'Late Cimmerian unconformity' 191
3.34 TWTT map of the base Cenozoic unconformity 192

3.35	TWTT map of the base Chalk	193
3.36	North-South section across the southern part of the NCSB in Irish waters	194
3.37	Tectonostratigraphic chart for the Celtic Sea region	195
4.1	Core porosity measurements for the Sherwood Sandstone from three locations in the North Porcupine and Slyne/Erris basins compared with average porosity measurements in the exhumed East Irish Sea Basin and Southern North Sea Basin	197
4.2	Techniques for estimating exhumation from sonic velocity data	199
4.3	Wells depicting Sherwood Sandstone Group lithostratigraphy, with geophysical logs	203
4.4	Wells depicting Mercia Mudstone Group lithostratigraphy, with geophysical logs	204
4.5	Logs of wells from the South Celtic Sea and Bristol Channel basins showing Lias Group stratigraphy	205
4.6	The effect of adding the density correction to the original density data	207
4.7	Calculated porosity data for offshore well 103/18-1	210
4.8	Calculated porosity data for offshore well 103/21-1	211
4.9	Comparison of the density derived porosities versus interval transit time (ITT) for the various wells and lithologies	212
4.10	Graph showing a linear relationship fitted to the porosity data derived from the density log	212
4.11	Graph showing a power relationship fitted to the porosity data derived from the density log	213
4.12	Graph showing an exponential relationship fitted to the porosity data derived from the density log	213
4.13	Graph showing the relationships between interval transit time and density derived porosity for the Mohcras borehole and the offshore wells 103/18-1 and 103/21-1	214
4.14	Graph showing a the 'hybrid' best fit relationship fitted to the porosity data derived from the density log	214
4.15	Transit time versus temperature relationships of NaCl brines	217
4.16	Calculation of supercurve for the offshore SW UK exploration wells	222
4.17	Typical curve for sonic travel time (Δt) and porosity vs. depth for Lias shales at maximum burial depth illustrating the method for estimating thickness of eroded overburden	223
4.18	A compilation of velocity-depth trends for the Bunter Shale Formation from various authors	225
4.19	Porosity evolution in a Chalk sequence	228
4.20	Example of 1:4000 scale sonic log used for picking the tops and bases of the stratigraphic units	231
4.21	Graph showing Interval Transit Time (ITT) against midpoint depth (D) for the Upper Cretaceous Chalk for exploration wells in the SW United Kingdom	232
4.22	Graph showing Interval Transit Time (ITT) against midpoint depth (D) for the Lower Cretaceous Greensand for exploration wells in the SW United Kingdom	233

4.23 Graph showing Interval Transit Time (ITT) against midpoint depth (D) for the Lower Jurassic Lias Group for exploration wells in the SW United Kingdom 233
4.24 Graph showing Interval Transit Time (ITT) against midpoint depth (D) for the Upper Triassic Mercia Mudstone Group for exploration wells in the SW United Kingdom 234
4.25 Graph showing Interval Transit Time (ITT) against midpoint depth (D) for the Triassic Sherwood Sandstone for exploration wells in the SW United Kingdom 234
4.26 Porosity data for well 93/02-3 and 93/06-1 using the Wyllie time-average equation and Raymer-Hunt-Gardner transform 238
4.27 Porosity data for the Burton Row borehole using the Wyllie time-average equation and Raymer-Hunt-Gardner transform 239
4.28 Total exhumation magnitudes calculated from Wyllie derived porosity (68µs/ft matrix velocity) for each of the offshore wells 240
4.29 Total exhumation magnitudes calculated from Wyllie derived porosity (60µs/ft matrix velocity) for each of the offshore wells 242
4.30 Total exhumation magnitudes calculated from Wyllie derived porosity (68µs/ft matrix velocity and no correction factor) for each of the offshore wells 245
4.31 Map showing total exhumation magnitudes calculated from Wyllie derived porosity (60µs/ft matrix velocity and no correction factor) for each of the offshore wells 246
4.32 Map showing total exhumation magnitudes calculated from Raymer derived porosity (68µs/ft matrix velocity) for each of the offshore wells 249
4.33 Map showing total exhumation magnitudes calculated from Raymer derived porosity (60µs/ft matrix velocity) for each of the offshore wells 250
4.34 Map showing total exhumation magnitudes calculated using the density log derived linear relationship for each of the offshore wells 253
4.35 Map showing total exhumation magnitudes calculated using the density log derived power relationship for each of the offshore wells 256
4.36 Map showing total exhumation magnitudes calculated using the density log derived exponential relationship for each of the offshore wells 257
4.37 Map showing total exhumation magnitudes calculated using the density log derived hybrid relationship for each of the offshore wells 260
4.38 Graph showing the calculated compaction trend and erosion amount for well 103/18-1 263
4.39 Graph showing the calculated compaction trend and erosion amount for the Burton Row 264
4.40 Map showing total exhumation magnitudes for each of the offshore wells as derived from the statistical curve fitting technique 265
4.41 Comparison of ITT for the shale sequences of wells 106/24-2, 106/28-1 and the Burton Row borehole with the supercurve derived for the SW UK 268
4.42 Map showing total exhumation magnitudes calculated for the Supercurve for each of the offshore wells 269
4.43 Map showing total exhumation magnitudes calculated using the Ware & Turner (2002) supercurve for each of the offshore wells 270

4.44 Comparison of interval transit time-depth values compared to the Lower Jurassic shale and Triassic Bunter shale trends of Japsen (2000) for wells 50/03-1, 93/02-2, 93/02-3 and 93/06-1 272
4.45 Map showing total exhumation magnitudes calculated for the Lower Jurassic Shale trend of Japsen (2000) for each of the offshore wells 274
4.46 Map showing total exhumation magnitudes calculated for the Japsen (2000) Bunter Shale trend for each of the offshore wells 275
4.47 Map showing total exhumation magnitudes for the post-Juarassic calculated using the Hillis approach for each of the offshore wells 278
4.48 Map showing total exhumation magnitudes for the post-Cretaceous calculated using the Hillis approach for each of the offshore wells 279
4.49 Velocity versus porosity in clay-free sandstones 283
4.50 Schematic burial diagrams for the Mesozoic succession illustrating the relationship between burial anomalies ('uplift') for the Chalk and the Triassic in the same well 294
4.51 Comparison of AFTA/VR and sonic velocity derived uplift-erosion estimates for wells in the Wessex Basin 297
4.52 Underplating map of Al-Kindi et al. (2003) converted to an exhumation map 300

5.1 Forward modelling method for measured apatite fission track age and track length distributions 306
5.2 Process for creation and interpretation of AFTA histograms I 307
5.3 Process for creation and interpretation of AFTA histograms II 308
5.4 Basic framework for calculating a thermal history plot to get maximum palaeotemperature data 309
5.5 Basic framework for calculating a thermal history plot to get timing of cooling data 310
5.6 Interpreting the thermal history plot – basics 311
5.7 Interpreting the thermal history plot – multiple episodes 311
5.8 Pitfalls of AFTA – multiple scenarios 312
5.9 Example of a thermal history plot and histogram 312
5.10 The relationship between mean track length and fission-track age for AFTA samples collected from across the SW UK. 314
5.11 Map showing locations of onshore AFTA samples from Pembrokeshire 316
5.12 Fission track length histograms from the Pembroke Peninsular 317
5.13 Map showing locations of onshore AFTA samples from North Devon 318
5.14 Fission track length histograms from North Devon 319
5.15 Map showing locations of onshore AFTA samples from South Wales 320
5.16 Fission track length histograms from South Wales 321
5.17 Map showing locations of onshore AFTA samples from North Somerset 322
5.18 Fission track length histograms from North Somerset 323
5.19 Map showing locations of onshore AFTA samples from South Devon, Somerset and Dorset 324
5.20 Fission track length histograms from South Devon, Somerset and Dorset 325
5.21 Location map showing the wells analysed in this study 326
5.22 Vitrinite reflectance profiles from wells and boreholes across the SW UK 329
5.23 Palaeotemperature constraints from AFTA and VR data from the Burton Row borehole plotted against depth 332

5.24 Amount of additional section and palaeogeothermal gradients required to explain the Paleogene palaeothermal episode at the Burton Row borehole 333
5.25 Palaeotemperature constraints from VR data from the Senghenydd borehole plotted against depth 334
5.26 Amount of additional section and palaeogeothermal gradients required to explain the palaeothermal episode at the Senghenydd borehole 335
5.27 Palaeotemperature constraints from VR data from the Gwendraeth Valley 2 borehole plotted against depth 337
5.28 Amount of additional section and palaeogeothermal gradients required to explain the palaeothermal episode at the Gwendraeth Valley 2 borehole 338
5.29 Map showing the distribution of VR temperature-depth plots which indicate elevated palaeotemperatures were due primarily to deeper burial 340
5.30 Map showing the distribution of VR temperature-depth plots which indicate elevated palaeotemperatures were due primarily to deeper burial but also with evidence of 'heat spikes' from fluid flow 341
5.31 Map showing the distribution and amount of additional section and palaeogeothermal gradients required to explain the palaeothermal episodes recognised in the VR data of the offshore wells 342
5.32 Map showing the distribution and amount of additional section and palaeogeothermal gradients required to explain the palaeothermal episodes recognised in the VR data of the offshore wells 343
5.33 Palaeotemperature constraints from VR data from well 42/21-1 plotted against depth 344
5.34 Palaeotemperature constraints derived from AFTA and VR data in individual samples from well 42/21-1 plotted against depth 345
5.35 Palaeotemperature constraints from VR data from well 48/30-1 plotted against depth 346
5.36 Palaeotemperature constraints from VR data from well 48/30-2 plotted against depth 347
5.37 Palaeotemperature constraints from VR data from well 49/26-1a plotted against depth 349
5.38 Geoseismic section through well 103/02-1 350
5.39 Palaeotemperature constraints from AFTA and VR data from well 103/02-1 plotted against depth 351
5.40 Palaeotemperature constraints from AFTA and VR data from well 106/28-1 plotted against depth 353
5.41 Fission-track length distribution and accompanying thermal history solution for AFTA sample from exploration well 106/28-1 in the SGCB 353
5.42 Palaeotemperature constraints from VR data from well 42/17-1 plotted against depth 355
5.43 Palaeotemperature constraints from VR data from well 49/09-1 plotted against depth 357
5.44 Palaeotemperature constraints from VR data from well 57/09-1 plotted against depth 358
5.45 Geoseismic section through well 102/28-1 359
5.46 Palaeotemperature constraints from AFTA and VR data from well 102/28-1 plotted against depth 360
5.47 Migrated seismic profile and interpreted geo-seismic section incorporating well 103/21-1 361

5.48 Palaeotemperature constraints from AFTA and VR data from well 103/21-1 plotted against depth 362
5.49 Seismic section incorporating well 106/24-1 in the main SGCB depocentre 364
5.50 Fission-track length distribution and accompanying thermal history solution for AFTA sample from exploration well 106/24-1 in the SGCB 365
5.51 Palaeotemperature constraints from AFTA and VR data from well 106/24-1 plotted against depth 366
5.52 Palaeotemperature constraints from AFTA and VR data from well 106/24a-2b plotted against depth 367
5.53 Fission-track length distributions and accompanying thermal history solutions for AFTA samples from exploration well 106/24a-2b in the SGCB 369
5.54 Seismic line through well 107/16-1 located in the NE SGCB 371
5.55 Fission-track length distribution and accompanying thermal history solution for AFTA sample from exploration well 107/16-1 in the SGCB 371
5.56 Palaeotemperature constraints from AFTA and VR data from well 107/16-1 plotted against depth 372
5.57 Migrated seismic profile and interpreted geoseismic section incorporating well 103/18-1 374
5.58 Palaeotemperature constraints from AFTA and VR data from well 103/18-1 plotted against depth 375
5.59 Map showing distribution of THR solutions for all SW UK samples 377
5.60 Estimates of the time at which cooling episodes began for each sample based on thermal history interpretation of the AFTA data 378
5.61 Timing of cooling episodes for a series of apatite samples collected from onshore SW Wales based on thermal history interpretation of apatite fission track data 379
5.62 Timing of cooling episodes for a series of apatite samples collected from onshore South Wales based on thermal history interpretation of apatite fission track data 380
5.63 Timing of cooling episodes for a series of apatite samples collected from onshore South Devon, Somerset and Dorset based on thermal history interpretation of apatite fission track data 381
5.64 Timing of cooling episodes for a series of apatite samples collected from onshore North Somerset and the Bristol Channel based on thermal history interpretation of apatite fission track data 383
5.65 Timing of cooling episodes for a series of apatite samples collected from onshore North Devon based on thermal history interpretation of apatite fission track data 383
5.66 Map showing distribution of palaeotemperatures derived from AFTA attained prior to cooling during the early Jurassic 385
5.67 Map showing distribution of palaeotemperatures derived from AFTA attained prior to cooling during the early Cretaceous 386
5.68 Map showing distribution of palaeotemperatures derived from AFTA attained prior to cooling during the Miocene 386
5.69 Maps of palaeotemperatures attained prior to early Jurassic, early Cretaceous and Cenozoic (Miocene) cooling episodes 389
5.70 Map showing the distribution of maximum palaeotemperatures from VR data in the BCB 390

5.71 Series of contour maps showing maximum and minimum estimates of the amount by which the SW UK region was more deeply buried prior to the Upper Triassic cooling episode 392
5.72 Series of contour maps showing maximum and minimum estimates of the amount by which the SW UK region was more deeply buried prior to the Lower Cretaceous cooling episode 393
5.73 Series of contour maps showing maximum and minimum estimates of the amount by which the SW UK region was more deeply buried prior to the Cenozoic cooling episode 394
5.74 Synoptic diagram of fault valve behaviour (Sibson, 2007) 399
5.75 Map showing the magnitude of exhumation in the offshore wells across the SW UK derived from AFTA and VR data 401
5.76 Comparison between Lower Jurassic Palaeogeographic setting of NW Wales andCardigan Bay as indicated by results from this study and those of Holford (2006), and that proposed by Dobson & Whittington (1987) 408
5.77 Model to account for the observation of the Upper Triassic-Lower Jurassic exhumation across the SW UK 409
5.78 Model to account for the observation of Lower Cretaceous exhumation across the SW UK 412
5.79 Table of tectonic stages 414
5.80 Model to account for the observation of the Cenozoic exhumation episodes across the SW UK 415
5.81 Schematic boundary conditions from the modelling work of Gölke & Coblentz, (1996) showing the two main stress fields acting on NW Europe during the late Cenozoic 416

6.1 Mesozoic event stratigraphy diagram for the SW UK 422
6.2 Palaeotemperature profile and reconstructed burial history from AFTA and VR data from the Wytch Farm wells 423
6.3 Middle Jurassic palaeogeographic reconstruction for the British Isles region 427
6.4 Cretaceous event stratigraphy diagram 429
6.5 Palaeotemperature profile and reconstructed burial history from AFTA and VR data from the Kimmeridge-5 well 431
6.6 Evidence for depth-dependent stretching SW of Britain during the early Cretaceous 434
6.7 Examples of models of landscape evolution at rifted continental Margins 435
6.8 Early Paleogene event stratigraphy diagram 438
6.9 Graph showing time of cooling from maximum palaeotemperature (from AFTA) for five wells compared to the timing of the Cenozoic igneous activity 439
6.10 Palaeotemperature profile and reconstructed burial history from AFTA and VR data from the Lulworth Banks well 441
6.11 Palaeotemperature profile and reconstructed burial history from AFTA and VR data from the Arreton-2 well 441
6.12 Apparent erosion magnitude from VR and AFTA data, modelled at four wells in the NCSB 442
6.13 Maps of the predicted thickness of early Paleogene underplating beneath the British Isles and expected magnitudes of exhumation 447

6.14	Examples of non-uniform shortening within sedimentary basins	453
6.15	Hillis's (1992) two-layer compressional deformation model for the Cenozoic exhumation of the British Isles	455
6.16	Schematic model relating the observations of data from logs, seismic, AFTA and VR to explain the current and palaeo-BCB	456
6.17	Cenozoic event stratigraphy diagram	458
6.18	Schematic model of the SGCB to account for the observations from logs, seismic, AFTA and VR as revealed by this study	465
6.19	Regional extent of Lower Cretaceous, Paleogene and Neogene exhumation episodes	467
6.20	Summary map of the main exhumation episodes that have affected the western UKCS	468
6.21	Comparison between timing of exhumation episodes and variations in sea level and surface temperature	469
6.22	Burial histories modelled for wells 48/19-1 and 50/03-1 in the NCSB	473
6.23	Top Lower Jurassic pre-uplift depth map with maturity estimation of the NCSB	474
6.24	Apatite fission-track age map for Southern Africa	478
6.25	Apatite fission-track age map for the Australian continent	480
6.26	Plot of fission track age vs. mean track length for the North Atlantic data	481
6.27	Lithospheric cross-sections linking Mesozoic-Cenozoic exhumation episodes with major coeval plate tectonic events	484

LIST OF TABLES

1.1	Table showing the data available in this study	5
1.2	Compilation of published exhumation estimates for the Irish and Celtic Sea basin systems	17
2.1	Lexicon of terms used to describe uplift and exhumation	57
2.2	Summary of techniques for measuring amount and timing of exhumation	58
2.3	Summary of techniques for measuring amount and timing of exhumation	59
2.4	Some common matrix velocities	74
2.5	Mineral velocities at room temperature and pressure	76
2.6	An example of density – porosity characteristics of a deep sea, terrigenous sediment	84
4.1	Data defining normal compaction relations	232
4.2	Exhumation magnitudes based on the Sclater and Christie (1980) trend using the Wyllie time-average equation and a matrix interval transit time of 68μs/ft to derive porosities	239
4.3	Exhumation magnitudes based on the Sclater and Christie (1980) trend using the Wyllie time-average equation and a matrix interval transit time of 60μs/ft to derive porosities	241
4.4	Exhumation magnitudes based on the Sclater and Christie (1980) trend using the uncorrected Wyllie time-average equation and a matrix interval transit time of 68μs/ft to derive porosities	244
4.5	Exhumation magnitudes based on the Sclater and Christie (1980) trend using the uncorrected Wyllie time-average equation and a matrix interval transit time of 60μs/ft to derive porosities	244
4.6	Exhumation magnitudes based on the Sclater and Christie (1980) trend using the Raymer-Hunt Gardner equation and a matrix interval transit time of 68μs/ft to derive porosities	248
4.7	Exhumation magnitudes based on the Sclater and Christie (1980) trend using the Raymer-Hunt-Gardner equation and a matrix interval transit time of 60μs/ft to derive porosities	248
4.8	Exhumation magnitudes based on the Sclater and Christie (1980) trend using the density derived linear relationship	252
4.9	Exhumation magnitudes based on the Sclater and Christie (1980) trend using the density derived power relationship	254
4.10	Exhumation magnitudes based on the Sclater and Christie (1980) trend using the density derived exponential relationship	255
4.11	Exhumation magnitudes based on the Sclater and Christie (1980) trend using the density derived hybrid relationship	259
4.12	Table showing the optimum shift constants and apparent and total exhumation magnitudes for the wells analysed using the statistical curve fitting technique	262
4.13	Table showing apparent and total exhumation magnitudes derived from the supercurve technique	267

4.14 Table showing apparent and total exhumation magnitudes derived from the Ware & Turner (2002) supercurve 267
4.15 Table showing apparent and total exhumation magnitudes derived from comparison with the Japsen (2000) Lower Jurassic shale trend 273
4.16 Table showing apparent and total exhumation magnitudes derived from comparison with the Japsen (2000) Triassic Bunter shale trend 273
4.17 Table showing apparent and total exhumation magnitudes derived from using the approach of Menpes & Hillis (1995) 277
4.18 Table showing a comparison of total exhumation values for each of the techniques used 280

5.1 Palaeogeothermal gradients derived for the offshore wells of the NCSB based on work by Corry & Brown (1998) 328
5.2 Exhumation estimates from the offshore wells and onshore boreholes of the SW UK using palaeothermal data 399
5.3 Compilation of published estimates of exhumation for 54 wells offshore Ireland 405

CHAPTER 1: INTRODUCTION

1.1: INTRODUCTION

The aim of this Chapter is to provide a background to the work presented in this thesis and to provide a full review of previous research. The Chapter outlines the main aims and objectives of the thesis and also the data utilised to meet those objectives.

A multitude of geological, geophysical and geomorphological observations at both constructive and destructive plate margins have been accounted for by application of plate tectonic theory, however these models are less successful at explaining many similar observations (e.g. topography and seismicity) of intra-plate regions (Allen & Allen, 2005). A major uncertainty is the origins of anomalous vertical motions (i.e. subsidence/burial and uplift/exhumation) within continental interiors and adjacent to passive margins (e.g. Cloetingh *et al.* 1990; Japsen & Chalmers, 2000). Recently the increased use of thermochronological tools such as Apatite Fission-Track Analysis (AFTA) across apparently stable intra-plate regions across the world (e.g. NW Europe, SW Australia, Southern Africa) has repeatedly revealed evidence for extensive phases of kilometre-scale exhumation with no obvious causal mechanisms (Green *et al.* 2002). This exhumation clearly has major implications for the interactions between Earth surface processes and geodynamic phenomena such as lithospheric plate motions and mantle convection and elucidating the driving mechanisms is clearly a problem of global tectonic significance (e.g. Cooper & Williams, 1989; Buchanan & Buchanan, 1995; Doré *et al*. 2002*a*).

Taking the south-western UKCS as its example, this thesis uses palaeothermal (AFTA and Vitrinite Reflectance (VR) data) and compactional (e.g. porosities inferred from sonic and

density logs) data to constrain the timing and magnitude of exhumation of a major intra-plate basin system (the Celtic Sea) whose development was influenced by both Alpine orogenesis and North Atlantic rifting. This exhumation can be achieved by a number of processes such as post-orogenic unroofing, rift-flank uplift, hotspot activity, compressive tectonics, eustatic sea-level change, glaciation and isostatic readjustment (Doré *et al.* 2002*a*).

As global oil and gas resources continue to deplete and 'easy oil' all but produced, hydrocarbon exploration is becoming increasingly focused on 'higher risk' sedimentary basins such as those in deeper water or those which have been affected by exhumation (Macgregor, 1995; Doré *et al.* 2002*b*). It is well known that exhumation can have profound effects, both positive and negative, on the hydrocarbon systems of sedimentary basins (e.g. Doré & Jensen, 1996; Doré *et al.* 2002*a*; Turner & Williams, 2004). For example, in inverted basins the timing of oil generation in relation to that of trap formation is a crucial factor in determining hydrocarbon prospectivity. It is therefore essential to reconstruct the thermal and tectonic histories of inverted basins as accurately and precisely as possible, particularly the time at which hydrocarbon generation effectively ceases (which can be taken to be synchronous with the onset of cooling from maximum palaeotemperatures). The relationship between this timing and episodes of uplift and erosion (e.g. due to inversion) is important in determining whether potential trapping structures have been produced particularly where multiple episodes may have occurred (Green *et al.* 1995). It is important to adopt a multi-parameter approach since studies of inverted basins which are based only on the preserved section using techniques such as back-stripping, structural analysis, section balancing etc. provide only partial insight into the thermal and tectonic history of basin development, although this approach is quite common (e.g. Chadwick, 1986; Karner *et al.* 1987*a*). Aside

from a scientific perspective therefore, establishing a better understanding of the causes and effects of exhumation is also of significant economic importance.

1.2: AIMS AND OBJECTIVES

The principle aim of this thesis is to investigate the Mesozoic-Cenozoic thermal and to a lesser extent structural evolution of the southwest UK primarily by the integrated analysis and interpretation of palaeothermal (i.e. AFTA and VR data) and compaction (i.e. sonic velocity and formation density logs) based proxies of formerly deeper burial thereby contributing to the understanding of the magnitude, timing and driving mechanisms of exhumation in intra-plate regions. The main objectives are as follows:

- Assess the timing of palaeothermal events and relate them to recognised tectonic events in NW Europe.

- Assess and compare the magnitude of exhumation derived by separate (thermal and mechanical) methods and thereby test the robustness of different methods for the calculation of exhumation magnitudes in basin studies.

- Investigate the distribution of exhumation values across the SW UK and assess the relative importance of nearby structural features on those values.

- Identify potential driving mechanisms for the observed distribution, timing and magnitude of exhumation.

- Place the results in the wider regional context and discuss their impact on the understanding of intra-plate exhumation and structural evolution of the North Atlantic region.

1.3: DATABASE

The majority of the palaeothermal data presented in this thesis comes from Geotrack open report #GC429 on the Bristol Channel. The palaeothermal database comprises 77 AFTA samples collected (by Geotrack) from outcrops across the SW UK and an additional 27 VR samples. There is also a set of 28 samples collected from across the Bristol Channel mainly from BGS shallow boreholes. In order to fill in some of the data gaps present in the Geotrack report the author undertook Summer Fieldwork in 2006 and collected a further 15 samples from the central Devon area. Of these 15 samples only 5 were of high enough quality to yield useful results for AFTA (other samples being affected by weathering or low uranium content). A summary of the data used is provided in Table 1.1. A set of 2D digital seismic data shot by Fugro was used for this study covering the NCSB and south-western SGCB. Well control in the NCSB is provided by 3 wells (48/29-1, 48/30-1 and 48/30-2) and these were used to tie the NCSB and SGCB lines together. The locations of the offshore wells are shown in Figure 1.1 whilst Figure 1.2 shows a location map for the seismic lines.

Well/borehole	VR	AFTA	Sonic	Density	Gamma
42/16-1	✓	✓	×	×	×
42/17-1	✓	✓	×	×	×
42/21-1	✓	✓	×	×	×
48/19-1	✓	×	×	×	×
48/30-1	✓	×	×	×	×
48/30-2	✓	×	×	×	×
49/09-1	✓	×	×	×	×
49/26-1	✓	×	×	×	×
50/03-1	✓	×	✓	×	×
50/03-2	×	×	✓	×	×
57/09-1	✓	×	×	×	×
93/02-2	×	×	✓	×	×
93/02-3	×	×	✓	×	×
93/06-1	×	×	✓	×	×
102/28-1	✓	✓	✓	×	×
102/28-2	×	×	✓	×	×
103/01-1	✓	×	✓	×	×
103/02-1	✓	✓	✓	×	×
103/18-1	✓	✓	✓	✓	✓
103/21-1	✓	✓	✓	✓	✓
106/18-1	×	×	✓	×	×
106/20-1	×	×	✓	×	×
106/24-1	✓	✓	✓	×	×
106/24-2	✓	✓	✓	×	×
106/28-1	✓	✓	✓	×	×
107/16-1	✓	✓	×	×	×
Burton Row	✓	✓	✓	✓	✓
Gwendraeth Valley 2	✓	×	×	×	×
Senghenydd	✓	×	×	×	×
Mohcras Farm	✓	✓	✓	✓	✓

Table 1.1 - Table showing the data available for each well or borehole used in this study.

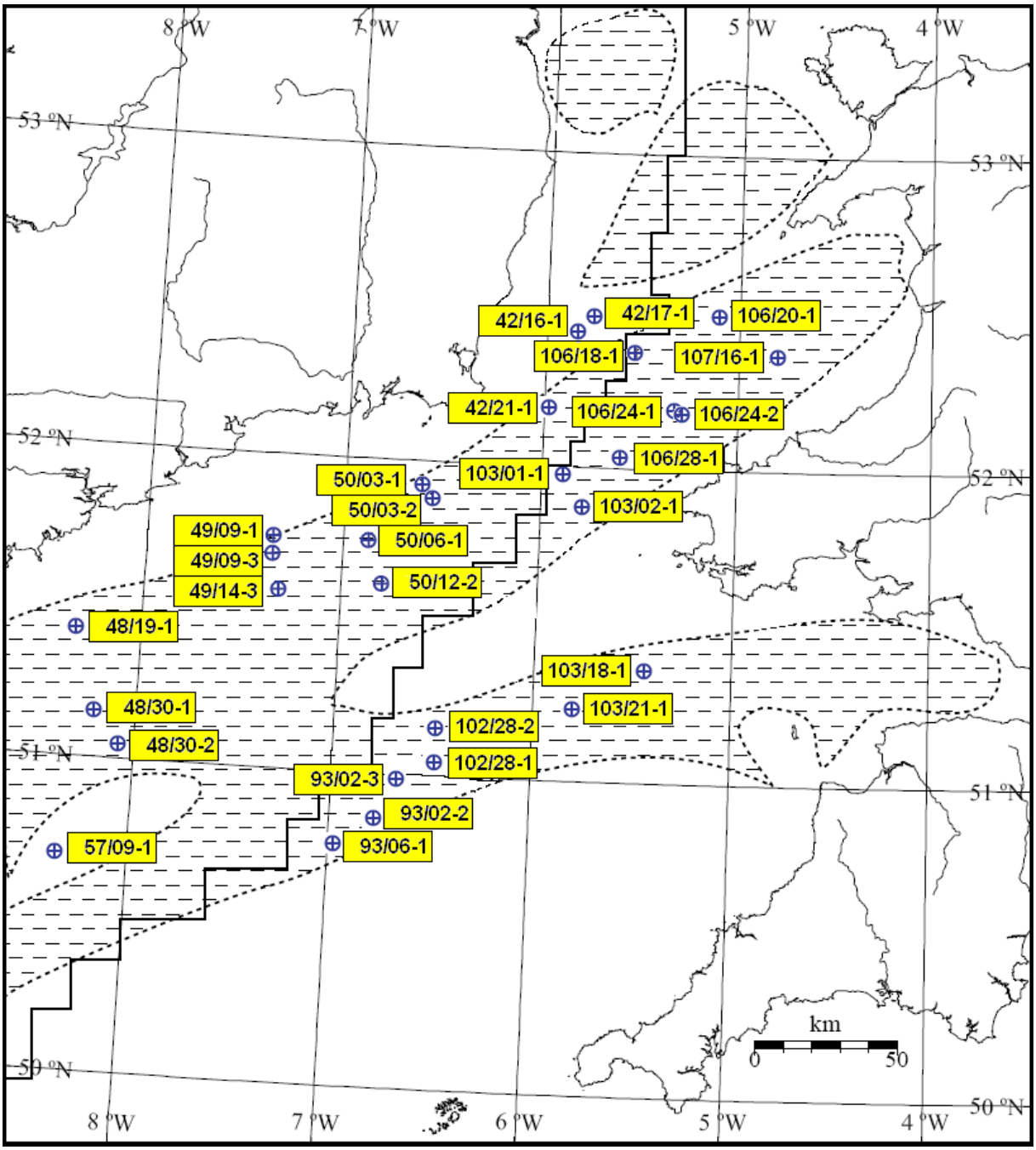

Figure 1.1 - Map showing the location of exploration wells used for evaluation of exhumation in the SW UK. The main Mesozoic-Cenozoic depocentres are shaded with a stippled fill (based on Williams, 2002).

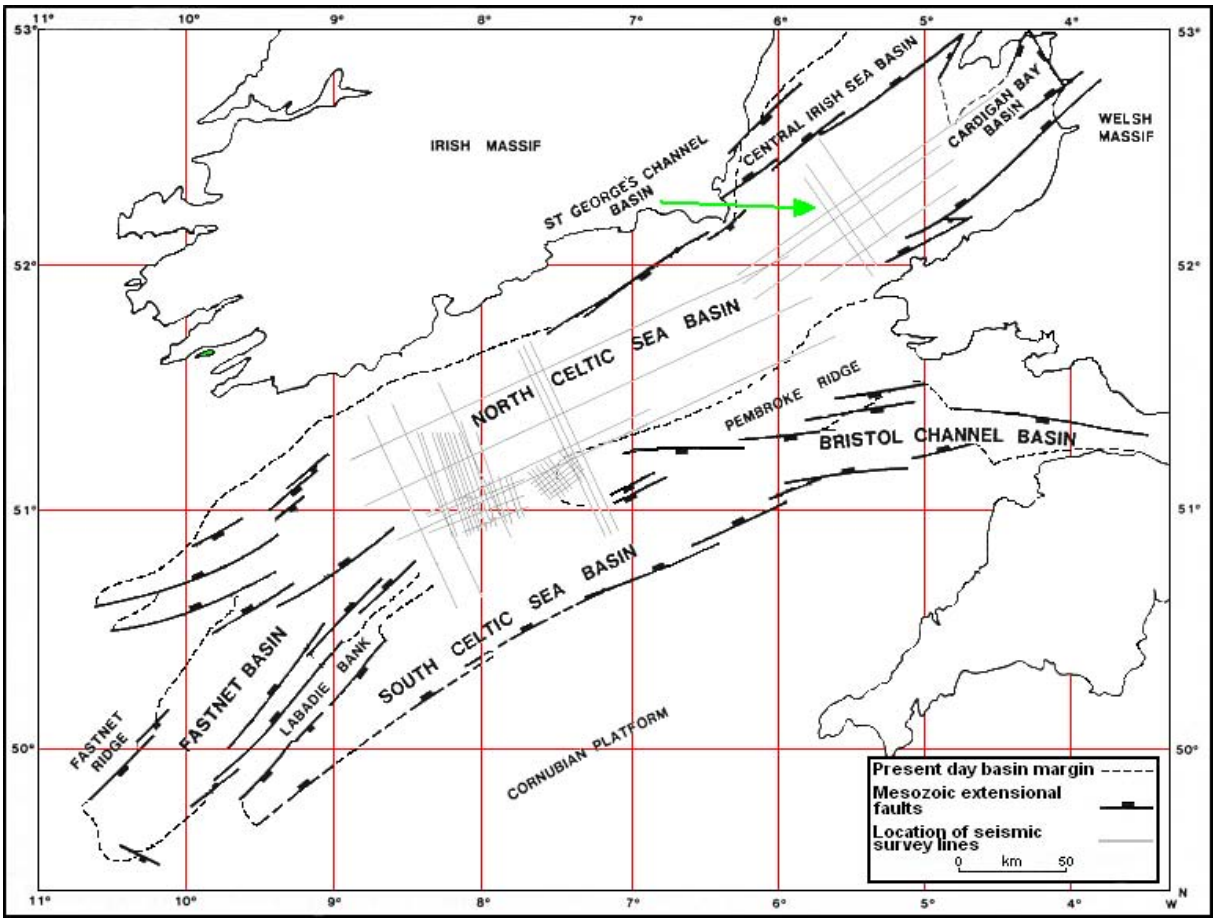

Figure 1.2 - Location map showing the seismic surveys that were used to constrain the timing of unconformities in the NCSB and SGCB. The approximate extents of the main sedimentary basins are shown as well as the positions of major faults (Based on Petrie *et al.* (1999)).

1.4: BASINS OF THE WESTERN APPROACHES-CELTIC SEA BASIN SYSTEM

The south-western UK region comprises a number of sedimentary basins mainly initiated during the Permian-Triassic. Each of these basins has major differences in their structural and stratigraphical characteristics particularly north and south of the 'Variscan Front' (Figure 1.3). North of the Variscan front basins have a 'Caledonide' structural trend; thick Permian-Triassic and Jurassic sequences are overlain with a marked unconformity by Cenozoic strata and Cretaceous beds are generally absent (i.e. SGCB, CBB, CISB). South of the Variscan front basins have a 'Variscide' structural trend; they are infilled by Permian-Triassic, Jurassic and litho and chrono-stratigraphically variable Cretaceous sequences with only relatively thin

Cenozoic strata (i.e. NCSB, SCSB, BCB) (Tappin *et al.* 1994). The SGCB and BCB, together with the North Celtic Sea Basin (NCSB), the South Celtic Sea Basin (SCSB), the Cardigan Bay Basin (CBB) and the Central Irish Sea Basin (CISB), form a chain of Mesozoic and Cenozoic depocentres (the Celtic Sea basin chain) stretching from 49°N to 54°N. The Celtic Sea is itself located within a much larger polyphase rift complex incorporating the western UKCS and part of the northwest Atlantic passive margin (Figure 1.3). This whole region is an important area of study, because it is transitional between underplated Atlantic margin basins such as the Rockall Trough and the inverted Wessex Basin-English Channel region. The Western UKCS has been the focus of much investigative work by the oil industry, with a considerable number of wells being drilled in the area.

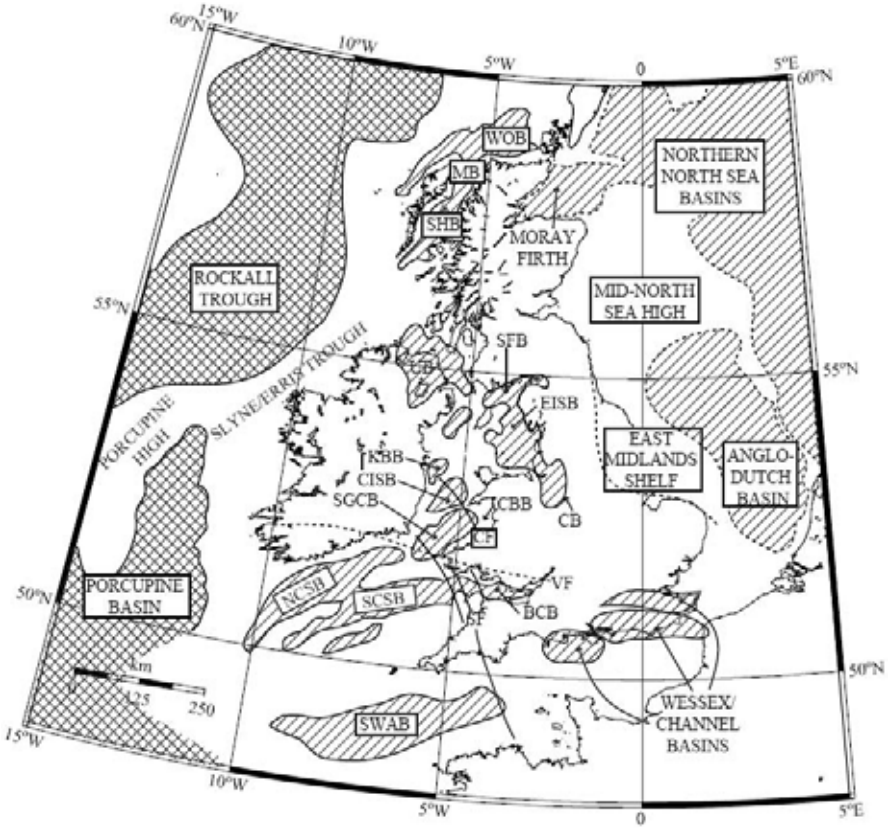

Figure 1.3 - Sedimentary basins of the UK and the NE Atlantic margin. Permian-Triassic and Jurassic basins are hatched, whereas the main Cretaceous depocentres west of Ireland are highlighted with a cross-hatch fill. KEY: WOB-West Orkney Basin; MB-Minch Basin; SHB-Sea of Hebrides Basin; SFB-Solway Firth Basin; EISB-East Irish Sea Basin; UB-Ulster Basin; KBB-Kish Bank Basin; CB-Cheshire Basin; CBB-Cardigan Bay Basin; CISB-Central Irish Sea Basin; SGCB-St. George's Channel Basin; NCSB-North Celtic Sea Basin; SCSB-South Celtic Sea Basin; SWAB-South Western Approaches Basin; CF-Codling Fault; VF-Variscan Front; SF-Sticklepath Fault (based on Williams, 2002).

1.4.1: NORTH CELTIC SEA BASIN (NCSB)

Lying astride the Variscan front thrust the basin is something of a structural hybrid it displays the 'Caledonide' trend but has a fairly thick Cretaceous sequence. The NCSB has the form of a rather symmetrical faulted downwarp lying for the most part in the hangingwall of the Variscan front thrust. It is thought that extensional reactivation of the thrust played a part in the structural evolution of the basin (Cheadle *et al.* 1987), but relict Caledonian structures were also significant in controlling basin morphology. A patchy cover of Cenozoic strata unconformably overlies the chalk. In cross section the NCSB forms a broad fault-bounded synclinal depression (Figure 1.4), with a Triassic fill up to 2000m thick (Tappin *et al.* 1994) overlain by 3000m of Jurassic and Lower Cretaceous syn-rift sediment. In places, over 2000m of Upper Cretaceous post-rift thermal subsidence deposits rest with pronounced unconformity on a series of tilted and eroded fault blocks. The NCSB is transitional between the SGCB to the north, which has a distinct Caledonian structural grain, and the SCSB and BCB in the south, which formed above Variscan basement. The NCSB is a significant hydrocarbon province, and a large number of exploration and production wells have been drilled in the region (e.g. Kinsale Head and Ballycotton fields).

1.4.2: SOUTH CELTIC SEA BASIN (SCSB)

The SCSB is separated from the NCSB by a narrow basement ridge and the basin axis swings from an ENE-WSW trend south of 51°N to a predominantly E-W trend as it passes into the BCB (Figure 1.3). In the east the basin has the form of an elongated faulted trough with a dominant east-north-east to west-south-west Variscide structural trend. Farther west an axial normal fault with northerly down-throw becomes a prominent structural feature. This fault is associated with a graben on the northern flank of the basin (Van Hoorn, 1987*a*). Subsequent minor compression and basin inversion in mid Cenozoic times produced a mild upwarp of the

basin depocentre with minor reversal of the faults on the southern margin of the basin. The sediment fill comprises a Triassic to Lower Cretaceous syn-rift sequence which was uplifted during the Early Cretaceous (Tappin *et al.* 1994), and the entire Mesozoic depocentre has been folded into a broad dome during a Cenozoic inversion event.

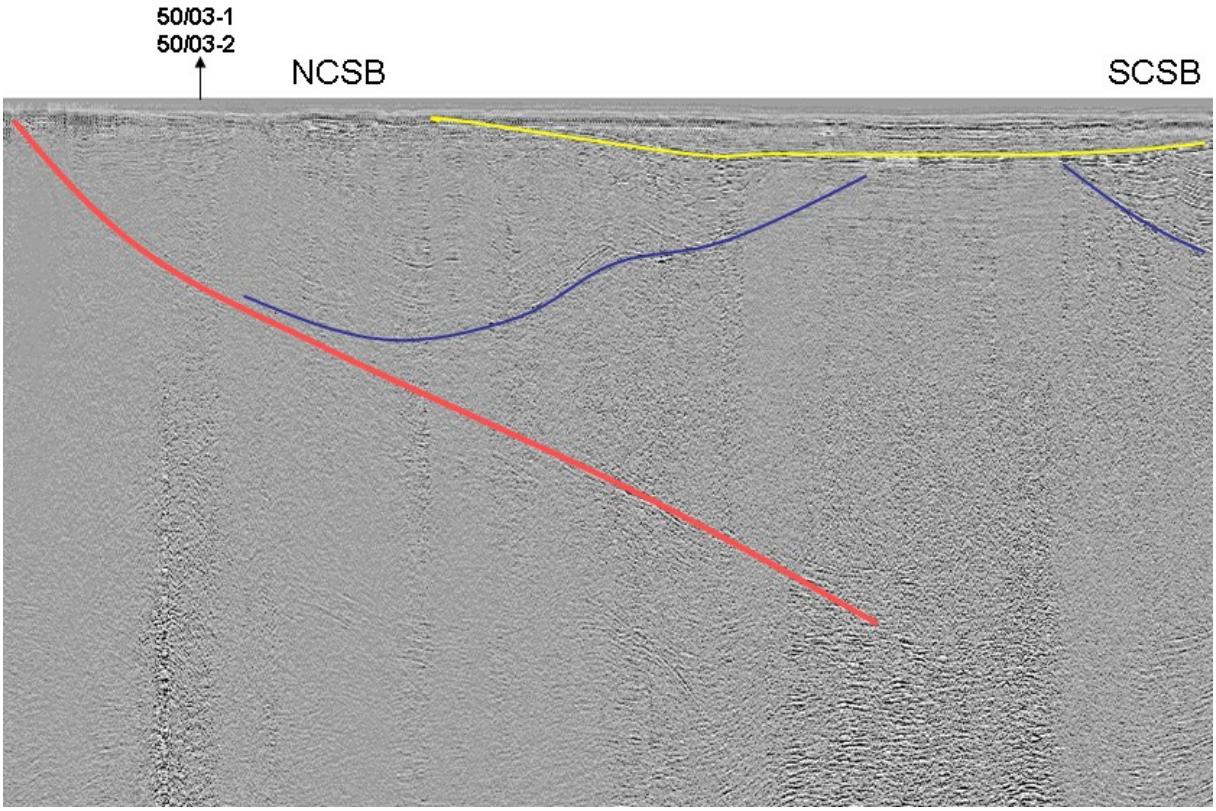

Figure 1.4 – Seismic cross-section through the NCSB AND SCSB (along the SWAT 4 seismic line (BIRPS & ECORS, 1986)) showing the general basin form. The red line represents the main basin bounding fault, the blue lines show the base of the Permian-Triassic and the yellow line represents the extent of preserved Cenozoic sediments.

1.4.3: BRISTOL CHANNEL BASIN (BCB)

The SCSB is juxtaposed with the BCB along the Sticklepath-Lustleigh fault zone, a strike-slip lineament which forms an accommodation zone between two adjacent Variscan thrust sheets. The fault complex has a long history of reactivation and shows around 5km of net dextral offset (Holloway & Chadwick, 1986). The WNW-ENE trending BCB deforms Mesozoic strata and is situated between two Variscan zones (Franke & Engel, 1982), the South Wales

Coalfield to the north and the Culm fold and thrust-sheet to the south (Gayer & Jones, 1989), of differing sedimentary facies, stratigraphy, structure and metamorphic grade. It is a markedly elongate east-west 'Variscide' basin which continues eastwards into the Glastonbury Trough and Wessex Basin. In the east it has the form of a northerly deepening asymmetric graben that is bounded to the north by the east-west trending Central Bristol Channel normal fault zone. This important structural feature has a length of more than 190km and is thought to have formed by extensional reactivation of an underlying Variscan thrust (Brooks *et al.* 1988). The basin structure is complicated by a set of north-westerly trending wrench faults that are probably reactivated Variscan structures. Towards its western end the basin has a more symmetrical cross section as it passes *en-échelon* into the SCSB (Kamerling, 1979). The main depocentre formed in the hanging wall block of a Variscan thrust fault (Brooks *et al.* 1988) and it comprises up to 3000 m of Triassic to Lower Cretaceous syn-rift sediment covered by a thin layer of Upper Cretaceous post rift. Recently work by Miliorizos *et al.* (2004), has shown that the Bristol Channel and Gravel Margin thrusts can be linked at depth with the Cannington Park thrust as syn-genetic structures formed immediately before, or at the same time as the Variscan root of the Watchet Fault (Figure 1.5) (Miliorizos *et al.* 2004).

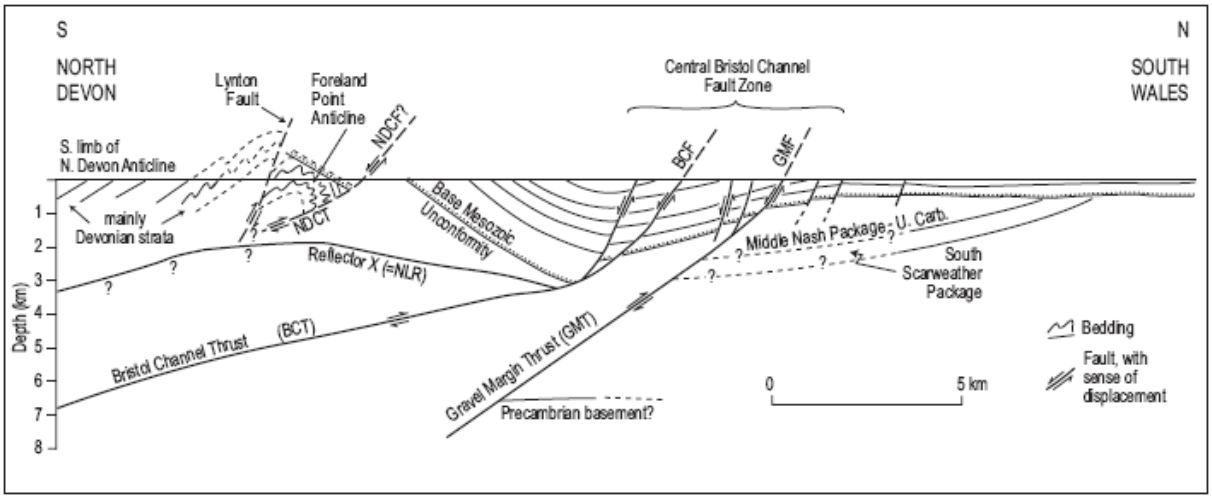

Figure 1.5 – Structural section across the inner Bristol Channel from North Devon to South Wales, west of the Watchet-Cothelstone-Hatch Fault, showing the positions and geometries of the main Variscan structures: NDCT-North Devon Coastal Thrust; BCT-Bristol Channel Thrust; GMT-Gravel Margin Thrust; NLR-North Ledge Reflector (after Miliorizos *et al.* 2004).

1.4.4: ST. GEORGE'S CHANNEL BASIN (SGCB)

The SGCB is a NE-SW trending Mesozoic half graben down faulted against the Palaeozoic rocks of Wales and is essentially contiguous with the NCSB (Figure 1.3). The basin is approximately 100km long, 50km wide and 12km deep and today forms a narrow trough, flanked on either side by the shallow shelves of the Irish and Welsh platforms (Figure 3.1). The south-eastern margin of the basin is marked by a major NE-SW trending fault zone comprising the Bala Fault and the *en-échelon* St George's Fault, which are probably reactivated Caledonian structures (Tappin *et al.* 1994; Williams *et al.* 2005). The north-western margin of the basin is marked by the similarly NW-SE trending Northwest Flank Fault, which serves to separate the SGCB from the CISB (Welch & Turner, 2000; Williams *et al.* 2005). The Triassic and Jurassic evolution of the SGCB has been described by Dobson & Whittington (1987), Barr *et al.* (1981), Tappin *et al.* (1994) and Welch & Turner (2000) and recently Holford (2006) presented a more comprehensive study of the Mesozoic to Cenozoic history of this basin.

1.4.5: SOUTH WALES COALFIELD AND PRE-MESOZOIC BASIN EVOLUTION

The South Wales Coalfield is a complex WNW-ENE trending and inwardly plunging synformal structure (Burgess & Gayer, 2000). The structure is asymmetric; the southern limb dips steeply north and the northern limb gently south. The coalfield represents an erosional remnant of the South Wales coal basin preserved within the Variscan fold belt. Variscan deformation is dominated by WNW-ESE striking thrusts and folds which produced approximately 30% shortening in the east of the coalfield (Jones, 1991) locally rising to 50-60% in the west (Frodsham & Gayer, 1997). Structures verge to the north in the northern limb but an important south-verging back-thrust zone occurs in the southern limb. Regionally, the thrusts propagate to the north in a piggyback sequence but locally break-back thrusts are dominant (Frodsham & Gayer, 1997). Various subsidence mechanisms have been proposed for British Late Carboniferous basins ranging from thermal subsidence following Early Carboniferous rifting (Leeder & McMahon, 1988), through active extension associated with transtension (Waters *et al.* 1994), to flexural subsidence in response to thrust-sheet loading (e.g. Gayer *et al.* 1993). Maynard *et al.* (1997) reviewed the Carboniferous of Western Europe and concluded that no single mechanism could explain all the Late Carboniferous basins in Britain, but that greater subsidence during the Namurian and Westphalian in the southern basins supported a flexural mechanism. Kelling (1988) first proposed a foreland basin model for the South Wales Coalfield. He cited as evidence high subsidence rates increasing with time, a northward migration of the basin depocentre towards the foreland and major immature clastic input sourced from the orogenic hinterland to the south. Later studies (Gayer & Jones, 1989; Gayer *et al.* 1993; Burgess & Gayer, 2000) have supported the flexural model for basin subsidence documenting propagation of the Variscan thrust deformation through the basin fill towards the foreland. However, variation in subsidence across major E-W fold structures (Jones, 1989) and across some of the NW-SE

trending cross-faults (Hartley, 1993*b*) suggests that subsidence was also influenced by intra-basinal inhomogeneity. Coward (1990) disputed the flexural model arguing that no adequate Variscan thrust-sheet load can be identified in SW England and that the presence of small basins and documented strike-slip structures favours a transpressive basin mechanism.

1.5: BACKGROUND TO RESEARCH AND PREVIOUS WORK

There is a substantial body of published work relating to the tectono-stratigraphic evolution of basins on the western UKCS, with the majority of these studies focusing on the NCSB, SCSB and East Irish Sea basins; little attention has been paid to the SGCB and the BCB. Specific studies of the SGCB have been published by Barr *et al.* (1981), Dimitropoulos & Donato (1983), Dobson & Whittington (1987), Tappin *et al.* (1994), Turner (1996, 1997) and Welch & Turner (2000). With the exception of Turner (1997) these have generally focused on the Mesozoic evolution of the basin and Cretaceous and Cenozoic tectonic events remain poorly constrained. Similarly, the geological evolution of the BCB-SCSB complex has been described by Tappin *et al.* (1994), Kamerling (1979) and Bulnes & McClay (1998), while Van Hoorn (1987b) presents evidence for Early Cretaceous and Cenozoic basin inversion. Related publications by Brooks *et al.* (1988) and Holloway & Chadwick (1986) have focused on basement fault reactivation, while Nemcok *et al.* (1995) and Dart *et al.* (1995) described the kinematics of reactivated faults along the exposed margins of the basin. At the regional scale, BIRPS & ECORS (1986), Dyment *et al.* (1990), Dyment & Bano (1991) and Ford *et al.* (1992) have all described the deep structure of the Celtic Sea basins, while other authors have focused on regional tectonics (Gardiner & Sheridan, 1981; Beach, 1987; Hillis, 1992), Mesozoic basin formation (Evans, 1990; Naylor *et al.* 1993; Tappin *et al.* 1994; McCann & Shannon, 1994; Rowell, 1995; Jackson *et al.* 1995; Maingarm *et al.* 1999; Hillis & Chapman, 1992) and hydrocarbon habitat (Jenner, 1981; Maddox *et al.* 1995; Shannon & Naylor, 1998).

Although it has long been recognised that the British Isles have been subjected to varying degrees of uplift and exhumation during Mesozoic and Cenozoic times (e.g. Davis, 1895; Geikie, 1901; Jones, 1936) it is only within the past few decades that concerted efforts have been made to elucidate the amount, timing and causes of exhumation. These efforts have been facilitated by both an abundance of information provided by hydrocarbon exploration (i.e. data from seismic surveys and exploration wells) and the development of new techniques such as AFTA which allow the former burial depths of rock sequences to be reconstructed. Subsequently, numerous attempts have been made to quantify the magnitude of exhumation and patterns of vertical motions across the sedimentary basins of the western UK and their onshore margins (Table 1.2).

A variety of techniques have been used in these investigations: thermally-based approaches have utilised purely AFTA (e.g. Green, 1986, 1989, 2002; Lewis *et al.* 1992; Thomson *et al.* 1999*a*; Allen *et al.* 2002), VR data (Cornford, 1986; Roberts, 1989; Hardman *et al.* 1993; Rowley & White, 1998; Corcoran & Clayton, 1999, 2001; Pearson & Russell, 2000) or a combination of both (e.g. Green *et al.* 1997, 1999, 2000, 2001*a*, *b*; Bray *et al.* 1998; Duncan *et al.* 1998). Less commonly, techniques like clay mineralogy indices have also been used to determine deeper burial (e.g. Kemp *et al.* 2005). Compaction-based techniques such as sonic velocity analyses have been employed extensively across this region and other parts of the British Isles (e.g. Hillis, 1991, 1995*a*, *b*; Chadwick *et al.* 1994; Menpes & Hillis, 1995; Murdoch *et al.* 1995; Thomson & Hillis, 1995; Japsen, 1997, 1998, 2000; Ware, 1999; Ware & Turner, 2002; Williams, 2002). Some studies have employed tectonic-based approaches i.e. subsidence modelling (e.g. McMahon & Underhill, 1995; McMahon & Turner, 1998; Rowley & White, 1998; Clift & Turner, 1998; Clift, 1999). Some workers have used seismic reflection data to infer magnitudes of erosion (e.g. Tucker & Arter, 1987; Van Hoorn, 1987*a*;

Bulnes & McClay, 1998). A small number of studies have combined data from different techniques in order to place tighter constraints on the burial and exhumation histories of individual basins (e.g. Corcoran & Mecklenburgh, 2005; Williams *et al.* 2005; Holford *et al.* 2005*a*, *b*; Holford, 2006). A compilation of exhumation estimates for the Western UK region is provided in Table 1.2.

The rationale behind this type of research was initiated following the early application of AFTA to rocks from Northern England and the EISB (e.g. Green 1986; Lewis *et al.* 1992; Green *et al.* 1993). These studies revealed that samples presently at outcrop or close to the sea bed had resided at palaeotemperatures between 80- 110°C or higher prior to cooling to which began at *c.* 60Ma. Because no samples from vertical sections (i.e. over a range of depths from an elevation profile or exploration well) were analysed in these studies, no constraints on palaeogeothermal gradients or the causes of heating were available. Assuming a palaeogeothermal gradient equivalent to the present-day value of *c.* 30°C/km and a palaeosurface temperature of 20°C, Lewis *et al.* (1992), estimated that this region had been buried by an additional 3km of section in early Cenozoic times. The requirement of a kilometre-scale Mesozoic cover over this region conflicted with palaeogeographic reconstructions which depicted this region as largely emergent throughout the Mesozoic (e.g. Ziegler 1990; Cope *et al.* 1992) and thus was met with criticism by some workers who considered a figure of 3km to be an overestimate by at least 1km (e.g. Holliday 1993, 1999).

Basin / Region	Authors	Method	Exhumation event		
			Early Cretaceous	Late-Cretaceous-Paleogene	Late Paleogene-Neogene
East Irish Sea Basin	Bushell, 1986	Basin modelling	*c.* 1km	*c.* 1km	
	Chadwick *et al.* 1994	Sonic & AFTA		>2.2km	
	Colter, 1978	Sonic		*c.* 2km	
	Cowan *et al.* 1999	Basin modelling		*c.* 1km	
	Green *et al.* 1997	AFTA & VR		1.5-2.0km	
	Hardman *et al.* 1999	Basin modelling	<0.3km	0.3-3.0km	
	Holford *et al.* 2005b	AFTA & VR	<2km	<1.5km	*c.* 1km
	Holliday, 1993	AFTA		0.7-1.7km	
	Knipe *et al.* 1993	Dipmeter/seismic		*c.* 2km	
	Lewis *et al.* 1992	AFTA		<3km	
	Rowley & White, 1998	VR		*c.* 3km	
		Subsidence analysis		0.4-2.1km	
	Ware & Turner, 2002	Sonic		0.6-2.1km	
Central Irish Sea Basin	Corcoran & Clayton, 1999	VR	0.35-1.9km		
	Floodpage *et al.* 2001	AFTA	*c.* 2km	*c.* 0.7km	
	Green *et al.* 2001	AFTA & VR	*c.* 3km	*c.* 2km	*c.* 1km
	Maddox *et al.* 1995	AFTA, VR & Sonic		1.0-2.5km	
	Williams *et al.* 2005	Sonic & seismic	*c.* 2.25km		*c.* 1km
St. George's Channel / Cardigan Bay basins	Barr *et al.* 1981	VR		*c.* 1km	
	Green *et al.* 2001	AFTA & VR		1.5km	1km
	Holford *et al.* 2005a	AFTA, VR & Sonic	<2.5km	?	<1.5km
	Tucker & Arter, 1987	Seismic		*c.* 1km	
	Welch & Turner, 2000	VR		0.6-1.8km	
	Williams *et al.* 2005	VR, seismic & sonic		*c.* 1km	*c.* 1km
Kish Bank Basin	Geotrack, 1995	AFTA & VR	2-3km	1km	
	Jenner, 1981	VR		3km	
	Naylor *et al.* 1993	VR		1.3km	
	Rowley & White, 1998	Subsidence analysis		0.9-1.5km	
	Ware, 1999	Sonic		0.5-0.8km	
North Celtic Sea Basin	Menpes & Hillis, 1995	Sonic		0.4-1.2km	
	Murdoch *et al.* 1995	Sonic & seismic		<1.1km	
	Tucker & Arter, 1987	Seismic		0.6-2.5km	
South Celtic Sea Basin	Bulnes & McClay, 1998	Seismic	>1km	*c.* 1km	
	Van Hoorn, 1987	Seismic	<3.3km		

Table 1.2 - Compilation of published exhumation estimates for the Irish and Celtic Sea basin systems.

Potential mechanisms driving Cenozoic uplift of the UKCS and the NE Atlantic margin have been the subject of considerable debate. A number of authors have presented structural evidence attesting to Cenozoic compression in basins throughout the region (e.g. Lake & Karner, 1987; Tucker & Arter, 1987; Roberts, 1989; Hillis, 1992, 1995; Menpes & Hillis, 1995; Doré & Lundin, 1996; Boldreel & Andersen, 1998; Vagnes *et al.* 1998; Lundin & Doré, 2002), the origin of these structures being variously attributed to intra-plate stresses associated with North Atlantic ridge-push and the Alpine orogeny. The mechanics of intra-plate

compression have been summarised by Cloetingh (1988) and Ziegler *et al.* (1998), while Ziegler (1989*b*), Knott *et al.* (1993) and Doré *et al.* (1999) have presented a series of plate reconstructions showing the geo-dynamic setting for Late Cretaceous and Cenozoic intra-plate deformations in NW Europe. Other workers (notably Brown, 1991; Brodie & White, 1994, 1995; Clift & Turner, 1998) have argued in favour of plume activity and magmatic underplating associated with the contemporaneous initiation of the Iceland mantle plume and thermal uplift connected with localised hot-spot activity (Cope, 1994), as the main cause of early Cenozoic exhumation. Brodie & White (1995) have discussed the link between sedimentary basin inversion and igneous underplating, and there is a substantial body of literature pertaining to the thermal and mechanical effects of plumes on the lithosphere. The reader is referred to White & McKenzie (1989), Courtney & White (1986) and Nadin *et al.* (1995), for a discussion of the role of transient thermal and dynamic uplift in modifying subsidence patterns in the vicinity of a plume head. White & McKenzie also presented a hotspot track for the Iceland Plume, which was subsequently modified by Lawver & Muller (1994).

Studies of the geology of the Celtic Sea-Bristol Channel basin system and the onshore Wessex Basin of southern England, where the Mesozoic and Cenozoic stratigraphic record is more complete, have identified multiple phases of exhumation with discrete events during the early Cretaceous (e.g. Kamerling, 1979; Van Hoorn, 1987*a*; Ruffell, 1992; McMahon & Turner, 1998), late Cretaceous-early Paleogene (e.g. Tucker & Arter 1987; Hillis 1992, 1995) and late Paleogene-Neogene (e.g. Chadwick 1993). Similarly timed erosional events have been reported from elsewhere in the British Isles, including regions as far afield as the northern North Sea during the early Cretaceous (e.g. Rawson & Riley, 1982; Kyrkjebø *et al.* 2004), the Moray Firth during the early Paleogene (e.g. Thomson & Underhill, 1993; Argent

et al. 2002) and the southern North Sea during Neogene times (e.g. Japsen, 1997, 2000; Green, 2005). These observations (e.g. the fact there are multiple unconformities) suggest that the Western Approaches-Celtic Sea basin system has experienced a complex, multiphase exhumation history which cannot be explained in terms of a single event or process. In the following parts of this chapter the evidence for the spatial extent, magnitude and possible driving mechanisms of each of the major exhumation episodes which have affected the southwest UK basin system are reviewed. To place these exhumation episodes in their wider plate-tectonic context, Figures 1.6-1.8 contain a series of maps depicting the tectonic evolution of the European and Mediterranean regions from early Jurassic to Miocene times.

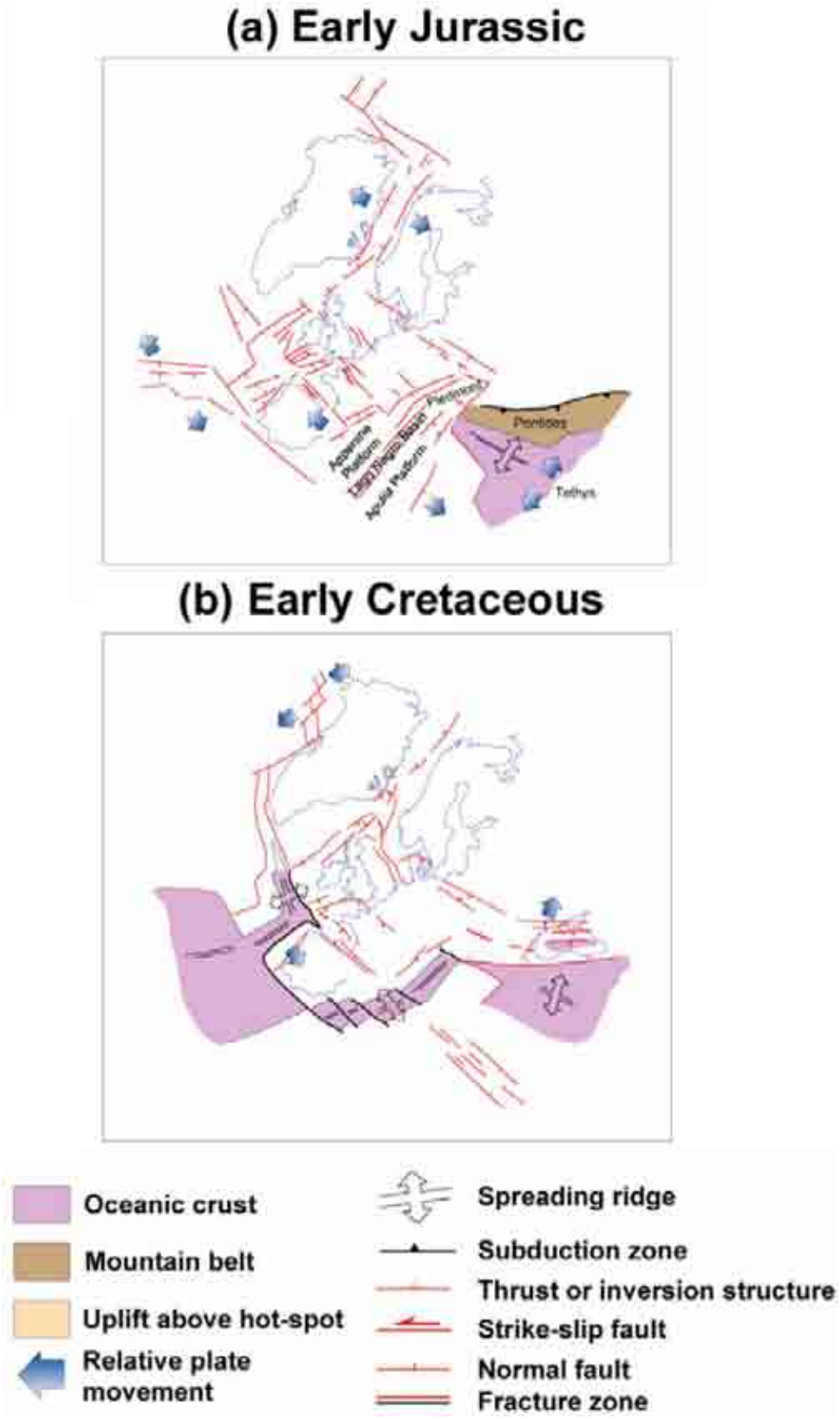

Figure 1.6 (and Figures 1.7-1.8) – A series of palaeotectonic reconstructions depicting the geological and tectonic evolution of the European and Mediterranean regions during (a) early Jurassic and (b) early Cretaceous times. The exhumation history of the southwest UK has been profoundly influenced by events such as the progressive opening of the Atlantic Ocean (b-f) and the lithospheric shortening resulting in the closure of the Tethys and the development of the Alpine orogeny (c-f) (after Coward *et al.* (2003)).

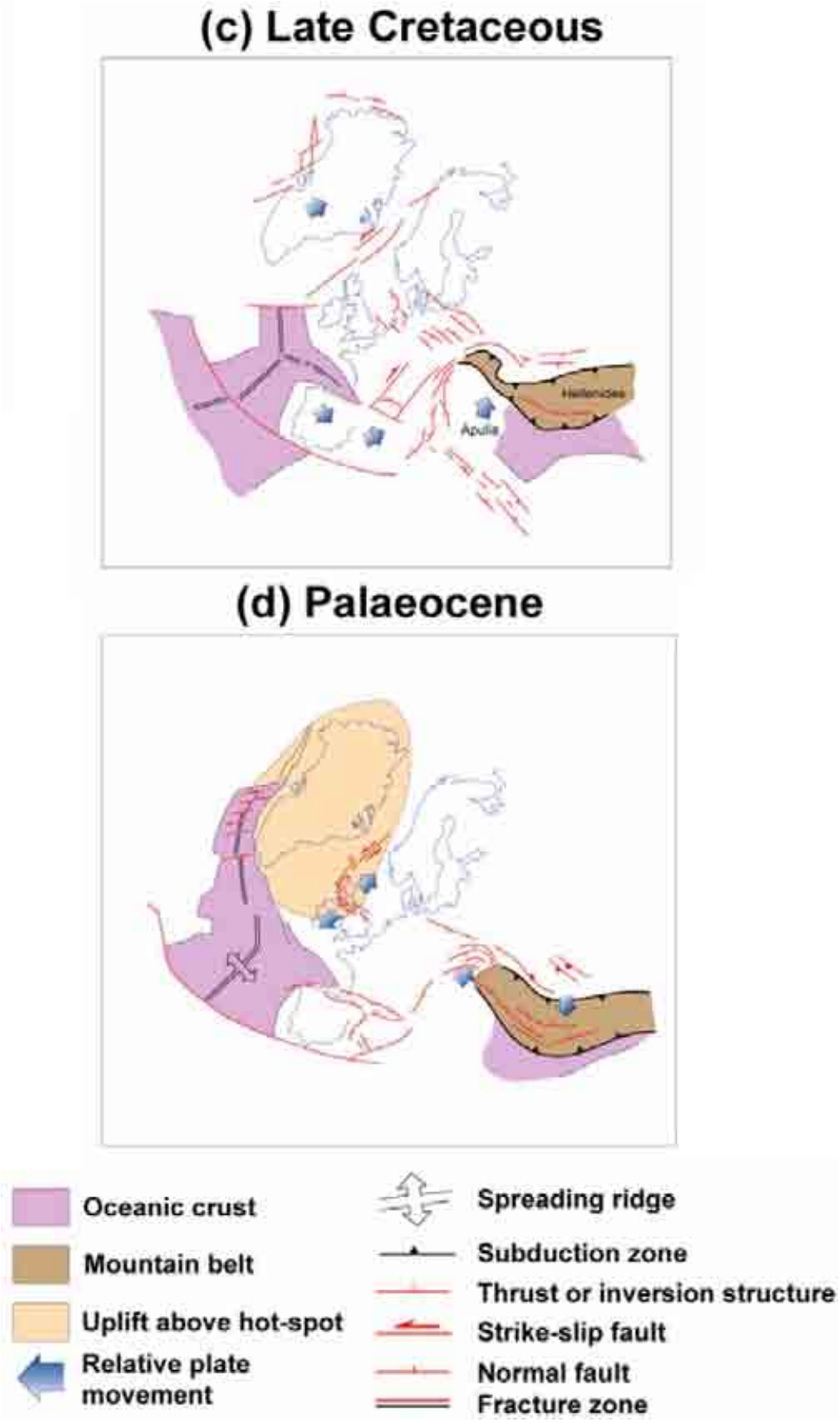

Figure 1.7 (and Figures 1.6 and 1.8) – A series of palaeotectonic reconstructions depicting the geological and tectonic evolution of the European and Mediterranean regions during (c) late Cretaceous and (d) Paleocene times. The exhumation history of the southwest UK has been profoundly influenced by events such as the progressive opening of the Atlantic Ocean (b-f) and the lithospheric shortening resulting in the closure of the Tethys and the development of the Alpine orogeny (c-f) (after Coward *et al.* (2003)).

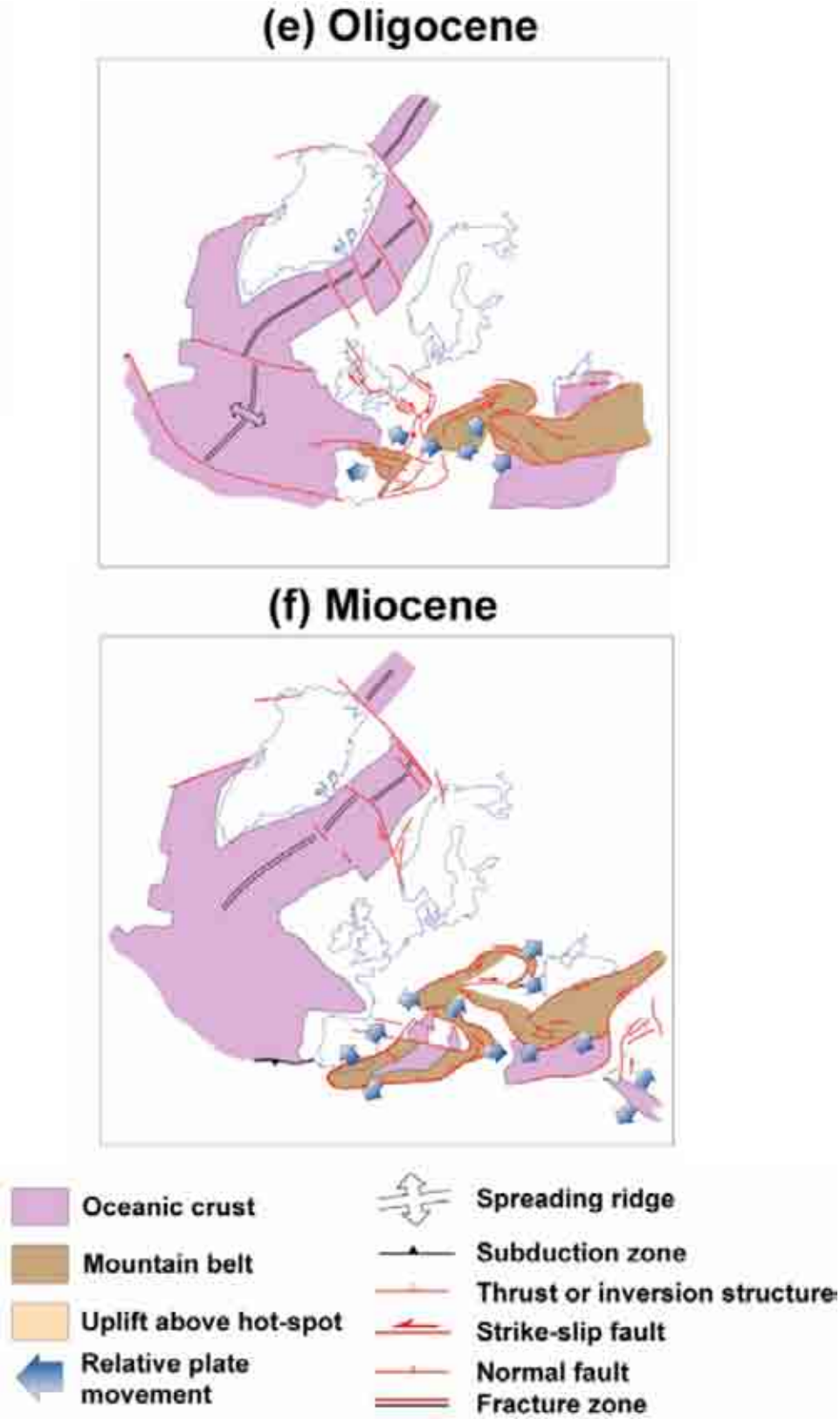

Figure 1.8 (and Figures 1.6-1.7) - A series of palaeotectonic reconstructions depicting the geological and tectonic evolution of the European and Mediterranean regions during (e) Oligocene and (f) Miocene times. The exhumation history of the southwest UK has been profoundly influenced by events such as the progressive opening of the Atlantic Ocean (b-f) and the lithospheric shortening resulting in the closure of the Tethys and the development of the Alpine orogeny (c-f) (after Coward *et al.* (2003)).

1.5.1: EARLY CRETACEOUS EXHUMATION

A number of authors have shown that the British Isles were affected by uplift and erosion during the early Cretaceous (e.g. Kamerling, 1979; Fyfe *et al.* 1981; van Hoorn, 1987*a*; Ruffell, 1992; Kyrkjebø *et al.* 2004; Corcoran & Mecklenburgh, 2005) and Ziegler (1990), has claimed that a major unconformity, often termed the "late Cimmerian unconformity", can be correlated across wide areas of Western and Central Europe. However, the use of the term "late Cimmerian unconformity" is considered misleading as it implies a single erosive phase related to a specific tectonic event Kyrkjebø *et al.* (2004) where detailed stratigraphic investigations in several parts of Britain have shown that the "late Cimmerian unconformity" actually consists of a number of regional and local unconformities which encompass a significant period of time (e.g. Rawson & Riley, 1982; Ruffell, 1992).

Two dominant phases of early Cretaceous uplift and erosion have been recognised and each correlates with tectonic activity along the incipient Atlantic margin of NW Europe (Figure 1.6b and Figure 1.9) (Ziegler, 1990; Doré *et al.* 1999; Roberts *et al.* 1999). McMahon & Turner (1998) identified two distinct early Cretaceous unconformities using seismic and stratigraphic data from the Wessex, Celtic Sea and Western Approaches basins (on and offshore southern England). The oldest and most significant of these unconformities is Berriasian in age whilst a younger (Aptian) unconformity, apparently associated with lower magnitudes of erosion, was also identified. A Jurassic-Cretaceous unconformity has been identified in the Bristol Channel and South Celtic Sea basins by various workers (e.g. Coward & Trudgill, 1989; Ziegler, 1990; Ruffell & Coward, 1992; Bulnes & McClay, 1998). The timing of erosion here is constrained as pre-Aptian by the transgression of Aptian shallow-marine to continental sands over deeply truncated Triassic and Jurassic strata (Ziegler 1990).

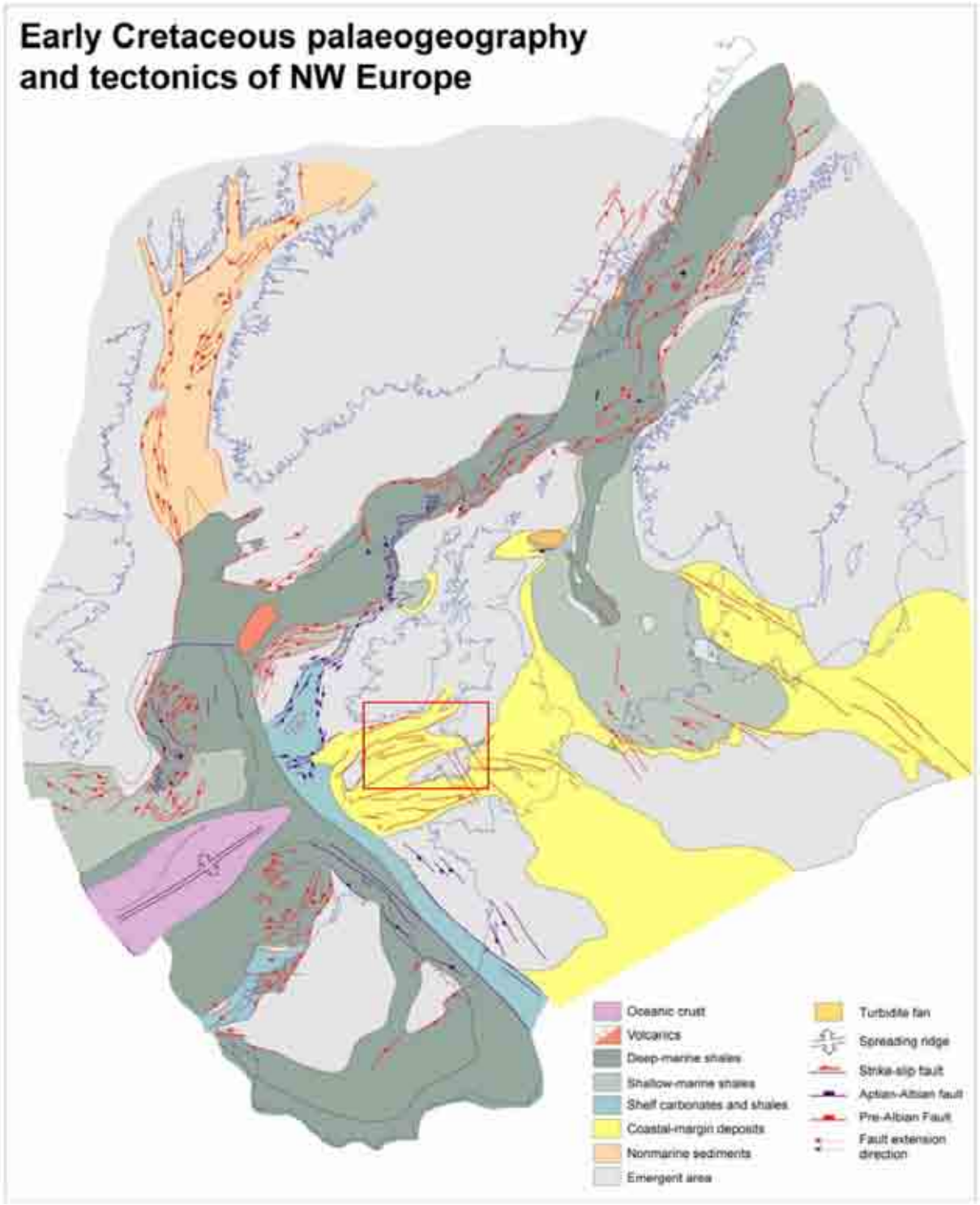

Figure 1.9 – Palaeogeographic reconstruction of NW Europe and the North Atlantic during early Cretaceous times, showing the distribution of active structures and sediment facies. NE-SW extension affected the North Sea and Central Europe during the early Cretaceous, whilst NW-SE extension along the Atlantic margin was responsible for the formation of the Faroe-Shetlands Basin. The cessation of extension in the central and northern North Sea, followed by the onset of post-rift thermal subsidence led to the development of a basal Cretaceous unconformity complex. Sedimentation in the Celtic Sea and southern England was dominated by coastal-marginal deposits, with most parts of the British Isles emergent. The area of interest in this study is highlighted by the red box (after Coward et al. (2003)).

Ruffell & Coward (1992) suggested that the Jurassic-Cretaceous unconformity in the Celtic Sea region was related to inversion which involved reverse movement along pre-existing Variscan thrusts. Ziegler (1990) claimed that dextral strike-slip movements along the basin margins and intra-basinal fault zones of the BCB and SCSB caused intense deformation, illustrated by the erosion of over 3km of Triassic-Jurassic sediments from the margins of these basins (Van Hoorn, 1987*a*). These deformations coincided with the last rift and wrench movements that preceded mid-Aptian crustal separation between Iberia and Europe and with the onset of sea-floor spreading in the Bay of Biscay (Figure 1.6b) (*cf.* Doré *et al.* 1999; Roberts *et al.* 1999).

1.5.2: LATE CRETACEOUS-CENOZOIC EXHUMATION

Figure 1.10 highlights the change in tectonic regime across NW Europe during the late Cretaceous which consisted of thermal subsidence and a major tectono-eustatic rise in sea-level (Ziegler, 1990). However, a major global sea level regression at the end of the Cretaceous (Haq *et al.* 1987) coupled with widespread surface uplift around NW Europe (Doré *et al.* 2002*a*) led to the emergence of most of the British Isles during the early Paleogene (Figure 1.12) (Murray, 1992; Anderton, 2000). This led to a well documented, rapid and considerable exhumation of many parts of Britain, encompassing a region which extends from the WAB, NCSB and SCSB (Hillis, 1991, 1995*a*), across central and northern England (Green, 1986, 1989, 2002; Chadwick *et al.* 1994; Green *et al.* 2001*b*) to the Scottish Highlands and Moray Firth (Thomson & Underhill, 1993; Thomson *et al.* 1999*b*; Argent *et al.* 2002). Late Cretaceous and Paleocene uplift affected the entire western UKCS, forming a pronounced basal Cenozoic unconformity over much of the area. Evidence for substantial early Cenozoic exhumation includes:

- Jurassic and Permian-Triassic syn-rift sediments outcrop at seabed in the SGCB, CISB and KBB (Figure 1.11); a substantial thickness of post-rift sediment is missing from these areas

- anomalous porosity-depth relationships derived from sonic transit times suggest that sediments have been exhumed

- Apatite fission-track and vitrinite reflectance measurements indicate that maximum palaeotemperatures occurred some 60Ma B.P. (Duncan *et al.* 1998).

Potential mechanisms driving Paleocene uplift of the UKCS and the NE Atlantic margin have been the subject of considerable debate complicated by the coincidence of two major continental-scale processes (Turner, 1997). Cenozoic compression has been cited by a number of authors (e.g. Lake & Karner, 1987; Tucker & Arter, 1987; Ziegler, 1987; Roberts, 1989; Hillis, 1992, 1995; Doré & Lundin, 1996; Boldreel & Andersen, 1998; Vagnes *et al.* 1998; Lundin & Doré, 2002), who have presented structural evidence (Figures 1.7-1.8 and 1.12) variously attributed to intra-plate stresses associated with North Atlantic ridge-push and the Alpine orogeny. Meanwhile other workers (White & McKenzie, 1989; Brodie & White, 1994, 1995; Rowley & White, 1998; Clift & Turner, 1998; Doré *et al.* 1999; Al-Kindi *et al.* 2003) have favoured plume activity and igneous underplating as the main cause of early Cenozoic exhumation. The evidence for these theories is examined in more detail below.

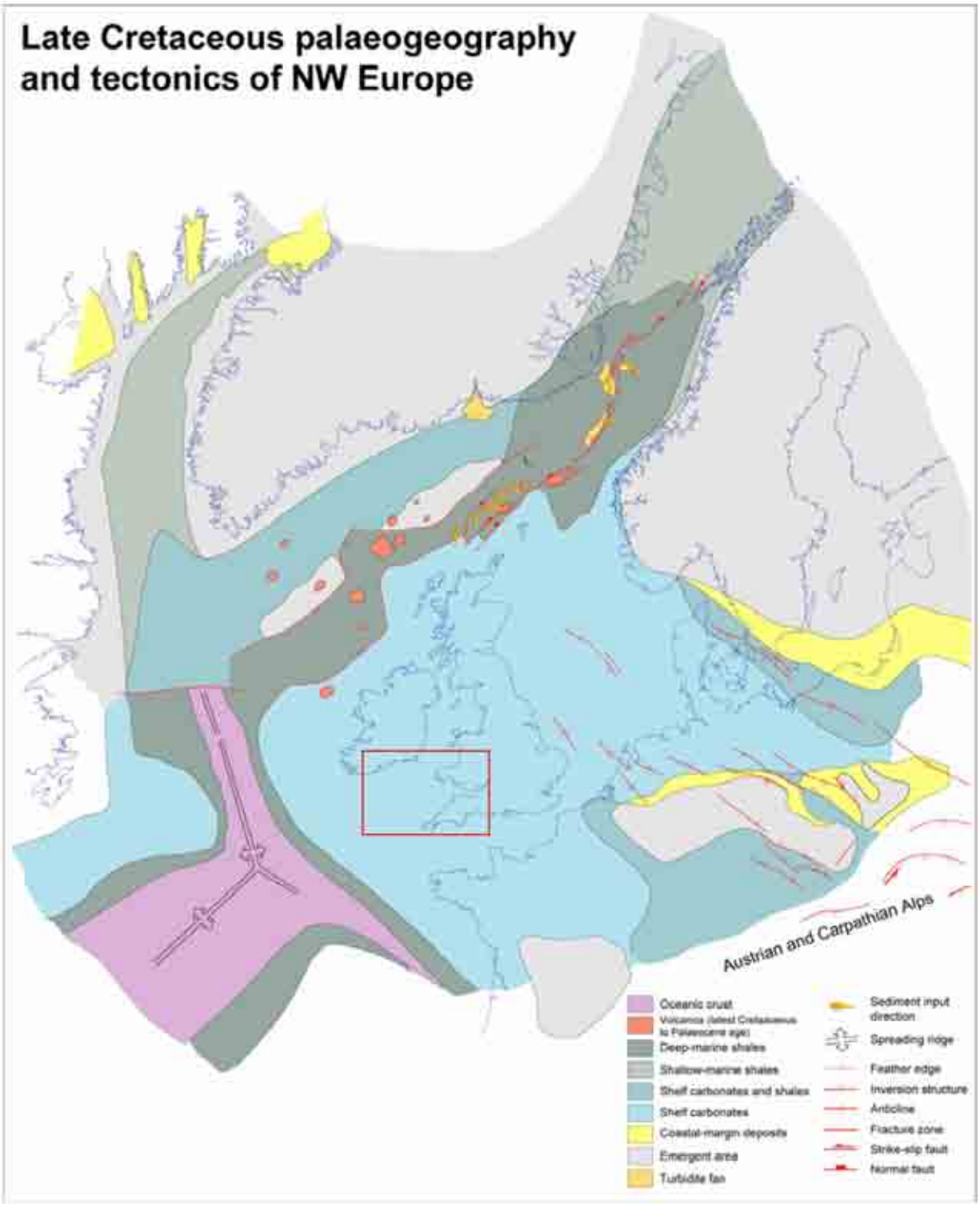

Figure 1.10 – Palaeogeographic reconstruction of NW Europe and the North Atlantic during late Cretaceous times, showing the distribution of active structures and sediment facies. There was relatively little rift activity in the North Atlantic during late Cretaceous times and the region experienced passive thermal subsidence, with chalk deposited across much of Europe. Some inversion occurred in the southern North Sea, probably related to early Alpine collision in Eastern Europe. The area of interest in this study is highlighted by the red box (after Coward *et al.* (2003)).

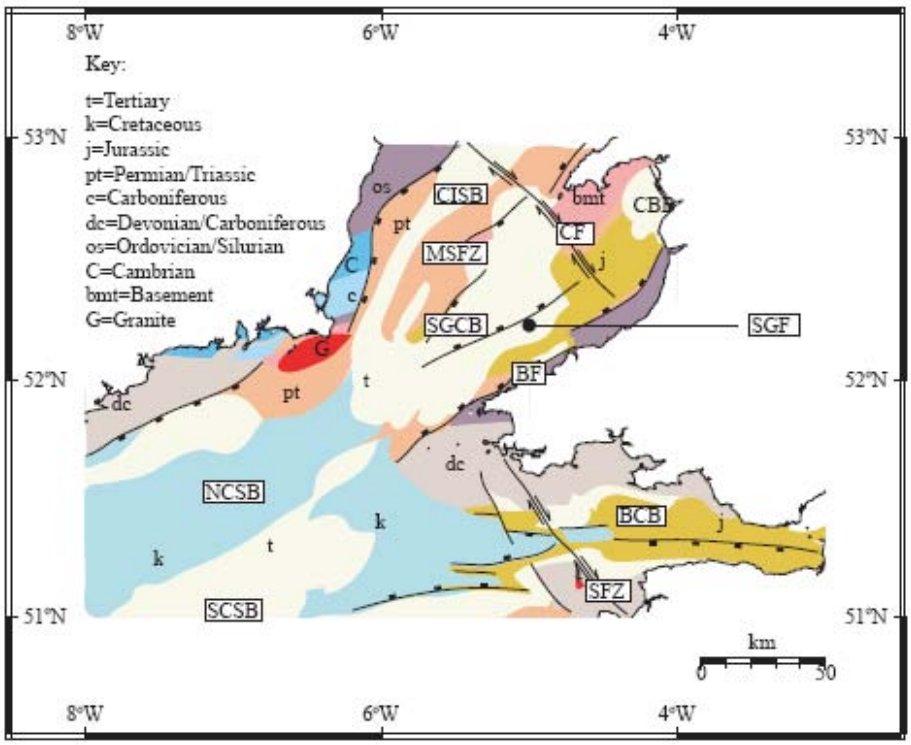

Figure 1.11 – Quaternary sub-crop map of the northern Celtic Sea region. Key: CISB-Central Irish Sea Basin; CBB-Cardigan Bay Basin; SGCB-St George's Channel Basin; NCSB-North Celtic Sea Basin; SCSB-South Celtic Sea Basin; BCB-Bristol Channel Basin; BF-Bala Fault; SGF-St George's Fault; SFZ-Sticklepath-Lustleigh Fault Zone; CF-Codling Fault; MSFZ-Menai Straits Fault Zone (after Tappin *et al.* 1994).

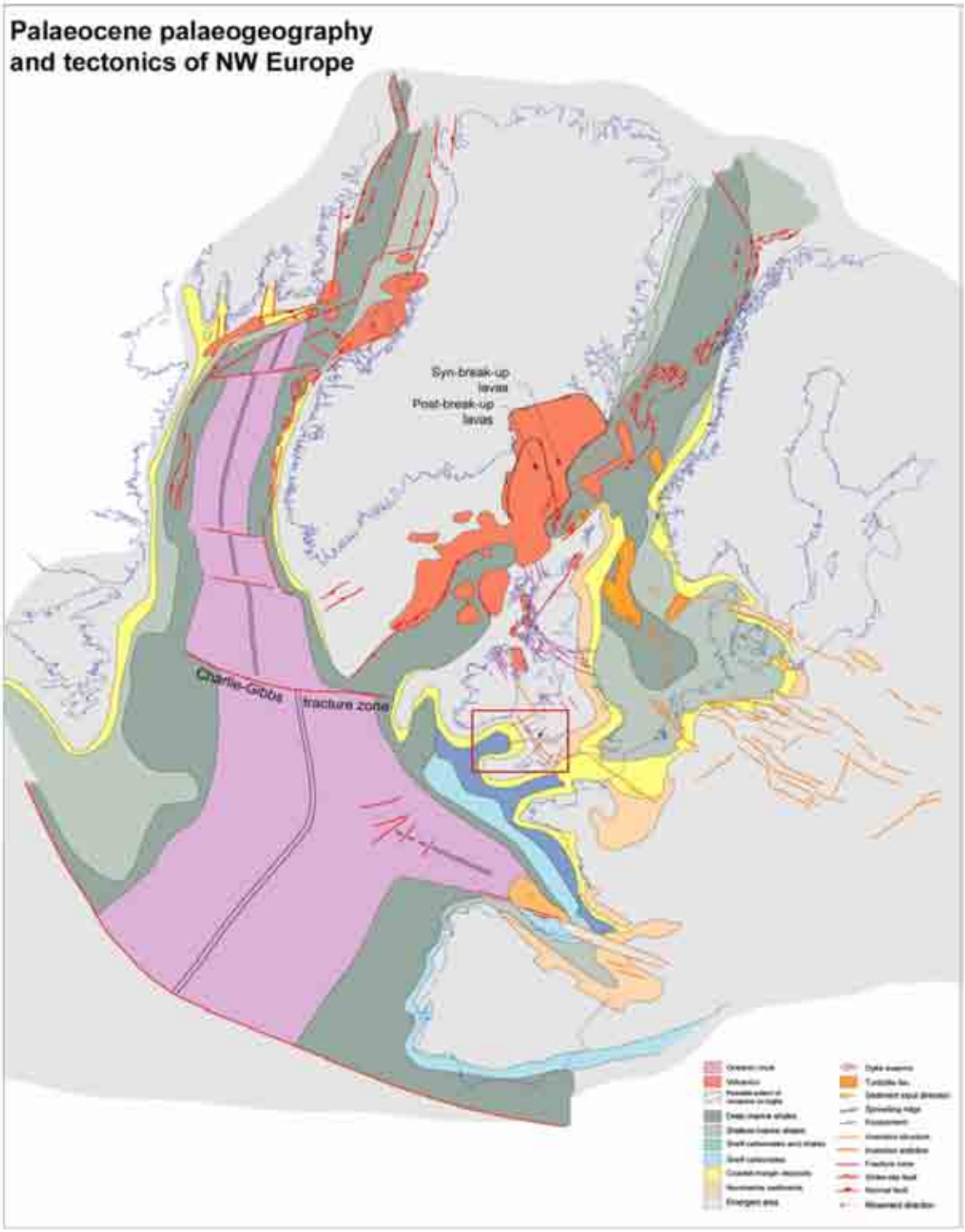

Figure 1.12 – Palaeogeographic reconstruction of NW Europe and the North Atlantic during Paleocene times, showing the distribution of active structures, sediment facies and volcanic rocks associated with plume activity. During the Paleocene, sea-floor spreading commenced in the Labrador Sea whilst extension continued along the incipient NE Atlantic margin. Large parts of NW Europe experienced uplift with an accompanying flux of sediments into the North Sea Basin. Intense igneous activity affected the North Atlantic during the Palaeocene. In Scotland, Ireland and their offshore areas major volcanism occurred between 61-57Ma associated with NW-trending dyke and fault activity. The plateau basalts of the Faeroes and East Greenland and Vøring and Rockall plateaus formed between 56-52Ma and continental separation between Greenland and Europe was achieved during the earliest Eocene (*c.* 53Ma). The area of interest in this study is highlighted by the red box (after Coward *et al.* (2003)).

1.5.2.1: Magmatic underplating and the role of the Iceland Plume

The opening of the North Atlantic Ocean at approximately 53Ma (earliest Eocene) (Doré *et al.* 1999) was preceded by voluminous magmatism along both oceanic margins (Figure 1.12). Magmatic activity occurred within the approximate interval of 63-52Ma, with the main phase of activity at 59Ma (Figure 1.13) (Mussett *et al.* 1988). Adding igneous material to the base of the crust beneath an extending basin can cause regional exhumation, assuming that the material has a lower density than the surrounding lithosphere (Brodie & White 1995; Clift & Turner, 1998). White *et al.* (1987) estimated that between 5-10×10^6 km³ of igneous rock was produced in the North Atlantic region during the early Paleogene and includes the onshore basalts and igneous complexes of Greenland, the Faeroes and NW Britain and the thick extrusive basaltic flows along the offshore east Greenland and Rockall Faeroes-Norwegian margins.

White & McKenzie (1989), showed that the production of such volumes of igneous rock during continental rifting requires the potential temperature of the asthenosphere to be elevated by 100-200°C above normal temperatures (*c.* 1280°C) in order to facilitate decompression melting of the hot asthenospheric mantle. Such elevations of temperature are provided by mantle plumes and White & McKenzie (1989) proposed that the early Paleogene initiation of the Iceland mantle plume was responsible for the massive magmatism along the Atlantic margins. Subsequently therefore, many workers have invoked the Iceland plume and associated phenomena to explain the uplift and exhumation of the British Isles during the early Paleogene (Brodie & White, 1994, 1995; Nadin *et al.* 1995; White & Lovell, 1997; Rowley & White, 1998; Jones *et al.* 2001, 2002). Brodie & White (1995) concluded that the most plausible method of generating permanent uplift of the western UKCS is to add gabbroic melt to the base of the crust (Figure 1.14). Rare earth element distributions in rocks from

various locations within the British Tertiary volcanic province suggest that there has been between 2-5 km of melt production beneath the western UKCS. It should be noted that in recent years, many inconsistencies associated with the 'plume' hypothesis have been acknowledged, whilst the existence of a long-lived plume beneath Iceland has also been explicitly questioned (Foulger, 2002; Foulger & Natland, 2003; Foulger & Anderson, 2005; Lundin & Doré, 2005*a*, *b*).

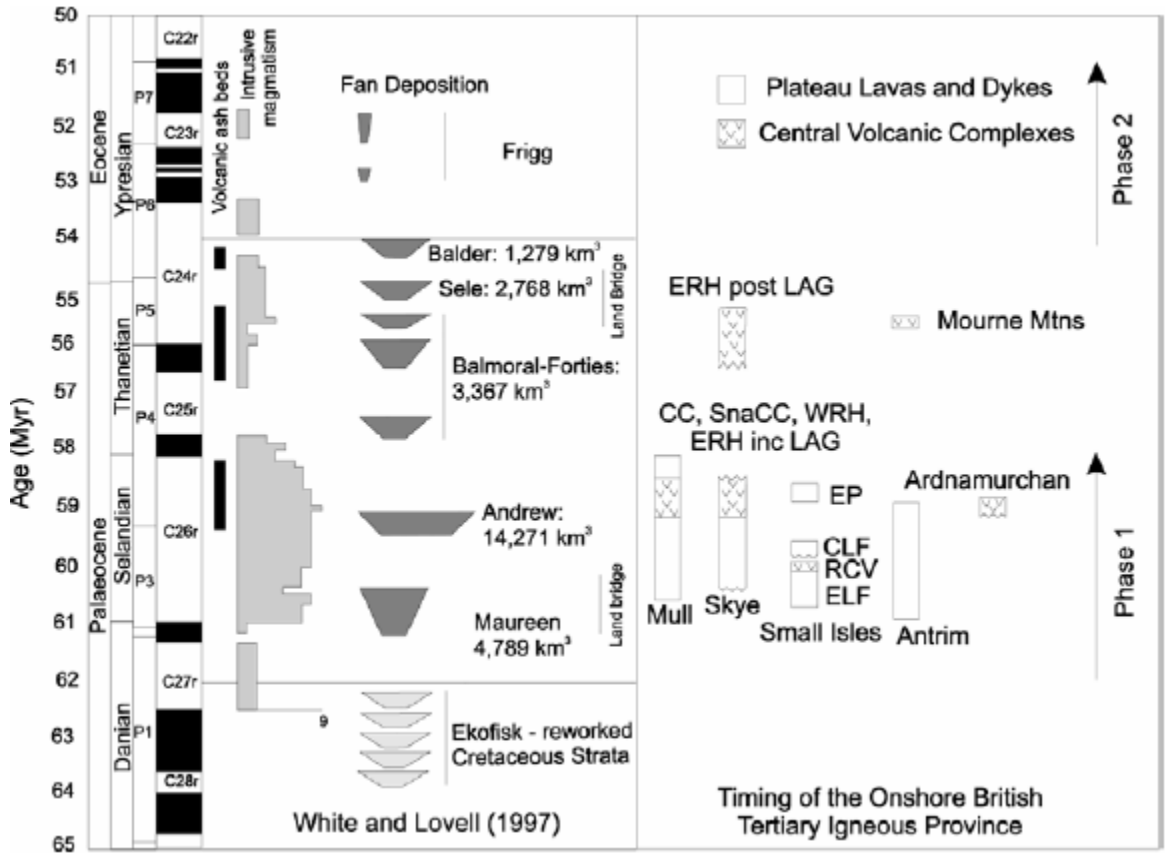

Figure 1.13 - Comparison of the timing of onshore magmatic activity of the British Tertiary Igneous Province (BTIP) (from Chambers *et al.* 2005) with the correlation of periods of Palaeocene-Eocene submarine fan deposition (sand pulses) in the North Sea and intrusive magmatism of White & Lovell (1997). Key: CC-Cuillin Centre; SnaCC-Strath na Creitheach Centre; WRH-Western Red Hills; ERH-Eastern Red Hills; LAG-Loch Ainort Granite; EP-Sgurr of Eigg Pitchstone; CLF-Canna Lava Formation; RCV-Rum central volcano; ELF-Eigg Lava Formation. Although the onset of magmatism corresponds to the first major influx of clastic sediments (Maureen, which comprises c. 20% of the total volume of Paleogene submarine fan deposits), and the largest sand pulse (Andrew, c. 50%) is coeval with the development of the central volcanoes of Mull and some of Skye, magmatism continues when there is no sediment in the North Sea (after Chambers *et al.* (2005)).

As illustrated by Figure 1.14, several types of epeirogenic uplift are associated with mantle plume activity (Nadin *et al.* 1995; Jones *et al.* 2001). Dynamic uplift above a convection cell can occur without the need for increased heat flow (Courtney & White 1986). Nadin et al. (1995) described an example of dynamic uplift from the northern North Sea, which was probably related to the proto-Iceland plume. The authors concluded that regional Paleocene uplift and subsequent Eocene subsidence can be explained by a model incorporating long-wavelength flexural uplift in response to the flow field generated by a mantle plume (Figure 1.5). Their models showed that the magnitude of the uplift is related to the viscosity of the lithosphere, but dynamic uplift could occur up to 1500m from the plume head. Close to the centre of the plume dynamic uplift combined with thermal buoyancy resulted in up to 2.5km of total uplift (Figure 1.15). More localised uplift will result due to thermal buoyancy from lithosphere heated by conduction from underlying hot asthenosphere (Nadin *et al.* 1995; Jones *et al.* 2001). The area affected by thermal uplift will be restricted to that above the narrow central plume (150-200km wide) of rising mantle with abnormally hot temperatures (White & McKenzie, 1989). The Iceland plume probably lay between 1000-1500 km away from the Celtic Sea at around 60Ma (White & McKenzie 1989; Lawver & Müller, 1994), although a separate plume could have been located in the vicinity of the Cenozoic Igneous Province around this time (Cope, 1994; Nadin *et al.* 1995; Clift & Turner, 1998). Both dynamic and thermal uplift are transient, and so will disappear when the convection wanes or the thermal anomaly dissipates (Jones *et al.* 2001). Permanent uplift can occur if adiabatic decompression of hot asthenosphere causes melting and the resultant igneous material is injected into the lithospheric column (Jones *et al.* 2001).

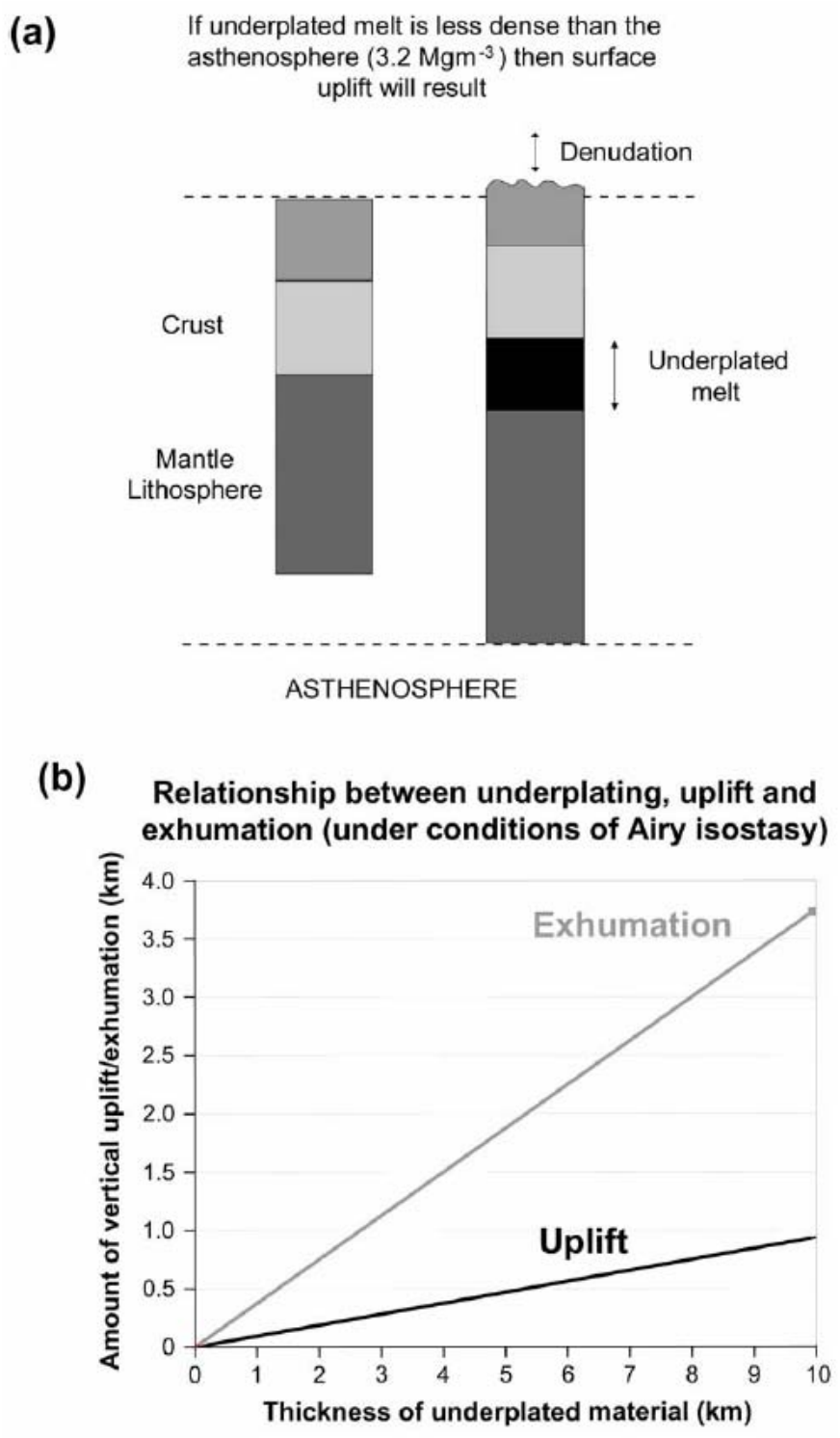

Figure 1.14 – (a) Diagram illustrating the effect of adding a thickness of underplated melt to the lithosphere. If the melt has a density lower than that of the asthenosphere (3.2Mg/m³), surface uplift will result. Erosion and subsequent isostatic readjustment can result in a maximum amount of exhumation, the value of which can be determined from equations 3.1 and 3.2. It should be noted that the precise distribution of underplating within the lithosphere does not affect the isostatic balance. (b) Graph showing the amount of vertical uplift and exhumation resulting from variable thicknesses of underplating. Calculated using equations 3.1 and 3.2 and the following assumed densities; crustal = 2.4MG/m³; asthenospheric = 3.2Mg/m³; underplating = 2.9Mg/m³. This modelling assumes i) Airy isostasy and ii) 'normal' crustal and lithosphere thicknesses of 35km and 125km (from Holford, (2006)).

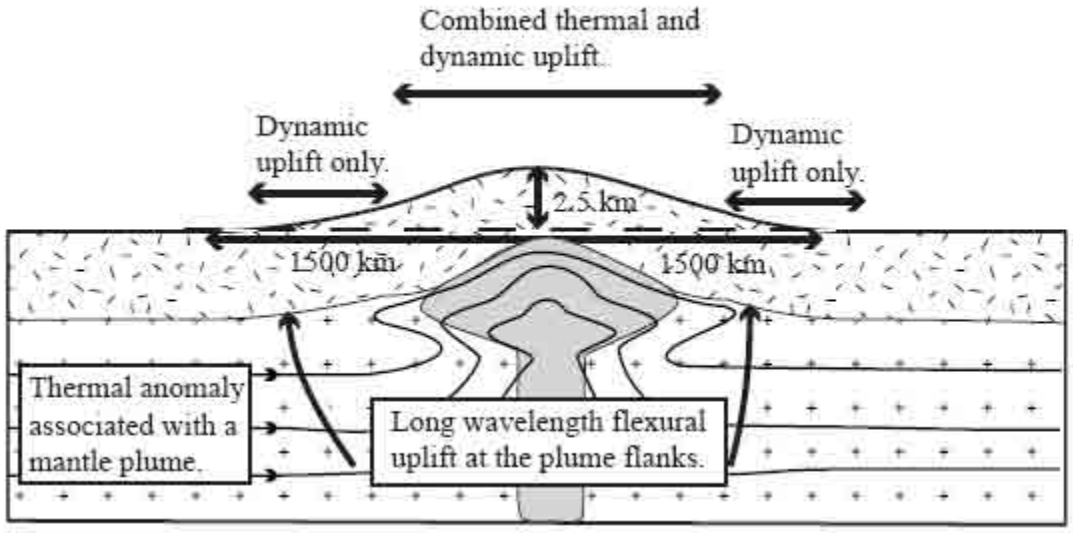

Figure 1.15 - Zones of thermal and dynamic uplifted associated with a mantle plume (after Nadin *et al.* 1995)

Brown (1991) first proposed magmatic underplating as a driving mechanism of Cenozoic exhumation in the British Isles in order to explain the elevated early Paleogene temperatures revealed by onshore AFTA samples in the East Midlands Shelf, UK (Green, 1989). The underplating hypothesis was subsequently expanded by Brodie & White (1994, 1995), in order to explain a number of observations regarding the geology of the British Isles, such as exhumation in the East Irish Sea (see also Rowley & White, 1998) and the apparent tilting of the British Isles along a NNE-SSW axis. Searching to explain these observations, Brodie & White (1994, 1995), discounted both flexural effects related to the early Paleogene opening of the North Atlantic and horizontal lithospheric shortening caused by Alpine orogenesis.

As discussed in more detail by Holford (2006), the British Isles are characterized by small-wavelength (<50km) gravity anomalies, which rules out lithosphere flexure as a cause of exhumation since flexural isostatic processes such as rift-flank uplift (*cf.* Weissel & Karner, 1989) should generate large amplitude gravity anomalies. Thermal effects related to Atlantic opening are also thought to be negligible (Nadin & Kusznir, 1995). In addition, Brodie & White (1995), contended that the observable Cenozoic shortening across the British Isles (*c.*

5% strain) is too small to generate sufficient crustal thickening and hence exhumation (e.g. *c.* 30% shortening required to produce 3km of exhumation).

In light of this information Brodie & White (1994, 1995), proposed magmatic underplating coeval with the magmatic activity of the British Cenozoic Igneous Provinces, as the most likely cause of exhumation. The geometry of this plume was originally imagined as roughly circular fed by a narrow central plume of rising material during early Paleogene times (White 1988; White & McKenzie 1989). Recently however, it has been re-envisaged in terms of a tetrad of linear, subvertical sheet-like plumes (Smallwood & White 2002; Al-Kindi *et al.* 2003) one of which may have extended from western Greenland to Lundy in the Bristol Channel (Figure 1.16) (Al-Kindi *et al.* 2003). Melt generated by this hot convective sheet is thought to be the source of the underplating (Al-Kindi *et al.* 2003).

In addition to the large amounts of apparent evidence to support the underplating hypothesis, there are an equally large number of observations which cast doubt on it being the sole driving mechanism of Cenozoic exhumation. As detailed more thoroughly by Holford (2006), although Al-Kindi *et al.* (2003) claim to have constrained the thickness of an underplated layer using wide-angle seismic refraction data, there is little evidence to support the existence of substantial lower crustal underplating from deep seismic reflection profiles acquired within the Irish Sea, which lack the reflectivity patterns associated with magmatic underplating (England & Soper, 1997; Chadwick & Pharaoh, 1998). Chambers *et al.* (2005) have also questioned White & Lovell's (1997) assertion of a correlative link between pulses of sedimentation in the North Sea and surface uplift caused by episodic magmatic underplating. New $^{40}Ar/^{39}Ar$ ages obtained from volcanic rocks in the British Cenozoic Igneous Province show that the majority of magmatic activity occurred within a short time span (3Myr) rather than in a pulsed manner (Figure 1.13). More importantly for the SW UK

region, despite Brodie & White's (1994, 1995) contention that shortening within the Irish Sea region is insufficient to account for the observed magnitudes of exhumation, a number of recent studies in the SGCB have demonstrated the important role of compressional deformation (tectonic inversion) in driving exhumation during late Cretaceous-early Paleogene times (Ware & Turner, 2002; Williams, 2002; Williams *et al.* 2005).

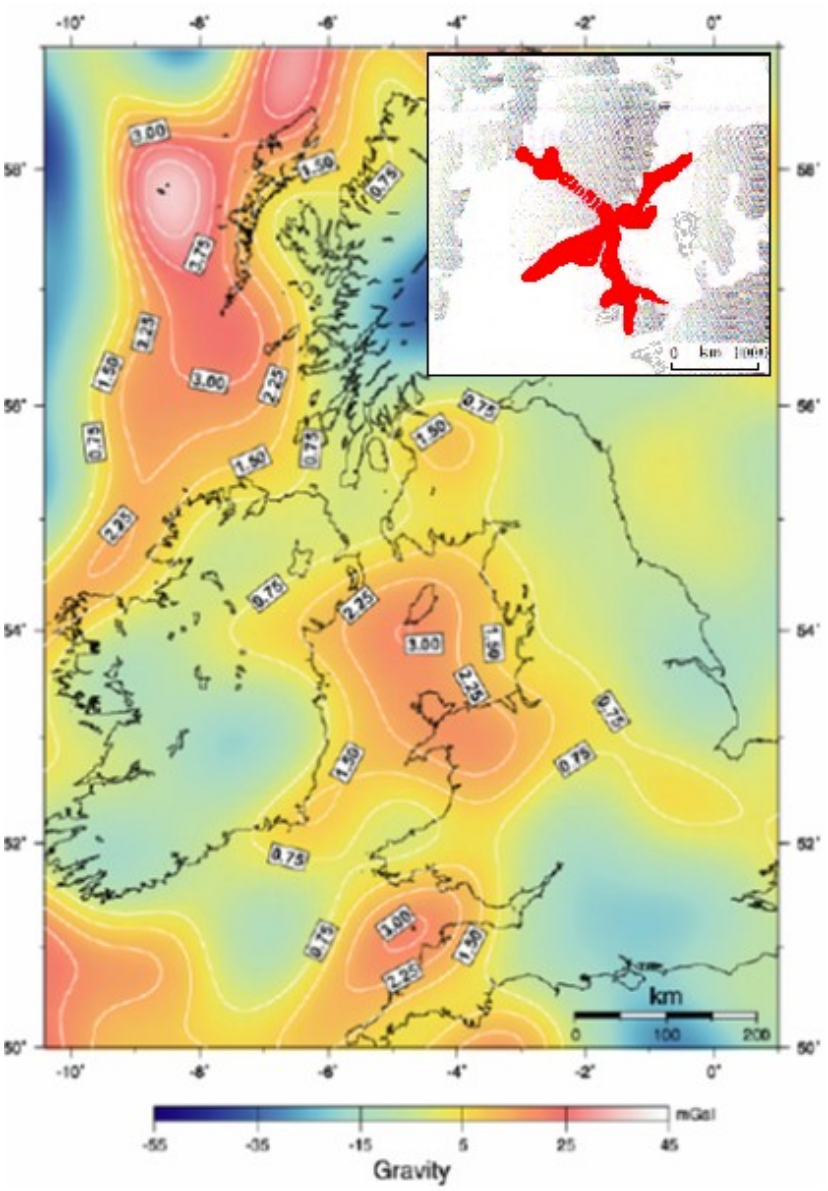

Figure 1.16 – Long-wavelength, free-air gravity map showing positive anomaly centred on the Irish Sea. Numbered white contours – predicted thickness of magmatic underplating determined by calibrating long-wavelength gravity data with wide-angle seismic model. Inset: Reconstruction of North Atlantic region at initiation of Iceland plume just before continental break-up. Solid red pattern – onshore-offshore distribution of magmatism which is the crustal manifestation of intersecting convective sheets. Note that this map predicts the thickest underplated material beneath the EISB where according to Holford *et al.* (2005a), AFTA indicate that exhumation was during the Cretaceous and not the Cenozoic (modified after Al-Kindi *et al.* 2003).

1.5.2.2: Localised hotspot-related uplift

Cope (1994) suggested that the exhumation of the western UKCS may have been caused by a localised latest Cretaceous to late Paleogene hotspot located beneath the Irish Sea (Figure 1.17). This hypothesis has been challenged by a number of workers such as Thomson (1995), who noted that because the thermal anomaly related to a hotspot is transient when, it decays the uplift will also decay. The erosion which occurred during the Paleogene means that most of the British Isles should be at or below sea level if the exhumation was driven by a transient hotspot (Thomson, 1995). Since most of the British Isles are presently above sea-level, with regions of notable relief including the Scottish Highlands, the Pennines and Snowdonia (e.g. Clayton & Shamoon, 1998, 1999), Cope's (1994) proposed erosion map showing a 'bull's-eye' pattern over the Irish Sea (Figure 1.17) is in poor agreement with these observations coupled with regional variation in early Cenozoic erosion magnitudes and palaeotemperatures revealed by other studies (e.g. Thomson 1995; Green 2002; Holford, 2006).

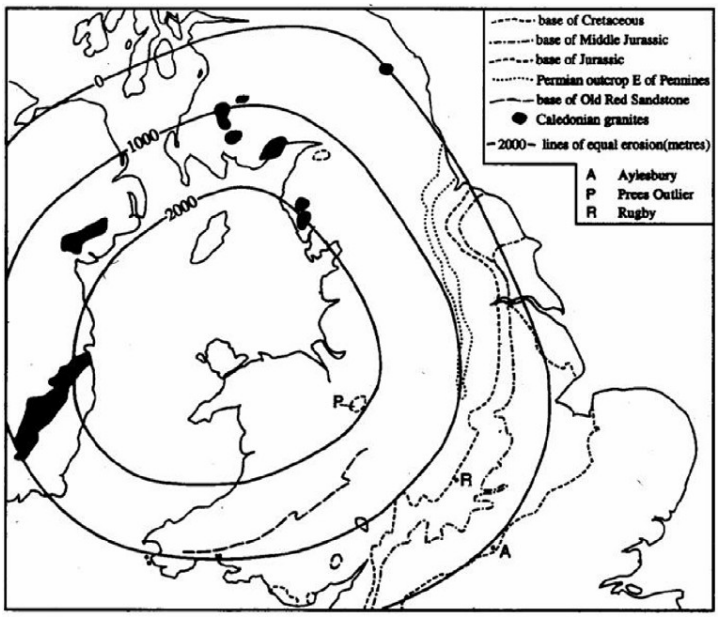

Figure 1.17 - Cope's (1994) estimation of the possible extent and amount of net erosion in the Irish Sea and surrounding areas, attributed to a localised late Cretaceous hotspot. Cope (1994) drew attention to the marked parallelism between his erosion contours and formation boundaries (with the exception of north Yorkshire, where the contours curve around the pre-existing Cleveland Basin). Many subsequent workers however, have shown that there is little agreement between Cope's (1994) predicted pattern of erosion and actual Cenozoic exhumation estimates (e.g. Thomson, 1995; Green *et al.* 1997, 2002; Green, 2002; Holford *et al.* 2005a; Holford, 2006).

1.5.2.3: Intra-plate shortening (tectonic inversion)

Many workers have argued that the post-Palaeozoic exhumation of the Western Approaches-Celtic Sea basin system and contiguous regions was driven by compressional and transpressional intra-plate shortening (tectonic inversion). The isostatic response to the crustal thickening caused by horizontal shortening is surface uplift (Figure 1.18a), which can subsequently be amplified by erosion (Figure 1.18b) (Brodie & White, 1995; Watts, 2001). Tectonic inversion is thus one of the main causes of exhumation in intra-plate regions and passive margins. As Figure 1.18b shows, to generate the amounts of exhumation generally observed across the Western Approaches-Celtic sea region (e.g. <3km), shortening strains of up to 30% are required (*cf.* Brodie & White, 1995). Within the upper crust, horizontal shortening is generally manifested by reversals in displacement (from normal to reverse) along dip-slip faults, changes in the polarity of structural relief (i.e. low-lying basin areas become positive structural culminations) and the inflation and expulsion of syn-rift sequences in sedimentary basins (Figure 1.19) (Hayward & Graham, 1989; Williams *et al.* 1989; Turner & Williams, 2004). On a larger-scale, compressional and transpressional shortening can result in whole lithosphere folding and buckling (Hillis, 1992; Ziegler *et al.* 1995).

The evidence for Mesozoic-Cenozoic tectonic inversion in the sedimentary basins of the British Isles has been well documented (e.g. the Irish Sea (Turner, 1997; Izzat *et al.* 2001; Cunningham *et al.* 2004; Williams *et al.* 2005), the Celtic Sea and Western Approaches (Tucker & Arter, 1987; van Hoorn, 1987*a*; Roberts, 1989; Hillis, 1991, 1992, 1995; Ziegler *et al.* 1995; Bulnes & McClay, 1998), the Wessex Basin (Lake & Karner, 1987; Chadwick, 1993; Underhill & Paterson, 1998; Gale *et al.* 1999; Blundell, 2002), the Inner Moray Firth (Thomson & Underhill, 1993; Hillis *et al.* 1994; Thomson & Hillis, 1995) and the southern North Sea (Glennie & Boegner, 1981; van Hoorn, 1987*b*; Nielsen & Hansen, 2000; Nielsen *et*

al. 2005; Worum & Michon, 2005)). Locations of Oligocene and Miocene-age inversion structures in NW Europe and along the Atlantic margin are identified in Figures 1.20 and 1.21. Several sources of the compressional stresses have been proposed such as Alpine orogenesis, particularly in Central and Western Europe (Roberts, 1989; Ziegler, 1989*a*; Ziegler *et al.* 1995) and Atlantic ridge-push, especially along the Atlantic margin (Boldreel & Anderson, 1993; Doré *et al.* 1996; Lundin & Doré, 2002). Assessing the contribution of these events to tectonic inversion is complicated however by the fact that deformation did not occur during one single event. Instead, a number of discrete phases of deformation throughout the late Cretaceous-Cenozoic have been identified (Figure 1.22) (e.g. Boldreel & Andersen, 1998; Dewey, 2000; Blundell, 2002; Worum & Michon, 2005).

There is abundant evidence for tectonic inversion in the Celtic Sea-Western Approaches region during Cenozoic times (Tucker & Arter, 1987; van Hoorn, 1987*a*; Hayward & Graham, 1989; Roberts, 1989; Hillis, 1991; Menpes & Hillis, 1995; Murdoch *et al.* 1995; Bulnes & McClay, 1998). Tectonic inversion in the NCSB was accommodated by a combination of compressive reactivation of pre-existing growth faults, and the broad regional upwarping of the Cretaceous depocentre (Figure 3.8d) (Tucker & Arter, 1987). Around 1km of erosion is associated with this inversion, which Tucker & Arter (1987) contended, on stratigraphical grounds, must have occurred between the late Maastrichtian and early Eocene. Roberts (1989), Murdoch *et al.* (1995) and Blundell (2002), however, argued that the inversion of the NCSB occurred during the Oligocene or Miocene, coeval with the inversion of the WAB (Hayward & Graham, 1989). This emphasizes the lack of precise control on the timing of inversion in many of these studies, with the preferred timing often assigned from consideration of regional geological trends.

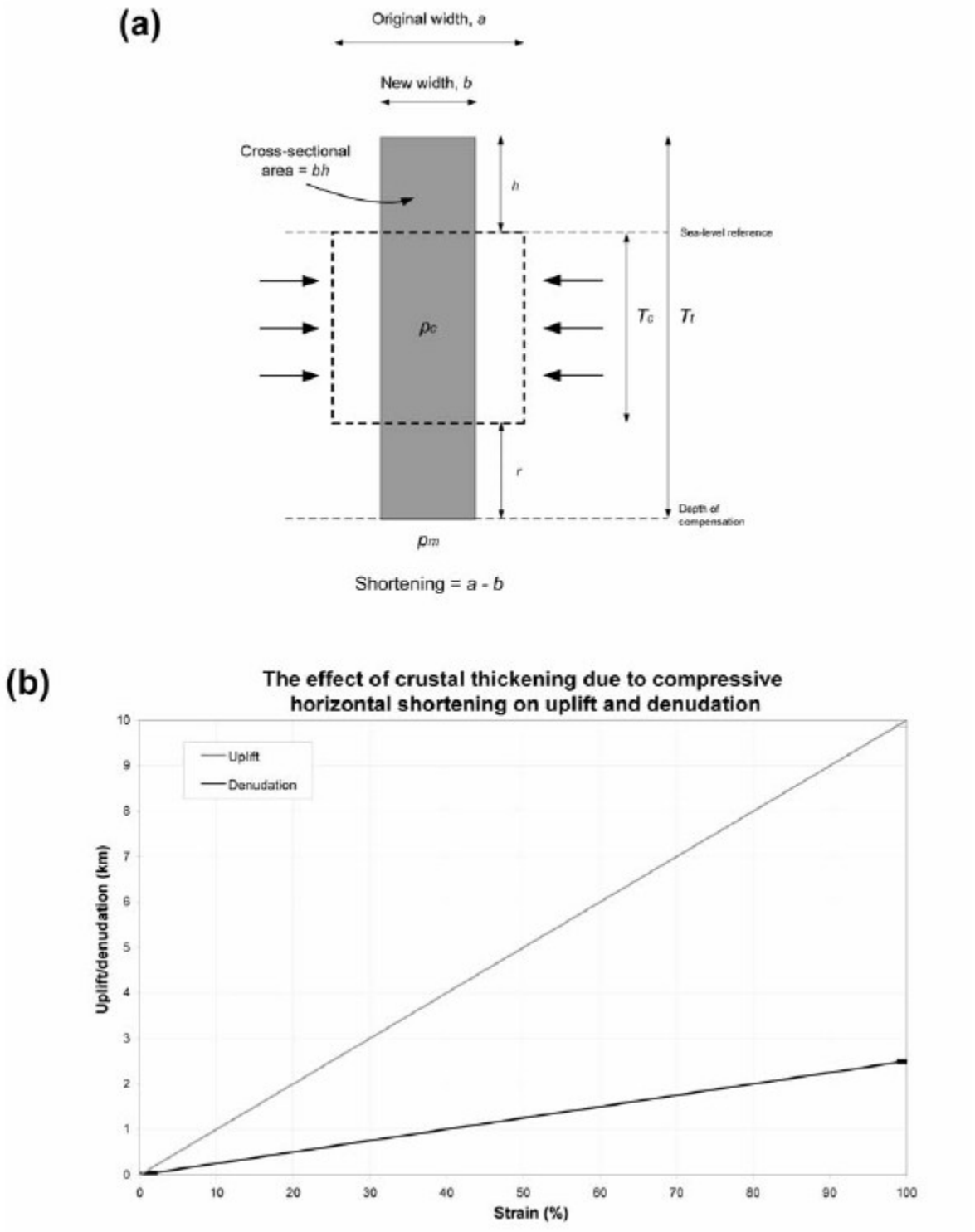

Figure 1.18 - (a) Diagram illustrating how shortening of a column of crust by horizontal compression (under conditions of Airy isostatic equilibrium) leads to an upwards movement of the surface with respect to sea level. (b) The amount of uplift and denudation resulting from horizontal shortening of a standard column of continental lithosphere 125 km thick (crustal thickness = 30 km) for varying amounts of compressional strain. Calculated using equations 1-5 of Brodie & White, (1995). Parameters are given in Table 1 of Brodie & White, (1995) (From Holford (2006)).

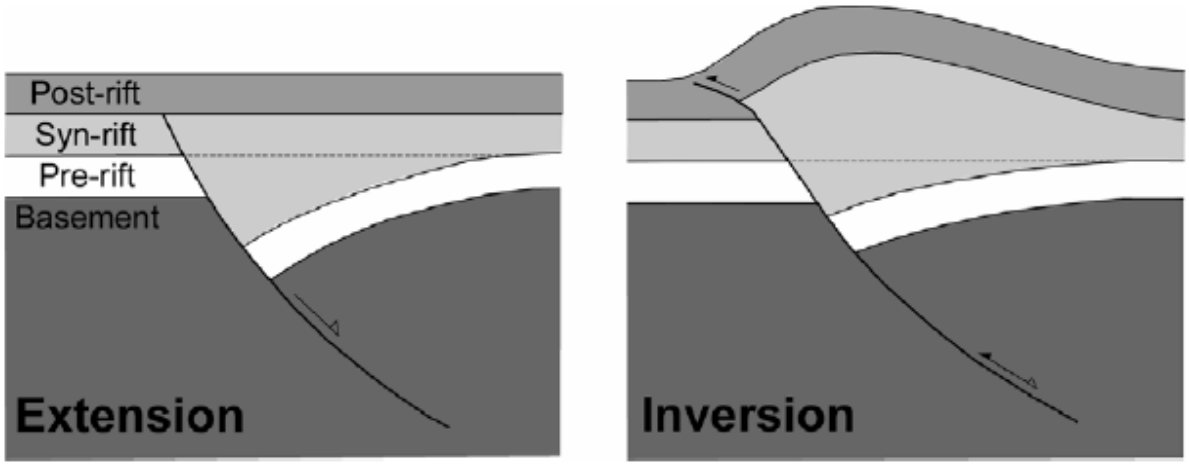

Figure 1.19 - Schematic diagram of a classical positive inversion structure. The sense of movement along a basin controlling extensional fault is reversed during compressional tectonics, leading to the expulsion of the syn-rift fill and the formation of a growth anticline whilst still retaining net extension at depth. In the bottom example, the position of the null point is identified. This marks the divide between reverse displacement above and normal displacement below. The progressive contractional inversion of an extensional syn-rift sequence will cause the null point to move down the syn-rift sequence (after Williams *et al.* (1989)).

The relative importance of Alpine orogenesis and Atlantic ridge-push as the primary driving mechanisms behind the Cenozoic compressional shortening in NW Europe and the Atlantic margin is a hotly debated subject. The World Stress Map shows that maximum horizontal compressive stresses in Europe and the North Atlantic are oriented uniformly NW-SE to NNW-SSE (Figure 1.23) (Müller *et al.* 1992; Zoback 1992), with local deviations in stress orientation largely explained by heterogeneity due to the detachment of sedimentary cover sequences from basement (Hillis & Nelsen, 2005). This is consistent with the directions of both Alpine continental convergence and sea-floor spreading in the Atlantic. Results from the geodynamic models of Bott (1993) and Bott & Bott (2004) have shown that oceanic ridges underlain by anomalously hot, buoyant mantle can generate horizontal compressive stresses of up to 100MPa which can extend great distances (<2000 km) from the site of the ridge. Bott & Bott (2004) therefore attribute the NW-SE compressive stresses to anomalously strong ridge-push associated with the Iceland mantle plume. The results of Bott's (1993) finite-element modelling imply that although the Alpine orogenic belt can provide resistance to this

far-field compression, thus allowing this stress regime to pervade the entire region, it cannot cause distant compression by itself (Bott & Bott 2004).

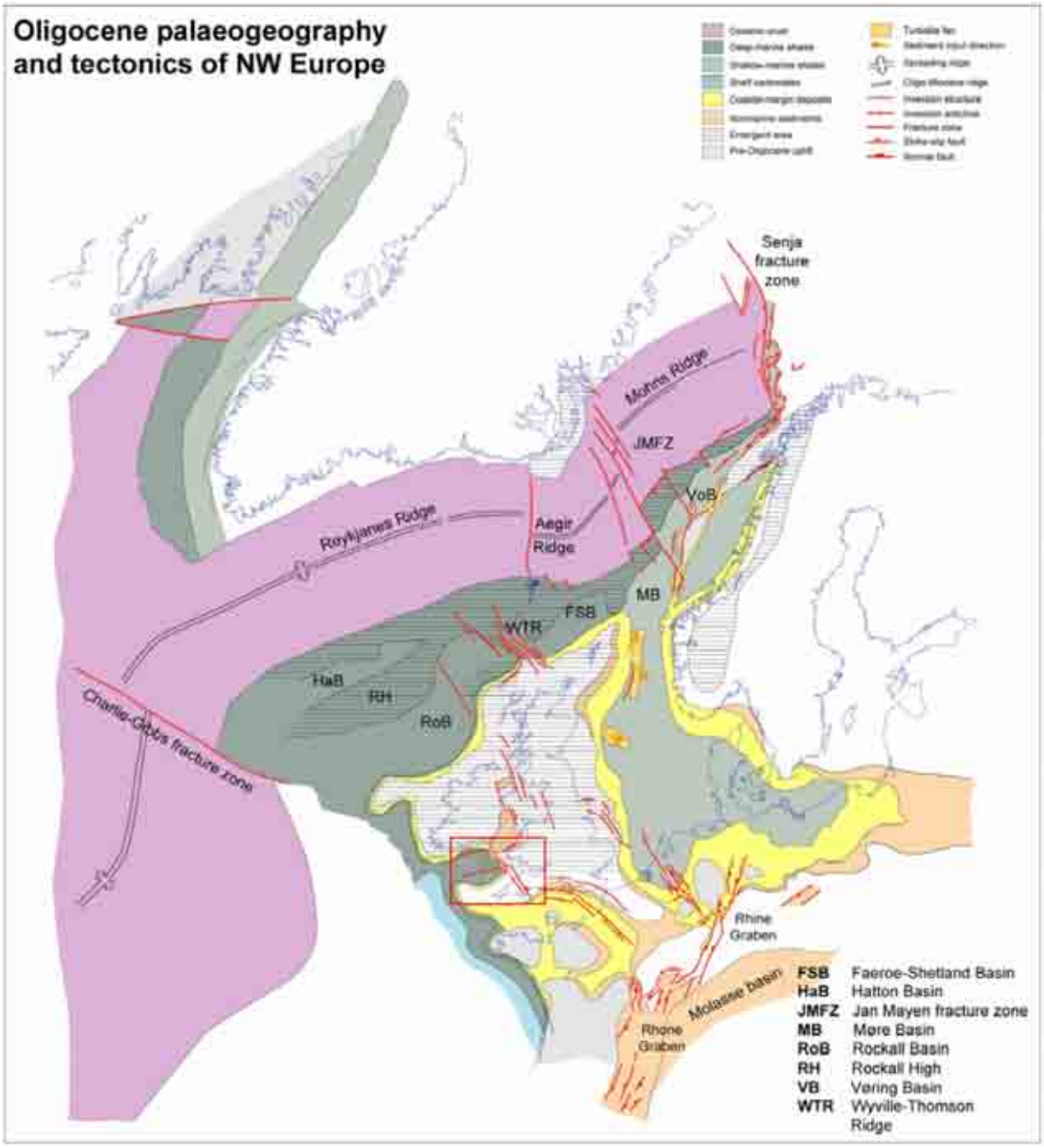

Figure 1.20 - Palaeogeographic reconstruction of NW Europe and the North Atlantic during early Oligocene times (*c.* 36 Ma), showing the distribution of active structures and sediment facies. A second phase of North Atlantic-Arctic opening started in mid-Oligocene times when relative plate motion changed to approximately east-west. This change in spreading direction was associated with the cessation of seafloor spreading in the Labrador Sea, causing Greenland to become part of the North Atlantic plate. Basin inversion occurred along the Atlantic margin of Norway and NW Britain, as well as in the western part of the southern North Sea and the English Channel, whilst strike-slip deformation in the western part of the British Isles led to the formation of a series of pull-apart basins. The area of interest in this study is highlighted by the red box (after Coward *et al.* (2003)).

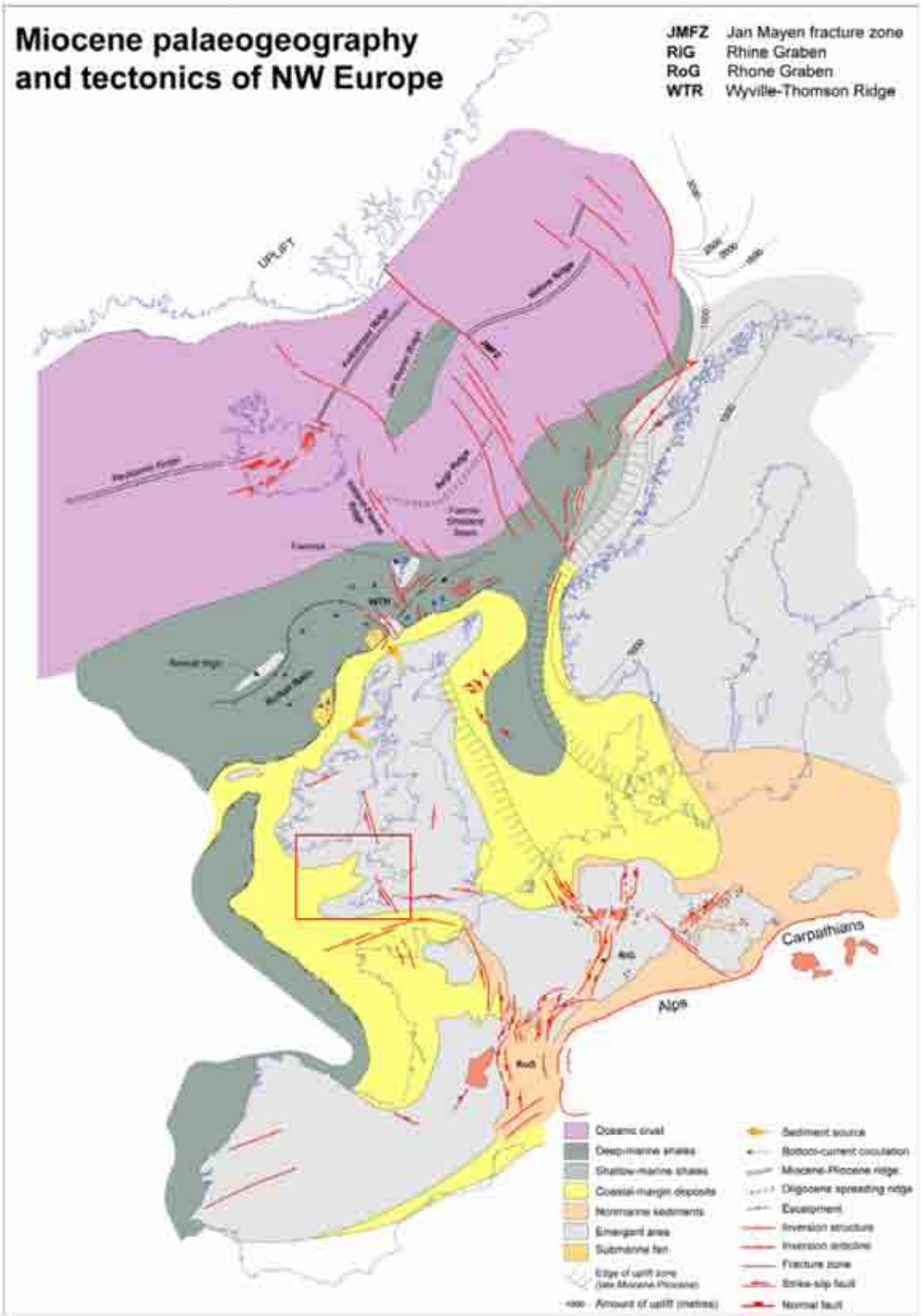

Figure 1.21 - Palaeogeographic reconstruction of NW Europe and the North Atlantic during early Miocene times, showing the distribution of active structures and sediment facies. Large parts of the British Isles, Scandinavia and Greenland were affected by late Neogene uplift and erosion, the by-products of which were redeposited as large sediment slumps along the continental shelf. This onshore uplift was accompanied continued (thermal) subsidence in the North Sea. The area of interest in this study is highlighted by the red box (after Coward *et al.* (2003)).

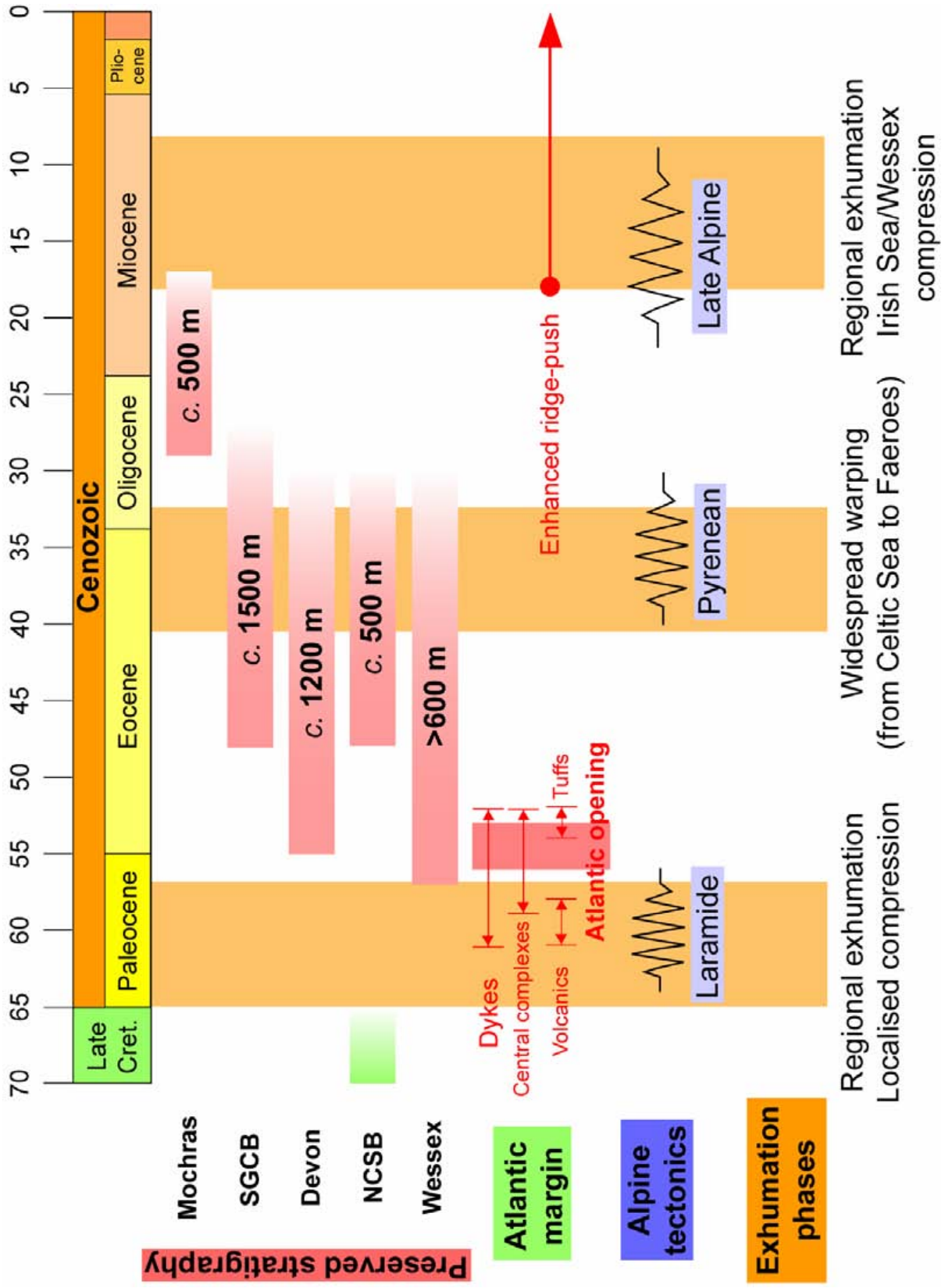

Figure 1.22 - Cenozoic event stratigraphy diagram for the southern British Isles showing ages and thicknesses of preserved Cenozoic sediments (compiled from various sources) compared against the timing of important regional tectonic events (e.g. timing of North Atlantic Igneous Province magmatism and major compressional pulses of the Alpine orogeny (from Doré *et al,* 1999)).

This contradicts the observations of Ziegler *et al.* (1995, 1998) however, of the development of important compressional intra-plate structures (e.g. in the NW European Alpine foreland) at distances of up to ±1600km away from orogenic fronts, the timing and patterns of which correlate directly with important phases of collisional plate coupling. Furthermore, since continental break-up in the North Atlantic was not achieved until *c.* 53Ma (earliest Eocene) (Doré *et al.* 1999), ridge-push forces cannot explain the development of late Cretaceous-Palaeocene compressional structures in NW Europe (Boldreel & Andersen, 1998).

Roberts (1989) contended that tectonic inversion during the late Cretaceous-Palaeocene was driven by the transmission of compressional stresses through the European foreland during the early phases of Alpine collision; this phase of deformation terminated during the Eocene, when the initiation of the extensional plate boundary along the Rhine-Rhone rift system prevented further transmissions of stress (Roberts, 1989; Coward *et al.* 2003). The timing of strike-slip movements along the Sticklepath-Lustleigh Fault Zone (Holloway & Chadwick, 1986; Turner, 1997; Dunford *et al.* 2001; Cunningham *et al.* 2004), and similar NW-SE trending structures along the Atlantic margin (i.e. the Anthon Dohrn Lineament) (Doré *et al.* 1997; Johnson *et al.* 2005; Kimbell *et al.* 2005) may correlate with the generation of the European Rift system and its associated stress field (Coward, 1994; Ziegler *et al.* 1995; Blundell, 2002; Coward *et al.* 2003).

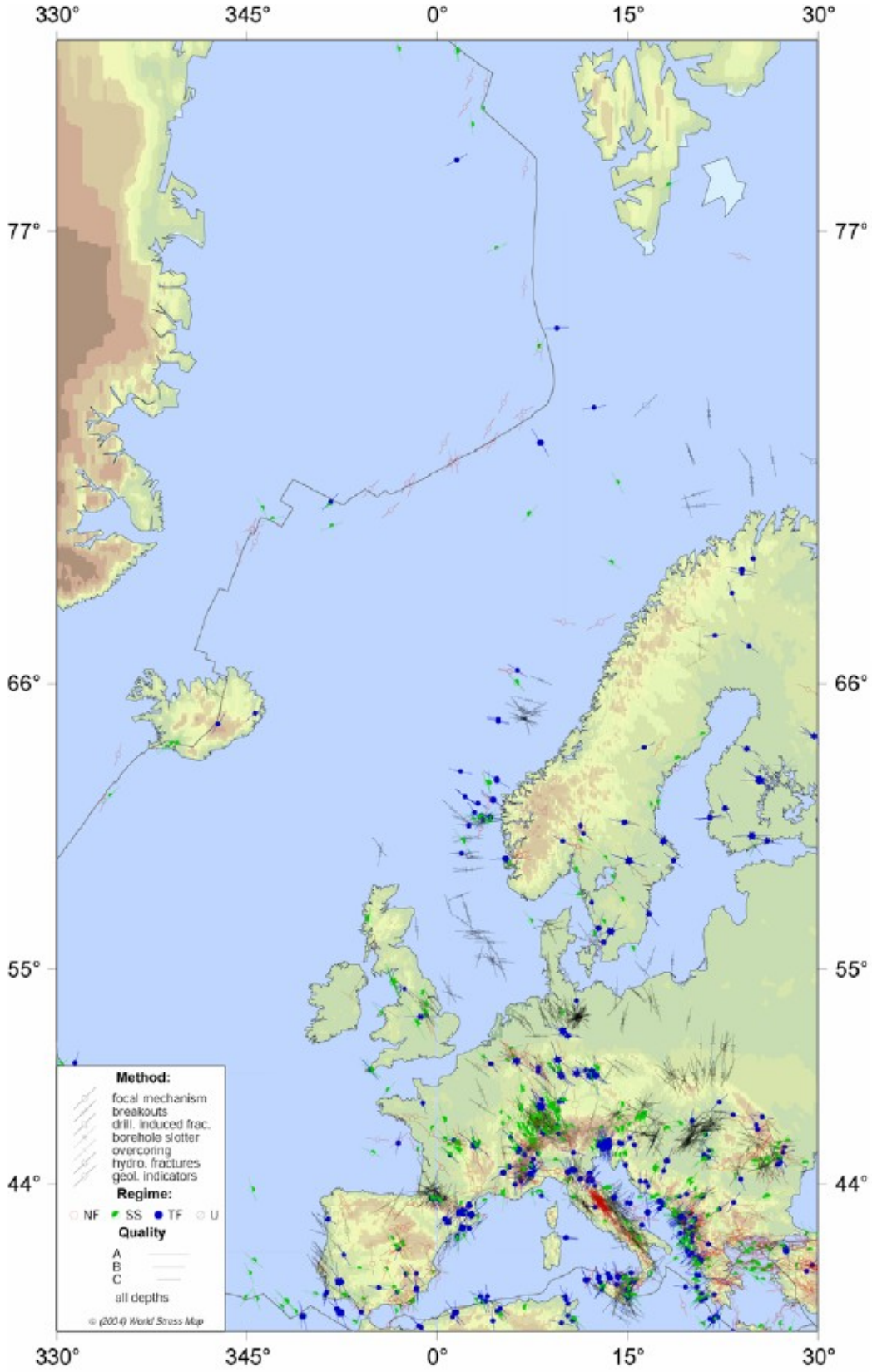

Figure 1.23 - Stress map of Europe and the North Atlantic, based on World Stress Map data from Reinecker *et al.* (2003). The long axes of the bars represent the maximum horizontal stress orientation and the length of the bars the quality ranking of that indicator. Maximum horizontal stresses are generally uniformly oriented NW-SE to NNW-SSE.

The collision in the Pyrenees and subduction along the northern margin of the Bay of Biscay initiated the next phase of inversion. The suturing of the Iberian and European plates during the Oligocene allowed the northward transmission of stresses which led to further inversion (Roberts, 1989). Neogene (Miocene) compressional deformation in NW Europe (e.g. in the Wessex Basin (Chadwick, 1993)) was coincident with an increase in the rate of African-European convergence beginning at 22Ma (Dewey *et al.* 1989; Dewey, 2000). Based largely upon the work of Ford *et al.* (1999), Blundell (2002) attempted to directly correlate the Cenozoic deformations of southern Britain with stages of the evolution of the North Alpine Foreland Basin (Figure 1.24). Periods of tectonic inversion occurred when stresses generated during Alpine collisional coupling could not be accommodated within the orogen or foreland basin, and were thus transmitted into the Alpine foreland (Blundell, 2002). The convergence of the Apulian plate with Europe during the mid to late Eocene (46-36Ma) resulted in the NW migration of the flexural foreland basin and the front of a low-angle external orogenic wedge, thereby permitting the transmission of stresses into the foreland (Ford *et al.* 1999). Blundell (2002) correlated this deformation phase with the Eocene uplift of the Weald Basin (*cf.* Nielsen & Hansen, 2000) and the uplift identified by Gale *et al.* (1999), along the Sandown Pericline. During the Oligocene and early Miocene shortening was largely accommodated within the thickness of the orogenic wedge, meaning that little or no stress would have propagated into the foreland (Blundell, 2002). Collapse of the outer orogenic wedge during the late Miocene to Pliocene (11-3Ma) and compressional deformation of the Jura fold belt allowed compressional stresses to propagate beneath the Jura décollement resulting in the inversions along the Abbottsbury-Purbeck line (*cf.* Underhill & Paterson, 1998) and the deformation of Eocene and older strata across southern Britain (Blundell, 2002).

It is apparent that the precise cause of Cenozoic inversion in Northwest Europe is extremely difficult to pinpoint and likely to be best explained by composite events involving compressive stresses from both sea-floor spreading and Alpine orogenesis. Several authors (e.g. Stoker *et al.* 2005*b*) have suggested an underlying mantle control on tectonics in Europe based on the coincidence of inversion and plate reorganisations. Stoker *et al.* (2005*b*) present an example of this where the cessation of sea-floor spreading in the Labrador Sea and the incipient extinction of the Ægir ridge was approximately coeval with the late Eocene to early Oligocene Pyrenean orogenic phase (Figure 1.20), whilst the late Alpine compressive pulse during the early Neogene was coincident with the separation of Jan Mayen and Greenland and the establishment of the Kolbeinsey Ridge (Figure 1.21).

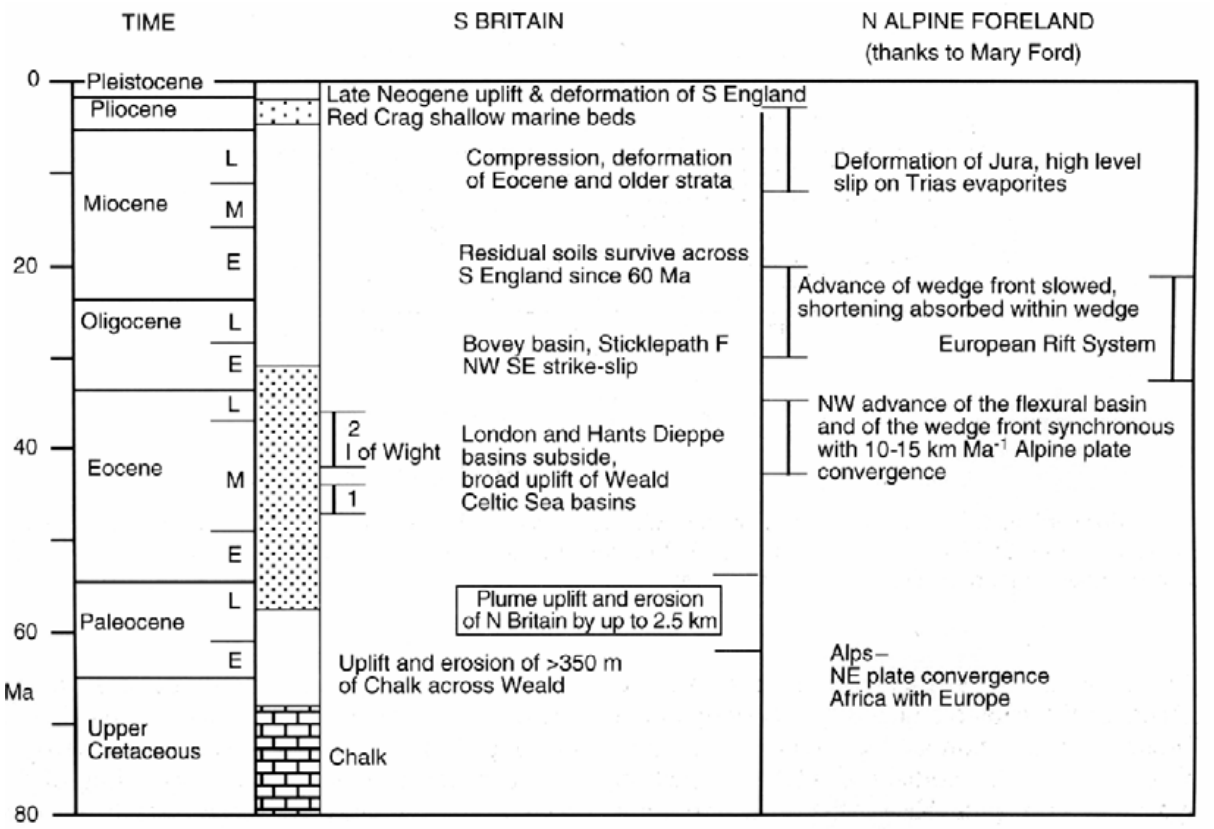

Figure 1.24 - Correlation of Cenozoic tectonic events in southern Britain and the Alpine Foreland Isle Of Wight uplift phases 1 and 2 refer to those identified by Gale *et al.* 1999) (after Blundell, 2002).

1.5.3: NEOGENE EXHUMATION ACROSS THE NORTH ATLANTIC REGION

It is widely accepted that NW Europe and the Atlantic margin experienced significant kilometre-scale uplift and exhumation during the Cenozoic and these events have been important in establishing the present configuration of sea and landmasses (Doré *et al.* 1999). As highlighted above important episodes occurred during the Paleogene and Miocene however significant uplift also occurred during the late Neogene, especially along the North Atlantic margins (Figure 1.25; Japsen & Chalmers, 2000).

The exhumation is recorded by the major prograding shelf-margin wedges which have been described from the UK Atlantic margin, the Norwegian margin, and the eastern and western Greenland margins (Stoker, 2002). It has also been noted by several authors that the onshore exhumation was accompanied by apparently anomalous, accelerated subsidence, particularly along the NW European margin (Figure 1.25) (e.g. Cloetingh *et al.* 1990; Hall & White, 1994; Ceramicola *et al.* 2005). Williams et al. (2005) presented evidence for significant Neogene exhumation in the SGCB where the preserved Paleogene rocks in this basin were themselves more deeply buried by at least 1km of additional section prior to Neogene exhumation. In other parts of the British Isles, Japsen (1997, 2000) has shown that the East Midlands Shelf and parts of the southern North Sea also experienced around 1km of exhumation during the late Neogene, an observation corroborated by palaeothermal analyses (Green *et al.* 2001*b*). In addition, it has been noted that much of the present-day topography of the British Isles is the result of differential neotectonic movements during the late Neogene (Clayton & Shamoon, 1999; Watts *et al.* 2000, 2005; Blundell, 2002). The magnitude and extent of the late Neogene uplift points strongly towards a tectonic origin (albeit probably enhanced by glacio-isostatic uplift (Eyles, 1996; Doré *et al.* 1999)), although the precise causes are as yet unknown (Japsen & Chalmers, 2000; Japsen *et al.* 2005).

A number of authors claim that the Iceland plume cannot be responsible for permanent uplift (e.g. Jones *et al.* 2002; Japsen *et al.* 2005) and instead variation of in-plane stress as a result of regional lithospheric compression has been invoked to explain the observations of accelerated subsidence in the basins around Greenland and Scotland as well as basin-flank uplift (Cloetingh *et al.* 1990), although the amounts of uplift and subsidence predicted by this model appear to be too small by an order of magnitude (Japsen & Chalmers, 2000). Rohrman & van der Beek (1996) suggested that the uplift of the Atlantic margins could be explained by a Rayleigh-Taylor instability. Whilst the driving mechanisms of this uplift and exhumation continue to be a topic of intense debate (e.g. Japsen & Chalmers, 2000; Doré *et al.* 2002*a*) it is clear that Neogene uplift is one of the most important tectonic events to have affected NW Europe during post-Palaeozoic times (Doré *et al.* 1999). It is important to note that ice sheets covered the Celtic Sea basins for much of the Quaternary, with attendant implications for post-glacial isostatic rebound in generating regional uplift and subsidence (Doré & Jensen 1996). The effect of Quaternary processes on sedimentary basin evolution and regional uplift is largely ignored in the UK.

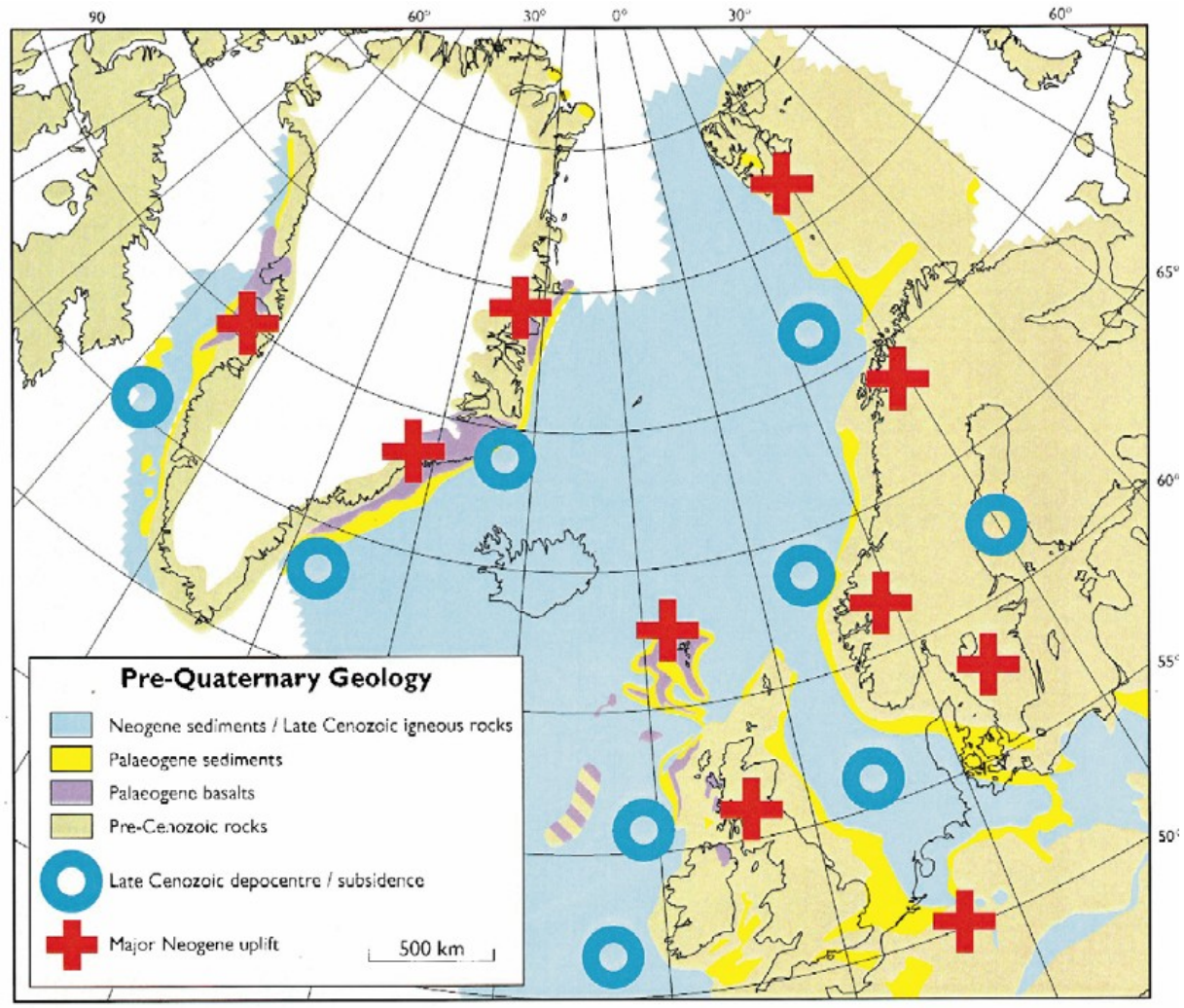

Figure 1.25 - Map of the pre-Quaternary geology around the North Atlantic region showing areas of Neogene/late Cenozoic uplift/erosion and of accelerated subsidence/deposition. From Japsen & Chalmers (2000), compiled from various sources.

CHAPTER 2: TECHNIQUES USED TO ESTIMATE THE MAGNITUDE AND TIMING OF EXHUMATION

2.1: INTRODUCTION

The aim of this chapter is to discuss the relative merits and application of the techniques used to estimate the timing and magnitude of exhumation in this study of the SW UK and its offshore basins. As discussed more fully by Corcoran & Doré (2005), most techniques for estimating exhumation in sedimentary basins utilise 'point' measurements (i.e. local estimates for an individual well or borehole) of vertical rock displacement relative to a specified frame of reference. In this study, the main frames of reference which have been used to estimate exhumation are thermal (e.g. Apatite Fission Track Analysis (AFTA) and Vitrinite Reflectance (VR)) and compactional (e.g. sonic velocity and formation density from wireline log data). Although many techniques can be used to estimate former burial depths in exhumed sedimentary basins, this Chapter will only focus on those used in this study; the interested reader is referred to the recent review paper by Corcoran & Doré (2005), for an up-to-date assessment of the most common methods which are used to measure exhumation. It should be noted at the outset that, taken individually, although 'point' measurements can provide quantitative constraints on the magnitude (and, if AFTA is used, the timing) of exhumation they can rarely be used to identify mechanisms of exhumation. Some mechanisms, most notably tectonic inversion, can be directly identified by seismic reflection data (Turner & Williams, 2004), but usually mechanisms have to be inferred from patterns of exhumation constructed from wide data coverage and combined with geological and geophysical observations (e.g. Argent *et al.* 2002; Ware & Turner, 2002). In many cases however, the superimposition of different types of driving mechanism (regional or local;

permanent or transient; compressional; thermal; isostatic or eustatic) make it difficult to isolate the contribution of individual processes (Turner & Williams, 2004; Corcoran & Doré, 2005).

2.1.1: DEFINITIONS

A wide lexicon of terms, which are often interchangeably used, has developed in recent years with respect to the exhumation of rocks (see Table 2.1, Doré *et al.* 2002*a* and Corcoran & Doré, 2005) however this study follows the terminology suggested by England & Molnar (1990) and Corcoran & Doré (2005).

2.1.1.1: Uplift

As emphasized by England & Molnar (1990), in studies of this kind, when attempting to estimate vertical displacements of uplift it is essential to specify both the object which is being displaced and the frame of reference. In particular, England & Molnar (1990), made important distinctions between the displacement of the Earth's surface (averaged over an area *c.* 103-104km²) with respect to the geoid (*surface uplift*), displacement of rocks with respect to the geoid (*uplift of rocks*) and displacement of rocks with respect to the surface (*exhumation*). These three types of displacement are related in the following way:

$$surface\,uplift = uplift\ of\ rock - exhumation \tag{2.1}$$

These quantities cannot be equal, except when all are zero (England & Molnar 1990). The relationship between surface uplift and crustal uplift depends upon the amount of denudation or deposition. If there is no denudation or deposition, then surface uplift and uplift of rocks (often also known as *crustal uplift* (e.g. Summerfield 1991)) will be equal. If denudation occurs (as is likely) then crustal uplift will be greater than surface uplift, and if denudation is

greater than crustal uplift surface elevation will be reduced (Doré *et al.* 2002*a*). It is important to discriminate between these different quantities, because only surface uplift requires a quantifiable amount of work against gravity, and hence a tectonic driving force; uplift of rock or exhumation can be caused solely by changes in sedimentary or erosional base level (e.g. eustatic sea level change) (England & Molnar 1990).

The interactions between some of the terms introduced in the preceding paragraph are illustrated in Figure 2.1 (modified from Molnar & England (1990)). This figure contains a series of schematic crustal cross-sections which indicate the possible isostatic effects of erosion on the elevation of a mountain belt. If a mountain range with an average elevation h and crustal thickness h_c (a) is instantaneously eroded, the erosion will reduce the surface elevation, but isostatic compensation will result in *crustal uplift* (uplift of rocks), as indicated by the upwards movement of the reference marker in (b) relative to (a). Note that the crust above the reference horizon has been eroded between stages (a) and (b). This is *exhumation* or *denudation* (D). As a result of the erosion and resultant isostatic readjustment, there has been a change in the mean surface elevation Δh. In this example the *surface uplift* is negative, as there has been a lowering of the mean surface level (Molnar & England 1990; Allen & Allen, 2005). Figure 2.1(c) illustrates the effects of dissection by river erosion on the mountain landscape. Rivers carve deep valleys down to sea level; whereas the mean elevation is the same as in situation (b) (i.e. $h - \Delta h$), the isostatic response to erosion uplifts the mountain peaks to an elevation of $2(h - \Delta h)$, meaning that the highest mountain peaks are considerably higher than the initial mean elevation.

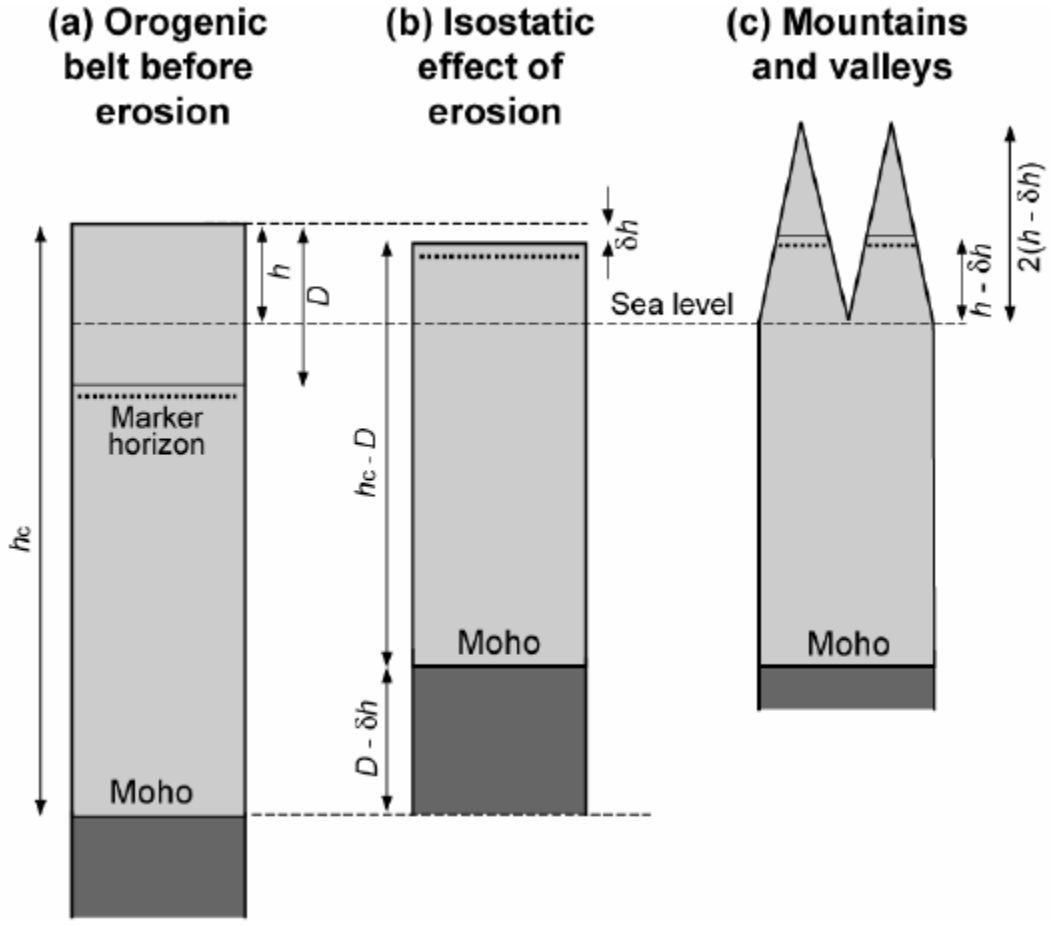

Figure 2.1 - A series of schematic crustal cross-sections illustrating the possible effects of erosion on the elevation of mountain belts and valleys. In situation (a) the crustal block is characterised by a surface elevation of h and contains a marker horizon located at depth D In situation (b) erosion of the crustal thickness D brings the marker horizon to the surface, resulting in a change in surface elevation Δh. In (c) the erosive activity of rivers has excavated a series of deep valleys to sea level. This results in the uplift of the mountain peaks to an elevation $2(h - \Delta h)$, while the marker horizon remains at an elevation of $h - \Delta h$ (modified after Molnar & England, 1990 and Allen & Allen, 2005).

2.1.1.2: Exhumation

As noted by England & Molnar (1990), very few studies have actually been able to quantify surface uplift (e.g. Abbott *et al.* 1997). Because of the problems involved in constraining an absolute datum, several workers (e.g. Nansen, 1904; Holtedahl, 1953; Harland *et al.* 1989; Ware & Turner, 2002; Corcoran & Doré, 2005) have suggested that exhumation is actually a far more useful parameter to constrain than uplift. The term *net exhumation* (*net uplift* – *sensu* Riis & Jensen, 1992; Doré & Jensen, 1996) refers to the vertical difference between the present-day burial depth of a reference unit/horizon and its maximum burial depth prior to

exhumation. This parameter is of particular importance in terms of hydrocarbon exploration because maximum burial depth is a key control on the maturation, compaction and diagenetic state of source, reservoir and seal rocks (Doré *et al.* 2002*b*). The term *gross exhumation* is used to define the magnitude of erosion which must have occurred at a particular unconformity prior to post-exhumation re-burial (Corcoran & Doré, 2005). Summary definitions of uplift, exhumation and other important terms like *erosion*, *denudation* and *inversion* are provided in Table 2.1.

In the rest of this Chapter, the methodologies and application of the main techniques which have been used in this study to estimate the timing – namely palaeothermal (AFTA and VR) and compactional (sonic velocity, porosity and formation density data) proxies of former burial depths are critically assessed. An overview of other available, but less commonly used methods of measuring exhumation is also provided in Table 2.2, which also lists the advantages and disadvantages of each method as well as providing examples of their application. A comparison of different techniques used to measure palaeotemperatures in sedimentary basins is provided in Table 2.3.

Term	Summary definition	Frame of reference	Spatial-wavelength
Uplift	Non-specific term referring to displacements "opposite to the gravity vector" (England & Molnar 1990)	Object displaced and/or reference frame not specified	Not specified
Surface uplift	Displacement of Earth surface averaged over area $>10^3$-10^4 km^2 (England & Molnar 1990)	Geoid or mean sea level	Long
Crustal uplift	Vertical displacement of rock column (Doré *et al.* 2002*a*)	Geoid or mean sea level	Short
Uplift of rocks	Vertical displacement of rock column (England & Molnar 1990)	Geoid or mean sea level	Short
Net uplift	Present elevation of a marker bed above its maximum burial depth (Riis & Jensen 1992; Doré & Jensen 1996)	Ground level or seabed	Short
Inversion	Compressional reactivation of formerly extensional fault systems leading ultimately to extrusion of syn-rift basin fill (Williams *et al.* 1989)	Pre-extensional regional elevation	Short and/or long
Epeirogeny	Large scale uplift of Earth's surface without significant folding or fracture (Summerfield 1991)	Geoid or mean sea level	Long
Erosion	Local subareal or submarine removal of material by both mechanical or chemical processes (Riis & Jensen 1992)	Fixed subsurface coordinates	Short
Denudation	Loss of mass from both surface and subsurface parts of a drainage system or regional landscape by all types of weathering, physical and chemical (Leeder 1999)	Fixed internal reference axes within bedrock	Long
Exhumation	A descriptive term describing removal of overburden material such that previously buried rocks are exposed (Doré *et al.* 2002*a*)	Ground level	Short and/or long
Net exhumation	Difference between present-day burial depth of a reference unit and its maximum burial depth prior to exhumation (Corcoran & Doré 2005)	Tectonic, thermal, compactional, stratigraphic (relative to seabed, ground level or stratigraphic marker)	Short
Gross exhumation	Magnitude of erosion which must have occurred at a particular unconformity prior to post-exhumation re-burial (Corcoran & Doré 2005)	Tectonic, thermal, compactional, stratigraphic (relative to seabed, ground level or stratigraphic marker)	Short

Table 2.1 - Lexicon of terms used to describe uplift and exhumation (modified after Corcoran & Doré, 2005).

Technique	Advantages	Disadvantages	Examples
Geomorphological analysis	Field-based, plentiful data, relates landform development to geological history	Difficult to obtain quantitative measures of erosion-denudation and to constrain timing; most effective when used with offshore analysis	Hall & Bishop (2002); Cunningham *et al.* (2003, 2004); Japsen *et al.* (2005)
Graphical reconstruction	Simple technique to estimate eroded thickness, correlate surfaces and determine onshore-offshore relationships	Relies on long distance extrapolation and assumption of thickness	Japsen *et al.* (2002)
Offshore sedimentary response	Provides indicator of denudation chronology of source areas; seismic data allow full sedimentary succession to be observed	Erosion and deposition of offshore successions complicate correlation with onshore denudation chronology; most effective when used together with onshore analysis	Huuse (2002)
Mass balance	Directly and quantitatively correlates denudation with offshore sedimentation	Loss off mass in solution; difficulty in assigning sediment to correct catchment area	Jones *et al.* (2002)
Vitrinite reflectance (VR)	Preserves record of higher temperatures (and therefore burial depths) than AFTA	Vitrinite absent from many sediments and all basement; often difficult to separate out components of heating due to deeper burial and elevated heat flow; reworked and oxidized vitrinite a problem; only a crude timing indicator	Green *et al.* (1997, 2001*a, b*, 2002)
Apatite fission-track analysis (AFTA)	Can establish detailed exhumation and burial chronology both onshore and offshore	Only records palaeotemperatures within *c.* 60-120°C window, therefore often unreliable in establishing recent events; difficult to separate changes in basal and transient heat flow from exhumation	Green *et al.* (1997, 2001*a, b*, 2002)
Cosmogenic nuclide	Used to obtain detail on geologically recent landform development not obtainable from AFTA	Onshore only, mainly limited to chronology of present land surface	Schaller *et al.* (2001)
Compaction	Plentiful source of well data (sonic and density logs); easier to distinguish changes in basal heat flow from exhumation compared with thermal methods	Unreliability of baseline compaction trends for a basin or lithology; difficulty in identifying 'typical' lithologies for analysis; mechanical compaction retarded by overpressure leading to erosion underestimates; only a crude timing indicator	Hillis (1991, 1995); Japsen (1998, 1999, 2000); Ware & Turner (2002)
Tectonic/subsidence modelling	Can provide insights into the geodynamic processes responsible for sedimentary basin subsidence and uplift	Numerous uncertainties regarding the generally applicability of relatively simple models of lithospheric deformation to complex basin sysytems	Rowley & White (1998); Jones *et al.* (2001)

Table 2.2 - Summary of techniques for measuring amount and timing of uplift and erosion (modified after Doré *et al.* 2002).

Palaeotemperature indicator	Sediment component analysed	Main rock type	Equipment required	Approximate maturity range (VR_{ro})	Palaeotemperature precision	Maximum measurable palaeotemperature	Time information	Limitations
VR	Vitrinite	Siltstone, shale	Reflecting light microscope, photometer	0.3-5.0	±5°C	>350°C	None	Geochemical suppression, pressure retardation
FAMM	Various macerals		Laser fluorescence microprobe	0.4-1.2		175°C		Small number of laboratories set up for technique
TAI	Palymorphs		Transmitting light microscope, non-colourblind operator	0.3-2.4	±20°C or higher	260°C		Subjective, poor temperature resolution
CAI	Conodonts	Carbonates		0.3-5.0+	±20-50°C	>600°C		Subjective, Cambrian-Triassic only, poor resolution
Illite crystallinity	Illite	Shale	X-ray diffraction instrument	0.4-5.5	±10°C	300°C		Clay composition changes due to fluids
Pyrolysis	Organic matter	All sediments	Gas-chromatograph mass spectrometer or RockEval tool	0.6-1.4	±5°C	200°C		Must use standard heating rate, results vary for sediment type
Fluid inclusions	Fluid inclusions in calcite, quartz, feldspar grains	Sandstone, limestone	Microscope, heating stage	n/a	±2°C	>1000°C	Relative timing of different inclusions	Only gives temperature at times of fluid migration
Biomarkers	Extracts and pyrloysates	All sediment	Gas-chromatograph mass spectrometer	0.3-2.0	±15°C	240°C	None	Most indices are poorly calibrated to VR
AFTA	Apatite	Sandstone	Microscope, thermo-nuclear reactor	0.3-1.0	±5°C	130°C	Absolute age of last cooling event	Composition of apatite must be determined

Table 2.3 - Summary of various techniques used to estimate palaeotemperatures in sedimentary basins, FAMM - Fluorescence analysis of multiple macerals; TAI-Thermal Alteration Index; CIA-Conodont Alteration Index (modified after Beardsmore & Cull, 2001).

2.2: ESTIMATING EXHUMATION USING COMPACTION DATA

Compaction-driven porosity reduction is an effective and widely used measure of former burial depths in sedimentary basins (Magara, 1976, 1978; Sclater & Christie, 1980; Senna, 1984; Bulat & Stoker, 1987; Hillis, 1991, 1995; Japsen, 2000; Japsen *et al.* 2002; Ware & Turner, 2002; Kelley, 2005; Holford *et al.* 2005*a*; Reed *et al.* 2005; Holford, 2006; Mavromatidis, 2007). Compaction is the largely irreversible process of sediment volume reduction due to overburden loading, grain rearrangement (packing), grain solution, porosity reduction, etc. and can be described primarily as a function of pore space (porosity) reduction (the reduction of the solids volume plays only a minor role). Giles *et al.* (1998) highlighted the importance of modelling this compaction in terms of three dimensional strain rather than the vertical change in sediment thickness. Compaction defined in this way is not the same as porosity loss which may be due to increase in solid volume (e.g. by introduction of cement) as well as to volume strains. As the pore space is filled with fluids which must be expelled during the compaction process the ability of the sediment to transmit fluids, or permeability, is the additional controlling parameter in compaction processes. In order to model compaction the general path of porosity, permeability and compressibility decrease with depth must be known.

Compaction studies require a plentiful (Ware & Turner (2002), suggested *c.* 2km of section) source of well data (porosity is usually inferred from geophysical logs acquired at exploration wells, most commonly from the sonic log which, provides the Interval Transit Time (ITT) ,Δt. ITT measures the formations capacity to transmit sound waves which varies with lithology and rock texture, notably porosity (Figure 2.2) (Doré *et al.* 2002)) and are especially useful in conjunction with thermally based burial proxies such as AFTA and VR since sedimentary porosities are largely unaffected by transient heating episodes which can often be

misinterpreted in terms of deeper burial (Ware & Turner, 2002). Thickness of sedimentary rocks removed by erosion in the geologic past can be estimated from shale compaction data. Such estimates are possible because shale compaction is related to overburden load or burial depth if pore pressure is normal or hydrostatic (Magara, 1976). This method cannot apply if the shales are undercompacted because shale compaction is not a simple function of burial depth in an undercompacted zone (Magara, 1976).

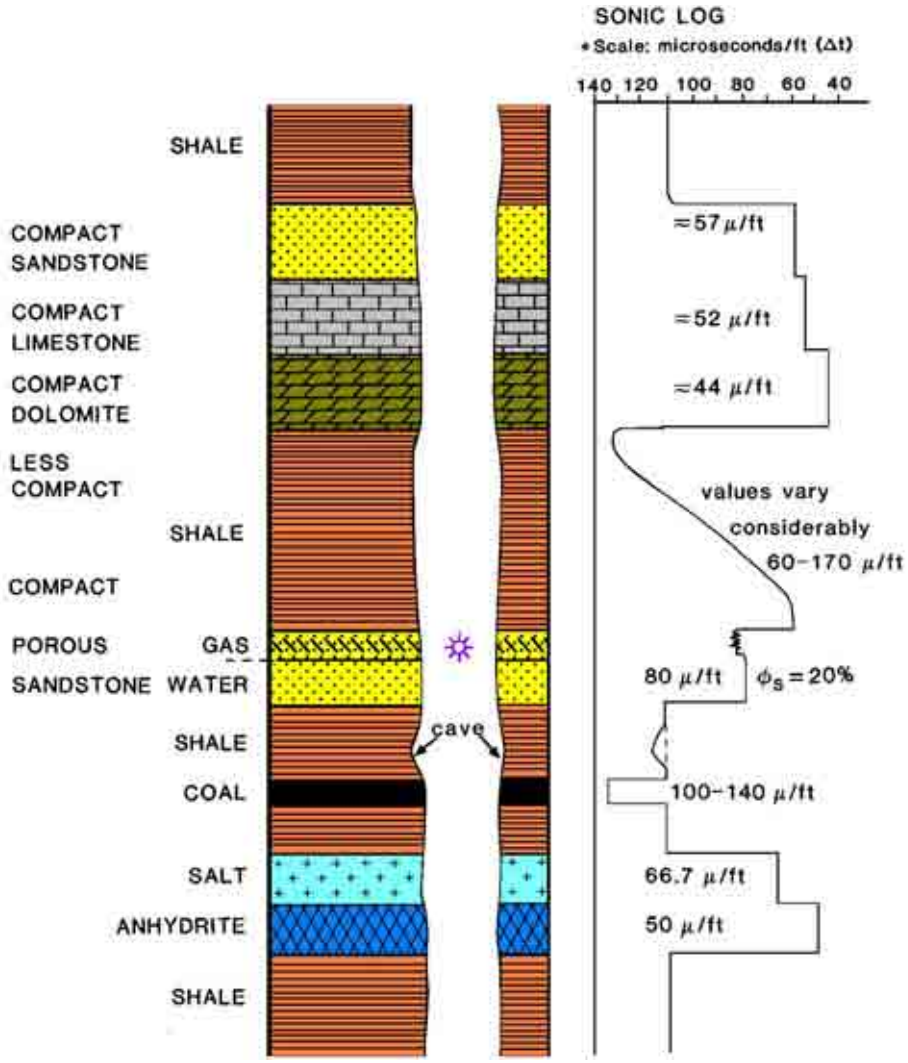

Figure 2.2 – Some typical responses of the sonic log. The sonic log shows a formations ability to transmit sound waves. It is expressed as interval transit time, Δt. ($1\times10^6/\Delta t$) = sonic velocity in ft/sec (after Rider, 1996).

2.2.1: COMPACTION

Compaction is generally expressed by the reduction in porosity with burial depth, or more correctly, as porosity variation with effective stress (Rubey & Hubbert, 1959; Corcoran & Doré, 2005). As sediment becomes compact so its velocity increases because acoustically slow fluid-filled voids are being replaced by faster rock matrix. The effect is most obvious on a reduced scale sonic log where in over-thick shale intervals there is a regular increase in velocity downwards due to compaction (Figure 2.3). In extremely homogenous intervals where ITT is plotted on a logarithmic scale and depth on an arithmetic scale there may be a straight-line relationship which represents a very regular compaction (Hottman & Johnson, 1965). Such regular relationships are especially visible in the Cenozoic sediments in many parts of the world (e.g. Herring, 1973; Magara, 1968; Issler, 1992).

Using general compaction trends it is possible to estimate erosion at unconformities or the relative amount of uplift (Lang, 1978; Magara, 1978; Vorren *et al.* 1991; Hillis, 1995). Compaction is generally accompanied by diagenetic effects which are irreversible (Schmidt, 1973) and stay frozen during uplift. The compaction of a sediment therefore represents its deepest burial. Using the general compaction curve for a particular interval any overcompaction can be explained by uplift. Tracking back to the general curve gives the amount of uplift (Figure 2.4).

Similarly any jumps in compaction as at unconformities or faults when compared to the general well trends can give some idea of the amount of missing section. However it should be stressed that such generalities should only be applied to one stratigraphic interval at a time and then in relatively consistent facies (*cf.* Hillis, 1995).

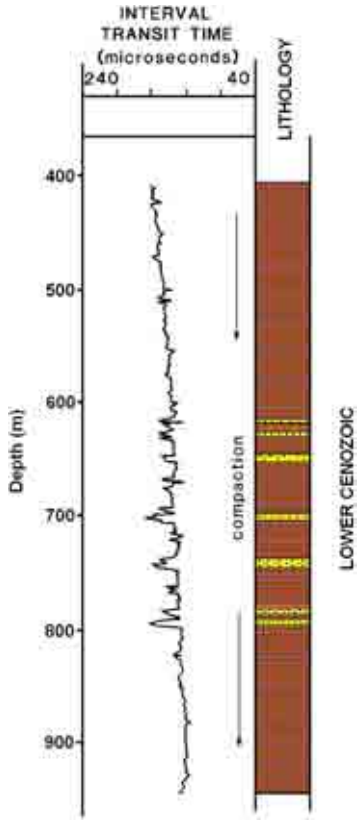

Figure 2.3 – Compaction in a shale sequence shown by a regular decrease in interval transit time with depth. The velocity decreases from approximately 160μs/ft to 140μs/ft over 500m (modified after Rider, 1996).

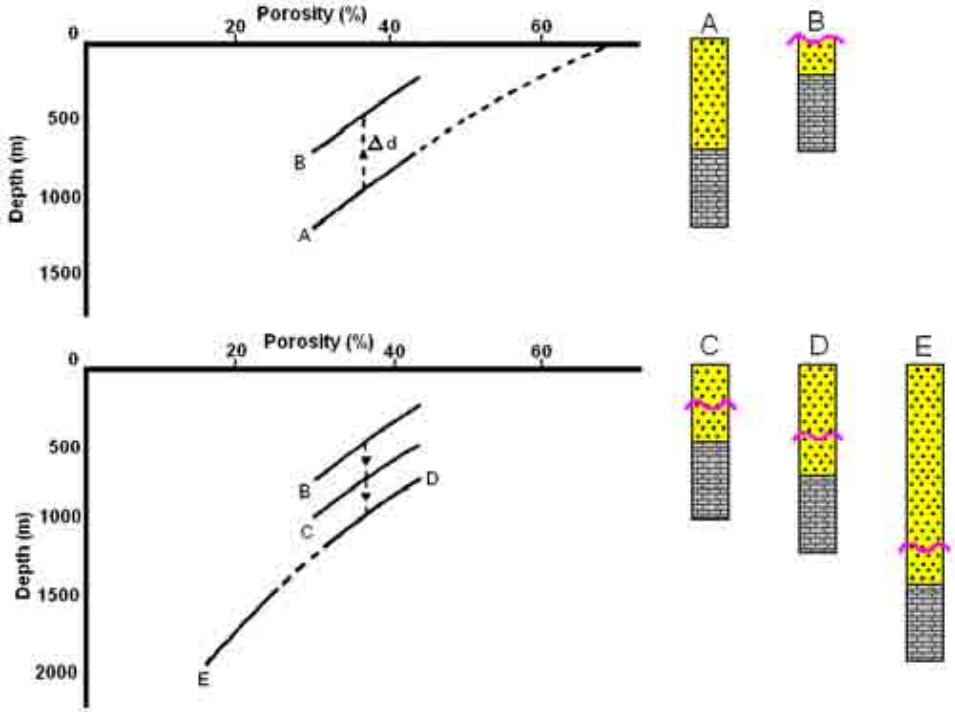

Figure 2.4 – Porosity evolution in a Chalk sequence during burial, (A) subsequent uplift (B), and post-uplift burial (C, D, E). The apparent uplift is the amount of uplift (Δd) not reversed by subsequent subsidence. It can be measured by the displacement along the depth axis of the porosity-depth relation of the uplifted sequence (B or C) from that of a reference or normally compacted sequence (A, D or E) (modified after Hillis, 1991).

Initial porosities of loosely packed (i.e. uncompacted and uncemented) sediments depend on sorting, grain shape, grain size and sedimentation rates and can range from approximately 25-55% for sandstones (Houseknecht, 1987), 50-90% for shales (mudstone, siltstone, clay, argillaceous mud), 40-95% for limestones (44% for grainstones, 55% for packstones (Enos & Sawatsky, 1981)) and 70-95% for deep sea calcareous ooze. The extreme range for carbonate rocks reflects the wide range of grain sizes and shapes of organic debris. The sediment to water contact is often transitional and is not always well defined for example argillaceous sediments can show a gradual upward transition from a sediment with a porosity exceeding 80% to a fluid with a gradually decreasing percentage of particles carried in suspension. Porosity values can vary widely within the uppermost sediments (Haenel, 1979). A definite boundary and therefore a definite initial porosity cannot be defined (Füchtbauer & Müller, 1970; Larsen & Chillingar, 1979; Chilingarian, 1983). However initial porosities are one of several parameters which are required to simulate compaction processes; a value must be defined which is a representative average.

General porosity values for sediments are mostly given as porosity-depth curves for a specific litho-type. These functions are purely empirical since no compaction mechanism links porosity and depth simply, directly and universally (Giles *et al.* 1998). Porosity loss with increasing depth is largely irreversible (Lang, 1978; Serra, 1984; Giles, 1996) with the exception of the creation of enhanced porosity by grain dissolution (Giles & de Boer, 1990) and hence is commonly determined by the maximum burial depth rather than the present day depth. However porosity-depth curves describe only the present condition and do not necessarily indicate the reduction of porosity versus time and/or depth i.e. the compaction history (Chapman, 1981). Decreasing porosities with depth can be a function of overburden thickness, time, lithology, depositional environment, pressure development (including

overpressure), diagenesis and tectonic stress (Chilingarian, 1983). A wide range of porosity-depth trends is possible and Figures 2.5-2.7 show examples of porosity depth trends for the basic lithotypes sand, shale and limestone.

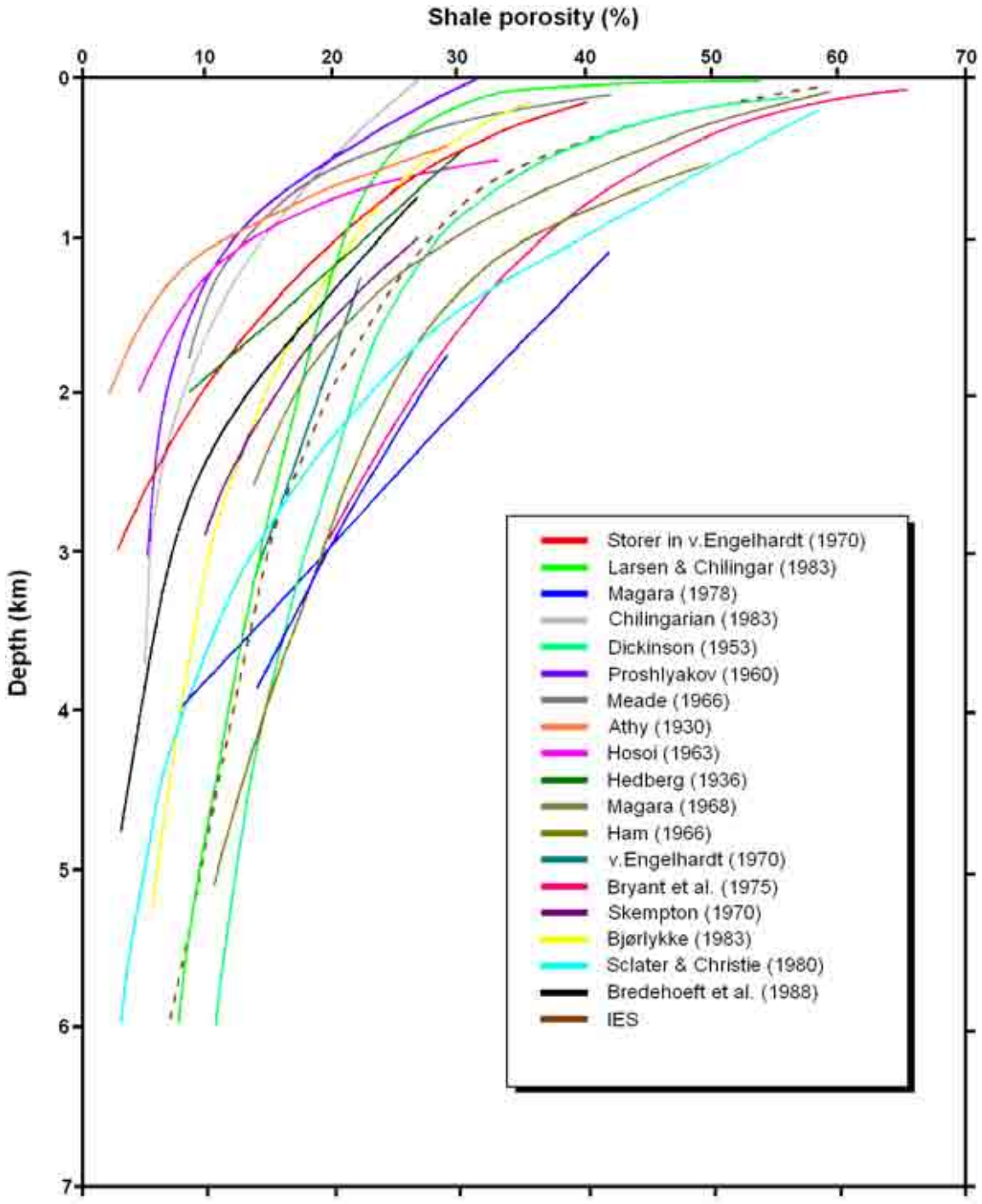

Figure 2.5 – Porosity-depth curves for shales from various published sources (modified after Wygrala, 1989).

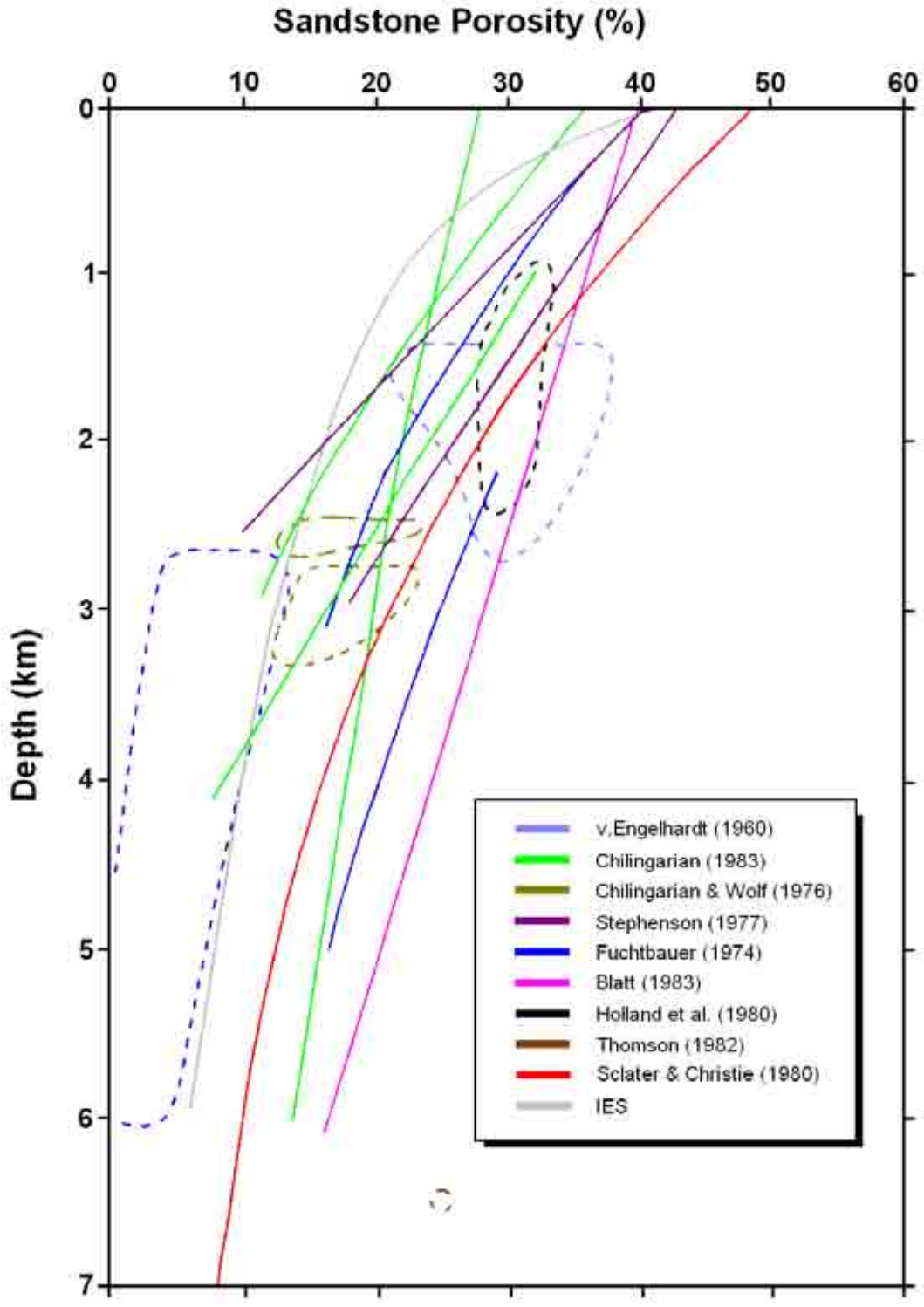

Figure 2.6 - Porosity-depth curves for sandstones from various published sources, dashed lines represent clusters of data points for which no trend line was fitted (modified after Wygrala, 1989).

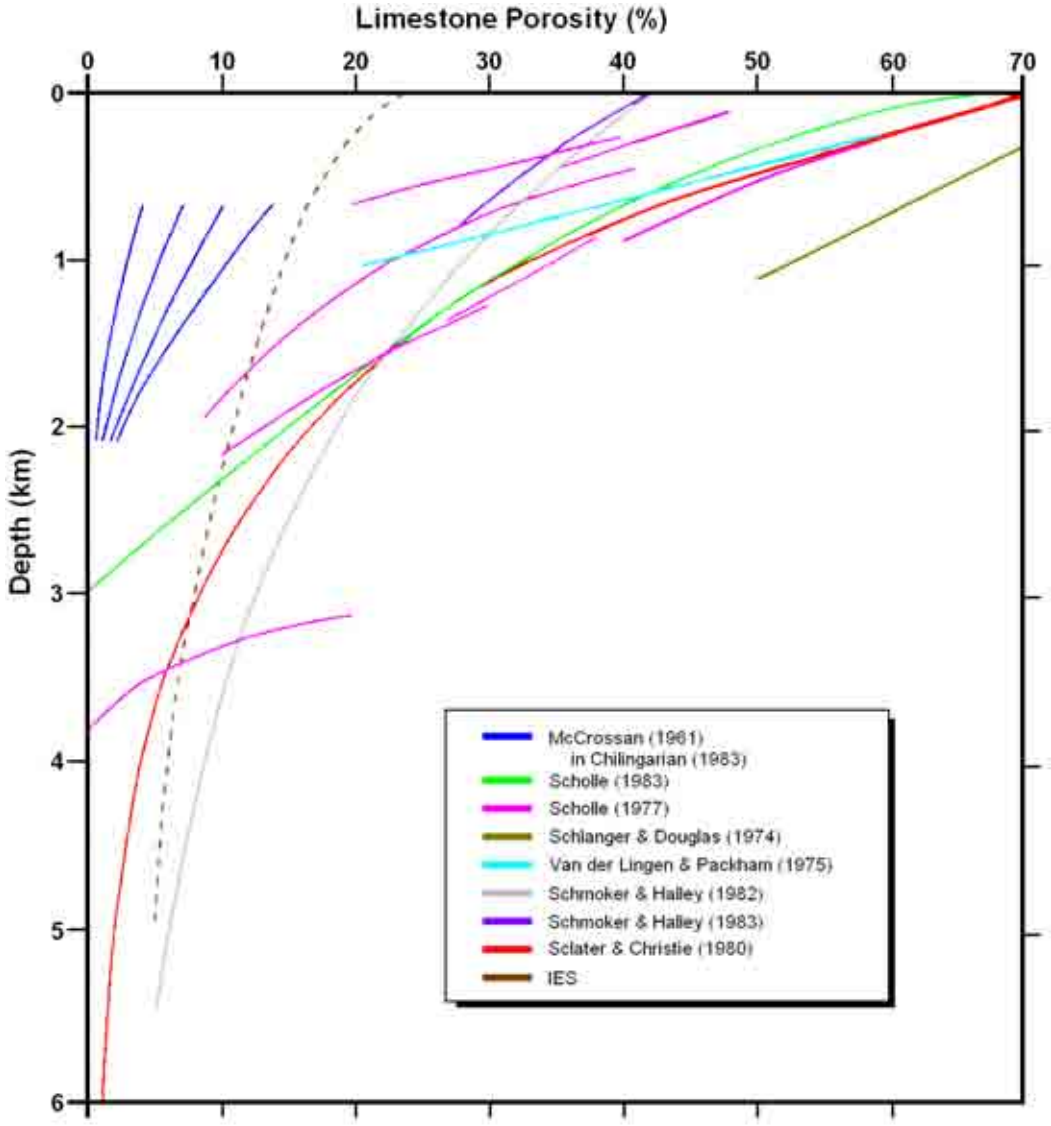

Figure 2.7 - Porosity-depth curves for limestones from various published sources (modified after Wygrala 1989).

A number of porosity-depth functions have been proposed for fitting field data. The simplest of these is a linear decrease in porosity with depth. Linear porosity-depth relationships have been used by Magara (1980) and Selley (1978) to account for diagenetic changes affecting compaction, whilst linear segments were used by Haung & Gradstein (1980) and Falvey & Deighton (1982). However a linear trend implies negative porosities below a certain depth and does not adequately represent the curved trends seen at shallower depths. However many attempts have been made in the past to present average scenario curves, typical of differing

lithologies. Most models recognise the marked differences between high porosity and low porosity sediments, however the ones which are discussed here represent the low porosity models, typically associated with shales and mixed shale/sandy sequences. Shale compaction is the result of physical, chemical and mineralogical phenomena in the subsurface. However it is known that in many parts of the world that the level of shale compaction is governed mainly by the burial depth (or overburden pressure) provided that the fluid pressure is near hydrostatic or the shale is near compaction equilibrium (*cf.* Magara, 1976, 1978).

The observation that porosity decreases more gradually at greater depth, led workers such as Athy (1930) and later other workers (Rubey & Hubbert, 1959; Magara, 1976; Sclater & Christie, 1980) to propose an empirical relationship:

$$\phi = \phi_0 \, exp^{-bz} \tag{2.2}$$

Where Φ is porosity, Φ_0 is the initial (surface) porosity, z is depth and b is the compaction coefficient describing the porosity decrease per unit depth. Sclater & Christie (1980) used this exponential function to fit porosity data from the North Sea. This model and the parameters used by Sclater & Christie have subsequently become the most commonly used. Falvey & Middleton (1981) noted that an exponential porosity-depth relationship does not provide a good fit to the data at high porosities. As an alternative they proposed a function based on the assumption that a differential change in porosity is proportional to the differential change in load:

$$\phi = \frac{\phi_0}{\left(1 = \phi_0 \lambda_{fm} z\right)} \tag{2.3}$$

where λ_{fm} is again a constant of proportionality. This function reproduces the general form of the porosity-depth curve but also predicts that some porosity is maintained down to depths of

10km. A similar approach was taken by Baldwin & Butler (1985) who chose to represent solidity (1-Φ) purely empirically as a power law function of depth. Rubey & Hubbert (1959) consider that Athy's (1930) curve – derived from the Late Carboniferous and Permian shales in northern Oklahoma – is the closest to the compaction-equilibrium conditions (where fluid pressure reaches normal hydrostatic pressure), because of its elapsed time since deposition. High porosity sediments, such as sandstones are worth only a passing mention, because they exhibit compaction curves that are remarkably different. Magara (1980) clearly demonstrates that sandstone porosity-depth relationships are on the whole linear in nature and presents a case for the reduction in sandstone porosity to be controlled primarily by chemical and mineralogical agents rather than mechanical compaction.

2.2.2: CALCULATION OF EXHUMATION MAGNITUDES

Measuring an absolute magnitude of exhumation at a well locality involves two steps (Figure 2.8). The first step involves the derivation of a 'normally buried' porosity versus depth plot for the unexhumed successions in the basin – a reference curve. A reliable porosity-depth trend (reference curve) requires a large number of porosity measurements distributed over a wide depth range, from samples that are at their present maximum burial depth (Giles *et al.* 1998). There are a number of ways in which porosity-depth curves can be generated however they are primarily made from direct porosity measurements on core samples or density measurements from a wireline log (though the sonic log can also be used). The second step involves comparing the calculated curve from the well location with the established reference curve. Stratigraphic units that are shallower than their maximum burial-depth will have anomalously low porosity with respect to present-day burial depth (Corcoran & Doré, 2005). The displacement along the depth axis of the observed porosity with respect to that predicted

from the reference trend will provide an estimate of net or apparent exhumation (E_A) (Figure 2.9).

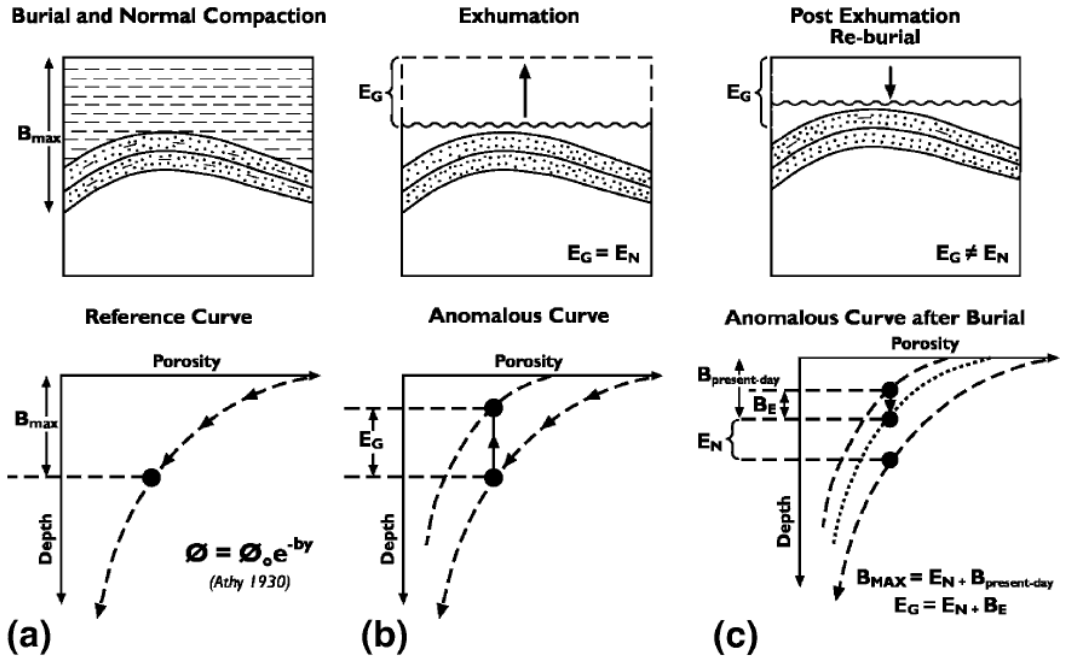

Figure 2.8 – Evolution of porosity vs. depth trends in exhumed sedimentary basins; a) 'normal' compaction (exponential decay of porosity with burial depth, under hydrostatic conditions) in subsiding basin – the reference curve; b) exhumation leads to anomalous porosity vs. depth trend with vertical displacement from the reference curve yielding E_G an estimate of gross exhumation; c) post-exhumation re-burial (B_E) reduces the vertical displacement between the anomalous curve and the reference curve to E_N the net exhumation at a given well location (after Corcoran & Doré, 2005).

As discussed by Menpes & Hillis (1995), there are simple relationships between apparent exhumation (E_A), present-day burial depth (B_P), maximum burial-depth (B_T) and total exhumation (E_T) (Figure 2.4).

Maximum burial depth (B_{max}) can be computed for the section by adding the net exhumation (E_N) to the present-day burial depth ($B_{present\text{-}day}$):

$$B_{max} = E_N + B_{present\text{-}day} \tag{2.4}$$

Net exhumation (E_N) will equal total or gross exhumation (E_G) only in the case where the erosional unconformity is at the seabed or present-day ground level. Where post-exhumational burial (B_E) has occurred, gross exhumation will be given by:

$$E_G = E_N + B_E \tag{2.5}$$

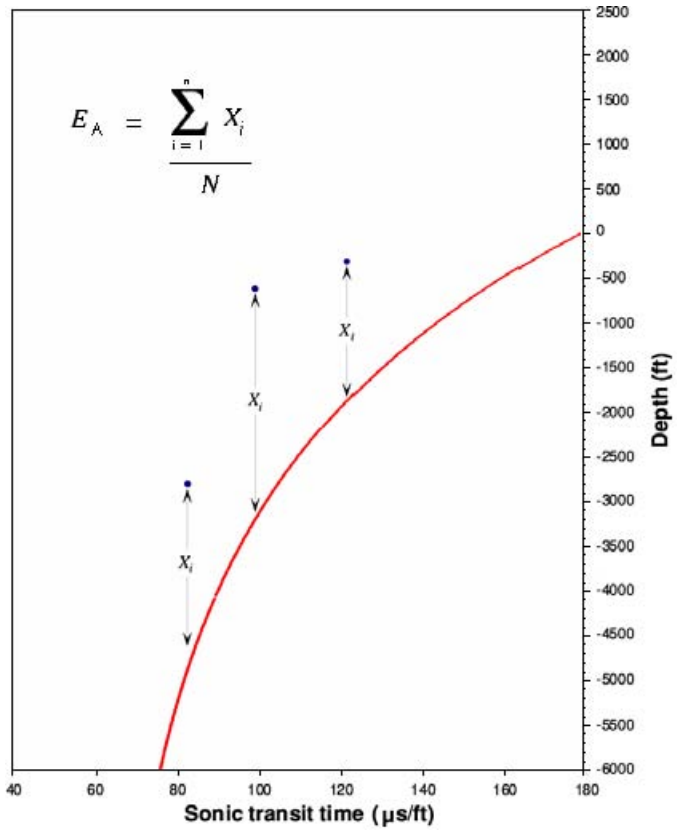

Figure 2.9 – Method used to calculate exhumation from compaction data for a well or borehole. The difference between every data point (i.e. sonic velocity, formation density or porosity measurement) and a specified reference compaction curve will give an individual exhumation estimate. An average of all the individual exhumation estimates gives a statistically derived mean exhumation value for the well or borehole (modified after Ware, 1999).

2.2.3: ESTIMATING POROSITIES FROM SONIC VELOCITY DATA

The importance of calibrating the porosity-depth curve for a given lithology can be illustrated by comparing the range of porosity-depth trend exhibited by sandstones and shales (Figures 2.5 and 2.6) from a variety of settings around the world. Different data sets may exhibit

differences in porosity of 20% at the same depth. A large number of possible causes may explain the differences between curves including differences in composition (Nagtegaal, 1978), age (Maxwell, 1960), geothermal gradient (Galloway, 1974), overpressure (Dickinson, 1953) and initial porosity and packing (Beard & Weyl, 1973; Atkins & McBride, 1992). A variety of transforms have been developed to convert measured ITT to porosity. The most widely used of these transforms are the Wyllie time-average equation (Equation 2.6; Wyllie *et al.* 1956) and the so called Raymer-Hunt-Gardner transform (Equation 2.8; Raymer *et al.* 1980). Equation 2.6 simply states that the transit time measured by the tool is the sum of the time spent in the solid matrix and the time in the fluid. This 'time' is a function of the matrix velocity and constituent's volumes (i.e. wave path lengths Figure 2.10).

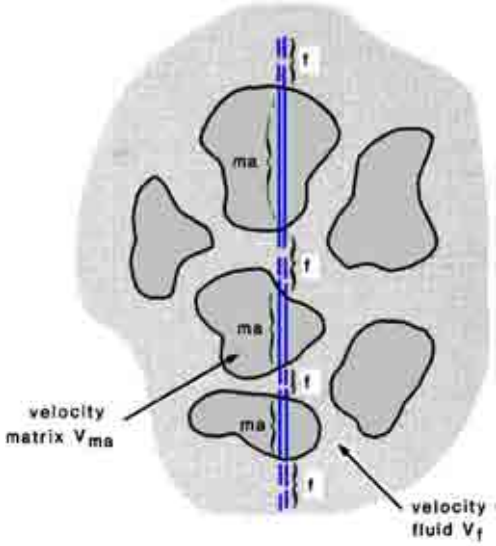

Figure 2.10 – Diagrammatic representation of the path of P-waves through a rock showing the relationship between time spent in the matrix (V_{ma}) and time in the fluid (V_f) giving the basis for the calculation of porosity from sonic velocities (modified after Rider 1996).

Practical application of the Wyllie time average equation:

$$\Delta t = \phi \Delta t_f + (1-\phi)\Delta t_{ma} \qquad (2.6)$$

in shales has led to the need to develop a correction factor to correct apparent porosity to true porosity (Alberty, 1994), since the Wyllie equation was developed for sandstones. The need

for this correction factor has generally been attributed to the effects of compaction or net effective stress. The so-called compaction factor (C_p) is derived through the normalisation of apparent sonic porosity to known porosity typically from core or density porosity. The resulting equation for the estimation of porosity from sonic ITT is:

$$\phi = \frac{\Delta t - \Delta t_{ma}}{\Delta t_f - \Delta t_{ma}} \bullet \frac{1}{C_p} \tag{2.7}$$

This correction has simply evolved as a result of poor match between apparent sonic porosity and independent measures of porosity (Alberty, 1994). Typical values for C_p range from 1.0-1.3 (Raymer *et al.* 1980). The relationship is best translated into graphic form where it becomes obvious that the measured ITT has a linear relationship with porosity (Figure 2.11). The relationship will vary depending on the velocity of the matrix material. Some of the more common matrix velocities are shown in Table 2.4.

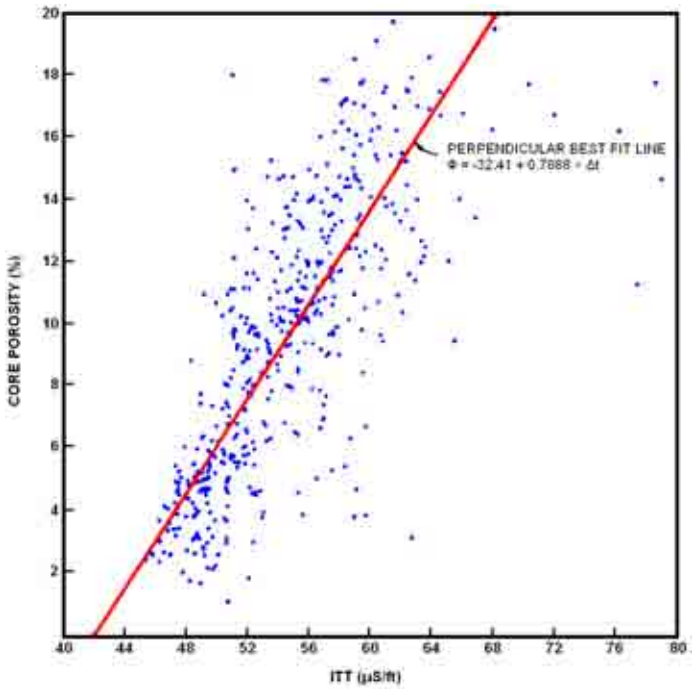

Figure 2.11 – Interval transit time compared to measured porosity in a dolomite (modified from McFadzean, 1973).

	Δt_{ma} (µs/ft)	V (m/s)	V (ft/s)
Sandstones	55.5-51	5490-5950	18000-19500
Quartz	55.1	5530	18150
Limestones	53-47.6	5800-7000	19000-23000
Calcite	46.5	6555	21500
Dolomites	45-38.5	6770-7925	22200-26000
Dolomite	40	7620	25000
Shale	167-62.5	1600-5000	500-16000

Table 2.4 – Some common matrix velocities (from Serra, 1979; Gearheart, 1983; Schlumberger, 1985).

The quantitative derivation of porosity using the time average equation relationship is usually imprecise and modifications are necessary (Raymer *et al.* 1980) although these are often only effective very locally (Brereton & McCann, 1990). Clearly the physical relationship between velocity and porosity is still to be explained. The effect which causes most deviation from the simple law is lack of compaction (i.e. external pressure) when porosities are very high especially in sandstones. However recent work has shown that the failure of the time average equation in fact covers the whole range of sandstones (Brereton & McCann, 1990 and Figure 2.12).

The Raymer-Hunt-Gardner (RHG) transform (Raymer *et al.* 1980) is an empirical fit of independently determined porosity to observed interval transit times. It expresses porosity as a function of measured ITT, matrix ITT and a constant:

$$\phi = C \bullet \frac{\Delta t - \Delta t_{ma}}{\Delta t} \qquad (2.8)$$

Practical use of the RHG-transform in a range of worldwide basins has resulted in a range of constants to normalise apparent porosity to independently determined porosity from cores (Alberty, 1994). Typical values of C vary from 0.625 to 0.700. Note that the transform makes no provision for different brine properties. For both equations the largest source of error is in determining the correct matrix ITT.

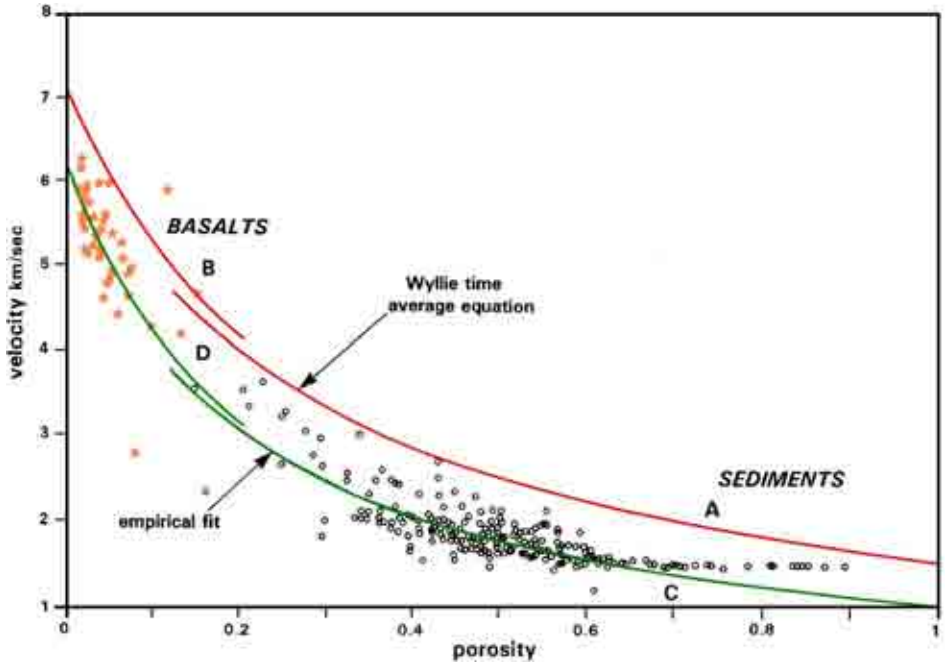

Figure 2.12 – Porosity predictions from the Wyllie time average equation in (A) sediments (calcareous oozes), (B) oceanic basalts. Empirical curve fit for (C) sediments and (D) oceanic basalts. The indication is that the Wyllie equation overestimates porosity across a wide range of values (from Brereton & McCann, 1990).

Wyllie *et al.* (1956, 1958) measured the observed directional velocity in a number of materials (Table 2.5). Wyllie (1956) suggested a matrix velocity of 19500ft/sec (51μs/ft) for sandstone with a pore-water velocity of 4800ft/sec (208μs/ft). Poelchau (1997) and Rider (1996) highlighted a number of typical matrix velocities for common lithologies (Table 2.4) which are consistent with extensive work by Magara (1976, 1978, 1980) whose work with shale sequences all over the world has led to a suggested matrix velocity of 68μs/ft to represent a typical shale and it is based on these authors that the values used in the study were chosen. The value for interstitial fluid was taken to be 188.85μs/ft in all cases (Schlumberger, 1989).

Mineral	Observed directional velocity (ft/sec)		
	X	Y	Z
Anhydrite ($CaSO_4$)	20340	20790	20360
Calcite ($CaCO_3$)	23060	21570	15740
Dolomite ($CaCO_3.MgCO_3$)	14960	-	-
Feldspar ($Na_2O.Al_2O_3.6SiO_2$)	14370	21920	-
K-Feldspar	12150	18760	12460
Gypsum ($CaSO_4.2H_2O$)	18970	17460	21300
Halite	15350	-	-
Mica Schist	500	16650	12860
Quartz	17650	17750	21400
Slate	16230	20600	-

Table 2.5 – Mineral velocities at room temperature and pressure. Quartz and calcite measured on crystal axis (after Wyllie *et al.* 1956).

2.2.4: DENSITY DERIVED POROSITY

The density log provides a continuous record of a formations bulk density. This is the overall density of a rock, which is a function of the density of the minerals forming a rock (i.e. matrix) and the volume of free fluid it encloses (i.e. porosity) (Rider, 1996). A radioactive source in the formation density logging tool emits gamma rays which are scattered and lose energy as a result of collisions with electrons in the formation (Allen & Allen, 2005). The number of scattered rays recorded at a detector on the logging tool depends on the electron density of the formation, which is related to the true bulk density of the formation (Schlumberger, 1989). Bulk density (ρ_b) can be calculated using the following relationship (Schlumberger, 1989):

$$\rho_b = \phi\rho_f + (1-\phi)\rho_{ma} \qquad (2.9)$$

Where ρ_f is the average density of the fluid occupying the pore space (a function of temperature, pressure and salinity) and ρ_{ma} is the average density of the rock matrix. Rearranging this equation enables porosity to be determined:

$$\phi = \frac{(\rho_{ma} - \rho_b)}{(\rho_{ma} - \rho_f)} \tag{2.10}$$

2.2.5: CONTROLS ON VELOCITY-DEPTH TRENDS

A comprehensive review of the primary controls on velocity-depth trends is beyond the scope of this thesis and after many years application in the oil and gas industry the problems are well known. The interested reader is referred to Ware (1999) who provided a detailed and useful review of these controls some of which are summarised below. Hamilton (1976) showed that porosity is the dominant control on velocity within sedimentary rocks; porosity decrease causes bulk modulus to increase and therefore despite the counteracting effect of bulk density increase, velocity to increase. The recognition of this porosity dominance led Wyllie *et al.* (1956) to introduce their empirical porosity/velocity relationship (Equation 2.6). This equation has been used to estimate porosity with relative success during the last fifty years. It does however fail under a variety of conditions:

1. atypical cementation, since it assumes average cementation in which change of frame modulus are implicit in changes of porosity

2. porosities greater than about 0.25 with an error that increases rapidly with further porosity increase

3. non spherical pores (e.g. cracks, joints)

4. anisotropy, which is particularly strong in shales

5. pore fluids other than water (e.g. the slow compressional velocities associated with the presence of gas)

6. pressure dependence of velocity, for both overburden pressures and excess pore pressures

These failures highlight the complexities of porosity changes within the sedimentary column and clearly demonstrate that porosity itself is dependent on further variables.

2.2.5.1: Dewatering, viscosity and critical porosity

The exponential function of shale porosity-depth, proposed by Rubey & Hubbert (1959), may be explained as follows. At the earliest stage of compaction, the shale retains high permeability, so that more pore-fluid can be squeezed from it for a given increase in burial depth (overburden pressure). As a consequence, a faster rate of porosity reduction occurs at shallower depths (Magara, 1980). With progressive depth increase more fluid is expelled from the shale and permeability loss accompanies the reduction in porosity. At deep burial depths, the amount of fluid expulsion is greatly reduced for a given increase in overburden pressure. Thus, in normally pressured rocks, permeability is not a control rather a consequence of compaction. Such changing rates of fluid expulsion can be shown as an exponential function of the form of Athy's (1930) equation however Rubey & Hubbert (1959) use a relationship in which effective stress is the control rather than depth. From work by Low (1976), on the viscosities of water in the clay mineral, Montmorillonite, water viscosity is shown to increase as the porosity decreases or as the compaction process progresses. Magara (1977) cites this as a useful addition to the dewatering story, by further slowing down rate of fluid expulsion, despite the slight reduction in viscosity that accompanies the higher geothermal temperatures at depth. In summary the reduced rate of shale compaction at depth

may be the result of the combined effect of decreasing shale permeabilities and increasing water viscosity. Further to this, there is a critical porosity change that occurs very early on within the burial history of sediment (Figure 2.13). This change is primarily associated with the change from matrix-supported to framework-supported conditions, brought on by increased overburden pressure and is described by Magara (1978).

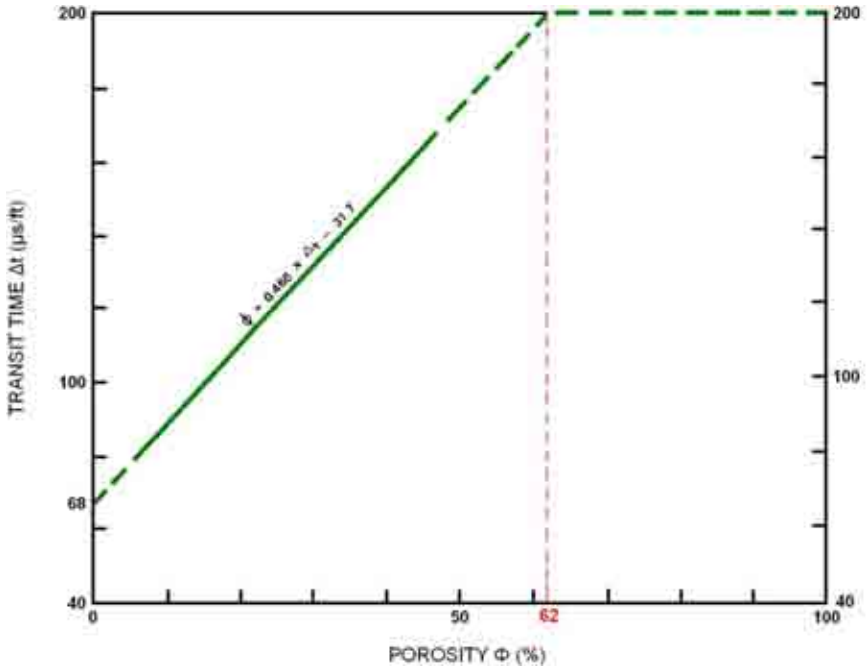

Figure 2.13 – Empirical relationship between porosity and transit time of the shales of Cretaceous age in western Canada (modified after Magara, 1976).

The transit-time for pure water or 100% porosity is about 200μs/ft (Magara, 1978). The addition of small amounts (5-10%) of clay sediment to the water will produce no significant change in transit time, since essentially the sound will travel through the water and not the clay. The transit time will stay at almost the same level until the amount of clay becomes 38% of the total bulk volume (or 62% porosity) – which is referred to as the critical porosity. This critical porosity separates mechanical and acoustic behaviour into two distinct domains (Nur *et al.* 1991; Chen & Nur, 1994; Nur *et al.* 1998). By definition Φ_c is the porosity below which the mineral grains in a sediment become load bearing. At porosities above Φ_c the sediment loses all rigidity and falls apart; the sediment is in suspension and the fluid phase is

load bearing (Japsen *et al.* 2007). The value of Φ_c is determined by the sediment type, grain sorting and angularity at deposition and can vary within the same rock type (Japsen, 2007). The transit time decreases (velocity increases) as the amount of clay content increases (or porosity decreases). This observation for shales is different from that made by Wyllie *et al.* (1956, 1958) for sandstones in which a linear relationship is established for the entire range of sandstone porosity (0-100%). In real life, the porosity of clay of the sea floor is known to be about 70-80% and such critical porosity changes are known to occur at different depths for different sedimentary basins (Magara, 1978). Dickinson (1953), shows that for the Gulf Coast, this is encountered at depths as little as 100ft (relative to the sea bed), whereas for other areas 400ft below sea floor are quoted (Pirmez *et al.* 1997).

2.2.5.2: Lithology and Clay content

The effects of clay content and porosity on compressional velocity have been examined in a variety of core-based studies (Tosaya & Nur, 1982). However Han *et al.* (1986), provide the most comprehensive study of porosity-velocity relationships in shales and sandy shale sequences. They concluded that for low porosity shale and shale/sand sequences even a relatively small clay fraction change (0.02 to 0.04) can lower the elastic moduli and velocity substantially. Marion *et al*. (1992) demonstrate that the influence of clay content on the velocity-porosity relationship becomes clear when looking at the data at a constant value of confining pressure (Figure 2.14). Figure 2.15 shows the logical follow on from this, whereby increased pressures are observed on the velocity-porosity relationship demonstrating expected increases of velocity with a decrease in porosity. The key observation from these two Figures is not so much the relationship trend (i.e. linear or curved), but rather that they converge at a single point, the point where clay volume fraction is equal to sand porosity. Since velocities are primarily governed by shear and bulk moduli of the matrix then in such instances

accepting similar grain packing distributions, velocities may not be much different to those of pure and member compositions. Heasler & Kharitonova (1996) were able to conclude from their exhumation estimates derived from sonic velocities of shales and mixed siltstone/shale/sandstone lithologies that magnitudes of exhumation did not differ significantly. This indicates that under appropriate circumstances, mixed shale/siltstone/sandstone lithologies, providing they contain clay matrices, may not yield significantly different velocities.

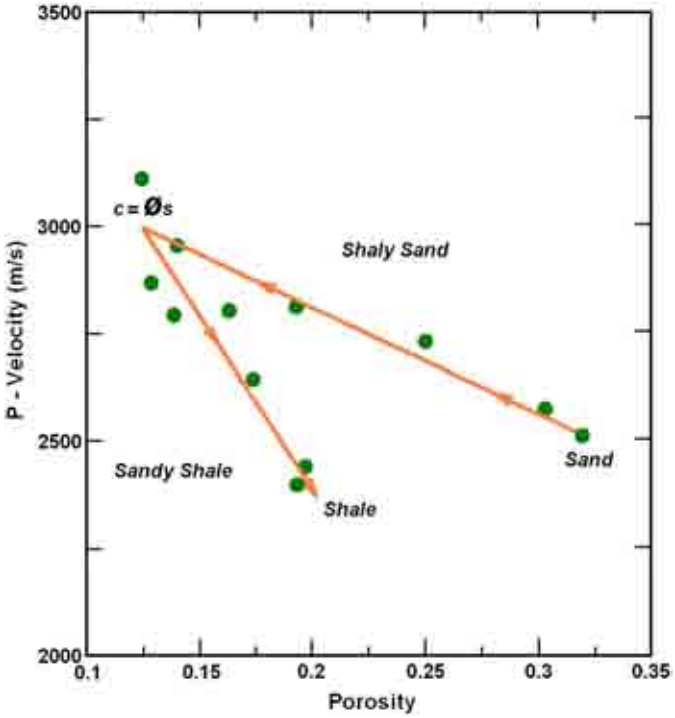

Figure 2.14 – Influence of clay content on the P-wave velocity-porosity relationship at a constant confining pressure (50MPa). Distinct trends for shaly sand and for shale can be observed. The trends intersect when clay content equals sand porosity, whilst the arrows indicate increasing shaliness (from Marion *et al.* 1992).

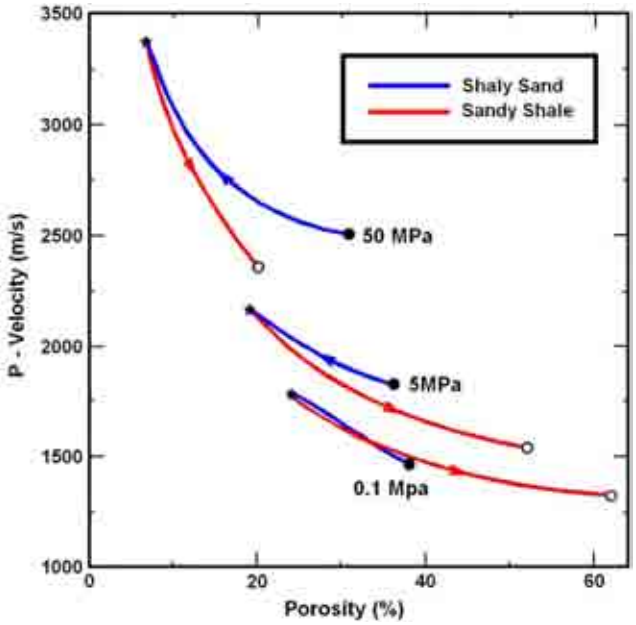

Figure 2.15 – Calculated velocity and porosity using a sand/clay model at various pressures. At each pressure solid lines represent trends for shale and shaly sand. Clean sand and pure shale are represented by a filled circle and an empty circle respectively (from Marion *et al.* 1992).

2.2.5.3: Abnormal Pressure

Overpressures develop when pore fluids cannot be expelled from low-permeability sediments which are exposed to rapid overburden pressure increases due to high sedimentation rates; compaction is retarded and porosities remain higher than normal as the overburden pressure is partially balanced by the increased pore pressures (Chapman, 1981). For elastic moduli the relevant skeletal pressure is the differential or effective pressure; the difference between overburden pressure and pore pressure (Wyllie *et al.* 1958). In the laboratory these terms are expressed as:

$$P_{eff} = P_{conf} - nP_{pf} \qquad (2.11)$$

Where P_{eff} is the effective pressure (differential), P_{conf} the confining pressure (overburden or lithostatic), P_{pf} the pore fluid pressure and where n is a local constant that is generally assumed to be 1 but more recently considered ≤1 (Erickson & Jarrard, 1998*a*). In relatively

permeable sequences, effective pressure increases with depth because lithostatic (overburden) pressure increases at about double the rate of hydrostatic pressure increase. Overpressured zones, therefore exhibit anomalously low velocities because of the decreased effective pressure. Conversely underpressured zones exhibit anomalously high velocities because of the increased effective pressure. A number of causes have been proposed for the generation of abnormal pressures as reviewed by several authors (Powers, 1967; Burst, 1969; Magara, 1976; Meissner, 1978; Osborne & Swarbrick, 1997) and are not repeated here.

2.2.5.4: Rebound, Exhumation and Micro-cracks

Much work in quantifying these effects has been done by Hamilton (1976), who points out that any equation or graph showing percent rebound will need to be constrained at zero rebound (0%) at zero depth. Certainly it has been proved that rebound tends to vary with lithology such that the most rebound is from pelagic clay; for example 6.9% at a depth of 300m, while the least rebound is in siliceous sediments; 1.7% for diatomaceous ooze at a depth of 300m (Hamilton, 1976). Schmertmann (1955), theorised that geologic rebound (removal of overburden due to erosion) if similar plots could be made, would also be parallel to laboratory tests.

Rebound estimates tend to be limited to the first 500m of strata. However data on the rebound of shale indicate that the amount of rebound at depth is significant (Hamilton, 1976). For example two values are estimated from the Bearpaw Shale, a marine clay shale in western Canada. The higher pressure value at about 1.0×10^{-4}kg/m² indicates a rebound of about 7% (from 34% to 41% porosity), whilst the lower pressure value at about 0.5×10^{-4}kg/m² (9.5% rebound) is from 31% to 40.5% (Peterson, 1958). On the whole, most curves of porosity rebound, e.g. Magara (1968); Dickinson (1953); tend to converge around 1200m in depth.

Table 2.6 lists estimated rebound percentages down to 1.3km, which have been calculated and estimated graphically from porosity-depth curves (Hamilton, 1976). It is worth noting that around 0.4 to 0.7km burial depth, the rebound porosities tend to fluctuate which coincides with the change from a semi-lithified to fully-lithified sediment. At this point rebound will no longer increase staying at this instance with a value of around 7%. The effect that this average rebound porosity value will have on exhumation estimates is discussed later.

Density (g/cm^2)	Porosity (%)	Depth (km)	Rebound Porosity (%)	Density gradient ($g/cm^3/m$)
1.53	72.0	0	0	0
1.59	68.2	0.05	0.7	13.0
1.66	64.4	0.10	1.6	13.0
1.72	60.9	0.15	2.4	12.7
1.78	57.4	0.20	3.3	12.5
1.90	50.6	0.30	5.2	12.5
2.00	44.4	0.40	7.0	11.8
2.10	38.9	0.50	8.6	11.3
2.17	34.5	0.60	9.5	10.7
2.20	32.5	0.70	8.5	9.6
2.24	30.5	0.80	7.9	8.9
2.26	29.0	0.90	7.3	8.2
2.29	27.5	1.00	7.2	7.6
2.30	26.5	1.10	7.2	7.1
2.32	25.8	1.20	7.2	6.6
2.32	25.8	1.30	7.2	6.1

Table 2.6 – An example of density –porosity characteristics of a deep sea, terrigenous sediment (from Hamilton, 1976).

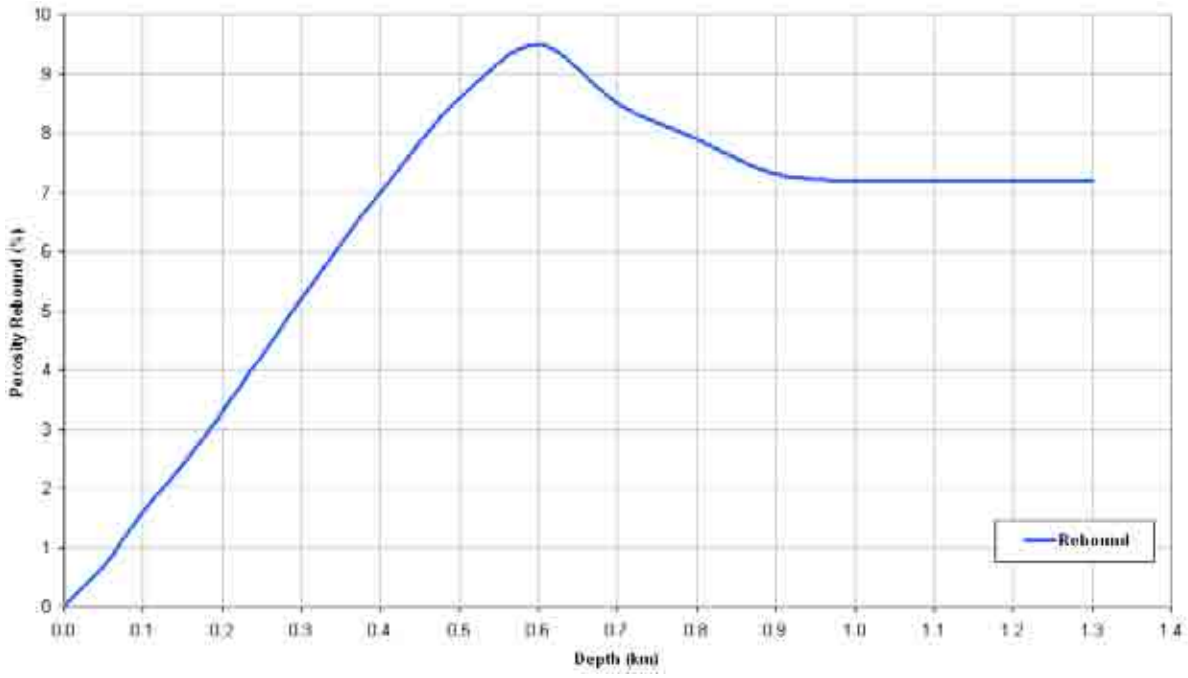

Figure 2.16 – A graph showing porosity rebound versus depth from the values in Table 2.8.

2.2.5.5: Additional controls

In addition to the preceding controls Ware (1999) also identified several additional controls on velocity-porosity relationships. Temperature (Shumway, 1958; Gregory, 1977; Stephenson, 1977; Timur, 1977; Schopper, 1982; Poelchau, 1997), anisotropy (Nur & Simmons, 1969; Tosaya & Nur, 1982; White *et al.* 1983; Erickson & Jarrard, 1998*a*), non-aqueous pore-fluids (Magara, 1976), biogenic components (Sheriff & Geldart, 1995; Figure 2.17), sedimentary facies (Erickson & Jarrard, 1998*b*) and continental glaciation (Figure 2.18) all play a minor role in affecting the trend. For the purposes of this thesis these effects have been considered minor components to the overall result and as a result have been ignored, however rigorous analysis of the data should consider these effects in the event of further, more detailed work.

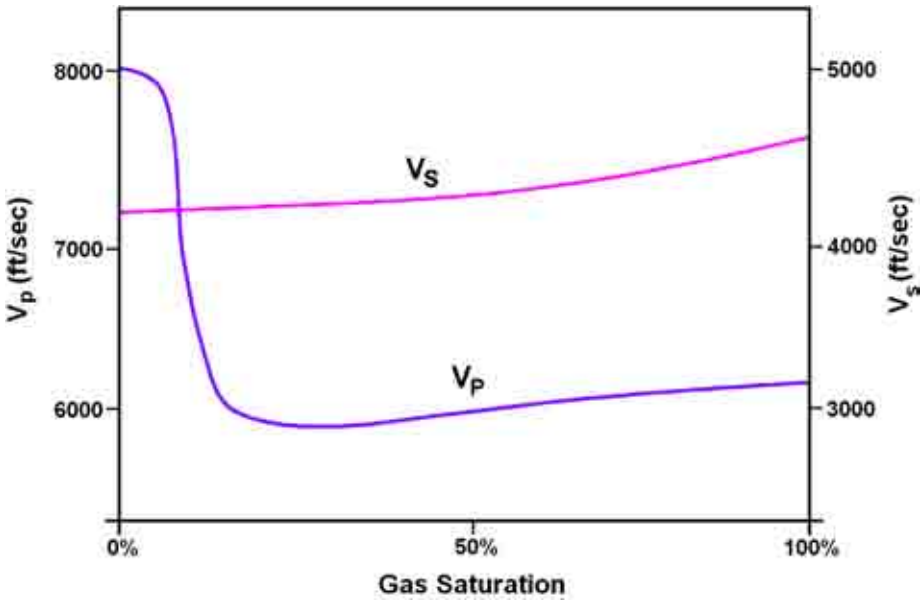

Figure 2.17 – Diagram showing the effects of gas saturation on the P-wave velocity of a rock. As a small amount of gas changes the compressibility (the bulk modulus) of the rock, the P-wave velocity will fall, whereas the shear-wave velocity will increase slightly as density drops (after Sheriff & Geldart, 1995).

Figure 2,18 – The maximum extent of the two major Pliestocene glaciations in the British terrestrial record. 1. The Anglian (*ca.* 450kya MIS12); 2. The Devensian (*ca.* 20kya MIS2) If the ice sheet had been added to the sedimentary column as part of the continuous loading history then its weight certainly would have contributed to additional compaction. If however the ice sheet developed after uplift and erosion shale compaction would be unchanged because the shales already had been overcompacted with reference to their depth of burial at that time. In this area the latter is believed to be the case as the maximum extent of the Pleistocene glaciation event barely reached the coast of Devon and also occurred sometime after Basin Inversion in the Oligocene-Miocene. The fact that the density of ice (0.9g/cc is significantly lower than that of average sediments (approximately 2.3g/cc) must also be remembered. In conclusion for the purposes of this research the effect of ice on compaction is believed to be insignificant and is ignored here (from http:///www.iceage.org.uk uncredited author).

2.2.6: LIMITATIONS OF COMPACTION STUDIES

Although compaction studies benefit from plentiful data and reduced susceptibility to transient thermal anomalies (Doré *et al.* 2002*a*; Corcoran & Doré, 2005), there are a number of important problems and sources of uncertainty associated with compaction based techniques:

1. Mavko *et al.* (1998) showed that the relationship between compressional velocity (sonic) and porosity depends critically on lithology. This means that the underlying assumption of the Wyllie time average equation is invalid in many cases. This was highlighted by Raymer *et al.* (1980) who suggest that the equation is only valid for consolidated sandstones over a limited porosity range of 25-30%.

2. Stratigraphic units must exhibit a consistent relationship between depth and compaction if they are to be of use in exhumation analysis (Corcoran & Doré, 2005). The absence of a consistent relationship suggests that the compaction trend is obscured by the 'data noise' of lithological variation, diagenetic imprint and other factors (Corcoran & Doré, 2005).

3. Compaction studies should preferably be conducted using fine-grained lithologies (i.e. shales rather than sandstones), as the porosities of fine grained rocks are less affected by diagenesis, are less likely to act as aquifers and are generally more uniform in terms of grain size and mineralogy (Japsen *et al.* 2002).

4. Unreliability in establishing the baseline compaction trend (reference curve) for a basin or rock unit is a key limitation, particularly in basins where pervasive regional exhumation has occurred (Corcoran & Doré, 2005). Existing methodologies which utilise statistical manipulation to establish a reference curve lack support from

physical models and in some cases assume that a heterolithic sedimentary sequence can be described by a single average compaction coefficient (Corcoran & Doré, 2005).

5. Removal of the overburden load may lead to poroelastic rebound (pore dilation and microfracturing) partially reversing the compaction process and leading to erroneous exhumation estimates (Japsen, 2000).

6. In basins which contain mobile salt layers care must be taken to separate the effects on the sonic velocity trends of halokinetically induced exhumation which is not relevant to the pre-salt stratigraphic units (Archard *et al.* 1998).

7. In sedimentary basins where successions are overpressured (defined simply as pore fluid pressures greater than would be calculated from a hydrostatic gradient (*c.* 10MPa/km)) the pore fluid reduces the effective stress on framework grains and thus retards compaction, resulting in anomalously high porosities (Corcoran & Doré, 2002; Turner & Williams, 2004; Allen & Allen, 2005).

8. During uplift, horizontal stress increases and drives significant porosity reduction (Turner & Williams, 2004). If exhumation has been primarily driven by compressional deformation (i.e. tectonic inversion), then it is likely that a fraction of the observed compaction can be attributed to a shortening-induced porosity reduction (Ware & Turner, 2002).

9. Whereas most compaction studies assume that mechanical compaction is the dominant control upon porosity reduction with increasing depth, above temperatures of around 80°C, for mudstones and shales and 100°C, for sandstones, thermochemical compaction (i.e. thermally controlled chemical diagenetic processes such as

cementation) exerts the primary control on sediment compaction (Bjørlykke & Høeg, 1997).

2.3: ESTIMATING EXHUMATION USING PALAEOTHERMAL DATA

Thermal history based techniques provide information about the movement of rocks relative to a thermal frame of reference by utilising the general principle that sedimentary rocks are heated as they are buried and cool as they are exhumed (Corcoran & Doré, 2005). A peak temperature profile derived from AFTA, VR (or indeed any other palaeothermal indicator such as fluid inclusion data) in a vertical succession of rocks can be used to extrapolate a palaeogeothermal gradient for that succession (at peak palaeotemperature exposure) and by extrapolation to an assumed palaeosurface temperature, the magnitude of exhumation at that location (Figure 2.19) (Corcoran & Doré, 2005). AFTA also provides a direct estimate of the timing of exhumation (cooling from maximum palaeotemperature (Green *et al.* 2002)) but in some cases, stratigraphic relationships can also be used to constrain timing (Evans & Clayton, 1998; Corcoran & Clayton, 1999). Furthermore, the style of the peak palaeotemperature profile may allow selection of appropriate profiles for exhumation analysis by identifying successions that have been heated by conductive, rather than advective processes (Bray *et al.* 1992; Duddy *et al.* 1994).

2.3.1: APATITE FISSION TRACK ANALYSIS (AFTA)

Apatite Fission Track Analysis (AFTA) is a relatively new method of thermal history analysis, applicable both to sediments and basement rocks, which provides a direct estimate of the time at which a rock began to cool from its maximum palaeotemperature as well as providing an estimate of maximum palaeotemperature. In many situations this knowledge is critical to the understanding of the timing of oil generation and migration in relation to trap

formation. Detrital apatite grains are incorporated into sedimentary rocks from three dominant sources – crystalline basement rocks, older sediments and contemporaneous volcanism. Apatites derived from the first two sources will, in general, contain fission tracks when they are deposited, with AFTA parameters characteristic of the source regions. However, apatites derived from contemporaneous volcanism, or from rapidly uplifted basement will contain no tracks when they are deposited. The kinetic response of the apatite fission track system is well understood having been extensively studied and calibrated in laboratory conditions (Green *et al.* 1986; Laslett *et al.* 1987; Duddy *et al.* 1988) and verified by testing against geological constraints (Green *et al.* 1989*a*, 1989*b*). The principles involved in the application of the technique have been described for example by Green (1989), Miller & Duddy (1989) and Kamp & Green (1991).

2.3.1.1: Basic Principles of Apatite Fission Track Analysis

Fission tracks are trails of radiation damage which are produced within apatite grains at a more or less constant rate through geological time as a result of the spontaneous fission of Uranium-238 impurity atoms. These damage zones form when the charged nuclear particles travel through insulating solids, leaving trails of disrupted atoms (Figure 2.20). Minerals such as apatite [$Ca_5(PO_4)_3(F,Cl,OH)$], zircon ($ZrSiO_4$) and sphene [$CaTiO(SiO_4)$] contain sufficient concentrations (c. 1-1000ppm) of uranium to produce a detectable amount of fission events. The number of fission events which occur within an apatite grain during a fixed time interval depends on the magnitude of the time interval and the uranium content of the grain. Each fission event leads to the formation of a single fission track, which forms with an initial length of ~16μm and a standard deviation of ~1μm (in the case of apatite, tracks in zircon are generally shorter c. 11-12μm) (Miller & Duddy, 1989). The widths of latent (i.e. unetched) fission-tracks, which can be observed with a transmission electron microscope, are only

between 3-14nm (Paul & Fitzgerald, 1992). Optical observation and measurement of tracks requires chemical etching which can enlarge the track to a width of c. 1µm, with nitric acid (5M HNO_3) the preferred etchant of most laboratories (Barbarand *et al.* 2003*a*).

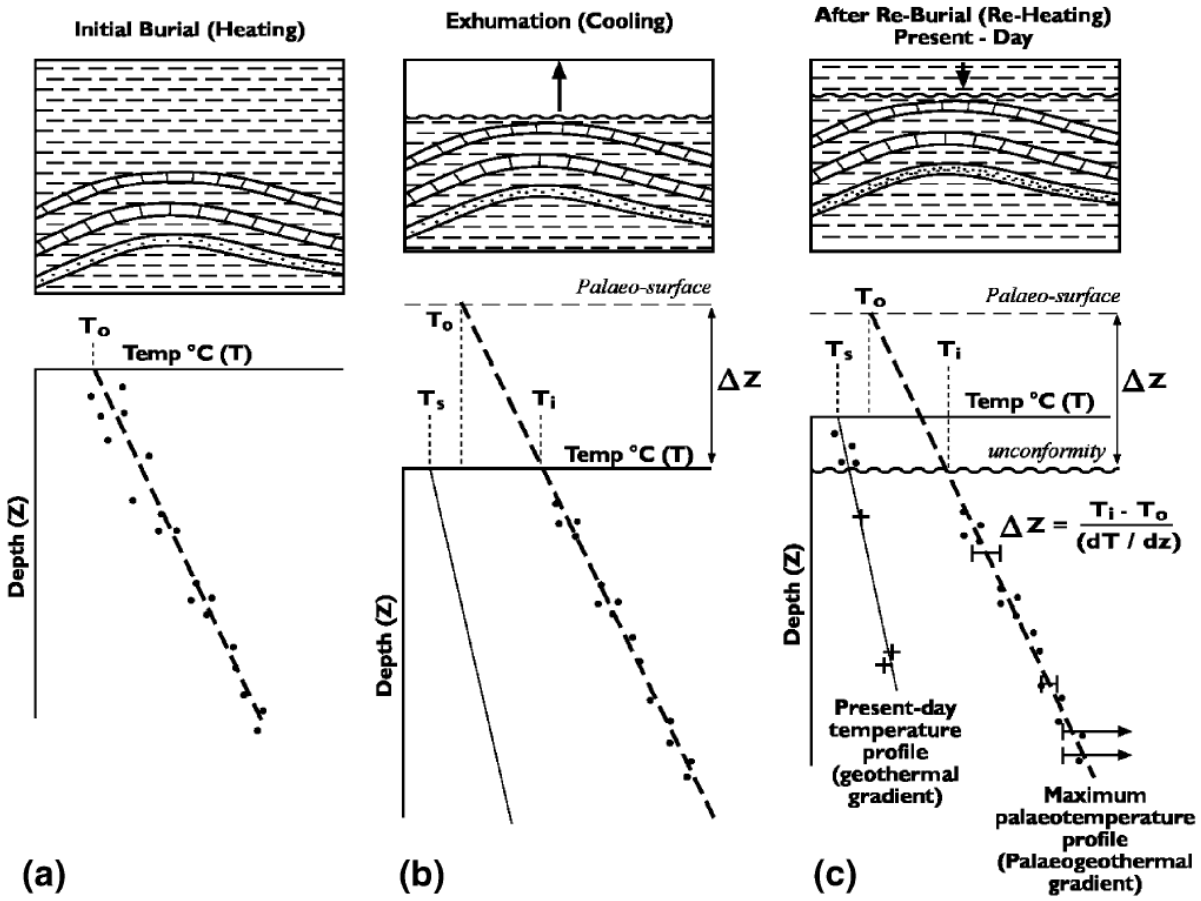

Figure 2.19 – Thermal history based techniques rely on the general principle that rocks are heated as they are buried but cool as they are exhumed. (a) Initial burial and heating recorded and 'locked-in' by thermal indicators followed by (b) exhumation and cooling of rocks which facilitates (c) determination of peak palaeotemperature vs. depth profile from VR and AFTA of a vertical sequence of sample data from the wellbore. Present-day temperature profile is established from corrected BHT measurements. By comparing the palaeogeothermal gradient with the present-day geothermal gradient it can be deduced if the preserved section has been hotter in the past and interpretations can be made with respect to the cause of the high palaeotemperatures and the subsequent cooling to present-day temperatures. Under certain conditions the peak palaeotemperatures (prior to exhumation) can be used to establish a palaeogeothermal gradient and by extrapolation to an assumed palaeosurface temperature can yield an estimate of exhumation (ΔZ) at unconformity. T_i = palaeotemperature intercept at unconformity; T_0 = palaeosurface temperature; T_s = present-day surface temperature; $(\delta T/\delta Z)$ = palaeogeothermal gradient. Magnitude of removed section (*gross exhumation*) is given by $\Delta Z = (T_i - T_0)/(\delta T/\delta Z)$. (after Corcoran & Doré, 2005).

2.3.1.2: Fission-track dating

Fission-tracks can be used to date minerals, although unlike other isotopic dating methods, the daughter product is the radiation damage rather than another isotope. The method relies upon the constant relative abundance of $^{235}U/^{238}U$ and since fission-track density is proportional to the amount of tracks, amount of Uranium and elapsed geological time it is possible to compute a fission track age for the apatite grain. There are a number of ways of determining this ratio but for practical purposes the Population Method (PM) and External Detector Method (EDM) are used almost exclusively. The EDM (Figure 2.21) involves attaching a low-uranium muscovite mica sheet to a polished and etched apatite surface. The sample is then irradiated with low-energy thermal neutrons, which induces fission in ^{235}U. After irradiation, the mica sheet is removed and etched to reveal the induced tracks, the density of which is proportional to the concentration of uranium in the apatite grain (Andriesen, 1995).

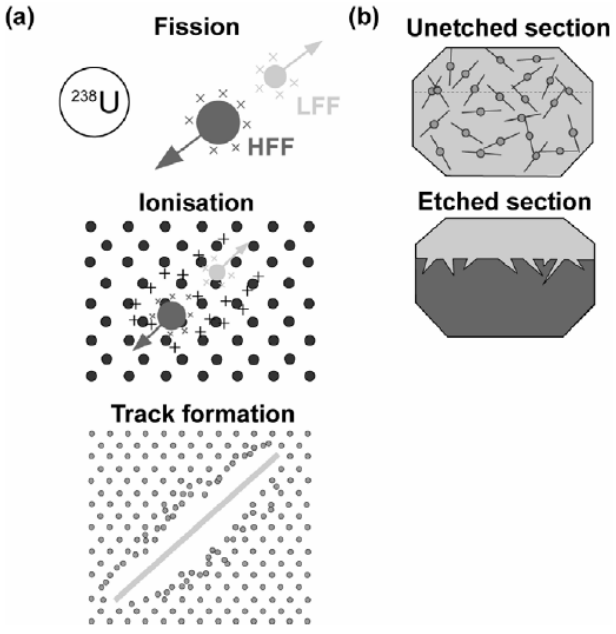

Figure 2.20 – The formation of fission-tracks in a uranium bearing mineral. (a) Spontaneous fission of ^{238}U produces two highly charged heavy particles of different masses, which recoil as a result of Coulomb repulsion and interact with other atoms within the crystal lattice by electron stripping or ionisation. This results in further deformation of the lattice as the ionised lattice atoms repel each other. As the fission particles capture electrons they slow down and begin to interact by atomic collisions, which further reduce the particles' energy until they come to rest, leaving a radiation damage trail or 'fission-track'. (b) These cannot be optically observed until the mineral has been treated with a chemical etchant (modified after Gallagher *et al.* 1998).

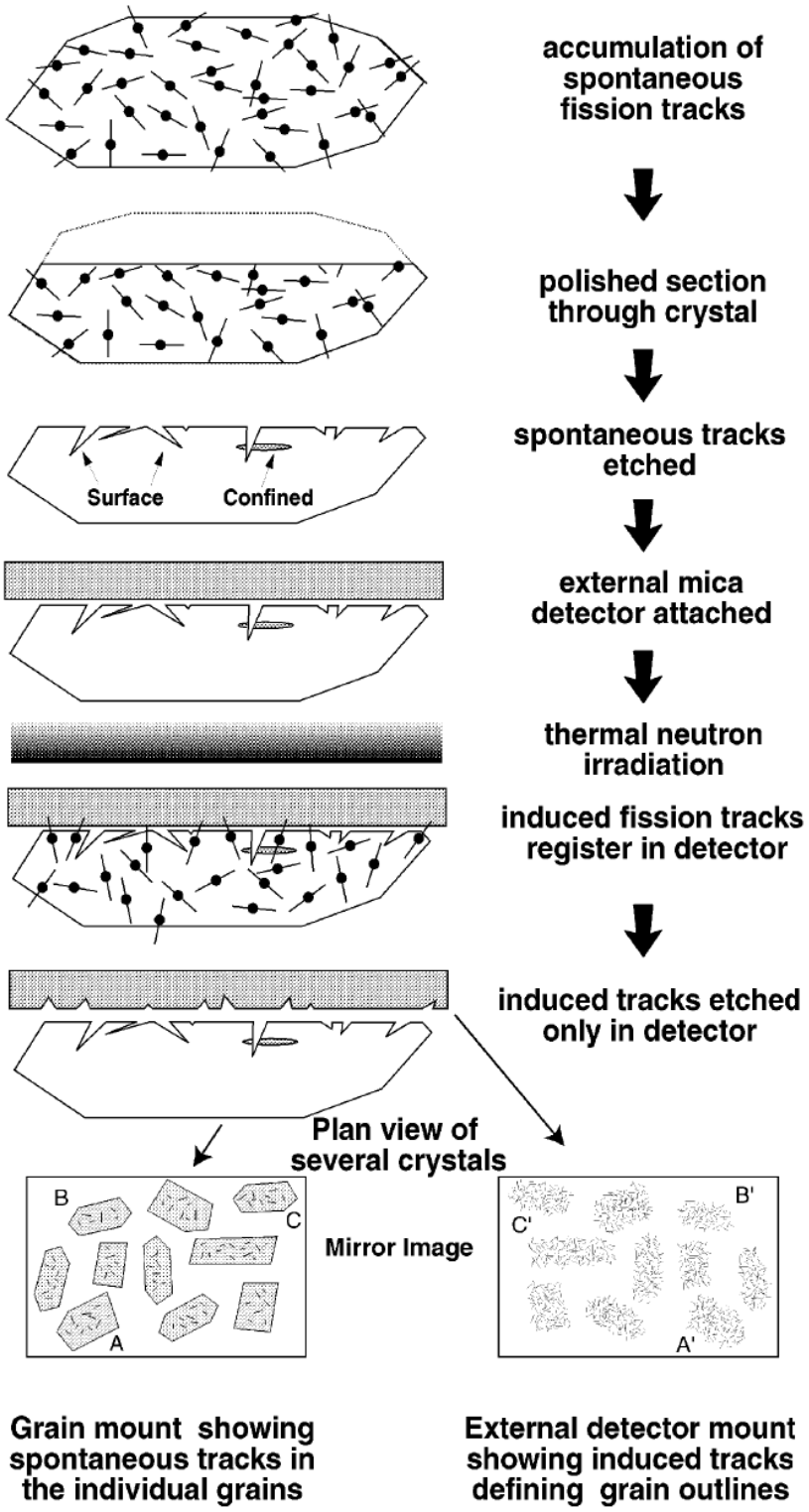

Figure 2.21 – Sequential diagram showing the application of the external detector method (Hurford & Green, 1983) in order to determine the fission-track age of a mineral. The surface of a mineral is polished and etched in order to reveal surface and confined spontaneous fission-tracks. The next stage involves attaching a uranium-free detector (usually muscovite mica) to the etched surface. The sample is then sent to a nuclear reactor where it is irradiated with low-energy neutrons which induce fission in the 235U. During fission, some heavy particles cross the interface between the mineral and the mica. Following this procedure, the mica is etched to reveal the induced tracks. By counting the number of induced tracks in the mica we estimate the concentration of the daughter product (after Gallagher *et al.* 1998).

The precise procedures for calculating a fission-track age of a sample are detailed in Hurford & Green (1982, 1983) and are not repeated here. A recent advance in determining fission-track ages has been the use of Laser Ablation-Inductively Coupled Plasma-Mass Spectrometry (LA-ICP-MS) (Hasebe *et al.* 2004). However, this approach has the considerable drawback of causing irreparable damage to the apatite sample, which often precludes further analyses.

Fission-track ages are normally reported as either a pooled age, which is a combined estimate of the age of the population where all grains are consistent with a single population, or the central age, which is an estimate of the modal age in a sample containing a distribution of age populations (Gailbraith, 1990). There is usually a spread in the ages determined for a number of apatite grains from a certain population, due to natural variations in the distribution and decay of uranium (Gailbraith, 1981; Green, 1981). Grains will also yield different ages if they are derived from different sources. It is therefore important to determine whether a group of apatite grains was derived from a single population (i.e. representing a single thermal history) or from a mixture of different sources (and therefore thermal histories). The χ^2 statistical test is used for this purpose (Gailbraith, 1981). This test determines the probability that all single grain ages belong to a single population. Less than 5% probability indicates a significant spread in single grain apparent ages (outside that allowed by the Poissonian variation in number of fission events) and is referred to as the central age (Gailbraith & Laslett, 1993). For values of χ^2 >5%, the pooled age is used, which is simply the sum of the spontaneous counts divided by the sum of the induced counts.

2.3.1.2.1: The significance of track age

A fission-track age is the time over which the spontaneous tracks in a sample would have taken to accumulate if they all had the same type of track length distribution as those of 'age standard' samples (Green, 2001). For apatite's, age standard samples come from volcanics or high level intrusives with independently known ages and which have experienced very simple geological histories involving rapid cooling to temperatures <50°C (e.g. Durango apatite, Fish Canyon Tuff (Green, 2001)). Generally this is not the case and thus the fission-track age usually has very little direct time significance, rather it provides a combined measure of both the time over which tracks have been retained and the degree of length reduction which has affected the tracks. It should be interpreted in combination with track length data in order to obtain information about the thermal history of a sample (Green, 2001).

2.3.1.3: Quantitative understanding of Fission-Track Annealing in Apatite

In sedimentary rocks which have not been subjected to temperatures greater than ~50°C since deposition, spontaneous fission tracks have a characteristic distribution of confined track lengths. In such samples by measuring the spontaneous track density and the Uranium content of a collection of apatite grains a "fission track age" can be calculated which will be equal to the time over which tracks have been accumulating. The technique is calibrated against other isotopic systems using age standards which also have this type of length distribution. In samples which have been subjected to temperatures greater than 50°C after deposition, fission tracks are shortened because of the gradual repair of the radiation damage which constitutes the unetched tracks. In effect, the tracks shrink from each end in a process which is known as fission track annealing. The final length of each individual track is essentially determined by the maximum temperature which that track has experienced. A time difference of an order of magnitude produces a change in fission track parameters which

is equivalent to a temperature change of only ~10°C, so temperature is by far the dominant factor in determining the final fission track parameters (Fleischer *et al.* 1965).

2.3.1.3.1: Annealing Kinetics and modelling the development of AFTA parameters

The understanding of the behaviour of fission tracks in apatite during geological thermal histories is based on study of the response of fission-tracks to elevated temperatures in the laboratory (Fleischer *et al.* 1965; Green *et al.* 1986; Laslett *et al.* 1987; Duddy *et al.* 1988; Green *et al.* 1989*b*), in geological situations (Green *et al.* 1989*a*), observations of the lengths of spontaneous tracks in apatites from a wide variety of geological environments (Gleadow *et al.* 1986) and the relationship between track length reduction and reduction in fission track age observed in controlled laboratory experiments (Green, 1988).

These studies resulted in the capability to simulate the development of AFTA parameters resulting from geological thermal histories for an apatite of average composition (Durango apatite - ~0.43wt% Cl). Full details of this modelling procedure have been explained in Green *et al.* (1989b). The following discussion presents a brief explanation of this approach.

Geological thermal histories involving temperatures varying through time are broken down into a series of isothermal steps. The progressive shortening of track length through sequential intervals is calculated using the extrapolated predictions of an empirical kinetic model fitted to laboratory annealing data. Contributions from tracks generated throughout the history (remembering that new tracks are continuously generated through time as new fissions occur) are summed to produce the final distribution of track lengths expected to result from the input history. In summing these components, care is taken to allow for various biases which affect revelation of confined tracks (Laslett *et al.* 1982). The final track length reduction of each component of tracks is converted to a contribution of fission track age using

the relationship between track length and density reduction determined by Green (1988). These age contributions are summed to generate the final predicted fission track age.

This approach depends critically on the assumption that extrapolation of the laboratory-based kinetic model to geological timescales, over many orders of magnitude in time, is valid. This was assessed critically by Green *et al.* (1989*b*), who showed that predictions from this approach agree well with observed AFTA parameters in apatites of the appropriate composition in samples from a series of reference wells in the Otway Basin of south-east Australia (Gleadow & Duddy, 1981; Gleadow *et al.* 1983; Green *et al.* 1989*a*). This point is illustrated in Figure 2.22. Green *et al*. (1989*b*), also quantitatively assessed the errors associated with extrapolation of the Laslett *et al.* (1987) model from laboratory to geological timescales (i.e. precision as opposed to accuracy). Typical levels of precision are ~0.5µm for mean lengths <10µm and ~0.3µm for lengths >10µm. These figures are equivalent to an uncertainty in estimates of maximum palaeotemperature derived using this approach of ±10°C. Precision is largely independent of thermal history for any reasonable geological history. Accuracy of prediction from this model is limited principally by the effect of apatite composition on annealing kinetics as explained in the next section.

2.3.1.3.2: Compositional effects

Natural apatite's essentially have the composition $Ca_5(PO_4)_3(F,OH,Cl)$. Most common detrital and accessory apatite's are predominantly Fluor-apatite's, but may contain appreciable amounts of Chlorine. The amount of Chlorine in the apatite lattice exerts a subtle compositional control on the degree of annealing, with apatites richer in Fluorine being more easily annealed than those richer in Chlorine. The result of this effect is that in a single sample, individual apatite grains may show a spread in the degree of annealing (i.e. length reduction and fission track age reduction). This effect becomes most pronounced in the

temperature range 90-120°C (assuming a heating timescale of ~10Ma) and can be useful in identifying samples exposed to palaeotemperatures in this range. At temperatures below ~80°C the difference in annealing sensitivity is less marked and compositional effects can largely be ignored.

The original quantitative understanding of the kinetics of fission track annealing, as described above, relates to a single apatite (Durango apatite) with ~0.43wt% Cl, on which most of the original experimental studies (Green *et al.* 1986; Gleadow *et al.* 1987; Duddy *et al.* 1989) were carried out. Recently this quantitative understanding has been extended to apatites with Chlorine contents up to ~3wt%. This new, multi-compositional kinetic model is based both on new laboratory annealing studies on a range of apatites with different Fluorine-Chlorine compositions (Figure 2.23) and on observations of geological annealing in apatite's from a series of samples from exploration wells in which the section is currently at maximum temperature since deposition. Details of the multi-compositional model are contained in a Technical Note available from Geotrack in Melbourne.

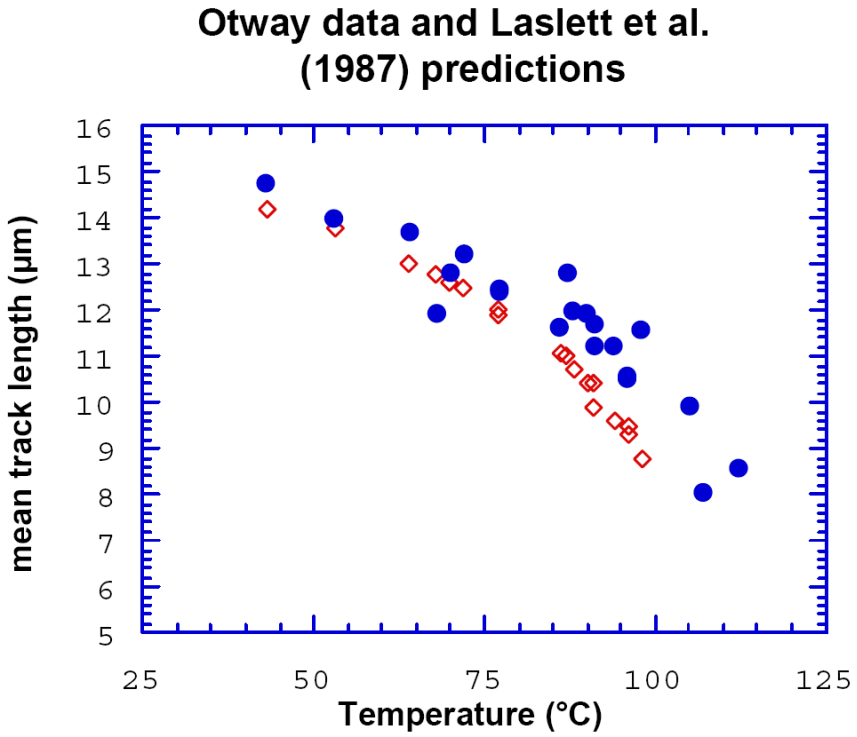

Figure 2.22a – Comparison of mean track length (solid circles) measured in samples from four Otway Basin reference wells (from Green *et al.* 1989a) and predicted mean track lengths (open diamonds) from the kinetic model of fission track annealing from Laslett *et al.* (1987). The predictions underestimate the measured values, but they refer to an apatite composition that is more easily annealed than the majority of the apatites in these samples, so this is expected.

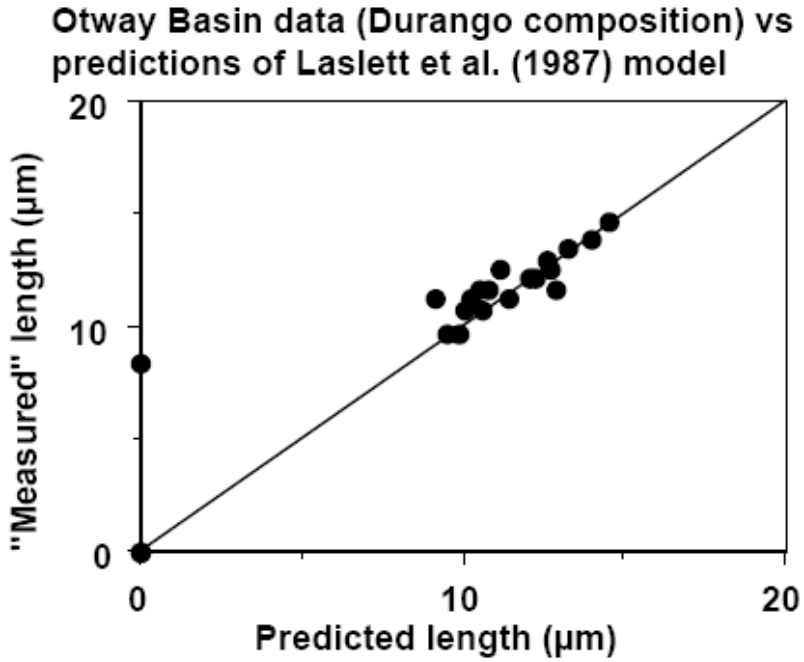

Figure 2.22b – Comparison of mean track length in apatite's of the same Chlorine content as Durango apatite from the Otway Group samples illustrated in Figure 2.25a with values predicted for apatite of the same composition by the model of Laslett *et al.* (1987). The agreement is clearly very good except possibly at lengths below ~10um.

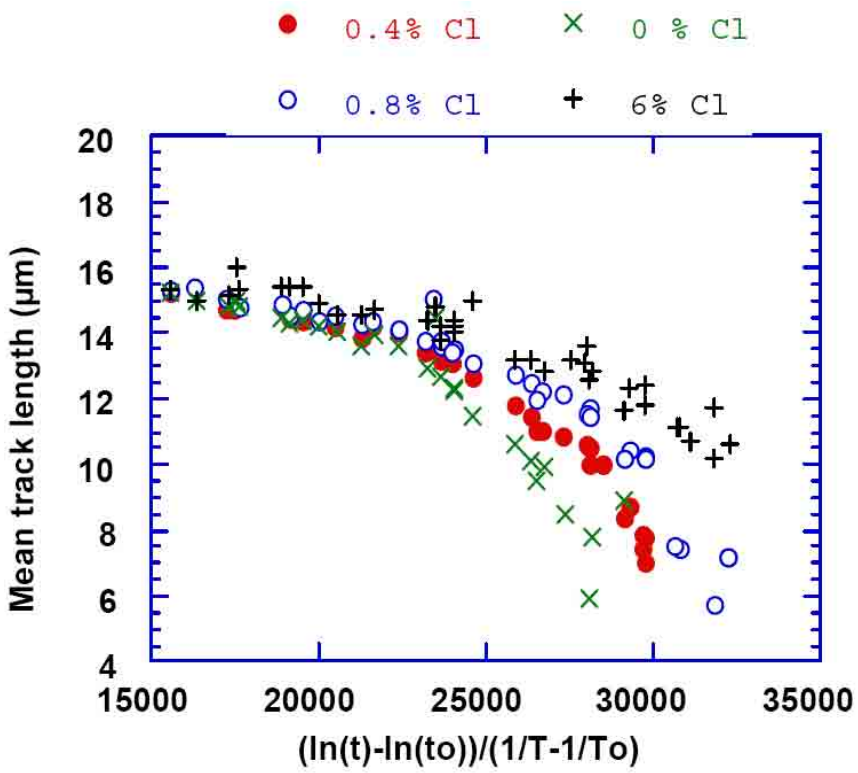

Figure 2.23 – Mean track length in apatite's with four different Chlorine contents as a combined function of temperature and time to reduce the data to a single scale. Fluor-apatite's are more easily annealed than chlor-apatite's and the annealing kinetics show a progressive change with increasing Cl content

The multi-compositional model allows prediction of AFTA parameters for any Chlorine content between 0 and 3wt% using a similar approach to that used in the original single composition modelling as outline above. The range of Chlorine contents from 0 to 3wt% spans the range of compositions commonly encountered as discussed in the next section.

Predictions of the new multi-compositional model are in good agreement with the geological constraints on annealing rates provided by the Otway Basin reference wells as shown in Figure 2.24. However note that the AFTA data from these Otway Basin wells were among those used in construction of the new model, so this should not be viewed as independent verification but rather as a demonstration of the overall consistency of the model.

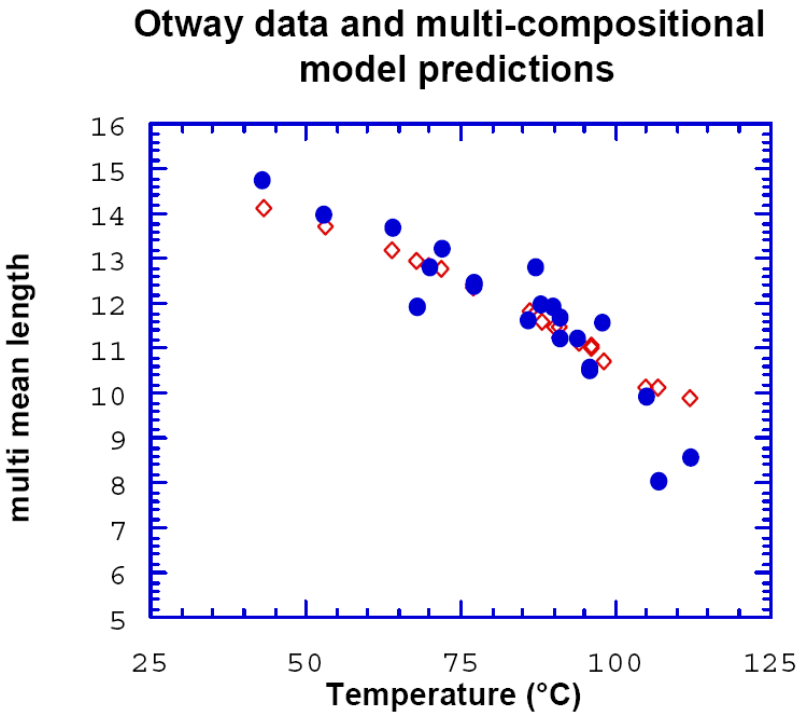

Figure 2.24 – Comparison of measured mean track length (solid circles) in samples from four Otway Basin reference wells (from Green et al. 1989a) and predicted mean track lengths (open diamonds) from the new multi-compositional kinetic model of fission track annealing described in section 2.3.1.3.2. This model takes into account the spread of Cl contents in apatite's from the Otway Group samples and the influence of Cl content on annealing rate. The agreement is clearly very good over the range of the data.

2.3.1.3.3: Distributions of Chlorine content in common AFTA samples

Figure 2.25a shows a histogram of Chlorine contents measured by electron microprobe in apatite grains from more than 100 samples of various types. Most grains have Cl contents less than ~0.5wt%Cl. The majority of grains with Cl contents greater than this come from volcanic sources and basic intrusives and contain up to ~2wt% Cl. Figure 2.25b shows the distribution of Cl contents measured in randomly selected apatite grains from 61 samples of 'typical' quartzo-feldspathic sandstone. This distribution is similar to that in Figure 2.25a except for a more rapid fall-off as Cl content increases. Apatites from most common sandstones give distributions of Cl content which are very similar to that in Figure 2.25b. Volcanogenic sandstones typically contain apatites with higher Cl contents with a much flatter distribution for Cl contents up to ~1.5wt% falling to zero at ~2.5-3wt% as shown in Figure 2.25c. Cl contents in granitic basement samples and high-level intrusives are typically

much more dominated by compositions close to end-member Fluor-apatite although many exceptions occur to this general rule.

2.3.1.3.4: Effects from other elements

Although, in terms of composition, Cl content is recognised as the dominant, major, first-order control on annealing rate (Hurford *et al.* 2005), Barbarand *et al.* (2003b), have investigated the effects of apatite composition on annealing in a suite of 13 apatite samples of different composition and crystalline structure. While Cl was found to have a dominant control on apatite structure, and thereby annealing rate above c. 0.35wt%, below this value other elements particularly Rare Earth Elements (REE), were claimed to exert an appreciable control on annealing rates. A similar experimental study of the annealing kinetics of 15 different apatite species carried out by Carlson *et al.* (1999) also identified the potential significance, albeit secondary, of elements other than Cl (such as Sr and Mn) in controlling annealing sensitivity.

It has been suggested by some workers that the apatite solubility, represented by the arithmetic mean etch-pit diameter parallel to the crystallographic c-axis (signified by the parameter D par) (e.g. Donelick, 1991; Carlson *et al.* 1999; Donelick *et al.* 1999) can be used as a proxy for the bulk chemical composition of an apatite sample. Indeed Ketcham *et al.* (1999, 2000), have developed an annealing model for apatite which attempts to account for the variation in annealing behaviour that exists between different apatite's as a result of compositional variations, as indicated by the D par parameter. However Green *et al.* (2002) have claimed that the performance of this model in geological conditions has yet to be rigorously demonstrated. Furthermore, in a discussion on the dataset provided by Barbarand *et al.* (2003b), Green *et al.* (2005), have claimed that Cl content provides a far more reliable method of describing the annealing sensitivity of a particular apatite species than etch-pit size.

Whereas it has been clearly demonstrated that samples which show significant variation in fission-track ages correlating very closely with Cl content over a range of compositions (e.g. Crowhurst *et al.* 2002), the data presented by Barbarand *et al.* (2003b), often show a wide range of etch-pit sizes for different apatite samples of the same composition (particularly at low (<0.1wt%) Cl contents) (Figure 2 in Green *et al.* 2005).

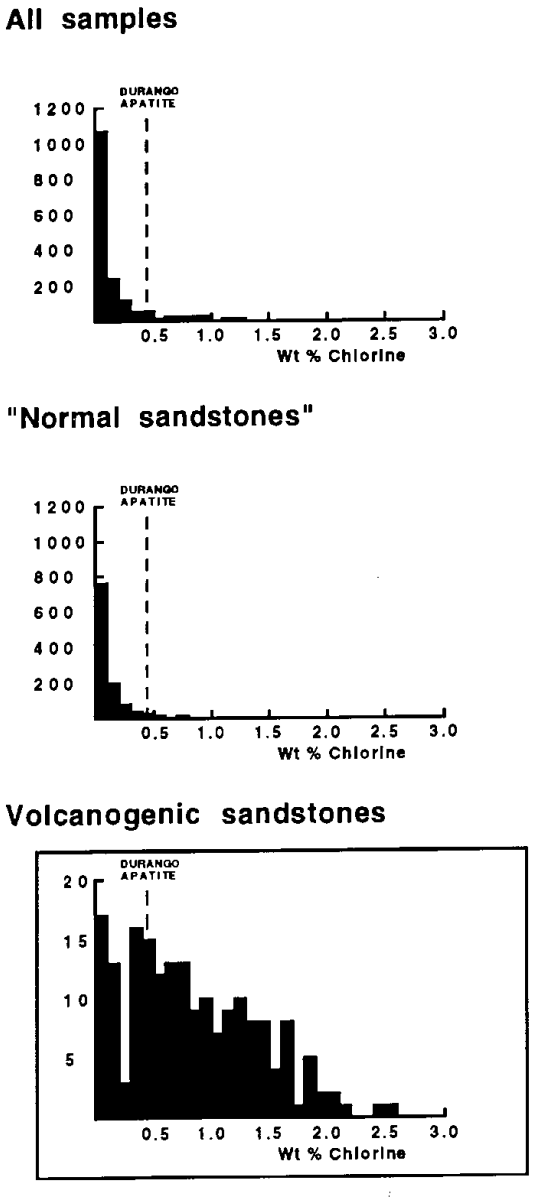

Figure 2.25 – a) Histogram of Cl contents (wt%) in over 1750 apatite grains from over 100 samples of various sedimentary and igneous rocks. Most samples give Cl contents below ~0.5wt%, while those apatites giving higher Cl contents are characteristic of volcanogenic sandstones and basic igneous sources. b) Histogram of Cl contents (wt%) in 1168 apatite grains from 61 samples which can loosely be characterised as 'normal sandstone'. The distribution is similar to that in a, except for a lower number of grains with Cl contents greater than ~1%. c) Histogram of Cl contents (wt%) in 188 apatite grains from 15 samples of volcanogenic sandstone. The distribution is much flatter than the other two with a much higher proportion of Cl-rich grains.

2.3.1.3.5: Pressure effects

Although the early experimental studies into the stability of fission-tracks in various minerals indicated that any effects of pressure upon annealing over geological timescales were insignificant in comparison to the effects of temperature (e.g. Fleischer *et al.* 1965; Naeser & Faul, 1969), the results of more recent experimental work on the pressure dependence of fission-track annealing by Wendt *et al.* (2002), have led these workers to suggest that fission-tracks in apatite are stable under conditions of hydrostatic pressure, but that the stability field of fission-tracks in apatite increases towards temperatures higher than 110°C depending on the absolute pressure. These results, if valid, have potentially far-reaching implications given that the accepted statistical models for fission-track annealing in apatite (e.g. Laslett *et al.* 1987) do not account for the influence of pressure. However Kohn *et al.* (2003) have discounted the results and conclusions of Wendt *et al.* (2002), on a number of grounds. Firstly, they question several fundamental aspects of the experimental design and execution employed by Wendt *et al.* (2002). Secondly, the results of Wendt *et al.* (2002) appear to be inconsistent with actual data from deep boreholes in regions characterised by relatively low geothermal gradients, where any effect due to pressure should be maximised. For example, apatite samples taken from depths of *c.* 7.06-7.66km from the very deep (*c.* 12.25km) SG-3 borehole on the Kola Peninsula in the Baltic Shield (geothermal gradient *c.* 18°C/km), where the present –day temperature is *c.* 122°C show fission-track ages which are reduced to zero. This indicates that any pressure effect on annealing in this environment (in this case approaching ~200MPa) can only be minor. Thirdly Wendt *et al.* (2002), make no attempt to extrapolate the results of their experiments to geologically relevant heating times and temperatures, which is generally considered to be the fundamental test that all annealing models must pass to ensure their reliability (e.g. Green *et al.* 1989). Finally, if any pressure dependence does exist, then annealing models which have been calibrated using actual

geological data from boreholes such as the Green *et al.* (1996), 'multi-compositional' annealing model should implicitly incorporate any effects of pressure dependence.

2.3.1.3.6: Alternative kinetic models

Recently both Carlson (1990) and Crowley *et al.* (1991) have published alternative kinetic models for fission track annealing in apatite. Carlson's model is based on laboratory data for Durango apatite (Green *et al.* 1986) and other (unpublished) data. In the abstract, Carlson claims that because his model is "based on explicit physical mechanisms, extrapolations of annealing rates to the lower temperatures and longer timescales required for the interpretation of natural fission track length distributions can be made with greater confidence than is the case for purely empirical relationships fitted to the experimental annealing data". As explained in detail by Green *et al.* (1993), all aspects of Carlson's model are in fact purely empirical and his model is inherently no 'better' for the interpretation of data than any other. In fact detailed inspection shows that Carlson's model does not fit the laboratory data set at all well (Figure 2.26). Therefore this model is not recommended for the interpretation of AFTA data.

The approach taken by Crowley *et al.* (1991) is very similar to that taken by Laslett *et al.* (1987). They have fitted models to new annealing data in two apatites of different composition; one close to end member Fluor-apatite (B-5) and one having a relatively high Sr content (113855). The model developed by Crowley *et al.* (1991) from their own annealing data for the B-5 apatite gives predictions in geological conditions which are consistently higher than the measured values as shown in Figure 2.27. Corrigan (1992) reported a similar observation in volcanogenic apatite's in samples from a series of West Texas wells.

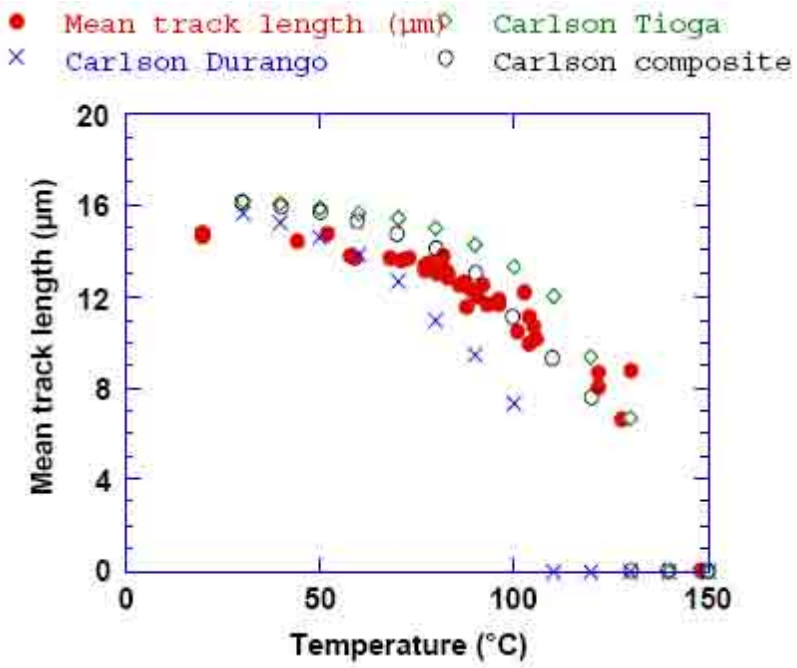

Figure 2.26 – Comparison of predictions of Carlson's models with data from a similar situation to the Otway Basin wells, from South Texas (Corrigan, 1993). The predictions of the composite model are closest to the data, although this seems to be fortuitous, as the two models for mono-compositional apatite fall well above and below the data.

Since the B-5 apatite is close to end-member Fluor-apatite, while the Otway Group apatite's contain apatite's with Chlorine contents from zero up to 3wt% (and the West Texas apatite's have up to 1wt%), the Fluor-apatite's should have mean lengths rather less than the measured values, which should represent a mean over the range of Chlorine contents present. Therefore the predictions of the Crowley *et al.* (1995), B-5 model appear consistently high. This is attributed to the rather restricted temperature-time conditions covered by the experiments of Crowley *et al.* (1991), with annealing times between 1 and 1000 hours in contrast to times between 20 minutes and 500 days in the experiments of Green *et al.* (1986). In addition few of the measured length values in the Crowley *et al.* (1991) study fall below 11µm (in only 5 out of 60 runs in which lengths were measured in apatite B-5) and their model is particularly poorly defined in this region. Crowley *et al.* (1991) also fitted a new model to the annealing data for Durango apatite published by Green *et al.* (1986). Predictions of their fit to the data are not very much different to those from the Laslett *et al.* (1987), model. The differences are

not important however as the multi-compositional model has rendered the single compositional model obsolete.

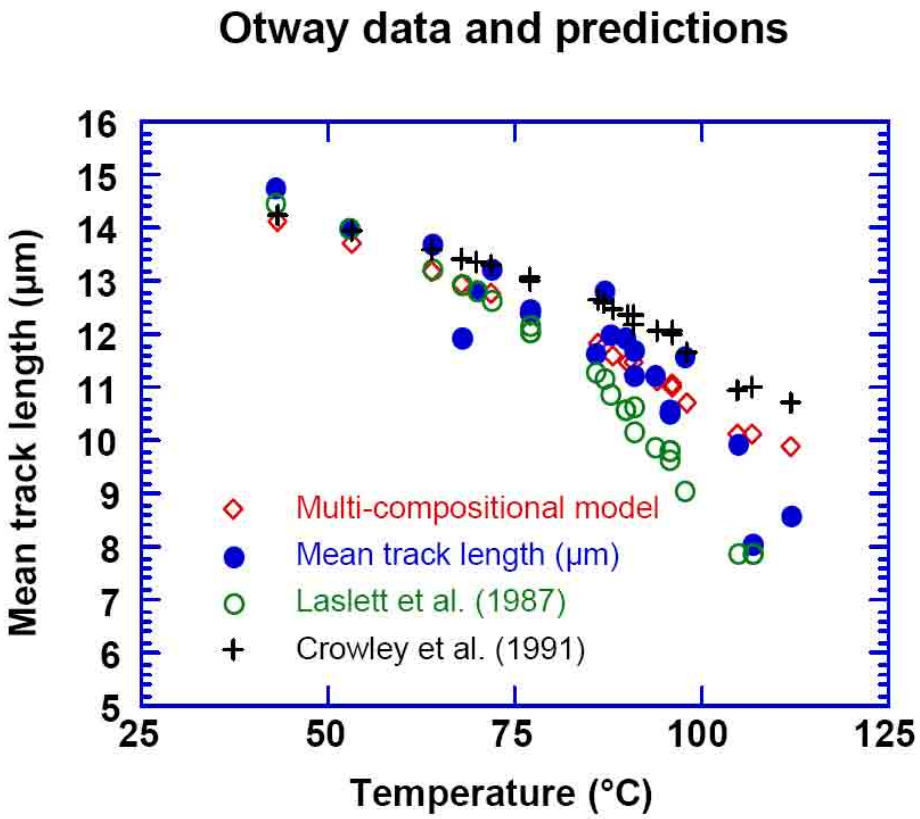

Figure 2.27 – Comparison of mean track length in samples from four Otway Basin reference wells (from Green et al. 1989a) and predicted mean track lengths from three kinetic models for fission track annealing. The Crowley et al. (1991) model relates to almost pure Fluor-apatite (B-5), yet over predicts mean lengths in the Otway Group samples which are dominated by Cl-rich apatite's. The predictions of that model are therefore not reliable.

2.3.1.4: Deriving thermal history information from fission-track data

A major advantage of AFTA is its ability to provide an estimate of the time at which a sample began to cool from its maximum post-depositional palaeotemperature, or a subsequent peak value (Green *et al.* 2002). Forward modelling programs have been developed by Green et al. (1989) which combine detailed knowledge of the kinetics of the fission-track annealing process and formal statistical procedures. These models can simulate fission track age and track length distributions consistent with input time-temperature pathways (Green *et al.* 1989). As Chlorine (Cl) content has an impact on the fission-track annealing kinetics in

apatite, the modelling procedure attempts to match fission-track age and length distributions for both the entire sample and for the individual apatite grains (within the sample) binned into discrete wt.% Cl intervals (Corcoran & Doré, 2005). Comparison of the model data with the measured age and track length distributions (Figure 2.28) allows estimates of maximum palaeotemperature interpretation for up to three palaeothermal episodes (Green *et al.* 2001, 2002). As there is a lack of constraints on low-temperature (below 60°C, corresponding to burial of less than 2km) history from AFTA, supplementary insights can be provided by low-temperature thermochrononometry such as the (U-Th)/He dating of apatite (Huuse, 2002). This system which is based on the accumulation and diffusive loss of Helium produced by the alpha decay of Uranium and Thorium impurities within apatite grains (Farley, 2000), offers potential for improved resolution in the timing of cooling events and independent estimation of maximum palaeotemperatures between 50-80°C (Corcoran & Doré, 2005). Palaeotemperature estimates derived using this approach usually have an absolute uncertainty of better than ±10°C.

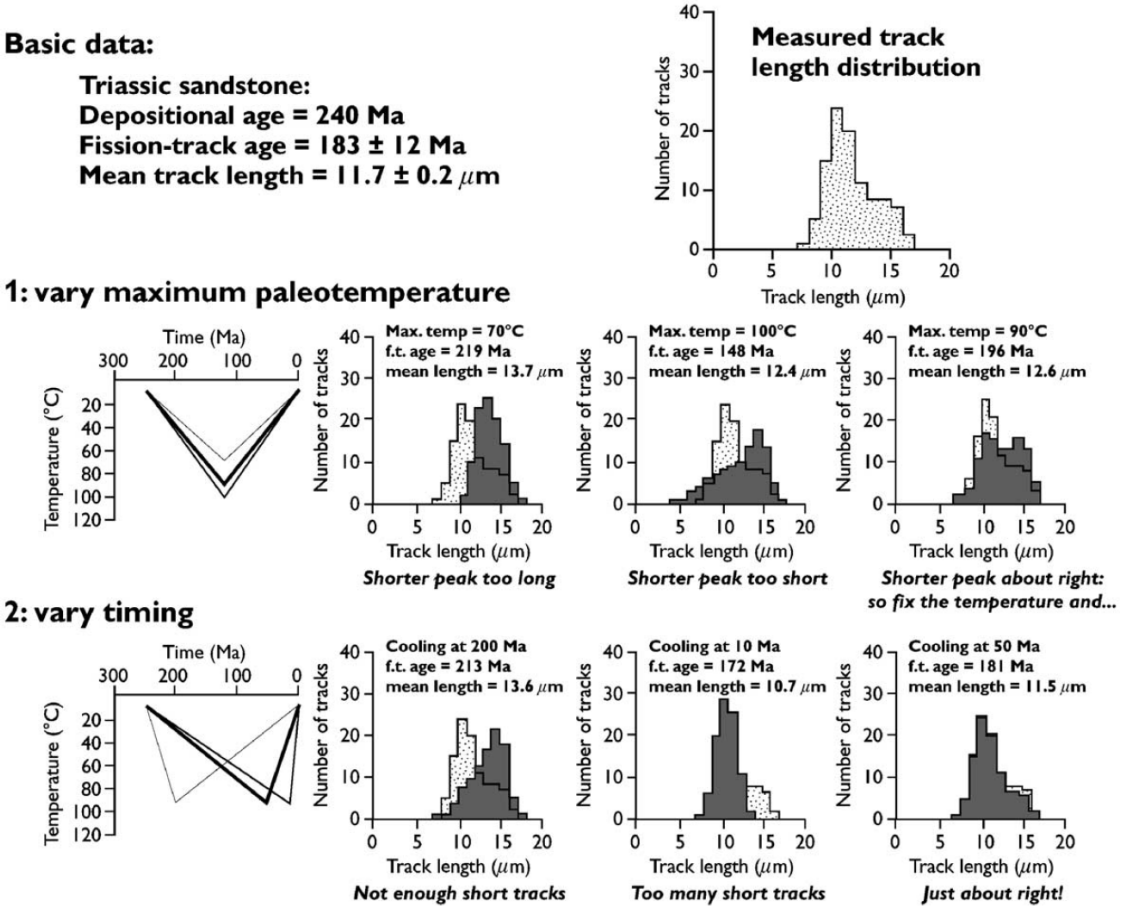

Figure 2.28 – Forward modelling methodology of Green et al. (1989) for measured apatite fission track age and track length distributions, in the case of a synthetic sample with no variation in Cl content. Formal statistical procedures are used to discriminate between a range of thermal history scenarios by firstly optimising magnitude of peak palaeotemperature and then optimising the timing of peak palaeotemperature. In this synthetic model, cooling from a peak palaeotemperature of 90°C from 50 Ma, gives the best fit to the observed track length distributions (after Green *et al.* 2002)

Because fission-tracks are formed continuously throughout geological time, in a sample which has been heated and cooled, the tracks produced up to the time at which cooling begins will be shortened to a length determined by the maximum palaeotemperature, whereas tracks produced subsequent to the onset of cooling will be longer (e.g. Sample 1 in Figure 2.29). The timing of cooling, in relation to the overall duration of the history, determines the proportion of shorter to longer tracks and the length of the shorter peak will be determined by the maximum palaeotemperature. It is necessary to combine information about the track lengths with a fission-track age measurement, since grains of apatite may well contain

'inherited' tracks at the time of deposition (Green *et al.* 2002). In a sample which has been totally annealed at some point (so that the track lengths have been reduced to zero), tracks will only be retained after cooling below this limit (e.g. Sample 2 in Figure 2.29). The track data will thus provide only a minimum estimate of the maximum palaeotemperature, although tight constraints on the time of cooling can often be provided by the fission-track age in such samples (Green *et al.* 2002).

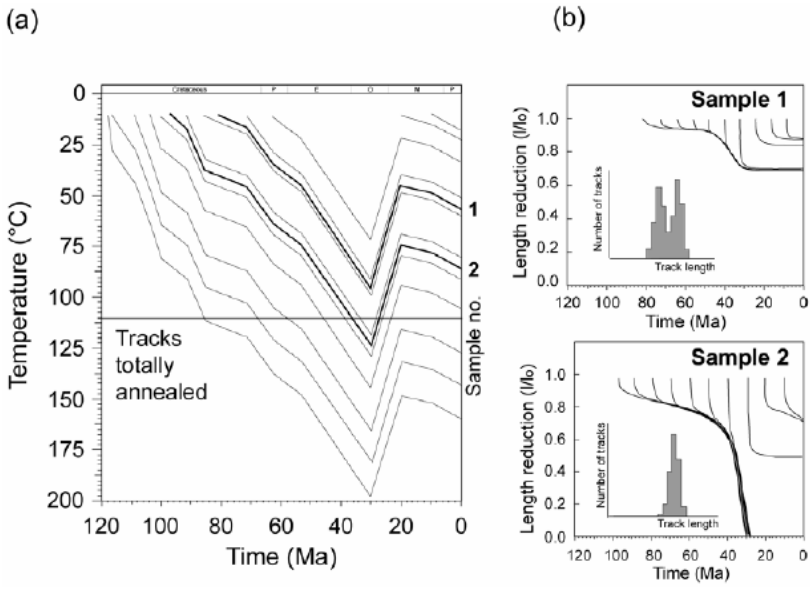

Figure 2.29 – The thermal response of fission-tracks in apatite to geological thermal histories. (a) Shows thermal histories for two samples in a hypothetical well sequence, with both samples undergoing heating and subsequent cooling, with minor reheating. (b) The resultant track length distributions and the associated track length reduction for both samples. See text for further discussion (modified after Green *et al.* 2002).

2.3.1.4.1: Cooling History

If the data are of high quality and provided that the cooling from maximum palaeotemperatures began sufficiently long ago (so that the history after this time is represented by a significant proportion of the total tracks in the sample), determination of the magnitude of a subsequent peak palaeotemperature and the timing of cooling from that peak may also be possible. A similar approach to that outlined above provides best estimates and corresponding ±95% confidence limits for this episode. Such estimates may simply represent part of a protracted cooling history and evidence for a later discreet cooling episode can only

be accepted if this scenario provides a significantly improved fit to the data. Geological evidence and consistency of estimates between a series of samples can also be used to verify evidence for a second episode. In practice, most typical AFTA datasets are only sufficient to resolve two discrete episodes of heating and cooling. One notable exception to this is when a sample has been totally annealed in an early episode and has then undergone two (or more) subsequent episodes with progressively lower peak palaeotemperatures in each. But in general, complex cooling histories involving a series of episodes of heating and cooling will allow resolution of only two episodes and the results will depend on which episodes dominate the data. Typically this will be the earliest and latest episodes, but if multiple cooling episodes occur within a narrow time interval the result will represent an approximation to the actual history.

It is important to emphasise the extent to which fission-track data are dominated by maximum palaeotemperatures. This is illustrated by Figure 2.30, which shows a series of track length distributions for mono-compositional apatite samples, predicted for a range of thermal histories. In the sample which has been heated to 70°C, the degree of length reduction in tracks formed before the onset of cooling is small, and it is difficult to resolve the short component of tracks from the longer tracks which formed after cooling. In samples such as this, it is often the case that a wide range of timings for the cooling episode will be consistent with the data. For the sample which has been heated to 100°C, the degree of length reduction is more severe and the shorter tracks can be more easily resolved, enabling tighter controls on the timing of cooling. The tightest constraints on the timing of cooling should be provided by the sample which was heated to 120°C (and so experienced total annealing); note how the predicted fission track age for this sample is much closer to the timing of cooling than for the other samples.

Although the continuous production of fission tracks throughout time enables some aspects of the thermal history of a sample following the onset of cooling to be inferred, it is not possible to provide any information on the approach to a palaeothermal maximum (Green *et al.* 2002). Therefore it is necessary to assume a value of heating rate to obtain an estimate of maximum palaeotemperature; the kinetics of the annealing process means that a change of an order of magnitude in the heating rate is equivalent to a change in the required palaeotemperature of 10°C (Green *et al.* 1989). Furthermore, fission-track data do not provide sufficient information to model the entire thermal history of a sample, despite attempts by some workers (e.g. Gallagher, 1995; Ketcham *et al.* 2000; Cunningham *et al.* 2003). This is because the effects of variation within one part of the thermal history can be compensated for by events at other times; this results in confidence limits which are so wide that the thermal history solutions provide no useful constraints. In practice, because of the inherent spread in the distribution of track lengths as a function of the degree of annealing (Green *et al.* 1986), the resolution of a maximum of two, or rarely, three, episodes of heating and cooling is often the limit allowed by even the highest quality data (Green *et al.* 2001*a*, 2002).

In summary two parameters are measured from fission track analysis - number of fission-tracks (from which the fission track age is derived – Hurford & Green, 1983) and distribution of fission track lengths (from which temperature history is elucidated – Laslett *et al*. 1987). AFTA data can also provide information on the likely magnitude of present-day temperatures by measuring the lengths of tracks formed since the last cooling episode and the degree of fission-track age reduction at present day temperatures of around 100-110°C where the fission-track age is expected to decrease rapidly towards zero (Green *et al.* 1999).

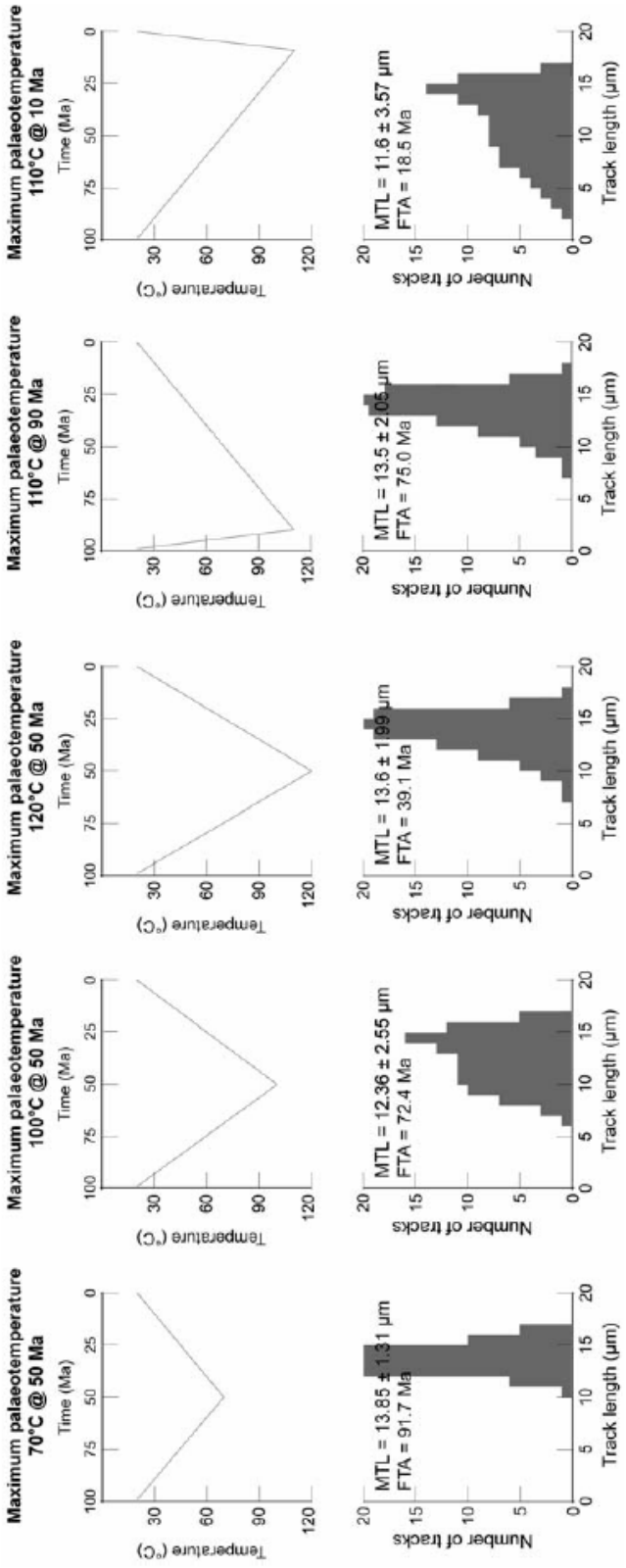

Figure 2.30 – This diagram shows a number of fission-track length distributions predicted for a series notional mono-compositional apatite samples using the Laslett *et al.* (1987) annealing algorithm and a variety of thermal history scenarios. These scenarios illustrate the extent to which apatite fission-track data are dominated by maximum palaeotemperatures; see text for further discussion (from Holford, 2006).

2.3.1.4.2: Allowing for tracks inherited from source areas

The effect of tracks inherited from source areas and present at the time the apatite is deposited in the host sediment is often posed as a potential problem for AFTA. However this can readily be allowed for in analysing both the fission track age and length data.

In assessing fission track age data to determine the degree of annealing, the only criterion used is the comparison of fission track age with the value expected on the basis of the Default Thermal History. From this point of view, inherited tracks do not affect the conclusion – if a grain or a sample gives a fission track age which is significantly less than expected, the grain or sample has clearly undergone a higher degree of annealing than can be accounted for by the Default Thermal History and therefore must have been hotter in the past whether the sample contained tracks when it was deposited or not.

The presence of inherited tracks does impose a limit on our ability to detect post-depositional annealing from age data alone, as in samples which contain a fair proportion of inherited tracks, moderate degrees of annealing may reduce the fission track age from the original value, but not to a value which is significantly less than the stratigraphic age. This is particularly noticeable in the case of Cenozoic samples containing apatite's derived from Palaeozoic basement. In such cases, although fission track age data may show no evidence of post-depositional annealing, track length data may well show such evidence quite clearly.

The influence of track lengths inherited from source areas can be allowed for by comparison of the fission track age with the value predicted by the Default Thermal History combined with inspection of the track length distribution. If the mean length is much less than the length predicted by the Default Thermal History, either the sample has been subjected to elevated palaeotemperatures, sufficient to produce the observed degree of length reduction or

else the sample contains a large proportion of shorter tracks inherited from source areas. However in the latter case, the sample should give a pooled or central fission track age correspondingly older than the stratigraphic age, while the length distribution should contain a component of longer track lengths corresponding to the value predicted by the Default Thermal History. It is important in this regard that the length of a track depends primarily on the maximum temperature to which it has been subjected, whether in the source regions or after deposition in the sedimentary basin. Thus any tracks retaining a provenance signature will have lengths towards the shorter end of the distribution where track lengths will not have "equilibrated" with the temperatures attained since deposition.

In general it is only in extreme cases that inherited tracks render track length data insensitive to post-depositional annealing. For example, if practically all the tracks in a particular sample were formed prior to deposition, perhaps in a Pliocene sediment in which apatite's were derived from a stable Paleozoic shield with fission track ages of ~300Ma or more, the track length distribution will, in general, be dominated by inheritance, as only ~2% of tracks would have formed after deposition. Post-depositional heating will not be detectable as long as the maximum palaeotemperature is insufficient to cause greater shortening than that which occurred in the source terrain. Even in such extreme cases, once a sample is exposed to temperatures sufficient to produce greater shortening than that inherited from source areas, the inherited tracks and those formed after deposition will all undergo the same degree of shortening and the effects of post-depositional annealing can be recognised. In such cases the presence of tracks inherited from source areas is actually very useful, because the number of tracks formed after deposition is so small that little or no information would be available without the inherited tracks.

2.3.1.5: Plots of fission track age and mean track length versus depth and temperature

AFTA data from well sequences are usually plotted as shown in Figure 2.31. This figure shows AFTA data for two scenarios: one in which deposition has been essentially continuous from the Carboniferous to the present and all samples are presently at their maximum palaeotemperature since deposition (Figure 2.31a); and one in which the section was exposed to elevated palaeotemperatures prior to cooling in the Early Cenozoic (Figure 2.31b).

In Figure 2.31a, for samples at temperatures below ~70°C, the fission track age is either greater than or close to the stratigraphic age and little fission track age reduction has affected these samples. Track lengths in these samples are all greater than ~13µm. In progressively deeper samples, both the fission track age and mean track length are progressively reduced to zero at a present temperature of around 110°C, with the precise value depending on the spread of apatite compositions in the sample. Track length distributions in the shallowest samples would be a mixture of tracks retaining information on the thermal history of source regions, while in deeper samples, all tracks would be shortened to a length determined by the prevailing temperature. This pattern of AFTA parameters is characteristic of a sequence which is currently at maximum temperatures.

The data in Figure 2.31b show a very different pattern. The fission track age data show a rapid decrease in age, with values significantly less than the stratigraphic age at temperatures of ~40-50°C, at which such a degree of age reduction could not be produced in any geological timescale. Below this rapid fall, the fission track ages do not change much over ~1km (30°C). This transition from rapid fall to consistent ages is diagnostic of the transition from partial to total annealing. Samples above the break in slope contain two generations tracks: those formed prior to the thermal maximum, which have been partially annealed (shortened) to a degree which depends on the maximum palaeotemperature; and those formed after cooling

which will be longer. Samples below the break in slope contain only one generation of tracks, formed after cooling to lower temperatures at which tracks can be retained. At greater depths, where temperatures increase to ~90°C and above, the effect of present temperatures begins to reduce the fission track ages towards zero, as in the "maximum temperatures now" (Figure 2.31a) case.

The track length data also reflect the changes seen in the fission track data. At shallow depths, the presence of the partially annealed tracks shortened prior to cooling causes the mean track length to decrease progressively as the fission track age decreases. However at depths below the break in slope in the age profile, the track length increases again as the shorter component is totally annealed and so does not contribute to the measured distribution of track lengths. At greater depths the mean track lengths decrease progressively to zero once more due to the effects of the present temperature regime. Examples of such data have been presented, for example, by Green (1989) and Kamp & Green (1990).

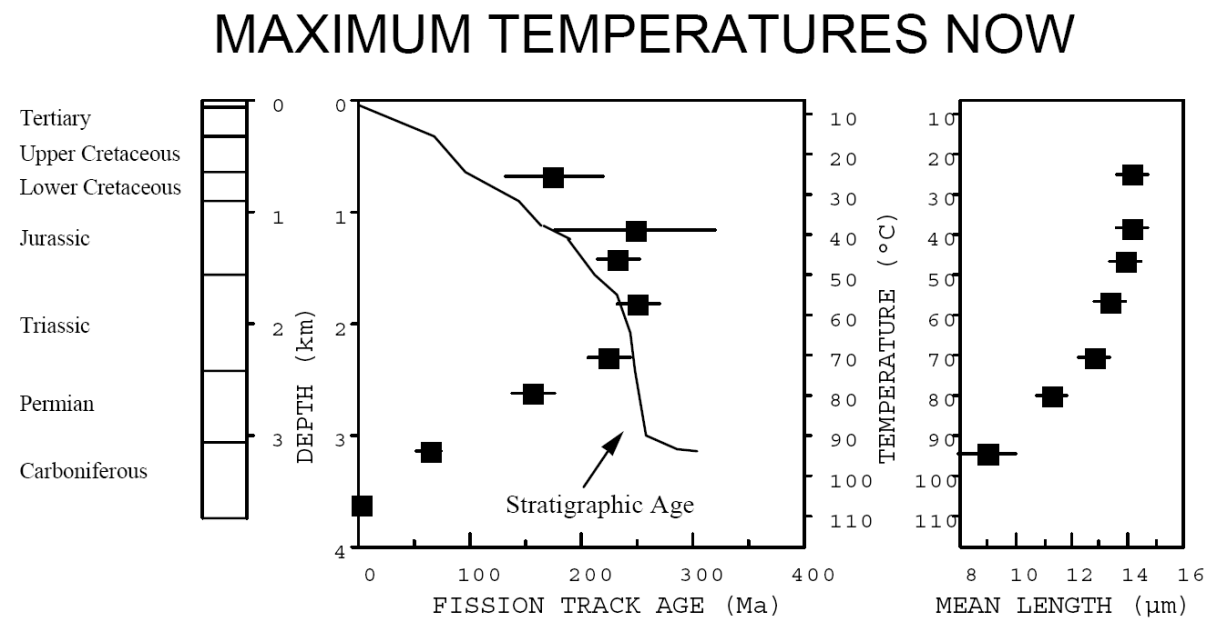

Figure 2.31a – Typical pattern of AFTA parameters in a well in which samples throughout the entire section are currently at their maximum temperatures since deposition. Both the fission track age and mean track length undergo progressive reduction to zero at temperatures of ~100-110°C, the actual value depending on the range of apatite compositions present (from Geotrack, 2001).

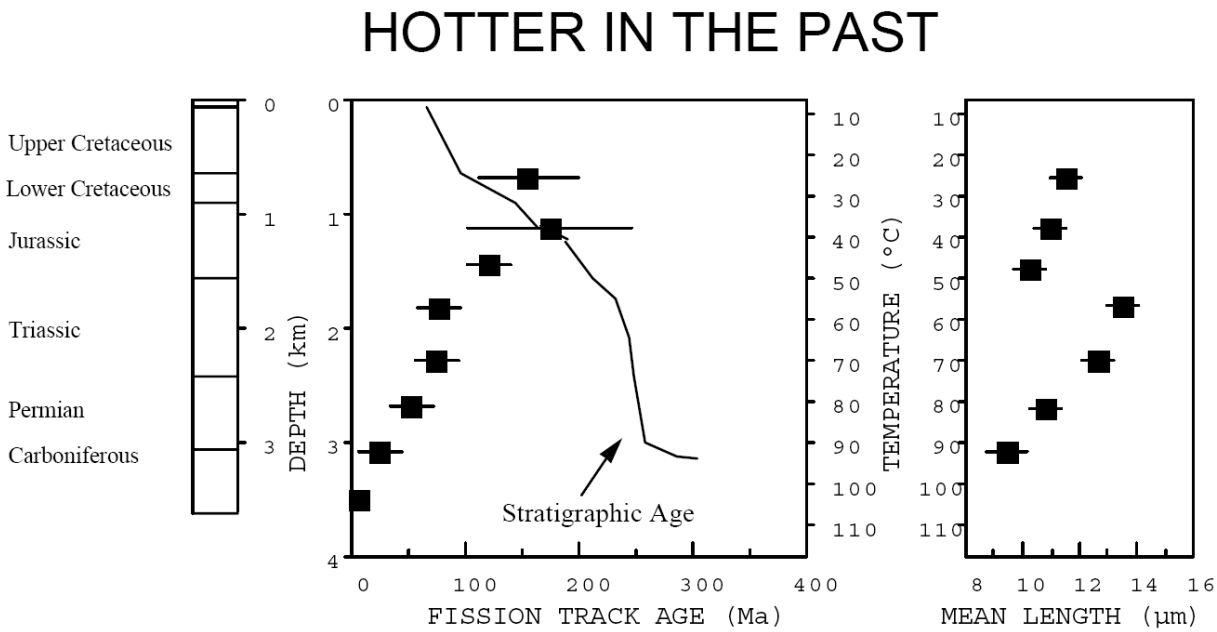

Figure 2.31b – Typical pattern of AFTA parameters in a well in which samples throughout the section were exposed to elevated palaeotemperatures after deposition (prior to cooling in the Early Cenozoic, in this case). Both the fission track age and mean track length show more reduction at temperatures of ~40-50°C than would be expected at such temperatures. At greater depths (higher temperatures), the constancy of fission track age and the increase in track length are both diagnostic of exposure to elevated palaeotemperatures (from Geotrack, 2001).

2.3.2: VITRINITE REFLECTANCE (VR)

Hydrocarbons are by-products of the metamorphism of organic material (kerogen) within sediments. This process involves the expulsion of volatiles, gases liquids and oils during the chemical alteration of buried organic matter and the thermal maturity of a rock is a measure of the degree to which this metamorphism has progressed (Tissot & Welte, 1984).

The most important controls on the maturation of organic matter are temperature and time (Tissot & Welte, 1984). The relationship between temperature and the rate of chemical reactions is given by the Arrhenius equation:

$$K = A\,exp^{\left(\frac{-E_a}{RT}\right)} \qquad (2.12)$$

Where K is the reaction rate, A is a constant sometimes referred to as the *frequency factor* (it is the maximum value that can be reached by K when given an infinite temperature), E_a is the *activation energy* (a parameter which can be thought of as an energy barrier ($Jmol^{-1}$) that must be overcome before the reaction can proceed), R is the Universal Gas Constant ($8.314JK^{-1}mol^{-1}$) and T is absolute temperature (K) (Beardsmore & Cull, 2001).

2.3.3: THERMAL HISTORY RECONSTRUCTION (THR)

Thermal History Reconstruction (THR) relies on application of AFTA and VR to identify the timing of dominant episodes of heating and cooling that have affected a sedimentary section, to quantify the palaeotemperatures through the section and to characterise the mechanisms of heating and cooling (Green *et al.* 1999). Sedimentary rocks are progressively heated during burial and begin to cool at the initiation of exhumation. AFTA and VR data (e.g. from an exploration well or borehole) provide quantitative estimates of the temperatures attained by individual rock samples at a palaeothermal maximum, prior to the onset of cooling (Green *et*

al. 1995, 2002). This combined approach is particularly useful in the reconstruction of the thermal and burial histories of sedimentary basins, especially if there are unconformities representing major time gaps (Duncan *et al.* 1998; Green *et al.* 2000). The integration of AFTA and VR data is especially useful in sedimentary succession where most AFTA samples have been totally annealed, since VR allows estimation of higher palaeotemperatures than those resolvable from AFTA alone (Duddy *et al.* 1994).

The first stage in the combined thermal history interpretation of AFTA and VR data from an exploration well or borehole begins by constructing a 'default thermal history' for each sample (e.g. Duddy *et al.* 1994; Green *et al.* 2002). The default thermal history is constructed using the preserved stratigraphy recorded in a well/borehole, assuming that all stratigraphic breaks represent hiatuses (i.e. no deposition or erosion). A thermal history is then derived by assuming that the present geothermal gradient has remained constant since the deposition of the oldest sediments. If the observed data (fission track age and length distribution, $\%R_0(max)$) are consistent with equivalent values predicted by the default thermal history, then the sample is at, or close to, its maximum post-depositional temperature. If however, a greater degree of annealing or maturity is observed than that predicted by the default history, then the samples have been hotter at some point during the past (Duddy *et al.* 1994; Green *et al.* 2002). If this is the case, AFTA can enable the timing of cooling to be estimated and both AFTA and VR can be used to constrain the magnitude of maximum palaeotemperatures. Examples of the 'default thermal history' approach are provided by Argent *et al.* (2002), Green *et al.* (2004) and Holford *et al.* (2005*a*).

Thermal history interpretation is based on a detailed knowledge of the kinetic responses of both AFTA and VR, which are well calibrated based on studies in both geological and laboratory conditions. THR information is extracted from the AFTA data by modelling

measured AFTA parameters through a variety of possible thermal history scenarios varying the magnitude and timing of the maximum palaeotemperature and defining the range of values of each parameter, which give predictions consistent with the measured data (Green *et al.* 1999). Observed VR values are converted to maximum palaeotemperatures using the kinetic model developed by Burnham & Sweeney (1989) and Sweeney & Burnham (1990). Information on the timing of these maximum palaeotemperatures is provided by the AFTA data.

2.3.3.1: Construction of geothermal gradients

Where samples are analysed over a range of depths, such as in a down-hole well section, the magnitude of exhumation (i.e. thickness of the eroded succession) can be determined by extrapolation of a linear palaeotemperature profile to an appropriate palaeosurface temperature (Bray *et al.* 1992) (Figure 2.32).

The form of the palaeotemperature profile provides key information on likely mechanisms of heating and cooling (Figure 2.33). By dividing the difference between the palaeosurface temperature and the palaeotemperature intercept at the appropriate unconformity by the palaeogeothermal gradient, the amount of section that was once deposited above the unconformity surface and has been removed subsequently by uplift and erosion can be calculated (Figure 2.34). Such an analysis assumes that:

1. The palaeotemperature profile is linear.

2. The palaeogeothermal gradient through the preserved succession can be extrapolated linearly through the eroded succession. This assumption can never be verified since

the section is no longer present and Holliday (1993) has recently challenged the validity of this assumption.

3. The palaeosurface temperature is known.

4. The heating rate used to estimate palaeotemperatures is correct.

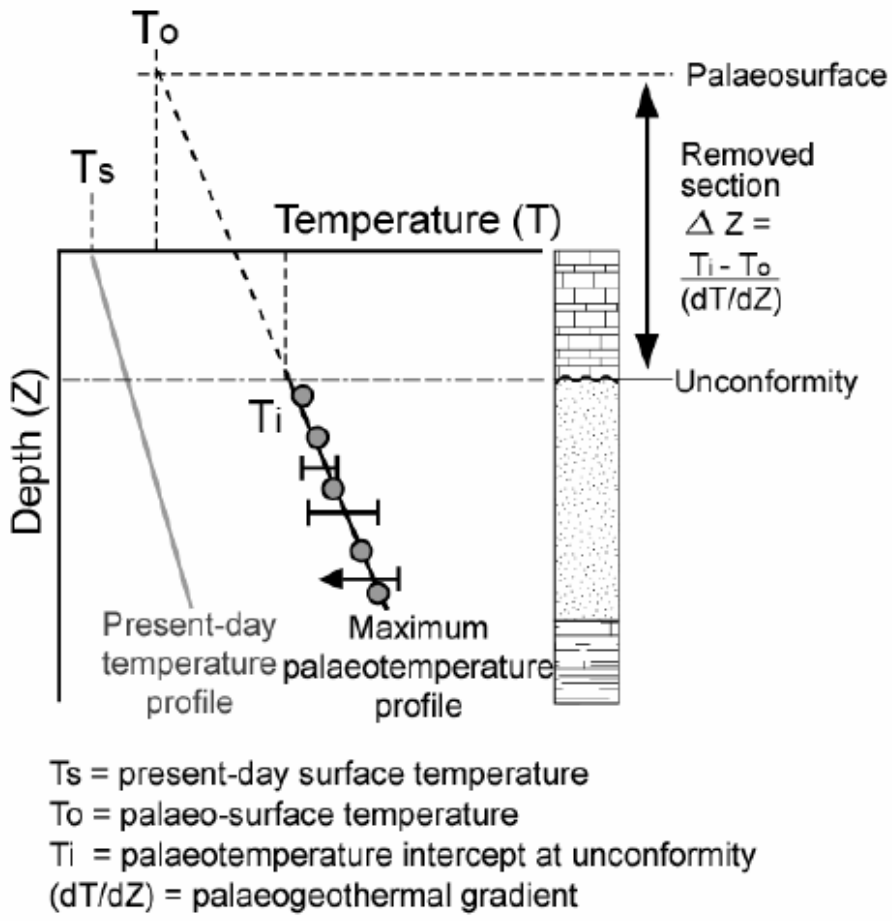

Figure 2.32 – If the palaeogeothermal gradient can be constrained by AFTA and VR, as explained in the text, then for an assumed value of surface temperature, T_s, the amount of section removed can be estimated as shown.

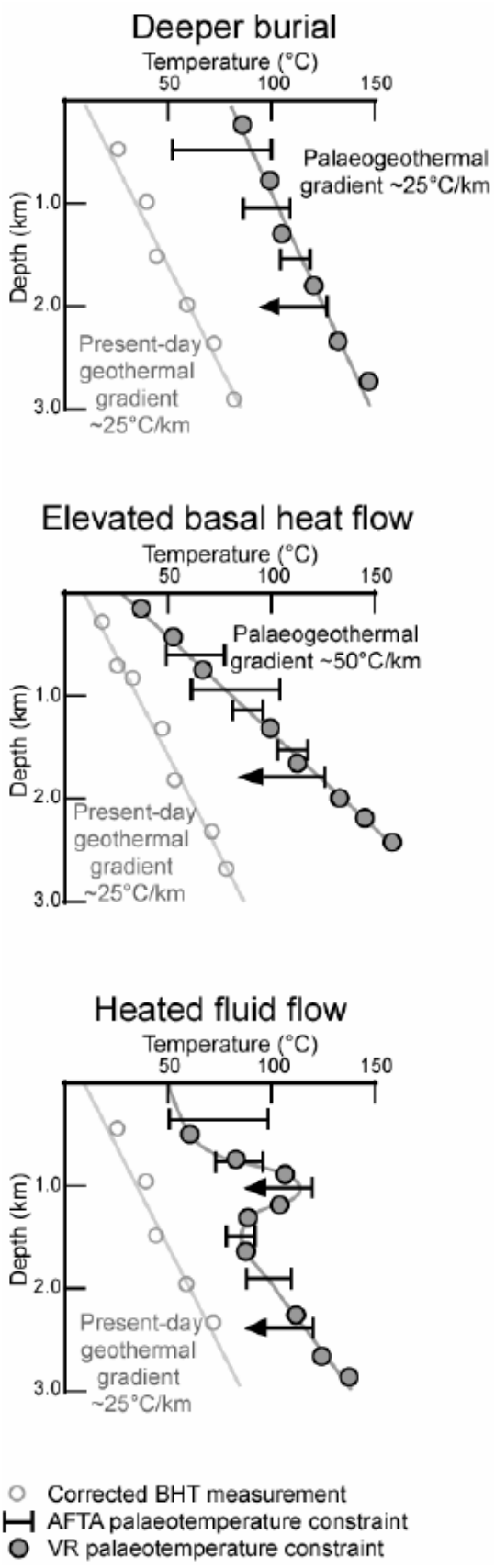

Figure 2.33 – Schematic examples of palaeotemperatures produced by heating related to deeper burial, elevated basal heat flow and the passage of heated fluids respectively (modified after Holford *et al.* 2005).

The degree to which the palaeogeothermal gradient can be constrained depends on a number of factors, particularly the depth range over which samples are analysed. If samples are only analysed over ~1km, then the palaeotemperature difference over that range may be only 20-30°C. Since maximum palaeotemperatures can often only be determined within ±10°C, this introduces considerable uncertainty into the final estimate of palaeogeothermal gradient (see Figure 2.35). In the case of outcrop samples interpreted in the absence of independent constraints on palaeogeothermal gradients, a range of likely values must be assumed.

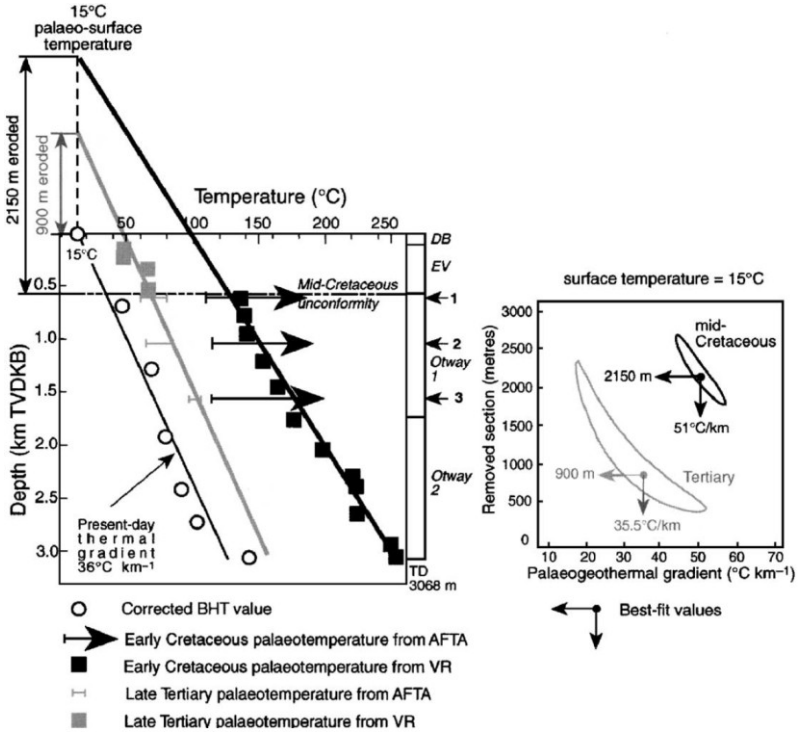

Figure 2.34 – Graphical construction of Green *et al*. (2002) for the derivation of exhumation estimates from maximum palaeotemperature profiles established from VR and AFTA. Left: Both AFTA and VR data clearly record two palaeothermal episodes in this example. The timing of the cooling episodes derived from AFTA , the presence of two unconformities in the well (Mid-Cretaceous and Late Cenozoic) and the linearity of the palaeotemperature profiles for each episode, indicate that the temperature and palaeotemperature distributions can best be explained by two episodes of deeper burial followed by exhumation in each case. Right: Plot of removed section vs. palaeogeothermal gradient for an assumed palaeosurface temperature. Best fit and allowed ranges (±95% confidence intervals) of exhumation estimates and palaeogeothermal gradients (for each event) are determined from statistical analysis and displayed as contoured banana-shaped regions on plot. In this exaple the best fit data indicates 2150m of *gross exhumation* at the Mid-Cretaceous unconformity followed by re-burial and subsequent *gross exhumation* of 900m at the Late Cenozoic unconformity (after Corcoran & Doré, 2005).

The pitfalls of the semi log plot (VR vs. depth advocated by Dow (1977) and Dow & O'Connor (1982)), can be avoided by using the graphical construct of Bray *et al.* (1992) (presented by Green *et al.* 2002) which allows for the assessment of exhumation at an unconformity. For comparisons to be made and also to avoid confusion, temperature and palaeotemperature measurements should be displayed with respect to the sea-bed (for offshore well; ground level for onshore well) and not TVDKB (True Vertical Depth below Kelly Bushing) as, in the offshore environment, sea-bed is the appropriate datum for the extrapolation to a palaeosurface temperature (Corcoran & Doré, 2005 and Figure 2.34). The earlier graphical construct of Dow (1977) has been adopted by a number of workers (e.g. Horstman, 1984; Unomah & Ekweozor, 1993; Thomson & Hillis, 1995; Corcoran & Clayton, 2001). The approach utilises the vertical depth separation (on a VR vs. depth semi-log plot) between the VR gradient value immediately above an unconformity and the intercept of the pre-unconformity VR gradient segment extrapolated to the same VR value as an estimate of the amount of eroded section (Corcoran & Doré, 2005 and Figure 2.36). As highlighted by Katz *et al*. (1988) argued that this construct is flawed as it since it discounts the reduced graphical separation (on a semi-log plot) resulting from increased absolute VR values and also does not allow for the actual 'annealing' of the VR profile discontinuity with increasing re-burial. Additionally Green *et al.* (2002) have stated such an approach should be avoided, as untransformed vitrinite can have a reflectance as high as 0.32%. Extrapolation to 0.2% will thus lead to overestimation of the amount of removed section. In contrast, the Green *et al.* (2002) approach uses only the pre-unconformity palaeotemperature segment (independent of 'annealing' process) and an assumed palaeosurface temperature to determine the magnitude of exhumation at an unconformity.

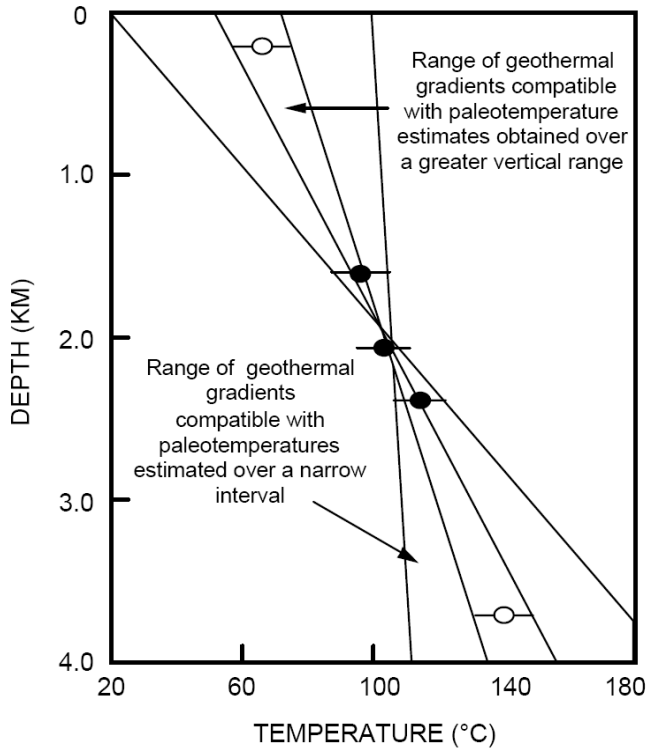

Figure 2.35 – It is important to obtain palaeotemperature constraints over as great a range of depths as possible in order to provide a reliable estimate of palaeogeothermal gradient. If palaeotemperatures are only available over a narrow depth range, then the palaeogeothermal gradient can only be very loosely constrained.

As stated by Corcoran & Doré (2005), one of the main advantages of a thermal framework approach to the assessment of exhumation is the widespread availability of palaeothermal indicators which provide insights into basin evolution that are not available from inspection of the remnant rock record (for example, palaeothermal indicators may yield information with respect to palaeogeothermal gradients which can be used to estimate the magnitude of missing section, independent of stratigraphic evidence). The oil exploration industry widely utilises VR data to constrain charge models in a basin and is the primary indicator of organic maturation recorded in wells offshore Ireland (Corcoran & Clayton, 2001). AFTA has been extensively applied in exhumed offshore basins (Floodpage *et al.* 2001; Green *et al.* 2001) and to deduce the fission track cooling chronologies of the onshore rock record (Allen *et al.* 2002). A further advantage is that, in the absence of a post-unconformity rock record, AFTA can provide a direct estimate of the timing of exhumation from the derived fission track age.

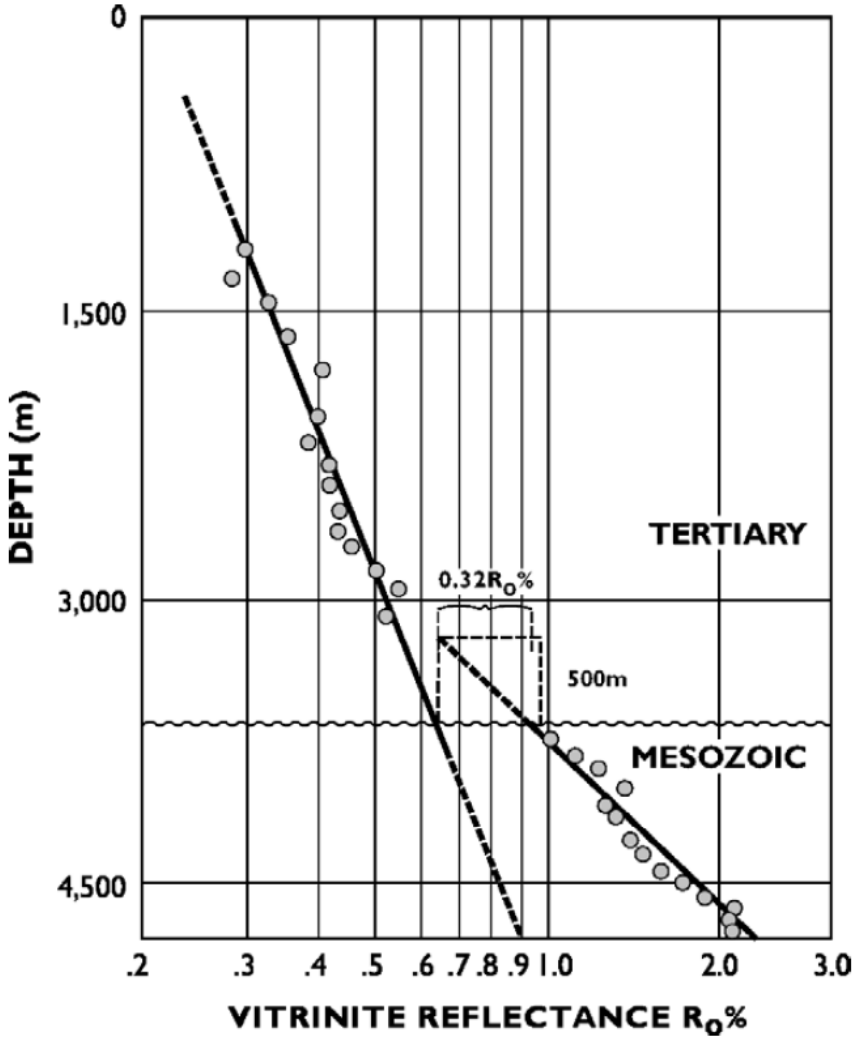

Figure 2.36 – A semi-log plot of vitrinite reflectance versus depth for a well containing an erosional unconformity contact between the Tertiary and the underlying Mesozoic section, with graphical construction of Dow (1977) for the estimation of removed section at an unconformity. This methodology suggests that the difference in depth between the VR segment value immediately above an unconformity and the intercept of the pre-unconformity VR segment extrapolated to the same VR value yields an estimate of the amount of erosion at the unconformity. This construct significantly underestimates the amount of section removed at the Base Tertiary unconformity as it does not allow for the 'annealing' in of the discontinuity in the VR profile that is caused by burial during the Tertiary (after Corcoran & Doré, 2005).

2.3.4: LIMITATIONS OF AFTA AND VR

There are a number of pitfalls and sources of uncertainty with respect to the use of a thermal framework approach (VR and AFTA) to estimate the magnitude of exhumation:

1. Palaeotemperature profiles which are non-linear (i.e. bell shaped profiles, dog-leg profiles or profiles with negative palaeogeothermal gradients) cannot be used to estimate the magnitude of exhumation at a given well location (Duddy *et al.* 1998). Profiles like these are clearly caused by transient thermal effects of various origin (such as emplacement of molten magma and/or hydro-thermal fluid flow) which can result in the distortion of conductive heat distribution in a basin (Wycherley *et al.* 2003).

2. VR and AFTA information is dominated by maximum palaeotemperatures and do not preserve information on thermal events that occurred prior to the achievement of peak palaeotemperatures (Corcoran & Doré, 2005). Complete annealing of fission tracks in apatite generally occurs in the 100-120°C range so apatite fission tracks cannot store information on exhumation (cooling) events that occurred prior to the most recent episode of 'complete annealing' of tracks (Green *et al.* 1986).

3. Systematic errors can be introduced in the estimation of palaeogeothermal gradients by the mathematical translation of VR values into absolute palaeotemperatures and consequently, the magnitude of exhumation (Green *et al.* 2002). Although the kinetic model (EASY%R0 algorithm) of Sweeney & Burnham (1990) is widely accepted as the most accurate VR to temperature translation method, within the range of organic maturity associated with oil and gas generation, other empirically based translation schemes are also used over wider maturity ranges (e.g. Barker & Pawliewicz, 1986; Barker, 1988; Barker & Goldstein, 1990). Using these translation schemes in general produces a higher gradient and thus a lower estimate of exhumation relative to the Sweeney & Burnham model (see Figure 3 of Green *et al.* 2002 and Figure 8 of Corcoran & Clayton, 2001).

4. One of the major underlying assumptions of thermal history techniques is that the measured palaeothermal profiles represent the distribution of temperature with depth immediately prior to exhumation (Corcoran & Doré, 2005). In highly stretched basins and for old (especially syn-rift) stratigraphy, the palaeothermal indicators may represent maximum palaeotemperatures attained early in basin history (due to heat-flow pulse from rifting) and not subsequently exceeded (Allen *et al.* 1998).

5. A major assumption of the thermal technique is the linearity of the palaeotemperature-depth profile through the preserved section and linear extrapolation though the removed section to the assumed palaeosurface temperature. This assumption is valid only in cases where the thermal conductivity of the removed and preserved sections is identical although Green *et al.* (2002) report that, in practice the assumption of linearity (of palaeogeothermal gradients) has yielded reliable results.

6. Geological factors such as changes in orogenic provenance, faulting or lithological variations can result in offsets to the palaeotemperature profile particularly in VR datasets. Additional variations in the profile can result from the limitations of the VR sampling and analytical techniques, such as the deficiencies of cuttings samples and maceral misidentification, which can result in low reproducibility of identical datasets (Figure 2.37) (Dembicki, 1984).

7. Overpressured sedimentary sequences can cause the retardation of VR (Hao & Chen, 1992; McTavish, 1998; Carr, 2000). This decreases the computed palaeogeothermal gradient and leads to an inaccurate estimate of exhumation since retardation violates the underlying assumptions of the profile modelling.

8. VR suppression (deviations of VR profile towards lower values of R_m%) can result from the presence of Hydrogen-rich vitrinites. Consequently, variations in the chemical composition of vitrinite, between well locations, may lead to invalid comparison of VR gradients and associated exhumation estimates (Corcoran & Doré, 2005).

9. Mobile salt layers in a basin (halite) can lead to complex present-day temperatures and palaeotemperature (Corcoran & Doré, 2005). For example, the high thermal conductivity of salt may result in the deviation of an anomalously high palaeogeothermal gradient for a well drilled on a salt dome-supported anticline and consequently, a spurious estimate for the magnitude of exhumation will result at that location (Corcoran & Doré, 2005).

This general approach has been criticised as oversimplified by some workers (e.g. Holliday, 1993; Smith *et al.* 1994; Gallagher *et al.* 1998). However, results in tightly controlled situations are usually highly consistent with estimates of deeper burial from other techniques thereby validating the use of AFTA and VR data in determining magnitudes of exhumation. For example, estimates of the amount of late Miocene exhumation at the Fresne-1 exploration well of the Taranaki Basin of New Zealand based on AFTA and (U/Th)/He data show excellent agreement with estimates from truncated reflectors observable on seismic data (Kamp & Green, 1990; Crowhurst *et al.* 2002), whilst Holford *et al.* (2005a) and Williams *et al.* (2005) present examples from the CBB and SGCB, where exhumation estimates based on AFTA and VR data from boreholes and exploration wells are highly consistent with independent estimates from compaction and seismic reflection profiles.

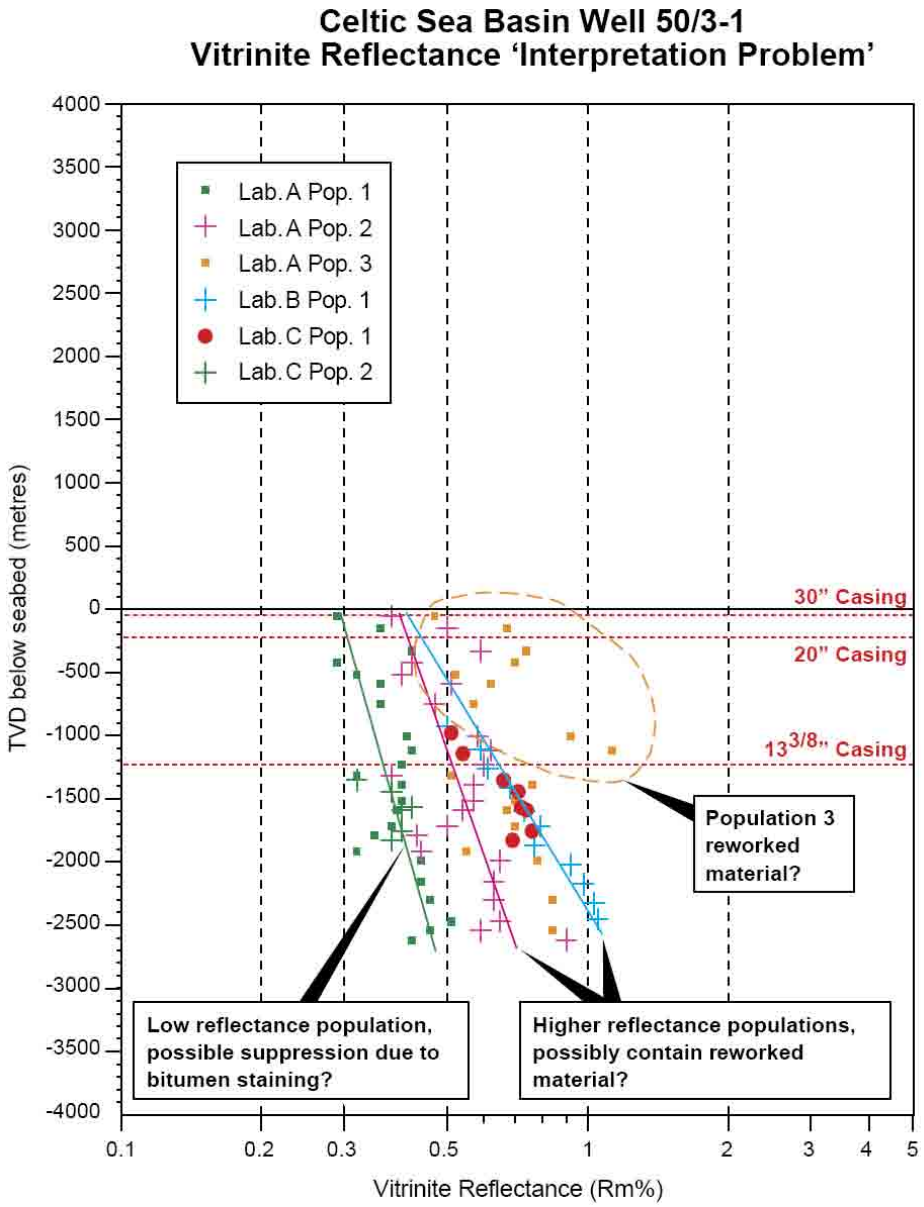

Figure 2.37 – Pitfalls in VR interpretation – VR analysis of cuttings data from well 50/03-1, offshore Ireland, by three different geochemical laboratories. Plot of VR (Rm%) vs. depth. A number of 'vitrinite populations' were identified in this Jurassic section (three populations by Lab A, one by Lab B and two by Lab C). No core data was available to address cavings dilemma; well casing points are included to help high grade cuttings data, but are of limited use. The occurrence of sub-parallel trends indicates uncertainty in maceral identification and requires cross-referencing with equivalent VR values defined from other thermal indicators such as SCI, pyrolysis Tmax etc. to help identify the 'true' indigenous vitrinite population. Selection of the appropriate VR population and trend is a critical step in the estimation of magnitude of exhumation (after Corcoran &Doré, 2005).

CHAPTER 3: REGIONAL GEOLOGY AND EXHUMATION HISTORY OF THE WESTERN APPROACHES-CELTIC SEA BASIN SYSTEM

3.1: INTRODUCTION

The southwestern UK comprises a series of linked Mesozoic-Cenozoic sedimentary basins located between the United Kingdom and Ireland. They extend from the Western Approaches Basin in the south, up through the Celtic Sea basins, East Irish Sea basin, Solway Firth and North Channel basins in the north (Figure 3.1). The Celtic Sea basin system is a linked complex comprising the North Celtic Sea Basin (NCSB), South Celtic Sea Basin (SCSB), Bristol Channel Basin (BCB), St. George's Channel Basin (SGCB), Cardigan Bay Basin (CBB), Central Irish Sea Basin (CISB) and Kish Bank Basin (KBB). To the south of the Celtic Sea the Fastnet, St. Mary's, Melville and Haig-Fras basins make up the southern part of the Western Approaches Basin (WAB), which continues northeast through the Plymouth Bay Basin into the Channel Basin. These basins are mainly of an extensional origin with margins controlled by major normal faults, which downthrown the basins against largely Palaeozoic-age basement massifs (Tappin *et al.* 1994). They form part of a much larger polyphase rift complex of sedimentary basins across NW Europe which were initiated during the Permian and Triassic (Shannon, 1991), in response to roughly E-W oriented lithospheric extension (Chadwick & Evans, 1995; Coward, 1995). Consequently, the tectonic history of the Western Approaches-Celtic Sea basin system is inextricably linked to that of the North Atlantic passive margin as a whole.

This extension was the result of plate reorganisation, which led to the breakup of the Caledonian and Variscan terranes of the short-lived Pangaean supercontinent along distinct

Arctic and Atlantic rifts throughout the Mesozoic (Ziegler, 1990) and ultimately culminated in full continental break-up along the North Atlantic margin during early Eocene times (Doré *et al.* 1999; Roberts *et al.* 1999) when it was accompanied by large volumes of volcanism and magmatic underplating. Regional subsidence occurred during the Jurassic and Cretaceous in response to extension in front of the northward propagating rift and the two rift systems coalesced in Late Jurassic to Early Cretaceous times when the North Atlantic Rift reached the Rockall Trough (Ziegler 1989; Knott *et al.* 1993; Roberts *et al.* 1999; Doré *et al.* 1999). During the Cenozoic, the Western Approaches and Celtic Sea basin complexes were subjected to several phases of compression and regional uplift, which inverted basin centres and led to the selective reactivation of Mesozoic extensional faults (e.g. Tucker & Arter, 1987; Van Hoorn, 1987*b*; Roberts, 1989; Tappin *et al.* 1994; Knipe *et al.* 1993; Dart *et al.* 1995; Nemcok *et al.* 1995; Stewart *et al.* 1997; Turner, 1997; Bulnes & McClay, 1998).

Whilst the preserved stratigraphy and structure of the Western Approaches-Celtic Sea basins has long been the subject of thorough investigation (e.g. Browne & Cooper, 1950; Powell, 1956; Donovan *et al.* 1961; Griffiths *et al.* 1961; Lloyd, 1963; Curry *et al.* 1967; Wood & Woodland, 1968; Bullerwell & McQuillin, 1969; Davey, 1970; Blundell *et al.* 1971; Woodland, 1971; Naylor & Mounteney, 1975; Doré, 1976; Penn & Evans, 1976; Kamerling, 1979; Barr *et al.* 1981; Van Hoorn, 1987b; Tappin *et al.* 1994; Jackson *et al.* 1995; Meadows *et al.* 1997; Welch & Turner, 2000, Williams, 2002; Williams *et al.* 2005; Holford *et al.* 2005; Holford, 2006), the Mesozoic-Cenozoic evolution of these basins remains poorly resolved. This is largely a result of interspersed phases of post-Palaeozoic rifting, thermal subsidence and uplift (Tappin *et al.* 1994; Jackson *et al.* 1995; Welch & Turner, 2000; Holford, 2006), which have led to marked regional variations in the preserved stratigraphic record across the basins. The Jurassic and Cenozoic sequences in these basins are bounded by major

unconformities which attest to several regionally extensive phases of uplift and erosion during the Mesozoic and Cenozoic (Figure 3.2 and 3.3). The marked stratigraphical compartmentalisation between adjacent basins over relatively short distances can, to some degree, also be attributed to the complex pattern of NW-SE, NE-SW and E-W trending basement lineaments which cross the basins (Figure 3.4) (Welch & Turner, 2002). These were variously active during the Caledonian, Variscan and Alpine compressional episodes and the reactivation of basement structures in response to extensional stresses during the intervening periods played a key role in the generation of accommodation spaces for sediment accumulation.

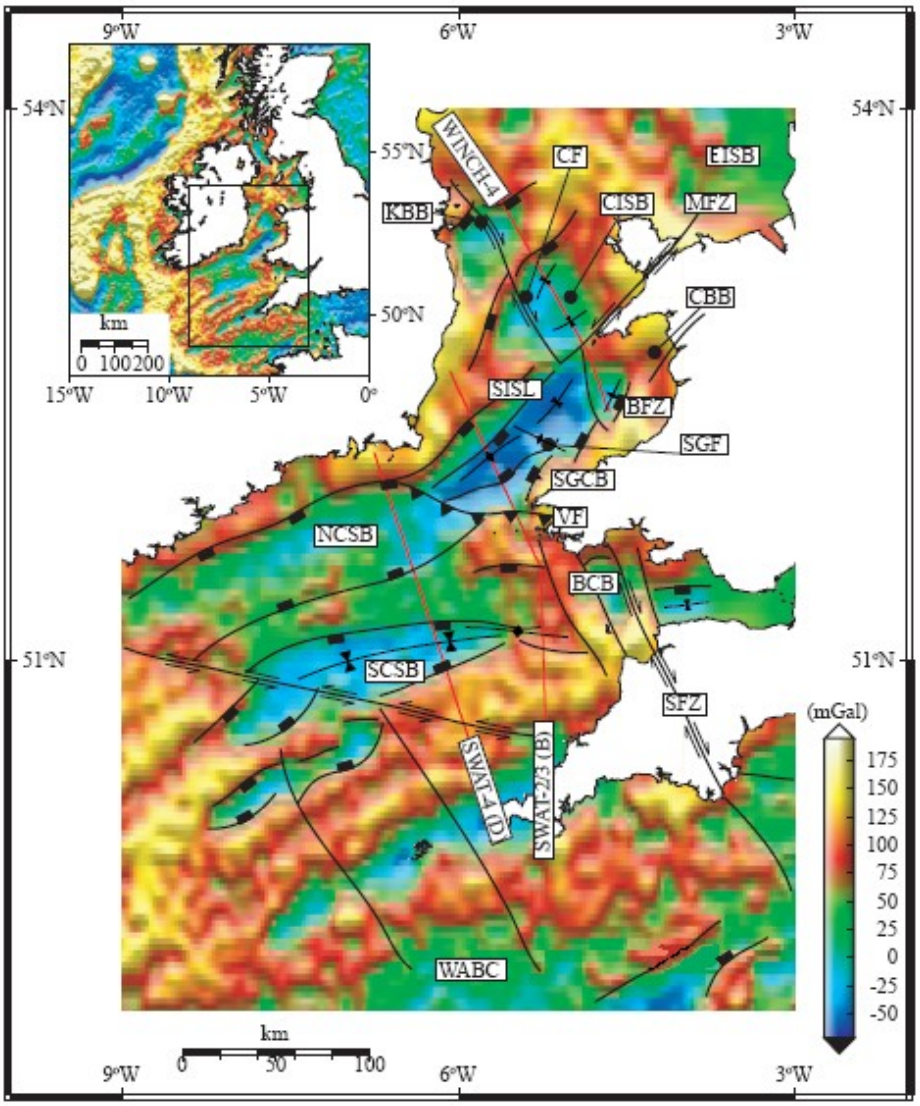

Figure 3.1 – Free-air gravity anomaly map of the offshore Western Shelves region. The gravity data are a compilation of ship track and satellite measurements sampled and gridded with one minute cell spacing, with artificial illumination from the north. Abbreviations: BFZ-Bala Fault Zone; BCB-Bristol Channel Basin; CBB-Cardigan Bay Basin; CISB-Central Irish Sea Basin; KBB-Kish Bank Basin; MFZ-Menai Straits Fault Zone; NCSB-North Celtic Sea Basin; SCSB-South Celtic Sea Basin; SFZ-Sticklepath-Lustleigh Fault Zone; SGF-St George's Fault; SGCB-St George's Channel Basin; SISL-South Irish Sea Lineament; WABC-Western Approaches Basin Chain. Also shown are selected deep seismic reflection survey lines (from Williams, 2002).

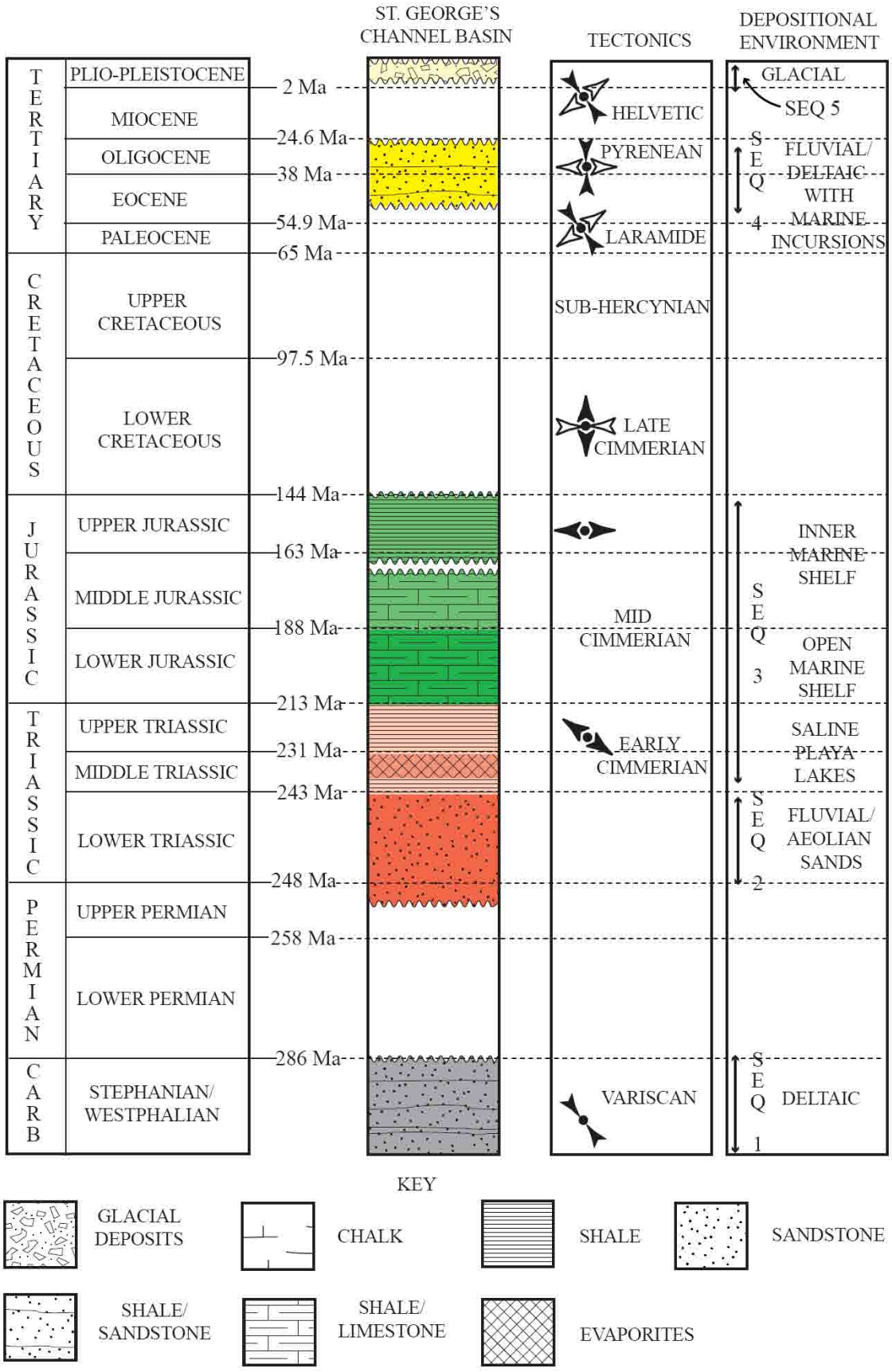

Figure 3.2 - Chronostratigraphic nomenclature, regional stress azimuths (Hibsch *et al.* 1995) and depositional environments (Ziegler, 1990) of the St. George's Channel Basin (after Williams, 2002).

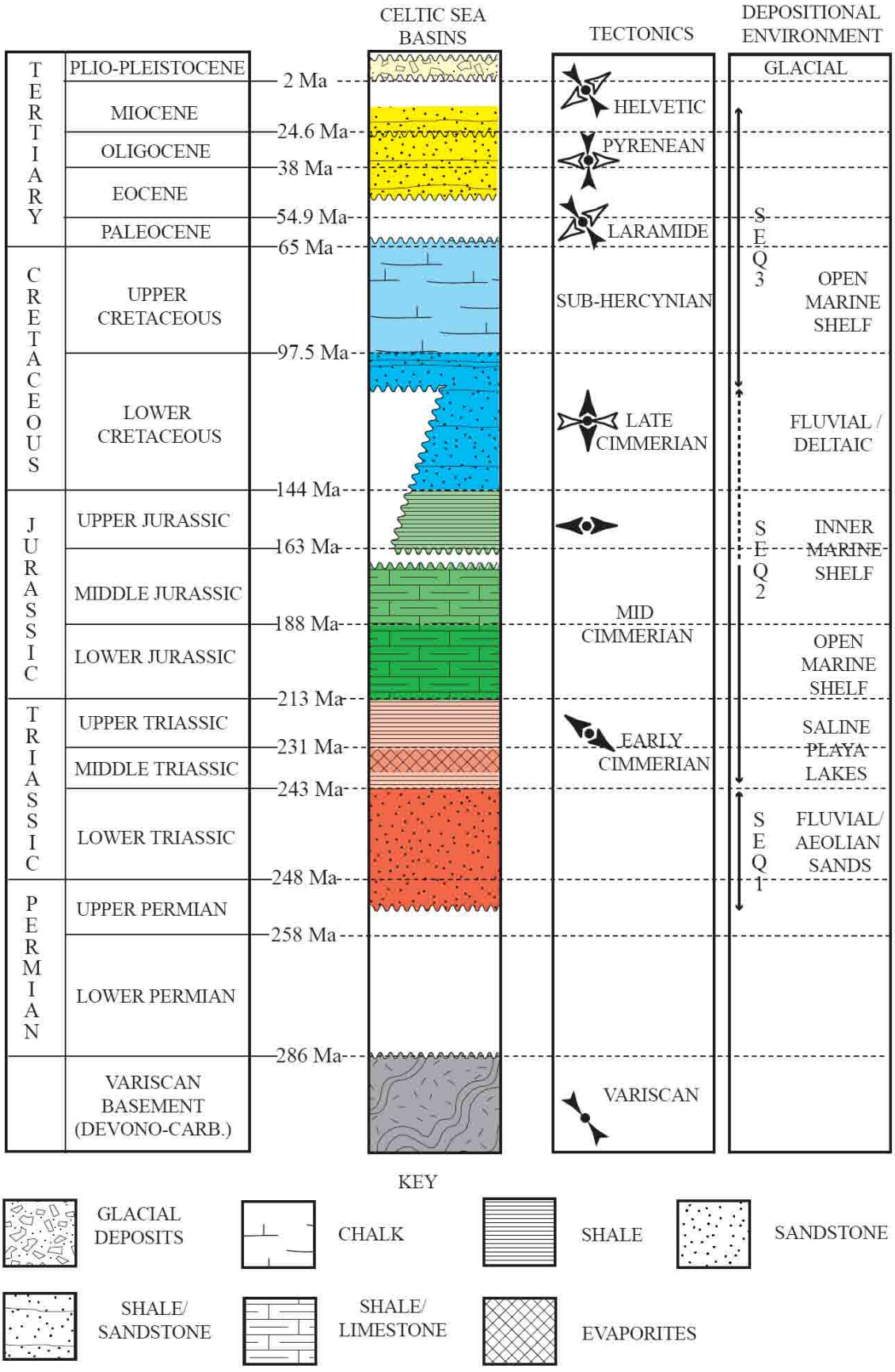

Figure 3.3 – Chronostratigraphic nomenclature, regional stress azimuths (Hibsch *et al.* 1995) and depositional environments (Ziegler, 1990) of the Celtic Sea basins (after Williams, 2002).

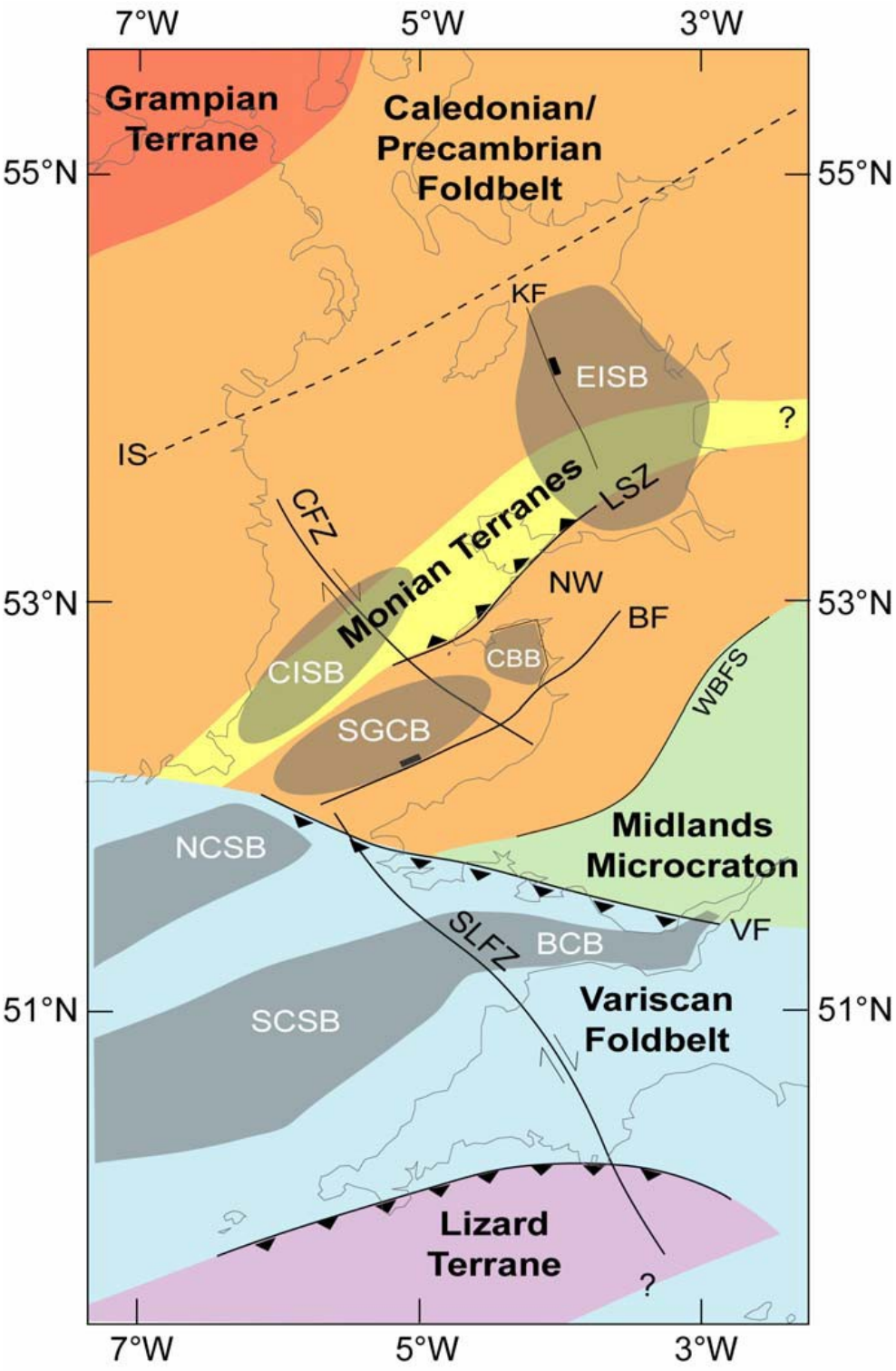

Figure 3.4 - Map showing terranes of the Caledonian and Variscan orogens in Britain and Ireland. The sedimentary basins of the western UK are underlain by various crustal blocks of varying age and mechanical properties, thereby exerting a profound structural heterogeneity on this region. The boundaries of these blocks are commonly marked by major, crustal-scale fault systems, a number of which have been highlighted along with other important crustal lineaments. Abbreviations: BF-Bala Fault; BCB-Bristol Channel Basin; CBB-Cardigan Bay Basin; CISB-Central Irish Sea Basin; CFZ-Codling Fault Zone; EISB-East Irish Sea Basin; IS-Iapetus Suture; KF-Keys Fault; LSZ-Lŷn Shear Zone; NCSB-North Celtic Sea Basin; NW-North Wales; SCSB-South Celtic Sea Basin; SGCB-St George's Channel Basin; SLFZ-Sticklepath-Lustleigh Fault Zone; VF-Variscan Front; WBFS-Welsh Borderland Fault System (after Bluck *et al.* 1992).

3.2: REGIONAL CRUSTAL STRUCTURE

The regional crustal structure beneath the SW UK has been described in detail previously and the interested reader is referred to Holford (2006) who presents a comprehensive review of the previous research and findings. What follows in this section is a brief summary based on Holford's (2006) review. The crust in the SW UK region can be viewed as comprising a number of suspect terranes whose exposed boundaries are marked by prominent fault systems of various kinds (Figure 3.4) (Bluck *et al.* 1992). Although the major tectonic character of the region reflects Mesozoic rifting, the Western Approaches-Celtic Sea basins inherited many of their structural characteristics from crustal-scale lineaments formed during Late Precambrian, Caledonian and Variscan orogenic episodes which shaped the Palaeozoic 'basement' and in many cases, controlled the nucleation of the later extensional basins (Gibbs, 1987; Sibuet *et al.* 1990; Dyment *et al.* 1990; Dyment & Bano, 1991; Ford *et al.* 1992; Naylor *et al.* 1993). During the Caledonian orogenic cycle, basement crust underlying the Celtic Sea formed part of the northern margin of the Gondwana continent. Palaeozoic rocks of Cambrian to Devonian age outcrop along the margins of the major basins and record the formation and destruction of the large Lower Palaeozoic Welsh and Irish basins. Post-Caledonian orogenic collapse led to crustal extension, which reactivated pre-existing Caledonian lineaments to form a network of small graben in the hanging wall of major structures such as the Johnston Thrust (Shannon, 1991; Tappin *et al.* 1994). North-directed late Carboniferous Variscan compression caused significant crustal shortening in the southern Celtic Sea region, initiating oblique transpressional reactivation of major basement lineaments such as the Bala Fault (Figure 3.5) (Fitches & Campbell, 1987; Corfield *et al.* 1996).

The acquisition of numerous deep multichannel seismic reflection profiles by the British Institutions' Reflection Profiling Syndicate (BIRPS) during the 1980's enabled significant

advances in the understanding of crustal structure in the south-western UK to be made (e.g. Beamish & Smythe, 1986; BIRPS & ECORS, 1986; McGeary *et al.* 1987; Coward & Trudgill, 1989; England & Soper, 1997). Traverses covering the Western Approaches-Celtic Sea basin system include SWAT profiles 2-11 (e.g. Figure 3.7; Klemperer & Hobbs, 1991). Data were recorded to 15 seconds two-way travel time (twtt), imaging reflectors from beneath the Moho, which lies at depths of between 28 and 32km within this study area (Figure 3.6; Chadwick & Pharaoh, 1998).

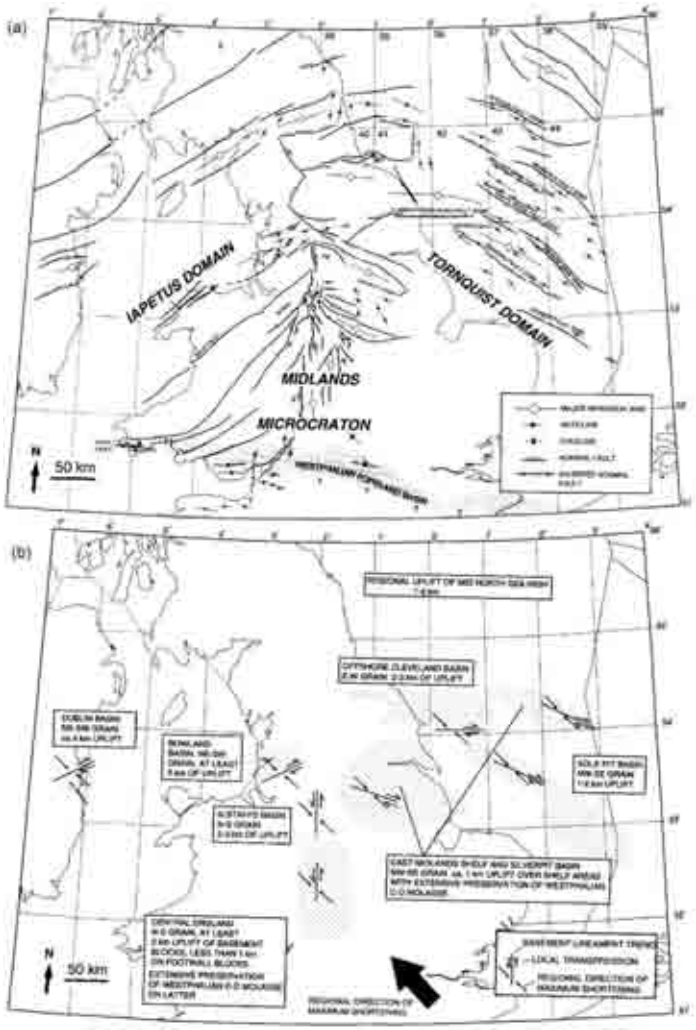

Figure 3.5 - (a) Variscan inversion tectonics and other structural elements of the British Isles and Ireland. Key: ML-Malvern Lineament; PL-Pendle Lineament; PM-Pennine Monocline; W/RRF-Wem/Red Rock Fault. (b) Summary map illustrating the variation in the amount of tectonic uplift and transpression relative to the regional direction of maximum shortening for inversion on the Variscan foreland. Basins trending NE-SW were roughly perpendicular to the NW-SE to NNW-SSE regional direction of maximum shortening and hence experienced strong inversion. Basins with N-S and NW-SE oriented controlling faults were oriented more obliquely to the direction of maximum shortening and as a consequence experienced less uplift and deformation (after Corfield *et al.* 1996).

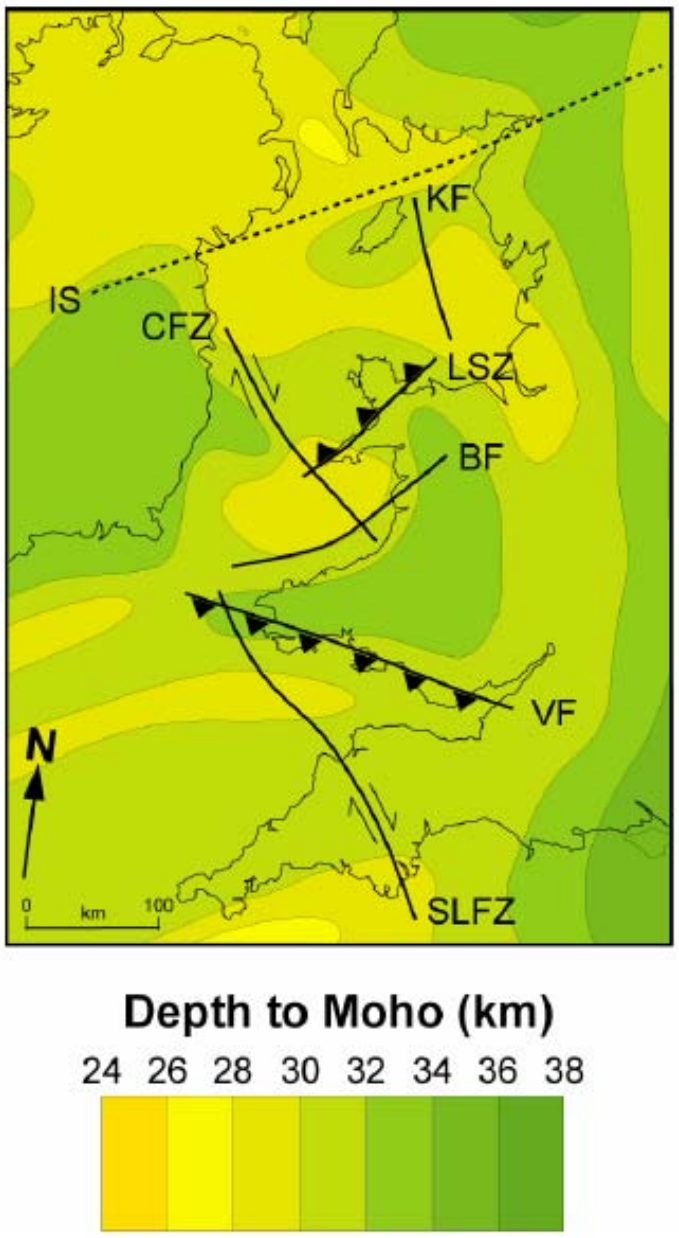

Figure 3.6 - Map showing depth to the seismic reflection Moho beneath the western UK region, This map indicates that crustal thicknesses in this region vary between c. 28 and 34km, with areas underlain by shallow Moho reflecting zones of crustal thinning (i.e. mostly offshore, Mesozoic-Cenozoic sedimentary basins such as the SGCB, EISB and Celtic Sea basins), and deeper Moho overlain by mostly onshore, Palaeozoic basement massifs in Wales, Ireland and Northern England (modified after Chadwick & Pharaoh, (1998) and Dèzes & Ziegler, (2002)).

Within the SCSB-BCB region, deep seismic reflection profiles reveal a number of prominent crustal structures which have played an important role in basin evolution in this area. A series of geological cross-sections through the western UK region, based mainly on deep seismic reflection are presented in Figure 3.8.

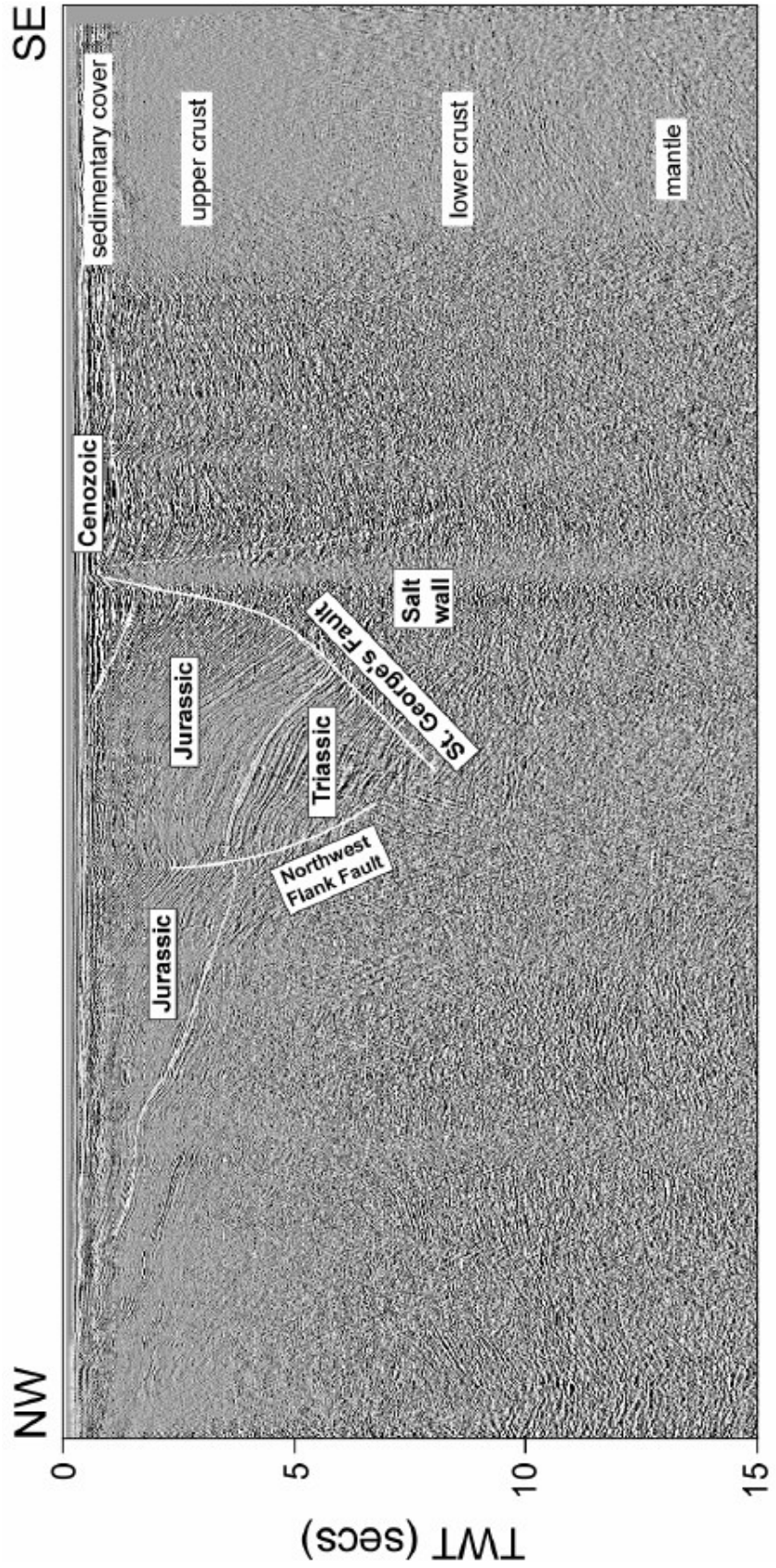

Figure 3.7 - Part of the BIRPS SWAT2 deep seismic reflection profile through the St. George's Channel Basin illustrating the structure of this basin and the seismic characteristics of the lithosphere beneath the Irish Sea basin system (after Williams, 2002).

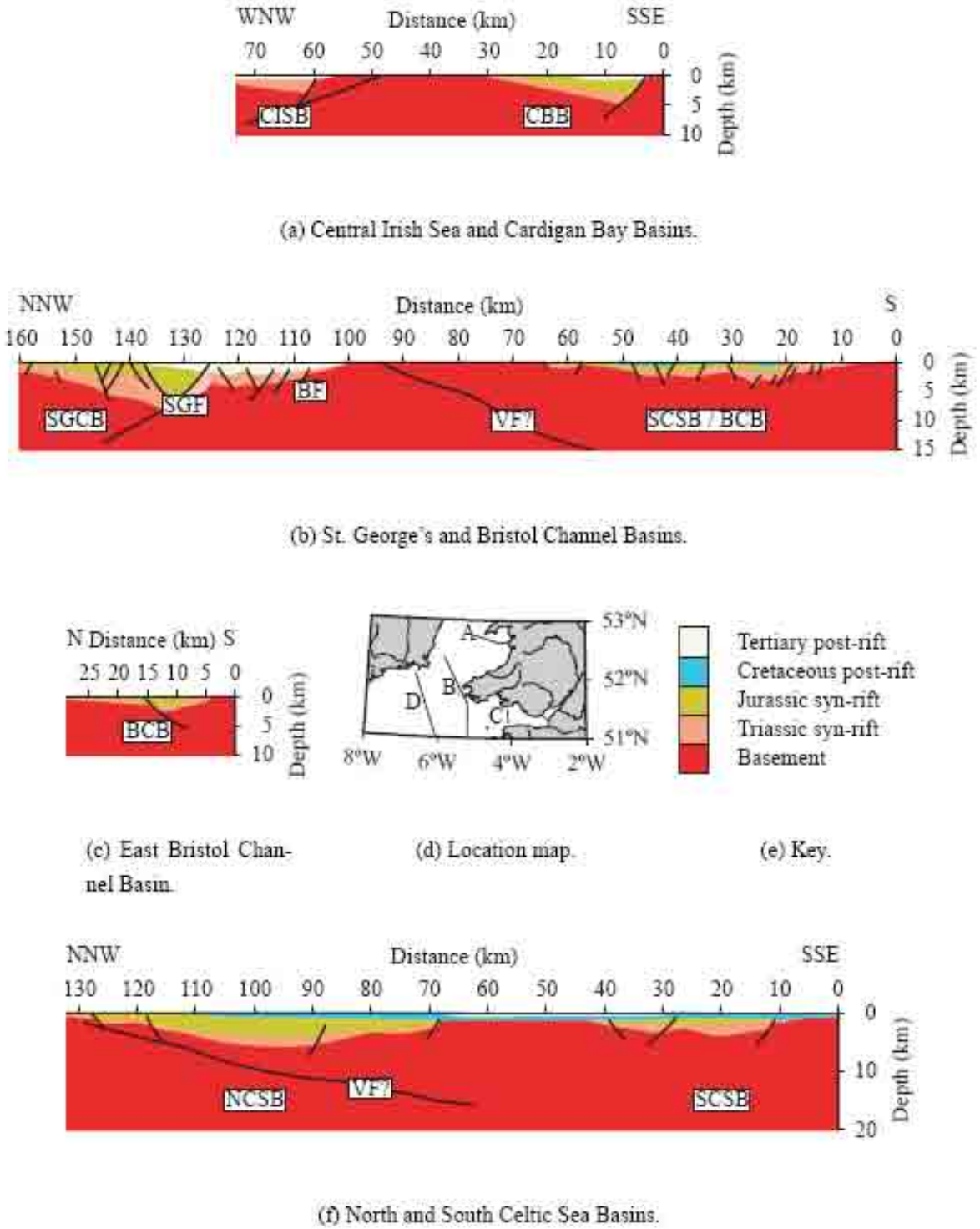

Figure 3.8 - Geological cross-sections through the principal basins of the Irish and Celtic Seas, based on depth conversions of BIRPS and BGS seismic data. (a) Central Irish Sea and Cardigan Bay basins. (b) St. George's and Bristol Channel basins. (c) Bristol Channel Basin. (d) North and South Celtic Sea basins (after Tappin *et al.* 1994).

3.3: TECTONO-STRATIGRAPHY OF THE WESTERN APPROACHES-CELTIC SEA BASIN SYSTEM

The main structural framework of southwest England formed in Devonian and Carboniferous times. The pre-Mesozoic evolution of the SW UK is largely beyond the scope of this thesis the interested reader is referred to Badham (1982); Ziegler (1982); Coward & Smallwood, (1984); Cazes & Torreilles (1988); Evans (1990); Tappin *et al.* (1994) and references therein for a complete account.

The Variscide basement of southern England comprises rocks which are folded, faulted and cleaved with an approximate east-west trend. Several major thrust zones can be identified within the region both at outcrop and in the sub-surface from seismic reflection profiles. The thrusts are commonly offset by strike slip faults. These may have formed during thrusting as transfer faults; alternatively they may be a very late Variscan feature displacing the earlier thrusts (Figure 3.9). South of the Variscan front (Figure 3.9) from the Mendip Hills and the southern margin of the London platform southwards, the marginal normal faults bounding the Wessex Basin may overlie Variscan thrusts which have been inferred from interpretation of seismic reflection profiles (Chadwick, 1983). Basin margin faults in this area are regarded as the consequence of extensional reactivation of these earlier thrust structures developed in the Variscan basement. Thus these Permian and Mesozoic basins are thought to lie above the former Variscan upthrust areas. It is also notable from Figure 3.9 that these bounding faults are not continuous structures but are offset both sinistrally and dextrally. These offsets in basin margins may overlie pre-existing transfer zones offsetting the thrust faults in the Variscan basement.

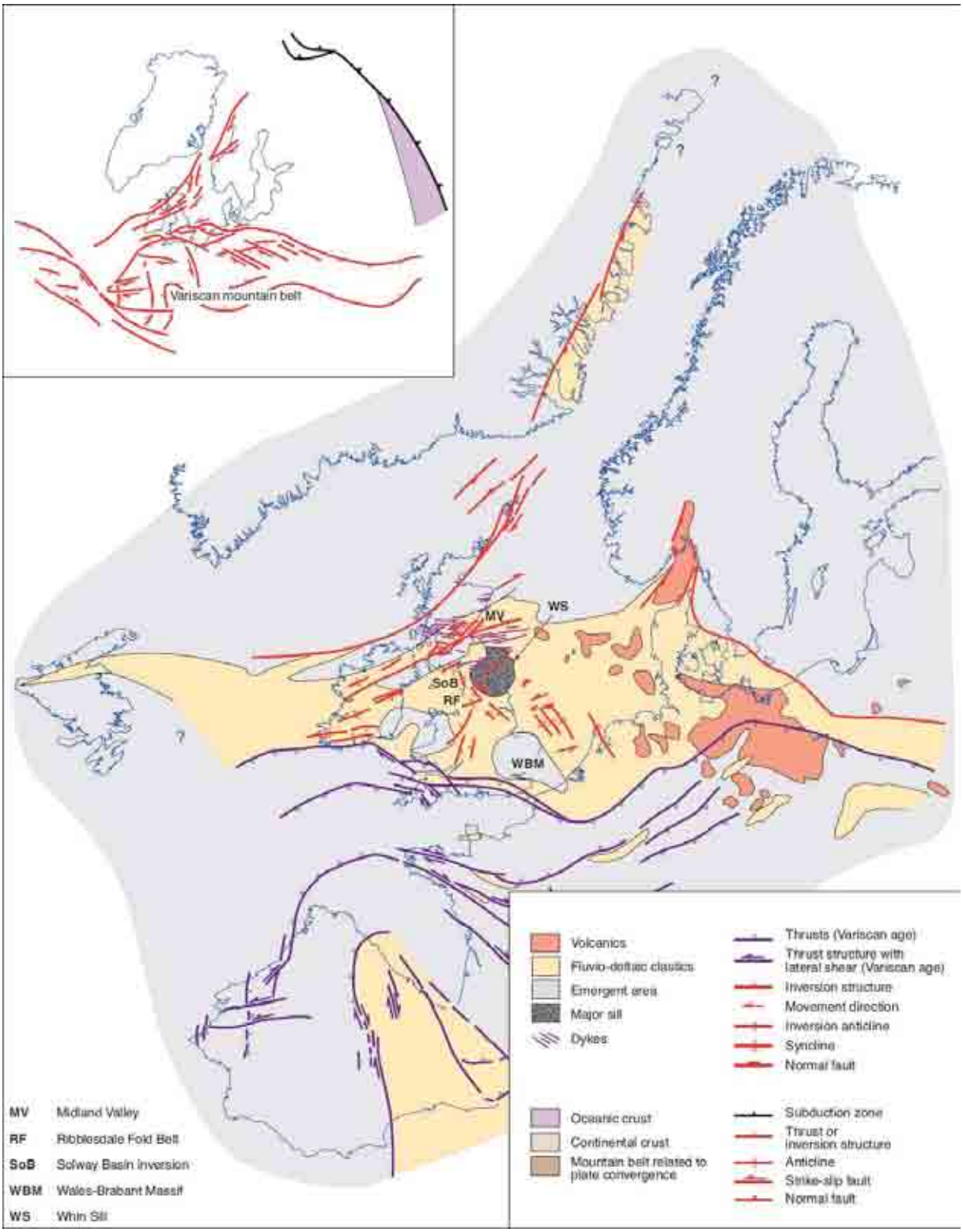

Figure 3.9 – Late Carboniferous palaeogeography showing the major structural features of the basement of England and Wales (after Coward *et al.* 2003). The inset shows the Late Carboniferous structures of NW Europe.

3.3.1: PERMIAN

In early Permian times a period of crustal subsidence was initiated which continued with only minor interruptions until the end of the Cretaceous. A system of rifts started to fracture the newly formed Pangaean Supercontinent. By Triassic time's, extension of the crust along these lines of weakness led to the formation of sedimentary basins across southern Britain and surrounding areas (Chadwick, 1985, 1986; Hillis, 1988; Coward *et al.* 2003). The rifts formed along the reactivated Variscan thrusts and northwest trending dextral strike-slip faults. The basins were part of an Arctic-North Atlantic rift system (Figure 3.10) linked with the development of basins in the Bay of Biscay and Rockall trough (Ziegler, 1987*a*). Regional and temporal variations in the rate of subsidence often associated with major normal faulting controlled the distribution of the Permian and Mesozoic basins and the nature of the sediments within them. In the area of the Western Shelves and the English Channel, Permian-Triassic red beds attain substantial thicknesses as indicated by reflection seismic data that are calibrated by a limited number of wells, paleontological control however, is generally poor. The absence of Late Permian marine deposits renders it difficult to subdivide this series and therefore palaeogeographic reconstructions for Early and Late Permian times have to remain conceptual (Figure 3.11) (Ziegler, 1990).

In south-western England, post-Variscan orogeny volcanic rocks are of early Permian age but the accumulations of the main overlying red-bed sequences did not commence until the late Permian (Warrington & Scrivner, 1988). This continental clastic sequence, consisting partly of wind-blown sands was deposited in initially separated basins that later began to coalesce. The main depocentres were the Wessex Basin and probably also the Channel Basin (Ziegler, 1990). As subsidence slowed there may have been a period of non-deposition prior to the onset of Triassic subsidence. The regional unconformities on seismic may be associated with

this (Evans, 1990). In southern Britain Permian subsidence can be related to the process of lithospheric extension.

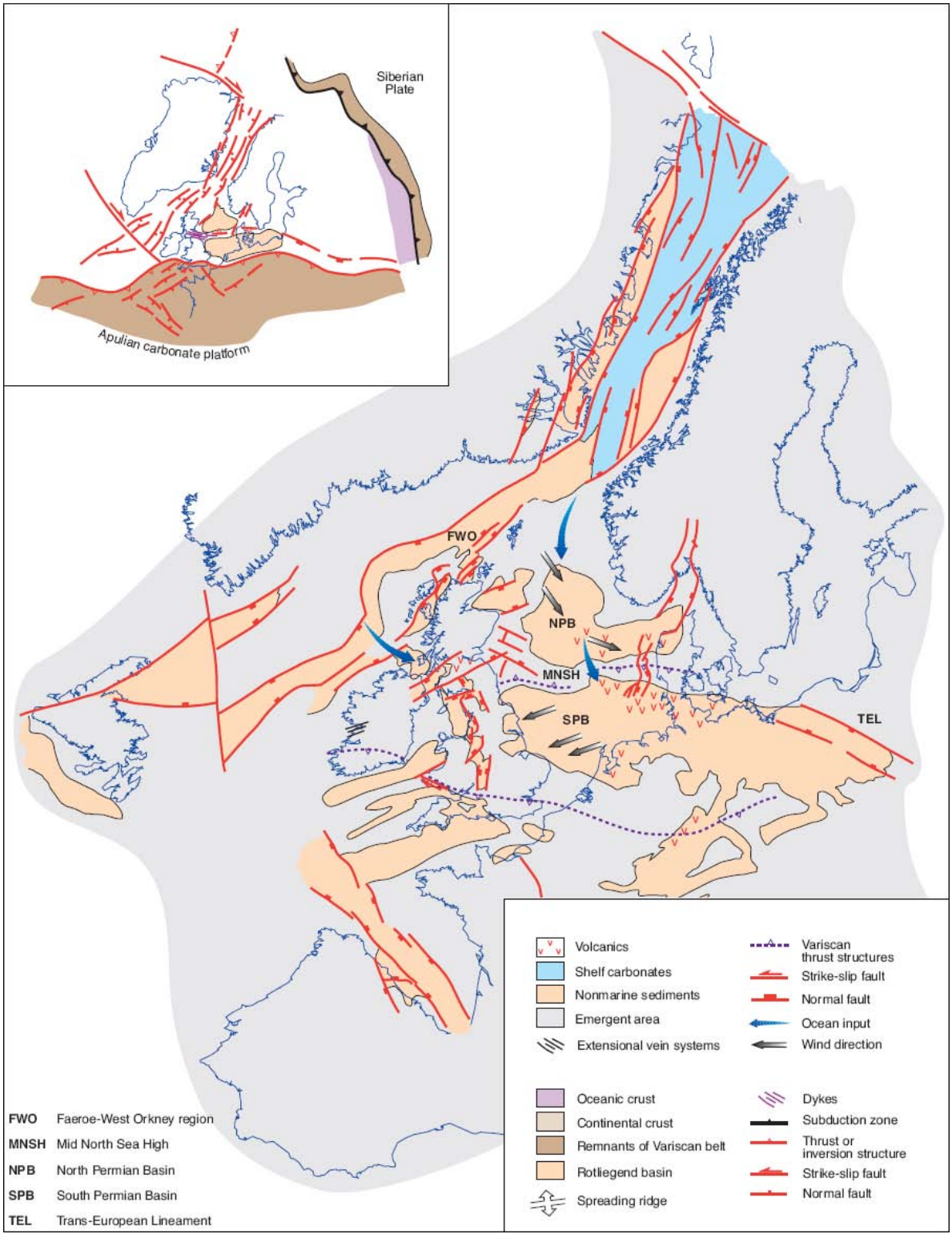

Figure 3.10 – Early Permian framework of the Arctic-North Atlantic domain showing the active structures and sediment facies. Principal areas of subsidence (deposition) are shown in the tan colour. Inset shows the latest Carboniferous to early Permian structures in NW Europe (after Coward *et al.* 2003).

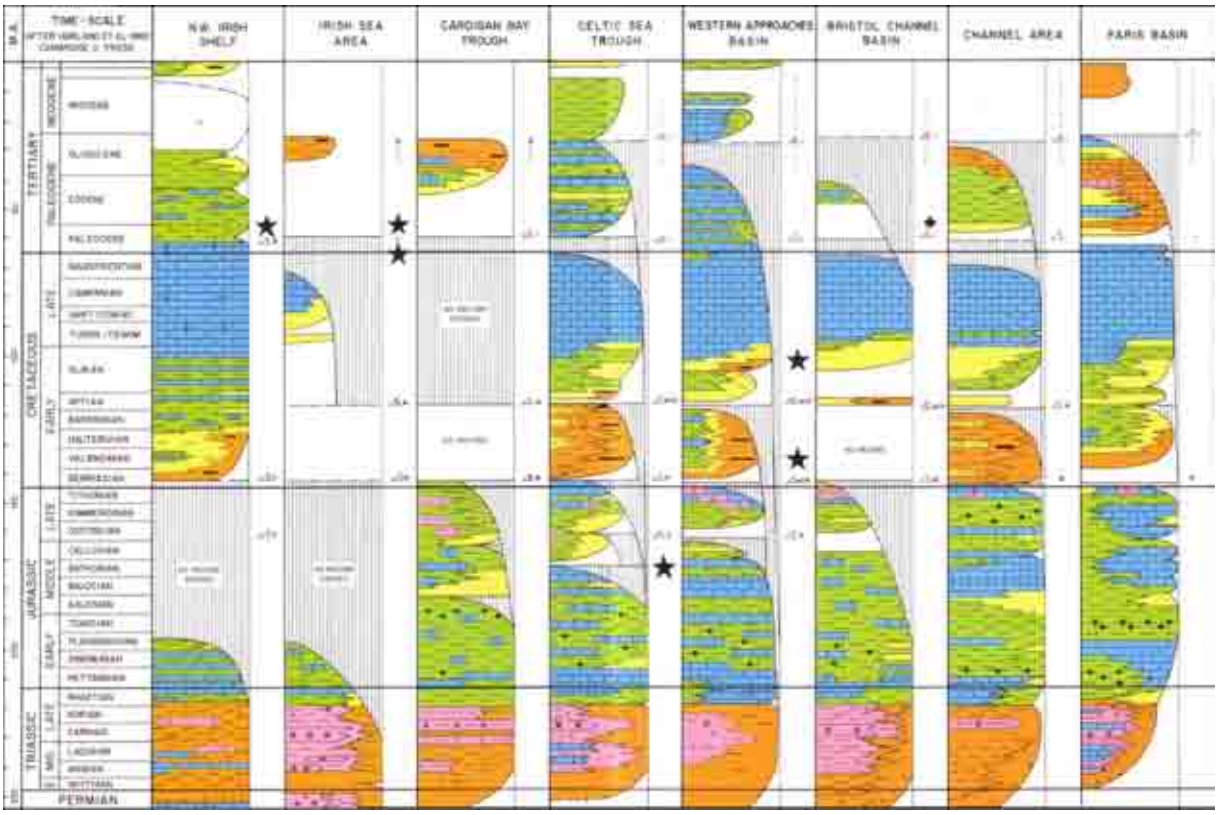

Figure 3.11 – Stratigraphic correlation chart of the Mesozoic-Cenozoic for the Western Shelves area. Key: Star – local volcanics; + - Batholiths; < - unconformity; Depositional Environments: Orange – Continental, lacustrine; Green – shallow-marine shales; Brown – Deep-marine clastics; Pink – evaporate; yellow – deltaic, coastal and shallow-marine clastics; light blue – Deep marine shales; Blue - carbonates (after Ziegler, 1990).

Normal faulting led to the accumulation of thick sequences of supposed Permian age in the Crediton trough and Dorset Basin (Figure 3.10). Resolution of the dip-slip vectors on the faults within these basins suggests lithospheric extension in a northwest-southeast direction (Chadwick, 1985).

In the WAB, Permian-Triassic sediments reach thicknesses of up to 5000m (Ziegler, 1990). Limited well control indicates that Early Permian conglomerates and volcanics are overlain by shaly red beds and a probable Late Permian sequence of up to 2000m of sand and shales (Ziegler, 1987*c*; Chapman, 1989). Deep reflection seismic data over the Permian Plymouth Bay Basin, located at the north-eastern termination of the WAB, show that subsidence of this basin, after an initial fault controlled phase, was governed by regional crustal down warping

(Pinet *et al.* 1987). A similar pattern is evident from reflection seismic data for the Melville Basin, which is located in the south-western part of the WAB (Chapman, 1989). The northern part of the Melville Basin remained a high throughout the Permian and did not receive any sediment until the Triassic subsidence phase. Likewise the Permian sediments in the southwest Channel and Brittany basins are thin and these basins may also have been end-Variscan topographic highs (Evans, 1990). The early Permian sediments in the southern part of the Melville Basin and the Plymouth Bay Basin were deposited in Variscan intermontane troughs with contemporaneous volcanics that were related to the final phases of the granite batholiths. The loading of Permian sediments on the crust amplified the initial magnitude of the topographic low in the southern part of the Melville Basin to accommodate up to 4km of sediments (Evans, 1990). Chapman (1988) dates the initiation of rifting in the Melville Basin as early Permian but unequivocal evidence for crustal extension of this age is lacking in many basins in the North Atlantic region (Masson & Miles, 1986).

The SCSB-BCB may also have started to subside during the Early to Late Permian and probably corresponded initially to a topographic depression in which Permian alluvial-fan deposits accumulated as known from outcrops on the Cornubian Platform (Van Hoorn, 1987*b*). In the NCSB a seismically defined basal clastic unit that is not calibrated by wells is thought to be of Permian age (Tucker & Arter, 1987; Petrie *et al.* 1989).

The Wessex Basin is characterised by a fairly complete Permian to Cretaceous sequence though with considerable local variation in sediment thickness, facies and stratigraphic preservation. The basin is transected by several east-west trending zones of normal faults. These fault zones which commonly comprise several individual normal faults showing 'en échelon' offsets allow subdivision of the Wessex Basin into smaller basins and highs. These faults were active from Permian to early Cretaceous times, down throwing strata to the south

and profoundly affected patterns of sedimentation. This is evidenced by the exposed western edge of the Dorset Basin where a thick sequence of continental red bed sediments containing volcanic rocks dated at 280-290Ma (Warrington & Scrivner, 1990) are preserved in the Crediton Trough and near Exeter. Elsewhere the subsurface distribution of Permian strata is not well known though deep borehole information indicates marked thickness changes indicative of an early graben system (Whittaker, 1985). However the predominantly argillaceous nature of the Permian sequence suggests that for much of the interval subsidence was regional with little contemporaneous fault activity.

Permian and Mesozoic subsidence in many of the basins in England and Wales is similar to that predicted by McKenzie (1978). Figure 3.12 illustrates a step-by-step backstrip of a typical succession found within the Dorset Basin. Deposition of sediment within each stratigraphical interval is triggered by an isostatically driven subsidence of the basement surface. Early in the development of the sedimentary basin (e.g. Permian) the thickness of sediment deposited is very similar to the amount of basement subsidence. Later in the basin's development, compaction under loading of the earlier sediments allows the accumulation of a thickness of new sediment considerably greater than the basin subsidence (e.g. between end-Albian and end-Maastrichtian times the basement subsidence was barely more than half the thickness of Chalk deposited). A simplified crustal subsidence history for the Dorset Basin is shown in Figure 3.13.

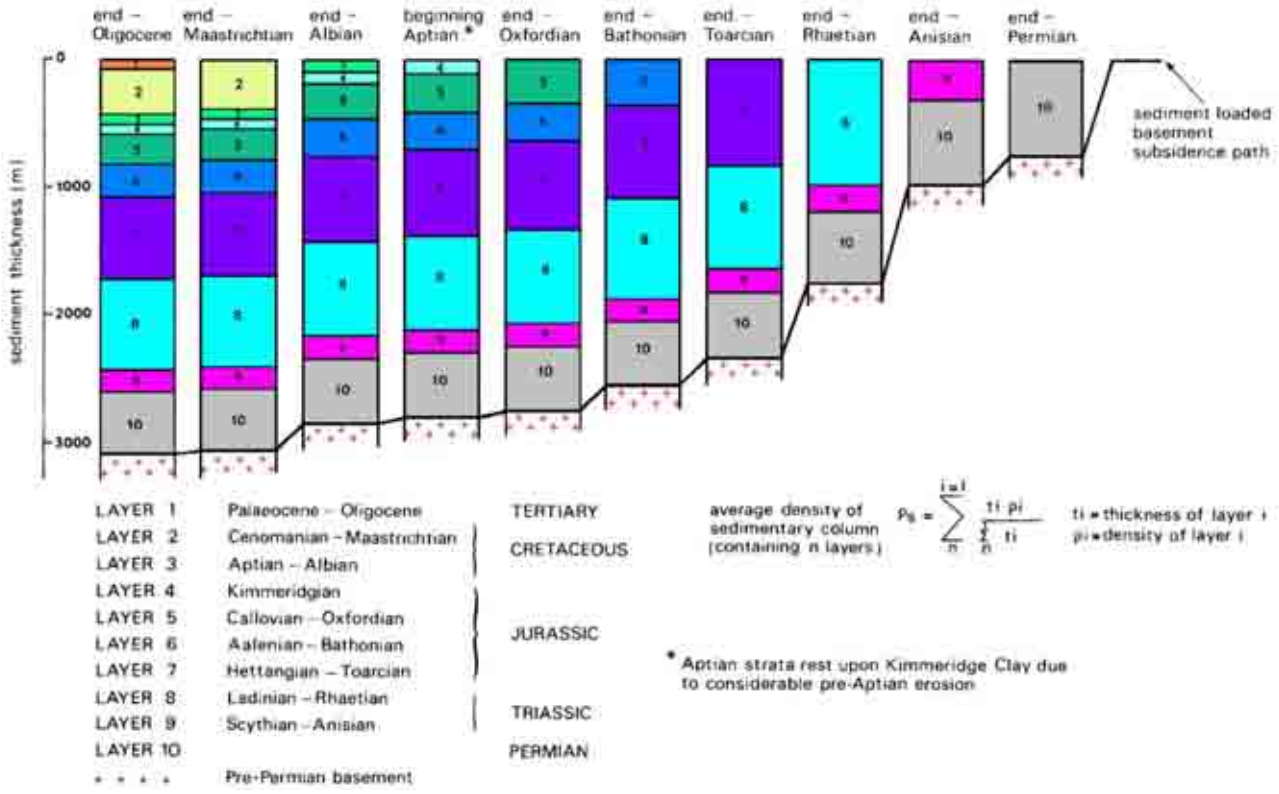

Figure 3.12 – Decompaction of a sedimentary sequence (Dorset Basin) by back-stripping (after Whittaker, 1985)

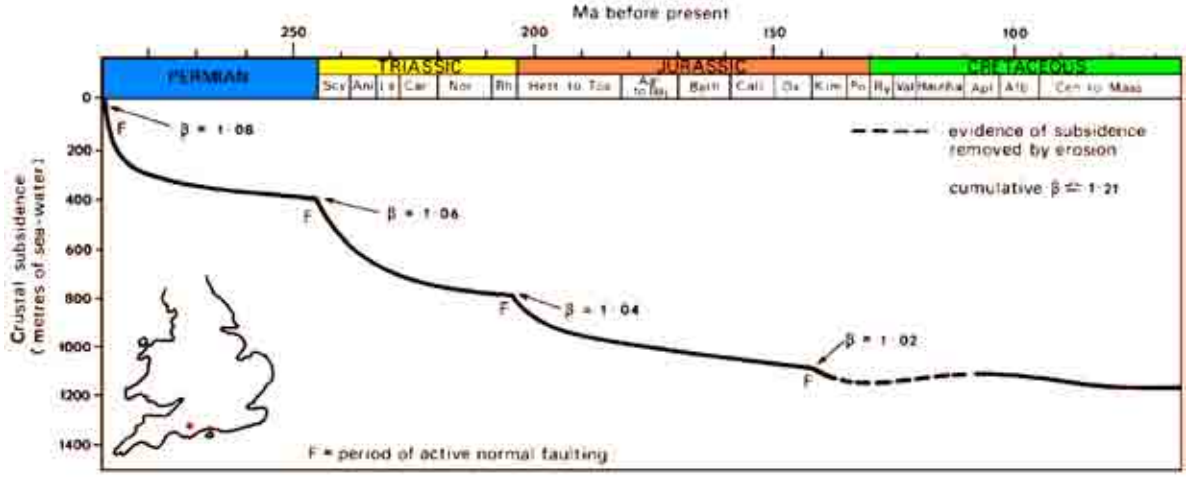

Figure 3.13 – Crustal subsidence history curve for Dorset Basin (after Whittaker, 1985).

3.3.2: TRIASSIC

In Western and Central Europe, the latest Permian-earliest Triassic corresponds to a period of regional regression of the Arctic Sea and the inception of a complex multi-directional rift system that transected the Variscan fold belt and the continuously subsiding Northern and Southern Permian Basins (Figure 3.10) (Ziegler, 1990). In the Arctic-North Atlantic, Central Atlantic and Tethys domains, Triassic regional stress fields affected wide areas around the future diverging plate margins that came into evidence during the Jurassic, Cretaceous and Early Cenozoic (Ziegler, 1990). This was particularly the case in Western and Central Europe where the build up of tensional stress patterns caused the extensional reactivation of the Permian-Carboniferous fracture systems; as such, they played an important role in the localisation of Triassic grabens in Western and Central Europe.

During early Triassic times renewed crustal extension led to a strongly rejuvenated fault scarp topography and the deposition of coarsely arenaceous sediments. Major faults active at this time include the Lyme Bay-Portland and Central English Channel faults with over 1000m and up to 800m of syn-depositional throw respectively (Hamblin *et al.* 1992). To the south of these faults the Portland-Wight Basin and the Central English Channel Basin developed as deep asymmetric graben. In late Triassic times fault activity gradually declined, surface topography diminished and argillaceous and evaporitic sediments were deposited. Permian-Triassic subsidence was concentrated in the western part of the Wessex-Channel Basin with up to 3000m of sediment preserved in the western portion of the Portland-Wight Basin and up to 2000m in the Dorset Basin. In many places erosion of the upthrown blocks coupled with rapid subsidence and tilting of the downthrown blocks led to the development of a minor unconformity at the base of the Triassic sequence. This unconformity is seen in many boreholes in southern England (e.g. Wytch Farm oilfield).

Viewed in the broader context of the Arctic-North Atlantic and Tethys rift systems, the area that was affected by extensional tectonics during the Triassic reaches from the Polish Trough in the northeast over a distance of 2000km to the Atlas grabens of Morocco and Algeria in the southwest and from the Grand Banks of eastern Canada in the northwest over a distance of 3500km to the margins of the Tethys Ocean in the southeast (Ziegler, 1990). It is inferred that the driving mechanism underlying the evolution of the Triassic rift systems that developed in the core of Pangaea is provided by gradually developing upwelling asthenospheric convection systems (Ziegler, 1990).

The Plymouth Bay Basin is almost circular in plan and has a particularly thick Permian-Triassic sequence (>9km) that shallows south against the Ouessant-Alderney fault zone. The basin overlies a southerly dipping crustal detachment zone related by Pinet *et al.* (1987), to an easterly extension of the Lizard Thrust. Major faulting and block tilting is absent and the basin in-filled a gradually subsiding crustal sag (Whittaker, 1985). The continuity of the Variscan thrust underlying the basin demonstrates that the lower crust did not undergo excessive horizontal extension during basin formation which implies that the form cannot be related easily to any rifting process (Evans, 1990).

The SCSB also formed along reactivated thrusts during the Permian-Triassic rifting. The basin contains up to 3.3km of Permian to Jurassic strata arranged in a series of synclinal faulted grabens. Seismic sections show a series of ENE oriented normal faults delimiting the southern margin of the basin (Van Hoorn, 1987). Gardiner & Sheridan (1981) equate this system of south easterly trending faults with the reactivation of underlying faults that are related to the south-westward extension of the Variscan Cannington thrust, which runs along the southern side of the Bristol Channel. The NCSB differs from basins to the NE in that Permian-Triassic sedimentary fill is generally much thinner than the overlying Mesozoic

strata (Tucker, 1987). Strongly fault controlled the Permian-Triassic sequence is locally in excess of 3000m thick but is generally less than 2000m thick. Compared with the WAB, the NCSB, SCSB, CBB and Haig Fras Basin grabens subsided somewhat more slowly during the Triassic (Ziegler, 1990). Based on limited well control, Lower Triassic sediments in these basins appear to consist of conglomerates and sandstones. These clastics pass up wards into Middle and Late Triassic evaporate playa-lake mudstones. Limestone stringers, representing possible Muschelkalk equivalents (Ziegler, 1990), have been encountered only in wells drilled on the Fastnet Basin, which is located at the south-western termination of the Celtic Sea Basin (Figure 3.14). Halites of presumed Ladinian and Carnian age occur in the Celtic Sea, Cardigan Bay and Bristol Channel basins. There is no evidence for syn-depositional Triassic volcanic activity in these basins, in which Triassic strata attain maximum thicknesses in the range of 2000-3000m (Kamerling, 1975; Robinson *et al.* 1981; Naylor & Shannon, 1982; Van Hoorn, 1987*b*; Tucker & Arter, 1987; Petrie *et al.* 1989).

Active normal faulting continued during the deposition of the Mercia Mudstone Group particularly along the marginal faults of the major basins. Adjacent to these faults are marginal breccias and conglomerates such as the Dolomite Conglomerate of the Mendip Hills. The generally decreasing rates of basin subsidence through the Triassic together with the tendency for younger formations of the Mercia Mudstone Group to overlie earlier ones suggest that a large proportion of later Triassic subsidence can be attributed to thermal relaxation effects inherited from the Scythian (and Permian) extensional pulses. However exposures on the Somerset coast and in the Mendip Hills suggest a renewal of normal faulting towards the end of Triassic times. In the Penarth Group small-scale growth faulting can be observed at outcrop at Lilstock, Somerset (Whittaker & Green, 1983) and there is some

further evidence of contemporary tectonic activity in that slumps are common in the Cotham and Langport members.

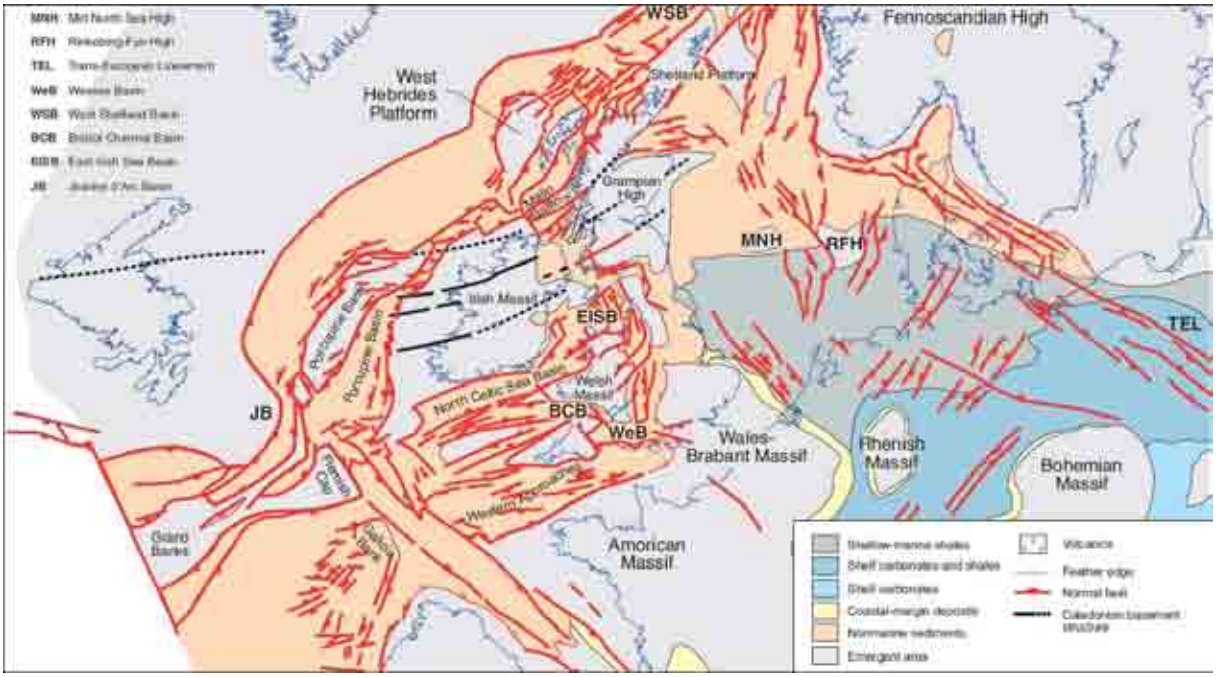

Figure 3.14 – Tectonic map of the Celtic Sea-Western Approaches area showing basin configuration and structural distribution from Mid-Late Triassic times (modified after Coward *et al.* 2003).

3.3.3: JURASSIC

Towards the end of Triassic times continued erosion and regional subsidence resulted in a change from continental conditions to a shallow marine environment in which a relatively uniform cyclical sequence of argillaceous and carbonate rocks was deposited. Renewed crustal extension in the early Jurassic led to important normal faulting and a change in depositional patterns as the loci of maximum subsidence shifted eastwards. In the Portland-Wight Basin the hitherto dormant Wight-Bray faults became active as the depocentre migrated east. Locally in the Western part of the basin above the Permian-Triassic depocentre listric normal faults developed detaching in the thick Triassic salt sequence. These listric faults are in marked contrast to the dominantly sub-planar normal faulting observed elsewhere. In Western and Central Europe, Lower Jurassic times were characterised by the

regional transgression of the Tethys Sea and the establishment of a broad, open-marine shelf sea that occupied much of the Paris Basin, the Celtic Sea-Western Approaches area, the Irish Sea, the central and southern North Sea, Denmark and Germany (Ziegler, 1990) (Figure 3.15). Well control in the Celtic Sea basins indicates that marine conditions were established during the Rhaetian as is evident from the deposition of shales and carbonates that persisted during the Hettangian. In the Fastnet Basin, Hettangian strata are developed in a shallow-marine carbonate facies (Millson, 1987; Ainsworth *et al.* 1987; Petrie *et al.* 1989).

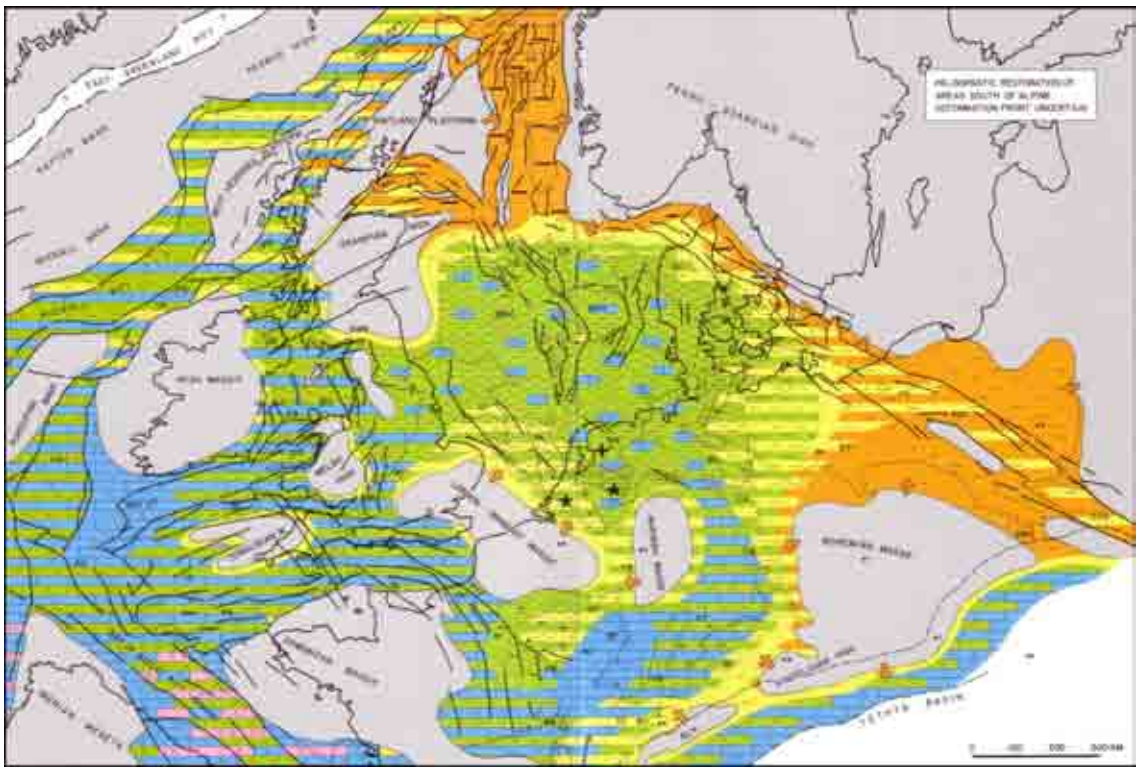

Figure 3.15 – Rhaetian-Hettangian palaeogeography (after Ziegler, 1990).

In the Channel and Wessex basins, Lower Jurassic sediments are developed predominantly in a shaly facies and contain only occasional carbonate and sand intercalations (Ziegler, 1990). Their thickness ranges from 300-500m. Subsidence of these basins was controlled by a system of east-west trending normal faults (Ziegler, 1990). These basins can be regarded as pull-apart features that developed between the left-stepping sinistral Sticklepath-Lustleigh and Pays-de-Bray Faults. Syn-depositional wrench faulting is evident by the development of the

anticlinal Mendip and Moreton-in-the-Marshes axis. Also the north-south trending Worcester Graben continued to subside during the Early Jurassic (Cope *et al.* 1980*a*; Holloway, 1985*b*; Sellwood *et al.* 1986; Lake & Karner, 1987).

In the Celtic Sea-Bristol Channel basins, Sinemurian to Toarcian strata consist predominantly of shales, marls and occasional limestones. In the axial parts of these rapidly subsiding grabens deeper water conditions gave rise to the deposition of partly kerogenous shales that have an oil source-rock potential. Clastic influx from the Irish, Cornubian, Amorican and Welsh massifs was generally at a low level although a few discrete regressive deltaic sands are evident for instance in the Fastnet and Bristol Channel basins during the Sinemurian and Pleinsbachian (Ziegler, 1990). Subsidence of these basins was accompanied by a progressive overstepping of their earlier margins (Kamerling, 1979; Millson, 1987; Van Hoorn, 1987; Tucker & Arter, 1987; Ziegler, 1987*c*; Petrie *et al.* 1989). Reflection seismic data indicate that Early Jurassic sediments attain thicknesses of up to 1500m in the Celtic Sea basins, 1000m in the BCB and 1500m in the WAB. The Mohcras borehole, drilled at the head of Cardigan Bay, penetrated 1300m of Hettangian to Toarcian shales (Barr *et al.* 1981; Holford, 2006). Despite the relatively high Early Jurassic rate of crustal extension across the Celtic Sea-Western Approaches area it is noteworthy that there is no evidence for contemporaneous volcanic activity (Ziegler, 1990).

The Jurassic and Early Cretaceous time span was characterised by major eustatic sea-level fluctuations (Vail *et al.* 1977; Hallam, 1978; Vail & Todd, 1981; Haq *et al.* 1987). In combination with increased tectonic instability of the Tethys and North Atlantic borderlands these gave rise to a number of regional unconformities, regressions and transgressions that can be correlated over large parts of Western and Central Europe (Ziegler, 1990).

During the Bajocian-Early Bathonian, crustal separation was achieved in the Central Atlantic and in the western Mediterranean domain. This important rifting event was paralleled by the upwarping of a major rift dome in the North Sea, from which erosion products were shed into the adjacent continuously subsiding grabens and troughs (Ziegler, 1990). In the Celtic Sea-Western Approaches area, control on the facies development of Aalenian to Bajocian sediments is limited to a relatively small number of wells. Bajocian and Bathonian open-marine shales, containing carbonate intercalations were deposited during a period of maximum transgression; there is no evidence for regional thermal doming of the area (Ziegler, 1990). However, accumulation of these strata was accompanied by continued crustal extension, which is emphasised by the occurrence of Bajocian olivine-diorite sills in the Fastnet Basin (Caston *et al.* 1981). Clastics derived from the Irish Massif occur in the Fastnet Basin and thick marginal marine sandstones, shed by the Welsh Massif were deposited in the CBB. Overall a general shallowing of the basins in the area is observed. Bajocian and Bathonian sediments attain maximum thicknesses of 800m in the CBB and 1000m in the south-western parts of the WAB (Barr *et al.* 1981; Robinson *et al.* 1981; Tucker & Arter, 1987; Van Hoorn, 1987*b*; Millson, 1987; Petrie *et al.* 1989).

By middle-late Jurassic times a tectonic regime of regional thermal subsidence had become established with only minor contemporaneous fault activity that increased gradually with time. During Bathonian and early Callovian times considerable subsidence took place in the Vale of Pewsey and Dorset basins. Differential subsidence in these areas associated with growth on faults is confirmed by differences in sequences encountered in deep boreholes. Farther south considerable growth took place on the Purbeck-Wight fault system giving a very thick Bathonian succession in the Central Channel Basin. Middle Jurassic sedimentation as a

whole continued the trend established in the early Jurassic of a gradually increasing area of deposition (Figure 3.16) accompanied by steadily declining subsidence rates (Figure 3.13).

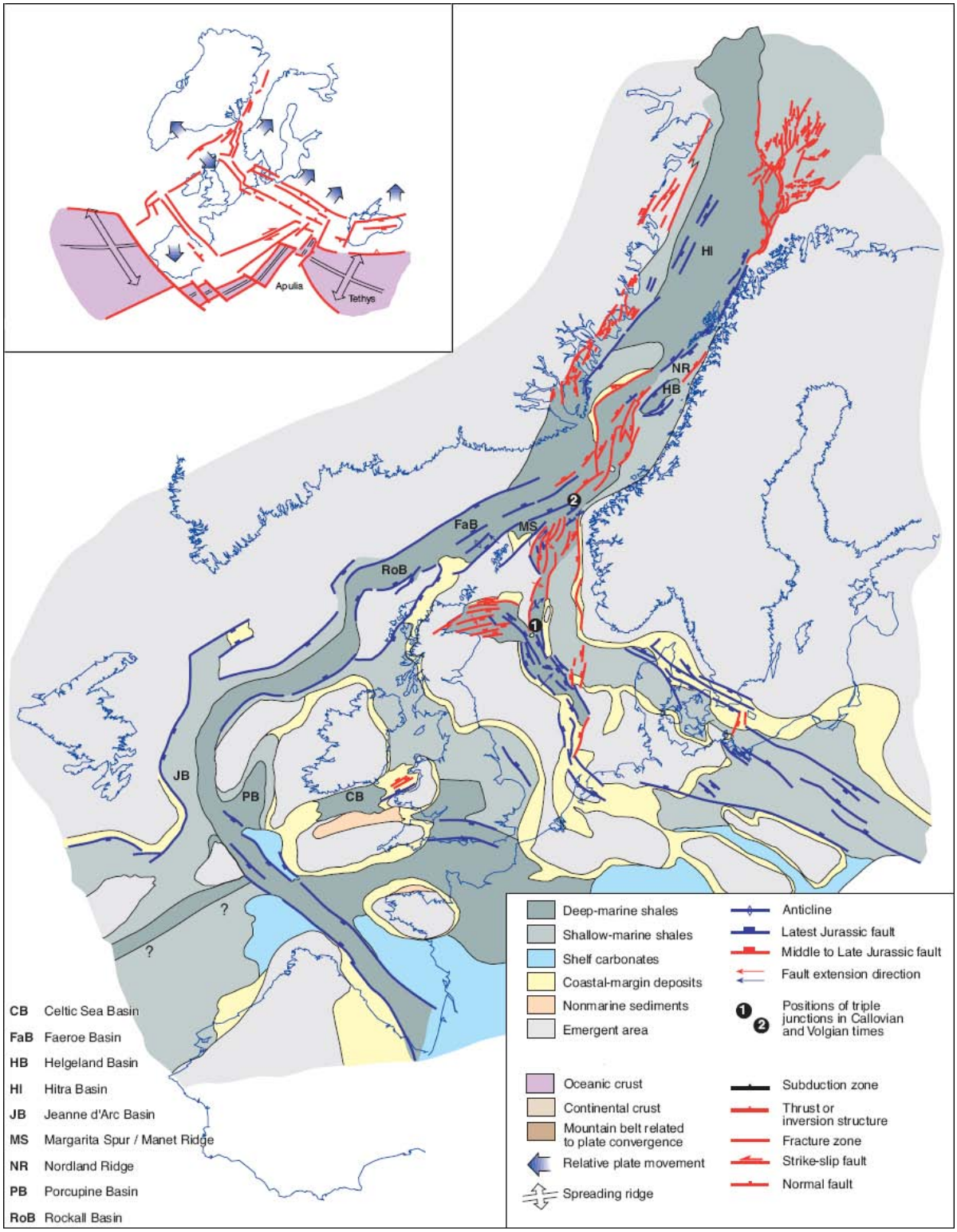

Figure 3.16 – Late Jurassic framework of Arctic-North domain showing the distribution of active structures and sediment facies (after Coward *et al.* 2003). Inset shows Latest Jurassic structures in Europe and the Mediterranean.

The late Middle and Late Jurassic evolution of the North Atlantic was governed by stress regimes that were similar to those of Bajocian and Bathonian times (Ziegler, 1990). Late Jurassic propagation of rifting into the Labrador Sea area is indicated by igneous activity in south-western Greenland and in the coastal areas of Labrador (Watt, 1969; King & McMillian, 1985). This suggests that tensional stresses built up at the northern termination of the Central Atlantic seafloor spreading axis between the Grand Banks-Flemish Cap and Iberia and in the area of the Bay of Biscay rift zone (Ziegler, 1990). During the Late Jurassic deep-water conditions became established in the axial zones of the Bay of Biscay rift, in the Porcupine Trough and probably also in the Rockall Trough and in the area of the Tagus Abyssal Plain (Figure 3.16). During the Callovian and Oxfordian, tectonic activity accelerated whereby differential movements between the Newfoundland Shelf and Iberia gave rise to wrench deformations that are reflected in the stratigraphic record of the Celtic Sea-Western Approaches basins.

Late Jurassic times saw a renewal of crustal extension with the Portland Wight basin subsiding rapidly along the London platform and Portland-Wight-Bray fault systems. In the Celtic Sea-Western Approaches area depositional patterns established during the Bajocian and Bathonian became disrupted by wrench movements during the early Callovian and again during the Oxfordian. Repeated partial uplift of basinal areas in the NCSB, SCSB, BCB and in the WAB where up to 2km of Permian to Jurassic sediments were eroded from the northern sub-basins gave rise to a system of unconformities that are, at least in part, correlative (Ziegler, 1990). The uplift was contemporaneous with the initiation of rifting on the continental margin. The uplift appears to have a symmetry centred on the Cornubian ridge. The basins immediately to the north and south of the ridge were subject to uplift during the late Jurassic-early Cretaceous but no significant unconformity can be traced in the NCSB.

The mechanism may have been focussed in the Cornubian ridge by the low density material within its batholiths (Hillis, 1988). In the southern basins of the WAB the magnitude of the local subsidence was much greater than that of regional uplift and up to 2.5km of sediments was rapidly deposited in a region which was undergoing broad uplift. Each of these hiatuses may correspond to a more or less discrete phase of deformation, however their significance is difficult to assess on a regional scale due to generally poor seismic resolution that does not always permit determination of the structural relationship between the respective depositional sequences. Local subsidence involving renewed reactivation of former Variscan thrusts and transfer faults also occurred while salt withdrawal in the Melville Basin served to preserve isolated Lias outliers. The faulted northern boundary of the Melville Basin formed at this time. The rapid accumulation of sediments in the southern basins of the WAB is related to sinistral strike-slip movement along the Ouessant-Alderney fault zone. Tectonic events were the result of lithospheric stresses related to the opening of the North Atlantic (Ziegler, 1987*a*). Within the Western Approaches area this has manifested as three events:

1. Middle Jurassic uplift of limited extent.
2. Major regional uplift towards the end of Jurassic times.
3. Localised rifting associated with strike-slip movement during the early Cretaceous.

During the Callovian and early Oxfordian, the clastic supply to the NCSB, SCSB, BCB, CBB and WAB increased; this reflects uplifting of the Irish Massif (Leinster Block), the Welsh Massif and the Amorican Massif and also the gradual emergence of the Cornubian Massif. In basinal areas, Callovian and Oxfordian shallow marine to lagoonal shales, partly containing carbonates, grade laterally into deltaic sands (Ziegler, 1990). After the mid-Oxfordian break, sedimentation resumed on a regional scale in the differentially subsiding NCSB, SCSB, CBB,

BCB and WAB with the deposition of shallow marine to lagoonal evaporitic shales and sands. Late Jurassic sediments attain thicknesses of up to 1500m in the Celtic Sea basins and 1000-1500m in the WAB (Kamerling, 1979; Barr *et al.* 1981; Van Hoorn, 1987*b*; Tucker & Arter, 1987; Millson, 1987; Ziegler, 1987*c*, Petrie *et al.* 1989). By late-Tithonian to early-Berriasian time, all basins shallowed out in response to falling sea-levels and a new phase of wrench induced deformation (Late Cimmerian unconformity (Ziegler, 1990)).

3.3.4: CRETACEOUS

The early Cretaceous evolution of Western and Central Europe was dominated, as in the Late Jurassic, by crustal extension across the Arctic-North Atlantic rift system. Consequently relatively few changes occurred in its structural framework and basin development continued along lines established during the Late Jurassic. However, major tectono-eustatic sea-level changes (Figure 3.17), as well as induced lithospheric deflections and the development of new thermal anomalies played an overriding role in the Early Cretaceous changes of basin outlines and sedimentation patterns (Ziegler, 1990).

The overall trend of falling Global Sea Level (GSL) (Figure 3.17) is reflected in the facies of the Purbeck Beds. Freshwater limestones, algal limestones, shales and evaporates are common in the Purbeck sequence and suggest, together with presence of fossil soils, a depositional environment of lagoons, sabhkas and shallow hyper-saline lakes. There is faunal and other evidence (e.g. the presence of glauconite) of occasional marine incursions the most important of which, the Cinder Bed, lies near the middle of the Purbeck sequence. The Cinder Bed is a thin marine deposit composed almost entirely of Oyster shells. Correlation with the complete marine sequence preserved in Europe (Casey, 1973) suggests that the Cinder Bed might be synchronous with a significant marine transgression which marks the

Jurassic-Cretaceous boundary. Above the Cinder Bed the upper parts of the Purbeck sequence are composed of shales with fibrous Calcite and thin fossiliferous freshwater limestones. These grade upwards into the Wealden Beds which were also deposited in a mostly non-marine environment but consist of a predominantly clastic sequence. Figure 3.18 illustrates the general palaeogeography accompanying the accumulation of the Wealden Beds.

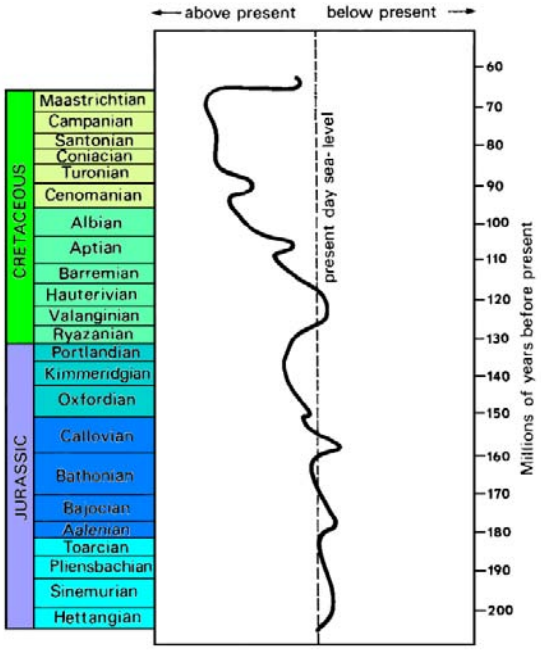

Figure 3.17 – Generalised variation in global sea-level for the Jurassic and Cretaceous periods (modified after Vail *et al.* (1977) and Hallam (1984)).

On a regional scale, tectonic activity increased at the transition from the Jurassic to the Cretaceous whereby the Bay of Biscay and the Rockall-Faroe-Møre grabens developed into the principal rift axes. However, persistent crustal extension across the North Sea Rift and the Celtic Sea-Western Approaches graben system resulted in a sharp accentuation of the marginal troughs, the Channel and Weald basins and the uplift of the London-Brabant-Rhenish-Bohemian Massif (Ziegler, 1990). The minimum horizontal stress during the early Cretaceous changed direction from NE-SW to N-S in response to the rotation of Iberia (Tappin *et al.* 1994) as the Central Atlantic spreading axis propagated northward (Figure 3.19) (Knott *et al.* 1993; Roberts *et al.* 1999; Doré *et al.*1999).

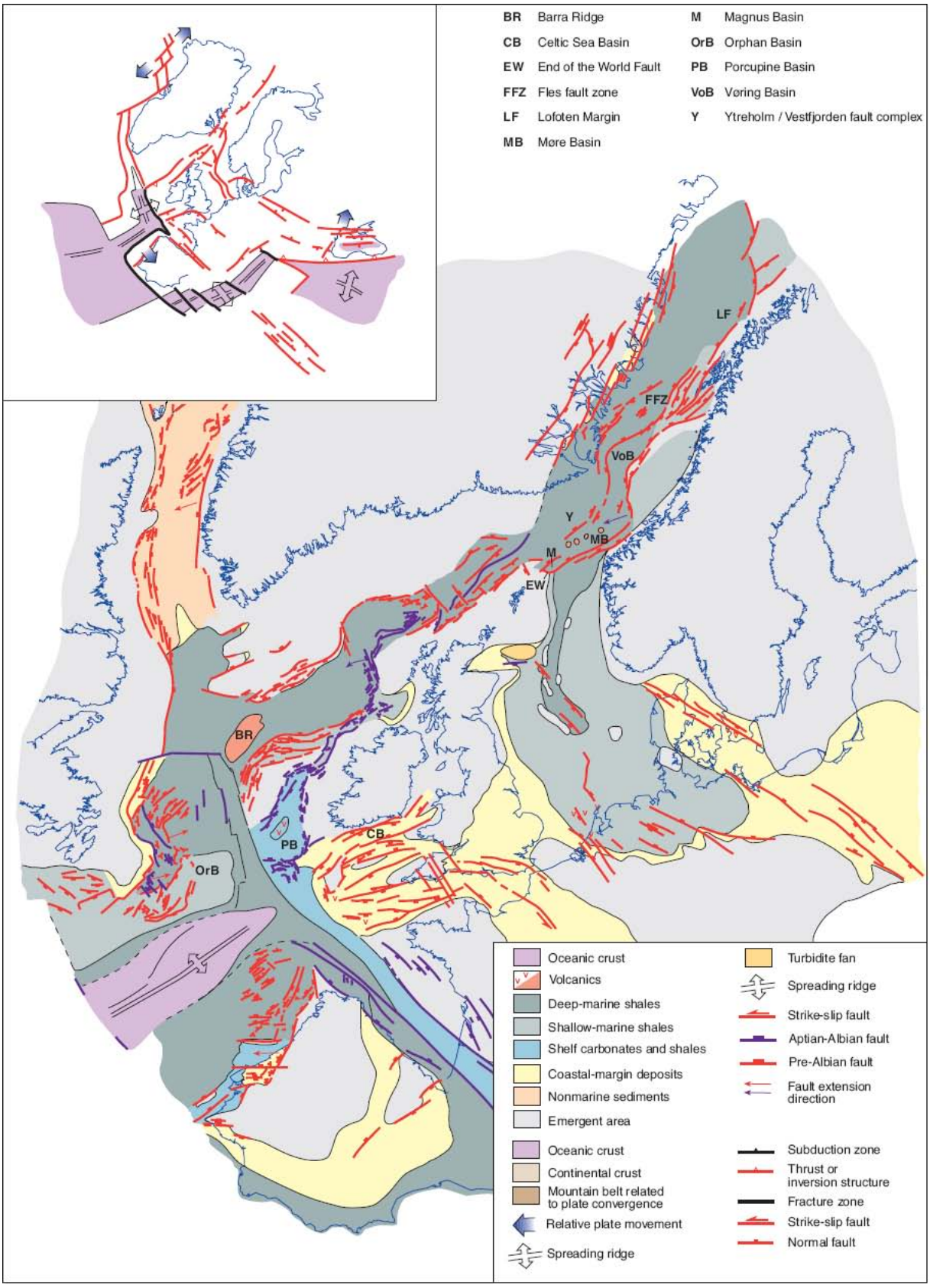

Figure 3.18 – Generalised palaeogeography during Early Cretaceous times showing the distribution of active structures and sediment facies (after Coward *et al.* 2003). Inset shows early Cretaceous structures in Europe and the Mediterranean.

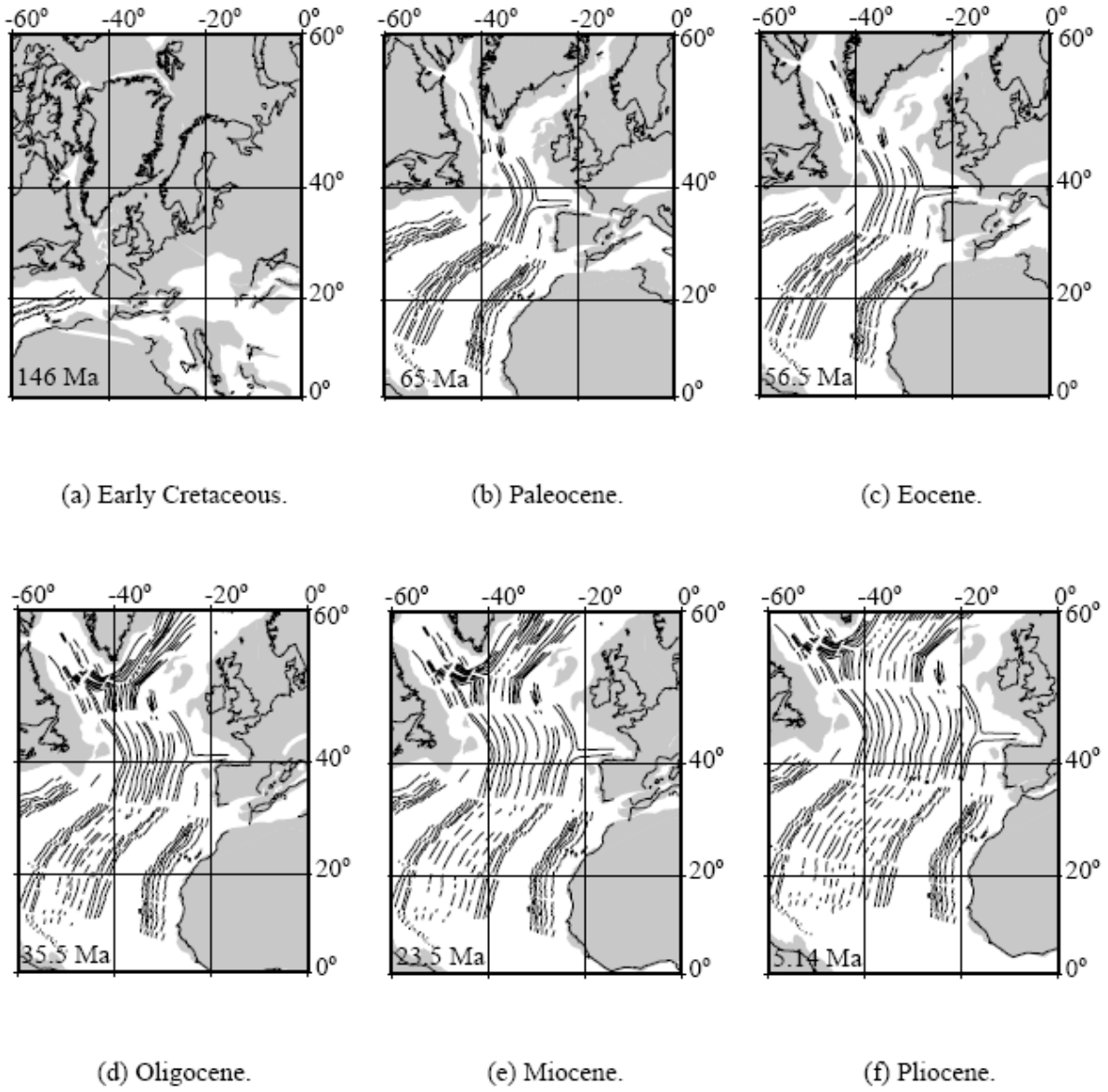

Figure 3.19– Plate reconstruction showing the opening of the North Atlantic (from Williams, 2002).

During the later parts of the Early Cretaceous, tectonic activity in Western and Central Europe abated gradually. Following mid-Aptian crustal separation between Iberia and the Amorican Shelf, the graben system of the Celtic Sea-Western approaches became inactive. A further tectonic event referred to as the 'Austrian' tectonic pulse (Kent, 1976) preceded and accompanied this crustal separation. During the middle Albian, sea-floor spreading commenced between the Irish and Newfoundland shelves and probably also in the southern

parts of the Rockall Trough (Figure 3.18) (Roberts *et al.* 1981; Olivet *et al.* 1984; Masson *et al.* 1985; Ziegler, 1989*c;* Coward *et al.* 2003).

Figure 3.18 illustrates that the WAB, NCSB, SCSB, Porcupine and Rockall troughs form the northern continuation of the graben system of the West-Iberian and Newfoundland shelves and that the Bay of Biscay Rift, with its prolongation into the Labrador Sea forms a cross-cutting element. During the Early Cretaceous, highs flanking this complex rift system, as well as positive elements separating the individual grabens, became uplifted whereas most of the grabens continued to subside (Ziegler, 1990). Regional doming of the North Atlantic area can probably be related to progressive lithospheric thinning in response to its mechanical stretching and thermal attenuation. This regional thermal doming effect is particularly evident in Iberia and in the area of the Cornubian and Amorican massifs (Ziegler, 1990). Neocomian to mid-Aptian crustal extension across the Celtic Sea-Western Approaches basins and rifting in the Rockall Trough, followed by limited sea-floor spreading in its southern parts during the late Albian, was compensated by wrench deformations in the Irish Sea, the Channel area and in the Paris Basin (Ziegler, 1988*b*).

In the NCSB, Late Jurassic marine and lagoonal sediments are separated by the Late Cimmerian unconformity from the overlying early Cretaceous Wealden clastics; only in the axial parts of this basin may sedimentation have been more or less continuous across the Jurassic-Cretaceous boundary (Figure 3.11). Neocomian to Barremian subsidence of the Celtic Sea was accompanied by extensional faulting as is evident from the thickness changes of the Wealden clastics. These attain maximum thicknesses of about 2000m in the central part of the basin however they are missing in the CBB and Caernarvon Basin presumably by non-deposition (Ziegler, 1990, Murdoch *et al.* 1995).

In the BCB and SCSB, Neocomian and Barremian sediments are missing. Aptian shallow-marine to continental sands transgress over deeply truncated Triassic and Jurassic series and are, in turn, overlain with an intervening hiatus by late Albian marine-deltaic sands. These are conformably overlain by the Late Cretaceous chalk series (Figure 3.11). To the west across the Pembrokeshire Ridge, the Aptian sand wedge expands and includes Valangian-Hauterivian sediments. This is taken as evidence that the main erosional phase in the BCB is of pre-Aptian age and probably results from Late Cimmerian deformation and uplift of the basin (Ziegler, 1990; Tappin *et al.* 1994). The structural style of the Triassic and Jurassic series indicates that their deformation involved dextral wrench movements along the basin margin and intra-plate basinal fault systems, and possibly sinistral movements along the Sticklepath-Lustleigh fault (Holloway & Chadwick, 1986). Erosion was particularly severe over the basin margins as illustrated by the erosion of some 3000m of Jurassic and Triassic sediments along the south-eastern margin where salt diapirism may have augmented uplift (Whittaker, 1985; Tappin *et al.* 1994; Murdoch *et al.* 1995). There is no evidence for major deformation during the early Albian break in sedimentation (Kamerling, 1979; Van Hoorn, 1987*b*; Coward & Trudgill, 1989). It is likely that the CBB and Caernarvon Basin also became deformed and uplifted during the earliest Cretaceous in response to wrench movements. The dating of the inversion of these basins however, is impeded by the total absence of Cretaceous sediments; a late Eocene clastic-dominated series overlays with an angular unconformity of deeply truncated Jurassic and Triassic strata (Barr *et al.* 1981; Tucker & Arter, 1987; Coward & Trudgill, 1989).

Mesozoic tectonics was dominated by crustal subsidence and normal faulting probably associated with a tensional stress field and extensional thinning of the continental crust and lithosphere. Conversely it is tempting to ascribe this early Cretaceous uplift to a compressive

stress field with consequent thickening of the crust and lithosphere. This type of uplift however is invariably associated with the inversion of pre-existing extensional structures that is the preferential uplift of former basinal areas primarily by reversal of normal faults. The early Cretaceous uplift in southern Britain was not associated with tectonic inversion for the following reasons:

1. Early Cretaceous uplift was most severe over earlier Mesozoic structural highs

2. Those basinal areas which had subsided most rapidly during the late Jurassic extensional phases continued to subside most rapidly during the early Cretaceous and continued to receive considerable amounts of sediment whilst erosion prevailed elsewhere

3. Normal faulting continued throughout the early Cretaceous

4. There is no evidence of early Cretaceous reverse faulting or the monoclinal folding usually associated with inversion tectonics (Chadwick, 1985*a*; Sellwood *et al.* 1986; Karner *et al.* 1987; Lake & Karner, 1987).

As a consequence of this earliest Cretaceous deformation, the Channel and Weald basins became isolated from the NCSB, SCSB and WAB. The Wealden series of the Channel and Weald basins is composed of fluvial and fluvial-deltaic sandstones and shales that were deposited in fresh to brackish-water lakes. Sands were derived across active fault-scarps from the London-Brabant Massif, the Cornish Platform and the Amorican Massif (Allen, 1959, 1976, 1981; Rawson *et al.* 1978). Syn-depositional faulting was apparently restricted to the earlier parts of the Neocomian. The Aptian transgression was preceded by crustal warping induced by wrench faulting, as is evident in the Channel area (Jeans *et al.* 1977). The

occurrence of Fullers Earth levels in the Neocomian to Aptian series of southern England may be related to activity of the Wolf Rock and Epsom Shoal volcanoes (Jeans *et al.* 1977). The Aptian and Albian shallow-marine greensands and shales attain thicknesses of c. 300m in the Channel and Weald basins. Differential subsidence of these basins was accompanied by mild sinistral wrench faulting. However, tectonic activity apparently abated during the Albian (Chadwick, 1985*b*; Sellwood *et al.* 1986; Lake & Karner, 1987). During Aptian and Albian time, rising sea-levels and possibly the relaxation of lithospheric stresses and thermal anomalies provided for the regional overstepping of Barremian basin margins and the re-establishment of shallow-marine connections between the basins of southern England, the Celtic Sea-Western Approaches basins, the Paris Basin and the North Sea (Ziegler, 1990).

Following intra-Aptian crustal separation in the Bay of Biscay rift, the Amorican Shelf and the Celtic Sea-Western Approaches basins became tectonically inactive and began to subside regionally in response to cooling and thermal contraction of the lithosphere. Carbonate sedimentation, which was already established along the margins of these shelves during the Late Jurassic and Early Cretaceous, spread by Cenomanian time over the entire area as well as the Paris Basin (Figure 3.11 and Figure 3.20). The chalk was probably deposited over most of southern Britain but subsequent erosion has restricted present outcrops to the south and east of England. Evidence from chalk exposed in quarries in southern England suggests that superimposed upon the broad picture of regional subsidence a new tectonic regime had a sporadic influence. Jarvis & Woodroff (1981) have inferred from the study of distributed hardgrounds periods of uplift and faulting in Coniacian and Santonian times. Though this very minor tectonic event does not relate in a simple way to the later, predominantly Cenozoic tectonic inversion in southern England, it may correlate with the major late Cretaceous inversion observed in northern Europe (Ziegler, in Bally, 1982). Chalks attain maximum

thickness of 1000m in the Celtic Sea basins, 500m in the WAB and 500-1000m along the northern shelf margin of the Bay of Biscay (Ziegler, 1990). On a regional scale, isopachs of the Late Cretaceous series reflect a south-westward tilting of the Celtic Sea-Western Approaches shelf. The general increase in the thickness of the chalk in the axial parts of the Celtic Sea and Western Approaches basins can be related to differential compaction of the underlying Mesozoic sediments (Ziegler, 1990).

In the Channel and Weald basins, a major unconformity separates Maastrichtian chalks from Late Paleocene fluvial clastics that were derived from the uplifted Welsh-Anglia High (Ziegler, 1990). This break in sedimentation coincides with the first phase of compressional deformation (inversion) of these Mesozoic depocentres (Lake & Karner, 1987; Karner *et al.* 1987). A similar hiatus straddling the Cretaceous-Cenozoic boundary is evident in the BCB, SCSB and NCSB where it is also associated with a mild phase of basin inversion (Van Hoorn, 1987*b*; Tucker & Arter, 1987).

In the regional framework of the more pervasive Laramide intra-plate deformations of Northwest and Central Europe, it is also likely that the mild compressional deformation of the Celtic Sea and Channel area, which involved dextral reactivation of the Sticklepath-Lustleigh and Pays-de-Bray fault systems, was induced by tangential stresses that were exerted onto the Alpine foreland as a consequence of the convergence and collision of the Alpine Orogen with the Helvetic Shelf (Ziegler, 1987*a*, 1988*b*, 1989*a*).

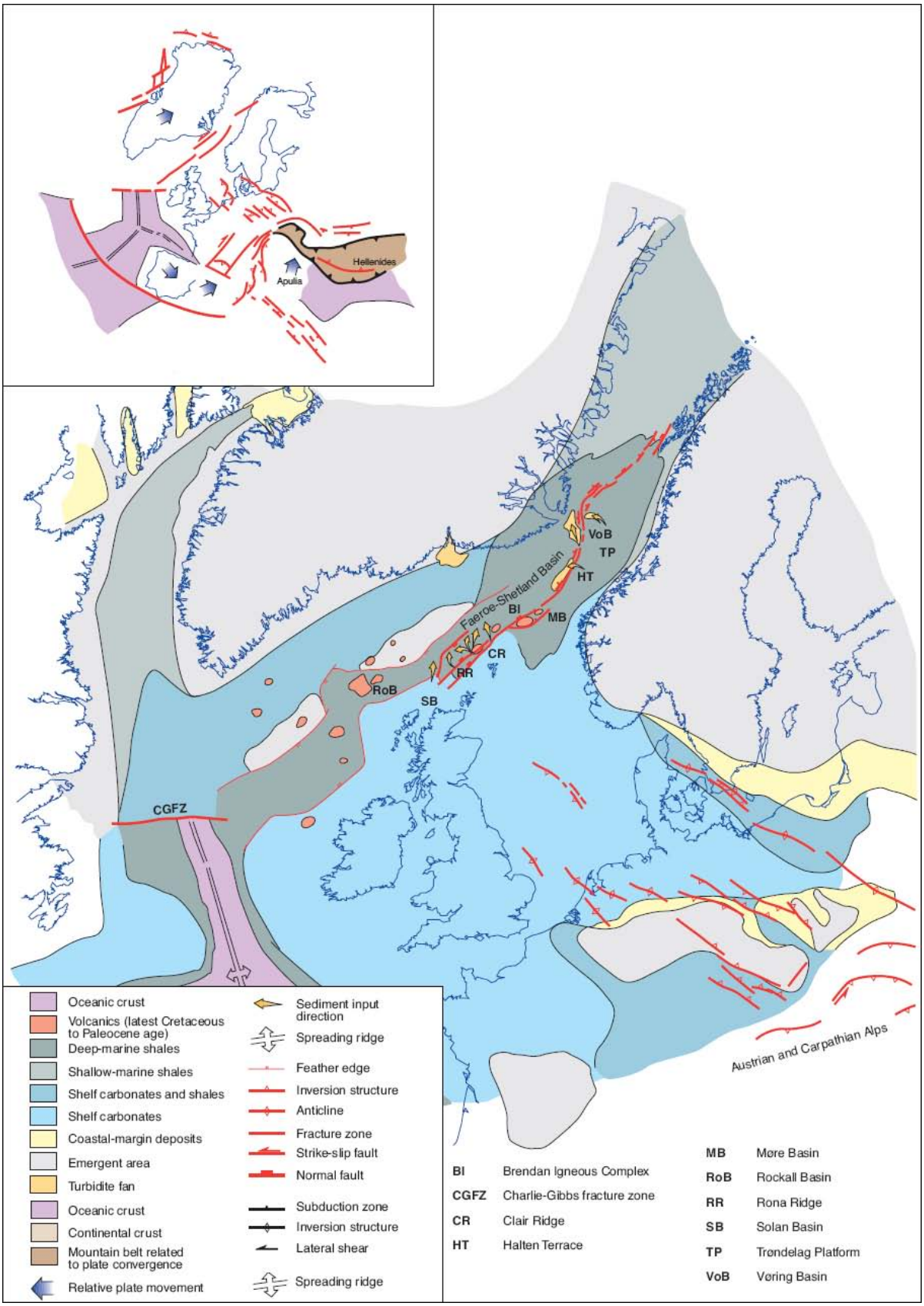

Figure 3.20 – Generalised palaeogeography during Late Cretaceous times showing the distribution of active structures and sediment facies (after Coward *et al.* 2003). Inset shows late Cretaceous structures in Europe and the Mediterranean.

3.3.5: CENOZOIC

In England and Wales the Cenozoic era saw important changes in tectonic framework. Following earliest Eocene crustal separation between the European Craton and Greenland, the evolution of Western and Central Europe was dominated by stress systems that were related to the convergence of the Africa-Arabian and Eurasian plates and their suturing along the Alpine fold belts and to changes in the rate of sea-floor spreading in the various segments of the North Atlantic Ocean (Ziegler, 1990). Continued northward drift and counter-clockwise rotation of Africa-Arabia relative to Eurasia gave rise to the Eocene-Miocene main orogenic phases of the Alpine fold belt (Tollmann, 1980; Trümpy, 1980; Livermore & Smith, 1985; Savostin *et al.* 1986; Dercourt *et al.* 1986). During the late Eocene and Oligocene the Alpine foreland was transected by the Rhine-Rhône and Eger rift system, which remained active until the present. Evolution of this rift system is broadly contemporaneous with the compressional deformation of Mesozoic grabens of the Western Approaches, Celtic Sea and Channel basins.

During the reorganisation of sea-floor spreading axes in the Norwegian-Greenland Sea, the pre-existing NNW-SSE trending fracture systems that transacted the Hebrides Shelf, the Irish Sea and the eastern parts of the Celtic Sea, became sinistrally reactivated and caused the subsidence of a string of isolated basins containing late Eocene and Oligocene sediments (Ziegler, 1990). In the CBB and SGCB, Paleogene clastics containing lignites and minor carbonate intercalations attain thicknesses of some 800m (Barr *et al.* 1981; Tucker & Arter, 1987). Their accumulation was associated with transtensional reactivation of fault systems that presumably came into evidence during the Mesozoic development of the NCSB and its Early Cretaceous inversion (Coward & Trudgill, 1989). The Mohcras borehole, drilled onshore at the head of Cardigan Bay, penetrated 525m of Oligocene clays, conglomerates and lignites (Curry *et al.* 1978). Along the trace of the Sticklepath-Lustleigh fault, a number of

small pull-apart basins contain in part sizable thicknesses of late Eocene and Oligocene clastics. The geometry of the fault systems that controlled the subsidence of these basins is indicative of sinistral wrenching (Holloway & Chadwick, 1986). In post-Oligocene time, these faults, however, became dextrally reactivated (Holloway & Chadwick, 1986; Lake & Karner, 1987, Van Hoorn, 1987*b*, Arthur, 1989; Turner, 1997; Dunford *et al.* 2001; Cunningham *et al.* 2004). Activity along this fault was accompanied by intrusion of the Lundy granite (53.4 ± 1.3Ma (Fitch *et al.* 1969)) and its associated dyke swarm which was the southernmost manifestation of the activity related to the Hebrideean igneous province (Curry, 1978). Although the igneous plug affecting the top chalk in the Fastnet Basin is more likely to be a younger Cenozoic intrusion (Caston, 1981). Fission track data indicate that the area of the Irish Sea, as well as much of England, became affected by a second late Eocene to Oligocene phase of regional uplift (Roberts, 1989; Green, 1989) that is contemporaneous with the resumption of inversion movements in the Sole Pit, Broad Fourteens-West Netherlands, Channel, Celtic Sea and Western Approaches basins (Ziegler, 1987*a*, 1988*b*).

The pattern of Paleocene, Oligocene and Miocene compressional deformations in the Alpine foreland of Western and Central Europe is summarised in Figures 3.21 - 3.23. Compared with the distribution of the sub-Hercynian and Laramide compressional foreland deformations, a clear westward shift in tectonic activity can be recognised (Ziegler, 1990). The observed general westward shift of intra-plate compressional tectonic activity is thought to be the expression of changes in the convergence direction between the Africa-Arabian and the European cratons (Ziegler, 1987*a*, 1988*b*, 1989*a*).

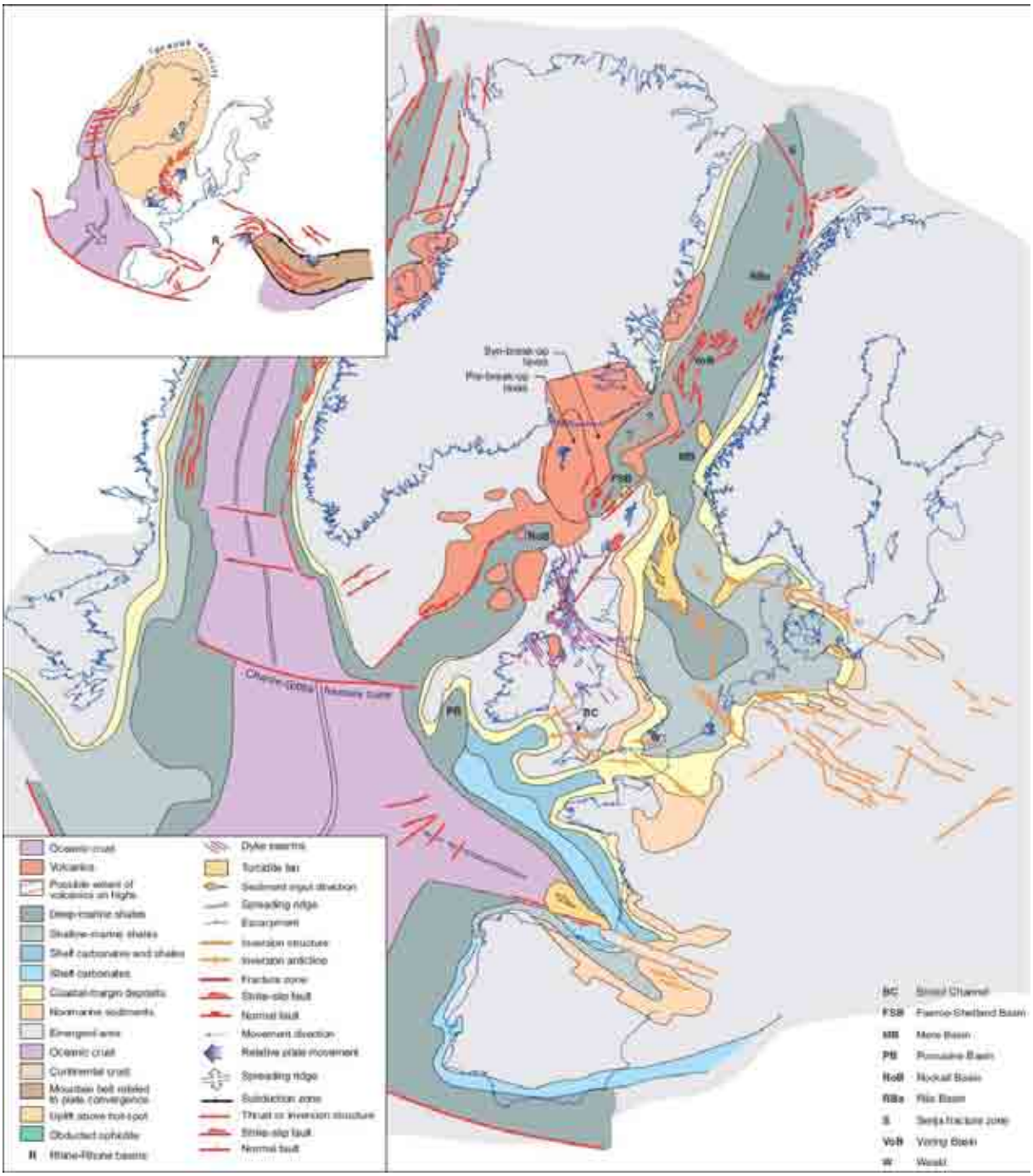

Figure 3.21 – Generalised palaeogeography during Paleocene times showing the distribution of active structures and sediment facies (after Coward *et al.* 2003). Inset shows Paleocene structures in Europe and the Mediterranean.

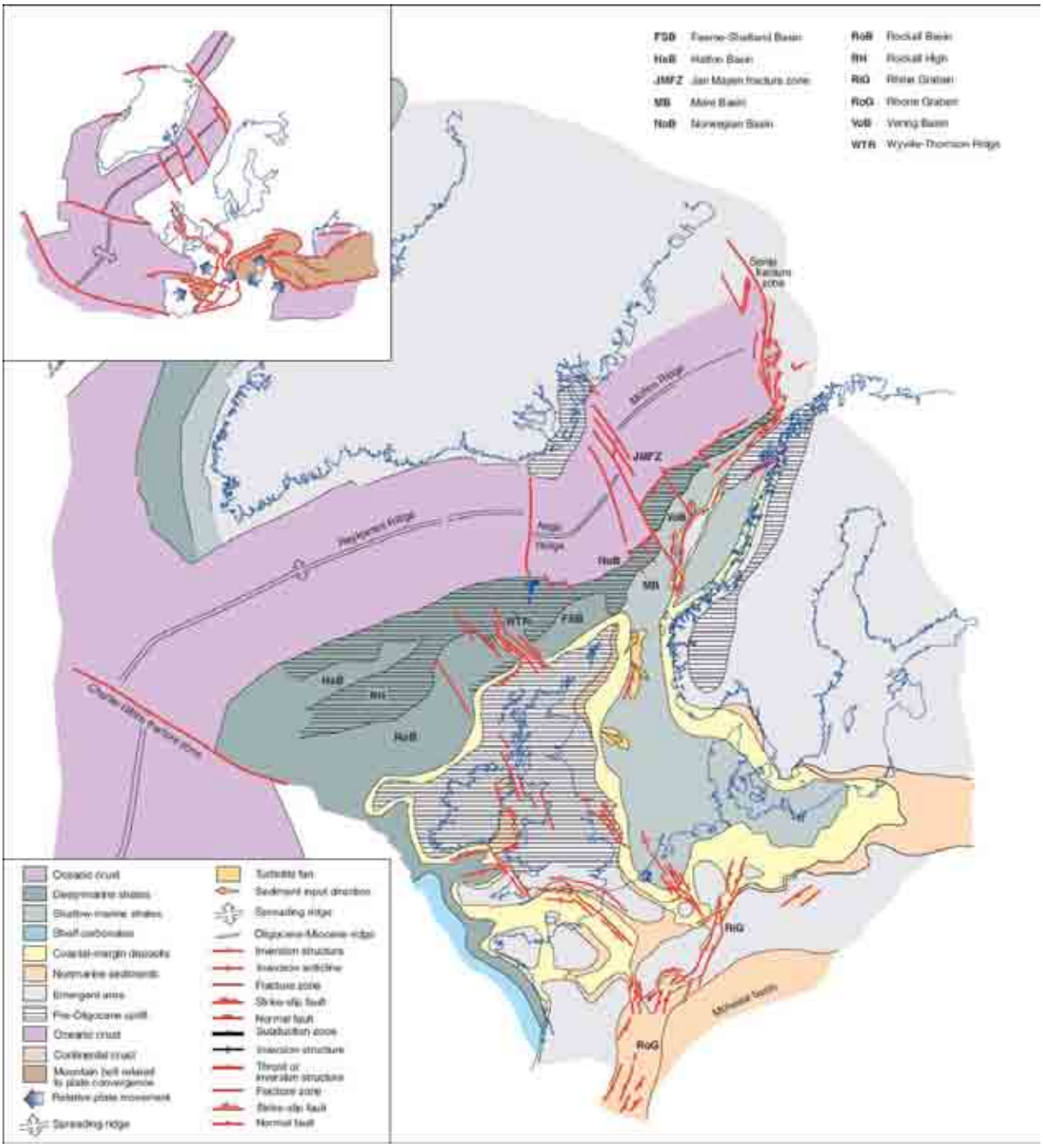

Figure 3.22 – Generalised palaeogeography during Oligocene times showing the distribution of active structures and sediment facies (after Coward *et al.* 2003). Inset shows Oligocene structures in Europe and the Mediterranean.

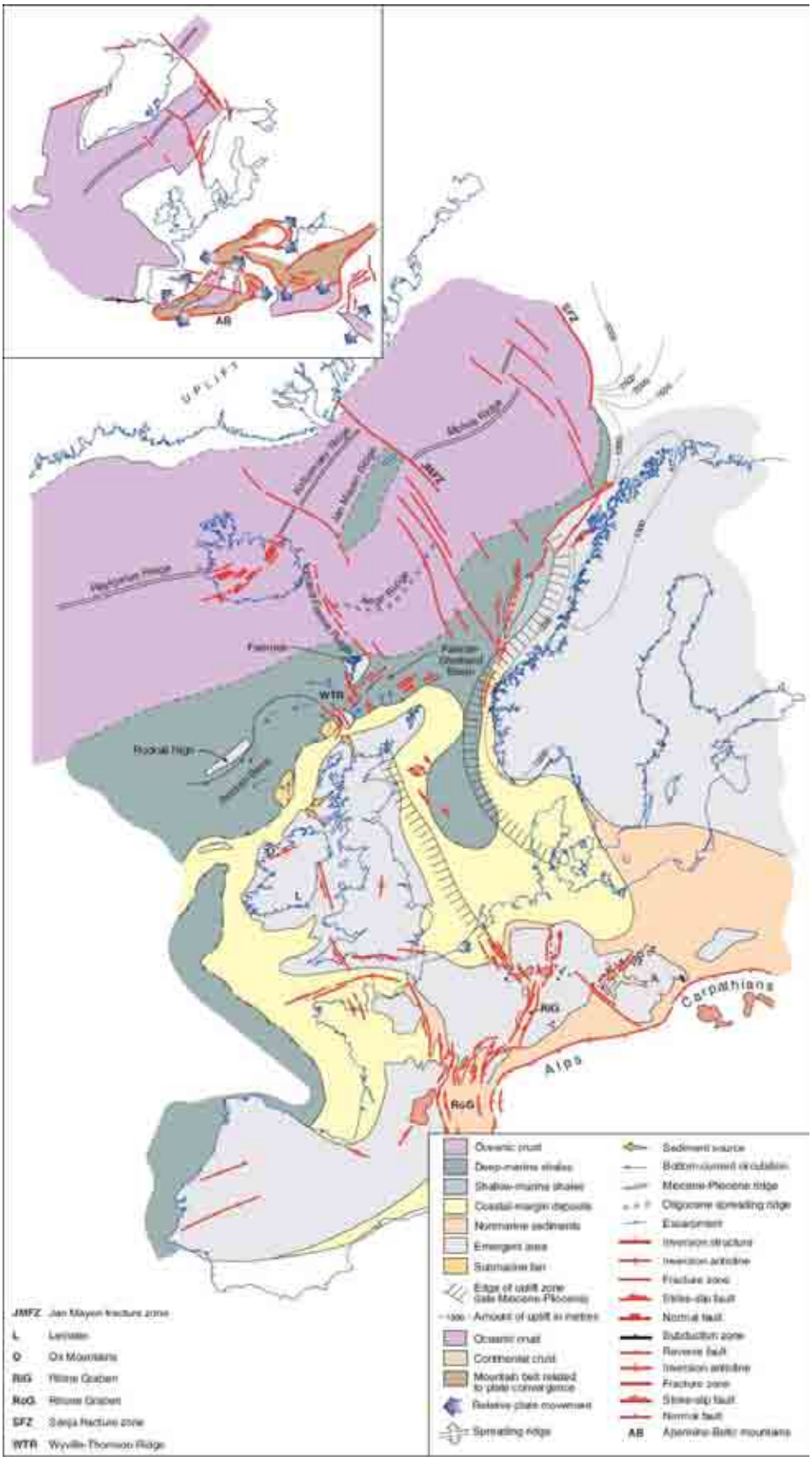

Figure 3.23 – Generalised palaeogeography during Miocene times showing the distribution of active structures and sediment facies (after Coward *et al.* 2003). Inset shows Miocene structures in Europe and the Mediterranean.

Cenozoic sedimentation was confined largely to the early and middle parts of the Cenozoic. The end Cretaceous fall in GSL (Vail, 1977, Hallam, 1984, Figure 3.17) resulted in a considerably decreased area of deposition and in marked changes of sedimentary facies. The lack of significant normal faulting suggest that subsidence was largely caused by relict thermal relaxation effects inherited from the Mesozoic extensional phases. Patterns of subsidence are difficult to establish in detail but probably differed considerably from those of Cretaceous times. The present occurrences of synclines of Cenozoic strata (Figure 3.23) which directly overlie Mesozoic structural highs are a consequence of tectonic inversion. The date of initiation of this inversion and the extent to which it influenced patterns of subsidence is uncertain (Woolridge, 1926; Curry, 1965; King, 1981; Plint, 1982). Inversion of the Channel and Weald basins had commenced during the mid-Paleocene as is evident from a regional unconformity spanning late Maastrichtian to late Paleocene times. Sedimentation resumed generally during the earliest Eocene with the deposition of transgressive sands and shallow-marine shales. Late Eocene and early Oligocene regressive conditions are indicated by the deposition of continental and deltaic clastics. The sedimentary record of the area terminates around the mid-Oligocene (Curry & Smith, 1975; Curry *et al.* 1978).

Mild intra-Eocene compressional deformations are evident from the gradual upwarping of the Wealden-Artois axis, which at the beginning of the Oligocene interrupted the marine connection between the southern North Sea and the area of the Western Approaches-Channel basins. Inversion movements persisted during the Oligocene and early Miocene. It involved the compressional reactivation of previously tensional faults. Net uplift of the basin axis amounts to some 1500m (Figure 3.24) (Karner *et al.* 1987*a*; Lake & Karner, 1987). The pre-Quaternary geological map given in Figure 3.25, illustrates the scope of these inversion movements in the Channel area (Smith, 1984).

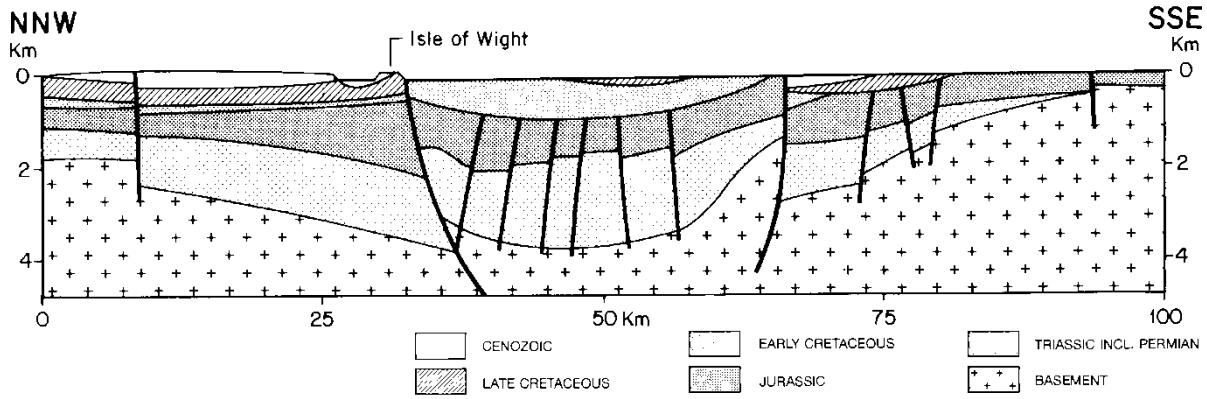

Figure 3.24 – Schematic structural cross-section of the Channel area (modified after Ziegler, 1990)

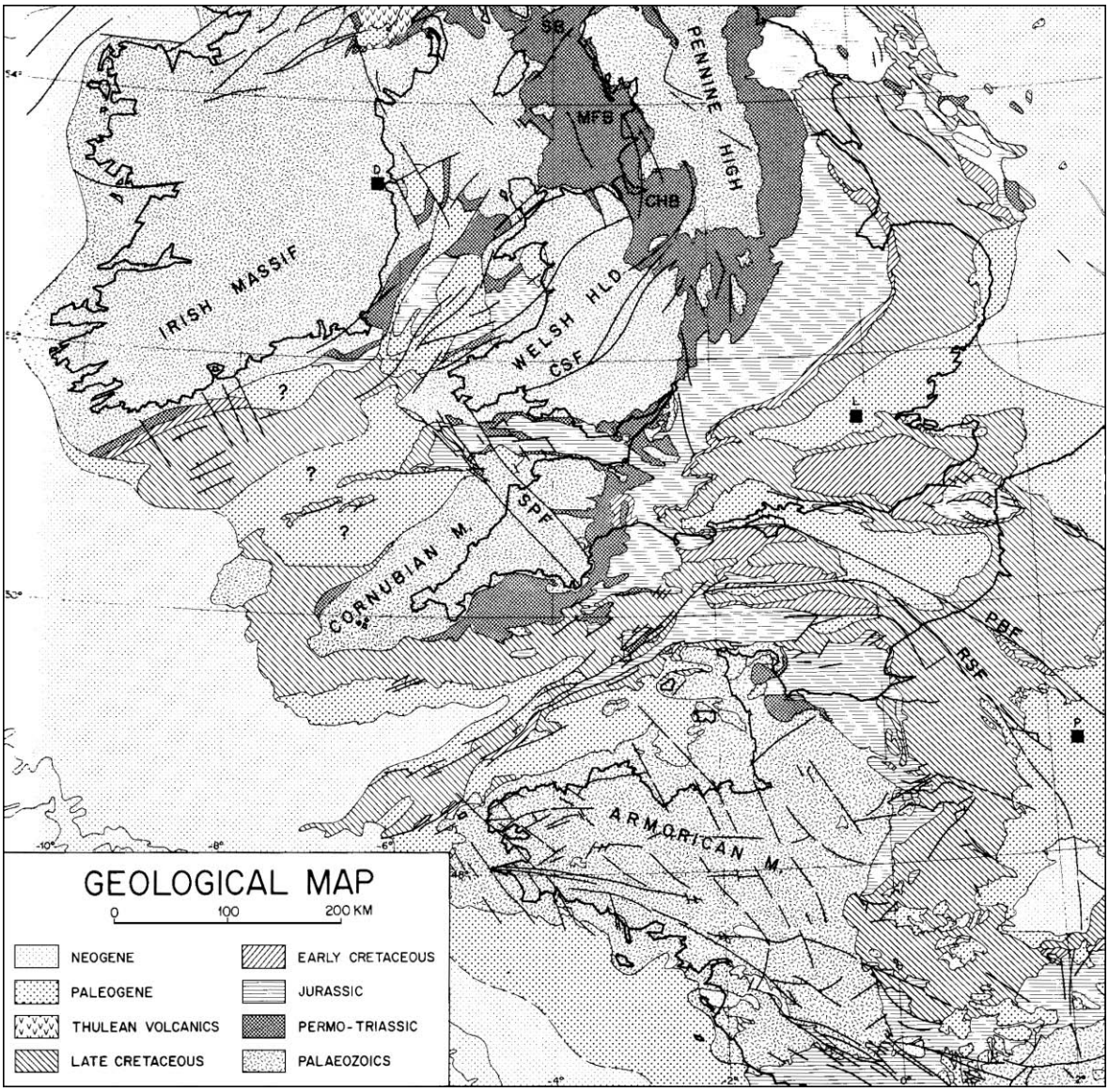

Figure 3.25 – Geological map of the Celtic Sea-Western Approaches area. Abbreviations: CHB-Cheshire Basin; CSF-Church-Stretton Fault; MFB-Manx-Furness Basin; PFB-Pays-de-Bray Fault; RSF-Rouen-Sennely Fault; SB-Solway Basin; SPF-Sticklepath-Lustleigh Fault (modified after Ziegler, 1990).

The balance of evidence indicates that the main episodes of inversion affected the Wessex-Channel basin from late Cretaceous times onwards coeval with the 'Laramide' inversions of northern Europe (Ziegler, 1981) but that major inversion did not take place until Miocene times associated with 'Helvetic' Alpine and Pyrenean orogenic events. The inversion of the Wessex Basin falls into two categories:

1. Regional up-warps such as the Portland-Wight High which comprises major flexures with the axial uplifts of more than 1000m. These features appear to be associated with regional pure-shear basin shortening and it is noteworthy that the greatest uplifts occur in basins which contain thick lower Cretaceous sequences. Basins containing older more competent sediments such as the Dorset and Western Portland-Wight were less affected by shortening and uplift.

2. Comprises lower east-west trending zones of faulted flexures which are related directly to the reversal of underlying basin controlling normal faults.

Following basin inversion which ended in mid Cenozoic times the surface of much of Wessex-Channel basin has probably stayed close to sea level. Considerable erosion of its western part may have continued as a result of regional eastward tilting and uplift of the Cornubian massif (Whittaker, 1985).

The amount of crustal shortening that was achieved during the Cenozoic inversion of the WAB is difficult to estimate but is unlikely to exceed a couple of kilometres South West England was probably uplifted during the late Eocene to early Oligocene inversion which affected the WAB (Ziegler, 1987*c*). Because of the almost complete removal of Mesozoic and Cenozoic sediments the magnitude of this uplift onshore cannot be assessed though it may have been hundreds of metres (Whittaker, 1985).

The timing of inversion in the NCSB differs significantly from that of the WAB. Inversion movements mainly affected the south-eastern flank of the NCSB and the axial parts of the Fastnet Basin (Robinson *et al.* 1981; Tucker & Arter, 1987). The main phase of inversion, resulting in buckling-up of broad anticlinal features, occurred during the middle-late Paleocene. A second, mild phase of inversion occurred during the late Oligocene to early Miocene (Ziegler, 1990). The structural relief generated during basin inversion is, at shallow levels, of the order of 2500m. Like other inverted basins the compressional deformation of the NCSB was accompanied by dip-slip reversal on normal faults as is evident from reverse displacements and monoclinal flexures at shallow levels, whereas normal fault geometries are preserved at deeper levels (Ziegler, 1990). As wrench faults play only a subordinate role in the structural style of the NCSB, compressional stresses causing its inversion were presumably oriented normal to the pre-existing basin axis (Tucker & Arter, 1987).

In the SCSB and BCB a regional unconformity separates the late Cretaceous chalks from late Eocene to Oligocene shales and carbonates. This unconformity truncates late Cretaceous sediments, which are involved in a gentle low-relief, asymmetric anticlinal structure that is superimposed on the south-eastern margin of the SCSB. In the BCB, Cretaceous sediments are missing. The pre-Quaternary geological map of the area (Figure 3.25) indicates that the Bristol Channel-SCSB was affected by a second mild phase of inversion during the late Oligocene-early Miocene (Van Hoorn, 1987*b*).

The crustal configuration of the Celtic Sea-Western Approaches area as derived from deep reflection-seismic data shows only moderate undulations of the Moho-Discontinuity (Lake & Karner, 1987). Considering the thickness of Permian-Carboniferous, Mesozoic and Cenozoic sediments contained in the NCSB, SCSB, WAB and BCB, which range from 4-15km (Ziegler, 1990) and assuming that these basins were in isostatic equilibrium prior to their

inversion, it is likely that substantial crustal thinning accompanied their subsidence (Cheadle *et al.* 1987; Pinet *et al.* 1987; Dyment, 1989; Coward & Trudgill, 1989; Bois *et al.* 1990; Ziegler, 1990). Although the amount of crustal shortening that was achieved in these basins during their Cenozoic inversion is difficult to estimate, it entailed, probably at the scale of several kilometres, the convergence of the Amorican Block and the Welsh-Anglia and Irish massifs and commensurate dextral displacements along the Pays-de-Bray and Sticklepath-Lustleigh fault systems. It is likely that at the same time, compressional stresses were exerted on the more rigid craton of the British Isles, which was progressively uplifted during the Oligocene and Neogene (Ziegler, 1990). Such a broad-scale positive lithospheric deflection is in keeping with the present-day, generally north-northwest-directed compressional stress regime of Europe (Klein & Barr, 1986) and the gravity field of the British Isles (Karner *et al.* 1987*b*).

3.4: THE TIMING OF MAXIMUM FORMER DEEPER BURIAL FROM SEISMIC

The compactional approach for estimating former deeper burial detailed in Chapter 4, reveals very little of the timing of the event (the age of the formation in which the burial anomaly is measured must predate the exhumation episode). Additionally multiple exhumation episodes are not catered for by any of the compactional approaches unless one computes exhumation separately from successions above and below a recognised unconformity (such as the Hillis approach, which seems to indicate a pre-Cretaceous episode and post-Cretaceous episode see Chapter 4), but realistically timing can only be constrained as post deposition of the youngest unit under analysis (i.e. post Lower Jurassic (Liassic) in the case of this study). Integration with other techniques is required to elucidate any timing of former deeper burial such as palaeothermal data (Chapter 5) and seismic data. Seismic data reveals evidence for two unconformities providing a timing constraint of post-Jurassic-Albian (i.e. Lower Cretaceous)

and post Maastrictian-Oligocene (inferred to be Paleogene based on preserved Cenozoic sediments and AFTA/VR data (Chapter5)).

The location of the seismic lines used in this study is provided in Figure 3.26. Three wells were available to tie the stratigraphy to the seismic data (e.g. Figure 3.27) in order to obtain the tightest constraint on the timing of the erosive episodes. The base Cenozoic unconformity (Figures 3.27-3.33) is the most obvious unconformity identified on the seismic data mainly due to the underlying Chalk reflectors being truncated by the unconformity. This is particularly well demonstrated in Figures 3.31 and 3.32 where the underlying reflectors are 'cut off' by the unconformity. The spatial distribution of this unconformity is shown in Figure 3.34.

The second unconformity is much more subtle in its recognition and evidence for its existence comes from lines typified by Figure 3.33. Well completion reports from Britoil recognise this unconformity as Wealden in age (termed 'Late Cimmerian'). It appears as an erosional unconformity with marked angular discordance on many seismic lines across the western NCSB however on most of the lines analysed in this project it is very hard to distinguish as shown in Figures 3.27-3.32.

In addition to identifying periods of exhumation from unconformities the seismic data also reveal evidence of the importance of compressional tectonics in the Celtic Sea basins. For example Figure 3.30 shows reactivation of a normal fault where horizons above the 'null point' show evidence for reverse movement compared to the net normal displacement below the 'null point'. A much clearer example of this is shown in Figure 3.32 which also demonstrates the net normal and net reverse displacement below and above the 'null point'

respectively. Some formations also show thinning onto structural highs as shown by the base Chalk isopach map (Figure 3.35).

Salt has long been recognised as being present in the Celtic Sea basins (e.g. Upshaw *et al.* 1974) and its influence on the tectonic evolution of the basins analysed (e.g. Turner, 1997; Bulnes & McClay, 1998; Welch & Turner, 2000). This study has also revealed evidence for salt diapirism by the presence of a 'salt plug' in the footwall of the fault shown in Figure 3.33. Independent seismic verification of the recognised unconformities comes from the work of Colin *et al.* (1981) who identified a number of unconformities in the western NCSB (Figure 3.36).

The validation of the exhumation episodes recognised in this study with those of Colin *et al.* (1981) provides a reasonable timing constraint on the exhumation episodes affecting the SW UK; a Lower Cretaceous episode (*c.* 125-100Ma) and a Paleocene episode (*c.* 65-55Ma). These results are in excellent agreement with the independently derived timings from AFTA and VR data (see Chapter 5). The seismic observations coupled with results from the AFTA and compactional data, as well as published literature have allowed for the creation of a tectonostratigraphic diagram for the Celtic Sea which is shown in Figure 3.37.

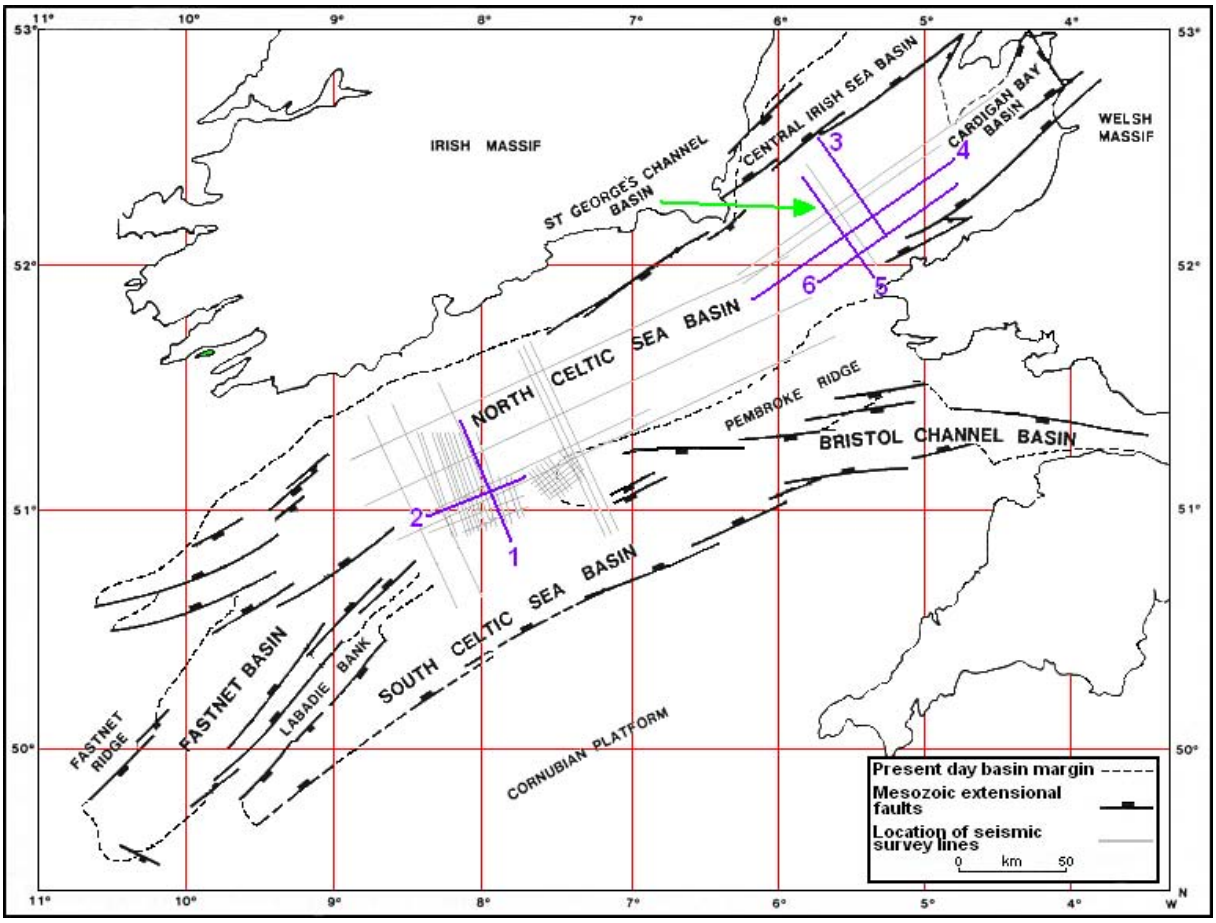

Figure 3.26 – Map highlighting the location of the seismic data used in this study. Overlay on a gravity anomaly map as it will very effectively highlight the principal basement lineaments; also draft the seismic line locations as the scanned grid used here is too low-res.; also show the locations of the wells you have used on this map The purple lines represent interpreted lines which are presented in this section (modified after Petrie *et al.* 1989).

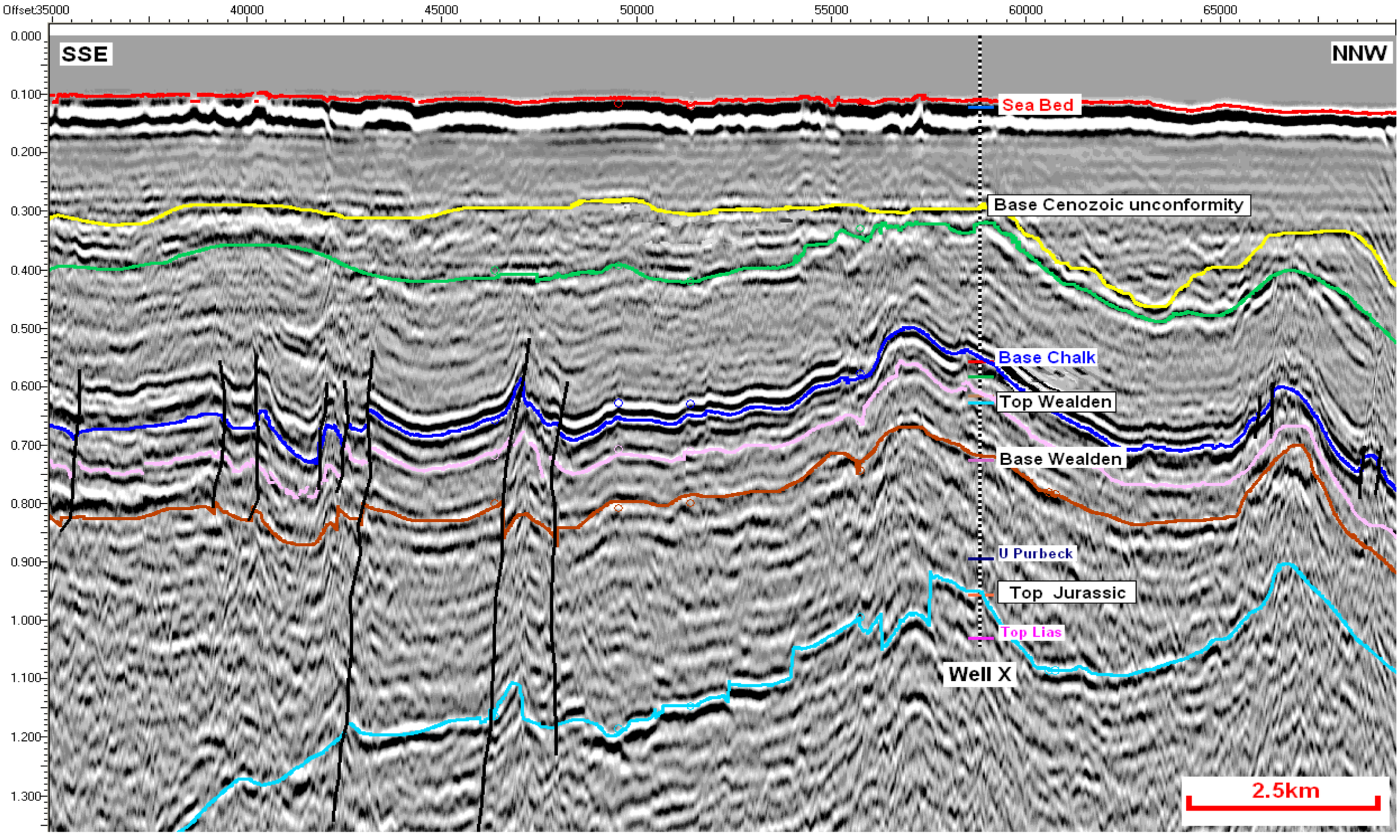

Figure 3.27– Line 1, showing main horizons mapped in this study and an example of the well data used to tie in the stratigraphy. Offset is horizontal scale in metres and vertical scale is TWTT in seconds.

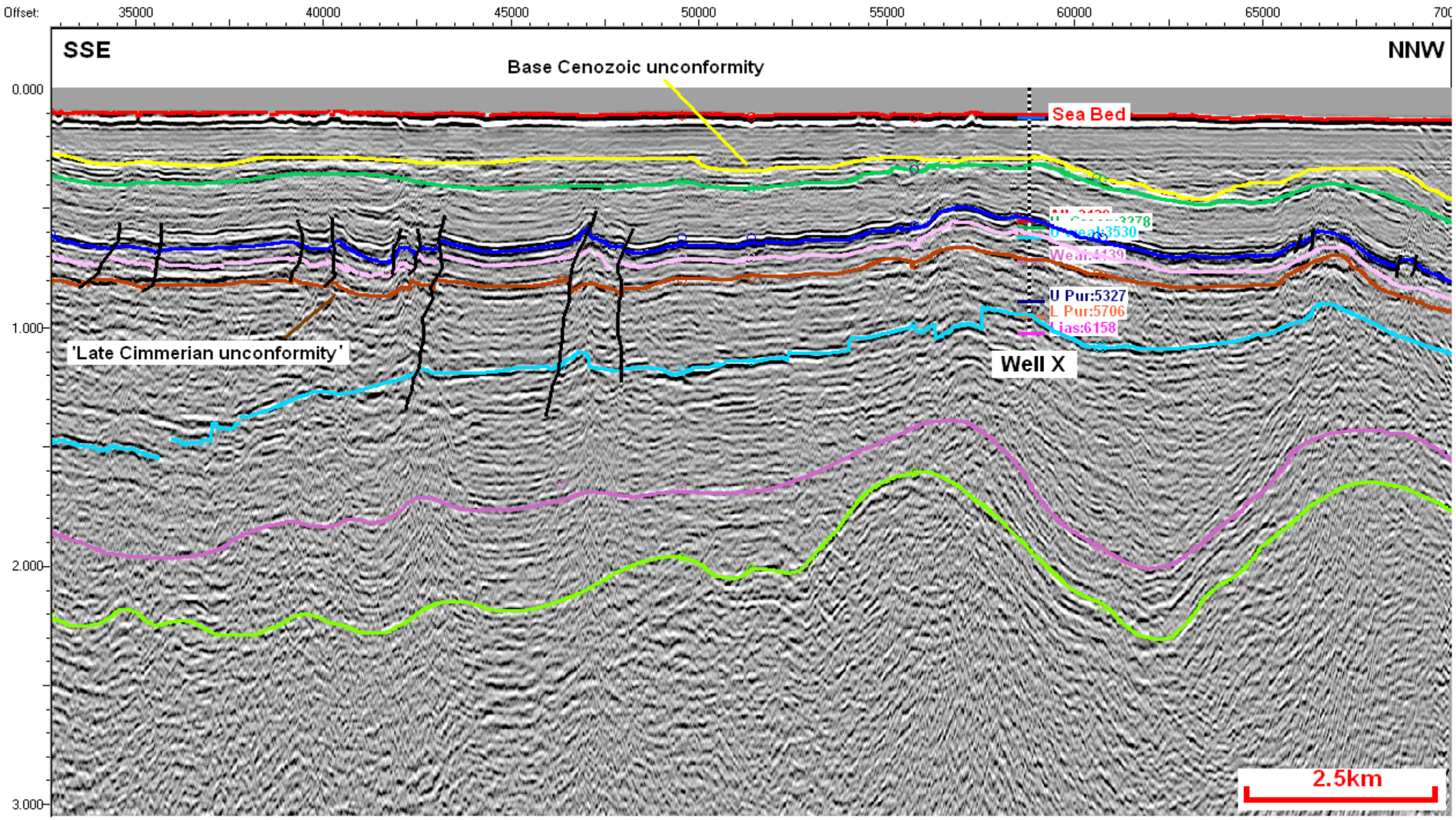

Figure 3.28 – Seismic line from the NCSB showing the two unconformities recognised in this study. The 'Late Cimmerian unconformity' is geologically equivalent to the base Wealden (see text) and is not immediately obvious as being an unconformity. The location of this section is line 1 in Figure 3.26. Offset is horizontal scale in metres and vertical scale is TWTT in seconds.

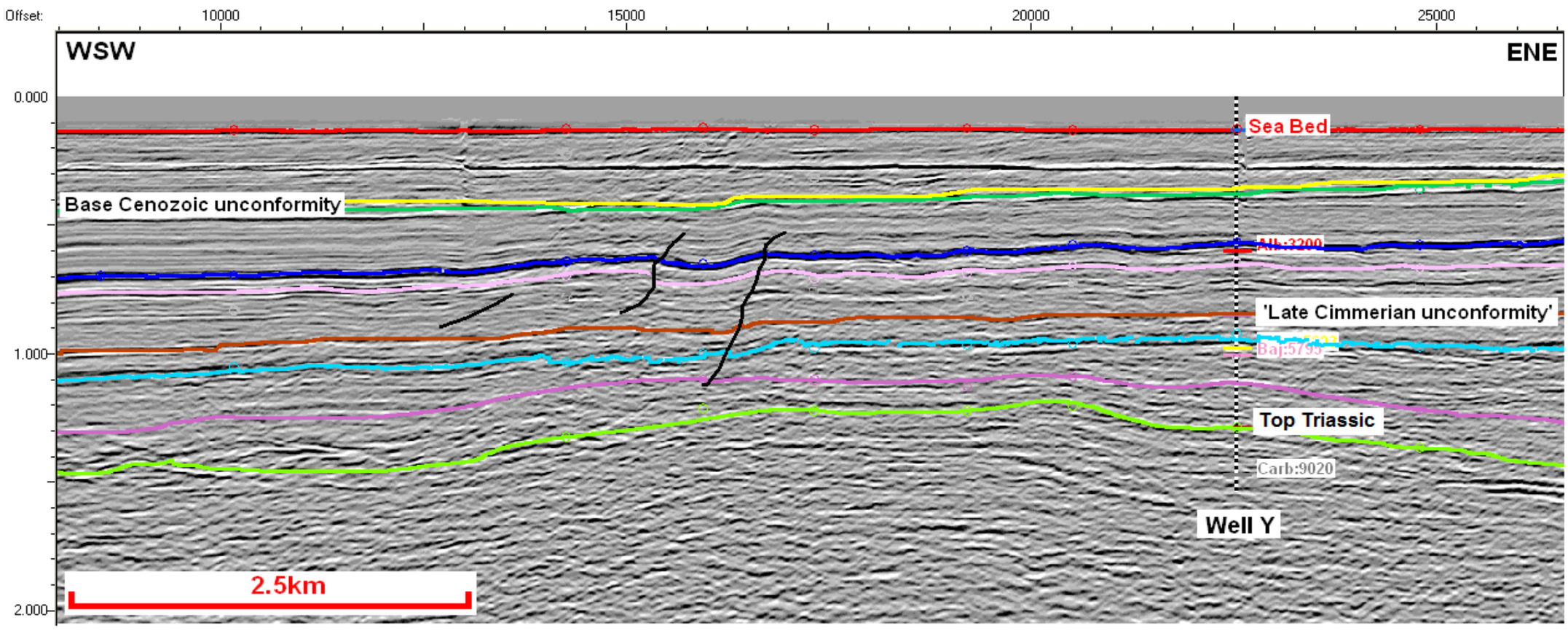

Figure 3.29 – Seismic line from the NCSB showing the two unconformities recognised in this study. Note the 'Late Cimmerian unconformity' is still difficult to identify and additionally the base Cenozoic unconformity is also disguised in this particular section. The location of this section is line 2 in Figure 3.26. Offset is horizontal scale in metres and vertical scale is TWTT in seconds.

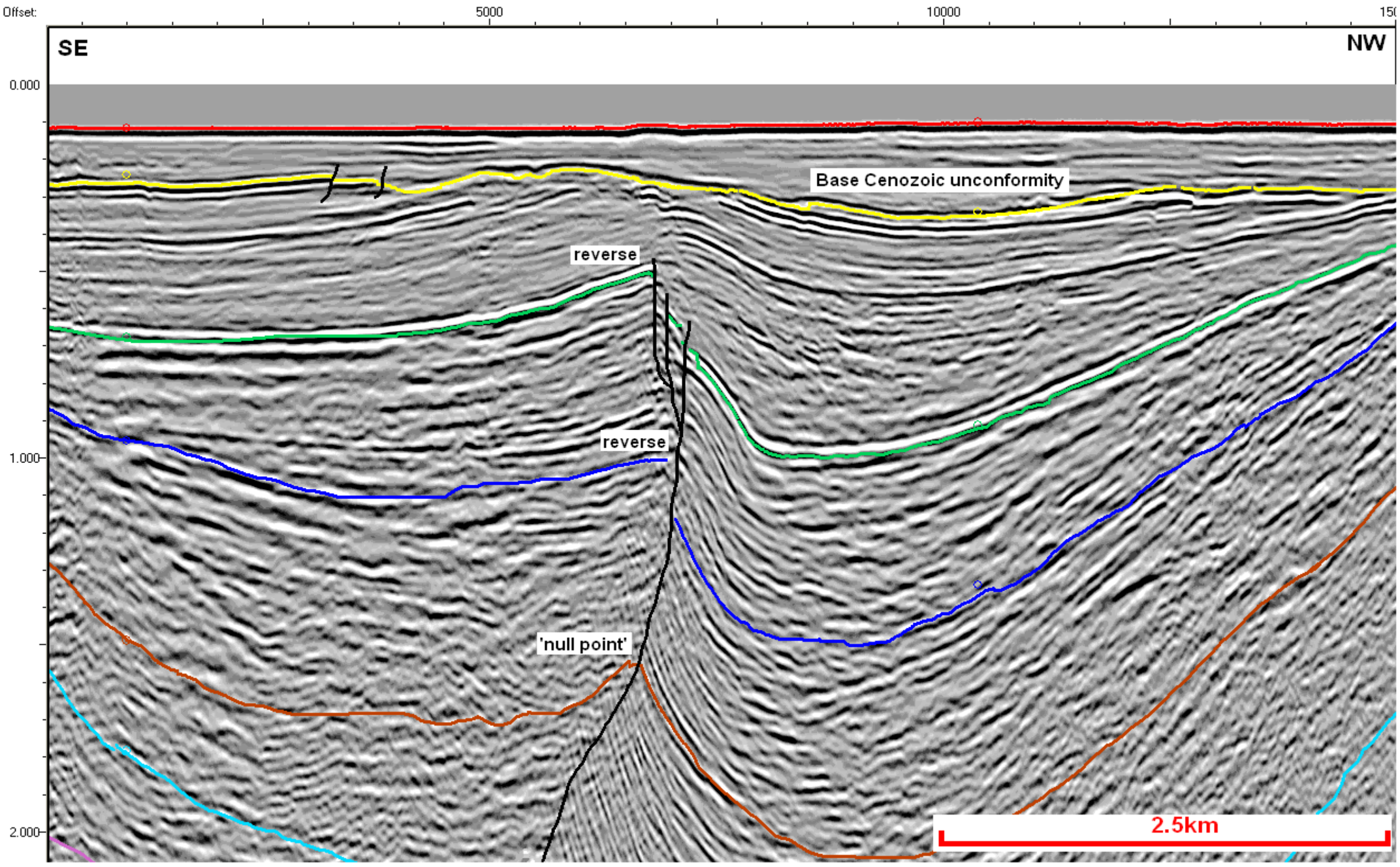

Figure 3.30 – Seismic section from the SGCB showing evidence of compressional reactivation of normal faults. Notice the net reverse movement above the 'null point', horizons below the 'null point' show net normal displacement. The location of this section is line 3 in Figure 3.26. Offset is horizontal scale in metres and vertical scale is TWTT in seconds.

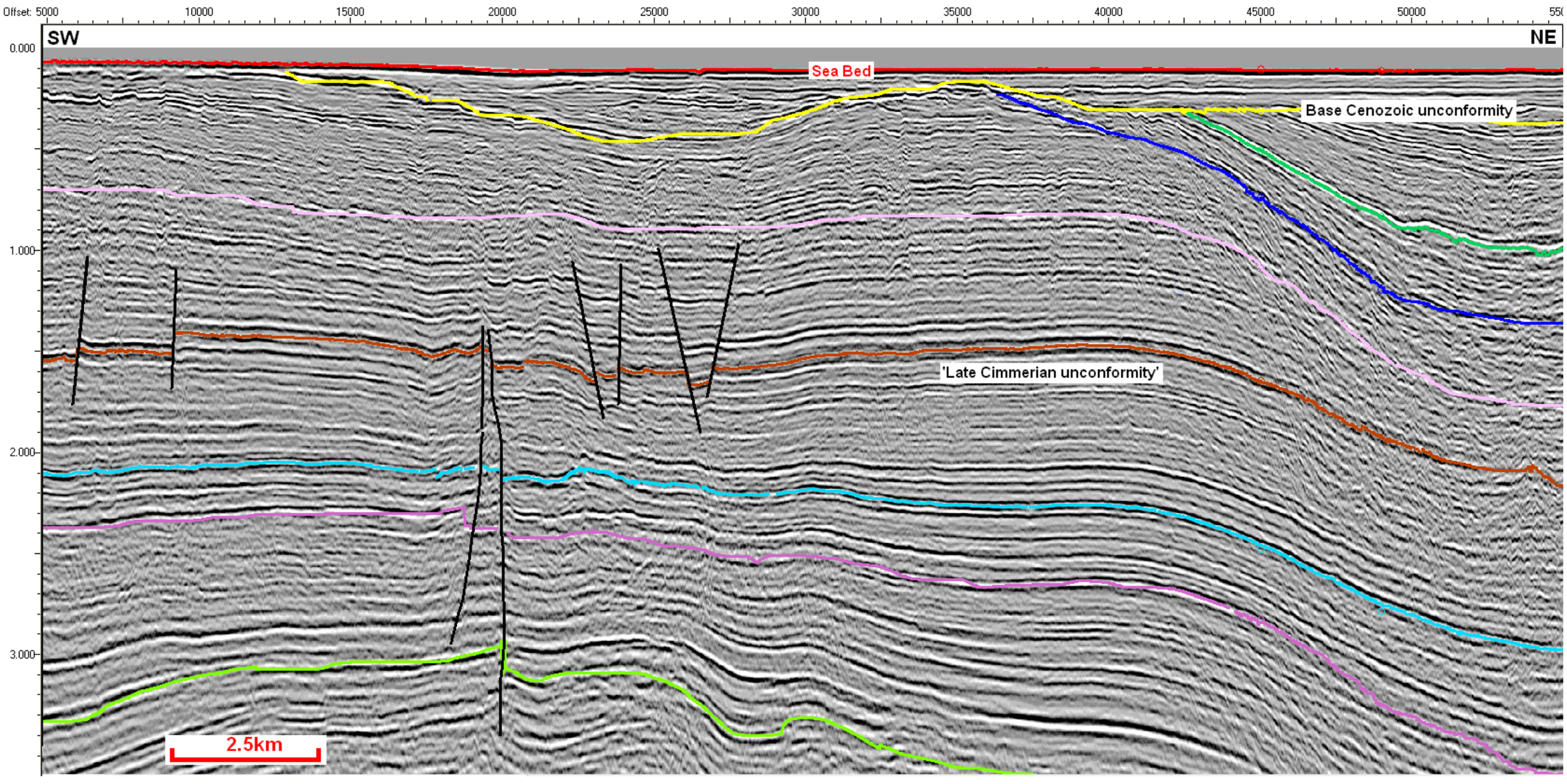

Figure 3.31 – Interpretation of Line 4 showing the onlapping of reflectors against the base Cenozoic unconformity. Offset is horizontal scale in metres and vertical scale is TWTT in seconds.

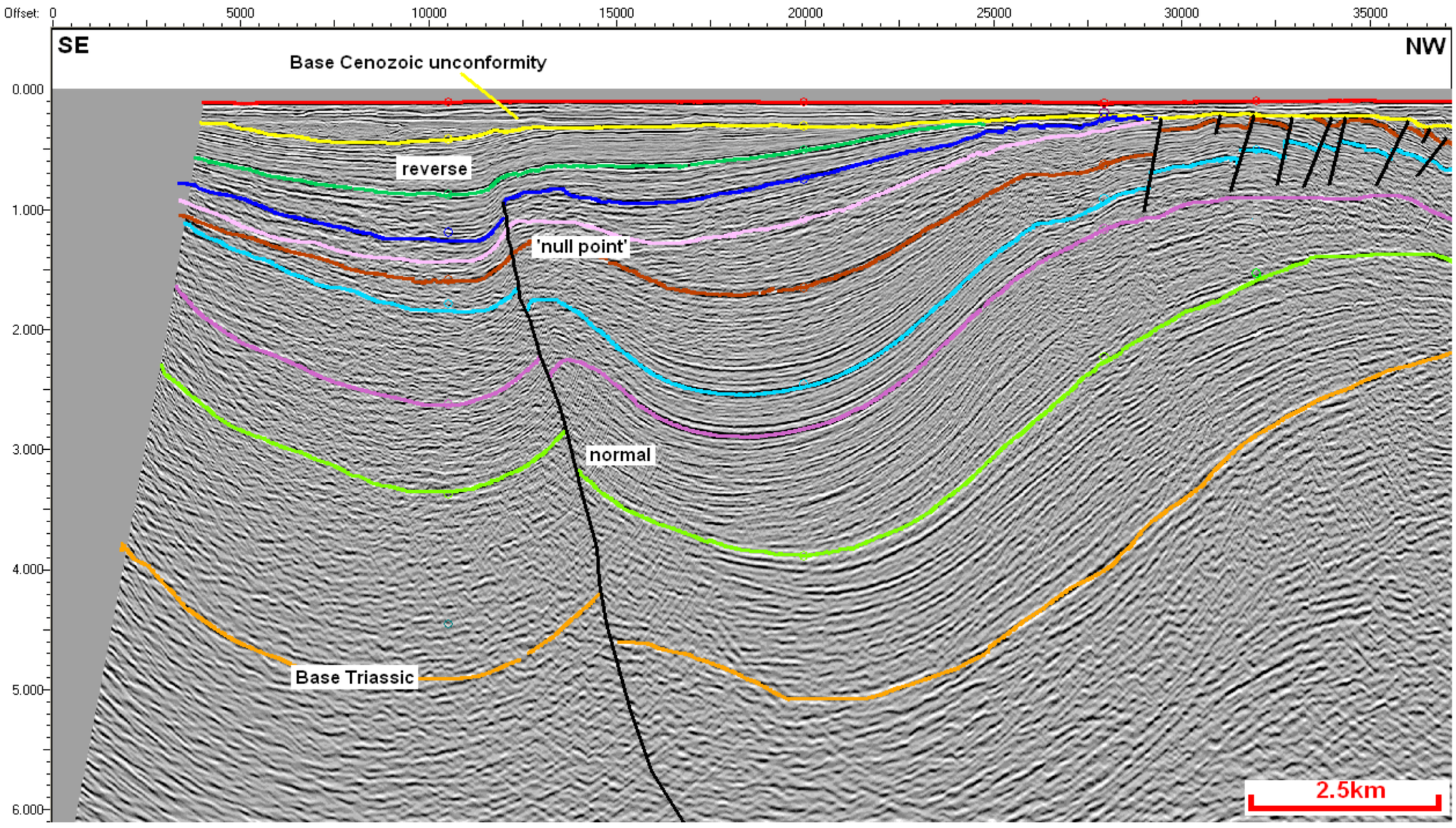

Figure 3.32 – Seismic section from the SGCB showing evidence of compressional reactivation of normal faults. Notice the net reverse movement above the 'null point', horizons below the 'null point' show net normal displacement. This section also highlights the on-lapping of reflectors against the base Cenozoic unconformity. Note also the reverse faults to the right of the section. The location of this section is line 5 in Figure 3.26. Offset is horizontal scale in metres and vertical scale is TWTT in seconds.

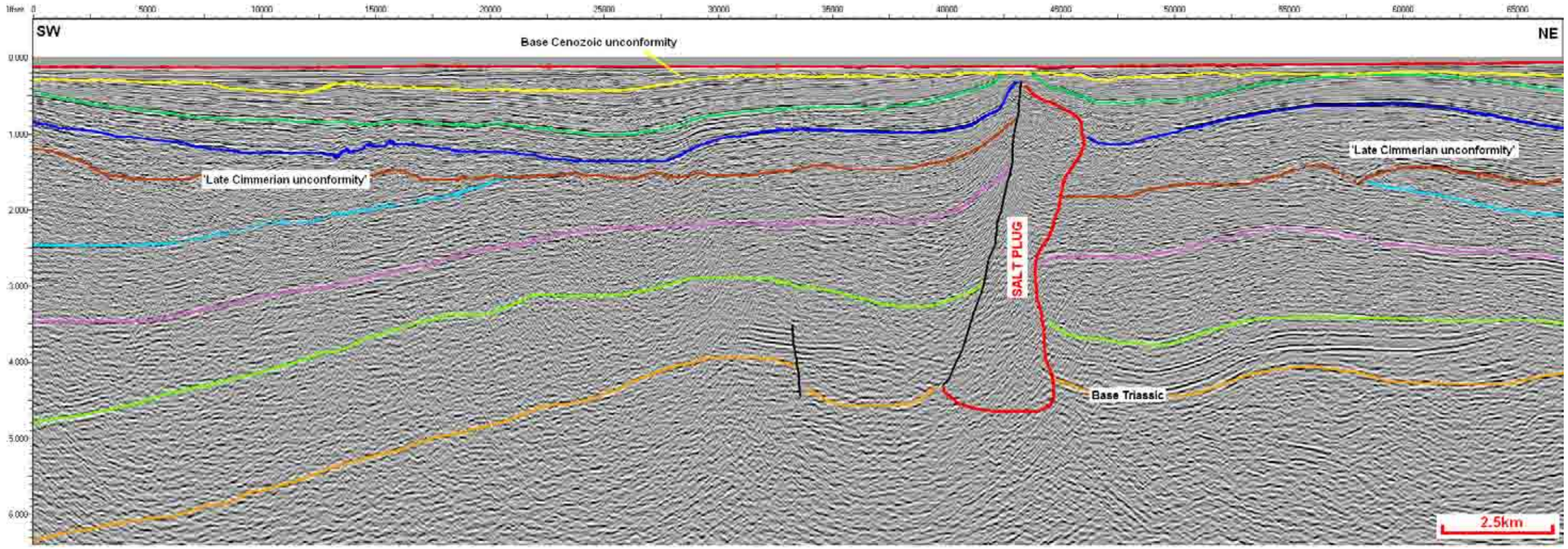

Figure 3.33 – Seismic section from the SGCB showing evidence of the erosional nature of the 'Late Cimmerian unconformity'. Note the termination of the top Jurassic reflector against the unconformity. This section also provides evidence for salt diapirism in the SGCB. The location of this section is line 6 in Figure 3.26. Offset is horizontal scale in metres and vertical scale is TWTT in seconds.

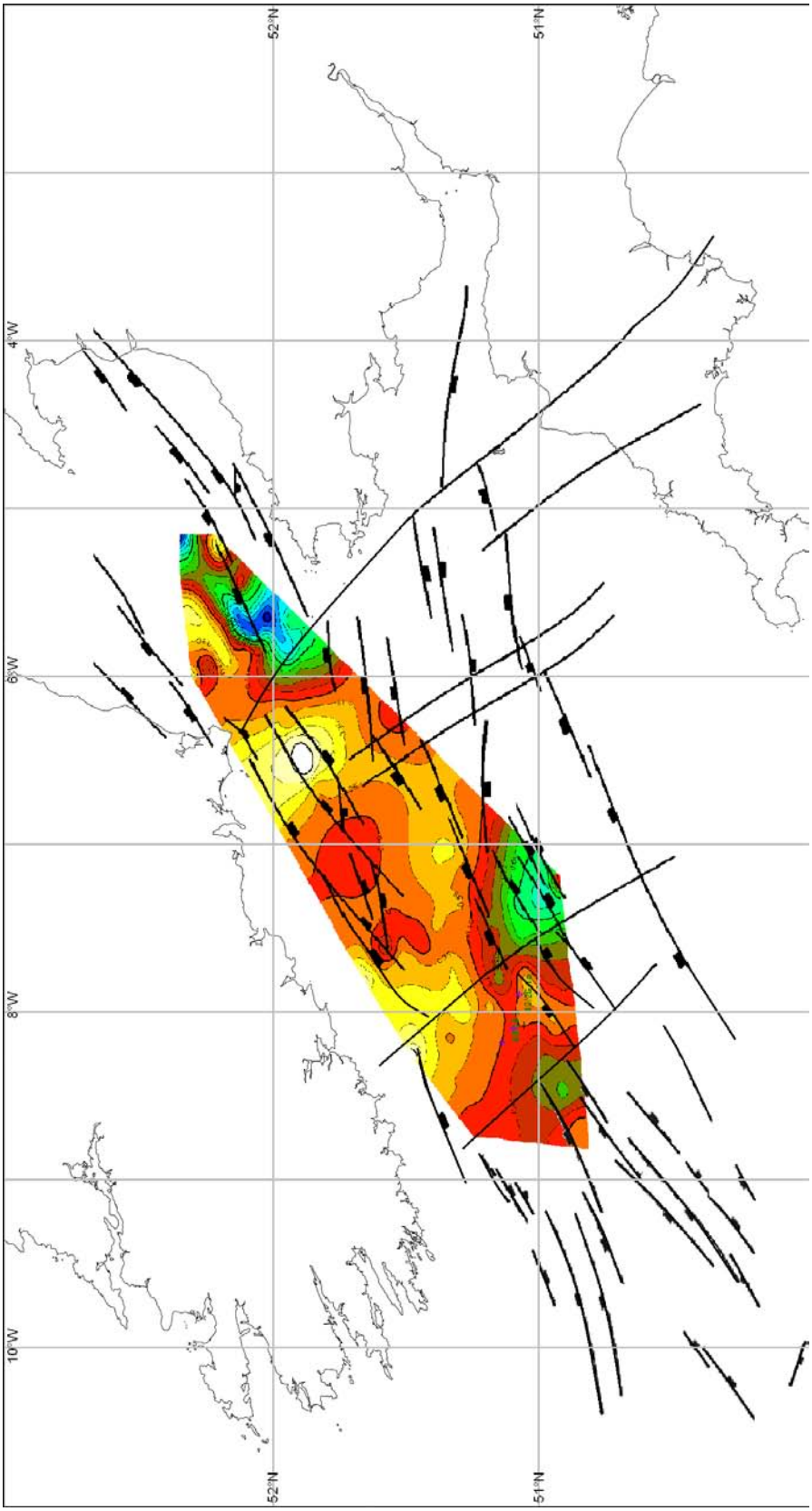

Figure 3.34 – TWTT map of the base Cenozoic unconformity showing its spatial distribution. Note the lows within the basin depocentres of the NCSB, SCSB and SGCB/CBB. Please note that there may be some edge effects at the extremes of the map due to the data coverage.

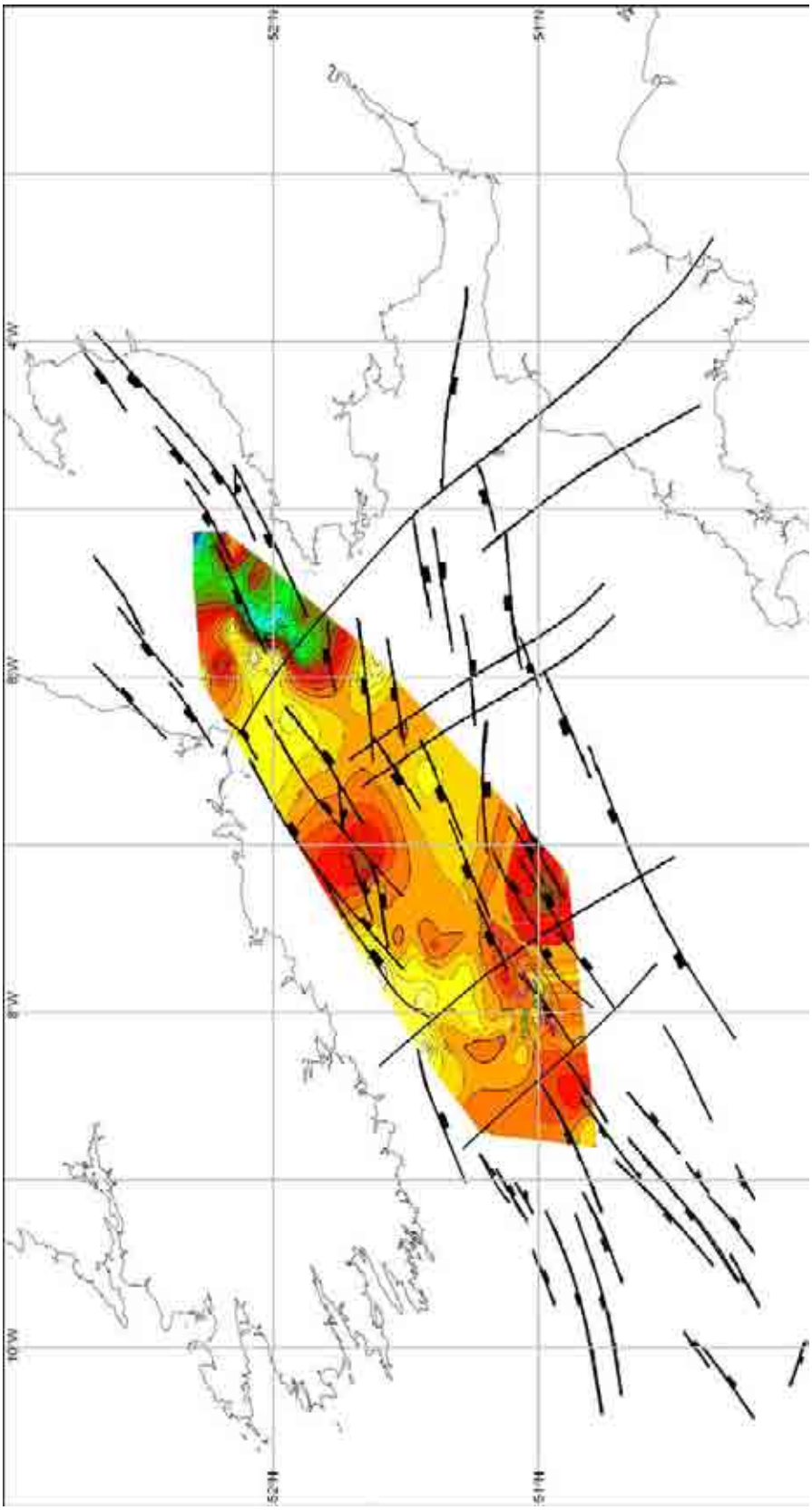

Figure 3.35 – TWTT map of the base Chalk. Note the shallowing of the formation against the basement high of the Pembroke ridge (southern edge of the coloured area) and the deepening of the unit within the main basin depocentres of the SGCB and NCSB.

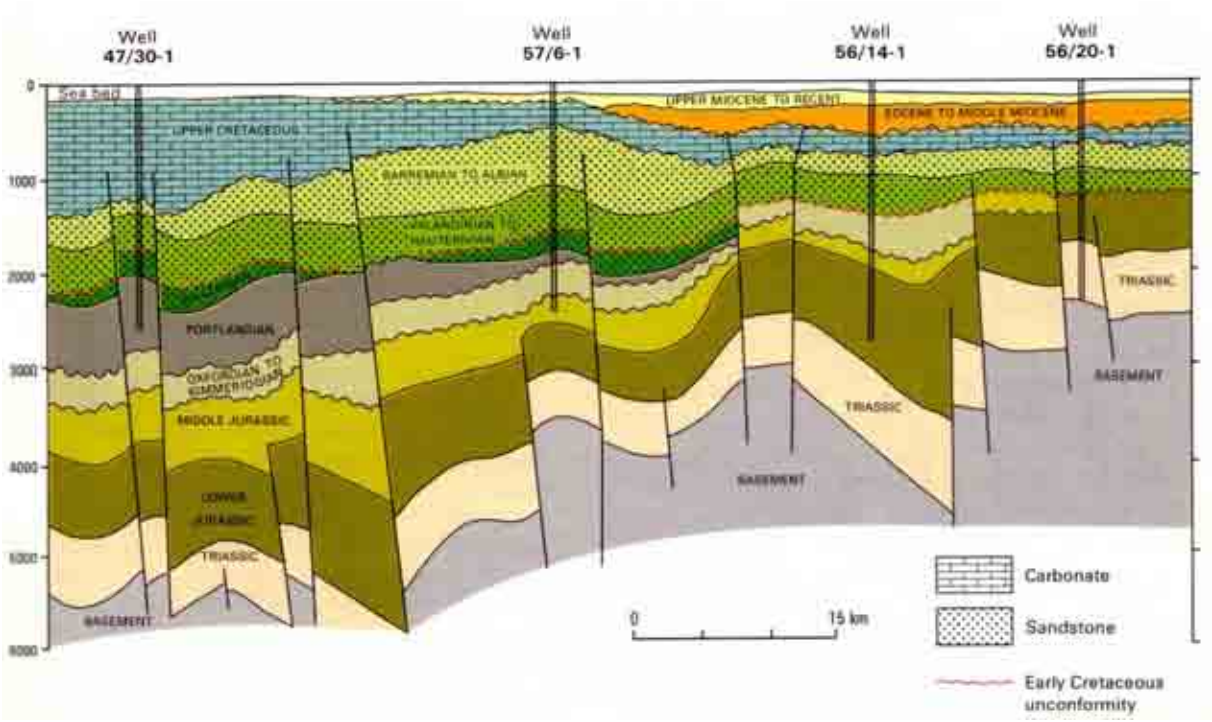

Figure 3.36 – North-South section across the southern part of the NCSB in Irish waters (after Colin *et al.* 1981).

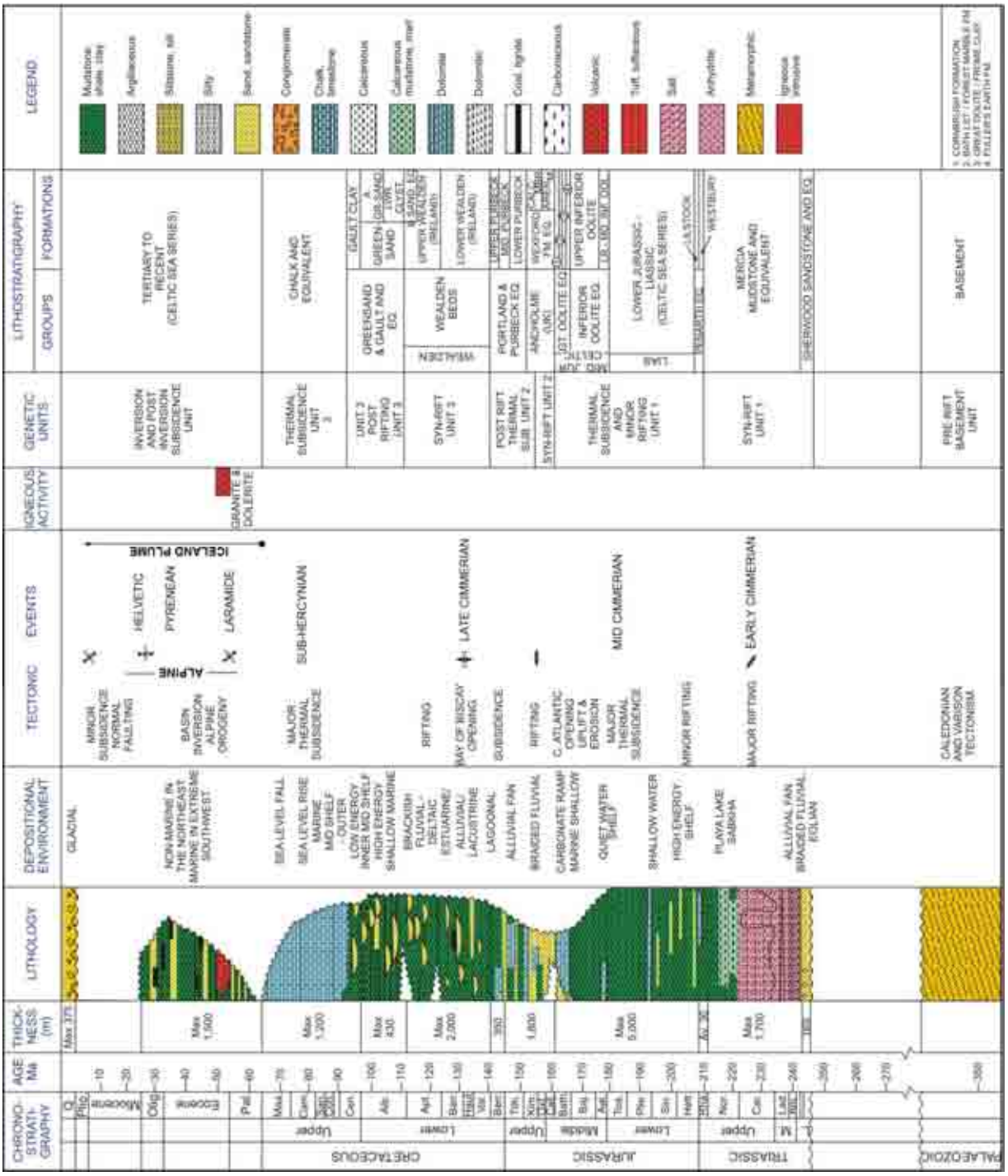

Figure 3.37 – Tectonostratigraphic chart for the Celtic Sea constructed from observations in this thesis and published literature (modified after Ziegler, 1990; Tappin *et al.* 1994; Williams, 2002; Holford, 2006).

CHAPTER 4: USING COMPACTIONAL DATA TO ESTIMATE EXHUMATION IN THE OFFSHORE BASINS OF THE SW UK

4.1: INTRODUCTION

The aim of this chapter is to present data of former deeper burial calculated from compactional data. The data was analysed using a range of techniques commonly used in studies of this type and as such has allowed the robustness of these methods to be compared and contrasted. Compaction is the reduction in sediment volume which occurs during burial and is the result of mechanical and thermomechanical processes (Magara, 1976; Sclater & Christie, 1980; Bulat & Stoker, 1987). Although some porosity 'rebound' can occur during exhumation (through recovery of the elastic component of deformation when effective stress is reduced), laboratory tests and empirical observations confirm that sediment compaction is largely irreversible (Luo & Vasseur, 1995; Giles *et al.* 1998). This observation, together with the fundamental assumption that the relevant stratigraphic units in the basin have experienced equilibrium compaction (i.e. compaction under hydrostatic conditions) with burial, forms the basis of compaction-based techniques for the assessment of former deeper burial.

A number of variations in methodology have evolved based upon the compaction parameter studied, approaches to selection of the normal compaction reference curve for an area and optimisation of curve fitting techniques. The most direct method involves the plotting of measured core-porosity from individual wells versus depth for a particular lithostratigraphic unit (Figure 4.1; Corcoran & Doré, 2005). Since no cores were available for analysis in the offshore wells this method has not been used in this thesis.

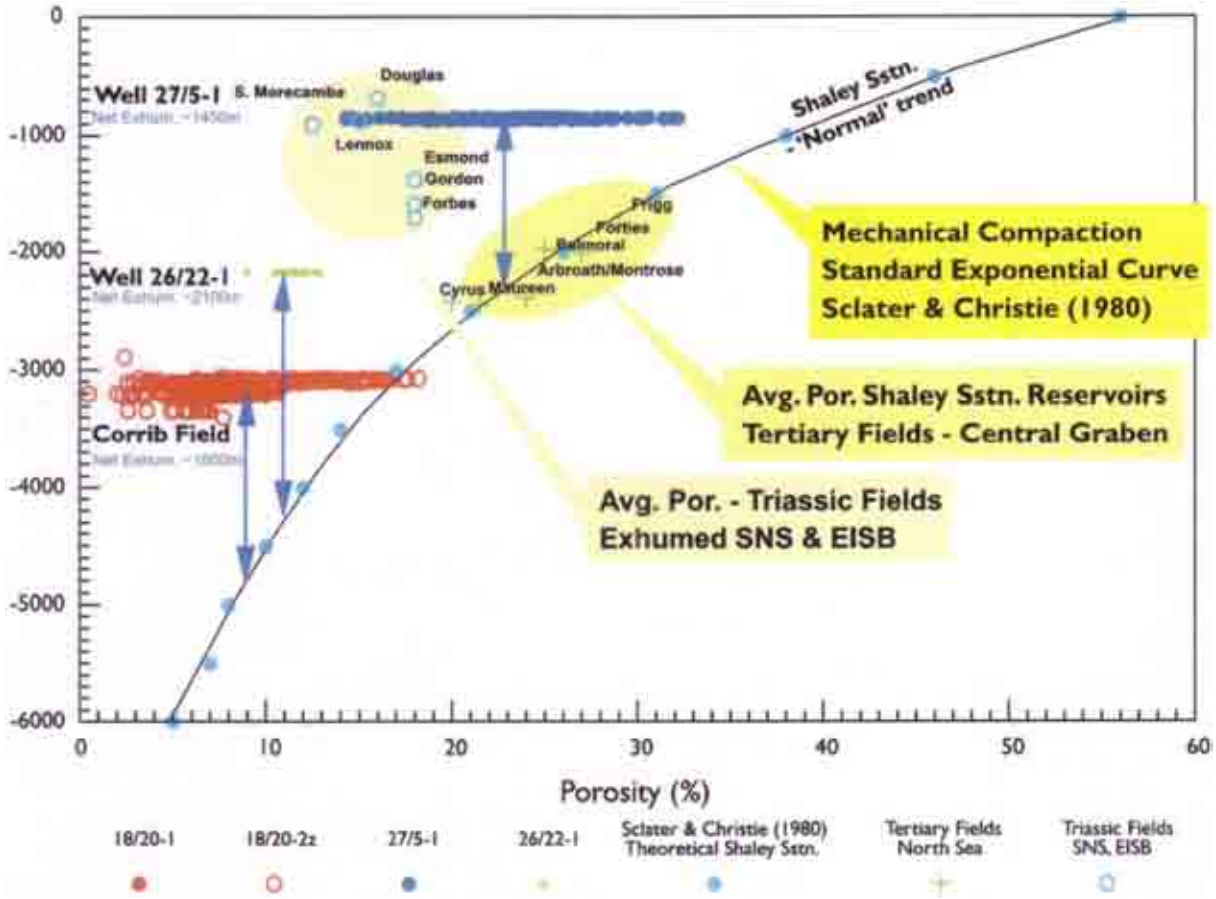

Figure 4.1 – Core porosity measurements for the Triassic Sherwood Sandstone reservoir, from three locations in the North Porcupine (26/22-1) and Slyne/Erris (Corrib Field 18/20-1 and 18/20-2; 27/05-1) basins compared with: average porosity measurements for Triassic gas fields in the exhumed East Irish Sea Basin and Southern North Sea Basin, average porosities for hydrocarbon bearing shaly sandstone reservoirs in the Central North Sea (from Abbotts, 1991) and a theoretical 'normal' compaction curve constructed from Sclater & Christie (1980) parameters for a typical shaly sandstone in the Central North Sea Basin – $\Phi=\Phi_0 e^{-cy}$, with surface porosity $\Phi_0=0.56$ and compaction coefficient $c=0.39$ (km^{-1}). Estimates of net exhumation at the 3 locations are as follows: Well 26/22-1 – 2100m; Well 27/05-1 – 1450m; Corrib Field area – 1600m (after Corcoran & Doré, 2005).

The widespread availability of sonic logs in offshore wells has rendered the sonic interval transit time or interval velocity parameter the most popular method for the estimation of former deeper burial from compaction trends. A common approach to estimating deeper burial at a well uses the sonic velocity log as a proxy for formation porosity:

$$\Delta t_{log} = \Delta t_{ma}(1-\phi) + \phi \Delta t_f \qquad (4.1)$$

where Φ is the porosity, and Δt_{log}, Δt_{ma} and Δt_f are the measured, matrix and fluid Interval Transit Time's (ITT) (Wyllie *et al.* 1956). There are two basic approaches to quantifying deeper burial from this relationship. The first seeks to establish a regional normal compaction curve for a ubiquitous uniform lithology, which is then used to estimate the burial anomaly (e.g. Menpes & Hillis, 1995). This is achieved by using two 'least exhumed' reference wells or an average velocity-depth gradient to constrain a linear ITT-depth relationship (Figure 4.2). It is important to remember that this technique estimates erosion relative to the 'least exhumed' reference wells, therefore if an entire area (including the 'reference wells') has undergone a regional uplift event this will be a minimum estimate of former deeper burial. The validity of burial anomaly magnitudes calculated for individual lithologies can be assessed by cross-plotting results from different stratigraphic units. For example, Menpes & Hillis (1995) used this technique to estimate burial anomalies for the Chalk, the Gault Clay and the Mercia Mudstone Group in the southern Celtic Sea and SW Approaches area of the UKCS. An alternative approach is to attempt to calculate the burial anomaly values at each well using a statistical curve-fitting technique. Heasler & Kharitonova (1996) and Ware (1999) used Athy's (1930) exponential compaction function of the form:

$$\Delta t = \Delta t_0 \, exp^{-bx} + c \qquad (4.2)$$

where Δt is the ITT, Δt_0 is the surface value of the ITT (taken to be 180-200μs/ft for sea water), x is the depth and c a shift constant which approximates to the ITT of the rock matrix. The curve fitting technique involves a logarithmic transformation of equation 4.1 to allow a simple linear analysis and the shift constant is varied to achieve an optimum fit based on the root mean square error. An estimate of former deeper burial is achieved by extrapolating the best-fit curve above the erosional unconformity to the value Δt_0 (Figure 4.2b). Again the

burial anomaly estimate must include the thickness of sediment deposited above the unconformity marking the uplift event.

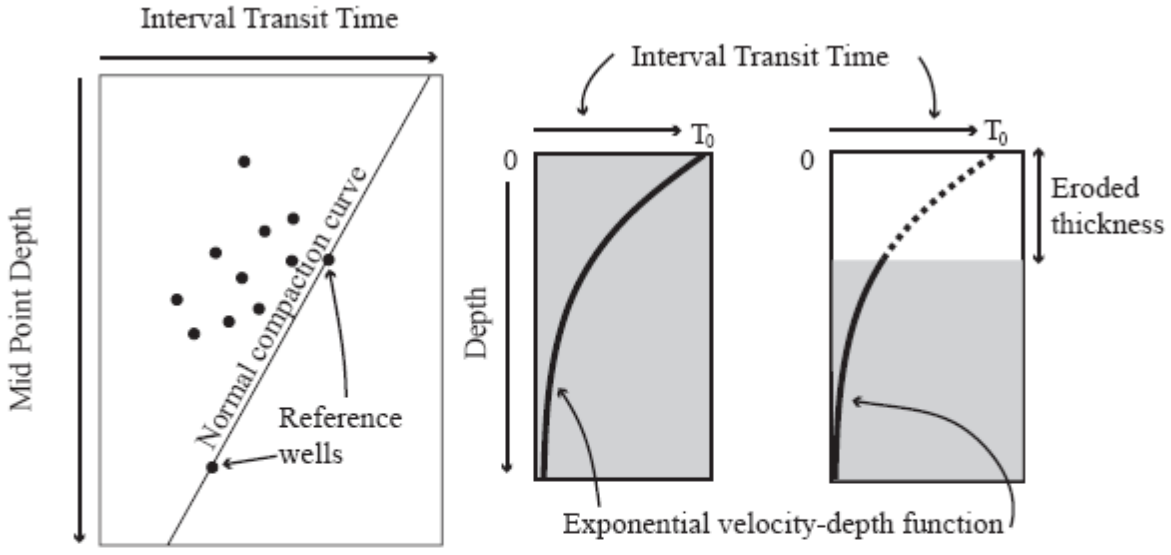

Figure 4.2 – Techniques for estimating exhumation from sonic velocity data (after Williams, 2002). (a) Estimating exhumation relative to two 'least exhumed' wells (after Menpes & Hillis, 1995); (b) Estimating exhumation from a single well using the sonic velocity log (after Heasler & Kharitonova, 1996).

The Celtic Sea contains a series of linked Mesozoic extensional basins that have been exhumed during the Early Cretaceous, the Paleogene and the Neogene. These basins are structurally diverse; for example the SGCB is filled with over 12km of Mesozoic rift sediments whereas the nearby BCB contains little more than 4km of sediment fill. Critically, structural and stratigraphic evidence suggests that each basin has undergone markedly contrasting amounts of exhumation, with Triassic syn-rift sediment exposed at the sea-floor in the CISB and in excess of 6km of Jurassic strata sub-cropping 2km of Cenozoic sediment in the adjacent SGCB. The NCSB, SCSB and BCB are characterized by thick Triassic and Jurassic syn-rift units that are unconformably overlain by an Upper Cretaceous, Chalk-dominated post-rift sequence. The Chalk decreases in thickness towards the north in the

Celtic Sea whereas Upper Cretaceous sediments are entirely absent north of the 'Variscan Front'.

It is clear that in order to elucidate the uplift and erosion history of the SW UK a clear understanding of the distribution and magnitude of exhumation in the offshore basins is vital for an effective tectonic synthesis of the region and 34 wells have been drilled in the UK Quads of the Celtic Sea region, allowing such a study to be carried out. Data from UK Quads 93, 102, 103 and 106, Irish Quad 50 and the onshore Burton Row borehole was used to calculate former deeper burial based on compactional data analysis.

4.2: DETERMINATION OF FORMER DEEPER BURIAL FROM POROSITY

The general methodology to compute an absolute estimate of the magnitude of former deeper burial at any given well location has been outlined in Chapter 2 (*cf.* Section 2.2). In order to estimate magnitudes of exhumation, porosity data from the Lower Jurassic Lias Group, Triassic Mercia mudstone Group and Triassic Sherwood Sandstone sequences have been compared to the compaction trend for North Sea (Central Graben) shales, expressed by the exponential porosity-depth relationship of Sclater & Christie (1980):

$$\phi = \phi_0 e^{-cy} \qquad (4.3)$$

Where Φ_0 is the porosity of sediments at the time of deposition, c is a constant compaction coefficient and y is depth. For North Sea shales, Sclater & Christie (1980) suggested values of 63% for Φ_0 and 0.00051 for c when y is expressed in metres. Re-arranging equation 4.3 to give depth for a calculated porosity gives:

$$y = \frac{1}{c}\log\left(\frac{\phi_0}{\phi}\right) \tag{4.4}$$

Shales are generally chosen for the analysis of maximum burial depths because they exhibit relatively simple (i.e. more predictable from being less prone to unwanted diagenetic effects) normal compaction trends with their porosity decreasing rapidly with depth (Magara, 1978). Coarser grained lithologies such as sandstones are susceptible to anomalous compaction behaviour due largely to diagenetic effects (Japsen *et al.* 2000).

Before the calculation of porosities the sonic log was filtered to remove spurious data and to ensure lithological consistency. In stratigraphic intervals with mixed lithologies it is necessary to separate the data into consistent lithological units which then can be compared against an appropriate compaction trend. The three stratigraphic intervals chosen were the Lower Jurassic Liassic shales, Triassic Mercia Mudstone Group and Triassic Sherwood Sandstone Group. In southern England, the Sherwood Sandstone Group was subdivided into three units by Whittaker *et al.* (1985); these are displayed well in the Burton Row borehole (Figure 4.3). The units are distinguished by their geophysical-log and lithological character and represent an overall upward-fining sequence.

At the base, unit SS1 is characterised by low gamma-ray values and relatively high sonic velocities which represent poorly bedded pebble beds and conglomerates, with sandstone inter-beds. Unit SS2 shows higher gamma-ray values, which increase upwards and sonic velocities which decrease upwards. The unit comprises sandstones with minor conglomerates and siltstone inter-beds (Tappin *et al.* 1994). Unit SS3 continues the trend of upward increase in gamma-ray values and decrease in sonic velocity, reflecting upward-fining into sandstones and siltstones. For the purposes of the analysis only unit SS3 was considered shaley enough

to analyse occurrences of the other units resulting in the values being discarded due to lack of shale.

In offshore wells, the base of the Mercia Mudstone Group is taken, by comparison with the Burton Row borehole (Whittaker *et al.* 1985), at a marked change on gamma-ray and sonic log profiles that reflects an upward passage from inter-bedded sandstones, siltstones and mudstones into mudstones (Figure 4.4). Four lithological units are distinguishable in offshore wells: in ascending order these are: (i) red mudstones and siltstones with subordinate sandstones, gypsum and halite; (ii) halites inter-bedded with claystones, mudstones, sandstones, dolomite and gypsum; (iii) red, commonly silty, claystones; and (iv) grey-green mudstones with subordinate dolomite and gypsum (Tappin *et al.* 1994).

The Lias Group consists of medium to dark grey, fossiliferous mudstones with variable carbonate content, inter-bedded with argillaceous limestones, siltstones and more rarely, fine-grained sandstones. The group is subdivided into the Lower, Middle and Upper Lias, the middle sequence being usually more arenaceous (Figure 4.5).

Two methods were used to filter the sonic data so that only data from shales was used in determining amounts of exhumation. Firstly the sonic log was manually edited (removal of null values and anomalous values) using operator's stratigraphic logs to separate fine grained units and coarser units and remove non-shale lithologies. Secondly data which exceeded the lower value for that of water (180μs/ft) and which were less than the matrix velocity for dolomites (40μs/ft) were removed. In the case of the wells 103/18-1 and 103/21-1 and the Burton Row borehole, the gamma log, a proxy for shale volume (e.g. Schlumberger, 1989; Rider, 1996) was used to remove parts of the log where the equivalent gamma ray response was less than 70 API units (i.e. GR>70 API = Shale). Unfortunately the GR log was not

available for any of the other wells used in this study. For logs where Triassic salt was present any data below the salt was discarded since salt does not compact with depth. Once filtered the sonic log was sampled and averaged at 20 metre intervals since the lithological data for the offshore wells was only correct to two metre intervals. Averaging the data over 20 metre intervals averaged out the effects of unwanted lithologies such as coarser lithologies and salt particularly where no GR log was available.

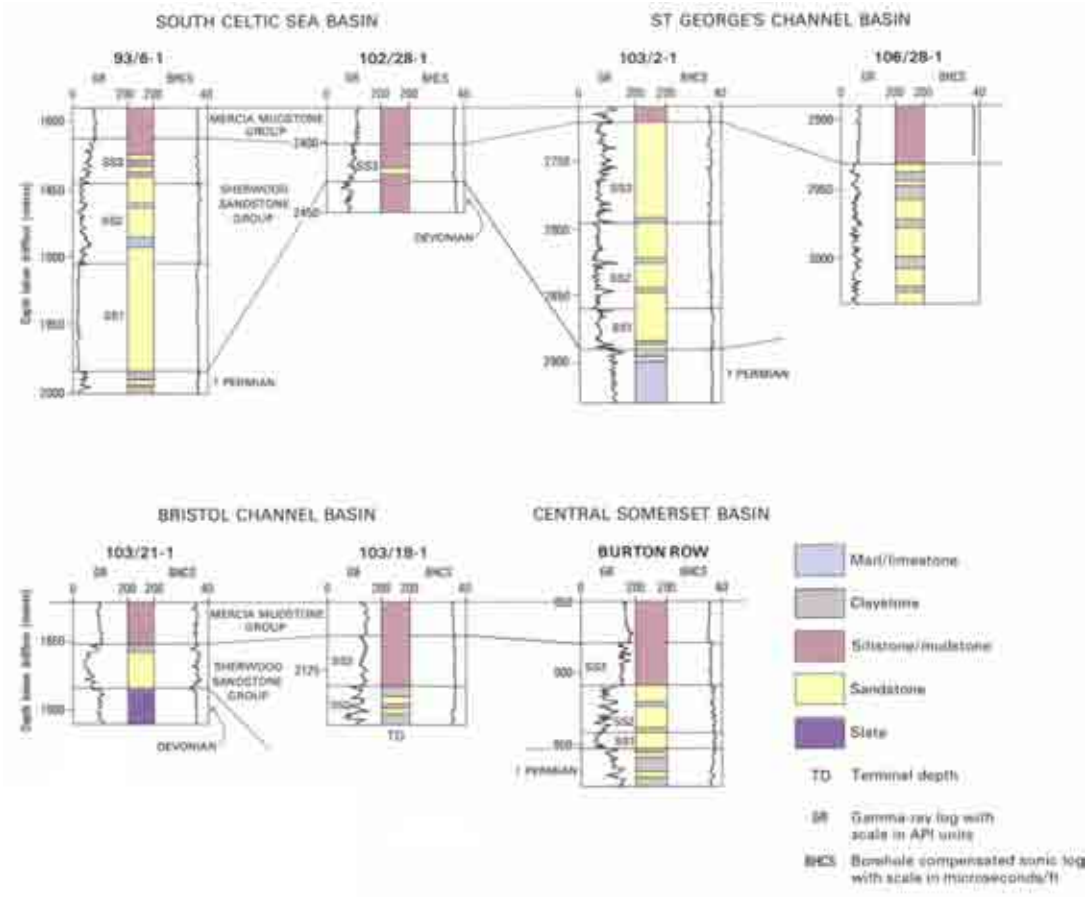

Figure 4.3 - Wells depicting Sherwood Sandstone Group lithostratigraphy, with geophysical logs (after Tappin *et al.* 1994).

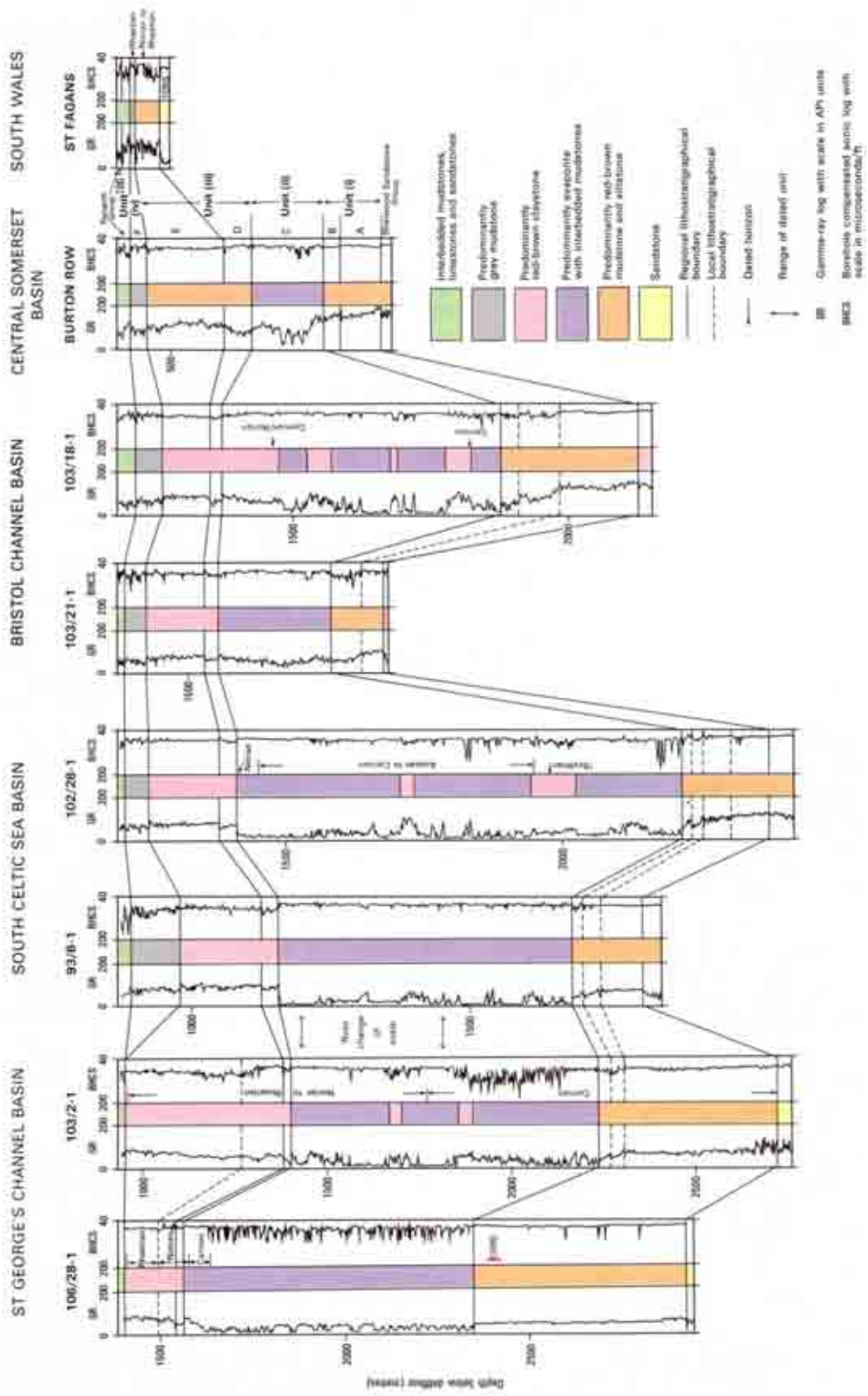

Figure 4.4 – Wells depicting Mercia Mudstone Group lithostratigraphy, with geophysical logs. Litho-stratigraphical units are based on the Burton Row borehole (after Whittaker et al., 1985) and geophysical units after Lott *et al.* (1982). Note the change of scale between wells 103/02-1 and 93/06-1 (after Tappin *et al.* 1994).

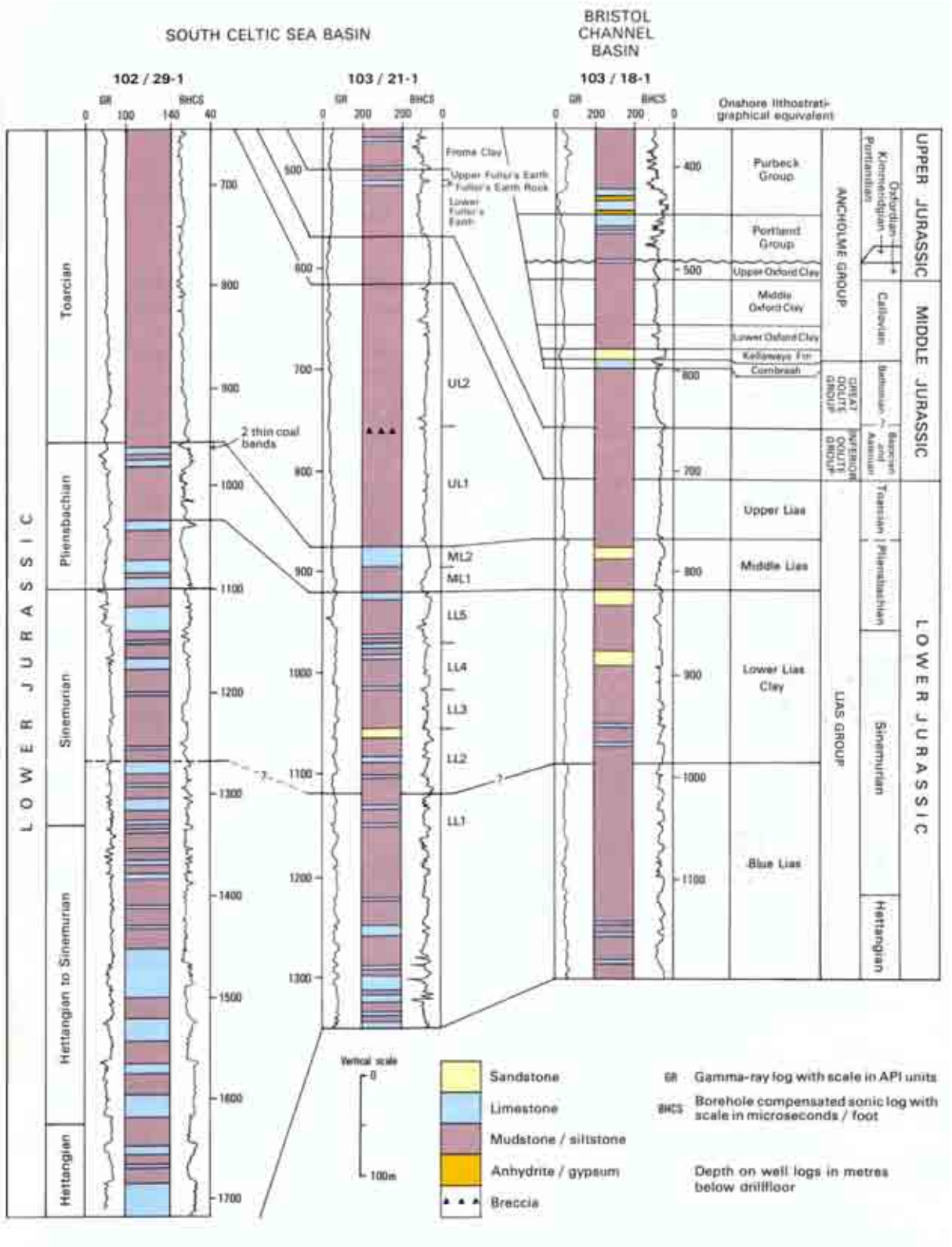

Figure 4.5 – Logs of wells from the South Celtic Sea and Bristol Channel basins showing Lias Group stratigraphy (after Tappin *et al.* 1994).

4.2.1: POROSITY CALCULATION

As with the sonic data the porosity was averaged at 20 metre intervals to smooth out anomalous porosities from unwanted horizons. The calculation of porosities has not been used to estimate exhumation in the Celtic Sea before and as such there is not an established correction factor to use in the equations. For this reason the Wyllie equation (Equation 2.7) calculated the average porosity based on correction factor of 1.0, 1.15 and 1.3 and the RHG-transform (Equation 2.8) an average based on the two end members 0.7 and 0.625. The parameters for bulk density and fluid density (see Chapter 2) were constants however to reflect the variation in shale lithology both the 68μs/ft and 60μs/ft constants were used for bulk density. It should be noted that the Wyllie equation in its unaltered form is still used by the hydrocarbon industry in estimating porosities. For this reason, as well as the fact that the correction factors should bring the results broadly in line with the Raymer equation, the exhumation values generated by the unaltered Wyllie equation were also recorded. For both equations the true value for exhumation of a particular unit can be thought of as falling somewhere between the upper and lower limits as defined by the correction factors which represent maximum and minimum porosities for that value. The ASCII data files and calculated values are included on the CD available with this thesis and the interested reader is referred to those files to see a practical example of the approach.

4.2.2: DENSITY DERIVED POROSITY

In order to try and get a more rigorous transform with which to calculate porosities and compare with the Sclater & Christie trend the density logs from two offshore wells (103/18-1 and 103/21-1) as well as the onshore Mochras borehole (Holford, 2006) were used to calculate porosities. As before the density log was filtered to remove spurious data and to ensure lithological consistency before the porosities were calculated. In addition the tool

measured density correction factor (Schlumberger, 1989) was added to the data, the effect on porosities that this has is demonstrated in Figure 4.6.

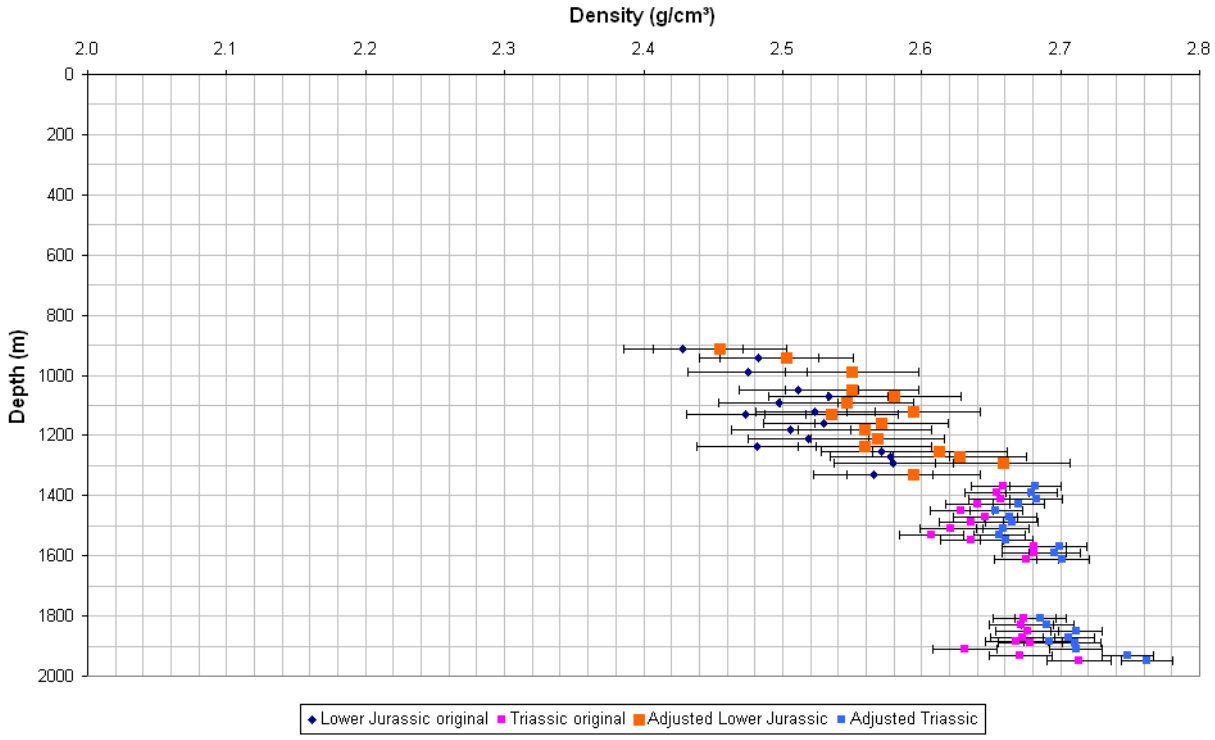

Figure 4.6 – The effect of adding the density correction to the original density data (in this case for well 103/21-1). Note how many of the outlying values scatter is reduced by addition of the correction factor.

Porosity (Φ) can be estimated from bulk density data using the following relationship (Schlumberger, 1989):

$$\phi = \frac{(\rho_{ma} - \rho_b)}{(\rho_{ma} - \rho_f)} \qquad (4.5)$$

Where ρ_{ma} is the matrix (or grain) density, ρ_b is the bulk density and ρ_f is the pore fluid density. For shales the largest source of error when converting density data to porosities arises from the highly variable nature of shale matrix densities (Rider, 1996). For this reason two sets of porosities have been calculated using the end member matrix densities of 2.67g/cm³ and 2.72g/cm³ (*cf.* Holford *et al.* 2005). For both sets of calculations pore fluid density (ρ_f) was assumed to be 1.01g/cm³. Again the porosities were calculated and averaged

across 20m intervals and these results are shown in Figure 4.7 and 4.8. Porosities calculated using a value of 2.72g/cm³ are between 2-3% higher than those calculated assuming a matrix density of 2.67g/cm³. All calculated porosities are much lower than those predicted for equivalent depths by the Sclater and Christie (1980) shale trend. Porosities within the Triassic successions generally show little decrease with depth (Figures 4.7 and 4.8), which mirrors the asymptotic tendency of the Sclater & Christie (1980) shale porosity-depth trend at depths greater than 4km.

4.2.2.1: Calculation of a density derived porosity trend

The density derived porosity was then plotted against the interval transit time corresponding to that porosity for both the offshore wells and Mochras borehole (Figure 4.9). From Figures 4.7 and 4.8 it can be shown that using the lower density of 2.67g/cm³ results in a number of porosities, despite errors, which are negative. Since the minimum state of a rock can only be 0% porosity i.e. totally compacted and representing bulk matrix density, the lower value of 2.67g/cm³ is not favoured as being a true representation of the matrix density in these particular rocks. For this reason the data for porosities calculated using the 2.72g/cm³ was used to determine the relative trends between ITT and porosity (Figure 4.10). This data was then analysed and fitted to a number of functions that have been proposed by many different workers (e.g. linear: Sulley, 1978; Magara, 1980; power: Baldwin & Butler, 1985; exponential: Athy, 1930; Rubey & Hubbert, 1959; Magara, 1976) in order to compute a function which transformed interval transit time into an equivalent porosity which could be applied to the data where only the sonic log was available. These relationships and their fits are shown in Figures 4.10-4.14.

The sonic data from all of the wells was converted into porosity using each of the transforms. This analysis also showed that rocks in the area still have porosity below 68μs/ft – the point at which the rocks should be fully compacted (Magara, 1978). As previously mentioned there is a wide range of possible matrix velocities for shales and in light of this evidence it was decided that the value of 60μs/ft should be used as the matrix velocity for shales in this area. For this reason each of the Wyllie and Raymer analyses were carried out again this time using the lower value of 60μs/ft as the matrix velocity in order to compare the different exhumation estimates. Figure 4.13 shows the resulting trends plotted with all the data from the wells. It demonstrates that no single trend fits all of the points satisfactorily. For this reason a 'hybrid' trend (Figure 4.14) was developed composed of various segments which fitted the data best:

linear – 60μs/ft – 74μs/ft

exponential – 74μs/ft – 115μs/ft

power – 115μs/ft – 135μs/ft

exponential – 135μs/ft – 180μs/ft

This trend was also used to calculate the resulting porosities from the sonic data. It should be noted that this is not the only way in deriving a fitted curve to the data, however due to the sparse coverage of data points available to fit the trend, this method was judged to be the most reliable. It may be the case that the data would give a statistically better fit using a derivation of one of the individual trends but due to this data absence a more sophisticated method of curve fitting has not been possible in this study.

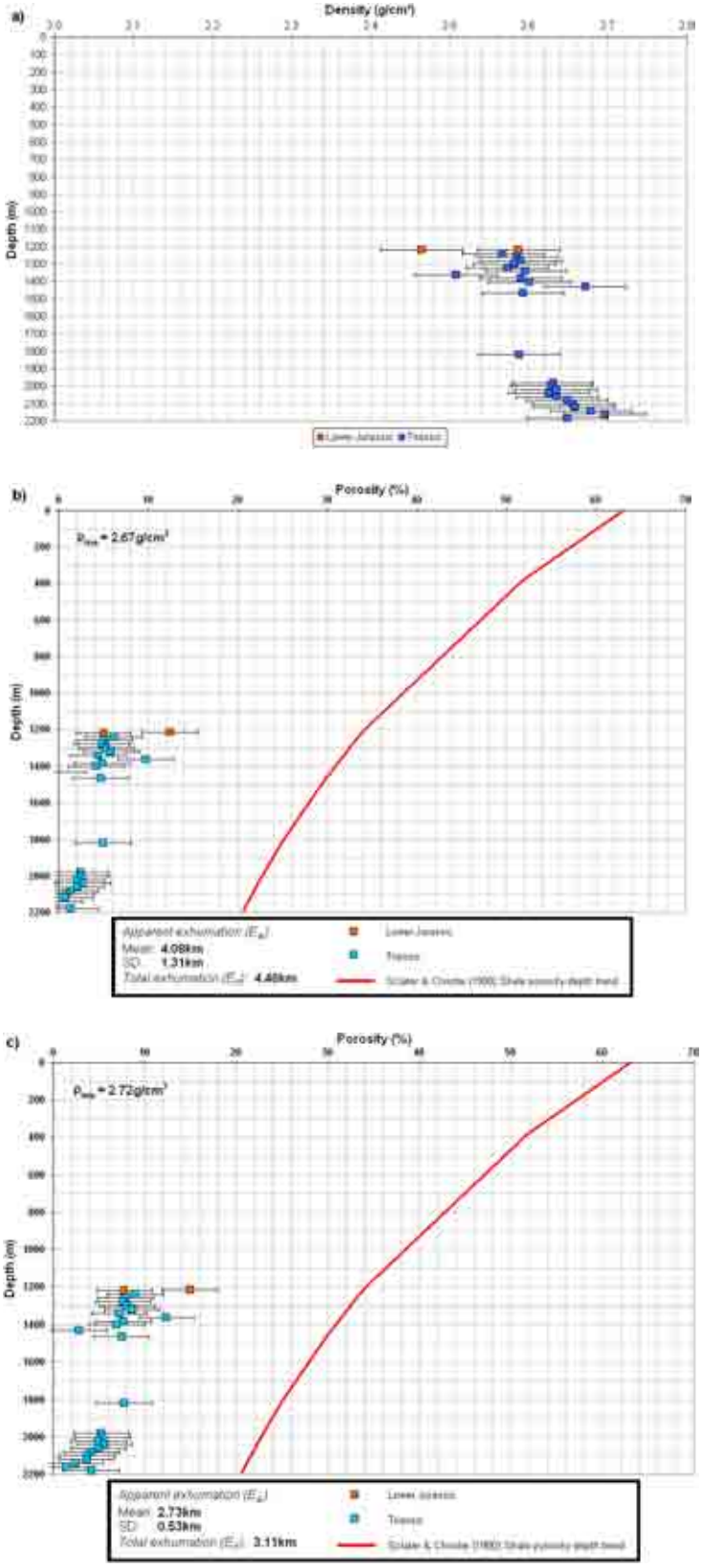

Figure 4.7 – Calculated porosity data for offshore well 103/18-1. Error bars represent ±1 standard deviation. (a) Bulk density (g/cm³) data for well 103/18-1 (b) Porosities calculated using equation (4.a) assuming a matrix density of 2.67g/cm³ (c) Porosity data and exhumation estimates calculated assuming a matrix density of 2.72g/cm³. Apparent and total exhumation estimates (*cf.* Hillis, 1995) relative to the Sclater & Christie (1980) shale porosity-depth trend.

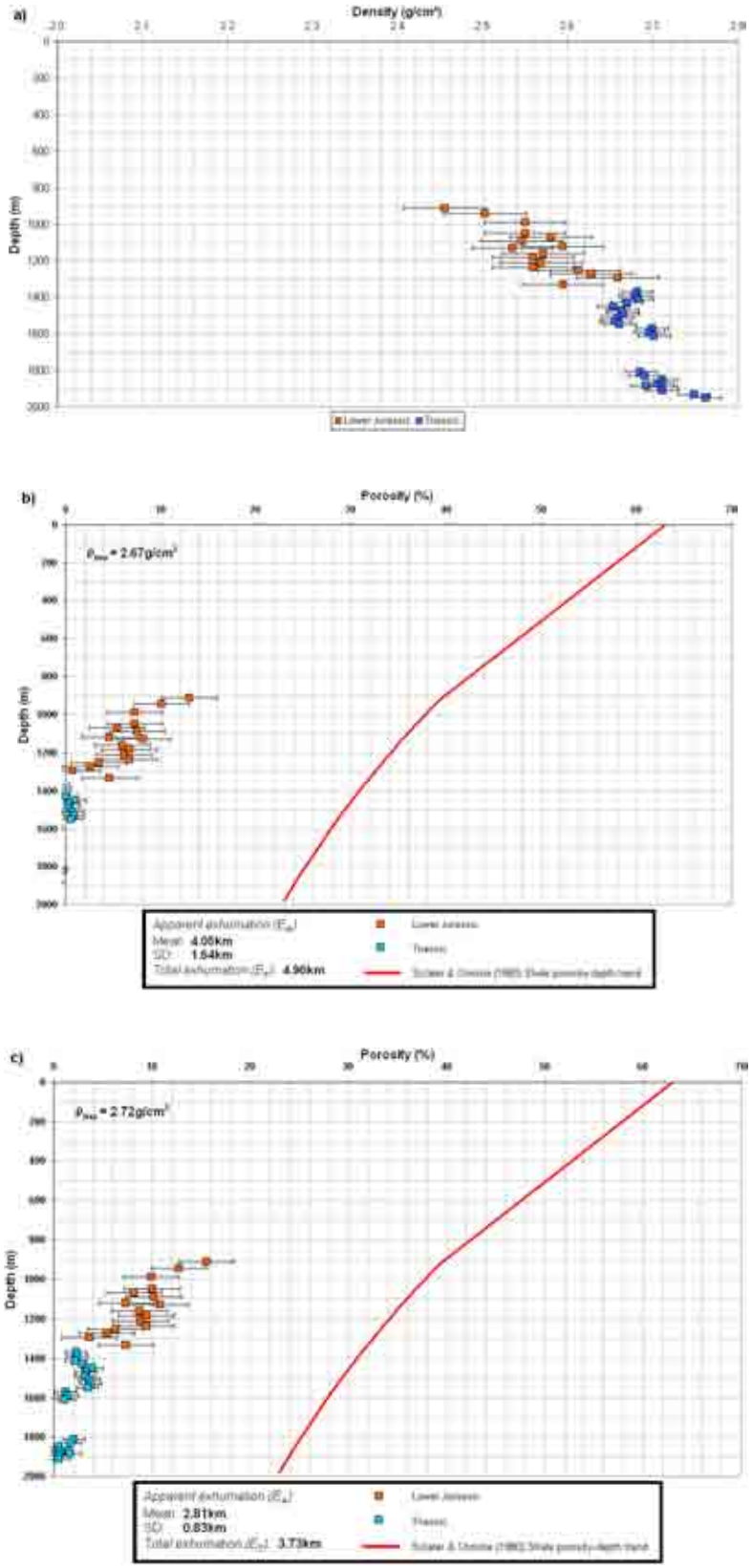

Figure 4.8 – Calculated porosity data for offshore well 103/21-1. Error bars represent ±1 standard deviation. (a) Bulk density (g/cm³) data for well 103/21-1 (b) Porosities calculated using equation (4.a) assuming a matrix density of 2.67g/cm³ (c) Porosity data and exhumation estimates calculated assuming a matrix density of 2.72g/cm³. Apparent and total exhumation estimates (*cf.* Hillis, 1995) relative to the Sclater & Christie (1980) shale porosity-depth trend.

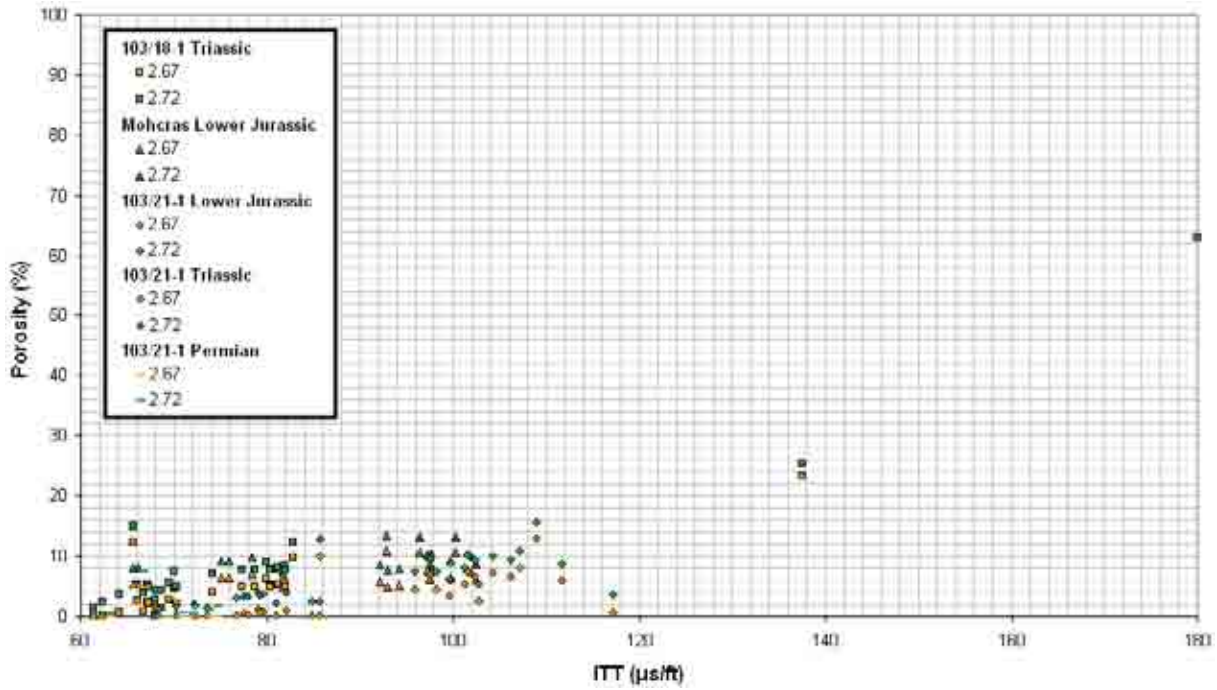

Figure 4.9 – Comparison of the density derived porosities versus interval transit time (ITT) for the various wells and lithologies.

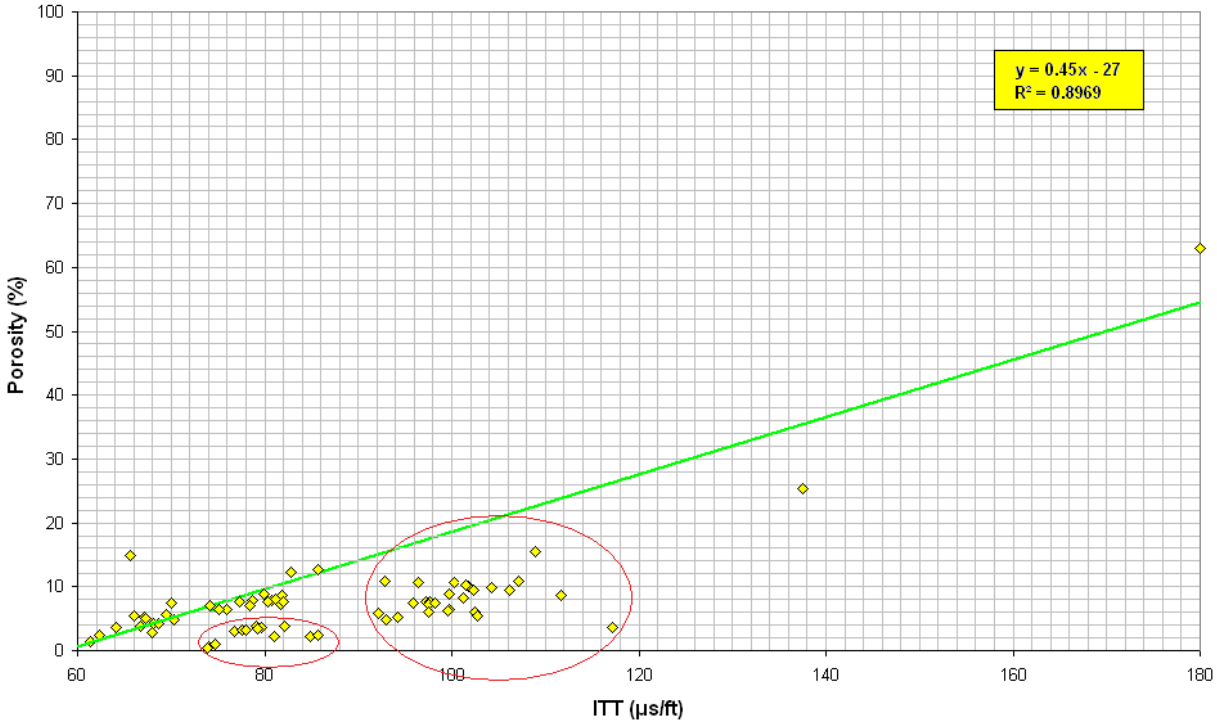

Figure 4.10 – Graph showing a linear relationship fitted to the porosity data derived from the density log. Note the Mochras borehole and 103/21-1 Triassic samples were omitted to generate this trend as they appear to lie on a different trend most likely related to lithological differences with the other wells used (two populations outlined by red circles). The fact that there are two trends already highlights the unlikelihood that a linear relationship is appropriate to model porosity in the SW UK.

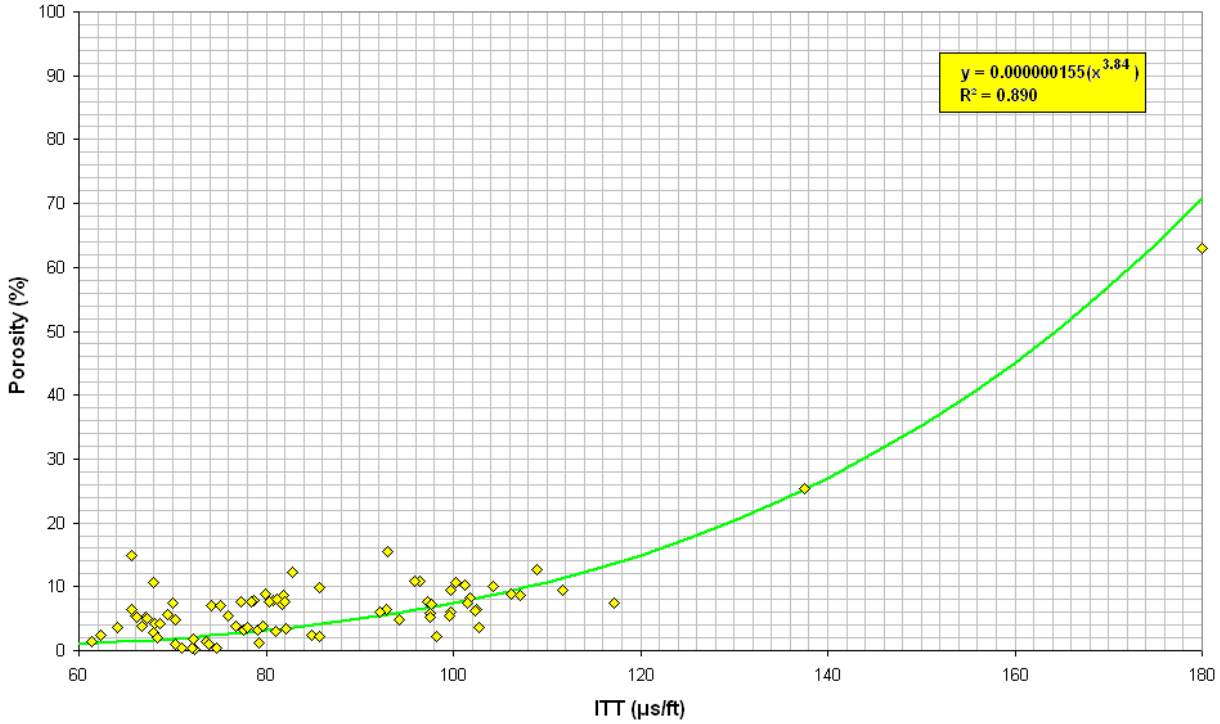

Figure 4.11 – Graph showing a power relationship fitted to the porosity data derived from the density log.

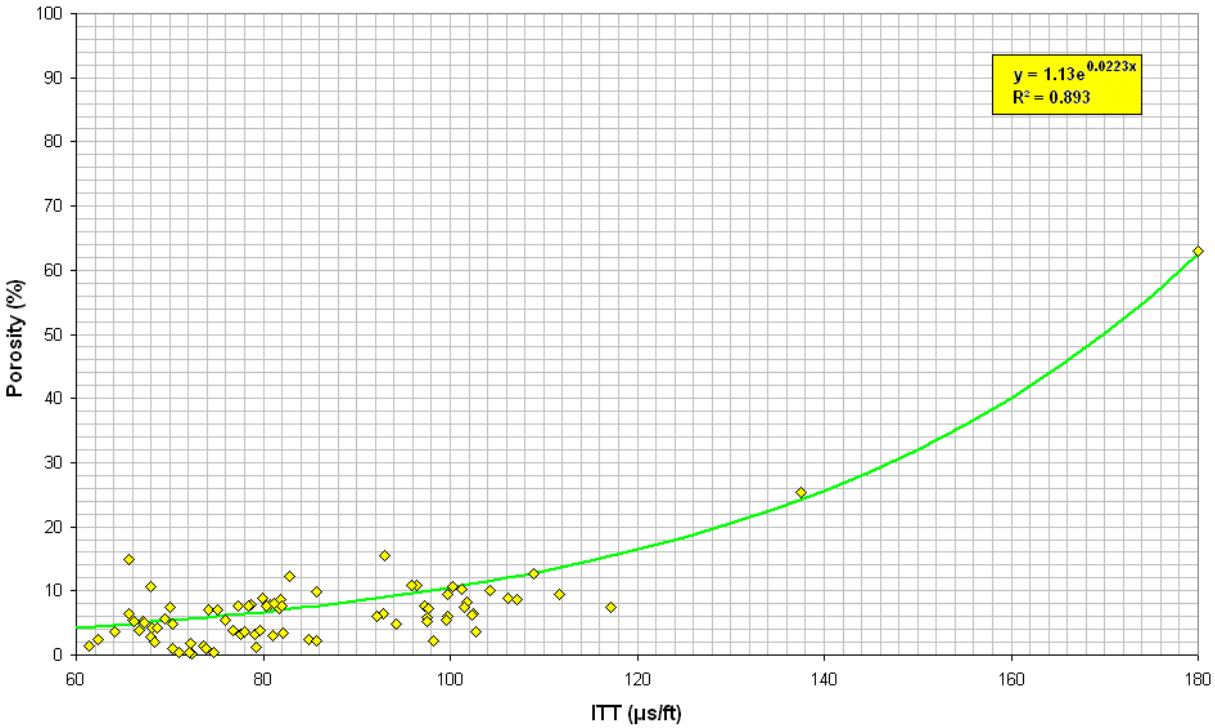

Figure 4.12 – Graph showing an exponential relationship fitted to the porosity data derived from the density log.

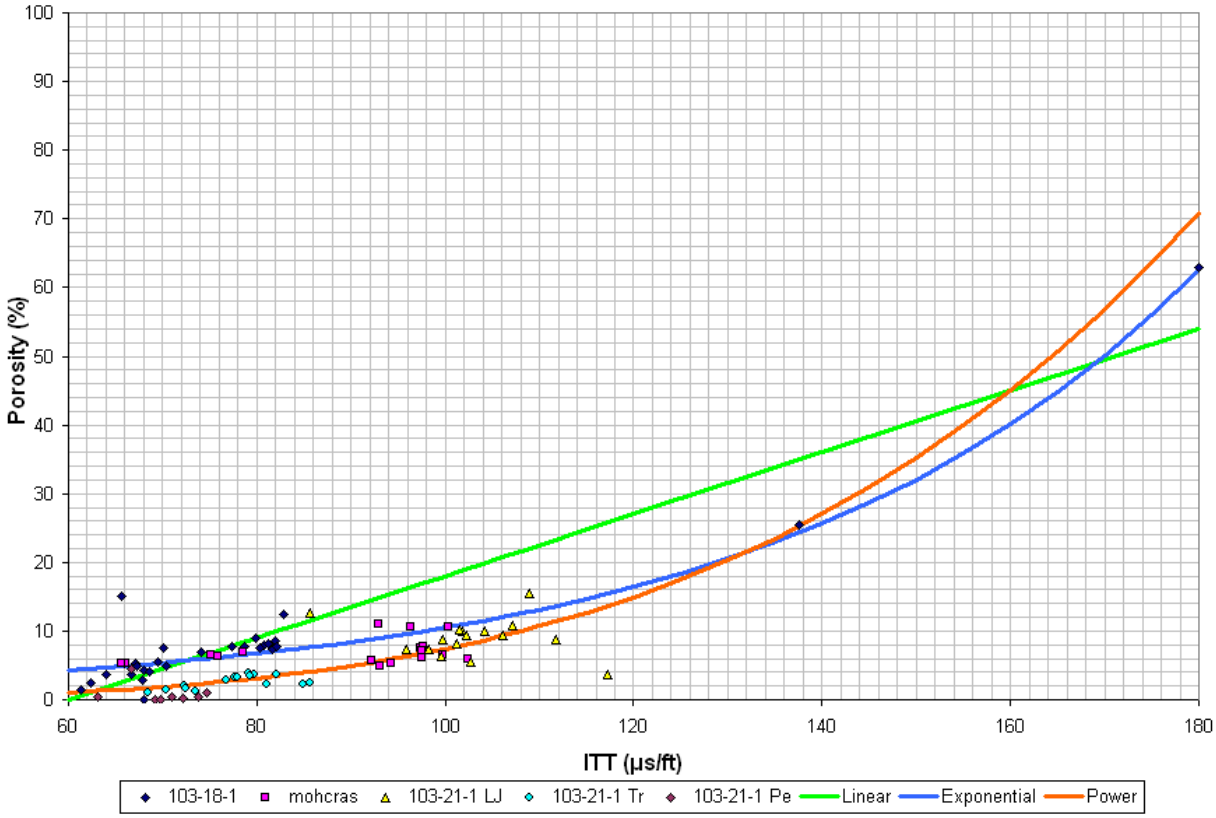

Figure 4.13 – Graph showing the relationships between interval transit time and density derived porosity for the Mochras borehole and the offshore wells 103/18-1 and 103/21-1. The graph shows that no single function adequately satisfies all the data.

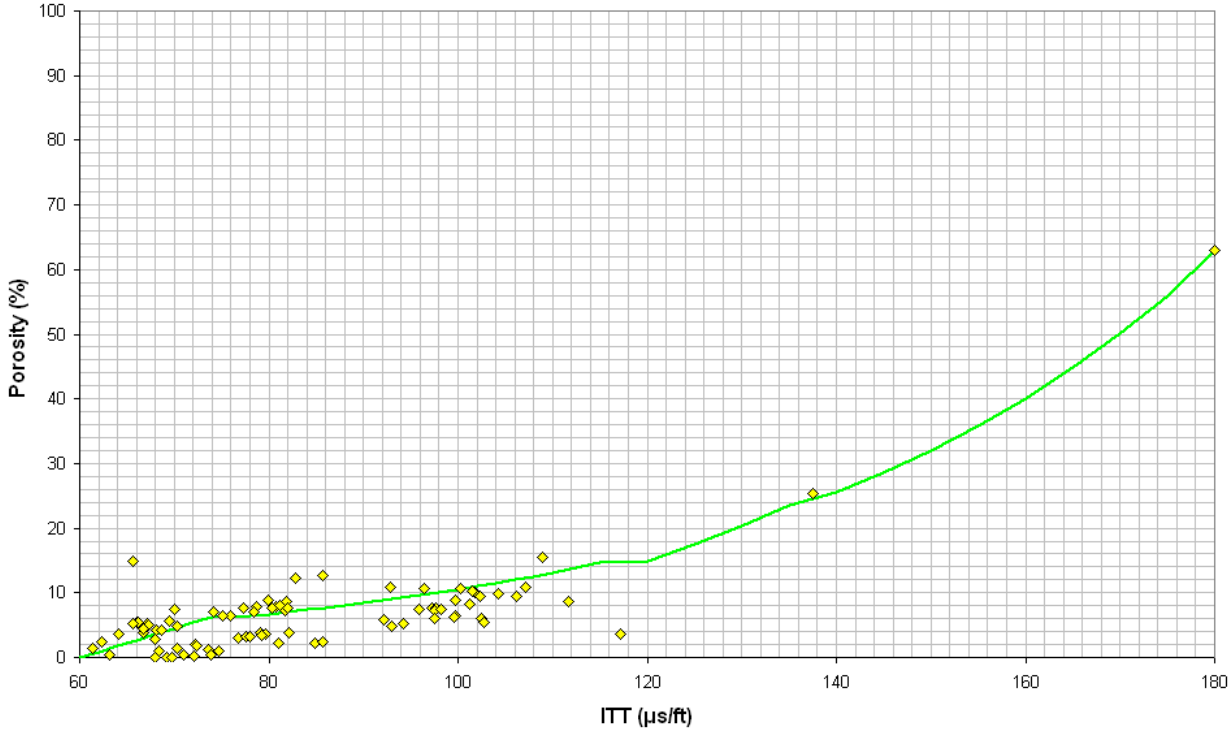

Figure 4.14 – Graph showing the 'hybrid' best fit relationship fitted to the porosity data derived from the density log.

4.3: DETERMINATION OF FORMER DEEPER BURIAL USING ITT

4.3.1: STATISTICAL CURVE FITTING TECHNIQUE

The first technique applied to the data was a purely mathematical statistical fit curve. An exponential relationship between porosity and depth was proposed originally by Athy (1930) and later by other workers (Rubey & Hubbert, 1959; Magara, 1976; Sclater & Christie, 1980; Korvin, 1984; Pittman & Larese, 1991) Athy's simple exponential model of porosity loss with depth is of the form:

$$\phi = \phi_0 \, exp^{(-bx)} \tag{4.6}$$

At the ground surface (x = 0), Athy's law predicts that porosity equals its surface value ($\Phi=\Phi_0$). At very great depths ($x \rightarrow \infty$), Athy's law predicts that porosity approaches zero. Since sonic velocity is directly dependent on porosity and the elastic moduli of sediments, a direct adaptation of this equation is performed to reflect sonic transit time:

$$tt = tt_0 \, exp^{(-bx)} \tag{4.7}$$

where *x* is depth (the independent variable), *tt* is sonic transit time (the dependent variable), tt_0 is the surface transit time (x = 0) and *b* is the exponential decay constant. However, as discussed by Kumer (1979) and Magara (1979) this equation diverges from the measured sonic data at depths greater than 5000-8000ft below the original depositional surface. Both these workers discussed the potential reasons for the divergence such as undercompaction and validity of individual data values. An important reason why the equation does not adequately describe the relationship between ITT and depth is that it incorrectly predicts the sonic transit time in a totally compacted (0% porosity) rock to be zero. The transit time for a rock with zero porosity approaches a constant value – the rock matrix velocity (Heasler & Kharitonova, 1996). Rock matrix transit times range from 39μs/ft for dolomites to 68μs/ft for shales

(Magara, 1976; Schlumberger, 1989). Consequently a more correct functional relationship between sonic transit time and depth is:

$$tt = tt_0 \, exp^{(-bx)} + c \tag{4.8}$$

where *c* is the so called shift constant and is equal to the sonic transit time of the rock matrix. On a linear plot of sonic transit time versus depth *c* approximates to the asymptote of the curve which generally flattens out at depths exceeding 8000ft. Porosity and shaliness normally decrease the sonic velocity in rock thus increasing the sonic transit time. A sandstone with 5% porosity for example will be characterised by a 60µs/ft ITT compared with 51-55µs/ft for non-porous sandstone (Ellis, 1987). If any shale is present within the sandstone the ITT of the rock is usually increased because the shale ITT is greater than that of the sandstone. Shale transit times vary greatly but most of the published values range between 59-143µs/ft (Ellis, 1987; Etnyre, 1989) however Magara (1976) suggests using 68µs/ft. Note that if Pittman & Larese (1991) are correct and compact rocks have a porosity of 5% or more if some amount of shale is present then the minimum ITT for the shale constant will be greater than the discussed values for zero porosity. The upper cut-off value (the intercept on the y-axis) represents the surface transit time and is here taken to be 180µs/ft. This termination as Magara (1976) points out must reflect the observation that the transit time values of a clay-water mix should not exceed the value for water alone. This is because in clay-water mixes, where bulk clay porosity is less than 38% (62% overall porosity) the sound will essentially travel through the water. The transit time for formation water (50ppk NaCl) at the surface is approximately 200µs/ft (Figure 4.15) and in the sub-surface this is usually less. For this reason Heasler & Kharitonova (1996) prefer a lower value of 180µs/ft but as Magara (1976) points out, this is the minimum value for a range whose upper limit should not exceed 210µs/ft. By choosing the lower estimate for surface transit time the method therefore

predicts minimum exhumation values. This analysis assumes that the sequence under analysis is composed of a lithologically monotonous sequence in both the preserved and eroded section.

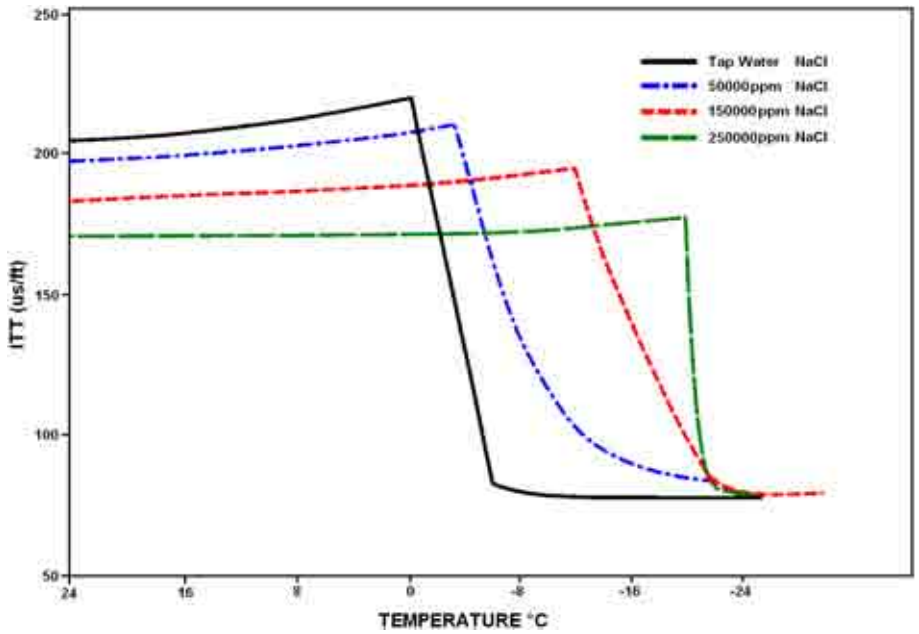

Figure 4.15 – Transit time versus temperature relationships of NaCl brines (after Magara, 1978)

4.3.1.1: Statistical fitting technique

In order to calculate the compaction curve, a least squares fitting technique is applied to Equation 4.8. However for numerical convenience the equation was first modified in the following manner:

$$tt - c = tt_0 \, exp^{(-bx)} \tag{4.9}$$

And taking the Naperian (natural) logarithm of both sides results in:

$$ln(tt - c) = ln\, tt_0 - bx \tag{4.10}$$

This is now a linear equation of the form $y = mx + c$ which can be easily fit using a standard least squares technique.

4.3.1.2: Error assessment of the statistical fit

The simplest technique for evaluating statistical fit would be the application of a correlation coefficient. However since the compaction curve has been calculated using logarithmically transformed sonic data values, a correlation coefficient for a least-squares fit is difficult to interpret. Consequently, Heasler & Kharitonova (1996) suggested that the Average Absolute Value (AAV) and the Root Mean Square (RMS) could be used to quantify the error of the logarithmically transformed sonic data. These two parameters both work by measuring the distance between the calculated and measured values and thus represent two different ways to evaluate the closeness of the calculated values to the measured ones.

The RMS is calculated using:

$$RMS = \sqrt{\frac{1}{N}\sum_{i=1}^{n}\left(D_i - C_i\right)^2} \tag{4.11}$$

The AAV is calculated using:

$$AAV = \frac{1}{N}\sum_{i=1}^{n}\left|D_i - C_i\right| \tag{4.12}$$

Where D_i represents measured values and C_i represents the corresponding calculated values of the logarithmically transformed data, whilst N is the sample size. The lower the RMS and AAV, then the closer the measured data points are to the calculated compaction curve and hence the greater degree of statistical fit. The AAV can be influenced by large errors but not as much as the RMS because the error is squared for the RMS calculation. Therefore if the RMS for two statistical fits is similar then the fit with the lower AAV is considered to be a better fit. Heasler & Kharitonova (1996) consider that the combination of these two values, RMS and AAV, represents a reliable tool to evaluate the exponential fits of logarithmically

transformed data. By cross posting the total exhumation (E_T) obtained for a particular shift constant it is also possible to see the overall distribution or trend that the changing shift constant makes to exhumation. In most cases where the AAV and RMS values are at their lowest then exhumation is also at a minimum.

Hamilton (1976) demonstrated that poroelasticity can lead to absolute porosity change of up to 7%. Converting this into transit time gives a reduction of 12.6μs/ft for unburied sediment, producing a maximum underestimate of denudation in the data of some 155m (510ft), depending on the decay constant of the compaction curve. P-wave velocities in low porosity sediments increase by up to 1.7% for a 100°C rise in temperature (Timur, 1977). Assuming a geothermal gradient of 33°C/km, this temperature-dependent velocity behaviour will lead to underestimation of denudation by up to 40m (129ft) in the dataset, again depending on the decay constant. In this study the maximum total geological error is therefore + 115 m (+377 ft). Given that geological errors are positive, all the exhumation values will be underestimates. The small magnitude of geological error with respect to the total denudation values means that they have been ignored in the subsequent interpretation. The main strength in this technique is the fact that it is applicable to a heterolithic sequence containing mudstone, siltstone and sandstone, meaning extensive filtering of the data was unnecessary (Heasler & Kharitonova, 1996). The ASCII data files, calculated values and calculate curves are included on the CD available with this thesis on an individual well by well basis and the interested reader is referred to those files to see a practical example of the approach.

4.3.2: THE SUPERCURVE TECHNIQUE

Only eight of the wells analysed contain sufficient (over 1500m of shale) thickness of shaley section and/or depth of well penetration to produce a statistically acceptable population of

sonic data to which a compaction curve could be fitted. The solution was to compare these data with a 'supercurve' (cf. Ware & Turner, 2002), a generic compaction curve for the offshore SW UK area derived from averaging normalized transit time vs. depth curves from the four most extensive available shale sections. This study uses a supercurve derived from sonic logs from wells 93/02-2, 93/02-3, 103/02-1 and 106/20-1 (Figure 4.16), each comprising more than 6000ft (1830m) of shaley section. Normalisation of each curve, such that they intersect the present surface with a transit time of 180µs/ft provides us with well-constrained approximations of the form of the unexhumed compaction curve, the average of which yields the supercurve (Figure 4.16). Normalisation was carried out by equating the curves to the following:

$$tt = (180 - c)e^{-bx} + c \tag{4.13}$$

Where c is the shift constant, x is the depth and b is the exponential decay constant. Note b and c remain the same as the un-normalised values. The difference between the supercurve and each datapoint on a sonic log gives a single denudation magnitude (Figure 4.17), the mean value of which yields apparent mean total exhumation. It must be acknowledged that this is an imperfect solution since the strength of the Heasler & Kharitonova (1996) sonic method was in generating a unique compaction curve per well. This method however still has significant merit since because of the use of a common baseline relative uplift between wells will still be observed. The ASCII data files and calculated values are included on the CD available with this thesis and the interested reader is referred to those files to see a practical example of the approach.

4.3.2.1: Corrections

The evaluation of experimental accuracy in any technique is of great importance. It is therefore vital that an estimate is made for the possible errors incurred so that the exhumation magnitudes can be quoted with an accuracy figure. Factor affecting the supercurve technique are critical porosity depth (determined by the critical porosity change which occurs at depths typically ranging from 100-400ft with the average at 250ft (76m) below the sea floor (Magara, 1976)), datum height above the sea-bed (typically KBE (Kelly Bushing Elevation or equivalent) of the drilling rig, which in most cases was 33.5m), water depth to reflect the true datum of the sea-floor, porosity rebound ((Hamilton, 1976) producing a maximum underestimate for exhumation of some 510ft (155m)) and temperature which gives a negligible effect on exhumation (see Chapter 2). This reveals a possible geological error of +115m (377ft) as the maximum case scenario. Since this is a positive figure it means that all burial anomaly values will be an underestimation of the actual figure reinforcing the notion that all calculated E_T values are minima. The resulting magnitudes of burial anomaly are shown in Table 4.13.

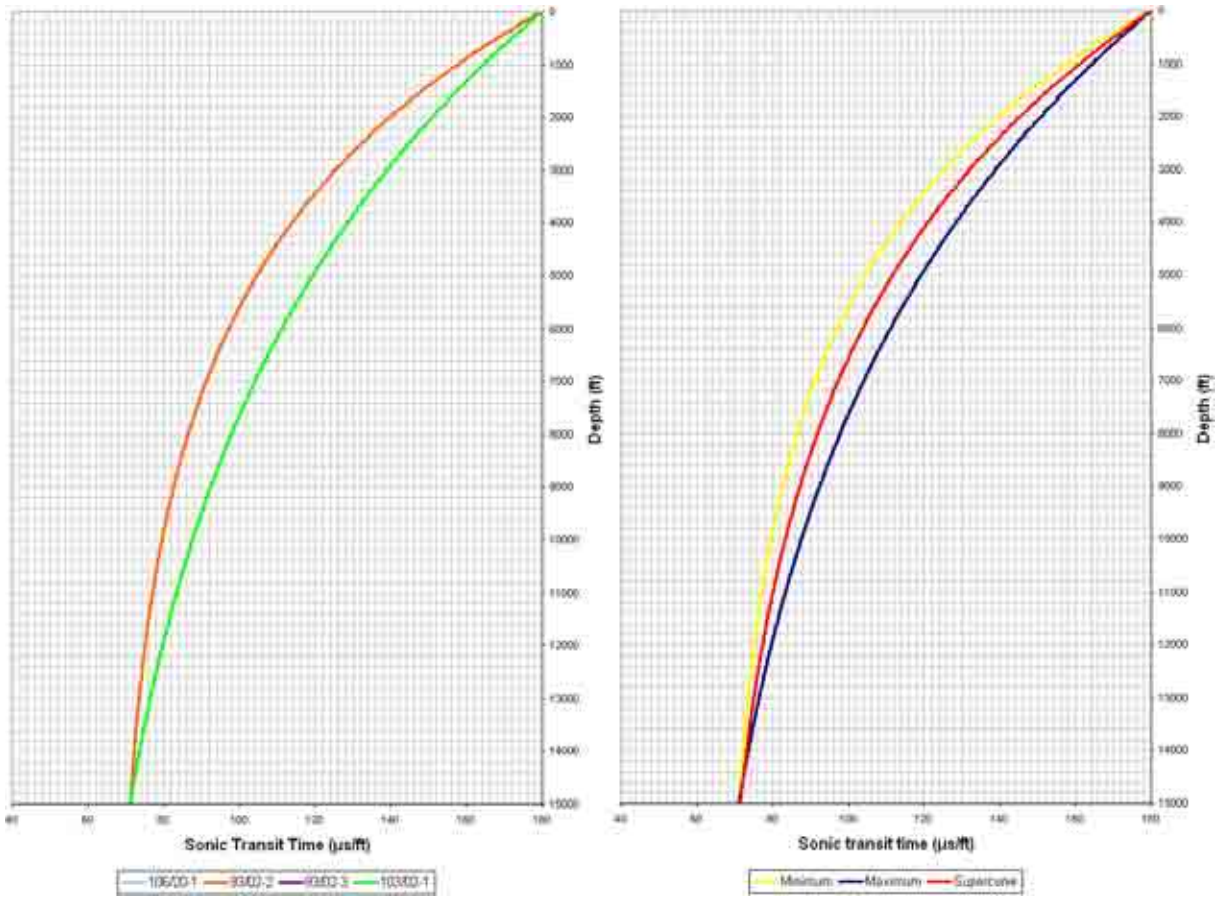

Figure 4.16 – Calculation of supercurve for the offshore SW UK exploration wells. (left) individual normalised well curves, (right) resulting supercurve with maxima and minima which mark the potential error range of ±300m for a calculated exhumation value. The parameters for the averaged curve are: exponential decay constant -0.00018ft^{-1} & shift constant 63µs/ft.

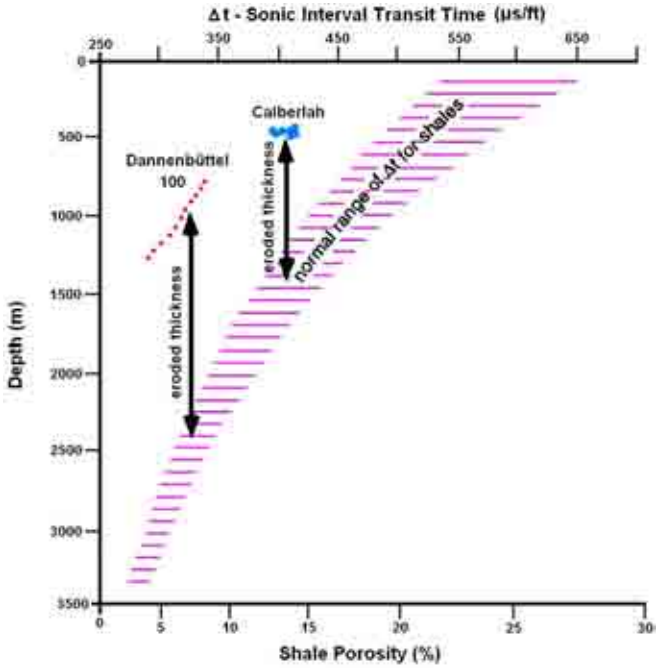

Figure 4.17 – Typical curve for sonic travel time (Δt) and porosity vs. depth for Lias epsilon (Jurassic) shales at maximum burial depth; this figure illustrates the method for estimating thickness of eroded overburden. Data from Gifhorn Trough, northwestern Germany (modified after Jankowsky, 1962).

4.3.3: THE JAPSEN RELATIONSHIPS

Using sonic velocity data from 123 wells in the British and Danish sectors of the southern North Sea, Japsen (2000) established a normal velocity-depth trend (i.e. reflecting a sedimentary succession which is at present at its maximum burial depth under conditions of hydrostatic pressure) for the Lower Triassic Bunter Shale Formation. The Bunter Shale Formation displays marked consistency in terms of thickness and lithology and is typically developed as an anhydritic red-brown mudstone with some minor greenish shales (Fisher & Mudge, 1998). In appearance therefore it is similar lithologically to the Mercia Mudstone Group of the Celtic Sea Basins, which comprises reddish brown silty mudstones and greenish grey mudstones with interbedded halites (Jackson *et al.* 1995). Sonic velocity data from the Bunter Shale Formation have commonly been used to estimate former burial depths in the Southern North Sea (e.g. Marie, 1975; Glennie & Boegner, 1981; Bulat & Stoker, 1987; Hillis, 1993, 1995) and a number of published velocity depth trends for the Bunter Shale

Formation are shown in Figure 4.18. Japsen's (2000) velocity-depth trend for the Bunter Shale Formation comprises a number of linear segments:

$V\ (m/s) = 1500 + 0.6z \qquad 0 < z < 1393m$

$V\ (m/s) = -400 + 2z \qquad 1393 < z < 2000m$

$V\ (m/s) = 2600 + 0.5z \qquad 2000 < z < 3500m$

$V\ (m/s) = 3475 + 0.25z \qquad 3500 < z < 5300m$

and displays a pronounced variation in velocity gradient with depth as illustrated in Figure 4.18. Japsen (2000) intimated that the reason for the segmentation in the velocity-depth trend may be the result of variations in mineralogy with depth. It is apparent from Figure 4.18 which compares Japsen's (2000) Bunter Shale Formation velocity-depth relationship with Ware and Turner's (2002) Mercia Mudstone Group 'supercurve', that Japsen's (2000) trend predicts lower velocities for depths <2km in comparison to the East Irish Sea Basin supercurve, although the difference is not significant for depths >2km. Since Lower Jurassic Lias Group rocks were also used in calculating exhumations Japsen's (2000) Lower Jurassic Shale trend was also used to calculate apparent exhumations. This is of the form:

$$V = \frac{10^6}{\left(460e^{\frac{-z}{2175}} + 185\right)} \qquad (4.14)$$

The trend fulfils reasonable boundary conditions at the surface (V_0=1550m/s) and at infinite depth (V_∞=5405m/s) and it is well defined at depths where velocity-depth data for normally compacted shale can be difficult to identify (2 < z <4km). The curve is also shown in Figure 4.18. Before the calculation of well exhumation magnitudes, the sonic logs were edited to remove spurious data and ensure lithological consistency. Salt, where present, was edited out of the dataset (although for illustrative purposes it is still included visually in the well plots Figure 4.44 and Appendix A).

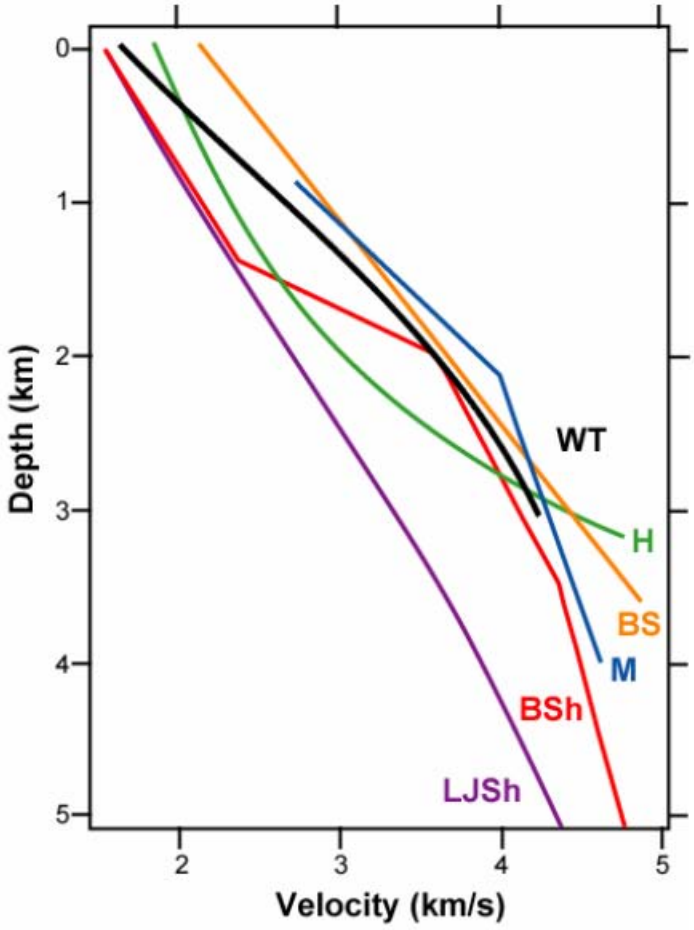

Figure 4.18 – A compilation of velocity-depth trends for the Bunter Shale Formation from various authors. Key: BS-Bulat and Stoker (1987); H-Hillis (1995); M-Marie (1975); BSh-Japsen (2000). Also shown for comparative purposes are Japsen's (2000) velocity –depth trend for the Lower Jurassic Shale of the Danish North Sea (LJSh) and Ware and Turner's (2002) averaged supercurve for the Mercia Mudstone Group of the EISB (WT) (after Holford, 2006).

Burial anomalies for individual wells have been calculated by comparing the difference between each data point on the sonic log and to both the Bunter Shale Formation and the Lower Jurassic shale velocity-depth relationship the mean value of which yields an estimate of former deeper burial. Following the approach of Ware & Turner (2002), burial anomalies have been corrected for post-exhumational burial relative to the sea-floor at each well location. Additionally, as before, exhumation has been corrected for present-day water depths, drill floor elevation and critical porosity and these values are shown in Table 4.15 and 4.16.

4.3.4: EXHUMATION MAGNITUDES RELATIVE TO INTERVAL TRANSIT TIME-DEPTH TRENDS DERIVED FOR THE OFFSHORE SW UK

As an alternative approach to estimating exhumation using porosity data, ITT's from the Triassic Mercia Mudstone Group and Sherwood Sandstone Group, Lower Jurassic Lias Group, Lower Cretaceous Greensand and Upper Cretaceous Chalk have been compared with linear ITT-d_m (midpoint depth) relationships constrained by data from two 'least exhumed' reference wells in the Southwest approaches-Celtic Sea Basins (*cf.* Menpes & Hillis, 1995). In an area subject to exhumation the wells with the lowest velocity for their given burial depth should be considered normally compacted provided their relatively low velocity is not merely due to phenomena which may inhibit normal compaction (such as overpressure or hydrocarbon-filled porosity). It should be noted however, that all wells in the study area of this thesis have been exhumed meaning that all burial anomalies will be relative and not absolute.

For a linear increase of velocity with depth the two wells which can be linked by a straight line that has no points falling to its right (less compacted) side define the normal compaction relationship (Hillis, 1993; Menpes and Hillis, 1995). Alternatively if there is a consistent intra-well rate of increase of velocity with depth in a given stratigraphic unit then the mean velocity-depth gradient within the unit in the wells analysed can be combined with the single well that shows the lowest velocity for its burial depth (allowing for the mean velocity-depth gradient) to determine the normal velocity-depth relationship (Hillis, 1991, 1993; Hillis *et al.* 1994). Since depth controlled compaction is largely irreversible units which are shallower than their maximum burial depth will be overcompacted with respect to their present burial depth (Magara, 1976; Lang, 1978; Bulat & Stoker, 1987; Hillis, 1991; Issler, 1992; Hillis *et al.* 1994).

It is assumed that all units follow a normal compaction trend with burial and that compaction is not reversed by subsequent exhumation (Figure 4.19 Well A and B). With these assumptions the amount of elevation of exhumed sedimentary rocks above their maximum burial depth (termed apparent exhumation) is given by the displacement along the depth axis of the observed compaction trend from the normal undisturbed trend. If further subsidence follows uplift the magnitude of the apparent uplift is reduced by the amount of post-uplift subsidence as shown by wells C and D (Figure 4.19). Although overburden weight following uplift does not cause any further porosity loss until the unit re-attains its previous maximum depth of burial (Hillis, 1991) the apparent uplift becomes smaller as the unit is progressively buried. In well D (Figure 4.19) the unit has re-attained its maximum depth of burial and no porosity anomaly is observed. With yet more subsidence the unit will once again begin to follow its normal compaction trend as shown by well E (Figure 4.19). Thus reference wells may have been subject to uplift of equal or lesser magnitude than the thickness of younger sediments (Hillis, 1991).

Regionally extensive stratigraphic units are the most useful for this type of study because the more widely occurring the unit the greater the likelihood of the reference wells being at or near their maximum burial depth (e.g. Jurassic-Lower Cretaceous units that are restricted to the inversion axes are never found at their maximum burial depth and hence reference wells defined by the following methodology would also be shallower than their maximum burial depth). In addition units with little to no lateral facies variation should be sought as they retain a regionally consistent (sonic) log character (Menpes & Hillis, 1995) and changes in mean ITT for the unit across the region are unlikely to be facies related. Finally given that log data are recorded every 15.2cm (6") thicker units are more desirable for the analysis because they tend to average out the effects of localised anomalous sonic log values (e.g. Chalk

hardgrounds) where the mean ITT for the entire unit is calculated. Shales have been widely used because they are believed to show the most simple (i.e. avoid the issues of cementation and diagenesis) velocity-depth relationships (Jankowsky, 1962; Marie, 1975; Magara, 1976; Lang, 1978; Cope, 1986; Wells, 1990; Issler, 1992; Japsen, 1993;) however because of the predictable faunal and mineralogical make-up and the broad uniform facies (Scholle, 1977) the Cretaceous chalk has also been used.

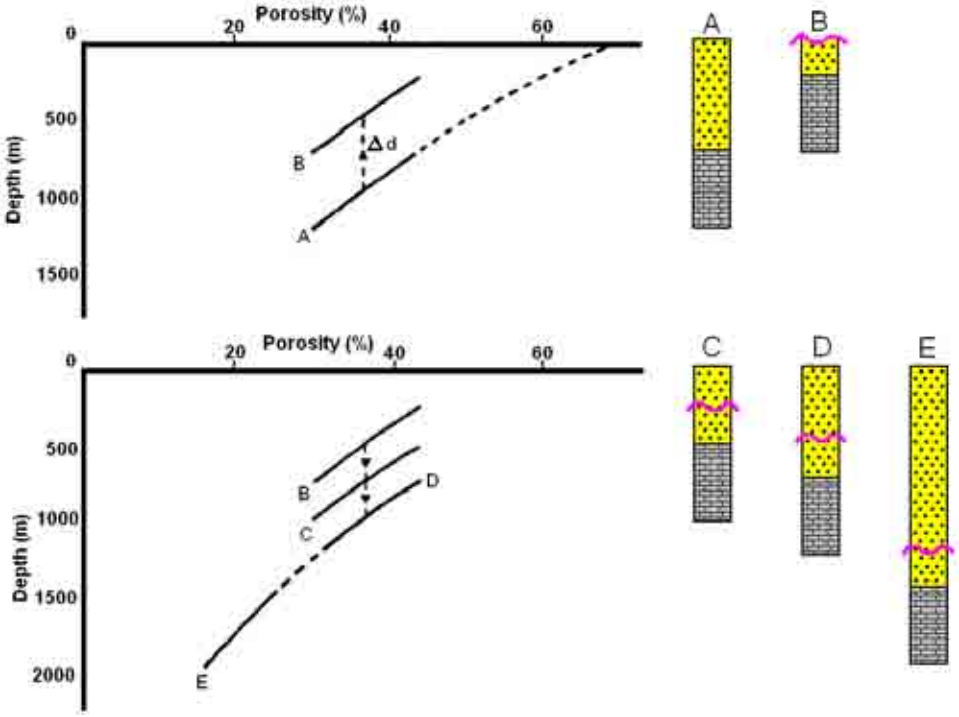

Figure 4.19 – Porosity evolution in a Chalk sequence during burial, (A) subsequent uplift (B), and post-uplift burial (C, D, E). The apparent uplift is the amount of uplift (Δd) not reversed by subsequent subsidence. It can be measured by the displacement along the depth axis of the porosity-depth relation of the uplifted sequence (B or C) from that of a reference or normally compacted sequence (A, D or E) (after Hillis, 1991).

The mean ITT (Δt_u) in combination with the depth of the formation midpoint below the seabed (d_u) can be used to calculate an apparent relative exhumation estimate (E_A) using the following equation:

$$E_A = \frac{1}{m}\left(\Delta t_u - \Delta t_o\right) - d_u \qquad (4.15)$$

where m is the gradient and Δt_o is the constant of the 'normal' compaction relationship (i.e. the ITT of uncompacted sediment). The normal compaction relationship should be verified by comparison to published compaction relationships (e.g. Scholle, 1977 for chalks, Baldwin & Butler, 1985 for shales) and reasonable surface values (e.g. Pryor, 1973 for sandstones). Further details of this approach can be found in e.g. Hillis, 1991. 1995; Hillis *et al.* 1994; Menpes & Hillis, 1995.

Williams *et al.* (2005) derived a linear ITT-dm relationship for the Mercia Mudstone Group of the SGCB and exhumation estimates relative to this trend for individual wells in that basin showed good agreement with exhumation estimates based on AFTA and VR data. ITT data from the MMG encountered in the Celtic Sea basins has therefore been compared with the ITT-dm trend of Williams *et al.* (2005). Menpes & Hillis (1995) derived linear ITT-dm relationships for the Upper Cretaceous Chalk, Lower Cretaceous Greensand/Gault Clay, MMG and Danian Chalk. Given the larger number of wells used in that study it was decided that the Cretaceous data would be compared to the Menpes & Hillis (1995) trends rather than a relationship derived from this study. The Menpes & Hillis (1995) MMG trend does not include well 103/01-1 and as such the Williams *et al.* (2005) trend is favoured since this trend accounts for the observations seen in that well and should thus be more representative of the area.

Though the Cenozoic is present across the area it is a relatively uneven mixture of relatively thin sand, shale and siltstone layers. To determine a normal compaction trend porosity or transit time depth curves are usually fitted to a single lithology such as shale (Magara, 1976; Issler, 1992), sandstone (Sclater & Christie, 1980; Hillis, 1993), chalk (Sclater & Christie, 1980) or limestone (Schmoker & Halley, 1982). Mavromatidis & Hillis (2005), concluded that the use of either sand or shale gave similar erosion results for their study of sonic

velocities in the Eromanga Basin, Australia and in the North Sea however to remain consistent in the approach the Cenozoic was discounted for analysis in this study. A Sherwood sandstone trend was derived from the wells used in this study.

Table 4.1 shows the relationships chosen to estimate the exhumation. It is noted explicitly that because this method only estimates erosion relative to 'least exhumed' reference wells, in a basin where the entire sedimentary succession (including the reference wells) has been affected by regional exhumation estimates derived using this approach will therefore be minima. If maximum burial depth is the principal control on the velocity of the units analysed and burial to and exhumation from maximum depth post dated the deposition of the youngest unit analysed than all units analysed in the same well should yield similar apparent exhumation values. Apparent exhumation results derived from velocities in the different stratigraphic units in the same well are cross plotted as a test of the validity of using different stratigraphic units/lithologies in maximum burial depth/exhumation studies.

As previously discussed thick Jurassic-Lower Cretaceous Wealden sequences in the Celtic Sea/South Western Approaches are localised in the regions of maximum inversion and hence are nowhere at maximum burial depth. Any compaction relationship determined for the Jurassic-Lower Cretaceous Wealden sequences would reflect exhumation from maximum burial depth and would yield low estimates of apparent exhumation. Hence the Jurassic-Lower Cretaceous Wealden sequences have not been considered in this study. The Cenozoic has also been omitted as it tends to be of laterally variable facies and is often not logged. Since salt does not compact with depth the analysis of the Mercia Mudstone has been limited to the shales above the salt.

The tops and bases of the Upper Cretaceous Chalk, Lower Cretaceous Greensand/Gault Clay, Lower Jurassic Lias Group, Triassic Mercia Mudstone Group and the Sherwood Sandstone were picked from sonic log plots at 1:4000 scale (e.g. Figure 4.20). The digital sonic log data was averaged over the picked interval to determine the mean interval transit times for each of the formations under consideration. It should be noted that the mean interval transit time refers to the quantity measured by the sonic log , the mean time required for a sound wave to traverse a foot of formation and not to the average velocity of a sonic wave in the formation under consideration as determined by one or two-way travel times. The mean transit times and depths to formation for each of the wells under consideration is shown in Appendix A.

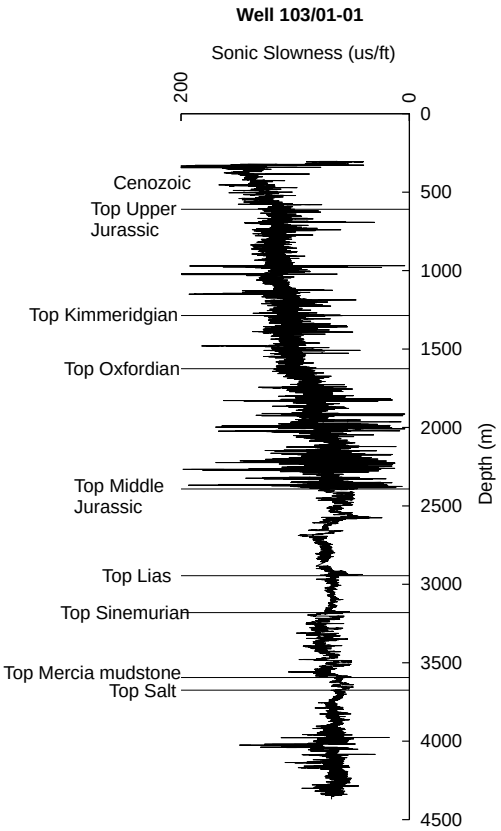

Figure 4.20 – Example of 1:4000 scale sonic log used for picking the tops and bases of the stratigraphic units.

The normal compaction relationship for each unit was defined by the straight line linking the two wells (termed the reference wells) with the highest ITT for their burial depth. The surface intercept of the normal compaction trend was checked to ensure it was less than 189μs/ft – the

ITT for salt water. The reference well data and the relationships describing normal compaction for each of the units analysed are given in Table 4.1 and the normal compaction relationships are shown in Figures 4.21-4.25.

Stratigraphic Unit	Reference Wells	Mean ITT (us/ft)	Mid-point depth (metres below sea bed)	Equation of normal compaction relationship
Upper Cretaceous Chalk	73/01-1	93.16	1137	ITT = 120-24D
	Kerluz	95.07	746	
Lower Cretaceous Greensand/Gault clay	Garlizenn	103.26	1521	ITT = 160-38D
	93/06-1	131.47	765	
Lower Jurassic Lias Group	103/02-1	116.82	621	ITT = 127-16D
	103/01-1	73.70	3260	
Triassic Mercia Mudstone	103/01-1	64.89	3621	ITT = 122-16D
	73/04-1	106.63	968	
Triassic Sherwood Sandstone	93/02-2	75.50	2441	ITT = 120-18D
	*	-	-	

Table 4.1 – Data defining normal compaction relations (ITT – interval transit time, D – mid-point depth (in km)). * Sherwood sandstone trend defined by single well (see text).

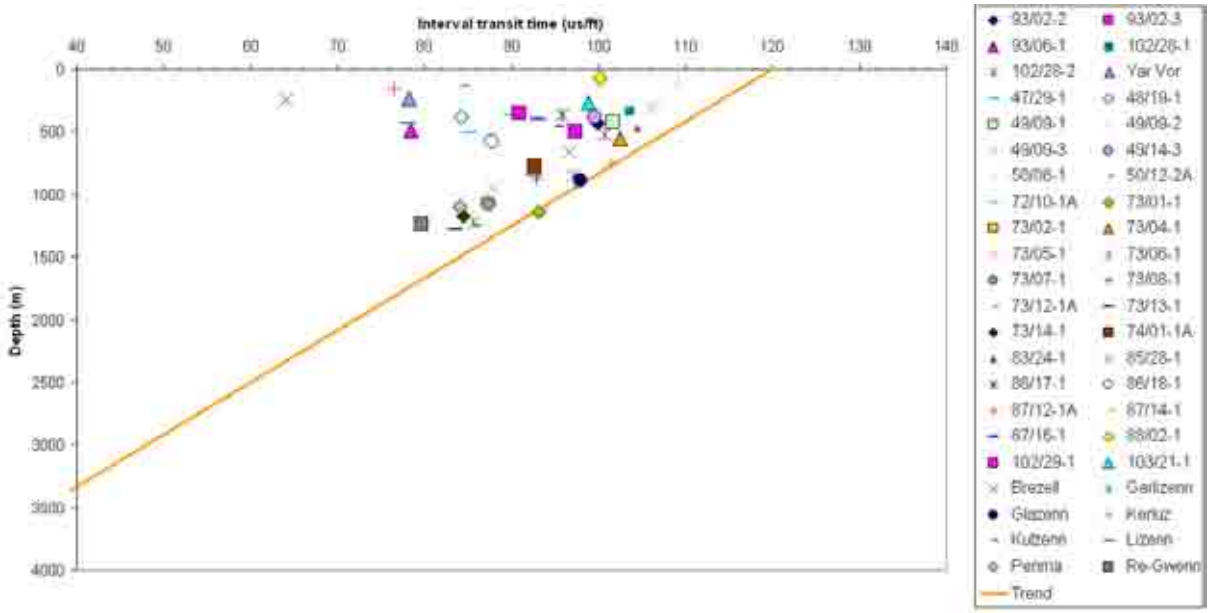

Figure 4.21 – Graph showing Interval Transit Time (ITT) against midpoint depth (D) for the Upper Cretaceous Chalk for exploration wells in the SW United Kingdom. Given that sonic velocities record maximum burial depths, the vertical difference between ITT and D of a well provides a measure of the amount by which the well has been uplifted above its maximum burial depth.

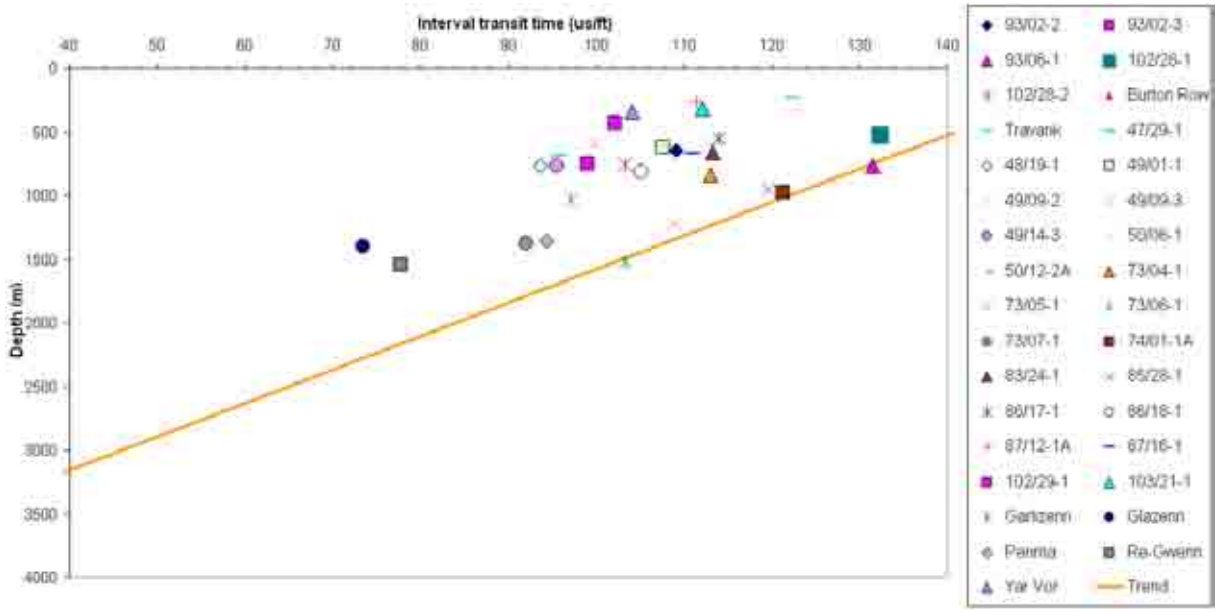

Figure 4.22 – Graph showing Interval Transit Time (ITT) against midpoint depth (D) for the Lower Cretaceous Greensand for exploration wells in the SW United Kingdom.

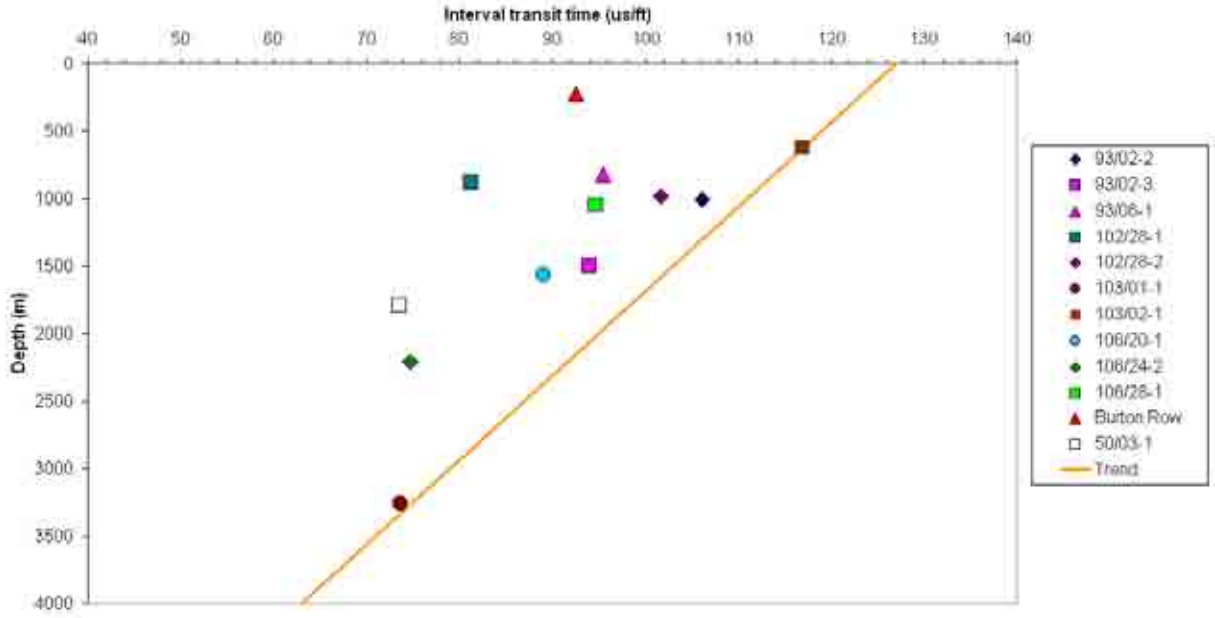

Figure 4.23 – Graph showing Interval Transit Time (ITT) against midpoint depth (D) for the Lower Jurassic Lias Group for exploration wells in the SW United Kingdom.

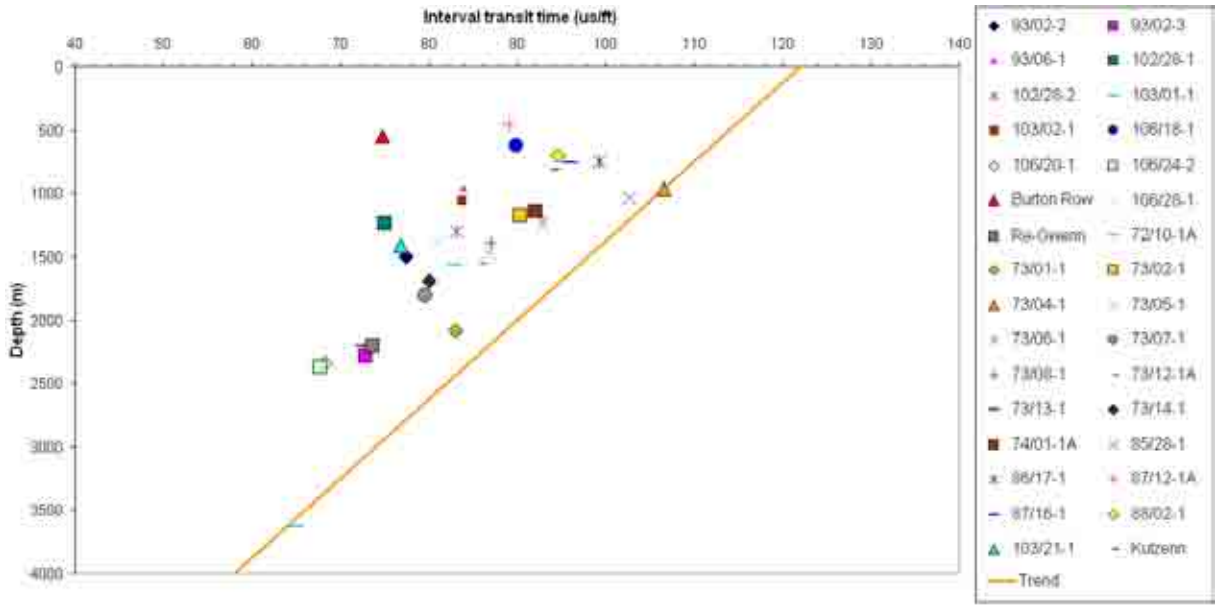

Figure 4.24 – Graph showing Interval Transit Time (ITT) against midpoint depth (D) for the Upper Triassic Mercia Mudstone Group for exploration wells in the SW United Kingdom.

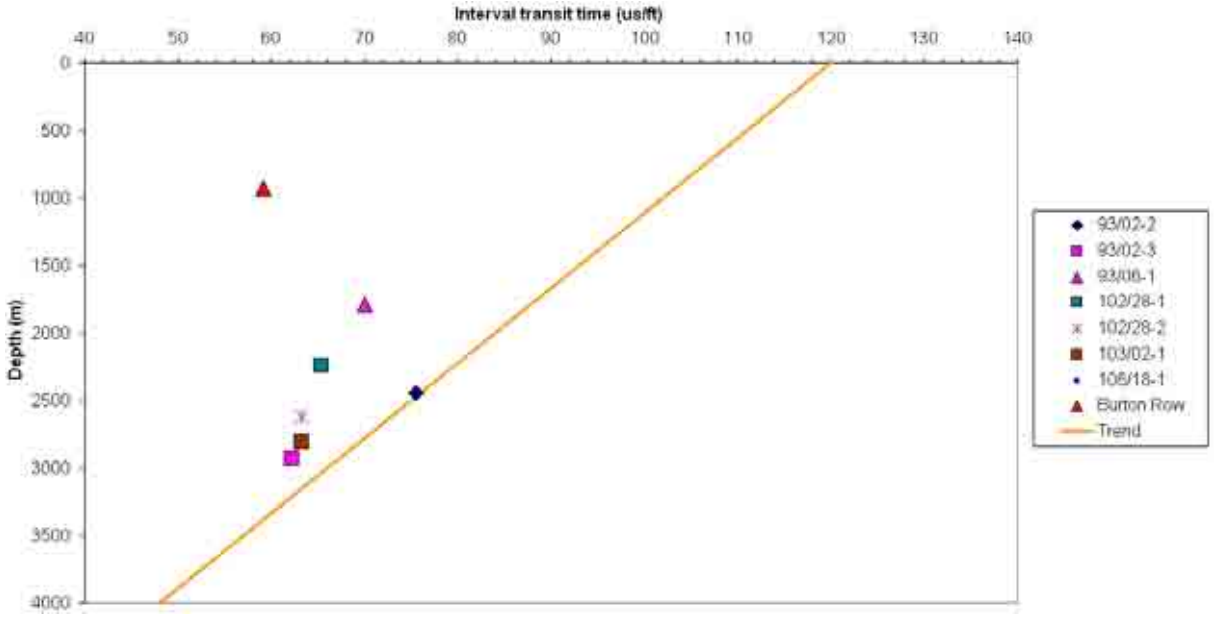

Figure 4.25 – Graph showing Interval Transit Time (ITT) against midpoint depth (D) for the Triassic Sherwood Sandstone for exploration wells in the SW United Kingdom.

Although the velocity-depth relationship is exponential over the depth range being considered a linear relationship between ITT and burial depth yields equivalent results (Bulat & Stoker, 1987). An empirical estimate of the accuracy of the normal compaction relationship was determined by examining the spread of the sonic logs of the reference wells around the

normal compaction trend. The error estimates are such that 95% of the sonic data lie within the error margins hence only large data spikes are outside the error margins. Since a lot of the data used in deriving the relationships was borrowed from Menpes & Hillis (1995) the error estimates are of the same magnitude too. For Upper Cretaceous chalk the error is ±250m, Lower Cretaceous Greensand/Gault clay it is ±450m, Lower Jurassic Lias Group ±400m, for the Mercia Mudstone ±400m and for the Sherwood Sandstone ±550m. The estimates for the Greensand, Lias and MMG are probably excessively high as the spread around the normal compaction trend is predominantly due to lithological variations within the formations assessed and hence should be considered the maximum potential error of the normal compaction relationship. If a particularly fast or slow portion of the formation were removed during exhumation the mean ITT calculated would correspondingly decrease or increase however the error induced by section removal would not exceed the errors above (Menpes & Hillis, 1995).

4.4: EXHUMATION RESULTS FROM THE POROSITY DATA OF THE OFFSHORE SW UK

The results from the 15 offshore wells used in the study are shown in Appendix A, two examples are shown in Figures 4.26 (offshore) and 4.27 (onshore). For the intervals under consideration all the calculated porosities are lower than those predicted for equivalent depths by the Sclater and Christie (1980) shale trend. The outliers represent unwanted lithologies such as sand lenses/channels, halite/anhydrite or interbedded limestone. Apparent (E_A) and total (E_T) exhumation estimates (*cf.* Hillis, 1995) relative to the Sclater & Christie (1980) trend are shown in Tables 4.2 – 4.11 for each of the techniques used (with a summary provided in Table 4.18). Apparent exhumation refers to exhumation which is not subsequently reversed by burial (Hillis, 1995). If exhumation is followed by renewed burial

the magnitude of apparent exhumation will be reduced by the amount of subsequent re-burial. Exhumation was calculated using the technique described in Chapter 2 (see e.g. Figures 2.8-2.9 and related text) where the difference between every data point and the Sclater & Christie (1980) shale compaction curve gives an individual exhumation estimate which when averaged, gives a statistically derived mean exhumation value for the well or borehole. In order to get total exhumation the value must be calibrated to a common datum. In the case of the offshore wells this datum was the sea bed. These values were then plotted on a map of the offshore area (Figures 4.28 – 4.37) to analyse the spatial distribution and relative values.

4.4.1: WYLLIE DERIVED EXHUMATION

Table 4.2 shows the exhumation values obtained using the Wyllie time-average equation (Equation 2.7) and assuming a matrix ITT of 68μs/ft. The largest value of exhumation is 3.69km in the case of the Burton Row borehole which is situated in the footwall of the BCB margin fault. The lowest value of 1.70km occurs in well 103/02-1 which lies in the footwall of the St. George's Fault and the hangingwall of the southern extension of the Bala Fault. Overall the data indicate that the area has experienced significant kilometres-scale exhumation. Figure 4.28 shows the spatial distribution of these values and their relation to major structural features. The distribution shows that there is a lot of small wavelength variation in exhumation style across the area especially in the SCSB. There do not appear to be clusters of exhumation values which would support magmatic underplating and indeed where underplating is predicted to be low there are a number of much larger values (compare Figure 4.28 with Figure 1.16, Chapter 1). In some cases there appears to be a marked difference in exhumation across major faults. Well 106/18-1, in the footwall of a fault, has a much higher exhumation value than well 106/20-1 which lies in the hangingwall. An interesting case concerns well 103/02-1 which lies in the footwall of the St. George's Fault

but in the hangingwall of the major basin bounding fault, the Bala Fault. The exhumation here represents the lowest of the values reported in the area. Less obviously the Burton Row borehole, which gives the largest value of exhumation, is also in the footwall of the fault which bounds the southern margin of the BCB.

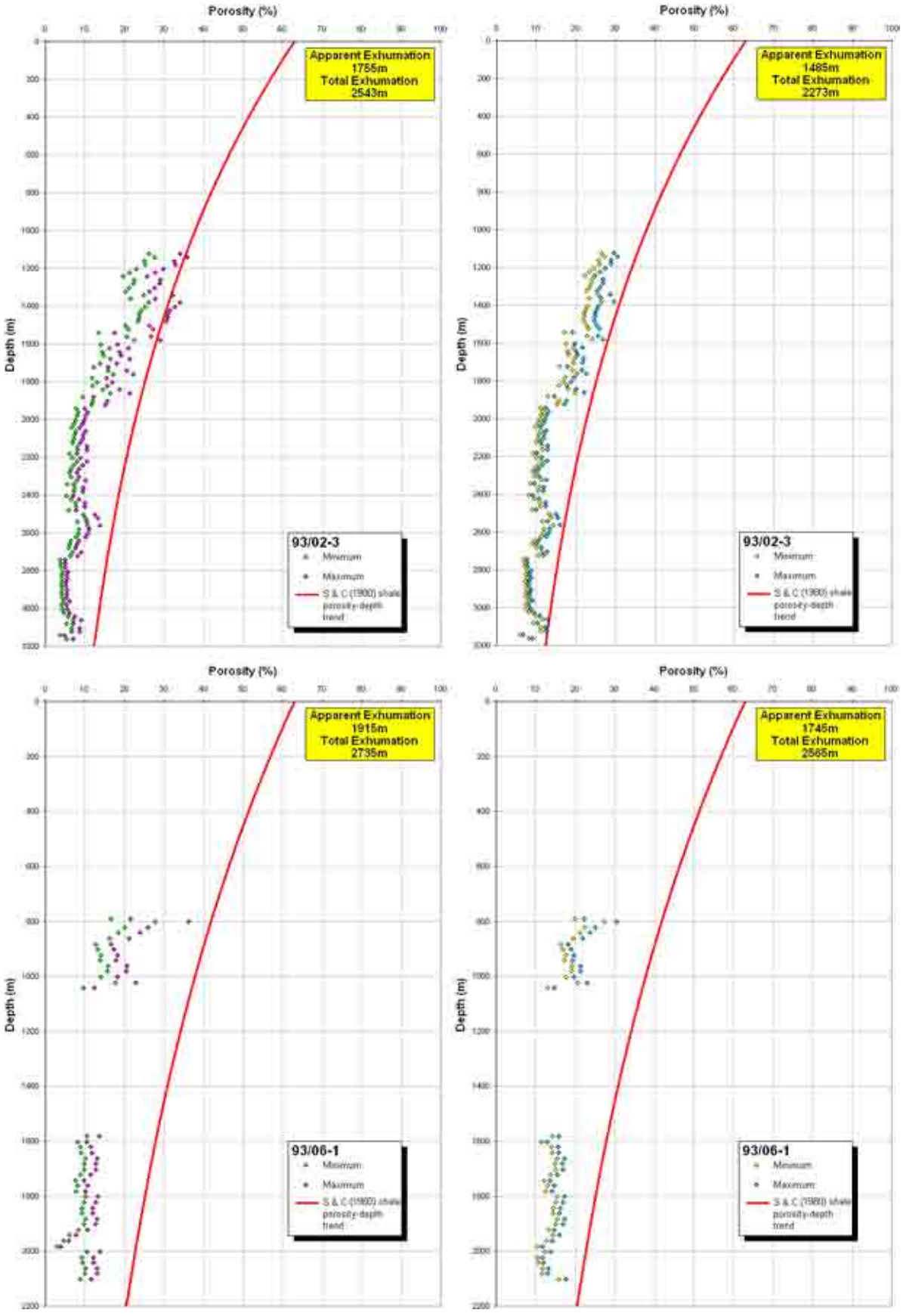

Figure 4.26 – Porosity data for well 93/02-3 and 93/06-1 using the (left) Wyllie time-average equation and (right) Raymer-Hunt-Gardner transform. Red line is the Sclater & Christie (1980) shale porosity depth trend.

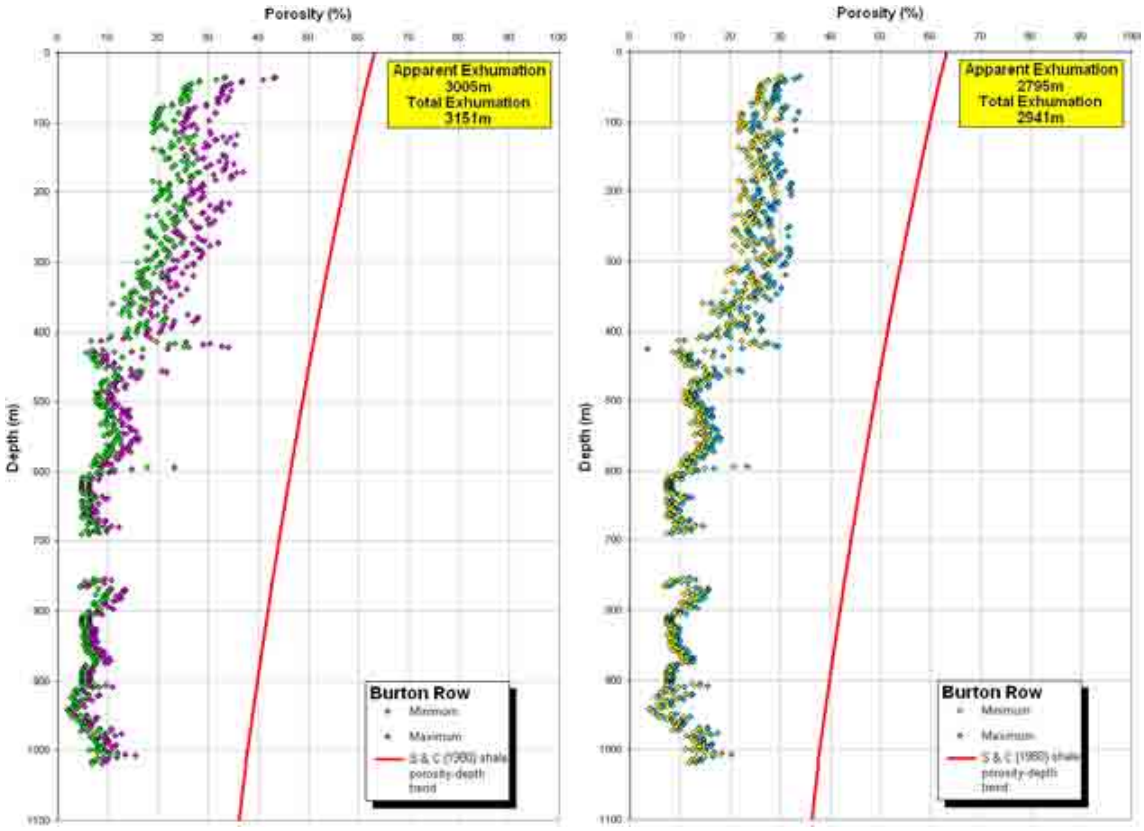

Figure 4.27 – Porosity data for the Burton Row borehole using the (left) Wyllie time-average equation and (right) Raymer-Hunt-Gardner transform. Red line is the Sclater & Christie (1980) shale porosity depth trend.

		Apparent exhumation (m)	Depth to u/c (m)	Water depth (m)	K.B.E (m)	Correction (m)	Total exhumation (m)
Well	50/03-1	2130	124	124	33.5	110	2240
	50/03-2	-	124	124	33.5	110	-
	93/02-2	2220	664	110	33.5	664	2884
	93/02-3	2390	788	110	33.5	788	3178
	93/06-1	2270	814	104	33.5	820	3090
	102/28-1	1550	570	97	26.0	575	2125
	102/28-2	1730	814	124	33.5	800	2530
	103/01-1	2580	616	148	33.5	578	3158
	103/02-1	1490	238	142	33.5	206	1696
	103/18-1	2100	362	94	22.9	367	2467
	103/21-1	1890	462	118	33.2	453	2343
	106/18-1	2640	100	100	33.5	110	2750
	106/20-1	1420	900	100	33.5	910	2330
	106/24-1	-	748	88	33.5	770	-
	106/24-2	2430	748	100	33.5	758	3188
	106/28-1	1850	932	109	24.0	923	2773
	Burton Row	3540	36	0	33.5	146	3686

Table 4.2 – Exhumation magnitudes based on the Sclater and Christie (1980) trend using the Wyllie time-average equation and a matrix interval transit time of 68μs/ft to derive porosities.

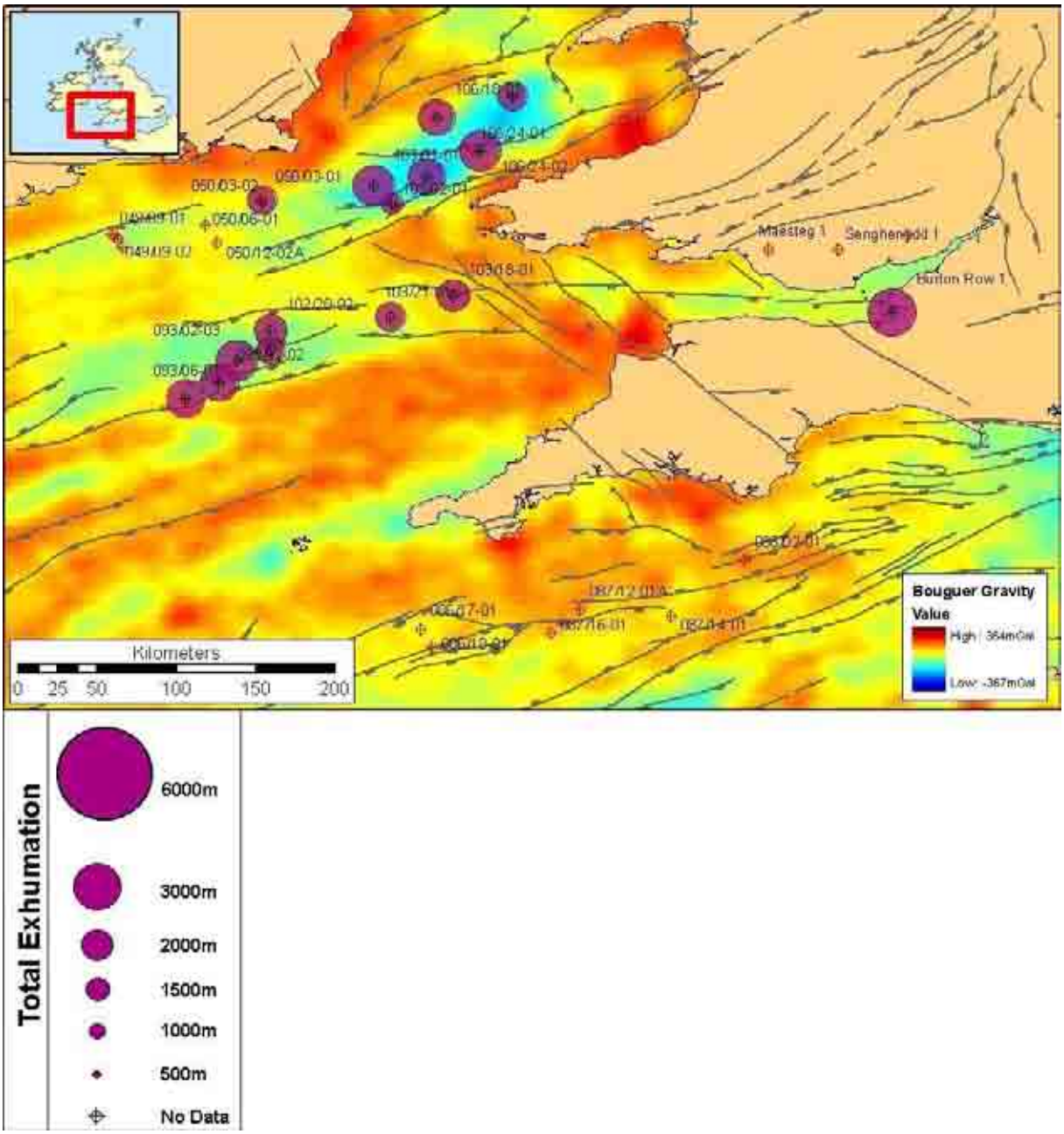

Figure 4.28 – Total exhumation magnitudes calculated from Wyllie derived porosity (68µs/ft matrix velocity) for each of the offshore wells. Wells for which no data was analysed are shown as purple cross-hairs. Coloured circles represent the total exhumation. In the SCSB exhumation appears to have been at its greatest at the basin centres. In the SGCB exhumation appears to be relatively uniform with the exception of well 103/02-1 and 106/18-1.

Table 4.3 shows the exhumation values obtained using the Wyllie time-average equation (Equation 2.7) and assuming a matrix ITT of 60µs/ft. The largest value of exhumation is 2.62km in the case of the Burton Row borehole which is situated in the footwall of the BCB margin fault. The lowest value of 1.58km occurs in well 50/03-1 which lies in the

hangingwall of the northern bounding fault of the NCSB. Overall the data indicates that the area has experienced significant kilometres-scale exhumation. Figure 4.29 shows the spatial distribution of these values and their relation to major structural features. The distribution shows that there is little variation in exhumation style across the area. Despite the much broader area of similar exhumation style again the predicted areas of large exhumation as a result of underplating do not manifest in the data. There is however still a number of places where exhumation varies across major faults. Well 93/06-1 has a much higher exhumation value than well 93/02-2 where the former lies in the footwall of a normal fault. Unlike Figure 4.28 (compare with Figure 4.29), well 103/02-1 does not appear to have differed markedly with the exhumation experienced by the surrounding wells. As before the Burton Row borehole records the largest value in exhumation across a major fault.

		Apparent exhumation (m)	Depth to u/c (m)	Water depth (m)	K.B.E (m)	Correction (m)	Total exhumation (m)
Well	50/03-1	1470	124	124	33.5	110	1580
	50/03-2	-	124	124	33.5	110	-
	93/02-2	1190	664	110	33.5	664	1854
	93/02-3	1120	788	110	33.5	788	1908
	93/06-1	1560	814	104	33.5	820	2380
	102/28-1	1110	570	97	26.0	575	1685
	102/28-2	1120	814	124	33.5	800	1920
	103/01-1	1040	616	148	33.5	578	1618
	103/02-1	1460	238	142	33.5	206	1666
	103/18-1	1400	362	94	22.9	367	1767
	103/21-1	1170	462	118	33.2	453	1623
	106/18-1	1830	100	100	33.5	110	1940
	106/20-1	770	900	100	33.5	910	1680
	106/24-1	-	748	88	33.5	770	-
	106/24-2	1210	748	100	33.5	758	1968
	106/28-1	980	932	109	24.0	923	1903
	Burton Row	2470	36	0	33.5	146	2616

Table 4.3 – Exhumation magnitudes based on the Sclater and Christie (1980) trend using the Wyllie time-average equation and a matrix interval transit time of 60μs/ft to derive porosities.

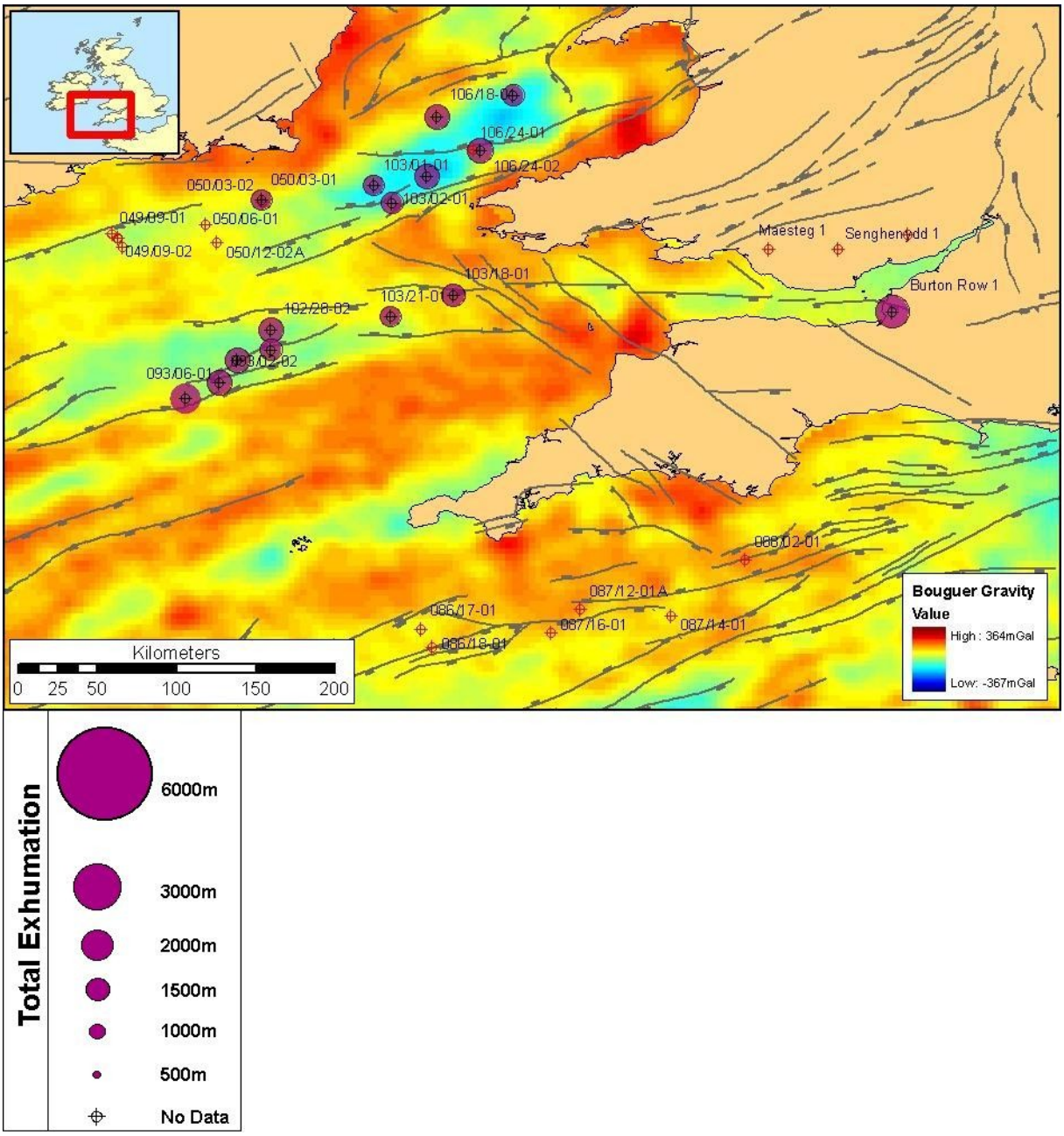

Figure 4.29 – Total exhumation magnitudes calculated from Wyllie derived porosity (60µs/ft matrix velocity) for each of the offshore wells. Wells for which no data was analysed are shown as purple cross-hairs. Coloured circles represent the total exhumation. Exhumation appears to be broadly similar across the area with the exception of some marked changes across major basin bounding faults as at Burton Row and well 93/06-1

As mentioned above it is still common in the hydrocarbon industry to use an uncorrected form of the Wyllie equation when dealing with maximum former deeper burial analyses and so for completeness this was also carried out in this analysis. Table 4.4 shows the exhumation values obtained using the Wyllie time-average equation (Equation 2.6) and assuming a matrix

ITT of 68μs/ft and Table 4.5 shows the exhumation values obtained using the Wyllie time-average equation (Equation 2.6) and assuming a matrix ITT of 60μs/ft. Since the correction factor multiplies the porosity by a constant value the spatial distribution of values is identical to those seen in Figures 4.28 and 4.29, only the values are different. For Figure 4.30, the largest value of exhumation is 3.46km for the Burton Row borehole. This compares to a value of 3.69km obtained with the correction factor (Figure 4.28). The lowest value of 1.44km for well 103/02-1 compared to 1.70km obtained with the correction factor. For Figure 4.31, the largest value of exhumation is 2.36km for the Burton Row borehole. This compares to a value of 2.62km obtained with the correction factor (Figure 4.29). The lowest value of 1.21km for well 50/03-1 compared to 1.58km obtained with the correction factor. Given the similarity of values it is difficult to separate the two different approaches. In order to assess which equation gives the better fit the absolute values must be compared against an independently derived estimate of exhumation. The values obtained from the density log (Figures 4.7 and 4.8) indicate exhumations of around 3km ±0.5km for wells 103/18-1 and 103/21-1. Based on this estimate the corrected equation (2.7) gives the much closer fit to the data. This supports Raymer's (1980) assertion that the original equation must be modified in order to estimate porosities in shales.

		Apparent exhumation (m)	Depth to u/c (m)	Water depth (m)	K.B.E (m)	Correction (m)	Total exhumation (m)
Well	50/03-1	1880	124	124	33.5	110	1990
	50/03-2	-	124	124	33.5	110	-
	93/02-2	1870	664	110	33.5	664	2534
	93/02-3	2140	788	110	33.5	788	2928
	93/06-1	2070	814	104	33.5	820	2890
	102/28-1	1300	570	97	26.0	575	1875
	102/28-2	1480	814	124	33.5	800	2280
	103/01-1	1760	616	148	33.5	578	2338
	103/02-1	1240	238	142	33.5	206	1446
	103/18-1	1850	362	94	22.9	367	2217
	103/21-1	1640	462	118	33.2	453	2093
	106/18-1	2390	100	100	33.5	110	2500
	106/20-1	1270	900	100	33.5	910	2180
	106/24-1	-	748	88	33.5	770	-
	106/24-2	2180	748	100	33.5	758	2938
	106/28-1	1600	932	109	24.0	923	2523
	Burton Row	3310	36	0	33.5	146	3456

Table 4.4 – Exhumation magnitudes based on the Sclater and Christie (1980) trend using the uncorrected Wyllie time-average equation and a matrix interval transit time of 68µs/ft to derive porosities.

		Apparent exhumation (m)	Depth to u/c (m)	Water depth (m)	K.B.E (m)	Correction (m)	Total exhumation (m)
Well	50/03-1	1100	124	124	33.5	110	1210
	50/03-2	-	124	124	33.5	110	-
	93/02-2	930	664	110	33.5	664	1594
	93/02-3	870	788	110	33.5	788	1658
	93/06-1	1350	814	104	33.5	820	2170
	102/28-1	850	570	97	26.0	575	1425
	102/28-2	870	814	124	33.5	800	1670
	103/01-1	840	616	148	33.5	578	1418
	103/02-1	1200	238	142	33.5	206	1406
	103/18-1	1150	362	94	22.9	367	1517
	103/21-1	920	462	118	33.2	453	1373
	106/18-1	1570	100	100	33.5	110	1680
	106/20-1	1130	900	100	33.5	910	2040
	106/24-1	-	748	88	33.5	770	-
	106/24-2	960	748	100	33.5	758	1718
	106/28-1	730	932	109	24.0	923	1653
	Burton Row	2210	36	0	33.5	146	2356

Table 4.5 – Exhumation magnitudes based on the Sclater and Christie (1980) trend using the uncorrected Wyllie time-average equation and a matrix interval transit time of 60µs/ft to derive porosities.

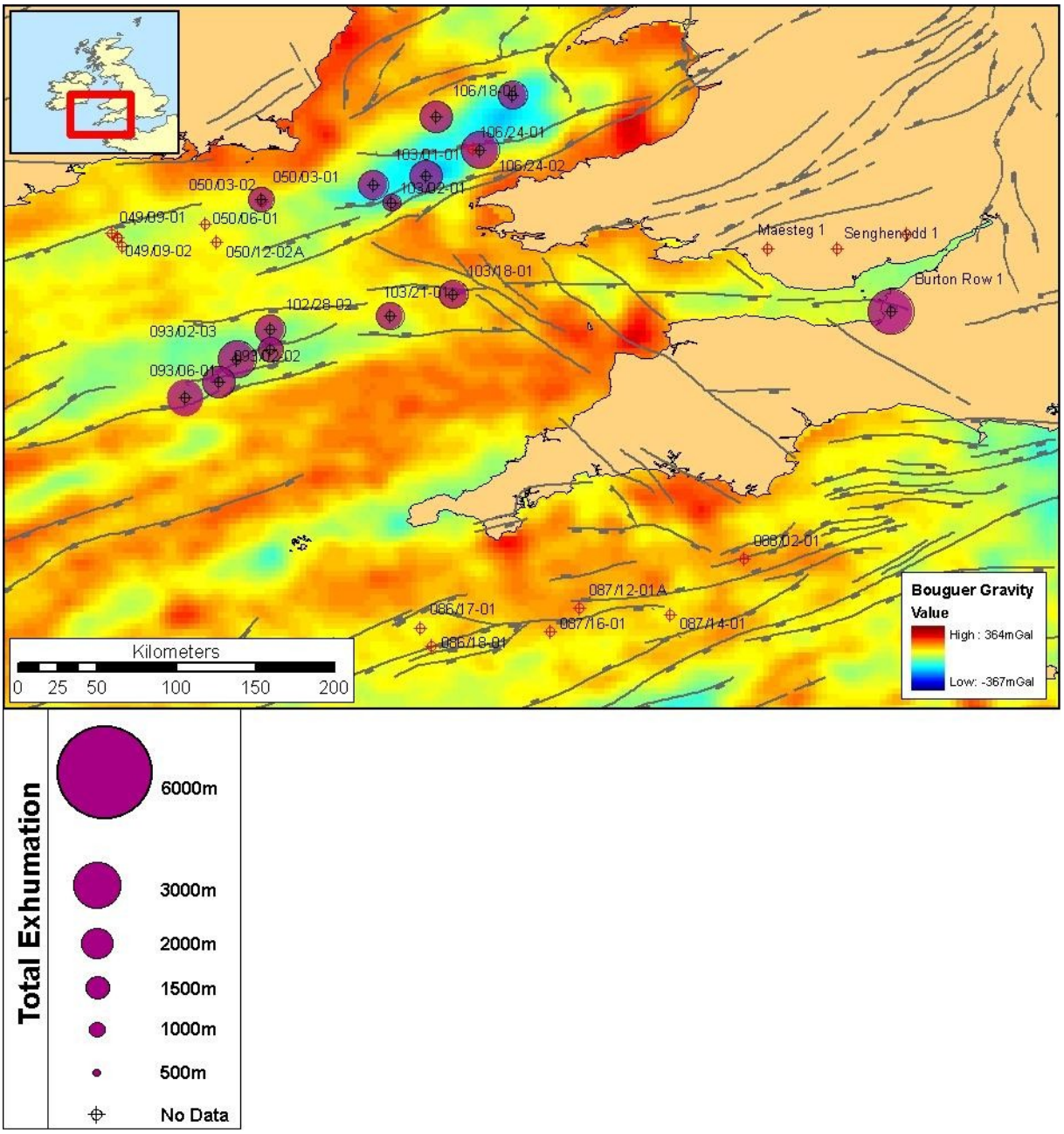

Figure 4.30 – Total exhumation magnitudes calculated from Wyllie derived porosity (68µs/ft matrix velocity and no correction factor) for each of the offshore wells. Wells for which no data was analysed are shown as purple cross-hairs. Coloured circles represent the total exhumation. Note the pattern is identical to Figure 4.28 only the values differ (see text for discussion).

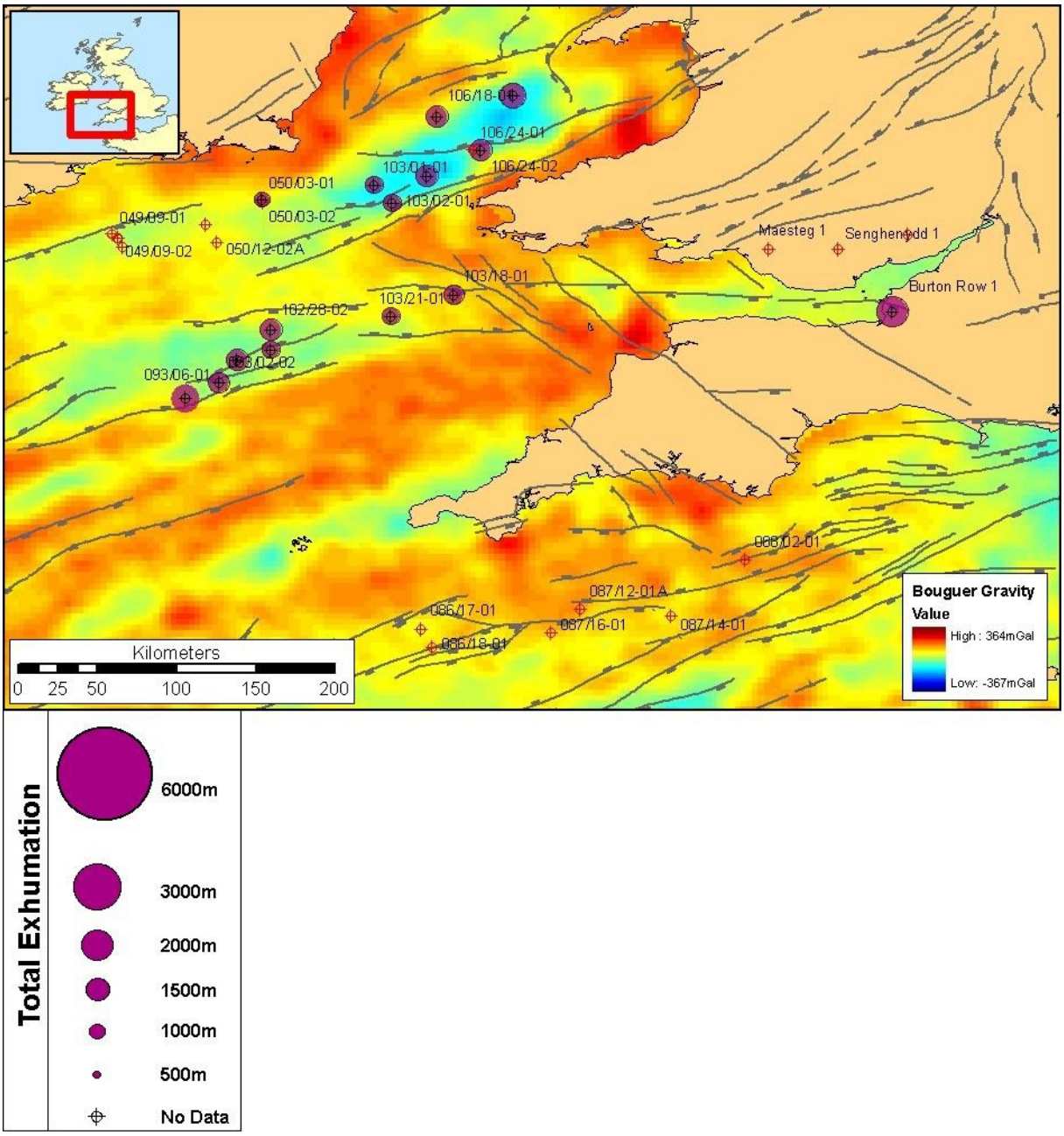

Figure 4.31 – Map showing total exhumation magnitudes calculated from Wyllie derived porosity (60µs/ft matrix velocity and no correction factor) for each of the offshore wells. Wells for which no data was analysed are shown as purple cross-hairs. Coloured circles represent the total exhumation. Note the pattern is identical to Figure 4.29 only the values differ (see text for discussion).

4.4.2: RAYMER DERIVED EXHUMATION

The Raymer-Hunt-Gardner equation is the corrected form of the Wyllie equation applied to shales thus the values obtained and subsequent spatial distribution should be broadly similar to the results in Figure 4.28, for a matrix velocity of 68μs/ft and Figure 4.29, for a matrix velocity of 60μs/ft. Table 4.6 shows the exhumation values obtained using the RHG transform (Equation 2.8) and assuming a matrix ITT of 68μs/ft. The largest value of exhumation is 3.55km in the case of the Burton Row borehole whilst the lowest value of 1.80km occurs in well 103/02-1. These compare to the Wyllie derived values of 3.69km and 1.70km. Figure 4.32 shows the spatial distribution of these values and their relation to major structural features. Overall the data indicates that the area has experienced significant kilometres-scale exhumation. Like the Wyllie derived exhumation values the Raymer derived exhumation distribution shows that there are small wavelength variations in exhumation style across the area (e.g. well 103/01-1 and well 103/02-1). Interestingly however, the observed differences in exhumation across major faults seem less pronounced with the exception of the values for Burton Row which retains a large difference between basin margin and basin centre. Table 4.7 shows the exhumation values obtained using the RHG transform (Equation 2.8) and assuming a matrix ITT of 60μs/ft. The largest value of exhumation is 2.34km in the case of the Burton Row borehole whilst the lowest value of 1.00km occurs in well 103/01-1. These compare to the Wyllie derived values of 2.62km and 1.62km. Figure 4.33 shows the spatial distribution of these values and their relation to major structural features. The data again highlights a number of small wavelength variations in exhumation which cannot be reconciled with the current model for underplating.

		Apparent exhumation (m)	Depth to u/c (m)	Water depth (m)	K.B.E (m)	Correction (m)	Total exhumation (m)
Well	50/03-1	2010	124	124	33.5	110	2120
	50/03-2	-	124	124	33.5	110	-
	93/02-2	2140	664	110	33.5	664	2804
	93/02-3	2180	788	110	33.5	788	2968
	93/06-1	2160	814	104	33.5	820	2980
	102/28-1	1520	570	97	26.0	575	2095
	102/28-2	1720	814	124	33.5	800	2520
	103/01-1	2200	616	148	33.5	578	2778
	103/02-1	1590	238	142	33.5	206	1796
	103/18-1	1960	362	94	22.9	367	2327
	103/21-1	1870	462	118	33.2	453	2323
	106/18-1	2510	100	100	33.5	110	2620
	106/20-1	1400	900	100	33.5	910	2310
	106/24-1	-	748	88	33.5	770	-
	106/24-2	2090	748	100	33.5	758	2848
	106/28-1	1650	932	109	24.0	923	2573
	Burton Row	3400	36	0	33.5	146	3546

Table 4.6 – Exhumation magnitudes based on the Sclater and Christie (1980) trend using the Raymer-Hunt Gardner equation and a matrix interval transit time of 68μs/ft to derive porosities.

		Apparent exhumation (m)	Depth to u/c (m)	Water depth (m)	K.B.E (m)	Correction (m)	Total exhumation (m)
Well	50/03-1	1100	124	124	33.5	110	1210
	50/03-2	-	124	124	33.5	110	-
	93/02-2	960	664	110	33.5	664	1624
	93/02-3	790	788	110	33.5	788	1578
	93/06-1	1330	814	104	33.5	820	2150
	102/28-1	970	570	97	26.0	575	1545
	102/28-2	980	814	124	33.5	800	1780
	103/01-1	420	616	148	33.5	578	998
	103/02-1	1210	238	142	33.5	206	1416
	103/18-1	1140	362	94	22.9	367	1507
	103/21-1	1020	462	118	33.2	453	1473
	106/18-1	1580	100	100	33.5	110	1690
	106/20-1	630	900	100	33.5	910	1540
	106/24-1	-	748	88	33.5	770	-
	106/24-2	740	748	100	33.5	758	1498
	106/28-1	670	932	109	24.0	923	1593
	Burton Row	2190	36	0	33.5	146	2336

Table 4.7 – Exhumation magnitudes based on the Sclater and Christie (1980) trend using the Raymer-Hunt-Gardner equation and a matrix interval transit time of 60μs/ft to derive porosities.

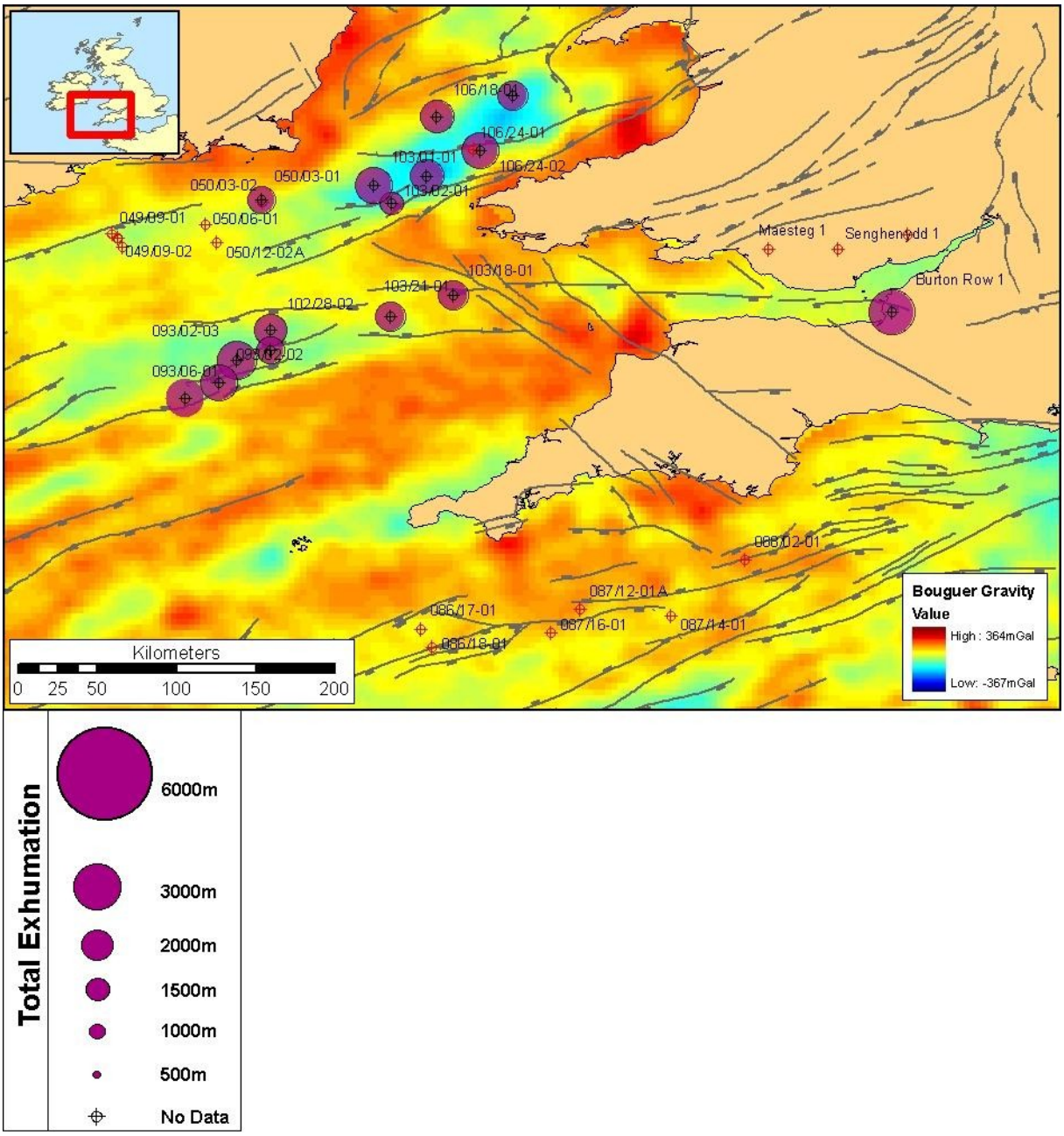

Figure 4.32 – Map showing total exhumation magnitudes calculated from Raymer derived porosity (68µs/ft matrix velocity) for each of the offshore wells. Wells for which no data was analysed are shown as purple cross-hairs. Coloured circles represent the total exhumation.

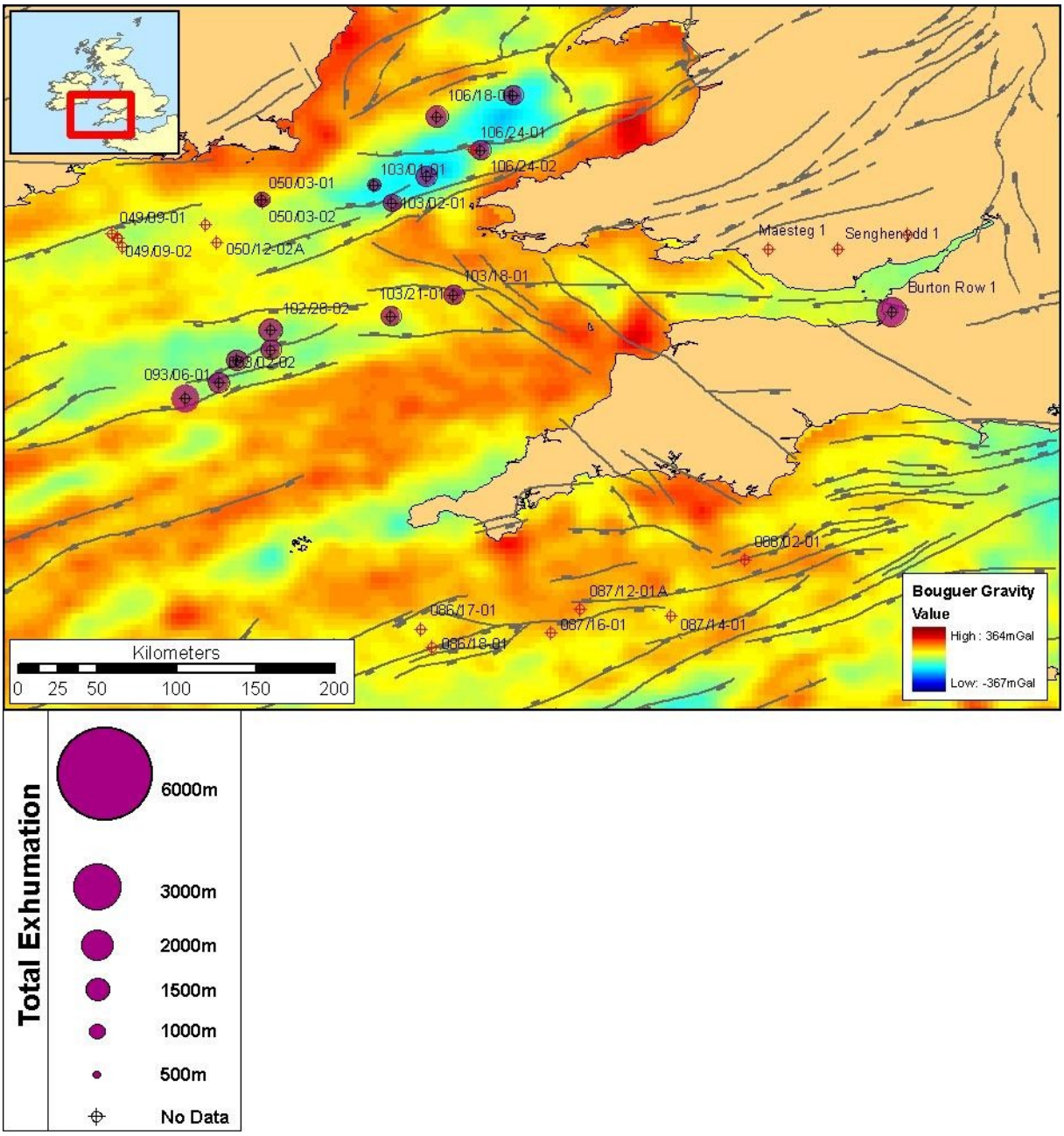

Figure 4.33 – Map showing total exhumation magnitudes calculated from Raymer derived porosity (60µs/ft matrix velocity) for each of the offshore wells. Wells for which no data was analysed are shown as purple cross-hairs. Coloured circles represent the total exhumation. Note the examples of small wavelength variation in burial anomaly between adjacent wells.

4.4.3: POROSITY RELATIONSHIP DERIVED EXHUMATION

As described above the most reliable of the porosity relationships should be the hybrid relationship as it is adjusted to fit the data it is however worth considering the results from each of the individual relationships to see how they compare. Table 4.8 shows the exhumation values obtained using the linear relationship. The largest value of exhumation is 3.86km in the case of well 102/28-2 whilst the lowest value of 1.76km occurs in well 103/01-1. Figure 4.34 shows the spatial distribution of these values and their relation to major structural features. Overall the data indicates that the area has experienced significant kilometres-scale exhumation. As with the Wyllie and Raymer derived exhumations values a lot of small wavelength variation in exhumation style can be observed across the area. The main difference is the stark differences in exhumation styles near faults. In some cases notably the Burton Row borehole and well 93/06-1, these differences occur in the footwall of major faults. However, there are some cases such as well 102/28-2 and well 106/24-2 where this large difference is in the hangingwall of a major fault or not apparently related to one. This may simply be a manifestation of different litho-types where sandier shale gives a lower porosity – and hence greater exhumation value – compared to a 'typical' shale. It is difficult to reconcile these differences based purely on the sonic log. A thorough analysis of other geophysical logs such as the Neutron density log should allow such a differentiation but these were not available for the wells where this distinction would be helpful.

		Apparent exhumation (m)	Depth to u/c (m)	Water depth (m)	K.B.E (m)	Correction (m)	Total exhumation (m)
Well	50/03-1	2420	124	124	33.5	110	2530
	50/03-2	-	124	124	33.5	110	-
	93/02-2	1940	664	110	33.5	664	2604
	93/02-3	1940	788	110	33.5	788	2728
	93/06-1	2930	814	104	33.5	820	3750
	102/28-1	2630	570	97	26.0	575	3205
	102/28-2	3060	814	124	33.5	800	3860
	103/01-1	1180	616	148	33.5	578	1758
	103/02-1	2500	238	142	33.5	206	2706
	103/18-1	2480	362	94	22.9	367	2847
	103/21-1	1990	462	118	33.2	453	2443
	106/18-1	2640	100	100	33.5	110	2750
	106/20-1	2130	900	100	33.5	910	3040
	106/24-1	-	748	88	33.5	770	-
	106/24-2	2570	748	100	33.5	758	3328
	106/28-1	1860	932	109	24.0	923	2783
	Burton Row	3450	36	0	33.5	146	3596

Table 4.8 – Exhumation magnitudes based on the Sclater and Christie (1980) trend using the density derived linear porosity/depth relationship.

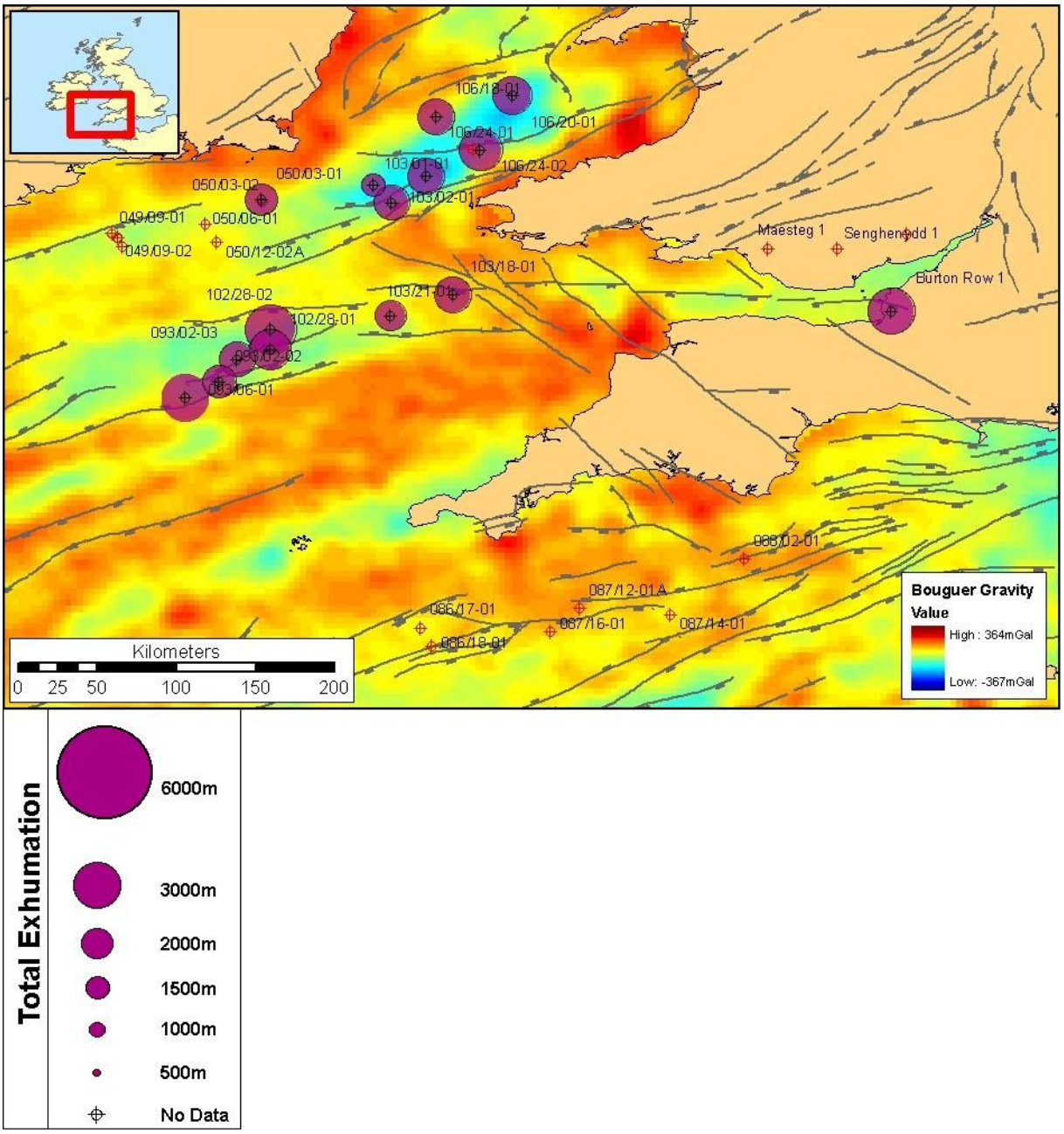

Figure 4.34 – Map showing total exhumation magnitudes calculated using the density log derived linear relationship for each of the offshore wells. Wells for which no data was analysed are shown as purple cross-hairs. Coloured circles represent the total exhumation. Exhumation appears to be greatest on the basin margins with significant differences across major faults.

Table 4.9 shows the exhumation values obtained using the power relationship. The largest value of exhumation is 5.58km in the case of well 93/06-1 whilst the lowest value of 3.65km occurs in well 103/01-1. Figure 4.35 shows the spatial distribution of these values and their relation to major structural features. The power distribution predicts extreme values of

exhumation across the area as a result of the way the function acts to keep low porosities at wide ranges of ITT as shown by Figure 4.11. A significant number of points deviate from the trend in the range 60-80µs/ft and it is these values which have acted to inflate the results. Comparing the values obtained with the density derived exhumation shows a difference of over 1.5km. For these reasons the power law is considered useful only in a narrow range of ITT and not useful to use as a standalone transform for sonic data to porosity data. It should however be noted that the transformed data displays the same small wavelength variations in burial anomaly that has been revealed by the other techniques.

		Apparent exhumation (m)	Depth to u/c (m)	Water depth (m)	K.B.E (m)	Correction (m)	Total exhumation (m)
Well	50/03-1	4370	124	124	33.5	110	4480
	50/03-2	-	124	124	33.5	110	-
	93/02-2	3680	664	110	33.5	664	4344
	93/02-3	3800	788	110	33.5	788	4588
	93/06-1	4760	814	104	33.5	820	5580
	102/28-1	4080	570	97	26.0	575	4655
	102/28-2	4200	814	124	33.5	800	5000
	103/01-1	3070	616	148	33.5	578	3648
	103/02-1	3960	238	142	33.5	206	4166
	103/18-1	4410	362	94	22.9	367	4777
	103/21-1	3860	462	118	33.2	453	4313
	106/18-1	4580	100	100	33.5	110	4690
	106/20-1	3970	900	100	33.5	910	4880
	106/24-1	-	748	88	33.5	770	-
	106/24-2	4360	748	100	33.5	758	5118
	106/28-1	3790	932	109	24.0	923	4713
	Burton Row	5280	36	0	33.5	146	5426

Table 4.9 – Exhumation magnitudes based on the Sclater and Christie (1980) trend using the density derived power law porosity/depth relationship.

Table 4.10 shows the exhumation values obtained using the exponential relationship. The largest value of exhumation is 3.98km in the case of the Burton Row borehole whilst the lowest value of 1.89km occurs in well 103/01-1. Figure 4.36 shows the spatial distribution of these values and their relation to major structural features. Overall the data indicates that the

area has experienced significant kilometres-scale exhumation. The data also shows the clearest evidence for major variation in exhumation across faults. In each case where a well is in the footwall of a major fault the well in the hangingwall shows a lower exhumation. This is demonstrated best across the BCB southern margin where the Burton Row borehole has experienced much greater exhumation than the basin centre but can also be seen with wells 93-02-2 and 93/06-1, 103/01-1 and 103/02-1 and wells 103/01-1 and 106/28-1. There is also evidence that basin centres have experienced significant uplift, a key observation of inversion, particularly in the SCSB and SGCB.

		Apparent exhumation (m)	Depth to u/c (m)	Water depth (m)	K.B.E (m)	Correction (m)	Total exhumation (m)
Well	50/03-1	2800	124	124	33.5	110	2910
	50/03-2	-	124	124	33.5	110	-
	93/02-2	2430	664	110	33.5	664	3094
	93/02-3	2360	788	110	33.5	788	3148
	93/06-1	3090	814	104	33.5	820	3910
	102/28-1	2790	570	97	26.0	575	3365
	102/28-2	2660	814	124	33.5	800	3460
	103/01-1	1310	616	148	33.5	578	1888
	103/02-1	2520	238	142	33.5	206	2726
	103/18-1	2930	362	94	22.9	367	3297
	103/21-1	2790	462	118	33.2	453	3243
	106/18-1	3330	100	100	33.5	110	3440
	106/20-1	2440	900	100	33.5	910	3350
	106/24-1	-	748	88	33.5	770	-
	106/24-2	2450	748	100	33.5	758	3208
	106/28-1	2440	932	109	24.0	923	3363
	Burton Row	3830	36	0	33.5	146	3976

Table 4.10 – Exhumation magnitudes based on the Sclater and Christie (1980) trend using the density derived exponential porosity/depth relationship.

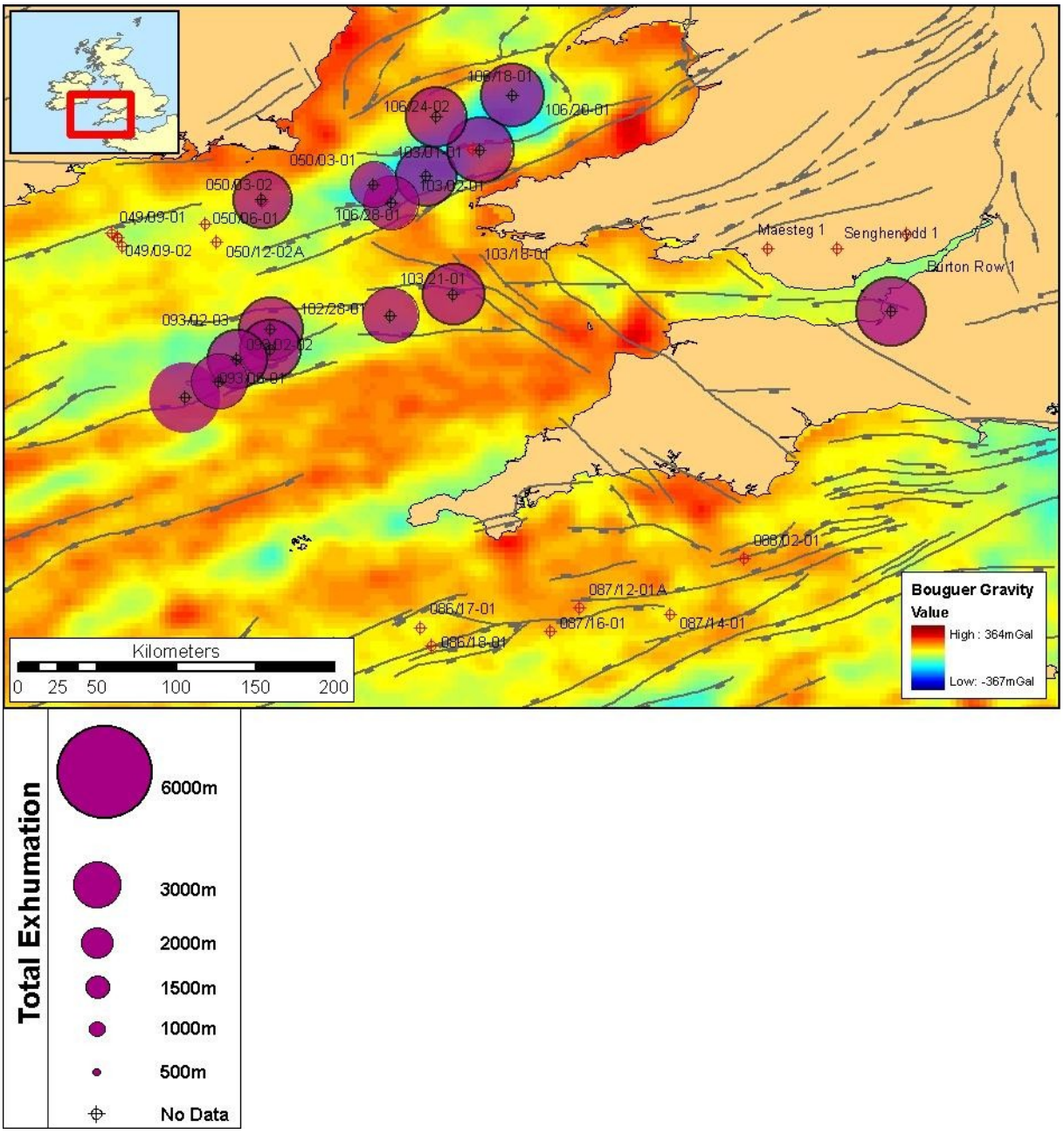

Figure 4.35– Map showing total exhumation magnitudes calculated using the density log derived power relationship for each of the offshore wells. Wells for which no data was analysed are shown as purple cross-hairs. Coloured circles represent the total exhumation. As discussed in the text the power law grossly overestimates exhumation at all well localities.

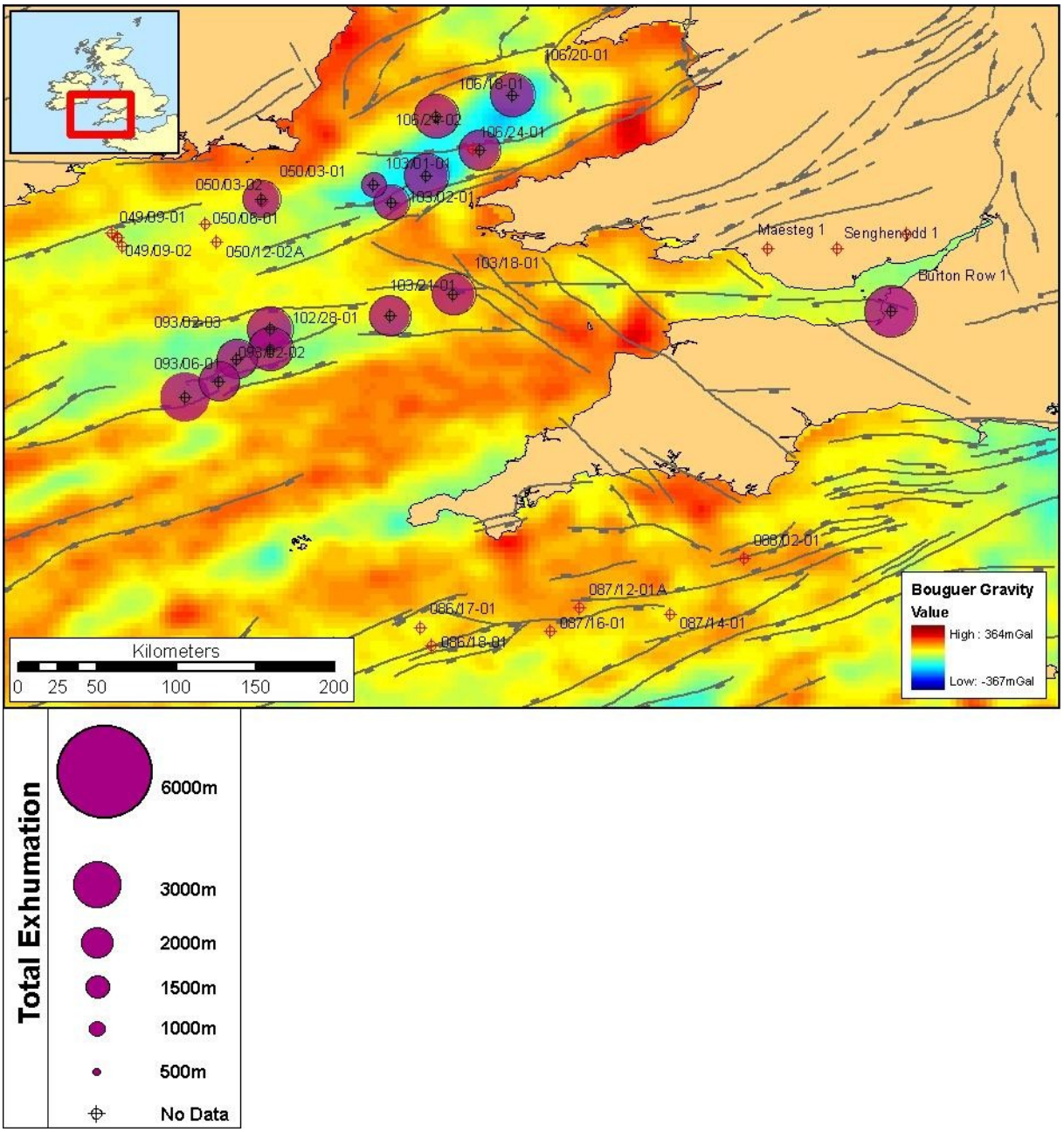

Figure 4.36 – Map showing total exhumation magnitudes calculated using the density log derived exponential relationship for each of the offshore wells. Wells for which no data was analysed are shown as purple cross-hairs. Coloured circles represent the total exhumation. Exhumation appears to be greatest in the basin centres but also shows a pattern of significant differences across major faults.

Table 4.11 shows the exhumation values obtained using the hybrid relationship. The largest value of exhumation is 4.40km in the case of well 102/28-2 whilst the lowest value of 2.03km occurs in well 103/01-1. Figure 4.37 shows the spatial distribution of these values and their relation to major structural features. Overall the data indicates that the area has experienced significant kilometres-scale exhumation. The data shows that the basin centres have experienced the most exhumation, evidence consistent with inversion. There is also evidence for major differences in exhumation across faults particularly with wells on the southern margin faults of the SCSB (wells 93/06-1 and 93/02-2) and BCB (Burton Row borehole and 103/18-1, 103/21-1). The hybrid relationship and exponential relationship also show the closest correlation with the independently derived exhumation from the density data. In the case of well 103/18-1 the density derived exhumation was 3.11km ± 0.53km compared with 3.30km for the exponential relationship and 3.40km with the hybrid relationship. For well 103/21-1 the density derived exhumation was 3.73km ± 0.83km compared with 3.24km for the exponential relationship and 3.26km with the hybrid relationship. As with the Wyllie and Raymer derived exhumations the distribution of exhumation in the area is not consistent with that proposed by the underplating theory since the largest exhumations occur in areas that, according to the underplating theory, should be lows. This, along with the small wavelength variations in exhumation, suggests that underplating alone is not responsible for the exhumation seen in the offshore SW UK area.

		Apparent exhumation (m)	Depth to u/c (m)	Water depth (m)	K.B.E (m)	Correction (m)	Total exhumation (m)
Well	50/03-1	2950	124	124	33.5	110	3060
	50/03-2	-	124	124	33.5	110	-
	93/02-2	2550	664	110	33.5	664	3214
	93/02-3	2410	788	110	33.5	788	3198
	93/06-1	3280	814	104	33.5	820	4100
	102/28-1	3200	570	97	26.0	575	3775
	102/28-2	3600	814	124	33.5	800	4400
	103/01-1	1450	616	148	33.5	578	2028
	103/02-1	2960	238	142	33.5	206	3166
	103/18-1	3030	362	94	22.9	367	3397
	103/21-1	2810	462	118	33.2	453	3263
	106/18-1	3340	100	100	33.5	110	3450
	106/20-1	2600	900	100	33.5	910	3510
	106/24-1	-	748	88	33.5	770	-
	106/24-2	2710	748	100	33.5	758	3468
	106/28-1	2420	932	109	24.0	923	3343
	Burton Row	3900	36	0	33.5	146	4046

Table 4.11 – Exhumation magnitudes based on the Sclater and Christie (1980) trend using the density derived 'hybrid' porosity/depth relationship.

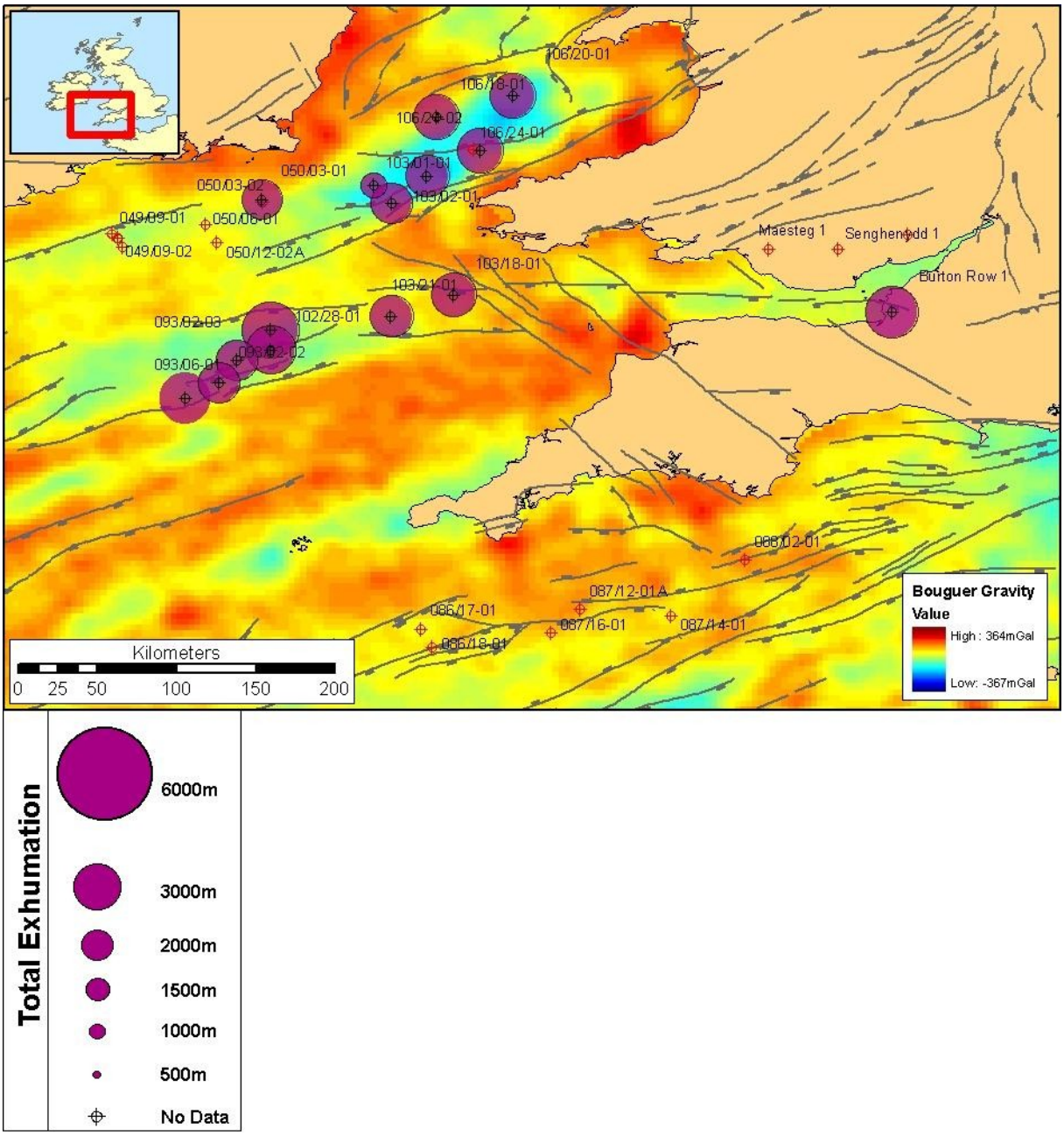

Figure 4.37 – Map showing total exhumation magnitudes calculated using the density log derived hybrid relationship for each of the offshore wells. Wells for which no data was analysed are shown as purple cross-hairs. Coloured circles represent the total exhumation. Exhumation appears to be greatest in the basin centres but also shows a pattern of significant differences across major faults.

4.5: BURIAL ANOMALY RESULTS FROM THE ITT DATA OF THE OFFSHORE SW UK

4.5.1: BURIAL ANOMALY DERIVED FROM COMPARISON WITH THE STATISTICAL CURVE FITTING TECHNIQUE

Figures 4.38 (offshore) and 4.39 (onshore) show examples of the sonic velocity-depth plots used in this study with a calculated normal compaction curve along with the corresponding error analysis (Plots for all the wells may be found in Appendix A). The latter is used to choose the optimum shift constant since the best fitting compaction curve should show the lowest variation between the calculated and the observed data. A shift constant for each of the 17 wells was determined using this method based on minimum AAV and RMS values. These error analysis plots can be ambiguous because low points in the AAV and RMS are sometimes poorly defined, show a broad range of values or they display several troughs. Reasons for this non-systematic behaviour reflect lithology variation and importantly the spread and distribution of the sample size. Interestingly the results presented by Heasler & Kharitonova (1996) for the Bighorn Basin, Wyoming, showed no apparent ambiguity. However the well data used there contained greater sample populations which were spread more uniformly throughout the sections analysed. Equation 4.10 was then used to calculate erosion amounts (Table 4.12).

The largest value of exhumation, 3.63km occurs in well 103/01-1 which is located in the footwall of the St Georges Fault and hangingwall of the southward continuation of the Bala Fault. The lowest value of 0.63km occurs in well 106/18-1. The total exhumation values were then plotted on a map (Figure 4.40) in order to analyse the distribution of exhumation. Overall the data suggest much lower magnitude of burial anomaly than the porosity derived values. The patterns of exhumation observed also vary considerably with those results. Burial anomaly differences across faults suggests that the hangingwall side has experienced a

greater burial anomaly than the footwall the only exception being Burton Row which still shows a marked positive difference in burial anomaly compared to the basin centre. The distribution suggests that basin centres experienced the lowest values of burial anomaly with the rocks closest to the basin margin faults experiencing the greatest burial anomaly. Interestingly the comparison of values for adjacent wells (50/03-1 with 50/03-2 and 106/24-1 with 106/24-2) show large variations in burial anomaly. The reason for this is likely due to the fact that wells 50/03-2 and 106/24-1 do not contain any extensive shale horizons in the Mesozoic rather they are composed of inter-bedded limestones, siltstones, mudstones and sandstones. These results challenge the assertion of Heasler & Kharitonova (1996) that the technique can be applied to heterolithic sequences. Alternatively the much shallower depth of penetration of the well may have led to an erroneous derivation of the correct 'normal compaction curve'.

		Shift Constant (µs/ft)	Decay Constant (1/ft)	Apparent exhumation (m)	Depth to u/c (m)	Water depth (m)	K.B.E (m)	Correction (m)	Total exhumation (m)
Well	50/03-1	48	0.00015	1610	124	124	33.5	110	1720
	50/03-2	67	0.00031	634	124	124	33.5	110	744
	93/02-2	67	0.00022	881	664	110	33.5	664	1545
	93/02-3	53	0.00013	1766	788	110	33.5	788	2554
	93/06-1	52	0.00020	1159	814	104	33.5	820	1979
	102/28-1	65	0.00026	766	570	97	26.0	575	1341
	102/28-2	55	0.00016	1406	814	124	33.5	800	2206
	103/01-1	47	0.00008	3047	616	148	33.5	578	3625
	103/02-1	64	0.00023	878	238	142	33.5	206	1084
	103/18-1	56	0.00021	1058	362	94	22.9	367	1425
	103/21-1	66	0.00025	787	462	118	33.2	453	1240
	106/18-1	62	0.00040	519	100	100	33.5	110	629
	106/20-1	54	0.00014	1623	900	100	33.5	910	2533
	106/24-1	70	0.00018	1034	748	88	33.5	770	1804
	106/24-2	45	0.00011	2257	748	100	33.5	758	3015
	106/28-1	60	0.00017	1251	932	109	24.0	923	2174
	Burton Row	30	0.00012	2336	36	0	33.5	146	2482

Table 4.12 – Table showing the optimum shift constants and apparent and total exhumation magnitudes for the wells analysed using the statistical curve fitting technique.

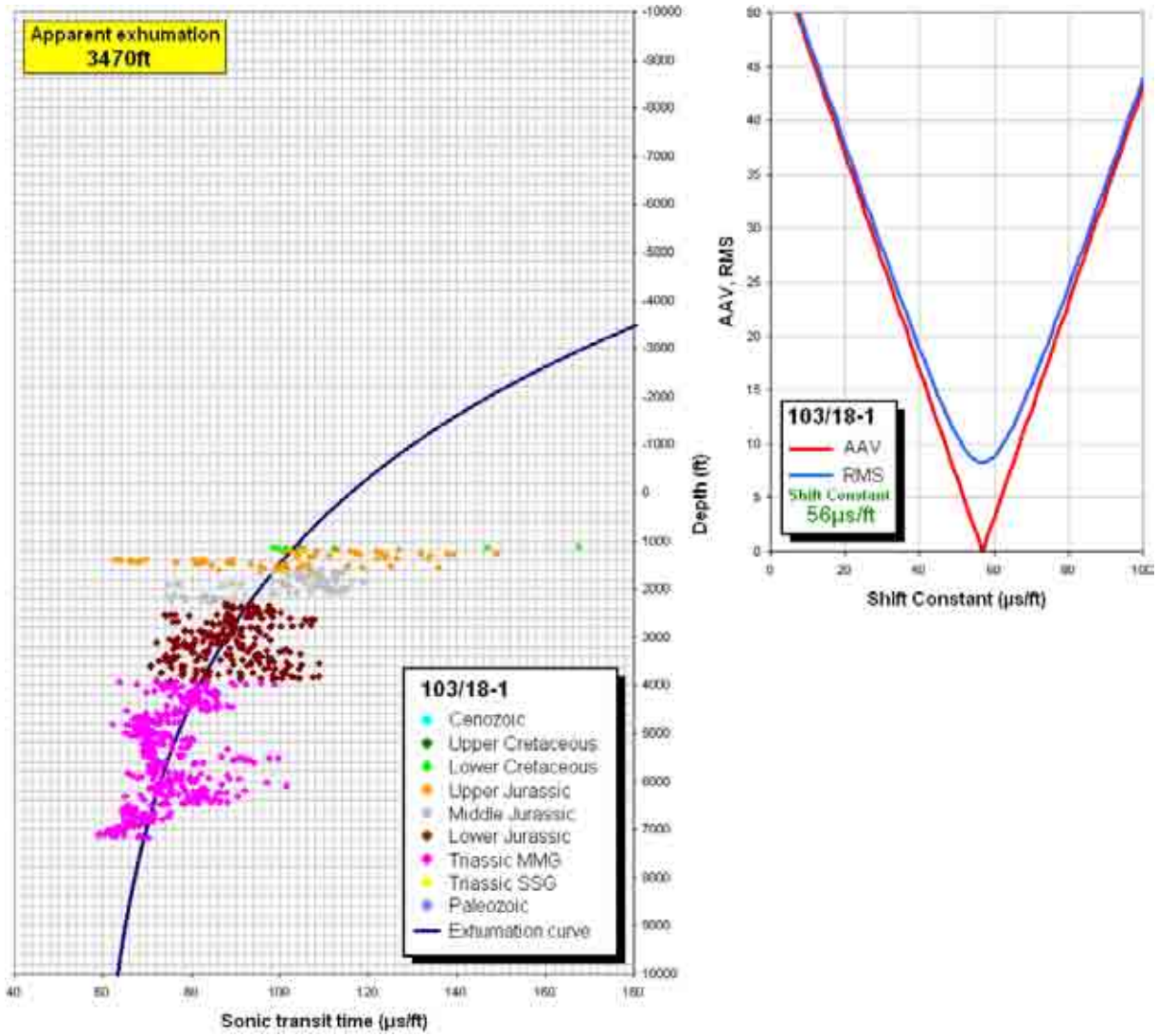

Figure 4.38 – (Above) Graph showing the calculated compaction trend and erosion amount for well 103/18-1 revealing an apparent exhumation of 3470ft (1058m). (Above, right) Error assessment of statistical fit showing the optimum shift-constant of 56µs/ft.

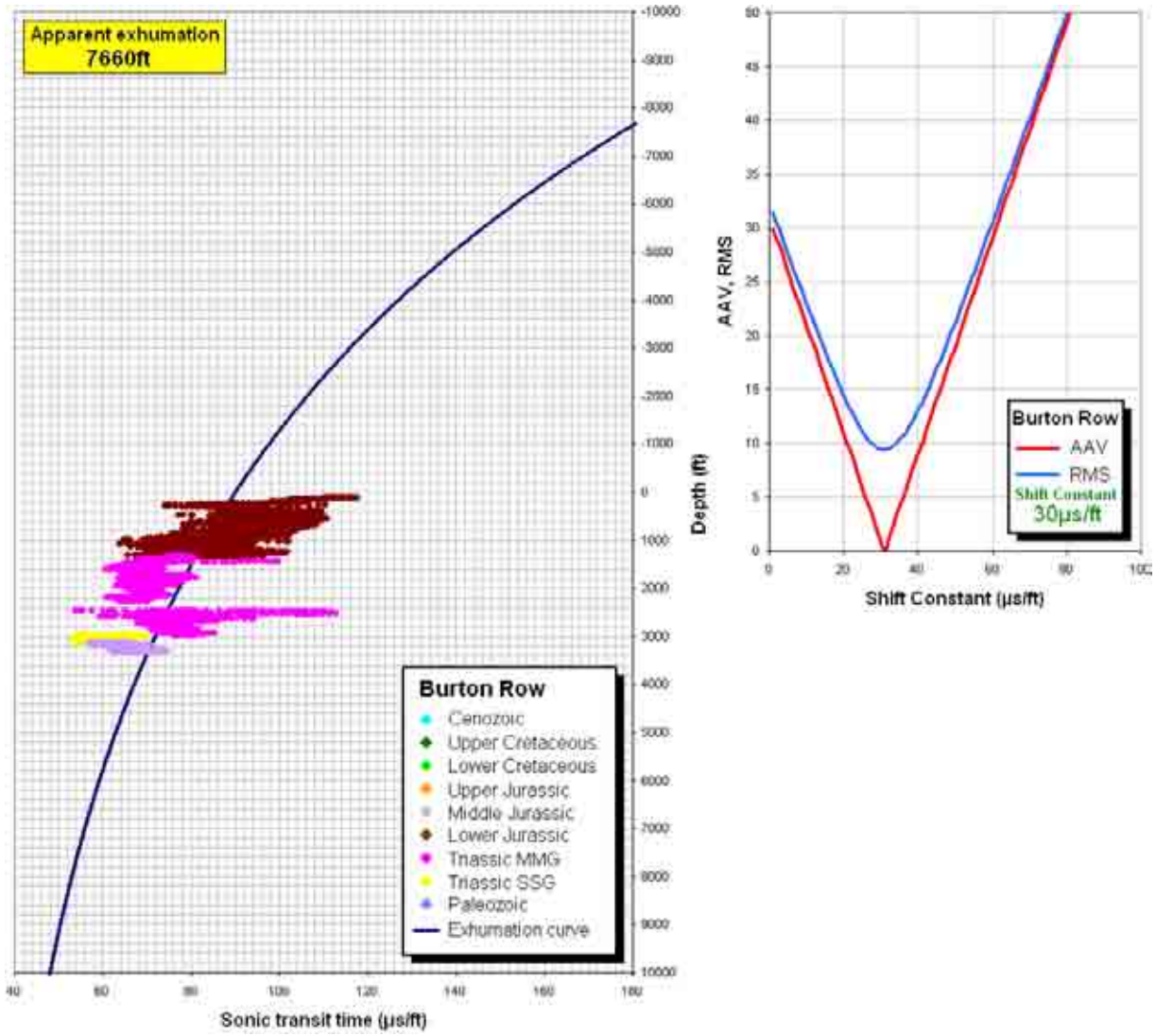

Figure 4.39 – (Above) Graph showing the calculated compaction trend and erosion amount for the Burton Row borehole revealing an apparent exhumation of 7660ft (2336m). (Above, right) Error assessment of statistical fit showing the optimum shift-constant of 30µs/ft.

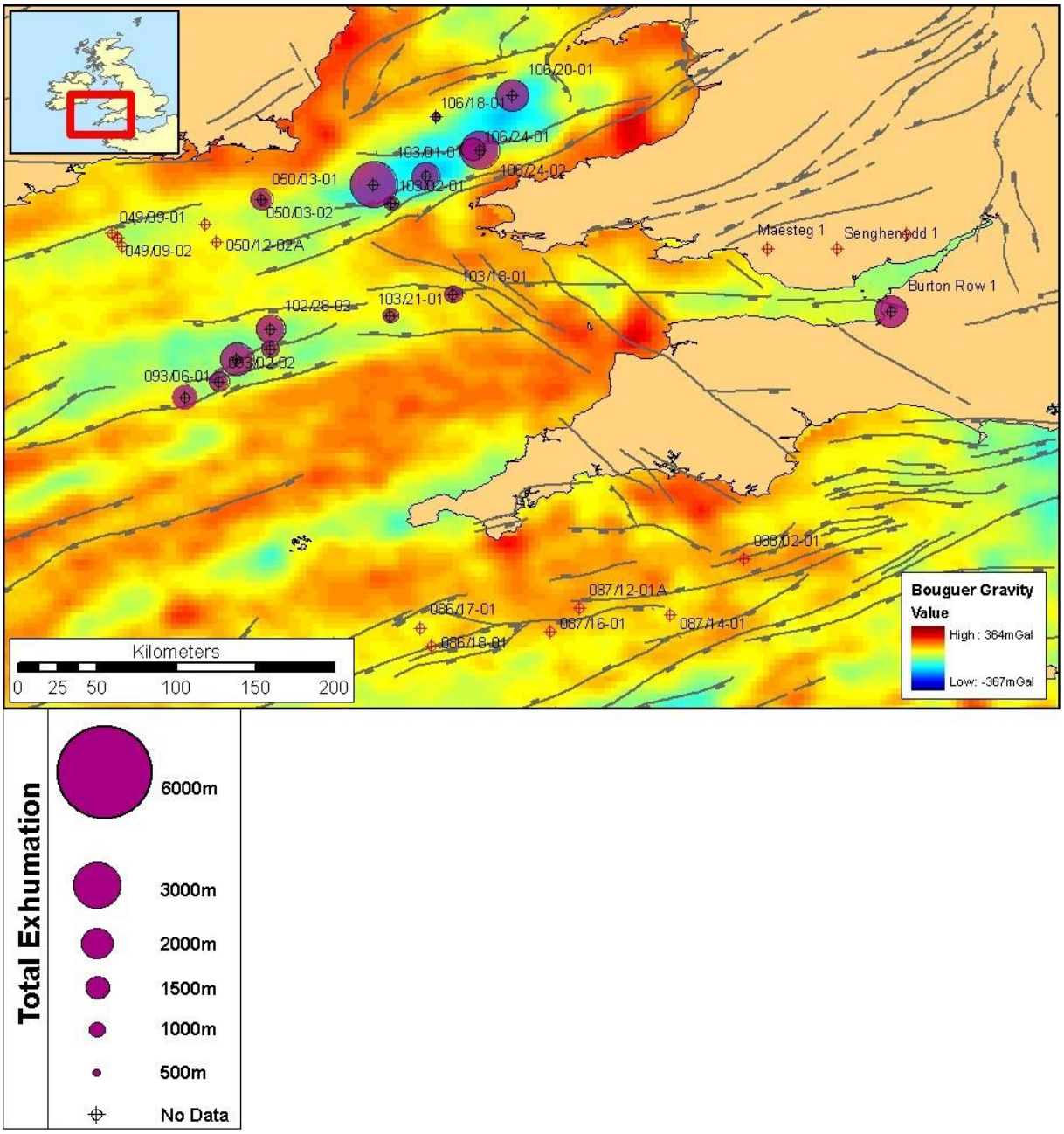

Figure 4.40 – Map showing total exhumation magnitudes for each of the offshore wells as derived from the statistical curve fitting technique. Wells for which no data was analysed are shown as purple cross-hairs. Coloured circles represent the total exhumation. Exhumation appears to have been at its greatest near to the normal faults with the smallest values of exhumation concentrated in basin centres. Note also the large variation in exhumation between adjacent wells (50/03-1, 50/03-2 and 106/24-1, 106/24-2).

4.5.2: INTERPRETATION OF RESULTS FROM THE SUPERCURVE

Figure 4.41 shows examples of the sonic velocity-depth plots for each of the wells compared to the supercurve derived for the SW UK (the full set can be found in Appendix A). Exhumation values are shown in Table 4.13. The largest value of exhumation, 3.29km occurs

in well 93/06-1 which is located in the footwall of a major fault. The lowest value of 2.05km occurs in well 103/21-1 which lies in the centre of the SCSB is the hangingwall of a major fault. The total exhumation values were then plotted on a map (Figure 4.42) in order to analyse the distribution of exhumation.

The data generated by the supercurve is generally consistent with that calculated from the porosity data Many of the distributional observations from that study are also evident here. The main observation of footwall uplift is apparent in the SCSB and at the Burton Row borehole. In the SGCB however the larger exhumation appears to have occurred in the hangingwall. Overall the data is much more consistent in regards to nearby wells. For example wells 103/01-1, 103/02-1 and 106/28-1 all show similar exhumation values for the same structural setting. The same is true for wells 93/02-3 and 102/28-1. This similarity was also displayed by the results from the Raymer derived porosity exhumation however the values here are much higher. This relationship should not be too surprising given the relationship between sonic velocity and porosity and suggests that the distribution of exhumation values is likely to be real rather than an artefact of the mathematically derived values.

Exhumation values were also calculated for the Ware & Turner (2002) supercurve for the East Irish Sea Basin (Table 4.14). The values recorded using this curve are considerably lower than any of the other techniques used. When plotting the data on a map (Figure 4.43) a similar distribution to the SW UK supercurve is observed. Due to the poor match between relative exhumation values the Ware & Turner (2002) supercurve is considered to be limited in its application to the East Irish Sea Basin. Similarly the SW UK supercurve is only applicable to the wells in this study and should not be applied to similar studies in different areas.

		Apparent exhumation (m)	Depth to u/c (m)	Water depth (m)	K.B.E (m)	Correction (m)	Total exhumation (m)
Well	50/03-1	2340	124	124	33.5	110	2450
	50/03-2	-	124	124	33.5	110	-
	93/02-2	1690	664	110	33.5	664	2354
	93/02-3	1720	788	110	33.5	788	2508
	93/06-1	2470	814	104	33.5	820	3290
	102/28-1	2130	570	97	26	575	2705
	102/28-2	2280	814	124	33.5	800	3080
	103/01-1	1480	616	148	33.5	578	2058
	103/02-1	2020	238	142	33.5	206	2226
	103/18-1	2210	362	94	22.86	367	2577
	103/21-1	1600	462	118	33.22	453	2053
	106/18-1	2170	100	100	33.5	110	2280
	106/20-1	1920	900	100	33.5	910	2830
	106/24-1	-	748	88	33.5	770	-
	106/24-2	2440	748	100	33.5	758	3198
	106/28-1	1160	932	109	24	923	2083
	Burton Row	3070	36	0	33.5	146	3216

Table 4.13 – Table showing apparent and total exhumation magnitudes derived from the supercurve technique. Wells 50/03-2 and 106/24-1 do not contain a shale section and as such were excluded from analysis.

		Apparent exhumation (m)	Depth to u/c (m)	Water depth (m)	K.B.E (m)	Correction (m)	Total exhumation (m)
Well	50/03-1	720	124	124	33.5	110	830
	50/03-2	-	124	124	33.5	110	-
	93/02-2	380	664	110	33.5	664	1044
	93/02-3	450	788	110	33.5	788	1238
	93/06-1	570	814	104	33.5	820	1390
	102/28-1	570	570	97	26	575	1145
	102/28-2	520	814	124	33.5	800	1320
	103/01-1	770	616	148	33.5	578	1348
	103/02-1	530	238	142	33.5	206	736
	103/18-1	570	362	94	22.86	367	937
	103/21-1	320	462	118	33.22	453	773
	106/18-1	760	100	100	33.5	110	870
	106/20-1	660	900	100	33.5	910	1570
	106/24-1	-	748	88	33.5	770	-
	106/24-2	400	748	100	33.5	758	1158
	106/28-1	400	932	109	24	923	1323
	Burton Row	1330	36	0	33.5	146	1476

Table 4.14 – Table showing apparent and total exhumation magnitudes derived from the Ware & Turner (2002) supercurve. Wells 50/03-2 and 106/24-1 do not contain a shale section and as such were excluded from analysis.

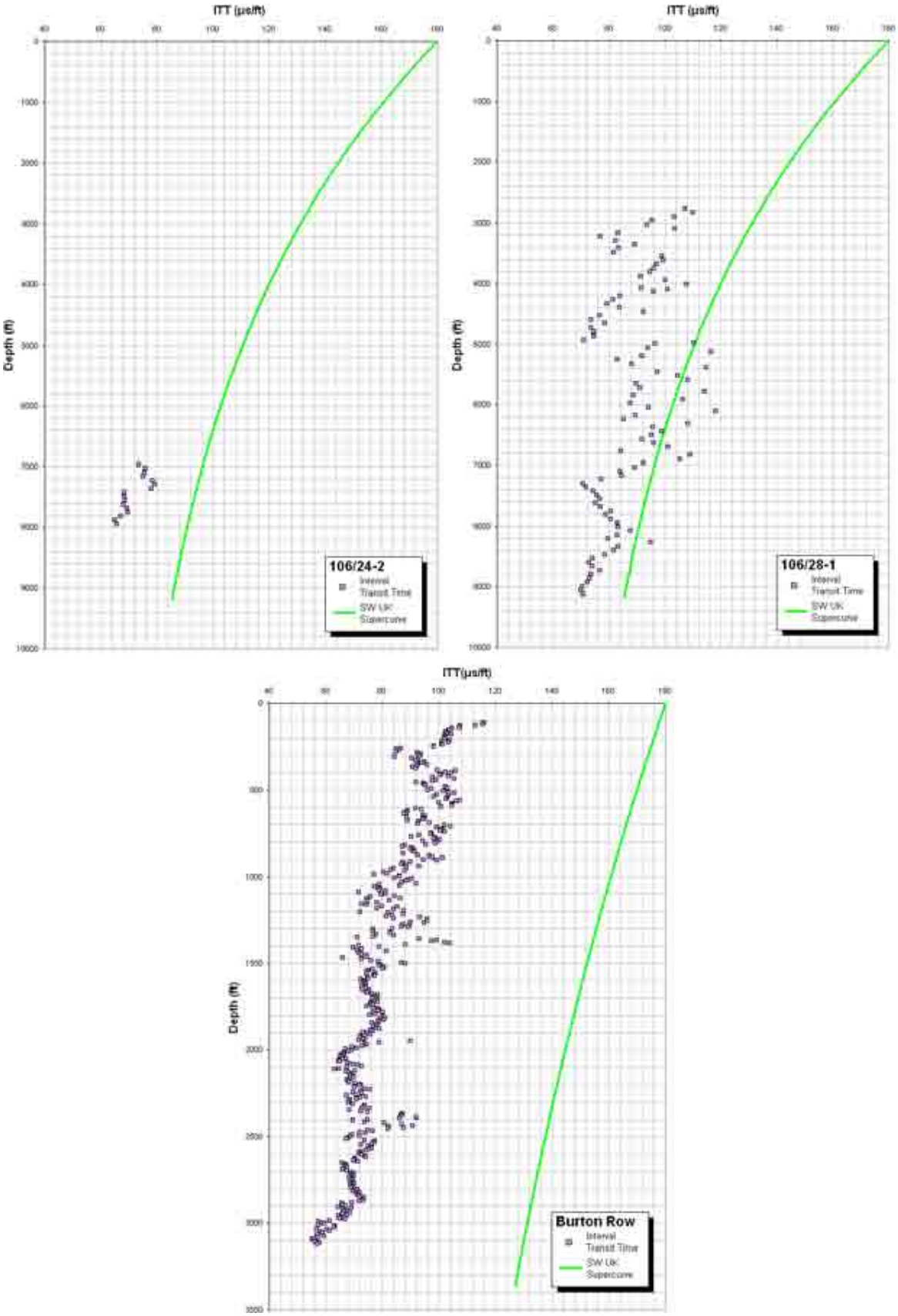

Figure 4.41 – Comparison of ITT for the shale sequences of wells 106/24-2, 106/28-1 and the Burton Row borehole with the supercurve derived for the SW UK.

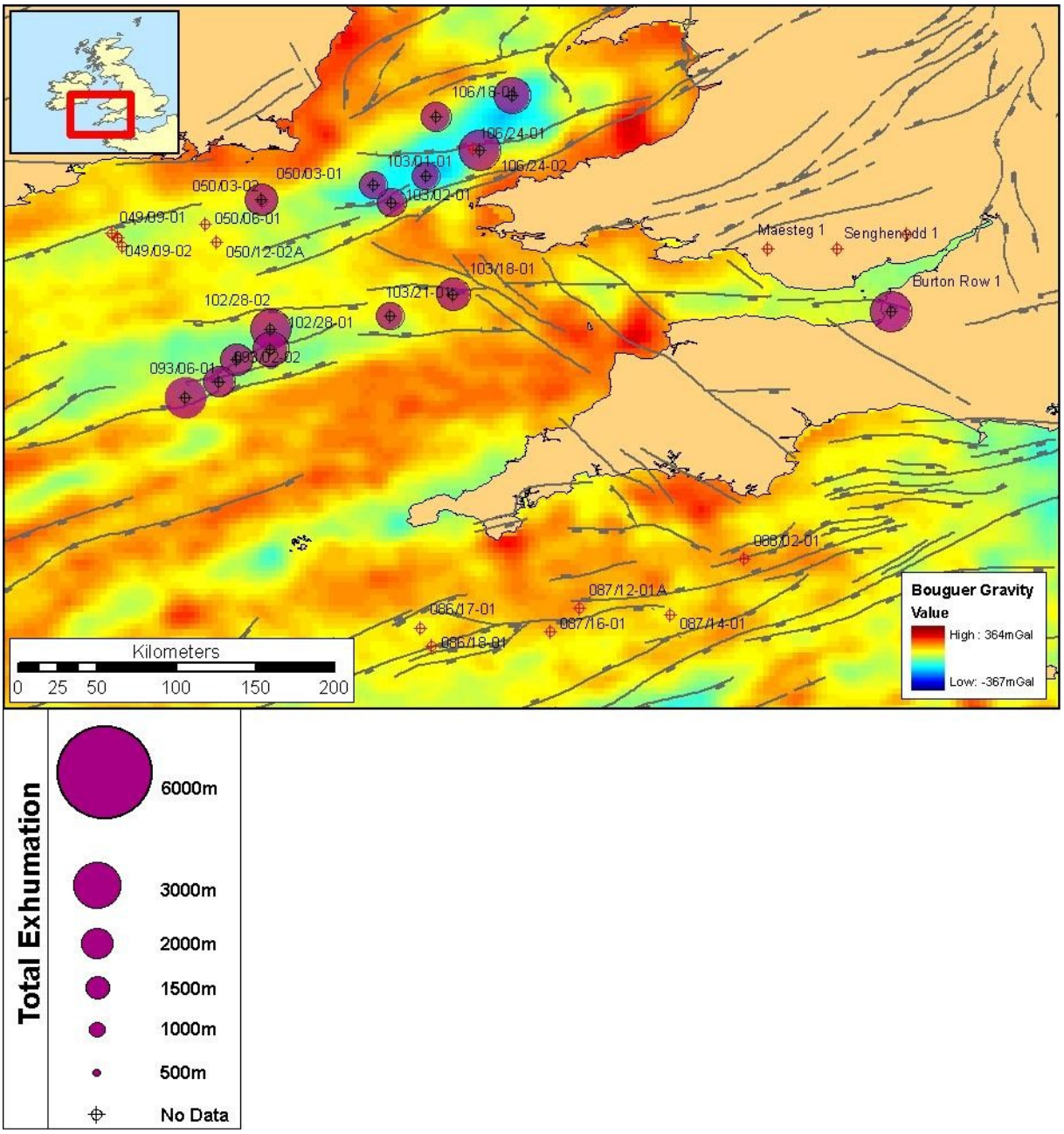

Figure 4.42 – Map showing total exhumation magnitudes calculated for the Supercurve for each of the offshore wells. Wells for which no data was analysed are shown as purple cross-hairs. Coloured circles represent the total exhumation. Exhumation appears to have been broadly similar across the area with the exception of the southern margin of the SCSB (Burton Row and 93/06-1) which have experienced noticeably higher exhumations.

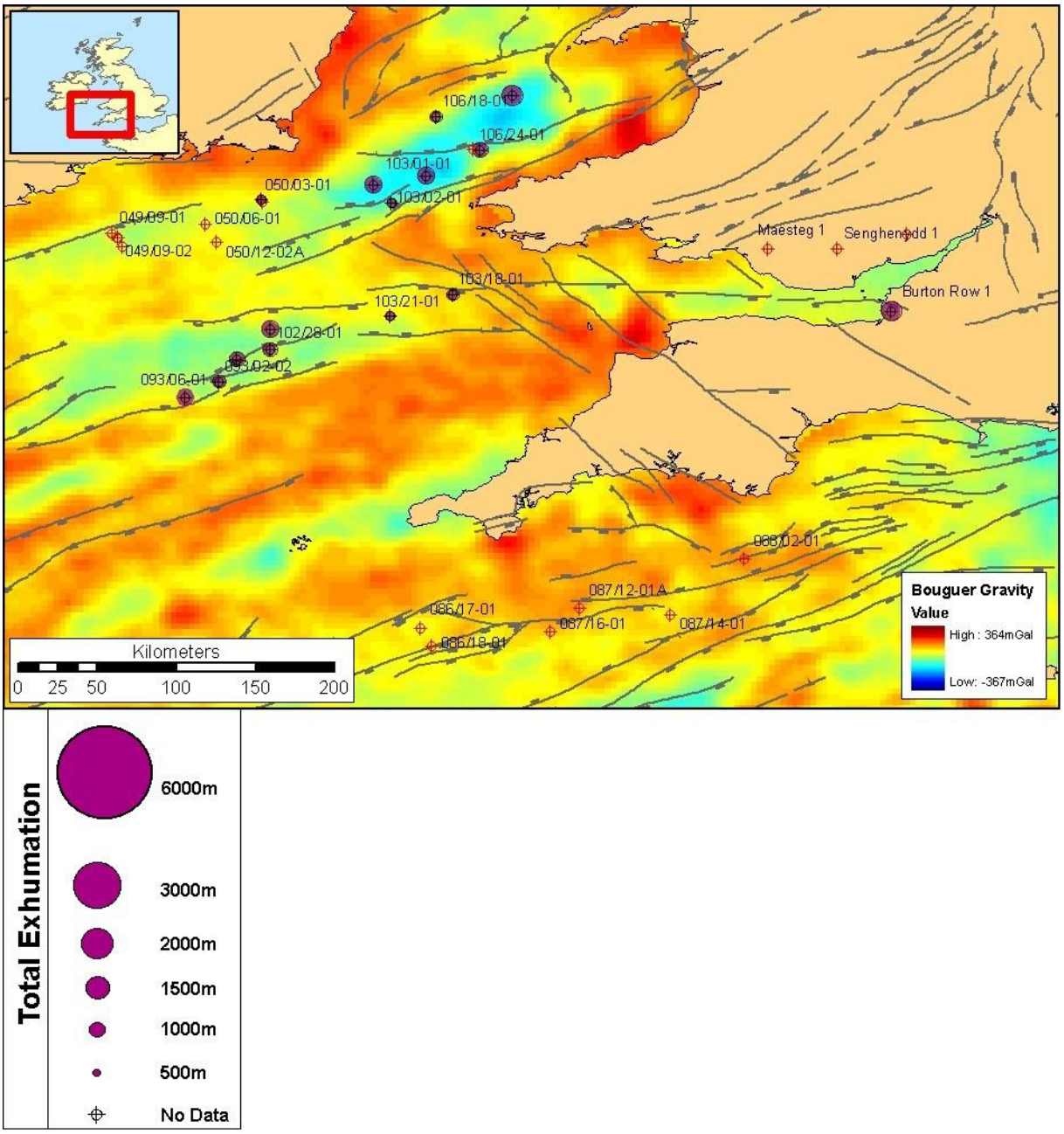

Figure 4.43 – Map showing total exhumation magnitudes calculated using the Ware & Turner (2002) supercurve for each of the offshore wells. Wells for which no data was analysed are shown as purple cross-hairs. Coloured circles represent the total exhumation. Exhumation values are the lowest calculated for the offshore region. This implies the velocity-depth relationship of the Celtic Sea shales is somewhat different to those found in the EISB.

4.5.3: JAPSEN RELATIONSHIPS

Figure 4.44 shows examples the sonic velocity-depth plots for each of the wells compared to the Lower Jurassic shale and Bunter Shale trends (the full set for all wells can be found in Appendix A). Burial anomalies are shown in Table 4.15 and 4.16. The largest value of burial anomaly for the Lower Jurassic trend is 3.73km and occurs in well 93/06-1 which is located in the footwall of a major fault. The lowest value of 2.11km occurs in well 103/01-1. For the Bunter Shale trend the largest value of burial anomaly is 3.34km and found in the Burton Row borehole in the footwall of the BCB southern margin fault. The lowest value of 1.19km is again found in well 103/01-1. The burial anomaly values were then plotted on a map (Figure 4.45 and 4.46) in order to analyse the distribution of former deeper burial. Figure 4.45 shows that former deeper burial was at its greatest in the basin centres consistent with inversion being the main driving mechanism. There is evidence in the SCSB for footwall uplift on the southern margin illustrated by well 93/06-1 and the Burton Row borehole. In the SGCB however hangingwall exhumation appears greater. Figure 4.46 shows large burial anomalies in the basin centres but also illustrates footwall uplift in both the SGCB and SCSB. Both trends give burial anomaly values which are similar to those derived from the porosity data. Overall the data show a decrease in burial anomaly magnitude towards the Pembroke Ridge increasing in value away from that structure.

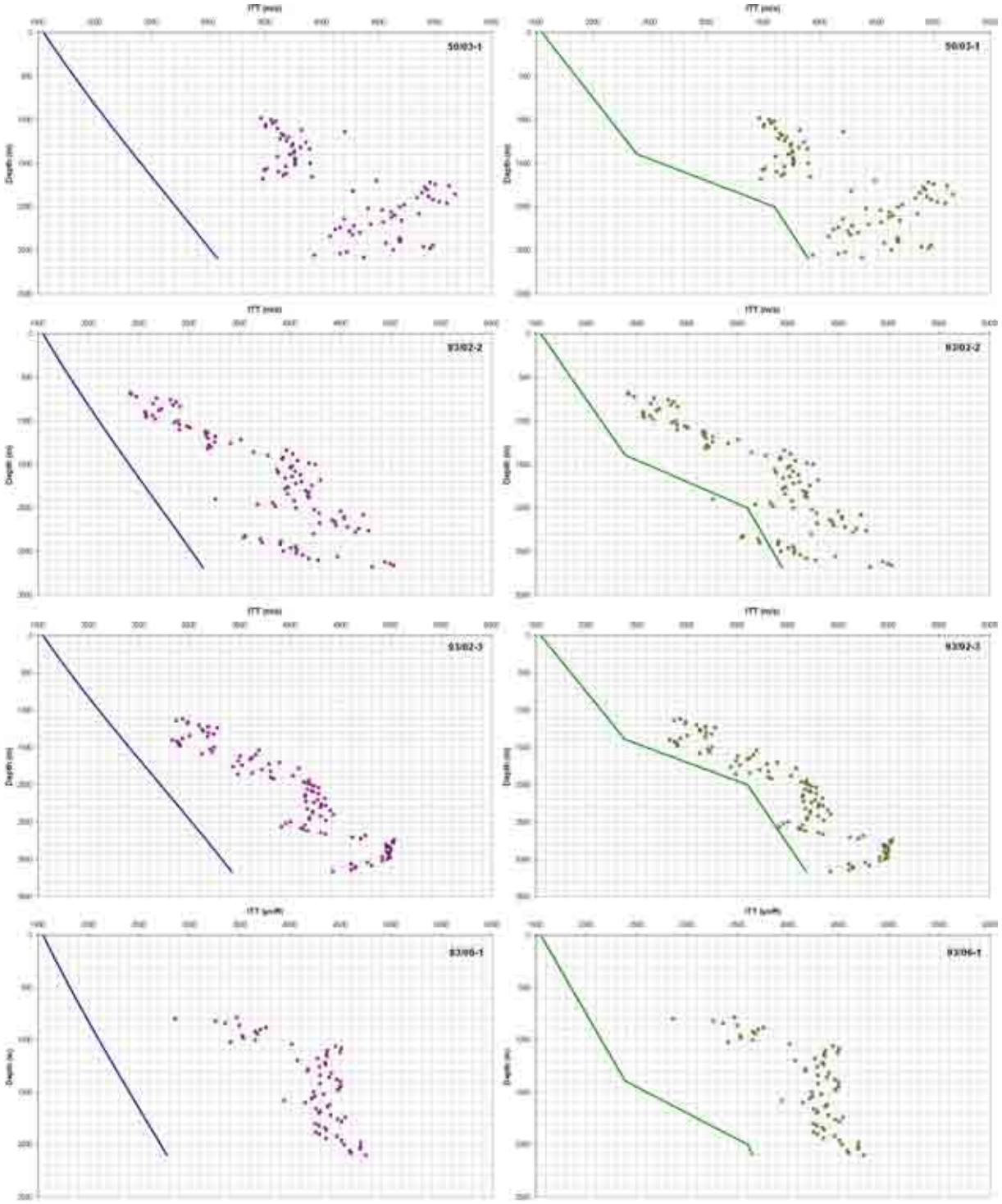

Figure 4.44 – Comparison of interval transit time-depth values compared to the Lower Jurassic shale and Triassic Bunter shale trends of Japsen (2000) for wells 50/03-1, 93/02-2, 93/02-3 and 93/06-1.

		Apparent exhumation (m)	Depth to u/c (m)	Water depth (m)	K.B.E (m)	Correction (m)	Total exhumation (m)
Well	50/03-1	3210	124	124	33.5	110	3320
	50/03-2	-	124	124	33.5	110	-
	93/02-2	2030	664	110	33.5	664	2694
	93/02-3	2510	788	110	33.5	788	3298
	93/06-1	2910	814	104	33.5	820	3730
	102/28-1	2510	570	97	26	575	3085
	102/28-2	2690	814	124	33.5	800	3490
	103/01-1	1530	616	148	33.5	578	2108
	103/02-1	2450	238	142	33.5	206	2656
	103/18-1	2620	362	94	22.86	367	2987
	103/21-1	2070	462	118	33.22	453	2523
	106/18-1	2740	100	100	33.5	110	2850
	106/20-1	2440	900	100	33.5	910	3350
	106/24-1	-	748	88	33.5	770	-
	106/24-2	2670	748	100	33.5	758	3428
	106/28-1	1920	932	109	24	923	2843
	Burton Row	3500	36	0	33.5	146	3646

Table 4.15 – Table showing apparent and total exhumation magnitudes derived from comparison with the Japsen (2000) Lower Jurassic shale trend. Wells 50/03-2 and 106/24-1 do not contain a shale section and as such were excluded from analysis.

		Apparent exhumation (m)	Depth to u/c (m)	Water depth (m)	K.B.E (m)	Correction (m)	Total exhumation (m)
Well	50/03-1	1410	124	124	33.5	110	1520
	50/03-2	-	124	124	33.5	110	-
	93/02-2	1120	664	110	33.5	664	1784
	93/02-3	980	788	110	33.5	788	1768
	93/06-1	1360	814	104	33.5	820	2180
	102/28-1	1960	570	97	26	575	2535
	102/28-2	1740	814	124	33.5	800	2540
	103/01-1	610	616	148	33.5	578	1188
	103/02-1	1550	238	142	33.5	206	1756
	103/18-1	1760	362	94	22.86	367	2127
	103/21-1	1500	462	118	33.22	453	1953
	106/18-1	2630	100	100	33.5	110	2740
	106/20-1	980	900	100	33.5	910	1890
	106/24-1	-	748	88	33.5	770	-
	106/24-2	1150	748	100	33.5	758	1908
	106/28-1	1280	932	109	24	923	2203
	Burton Row	3290	36	0	33.5	146	3436

Table 4.16 – Table showing apparent and total exhumation magnitudes derived from comparison with the Japsen (2000) Triassic Bunter shale trend. Wells 50/03-2 and 106/24-1 do not contain a shale section and as such were excluded from analysis.

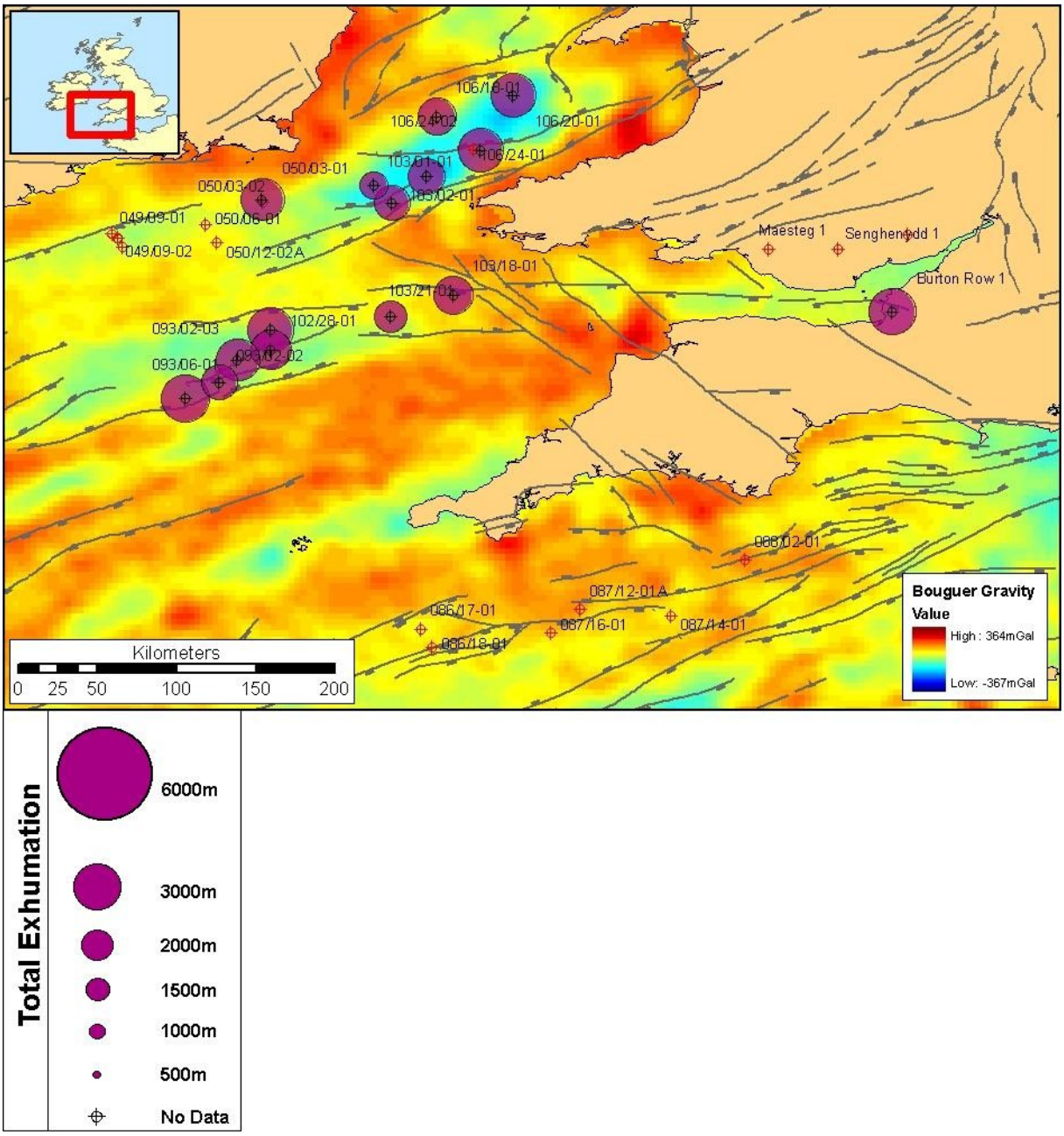

Figure 4.45 – Map showing total exhumation magnitudes calculated for the Lower Jurassic Shale trend of Japsen (2000) for each of the offshore wells. Wells for which no data were analysed are shown as purple cross-hairs. Coloured circles represent the total exhumation. Exhumation appears to have been broadly similar across the area though the values are much higher than the other techniques (excluding the Quad 103 derived exhumation estimates). Burton Row here appears to have a much more similar value to the rest of the area rather than a conspicuously high exhumation value.

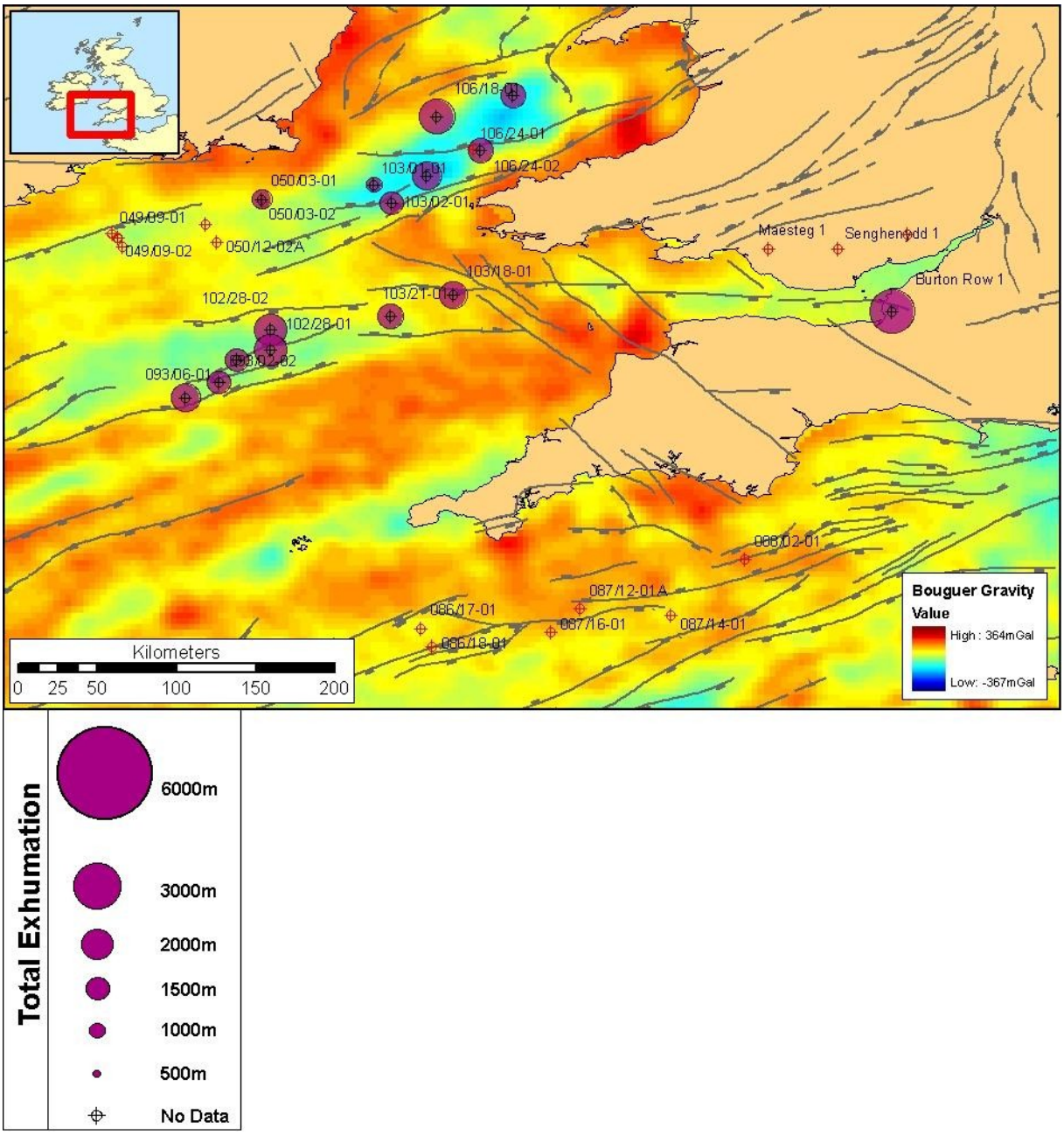

Figure 4.46 – Map showing total exhumation magnitudes calculated for the Japsen (2000) Bunter Shale trend for each of the offshore wells. Wells for which no data was analysed are shown as purple cross-hairs. Coloured circles represent the total exhumation. Burton Row again appears to have the largest exhumation value as does the Margin of the SCSB. The centre of the SCSB also appears to have experienced significant exhumation. In the North the CBB appears to have experienced large exumations on its northern margin whilst the rest of the basin has experienced a broadly similar exhumation.

4.5.4: HILLIS TREND

Table 4.17 shows the exhumation values calculated for each of the wells in this study as well as a suite of wells from the study of Menpes & Hillis (1995). The ability of this approach to consider other stratigraphic intervals other than shales allows separation of exhumation across the Jurassic-Cretaceous unconformity where present. This has resulted in two values for total exhumation to be calculated – one for post-Jurassic exhumation (inferred as a Cretaceous inversion event) and one for the post-Cretaceous (inferred to represent Cenozoic inversion).

For the post-Jurassic, the largest value of exhumation is 2.30km occurring in the Burton Row borehole. Larger values of exhumation are reported in the Western Approaches Basin (up to 2.70km) however values are based on data from Menpes & Hillis (1995). The largest value of exhumation for the post-Cretaceous is 2.30km and occurs in well Brezell which is located in French territorial waters in the Western Approaches Basin. In the Celtic Sea basins the largest value is 1.48km which occurs in well 50/12-2a in the NCSB. As mentioned above both these estimates are based on the reference trend and since it is likely that the whole area has experienced exhumation these values should be considered the minimum amount of exhumation. The total exhumation values were then plotted on a map (Figure 4.47 and 4.48) in order to analyse the distribution of exhumation.

Figure 4.47 shows that post-Jurassic exhumation was broadly similar across the area. There are some localised examples of basin centre exhumation being greatest but also, particularly in the SCSB, for footwall uplift (illustrated by well 93/06-1 and the Burton Row borehole). In the SGCB however hangingwall exhumation appears greater. Figure 4.48 shows that post-Cretaceous exhumation was broadly similar across the area with only the SGCB showing a slightly larger amount of exhumation compared to the general trend. Both trends give

exhumation values which are in line with those derived from the analysis of exhumation from porosity using the lower value of matrix ITT of 60µs/ft.

		Apparent Exhumation (m)							ET Jurassic (m)	ET Cretaceous (m)
		Upper Cretaceous	Lower Cretaceous	Lower Jurassic	Mercia Mudstone	Sherwood Sandstone	Post Jurassic Mean	Post Cretaceous mean		
Celtic Sea Wells	47/29-1	951	1008	-	-	-	-	980	-	1199
	48/19-1	1105	977	-	-	-	-	1041	-	1260
	49/09-1	340	758	-	-	-	-	549	-	768
	49/09-2	270	646	-	-	-	-	458	-	677
	49/09-3	262	995	-	-	-	-	629	-	848
	49/14-3	471	932	-	-	-	-	702	-	921
	50/03-1	-	-	1553	-	-	1553	-	1677	-
	50/06-1	350	634	-	-	-	-	492	-	711
	50/12-2A	1362	1164	-	-	-	-	1263	-	1482
	93/02-2	407	687	292	1287	REF	790	547	1410	766
	93/02-3	449	855	563	795	282	547	652	1287	871
	93/06-1	1242	REF	1148	1422	987	1186	1242	1926	1461
	102/28-1	351	202	1984	1697	797	1493	277	1973	496
	102/28-2	283	732	602	1131	535	756	508	1436	727
	102/29-1	868	1093	-	-	-	-	981	-	1200
	103/01-1	-	-	REF	REF	-	-	-	-	-
	103/02-1	-	-	REF	1340	347	844	-	1082	-
	103/18-1	-	-	-	1668	-	1668	-	2030	-
	103/21-1	609	938	-	1412	-	1412	774	1712	993
	106/18-1	-	-	-	1379	-	1379	-	1479	-
	106/20-1	-	-	806	1020	-	913	-	1813	-
	106/24-2	-	-	1060	1026	-	1043	-	1791	-
	106/28-1	-	-	976	1176	-	1076	-	2008	-
	Burton Row	-	-	1924	2401	2451	2259	-	2295	-
Southwestern Approaches Wells	72/10-1A	337	-	-	881	-	881	337	1981	556
	73/01-1	REF	-	-	354	-	354	-	1654	-
	73/02-1	339	-	-	799	-	799	339	1799	558
	73/04-1	174	392	-	REF	-	-	283	-	502
	73/05-1	389	125	-	726	-	726	257	1826	476
	73/06-1	113	626	-	596	-	596	370	1696	589
	73/07-1	282	415	-	846	-	846	349	2046	568
	73/08-1	250	-	-	793	-	793	250	1993	469
	73/12-1A	180	-	-	707	-	707	180	1907	399
	73/13-1	240	-	-	884	-	884	240	2384	459
	73/14-1	310	-	-	925	-	925	310	2425	529
	74/01-1A	366	40	-	729	-	729	203	1629	422
	83/24-1	175	563	-	-	-	-	369	-	588
	85/28-1	358	113	-	170	-	170	236	1070	455
	86/17-1	641	663	-	674	-	674	652	1274	871
	86/18-1	766	627	-	-	-	-	697	-	916
	87/12-1A	1662	1017	-	1595	-	1595	1340	2695	1559
	87/14-1	917	-	-	-	-	-	917	-	1136
	87/16-1	728	620	-	869	-	869	674	1569	893
	88/02-1	752	-	-	1012	-	1012	752	1112	971
	Brezell	2082	-	-	-	-	-	2082	-	2301
	Garlizenn	208	REF	-	-	-	-	208	-	427
	Glazenn	34	878	-	-	-	-	456	-	675
	Kerluz	REF	-	-	-	-	-	-	-	-
	Kulzenn	582	-	-	942	-	942	582	1542	801
	Lizenn	1314	-	-	-	-	-	1314	-	1533
	Penma	402	369	-	-	-	-	386	-	605
	Re-Gwenn	447	622	-	819	-	819	535	2219	754
	Travank	-	763	-	-	-	-	763	-	982
	Yar Vor	1502	1131	-	-	-	-	1317	-	1536

Table 4.17 – Table showing apparent and total exhumation magnitudes derived from using the approach of Menpes & Hillis (1995). The Jurassic and Cretaceous are separated by an unconformity allowing two separate total exhumations to be calculated (both corrected to the common datum of the sea-floor). The Post Jurassic total is composed of an average of the Lower Jurassic Lias Group, Mercia Mudstone Group and Sherwood Sandstone Group. The Post Cretaceous total is an average of the Upper and Lower Cretaceous. **REF** refers to wells which have been used as the 'reference wells' (see text).

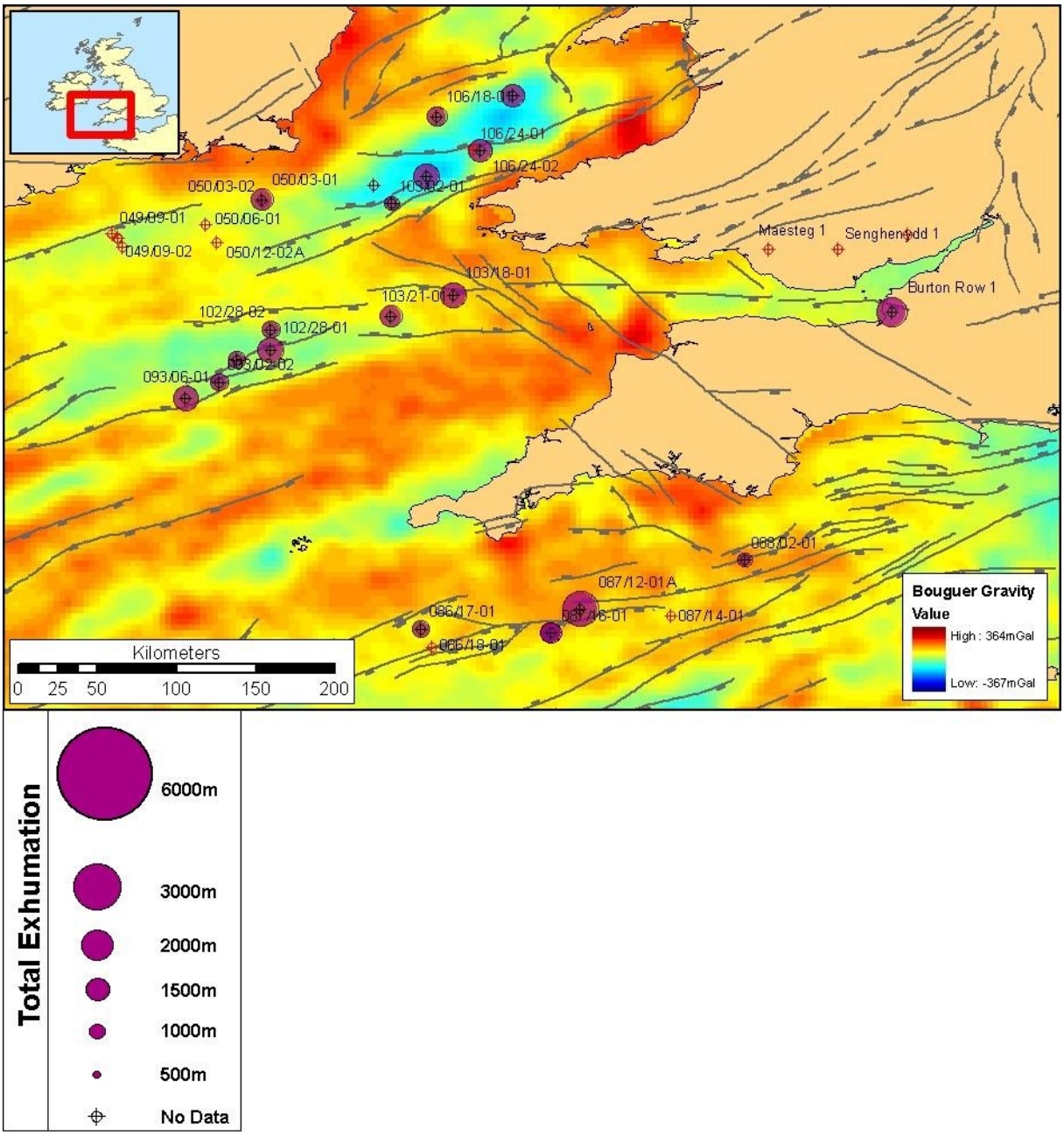

Figure 4.47 – Map showing total exhumation magnitudes for the post-Juarassic calculated using the Hillis approach for each of the offshore wells.

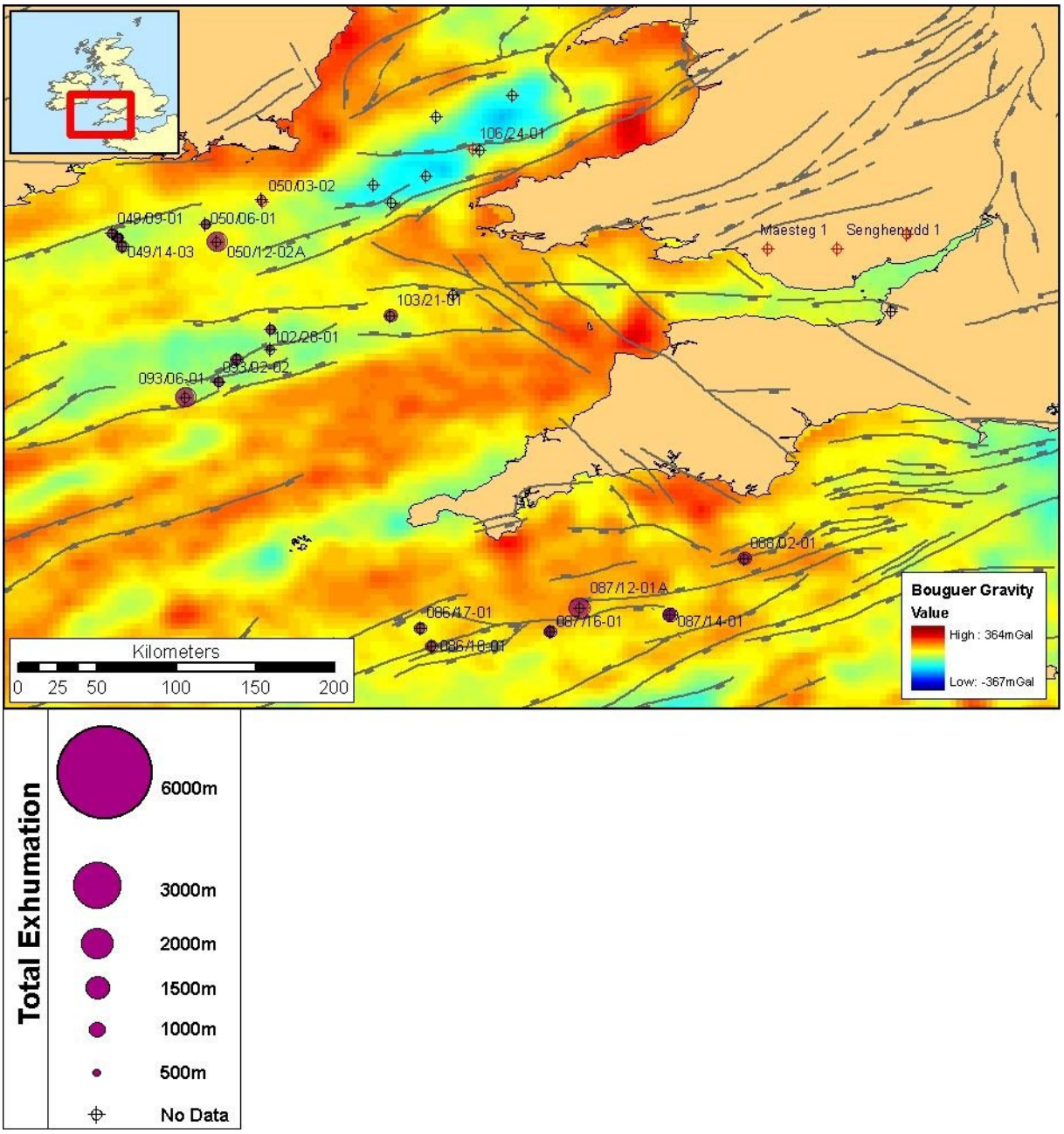

Figure 4.48 – Map showing total exhumation magnitudes for the post-Cretaceous calculated using the Hillis approach for each of the offshore wells.

4.6: DISCUSSION – VALIDITY OF COMPACTIONALLY DERIVED EXHUMATION AND IMPLICATIONS FOR THE EXHUMATION OF THE OFFSHORE SW UK

The Mesozoic-Cenozoic burial histories of the NCSB, SCSB, BCB and SGCB have been investigated using sonic log data from fifteen exploration wells and in the case of wells 103/18-1 and 103/21-1 bulk density log data. A number of different approaches (such as analysis using porosity and analysis using ITT) commonly used by maximum burial depth analysis workers have been compared with each other both to test their validity and absolute values. Table 4.18 shows a comparison of the values obtained by each of the techniques.

Well	Exhumation Corrie 66	Exhumation Corrie 68	Wylie 66	Wylie 80	RHG 66	RHG 80	Linear	Power	Exp	Hybrid	Superposition	Wase and Turner Superpositn	Japsen LJ	Japsen Trias
50/03-1	1700	1525	2240	1560	2726	1210	2530	4480	2510	3060	2460	830	3320	1520
50/03-2	744	646	-	-	-	-	-	-	-	-	-	-	-	-
53/02-2	1540	1408	2584	1854	2894	1634	2804	4344	3094	3214	2354	1044	2894	1784
53/02-3	2054	2318	3178	1908	2958	1678	2728	4588	3148	3188	2588	1238	3298	1768
53/06-1	1979	1803	3080	2380	2980	2150	3750	5080	3910	4100	3250	1290	3730	2180
102/28-1	1341	1225	2125	1660	2036	1545	3200	4655	3365	3771	2736	1145	3086	2535
102/28-2	2206	2026	2530	1920	2520	1780	3860	5000	3405	4400	3080	1320	3490	2540
103/01-1	3625	3235	3518	1618	2778	998	1753	3648	1888	3025	2058	1348	2108	1188
103/02-1	1584	953	1686	1666	1796	1416	2796	4186	2726	3166	2228	736	2634	1784
103/18-1	1425	1279	2467	1767	2227	1557	2947	4777	3287	3397	2577	937	2987	2127
103/21-1	1240	1118	2343	1623	2323	1473	2443	4313	3243	3263	2053	773	2523	1963
106/18-1	629	552	2750	1940	2826	1656	2752	4990	3440	3450	2230	870	2858	2740
106/20-1	2533	2305	2730	1680	2310	1540	3040	4880	3350	3570	2836	1470	3350	1880
106/24-1	1864	1636	-	-	-	-	-	-	-	-	-	-	-	-
106/24-2	3015	2726	3188	1968	2848	1456	3329	5118	3256	3468	3198	1158	3428	1968
106/28-1	2174	1994	2773	1903	2673	1560	2763	4713	3353	3543	2083	1323	2843	2203
Burton Row	2482	2263	3686	2516	3546	2336	3596	5426	3576	4046	3216	1476	3646	3436

Table 4.18 – Table showing comparison between total exhumation values for each of the compactional techniques used. This table should be read with Table 4.17 to enable comparison with the Hillis technique too. The table shows the wide range of values obtained depending on the compactional technique used and highlights the caution required when carrying out a compactional study of former deeper burial.

The advantages of compaction methods for the study of exhumation in offshore basins are the widespread availability of sonic logs and independence from rock sample collection, processing and associated pitfalls. New analyses of sonic velocity data from 15 offshore exploration wells indicate that the SW UK Triassic-Lower Jurassic strata have been more deeply buried by at least 0.6km with the average being 1.5km. An upper limit on the magnitude of deeper burial is ~4km with the average being 3.4km. There is a clear basin-wide variation in the amount of deeper burial indicated by the sonic velocity data highlighting short-wavelength variations in former deeper burial across major faults. The fact that this pattern is replicated when sonic velocity data are compared with a number of independent reference-trends strongly suggests that this is a real effect (Figure 5.75).

4.6.1: ROBUSTNESS OF THE METHODS USED

4.6.1.1: Porosity approach

The use of the porosity transforms to calculate porosity remains the most popular method for calculating former deeper burial in the hydrocarbon industry. However, formulae such as the Wyllie time-average equation and Raymer-Hunt-Gardner transform are a simplification of a complex process. For example, there is no physical reason for the total travel time of a wave in a two-component composite (matrix and pore-fluid) to be the sum of the travel times in the individual components (unless the two components are arranged in layers normal to the direction of propagation and the wavelength is small as compared to the thickness of an individual layer) which is fundamental in determining the porosity from sonic data. A number of models have been developed which highlight the interaction of velocity, porosity and pore-fluid compressibility and such relationships explicitly take into account the internal structure of rock. Examples of effective medium models are Hudson (1990) for cracked rocks; Kuster & Toksöz (1974) for low-porosity rocks; Berryman (1980), for low to medium-porosity rocks; Digby (1981), Walton (1987) and Dvorkin *et al.* (1994), for high-porosity granular rocks. Reviews of such theories are given by Zimmerman (1991) and Wang & Nur (1992).

Nevertheless the application of these formulas in many different parts of the world has provided a useful insight into the vertical motion of rocks over time. The key approximation tested in this analysis was the validity of choosing the often quoted value of 68µs/ft (Magara, 1978) as being the matrix velocity of a 'typical' shale. As has been highlighted in Chapter 2 as well as in the earlier parts of this chapter previous workers have acknowledged the wide range of matrix velocities possible for shales. This study has found, that in the case of the SW UK, the typical matrix velocity of a Mesozoic shale is 60µs/ft. This is based on the

conversion of density derived porosity into ITT. Based on this finding the results generated by the higher matrix velocity of 68µs/ft should be considered invalid. With this information it is then simply a case of deciding which equation gives the more accurate value of porosity and hence exhumation.

Work by Dvorkin & Nur (1998) has shown that the Wyllie equation consistently underestimates porosity and hence overestimates exhumation in sandstones. The RHG equation accurately predicts low-frequency saturated rock velocity in consolidated sandstones and in cemented high-porosity rocks. The accuracy of the Wyllie equation is not as good. Neither equation can adequately predict velocity in the high-porosity uncemented sands (Dvorkin & Nur, 1998) (Figure 4.49). Dvorkin & Nur (1998) go on further to show that the accuracy of the Wyllie equation can be increased by the appropriate choice of matrix velocity. Dvorkin & Nur (1998) conclude that the Raymer *et al.* (1980) velocity-porosity transform, with a reasonably chosen solid-phase velocity, can be reliably used for estimation of porosity in the interval from 0-35% and the Wyllie *et al.* (1956) time-average equation while less accurate, can be used to evaluate porosity from sonic logs. Thus in the case of the SW UK the Raymer derived exhumation, with a matrix velocity of 60µs/ft, is considered to give the most accurate values of exhumation in the absence of any further data. As shown above the density log derived porosity indicates that the wells 103/18-1 and 103/21-1 have experienced exhumation of 3km ± 0.5km. With this additional information it is clear that that exhumation values are grossly underestimated by ~1km using these parameters illustrating the complexity of assigning a single value to a succession.

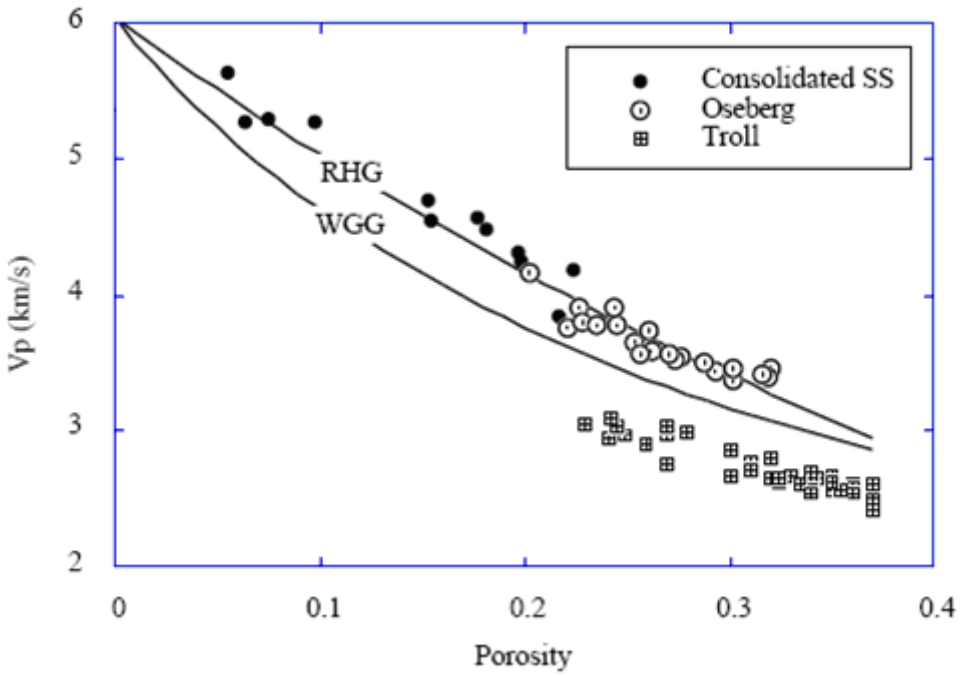

Figure 4.49 – Velocity versus porosity in clay-free sandstones. The symbols represent the three datasets. The solid lines are theoretical predictions Key: RHG-Raymer-Hunt-Gardner transform; WGG-Wyllie time-average equation(modified after Dvorkin & Nur, 1998).

4.6.1.2: Porosity relationships

The approach of using multiple parameters to better constrain porosity from ITT is manifested in the construction of the 'porosity relationships'. These trends were developed primarily from the density log, whose parameters are more tightly constrained than the equivalent matrix ITT for shales. This should mean that the former deeper burial values are much more accurate, however since the data in this study was limited to 2 wells from the same basin in the study area and one onshore well from outside of the study area their application to the whole region is questionable. A much more robust analysis could be carried out with a greater density of data points from a wider range of wells. For these reasons the porosity relationship estimates of former deeper burial are not considered to be the best approach for estimating former deeper burial in the SW UK. The following sections critically assess each of the four relationships properties.

4.6.1.2.1: Linear Relationship

The linear relationship by its very nature implies that there is a definite cut off where a rock is totally compacted and will not contain any pore space. Based on the data available this set the lower limit of shale matrix velocity as 60μs/ft. Extrapolation of the final fit however leads to a surface porosity of 54% compared to 63% for the Sclater & Christie (1980) shale trend. This illustrates the need for a locally derived normal compaction trend, since based on this information the Sclater & Christie (1980) trend does not seem to fit. It is interesting to note that Corcoran & Doré (2005) reported a surface porosity of 56% for the Sclater & Christie (1980) trend applied to the North Porcupine and Slyne/Erris basins (Figure 4.1) which would validate the linear trend and it may be that this lower initial porosity is more accurate in the case of the SW UK basins. It should be pointed out however, that the linear trend greatly exaggerates the porosity of mid-range ITT values (Figure 4.10). For these reasons it is not favoured as an appropriate trend to estimate former deeper burial in the SW UK.

4.6.1.2.2: Power Relationship

The power relationship was shown to give very poor results when applied to ITT data. This is mainly due to the rather slow increase in porosity over a wide range of values (Figure 4.11) thus resulting in grossly overestimated exhumations. If the power relationship is correct it implies that rocks never reach 0% porosity and maintain a residual porosity of ~2%. The concept of residual porosity has been explored as plausible by Pittman & Larese (1991) so discounting the relationship on this basis alone is not possible. Again the decision must be based on the fit of the data. The density log derived exhumation varies considerably with the values obtained from the power law relationship and it based on this fact that the relationship has been discounted. This differs from the findings of Baldwin & Butler (1985) who found

that power law equations seem to fit data for argillaceous sediments better than do simple exponential equations.

4.6.1.2.3: Exponential Relationship

The exponential relationship has long been favoured (e.g. Athy, 1930) as the best fit to shale data. As with the power law the exponential relationship implies that a residual porosity (~4%) will be present (Pittman & Larese, 1991) but extrapolation to initial surface porosity fits with the Sclater & Christie (1980) trend. Comparing the values obtained from this relationship with the values derived from the density log also shows a close fit (difference of ~0.2km in the case of well 103/18-1) meaning that the exhumation values generated must be considered with much more confidence.

4.6.1.2.4: Hybrid Relationship

It is premature to infer whether the process of compaction is indeed continuous rather than segmented and as such a hybrid relationship was constructed. Clearly the most confidence must be placed in an exponential relationship since generally this offers the best fit to the data and indeed to the Sclater & Christie (1980) trend which represents 'normal' compaction. The hybrid trend comprises 4 segments:

- The basis of excluding and filtering data precludes the possibility of having a residual porosity. For this reason the linear relationship was used to cut off the transform at the point where the data implied porosity was reaching zero.

- As mentioned above the linear relationship quickly deviates from the observed values once higher ITT are reached, so the point at which the linear and exponential relationships cross was used as the first turning point.

- The power law crosses the exponential trend over a wide range of values and as such it was decided to integrate this cross-over area and try and best-fit the trend of well 103/21-1 and Mochras, which clearly seem to lie on a much lower trend than the exponential relationship implies. This transitional area thus formed the third segment of the hybrid relationship.

- Where the trends began to deviate marked the fourth segment of the relationship which again followed the exponential trend. The reasoning behind this final segment was to fit the data into the framework of the 'normal' compaction trend and thus allow the initial porosity to equal that of the Sclater & Christie (1980) trend.

The resulting hybrid relationship fits the data well and also corroborates the independently derived density values of exhumation. For all of these reasons, in the absence of further data, the hybrid relationship is considered to be the most accurate porosity relationship technique to use for estimating exhumation in the SW UK.

However as mentioned before, the limited scope of the data puts a question over the applicability of these trends to the wider area and the large gap in the data for higher ITT's does not allow for a statistically acceptable fit. For this reason the results generated by these trends should be treated with caution and are not recommended in their current state, to estimate former deeper burial in the SW UK. Better answers will come from data that extend from the surface to depths of 7km (23000ft) and where the published curves are supported with the envelope of data as there are sparse data points above ~100µs/ft.

4.6.1.3 The use of a 'normal' compaction trend

The use of the default (normal) compaction curves can introduce significant errors into former deeper burial analysis particularly where little well data are available to calibrate the model. The use of locally calibrated porosity-depth curves will reduce calculation errors but not eliminate them because the present observed porosity-depth curve represents a series of samples with different effective stress histories and hence it does not describe the precise route by which a given sample achieved its present day porosity (Giles *et al.* 1998). High side and low side scenarios should ideally be run to check the scale of uncertainties. Porosity-effective stress relationships are to be preferred over porosity-depth relationships since, such equations are more physically realistic, able to handle porosity hysteresis and therefore, uplift and inherently take overpressures into account (Giles *et al.* 1998).

The assumption that porosity loss is equivalent to compaction is fundamentally flawed. Such a hypothesis requires that solid volume is constant. Dehydration reactions within shales and evaporites and cementation/dissolution reactions in sandstone all violate this assumption (Chapman, 1981; Giles *et al.* 1998). Local calibrations of porosity-depth/effective stress functions are needed. Porosity loss and by extension compaction cannot be considered to be time independent processes. Experimental and natural data all point to a clear time-dependence where porosity falls and compaction increases with time at constant effective stress. Current compaction models do not provide good descriptions of either compaction or porosity loss. Thus new equations to describe compaction are required which are firmly based on the underlying physical processes contributing to compaction.

These issues are significant in the case of the SW UK since no previous study has sought to describe the 'normal' compaction trend and the choice of compaction curve (Sclater & Christie, 1980 shale trend) has been based mainly on lithological similarity between the

Central Graben shales of the North Sea and those present in the SW UK. As shown in Chapter 2 (Figure 2.5) there are many possible normal compaction trends to choose from and part of the rationale behind choosing the Sclater & Christie (1980) trend is that it lies in the middle of these estimates. Since the basins of the SW UK have all been uplifted it is not possible to calibrate a local 'normal' compaction curve and as such the error cannot be quantified but by taking this approach it is hoped that such errors are minimised. The conclusion here is that no single factor is sufficient to determine the porosity-depth values and no generally valid porosity-depth functions exist (Bjørlykke *et al.* 1989). A qualitative multi-parameter approach is required.

4.6.1.4: The use of ITT to estimate former deeper burial

The process of estimating exhumation from sonic velocity logs is subject to error and it is difficult to distinguish the effects of multiple phases of uplift and subsidence. In addition, it is not possible to quantify erosion across an unconformity if post-exhumation subsidence exceeded uplift because in this case the sedimentary section will follow a normal compaction curve. This poses a particular problem in the SW UK area where most of the major sedimentary basins were subject to numerous exhumation episodes (see Chapter 5).

Additional sources of error occur because sonic velocity analysis seeks to identify anomalously over-compacted units with respect to a normal compaction trend (e.g. in this case the Sclater & Christie, 1980 shale trend). Therefore anything that causes a deviation from the 'normal' regional porosity-depth curve will invalidate the results. Consequently fluid overpressure, the presence of a non-compactable horizon, such as a salt layer, cementation, anomalously high porosity, porosity rebound and thermal effects are all potential sources of error.

Ware (1999) suggested that porosity rebound and temperature dependent velocity effects act to minimise the calculated exhumation value, whereas cementation and non-aqueous pore fluids can increase or decrease erosion estimates depending on their composition and mechanical properties (Williams, 2002). Finally because sonic velocity analysis assumes one-dimensional compaction in response to a vertical maximum compressive stress, horizontal compression might result in anomalous p-wave velocities throughout a sedimentary section without necessarily causing significant uplift (Williams, 2002). This is clearly a problem in sedimentary basins which have experienced inversion such as those in the SW UK and particularly basins such as the SGCB which contains thick shale sequences.

4.6.1.4.1: The statistical curve fitting approach

The statistical curve fitting technique provides results in line with those derived from porosity. The fitted curves also show a good relationship between the various different stratigraphic intervals which would seem to support Heasler & Kharitonova's (1996) assertion that their technique can be applied to heterolithic sequences of sandstones, mudstones and siltstones. However, it is also clear from the data that limestones deviate greatly from the compaction of shales (see Appendix A). The fact that limestone intervals are present in the sequences of the Middle and Upper Jurassic may explain why the subsequent curves fitted to those intervals in wells 50/03-2 and 106/24-1 generate exhumation values which deviate significantly from their adjacent wells which have shales to fit the curves to. Therefore the technique should be used with caution when considering heterolithic sequences and ideally the data should be separated to assess whether it is appropriate to include these mixed lithologies when fitting the curve. In addition the suitability of the curve representing the whole section can be questioned when dealing with such a limited (in some cases <500m)

section and where salt is known to be present. It is for these reasons that the statistical curve fitting technique is not recommended for assessing former deeper burial in the SW UK.

4.6.1.4.2: The supercurve and Japsen approach

Japsen *et al.* (2002) have suggested that the functional form of the transit time-depth relationship represented by equation 4.14 may be applied to marine shales dominated by smectite/illitie but is inappropriate for kaolinite rich shales or heterolites of continental origin like the Triassic Bunter Shale. Furthermore Japsen (1998) has shown that realistic compaction trend baselines are best achieved through evaluating physical models for a given lithology and not via an arbitrary choice of mathematical functions and regression parameters. The advantage of a significant well database and good stratigraphic control has allowed Japsen (1998) and Japsen (1999) to adopt a more refined methodology to accommodate burial anomalies associated with lithological variations and overpressuring in the formulation of normal velocity-depth baselines for Cretaceous and Cenozoic sediments in the North Sea Basin and reveals that the trend for chalk is best accommodated by a series of linear segments, rather than a single mathematical function.

The analysis of erosional history based on sonic data can be developed further where two homogenous units are encountered in the same wells because the two units may or may not have been simultaneously at maximum burial at a given location (Japsen, 2000). If the two units were at maximum burial depth simultaneously prior to the most recent erosional event the burial anomalies for the two units should be identical. If however the lower unit was at maximum burial before the upper unit due to an intervening erosional event the burial anomaly for the lower unit should exceed that of the upper unit (Figure 4.50). The burial anomaly dZ_B is the difference between the present-day burial depth of a rock, z and the depth

z_N (V) corresponding to normal compaction for the measured velocity V of the formation in question (Japsen, 1998 and Figure 4.77):

$$dZ_B = z - z_N(V) \tag{4.15}$$

The burial anomaly is zero for normally compacted sediments whereas high velocities relative to depth give negative burial anomalies which may be caused by a reduction in overburden thickness where the lithology is relatively homogenous over the study area and if lateral variations in heat flow and horizontal stress are minor ('apparent uplift', Bulat & Stoker, 1987; 'net uplift and erosion', Riis & Jensen, 1992; 'apparent exhumation', Hillis, 1995). A true burial anomaly may indicate undercompaction due to overpressure. Whether a burial anomaly is a measure of erosion or is caused by other factors (e.g. lithological changes) needs to be studied by an integrated evaluation of the area in question. Apart form matching other estimates of erosion the burial anomalies should principally correspond geographically to where there is missing section in the stratigraphic record. It must however be observed that any post-exhumational burial B_E (m) will mask the magnitude of the missing overburden section Δz_{miss} (m) and we get:

$$\Delta z_{miss} = -dZ_B + B_E \tag{4.16}$$

where the minus indicates that erosion reduces depth (Hillis, 1995; Japsen, 1998). Knowledge of the timing of the erosional events thus becomes a critical aspect not only for understanding the succession of events but also for understanding their true magnitude and for identifying the age of the eroded succession.

The increase of velocity with depth is often approximated by linear relationships between different transformations of velocity and depth but the most common expressions predict velocity to approach infinity with depth. The increase of velocity with depth should however

approach zero. This constraint becomes important when considering depth intervals over several kilometres (Japsen, 2000). Disregarding a proper mathematical formulation thus may lead to a severe underestimate of the amount of erosion because unconstrained trends predict too high velocities at depth. However, it must also be considered that the estimate of removed overburden becomes very sensitive to minor variations in velocity at great depth where a constrained baseline becomes ever steeper (Japsen, 2000).

This segmented approach seems to provide the closest relationship between the porosity relationships of Raymer *et al.* (1980) and Wyllie *et al.* (1956) with broadly similar exhumation values being reported from all these techniques. More importantly it suggests a number of stages in the compaction of a sediment rather than a continuous rearrangement of grains reducing porosity in a simple way. For these reasons the Japsen Bunter Shale trend and the subsequent method for calculating burial anomaly is judged to be the most reliable when estimating former deeper burial in the SW UK.

It is clear that many more studies need to be carried out before the relationship between stress and porosity is understood well enough to offer a truly representative compaction relationship for any type of sediment. These studies will have to be local in their approach as has been demonstrated in this study by application of the Ware and Turner (2002) supercurve – derived for the East Irish Sea Basin – to the SW UK. This study has shown that comparison of the trend with the shales found in the SW UK results in a large underestimation of exhumation (Table 4.14). The trend also suggests overpressure where none exists (according to well operators logs) based on the calibration of the curve to the properties of the East Irish Sea Basin shales. These concerns have also been raised by Corcoran & Doré (2005) when comparing the Ware & Turner (2002) supercurve with the 'Brockelschiefer' curve derived for North Sea shales.

4.6.1.5: Choice of compactional technique relevant to estimating former deeper burial in the SW UK.

As has been shown in this chapter a range of techniques, each with their own merits, is available to estimate former deeper burial from compactional data. The discussion above has highlighted a number of pitfalls associated with these techniques and critically assessed their application to the SW UK. Two approaches stand out as being most reliable in estimating former deeper burial in the SW UK; the technique using the RHG equation (with a matrix velocity of 60us/ft) and the Japsen Bunter Shale relationship. In order to allow a critical assessment of the burial history of the SW UK only one of these techniques can be chosen which fairly represents the whole area. Whilst the RHG derived former deeper burial magnitudes show the best fit with the palaeothermal data the uncertainty in assignment of the matrix velocity remains a possible shortfall of the technique.

As mentioned above, the Japsen Bunter Shale trend has been rigorously derived using rock physics and is subject to less error than the RHG mathematical transform. Thus the synthesis provided below is based on the Japsen Bunter Shale trend representing the magnitude of former deeper burial of the SW UK.Menpes & Hillis (1995) highlighted the importance of comparing the results of similar studies both to address whether there is a systematic error in the placement of the normal compaction relationship (i.e. whether reference wells are indeed at maximum burial depth) in their study and also to test the validity of the various methods. Overall each of the studies has provided a total exhumation episode which is in line with all of other approaches. These exhumations lie in the range of 1-3km of exhumation since the Jurassic. Another important observation that has arisen from this study is that the distribution of exhumation is similar regardless of the approach taken. This suggests that the strength of using the sonic log alone is in determining relative exhumation magnitudes. It is clear that in order to get a quantitative value of exhumation that the analysis of sonic data must be

combined with other techniques (such as seismic, AFTA, VR) in order that the most appropriate technique for the estimation of exhumation in an area can be found. The advantage of combining these different studies lies in being able to determine the timing of the exhumation episodes as well as the absolute magnitude both of which are critical factors in hydrocarbon exploration.

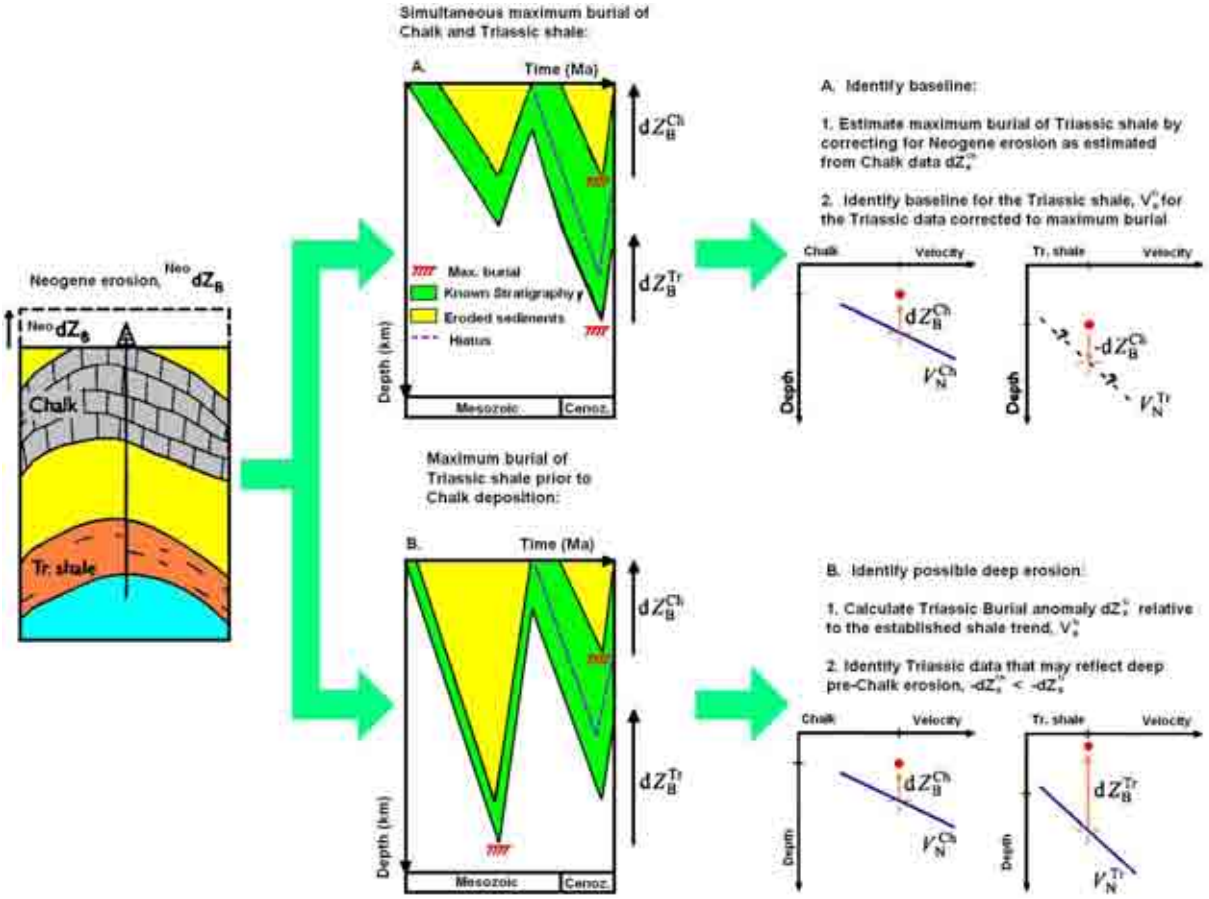

Figure 4.50 – Schematic burial diagrams for the Mesozoic succession illustrating the relationship between burial anomalies ('uplift') for the Chalk and the Triassic in the same well, dZ_B^{Ch} and dZ_B^{Tr}. Either the two units in the same well have been at maximum burial depth simultaneously or the lower unit has been at maximum burial prior to the upper unit due to an intervening erosional event. (A) The baseline for a Triassic formation V_N^{Tr}, can be traced more easily if we correct the depth to the formation for the effect of Neogene erosion as estimated from the Chalk burial anomaly dZ_B^{Ch}. (B) We can now calculate the burial anomaly for the Triassic formation dZ_B^{Tr} for all data points relative to V_N^{Tr} and identify the wells where the magnitude of the Triassic anomaly exceeds that of the Chalk. These cases may reflect deep pre-Chalk erosion. Legend: ●, present-day velocity-depth data point; +, velocity-depth data point at time of maximum burial (after Japsen, 2000).

4.6.2: THE MAGNITUDE AND DISTRIBUTION OF BURIAL ANOMALIES IN THE SW UK

The compactional data presented in this study indicates that the SW UK has experienced kilometre-scale exhumation since the Lower Jurassic. The data shows that the SW UK was more deeply buried by 1.19-3.44km (Table 4.18). The largest value of former deeper burial can be found in the Burton Row borehole which is in the southern margin fault of the BCB. The distribution of former deeper burial is broadly similar in each of the basins. In the BCB, as previously mentioned, the largest burial anomaly is to in the southern margin fault system footwalll with the basin centre experiencing a much smaller (*c.* 2km) burial anomaly. In the SCSB the magnitude of burial anomaly is broadly similar (2.0km ±0.25km) with the largest burial anomalies (*c.* 2.5km) in the basin centre. It is likely that the footwall of the SCSB margin faults would yield a similar burial anomaly to that of the BCB (Burton Row) but since no wells penetrate this succession it is not possible to place any constraints on it. The NCSB has only one value posted (1.52km) so it is not possible to discuss the distribution based on this single data point but it is expected to follow a similar trend as the en-échelon SGCB. In the SGCB again the largest burial anomaly is found in the basin bounding fault footwall (2.74km in well 106/18-1 on the northern margin and 2.20km in well 106/28-1 on the southern margin) compared to smaller anomalies (1.19-1.91km) in the basin centre.

If the method used to quantify denudation is internally consistent, the relative magnitude of exhumation can be used to investigate regional patterns of uplift. The dataset shows that the magnitude of apparent exhumation reflects a significant component of structural control. Exhumation highs occur in the vicinity of reactivated faults, folds and in the footwall blocks of extensional faults. This is particularly true of the SCSB and BCB where exhumation highs coincide with structures that formed during basin inversion.

Looking more closely at the distribution of exhumation across the area it is clear that faults have played an important part in controlling basin evolution. Seismic reflection data shows that tectonic inversion was the chief driving mechanism behind exhumation in the area (Williams 2002; Williams *et al.* 2005) and it should be noted that compressional shortening in sedimentary basins is characteristically non-uniform (Turner & Williams 2004) e.g. due to selective fault reactivation (Sibson, 1995). The compactional data provides clear evidence that marked differences in exhumation occur across major faults. This is particularly clear across the main basin bounding faults. Generally wells located in the footwall of the fault experienced larger burial anomalies than those located in the hangingwall. There are three possible explanations for increased exhumation in the footwall blocks of major basin bounding faults, these are:

1. That condensed footwall successions have influenced calculated values of exhumation.

2. That a component of footwall uplift augmented regional exhumation in the vicinity of major fault zones.

3. That uplift was concentrated along the basin margins.

Thin sedimentary units introduce a significant error into sonic-based denudation estimates because small-scale features such as hard grounds or salt stringers have a disproportionate effect on the average ITT. Under such circumstances small zones of low porosity will often lead to anomalously high estimates of burial anomaly. This does not however account for the discrepancy in exhumation observed across major fault zones in the SGCB because the Triassic Mercia Mudstone formation maintains a relatively constant thickness throughout the basin. It is far more likely that the spatial distribution of exhumation was established during

the early Cretaceous in this basin, when regional uplift coincided with a phase of N-S directed extension and led to severe erosion along the basin margins (Tappin *et al.* 1994). Locally, denudation was enhanced by footwall uplift along the St. George's Fault and the Northwest Flank Fault (Holford *et al.* 2005*a*). In contrast to the SCSB, early Cretaceous uplift did not constitute true basin inversion (Williams, 2002). Throughout the SGCB over 3km of Jurassic sediment are preserved in the main depocentre with only a thin cover of Liassic shale over the rest of the basin.

In a regional framework deeper burial from compactional data of up to 3km is consistent with results from the Kish Bank Basin (Ware, 1999), EISB (Ware & Turner, 2002; Holford *et al.* 2005*b*), Wales (Holford *et al.* 2005*a*; Holford, 2006), onshore Ireland (Green *et al.* 2001) and the Wessex Basin (Law, 1998; Figure 4.51).

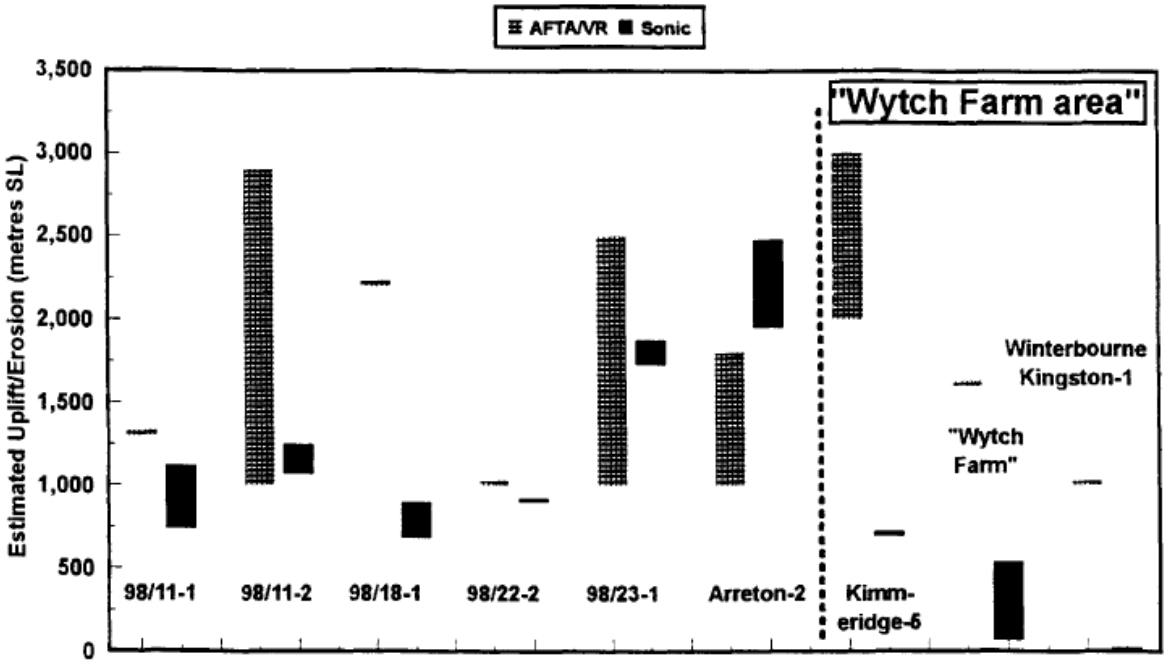

Figure 4.51 – Comparison of AFTA/VR and sonic velocity derived uplift-erosion estimates for wells in the Wessex Basin. Results are shown in pairs with error ranges for each selected well (after Law, 1998).

4.6.3: IMPLICATIONS FOR THE RELATIVE ROLE OF INVERSION VERSUS UNDERPLATING AS THE CAUSE OF EXHUMATION IN THE SW UK

Whilst none of the techniques necessarily reflect the accurate values of exhumation experienced at each particular location, the overall distribution of exhumation highlights some important observations. The first observation is that regardless of the technique used all of the techniques show evidence of short wavelength variation in exhumation across the area where wells separated by ~10km can show up to 1km of difference in burial anomaly. For example well 103/01-1 (1188m) and well 103/02-1 (1756m) show a variation of *c.* 550m whilst on a slightly larger (up to 50km) scale adjacent Quads can show variations of up to 1km (e.g. 102 vs. 93; 103 vs. 106). This observation is contrary to what would be expected if exhumation was driven solely by underplating and/or hot spot activity. Such activity would be expected to provide broad areas of similar exhumation as the crust flexes due to the thermal anomaly. As discussed above it is impossible to isolate individual events in a study of this kind and as such competing tectonic events cannot be resolved. All that can be stated is that exhumation in the SW UK was not due solely to igneous underplating or hot spot activity but is likely to be a combination of competing events.

The data also reveal evidence for inversion in the area which has been confirmed by seismic data (Williams, 2002) but yet again it cannot be confidently stated that this was the sole driving force of exhumation. This evidence is in the form of fault compartmentalisation where individual faults have been reactivated preferentially and others have remained in extension. This is manifested as a marked difference in burial anomaly across the fault. For example well 103/01-1 in the hangingwall of a fault experienced a much lower burial anomaly (1.19km) compared to well 103/02-1 in the footwall of the same fault (1.76km) and well 106/18-1 in the footwall of a fault experienced much deeper burial (2.74km) compared to well 106/20-1 (1.89km).

As a standalone technique, the compactional data presented in this thesis provides damning evidence against the proponents of the underplating theory since these small scale (10-20km) variations in burial anomaly cannot be explained by the models suggested for the emplacement of underplated material and show burial anomalies clearly at odds with currently published maps of burial anomaly across the SW UK (e.g. Al-Kindi *et al.* 2003; Figure 4.52). Even if these small scale variations are ignored the individual estimates of former deeper burial are at odds with what the magnitude of former deeper burial should be at a particular location due to underplating. For example according to Al-Kindi *et al.* (2003) the Burton Row borehole should at most be experiencing a burial anomaly of 0.75km. Results from this study show that the Burton Row borehole has experienced up to 3.5km of former deeper burial. Similarly the BCB should have experienced a burial anomaly of *c.* 3km centred on Lundy Island (Figure 4.52) whereas data from this study suggests the burial anomaly is closer to 2km. Each of these observations casts serious doubt on the validity of the underplating model to account for the exhumation in the SW UK. Whilst it is likely that it will have had some effect the relative importance and magnitude of this event has been overstated in previous studies and it is much more likely that horizontal compression (inversion) was the main driving force behind the distribution of burial anomalies across the SW UK, especially since it can reconcile the small-scale observations as well as the long scale ones.

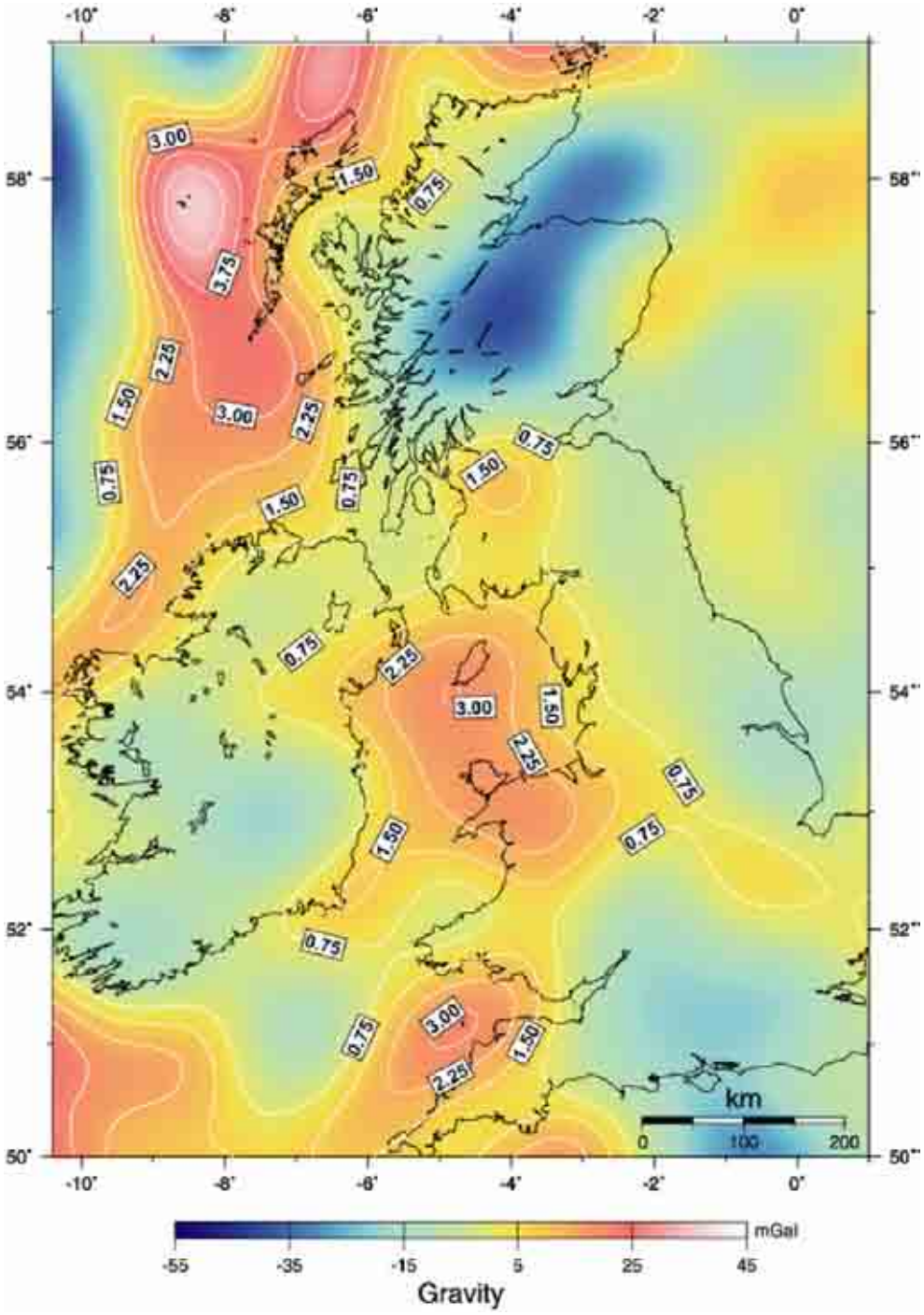

Figure 4.52 - Underplating map of Al-Kindi *et al.* (2003) converted to an exhumation map, assuming Airy isostasy and assuming uniform densities of 2.4, 2.9 and 3.2Mg/m³ for crustal sediments, gabbroic underplate and asthenospheric material respectively.

4.7: CONCLUSIONS

- Sonic log data from fifteen exploration wells in the offshore SW UK indicate that the area has experienced kilometres-scale exhumation since the Late Jurassic.

- The preferred method for calculating exhumation from compactional data in this study is to use the Japsen Bunter Shale trend. This relationship suggests that the SW UK region has experienced deeper burial of 1.19- 3.40km and is independently corroborated by palaeothermal data (Chapter 5).

- The distribution of this exhumation suggests that exhumation caused solely by igneous underplating or hot spot activity is incorrect due to multiple examples of small wavelength (<50km) variations in exhumation.

- Distribution of exhumation supports evidence seen on seismic data for inversion being a dominant driving force for this exhumation. The evidence also suggests that fault compartmentalisation and footwall uplift have been important in controlling the distribution of exhumation with the largest values of exhumation located in the footwalls of basin margin faults.

- The Raymer *et al.* (1980) equation which is an improved version of the Wyllie *et al.* (1956) time-average equation has been shown to provide more accurate determinations of porosity and hence exhumation. Comparison of corrected and uncorrected variants of the Wyllie equation highlights the need to apply the appropriate correction factor in order to more accurately estimate porosity from the sonic log.

- The assumption that a 'typical' shale has a matrix transit time (slowness) of 68µs/ft (Magara, 1978) has been shown to be an adequate assumption where limited data exists. Whilst it has been shown that some rocks in the SW UK exhibit porosity down to 60µs/ft the higher value provides the better fit to the data. More rigorous analysis of geophysical logs is needed in order to further constrain this quantity and arrive at a representative value for the rocks of the SW UK.

- The longstanding theory that shale compaction follows an exponential relationship has been shown to be valid for the SW UK.

- The comparison of the different approaches to exhumation highlights the difficulty in using a single approach to estimate total exhumation in sedimentary basins. The advantages of a multi-parameter approach allow for much tighter constraints to be placed on absolute values where limited data exists. It also highlights the need to combine compaction studies with other independent techniques such as AFTA, VR and seismic in order to obtain a meaningful absolute value.

- The application of supercurves derived for particular basins should not be applied to other basins in similar studies. Application of these curves will result in erroneous values of exhumation.

- The application of the statistical curve fitting technique to heterolithic sequences should be applied with caution especially where limestone beds are present.

CHAPTER 5: THE THERMAL AND EXHUMATION HISTORY OF THE SW UK

5.1: INTRODUCTION

The aim of this chapter is to provide a thermal history framework for the uplift and exhumation of the SW UK and thus provide an independent assessment of the timing of exhumation episodes revealed by the seismic data (*cf.* Chapter 4).

The coincidence between the temperature range in which fission tracks in apatite are annealed over time and that in which liquid hydrocarbons are generated (Gleadow *et al.* 1983) has led to the emergence of AFTA as a tool of unique ability in the study of thermal histories in sedimentary basins. Because of this temperature dependence, AFTA can provide detailed information on the low-temperature thermal histories of rocks, between *c.* 60-120°C for apatite and *c.* 350°C for zircon (Gallagher *et al.* 1998).

In contrast to other techniques used for the estimation of palaeotemperatures and/or former burial depths however, fission-track analysis, specifically of apatite, has the advantage of providing an independent estimate of the time at which a sample began to cool from its maximum palaeotemperature, and can therefore provide information on the timing of exhumation episodes (Green *et al.* 2002). AFTA allows a constraint to be placed on the timing of exhumation episodes and where a vertical profile exists (e.g. from a well or borehole (*cf.* Bray *et al.* 1992)), the magnitude.

Total annealing of apatite corresponds to VR values of *c.* 0.7-0.9% (depending on apatite composition) thus by combining AFTA with VR data a direct estimate of maximum

palaeotemperatures in the range where fission-tracks in apatite are totally annealed is possible. In the absence of VR data AFTA only provide minimum estimates of palaeotemperature (Duddy *et al.* 1994).

5.2: METHODOLOGY

For the purpose of this study, 77 samples were collected from the Southwest UK for AFTA. Samples were taken from a variety of stratigraphic levels including the Precambrian of southwest Wales, the Devonian and Silurian, the Carboniferous of the South Wales Coalfield, the Mesozoic and the Cenozoic. This number includes three samples previously reported by Holford (2006).

Analytical procedures were similar to those outlined in detail in Green (1986). Neutron irradiations were performed in a well thermalised flux (X-7 facility) in the HIFAR research reactor at Lucas Heights New South Wales, Australia. The apatite mounts were analysed by the external detector method and apatite ages were calculated using the zeta calibration method described by Hurford & Green (1982, 1983) and Green (1985). Age errors were calculated using either the conventional method of Green (1981) for samples with $P(\chi^2)$ greater than 5% or the central age approach of Gailbraith & Laslett (1993) for samples with $P(\chi^2)$ values less than 5%. Confined track lengths were measured only on prismatic surfaces using the technique described in Gleadow *et al.* (1986). All laboratory analysis (track counting, etching etc.) was carried out by the team at Geotrack in Australia and the forward modelling process followed the approach shown in Figure 5.1. Examples of the data sent back to Birmingham are shown in Tables B1-B5 in Appendix B.

This raw data was used to construct histograms for inclusion in this thesis; however the modelling behind these numbers (which provides the framework for the construction of the

thermal history plots) was done by Geotrack using their proprietary software. This modelling was used as the basis for the thermal histories created for use in this thesis. The creation and use of histograms was done in order to give an overall framework for creation of the thermal history plots. The process and theory behind AFTA histograms is shown in Figures 5.2 and 5.3. Once the histograms were created it was possible to generate the thermal history plots. The kinetics of both AFTA and VR are such that measured parameters are dominated by the maximum temperature to which a sample is subjected and as a result, no information is preserved on the history prior to the time at which cooling from maximum palaeotemperature begins.

For this reason all thermal history plots prior to the cooling episode are simplistic approximations and all that can be really accepted is the time and temperature of initial deposition of the sediment containing the sample (the stratigraphic age). Figures 5.4 – 5.9 highlight the basic framework used in calculating the thermal history plot.

Data points come from the raw data supplied by Geotrack (Appendix B) which allow confidence boxes to be drawn around the value supplied. The only certainty in the plot for samples is the current temperature (since this will be the temperature the sample resided at before being analysed) all other parameters should be considered simplifications since the technique cannot resolve an infinite amount of discrete events (the general limit being two episodes, three episodes may be separated in good samples). Analysis of samples (*cf.* Chapter 2) and determination of palaeotemperatures over a range of depths within a vertical well section allows determination of the palaeogeothermal gradient at the onset of cooling.

Extrapolation of the palaeogeothermal gradient to an assumed palaeosurface temperature allows estimation of the amount of missing section. This provides a measure of the magnitude of exhumation. Combining results from AFTA and VR has two advantages. First,

because each technique is calibrated independently each of the two methods provides independent verification of the results from the other. Second, the joint approach also affords the opportunity to obtain data from various lithologies (VR mostly from fine-grained rocks, AFTA from crystalline rocks and sandstones) through the well to provide palaeotemperature assessment over as wide a depth interval and palaeotemperatures range as possible (allowing more precise constraints on palaeogeothermal gradients and amounts of removed section).

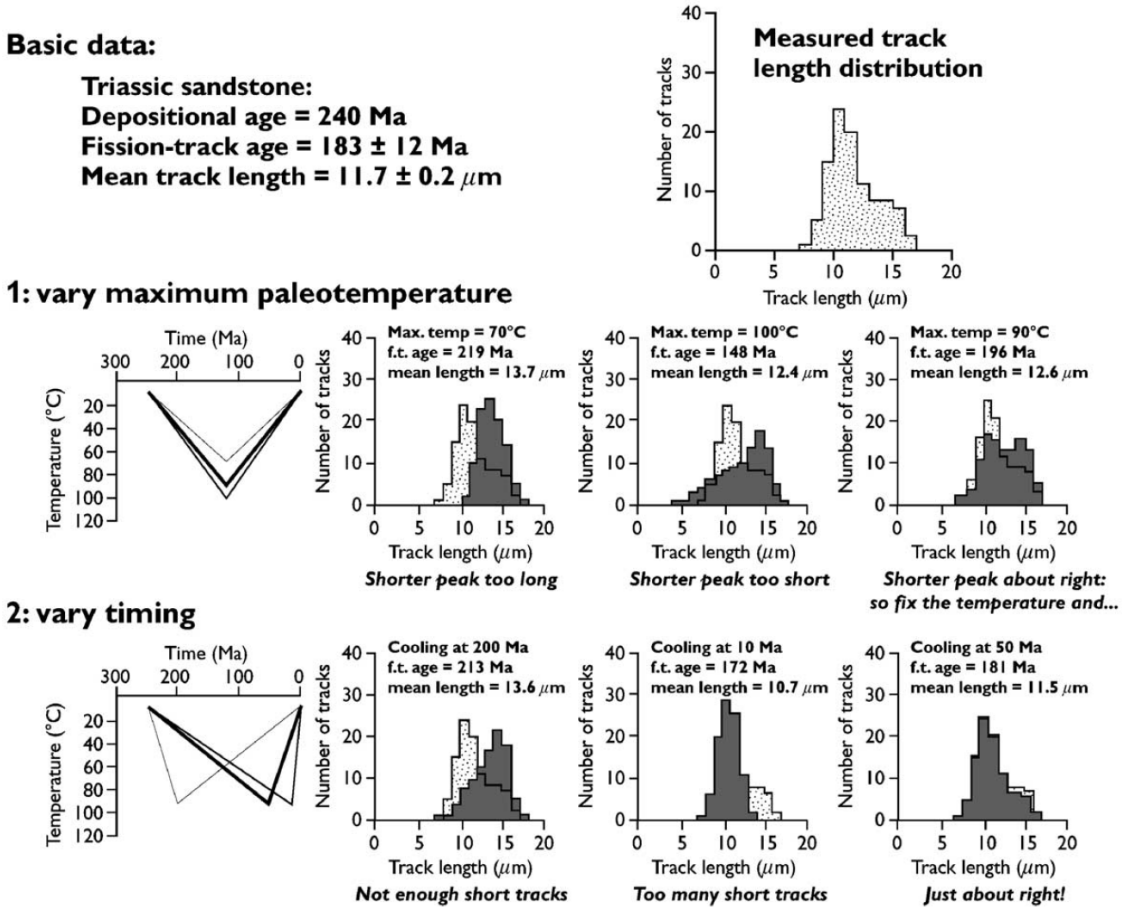

Figure 5.1 – Forward modelling methodology of Green et al. (1989) for measured apatite fission track age and track length distributions, in the case of a synthetic sample with no variation in Cl content. Formal statistical procedures are used to discriminate between a range of thermal history scenarios by firstly optimising magnitude of peak palaeotemperature and then optimising the timing of peak palaeotemperature. In this synthetic model, cooling from a peak palaeotemperature of 90°C from 50 Ma, gives the best fit to the observed track length distributions (after Green *et al.* 2002). All modelling in this thesis was carried out by Geotrack in Australia with the final outputs (Maximum temperature, Cooling episodes) sent back to Birmingham for compilation and context.

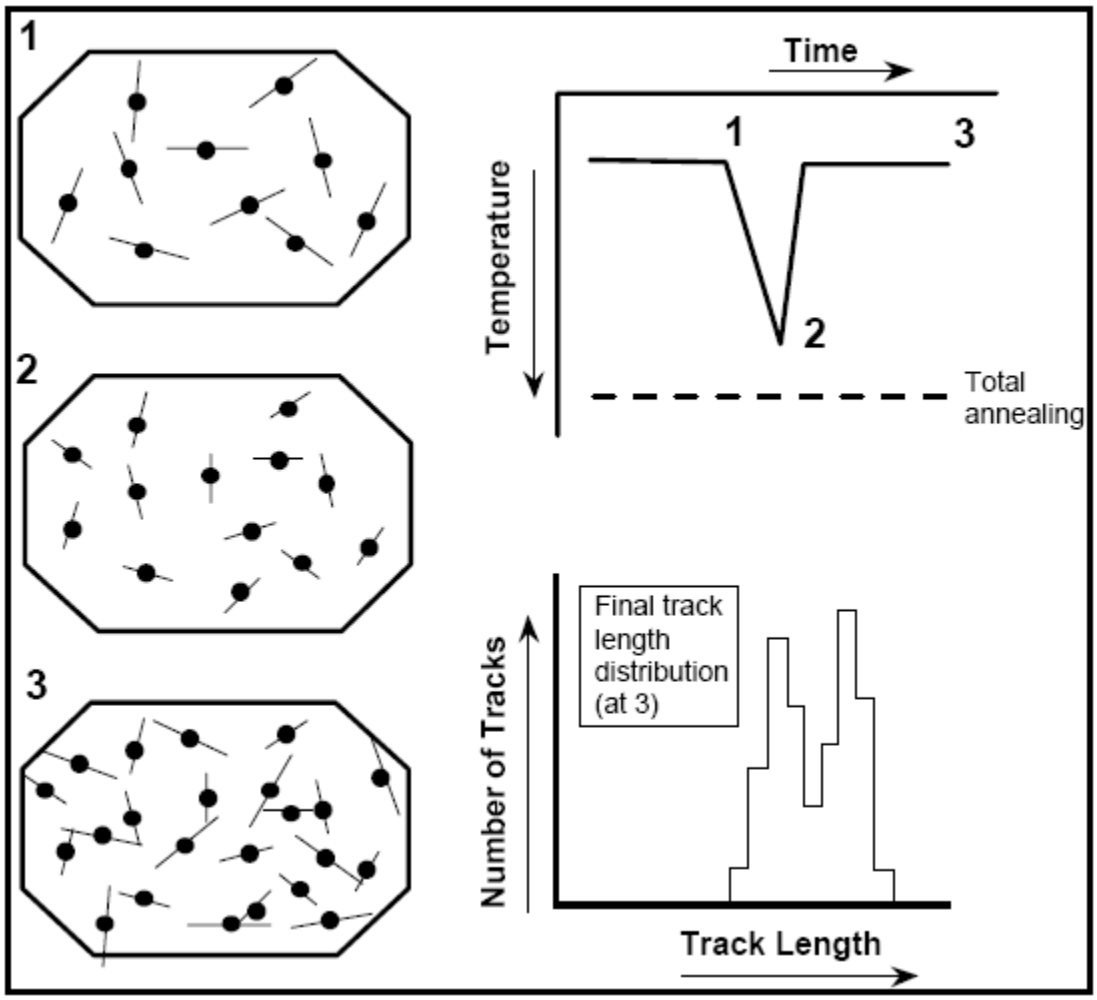

Figure 5.2 – Process for creation and interpretation of AFTA histograms. Tracks formed up to time 1 at low temperature are long. At time 2 after temperature increase all tracks shortened to more or less the same length. At time 3 tracks formed prior to cooling from maximum temperature are 'frozen' at short lengths while tracks formed after cooling at low temperature are long. Final length distribution at present day consists of two components (a bimodal distribution); short tracks formed prior to the onset of cooling and long tracks formed after cooling.

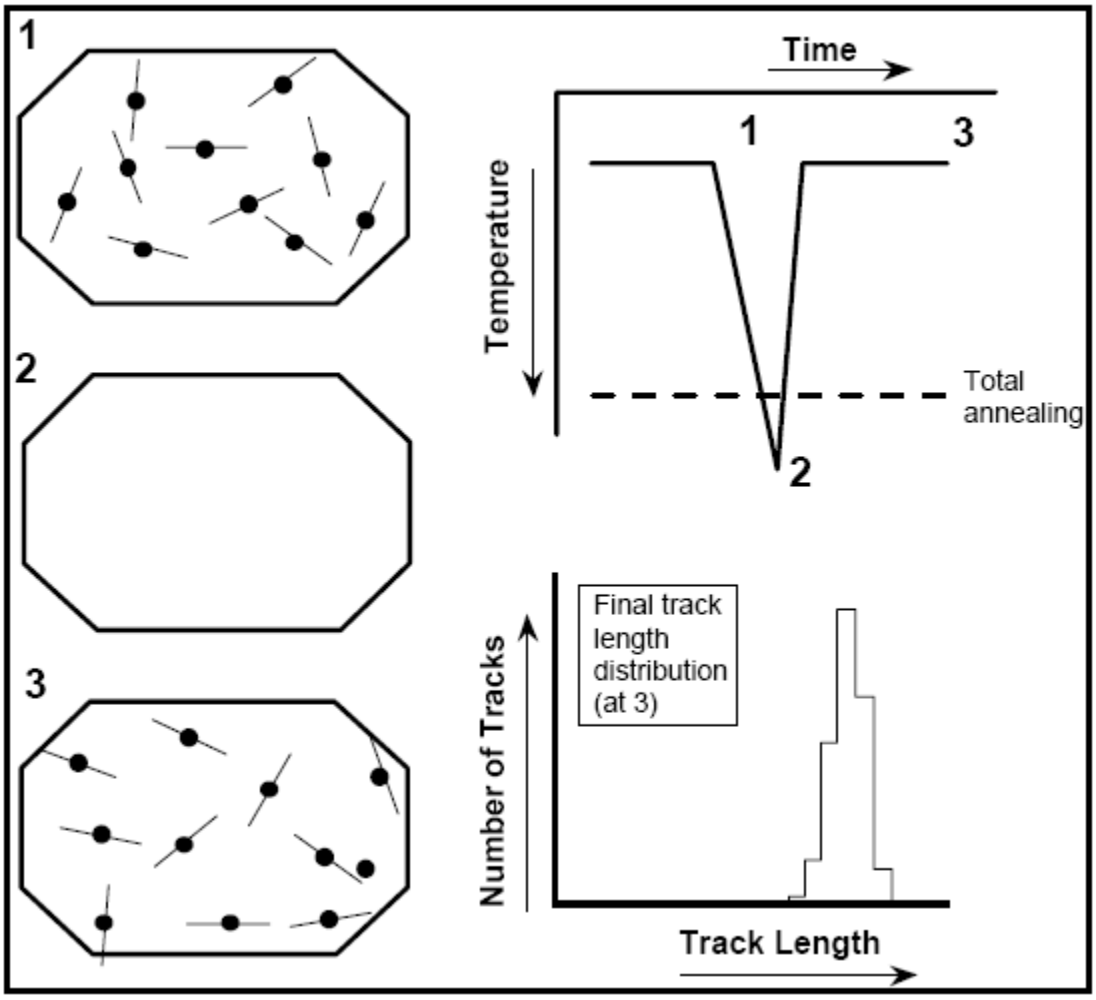

Figure 5.3 – Process for creation and interpretation of AFTA histograms. Tracks formed up to time 1 at low temperature are long. At time 2 after temperature increase all tracks are reduced to zero length due to annealing temperature (120°C) being reached and all damage being repaired. At time 3 the only tracks present are those formed after cooling at low temperature and these are long. Final length distribution at present day consists of a single component (a unimodal distribution).

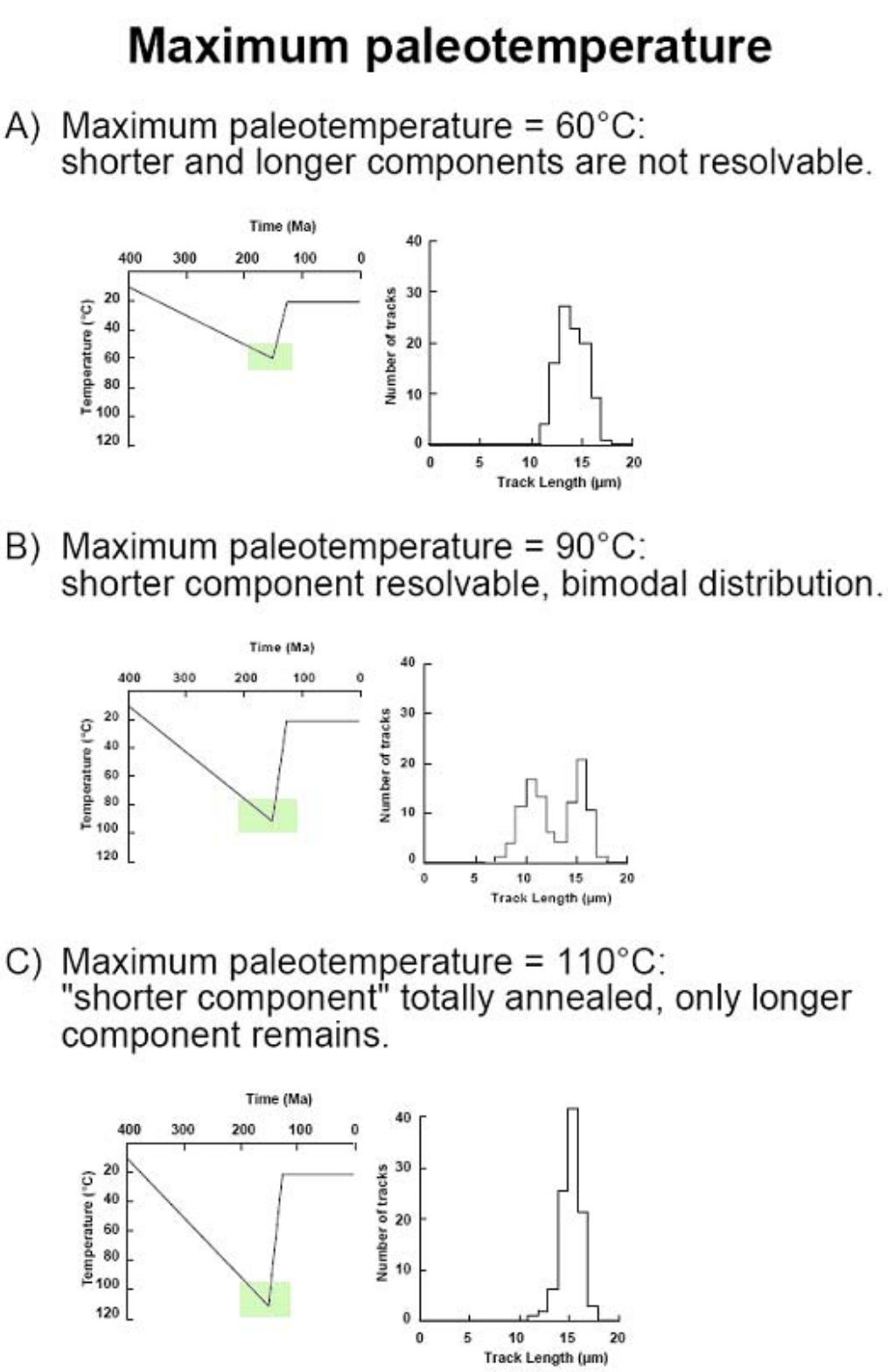

Figure 5.4 – Basic framework for calculating a thermal history plot of maximum palaeotemperatures. Timing and temperature figures were supplied by Geotrack (Appendix B) and the plots calculated from those figures. In terms of maximum palaeotemperature confidence boxes were drawn around the figure given based on the error in the technique (typically ± 10°C, the confidence in age is provided by the analysis). For simplification purposes the plots used in this thesis assumed that the given value was the track point for the thermal history curve, however in practice the curve could lie anywhere within the confidence box. (Figure taken from Geotrack Manual (1996)).

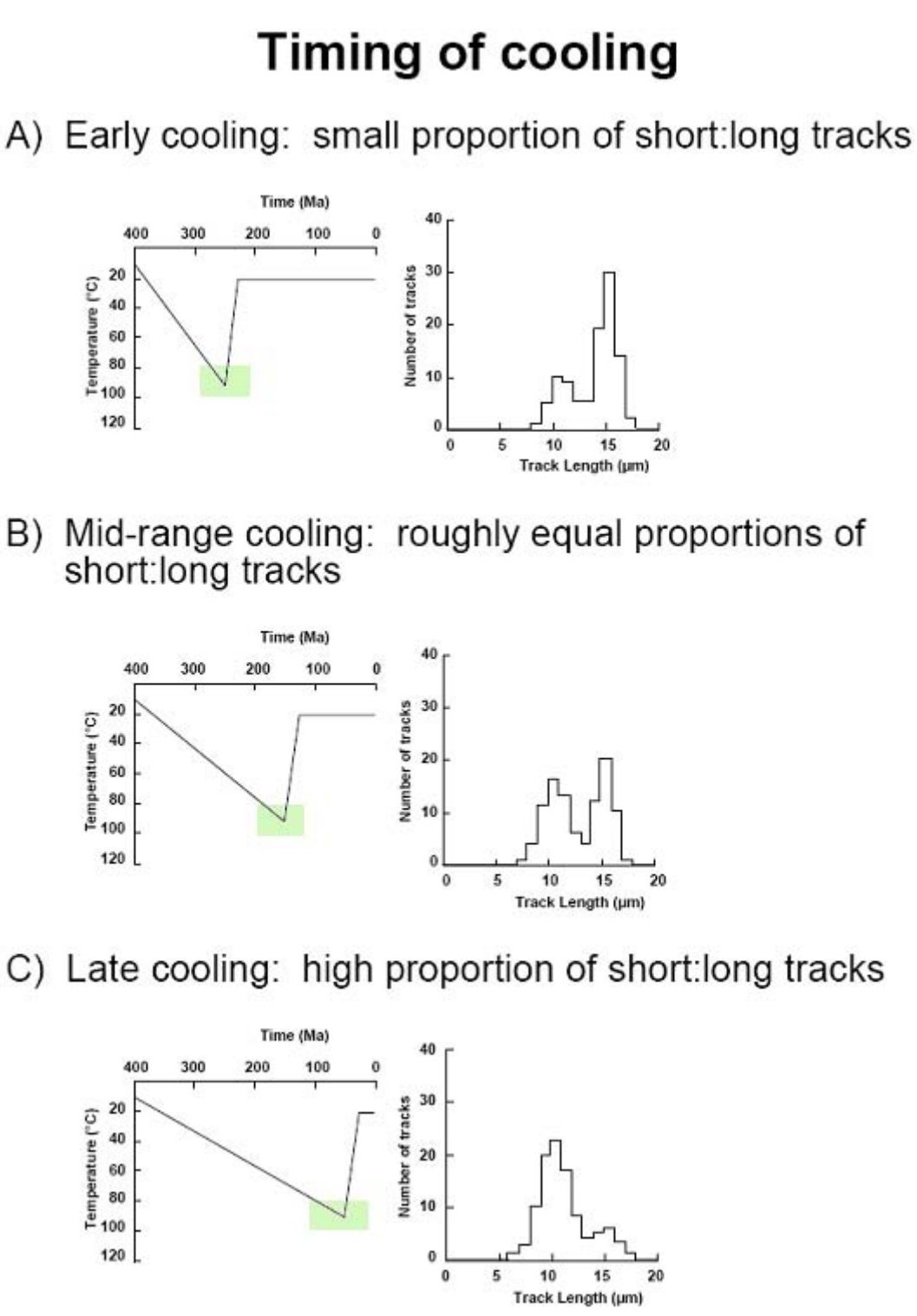

Figure 5.5 – Basic framework for calculating thermal history timing. Timing and temperature figures were supplied by Geotrack (Appendix B) and the plots calculated from those figures. In terms of timing, confidence boxes were drawn around the figure given based on the error in the technique (quoted with the values in the tables Appendix B). For simplification purposes the plots used in this thesis assumed that the given value was the track point for the thermal history curve, however in practice the curve could lie anywhere within the confidence box. (Figure taken from Geotrack Manual (1996)).

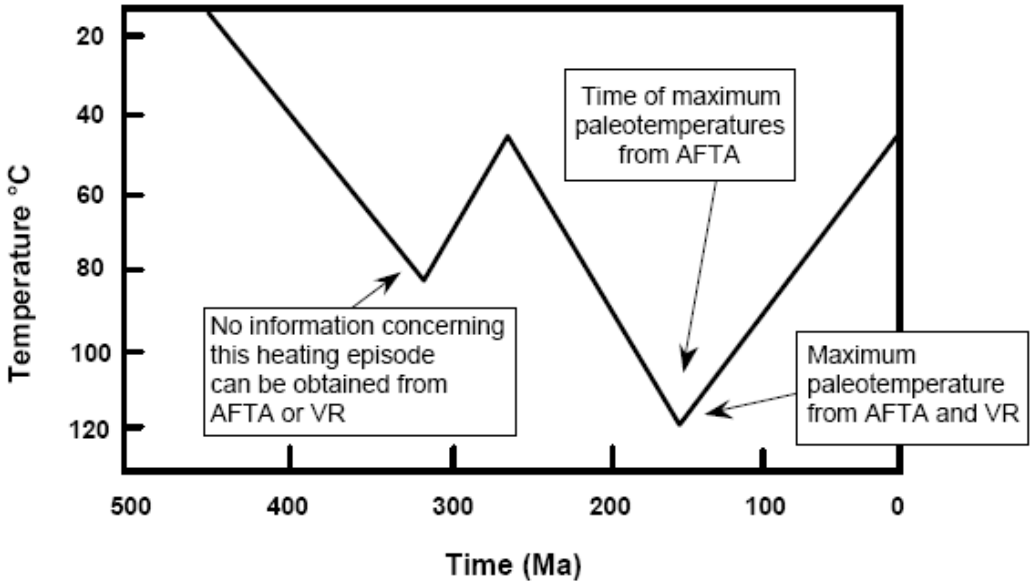

Figure 5.6 – AFTA and VR data preserve no information on heating and cooling episodes prior to cooling from the maximum palaeotemperature, duration of heating (except where present temperatures are maximum since deposition), any aspect of the thermal history prior to cooling from maximum temperature. In particular, in a sample currently at its maximum temperature since deposition, AFTA and VR data preserve no information on possible earlier heating episodes. These considerations establish the framework within which Thermal histories can be plotted. Note the starting point of the curve is taken to be the palaeosurface temperature at the time of deposition of the formation.

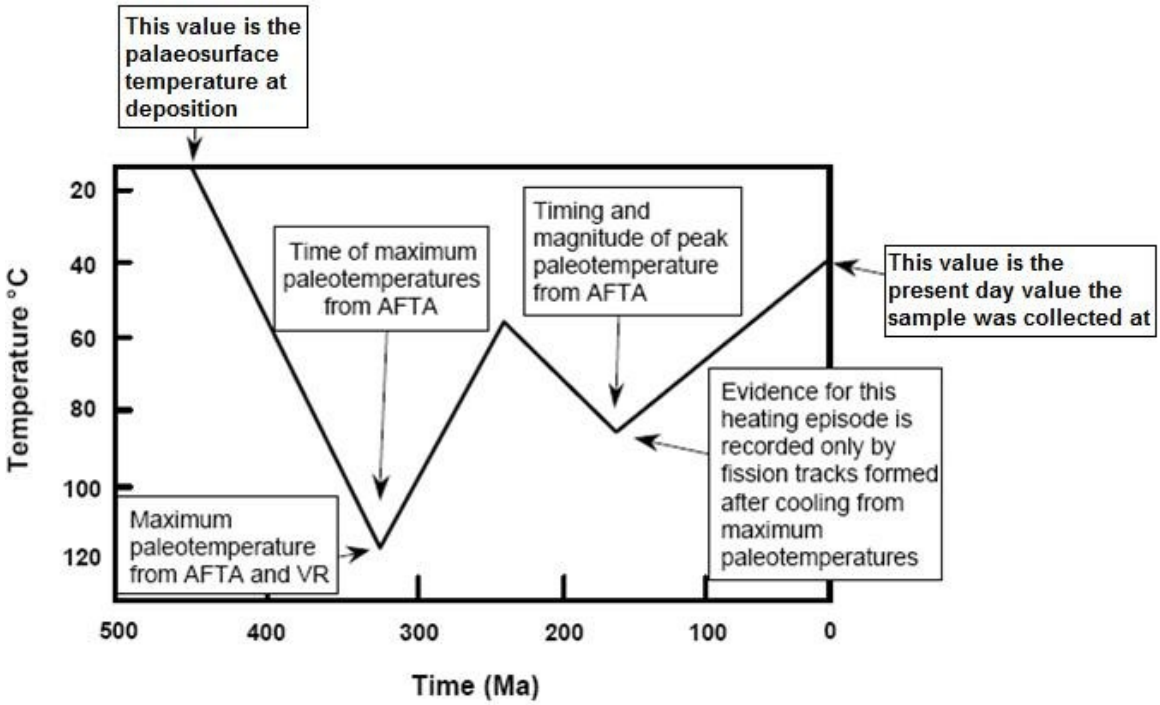

Figure 5.7 – AFTA can reveal multiple episodes particularly when combined with VR. Note that multiple scenarios are possible for any given values (Figure 5.6). In practice palaeotemperatures are accurate to ±10°C which compares favourably with the accuracy of present-day temperatures, which under normal exploration circumstances could be expected to be ±5°C. A prime consequence of being able to constrain palaeotemperatures to ±10°C is that even under ideal circumstances, estimates of eroded section made from a thermal history reconstruction can only be precise to ±100's of metres. For example: For a typical palaeogeothermal gradient of ~30°C/km, 10°C is equivalent to 300 metres of inherent uncertainty in the estimate of section removed. For a gradient of 10°C/km 10°C is equivalent to 1000 m.

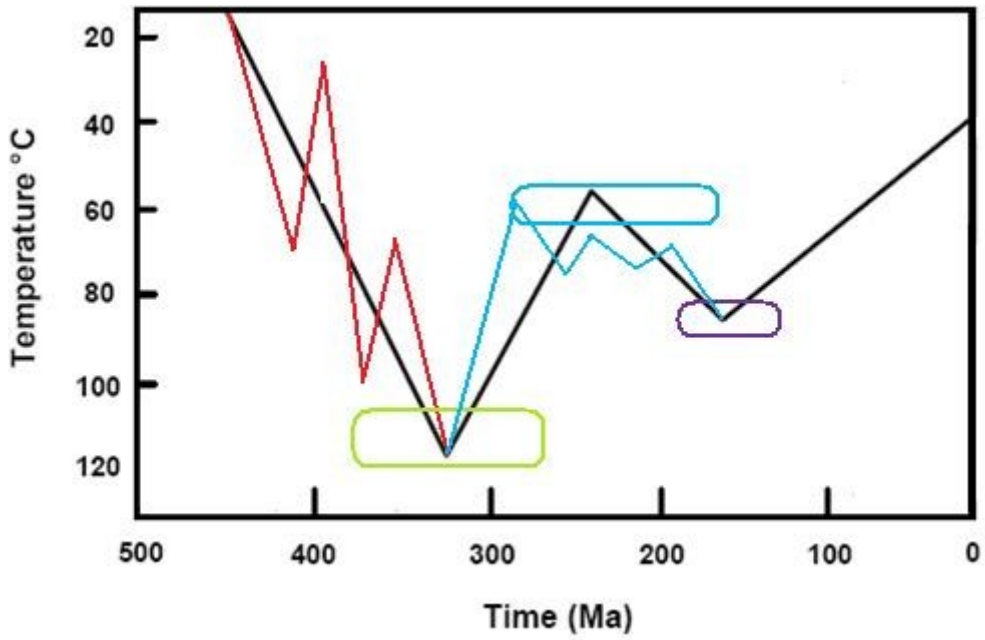

Figure 5.8 – Multiple scenarios are possible for any given sample once the basic framework is established (black line). This is often taken as the thermal history since the technique cannot resolve episodes prior to maximum palaeotemperature (red line), small scale movements where the maximum and minimum do not exceed the framework (blue line), resolution is limited in terms of timing and temperature (coloured boxes) meaning the default plot could fall anywhere within the boxed area. For simplicity this thesis uses a basic framework when creating the thermal history plots. A real example is shown in Figure 5.9 with the rest to be found in Appendix B.

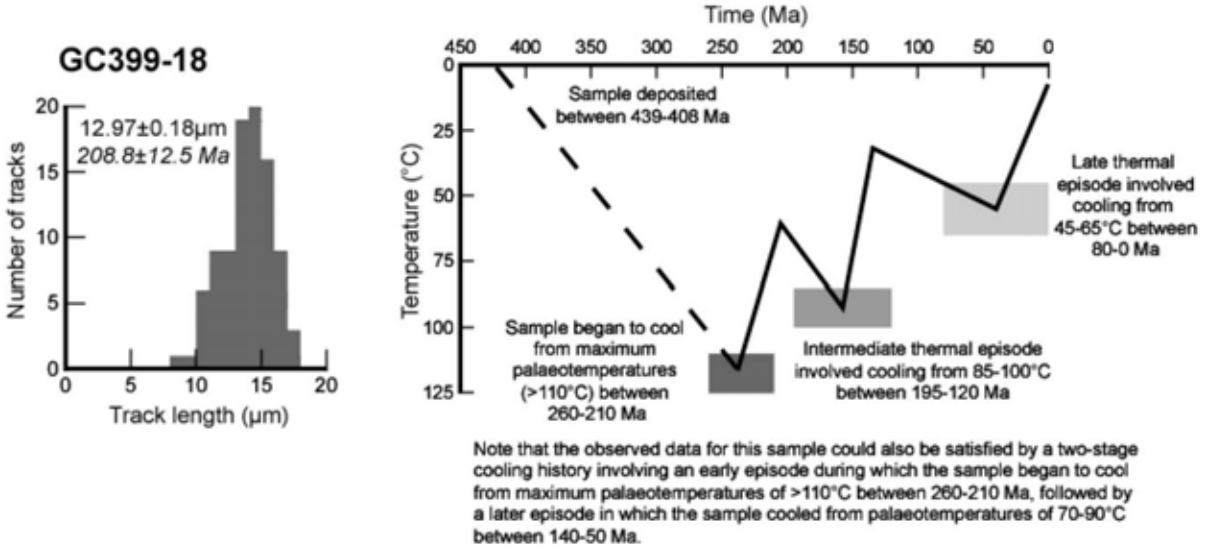

Figure 5.9 – Example Thermal history plot and histogram based on the raw data supplied by Geotrack for sample GC399-18 in SW Wales (after Holford, 2006).

5.3: THERMAL HISTORY DATA RESULTS FROM THE SW UK

5.3.1: REGIONAL AFTA DATASET ANALYSIS - 'BOOMERANG PLOTS'

A useful, qualitative way of assessing regional fission-track datasets can be achieved by plotting Mean Track Length (MTL) against fission-track age data for a suite of samples. This method, often referred to as the 'boomerang plot' (e.g. Gallagher & Brown, 1997; Gallagher *et al.* 1998) was introduced by Green (1986) in his influential study of fission track data from across northern England.

Green (1986) demonstrated that when a region is affected by a discrete phase of accelerated cooling, the apatite fission-track age and MTL data should define a distinctive pattern (assuming samples are distributed more or less uniformly across the *c.* 60-120°C zone of partial annealing). The pattern is characterised by an initial decrease in the MTL with decreasing age to a minimum mean length for intermediate ages, followed by a progressive increase in mean length for successively younger ages.

Perhaps most importantly, it should be recognised that if the dataset does not plot along the boomerang trend, a more complex history than coeval cooling during a single event is indicated. If the data do define a distinctive pattern, the plot can be used to estimate the timing of the last major cooling episode, which is indicated by the youngest fission-track ages (providing the mean confined track lengths are *c.* 14-15µm). If a suite of rocks has experienced a similar history, then the track length distribution will show a systematic shift through the trend of the data as illustrated by Green (1986), with only the maximum palaeotemperatures differing between the samples (as the samples will most likely have been collected from different elevations/sections of the stratigraphic column). The fission-track ages at the extremes of the plots have low Standard Deviations (SD's) as indicated by the

width of the error bars in Figure 5.10, whereas data in the middle of the plots exhibit high SD's.

Figure 5.10 shows plots of fission track age against mean track length for apatite samples collected from across the SW UK by both Geotrack (77) and the author (5). A simple visual inspection of the data (Figure 5.10) suggests a more complex thermal history than the northern England dataset of Green (1986). It is apparent that the SW UK data do not plot along a coherent 'boomerang' trend, as the mean track lengths of the samples tend to decrease at the same time as a reduction in fission track ages and the data do not show a transition between the 'original age' and 'reset age' components.

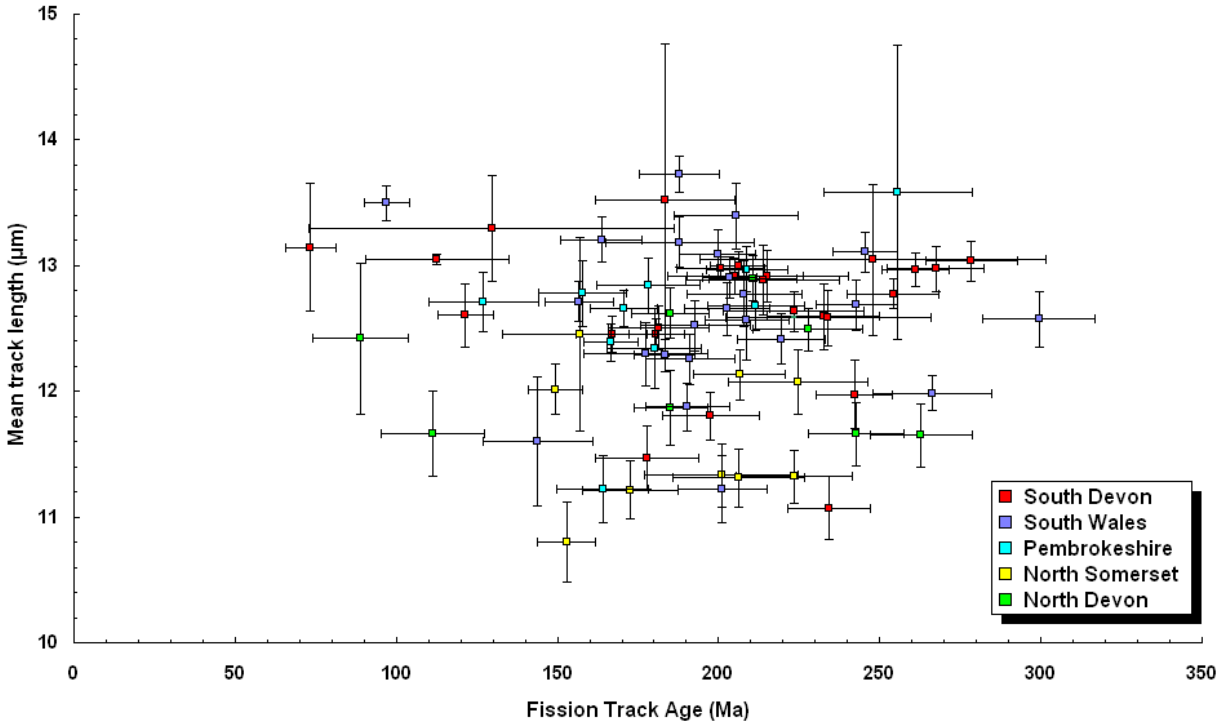

Figure 5.10 – The relationship between mean track length (µm) and fission-track age (Ma) for AFTA samples collected from across the SW UK.

5.3.2: PALAEOTHERMAL HISTORY OF THE SW UK

As explained more fully in Chapter 2, fission-track length histograms provide important information about the palaeothermal history of an apatite sample. During heating, track lengths are progressively reduced (annealed) and if temperature drops and stays low, then track length is "frozen" at the length to which it was reduced at maximum temperature. During continuous cooling, track length reduction is most rapid early in the thermal history of the sample when temperature is high, thus track length is dominated by maximum temperature. This observation means that the distribution of the tracks will give the thermal history of the sample (*cf.* Chapter 2).

5.3.2.1: Results from SW Wales

In order to determine the thermal and exhumation history of the southwest margin of the SGCB several samples were analysed from the Pembroke Peninsula, SW Wales, in the Lower Palaeozoic footwall of the Bala Fault (Figure 5.11).

The fission track ages of apatite fission track samples GC399-18, 19 and 20 (locations in Figure 5.11) are significantly younger than their Ordovician-Silurian stratigraphic ages (Table B.1, Appendix B), suggesting that they attained post-Silurian palaeotemperatures in excess of 110°C i.e. the total annealing temperature of apatite fission tracks. All three samples record protracted cooling histories.

For example, GC399-18 (central fission track age of 208.8 ±12.5Ma) cooled from maximum palaeotemperatures exceeding 110°C between 260-230Ma (late Permian-early Triassic). Assuming that palaeotemperatures during this early thermal episode were sufficient to anneal all fission tracks within the sample, two further discrete palaeothermal episodes can be inferred from the data. Following the first phase of total annealing, the sample was reheated

to 85-100°C between 195-130Ma (Middle-Late Jurassic), inducing partial annealing of new tracks formed since the first heating episode. Subsequently, the sample cooled from a third heating episode, attaining 45-65°C between 70Ma and the present-day.

Similar cooling histories are inferred for samples GC399-19 and GC399-20 and the other samples around the Pembrokeshire Coast (Appendix B). Figure 5.12 shows the spatial variation across the Pembroke Peninsular of the fission-track histograms highlighting the similarity in thermal history across the area.

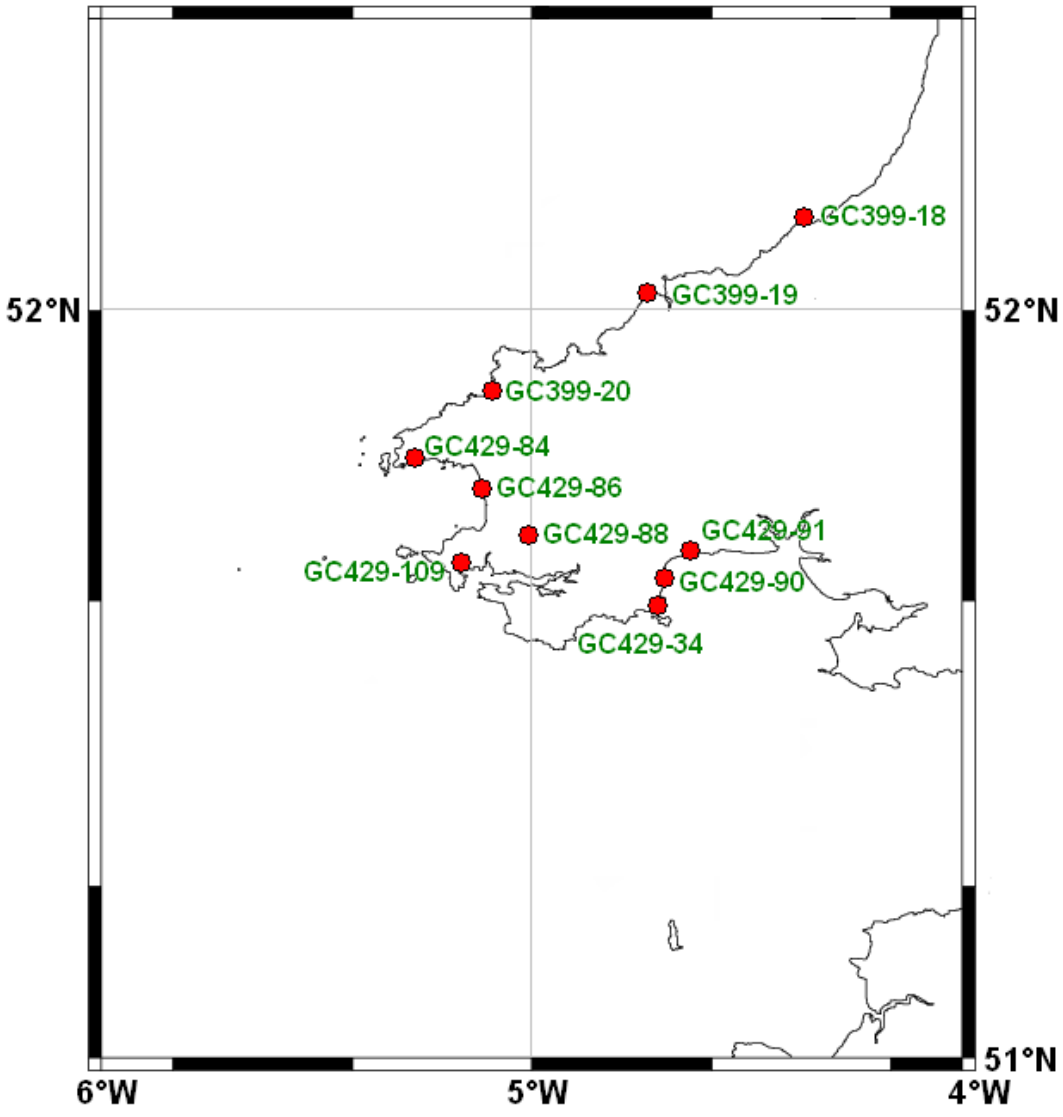

Figure 5.11 – Map showing locations of onshore AFTA samples from Pembrokeshire.

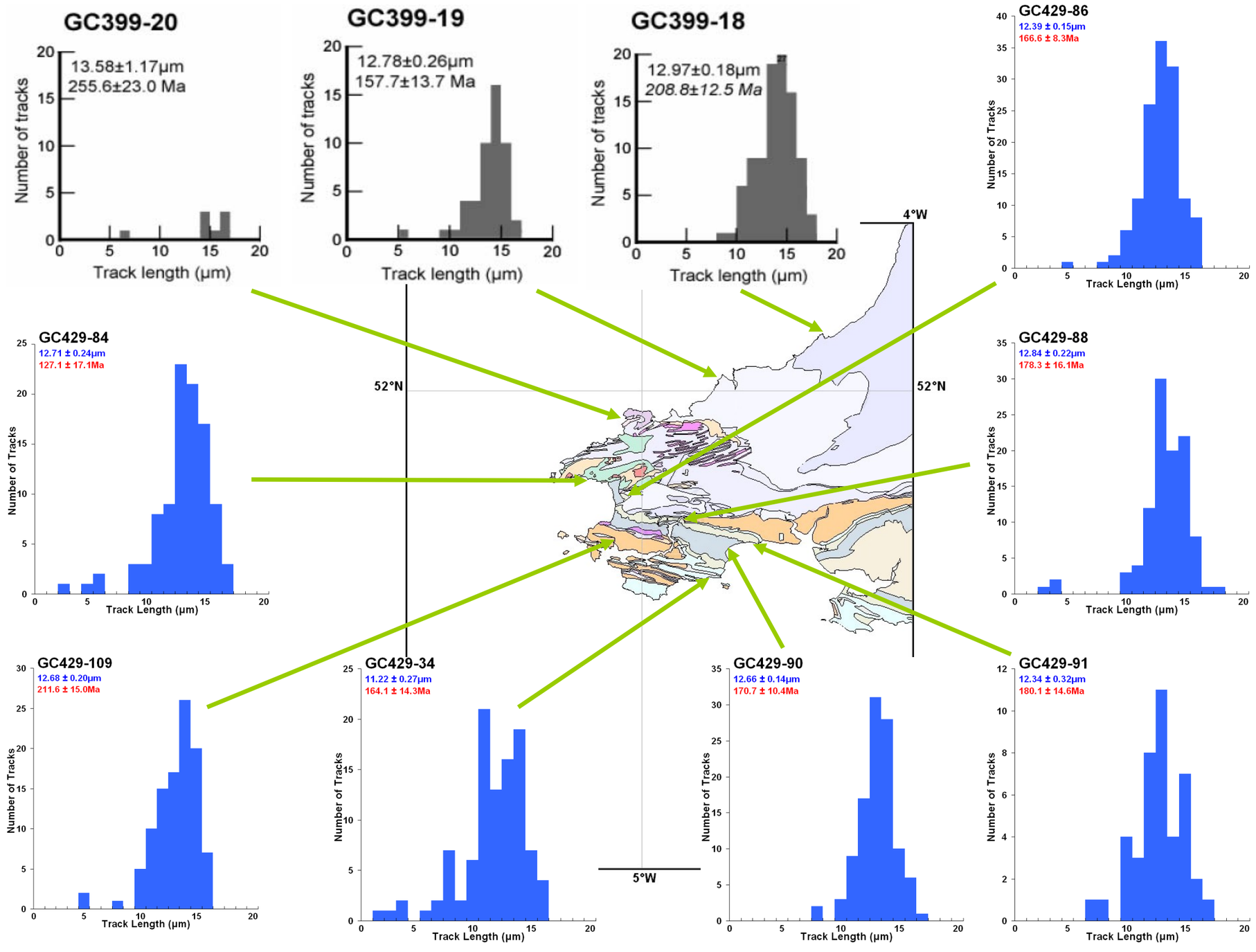

Figure 5.12 - Fission track length histograms from the Pembroke Peninsular. Most samples display unimodal distributions related to a high palaeotemperature and early post-depositional cooling. Sample numbers are shown in bold, fission-track ages in red, fission-track lengths in blue (bedrock geology after BGS, 2008).

5.3.2.2: Results from North Devon

In order to determine the thermal and exhumation histories of the northeast margin of the SCSB and southern margin of the BCB several samples were analysed from North Devon (Figure 5.13). The fission track ages of apatite fission track samples GC429-75, 76 and 83 (locations in Figure 5.13) are significantly younger than their Namurian stratigraphic ages (Table B.2, Appendix B), suggesting that they attained post-Namurian palaeotemperatures in excess of 110°C i.e. the total annealing temperature of apatite fission tracks. THR solutions and histograms are presented in Appendix B and Figure 5.14 shows the spatial variation across North Devon, of the fission track histograms highlighting the similarity in thermal history across the area.

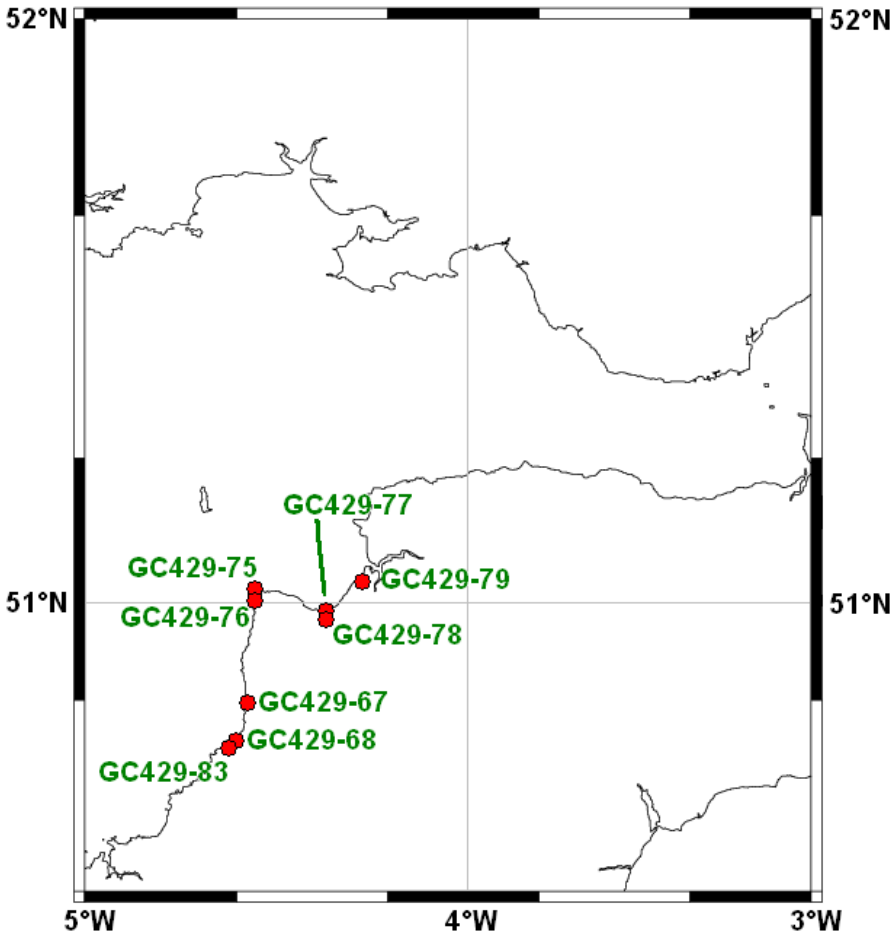

Figure 5.13 – Map showing locations of onshore AFTA samples from North Devon.

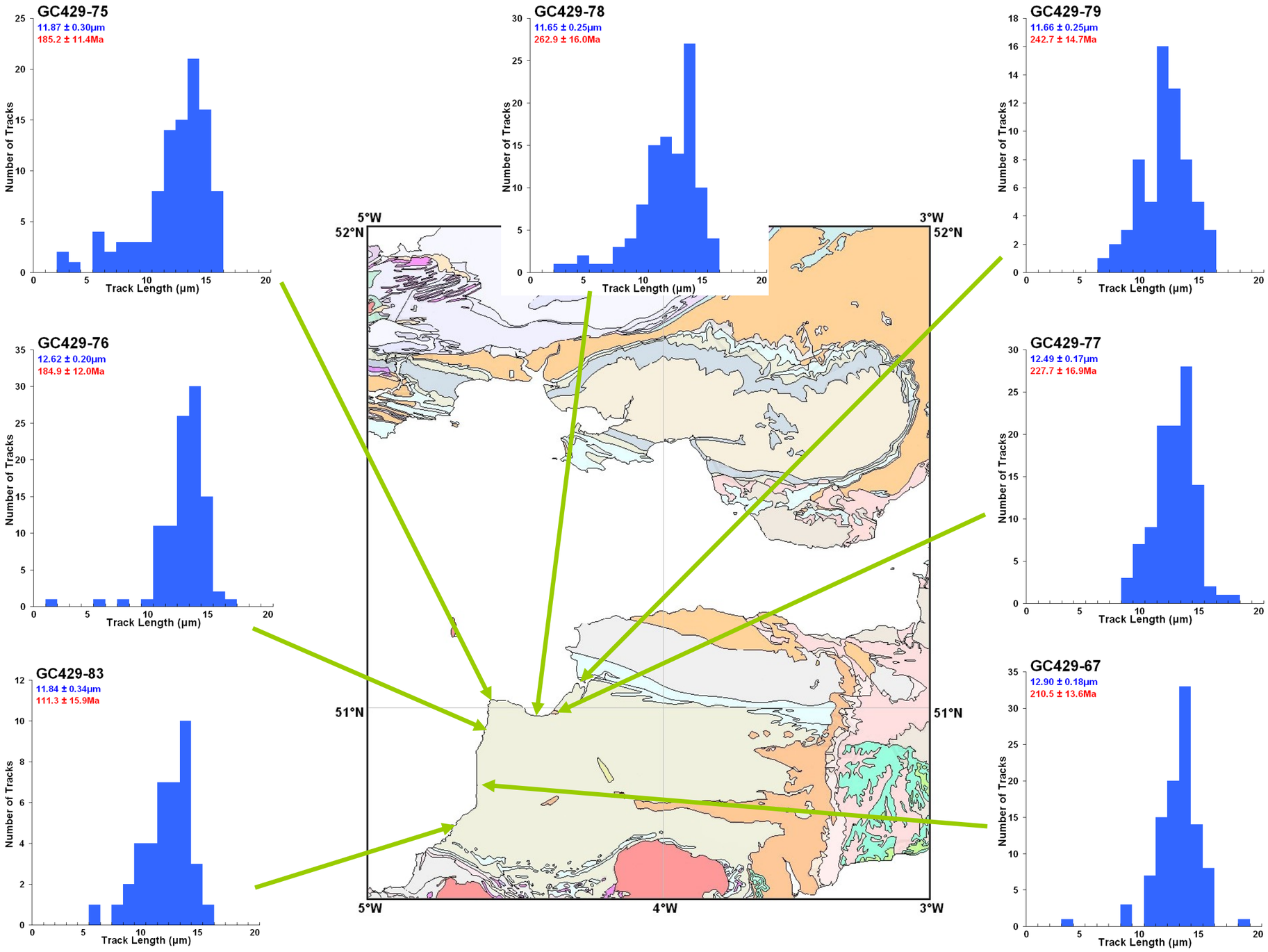

Figure 5.14- Fission track length histograms from North Devon. Most samples display unimodal distributions related to high palaeotemperatures and early post-depositional cooling. Sample numbers are shown in bold, fission-track ages in red, fission-track lengths in blue (bedrock geology after BGS, 2008).

5.3.2.3: Results from South Wales

In order to determine the thermal and exhumation histories of the northern margin of the BCB several samples were analysed from South Wales, the South Wales Coalfield and the Severn Estuary (Table B.3, Appendix B and Figure 5.15). Across the area there appear to be three separate distributions of thermal history; one of which is similar to the results reported for North Devon and Pembrokeshire, one which records an earlier cooling episode and one which records clear Paleocene cooling. THR solutions and histograms are shown in Appendix B, whilst Figure 5.16 shows the spatial variation across South Wales, of the fission track histograms highlighting the different thermal history styles across the area.

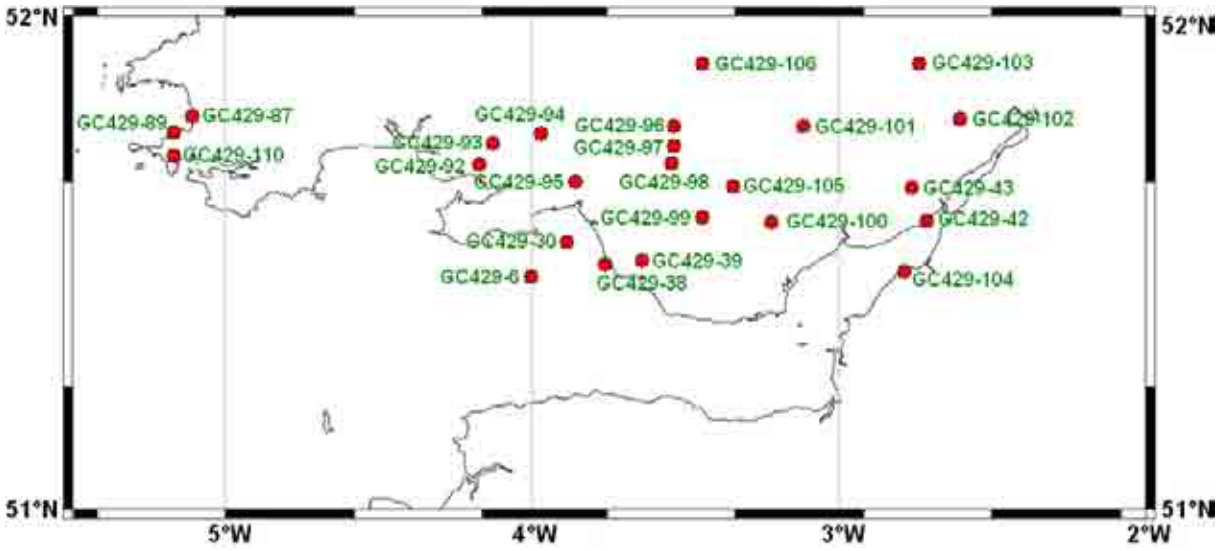

Figure 5.15 – Map showing locations of onshore AFTA samples from South Wales.

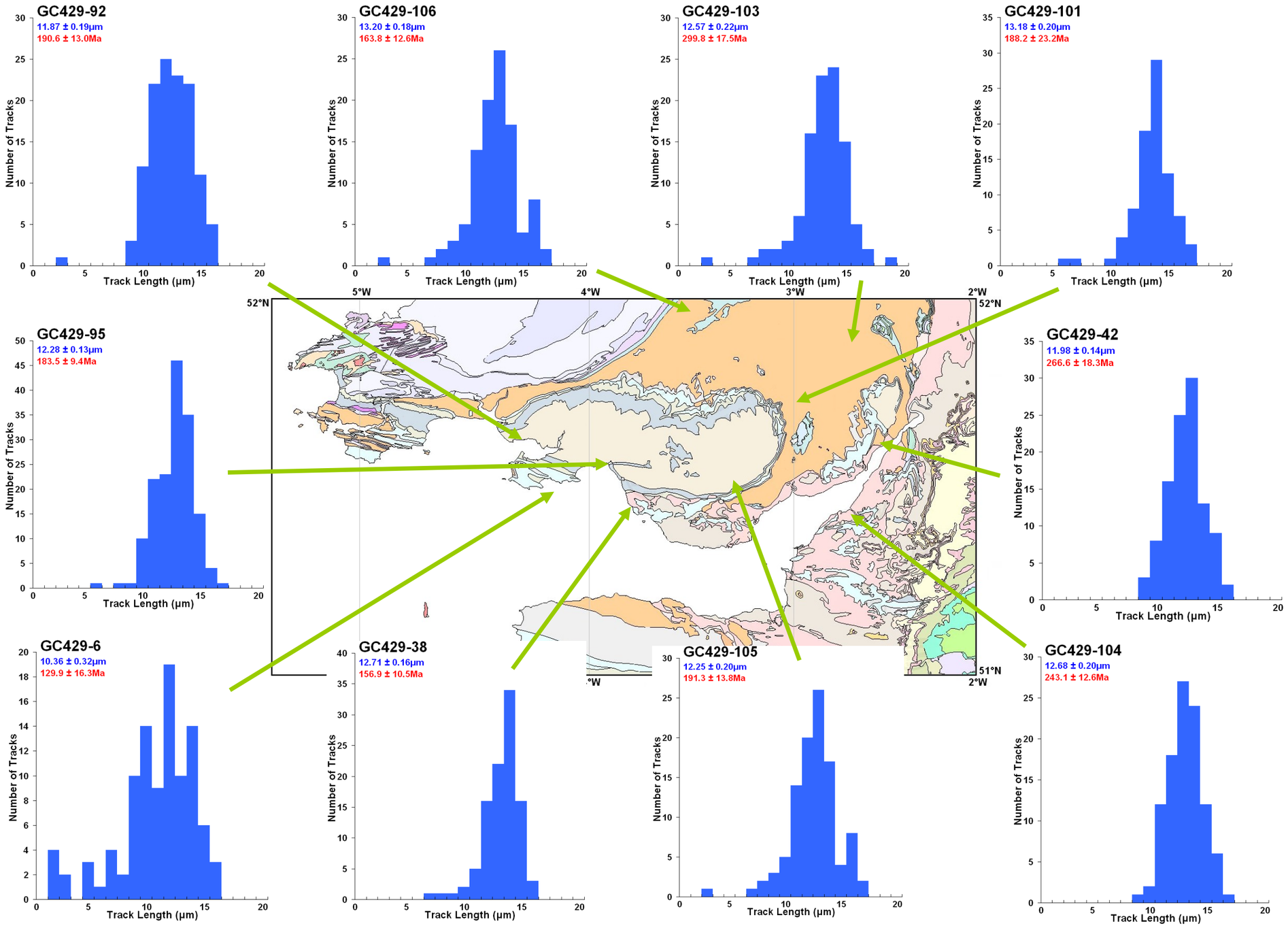

Figure 5.16- Fission track length histograms from South Wales. Most samples display unimodal distributions related to a high palaeotemperature and early post-depositional cooling. Sample GC429-6 provides evidence for mid-range cooling at a lower palaeotemperature giving a polymodal distribution. Sample numbers are shown in bold, fission-track ages in red, fission-track lengths in blue (bedrock geology after BGS, 2008).

5.3.2.4: Results from North Somerset

In order to determine the thermal and exhumation histories of the southern margin of the BCB several samples were analysed from North Somerset and the Bristol Channel (Table B.4, Appendix B and Figure 5.17). Across the area there appear to be two distinct thermal history distributions; one which is similar to the results reported for North Devon and Pembrokeshire and one which records clear Paleocene cooling. As before THR solutions are shown in Appendix B and Figure 5.18 shows the spatial variation across North Somerset, of the fission track histograms highlighting the different thermal history styles across the area.

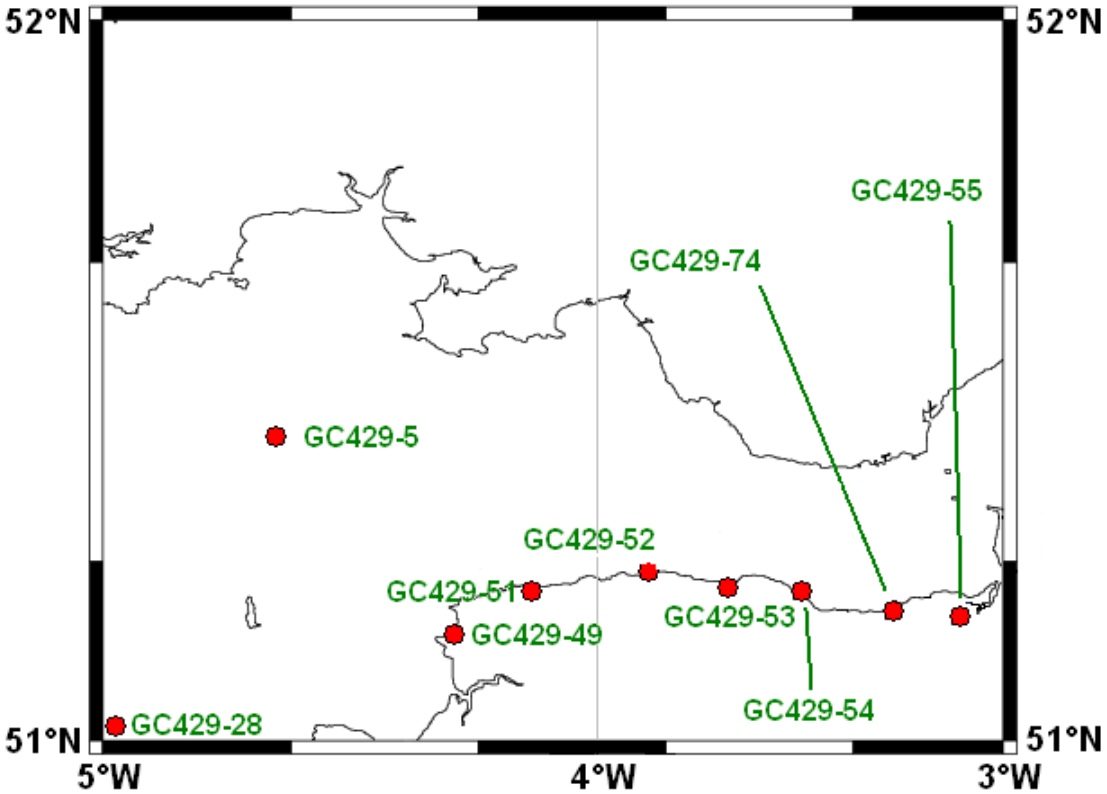

Figure 5.17 – Map showing locations of onshore AFTA samples from North Somerset.

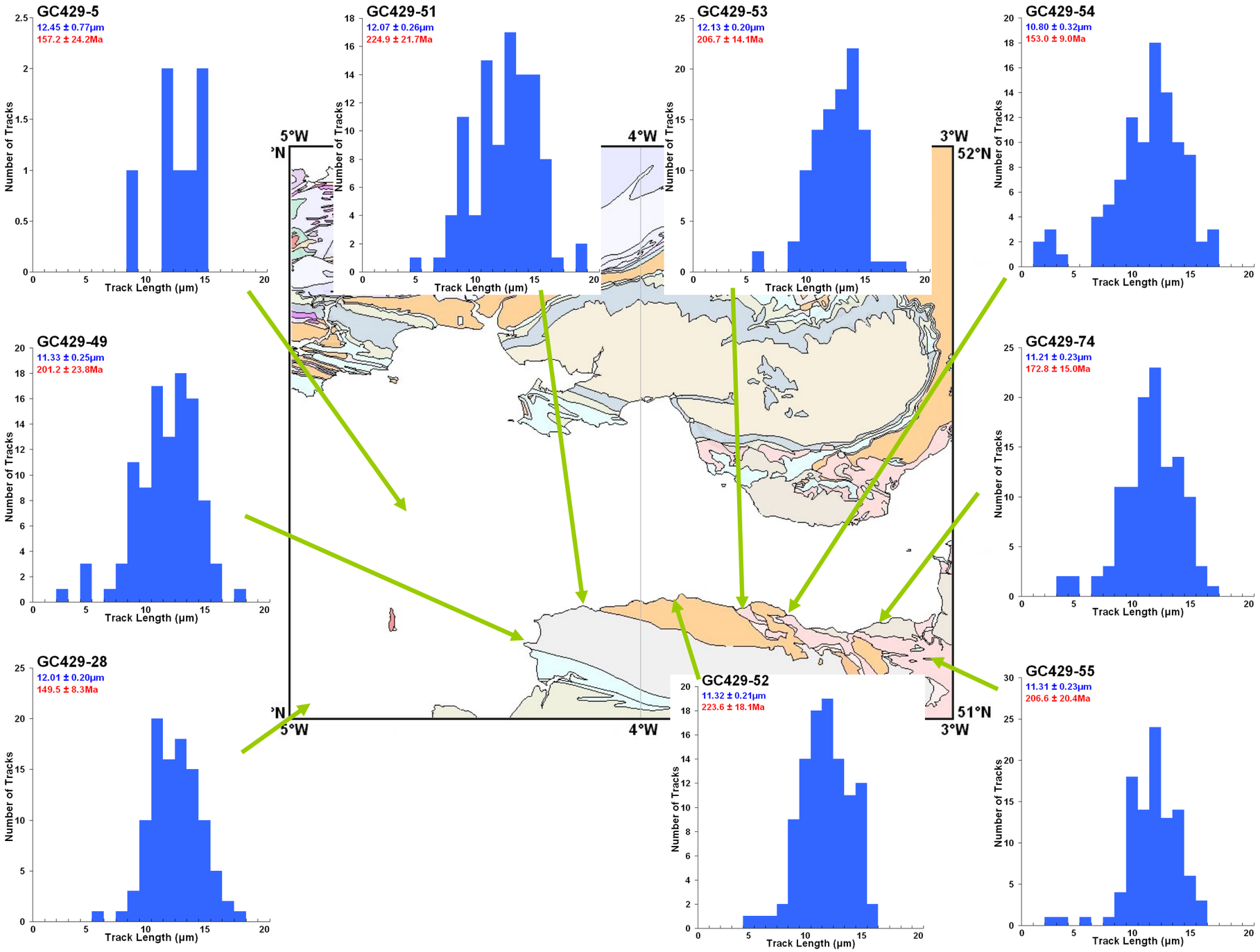

Figure 5.18- Fission track length histograms from North Somerset. Most samples display unimodal distributions related to a high palaeotemperature and mid-range post-depositional cooling. In a number of cases the distribution appears polymodal (particularly GC429-5, GC429-49, GC429-51) consistent with a lower maximum palaeotemperature and/or mid-range cooling. Sample numbers are shown in bold, fission-track ages in red, fission-track lengths in blue (bedrock geology after BGS, 2008).

5.3.2.5: Results from South Devon

In order to determine the thermal and exhumation histories of the western margin of the Wessex Basin and northern margin of the Western Approaches Basin several samples were analysed from South Devon, Somerset and Dorset (Table B.5, Appendix B and Figure 5.19). Across the area there appear to be three separate distributions of thermal history; one which is similar to the results reported for North Devon and Pembrokeshire, one which records an earlier cooling episode and one which records clear Paleogene cooling (Appendix B). Figure 5.20 shows the spatial variation across South Devon, Somerset and Dorset of the fission track histograms highlighting the different thermal history styles across the area.

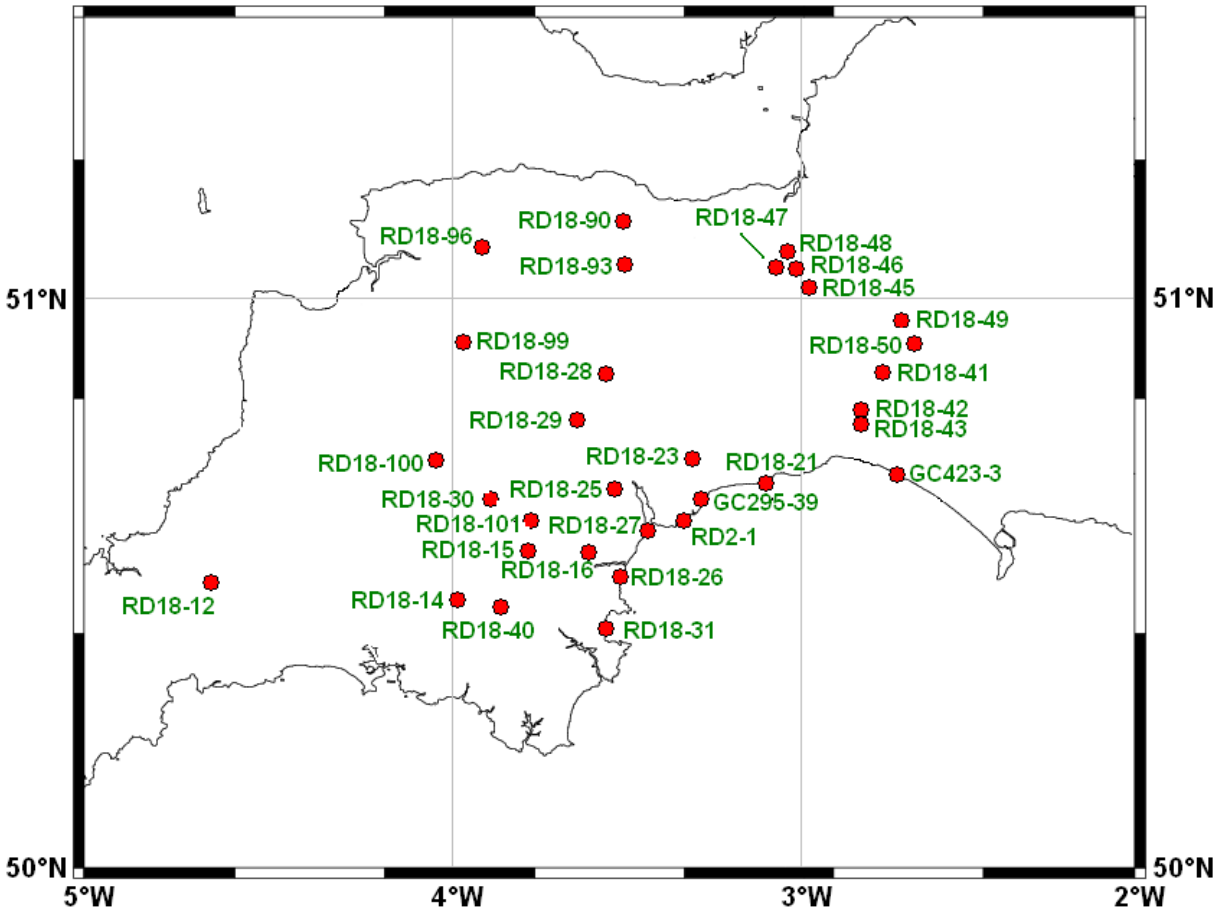

Figure 5.19 – Map showing locations of onshore AFTA samples from South Devon, Somerset and Dorset.

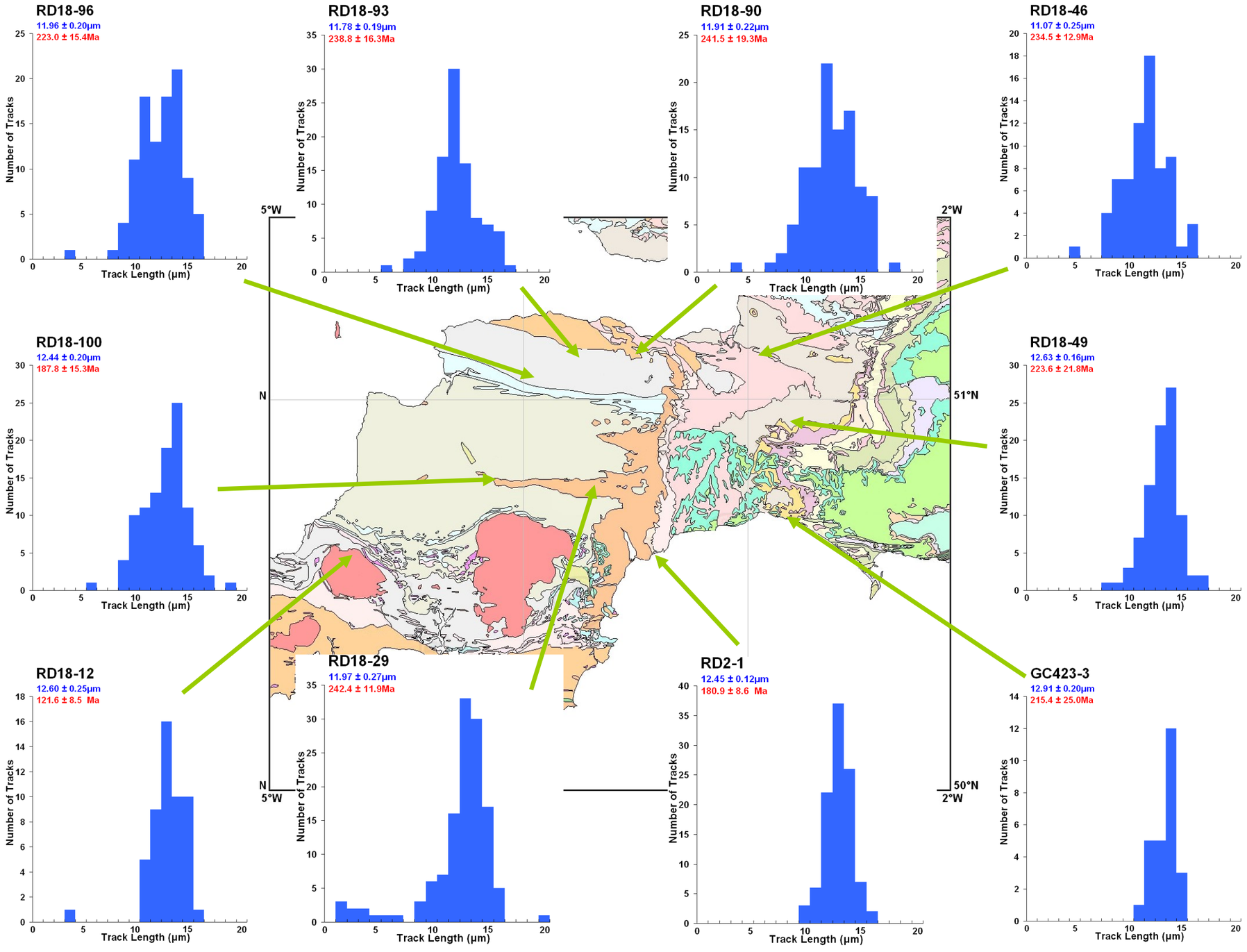

Figure 5.20 - Fission track length histograms from South Devon, Somerset and Dorset. The majority of the samples show a unimodal distribution related to early post-depositional cooling. The broad distributions indicate that palaeotemperatures were much more variable across this area than in others. Sample RD19-96 shows a polymodal distribution consistent with mid-range cooling. Sample numbers are shown in bold, fission-track ages in red, fission-track lengths in blue (bedrock geology after BGS, 2008).

5.3.3: ESTIMATING THE MAGNITUDE OF EXHUMATION USING PALAEOTHERMAL PROFILES FROM BOREHOLES

In this section of this chapter, the first study of palaeothermal (AFTA and VR) data from the Burton Row, Senghenydd and Gwendraeth Valley boreholes onshore SW UK is presented along with VR (and in some cases AFTA) data from 19 wells in the offshore basins (Figure 5.21). The principle aim of this study is to improve the regional understanding of the timing and magnitude of exhumation across the SW UK region by reconstructing the burial and exhumation history of the sedimentary section intersected by the boreholes and wells.

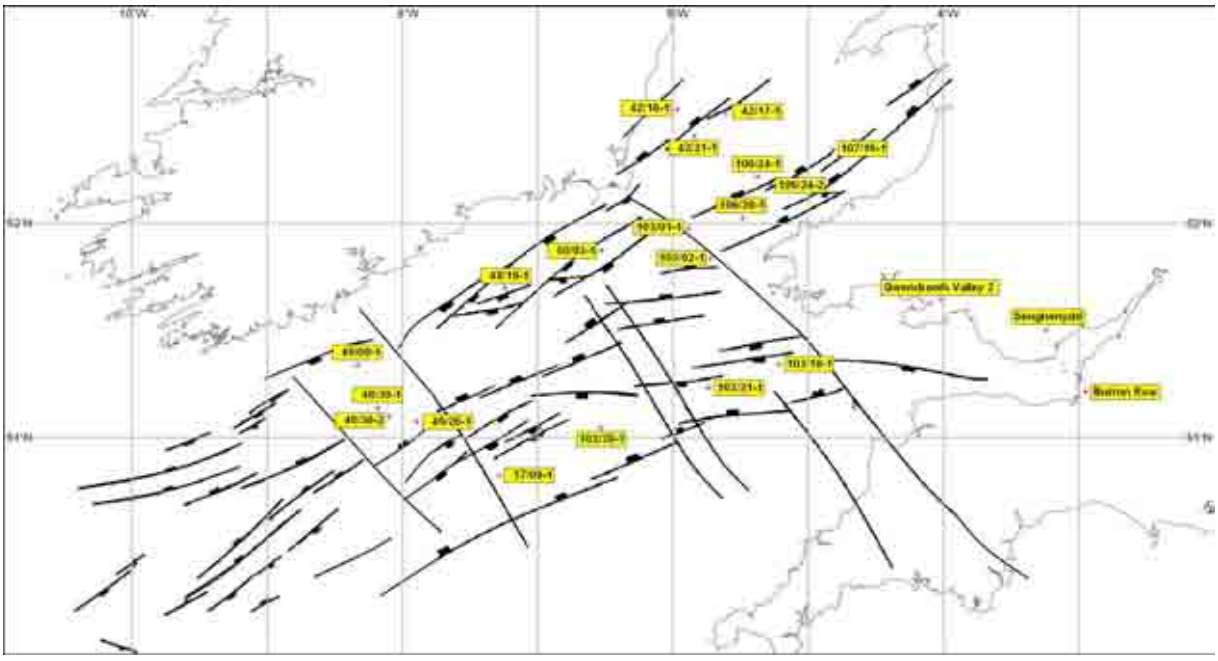

Figure 5.21 – Location map showing the wells analysed in this study (faults based on Van Hoorn, 1987*a* and Petrie *et al.* 1989).

VR profiles suggest that up to three distinct 'thermal episodes' can be identified in the Celtic Sea region (Figure 5.22). Measurements from Cenozoic sediments in wells 106/24-1, 106/28-1 and 49/09-1 indicate that a steeper geothermal gradient (of between 40-50°C/km) was prevalent during the Neogene. This is consistent with Holliday (1993) and Green *et al.* (1999), who have proposed an elevated palaeogeothermal gradient of around 50°C/km for the

Cenozoic, due in part to higher palaeosurface temperatures at this time. VR values from Jurassic strata are remarkably consistent throughout the Celtic Sea, indicating a regional palaeogeothermal gradient in the range 22-26°C/km which is thought to represent the Lower Cretaceous gradient. This is lower than the present day regional average of 32°C/km established by Corry & Brown (1998) (Table 5.1) and probably reflects lower thermal conductivities within the thick Jurassic shale sections. It should be noted that maturity measurements from well 042/21-1 define a remarkably linear trend with very little scatter; for this reason the data should be treated with caution (although the values are consistent with measurements from other wells in the region).

In addition, $\%R_0$ values from well 107/16-1 decrease with depth in the Upper Jurassic Kimmeridge and Oxford Clay formations. This is likely to reflect another process such as sediment reworking and/or fluid flow rather than deeper burial. The influence of syn-kinematic fluids in promoting fault reactivation and their effect on thermal maturity proxies has been highlighted by Turner & Williams (2004). In studies from the British continental shelf and Atlantic margins (e.g., Parnell *et al.* 1999; Middleton *et al.* 2001; Green *et al.* 2001) short-lived episodes of migration of anomalously hot reservoir fluids have been recorded in the relatively shallow subsurface. In their study of the Apley Barn borehole, southern England, Green *et al.* (2001) present a highly non-linear Cenozoic geothermal gradient, reminiscent of the temperature versus depth profiles modelled by Ziagos & Blackwell (1986), with a thermal 'spike' centred on a major permeability boundary (in this case an unconformity). Similar effects have been reported by Lampe *et al.* (2001) from the Rhine Graben who ascribe locally elevated VR anomalies to episodic fluid flow through shallow (1000–1500m) aquifers during Alpine-related basin inversion.

VR within Westphalian coals suggest elevated palaeogeothermal gradients in the range of 40-60°C/km. In most of the wells (e.g. 42/16-1, 42/12-1 and 103/02-1) there is significant scatter in measured maturity values, leaving the results open to interpretation. Corcoran & Clayton (1999) suggested that $\%R_0$ values derived from Westphalian sediments in wells 42/12-1, 42/16-1 and 42/17-1 reflect elevated geothermal gradients of 74-78°C/km established during Late Carboniferous uplift. Conversely, Green *et al.* (2001) concluded that a geothermal gradient of around 32°C/km can adequately account for fission track and VR data from the same wells. This study follows Green *et al.* (2001) in interpreting these maturity measurements in terms of subsequent Mesozoic and Cenozoic burial and the observed gradient is thought to represent the Paleogene. It remains feasible, however, that Westphalian sediments reached their maximum burial depth prior to Late Carboniferous exhumation, and it is impossible to rule out elevated basal heat flow during the Permian and Triassic in response to rifting.

Stratigraphic Age	Geothermal gradient (°C/km)	Error (°C/km)
Quaternary	53.4	5.2
Cenozoic	46.7	3.1
Upper Cretaceous Chalk	41.0	1.9
Cretaceous Greensand	37.2	3.0
Lower Cretaceous Wealden	21.1	1.6
Upper Jurassic	36.9	1.5
Middle Jurassic	24.5	4.0
Lower Jurassic	35.4	2.0
Triassic	38.0	1.9
Paleozoic	6.9	0.4

Present-day = 32°C/km

Table 5.1 – Palaeogeothermal gradients derived for the offshore wells of the NCSB based on work by Corry & Brown (1998).

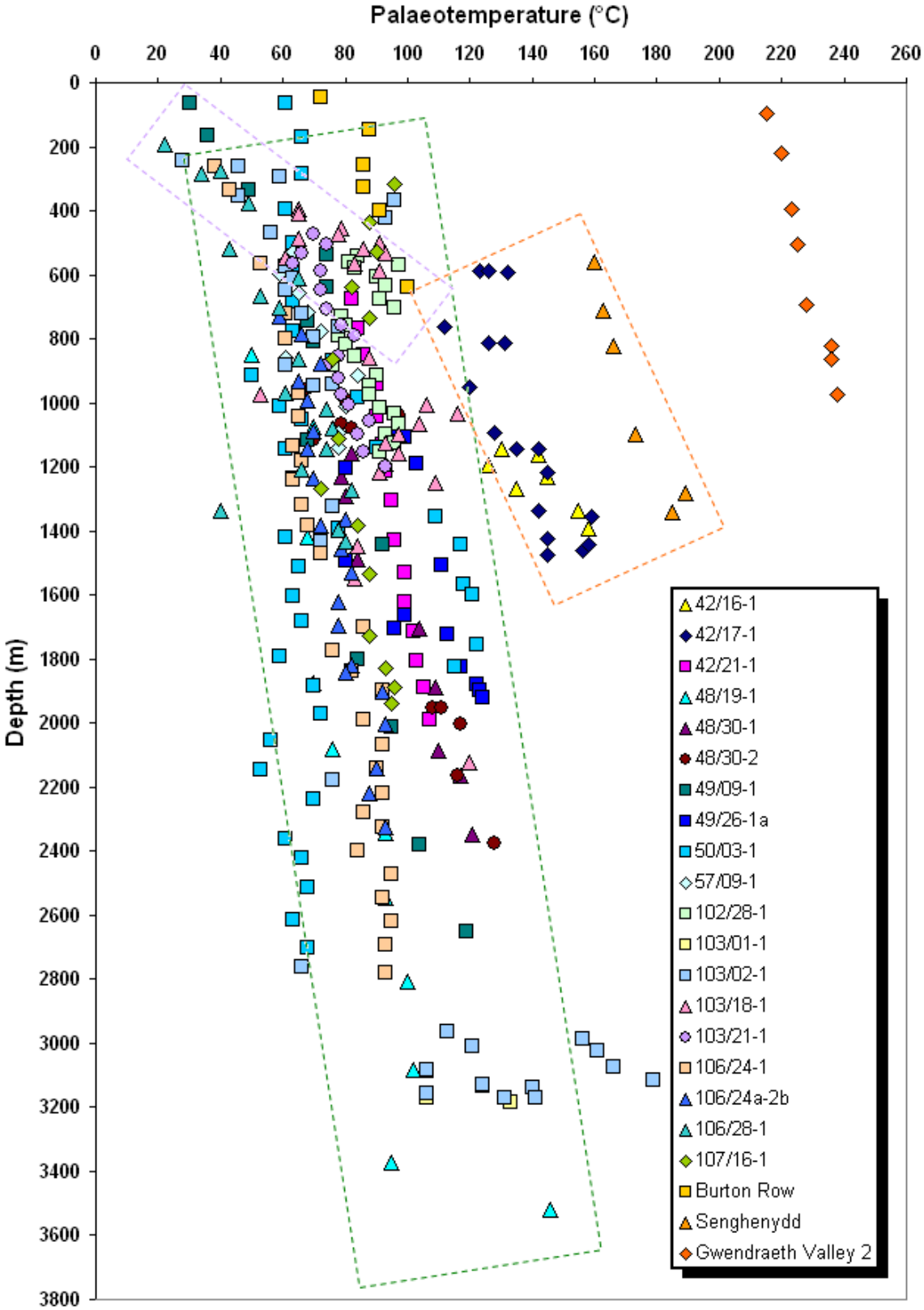

Figure 5.22 – Vitrinite reflectance profiles from wells and boreholes across the SW UK. Three distinct maturity gradients can be identified in the VR profiles from these wells (illustrated by the dashed boxes). These reflect palaeogeothermal gradients which were established during the Neogene (Purple box), the Paleogene (Orange box) and the Lower Cretaceous (Green box). Coloured symbols represent the VR measurements from particular wells.

5.3.3.1: Burton Row borehole

The Burton Row Borehole, Brent Knoll (Whittaker & Green, 1983) is located 25km to the east of St Audries Bay (Figure 5.21). The Burton Row borehole and the Somerset coast in general comprise extensive exposures of Upper Triassic to Lower Jurassic strata and form part of the southern margin of the BCB. The exposures have been studied for more than 130 years and are well documented (Richardson, 1911; Whittaker & Green, 1983; Warrington & Ivimey-Cook, 1995; Swift & Martill, 1999; Hounslow *et al.* 2004) and form part of a geological Site of Special Interest. The succession exposed on the coast and present in the borehole comprises formations assigned to the Mercia Mudstone, Penarth and Lias groups which occur widely at outcrop and beneath younger deposits in England and parts of South Wales, western Scotland and Northern Ireland and in the adjoining offshore areas (Warrington *et al.* 1980). The thermal history dataset consists of 6 VR samples (Appendix B) and 1 AFTA sample taken from the core of the Burton Row borehole.

An assumed present-day geothermal gradient of 30°C/km has been defined for the Burton Row borehole (Figure 5.23) due to the absence of any BHT data. When compared to palaeotemperature estimates from VR it is clear that all parts of the preserved section at Burton Row have been hotter at some point in the past. VR values from the Lias vary between 0.43-0.61% Corresponding to 72-100°C (Appendix B). VR derived palaeotemperatures are generally *c.* 40-70°C higher than present-day temperatures and in a plot of palaeotemperature against depth (Figure 5.23), they define a profile that is sub-parallel with the present-day palaeotemperature profile (Figure 5.23). This suggests that heating was due primarily to deeper burial rather than the result of a period of elevated heat flow or hot fluid circulation (*cf.* Green *et al.* 2002).

It is apparent from Figure 5.23 that the VR-derived palaeotemperatures show some variation with depth, especially within the Liassic section. Analysis of the maceral-compositions of the Liassic vitrinite samples indicate that the organic matter is dominated by lamalginite, which is usually a sign that measured reflectance's are suppressed (Carr, 2000). Suppression commonly affects marine hydrogen-rich facies such as the Lower Jurassic mudstones which are present in the Burton Row borehole and are widely distributed across the British Isles (Scotchman, 2001) and is due to the marine vitrinite remaining relatively perhydrous (i.e. having a high hydrogen to carbon ratio) (Beardsmore & Cull, 2001). Suppression also results from a number of other factors including high liptinite contents and the presence of aliphatic lipids and bitumen's derived from associated lipids (Carr, 2000). Suppression occurs immediately after a sediment has been deposited as a result of a negative feedback process; excess volatiles generated by aromatisation and condensation reactions saturate the micro-porous network, and restrict further aromatisation and condensation processes within the vitrinite (Carr, 2000). Suppression will continue to reduce reflectance until the hydrogen/bitumen has been removed from the vitrinite structure (Carr, 2000) and results in lower reflectances in comparison to thermally equivalent terrestrially derived vitrinite (Beardsmore & Cull, 2001). The lower VR values within the overall trend may be interpreted to have been affected by geochemical suppression, resulting in anomalously low reflectance's (Carr, 2000). However the measured reflectances agree with the AFTA suggesting no suppression.

Only one AFTA sample was available for the Burton Row borehole (from the Sherwood Sandstone Group at depth 909.9-933.6m). The process involved in extracting the thermal history solution is described in Chapter 2. A thermal history involving one episode of heating and cooling provides the best-fit to the measured data, although there are a couple of short

lengths that are very difficult to fit in detail. Their presence shows that the sample was not totally annealed prior to cooling, showing that the maximum palaeotemperature was <110°C.

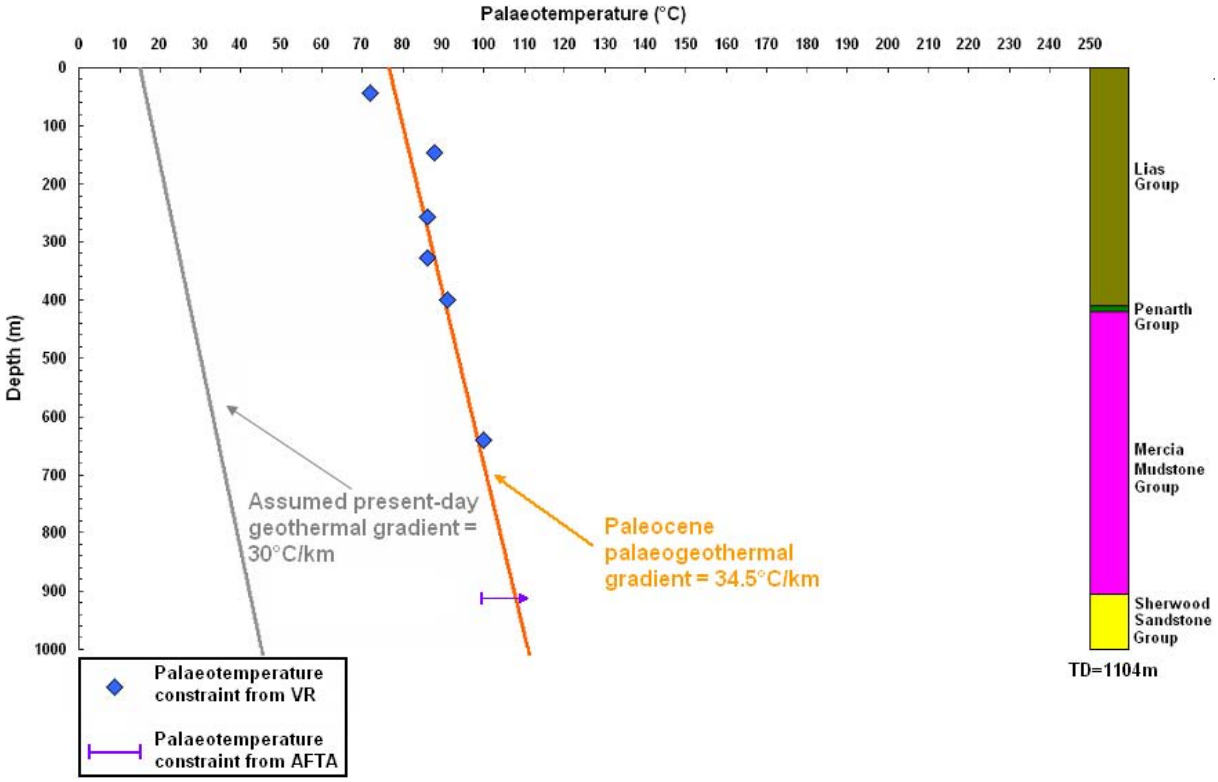

Figure 5.23 – Palaeotemperature constraints from AFTA and VR data from the Burton Row borehole plotted against depth. These are used to infer palaeotemperature profiles prior to the Paleogene cooling episode. A simplified stratigraphic column is also shown.

AFTA suggests that following deposition in the late Triassic (*c.* 230Ma), sample RD18-67 began to cool from its maximum post-depositional temperature of between 100-110°C in the interval of 65-40Ma (i.e. late Paleocene-Eocene). Since the Jurassic and Triassic units within the Burton Row borehole had been deposited by *c.* 180Ma (i.e. 115Ma prior to the onset of the cooling episode suggested by AFTA), it can be assumed that the style of thermal history indicated by this sample applies to the entire preserved Mesozoic section within the Burton Row borehole.

The maximum likelihood estimate of palaeogeothermal gradient prior to Paleogene exhumation is 34.5°C/km (26.5-41.5°C/km at 95% confidence limits) (Figure 5.24). A value of 20°C has been used for the surface temperature for the Paleogene, based on palaeoclimatic evidence presented by Yalçin *et al.* (1997). Extrapolating the fitted palaeotemperature profiles to this value indicates that the preserved Mesozoic succession was more deeply buried by 1950m ±200m (1300-2200m ±200m at 95% confidence limits) prior to Paleogene exhumation (Figure 5.24).

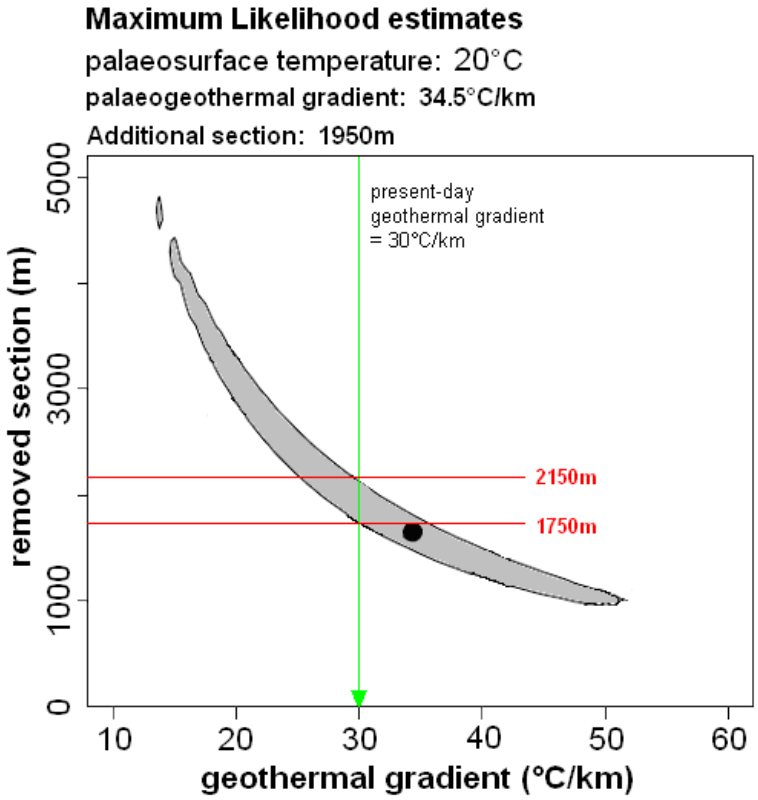

Figure 5.24 – Amount of additional section and palaeogeothermal gradients required to explain the Paleogene palaeothermal episode. The shaded region defines the allowed range of values for each parameter that are consistent with the measured palaeotemperature constraints within 95% confidence limits. Black dots represent the maximum likelihood estimates. Red horizontal bars indicate the range of exhumation estimates assuming no change in the present-day geothermal gradient. The range of values for additional section shows an excellent correlation with those derived from the compactional data (*c.* 1.8-2.8km).

5.3.3.2: Senghenydd borehole

The Senghenydd borehole is located in the Vale of Glamorgan in the South Wales Coalfield (Figure 5.21). It was drilled in the 1970s by Cambrian Exploration Limited and penetrates to Silurian rocks (though the VR data extends down to the Devonian only). The borehole indicates Carboniferous Limestone thicknesses of 330m whereas at Barry, on the south coast of the Vale of Glamorgan, the Carboniferous Limestone is over 1200m thick (Wilson *et al.* 1990) whilst Old Red Sandstone thicknesses of about 970m are indicated north of the Vale and this compares with a thickness estimate of about 900m in the Cardiff district (Waters & Lawrence, 1987). The thermal history dataset consists of 6 VR samples taken from cuttings of the Senghenydd borehole (Appendix B). An assumed present-day geothermal gradient of 30°C/km has been defined for the Senghenydd borehole (Figure 5.25) due to the absence of any BHT data.

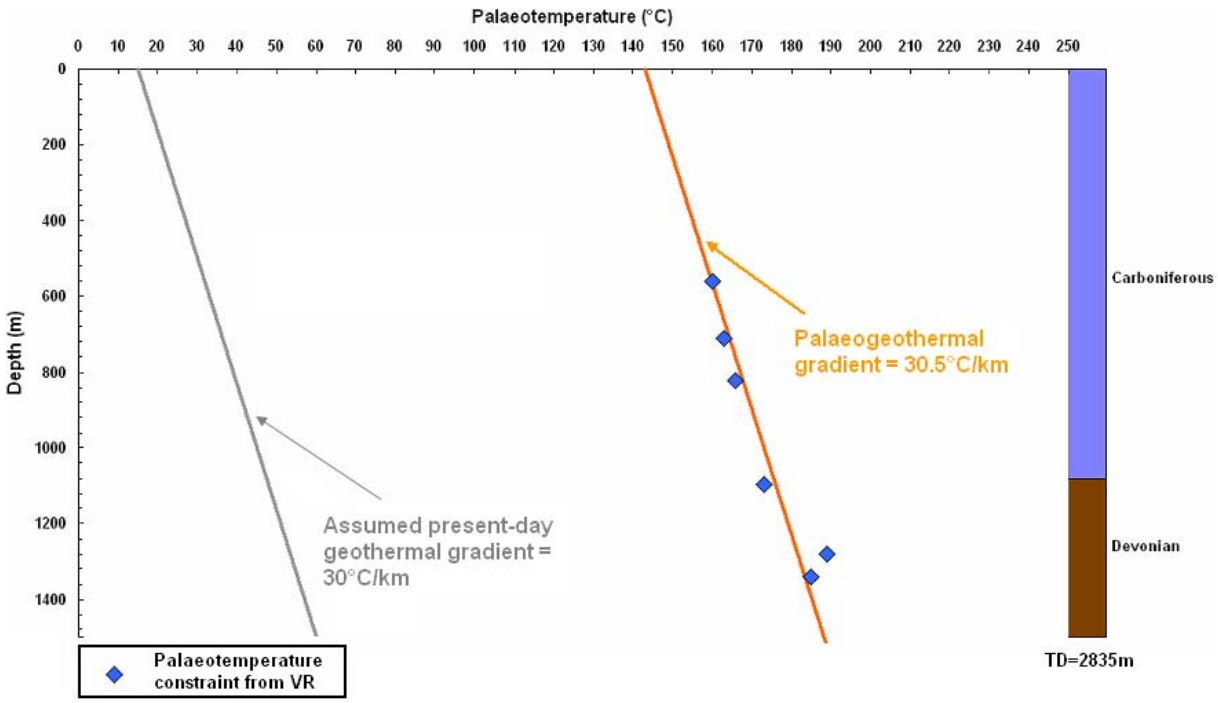

Figure 5.25 – Palaeotemperature constraints from VR data from the Senghenydd borehole plotted against depth. These are used to infer palaeotemperature profiles prior to the cooling episode. A simplified stratigraphic column is also shown.

Since no AFTA samples are available for the borehole there is no timing constraint on the exhumation episode(s) and the timing can only be constrained as post-Carboniferous. The maximum likelihood estimate of palaeogeothermal gradient prior to exhumation is 30.2°C/km (20.0-40.4°C/km at 95% confidence limits) (Figure 5.26). A value of 15°C has been used for the surface temperature for the Mesozoic, based on palaeoclimatic evidence presented by Yalçin *et al.* (1997). Extrapolating the fitted palaeotemperature profiles to this value indicates that the preserved Paleozoic succession was more deeply buried by 4250m ±400m (3050-6700m ±400m at 95% confidence limits) prior to exhumation (Figure 5.26).

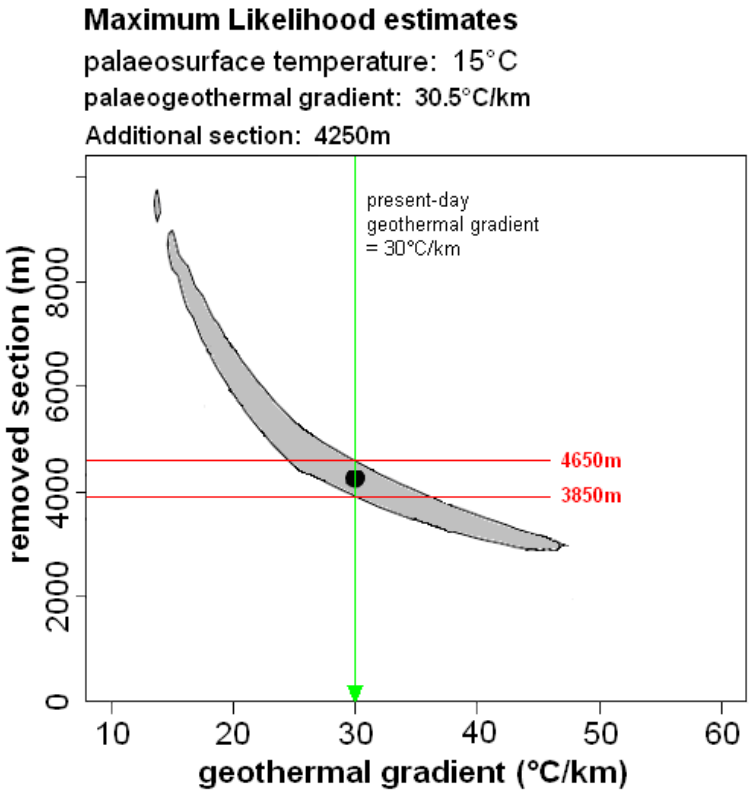

Figure 5.26 – Amount of additional section and palaeogeothermal gradients required to explain the palaeothermal episode. The shaded region defines the allowed range of values for each parameter that are consistent with the measured palaeotemperature constraints within 95% confidence limits. Black dots represent the maximum likelihood estimates. Red horizontal bars indicate the range of exhumation estimates assuming no change in the present-day geothermal gradient.

5.3.3.3: Gwendraeth Valley 2 borehole

The Gwendraeth Valley 2 borehole is located in the western part of the South Wales Coalfield (Figure 5.21). It comprises Silesian sediments in a structurally complex E-W trending syncline (Hartley, 1993). Over the last century the commercial exploitation of these coal-bearing sediments has resulted in the development of an extensive basin-wide data base (e.g. Robertson, 1933; Moore & Cox, 1943; Moore 1945, 1947; Blundell, 1952; Woodland & Evans, 1964; Parry, 1966; Thomas, 1967, 1974; Archer, 1968; Squirrel & Downing, 1969; Barclay, 1989) and in recent years this has been used to help elucidate the Silesian sedimentological and tectonic development of the area (e.g. Kelling, 1974, 1988; Jones 1989*a*, *b*, 1991; Hartley & Warr, 1990; Hartley, 1993). These studies have shown that Silesian sediments were deposited in a foreland basin initiated in the early Namurian and developed to the north of the Variscan orogen and south of the cratonic Wales-Brabant Massif (Kelling, 1988; Gayer & Jones, 1989; Hartley, 1993). In general, the 3.2 km thick Silesian basin-fill sequence shallows and coarsens upwards. The thermal history dataset consists of 8 VR samples (Appendix B) taken from the core of the Gwendraeth Valley 2 borehole. An assumed present-day geothermal gradient of 30°C/km has been defined for the Gwendraeth Valley 2 borehole (Figure 5.27) due to the absence of any BHT data.

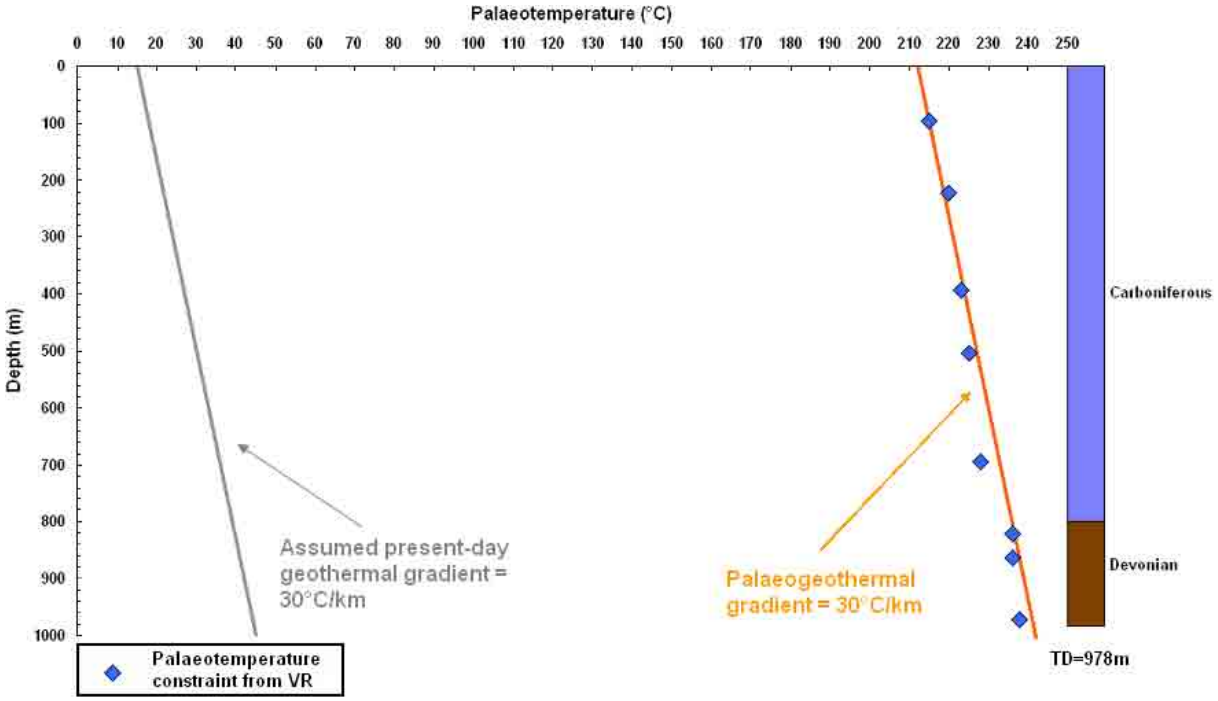

Figure 5.27 – Palaeotemperature constraints from VR data from the Gwendraeth Valley 2 borehole plotted against depth. These are used to infer palaeotemperature profiles prior to the cooling episode. A simplified stratigraphic column is also shown.

As with the Senghenydd borehole, since no AFTA samples are available there is no timing constraint on the exhumation episode(s). The maximum likelihood estimate of palaeogeothermal gradient prior to exhumation is 30.0°C/km (21.5-42.5°C/km at 95% confidence limits) (Figure 5.28). A value of 15°C has been used for the surface temperature for the Mesozoic, based on palaeoclimatic evidence presented by Yalçin *et al.* (1997). Extrapolating the fitted palaeotemperature profiles to this value indicates that the preserved Mesozoic succession was more deeply buried by 6550m ±400m (4700-9300m ±400m at 95% confidence limits) prior to exhumation (Figure 5.28).

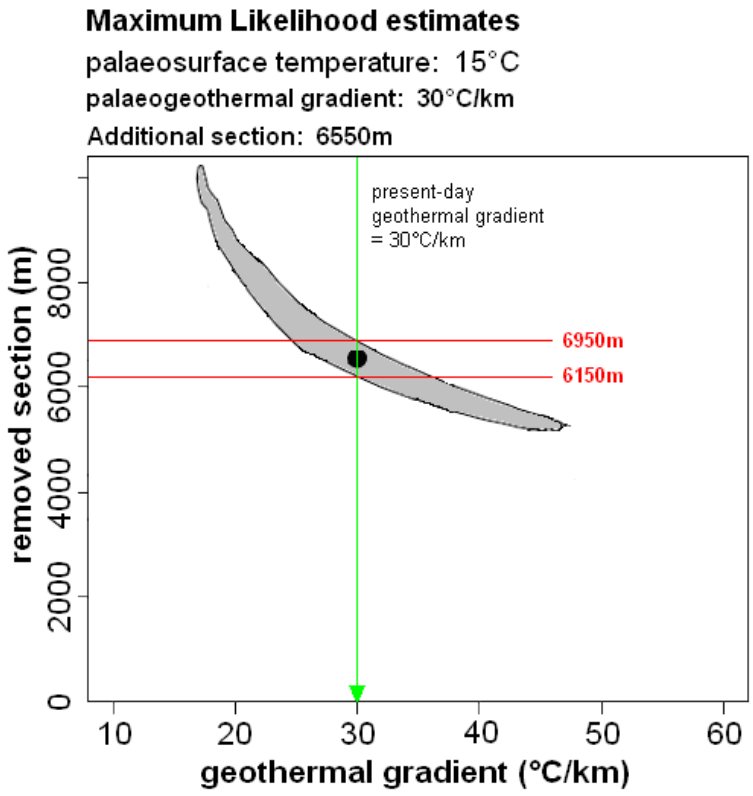

Figure 5.28 – Amount of additional section and palaeogeothermal gradients required to explain the palaeothermal episode. The shaded region defines the allowed range of values for each parameter that are consistent with the measured palaeotemperature constraints within 95% confidence limits. Black dots represent the maximum likelihood estimates. Red horizontal bars indicate the range of exhumation estimates assuming no change in the present-day geothermal gradient.

5.3.3.4: Offshore Exploration wells

The VR plots for each of the wells analysed are shown in Figures 5.29 and 5.30. The interpreted data fall into two trends – those which can be fitted to a single palaeogeothermal gradient (Figure 5.29) and those which show evidence of 'heat spikes' caused by fluid flow (Figure 5.30). In the case of the latter an assumed palaeogeothermal gradient is fitted through the data which is not affected by the 'heat spike'. Present-day geothermal gradient is calculated using corrected BHT measurements but where this data are not available an assumed present-day gradient of 32.0°C/km has been plotted based on the work of Corry & Brown (1998). It should be noted that where this assumed gradient is present it is for illustrative purposes only since there is no reason for the gradient in the NCSB to apply to all

wells in the area (as illustrated by the wide range of present-day gradients from the wells with BHT data). Where the palaeotemperature vs. depth plots define a palaeogeothermal gradient which is sub-parallel with the present-day gradient, this is suggestive of the heating being due primarily to deeper burial rather than the result of a period of elevated heat flow or hot fluid circulation (*cf.* Green *et al.* 2002).

It should be noted that unless AFTA data is present the timing of the palaeogeothermal gradient cannot be constrained in all but general terms (depending on the extent of continuous measurements from different stratigraphic intervals). Extrapolation of the palaeogeothermal gradient to a surface temperature allows the amount of additional section required to explain the elevated palaeotemperatures to be determined. This study has used the palaeoclimatic evidence of Yalçin *et al.* (1997) to determine appropriate surface temperatures for the calculation of additional section and this data is illustrated in Figures 5.31 and 5.32.

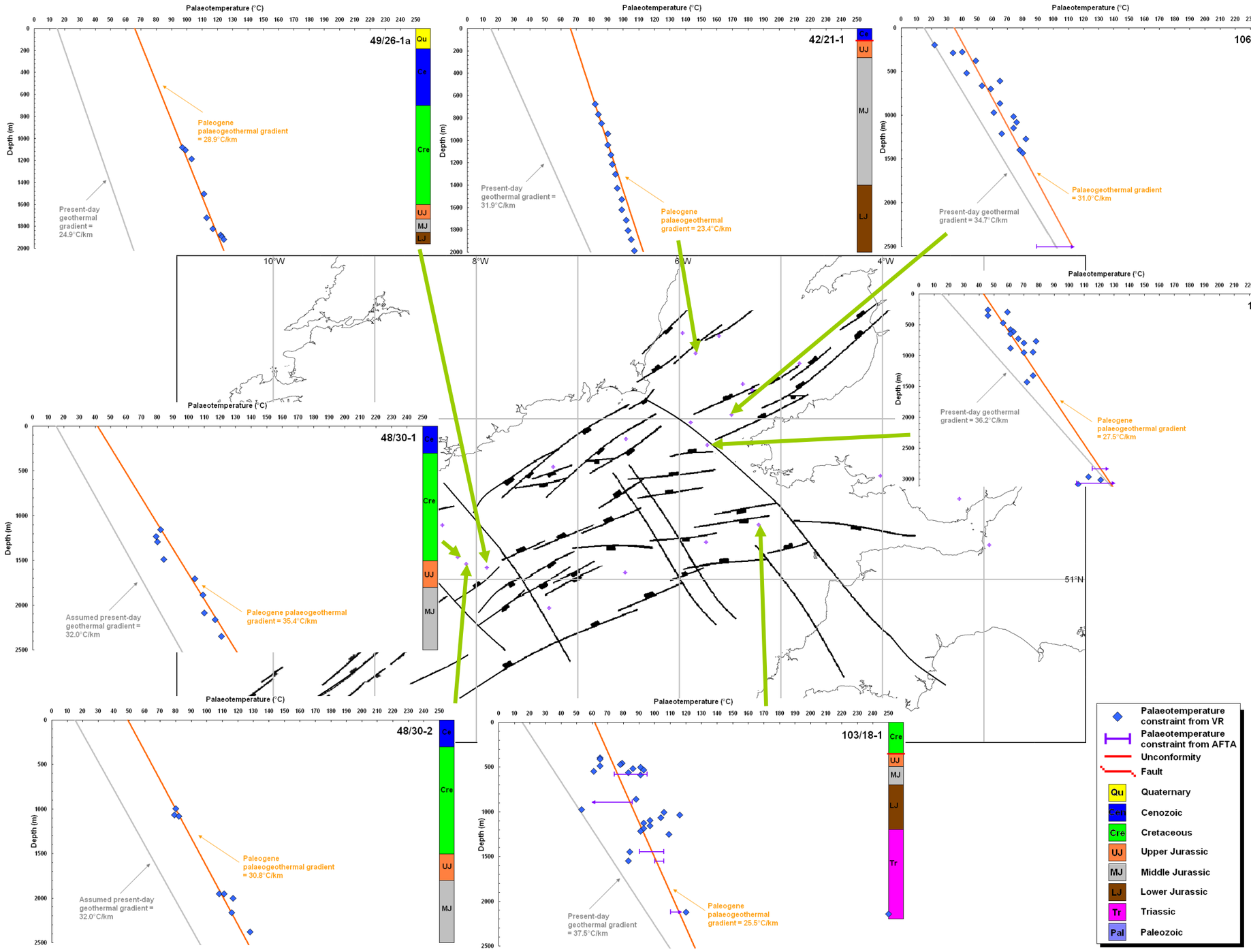

Figure 5.29 - Map showing the distribution of VR temperature-depth plots which indicate elevated palaeotemperatures were due primarily to deeper burial. (faults based on Van Hoorn, 1987*a* and Petrie *et al.* 1989).

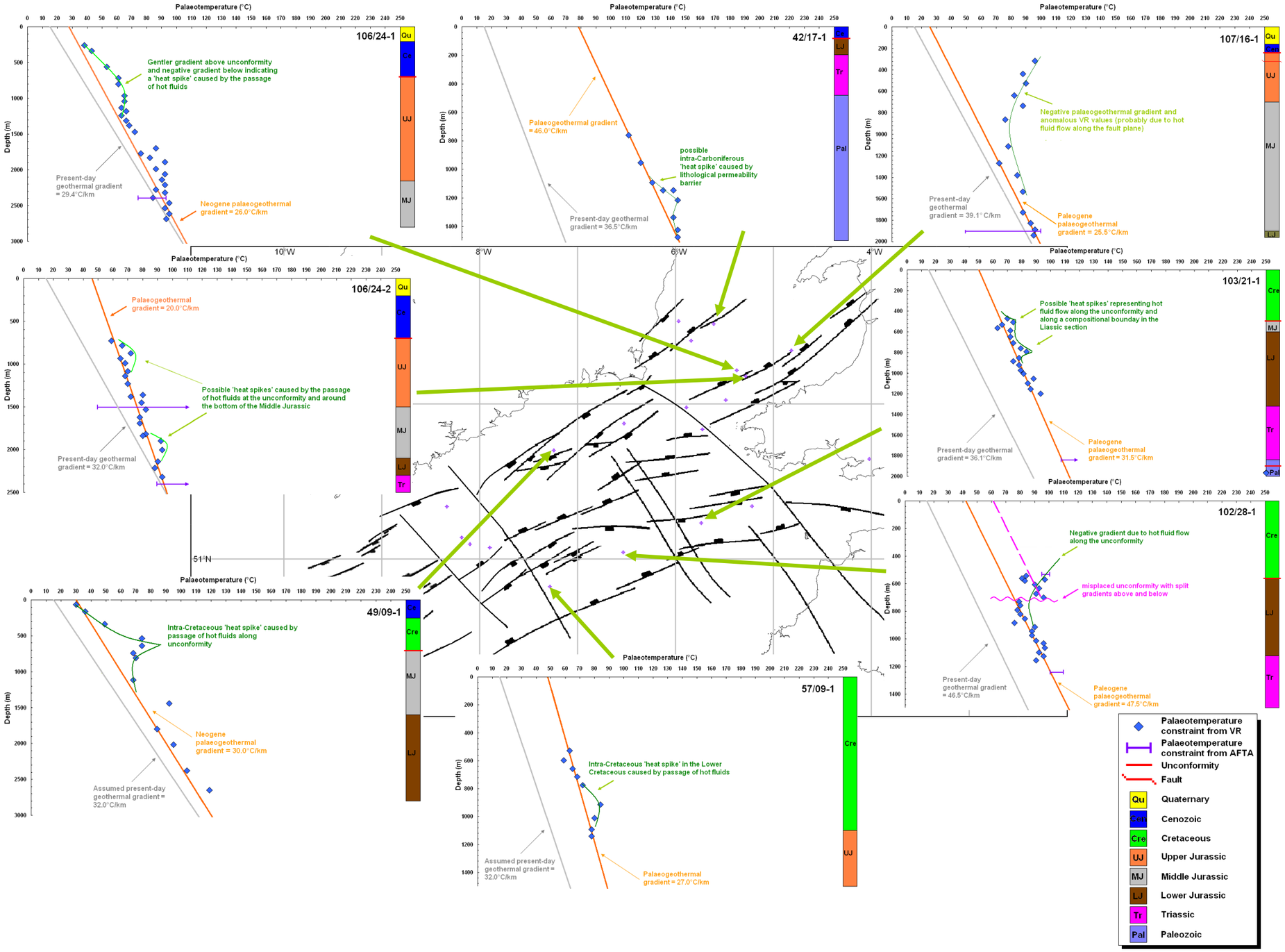

Figure 5.30 - Map showing the distribution of VR temperature-depth plots which indicate elevated palaeotemperatures were due primarily to deeper burial but also with evidence of 'heat spikes' from fluid flow. (faults based on Van Hoorn, 1987*a* and Petrie *et al.* 1989).

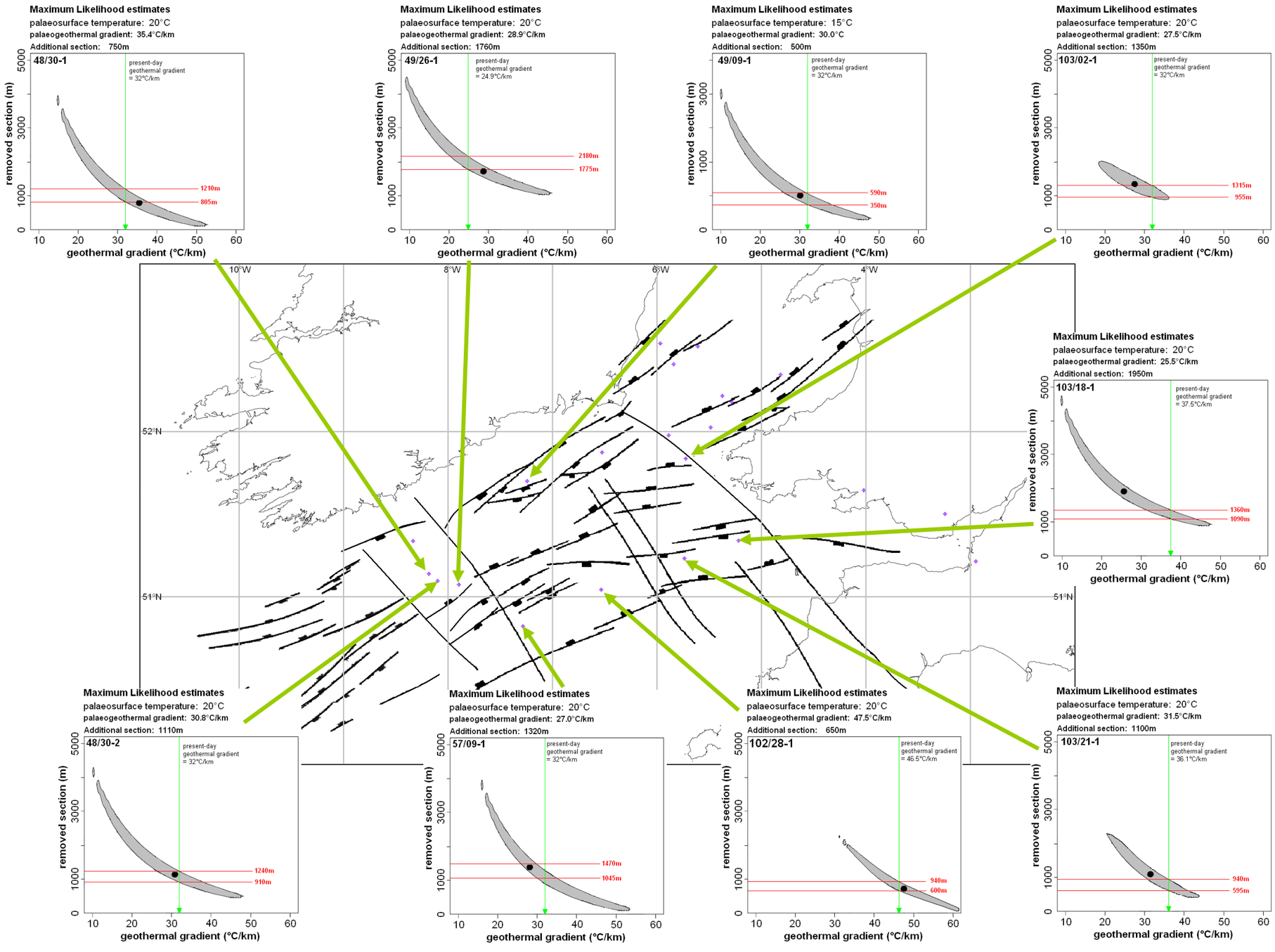

Figure 5.31 – Map showing the distribution and amount of additional section and palaeogeothermal gradients required to explain the palaeothermal episodes recognised in the VR data. The shaded region defines the allowed range of values for each parameter that are consistent with the measured palaeotemperature constraints within 95% confidence limits. Black dots represent the maximum likelihood estimates. Red horizontal bars indicate the range of exhumation estimates assuming no change in the present-day geothermal gradient.

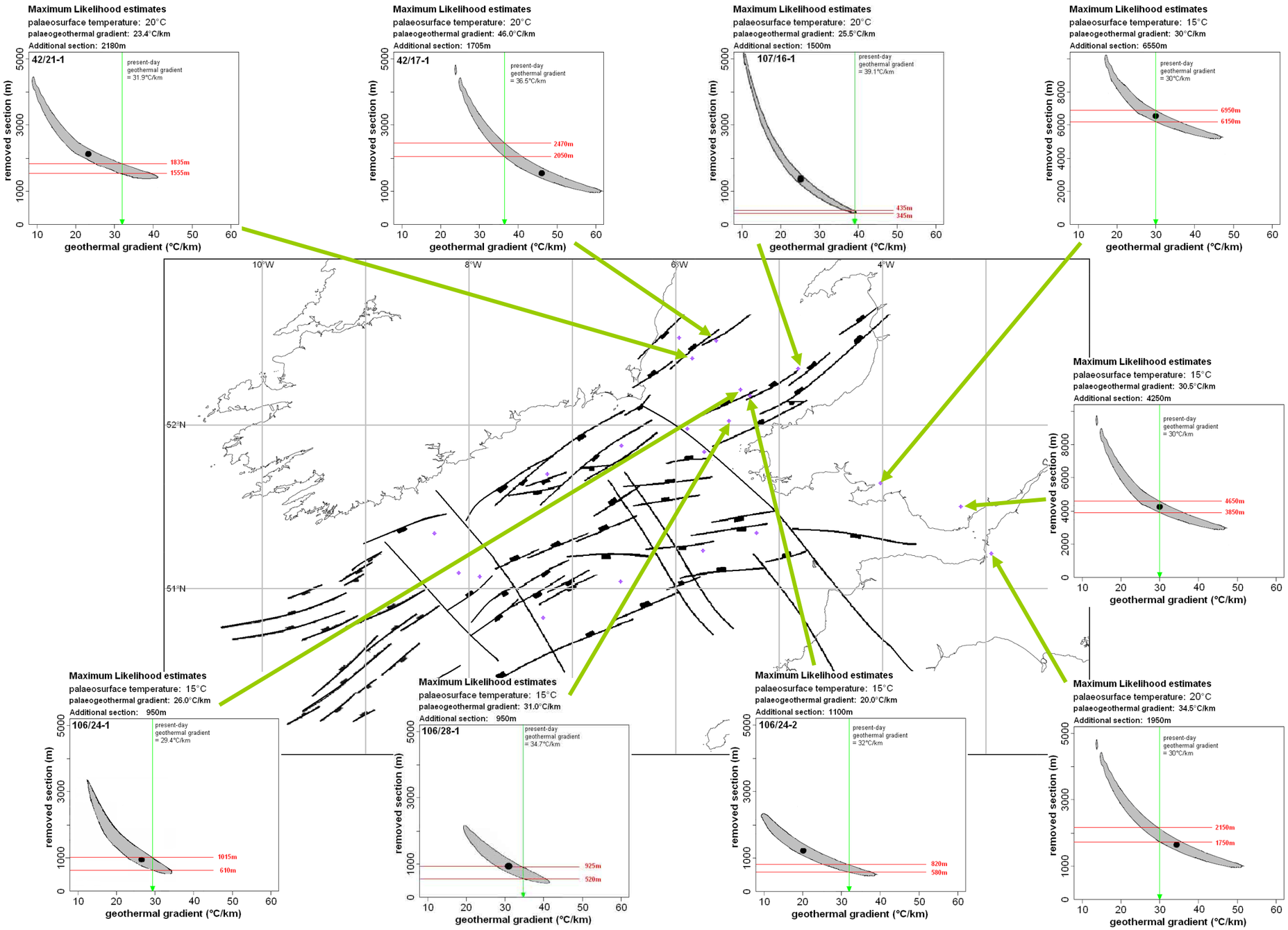

Figure 5.32 – Map showing the distribution and amount of additional section and palaeogeothermal gradients required to explain the palaeothermal episodes recognised in the VR data. The shaded region defines the allowed range of values for each parameter that are consistent with the measured palaeotemperature constraints within 95% confidence limits. Black dots represent the maximum likelihood estimates. Red horizontal bars indicate the range of exhumation estimates assuming no change in the present-day geothermal gradient.

5.3.3.4.1: Wells which show evidence of elevated palaeotemperature due to deeper burial

5.3.3.4.1.1: Exploration well 42/21-1

Well 42/21-1 tested the southern SGCB, where it penetrated a Middle and Lower Jurassic sequence consisting largely of shale (Figure 5.33). Fission-track data published by Green *et al.* (2001) suggests that only two uplift events occurred in the region surrounding this well, with around 2000m of uplift at the end of the Cretaceous and another 1000m during the Miocene. Williams (2002) reported that a geothermal gradient of 26°C/km, together with 2200m of Paleocene and 1000m of Miocene exhumation provides the best fit to the data. There are little Upper Jurassic sediments preserved in well 42/21-1, even though a very thick sequence (up to 3000m) occurs in the hangingwall of the St. George's Fault on the opposite flank of the basin. This partially reflects the fact that this part of the SGCB is a large half-graben hinged along the western flank of the basin; even so, a large proportion of the section eroded during Paleogene basin inversion must have consisted of Upper Jurassic rocks.

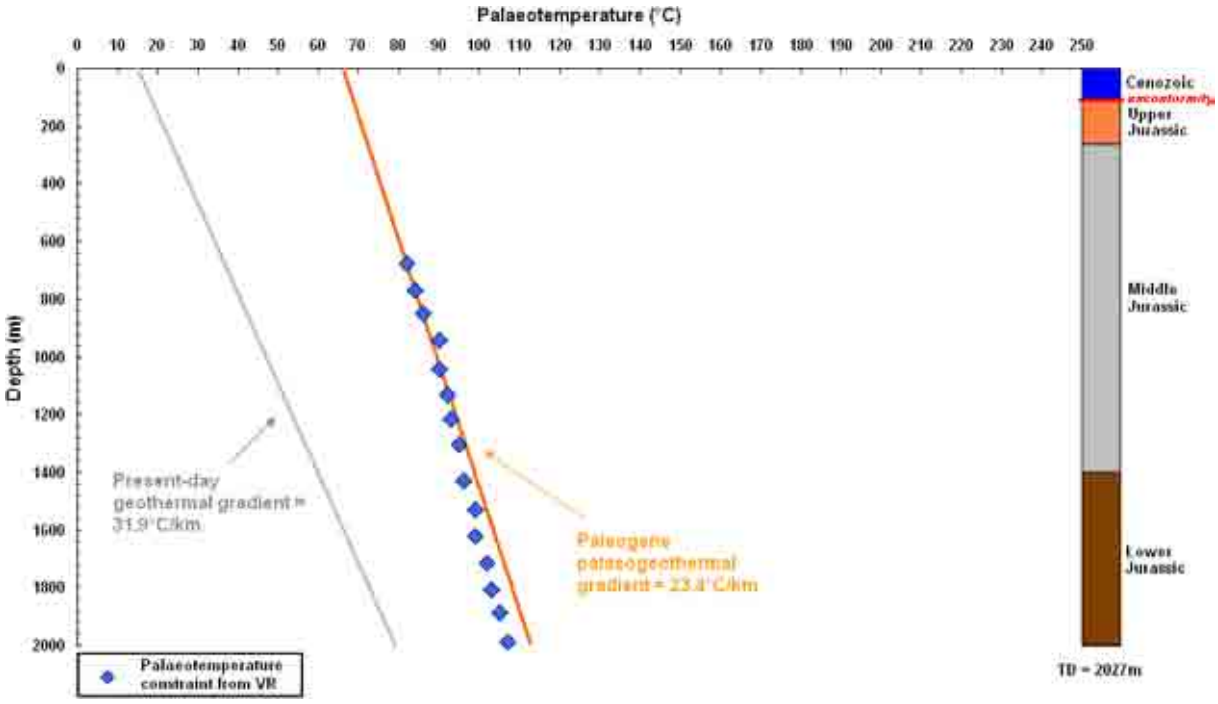

Figure 5.33 – Palaeotemperature constraints from VR data from well 42/21-1 plotted against depth. These are used to infer palaeotemperature profiles prior to the Paleogene cooling episode as defined by the AFTA data of Green *et al.* (2001). A simplified stratigraphic column is also shown.

A present-day geothermal gradient of 31.9°C/km has been defined for well 42/21-1 based on BHT data. As reported by Green *et al.* (2001) in well 42/21-1 an additional 2000m of post-Oxfordian sediment was deposited between 155-65Ma, 1500m of which were removed by uplift and erosion between 65-60Ma. This was followed by deposition of 500m of sediment between 60-15Ma with 1000m removed by uplift and erosion in the Neogene (15-2Ma). Based on the VR data presented in this study the maximum likelihood estimate of palaeogeothermal gradient prior to Paleogene exhumation is 23.4°C/km (17.4-30.0°C/km at 95% confidence limits) (Figure 5.32). Extrapolation of this gradient to the surface indicates that the preserved Mesozoic succession was more deeply buried by 2180m ±200m (1560-3180 ±200m at 95% confidence limits) prior to Paleogene exhumation (Figure 5.32). This is in excellent agreement with the data presented by Green *et al.* (2001) (Figure 5.34).

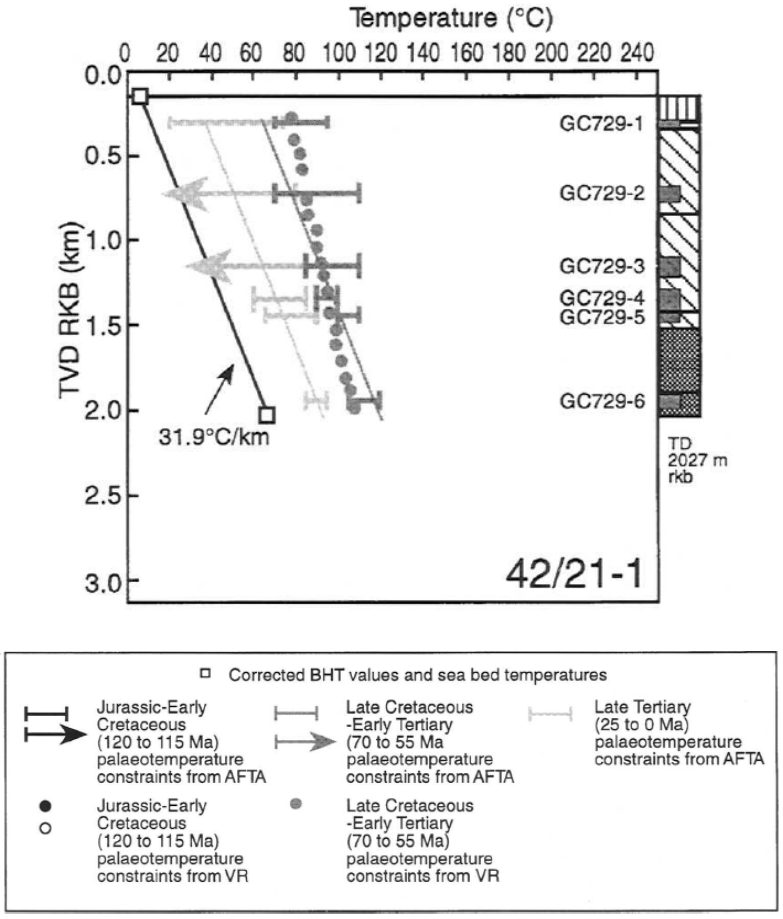

Figure 5.34 - Palaeotemperature constraints derived from AFTA and VR data in individual samples from well 42/21-1 plotted against depth (after Green at al. (2001)).

5.3.3.4.1.2: Exploration well 48/30-1

Well 48/30-1 was drilled on an anticline in the NCSB and consists of a thick Chalk section overlying Jurassic sediments (Figure 5.35). Since no AFTA samples are available for the borehole there is no timing constraint on the exhumation episode(s) but on the basis of preserved stratigraphy (the profile extends up through the Lower Cretaceous into the Chalk) it is inferred to be a Paleogene event The maximum likelihood estimate of palaeogeothermal gradient prior to Paleogene exhumation is 35.4°C/km (30.5-40.3°C/km at 95% confidence limits; Figure 5.31) and extrapolation of this gradient to the surface indicates that the preserved Mesozoic succession was more deeply buried by 750m ±200m (510-1060 ±200m at 95% confidence limits) prior to early Paleogene exhumation (Figure 5.31). Independent verification of this value comes from Spore Colour Index (SCI) data which indicate up to 1432m of additional section prior to Paleogene exhumation.

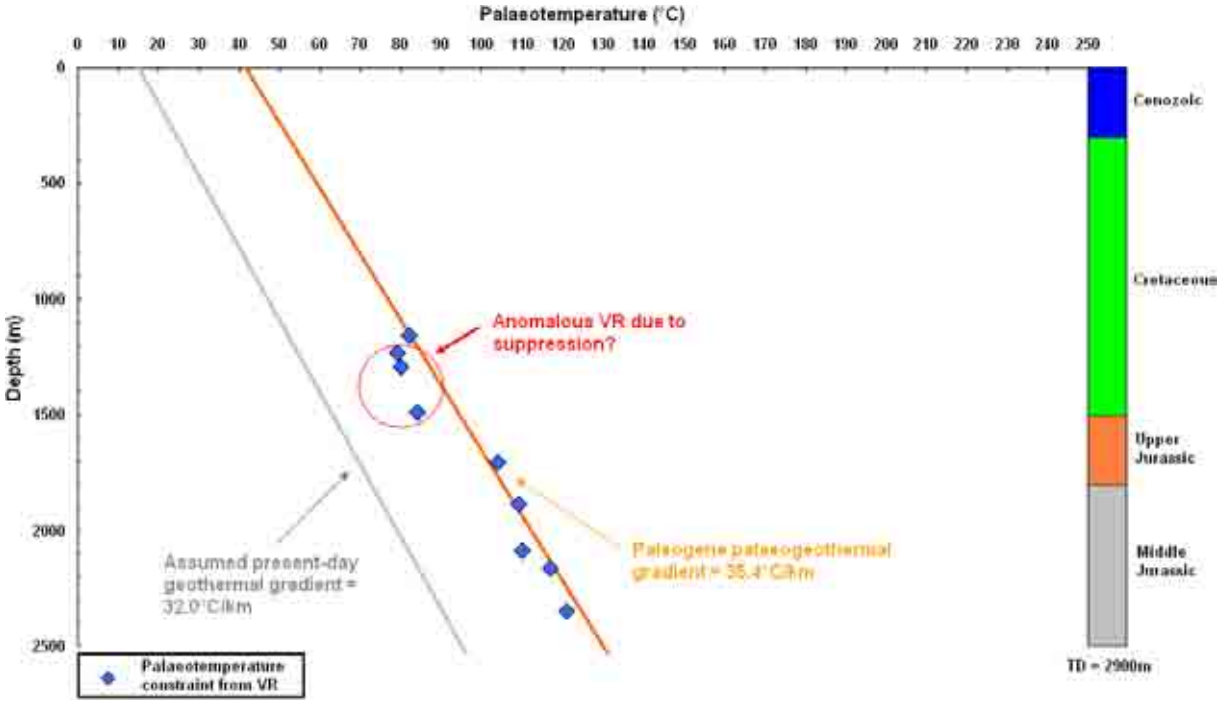

Figure 5.35 – Palaeotemperature constraints from VR data from well 48/30-1 plotted against depth. These are used to infer palaeotemperature profiles prior to the Paleogene cooling episode. A simplified stratigraphic column is also shown.

5.3.3.4.1.3: Exploration well 48/30-2

As with well 48/30-1 this well was drilled near the northern margin of the NCSB. It tested a faulted anticline with the principal objective being Lower Cretaceous Wealden sandstones and secondary objective being Middle-Upper Jurassic sandstones (Figure 5.36).

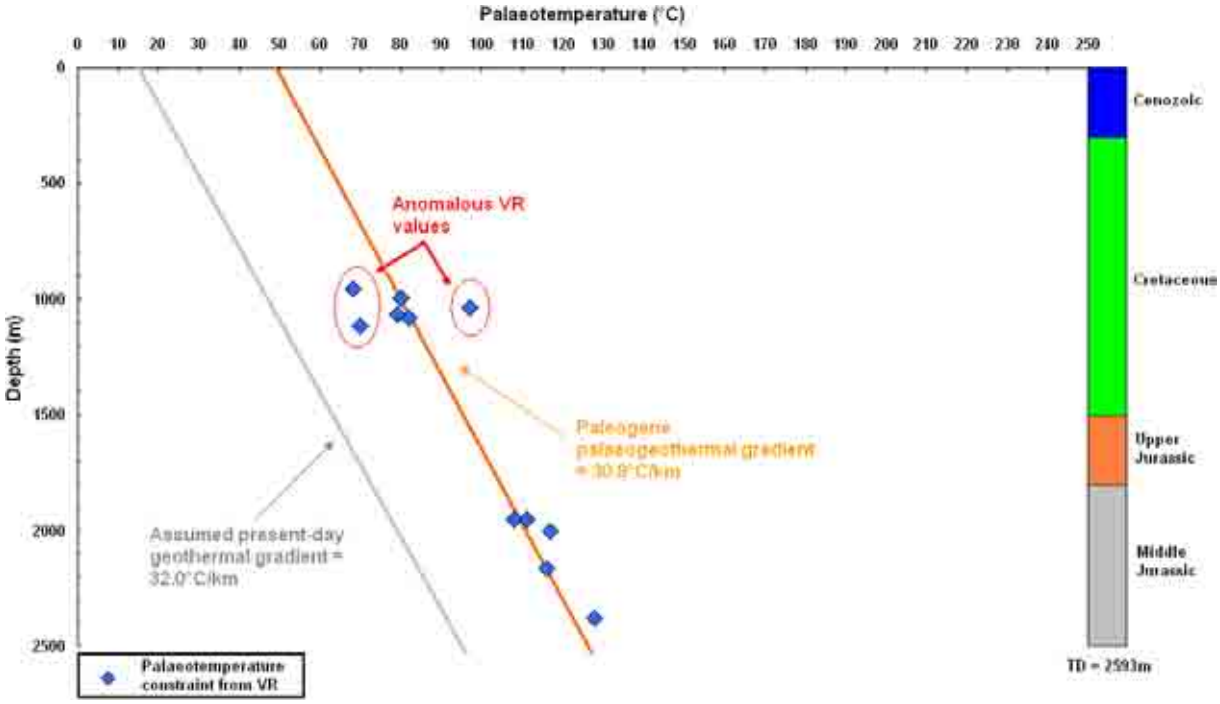

Figure 5.36 – Palaeotemperature constraints from VR data from well 48/30-2 plotted against depth. These are used to infer palaeotemperature profiles prior to the Paleogene cooling episode. A simplified stratigraphic column is also shown.

Since no AFTA samples are available for the borehole there is no timing constraint on the exhumation episode(s) but as with well 48/30-1 it is inferred to be a Paleogene event. There is the possibility of two episodes and/or a 'heat spike' in the Upper Cretaceous as the profile is not continuous through the Cretaceous. However the interpretation here assumes that the wayward VR data in the Cretaceous is detrital or suppressed. The maximum likelihood estimate of palaeogeothermal gradient prior to Paleogene exhumation is 30.8°C/km (25.2-36.4°C/km at 95% confidence limits; Figure 5.31). Additional section of 1110m ±200m (790-1580 ±200m at 95% confidence limits) prior to Paleogene exhumation (Figure 5.31) is inferred for the Mesozoic section. As with well 48/30-1 SCI data offer independent

verification of the amount of additional section. For this well SCI allows up to 1487m of additional section prior to Paleogene exhumation.

5.3.3.4.1.4: Exploration Well 49/26-1a

Well 49/26-1a tested the Blackrock structure in the NCSB. The primary objective was the Wealden sands. Corrected BHT data define a linear present-day geothermal gradient of 24.9°C/km (Figure 5.37). Since no AFTA samples are available for the borehole there is no timing constraint on the exhumation episode(s) but since the VR data extend throughout the Cretaceous into the Upper Cretaceous Chalk the event is inferred to be Paleogene. There appears to be a second gradient fitting the data to the left of the preferred gradient. This data is interpreted as being anomalous due to detrital VR and has been discounted in further analysis of this well. The maximum likelihood estimate of palaeogeothermal gradient prior to Paleogene exhumation is 28.9°C/km (24.8-33.0°C/km at 95% confidence limits; Figure 5.31) Extrapolating of the palaeogeothermal gradient indicates that the preserved Mesozoic succession was more deeply buried by 1760m ±200m (1400-2240 ±200m at 95% confidence limits) prior to Paleogene exhumation (Figure 5.31). This is consistent with independent evidence from SCI data which indicates the preserved section has been more deeply buried by 2221m prior to Paleogene exhumation.

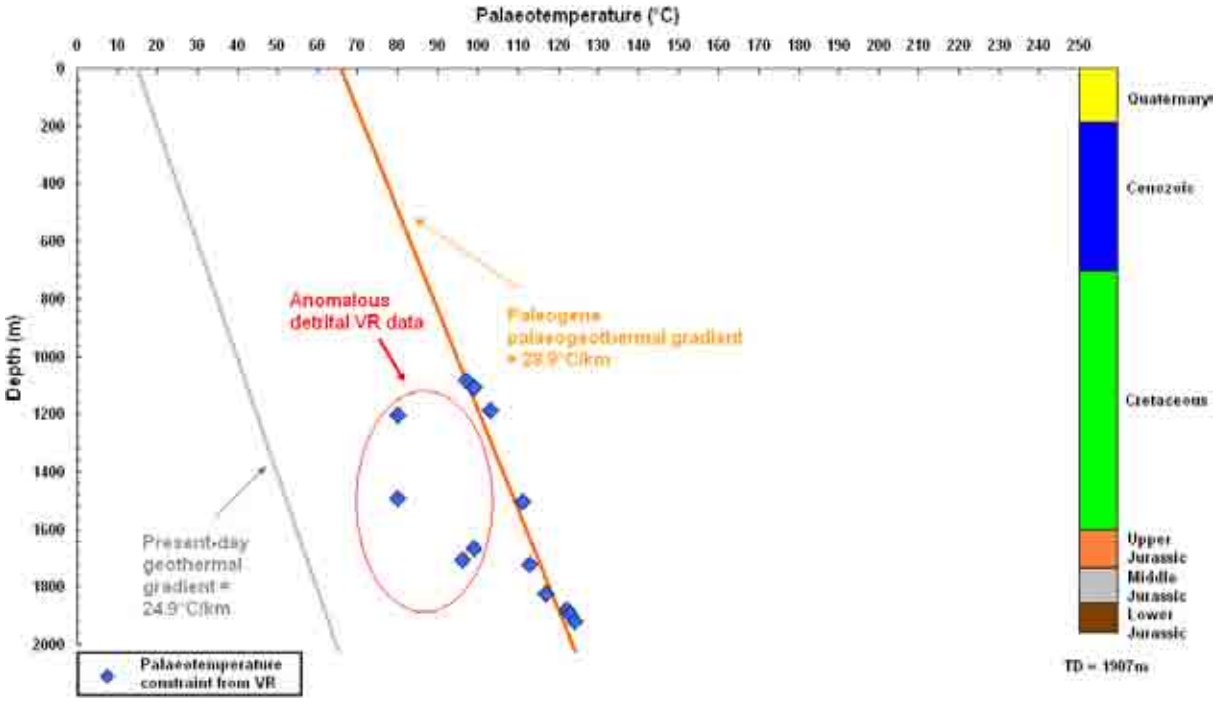

Figure 5.37 – Palaeotemperature constraints from VR data from well 49/26-1a plotted against depth. These are used to infer palaeotemperature profiles prior to the Paleogene cooling episode. A simplified stratigraphic column is also shown.

5.3.3.4.1.5: Exploration Well 103/02-1

This well, which is located on the SE margin of the SGCB, drilled the crest of a large rollover anticline cored by a salt dome (Figure 5.38; Williams, 2002). Middle Jurassic rocks subcrop a Quaternary glacial sequence on the crest of the anticline, and it is likely that three phases of exhumation combined to remove a thick Upper Jurassic, Cretaceous and Cenozoic sequence. Williams (2002) presented a burial history model for this well incorporating 800m of Miocene, 1000m of Paleocene and a further 1000m of Early Cretaceous uplift which gave a reasonably good fit to measured maturity data when combined with a constant geothermal gradient of 26°C/km. The complete absence of Cenozoic sediments from the crest of this fold probably reflects enhanced uplift in response to salt diapirism during the Miocene. Again, this interpretation is not unique; for example, the exact timing of salt movement is difficult to constrain because such movement could have occurred during Paleogene exhumation. This

dataset is re-evaluated in light of new palaeothermal data available in the form of 2 AFTA samples as well as the 32 VR samples taken from the core of well 103/02-1.

Five corrected bottom-hole temperature (BHT) measurements have been used to define a present-day geothermal gradient of 36.2°C/km for well 103/02-1 (Figure 5.39). It is apparent from Figure 5.39 that the VR-derived palaeotemperatures show some variation with depth. This could be indicative of suppression which results in lower reflectances of marine derived vitrinite in comparison to thermally equivalent terrestrially derived vitrinite (Beardsmore & Cull, 2001). However the measured reflectances agree with the AFTA suggesting no suppression in the interpreted interval.

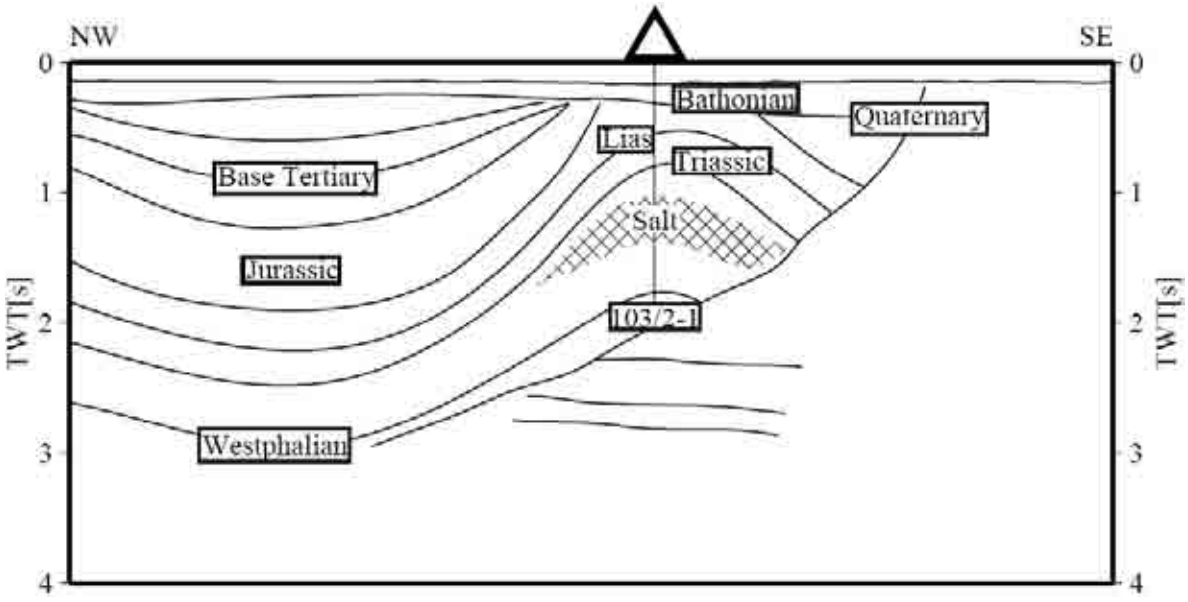

Figure 5.38 - Geoseismic section through well 103/02-1. The well penetrated the crest of an anticline which has been exhumed during three phases of basin inversion. Cenozoic exhumation was probably enhanced by salt diapirism (after Williams, 2002).

Two AFTA samples are available for well 103/02-1 both near the bottom of the well. At first sight, both samples suggest maximum temperature at the present-day. But VR data clearly show that the units from which these samples were taken have been hotter in the past, indicating that present-day temperatures have been overestimated. Track length data suggest

that a present-day geothermal gradient of 32°C/km may be more appropriate, and it is this value which has been used for interpreting the AFTA data. Sample GC420-107 cooled from maximum palaeotemperatures of 105-115°C beginning between 85 and 35Ma. Sample GC420-108 shows a similar history cooling from maximum palaeotemperatures of>105°C between 80-15Ma.

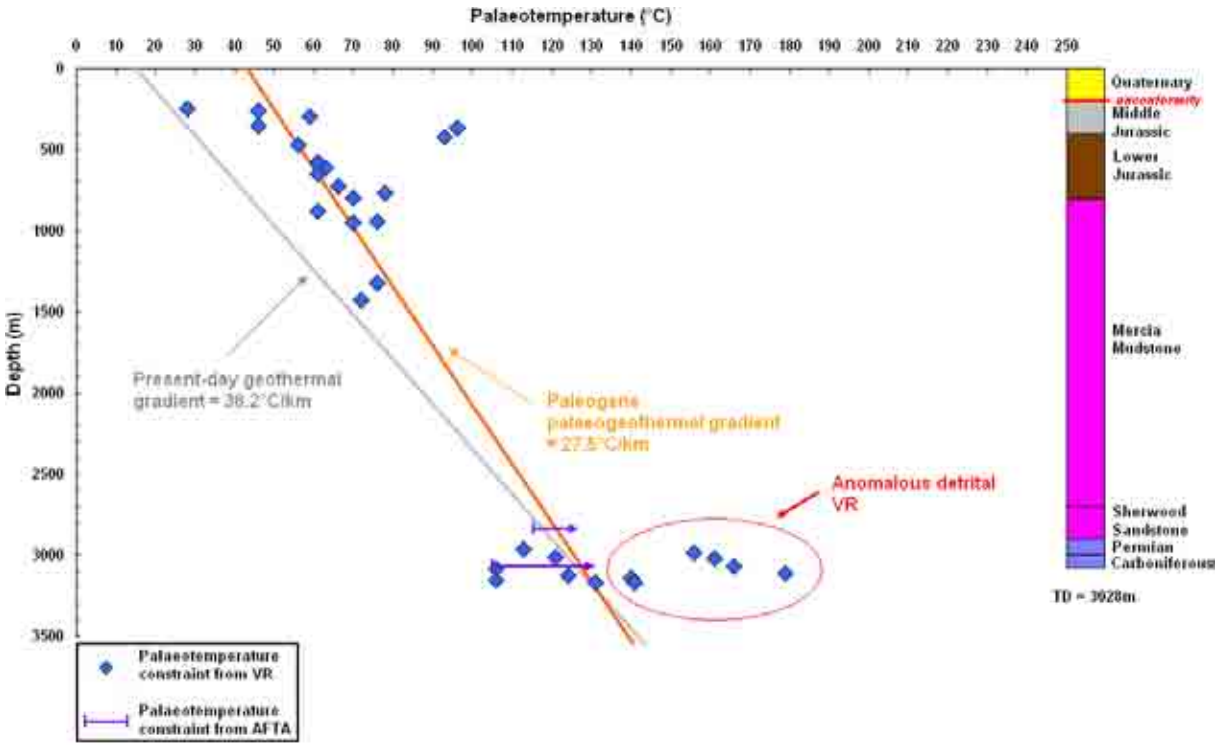

Figure 5.39 – Palaeotemperature constraints from AFTA and VR data from well 103/02-1 plotted against depth. These are used to infer palaeotemperature profiles prior to the Paleogene cooling episode. A simplified stratigraphic column is also shown.

The maximum likelihood estimate of palaeogeothermal gradient prior to Paleogene exhumation is 27.5°C/km (26.0-29.5°C/km at 95% confidence limits; Figure 5.31). Extrapolating the fitted palaeotemperature profiles to the surface indicates that the preserved Mesozoic-Paleozoic succession was more deeply buried by 1350m ±200m (1200-1550 ±200m at 95% confidence limits) prior to Paleogene exhumation (Figure 5.31).

5.3.3.4.1.6: Exploration Well 106/28-1

Well 106/28-1 was drilled in the footwall of the St. George's Fault, on the SE margin of the SGCB. It penetrated a thick Triassic succession overlain by a thin Lower Jurassic sequence and approximately 0.7km of Eocene-Oligocene sediments. Williams (2002) claimed that this location experienced exhumation during both the early and late Cenozoic. Sonic velocity data from the Triassic succession indicate deeper burial by 1.24km of now eroded overburden (Williams, 2002).

Available thermal history data comprises 18 vitrinite samples, one apatite sample and three BHT measurements. Corrected BHT data allow the definition of a linear present-day geothermal gradient with a value of 34.7°C/km (Figure 5.40). VR derived palaeotemperatures define an approximately linear palaeogeothermal gradient. The palaeotemperature data appear to be largely consistent either side of the Paleogene/Lower Jurassic unconformity, which suggests that maximum palaeotemperatures and probably burial depths were reached following Paleogene/post-Paleogene burial.

The single AFTA sample from this well (GC399-5) provides useful constraints on palaeotemperatures in the deeper parts of the section, where VR data are unavailable due to the terrestrial origin of the Triassic succession. The fission track age of this sample (129.3 ±21.6Ma) is significantly younger than its Lower Triassic depositional age and thermal history modelling of AFTA parameters reveals evidence for one palaeothermal episode, involving cooling from a palaeotemperature of 90-110°C at some point following deposition (Holford, 2006; Figure 5.41).

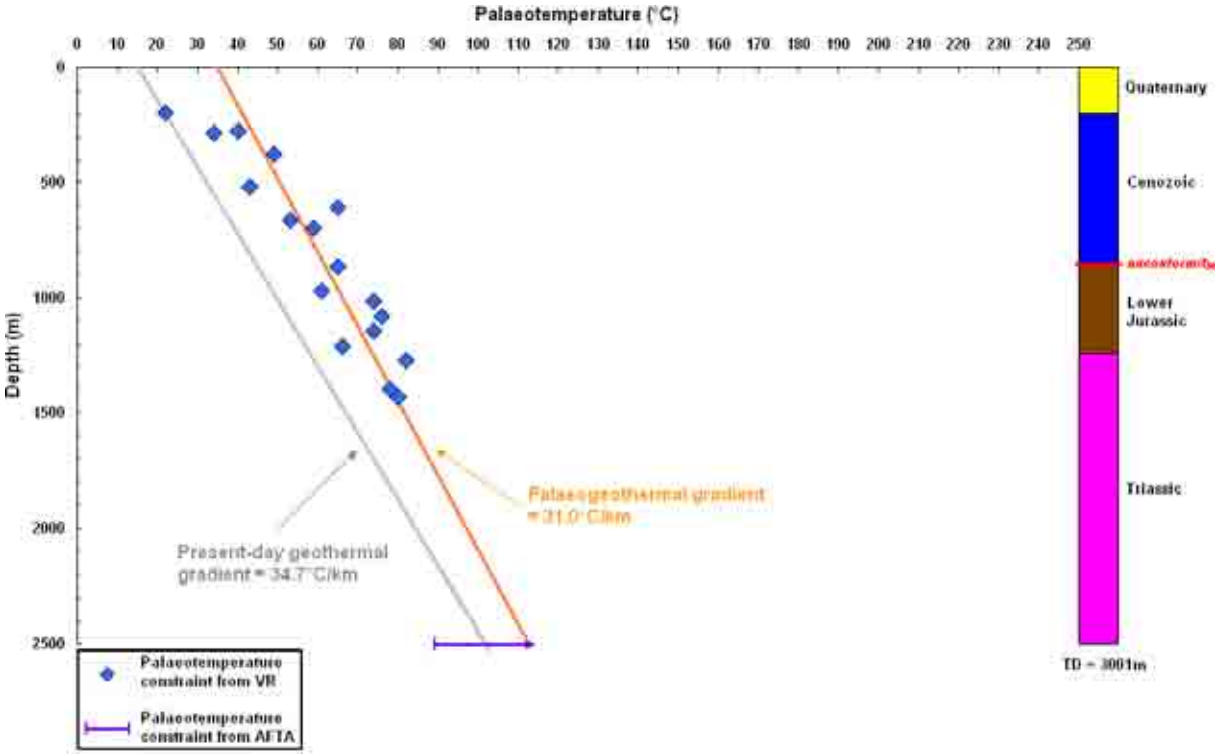

Figure 5.40 – Palaeotemperature constraints from AFTA and VR data from well 106/28-1 plotted against depth. These are used to infer palaeotemperature profiles prior to the Neogene cooling episode. A simplified stratigraphic column is also shown.

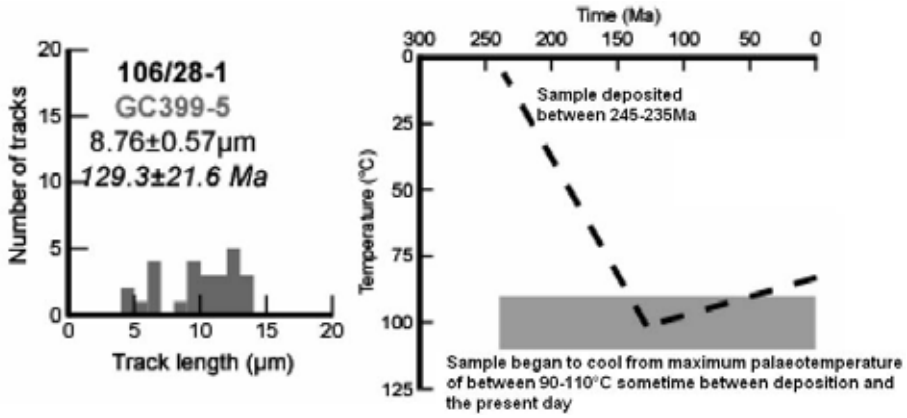

Figure 5.41 – Fission-track length distribution and accompanying thermal history solution for AFTA sample from exploration well 106/28-1 in the SGCB (after Holford, 2006).

Although this sample provides no constraint on the timing of cooling therefore, the range of palaeotemperatures indicated by AFTA are in good agreement with a palaeotemperature profile fitted to the palaeothermal constraints from VR (Figure 5.40). This suggests that the palaeotemperatures from AFTA record deeper burial during the Paleogene or later. The maximum likelihood estimate of the value of the palaeogeothermal gradient is 31°C/km (21-

39.5°C/km within 95% confidence limits), whilst extrapolation of this profile to an assumed palaeosurface temperature of 15°C yields a maximum likelihood estimate of 0.95km of additional section (0.55-1.75km within 95% confidence limits) deposited prior to post-Oligocene exhumation (Figure 5.32).

Assuming a palaeogeothermal gradient with a value equivalent to that of the present-day gradient (34.7°C/km) indicates that the preserved section in this well was more deeply buried by an additional 650-900m of Paleogene-Neogene section which was removed during mid-Miocene exhumation. This estimate is in broad agreement with the amount of deeper burial inferred from sonic velocity data (*c.* 1.24km). Holford (2006) presented a burial history plot for this well which incorporated *c.* 0.7km of late Cretaceous-early Paleogene exhumation (inferred on the basis of seismic reflection data (*cf.* Williams, 2002)), but since maximum palaeotemperatures and burial depths were attained following Eocene-Oligocene burial, no useful constraints on the magnitude of this exhumation can be determined from palaeothermal data.

5.3.3.4.2: Wells which show evidence of the passage of hot fluids

5.3.3.4.2.1: Exploration well 42/17-1

This well penetrated the NW margin of the SGCB (though some workers have considered the well to lie in the Central Irish Sea Basin e.g. Corcoran & Clayton, 1999 and Green *et al.* 2001) where Mercia Mudstone Group sediments subcrop a thin veneer of Lower Jurassic and Quaternary deposits (Figure 5.42). Williams (2002) reported that a burial history incorporating 2000m of exhumation and a geothermal gradient of 40°C/km provides the best fit to measured maturity values in well 42/17-1.

Westphalian coal-bearing sediments offer the only source of vitrinite in this well; maximum palaeotemperatures could therefore have occurred at any time from the Stephanian to the Neogene. Williams' (2002) model assumes that the Carboniferous section reached its maximum burial depth prior to Early Cretaceous exhumation and subsequent uplift events did not exceed 2000m. Regional post-rift thermal subsidence occurred throughout the Upper Cretaceous and Palaeogene, and sediment units deposited throughout both of these periods would have had a relatively constant thickness over the entire region. A maximum of 2000m of denudation is in good agreement with estimates of exhumation based on the sonic velocity log, although Green *et al.* (2001) favoured 3000m of Early Cretaceous and 2000m of Late Cretaceous exhumation based on a lower geothermal gradient of 36.5°C/km and a palaeosurface temperature of 6°C.

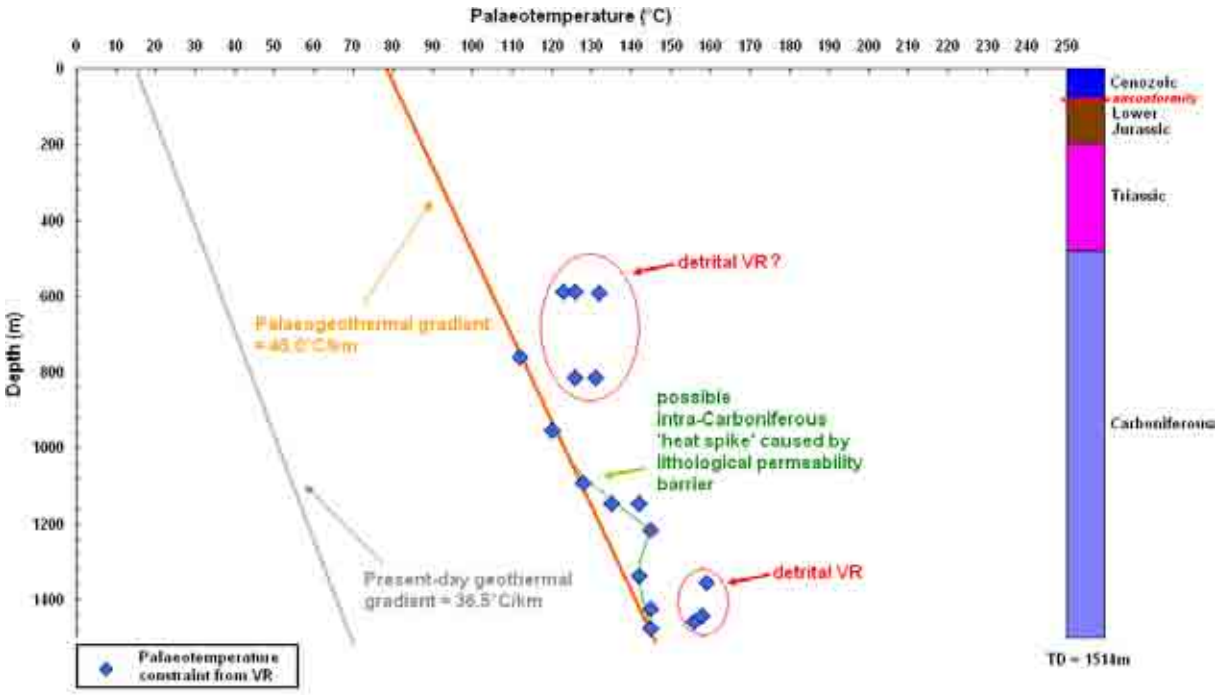

Figure 5.42 – Palaeotemperature constraints from VR data from well 42/17-1 plotted against depth. These are used to infer palaeotemperature profiles prior to the cooling episode. A simplified stratigraphic column is also shown.

The VR data allows a number of different interpretations to fit the data in addition to the favoured gradient. For instance there is the possibility of a 'heat spike' being present in the Carboniferous section. The reason for this spike could be due to a change of lithology in the section (e.g. sand encased in mudstone acting as a conduit for hydrothermal fluid) or could represent anomalous VR values due to caving or chemical effects such as suppression. Additionally a much steeper gradient could be fitted to the VR which supports the 'heat spike' meaning the rocks will have been more deeply buried than indicated by the favoured gradient. However the favoured interpretation discounts these possibilities. The results of this study are in close agreement with those of Green *et al.* (2001) with a best fit gradient of 46.0°C/km (26.8-62.0°C/km at 95% confidence limits) (Figure 5.32). Extrapolation of this gradient to a surface value of 20°C indicates that the preserved Paleozoic-Mesozoic succession was more deeply buried by 1705m ±200m (1120-4370 ±200m at 95% confidence limits; Figure 5.32).

5.3.3.4.2.2: Exploration Well 49/09-1

Well 49/09-1 was drilled on the northern margin of the NCSB in the hangingwall of the main basin controlling fault and encountered a thick Jurassic succession overlain by Cretaceous Chalk and Cenozoic rocks (Figure 5.43).

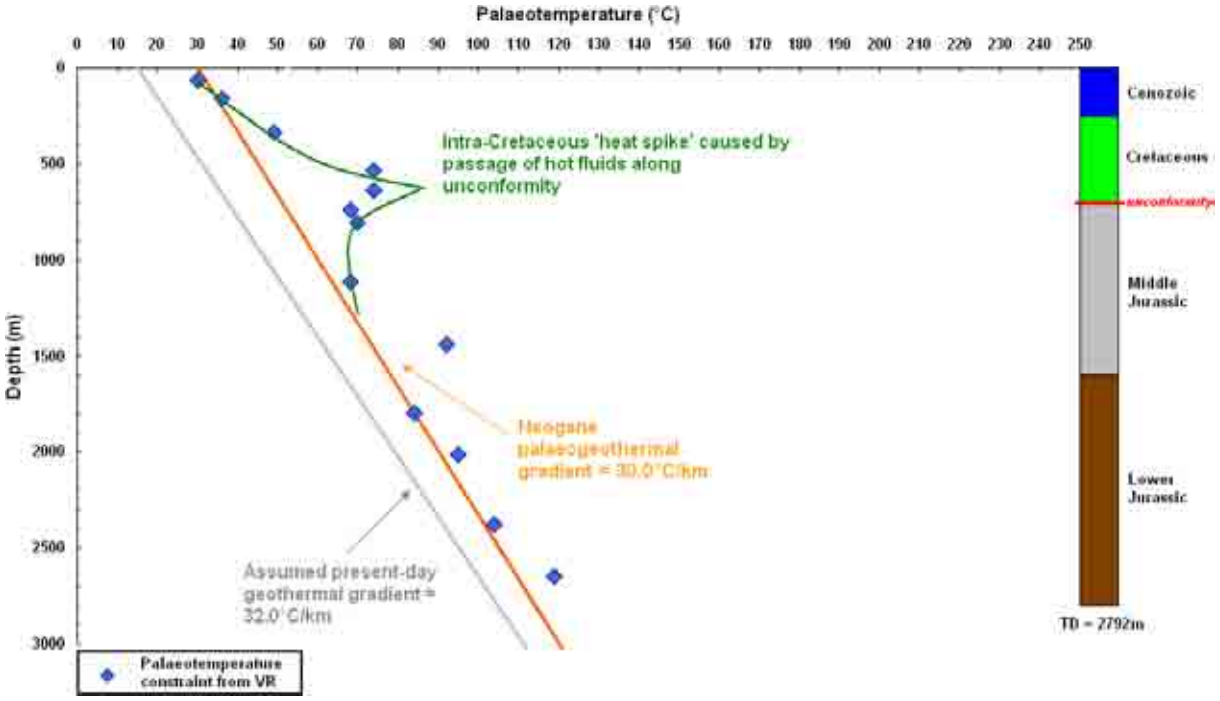

Figure 5.43 – Palaeotemperature constraints from VR data from well 49/09-1 plotted against depth. These are used to infer palaeotemperature profiles prior to the cooling episode. A simplified stratigraphic column is also shown. Note the intra-Cretaceous 'heat spike' just above the unconformity. This is interpreted as having been caused by the passage of hot fluids.

This well shows clear evidence for a 'heat spike' in the Cretaceous section and additionally it is possible to see a shallower gradient in the section above the unconformity. Those VR samples above the unconformity are inferred to have been affected by the passage of hot fluids along the unconformity. Since the well does not lie near to any igneous intrusions or volcanic centres the source of this hot fluid is due to the expulsion of fluids during compression which is consistent with the location of the well in the hangingwall of the basin controlling normal fault.

The passage of this hot fluid makes interpretation of the palaeogeothermal gradient difficult; however in this study a Neogene gradient close to the present-day gradient is inferred. The palaeogeothermal gradient prior to Neogene exhumation gives a best fit gradient of 30.0°C/km which corresponds to deeper burial of *c.* 500m (Figure 5.31).

5.3.3.4.2.3: Exploration Well 57/09-1

Well 57/09-1 was drilled near the southern margin of the NCSB close to the basin bounding fault and encountered a thick sequence of Cretaceous and Jurassic rocks (Figure 5.44).

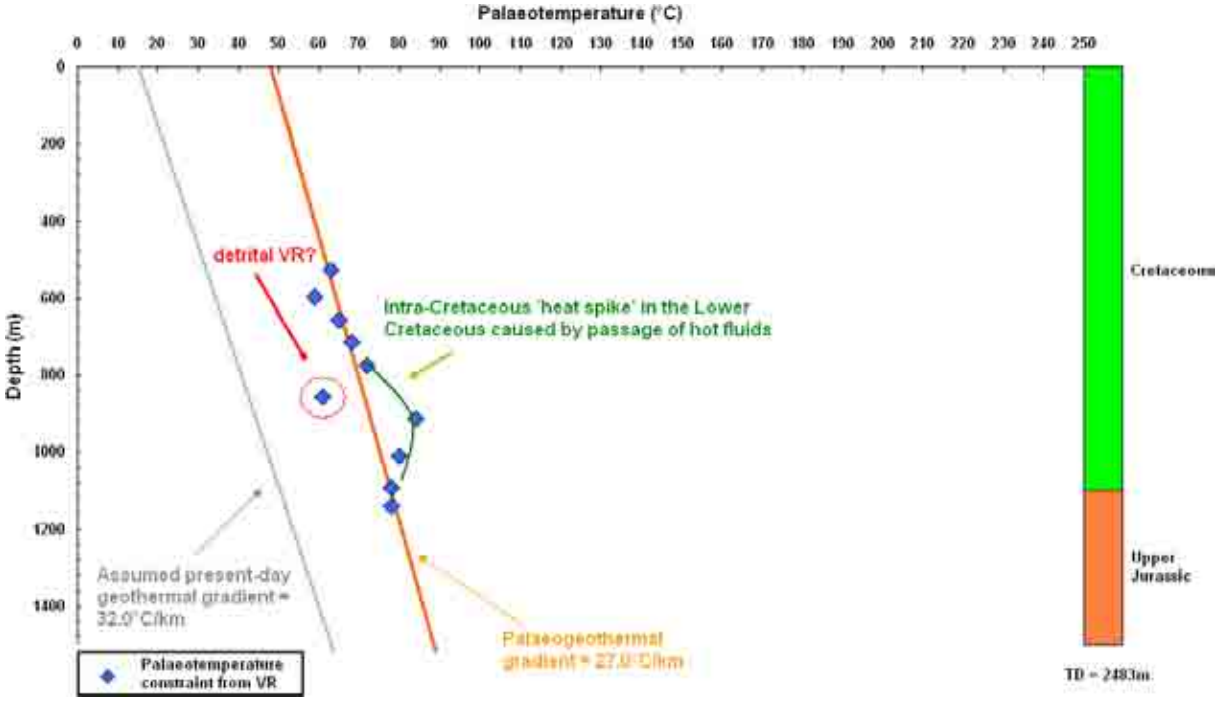

Figure 5.44 – Palaeotemperature constraints from VR data from well 57/09-1 plotted against depth. These are used to infer palaeotemperature profiles prior to the cooling episode. A simplified stratigraphic column is also shown. The point highlighted as detrital VR? could be due to a cave in of the borehole (since it lies on trend with the upper sequence) but without further analysis it is not possible to say much more other than it is 'anomalous'

Since no AFTA samples are available for the borehole there is no timing constraint on the exhumation episode(s) but given the thick sequence of Cretaceous rocks and the absence of Cenozoic rocks the episode is inferred to be Paleogene or later. Additionally there appears to be a 'heat spike' at the base of the Chalk. It is likely to have been caused by the passage of hot fluids and may be localised here as the higher porosity chalk lies above the less permeable Lower Cretaceous clays. The maximum likelihood estimate of palaeogeothermal gradient prior to exhumation is 27.0°C/km (24.8-54.6°C/km at 95% confidence limits; Figure 5.31). Extrapolation of this gradient to the surface indicates that the preserved Mesozoic succession

was more deeply buried by 1320m ±200m (350-1410 ±200m at 95% confidence limits) prior to exhumation (Figure 5.31).

5.3.3.4.2.4: Exploration Well 102/28-1

Well 102/28-1 was drilled in the SCSB and encountered a thick Cretaceous sequence lying unconformably above Lower Jurassic and Triassic rocks (Figure 5.45). Here, the first study of palaeothermal (AFTA and VR) data from well 102/28-1 is presented. The thermal history dataset consists of 13 VR samples and 2 AFTA samples taken from the core of well 102/28-1.

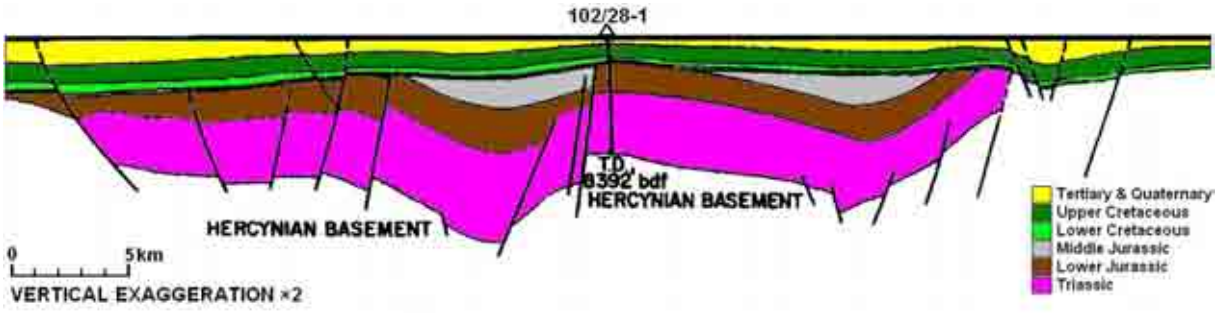

Figure 5.45 - Geoseismic section through well 102/28-1. The well penetrated the eroded northern limb of a syncline formed during Early Cretaceous basin inversion (modified after Kamerling, 1979).

Five corrected bottom-hole temperature (BHT) measurements have been used to define a present-day geothermal gradient of 46.5°C/km for well 102/28-1 (Figure 5.46). It is apparent from Figure 5.46 that the VR-derived palaeotemperatures show some variation with depth, especially within the Liassic section close to the unconformity. This could indicate that the lower samples are suppressed since suppression commonly affects marine hydrogen-rich facies such as the Lower Jurassic mudstones (Scotchman, 2001). Alternatively hot fluid circulation could have led to the higher VR values close to the unconformity. Since the measured reflectances agree with the AFTA it is suggested that hot fluid flow has affected both the VR and AFTA in this section rather than the anomalies being due to suppression. An alternative view is that the higher values correspond totally to Cretaceous deposition and as such the position of the unconformity has been misinterpreted. This would allow for two

clear palaeogeothermal gradients across the unconformity though no independent evidence for this scenario currently exists.

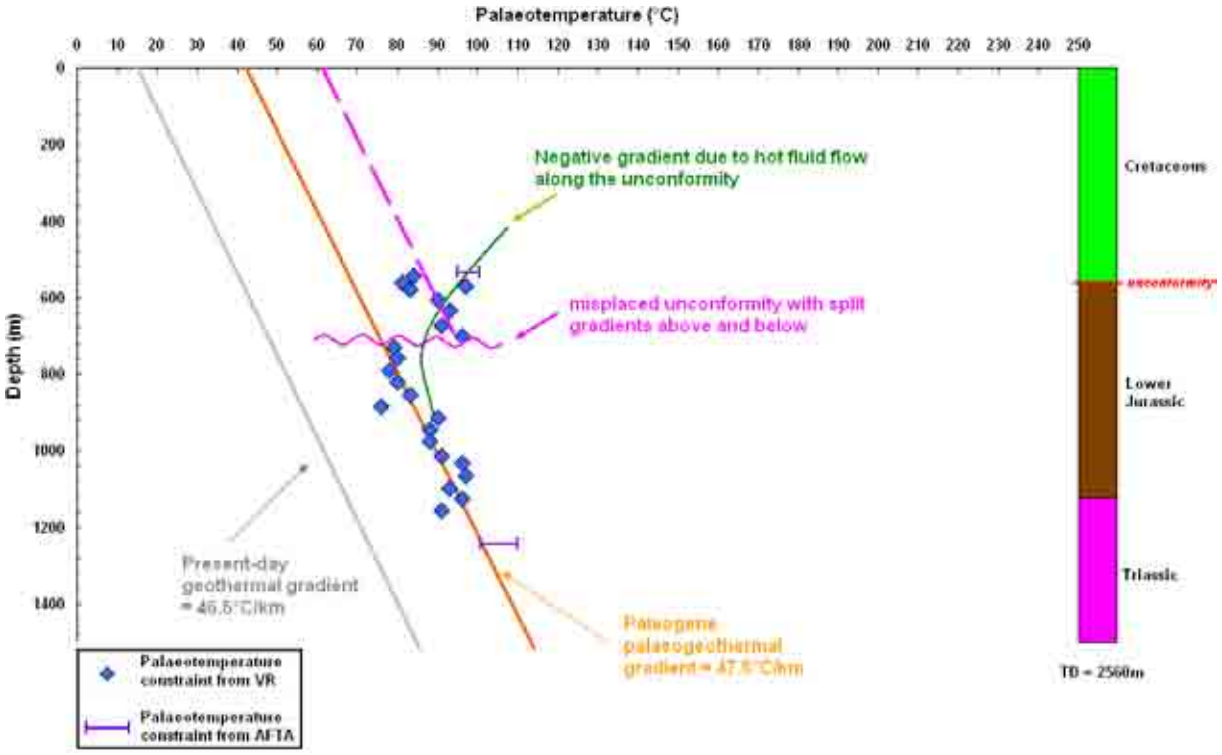

Figure 5.46 – Palaeotemperature constraints from AFTA and VR data from well 102/28-1 plotted against depth. These are used to infer palaeotemperature profiles prior to the Paleogene cooling episode. A simplified stratigraphic column is also shown. The data allow for a number of different interpretations for this well such as hot fluid flow, VR suppression, detrital source for the upper samples and incorrect recognition of the unconformity (see text for discussion).

AFTA sample GC420-84 from the Lower Cretaceous indicates that it cooled from maximum palaeotemperatures of 95-100°C, beginning some time between 65 and 0Ma. For sample GC420-105, AFTA suggests that following deposition in the late Triassic (*c.* 230Ma), sample GC420-105 began to cool from its maximum post-depositional temperature of between 100-110°C in the interval of 100-25Ma (i.e. late Paleocene-Eocene). These results indicate that the palaeogeothermal gradient is Paleogene.

The maximum likelihood estimate of palaeogeothermal gradient prior to Paleogene exhumation is 47.5°C/km (41.0-54.5°C/km at 95% confidence limits; Figure 5.31). Given that the present-day geothermal gradient at well 102/28-1 is 46.5°C/km these results imply

that geothermal gradients at well 102/28-1 have remained relatively constant over time. Extrapolating the fitted palaeotemperature profiles to the surface indicates that the preserved Mesozoic succession was more deeply buried by 650m ±200m (450-900 ±200m at 95% confidence limits) prior to Paleogene exhumation (Figure 5.31).

5.3.3.4.2.5: Exploration Well 103/21-1

Well 103/21-1 was drilled in the southwestern part of the BCB and encountered a sequence of Cretaceous rocks lying unconformably over Jurassic-Triassic rocks which in turn unconformably overly Carboniferous and Devonian rocks (Figure 5.47).

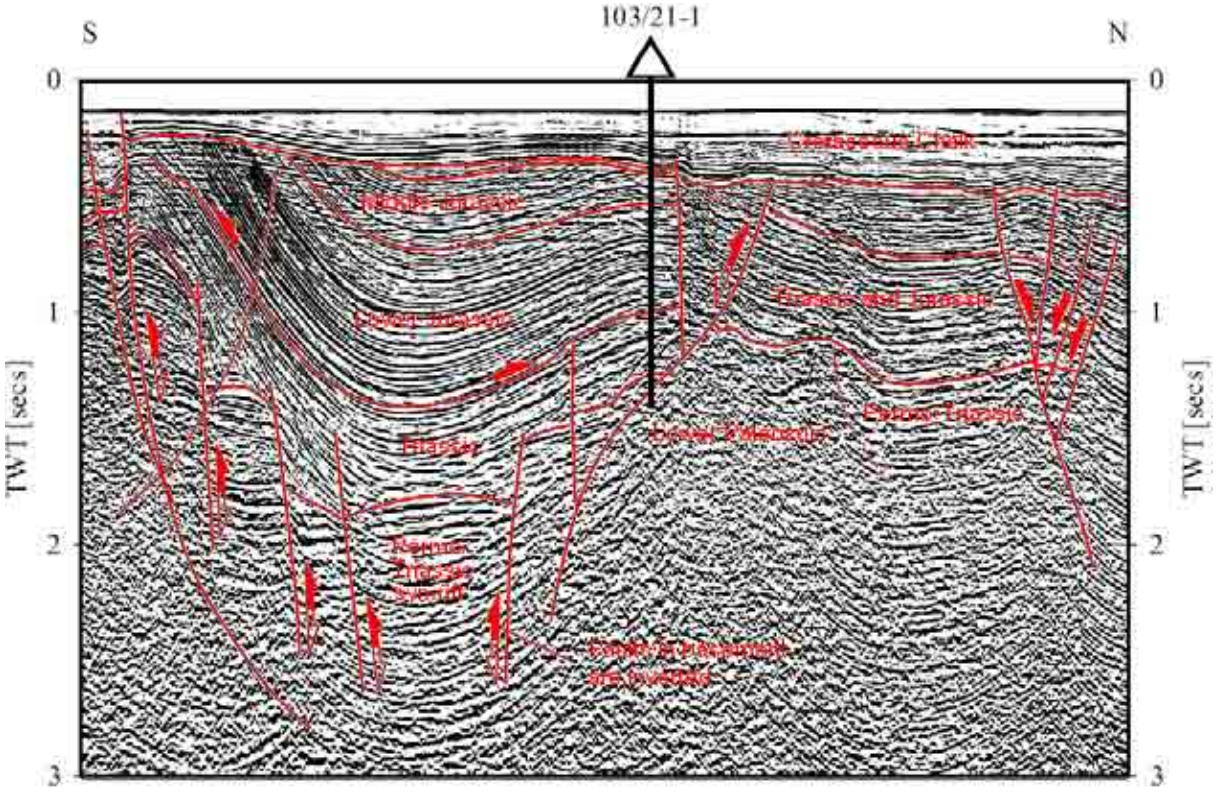

Figure 5.47 - Migrated seismic profile and interpreted geo-seismic section incorporating well 103/21-1 (modified after Williams, 2002).

This study presents the first analysis of palaeothermal (AFTA and VR) data from well 103/21-1. The thermal history dataset consists of 23 VR samples and 1 AFTA sample taken from the core of well 103/21-1. Three corrected bottom-hole temperature (BHT)

measurements have been used to define a present-day geothermal gradient of 36.1°C/km for well 103/21-1 (Figure 5.48). In a plot of palaeotemperature against depth (Figure 5.48), the VR data define a profile that is sub-parallel with the present-day palaeotemperature profile (Figure 5.48). This suggests that heating was due primarily to deeper burial rather than the result of a period of elevated heat flow or hot fluid circulation (*cf.* Green *et al.* 2002). However there is evidence for a small 'heat spikes' in the Lower Jurassic section and around the unconformity, indicating there has been some fluid flow. Additionally there has been significant fluid flow along the Permian-Devonian unconformity resulting in VR derived palaeotemperatures in excess of 250°C probably related to igneous activity, however this episode and the causes of it are beyond the scope of this thesis.

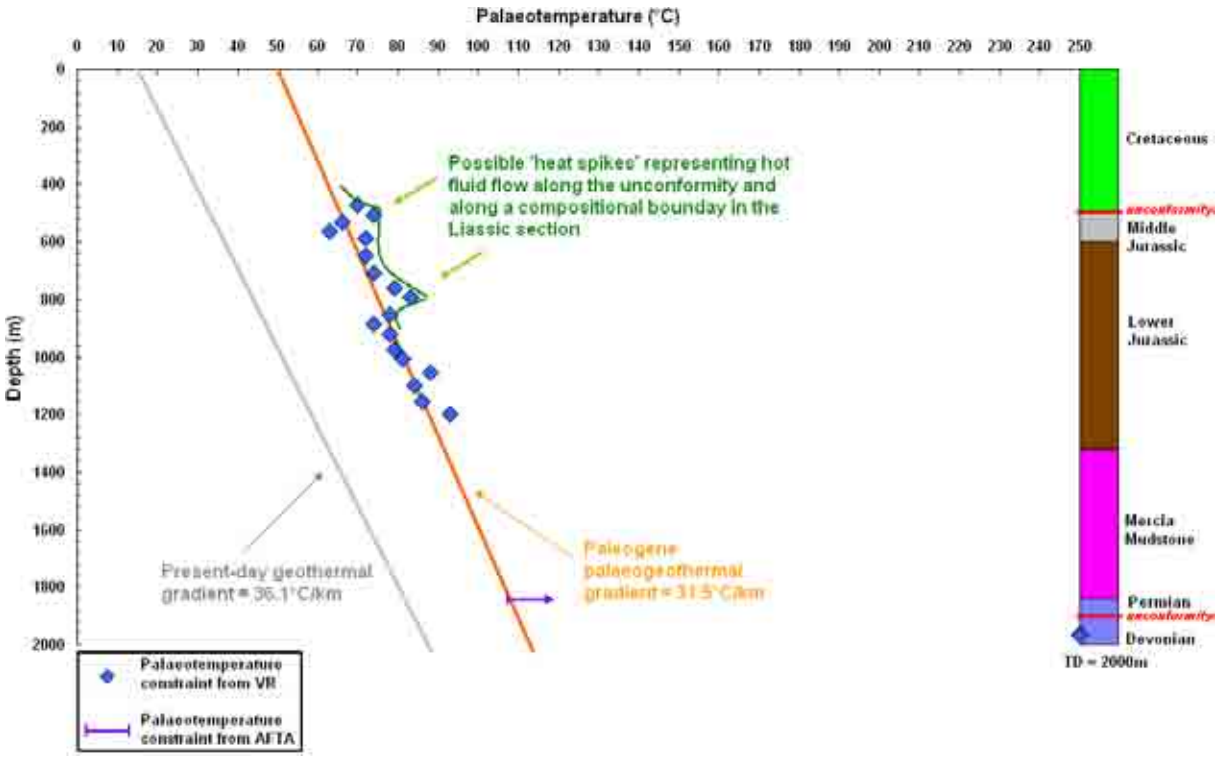

Figure 5.48 – Palaeotemperature constraints from AFTA and VR data from well 103/21-1 plotted against depth. These are used to infer palaeotemperature profiles prior to the Paleogene cooling episode. A simplified stratigraphic column is also shown.

Only one AFTA sample was available for well 103/21-1. AFTA suggests that sample GC420-126 began to cool from its maximum post-depositional temperature of >110°C in the

interval of 75-25Ma (i.e. late Cretaceous-Oligocene). Since the Jurassic and Triassic units within well 103/21-1 had been deposited by *c.* 160Ma (i.e. 95Ma prior to the onset of the cooling episode suggested by AFTA), it can be assumed that the style of thermal history indicated by this sample applies to the entire preserved Mesozoic section within well 103/21-1. The maximum likelihood estimate of palaeogeothermal gradient prior to Paleogene exhumation is 31.5°C/km (28.5-35.0°C/km at 95% confidence limits; Figure 5.31). Extrapolating this gradient to the surface indicates that the preserved Mesozoic-Paleozoic succession was more deeply buried by 1100m ±200m (950-1300 ±200m at 95% confidence limits) prior to Paleogene exhumation (Figure 5.31).

5.3.3.4.2.6: Exploration Well 106/24-1

Well 106/24-1 is located within the main depocentre of the SGCB and penetrated the crest of an anticline which formed during post-Paleogene basin inversion. This well encountered >0.6km of Eocene-Oligocene sediments which rest unconformably upon almost 2km of Upper-Middle Jurassic mudstones (Figure 5.49). Williams (2002) estimated exhumation at this location using seismic reflection data, which shows that ≥0.4s of Paleogene strata has been eroded by the hinge of the anticline penetrated by this well. Interval velocities of the preserved Paleogene succession vary between 2000 and 2500m/s, which equates to >0.4-0.5km of removed section.

Available thermal history data for this well comprise 29 VR samples, a single (Figure 5.50) Middle Jurassic aged AFTA sample (GC399-4; 2408m) and three BHT measurements which define a present-day temperature profile of 29.4°C/km. The VR data from this well indicate a 'heat spike' within the Paleogene and uppermost Jurassic sections (Figure 5.51). Below 1.5km however, the palaeotemperature estimates from VR converge with the present-day temperature profile. The lower VR values within the overall trend have been interpreted to

have been affected by geochemical suppression, resulting in anomalously low reflectances (Carr, 2000). Suppression commonly affects marine hydrogen-rich facies such as the Lower Jurassic mudstones which are widely distributed across the British Isles (Scotchman, 2001).

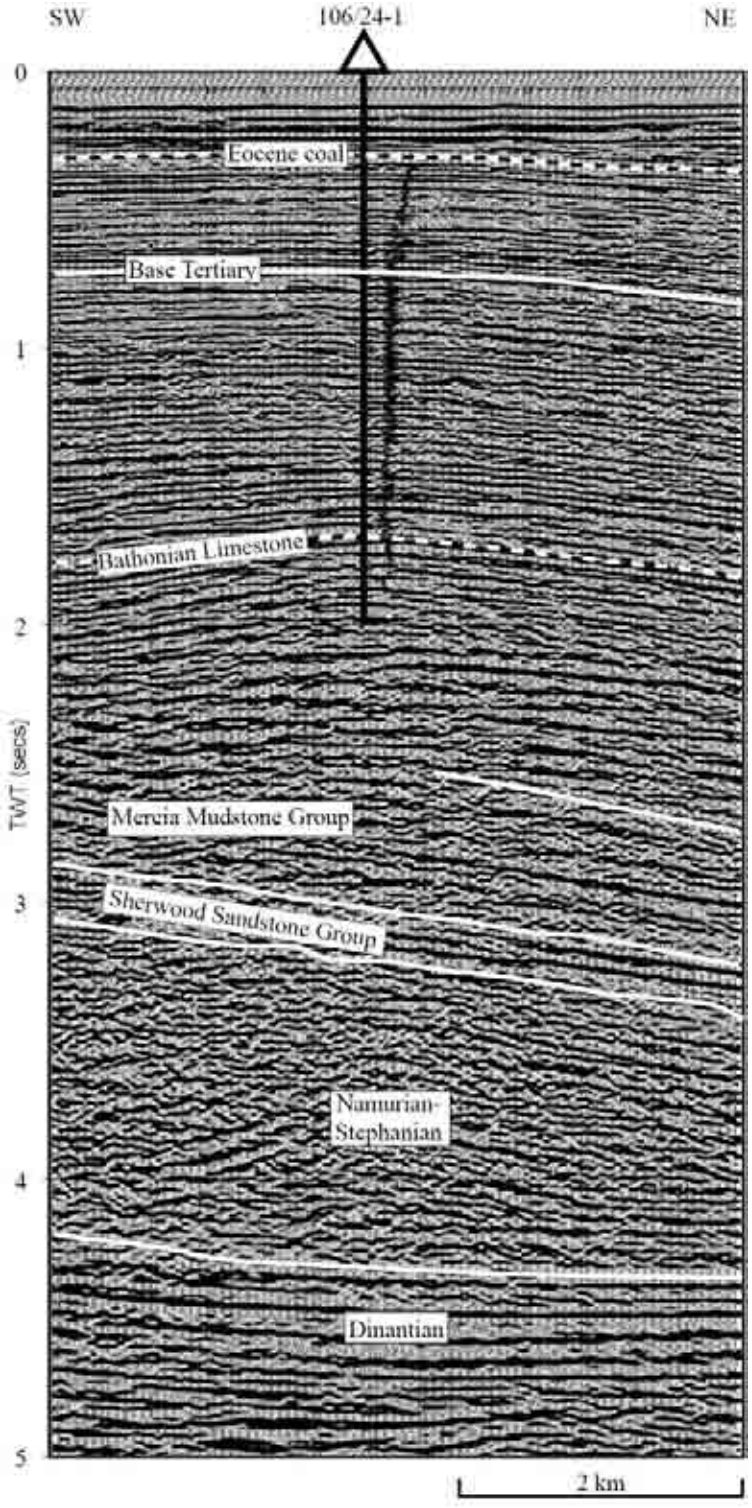

Figure 5.49 - Seismic section incorporating well 106/24-1 in the main SGCB depocentre (after Williams, 2002).

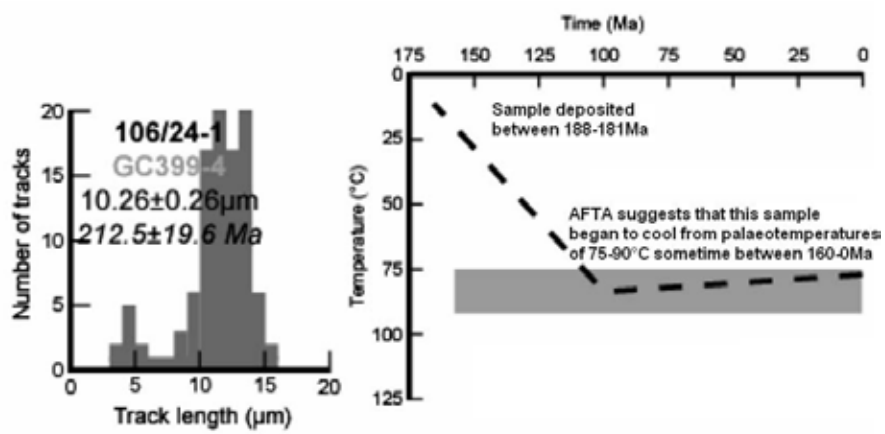

Figure 5.50 – Fission-track length distribution and accompanying thermal history solution for AFTA sample from exploration well 106/24-1 in the SGCB (after Holford, 2006).

As reported by Holford (2006), AFTA sample GC399-4 yielded a central fission track age of 212.5 ±19.6Ma, which is considerably older than the stratigraphic age of this sample (Bathonian; 167.7-164.7Ma). The fission track age therefore provides no direct evidence for this formation having experienced temperatures significantly higher than that at which it currently resides (*c.* 76°C). Thermal history modelling of AFTA parameters from this sample cooled from a maximum palaeotemperature of between 75-90°C at some time between deposition and the present-day. Assuming that the palaeotemperatures from the vitrinite samples at depths >1.5km are erroneous due to suppression and combining the shallower VR data with the palaeotemperature constraints from AFTA enables the determination of a palaeogeothermal gradient related to Paleogene/post-Paleogene burial-related heating. Palaeotemperatures from VR show no significant variation across the Paleogene/Jurassic unconformity, which suggests that maximum burial at this location was reached during the Paleogene (Figure 5.51).

The maximum likelihood estimate of palaeogeothermal gradient during Paleogene burial is 26°C/km (13-32.5°C/km within 95% confidence limits), corresponding to a maximum likelihood estimate of 950m of additional section prior to Neogene exhumation (600-2500m

±200m at 95% confidence limits) assuming a palaeosurface temperature of 15°C (Figure 5.32). This estimate is in excellent agreement with exhumation estimates derived by the sonic velocity analysis. Holford (2006) provided a burial history plot for this well, showing maximum burial depths attained prior to Neogene exhumation (mid-Miocene). His burial history also incorporates significant (*c.* 0.7km) exhumation during the late Cretaceous-early Paleogene, prior to deposition of the preserved Eocene-Oligocene section and points out similar amounts of exhumation can also be modelled during the early Cretaceous. However, it should be noted that palaeothermal data only provide constraints on the amount of Neogene exhumation, prior to which maximum burial depths were attained.

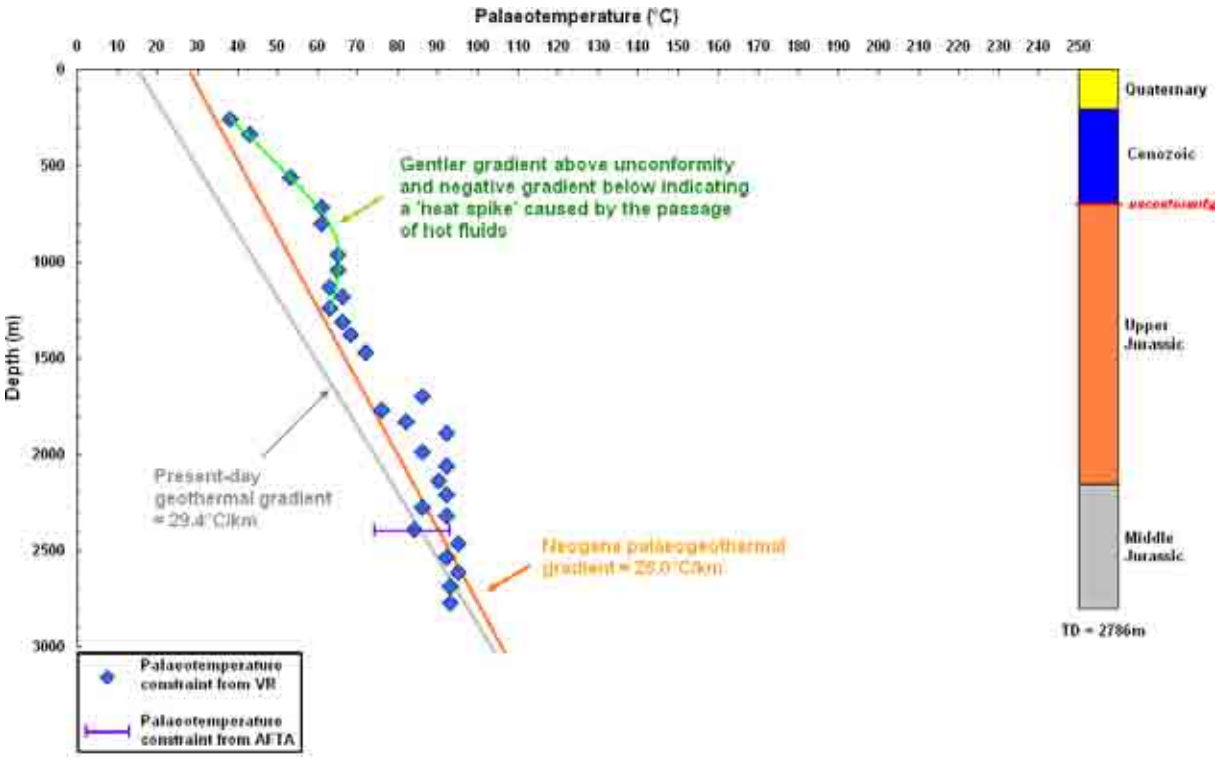

Figure 5.51 – Palaeotemperature constraints from AFTA and VR data from well 106/24-1 plotted against depth. These are used to infer palaeotemperature profiles prior to the Neogene cooling episode. A simplified stratigraphic column is also shown.

5.3.3.4.2.7: Exploration Well 106/24a-2b

Well 106/24a-2b is located within the main basin depocentre of the SGCB and seismic reflection data indicates that it penetrates the crest of an inversion-related anticline composed of deformed Paleogene (probably Eocene) sediments (Williams *et al.* 2005). Based on the analysis of anomalously high sonic velocities within the Upper Triassic Mercia Mudstone Group succession encountered by this well, Williams (2002) estimated that the pre-Jurassic units in this well had been more deeply buried by *c.* 1km of now removed overburden.

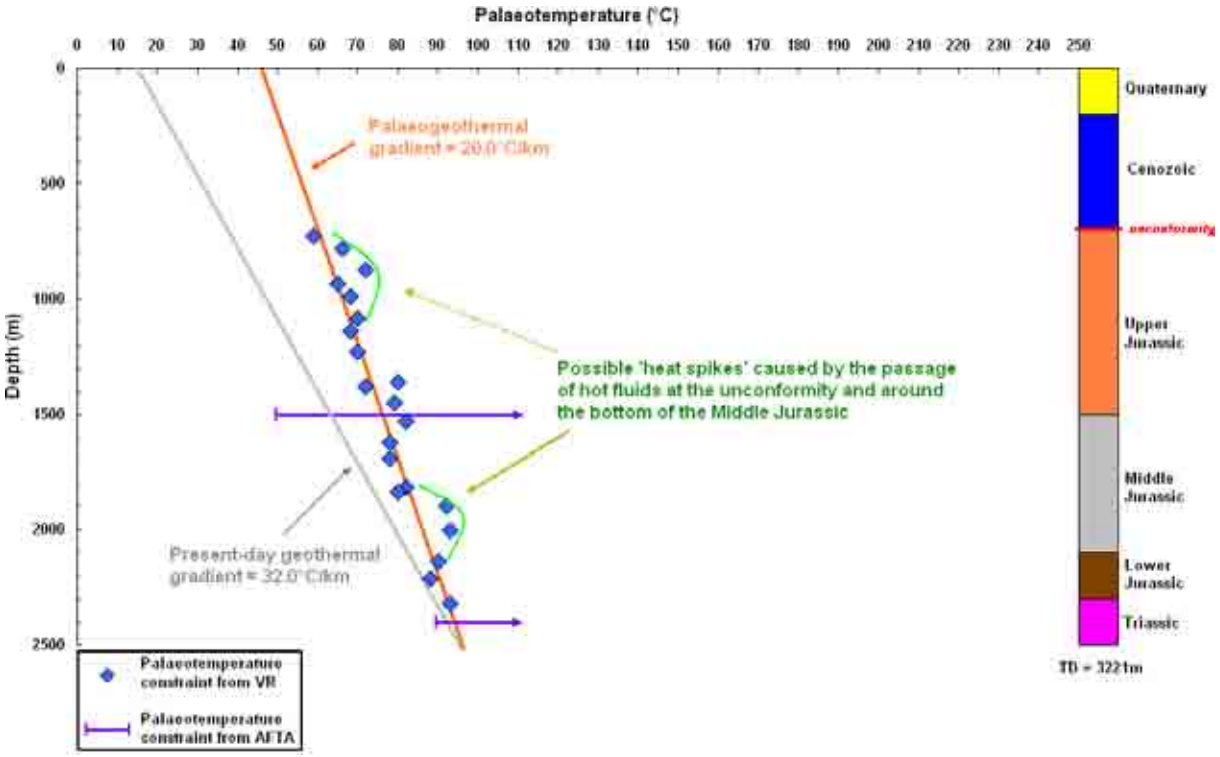

Figure 5.52 – Palaeotemperature constraints from AFTA and VR data from well 106/24a-2b plotted against depth. These are used to infer palaeotemperature profiles prior to the cooling episode. A simplified stratigraphic column is also shown.

Corrected BHT data indicate that the present-day geothermal gradient in this well has a value of 32.0°C/km. The thermal history of the well was determined using 22 vitrinite samples from the Paleogene and Jurassic intervals and two AFTA samples (Figure 5.52). The two AFTA samples available for this well (Figure 5.53) provide useful constraints on palaeotemperatures but poor constraints on the timing of cooling, probably because they have

only experienced moderate amounts of post-depositional cooling (Holford, 2006). Thermal history modelling of AFTA parameters from sample GC399-2, obtained from just above the base of the Upper Jurassic provide evidence for one palaeothermal episode from a palaeotemperature peak of <100°C between 145-0Ma. As the pooled fission track age (270.1 ±53.7Ma) of this sample is significantly higher than its stratigraphic age (*c.* 160-155Ma), this indicates that the sample has not been subjected to significantly higher temperatures (e.g. >110°C) than the temperature at which it presently resides (~52°C). The fission track age of the deeper sample, GC399-13 (87.5 ±14.7Ma) is significantly lower than its Triassic stratigraphic age, although this age reduction could be in part attributed to the fact that the sample presently resides at a temperature of *c.* 80°C. Modelling AFTA parameters from this sample suggests that it began to cool from a palaeotemperature peak of between 90-110°C (i.e. higher than the present-day temperature at this depth) between 170-5Ma. As Figure 5.52 shows, the palaeotemperature profile is approximately parallel to the present-day geothermal gradient but there is the possibility of a small 'heat spike' near the Jurassic/Cenozoic unconformity suggesting that there was some passage of hot fluids.

Fitting a linear profile to the palaeotemperature constraints from AFTA and VR yields a maximum likelihood estimate of 20.0°C/km for the palaeogeothermal gradient during Paleogene burial (18.5-33.1°C/km at 95% confidence limits). Extrapolating this profile to an assumed palaeosurface temperature of 15°C provides a maximum likelihood estimate of 1100m ± 200m of additional Paleogene-Neogene section removed during exhumation (600-1660m ±200m at 95% confidence limits; Figure 5.32). This is in excellent agreement with exhumation estimates based on compactional and seismic reflection data. Although thermal history data provide no direct evidence for late Cretaceous-early Cenozoic cooling, they are consistent with appreciable exhumation having occurred, assuming that the thickness of

eroded section did not exceed that accumulated during subsequent burial (Holford, 2006). An exhumation episode at this time is supported by seismic reflection data presented in Williams *et al.* (2005) which document the existence of a marked Jurassic/Paleogene unconformity within the basin due to late Cretaceous-Paleogene inversion.

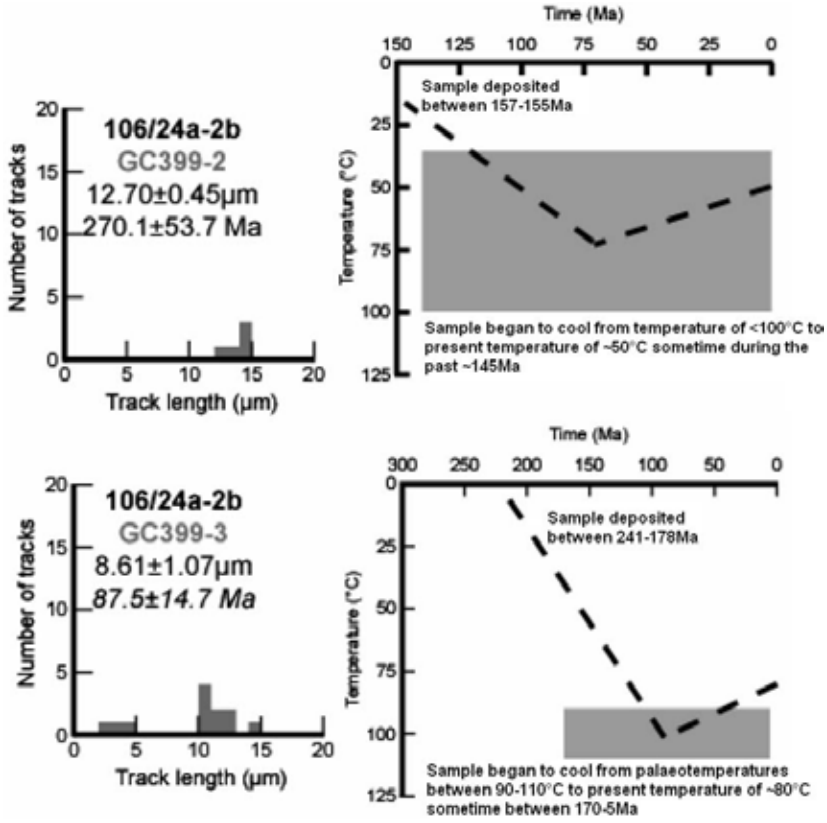

Figure 5.53 – Fission-track length distributions and accompanying thermal history solutions for AFTA samples from exploration well 106/24a-2b in the SGCB (after Holford, 2006).

5.3.3.4.2.8: Exploration Well 107/16-1

This well, located towards the northern margin of the SGCB encountered 69m of Paleogene sands and clays which unconformably overlay thick sequences of Upper and Middle Jurassic strata (532m and 1165m respectively). A seismic reflection profile through this well indicates that it cuts through a normal fault which has been contractionally reactivated, probably during Neogene tectonic inversion (Figure 5.54). An estimate of at least 0.8km of Cenozoic

sediments removed during exhumation is possible based on this profile (Williams, 2002; Williams *et al.* 2005).

Available palaeothermal data for this well comprises one AFTA and 15 VR samples. Corrected BHT measurements indicate that the present-day geothermal gradient at this location is 39.1°C/km (Figure 5.56). AFTA sample GC399-7 provided a pooled fission track age of 221.3 ±15.1Ma. This is older than the stratigraphic age of the sample (Aalenian 175.6-171.6Ma) and hence it is unlikely that this sample has been exposed to palaeotemperatures in excess of 110°C at any time post-deposition (Figure 5.55). Thermal history modelling of this sample provides evidence of cooling from a palaeotemperature of <100°C at some point between deposition and the present-day. All VR data from this well is from the Jurassic. VR derived palaeotemperatures do not however show a progressive increase with depth as would be expected for a palaeotemperature profile resulting from vertical conductive heat flow. As indicated by Figure 5.56, palaeotemperatures decrease from values of *c.* 95°C in the uppermost Jurassic to *c.* 70°C at depths of around 1km (Middle Jurassic). Below this, palaeotemperatures progressively increase to *c.* 95°C towards the base of the well.

These data define a highly non-linear 'dog-leg' palaeotemperature profile which cannot be explained in terms of variable thermal conductivities of the preserved or removed section since the well penetrated an essentially uniform lithological succession.

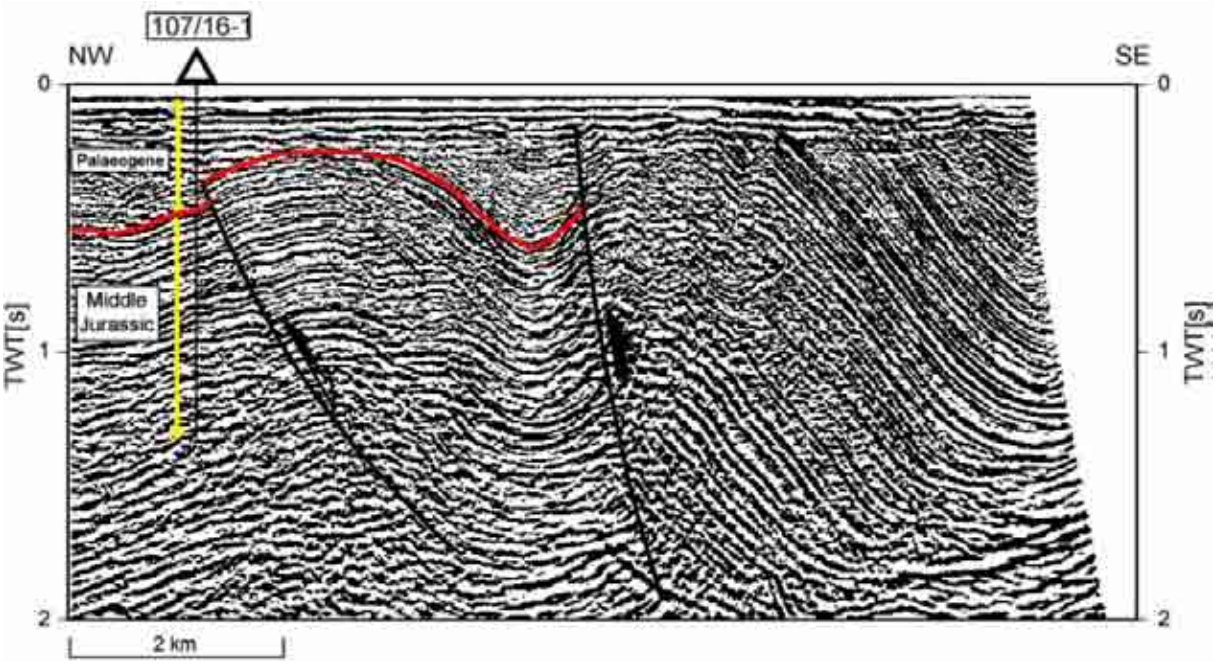

Figure 5.54 – Seismic line through well 107/16-1 located in the NE SGCB. The section is displayed with a significant component of vertical exaggeration to highlight the reactivated fault plane that cuts well 107/16-1. The red horizon represents the Mesozoic/Paleogene unconformity (after Williams, 2002).

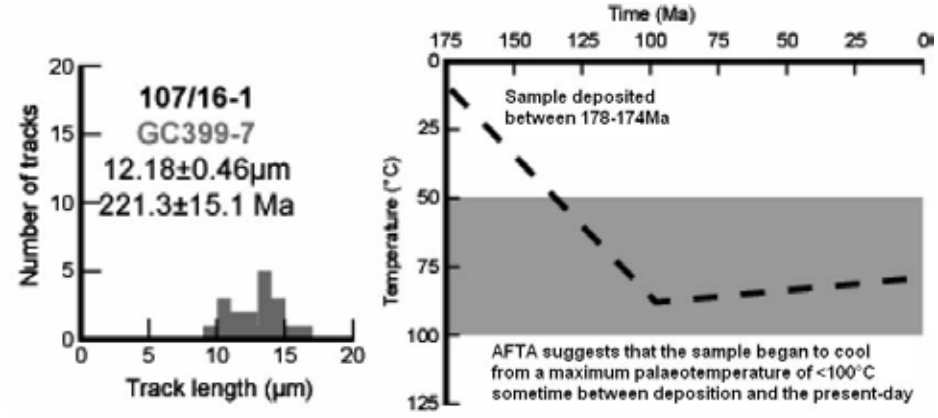

Figure 5.55 – Fission-track length distribution and accompanying thermal history solution for AFTA sample from exploration well 107/16-1 in the SGCB (after Holford, 2006).

The apparently anomalous VR values in the higher parts of the succession could reflect operator error. An alternative explanation is that the negative part of the palaeotemperature profile has resulted from a transient increase in lateral heat flow (e.g. due to a hot fluid flow event) in a constant basal heat flow regime.

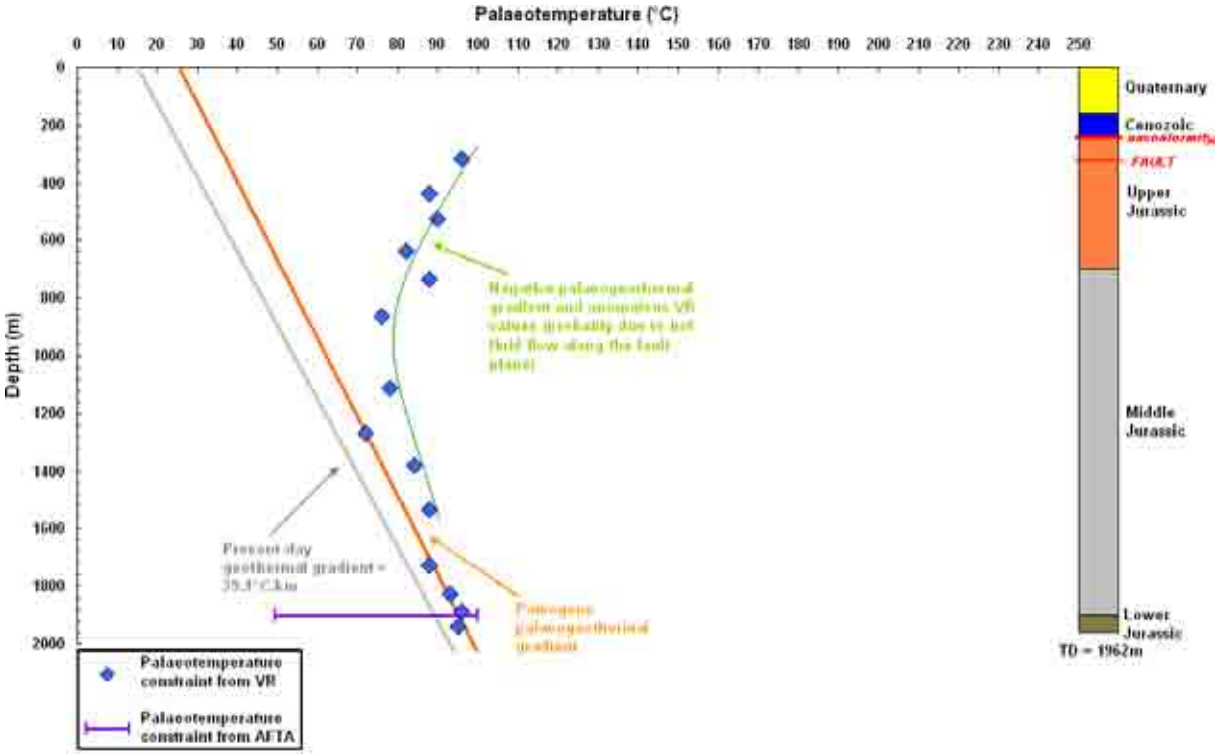

Figure 5.56 – Palaeotemperature constraints from AFTA and VR data from well 107/16-1 plotted against depth. These are used to infer palaeotemperature profiles prior to the Paleogene cooling episode. A simplified stratigraphic column is also shown. Note also the approximate position of a fault plane which was reactivated during Neogene compressional shortening.

Duddy *et al.* (1994, 1998) have demonstrated how a short-lived heated fluid flow event through a confined part of a vertical section (e.g. an aquifer or a permeability barrier such as an unconformity or fault place) can result in negative geothermal gradients below the fluid flow horizon. If this is the case, a transient period of fluid-related heating focussed along either the Paleogene/Upper Jurassic unconformity which acted as a permeability barrier juxtaposing Cenozoic sandstones against Mesozoic mudstones, or the reactivated fault plane shown in Figure 5.54, which could have acted as a conduit for heated fluids sourced from greater depths, possibly accompanying inversion (*cf.* Sibson, 1995; Turner & Williams, 2004) could explain the observed thermal effects in well 107/16-1 (Figure 5.56).

In order to estimate deeper burial using palaeothermal data, VR data from depths of <1km have been excluded from further analyses whilst it is assumed that VR values at depths >1km

record the signal of formerly deeper burial, since the deepest VR data are in good agreement with palaeotemperatures from AFTA. Unlike in the other wells from the SGCB, palaeotemperature data do not show consistency across the Cenozoic/Jurassic unconformity, hence it is not possible to attribute the palaeotemperature constraints to pre- or post-Paleogene maximum burial. The reliable constraints from VR and AFTA define a palaeogeothermal gradient with a maximum likelihood value of 25.5°C/km (12.5-37°C/km at 95% confidence limits). Extrapolating this gradient above the Quaternary/Paleogene unconformity to a palaeosurface temperature of 15°C yields a maximum likelihood estimate of 1500m of additional section prior to exhumation (500-4450m ±200m at 95% confidence limits; Figure 5.32). This estimate is in excellent agreement with the estimates based on seismic reflection data (*c.* 800m).

5.3.3.4.3: Wells in which VR data is unreliable

The VR profiles of 5 wells were deemed to have inherent problems in their data so as not to provide a reliable result when estimating palaeogeothermal gradients and removed section. Only one well is presented below as there is independent verification of palaeotemperatures from AFTA data. The other well data is presented in Appendix C.

5.3.3.4.3.1: Exploration Well 103/18-1

Well 103/18-1 was drilled in the western BCB and encountered Cretaceous rocks unconformably overlying a Jurassic-Triassic succession (Figure 5.57). This study presents the first analysis of palaeothermal (AFTA and VR) data from well 103/18-1. The thermal history dataset consists of 26 VR samples and 5 AFTA sample taken from the core of well 103/18-1. Three corrected bottom-hole temperature (BHT) measurements have been used to define a present-day geothermal gradient of 37.5°C/km for well 103/18-1 (Figure 5.58). It is apparent from Figure 5.58 that the VR-derived palaeotemperatures show a great deal of variation with

depth suggesting that measured reflectances are suppressed (Carr, 2000), affected by 'heat spikes' caused by circulation of hot fluids, detrital in origin or a combination of these. For this reason although a palaeogeothermal gradient can be fitted to the data (mainly thanks to the abundant AFTA data) the results from this well should be treated with caution.

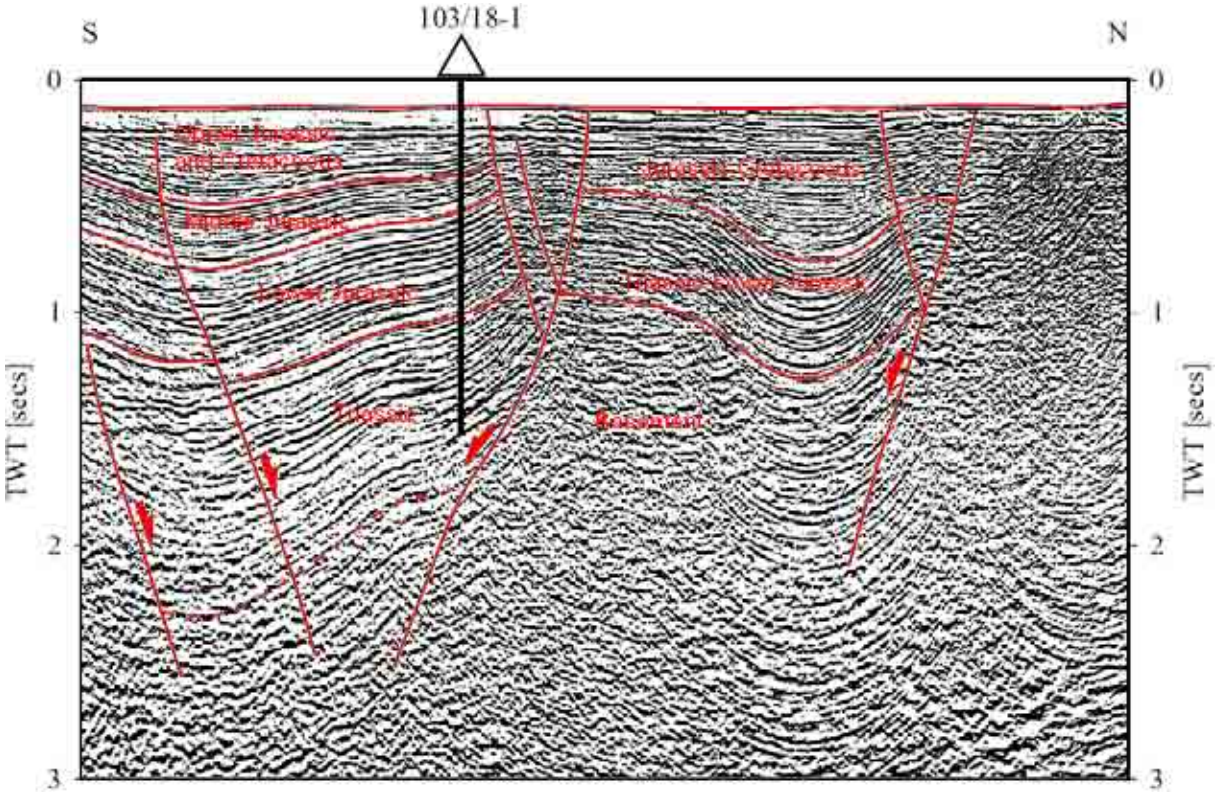

Figure 5.57 - Migrated seismic profile and interpreted geoseismic section incorporating well 103/18-1 (modified after Williams, 2002).

Five AFTA samples are available for well 103/18-1 from a variety of horizons and depths (Figure 5.58). Sample GC429-64 from the Middle Jurassic indicates cooling from maximum palaeotemperatures of 75-95°C, beginning some time between 75 and 0Ma. Sample GC429-65 is dominated by tracks inherited from source regions but tentative evidence suggests cooling from maximum palaeotemperatures of 60-85°C some time after deposition in the Lower Jurassic (200-175Ma). Sample GC420-76 cooled from maximum palaeotemperatures of 90-105°C some time between 85 and 10Ma. Sample GC420-42 indicates cooling from maximum palaeotemperatures of 100-105°C some time between 65 and 0Ma. Sample

GC420-43 provides evidence of being hotter at some time after deposition than now, but the track lengths are dominated by the present-day thermal regime. This sample indicates cooling from 110-115°C some time between 55-25Ma. All the samples indicate that maximum burial depth was achieved in the Paleogene.

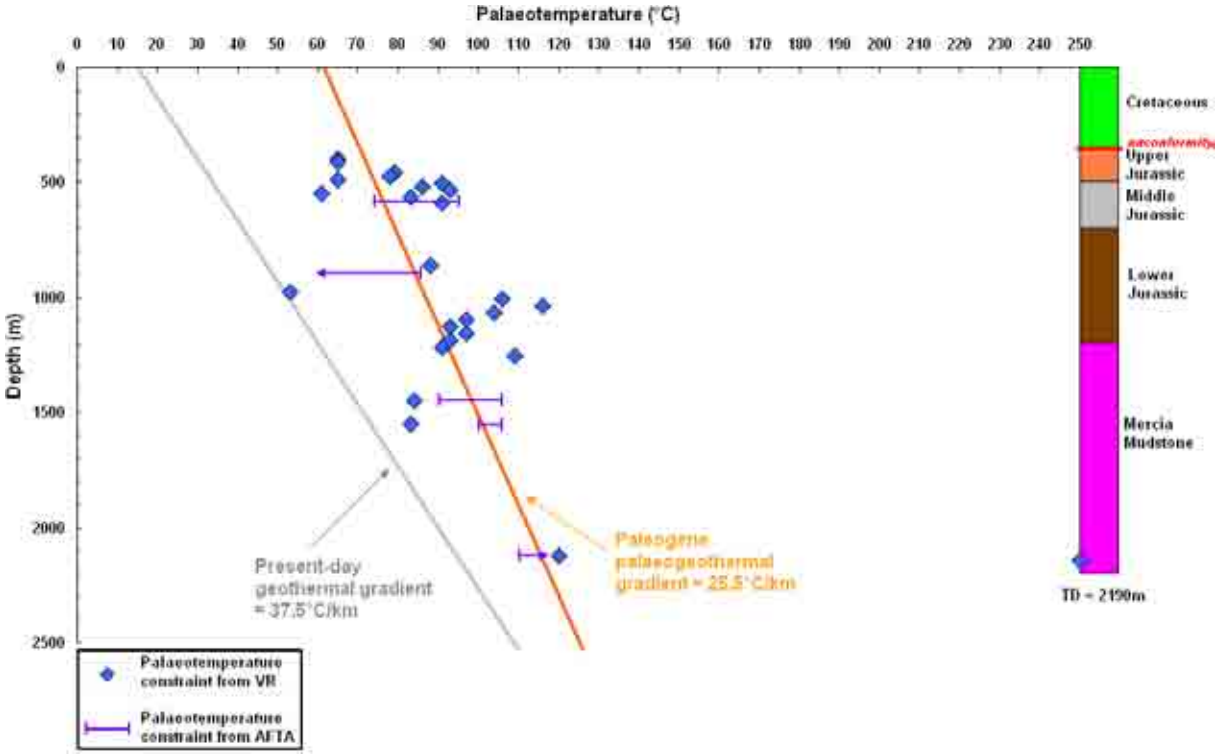

Figure 5.58 – Palaeotemperature constraints from AFTA and VR data from well 103/18-1 plotted against depth. These are used to infer palaeotemperature profiles prior to the Paleogene cooling episode. A simplified stratigraphic column is also shown.

The maximum likelihood estimate of palaeogeothermal gradient prior to Paleogene exhumation is 25.5°C/km (21.0-29.5°C/km at 95% confidence limits) (Figure 5.32). A value of 20°C has been used for the surface temperature for the Paleogene, based on palaeoclimatic evidence presented by Yalçin *et al.* (1997). Extrapolating the fitted palaeotemperature profiles to this value indicates that the preserved Mesozoic succession was more deeply buried by 1950m ±200m (1550-2500 ±200m at 95% confidence limits) prior to Paleogene exhumation (Figure 5.32).

5.3.4: THERMAL HISTORY MODELLING OF AFTA DATA

It must be noted that, in most cases, the fission track age is not indicative of a single, discrete event and should therefore be interpreted together with track length data in order to yield more meaningful information about the thermal history of a sample. Tables B.1-B.5 (Appendix B) show estimates of the maximum palaeotemperatures reached prior to cooling and the timing of the onset of cooling in each AFTA sample and the thermal history solutions for all samples and their special distribution are provided in Figure 5.59.

5.3.4.1: The timing of cooling episodes

The Upper Triassic episode (215-195Ma) seems to be limited to the northern margin of the BCB (South Wales and Pembrokeshire) and South Devon. Figures 5.61-5.63 show the timing constraints for the episode in those areas and show that the timing is constrained to Upper Triassic to earliest Lower Jurassic. Palaeogeographic reconstructions (*cf.* Ziegler, 1990; Chapter 3) show that the SW UK was experiencing rifting at this time due to tensional stresses caused by an asthenospheric plume (Ziegler, 1990) and as such this uplift is puzzling in an otherwise extensional setting. One possible mechanism for this uplift is footwall uplift (*cf.* Jackson & McKenzie, 1983) and is inferred to be the process responsible for the uplift in the SW UK at this time (see Section 5.4 for further discussion). In South Wales the cooling episode is inferred to correspond to extensional movements along the Bala Fault and northern BCB margin fault which respectively controlled the subsidence of the SGCB/CBB and BCB during this time. Although most of the Permian-Triassic subsidence within the SGCB is thought to have been accommodated by pure shear (i.e. sub-seismic scale) deformation rather than normal faulting (*cf.* Welch & Turner, 2000), there is clear evidence from seismic data presented by Williams (2002) for thickening of Triassic sequences into the Bala Fault.

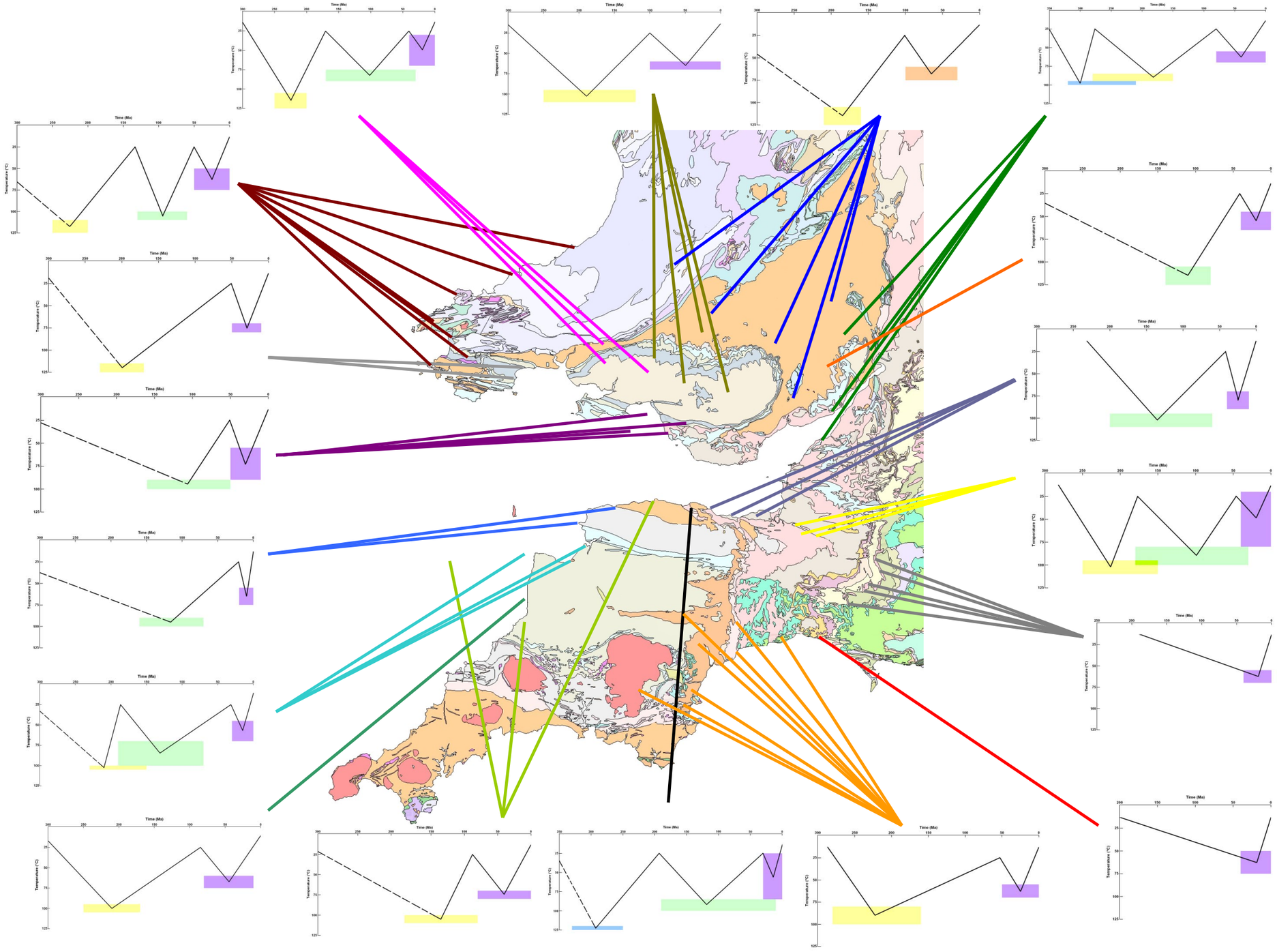

Figure 5.59 – Map showing distribution of THR solutions for all SW UK samples. Where many samples share a similar thermal history a single plot has been included and directed to the locations where it is applicable (bedrock geology after BGS, 2008).

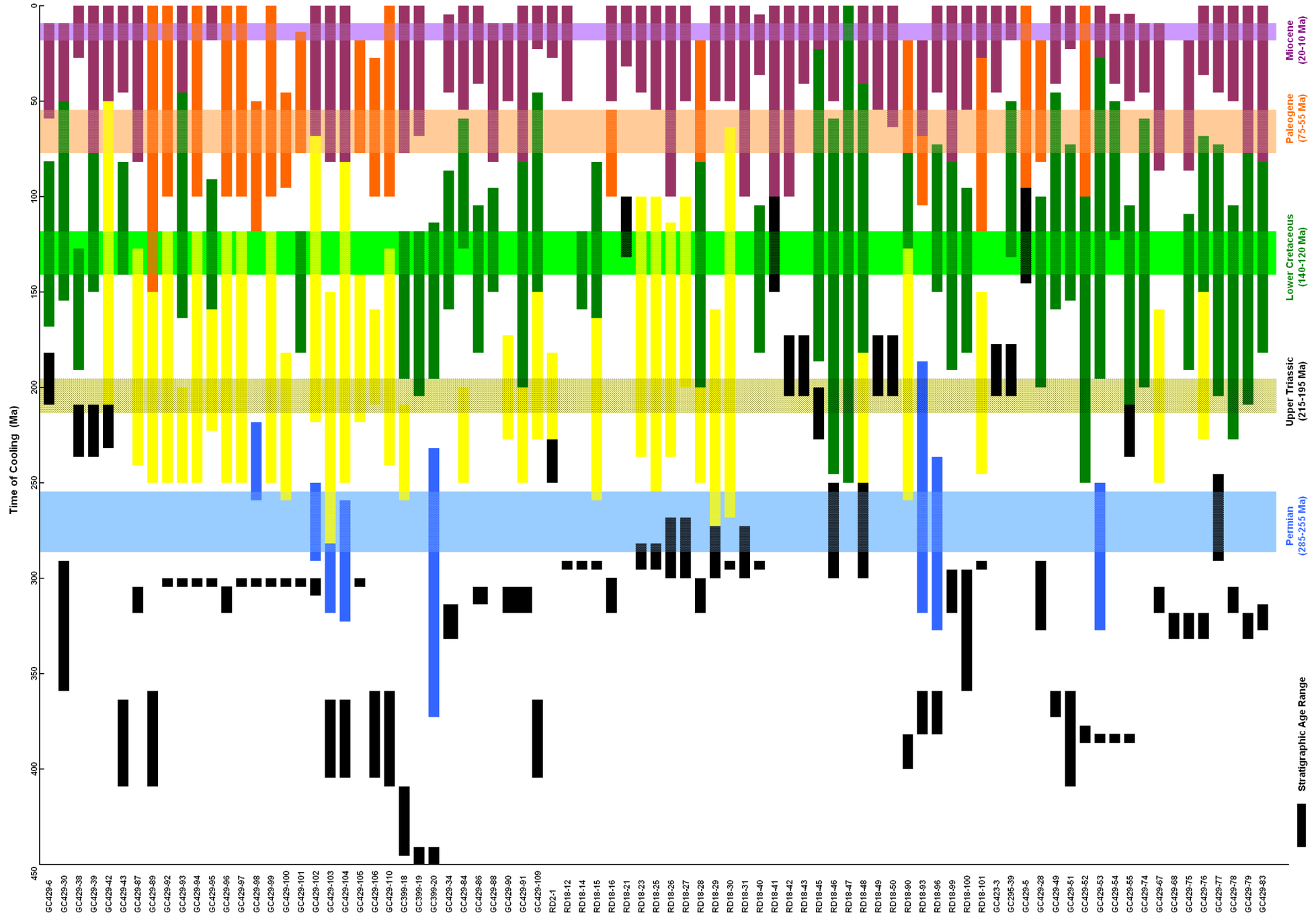

Figure 5.60 –Estimates of the time at which cooling episodes began for each sample based on thermal history interpretation of the AFTA data. The ranges shown correspond to ±95% confidence limits. Overlap of timing constraints from individual samples allows definition of regional cooling episodes beginning between 285-255Ma (Permian), 215-195Ma (Upper Triassic), 140-120Ma (Lower Cretaceous), 75-55Ma (Paleogene) and 20-10Ma (Miocene).

Movement along the former fault has been demonstrated to have affected North Wales by Holford (2005*b*, 2006).

Holford (2005*b*) asserted that as the Triassic–early Jurassic sediments of Cardigan Bay were deposited in fairly shallow-marine environments where the uplifted basin margins would have been exposed above sea-level and susceptible to erosion. Such erosion would have served to increase the magnitude of this footwall uplift and thus the exhumation experienced by the basin margins. This might serve to explain the large values of exhumation identified by the VR data in the South Wales Coalfield boreholes where up to *c.* 6km of section has been removed since the Carboniferous.

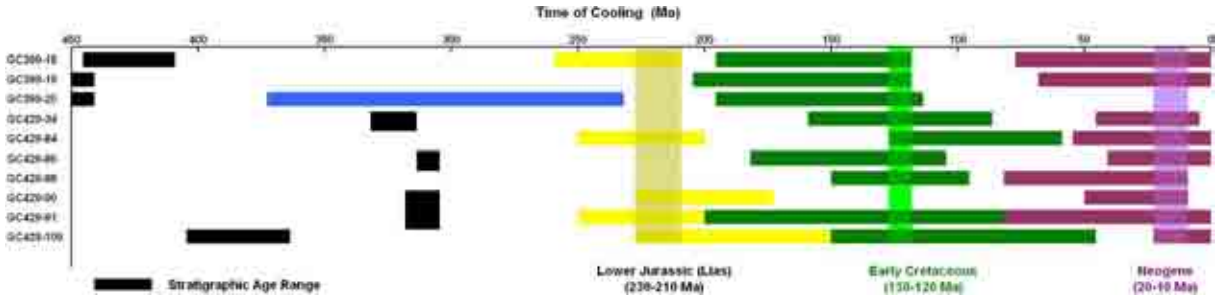

Figure 5.61 – Timing of cooling episodes for a series of apatite samples collected from onshore SW Wales based on thermal history interpretation of apatite fission track data. Horizontal bars represent estimates (within 95% confidence limits) of the time at which individual samples began to cool from palaeotemperature peaks. Vertical bars correspond to the time ranges which are consistent for each sample. In this case, three distinct cooling episodes are recognised beginning during the Upper Triassic (230-210Ma), Early Cretaceous (130-120Ma) and the Neogene (20-0Ma). Data for samples GC399-18, 19 and 20 taken from Holford (2006).

A possible problem with this interpretation is in assessing the extent of the cooling episode across the SW UK. Where the data do not show this Upper Triassic episode there are three possibilities:

- The cooling episode did not affect that location
- A subsequent palaeothermal episode over printed this episode
- The episode was not resolvable from the data

Some insight can be gained from analysing the granites in South Devon and Cornwall. These were emplaced at the same time across the area and should record the same thermal history. Sample RD18-14 and RD18-40 do not record this Upper Triassic episode despite being from the same granite formations as samples RD18-15 and RD18-101 which do. Another reason for the absence of the event in the data is explained by the age of the sediments which contain the apatite. Particularly in South Devon, Somerset and Dorset the samples stratigraphic ages are far younger than the cooling episode observed though its absence in older sediments in North Devon and Somerset is conspicuous (Figure 5.64 - 5.65). Clearly there is a lot more work to do in assessing the distribution of Upper Triassic exhumation across the SW UK.

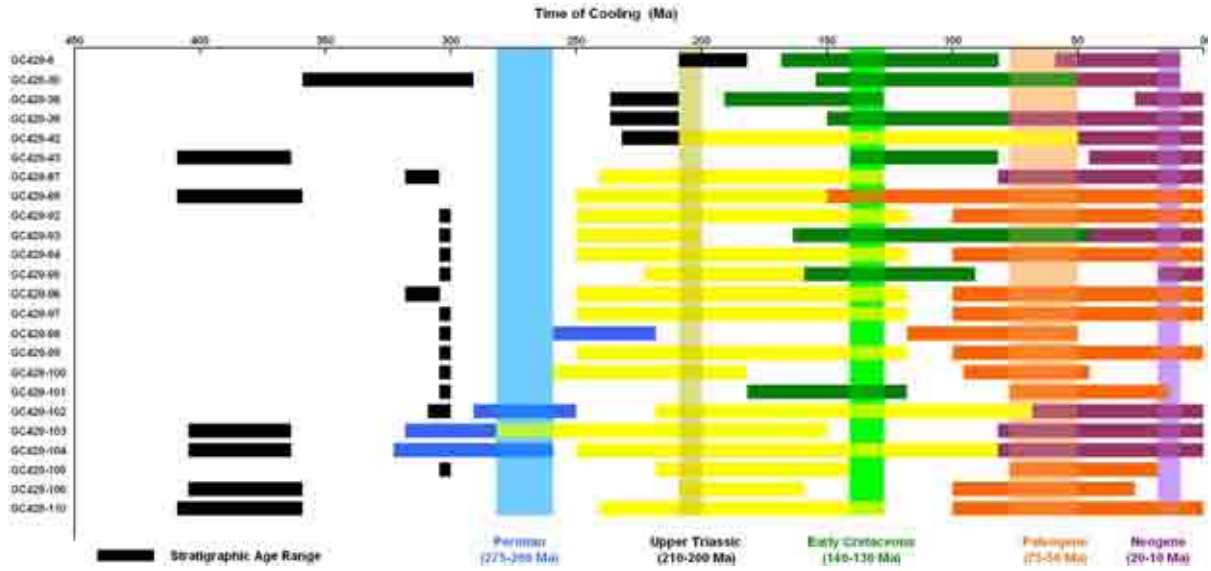

Figure 5.62 – Timing of cooling episodes for a series of apatite samples collected from onshore South Wales based on thermal history interpretation of apatite fission track data. Horizontal bars represent estimates (within 95% confidence limits) of the time at which individual samples began to cool from palaeotemperature peaks. Vertical bars correspond to the time ranges which are consistent for each sample. In this case, five distinct cooling episodes are recognised beginning during the Permian (275-250Ma), Upper Triassic (210-200Ma), Lower Cretaceous (140-130Ma), Paleogene (75-50Ma) and the Neogene (20-10Ma).

The Lower Cretaceous (140-120Ma) palaeothermal episode is observed across the whole of the SW UK and is only absent where a clear Paleogene is present (Figure 5.62). The ubiquitous nature of this episode reflects that fact that it must have been the major episode to have affected the SW UK in post-Triassic times and represents for most rocks their time of

deepest burial. Where the episode is not present this is due to the data being unable to resolve the event (especially since its omission generally corresponds to identification of a Paleogene episode in the data).

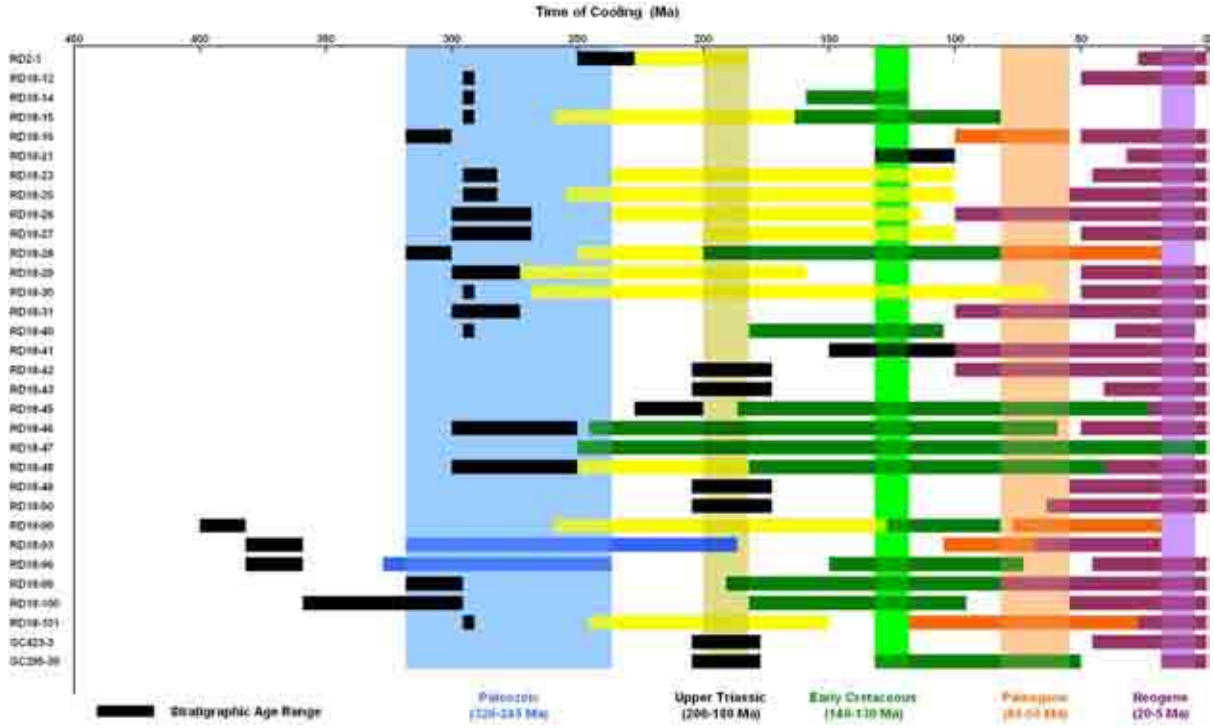

Figure 5.63 – Timing of cooling episodes for a series of apatite samples collected from onshore South Devon, Somerset and Dorset based on thermal history interpretation of apatite fission track data. Horizontal bars represent estimates (within 95% confidence limits) of the time at which individual samples began to cool from palaeotemperature peaks. Vertical bars correspond to the time ranges which are consistent for each sample. In this case, four distinct cooling episodes are recognised beginning during the Upper Triassic (200-180Ma), Lower Cretaceous (140-130Ma), Paleogene (85-55Ma) and the Neogene (20-5Ma).

Tectonically the Lower Jurassic cooling episode corresponds to initiation of sea-floor spreading in the Bay of Biscay and off the Goban Spur. A possible consequence of this sea-floor spreading would be a compressive stress regime leading to fault reactivation and basin inversion (see Chapter 6 for further discussion). However, Williams (2002) attributed the exhumation observed on seismic data to renewed footwall uplift. Williams (2002) goes on to describe how inversion in the BCB/SCSB occurred as a response of uplift of the Cornubian Platform without significant fault reactivation. This means that very little sediment was removed from the main depocentre allowing Upper Jurassic sediments to be preserved in the

core of the Bristol Channel syncline. However, Brooks *et al.* (1988) proposed that the Bristol Channel Fault Zone is actually a Variscan thrust fault reactivated during the Early Cretaceous, when it cut up through a faulted sequence of Triassic and Jurassic sediments. This is consistent with observations from the southern margin of the Eastern BCB, where a series of eroded Permo-Triassic fault blocks have been tilted towards the north. This suggests that the entire southern margin of the basin was uplifted during the Early Cretaceous (due to the uplift of the Cornubian Platform) and that the Variscan thrust fault was reactivated in response to gravitational forces associated with this uplift (*cf.* Knott, 2001).

It is clear that these local events have had a part to play in the tectonic history of these basins but it is suggested here that basin inversion is the more suitable candidate for the distribution of the palaeothermal episode across the whole of the SW UK and indeed the initial uplift of the Cornubian Platform is likely to have been caused by the compressive stresses transmitted from the spreading centres.

The Cenozoic palaeothermal episodes, of which two are clearly resolvable in the AFTA data are likely to represent a number of composite events. The evidence for this comes in the very broad ranges of the palaeothermal episodes recognised by the AFTA data. Closer scrutiny of the timing diagrams (Figures 5.60-5.65, particularly Figure 5.62) highlights three clear episodes identified by the AFTA; a Paleocene (75-55Ma), Oligocene (35-20Ma) and a Neogene (20-10Ma) episode.

Tectonically these timings correspond to basin inversion events related to the Alpine Laramide deformation episode, Pyrenean orogeny and Late Alpine orogeny respectively. Such close coincidence suggests a genetic link between these events and the palaeothermal episodes. This observation is also consistent with the conclusions of Van Hoorn (1987*a*) and

Williams (2002). From Figures 5.60-5.65 it is clear that different parts of the SW UK responded to the individual events in different ways with the SCSB, NCSB, EISB (Holford, 2006) responding to the Laramide inversion and with Devon, Somerset and the Wessex Basin (Bray *et al.* 1998) responding to the Pyrenean orogeny.

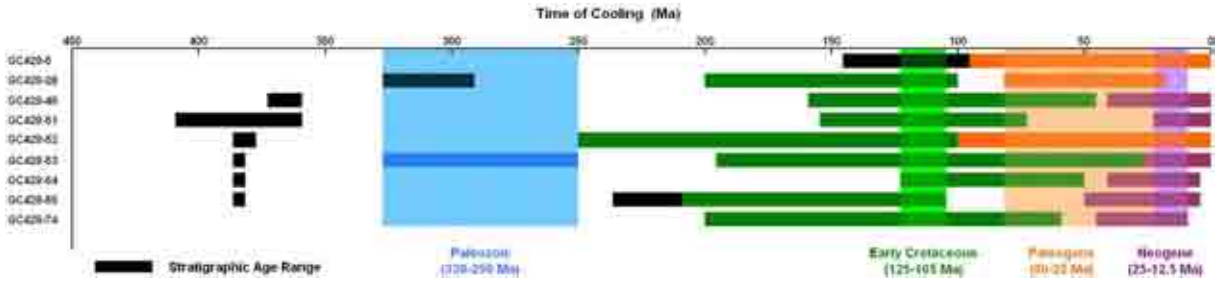

Figure 5.64 – Timing of cooling episodes for a series of apatite samples collected from onshore North Somerset and the Bristol Channel based on thermal history interpretation of apatite fission track data. Horizontal bars represent estimates (within 95% confidence limits) of the time at which individual samples began to cool from palaeotemperature peaks. Vertical bars correspond to the time ranges which are consistent for each sample. In this case, four distinct cooling episodes are recognised beginning during the Paleozoic (330-250Ma), Lower Cretaceous (125-105Ma), Paleogene (80-25Ma) and the Neogene (25-12.5Ma).

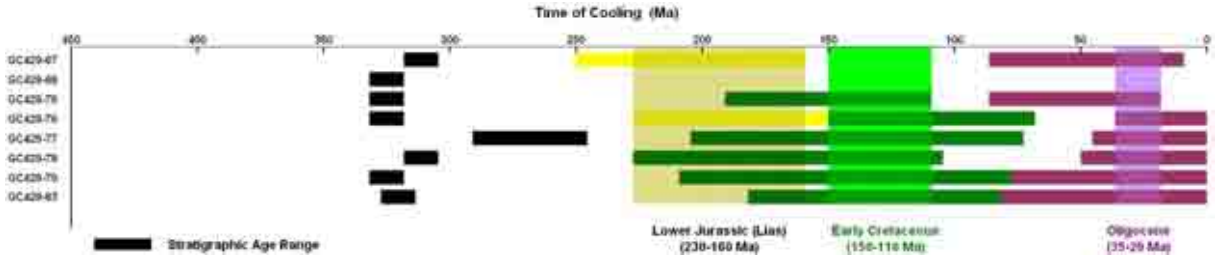

Figure 5.65 – Timing of cooling episodes for a series of apatite samples collected from onshore North Devon based on thermal history interpretation of apatite fission track data. Horizontal bars represent estimates (within 95% confidence limits) of the time at which individual samples began to cool from palaeotemperature peaks. Vertical bars correspond to the time ranges which are consistent for each sample. In this case, three distinct cooling episodes are recognised beginning during the Upper Triassic-Upper Jurassic (230-160Ma), Lower Cretaceous (150-110Ma) and the Oligocene (35-20Ma).

It is suggested here that the reason for the separation of events is due to the structural control of the main basin bounding faults. It is likely that the whole of the SW UK was affected by the compressive stresses generated by these events but depending on the orientation of the faults the relative importance of these events as recorded by the AFTA data differed. In the BCB faults trend approximately E-W, and were thus favourably orientated for reactivation during the Oligocene-Miocene, when the principal compression axis was N-S.

In this stress field NE-trending fault zones would have had a component of sinistral strike-slip motion; while NW-orientated lineaments such as the Sticklepath-Lustleigh Fault underwent net dextral displacement. Thus zones of transtension developed along fault zones that were previously inverted during Early Cretaceous dextral transpression. The preservation of Cenozoic strata along the southern margin of the SCSB is consistent with this interpretation (Van Hoorn 1987*b*).

A field based study conducted on the southern margin of the BCB by Dart *et al.* (1995) shows good agreement with the regional tectonic model proposed above. They determined that a three-phase tectonic history adequately accounted for observed patterns of extension and inversion along the North Somerset coast. The direction of extension and inversion were determined from a number of kinematic indicators measured at outcrop scale. The data obtained was consistent with initial N-S extension during the Jurassic, followed by N-S orientated compression during Miocene basin inversion. This latter event was accompanied by dextral strike-slip on NW-trending faults, together with sinistral strike-slip on conjugate NE- trending lineaments.

The broad distribution of the Neogene (20-0Ma) cooling episode is suggested here to represent a number of competing stress regimes from both ridge-push forces and Late Alpine compression meaning that all faults will have been in a favourable orientation to be reactivated by one stress field or the other.

5.3.4.2: The magnitude and distribution of exhumation episodes

Figures 5.66 - 5.68 show the spatial variation of palaeotemperatures derived from AFTA associated with the Early Jurassic, Early Cretaceous and Cenozoic (Miocene) cooling episodes, based on data reported in Tables B.1-B.5 (Appendix B). Utilising additional

information from VR (Appendix B, Tables B6-B13) as well as data presented by Holford (2006) it has been possible to construct palaeotemperatures maps of the whole SW UK region (Figure 5.69). Palaeotemperatures for individual samples prior to early Jurassic cooling are generally 20-30°C higher than those prior to Cenozoic cooling. Furthermore early Jurassic palaeotemperatures appear to be highest around the Pembroke Peninsula and near to the Bala Fault suggesting that the observed cooling may be related to activity along this fault system. This would suggest a causative mechanism of footwall uplift similar to what Holford (2006) assigned as being responsible for Jurassic uplift in NW Wales. Further evidence for footwall uplift is the raised palaeotemperatures around north Somerset and north Devon (Figure 5.69) in the proximity of the southern margin fault of the BCB.

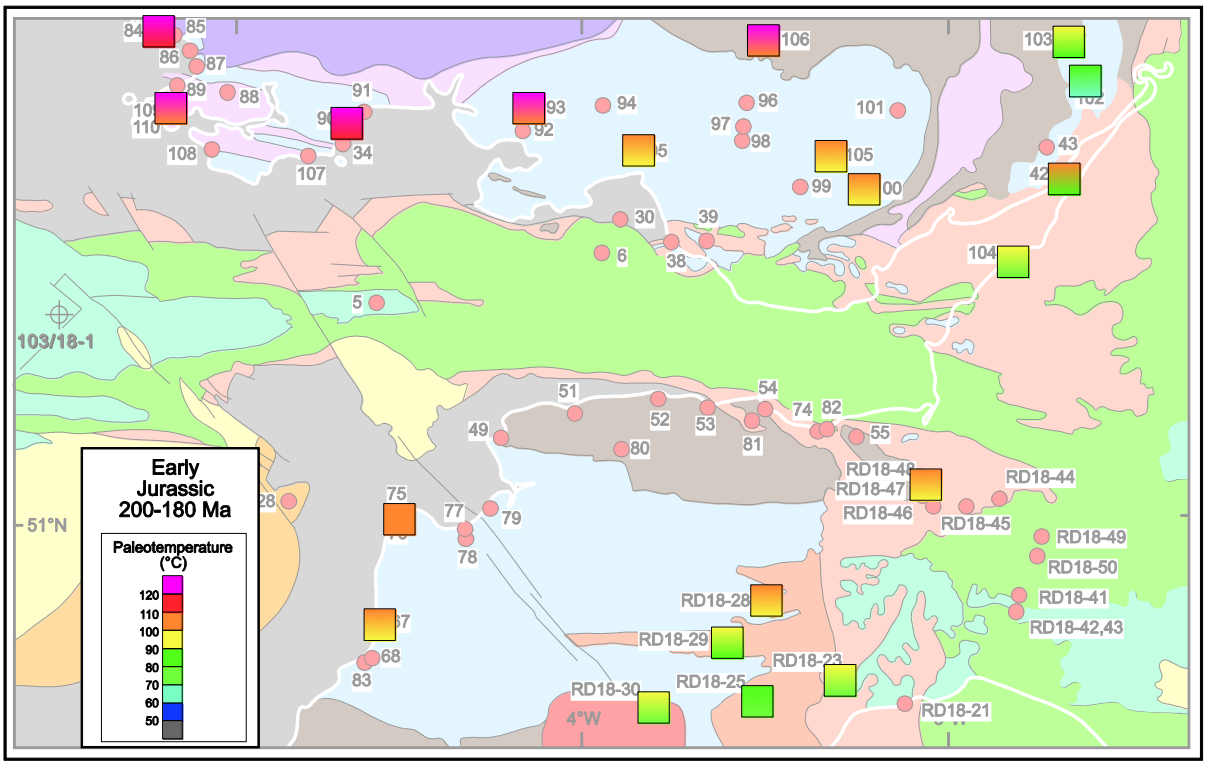

Figure 5.66 –Map showing distribution of palaeotemperatures derived from AFTA attained prior to cooling during the early Jurassic.

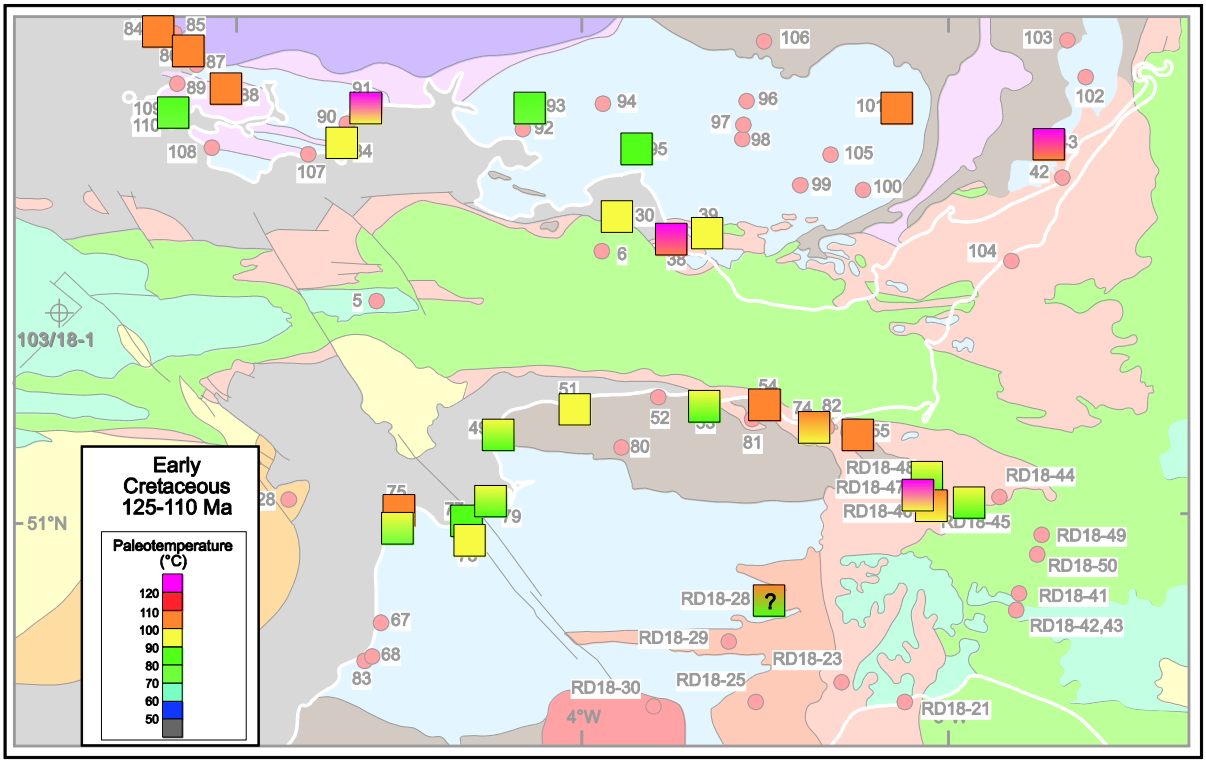

Figure 5.67 – Map showing distribution of palaeotemperatures derived from AFTA attained prior to cooling during the early Cretaceous.

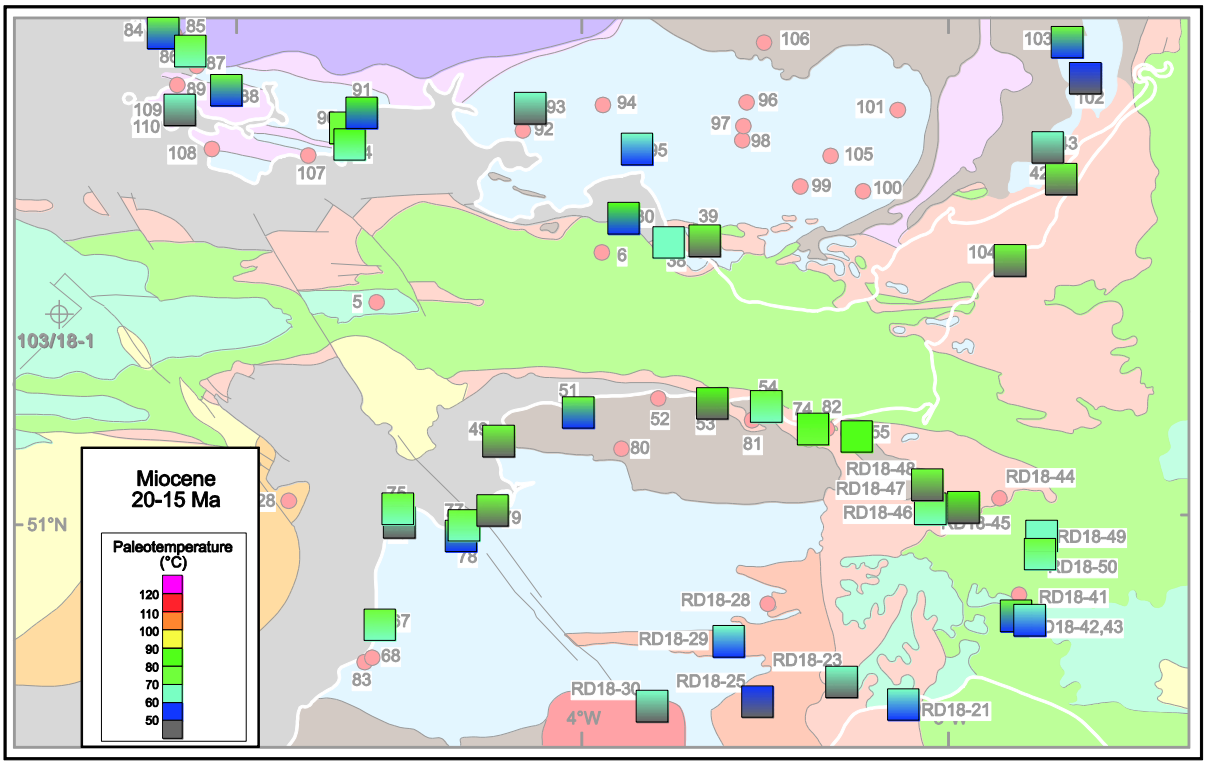

Figure 5.68 – Map showing distribution of palaeotemperatures derived from AFTA attained prior to cooling during the Miocene.

An alternative observation is that the palaeotemperatures appear to show a radial symmetry perhaps suggesting that thermal doming was important at this time. This has been discussed by Holford (2006) to have possibly affected Northern Ireland in the area around the Larne Number 2 borehole, thus its lateral extent may be manifested as this radial pattern.
The distribution of results from North Wales (Holford, 2006) would also support this assertion, though Holford (2006) cited footwall uplift as the primary cause of exhumation across this area.

Early Cretaceous palaeotemperatures appear to be quite variable across the area though there is evidence for a number of 'hot spots'. The most notable of these are in Pembrokeshire, Somerset and the Vale of Glamorgan. It is notable that these areas correspond with major faults the Johnston Thrust, Watchet-Cothelstone Fault and Swansea Valley Fault respectively. The presence of the hot spots in these areas suggests that Cretaceous reactivation of the faults has led to the difference in palaeotemperatures. Cenozoic palaeotemperatures are broadly similar across the area though there appears to be a subtle trend present whereby there is a decrease in palaeotemperature away from the main basin margin faults particularly in Pembrokeshire and the northern and southern BCB marginal faults. There is however an anomalously high area of elevated palaeotemperatures around Yeovil in Somerset. This corresponds to an area of E-W trending normal faults which again suggests inversion of these features has resulted in the difference in palaeotemperatures.

In order to deduce the thermal history of the BCB a palaeotemperatures map was created using 28 VR samples from the Bristol Channel (Appendix B, Table B11). As previously mentioned VR data only reveal maximum palaeotemperature information and thus no definitive timings can be deduced from the data however the data reveal some interesting patterns (Figure 5.70). Highest palaeotemperatures appear to be concentrated on the margins

of north Devon and Pembrokeshire whilst the lowest palaeotemperatures appear to be centred on Lundy Island. This result could be considered surprising given the fact that the Lundy granite was intruded during the Paleogene (53.4 ± 1.3Ma (Fitch *et al.* 1969)). However since the palaeotemperature 'spot samples' can be interpreted in terms of; i) variations in heat-flow or ii) variations in exhumation magnitude, if the buoyant Lundy granite generated local uplift pre-exhumation temperatures might be expected to be lower locally. In the absence of a palaeogeothermal gradient it is not possible to discriminate between these two processes.

In Figures 5.71-5.73, the palaeotemperature information derived from thermal history modelling of AFTA samples have been converted to maps of formerly deeper burial across the SW UK region prior to early Jurassic, early Cretaceous and Cenozoic cooling, respectively. Because of the lack of direct constraints on palaeogeothermal gradients, palaeoburial depths have been estimated using a range of realistic upper crustal geothermal gradients (20, 30, 40 and 50°C/km). A palaeosurface temperature was assigned to each episode based on palaeoclimatic evidence presented by Yalçin *et al.* (1997) (20°C for the Jurassic, 20°C for the Lower Cretaceous and 15°C for the Miocene). The maps have been produced by implementing a Kriging gridding algorithm within the Surfer software package. As indicated by Tables B.1-B.5 (Appendix B), palaeotemperature constraints are generally quoted as ranges (the exception being where samples have been completely annealed prior to cooling in which case the palaeotemperatures represent a minimum estimate). In Figures 5.71-5.73 therefore, both minimum and maximum estimates of palaeoburial depths prior to cooling have been calculated.

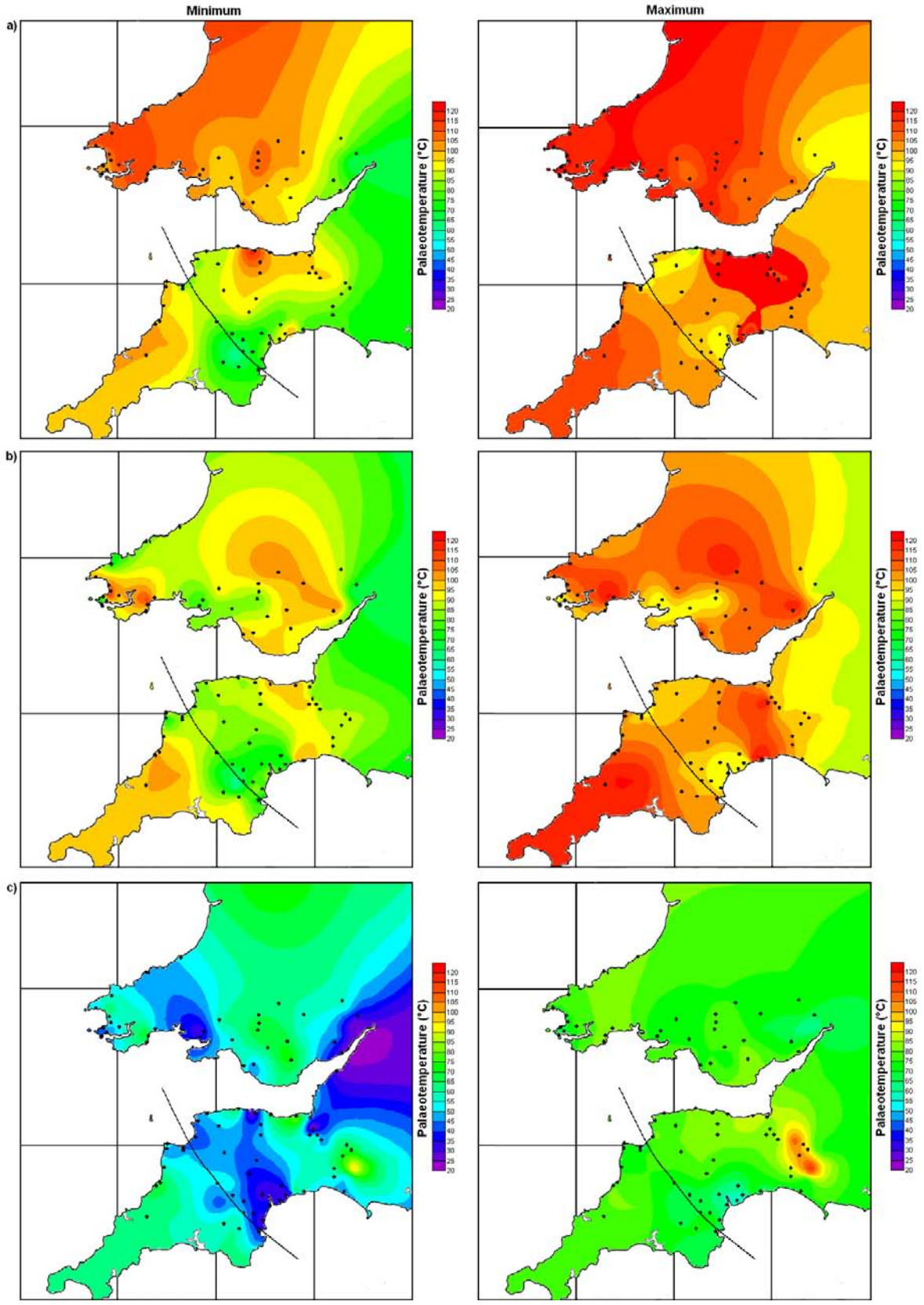

Figure 5.69 –Maps of palaeotemperatures attained prior to a) early Jurassic, b) early Cretaceous and c) Cenozoic (Miocene) cooling episodes. The maps were created by combining estimates from AFTA and VR both from this study and from that of Holford (2006). The maximum and minimum represent the absolute value within 95% confidence limits. Black dots show sample locations, whilst the black line shows the Sticklepath Fault.

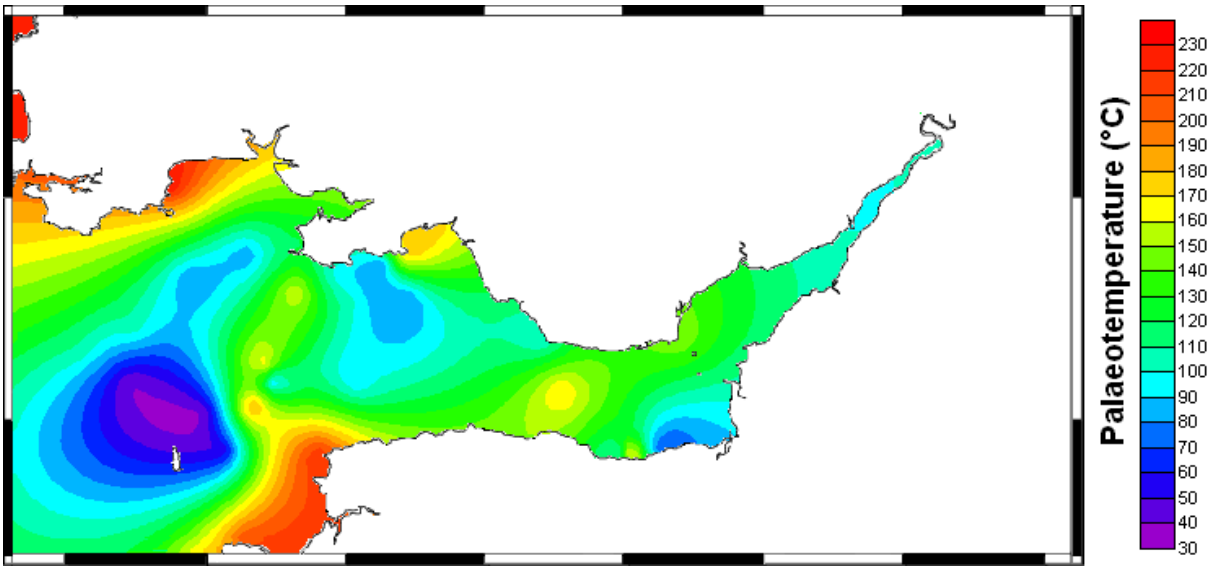

Figure 5.70 – Map showing the distribution of maximum palaeotemperatures from VR data in the BCB.

As shown by Figure 5.71 palaeotemperature information from AFTA indicates that samples which crop out across the SW UK region at the present-day were more deeply buried by *c.* 5km of overburden prior to early Jurassic cooling assuming a palaeogeothermal gradient of 20°C/km and by generally more than 1km of overburden for a palaeogeothermal gradient of 50°C/km. The data appears to show that the Sticklepath-Lustleigh Fault exerted some control on the amount of exhumation in its vicinity as evidenced by the lower exhumation estimates proximal to it. Highest amounts of exhumation are concentrated on major basin margin faults suggesting that footwall uplift was the primary driving mechanism for the exhumation.

Figure 5.72 indicates that samples which crop out across the SW UK region at the present-day were more deeply buried by *c.* 5km of overburden prior to Lower Cretaceous cooling assuming a palaeogeothermal gradient of 20°C/km and by generally more than 1.4km of overburden for a palaeogeothermal gradient of 50°C/km. The data appears to show that the basin margins of the BCB experienced the greatest amount of exhumation. Major faults such as the Watchet-Cothelstone Fault also appear to have experienced comparatively large exhumation amounts whilst the rest of the area experienced broad exhumation. This is likely

due to compartmentalisation of basins where individual faults may not be reactivated but where a fault is reactivated large values of exhumation are associated with that movement.

Palaeoburial maps based on palaeotemperature constraints prior to Cenozoic cooling for palaeogeothermal gradients of 20-50°C/km are provided in Figure 5.73. It is immediately apparent that the highest amounts of deeper burial prior to Cenozoic cooling are *c.* 2km. It must be acknowledged that the 'Cenozoic' cooling episode is less well defined temporally than the early Jurassic and early Cretaceous episodes and may in fact record a number of separate events (i.e. a combination of discrete cooling episodes during the Paleogene and Neogene).

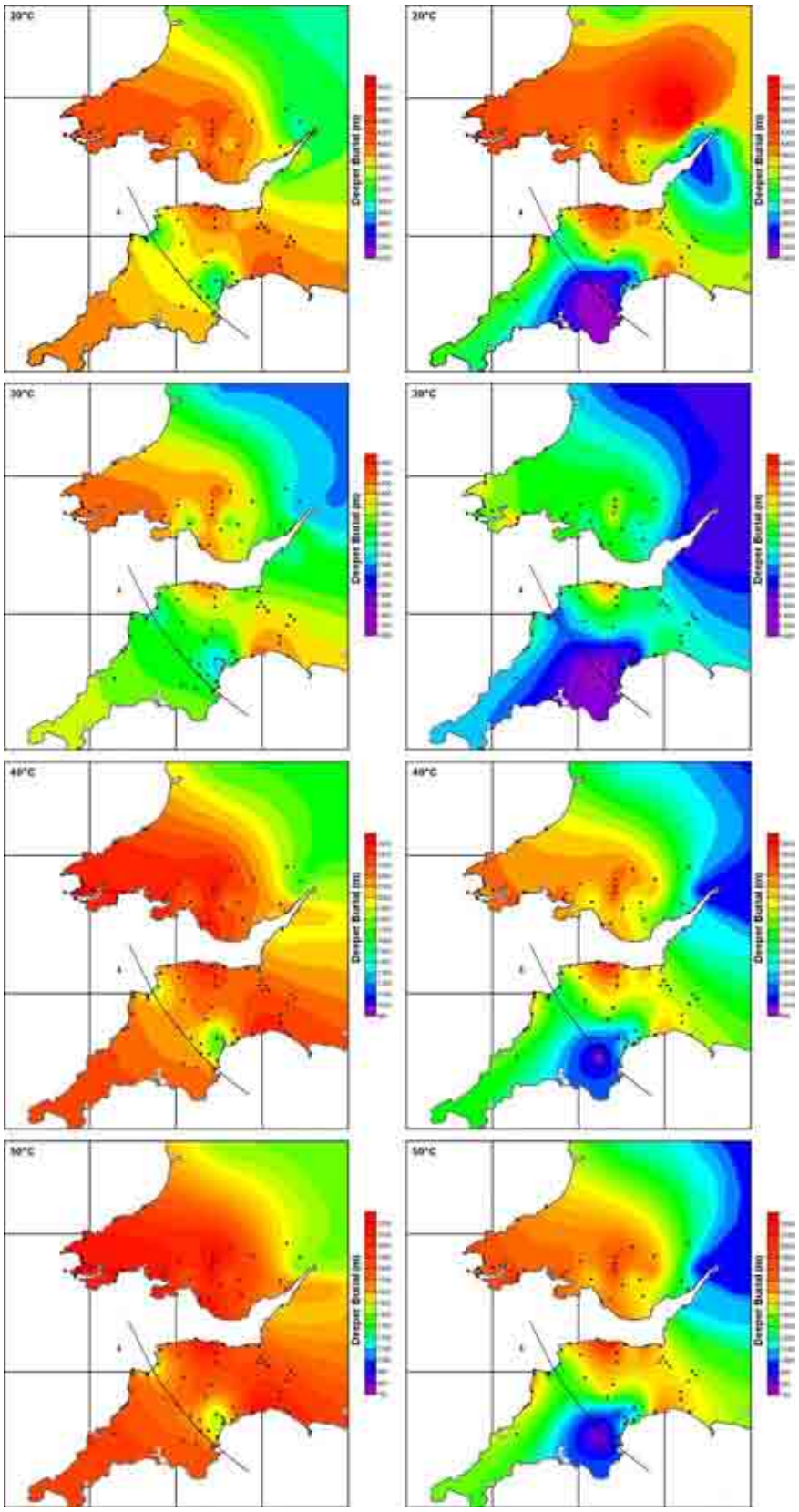

Figure 5.71 - Maps showing maximum (left) and minimum (right) estimates of the amount by which the SW UK region was more deeply buried prior to the Upper Triassic cooling episode. Maps have been produced for palaeogeothermal gradients of 20, 30, 40 and 50°C/km with an assumed palaeosurface temperature of 20°C applied in all cases. Black dots show sample locations, whilst the black line shows the Sticklepath Fault.

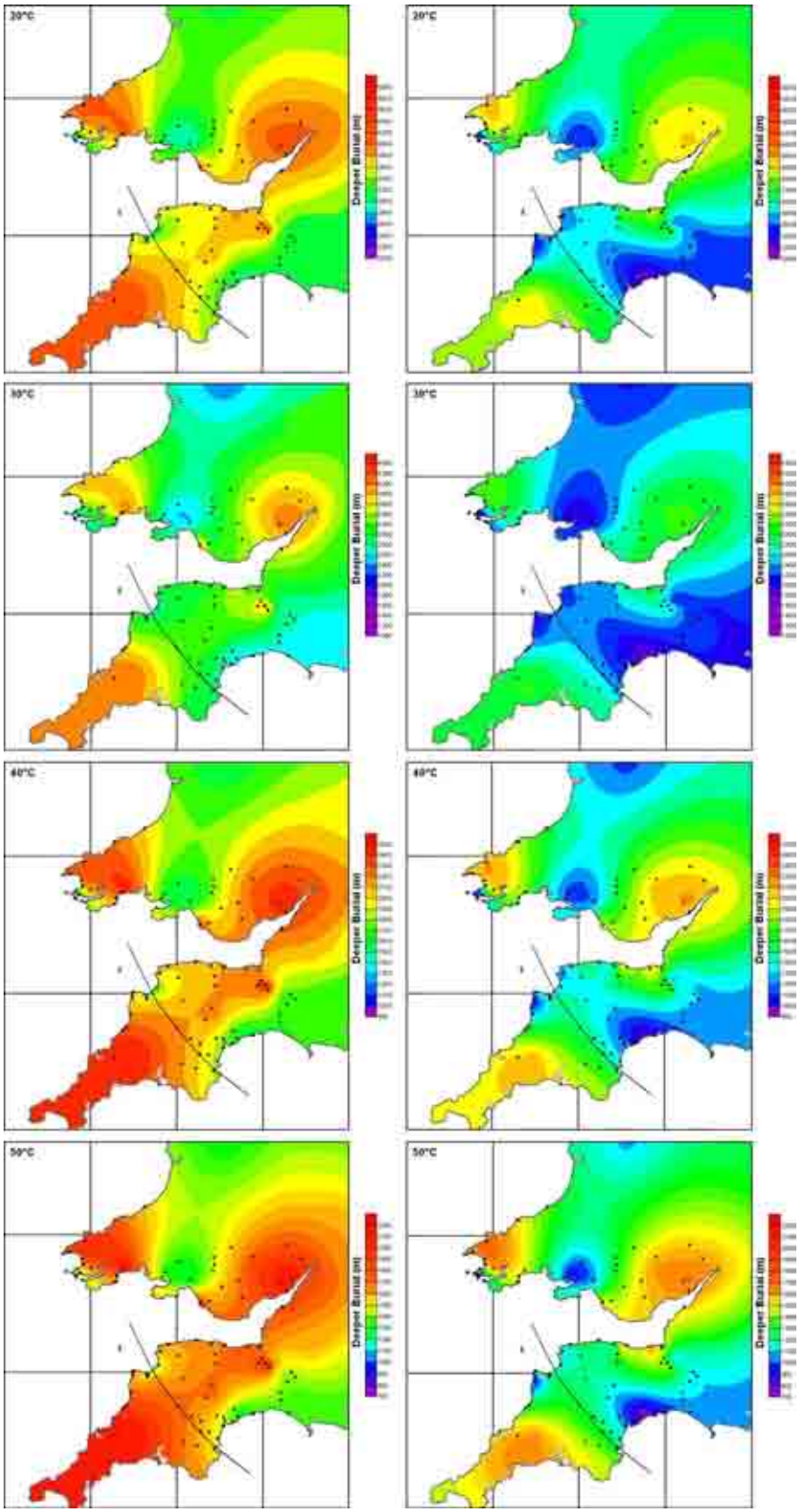

Figure 5.72 - Maps showing maximum (left) and minimum (right) estimates of the amount by which the SW UK region was more deeply buried prior to the Lower Cretaceous cooling episode. Maps have been produced for palaeogeothermal gradients of 20, 30, 40 and 50°C/km with an assumed palaeosurface temperature of 20°C applied in all cases. Black dots show sample locations, whilst the black line shows the Sticklepath Fault.

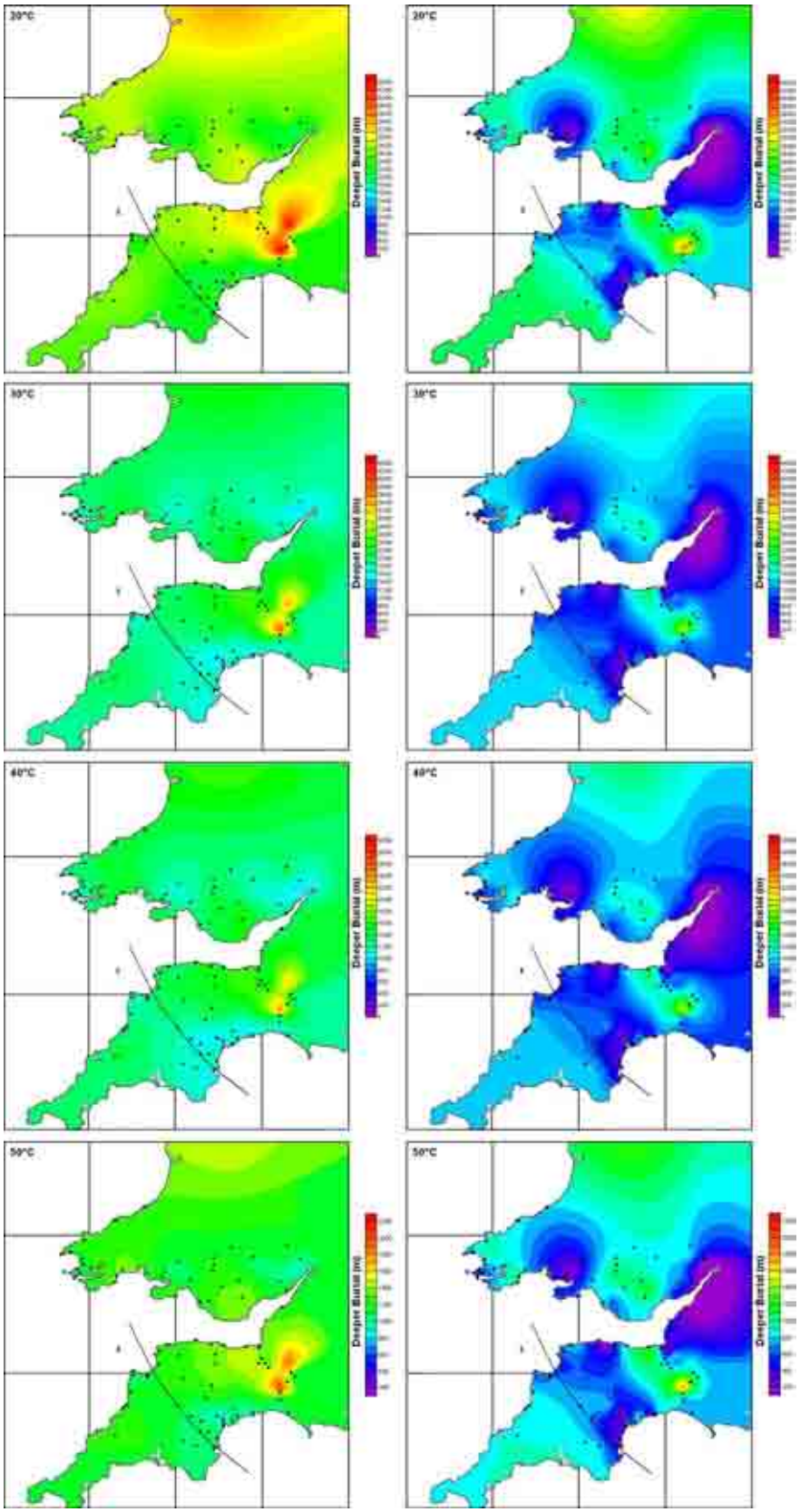

Figure 5.73 - Maps showing maximum (left) and minimum (right) estimates of the amount by which the SW UK region was more deeply buried prior to the Cenozoic cooling episode. Maps have been produced for palaeogeothermal gradients of 20, 30, 40 and 50°C/km with an assumed palaeosurface temperature of 15°C applied in all cases. Black dots show sample locations, whilst the black line shows the Sticklepath Fault.

5.4: DISCUSSION – THE MESOZOIC-CENOZOIC EXHUMATION OF THE SW UK AS INFERRED FROM AFTA AND VR

The Mesozoic-Cenozoic exhumation histories of the SW UK has been investigated using AFTA and VR data from nineteen offshore wells, three onshore boreholes and palaeothermal data from outcrop samples. AFTA data from SW UK provide evidence for at least three important phases of cooling across this region during the Mesozoic-Cenozoic.

5.4.1: TIMING

The Upper Triassic-Lower Jurassic (210-200Ma) cooling event is observed across the SW UK. It is important to note however that there appears to be a disparity between the timing of the event to the north and the south of the area. The event is recognised in the north onshore SW Wales (230-210Ma), South Wales (210-200Ma), North Devon (230-160Ma) and Central Devon/Somerset (245-150Ma). This compares with the south where, in South Devon (200-180) the event appears to be much later. This later timing is consistent with a similarly timed event in the Wessex Basin (some time before 170Ma; Bray *et al.* 1998) and one recognised onshore Ireland (180-170Ma; Green *et al.* 2000). The timings are reported within 95% confidence limits; therefore this time 'gap' is inferred to be real.

The Lower Cretaceous (140-120Ma) cooling event is observed right across the whole of the SW UK and the timing is relatively consistent. The results presented here are also synchronous with events over the entire western UKCS. For example similarly timed exhumation has been recognised in the EISB (125-110Ma; Holford, 2006), onshore Ireland (125-110Ma; Green *et al.* 2000) and in the Wessex Basin (140-100Ma; Bray *et al.* 1998). The timing is also consistent with major stratigraphic breaks across the western UKCS (e.g. Aptian-mid Albian in southern England (Bray *et al.* 1998)). This evidence strongly suggests that the whole of the UKCS was affected by the same event that is recognised in this study.

The cooling episode in the Cenozoic is likely to be composed of a number of discrete palaeothermal episodes, however in some cases it is beyond the ability of the AFTA technique to separate individual events. Evidence presented in this study indicate at least two, possibly three exhumation episodes in the Cenozoic; a late Cretaceous-early Palaeogene (75-55Ma) event, a possible Eocene-Oligocene event (45-25Ma) and a Neogene (Miocene, 20-10Ma) event. The Paleogene event appears most prominently in the offshore wells, however onshore it is recognised in the South Wales Coalfield (75-50Ma), parts of North Somerset (80-25Ma) and South Devon (85-55Ma). Similar studies of palaeothermal data have also revealed a Palaeogene palaeothermal event notably Holford (2006), who presented evidence of a Palaeogene event across the EISB (65-60Ma). The Eocene-Oligocene event is only inferred by outcrop samples in Central Devon (45-20Ma), however other studies have also revealed evidence for an exhumation episode at this time (e.g. Bray *et al.* 1998; in the Wessex Basin and Holford, 2006 in the Mohcras borehole). As mentioned previously AFTA is only able to resolve two individual palaeothermal episodes and more rarely three and it is likely that in most cases this event, where present, is masked by the earlier Paleogene event and later Neogene event. The Neogene (20-10Ma) event is similar to the Lower Cretaceous episode in that it is widely recognised across the western UKCS. Timing of this event across the SW UK is also relatively consistent though it is possible that the event ascribed to the Neogene in North Devon (35-20Ma) actually represents the Eocene-Oligocene event. Again similar studies have recognised the existence of a Neogene exhumation episode which affected the western UKCS (Bray *et al.* 1998; Green *et al.* 2000; Holford *et al.* 2005*a*; Holford, 2006) and the British Isles in general (Menpes & Hillis, 1995; Green *et al.* 1999; Japsen, 2000; Green *et al.* 2001; Williams, 2002).

5.4.2: MAGNITUDE AND DISTRIBUTION

This study has provided evidence for an Upper Triassic-Lower Jurassic cooling event within the SW UK. However, because onshore samples were mostly collected from outcrops rather than vertical sections (i.e. over a range of depths in a well/borehole or elevation profile), it is not possible to place direct constraints upon palaeogeothermal gradients (which can provide important insights into the causes of palaeothermal episodes; Chapter 2) associated with the cooling observed across the SW UK. This means that absolute magnitudes of exhumation related to this event are not possible.

In order to resolve the issue, this study has calculated exhumation based on a range of palaeogeothermal gradients which allow the magnitude and distribution of the exhumation to be assessed (Figure 5.71). The closest estimate to palaeogeothermal gradient during the Upper Triassic-Lower Jurassic exhumation episode of *c.* 35°C/km has been derived from work by Corry & Brown (1998) in the NCSB. Based on this estimate the SW UK has experienced exhumation of 1-3km. As illustrated in Figure 5.71 the distribution in the magnitude of palaeotemperatures (and exhumation) shows a definite trend. The largest values of palaeotemperatures (and by proxy deepest former burial) are found in SW Wales in the Pembrokeshire Peninsular. Additional areas of high palaeotemperature (compared to the surrounding region) can be found in North Somerset and on the South Devon coast. All of these areas are located close to major basin bounding faults and a genetic relationship is therefore inferred. AFTA and VR data suggest the SW Wales region experienced exhumation of 2.5-3.0km and North Somerset, South Devon and Dorset experienced 2.0-2.5km of exhumation. Interestingly, the lowest values for exhumation in the SW UK come from along the trace of the Sticklepath-Lustleigh fault (1.0-1.5km) suggesting that this fault played some

part in suppressing exhumation along its length perhaps by accommodating stresses via lateral displacement rather than uplift.

As with the Upper Triassic-Lower Jurassic event the Lower Cretaceous event was also limited by spot samples, however, offshore well profiles (Table 5.2) provide some insight into possible geothermal gradients, therefore, the same approach of presenting the data was taken as for the Upper Triassic-Lower Jurassic episode. The offshore wells reveal a potential Lower Cretaceous palaeogeothermal gradient of between 34.6-21.4°C/km. This is in excellent agreement with gradients proposed by Corry & Brown (1998), of 37.2-21.1°C/km. For the purposes of this study a gradient of 30°C/km is assumed to be applicable to the SW UK at this time. Figure 5.67 and 5.69 highlight the distribution of palaeotemperatures across the SW UK. The results show that there has been generally similar palaeotemperatures across much of the SW UK at this time with some notable 'hot spots'. These hotspots correspond to areas proximal to large scale faults such as the Bala Fault and Pembrokeshire, Watchet-Cothelstone Fault and North Somerset and Swansea Valley Fault and the Vale of Glamorgan.

This distribution is suggestive of preferential fault reactivation as a result of compression where individual faults control the level of local exhumation superimposed on a much broader uplift event (*cf.* Argent *et al.* 2002). These 'hot spots' could also be thought of as areas where fluid flow has caused elevated palaeotemperatures much like the 'heat spikes' which appear in the vertical well sections. The correlation with major faults suggests that these acted as conduits for fluid flow with a mechanism similar to the 'Fault valve' behaviour proposed by Sibson (2007) (Figure 5.74).

		Exhumation Episode Timing	Palaeogeothermal gradient (°C/km)	Apparent exhumation (m)	Depth to u/c (m)	Water depth (m)	K.B.E (m)	Correction (m)	Total exhumation (m)
Well	42/16-1	Paleogene	57.6	1050	1000	61	33.5	1049	2099
	42/17-1	post-Jurassic	34.6	2540	500	59	33.5	551	3091
	42/21-1	Paleogene	23.4	2180	300	56	33.5	354	2534
	48/19-1	-	-	-	-	-	-	-	-
	48/30-1	Paleogene	35.4	750	1500	123	33.5	1487	2237
	48/30-2	Paleogene	30.8	1110	1500	123	33.5	1487	2597
	49/09-1	post-Jurassic	21.4	1750	750	198	33.5	662	2412
	49/26-1	Paleogene	28.9	1760	1600	120	33.5	1590	3350
	50/03-1	Paleogene	38.1	850	124	124	33.5	110	960
	57/09-1	post-Cretaceous	27.0	680	124	124	33.5	110	790
	102/28-1	Paleogene	47.5	650	570	97	26.0	575	1225
	103/01-1	-	-	-	-	-	-	-	-
	103/02-1	Paleogene	27.5	1350	238	142	33.5	206	1556
	103/18-1	Paleogene	25.5	1950	362	94	22.9	367	2317
	103/21-1	Paleogene	31.5	1100	462	118	33.2	453	1553
	106/24-1	Neogene	26.0	950	748	88	33.5	770	1720
	106/24-2	post-Jurassic	20.0	1100	748	100	33.5	758	1858
	106/28-1	Neogene	31.0	950	932	109	24.0	923	1873
	107/16-1	Paleogene	25.5	1500	300	140	33.5	270	1770
	Senghenydd	Mesozoic	30.5	4250	0	0	33.5	110	4360
	Gwendraeth Valley 2	Mesozoic	30.0	6550	0	0	33.5	110	6660
	Burton Row	Paleogene	34.5	1950	36	0	33.5	146	2096

Table 5.2 – Exhumation estimates from the offshore wells and onshore boreholes of the SW UK using palaeothermal data. Individual best-fit geothermal gradients are indicated as well as the relative timing of the exhumation episode. The correction value follows the same approach as used for the sonic data (Chapter 4). Data highlighted in red should be treated with caution as it is based on limited data (see section 5.3.3.4.3 and discussion therein).

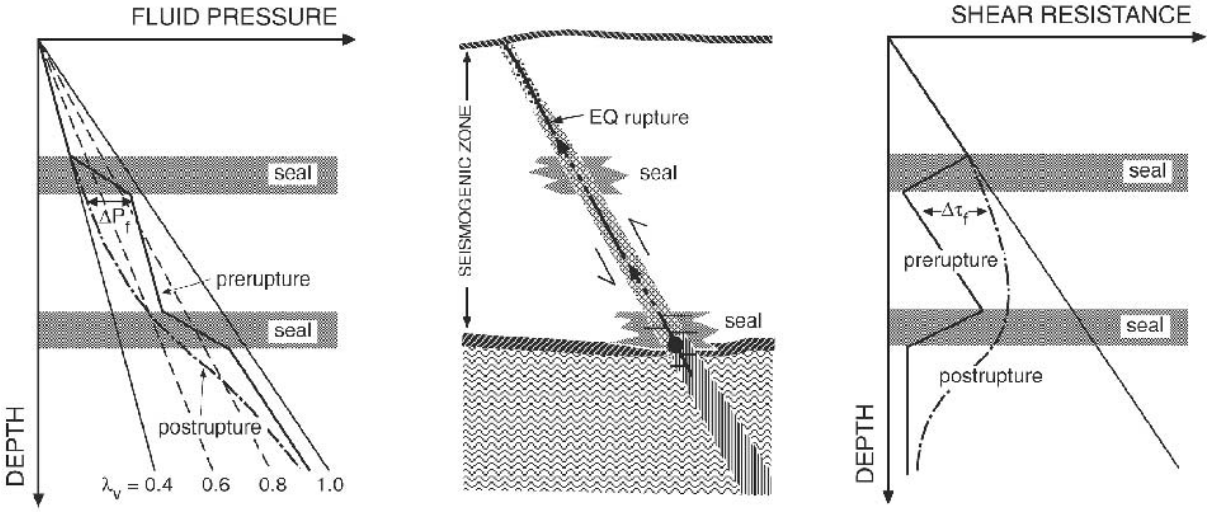

Figure 5.74 - Synoptic diagram of fault-valve behaviour relating pre-rupture and post-rupture fluid-pressure and frictional shear resistance profiles to the presence of two low permeability seals (after Sibson, 2007). Arrows denote post-failure discharge along rupture. In nature multiple seals may occur at different levels, varying laterally along strike.

This study (Figure 5.72) suggests exhumation of *c.* 3km across South Wales (Pembrokeshire and the Vale of Glamorgan) proximal to the major fault boundaries, while more distal areas experienced *c.* 2km of exhumation. Along the Watchet-Cothelstone Fault exhumation of

*c.*3km is suggested compared with *c.* 2.0-2.5km across the rest of Devon, Somerset and Dorset. This is in good agreement with estimates derived from VR data for the offshore wells (Table 5.2; Figure 5.75) which suggests exhumation of *c.* 1.5-3.5km in the offshore basins.

Much of the structural evidence presented by Frodsham & Gayer (1997) shows that coal seams acted as weak, easy-slip horizons during Variscan deformation. This lithological control may have resulted from fluid overpressures in the coals, generated initially during the compaction and devolatilisation of the coals and later by fluids arising from depth along the deep-seated disturbance zones (Gayer *et al.* 1991).

Though an alternative explanation is that, like salt, coal has very low shear strength irrespective of the effective stress. It is suggested here that exhumation is higher across the South Wales Coalfield due to the fact that weak coals promote easy slip an observation which has been made by other workers both in South Wales (Salih & Lisle, 1988; Davies, 1995) and in other coalfields around the world (e.g. Daniels *et al.* 1990 in the Pennsylvanian coalfield). Fluid flow along coal seams has also been demonstrated (Frodsham & Gayer, 1997) and this mechanism could be responsible for the much larger values of exhumation recorded at the Senghenydd and Gwendraeth Valley 2 boreholes compared to exhumation estimates for the rest of the SW UK area. However it should be noted that the VR profiles do not show the classical shapes expected of VR profiles when hot fluids have been circulating (*cf.* Figure 2.33).

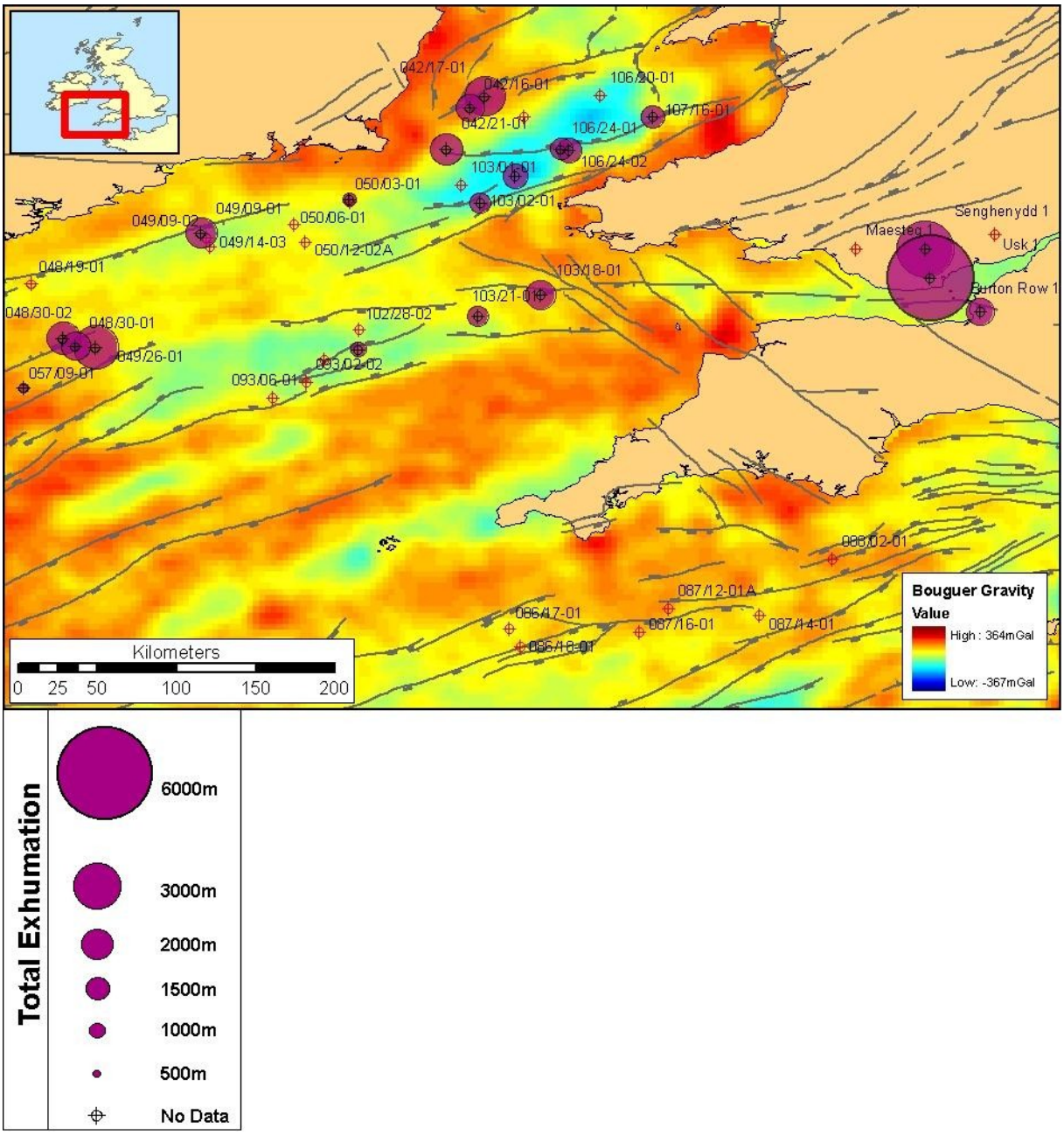

Figure 5.75 – Map showing the maximum burial anomaly in the offshore wells across the SW UK derived from AFTA and VR data. The distribution shows largest exhumation occurred in the South Wales Coalfield. The thermally derived data does not show the same short wavelength variations across faults which the compactional data does (though it could be argued the wells in the NW SGCB do) however the data are still at odds with the distribution of exhumation which would be expected if underplating was the sole driving mechanism of exhumation. Results are superimposed on a regional Bouger gravity anomaly map (BGS, 1997).

Due to the multi-phase nature of the Cenozoic episode it is difficult to estimate absolute values of exhumation. The Paleogene and Eocene-Oligocene episodes are very sparse in their record in the onshore samples making it difficult to constrain a map of palaeotemperatures

across the area. Ironically, it is possibly the best constrained in terms of geothermal gradient thanks to its almost ubiquitous nature across the offshore basins (Table 5.2). For the onshore region the event is best constrained by results from the Burton Row borehole which indicates exhumation of 1.5-2.5km. This is consistent with results from the offshore region (Table 5.2) indicative of 1.0-2.5km of exhumation across the area. No constraints can be placed on the Eocene-Oligocene episode as no vertical sections which record the event exist due to its record in outcrop samples only, however it is likely to be of similar magnitude to the Paleogene episode based on palaeotemperature data from those samples.

Neogene (Miocene) exhumation appears to have broadly affected the entire western UKCS based on palaeotemperature data (Figures 5.69 and 5.73). The data are very similar across the SW UK however there is evidence for slightly higher palaeotemperatures (and hence exhumation) on the basin margins of the BCB (both along the South Wales coast and the North Devon-Somerset coast). Additionally there appears to be a 'hot spot' centred in the Yeovil area of Somerset which could be related to the influence of the nearby Watchet-Cothelstone Fault or, as revealed by BGS maps, a series of normal faults. As with the previous episodes, there are few constraints on the palaeogeothermal gradient and as such once again the gradient has been based on the work of Corry & Brown (1998) who inferred a Cenozoic palaeogeothermal gradient of 41.0-46.7°C/km, based on data from the exploration wells of the NCSB. Based on this gradient the SW UK has experienced fairly uniform exhumation of 0.5-1.5km. The margins of the BCB experienced a slightly higher amount of exhumation (1.0-1.8km) with the 'hot spot' of Yeovil recording the highest value of exhumation at *c.* 2.2km.

This is in excellent agreement with estimates derived from other studies. For example, Williams (2002) presented seismic evidence for over 1km of exhumation in the BCB and SGCB. Up to 1.5km of Eocene and Oligocene strata blanket the base Cenozoic unconformity surface in the SGCB, suggesting that in this part of the Celtic Sea the Mercia Mudstone might have reached its maximum burial depth prior to Miocene uplift and denudation. VR profiles from wells in the SGCB suggest that thermal maturity in the Jurassic section were established prior to the Cenozoic, probably during burial beneath Cretaceous sediments which were removed during Paleogene exhumation. In these wells the best fit to the VR data can be achieved with around 1km of Paleogene erosion followed by the deposition of a similar amount of Eocene and Oligocene sediments, 400m of which were eroded during the Miocene. It should be noted however that the offshore wells record the Neogene palaeogeothermal gradient as closer to 30°C/km based on the SGCB wells (Table 5.2) so this amount of exhumation should be regarded as the most likely minimum amount.

5.4.3: DRIVING MECHANISMS FOR MESOZOIC-CENOZOIC EXHUMATION IN THE SW UK

In areas where the post-rift record is severely eroded, estimating the magnitude and timing of exhumation is difficult when more than one phase of uplift has occurred unless AFTA data are available. This limitation is clearly demonstrated in the Irish offshore. The relatively consistent picture that emerges from the study of Murdoch *et al.* (1995) of the NCSB is in strong contrast to the broad range in estimates of the magnitude and timing of exhumation at well locations in the Kish Bank, Central Irish Sea and St. George's Channel basins (Table 5.3). Estimates from tectonic and thermal methods are available for a single well, 42/21-1, in the St. George's Channel Basin (Table 5.3). Good agreement exists between thermal estimates (1600m – Corcoran & Clayton (1999) versus 1500m – Green *at al.* (2001)) for the main phase of exhumation and there is broad consensus with respect to the timing of this

episode (Palaeogene) with an additional event (Late Cenozoic) resolved by the AFTA data (Green *et al.* 2001). Insights gained from seismic interpretation in the SGCB has allowed Williams *et al.* (2005) to highlight multiple causes and timings for the observed exhumation in this basin to better understand inter-well variations in the magnitude of the exhumation and importantly to describe differences in the contribution of inversion to exhumation within the same basin, attributable to strain partitioning along major bounding faults. This is a key observation that is likely to apply to other basins that are both exhumed and inverted. This study suggests that erosion of the SCSB and BCB occurred in response to early Cretaceous, Paleogene and Neogene uplift, the magnitude of which, depending on the location of the wells relative to major inversion axes.

Basin	Well	Net exhumation	Timing	Method	Author
Kish Bank Basin	33/17-1	>1500	Paleogene	Tectonic	Rowley & White, 1990
	33/17-1	350	Cenozoic	Sonic ITT	Dunford et al. 2001
	33/17-2a	675	Cenozoic	Sonic ITT	Dunford et al. 2001
	33/21-1	>900	Paleogene	Tectonic	Rowley & White, 1990
	33/21-1	1500	Cenozoic	Sonic ITT	Dunford et al. 2001
	33/22-1	980	Cenozoic	Sonic ITT	Dunford et al. 2001
	33/22-1	3000	Post Jurassic	VR	Jenner, 1981
	33/22-1	1300	Post Liassic	VR	Naylor et al. 1993
	33/22-1	1200-1550	Early Permian	VR	Corcoran & Clayton, 1999
Central Irish Sea Basin	42/12-1	2250	Early Permian	VR & Stratigraphic	Corcoran & Clayton, 1999
	42/12-1	3000	Mid Cretaceous	AFTA & VR	Duncan et al. 1998
	42/12-1	1300	Early Cenozoic	AFTA & VR & Stratigraphic	Duncan et al. 1998
	42/16-1	2975	Early Cretaceous	AFTA & VR	Green et al. 2001
	42/16-1	2250	Early Cenozoic	AFTA & VR	Green et al. 2001
	42/16-1	1300	Late Cenozoic	AFTA & VR	Green et al. 2001
	42/16-1	2240	Early Cretaceous	Sonic ITT	Williams et al. 2005
	42/17-1	1000	Early Permian	VR & Stratigraphic	Corcoran & Clayton, 1999
	42/17-1	1900	Post Sinemurian	VR & Stratigraphic	Corcoran & Clayton, 1999
	42/17-1	2080	Early Cretaceous	Sonic ITT	Williams et al. 2005
St. George's Channel Basin	42/21-1	1000	Post Bathonian	VR & Stratigraphic	Corcoran & Clayton, 1999
	42/21-1	>2000	Early Cenozoic	Tectonic	Allen et al. 1998
	42/21-1	600	Paleogene	Tectonic & VR	Welch & Turner, 2000
	42/21-1	1500	Early Cenozoic	AFTA & VR	Green et al. 2001
	42/21-1	1000	Late Cenozoic	AFTA & VR	Green et al. 2001
North Celtic Sea Basin	47/29-1	910	Cenozoic	Sonic ITT	Menpes & Hillis, 1996
	47/30-1	500	Paleogene & Oligo-Miocene	Stratigraphic & Sonic ITT	Murdoch et al. 1995
	48/19-1	120	Paleogene & Oligo-Miocene	AFTA & VR	Murdoch et al. 1995
	48/19-1	507	Paleogene & Oligo-Miocene	Stratigraphic & Sonic ITT	Murdoch et al. 1995
	48/19-1	980	Cenozoic	Sonic ITT	Menpes & Hillis, 1996
	48/20-1	573	Paleogene & Oligo-Miocene	Stratigraphic & Sonic ITT	Murdoch et al. 1995
	48/22-1	252	Paleogene & Oligo-Miocene	Stratigraphic & Sonic ITT	Murdoch et al. 1995
	48/23-1	677	Paleogene & Oligo-Miocene	Stratigraphic & Sonic ITT	Murdoch et al. 1995
	48/24-1	787	Paleogene & Oligo-Miocene	Stratigraphic & Sonic ITT	Murdoch et al. 1995
	48/24-2	907	Paleogene & Oligo-Miocene	Stratigraphic & Sonic ITT	Murdoch et al. 1995
	48/25-2	672	Paleogene & Oligo-Miocene	Stratigraphic & Sonic ITT	Murdoch et al. 1995
	48/26-1	692	Paleogene & Oligo-Miocene	Stratigraphic & Sonic ITT	Murdoch et al. 1995
	48/30-1	653	Paleogene & Oligo-Miocene	Stratigraphic & Sonic ITT	Murdoch et al. 1995
	49/09-1	300	Paleogene & Oligo-Miocene	AFTA & VR	Murdoch et al. 1995
	49/09-1	295	Paleogene & Oligo-Miocene	Stratigraphic & Sonic ITT	Murdoch et al. 1995
	49/09-1	880	Cenozoic	Sonic ITT	Menpes & Hillis, 1996
	49/09-2	341	Paleogene & Oligo-Miocene	Stratigraphic & Sonic ITT	Murdoch et al. 1995
	49/09-2	640	Cenozoic	Sonic ITT	Menpes & Hillis, 1996
	49/09-3	830	Cenozoic	Sonic ITT	Menpes & Hillis, 1996
	49/10-1	294	Paleogene & Oligo-Miocene	Stratigraphic & Sonic ITT	Murdoch et al. 1995
	49/11-1	573	Paleogene & Oligo-Miocene	Stratigraphic & Sonic ITT	Murdoch et al. 1995
	49/13-1	793	Paleogene & Oligo-Miocene	Stratigraphic & Sonic ITT	Murdoch et al. 1995
	49/14-1	936	Paleogene & Oligo-Miocene	Stratigraphic & Sonic ITT	Murdoch et al. 1995
	49/14-2	983	Paleogene & Oligo-Miocene	Stratigraphic & Sonic ITT	Murdoch et al. 1995
	49/14-3	441	Paleogene & Oligo-Miocene	Stratigraphic & Sonic ITT	Murdoch et al. 1995
	49/14-3	820	Cenozoic	Sonic ITT	Menpes & Hillis, 1996
	49/16-1	557	Paleogene & Oligo-Miocene	Stratigraphic & Sonic ITT	Murdoch et al. 1995
	49/16-2	557	Paleogene & Oligo-Miocene	Stratigraphic & Sonic ITT	Murdoch et al. 1995
	49/17-1	632	Paleogene & Oligo-Miocene	Stratigraphic & Sonic ITT	Murdoch et al. 1995
	49/19-1	747	Paleogene & Oligo-Miocene	Stratigraphic & Sonic ITT	Murdoch et al. 1995
	49/20-1	1016	Paleogene & Oligo-Miocene	Stratigraphic & Sonic ITT	Murdoch et al. 1995
	49/29-1	173	Paleogene & Oligo-Miocene	Stratigraphic & Sonic ITT	Murdoch et al. 1995
	49/30-1	765	Paleogene & Oligo-Miocene	Stratigraphic & Sonic ITT	Murdoch et al. 1995
	50/03-1	1300	Paleogene & Oligo-Miocene	AFTA & VR	Murdoch et al. 1995
	50/06-1	666	Paleogene & Oligo-Miocene	Stratigraphic & Sonic ITT	Murdoch et al. 1995
	50/06-1	690	Cenozoic	Sonic ITT	Menpes & Hillis, 1996
	50/11-1	1121	Paleogene & Oligo-Miocene	Stratigraphic & Sonic ITT	Murdoch et al. 1995
	50/11-2	1079	Paleogene & Oligo-Miocene	Stratigraphic & Sonic ITT	Murdoch et al. 1995
	50/12-2	806	Paleogene & Oligo-Miocene	Stratigraphic & Sonic ITT	Murdoch et al. 1995
	50/12-2a	1170	Cenozoic	Sonic ITT	Menpes & Hillis, 1996
	55/09-1	440	Paleogene & Oligo-Miocene	Stratigraphic & Sonic ITT	Murdoch et al. 1995
	55/12-1	419	Paleogene & Oligo-Miocene	Stratigraphic & Sonic ITT	Murdoch et al. 1995
	55/14-1	661	Paleogene & Oligo-Miocene	Stratigraphic & Sonic ITT	Murdoch et al. 1995
	55/19-1	0	Paleogene & Oligo-Miocene	Stratigraphic & Sonic ITT	Murdoch et al. 1995
	55/20-1	287	Paleogene & Oligo-Miocene	Stratigraphic & Sonic ITT	Murdoch et al. 1995
	55/21-1	262	Paleogene & Oligo-Miocene	Stratigraphic & Sonic ITT	Murdoch et al. 1995
	55/21-2	0	Paleogene & Oligo-Miocene	Stratigraphic & Sonic ITT	Murdoch et al. 1995
	56/26-1	142	Paleogene & Oligo-Miocene	Stratigraphic & Sonic ITT	Murdoch et al. 1995
	56/26-2	164	Paleogene & Oligo-Miocene	Stratigraphic & Sonic ITT	Murdoch et al. 1995
	57/02-1	585	Paleogene & Oligo-Miocene	Stratigraphic & Sonic ITT	Murdoch et al. 1995
	57/06-1	945	Paleogene & Oligo-Miocene	Stratigraphic & Sonic ITT	Murdoch et al. 1995
	57/09-1	550	Paleogene & Oligo-Miocene	AFTA & VR	Murdoch et al. 1995
	57/09-1	497	Paleogene & Oligo-Miocene	Stratigraphic & Sonic ITT	Murdoch et al. 1995
	58/03-1	499	Paleogene & Oligo-Miocene	Stratigraphic & Sonic ITT	Murdoch et al. 1995

Table 5.3 – Compilation of published estimates of exhumation for 54 wells offshore Ireland. Method used to estimate the magnitude of exhumation at each well location is specified together with author's analysis of the timing of individual exhumation events (modified after Corcoran & Doré, 2005).

5.4.3.1: The Upper Triassic-Lower Jurassic episode

This study has provided evidence for an Upper Triassic-Lower Jurassic cooling event within the SW UK. Application of AFTA in various types of geological setting (e.g. Green *et al.* 2000, 2001*a*, 2001*b*) has shown that cooling of samples from palaeotemperature peaks can usually be attributed to either a decline in basal heat flow or exhumation (Green *et al.* 2002). It is possible that the observed cooling during the Upper Triassic-Lower Jurassic could reflect the decay of a thermal anomaly induced by the initial stages of rifting in the adjacent extensional sedimentary basins, but as discussed earlier, previous AFTA studies of these basins have revealed no evidence for a similarly timed thermal event. Additionally Gallagher *et al.* (1998) have suggested that the subsurface thermal effects of extension and associated magmatism related to the process of continental rifting are largely restricted to the region undergoing extension, crustal thinning and subsidence and that thermal gradients in the shallow crust of the marginal areas (i.e. ≤10km) are usually unaffected by rifting processes. The results of this study would appear to challenge that assertion since the distribution of the Upper Triassic episode appears much broader than 10km and may indeed extend over the whole of the SW UK. However, it is suggested here therefore that the elevated palaeotemperatures across the SW UK region prior to Triassic-early Jurassic cooling are better explained in terms of deeper burial followed by exhumation, rather than variations in basal heat flow.

Several authors (e.g. Eynon, 1981; Underhill & Partington, 1993) have argued for thermal doming of the UK during the Mid-Jurassic. Although this doming was centred on the North Sea (probably driven by a transient plume head), on the basis of stratigraphic evidence Underhill & Partington (1993) suggested that the elevation anomaly created by the doming had a diameter in the region of >900->1250km and therefore could have extended to SW UK.

A more likely candidate for thermal doming would be the proposed thermal dome of Tate & Dobson (1988) which was envisaged as offshore SW Ireland. However, the AFTA data from SW UK indicates a consistent time range of 210-200Ma for the onset of cooling from maximum palaeotemperatures, at least 20Ma earlier than the timing of the North Sea doming. In addition, an extensive AFTA dataset from across the Midland Platform and the East Midlands Shelf, which are more proximal to the centre of the projected domal area, reveals no evidence for an Upper Triassic-Lower Jurassic episode of cooling (Green *et al.* 2001*b*). It is possible that although a large area was significantly uplifted during Jurassic thermal doming, it was accompanied by relatively little erosion and therefore negligible cooling, thereby explaining the absence of a thermal signature for this event.

An alternative explanation is that the SW UK cooling event represents localised exhumation driven by footwall uplift along the major basin margin faults such as the Bala Fault. As explained more fully by Holford (2006), the CBB was a major depocentre throughout the Triassic and Jurassic, with subsidence controlled by normal movements along the Mohcras-Tonfanau-Bala fault system. The timing of the cooling event identified in the SW UK (215-195Ma) is coeval with subsidence in the adjacent basins (*cf.* Holford, 2006) and consistent with a localised exhumation event driven by uplift along the basin margins.

This observation allows modifications to be made to Holford's (2006) palaeogeographic reconstruction of Wales in light of this new evidence (Figure 5.76) further casting doubt on the validity of the Dobson & Whittington (1987) model and having major implications for palaeogeographic and tectonic reconstructions of the SW UK during the Mesozoic. The results presented in this study agree with those of Holford (2006) in suggesting that the area of subsidence was likely to have been far more restricted and predominantly controlled by normal displacements along the Bala Fault (*cf.* Cope, 1984) and southern margin fault of the

BCB with the footwalls of these faults almost certainly emergent. A model has been envisaged whereby the Upper Triassic-Lower Jurassic exhumation represents the effects of footwall uplift superimposed on a broader regional uplift caused by asthenospheric upwelling which initiated the rifting in the Permian-Triassic (Figure 5.77).

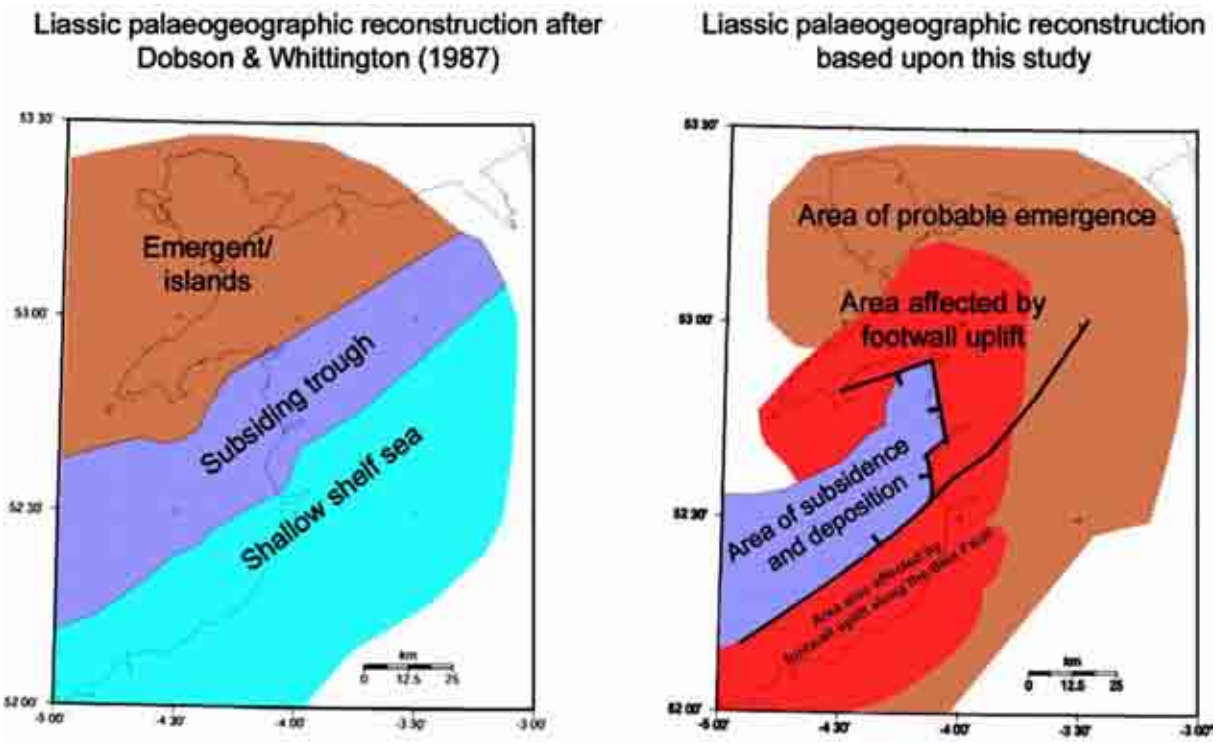

Figure 5.76 - Comparison between Lower Jurassic Palaeogeographic setting of NW Wales and Cardigan Bay as indicated by results from this study and those of Holford (2006), and that proposed by Dobson & Whittington (1987). Results from AFTA indicate that the region of Lower Jurassic subsidence and deposition was far more restricted than previously supposed and imply that the Mochras-Tonfanau-Bala fault system actively controlled Mesozoic subsidence (modified after Holford, 2006).

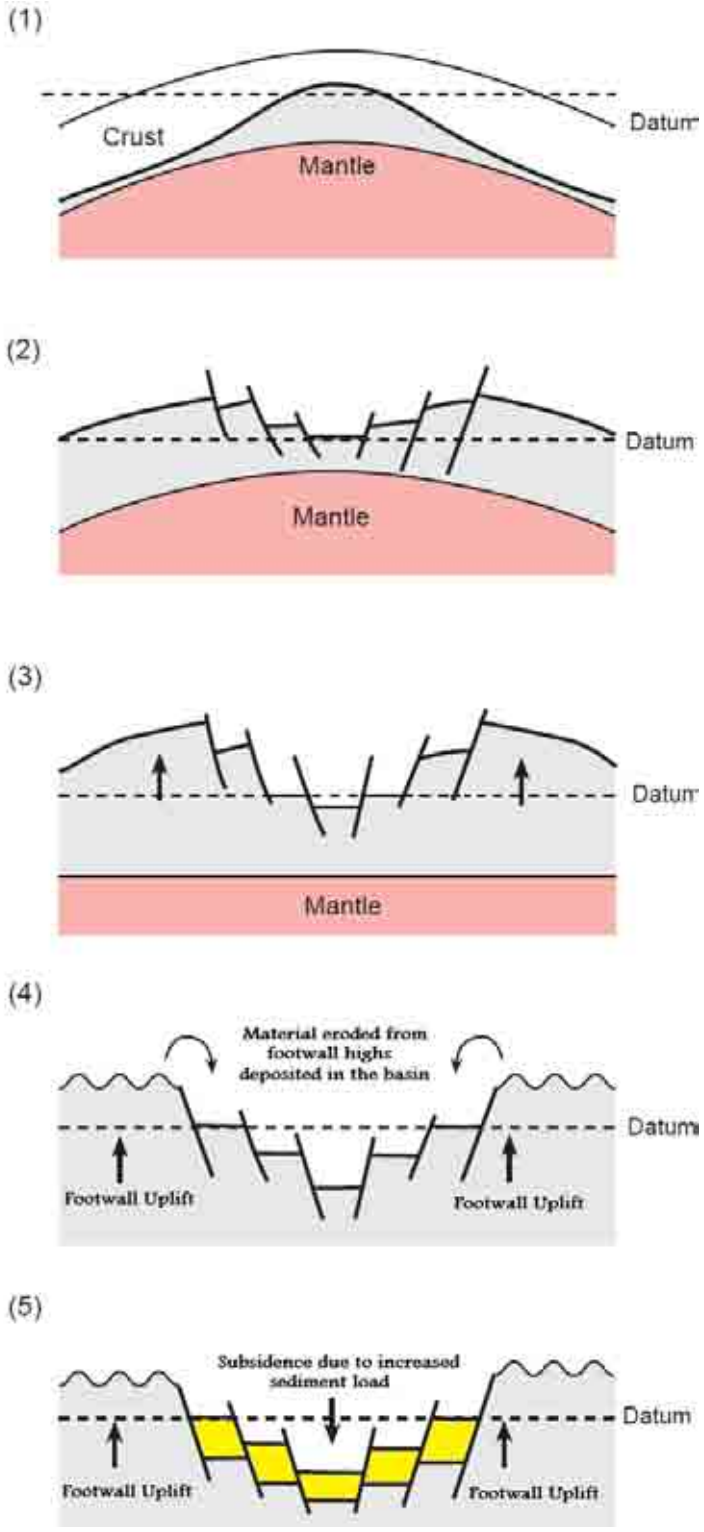

Figure 5.77 – Model to account for the observation of the Upper Triassic-Lower Jurassic exhumation across the SW UK. (1) Prior to rifting asthenospheric upwelling or crustal thinning causes regional epeirogenic uplift (2) Initiation of rifting and basin formation. The thermal anomaly from the asthenosphere/crustal thinning continues to cause epeirogenic uplift. (c) As the thermal anomaly decays regional subsidence begins in the rift basin and footwall uplift is initiated. (d) The eroded footwall highs deposit material into the basin causing further subsidence and enhanced footwall uplift. (5) The end result is a broad uplift event recognised away from basin margin faults due to epeirogenic uplift but more prominent uplift at the basin bounding faults due to enhanced footwall uplift.

5.4.3.2: The Lower Cretaceous episode

Another phase of exhumation, which on the basis of local and regional AFTA data appears to have begun during the early Cretaceous (140-120Ma) and removed up to 3km of mid Jurassic-early Cretaceous sediments, has also been identified across the SW UK. Kilometre-scale early Cretaceous exhumation is being increasingly documented across the offshore UK basins (e.g. Duncan *et al.* 1998; McMahon & Turner, 1998; Green *et al.* 2001*a*; Holford, 2006; this study). As discussed in more detail in Chapter 6, the early Cretaceous exhumation episode coincided temporally with a number of important rifting events along the incipient NE Atlantic margin (Doré *et al.* 1999), such as the onset of sea-floor spreading between Iberia and the Grand Banks, suggesting a causative link between these events. Additionally, as mentioned above footwall uplift is likely to have continued until this time.

It is important to note that, although kilometre-scale early Cretaceous exhumation has been identified across the margins of the SGCB (where sonic velocity data provide evidence for up to 2.25km of exhumation at this time (Williams *et al.* 2005)), the main depocentre of the SGCB seems to have been unaffected by exhumation at this time. One possible explanation for this is that the deep bathymetry which developed within the SGCB during the Jurassic (Turner, 1996) meant that uplift during the early Cretaceous was not necessarily accompanied by erosion (Williams *et al.* 2005). Furthermore, it is possible that the SGCB was actually undergoing subsidence during the early Cretaceous, since the SGCB has a similar NE-SW structural trend to the en-echelon NCSB where thick Lower and Upper Cretaceous successions are preserved (Tappin *et al.* 1994) and similarly no early Cretaceous palaeothermal effects are detected (Green *et al.* 2001*a*). As the deepest parts of the SGCB depocentre have not been drilled, it remains a possibility that Lower Cretaceous rocks are preserved in the axial parts of the basin (Tappin *et al.* 1994). The results presented in this

study seem to favour continued footwall uplift to be the causal mechanism of Cretaceous exhumation, however some well data seems to provide evidence of compression being a contributory mechanism of Lower Cretaceous exhumation (Figure 5.78), suggesting some reverse movement on faults may also be a cause. Wells 49/09-1 and 57/09-1 (Figures 5.43-5.44) show evidence of an intra-Cretaceous 'heat spike' which is inferred to have been caused by the passage of hot fluids. Since there is no evidence for igneous activity proximal to these wells during the Cretaceous the hot fluids are suggested to have been expelled from the pores of rocks during compression.

5.4.3.3: The Cenozoic episodes

AFTA studies carried out over the last few years have shown that over much of the UK region, Late Cretaceous-Early Cenozoic heating was not restricted to the developing continental margin, to the vicinity of Cenozoic igneous activity or to discrete inversion axes. Elevated palaeotemperatures prior to early Cenozoic cooling typically around 40-110°C higher than present temperatures have now been detected by application of AFTA over a wide region including northern and eastern England, southern Scotland, the Irish Sea, the Moray Firth, Northern Ireland, the Celtic Sea, the Wessex Basin and the southern North Sea in locations well away from any obvious source of heat and in rocks of various stratigraphic ages from Jurassic-Precambrian (Green *et al.* 1993). This study has identified three separate Cenozoic events; Paleogene, Eocene-Oligocene and Neogene.

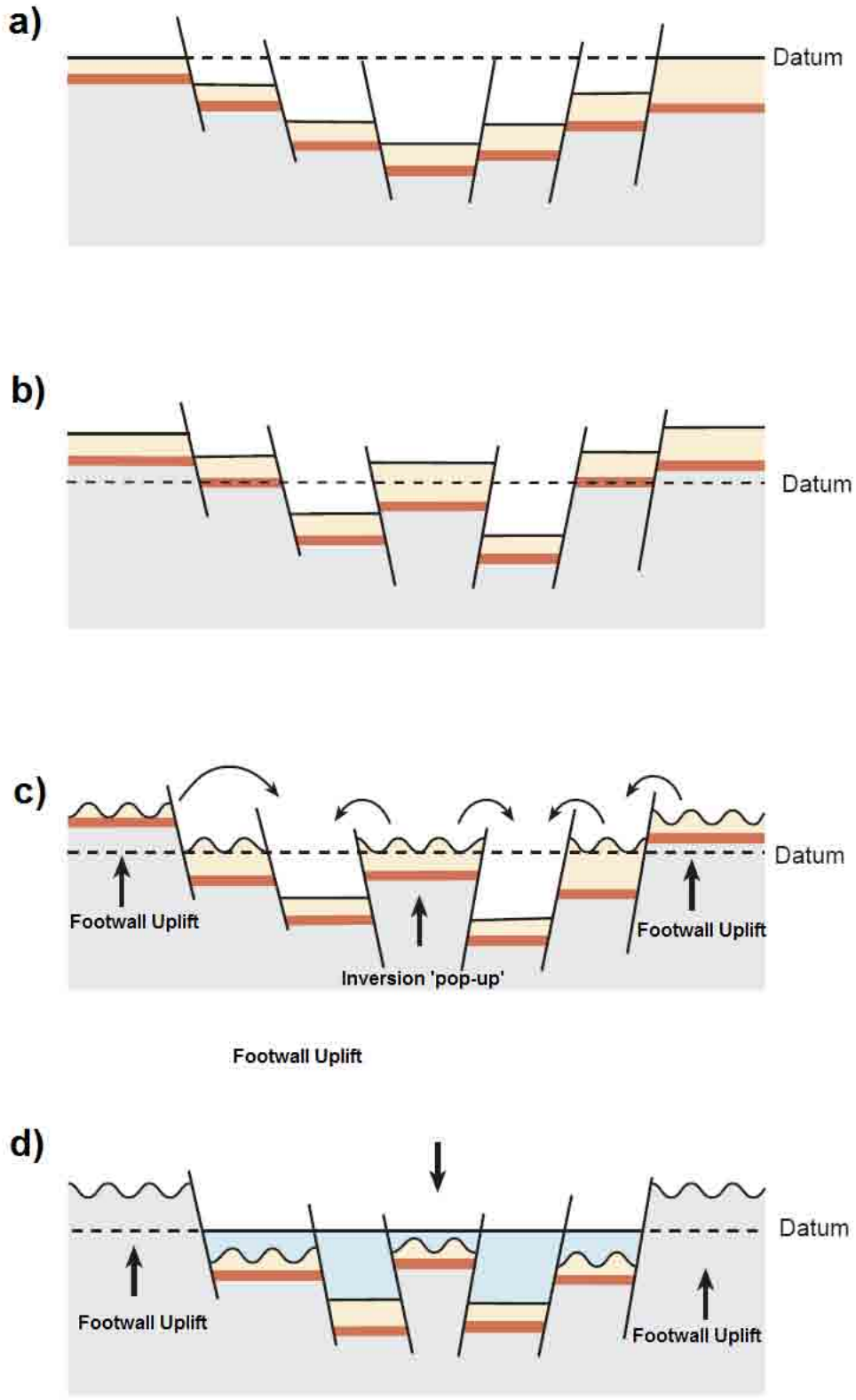

Figure 5.78 – Model to account for the observation of the Lower Cretaceous exhumation across the SW UK. (a) Late Jurassic pre-inversion basin configuration. (b) Inversion causes reactivation of faults. Basin compartmentalisation occurs due to selective fault reactivation. (c) As inversion continues regional highs get eroded counteracting inversion uplift and causing net subsidence. Footwall uplift allows basin margins to continue uplifting. (d) As inversion continues eroded material fills the basin and uplift becomes restricted to basin margins due to footwall uplift.

Previous workers (Williams, 2002; Turner & Williams, 2004; Williams *et al.* 2005; Holford *et al.* 2005*a*, *b*; Holford, 2006) have shown that Cenozoic exhumation in the western UK is largely due to tectonic inversion as evidenced by seismic reflection profiles and this evidence is supported by compactional and palaeothermal data (Williams, 2002; Holford, 2006). This study has shown that the 'Cenozoic' exhumation is actually a composite event made up of a number of separate cycles of exhumation. It is suggested that the cyclicity observed is due to the orientation of faults in relation to the prevailing stress direction.

Hibsch *et al.* (1995) have provided evidence for a changing stress-field throughout NW Europe during the Mesozoic-Cenozoic (Figure 5.79). Compressional shortening has been shown to be non-uniform (Turner & Williams, 2004) e.g. due to selective fault reactivation (Sibson, 1995) and it is suggested here that preferential reactivation of faults due to the orientation of the stress-field is what is responsible for the exhumation episodes identified by the palaeothermal data (Figure 5.80).

Hibsch *et al.* (1995) presented a number of maps which would seem to support this hypothesis and modelling by Gölke & Coblentz (1996) also highlight the effect of competing compressional stress directions (Figure 5.81) further commenting that a combination of ridge-push and collisional boundary forces (i.e. Alpine orogenesis) are found to establish the broad-scale features of the observed stress field. Maximum exhumation from fault reactivation will occur where faults are oriented perpendicular to the prevailing stress-field. The Hibsch *et al.* (1995) maps show that during the 'Laramide' phase of Alpine deformation the NCSB, SCSB, Channel Basin and WAB were all oriented favourably to the stress field which explains why the Paleogene exhumation episode is recorded by samples from these basins. During the Pyrenean orogeny the stress field indicates that the Wessex Basin and BCB were oriented favourably and likely experienced fault reactivation at this time explaining why the AFTA

samples from across central Devon record this event. As shown by the AFTA data this event is not as easily resolvable in the data and is interpreted to be due to either a weaker stress field compared to the 'Laramide' phase of the Alpine orogeny and thus smaller exhumation overall or the fact that the later Neogene event was much larger and overprinted this event.

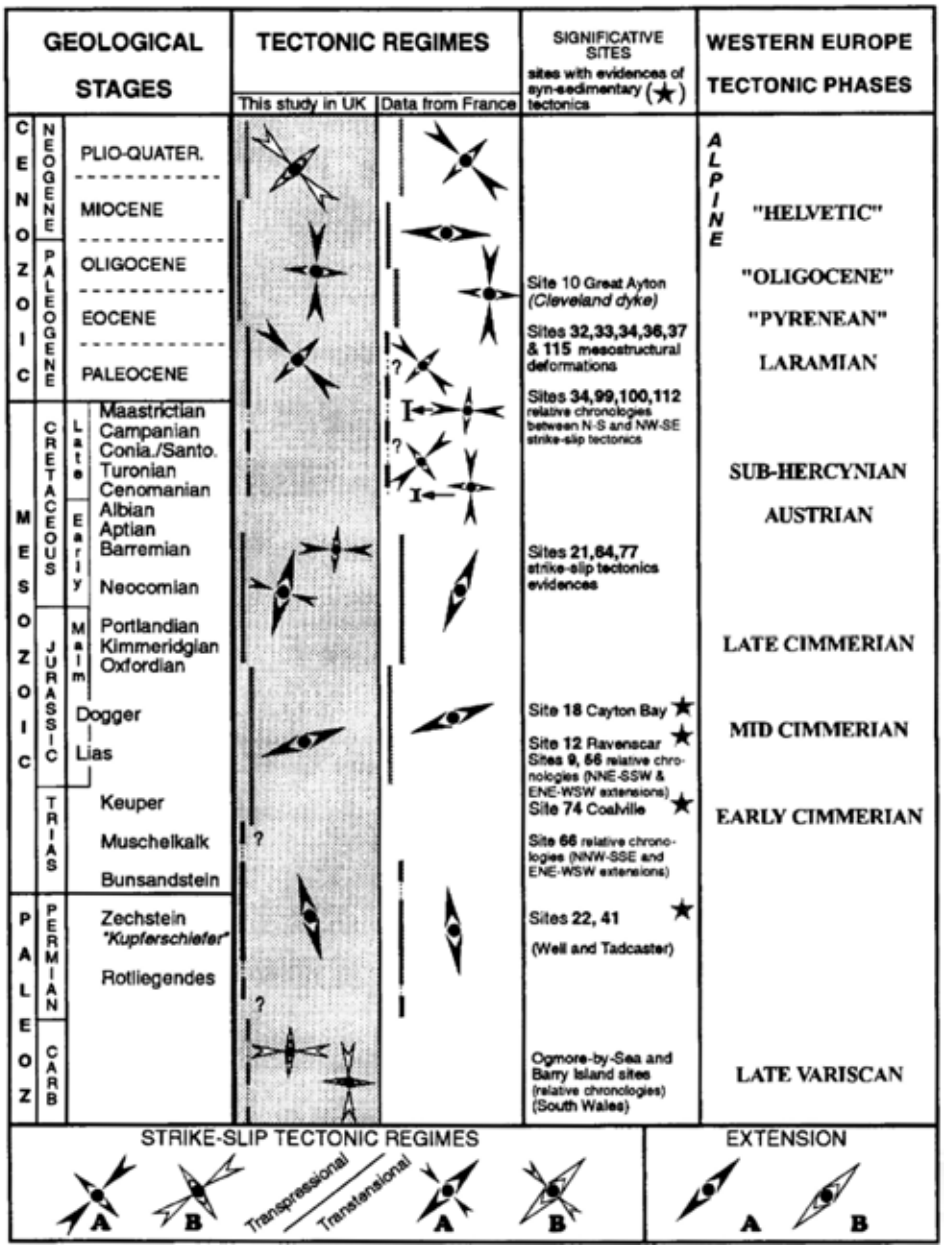

Figure 5.79 – Table of tectonic stages. A = palaeostress tensor, B = other tectonic data (after Hibsch *et al.* 1995).

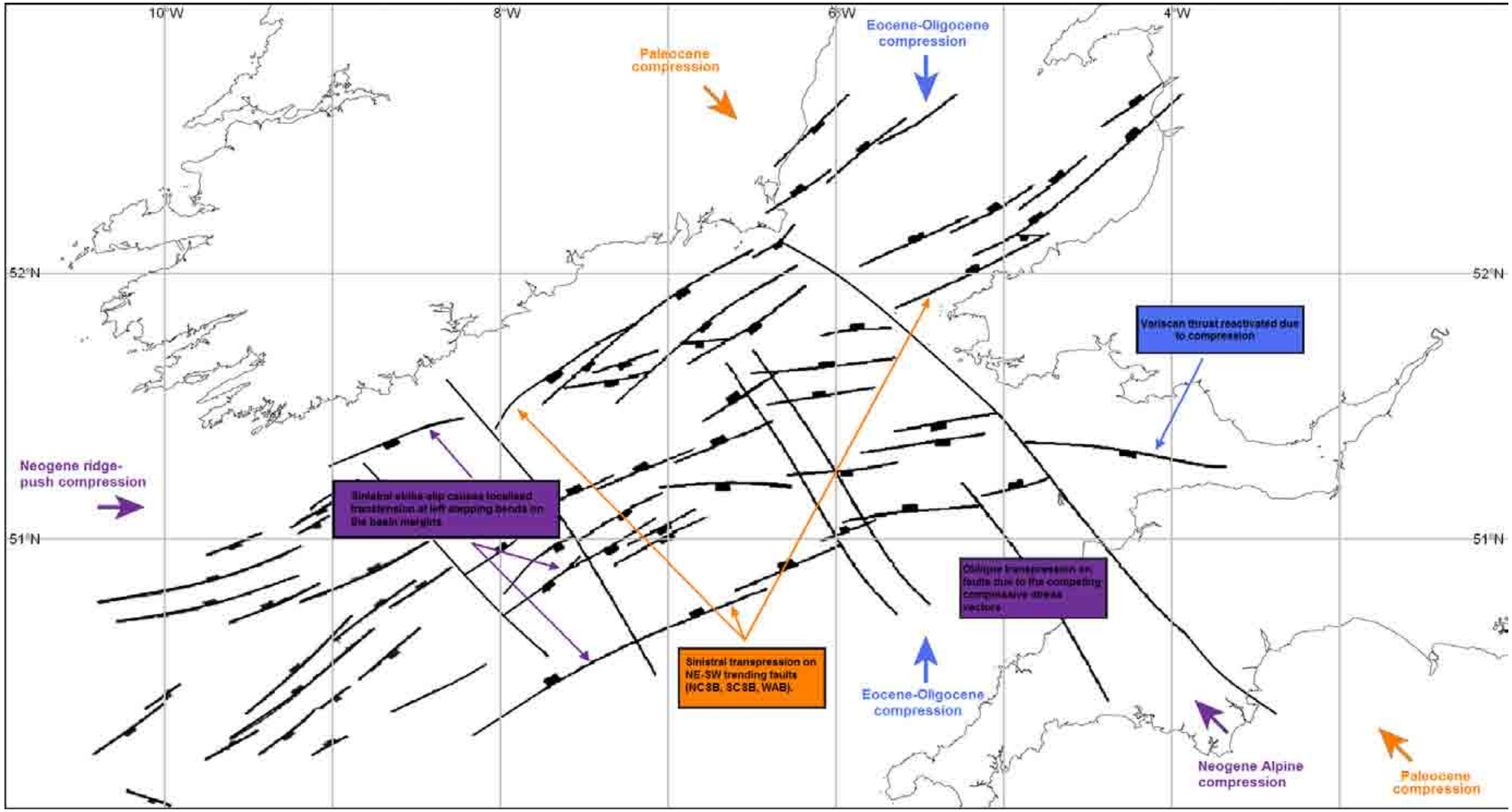

Figure 5.80 – Model to account for the observation of the Cenozoic exhumation episodes across the SW UK. The coloured arrows refer to the three Cenozoic episodes recognised by the AFTA; Orange – Paleogene, Blue – Eocene-Oligocene, Purple – Neogene (Miocene). Palaeostress directions are inferred from the work of Hibsch *et al. (*1995). Coloured caption boxes refer to events caused by the similarly coloured stress fields. This study suggests that fault reactivation and uplift was directly controlled by the prevailing stress field over time. Favourably oriented faults achieved maximum relative uplift whilst faults out of phase with the stress field suffered oblique uplift.

Figure 5.81 show the directions of ridge-push and Alpine orogeny used by Gölke & Coblentz (1996) and show that there is a stress field to act favourably on both fault orientations explaining why the Neogene event is so ubiquitous across the SW UK.

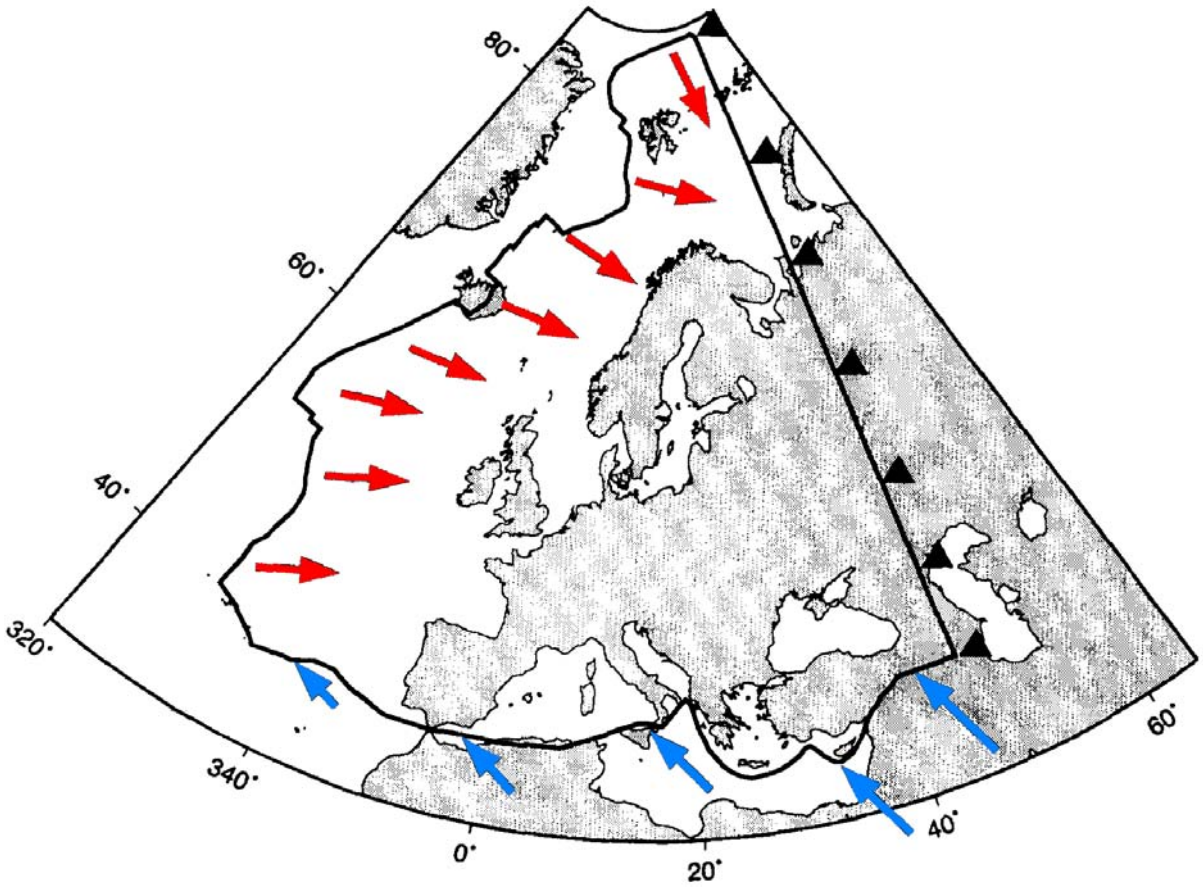

Figure 5.81 – Schematic boundary conditions from the modelling work of Gölke & Coblentz, (1996) showing the two main stress fields acting on NW Europe during the late Cenozoic; ridge push (red arrows) and Alpine orogenesis driving inversion (blue arrows). Force arrows are not drawn to scale. Triangles indicate the pinned elements along the eastern margin.

Understanding the petroleum systems of exhumed sedimentary basins requires quantification of the timing and magnitude of exhumation and a holistic approach is recommended as each of the methodologies used to measure exhumation (tectonic, thermal, compaction and stratigraphic) give useful insights into the exhumation and large uncertainties result from using individual techniques. As explained in more detail by Corcoran & Doré (2005) tectonic based techniques such as subsidence analysis are largely dependent on crustal models (e.g. McKenzie) and may therefore be inappropriate to use in terrains where such models do not

apply or require modification, whilst compaction and thermal techniques also have their drawbacks (Chapter 2).

Where convergence of the estimates from the different techniques occurs, more reliable values for the magnitude of exhumation can be achieved. Regional stratigraphic correlation, palaeogeographic analysis and extrapolation of sub-unconformity erosional truncation patterns on seismic data offer critical 'sense' checks on exhumation estimates derived from other techniques (Corcoran & Doré, 2005). These stratigraphic insights may be particularly important where exhumation at a given point in a basin has multiple causes – for example in the case where local tectonic inversion is superimposed upon epeirogenic uplift on a basin scale (Corcoran & Doré, 2005).

These assertions are supported by the work presented in this thesis for the offshore basins around the SW UK and Ireland and highlight the inherent difficulty in using individual exhumation estimation techniques in isolation. Cross referencing estimates of timing and magnitude between different methods (e.g. subsidence modelling, AFTA, VR and sonic velocity analyses) is an essential step in reducing uncertainty in the exhumation estimate, but assessing stratigraphic and seismic evidence together with these proxies is a critical factor in validating the exhumation estimate (Corcoran & Doré, 2005). On the other hand where systematic divergence occurs between exhumation estimates from different techniques this discrepancy itself may provide a valuable insight into the geological history of the basin as shown in the Slyne-Erris Basin by Corcoran & Doré (2005) where consistently higher exhumation estimates from thermal indicators are probably locally indicative of igneous and hydrothermal activity.

5.5: CONCLUSIONS

- Results from regional AFTA and VR data reveal evidence for five important cooling episodes during the Permian (285-255Ma), Upper Triassic (215-195Ma), Lower Cretaceous (140-120Ma), early Paleogene (75-55Ma) and the Neogene (20-10Ma).

- AFTA and VR data from three exploration wells on the margins of the BCB indicate that maximum burial depths in this basin were reached on the southern margin during the end Cretaceous to earliest Paleogene, prior to Paleogene exhumation which removed up to 2km of Paleogene-Neogene strata from the basin footwall, and on the northern margin during the Mesozoic, prior to early Cretaceous exhumation which removed up to 6.5km of Carboniferous-Cretaceous strata from the basin footwall.

- Estimates of exhumation magnitude from palaeothermal data show excellent agreement with those from compaction and seismic reflection data. Furthermore, seismic reflection data indicate that the principal driving mechanism of Neogene exhumation was compressional shortening (tectonic inversion).

- AFTA data from the SW margin of the SGCB (in the footwall of the basin-bounding Bala Fault) reveal evidence for a number of Mesozoic cooling episodes which correspond to phases of fault-controlled subsidence in the offshore basin and are hence interpreted as resulting from footwall uplift

- Palaeothermal data indicate that early Jurassic exhumation removed up to 3km of Jurassic-Permian section from the vicinity of Pembrokeshire. Early Cretaceous exhumation removed up to 2.5km of mid-Jurassic-early Cretaceous section and

Neogene exhumation can be explained by removal of up to 2.2km of mid-Miocene-Pliocene sediments.

- Whilst the North Atlantic margins have been affected by a number of important, and apparently anomalous phases of subsidence/burial and uplift/exhumation during the Cenozoic (e.g. Cloetingh *et al.* 1990; Hall & White 1994; Japsen & Chalmers 2000; Japsen *et al.* 2005), results from the SW UK add to an increasing body of evidence which suggests that the western UKCS and surrounding areas has experienced a much longer history of complex vertical motions, extending back through the Jurassic and Cretaceous. These results confirm the multi-phase nature of post-Palaeozoic exhumation across the SW UK but they also question the driving mechanisms proposed by previous studies, in particular those involving underplating.

- Distribution of exhumation estimates from across the SW UK suggest that local activity related to nearby faults is crucial in defining the character of exhumation which affects large regions. This study suggests that the effect of footwall uplift during the early Cretaceous and basin compartmentalisation due to reactivation of selected faults during Cenozoic inversion has been particularly important.

- This study provides new insights into the nature of the Cenozoic exhumation episode. Results suggest that it is composed of at least 3 distinct components; a Paleogene event (65-55Ma) related to Laramide compression, an Eocene-Oligocene (45-25Ma) event related to the Pyrenean orogeny and a Neogene event (20-10Ma) related to late Alpine compression and Atlantic ridge-push.

CHAPTER 6: DISCUSSION & SYNTHESIS

6.1: INTRODUCTION

The aim of this thesis was to elucidate the post-Triassic burial and exhumation history of the SW UK offshore and onshore basins. This was accomplished by using a combination of mechanical (compaction based techniques such as log-derived porosities), thermal (i.e. AFTA and VR) and seismic data. The combination of these complimentary techniques has allowed the timing, magnitude and distribution of exhumation to be constrained across the whole of the SW UK. This study has demonstrated that:

- The SW UK experienced a number of vertical movements suggesting a complex post-Triassic history.

- The preserved sedimentary section of Mesozoic-Cenozoic age has been more deeply buried than the depth at which it currently resides.

- A series of exhumation episodes removed significant overburden during the late Triassic, early Cretaceous, early Paleogene, Eocene-Oligocene and Neogene times.

The study has also revealed the spatial and temporal variety in this exhumation with some of the episodes restricted to distinct provinces (e.g. the late Triassic, early Paleogene and particularly the Eocene-Oligocene exhumation episode), whilst others are much broader in their effect (e.g. those beginning during the early Cretaceous and Neogene). Along with previous work at Birmingham (e.g. Holford, 2006) this study provides new insights into the geological evolution of the British Isles and NW Europe as well as contributing to the wider

geological debate regarding Paleogene and Neogene exhumation in the Atlantic Margin region, intra-plate stability and the relationship between plate boundary processes and far field effects (*cf.* Japsen & Chalmers, 2000; Doré *et al.* 2002*a,* Corcoran & Doré, 2005; Holford, 2006). This chapter summarises the results of the previous sections and adds analysis and discussion as to the driving mechanisms and processes responsible for the exhumation of the SW UK.

6.2: UPPER TRIASSIC-LOWER JURASSIC EXHUMATION

6.2.1: TIMING OF UPPER TRIASSIC-LOWER JURASSIC EXHUMATION

Onshore samples collected from across the SW UK were revealed to have cooled from maximum palaeotemperatures of >100°C between 215 and 195Ma (i.e. Upper Triassic-Lower Jurassic) (Figure 6.1) according to the AFTA data. A similarly timed exhumation event was noted by Green *et al.* (2000), based on data collected from across Ireland. In this study a regional mid-Jurassic cooling episode was identified which began between 180-170 Ma. Holford (2006) identified a regional cooling episode affecting NW Wales (230-185Ma) and the Larne Number 2 borehole, Northern Ireland (200-135Ma) also during Jurassic times. Bray *et al.* (1998) recorded a mid-Triassic-early Jurassic episode in the Permian-Triassic rocks of the western Wessex Basin, SE Devon which began some time before 170Ma and involved cooling from maximum palaeotemperatures of between 65-95°C. It is the interpretation of this study that all these events record the same regional cooling episode. There appears to be a difference in the timing of the exhumation episode either side of the offshore basins with the Irish event happening much later than in England and Wales. This difference is interpreted as representing differential movements on the basin controlling faults. The timing of the SW UK cooling episode is interesting as the thermal signature is not

noted in the offshore basins (e.g. Celtic Sea basins) and this has been investigated in Chapter 5. The offshore basins surrounding Wales and the Cornubian Peninsular contain thick sequences of Triassic and Jurassic sediments (Tappin *et al.* 1994) (Figure 6.1) as indicated on seismic data which show the BCB contains up to 2km of Triassic strata (Tappin *et al.* 1994) and up to *c.* 1km of Lower Jurassic strata.

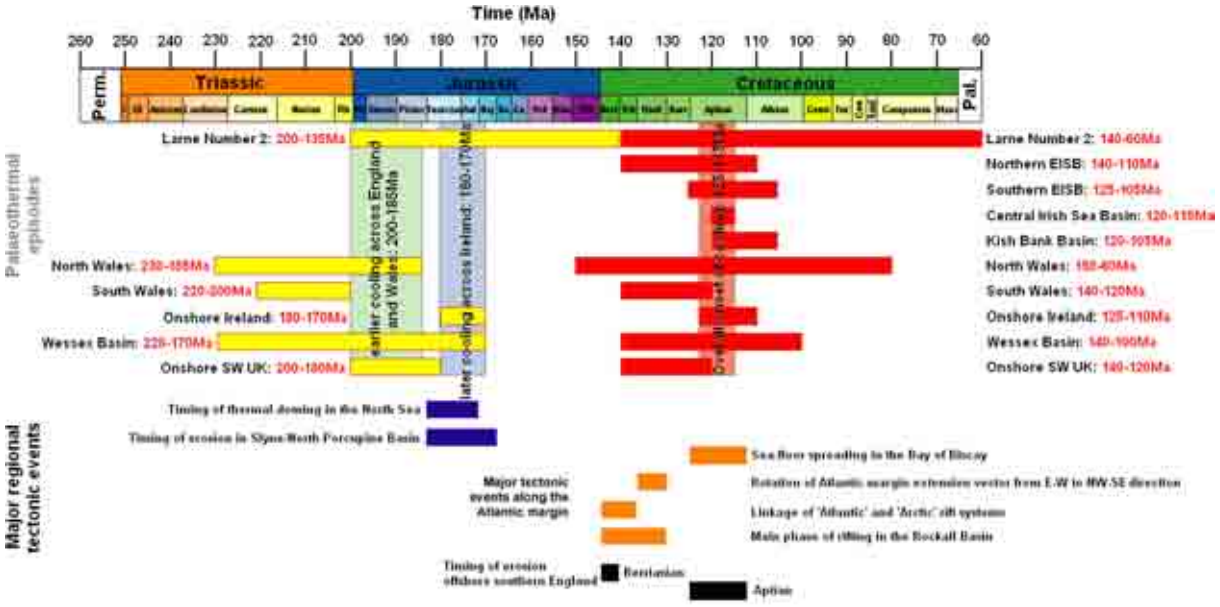

Figure 6.1 – Summary event stratigraphy for the Mesozoic of the SW UK, comparing the timing of cooling from AFTA with preserved section and important regional tectonic events, as discussed in this Chapter. Additional timings come from Holford, (2006), Bray *et al.* (1998) and Green *et al.* (2000). Timescale after Gradstein *et al.* (2004).

6.2.2: MAGNITUDE AND DISTRIBUTION OF UPPER TRIASSIC-LOWER JURASSIC EXHUMATION

Evidence for the magnitude of this exhumation comes primarily from the palaeothermal data from outcrop samples across the SW UK. As shown in Chapter 5, AFTA and VR data indicate that the area experienced up to 5km of deeper burial prior to this exhumation event depending on the choice of geothermal gradient. This choice of gradient is complicated by the fact that none of the offshore wells record the Jurassic event and as such no definitive palaeogeothermal gradient exists. The closest proxy for a realistic geothermal gradient comes from work by Corry & Brown (1998), who estimated palaeogeothermal gradients over time

using data from a number of offshore exploration wells in the NCSB. For the Lower Jurassic the gradient is estimated to be 35.4 ± 2.0°C/km and for the Triassic 38.0 ± 1.9°C/km. This indicates that a realistic gradient over this time period would be *c.* 36°C/km. Using this constraint the Upper Triassic-Lower Jurassic exhumation episode will have removed a maximum of 2.5-4.4km of overburden. The average value of former deeper burial across the SW UK would be up to 2km. This is in good agreement with data presented by Bray *et al.* (1998), for the Wytch Farm oil well which indicates former deeper burial of 2300m prior to Cretaceous reburial (Figure 6.2).

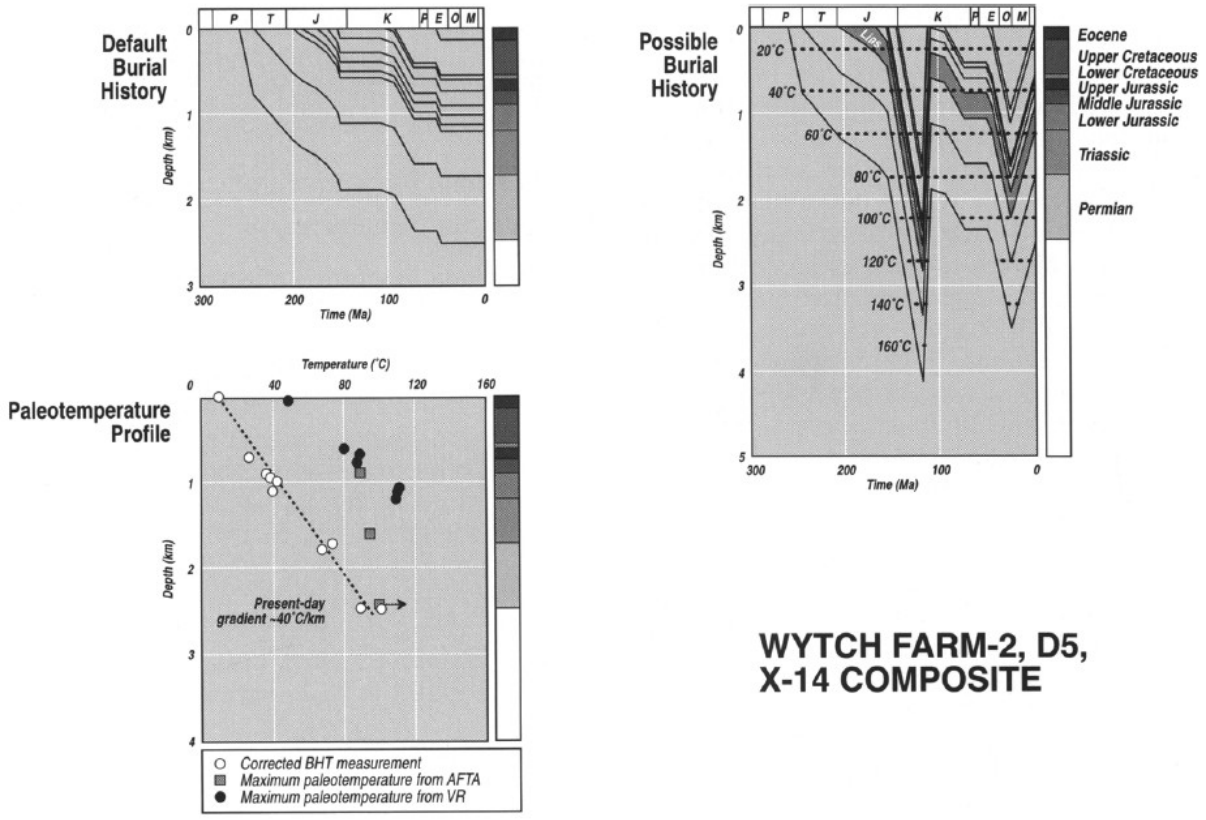

Figure 6.2 - Palaeotemperature profile and reconstructed burial history from AFTA and VR data from the Wytch Farm wells. The 'Default' burial history is constructed based on the preserved stratigraphy alone (i.e. by assuming no uplift and erosion at unconformities) (after Bray *et al.* 1998).

6.2.3: CAUSES OF UPPER TRIASSIC-LOWER JURASSIC EXHUMATION

The following discussion seeks to investigate the possible causal mechanisms for the cooling episode observed across the SW UK, and whether this event may be related to that observed in the Wessex Basin, Ireland and NW Wales. Thermal history modelling of AFTA data from the SW UK shows maximum Upper Triassic-Lower Jurassic palaeotemperatures increasing from Weymouth in the southeast of the region across Somerset and North Devon towards the Pembroke Peninsular and Bala Fault, normal displacements along which accommodated the Mesozoic subsidence within the SGCB (see Holford, 2006). Bray *et al.* (1998), also noted a widespread regional heating event in the mid-Triassic-early Jurassic in the Wessex Basin which they argue comprises a regional uplift and erosion, a regional hydrothermal event and elevated heat flow combined with Triassic rifting. Bray *et al.* (1998), point to evidence of E-W extension which caused N-S cross cutting vein system in Cornwall and East Devon with vein mineralisation during the Triassic. Sandeman *et al.* (1995) present $^{40}Ar/^{39}Ar$ data from the Lizard complex which, suggest a low-temperature thermal overprint at *c.* 220Ma. They note that this is in good agreement with the age estimated for an episode of hydrothermal activity affecting the Lizard as reported by Halliday & Mitchell (1976) and suggest that this was caused by fluxing of hydrothermal fluids relating to rifting of the North Atlantic in the late Triassic.

The cooling across the SW UK is interpreted by this study as recording exhumation caused by footwall uplift of the basin margins which can also potentially explain the thick Mesozoic successions in the CBB and SGCB as being eroded material carried off these palaeo-highs and a broader hydrothermal event whose activity was mainly restricted to the south and possibly related to thermal doming (see below). Holford (2006) commented that these results have important implications for both palaeogeographic reconstructions and the mode of

crustal extension within the western UK during the Mesozoic based on his work in the EISB and the noted observations of previous workers involved with Jurassic rocks (e.g. Arkell, 1933; Hallam, 1959; Cope 1984). Further support for footwall uplift as the driving mechanism comes from seismic reflection data (western UK lines show emergent footwall topography which would be susceptible to erosion) and also work by Ziegler & Cloetingh (2004), who stated that upon crustal separation the diverging continental margins (pre-continental rifts) and the 'unsuccessful' intra-continental branches of the respective rift system become tectonically inactive. However during subsequent tectonic cycles, such aborted rifts can be tensionally as well as compressionally reactivated (Ziegler *et al.* 1995, 1998, 2001, 2002). Work by Hibsch *et al.* (1995), showed that there was a prevailing stress field of extension present at the time of this exhumation event thus it is entirely possible that the scenario envisaged by Ziegler & Cloetingh (2004) is possible.

Massive thermal doming of rift zones can commence 15-60My after the beginning of crustal extensions (e.g. Gulf of Suez, 15-20My; East African rift, 20-25My; Baikal rift, 20-30My; Rhenish Shield, 25-30My; Central Atlantic rift, 30-40My; North Sea, 60My; (Ziegler, 1992)). Uplift of rift flanks can exceed 2km whereas grabens may be elevated by nearly as much above sea-level. This subsidence pattern can be reversed if the rate of thermal uplift exceeds the rate of isostatic subsidence caused by lithospheric extension (Ziegler, 1992) and can result in uplift above the erosional base level and truncation of a rift basins sedimentary fill (e.g. mid-Jurassic Central North Sea rift dome (Ziegler, 1990; Underhill & Partington, 1993)). Most rift domes straddle more or less symmetrically the zone of upper crustal extension with volcanic activity showing no marked concentration on one of the rift flanks (e.g. Rhine Graben, (Prodehl *et al.* 1992, 1995); Central North Sea, (Ziegler, 1990)). Such a scenario was considered by Tate & Dobson (1989) who commented on the similarity in alignment of a

crustal dome in the North Sea (formed during Toarcian-Aalenian (mid-Jurassic) times), whose formation resulted in the development of the 'mid-Cimmerian' unconformity (Hallam & Sellwood, 1976; Ziegler, 1990; Underhill & Partington, 1993) and their proposed mid-Jurassic Irish uplift axis. Underhill & Partington (1993), suggested that this crustal doming resulted from the obstruction of a broad (>1250 km diameter) transient plume head at the base of the lithosphere (Figure 6.3) the deflation of which caused the trilete rift system of the North Sea during the mid to late-Jurassic (Davies *et al.* 2001). Uncertainty remains as to whether the North Sea dome could have extended across Britain (AFTA data from the East Midlands suggests not (Green, 1989, 2005; Green *et al.* 2001*b*)) and Tate & Dobson (1989) questioned whether the proposed doming of Ireland evolved as a separate entity rather than as a result of the North Sea dome. Regardless, Underhill & Partington (1993), suggest that the intra-Aalenian, 'mid-Cimmerian' unconformity extended westwards across the Lake District, much of Scotland and the East Shetland Platform (Figure 6.3) and was caused by this dome. The results of this study favour some form of epeirogenic uplift (Chapter 5; Figure 5.77) alongside the footwall uplift concept, however the exact nature of this epeirogenic uplift is not clear and merits further investigation.

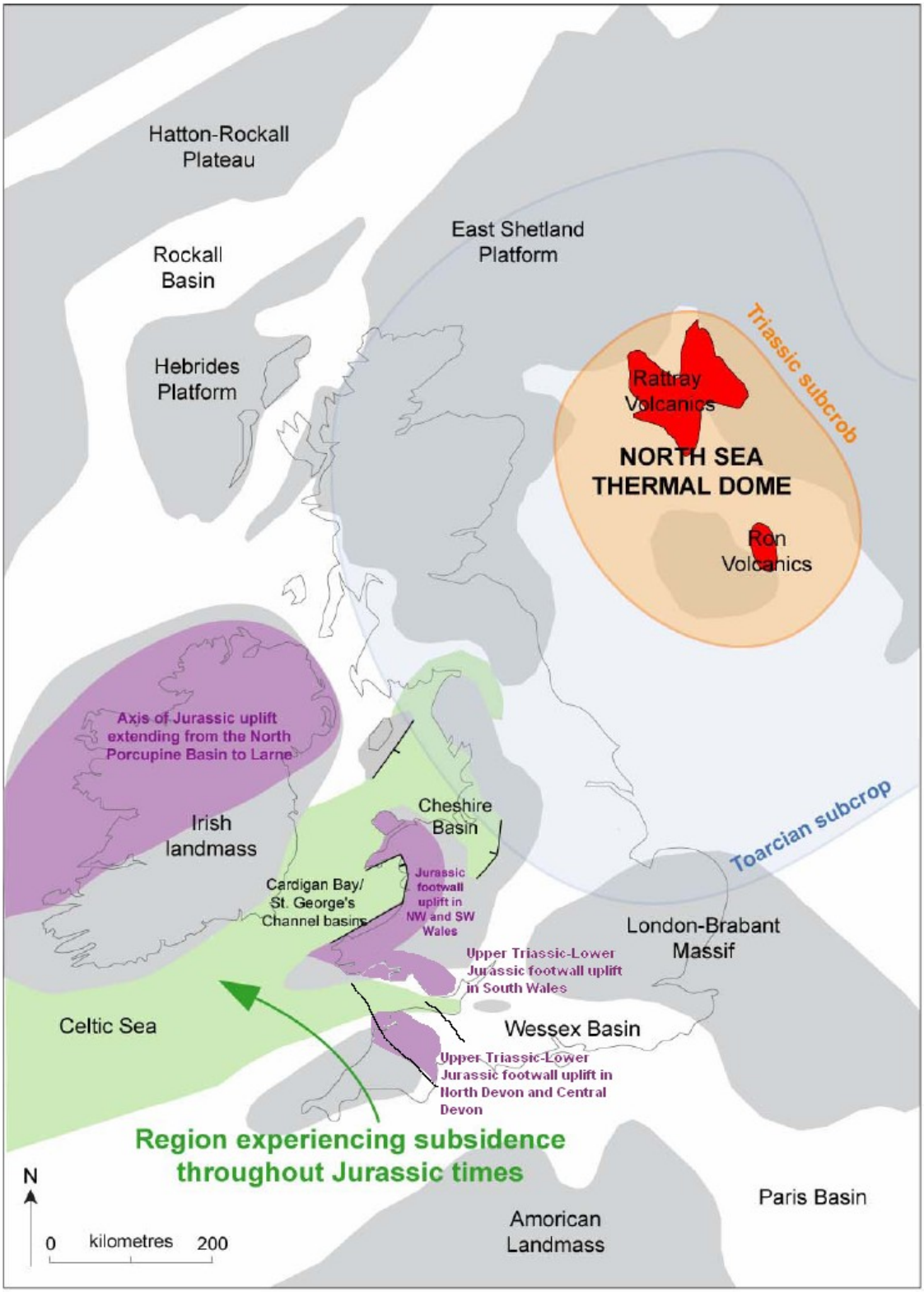

Figure 6.3 – Palaeogeographic reconstruction of the British Isles during the Middle Jurassic showing areas of emergence (shaded grey), areas for which AFTA data provide evidence for cooling (shaded purple), and the extent of the Toarcian and Triassic subcrop beneath the 'mid-Cimmerian' unconformity, which has been ascribed to plume-related thermal doming in the North Sea (based on Underhill & Partington, (1993); Coward *et al.* (2003), Simms *et al.* (2004) and Holford, (2006)).

6.3: LOWER CRETACEOUS EXHUMATION

6.3.1: TIMING OF LOWER CRETACEOUS EXHUMATION

AFTA data from the onshore SW UK region reveal evidence for a cooling episode during the Lower Cretaceous. Most of the samples collected from outcrops across the SW UK began to cool from palaeotemperatures of around 80-100°C between 140 and 120 Ma (Figure 6.4). Green *et al.* (2000), identified a regional Lower Cretaceous cooling episode across the Irish landmass which began between 125-110Ma and Holford (2006), identified a regional cooling episode affecting the Mohcras borehole NW Wales (160-80Ma), the northern EISB (140-110Ma), the southern EISB (125-105Ma), the CISB (120-115Ma) and the Larne Number 2 borehole, Northern Ireland (140-60Ma) also during Cretaceous times. Bray *et al.* (1998), recorded a Lower Cretaceous (140-100Ma) episode in the Wessex Basin and involved cooling from maximum palaeotemperatures of 65-80°C, a range also exhibited in the Cornish granites at this time (Chenet *et al.* 1996). This exhumation episode also coincides with a major unconformity (e.g. McMahon & Underhill, 1995; McMahon & Turner, 1997) and AFTA data show cooling coincides with the area where Wealden stratigraphy is absent and traditionally considered to have not been deposited. The results presented in this thesis suggest that the cooling recorded by AFTA data from the SW UK records these regional palaeothermal events.

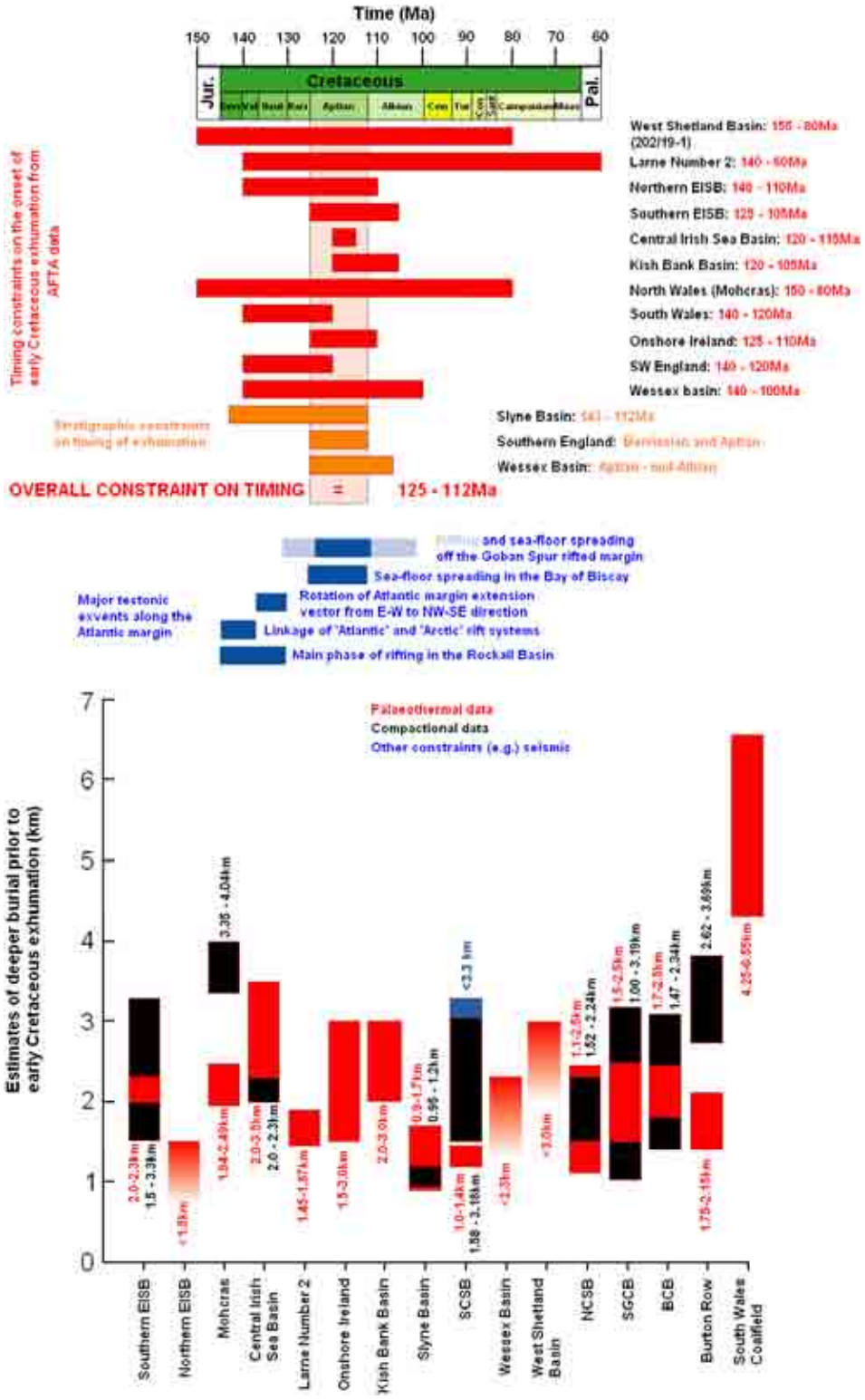

Figure 6.4 – Event stratigraphy diagram for the UK showing the regional signature of the Cretaceous cooling event recorded by AFTA. A UK wide comparison is made between stratigraphic constraints on the timing of exhumation and cooling revealed by AFTA in an attempt to identify the timing of regional early Cretaceous exhumation. This analysis suggests a regional onset of exhumation beginning between 125 to 112Ma. The timing of important regional tectonic events (from Doré *et al.* (1999) and Roberts *et al.* (1999)) is highlighted for comparative purposes. This diagram also shows estimates of the amount of deeper burial prior to early Cretaceous exhumation across the British Isles, as determined using various techniques. Further details are provided in the text (modified after Holford, (2006), Timescale after Gradstein *et al.* (2004)).

6.3.2: MAGNITUDE AND DISTRIBUTION OF LOWER CRETACEOUS EXHUMATION

Many previous studies have placed maximum burial depth of the Mesozoic section of the Celtic Sea-Western Approaches during early Paleogene times (e.g. Murdoch *et al.* 1995). This study however favours maximum burial during early Cretaceous times (Figure 6.4). As documented in Chapters 4 and 5, up to 3.5 km of Jurassic-early Cretaceous sediments appear to have been deposited across the SW UK, prior to exhumation beginning between 140 and 120Ma (Figure 6.4). Work by Holford (2006) has shown that significant early Cretaceous exhumation also affected the Irish Sea basin system (Green *et al.* 2001*a*), Larne Basin and other parts of onshore Ireland (Green *et al.* 2000). As with the Upper Triassic-Lower Jurassic episode it is difficult to constrain the palaeogeothermal gradient affecting the SW UK at this time. Data from the offshore wells indicates a range of palaeogeothermal gradients which have been attributed to the Lower Cretaceous ranging from 21.2°C/km to 35.4°C/km. This range is consistent with the range of gradients presented by Corry & Brown (1998), which range from 21.1 ± 1.6°C/km for the Lower Cretaceous Wealden to 37.2± 3.0°C/km for the Cretaceous Greensand. This means absolute magnitude of Cretaceous exhumation is hard to define but is likely in the range 2500-3000m. This is consistent with evidence presented by Bray *et al.* (1998), for 2000-3400m of Eocene-Oligocene exhumation in the Wessex Basin (Figure 6.5). In terms of distribution it should be noted that some parts of the SW UK most notably South Wales and the South Wales Coalfield do not show evidence (through AFTA) of Cretaceous cooling rather the AFTA indicates cooling during the Paleogene. This does not mean that uplift did not occur at this time indeed as noted in Chapter 5 it is entirely possible that the later Paleocene thermal episode completely overprinted a Cretaceous event. In the surrounding areas this Cretaceous exhumation is also observed with Williams *et al.* (2005) demonstrating that the SGCB experienced up to 2.5km of early Cretaceous exhumation at its margins. It is important to note however that the central parts of the basin appear not to have

been affected by this exhumation event (*cf.* Tappin *et al.* 1994; Turner, 1996; Green *at al.* 2001*a*; Holford, 2006).

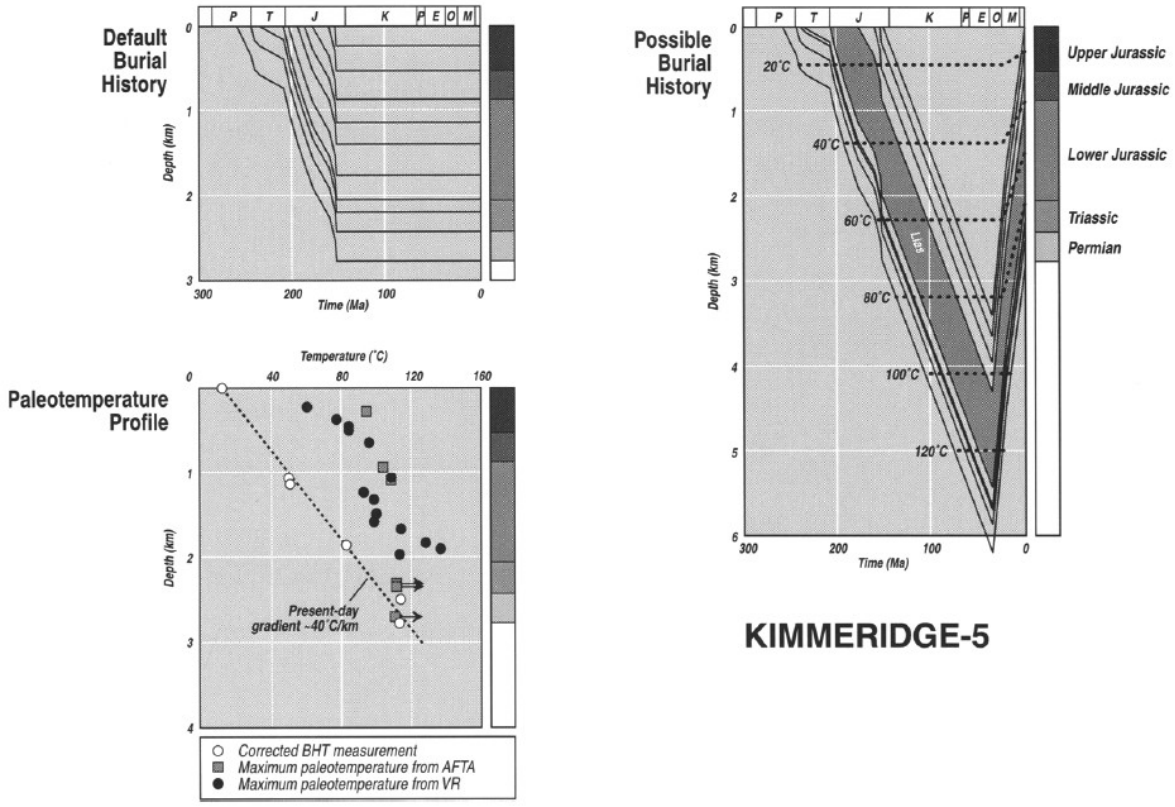

Figure 6.5 - Palaeotemperature profile and reconstructed burial history from AFTA and VR data from the Kimmeridge-5 well. The 'Default' burial history is constructed based on the preserved stratigraphy alone (i.e. by assuming no uplift and erosion at uncomformities) (after Bray *et al.* (1998)).

6.3.3: POTENTIAL DRIVING MECHANISMS OF LOWER CRETACEOUS EXHUMATION

The coincidence with the lower Cretaceous exhumation event recorded in the SW UK and that of seafloor spreading to the southwest of the British Isles highlights one possible causal mechanism for driving the exhumation (Figure 6.4). De Graciansky *et al.* (1985) by analysis of cores from the DSDP-IODP drilling program in the Goban Spur timed this spreading as early Aptian-early Albian (Figure 6.6). Sea-floor spreading was also occurring around this time between Iberia and Grand Banks (Johnston et al. 2001) and the Labrador Sea and could also have contributed to exhumation in the SW UK though it is much more distant to the study area than that in the Bay of Biscay and Goban Spur which are interpreted as being the

primary driving mechanism for exhumation in the SW UK at this time. Effects from the Labrador sea rifting are not thought to have contributed to exhumation since the mid-Atlantic ridge was already established at this point (Figure 6.4) and any stresses are not thought to have crossed it. It should be noted that this exhumation is not limited to the SW UK and similar events are recorded across the on and offshore basins of the British Isles (e.g. Irish Sea Basin (Holford *et al.* 2005; Holford, 2006); Slyne Basin (Corcoran & Mecklenburgh, 2005), southern England (Rawson & Riley, 1982; Ruffell, 1992; Bray *et al.* 1998; McMahon & Turner, 1998; Kyrkjebø *et al.* 2004)). A thermal mechanism has been proposed by McMahon & Turner (1998) as causing uplift around the Cornubian Platform based on Hauterivian-Barremian volcanics and intrusives so it is possible that multiple mechanisms were acting in unison to cause the exhumation observed.

Another possible mechanism has been proposed by Ziegler (1990) in which dextral strike slip motions along the margins of E-W trending basin faults (such as in the BCB and SCSB) cause intense deformation and removal of overburden (up to 3km in the BCB-SCSB case *cf.* Van Hoorn, 1987*a*; Figure 6.4). Another theory has been proposed by Holford (2006) in which rifting of the Rockall Basin (Scrutton & Bentley, 1988) caused a rotation of the direction of extension from E-W to NW-SE which orients favourably with the Celtic Sea basins and could have caused uplift (for further discussion see Roberts *et al.* 1999; Holford, 2006). Several other candidates for driving mechanism exist such as volcanic rift activity (Gallagher & Brown, 1997; Watts, 2001), magmatic underplating (Cox, 1993; White, 1992), flexural uplift (Weissel & Karner, 1989; Brodie & White, 1995; Tiley *et al.* 2003) and depth dependent stretching (Davis & Kusznir, 2004; Kusznir *et al.* 2004, 2005). Holford, 2006 highlights the short comings of these driving mechanisms with only depth dependent stretching being a remaining candidate, however as highlighted by Davis & Kusznir (2004) and Kusznir *et al.*

(2005) only regions *c.* 100-200km inboard from the continent ocean boundary should be affected by this mechanism and since the most proximal parts of the study area are located >300km from the COB this mechanism is not likely to have played a part in the Lower Cretaceous exhumation of the SW UK (Figure 6.6).

Further doubt on it being a valid mechanism comes from Gallagher et al. (1998) who reaffirm the notion that erosion is restricted to a maximum of 200km inboard of the COB (Figure 6.7) and also from discussions in Persano *et al.* (2002) and Balestrieri *et al.* (2005). The model for the Lower Cretaceous episode presented in this thesis (Figure 5.78) suggests continued footwall uplift combined with selective fault reactivation and limited reverse movement on faults related to the opening of the Bay of Biscay was chiefly responsible for the exhumation episode (see also Figure 6.16 and 6.18).

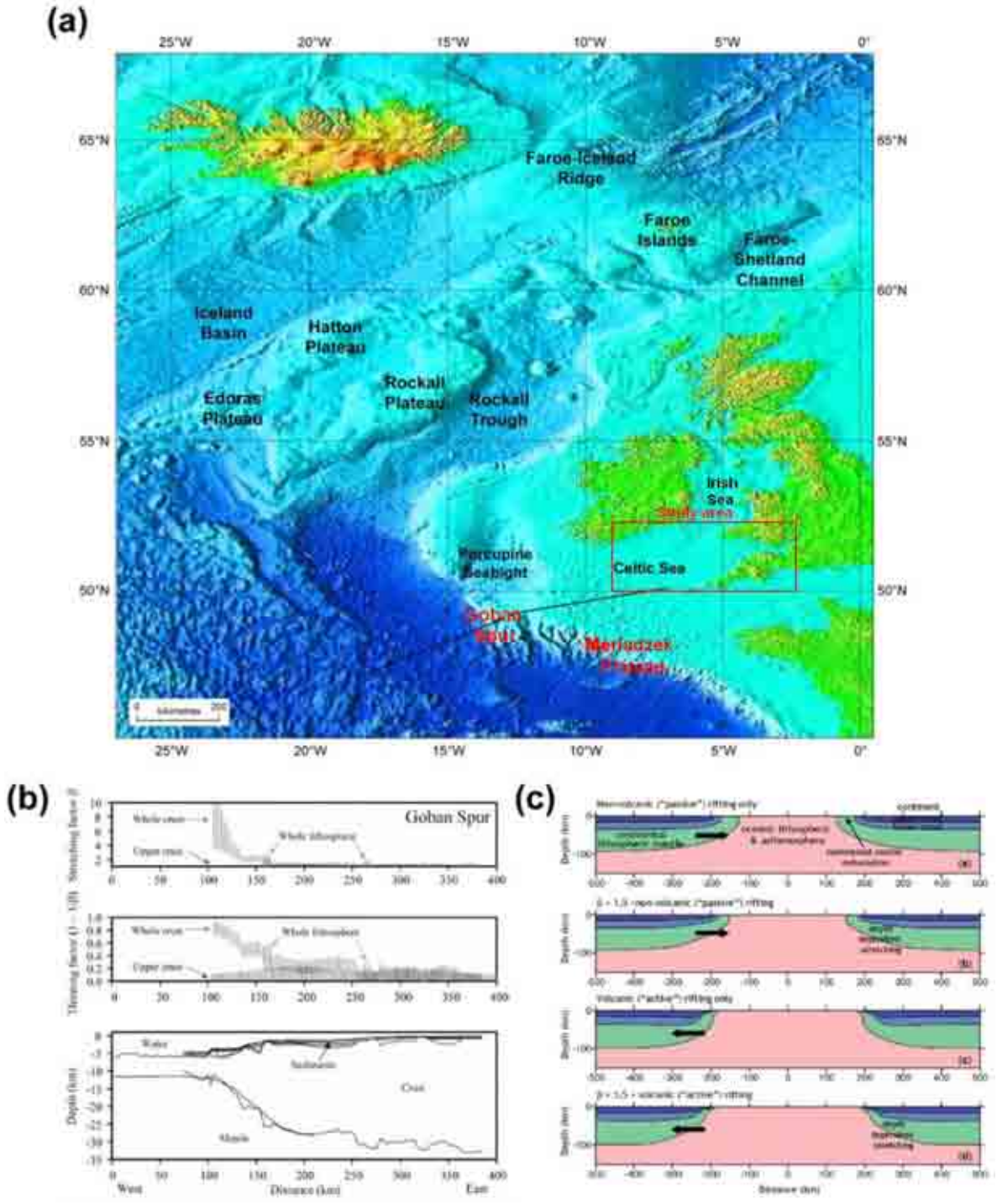

Figure 6.6 - (a) Major bathymetric features of the North Atlantic region. Locations referred to in the text are highlighted in red. The position of the geological cross section shown in (b) is indicated. (b) Stretching and thinning factors for the upper crust, whole crust, and whole lithosphere for a geological cross section across the Goban Spur rifted margin. Note that whilst estimates are similar towards the continental interior, there are significant discrepancies within *c.* 75 km of the ocean-continent boundary. This delimits the region over which depth-dependent stretching has occurred (after Davis & Kusznir, (2004). (c) Application of a two-phase fluid flow model for seafloor spreading initiation to 'passive' and 'active' rifted margin formation without and with pre-breakup pure-shear lithospheric stretching. Details of individual models are provided in Kusznir *et al.* (2005). All models show depth-dependent stretching. Note however that the region of lithosphere affected by depth-dependent stretching is generally restricted to <200 km within the ocean-continent boundary (after Kusznir *et al.* (2005)).

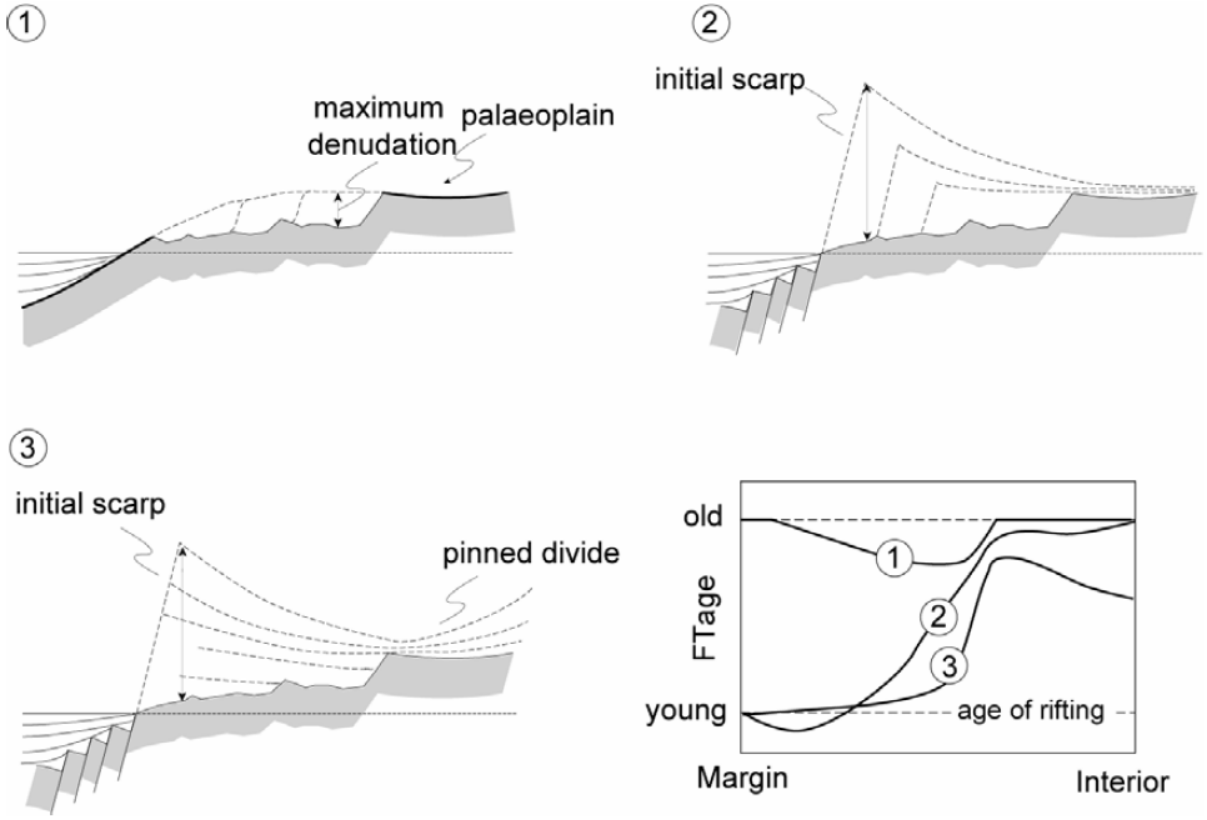

Figure 6.7 - Schematic representation of passive margin landscape evolution and the spatial distribution of expected fission track ages. Model 1 represents a 'downwarp model', which proposes that the passive margin is initially formed by long-wavelength down-flexing of the lithosphere with limited faulting, leading to the formation of a broad monocline. Denudation is expected to occur between remnants of the initial land surface preserved along the coast and the crest of the escarpment, inland of which only negligible amounts of denudation occur. The 'scarp-retreat model' (2) proposes that an initial escarpment is formed at the new continental margin by vertical displacement across normal faults separating the subsiding rift from the uplifted margin. Highest denudation rates are predicted immediately seaward of the initial scarp as a consequence of high relief. Relief-dependent erosion results in scrap-retreat, since the scarp front always has the highest relief. Seaward of the retreating scarp, the coastal region is characterized by more moderate denudation rates, whilst interior regions experience relatively slow denudation. The 'pinned divide model' (3) is similar to the scarp-retreat model, but additionally incorporates an inland drainage divide defined by a gentle slope toward the rift scarp. The presence of this drainage divide leads to rapid incision of streams draining seaward of the divide and the formation of a new scarp close to the initial position of the drainage divide. This leads to relatively uniform rates of denudation in the region seaward of the drainage divide, resulting in a down-wearing rather than scarp-retreat pattern of denudation (after Gallagher & Brown, (1999)).

6.4: PALEOGENE EXHUMATION

6.4.1: TIMING OF PALEOGENE EXHUMATION

The next phase of exhumation episode recognised by this study to affect the SW UK began during the late Cretaceous-early Paleogene. Unlike the Upper Triassic-Lower Jurassic and Lower Cretaceous, this palaeothermal episode is localised in its distribution appearing only in

the South Wales Coalfield, the offshore basins and isolated samples in Devon, Somerset and Dorset. AFTA data from the onshore SW UK region indicates that samples began to cool from palaeotemperatures of around 50-75°C between 75 and 55Ma (Figure 6.8). The offshore samples indicate much higher palaeotemperatures (from 85°C though most samples indicate temperatures in excess of 110°C) between 55-35Ma. These higher palaeotemperatures are likely related to the deeper burial experienced by samples in the Mesozoic depocentres of the offshore basins as opposed to the variably emergent basin flanks. The Irish landmass study of Green *et al.* (2000) identified a regional Paleogene cooling episode which began between 65-55Ma and Holford (2006), identified a regional cooling episode affecting the EISB (65-60Ma), the CISB (70-55Ma) and the Kish Bank Basin (65-40Ma) also during Paleogene times. However Bray *et al.* (1998), reports no palaeothermal episode from the Wessex Basin at this time. Instead an unconformity exists between the Late Cretaceous and Cenozoic dated at 80-60Ma. This unconformity could represent either non-deposition or erosion as with the Wealden unconformity which is recognised by AFTA as a palaeothermal event. Overall the Cenozoic is interpreted as recording a number of discrete exhumation episodes but due to the limit of resolution of AFTA it is not always possible to resolve the individual episodes. Further evidence for this theory of multiple events comes from work by Ford *et al.* (1999) and Blundell (2002), on the stratigraphic and structural evolution of the North Alpine Foreland Basin (Figure 1.24). Ford *et al.* (1999) recognized four stages of progressive deformation:

1. Mid-Late Eocene (46-36Ma) stage, when the convergence of the Apulian Plate with Europe resulted in the migration of the flexural basin and the front of a low-angle external orogenic wedge, allowing the northward propagation of stress into the foreland.

2. Early-Late Oligocene (33-23Ma) stage, when the migration of the flexural basin and wedge front slowed significantly; no growth structures developed and shortening was accommodated within the thickness of the orogenic wedge; no stress would have propagated into the foreland.

3. Early-Mid Miocene (16-11Ma) stage, when the system remained in much the same state as in the previous stage, with the wedge front stationary, so that little or no stress would have propagated into the foreland.

4. Late Miocene-Pliocene (11-3Ma) stage; around 11Ma the outer orogenic wedge effectively collapsed and compressional deformation concentrated on the Jura fold belt, which detached on high-level Triassic evaporites, to accommodate some 30km of NW shortening; beneath the Jura décollement, stress within the lithosphere is likely to have propagated into the foreland.

A similar unconformity was noted by Murdoch *et al.* (1995) in their study of the NCSB. They reported that the Cenozoic-Cretaceous boundary is in all areas an unconformity with angularity developed to the northeast in the CBB. This unconformity was caused by a broad regional uplift event which was not associated with any significant inversion, compression or reverse faulting. Timing can only be constrained as Paleocene to Eocene (65-35Ma), however data from AFTA further constrained this timing to 60-40Ma (Figure 6.9) suggesting there may be a link with the UK Cenozoic Igneous province occurring at approximately 60-55Ma.

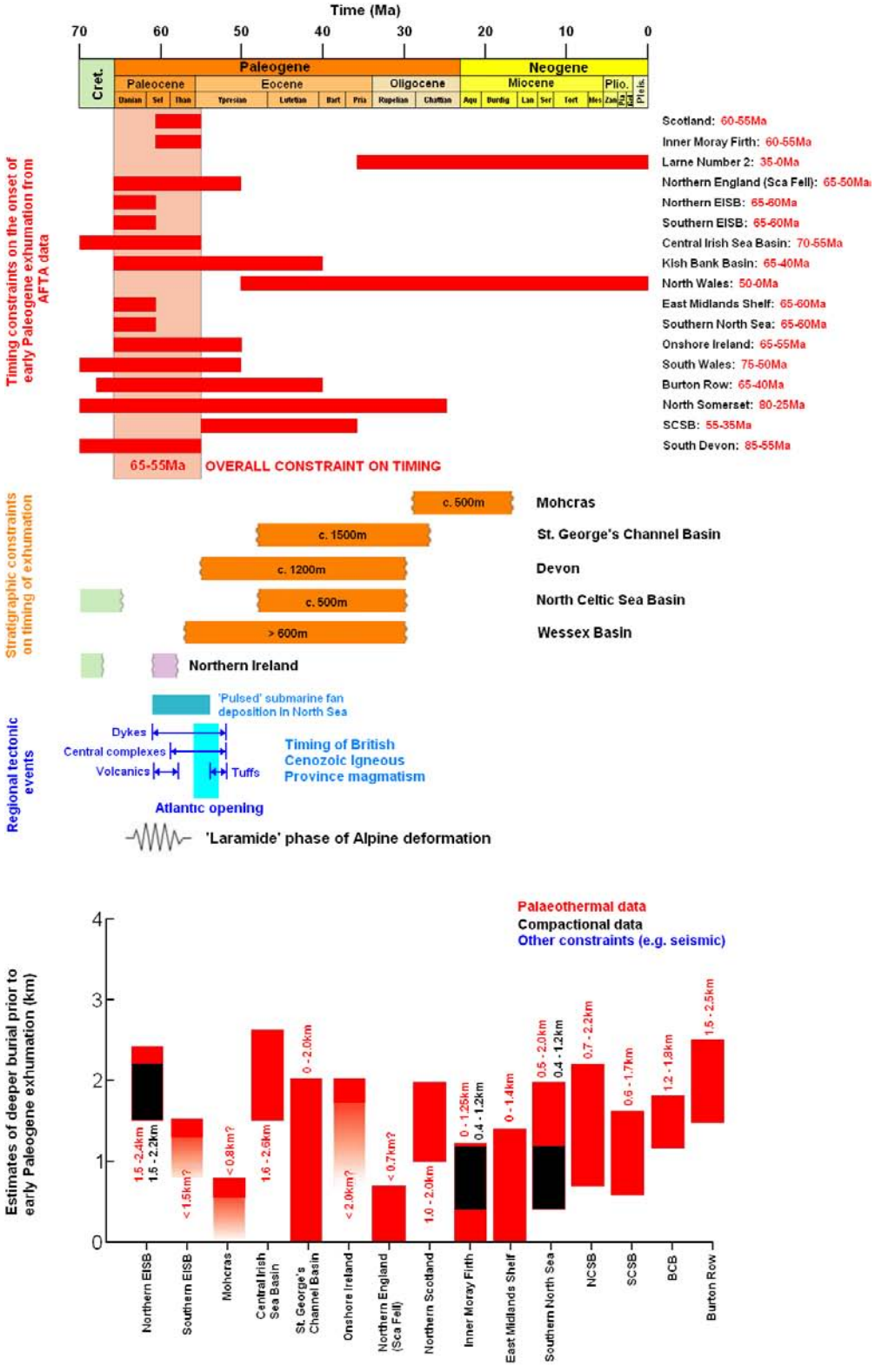

Figure 6.8 - Early Paleogene event stratigraphy diagram. Constraints on the onset of exhumation-related cooling provided by AFTA data from around the western UKCS are compared with stratigraphic constraints on the timing of exhumation in an attempt to identify the timing of regional early Cretaceous exhumation. The timing of important regional tectonic events (derived from White & Lovell, 1997 and Doré *et al.* 1999) is highlighted for comparative purposes. This diagram also shows estimates of the amount of deeper burial prior to early Paleogene exhumation across the British Isles, as determined using various techniques. Further details are provided in the text (modified after Holford, 2006).

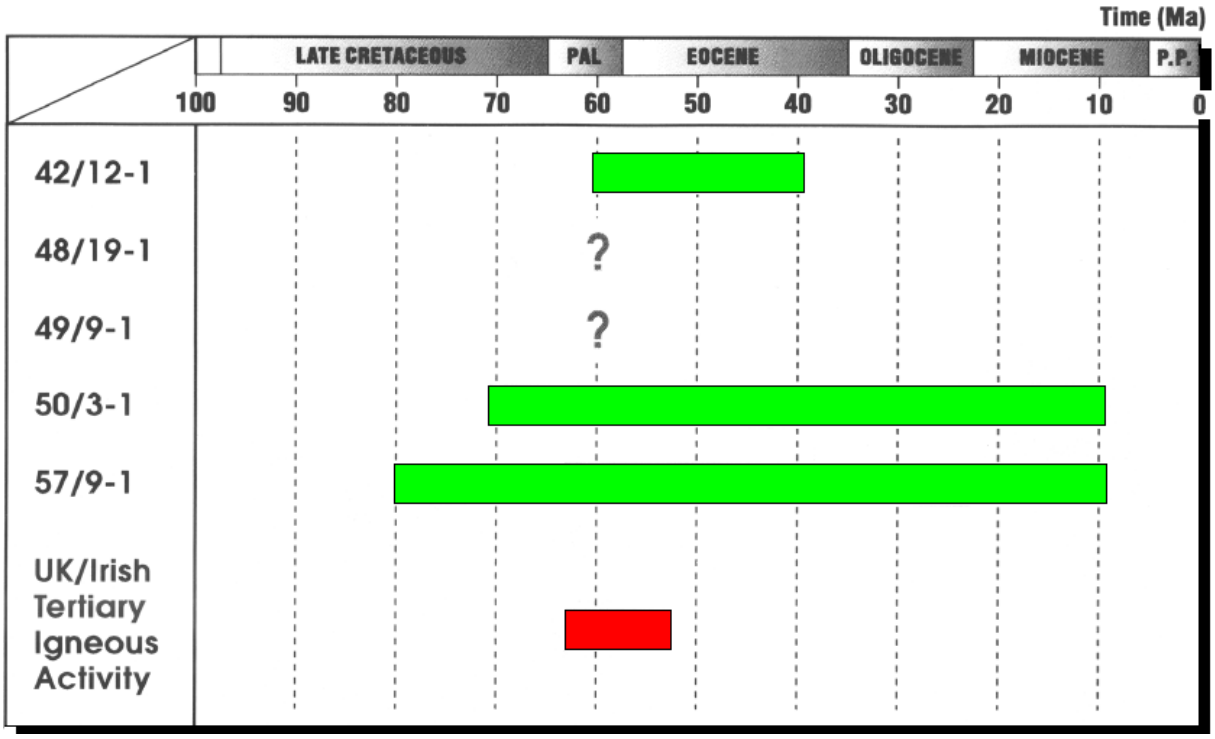

Figure 6.9 – Graph showing time of cooling from maximum palaeotemperature (from AFTA) for five wells compared to the timing of the Cenozoic igneous activity. Results are consistent with a widespread early Cenozoic uplift at around 60-55Ma, the time of the UK/Irish Cenozoic igneous activity. For two of the NCSB wells, results are also consistent with a later episode of uplift at 20Ma (modified after Murdoch *et al.* 1995).

6.4.2: MAGNITUDE AND DISTRIBUTION OF PALEOGENE EXHUMATION

There is some consensus that the uplift of the British Isles was driven primarily by tectonics during the early Paleogene (Praeg *et al.* 2005) though there is some debate as to the exact cause of this tectonic uplift. Considerable exhumation has been recorded across the whole of the British Isles from the Southwestern Approaches and Celtic Sea (Hillis, 1991, 1995a), across central (Green *et al.* 2001*b*), eastern (Green, 2005) and northern England (Green, 1986, 2002) towards the Scottish Highlands and Moray Firth (Thomson *et al.* 1999b; Argent *et al.* 2002). Those areas unaffected by uplift, such as the northern North Sea Basin, acted as important sinks for Cenozoic sediments (Morton *et al.* 1993; White & Lovell, 1997).

Brodie & White, (1994, 1995), Rowley & White, (1998) and Holford (2006) highlighted the EISB as being the locus point for this exhumation with evidence of up to 3km of erosion

during the Paleogene. Chapter 1 summarised the various theories of what caused this tectonic uplift and a major aim of this thesis has been to shed light onto which theories are more credible based on the geological evidence.

AFTA and VR data from the Burton Row borehole, on the margin of the BCB reveal that the preserved Mesozoic succession in this part of UK was more deeply buried by up to 2km of additional section prior to Paleogene cooling (65- 40Ma) (Figure 6.8) and it is likely that much of this section was removed during early Paleogene times. Evidence from the Wessex Basin is consistent with this estimate indicating deeper burial of 1800m of Cenozoic section in the Lulworth Banks borehole (Figure 6.10) and 1000-2000m of exhumation in the Arreton-2 borehole (Figure 6.11) (Bray *et al.* 1998).

Williams et al. (2005) showed that there is a lack of evidence for early Paleogene exhumation in the SGCB, where maximum burial depths were reached during the Cenozoic, prior to Neogene exhumation. Seismic data provides much evidence for compression of the basin during the Paleogene (Williams *et al.* 2005) suggesting that whilst the basin was affected by this exhumation event the Cenozoic burial (Chapter 5) caused the thermal signature of the Paleogene to be overprinted. Results presented by Murdoch *et al.* (1995) suggest exhumation values of up to 1300m (Figure 6.12) in the NCSB and further comment that Chalk erosion occurred during both this episode (which they suggest is Paleocene in age) and a later Cenozoic uplift episode with the greatest erosion (up to 1100m) taking place in the basin centre.

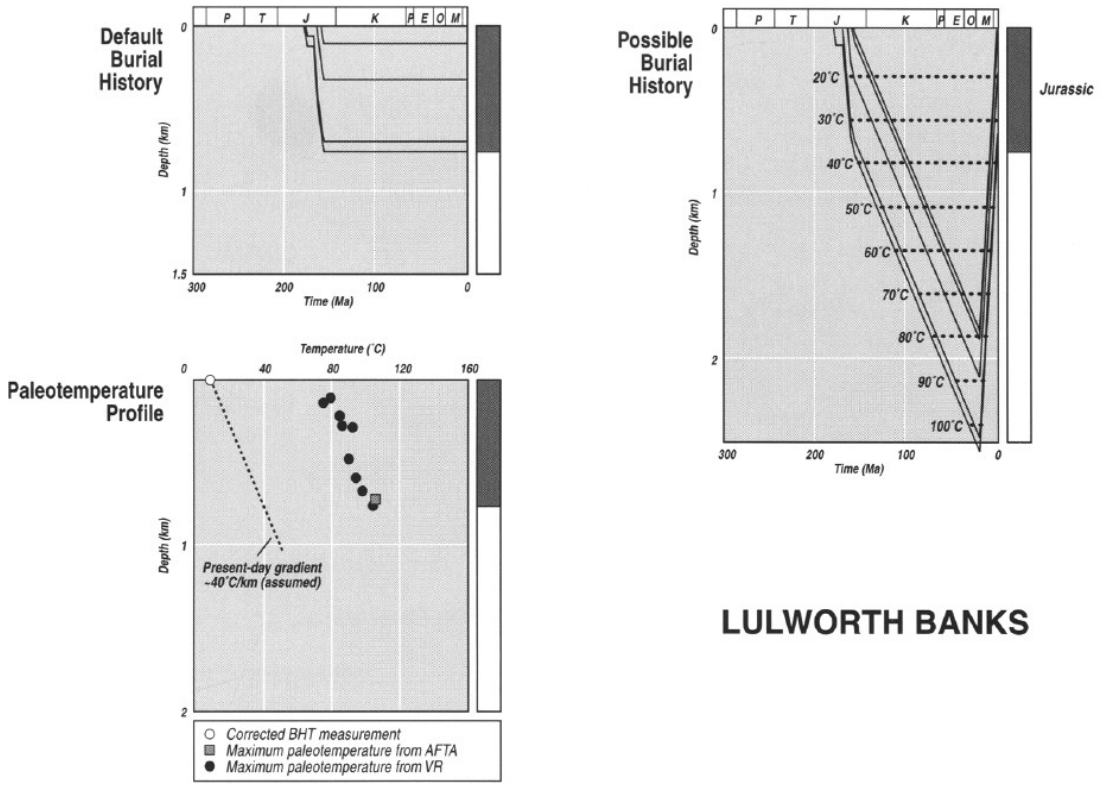

Figure 6.10 - Palaeotemperature profile and reconstructed burial history from AFTA and VR data from the Lulworth Banks well. The 'Default' burial history is constructed based on the preserved stratigraphy alone (i.e. by assuming no uplift and erosion at uncomformities) (after Bray *et al.* (1998)).

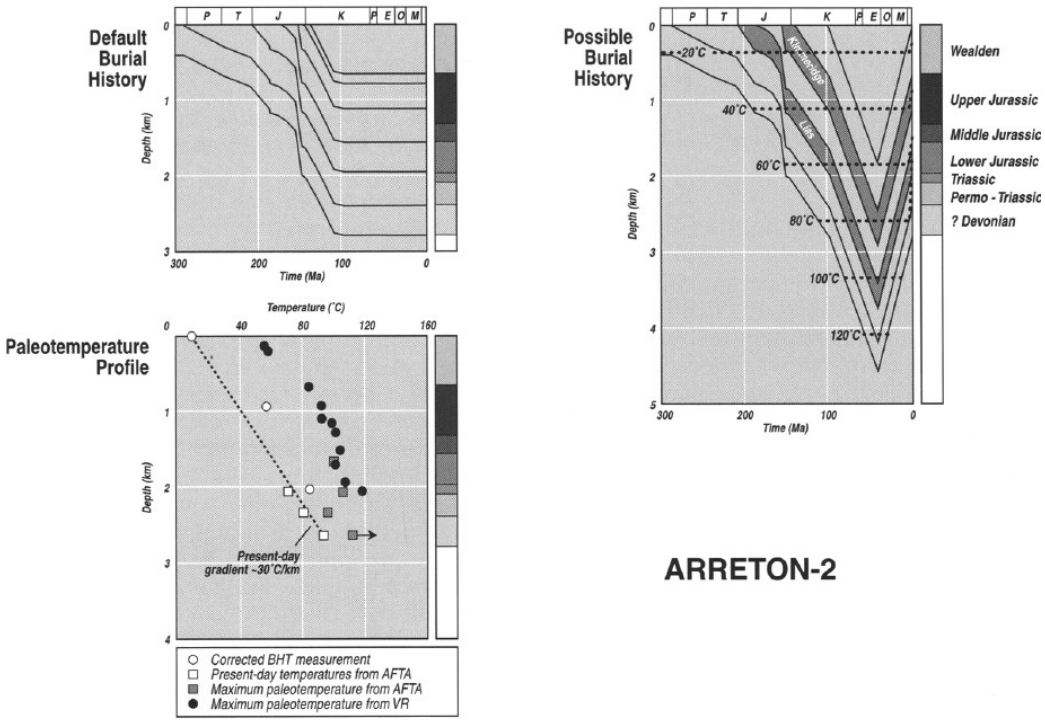

Figure 6.11 - Palaeotemperature profile and reconstructed burial history from AFTA and VR data from the Arreton-2 well. The 'Default' burial history is constructed based on the preserved stratigraphy alone (i.e. by assuming no uplift and erosion at uncomformities) (after Bray *et al.* (1998)).

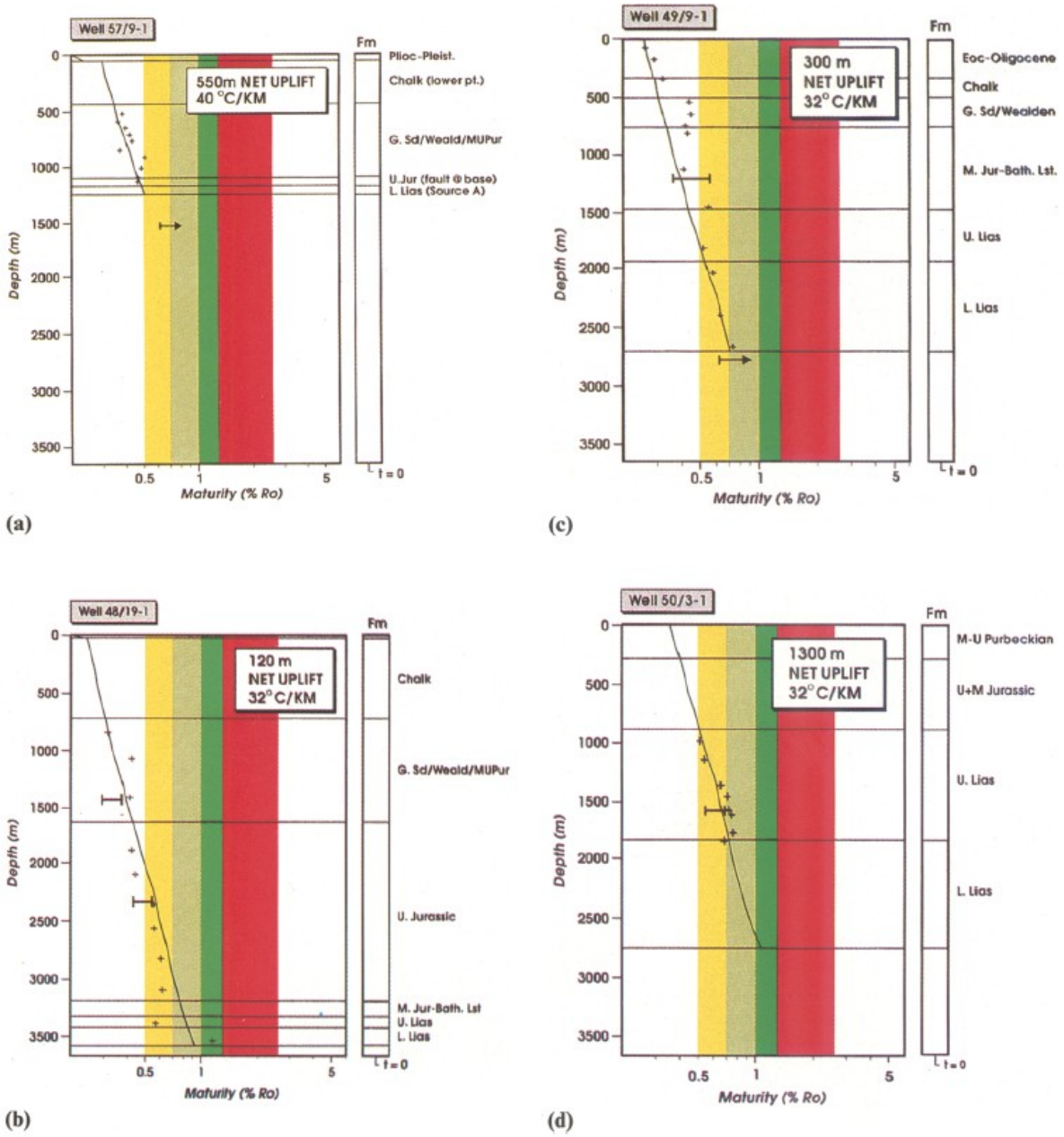

Figure 6.12 - Apparent erosion magnitude from VR (+) and AFTA (~) data, modelled at four wells in the NCSB. Yellow represents early mature oil (R_0 = 0.5-0.7%); light green represents mid-mature oil (R_0 = 0.7-1.0%); dark green represents late mature oil (R_0 = 1.0-1.3%); and red represents the main gas generation phase (R_0 = 1.3-2.6%). Insets show net uplift magnitude and geothermal gradients used in the model (after Murdoch *et al.* 1995).

The results presented in this study from across the SW UK suggest that there are major differences in the pattern of exhumation particularly over short (<100 km) distances. This spatial variation is mirrored in other parts of the British Isles such as the Scottish Highlands (*cf.* Thomson *et al.* 1999*b*; Green *et al.* 1999; Parnell *et al.* 2005*a*).

6.4.3: POTENTIAL DRIVING MECHANISMS OF EARLY PALEOGENE EXHUMATION

A number of authors (e.g. Ziegler, 1990; Drozdzewski, 1988; Chadwick, 1993; Nalpas *et al.* 1995) have proposed that the bulk of Late Cretaceous and younger intra-plate compressional deformations observed in western and central Europe developed in response to stresses that developed as a consequence of collisional coupling of the Alpine and Pyrenean orogens and their forelands and that the minor inversion structures evident along the Norwegian and Scottish continental margins are related to differential movements across intra-oceanic transform faults which project under the continent (Ziegler *et al.* 1995). This view was challenged by Cartwright (1989) who visualises a much stronger contribution of ridge-push forces associated with the sea-floor spreading axes of the North Atlantic, a view shared by Nielsen *et al.* (2007), who demonstrated a causal relationship between North Atlantic rifting and a change in deformation style *c.* 62Ma. Gillcrist *et al.* (1987) proposed a genetic relationship between the timing of basin inversion in the Channel-Western Approaches-Celtic Sea and the development of the Rhine-Rhone rift system. A major concern of Dewey & Windly (1988) was that the intense Paleocene compressional deformation of the Alpine foreland apparently does not correlate with major orogenic activity in the Alps (see Paleocene restoration of Trümpy, 1960).

However Paleogene exhumation of the UKCS occurred at the same time as an intense period of igneous activity (65-55Ma), which formed the British Cenozoic Igneous Province. The spatial distribution and timing of Paleogene denudation and Eocene-Oligocene subsidence therefore supports the idea that uplift was somehow related to thermal effects associated with an Early Cenozoic plume. Paleocene volcanism in the North Atlantic is widely attributed to the 'proto-Iceland plume', which was located somewhere beneath Greenland at around 60Ma (White & McKenzie, 1989; Lawver & Müller, 1994). As reported more fully by Holford

(2006) the distribution of igneous rocks suggests that a large part of northern England and Scotland (including the EISB, the Solway Firth, the Ulster Basin and the Sea of Hebrides Basin) lay within the zone of influence of the plume head. This region would have experienced transient thermal uplift (e.g. Nadin *et al.* 1995) together with igneous underplating (Brodie & White, 1995). In addition, a wider region incorporating the SGCB, the Celtic Sea and a large part of the North Sea would have been subjected to long-wavelength flexural uplift caused by the mantle flow field in the vicinity of the plume head (Courtney & White, 1986). Nadin *et al.* (1995) concluded that regional Paleogene uplift and subsequent Eocene subsidence in the northern North Sea can be explained by these 'transient dynamic uplift' effects. Thus, to date, early Paleogene exhumation has most commonly been attributed to vertical motions related to the initiation of the Iceland mantle plume (e.g. White & Lovell, 1997; Jones *et al.* 2002; Mackay *et al.* 2005).

Williams (2002) commented that the pattern of uplift and denudation predicted by the plume model can readily account for the following observations from the western UKCS:

1. The magnitude of Paleogene exhumation increased toward the north because this region was located closer to the main zone of thermal uplift and igneous underplating associated with the plume head.

2. Exhumation of the SGCB occurred in response to transient dynamic uplift, consequently the thick succession of Eocene and Oligocene sediments reflects post-exhumation subsidence. Subsidence following dynamic uplift occurred over a much shorter timescale than thermal relaxation of the lithosphere (Nadin *et al.* 1995), which would have been too slow to account for rapid Eocene and Oligocene subsidence in the SGCB.

3. The magnitude of Paleogene exhumation and Eocene-Oligocene subsidence decreased toward the south in the Celtic Sea, because this region lay on the edge of the zone of dynamic uplift.

4. Igneous underplating could account for the flat moho and reflective lower crust beneath the majority of the Celtic Sea basins (Brodie & White, 1995). It is important to note that the SGCB has an elevated moho, despite the fact that it experienced significant Paleogene exhumation. This could, however, reflect localised Cenozoic extension in this basin.

There are, however, a number of objections to the plume model. These are:

1) the magnitude of exhumation would be expected to decrease gradually over a wide region, consequently plume-induced uplift cannot account for local exhumation highs observed across the SW UK offshore basins

2) Williams (2002), showed that there is good evidence for Paleocene tectonic shortening in the SGCB, while other workers have identified inversion structures in the CISB and the EISB (Knipe *et al.*1993; Maingarm *et al.* 1999);

3) If igneous underplating is responsible for the uniform lower crustal structure beneath basins on the western UKCS, one would expect a similarly uniform pattern of exhumation throughout the region. Some of these objections can be overcome if regional epeirogenic uplift associated with a mantle plume is combined with a component of tectonic shortening.

A more detailed analysis of the short-falls of the plume model is presented by Holford (2006) and the interested reader is referred to Holford (2006 and references therein). In addition to the problems identified in Holford (2006) a number of other issues must be considered:

1. The need for the plume to 'morph' constantly through time to explain all the observations.

2. Why areas such as southern England are shown as undenuded?

3. If the Irish Sea is the focus of the underplating why is the area currently submerged?

4. If underplating is so widespread why does the only evidence for its existence appear to be confined to the immediate continental margins and diminish inboard?

Recently Al-Kindi *et al.* (2003) attempted to address this final point and the results of this study are shown in Figure 6.13a with this data converted to exhumation in Figure 6.13b. Holford (2006), showed the inconsistency between exhumation predicted by AFTA, VR and sonic data and that of the underplating model in the Irish Sea basin system however these discrepancies can be seen in other parts of the British Isles (e.g. Cleveland Basin, Green *et al.* 1993, 2001*b*) questioning the validity of the current model.

Many authors have cited the Iceland Plume as being responsible for uplift during the Cenozoic (e.g. Hall & White, 1994; Nadin *et al.* 1995; White & Lovell, 1997; Jones *et al.* 2001, 2002; Smallwood & White, 2002; Mudge & Jones, 2004; Mackay *et al.* 2005), however this theory has also come under scrutiny (Foulger, 2002; Foulger & Natland, 2003; Foulger & Andersen, 2005; Lundin & Doré, 2005*a*, *b*; Nielsen *et al.* 2007). The results of this study appear to contribute to the mass of evidence mounting against plume-related underplating being the dominant process causing exhumation during the early Paleogene.

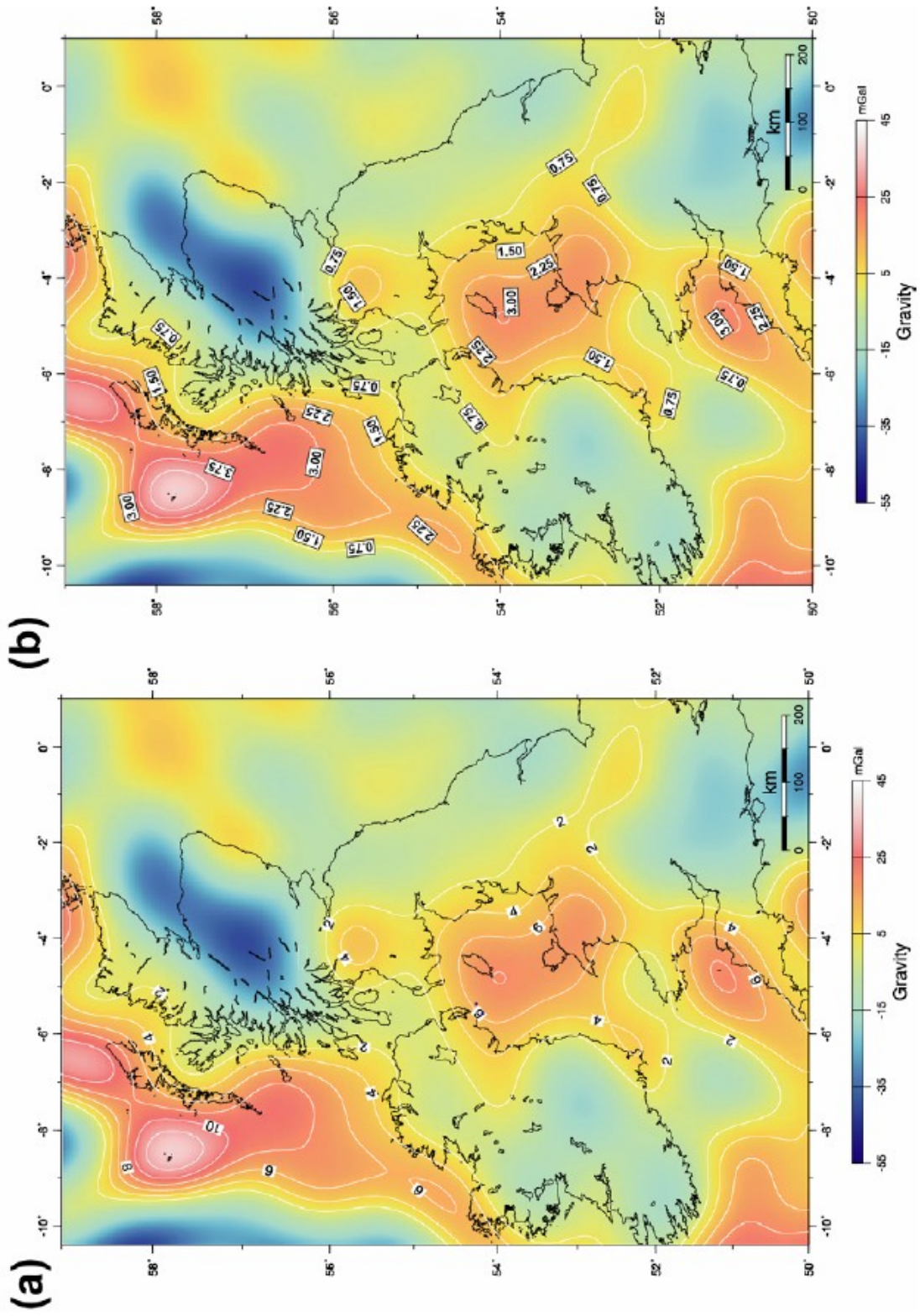

Figure 6.13 - (a) Map showing the predicted thickness of magmatic underplating beneath the British Isles determined by calibrating long-wavelength gravity data with wide-angle seismic data. This map predicts greatest amounts of underplating beneath the EISB, and the volcanic islands of St. Kilda off NW Scotland and Lundy in the Bristol Channel (after Al-Kindi *et al.* (2003)). (b) Underplating map of Al-Kindi *et al.* (2003) converted to an exhumation map, assuming Airy isostasy and the assuming uniform densities of 2.4, 2.9 and 3.2Mg/m³ for crustal sediments, gabbroic underplate and asthenospheric material respectively. Note that the negative gravity anomaly centred on Scotland predicts negligible exhumation across this part of the British Isles.

The other favoured driving mechanism for early Paleogene exhumation is intra-plate compressional shortening caused by the Alpine orogeny (Roberts, 1989; Hillis, 1992, 1995; Dercourt *et al.* 1993; Ziegler *et al.* 1995; Williams *et al.* 2005). Critics of this mechanism cite the lack of observed shortening needed to accommodate the magnitudes of exhumation (Brodie & White, 1994, 1995) however evidence presented by Williams *et al.* (2005) in the SGCB suggests that this has been overstated and indeed the results of this study would be consistent with the kinematics of early Alpine convergence as presented by Ziegler *et al.* (1995).

In western and central Europe structures which evolved in response to late Cretaceous and Cenozoic intra-plate compression include an array of inverted Mesozoic tensional and transtensional basins as well as the upthrusted basement blocks of the Bohemia Massif and Scania (Ziegler *et al.* 1995). A second more important phase of foreland deformation occurred during the late Paleocene. During this so-called 'Laramide' phase the foreland of the Northern Carpathians and the Eastern Alps was intensely deformed. A contemporaneous second phase of basin inversion is evident in the Central Graben of the North Sea and the most distal inversion structures observed in the central North Sea are located 1400km to the northwest of the present Alpine thrust front. Intra-Paleocene inversion movements are also evident in the Channel, Hampshire, Celtic Sea and Bristol Channel basins (Ziegler *et al.* 1995). The Laramide deformation of the Alpine-Carpathian foreland gave rise to a regional regression that is clearly tectonic in nature. To what degree this stress regime contributed to the Paleocene upwarping of the British Isles is uncertain in view of the intense volcanic activity which was associated with the development of the Iceland hot spot (Ziegler, 1990). The latter evolved during the late Senonian and persisted during Paleocene times and caused thermal uplift of surrounding areas (Morton & Parson, 1988). However the orientation of

northwest trending Paleocene dyke systems extending from Scotland and Northern Ireland to the North Sea coast and crossing the Irish Sea, suggests that the Laramide stress field also affected these areas. This hypothesis is also compatible with the Senonian and Paleocene compressional deformation observed in the Rockall and Faroe troughs (Boldreel & Andersen, 1993). Moreover as the latest Paleocene termination of inversion movements coincides closely with crustal separation between Europe and Greenland at the transition to the Eocene, it is postulated that the Laramide stress system impeded the early opening of the northern North Atlantic and the Norwegian-Greenland Sea (Zielger, 1988, 1990).

Compressional and transpressional intra-plate structures can occur at distances of up to 1600km from a collisional margin (Ziegler *et al.* 1998) as indicated for instance by the Paleocene deformation of the northern Alpine foreland (Ziegler, 1990) and the latest Carboniferous-Early Permian development of the Ancestral Rocky Mountains in the foreland of the Appalaciajn-Ouchita-Marathon orogen (Ross & Russ, 1985, 1986; Kluth, 1986; Stevenson & Baars, 1986; Oldow *et al.* 1989; Ziegler, 1989). Stress-induced whole lithospheric buckling leading to the uplift of arches with a wavelength of 500-750km (Nikishin *et al.* 1993; Burovet *et al.* 1993) can affect even broader areas of continental cratons as shown by the end-Silurian development of the Transcontinental and Labrador arches of North America (Ziegler *et al.* 1995). Similarly Pliocene-Pleistocene accelerated subsidence of the North Sea Basin and contemporaneous uplift of the Fennoscandian Shield can be related to deflections of the lithosphere in response to the build-up of the present-day compressional stress field of northwestern Europe (Cloetingh & Koor, 1992; Van Wees & Cloetingh, 1996). This stress field reflects a combination of forces related to collisional coupling of the Alpine orogen with its foreland and Atlantic ridge-push forces; the latter appear to play a dominant role only along the Atlantic margins (Müller *et al.* 1992; Gölke &

Coblentz, 1996). Ziegler *et al.* (1998) have shown that the nature of the resulting intra-plate deformation reflects the depth and degree of coupling along the plate boundary, with deformations ranging from crustal-scale tectonic shortening to whole lithosphere compressional doming. They also found that the spatial and temporal distribution of tectonic shortening in the upper crust reflects the following factors, which combine to determine the strength of the lithosphere:

1. The thermal regime controls the rheology and strength of the crust and mantle. Regions dominated by high basal heat flux are readily deformed in response to intra-plate compression.

2. Crustal thickness variations can result in rheologically weak crustal blocks prone to tectonic shortening.

3. Discontinuities in the crust and mantle can act as a focus for intra-plate stresses causing them to be reactivated in compression. The amount of tectonic shortening across these structures will be a function of the material properties of the discontinuity surface, fluid pressures and the orientation of the discontinuity with respect to the regional stress field.

4. The composition of the mantle (particularly where typical Peridotites have been replaced by mechanically weaker Serpentinite) can have an important effect on the mechanical properties of the lithosphere. Depleted mantle, mantle contaminated by subducted crust and underplated mantle can all influence the regional pattern of deformation.

It is clear that rifted crust and sedimentary basins are particularly susceptible to horizontal shortening in response to intra-plate compression. The Late Cretaceous and Cenozoic stress field of NW Europe was dominated by far-field compressive stresses generated by the Alpine orogeny and Atlantic ridge-push. Ridge-push forces were further enhanced during the Cenozoic by the coincidence of the Iceland Plume with the North Atlantic spreading axis (Bott, 1993; Lundin & Doré, 2002). The timing of inversion in basins on the UKCS can consequently be correlated with large-scale plate reorganisations during this period. This coincidence has been noted by Stoker *et al.* (2005) who correlated phases of Alpine orogenesis and the direction and rates of North Atlantic spreading, for example the late Alpine orogenic phase in Neogene times was coincident with separation of Jan Mayen and Greenland and the final establishment of the Kolbeinsey Ridge (Stoker *et al.* 2005). It follows that the interaction between Alpine collision and the opening Atlantic Ocean contributed to the exhumation and inversion of basins on the UKCS and the NE Atlantic margin throughout the late Cretaceous and Cenozoic. Additionally shortening has been demonstrated as characteristically non-uniform and exhumation patterns heterogeneous (Turner & Williams, 2004) and this is demonstrated on a number of scales (Figure 6.14; Williams *et al.* 1989; Sibson, 1995; Nielsen & Hansen, 2000).

The spatial and temporal distribution of basin inversion in the NCSB, SCSB and SGCB can be partially explained by the effects of intra-plate compression on highly heterogeneous basement. The SGCB is the deepest sedimentary basin on the western UKCS, and thus is more susceptible to basin inversion in response to intra-plate compression than other, shallower, depocentres. The fact that the SGCB formed by the reactivation of NE-trending Caledonian basement lineaments means that it was orientated at a high angle to the maximum compressive stress which was probably directed NW-SE during the Paleocene (Hibsch *et al.*

1995). Conversely, the NCSB, SCSB and BCB were predominantly inverted during the Oligocene-Miocene, in response to N-S directed tectonic shortening. Their E-W to NNE-WSW regional strike was more favourable for inversion under this stress field.

This observation of localised compression and regional exhumation led Hillis (1992), to develop a two-layer (i.e. depth-dependent) model of lithospheric compression (Figure 6.15), analogous to more familiar two-layer models of lithospheric extension (e.g. Kusznir *et al.* 1991; Kusznir & Ziegler, 1992).

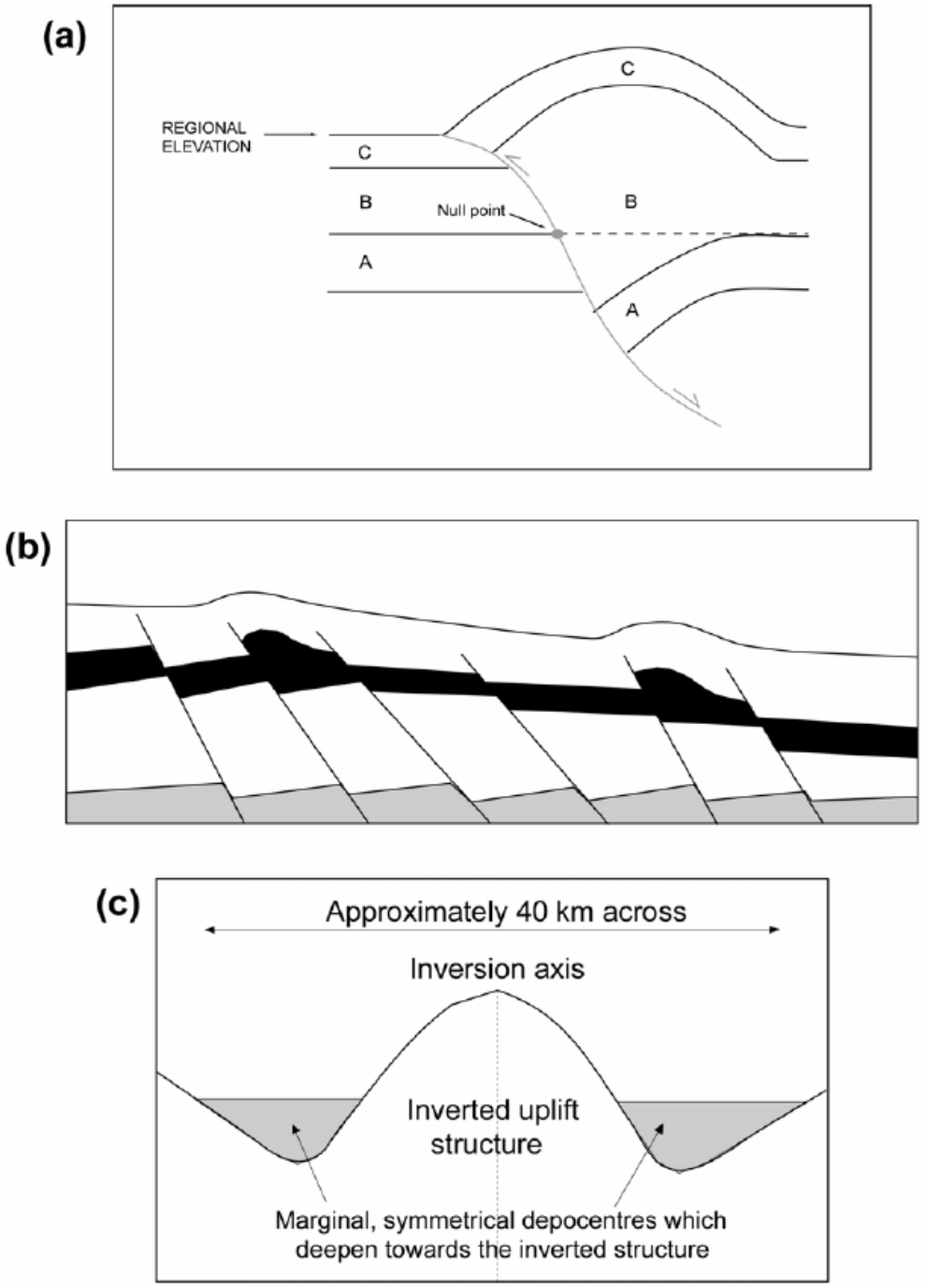

Figure 6.14 - Examples of non-uniform shortening resulting from the compressional deformation of a formerly extensional sedimentary basin. (a) Schematic diagram of a contractionally-reactivated normal fault. Parts of the hangingwall block will be preferentially elevated above the footwall and pre-deformation regional elevation (Williams *et al.* 1989). This will result in greater magnitudes of denudation over the hangingwall. (b) Diagram illustrating selective fault reactivation across an array of normal faults (cf. Sibson 1995). As only some of the faults have been contractionally reactivated, overall shortening across the section is highly non-uniform. (c) Schematic diagram illustrating the formation of marginal troughs on either side of an inversion structure. Such features are common throughout the Alpine foreland in NW Europe. Nielsen & Hansen (2000) have suggested that their formation is related to the differential shortening of the lithosphere.

In this model, compressional shortening and thickening in the lithospheric mantle, driven by either Alpine orogenesis or Atlantic ridge-push, is decoupled and laterally displaced from that in the crust. Crustal-scale lineaments are contractionally reactivated resulting in the formation of pronounced inversion axes (e.g. the inversion of the NCSB due to the reactivation of a major underlying Variscan thrust fault (Tappin *et al.* 1994; Blundell, 2002)), whilst shortening in the lithospheric mantle is laterally displaced from the inversion axes, explaining the regional exhumation patterns (Hillis, 1992). This model can also account for the regional subsidence and burial which preceded exhumation (*cf.* Green *et al.* 2002), since the submersion of the cold and dense mantle lithosphere into the surrounding asthenosphere would have caused an initial, isostatically-driven subsidence followed by uplift as a result of the subsequent warming of the lithosphere (Hillis, 1992). If thick-skinned compressional deformation of the Celtic Sea did occur during the Cenozoic, then the highly reflective lower crust and uniform reflection Moho might have originated in response to lower crustal flow, with mechanically weak mantle material flowing along pressure gradients to areas of thinned lithosphere beneath sedimentary basins (Hall & White, 1994). This process would have been facilitated by high mantle temperatures caused by igneous underplating during the early Cenozoic, and could conceivably explain regional epeirogenic uplift of the Celtic Sea region. In this study, evidence from AFTA and VR data combined with geological observations (Williams, 2002; Ziegler, 1995, Izatt *et al.* 2001; Green *et al.* 2001; Holford, 2006) suggests that the early Paleogene exhumation was driven by a combination of localised tectonic inversion and crustal shortening related to Alpine convergence (*cf.* Ziegler *et al.* 1995) with a component of regional uplift which may be associated with plume activity of the initial effects of North Atlantic continental break-up (which was achieved by *c.* 53Ma (Doré *et al.* 1999)) (see Figure 5.77, 5.78 and 5.80). A schematic model highlighting the observations of this study is shown in Figure 6.16.

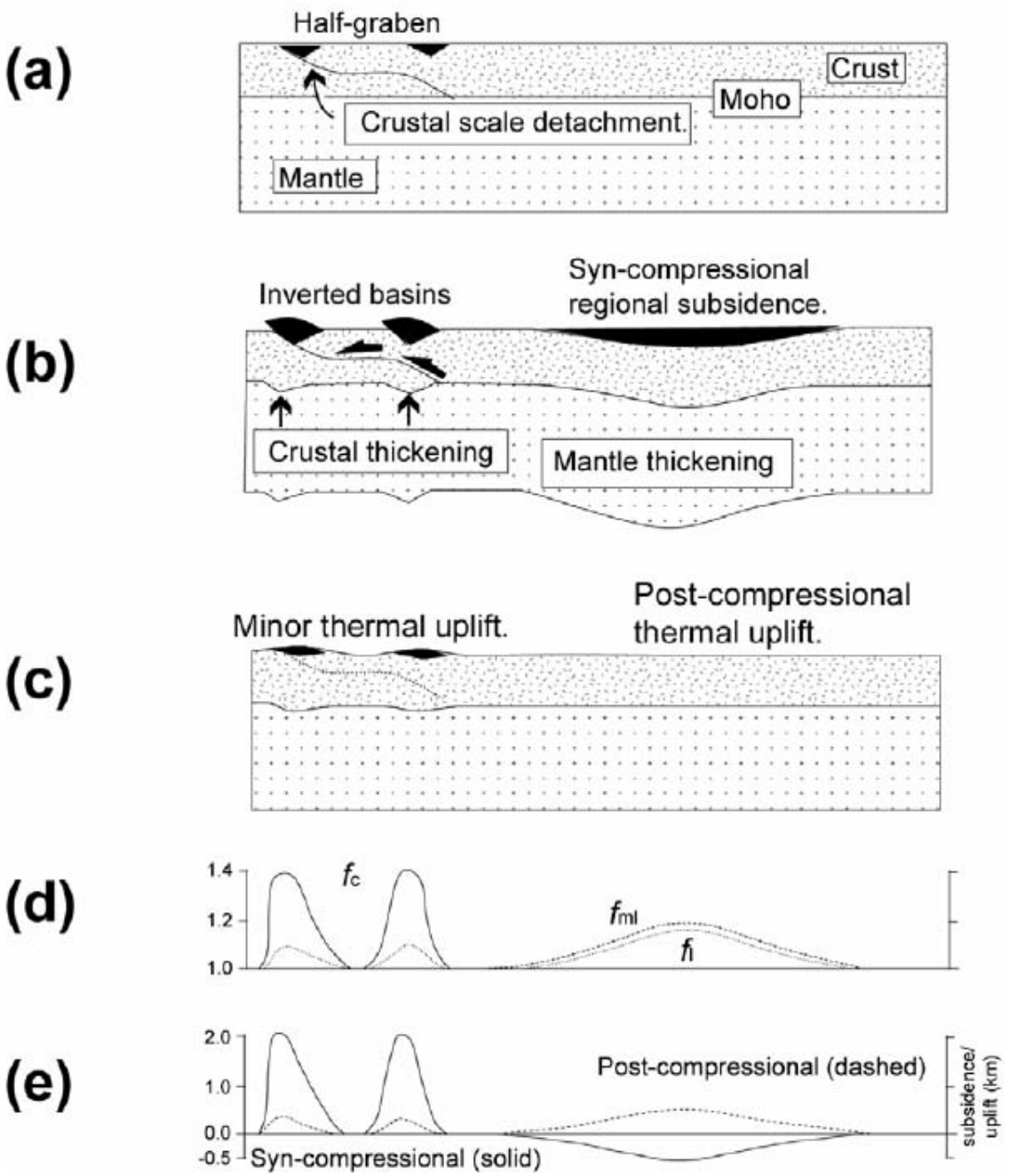

Figure 6.15 - Decoupled, two-layer modelling of lithospheric compression and thickening (Hillis, 1992). (a) Jurassic-early Cretaceous depocentres around the British Isles such as the southern Western Approaches Trough, the North and South Celtic Sea basins, and the Cleveland and Sole Pit axes formed above ramps in a major fault during extension. (b) These major faults are reactivated in compression, leading to the inversion of the Jurassic early Cretaceous depocentres. Thickening in the mantle lithosphere is decoupled and laterally displaced from that in the crust, causing initial subsidence. (c) Thermal re-equilibration of the lithosphere to its pre-compressional levels leads to the uplift of the region of mantle lithosphere thickening. (d) Balanced distribution of lithospheric thickening similar to that illustrated schematically in (a-c). The crustal thickening factor *f*c (solid line) is the ratio of the thickness of the deformed crust to its initial thickness. *f*ml is mantle lithospheric thickening (dashed) and *f*l is the whole lithospheric thickening (dotted). (e) The changes in surface elevation resulting from the distribution of lithospheric thickening shown in (d), assuming local isostasy and no surface loading. Syn-compressional elevation changes are shown by the solid lines, and post-compressional thermal uplift is shown by the dashed line.

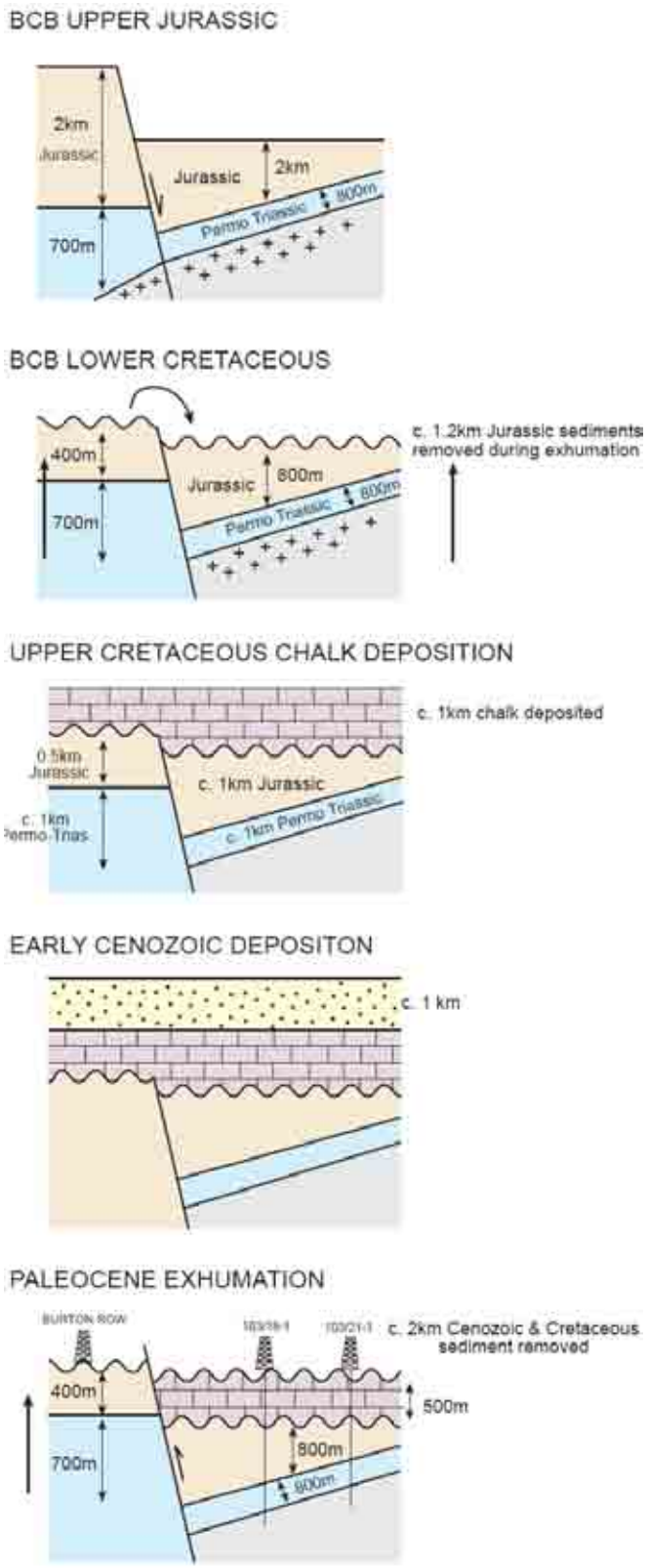

Figure 6.16 – Schematic model relating the observations of data from well logs, seismic, AFTA and VR to explain the current and palaeo-BCB. The model shows that the BCB has experienced a complex post-Triassic history involving multiple episodes of uplift and erosion. This study suggests that Cretaceous chalk deposition was much more extensive than that which is preserved. Footwall uplift and reactivation of the Bristol Channel Fault Zone has played an important part in determining the present day configuration.

6.5: NEOGENE EXHUMATION

6.5.1: TIMING OF NEOGENE EXHUMATION

The final episode of exhumation recognised by AFTA data in the SW UK indicates a cooling episode during the Neogene. The majority of outcrop samples collected from across the SW UK began to cool from palaeotemperatures of *c.* 50-80°C between 20 and 10Ma (Miocene) (Figure 6.17). Green et al. (2000) provided evidence for a regional cooling episode across Ireland between 25 and 15Ma (Figure 6.17) and there is also evidence of a similarly timed event in Northern Ireland (George, 1967; Roberts, 1989). Holford (2006) identified a regional cooling episode affecting the EISB (30-10Ma), CISB (25-0Ma) and the Kish Bank Basin (50-10Ma) also during Neogene times. Holford (2006) also asserted that although there is evidence across NW Wales for exhumation during the Cenozoic the resolution of the AFTA data does not allow for a tight constraint (*c.* 50-0Ma; Holford, 2006). Bray *et al.* (1998), recorded a mid-Cenozoic-Neogene episode in the Wessex Basin, which began around 40Ma related to the major phases of mid-Cenozoic structuring along the Portland-Wight monocline and inversion of Channel Basin. They also presented evidence of later episode *c.* 20Ma which is inferred to be related to the episode recognised in this study. There is evidence for similarly timed exhumation in the English Midlands (25-0Ma) and the UK Atlantic margin (*c.* 16Ma, Stoker *et al.* 2002, 2005*a*, *b*).

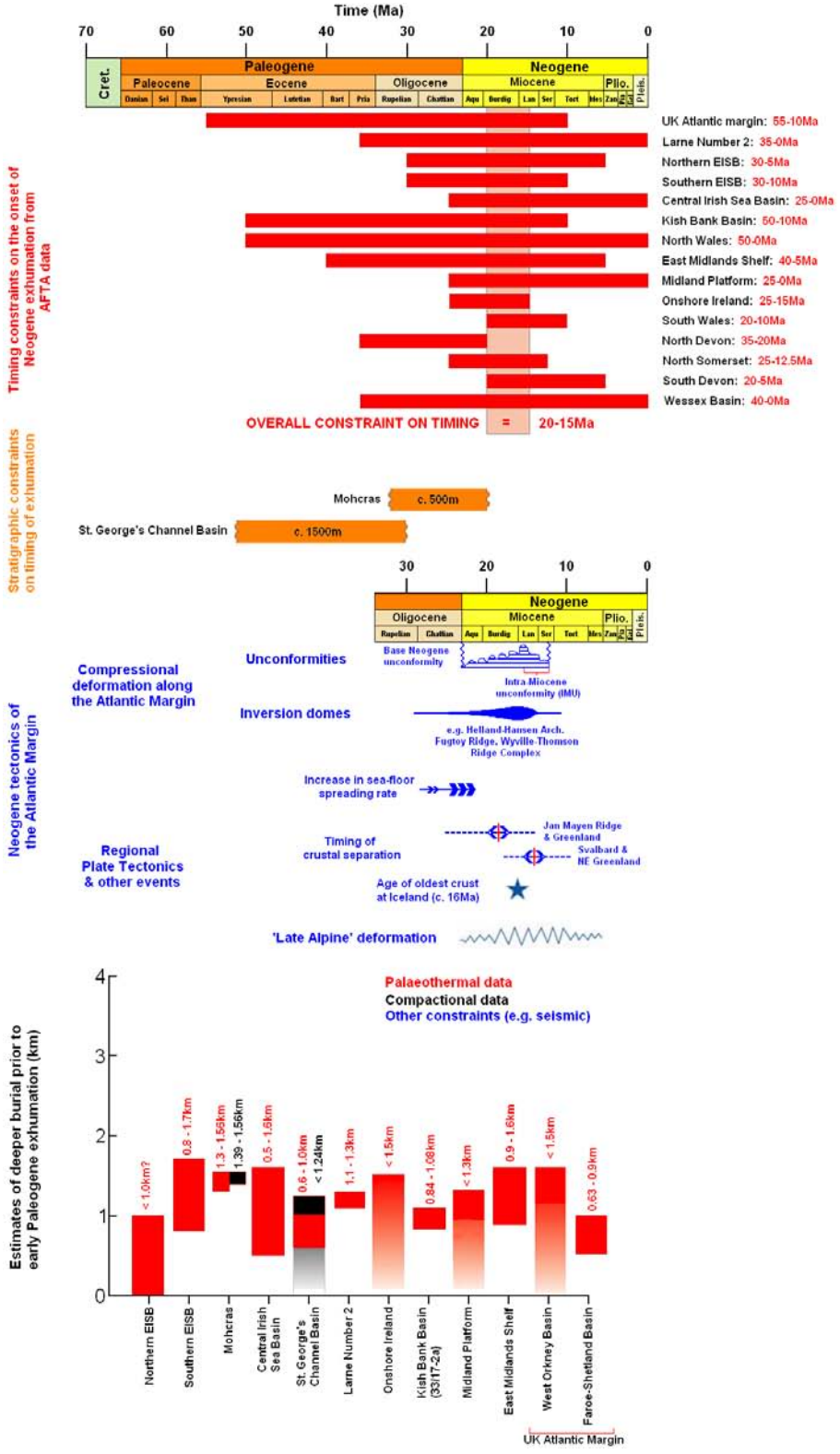

Figure 6.17 - Cenozoic event stratigraphy diagram. Constraints on the onset of exhumation-related cooling provided by AFTA data from across the western UKCS are compared with stratigraphic constraints on the timing of exhumation in an attempt to identify the timing of regional Neogene exhumation. This analysis suggests a regional onset of exhumation beginning between 20 and 15Ma. The timing of important regional tectonic events, derived from Lundin & Doré (2002) and Stoker *et al.* (2005*b*) are highlighted for comparative purposes. This diagram also shows estimates of the amount of deeper burial prior to Neogene exhumation across the British Isles, as determined using various techniques. Further details are provided in the text.

6.5.2: MAGNITUDE AND DISTRIBUTION OF NEOGENE EXHUMATION

The most important observation regarding the Neogene exhumation recorded in the SW UK is that this event is observed over the whole area in comparison to the other Mesozoic-Cenozoic episodes which show marked spatial variation. The relationship between tectonic events in the Cenozoic and timing is shown in Figure 6.17.

Evidence for the magnitude of this exhumation comes primarily from the palaeothermal data from outcrop samples across the SW UK. As shown in Chapter 5, AFTA and VR data indicate that the area experienced 0.8-2.0km of deeper burial prior to this exhumation event. Similar values of exhumation are recorded in the English Midlands (0.91-1.65km, Green et al. 2001), North Sea Basin (c. 1km, Japsen, 1997), Faeroe-Shetland Basin (0.63-0.9km, Parnell *et al.* 2005), the West Orkney Basin (*c.* 1.5km, Holford, 2006) and the Mohcras borehole where Holford (2006) demonstrated that the preserved Oligocene-Miocene succession had been more deeply buried by *c.* 1km prior to exhumation. There is also evidence for similarly timed exhumation across the whole of the circum North Atlantic margin (e.g. West Greenland (Japsen *et al.* 2005), East Greenland (Thomson *et al.* 1999*b*), Scandinavia (Riis & Fjeldskaar, 1992; Japsen *et al.* 2002) and NW Britain (Stoker, 2002)

Recently, some studies have argued that Cenozoic basin inversion and associated uplift in and around the UK were localised processes superimposed on Cenozoic regional uplift and associated exhumation (e.g. Bulat & Stoker, 1987; Hillis, 1991, 1993, 1994, 1995; Lewis *et al.* 1992; Keeley *et al.* 1993; Menpes & Hillis, 1995). Hillis (1995) and Menpes & Hillis (1995) used two wells located in the SCSB (102/28-1 and 102/29-1) to estimate the amount of missing section removed by erosion (apparent exhumation) in the SCSB. The value obtained from these two wells is 1100 ±400m and 980 ±150m respectively.

6.5.3: POTENTIAL DRIVING MECHANISMS OF NEOGENE EXHUMATION

Many studies have focussed on Neogene uplift yet the process driving the exhumation is still unresolved (Japsen & Chalmers, 2000; Doré *et al.* 2002; Japsen *et al.* 2005; Stoker *et al.* 2005*a*). What has been found however is that the uplift comprises two components:

1. Compressional deformation recorded by inversion features (e.g. Boldreel & Andersen, 1993, 1998; Doré & Lundin, 1996; Lundin & Doré, 2002; Ritchie *et al.* 2005; Stoker *et al.* 2005*b*).

2. Widespread seaward tilting (<1°) from the early Pliocene onwards (<4 ± 0.5Ma) (Praeg *et al.* 2005; Stoker *et al.* 2005*a*) resulting in the removal of several kilometres of overburden (Rohrman *et al.* 1995) and rapid basin subsidence (Japsen & Chalmers, 2000; Stoker *et al.* 2005*a*) the causes of which are debated (Cloetingh *et al.* 1990; Rohrman & van der Beek, 1996; Japsen & Chalmers, 2000; Nielsen *et al.* 2002; Rohrman *et al.* 2002; Praeg *et al.* 2005; Stoker *et al.* 2005*a*).

Stoker *et al.* (2005*a*) commented that the timing of the exhumation is poorly resolved however the results presented in this study have allowed a tight constraint to be placed on exhumation during the Neogene in the SW UK (Figure 6.17). The coincidence of the AFTA defined exhumation episode presented in this thesis and several instances of compressional tectonics suggests that Miocene compressional deformation was primarily responsible for the Neogene exhumation of the SW UK (see Figure 5.80 and 6.18) and probably the rest of the British Isles (Badley *et al.* 1989; Chadwick, 1993; Stewart & Bailey, 1996; Underhill & Paterson, 1998; Blundell, 2002). It should be noted however that this Neogene exhumation episode appears to have a broad regional component accompanying it (which to a lesser degree could also be argued for the early Cretaceous and Paleogene episodes) which is

necessary in order to reconcile the observations of exhumation across onshore Ireland (Green *et al.* 2000), NW Wales (Holford, 2006) and the English Midlands (Green *et al.* 2001*b*) which unlike the SW UK do not have evidence for late Cenozoic compressional structures. It is also possible that this cooling represents the tilting of the Atlantic margin rather than an exhumation event. In addition to Alpine tectonics extension and subsidence within the European Rift System, involving the Lower Rhenish Basin, the Rhine, Rhône and Limogne Graben, occurred mainly in Oligocene time through to Miocene time (Meier & Eisbacher, 1991). As the graben are oriented N-S, rifting is inferred to have resulted from E-W tension. As shown in Figure 1.24, inversion events in southern Britain can be correlated in time with events in the Alps to explain:

1. The uplift and erosion of the Chalk between 68 and 60Ma as due to stress generated by convergence between Africa and Europe.

2. The uplift of the Weald and subsidence of the London Basin and the uplift of the Sandown pericline and subsidence of the Hampshire-Dieppe Basin in a succession of short pulses of deformation as a consequence of Alpine stresses that could not be accommodated within the North Alpine Foreland Basin

3. Further uplift of the Weald, generation of thrusts extending into the London Basin capped by thrust anticlines, inversion on faults in the Wessex Basin and tightening of folds, folding of the Eocene strata associated with the compression of the Jura fold belt and northward propagation of stress.

The source of the compressional stresses responsible for this deformation have largely been attributed to both late Alpine convergence and North Atlantic sea-floor spreading (e.g. Boldreel & Andersen, 1993, 1998; Ziegler *et al.* 1995; Doré & Lundin, 1996; Lundin & Doré,

2002; Mosar *et al.* 2002; Johnson *et al.* 2005; Stoker *et al.* 2005*b*). Ziegler *et al.* (1995), suggested that Alpine compression affected basins up to 1600km from the orogen, and Blundell (2002), directly linked the Neogene deformational uplift of the Wessex Basin with the transmission of compressional stresses related to the collapse of the outer Alpine orogenic wedge during the late Miocene-Pliocene (*c.* 11-3Ma). Alternatively, Coward (1994) and Coward *et al.* (2003) specifically linked the compressional deformation of the SGCB to Oligocene-Miocene strike-slip deformation along a NW-SE trending transfer zone (including the Watchet-Cothelstone, Codling and Sticklepath-Lustleigh fault zone) which linked the opening of the North Atlantic with extension within the Rhine-Rhône basin system. The late Eocene to Oligocene transtensional basins of the Cardigan Bay and SW England, which subsided in response to sinistral reactivation of a pre-existing fracture zone during the reorganisation of sea-floor spreading axes in the Arctic-North Atlantic (Ziegler *et al.* 1995), became partly inverted during post-Oligocene times in response to dextral reactivation of their controlling fault systems. The timing of this episode is also coincident with the culmination of the Pyrenean orogeny which may also have contributed to the change is stress regime (Galloway *et al.* 1993). Late Eocene to Oligocene uplift of the British Isles (Roberts, 1989) is contemporaneous with the resumption of inversion movements in the southern North Sea and the Channel, Celtic Sea and Western Approaches areas.

The gravitational potential exerted by the significant topography which developed following the *c.* 16Ma formation of the Iceland 'anomaly' (*cf.* Lundin & Doré, 2005*a*, *b*) caused the Atlantic margin and inboard intra-plate regions to be placed under enhanced ridge-push forces (Bada *et al.* 2001; Bott, 1993; Kusznir, 2005; Foulger, 2006). These compressive stresses caused lithospheric shortening, and ultimately resulted in exhumation. Richardson (1992) calculated the torque acting on the Eurasian plate due to ridge-push forces and collisional

resistance along the Himalayan, Zagros and Mediterranean portions of the plate boundaries between the Indo-Australian, Arabian and African plates with the Eurasian plate. Richardson (1992) argued that while it is difficult to distinguish between the contributions of these two forces types, for Western Europe ridge-push may dominate for two reasons. First, much of the intra-plate stress data for Italy, the Adriatic and the Aegean Sea are at nearly 90° to the convergence direction for Africa-Eurasian plate motion. Secondly ridge-push forces seem adequate to also explain the compressional stresses in stable North and South America and have been shown to be an important part of all global models that provide an acceptable fit to the intra-plate stress field. The general scarcity of compressional deformations along passive margins suggests that ridge-push forces, even if enhanced by a ridge-centred hot spot (e.g. Iceland) (Bott, 1993) are on their own, not responsible for major intra-plate deformations but may contribute towards the deformation of the lithosphere if they act in constructive interference with other far-field stresses. Overall circumstantial evidence suggests that the most important intra-plate compressional/transpressional deformations, involving large-scale basin inversion and the upthrusting of major basement blocks, often deep in the interior of continental cratons are indeed related to collisional plate interaction (Green *et al.* 2002).

Examples of compressional and transpressional structures occurring on passive continental margins which clearly post-date the onset of sea-floor spreading, come mainly from the continental slopes of the British Isles (Porcupine Bank, Faroe-Rockall area: Roberts, 1989; Boldreel & Andersen, 1993) and the mid-Norway shelf (Ziegler, 1990). Whereas the broad anticlinal feature of the Mølde high is interpreted as a partly inverted basin (Bukovics & Ziegler, 1985), wrench faults, small-scale folds and thrust-faulted structures are evident on the Wyville-Thomson ridge, which separates the Rockall from the Faroe-Shetland trough and within the Faroe basin (Earle *et al.* 1989; Boldreel & Andersen, 1993). These structures

developed mainly during the late Eocene to Oligocene opening phases of the northern North Atlantic and Norwegian-Greenland Sea (Ziegler *et al.* 1995). During this time sea-floor spreading axes had not yet stabilised to their present arrangement; gradual abandonment of the Aegir Ridge at the expense of the newly developing Kolbeinsey Ridge was accompanied by transform motions along the Jan Mayen and the Iceland fracture zones. In areas where these fracture zones project into the continental margins, these were apparently tectonically destabilised as evident by their deformation. That such deformations can reach deep into a continent is illustrated by the late Eocene-Oligocene activity along a zone of wrench faulting which extends over a distance of 1000km from the Hebrides shelf through the Irish Sea to Cornwall, as indicated by subsidence of a chain of pull-apart basins such as the Petrockstow and Bovey Tracey basins in Devon (Ziegler, 1988, 1990; Roberts, 1989).

The World Stress map (Zoback, 1992) demonstrates that large parts of the lithosphere are at present affected by regionally persistent compressional horizontal stress regimes. Although many geodynamic processes contribute to the build-up of intra-plate horizontal compressional stresses, the pattern and timing of corresponding lithospheric deformations suggest that stresses related to collisional coupling of interacting plates play a dominant role in their development. Moreover palaeostress analyses show that stress patterns can change at the scale of a few million years in response to changes in plate interaction. By analogy with the Senonian and Paleocene compressional deformations of the northern and northwestern Alpine foreland, the Late Eocene to Miocene inversion of wrench and rift induced Mesozoic basins in the southern North Sea, the Channel and the Celtic Sea-Western Approaches areas are probably the effect of an intermittent build-up of horizontal compressional stresses which were transmitted from the Alpine collision front into the foreland. The observed systematic westward shift along these basins (North Sea, Channel, Wessex, Celtic Sea) of compressional

deformation is partly the expression of an increasingly important dextral translational component during the late Eocene to Pliocene convergence of Africa-Arabia and Europe (Ziegler, 1988).

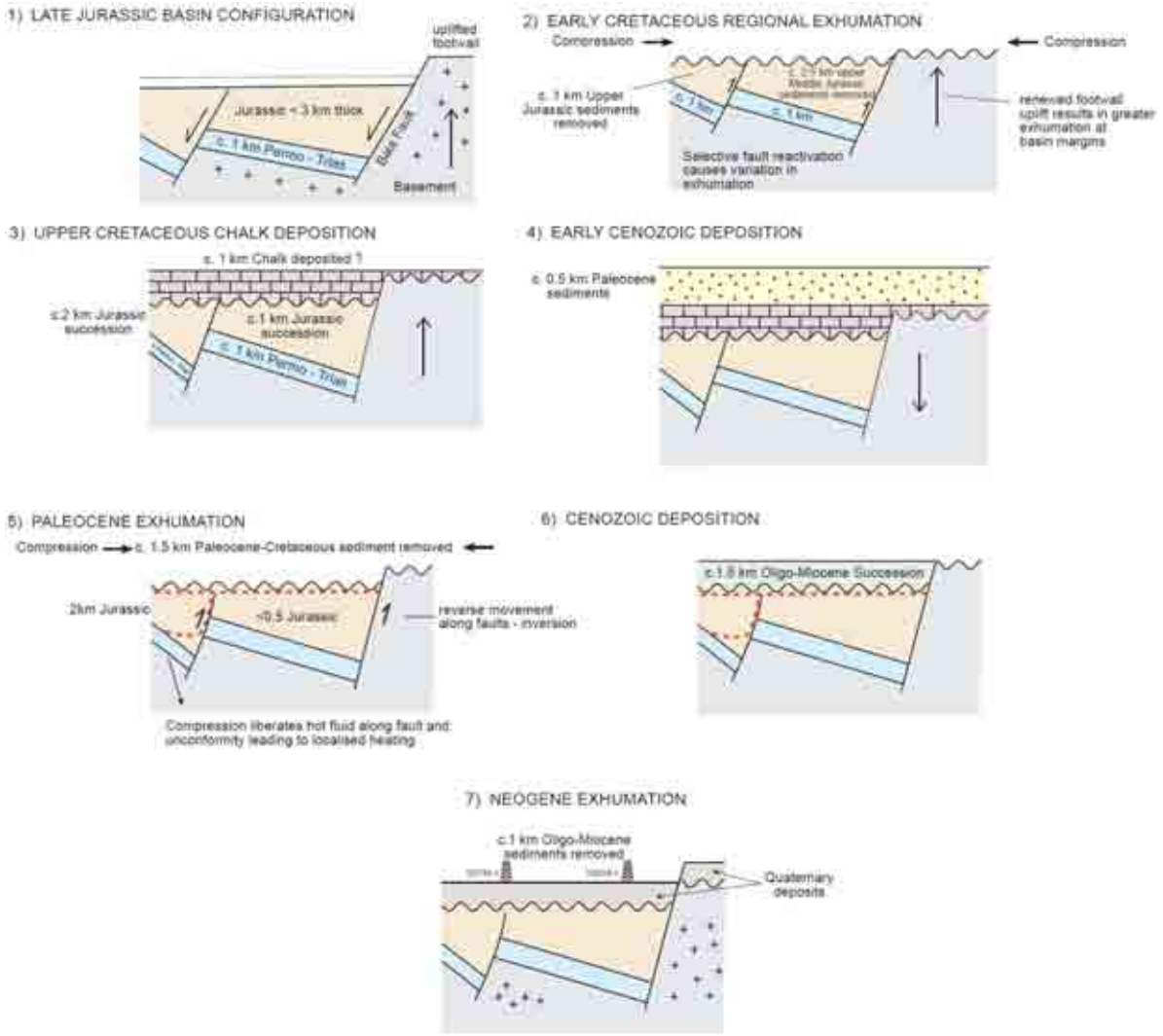

Figure 6.18 – Schematic model of the SGCB to account for the observations from well logs, seismic, AFTA and VR as revealed by this study. 1) Footwall uplift combined with a more regional epeirogenic episode (see Figure 5.77) causes greater uplift to occur at the Bala Fault footwall compared with the hangingwall. Eroded material from this high fills the SGCB depositing in excess of 3km of Jurassic section. 2) Early Cretaceous inversion related to the opening of the Bay of Biscay (see Figure 5.78) removed *c.* 2.5km of Jurassic section from the basin with variations in removed section controlled by selective fault reactivation. Continued footwall uplift at the basin margin coupled with inversion causes greater exhumation at the basin margins. 3) Following inversion deposition of the Upper Cretaceous Chalk begins resulting in *c.* 1km of Chalk deposition across the basin and SW UK. 4) Early Cenozoic deposition of *c.* 0.5km of clastic sediments occurs prior to Paleocene exhumation episode. 5) Paleocene exhumation removes *c.* 1.5km of sediment removing the Chalk deposition record from much of the basin. This exhumation is related to 'Laramide' compression and results in liberation of hot fluids from the compressed rocks which in the presence of local faults (as at 107/16-1) results in localised heating of the rocks. 6) Following Paleocene inversion deposition of *c.* 1.5km of Oligocene-Miocene clastics occurs. 7) Neogene exhumation related to Late Alpine compression and Atlantic ridge push causes oblique reactivation of faults leading to marked differences in exhumation depending on fault orientation and removal of up to 1km of sediments.

6.6: IMPLICATIONS

6.6.1: GENERAL COMMENTS ON THE NATURE OF EXHUMATION EPISODES

In researching this thesis a number of general observations regarding the nature of post-Triassic exhumation episodes in the SW UK and indeed the North Atlantic margin as a whole have been uncovered:

- Several kilometres of overburden are typically removed (generally of the order of ~3km).

- The exhumation occurs over a wide area (hundreds to thousands of kilometres horizontally) (Figure 6.19).

- Holford (2006) recognised an apparent periodicity in exhumation episodes of *c.* 50 to 60Myr. These cycles have also been reported from onshore Ireland (Green *et al.* 2000), northern Scotland (Thomson *et al.* 1999), the Falkland Islands (Thomson *et al.* 2002), northern Australia (Duddy *et al.* 2003) and SE Arabia (George *et al.* 2005). Such coincidence across a wide geographic area suggests a macro scale process being responsible.

- As highlighted by Green *et al.* (2002) exhumation is often preceded by accelerated burial. This has been dismissed as an artefact by some workers (e.g. Japsen, (1997)) however work presented by Holford (2006) in the Irish Sea as well as by Green *et al.* (2002) from other parts of the British Isles suggests that this is not the case and it is in fact a real observation.

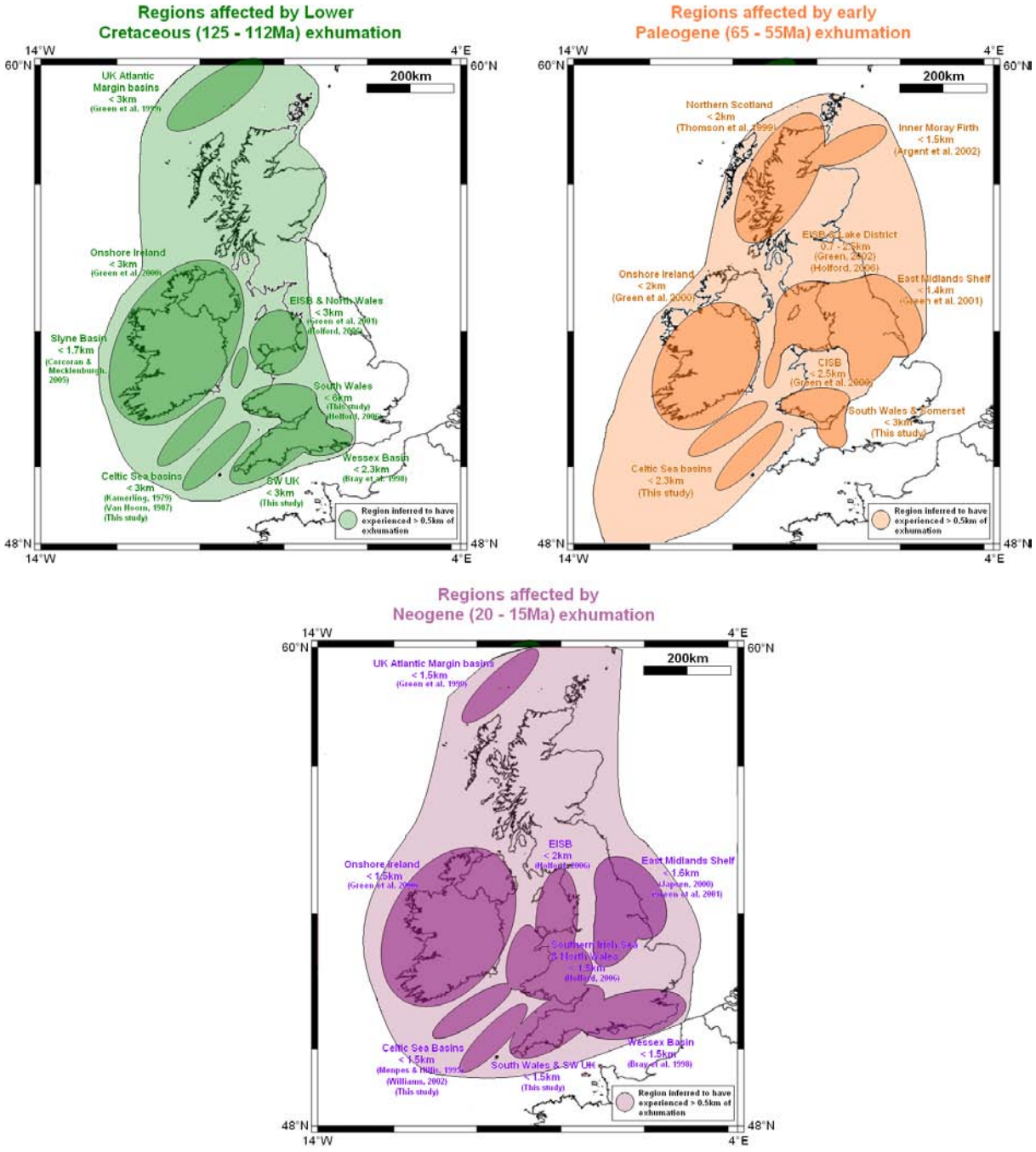

Figure 6.19 - Regional extent of the Lower Cretaceous, early Paleogene and Neogene exhumation episodes. Each of these events is characterised by kilometre-scale exhumation over horizontal distances in the range 500-1000km.

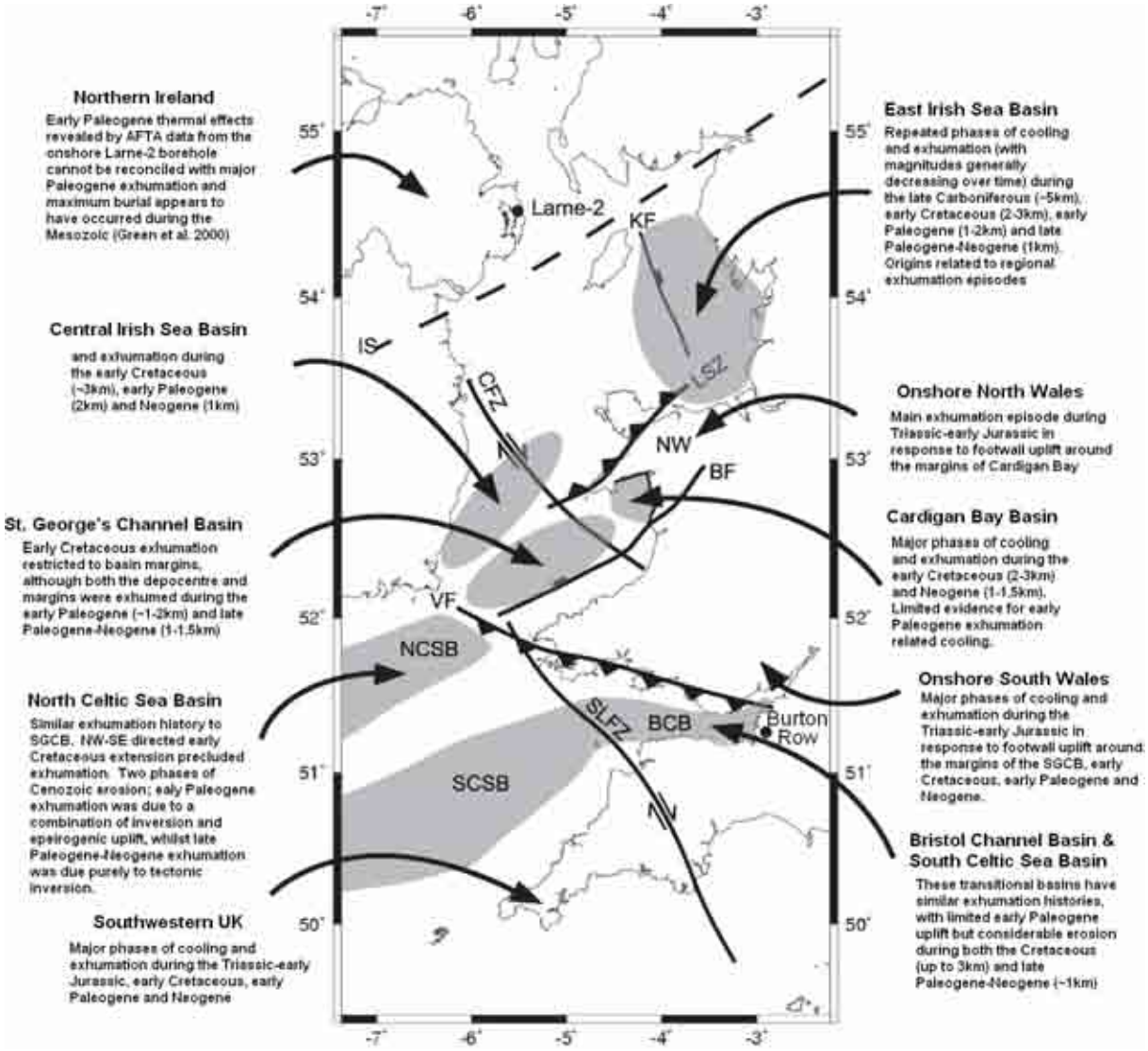

Figure 6.20 - Summary map of the main exhumation episodes that have affected the western UKCS. Major crustal-scale lineaments are also highlighted, the repeated reactivations of which have influenced repeated cycles of burial and exhumation across this region. BF, Bala Fault; CFZ, Codling Fault Zone; IS, Iapetus Suture; KF, Keys Fault; LSZ, Llyn Shear Zone; SLFZ, Sticklepath–Lustleigh Fault Zone; VF, Variscan Front (modified after Holford *et al.* 2005).

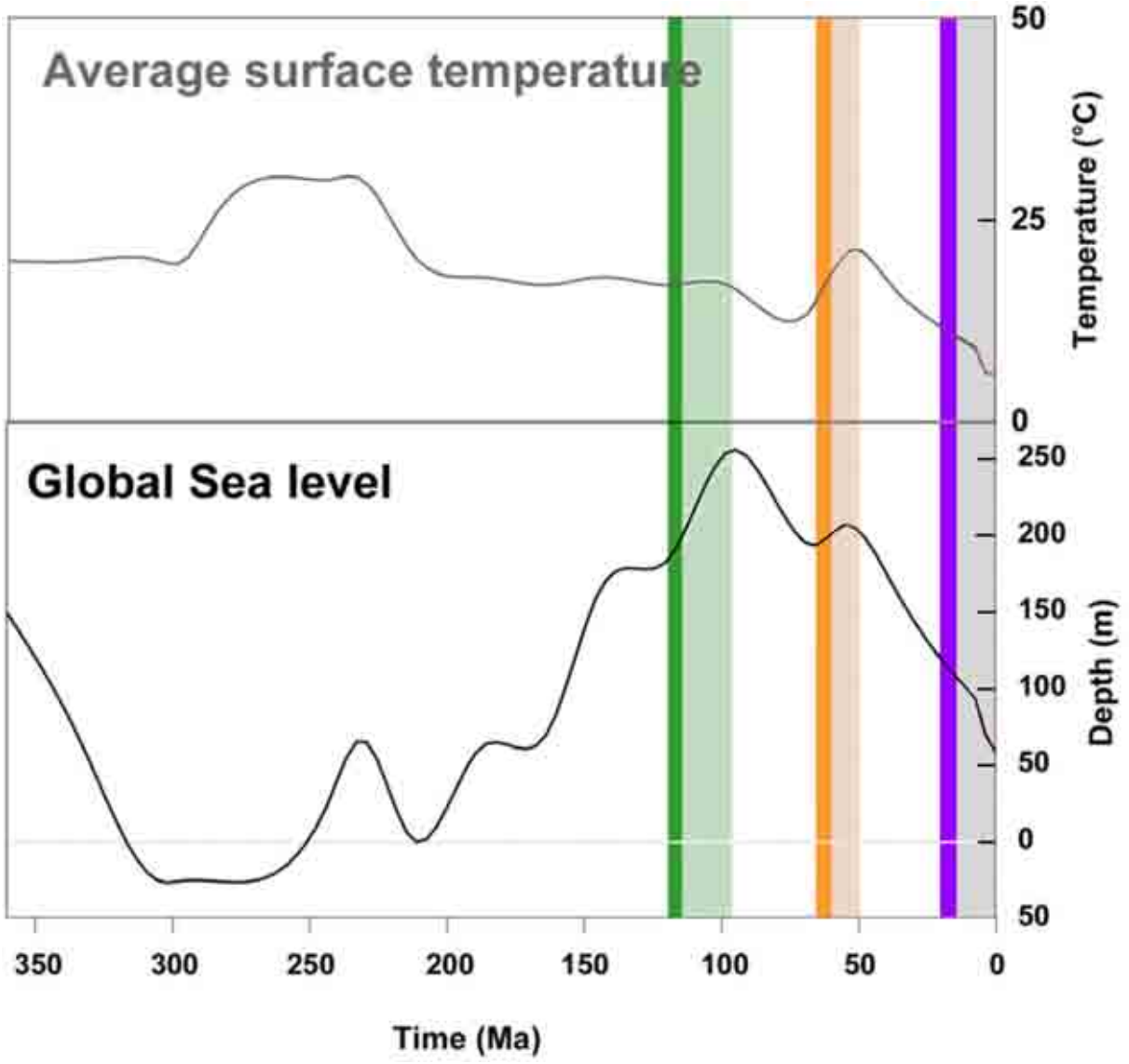

Figure 6.21 - Comparison between the timing of Mesozoic-Cenozoic exhumation episodes identified in this study with variations in average surface temperature for the British Isles (modified from Yalçin *et al.* 1997) and global sea-level curve (Haq *et al.* 1987). Dark vertical shaded bars indicate the time at which the regional exhumation episodes began, as discussed in the text, whilst the lighter shading indicates their inferred duration.

- The consistency of the temporal correlations between periods of widespread exhumation across the western UK (Figure 6.20) and major tectonic stress events at incipient or pre-existing plate boundaries implies that regional exhumation of intra-plate regions are probably driven by major tectonic events at plate margins.

- Holford (2006) also commented that exhumation episodes are often associated with falls in sea-level and other climatic factors (Figure 6.21).

6.6.2: IMPLICATIONS FOR PETROLEUM PROSPECTIVITY

The generation and maturation of petroleum are known to be temperature and geological-time dependent (Connan, 1974) so that the estimation of maximum burial depth or the maximum temperature the bed has ever attained is an important function in assessing hydrocarbon potential and is just as important as the basic factors of source, reservoir and seal. Unfortunately, consideration of thermal history is often relegated to one of the last and least important factors in prospect evaluation, such that even damning evidence of unsuitability of a region for significant hydrocarbon discoveries may not have much influence on the decision to drill. Proper analysis of maximum burial depth is essential in evaluating the palaeostructural configuration and structural timing which are important in a prospect evaluation.

Furthermore, the maximum temperature to which a rock has been subjected is the fundamental parameter for the assessment of source rock maturation. Temperature is the primary factor governing the degree of maturation and hence hydrocarbon generation and once a rock unit cools below its maximum temperature maturation ceases. Maturation will not recommence until the sample is re-heated to temperatures higher than the previous maximum. Further, if liquid hydrocarbons have been generated and reservoired in a sequence then temperature will again be a primary factor governing whether these liquids will be preserved or cracked to gas.

Another critical aspect of the thermal history of potential hydrocarbon source rocks is the timing of generation in relation to trap formation. Potential source rock horizons within the SW UK are found in the Carboniferous and Lower Jurassic sequences (Cornford, 1986; Cornford *et al.* 1987; Penn *et al.* 1987; Selley & Stanley, 1987). In southern England, Sinemurian and Pleinsbachian shales have an oil source rock potential whereas Toarcian

shales have a much lower content of organic matter than in the Paris Basin. The late Toarcian Bridport Sands contain the shallower oil accumulations of the Wytch Farm field which also produces from the Triassic Sherwood Sandstone (Ziegler, 1990).

In the EISB and adjacent areas, Green *et al.* (1997) showed that the area in which source rocks reached maximum maturity levels immediately before early Cenozoic inversion is restricted largely to the main EISB hydrocarbon province. In surrounding areas, by contrast, the main phase of hydrocarbon generation occurred during earlier episodes (from latest Carboniferous to early Cretaceous time). The lack of hydrocarbon discoveries in these regions suggests either that the hydrocarbon generation pre-dated structure formation or that any hydrocarbons accumulated in earlier episodes were lost during subsequent uplift and/or tilting.

Results presented here indicate that potential source rocks within most of the SW UK reached maximum maturity levels during early Cretaceous time, which represents the termination of the main phase of hydrocarbon generation. Any hydrocarbons accumulated at that time are likely to have undergone phase changes and redistribution during at least three discrete phases of uplift and erosion, significantly decreasing the chances of commercial amounts surviving to the present day. In the case of Carboniferous source rocks, all hydrocarbon generation occurred at an early stage, during Hercynian heating and prior to formation of any trapping structures. Maturity levels vary across the region from post-mature for gas generation over much of the offshore region to the west and onshore in North Devon and South Wales, to early mature for oil generation in the east around the Forest of Dean. However maximum hydrocarbon generation will have occurred early (even in the eastern region) and subsequent heating has not been sufficient to produce additional generation since Hercynian times.

In the SGCB to the north in the vicinity of well 42/21-1, the early Cenozoic episode appears to become dominant, raising the possibility that in this region, conditions similar to those characterising the main EISB hydrocarbon province may apply. However, because of the much larger thicknesses of preserved Jurassic section, any Carboniferous source rocks in most of this region are likely to have reached much higher maturity levels than in the EISB, whereas Jurassic source rocks are only marginally mature. These factors suggest much higher levels of exploration risk in this area, although the Dragon discovery (103/02-1) in UK Quad 103 (Tanner, 1999), shows that conditions suitable for operation of a viable petroleum system existed in this region at some stage.

Clearly, prospects of finding significant hydrocarbon reserves within the SCSB and BCB appear to depend either on the preservation of early formed hydrocarbons through several episodes of uplift and erosion, or on identification of areas in which Cenozoic palaeotemperatures were higher than those reached during earlier episodes. It seems unlikely that any hydrocarbons generated from Carboniferous source rocks during Hercynian heating will have survived through the subsequent tectonic history anywhere within the region. The prospect of hydrocarbons generated from Jurassic source rocks being preserved to the present day also appears slim for the main basinal region. Only in areas where Cenozoic palaeotemperatures exceeded early values will an appreciable proportion of hydrocarbons have been generated after trap formation, increasing the potential for preservation to the present day. Such conditions are more likely to the east (Dorset and the Wytch Farm oil field (e.g. Figure 6.2) and west (NCSB (e.g. Figures 6.22-6.23) and fields such as Kinsale Head and Ballycotton) of the study area and these areas may be more prospective in terms of the relative timing of maximum palaeotemperatures (maturity development) and formation of trapping structures, based on trends within the data from this study.

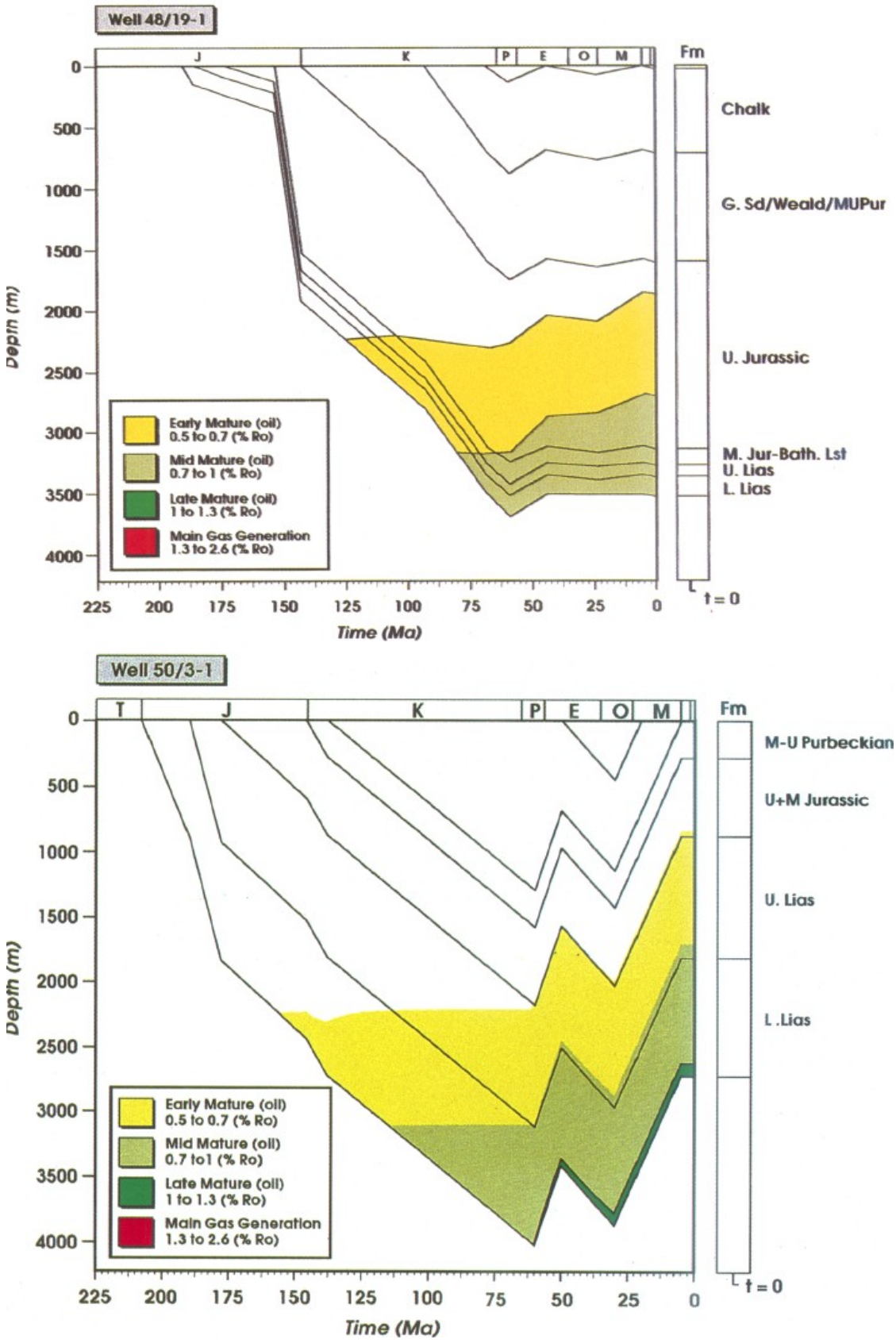

Figure 6.22 - Burial histories modelled for wells 48/19-1 and 50/03-1 in the NCSB. Well locations are shown in Figure 6.23. These models along with two others produced the maturity lines shown matched to VR and AFTA data in Figure 6.23 (after Murdoch *et al.* 1995).

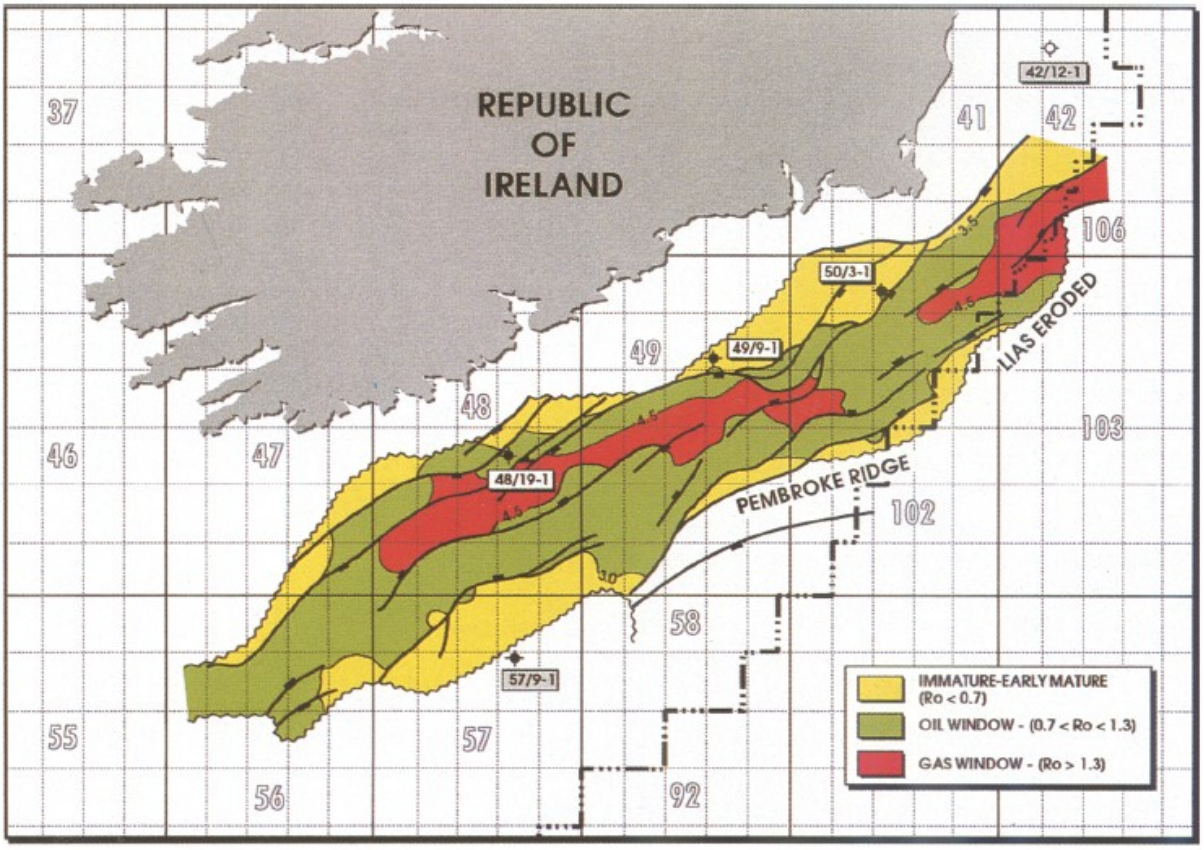

Figure 6.23 - Top Lower Jurassic pre-uplift depth map with maturity estimation of the NCSB. Contour values are in kilometers (after Murdoch et al. 1995).

Careful application of AFTA in combination with VR in the early phases of exploration is undoubtedly of great benefit to sophisticated hydrocarbon exploration in frontier areas.

6.6.3: GENERAL IMPLICATIONS OF THE RESULTS OF THIS STUDY FOR UNDERSTANDING THE EXHUMATION HISTORIES OF PASSIVE MARGIN AND INTRAPLATE REGIONS

Developing an improved understanding of the patterns of burial and exhumation within intra-plate regions and passive continental margins carries major implications for understanding the interactions between Earth surface processes and fundamental geodynamic phenomena such as lithospheric plate motions and mantle convection (e.g. Cooper & Williams, 1989; Buchanan & Buchanan, 1995; Doré *et al.* 2002). By combining constraints on former burial depths from several independent methods, this study has been able to reconstruct the post-

Triassic exhumation history of the intra-plate SW UK with considerably improved accuracy in comparison to previous studies. The integration of AFTA data with stratigraphic constraints has revealed evidence for three regional kilometre-scale exhumation events. These separate phases of exhumation began during the Lower Cretaceous (140-120Ma), early Paleogene (75-55Ma) and Neogene (20-10Ma), respectively (Figure 6.19). In addition, an earlier more localised exhumation event has also been identified during the Upper Triassic-Lower Jurassic (215-195Ma).

This SW UK has clearly experienced a Mesozoic-Cenozoic tectonic history of great complexity, characterised by repeated cycles of burial and exhumation. Results from this study support the view that extensional sedimentary basins comprise zones of long-term crustal weakness which are susceptible to repeated reactivations depending upon the prevailing stress regime (Ziegler *et al.* 1995; van Wees & Beekman, 2000; Turner & Williams, 2004). As demonstrated in this study (and similar studies e.g. Holford, 2006), each of the major exhumation episodes coincides temporally with major plate reorganisations or important periods of extensional or compressional deformation at pre-existing or incipient plate boundaries. This suggests that events at plate margins have exerted the primary control upon the exhumation, despite the considerable distances between this region and the most proximal plate boundaries (e.g. *c.* 1000 km from the late Alpine deformation front, *c.* 1800km from the Iceland spreading ridge). However, in each of the Mesozoic-Cenozoic exhumation episodes which have affected this study area, there appears to have been a component of regional uplift which cannot be accounted for solely by plate boundary forces and processes. A good example of this occurs with the early Cretaceous (140-120Ma) exhumation episode which was coeval with sea-floor spreading and the formation of the rifted continental margin SW of Britain. The observed magnitude and distribution of exhumation however (up to 3km

at distances >500 km from the plate margin) cannot be explained by processes such as rift-flank uplift (*cf.* Weissel & Karner, 1989) or thermal uplift associated with depth-dependent lithospheric extension (*cf.* Kusznir *et al.* 2005).

Hillis (1992) developed a two-layer model of lithospheric shortening, analogous to models of depth-dependent lithospheric extension (*cf.* Kusznir *et al.* 2004, 2005) in order to reconcile the occurrence of localised compression and regional exhumation. This model is not without its flaws (e.g. the existence of intra-lithospheric detachments beneath the inverted basins of the UK, remain unproven) however the recognition that the lithosphere may deform heterogeneously with depth during collision-related shortening has profound implications for understanding the mechanics of continental deformation.

Periods of widespread intra-plate exhumation, approximately coeval with phases of plate boundary deformation but with no obvious tectonic driving mechanism, have been documented from many other parts of the world. For example, continental break-up leading to seafloor spreading in the South Atlantic, offshore SW Africa, occurred at approximately 130Ma (Gallagher & Brown, 1999). Apatite fission-track data from the SW African rifted continental margin document the occurrence of kilometre-scale exhumation, coeval with the timing of break-up, extending considerable distances (i.e. >400 km) away from the ocean-continent divide, towards the supposedly stable cratonic interior of southern Africa (Figure 6.24) (Gallagher & Brown, 1999; Cockburn *et al.* 2000).

One of the best-studied rifted continental margins in the world is that of SE Australia. A prominent escarpment, with elevations of around 1000m, separates an upland surface of low to medium relief in the SE Australian highlands from a narrow, low-elevation coastal region (Ollier, 1982). Continental break-up between the Australian and Antarctic plates leading to

the formation of this margin and the Tasman Sea occurred during the mid Cretaceous, at approximately 95Ma (Veevers, 2000). Break-up was accompanied by considerable exhumation along the SE Australian margin. AFTA, VR and apatite (U-Th)/He data from the Otway Basin reveal evidence for a mid Cretaceous exhumation episode, beginning between100 and 90Ma, during which around 2km of early Cretaceous overburden was eroded (Green *et al.* 2004). Similar amounts of coeval exhumation are recorded by AFTA data from various parts of the SE Australian margin, including the Bass Strait (O'Sullivan *et al.* 2000), the Lachlan Fold Belt (O'Sullivan *et al.* 1996) and the Snowy Mountains, New South Wales (Kohn *et al.* 1999). However, maps illustrating the variation in AFTA ages across the Australian continent (Gleadow *et al.* 2002) show that young (i.e. <150Ma) fission-track ages, representing the effects of early Cretaceous exhumation, are not just restricted to the rifted margin of SE Australia (where ages are commonly <100Ma) but extend many hundreds of kilometres inland from the margin (Figure 6.25).

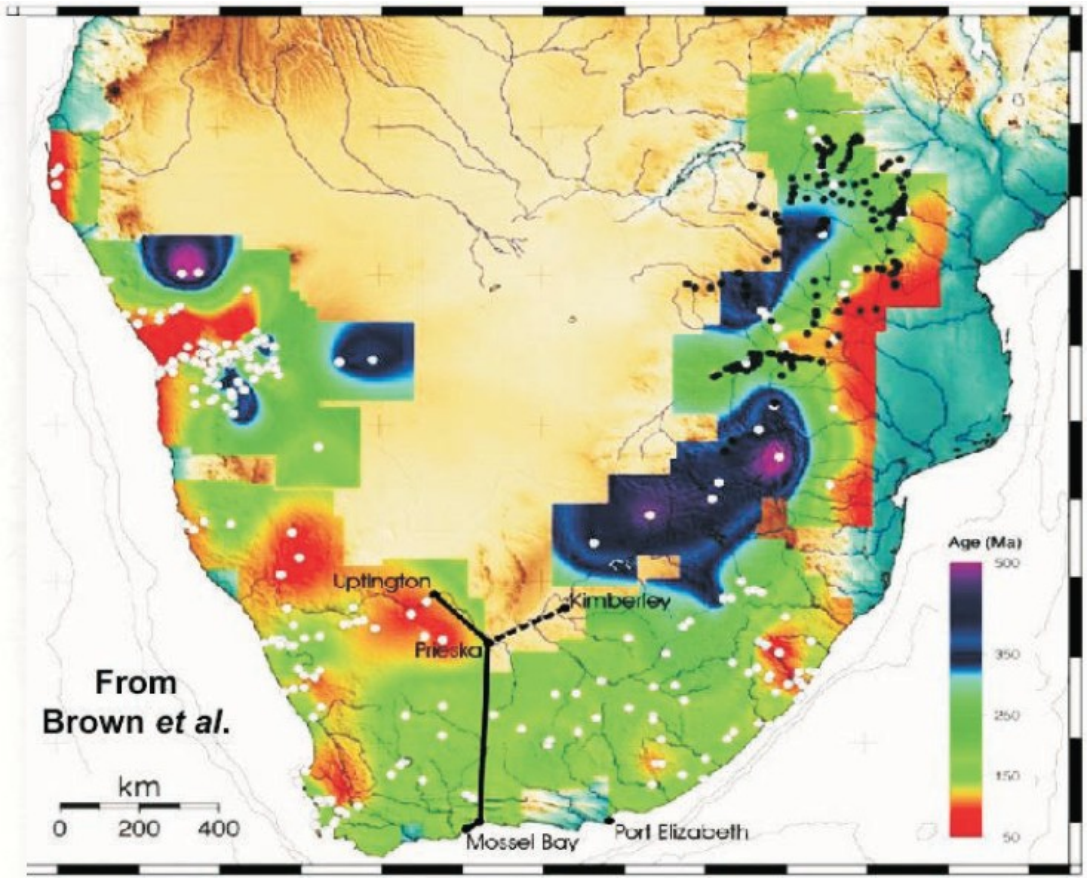

Figure 6.24 – Apatite fission track ages less than 200Ma in rocks of Permian age or older from outcrops across much of southern Africa reveal cooling from around 110°C or above in the early Cretaceous. This event is similar in character to that identified in SE Australia and must be related in some way to continental break-up since the early Cretaceous, although the precise processes and mechanisms which produce cooling (which must involve kilometre-scale exhumation) over such a wide area remain enigmatic (modified after Brown *et al.* (1997)).

The consistency in timing between the intra-plate exhumation episodes observed across the Western UK, SW Africa and SE Australia, with continental break-up and rifted margin formation during the early and mid Cretaceous, respectively, is highly suggestive of a causative link between these events. However, the apparently anomalous vertical motions recorded by AFTA data, demonstrating the occurrence of kilometre-scale exhumation extending great distances (i.e. >500 km) away from the ocean-continent boundary, cannot be explained by existing and accepted models of rifted continental margin and evolution.

A similar example of widespread exhumation across apparently stable continental platforms is provided by the Arabian plate. A recent tectonostratigraphic study of the Mesozoic-Cenozoic evolution of this region has revealed evidence for five major platform-wide Jurassic-Cretaceous unconformities, each associated with exhumation exceeding 0.3 km across broad areas (>50000km²) (George *et al.* 2005). These unconformities, which cannot be accounted for by plate boundary processes, developed over relatively short periods (2-10Ma) in comparison to the intervening phases of tectonic quiescence (25-50Ma) and are characterised by low-angle structural dips (typically <1°), which contributes to the perception that the Arabian platform has been tectonically stable for long periods of time (George *et al.* 2005). Similar low-angle unconformities have been documented in West Greenland (Sorenson, 2006), offshore Norway (Faleide *et al.* 2002), South America (Cobbold *et al.* 2001) and West Siberia (Allen & Davies, 2007).

AFTA data from many of the present-day topographic highs around the periphery of the North Atlantic define a common trend in a plot of mean track length vs. fission track age. This implies surprisingly similar styles of thermal history across an enormous area from West Greenland through the UK to Scandanavia. Thermal history solutions derived from these data suggest a series of exhumation episodes coeval with the ones derived in this study. These episodes appear to be broadly synchronous over a wide area. Variation in the magnitude of individual episodes defines the position of individual samples (Figure 6.26).

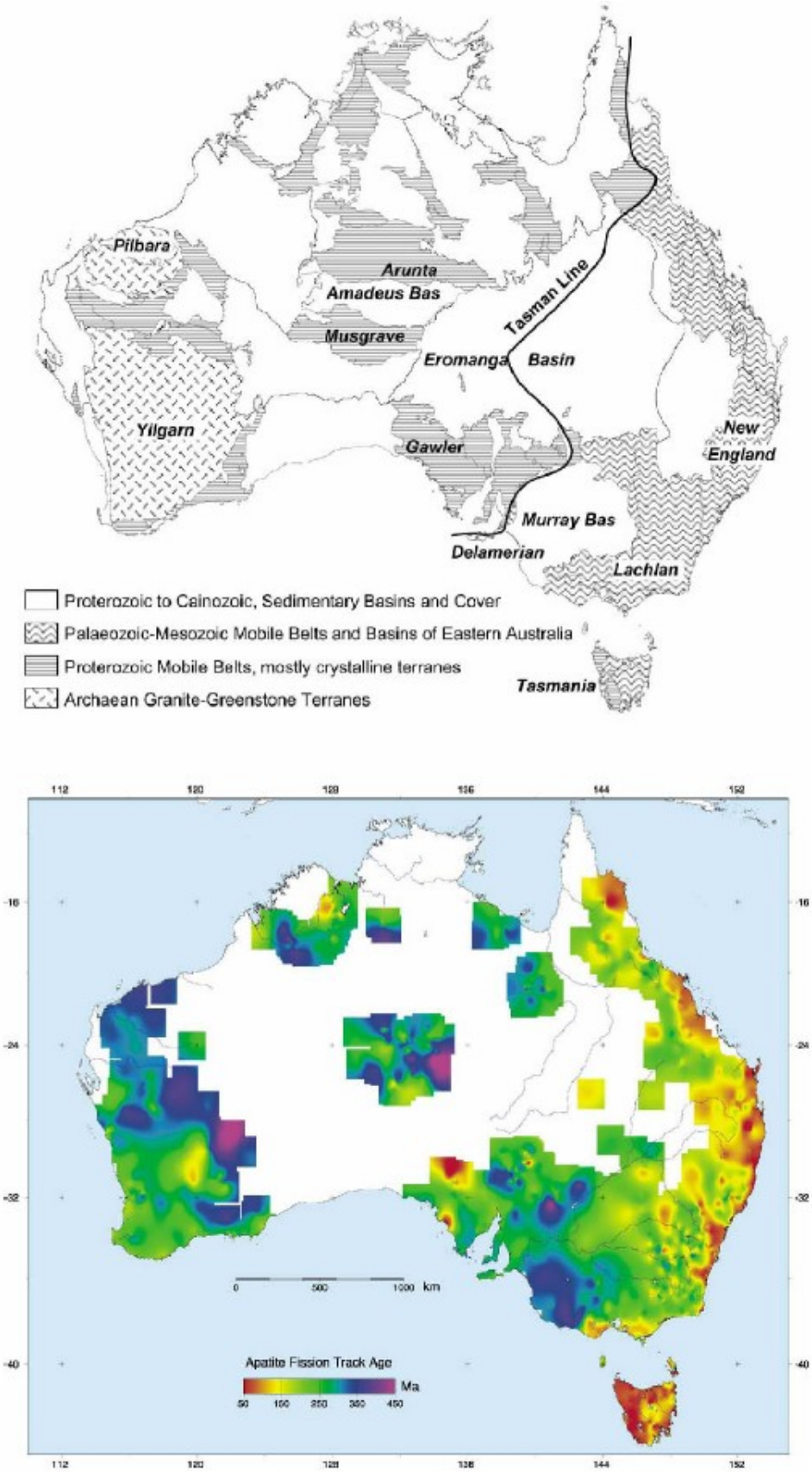

Figure 6.25 - Main geological regions of Australia compared with interpolated image of apatite fission track age across the Australian continent (results are calculated as the central age in Ma) (after Gleadow *et al.* (2002)).

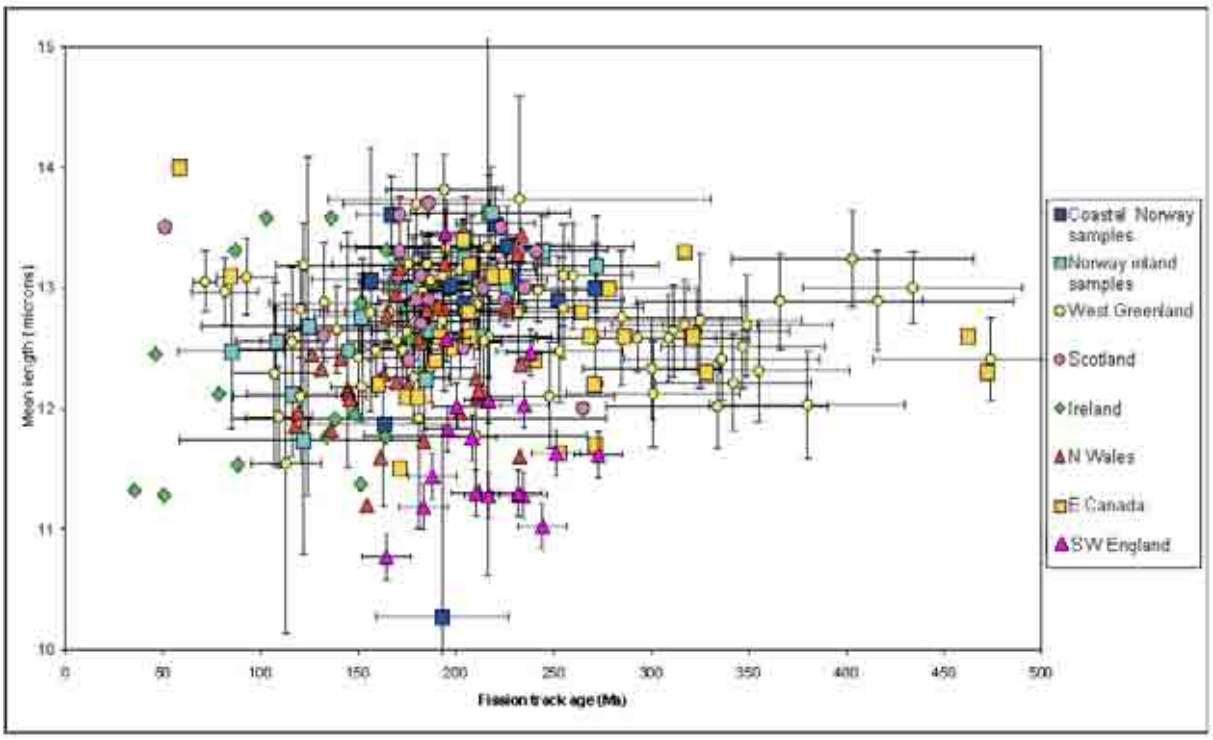

Figure 6.26 – Plot of fission track age vs. mean track length for the North Atlantic data. In regions where samples have undergone a single episode of cooling, these so called boomerang plots provide a record of a partial annealing zone (PAZ). PAZ's combine data from relatively shallow, unannealed samples with pre-cooling FT ages to deeper, fully annealed samples with correspondingly lower FT ages. The data presented here indicate a more complicated thermal history.

As discussed more fully by Holford (2006), although the phenomena of apparently periodic global tectonic deformation episodes and large-scale uplifts and subsidences within continental interiors have long been recognised (e.g. Stille, 1924; Umbgrove, 1947; Beloussov, 1962), since the advent of plate-tectonic theory, it has become common practice to explain the vertical motions of continental interiors in terms of secondary responses to lateral motions (i.e. the extension and shortening of the lithosphere) rather than primary responses to vertical motions (e.g. Dewey, 1982). Despite this, it is increasingly apparent that many global intra-plate regions (e.g. the SW UK (this study), the Irish Sea (Holford, 2006), NE Atlantic margin (Praeg *et al.* 2005), SE Australia (Green *et al.* 2004), Africa (Lithgow-Bertelloni & Silver, 1998) and Arabia (George *et al.* 2005)) have experienced complex vertical motions which, although coincident with plate reorganisations, cannot be explained by plate boundary

forces or processes. This has led a number of workers to infer dynamic and convective motion of the mantle, in order to explain the vertical motions of intra-plate regions, as well as a number of other phenomena associated with the formation of rifted continental margins (e.g. Lithgow-Bertelloni & Silver, 1998; King & Andersen, 1998; Boutilier & Keen, 1999; Wheeler & White, 2000; King *et al.* 2002; Praeg *et al.* 2005; Stoker *et al.* 2005*a*). These models are described in detail by Holford (2006) but the reader is also referred to King & Andersen, (1998), Andersen, (2001) and King *et al.* (2002). The findings of this thesis would seem to support the argument for small-scale convective flow initiating kilometre-scale vertical motions in the upper crust as envisaged by Praeg et al. 2005. This flow will evolve over time (Boutilier & Keen, 1999) and has been proposed as a potential underlying cause of rapid (<5Ma) plate reorganisations (King *et al.* 2002; Bercovici, 2003, Stoker *et al.* 2005*b*) with changes in mantle convection patterns being cited as initiating this reorganisation (*cf.* King *et al.* 2002).

As noted at the beginning of this section, the early Cretaceous, early Paleogene and Neogene exhumation episodes identified in this study are coeval with important phases of deformation at pre-existing or incipient plate boundaries, which suggests a causal relationship. However, these episodes cannot be explained solely in terms of plate boundary forces and processes. Holford (2006) noted that Praeg *et al.* (2005) and Stoker *et al.* (2005*a*) had recently documented a series of Cenozoic epeirogenic movements on the NW European Atlantic margin (early and late Cenozoic tilting, and mid-Cenozoic sagging) which they interpret in terms of dynamic topographic responses to the evolution of small-scale convection cells operating in the upper mantle beneath the Atlantic margin. Holford (2006) went on to state that it is possible that such a model of evolving convective flow could also account for the Mesozoic-Cenozoic exhumation history of the Irish Sea Basin through a combination of

regional dynamic uplift related to the normal stresses exerted on the base of lithosphere by upper mantle convection, with plate reorganisations and associated intra-plate stresses initiated by the evolving flow cells responsible for the compressional deformation which is superimposed upon the more regional uplift. The findings of this thesis would seem to reinforce this idea and further extend the influence of such a system to the SW UK basin system. A model compiled by Holford (2006) for the Mesozoic-Cenozoic evolution of the western UKCS, in which exhumation was driven by a combination of evolving upper mantle convective flow and intra-plate stress fluctuations is presented in Figure 6.27. This model implies that the exhumation of this region has been driven by a combination of horizontal and vertical forces, all of which are linked to important phases of deformation at plate boundaries, possibly as a result of upper mantle convection. To date, there have been few attempts to reconcile the patterns of vertical motions predicted by theoretical models of upper mantle convection with actual constraints on the spatial and temporal patterns of uplift and exhumation as provided by studies such as this. In order to gain a greater understanding of the interplay between mantle convection processes and vertical motions of intra-plate regions, it is essential to incorporate the constraints on the timing, magnitudes and patterns of exhumation provided by AFTA and related techniques.

Figure 6.27 (shown overleaf): Schematic lithospheric cross-sections presented by Holford (2006), attempting to link the Mesozoic-Cenozoic exhumation episodes identified within the Irish Sea basin system with major coeval plate tectonic events. A topographic and bathymetric map of the North Atlantic region is provided, upon which the locations of cross sections are superimposed. Important tectonic features have been highlighted. Present-day spreading ridges are indicated by thick solid red lines, whilst ancient spreading ridges are highlighted in pink. The location of the ocean-continent boundary along the NE Atlantic margin is indicated by the broken red line. Important oceanic fracture zones, and the position of the Alpine and Pyrenean deformation fronts are also highlighted. The early Cretaceous exhumation of the southern British Isles is interpreted to be driven by dynamic uplift generated by edge-driven convection associated with the onset of seafloor spreading to the SW of Britain (modified after Praeg *et al.* 2005). Early Paleogene exhumation is interpreted in terms of depth-dependent lithospheric shortening related to Alpine orogenesis (*cf.* Hillis, 1992), whilst Neogene exhumation is interpreted to be a response to plume-enhanced ridge push (*cf.* Lundin & Doré, 2002). Dynamic uplift associated with evolving edge-driven convection patterns provided the regional component of exhumation, upon which more localised compressional shortening is superimposed. The results presented in this thesis are consistent with the models proposed by Holford (2006) to explain results in the Irish Sea and North Wales, suggesting that they are valid over a wider area of the western UKCS.

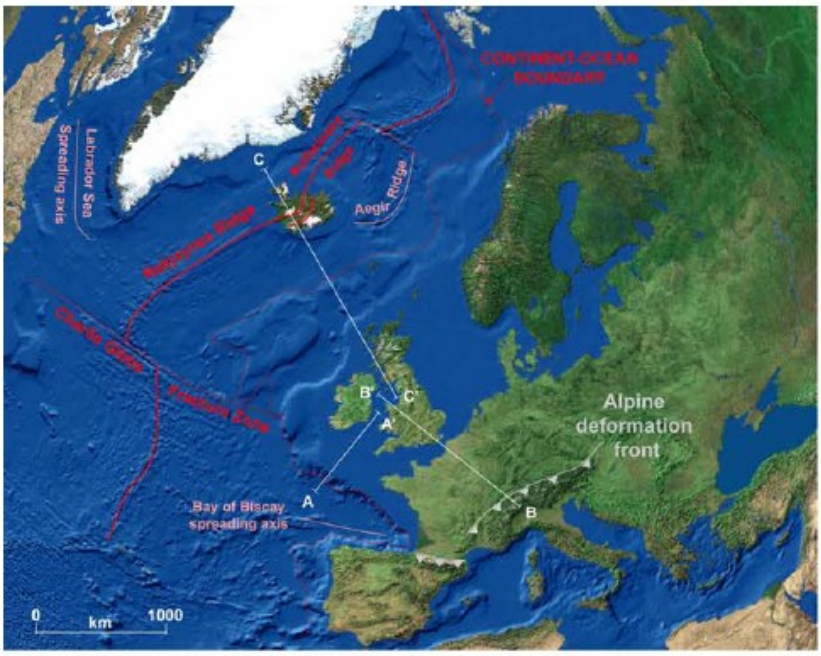
CONTINENT-OCEAN BOUNDARY
Labrador Sea Spreading axis
Aegir Ridge
Alpine deformation front
Bay of Biscay spreading axis
A
A'
B
B'
C
C'
0 km 1000

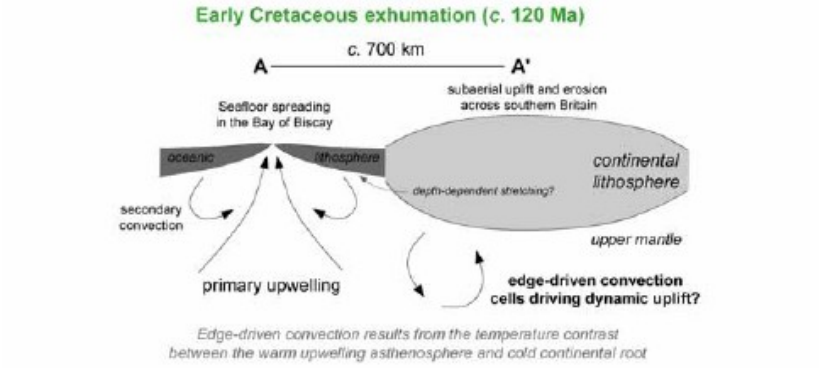
Early Cretaceous exhumation (c. 120 Ma)
c. 700 km
A
A'
Seafloor spreading in the Bay of Biscay
subaerial uplift and erosion across southern Britain
oceanic
lithosphere
continental lithosphere
depth-dependent stretching?
secondary convection
upper mantle
primary upwelling
edge-driven convection cells driving dynamic uplift?
Edge-driven convection results from the temperature contrast between the warm upwelling asthenosphere and cold continental root

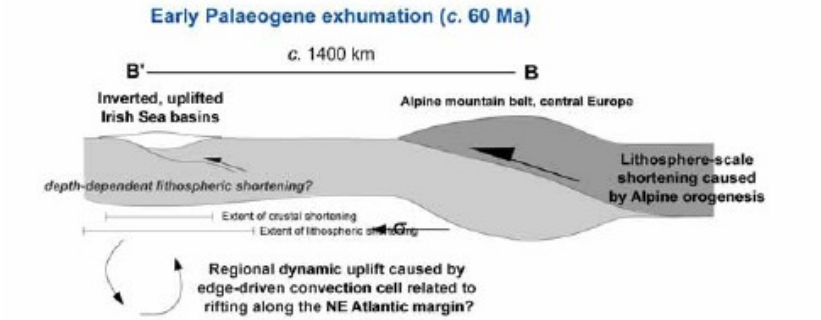
Early Palaeogene exhumation (c. 60 Ma)
c. 1400 km
B'
B
Inverted, uplifted Irish Sea basins
Alpine mountain belt, central Europe
depth-dependent lithospheric shortening?
Lithosphere-scale shortening caused by Alpine orogenesis
Extent of crustal shortening
Extent of lithospheric shortening
Regional dynamic uplift caused by edge-driven convection cell related to rifting along the NE Atlantic margin?

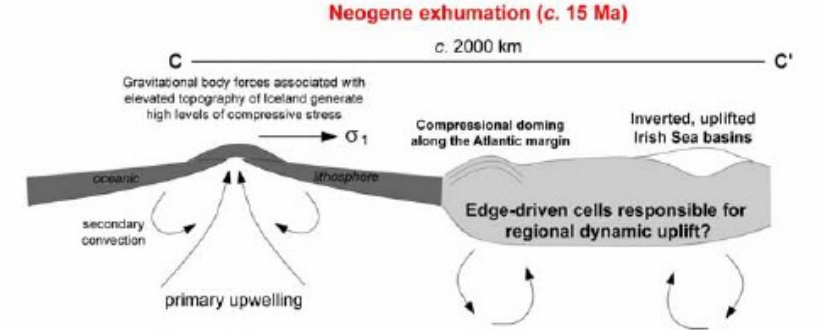
Neogene exhumation (c. 15 Ma)
c. 2000 km
C
C'
Gravitational body forces associated with elevated topography of Iceland generate high levels of compressive stress
σ1
Compressional doming along the Atlantic margin
Inverted, uplifted Irish Sea basins
oceanic
lithosphere
secondary convection
Edge-driven cells responsible for regional dynamic uplift?
primary upwelling

CHAPTER 7: CONCLUSIONS

7.1: CONCLUSIONS

The aim of this thesis has been to investigate the post-Triassic burial and exhumation history of the onshore SW UK and offshore Celtic Sea-Western Approaches basin system integrating data from palaeothermal techniques (i.e. AFTA and VR), mechanical/compactional techniques (i.e. log-derived porosities) and seismic data. The following conclusions can be drawn from this study:

- The offshore extensional basins of the Celtic Sea formed during Permian-Jurassic rifting. Maximum burial depths of the Triassic-Jurassic sediments contained within these basins were reached during the late Jurassic-early Cretaceous. As also noted by Holford (2006) most previous studies have assumed that maximum Mesozoic burial depths were reached during the late Cretaceous-Paleogene.

- The SW UK experienced a number of exhumation episodes beginning during the Upper Triassic with additional episodes occurring in the Lower Cretaceous, early Paleogene and Neogene. This study has also shown that the magnitude and distribution of erosion during these events is quite diverse. Comparison of regional stratigraphic and tectonic observations along with the timing of exhumation related cooling from AFTA constrains the onset of these exhumation episodes to 215-195Ma, 140-120Ma, 75-55Ma and 20-15 Ma, respectively.

- Integration of timing data from this study with similar studies around the western UKCS has further constrained the timing and distribution of the palaeothermal episodes. The Upper Triassic-Lower Jurassic episode has been constrained to 200-195Ma across England and Wales with the same episode appearing in Ireland at 180-170Ma. The Lower Cretaceous episode is constrained to 125-112Ma and affected all parts of the western UKCS at this time. The early Paleogene episode is constrained to 65-55Ma but is notably absent from North Wales, Northern Ireland (Larne-2 borehole) and the Wessex Basin. The Neogene episode is constrained to 20-15Ma across the whole of the western UKCS, though there is evidence to suggest that in some places this episode started during late Eocene-Oligocene times (35-30Ma) particularly in North Wales and the Wessex Basin.

- As part of this study the first thermal history analysis of the Burton Row borehole, onshore Somerset, Gwendraeth Valley-2 and Senghenydd boreholes, South Wales Coalfield have been carried out. Burton Row is located on the footwall of the BCB bounding fault whilst the two South Wales Coalfield boreholes are located in the main depocentre of that basin. Analysis of the compactional and palaeothermal data reveal that the preserved Mesozoic succession within the Burton Row borehole was more deeply buried by *c.* 2.0 km of additional section prior to Paleogene exhumation. Palaeothermal data from the South Wales Coalfield boreholes reveal deeper burial of 4.2-6.5km of additional section prior to Mesozoic exhumation.

- As originally noted by Holford (2006) and further backed up by this study, AFTA of the Lower Palaeozoic basement rocks which form the onshore footwall block to the SGCB in SW Wales were uplifted and eroded during the Triassic-early Jurassic (215-195Ma). It is inferred that this uplift was due to footwall uplift in response to rift

related subsidence in the offshore basins. This event also affected the SW UK particularly in South Devon between the Sticklepath-Lustleigh and Watchet faults suggesting a link. However since this analysis is based only on spot samples from outcrops it is not possible to constrain the gradient of the palaeogeothermal profile and hence determine the magnitude of erosion associated with this cooling.

- Analysis of data from the exploration wells of the SCSB-BCB shows that this basin has experienced a complex history of exhumation (Chapter 5). VR data from this basin indicates exhumation of up to 2km whilst compactional data derived from the sonic velocity data of the Upper Triassic Mercia Mudstone Group indicates preserved Permian-Lower Jurassic section has been more deeply buried by *c.* 1.5km of additional section, corresponding to a total exhumation of *c.* 2km within the basin. Timing of maximum burial derived from AFTA data indicates this occurred during the Paleogene. There is no evidence for Lower Cretaceous exhumation in the SCSB-BCB, however this may be a result of overprinting by elevated palaeogeothermal gradients (>50% higher than present-day values), combined with renewed late Cretaceous burial. A similar conclusion was reached by Holford (2006) for the SGCB who further asserted that these areas may have acted as depocentres for Cretaceous sediments and as a result were subsiding during the uplift episode.

- The work carried out in this thesis validates the approach of integrating palaeothermal, compactional and seismic data to elucidate burial and exhumation histories of basins. The constraints achieved by this integration allows for a much more detailed analysis of hydrocarbon maturation, fluid migration and trap formation and can also provide insights into potential retention issues. These items are of fundamental importance in assessing prospectivity of frontier basins particularly in inversion tectonic settings.

Additionally correlation of uplift magnitudes validates the individual techniques and in the approach overall.

- The temporal coincidence of the post-Triassic exhumation episodes in the SW UK and extensional or compressional deformation at existing or forming plate boundaries is a fundamental finding of this thesis. This is despite the great distances between deformation zones and the study area (500-2000km). These episodes involve the removal of several kilometres of overburden over considerable (i.e. 100-1000km) horizontal distances.

- The Lower Cretaceous exhumation episode identified in this study began between 140 and 120Ma and resulted in the removal of up to 3.5km of overburden from parts of the SW UK. As highlighted by Holford (2006), this exhumation was coeval with the onset of sea-floor spreading in the Bay of Biscay and the formation of a rifted continental margin SW of Britain during the Aptian, suggesting a genetic relationship between these events. Other workers have invoked the model of depth dependant stretching as being responsible for the formation of this margin however this model cannot explain the exhumation of the SW UK, some >300km away since numerical modelling results predict that depth-dependent stretching is only important within *c.* 200km of the ocean-continent boundary (for further clarification and background the reader is referred to Holford, 2006). More recent research suggests an intrinsic link between mantle convection processes and dynamic uplift (Holford, 2006).

- Exhumation in the early Paleogene began between 65-55Ma and was responsible for the removal of up to 2km of overburden. It should be noted however that marked spatial variability is characteristic of this episode with data from different basins

displaying remarkably different burial depths. For instance *c.* 2km of overburden has been removed from the NCSB whilst Holford (2006) demonstrated that no exhumation of North Wales and the SGCB occurred at this time. Magmatic underplating has been cited as the primary cause of exhumation at this time related to the emplacement of the Iceland mantle plume however as demonstrated by Holford (2006) who worked in the EISB a supposed locus of underplating activity there is little direct evidence of an underplated layer beneath this region. Data from this study further casts doubt on underplating being responsible since this mechanism should produce relatively smooth patterns of exhumation across a large region whereas it has been shown that over short distances large variation in exhumation across the SW UK has been observed. A more likely mechanism which would fit with observed field data across the SW UK is that of compressional shortening which is inferred here to be the principal cause of exhumation across the SW UK during the Paleogene.

- The final phase of exhumation resulting in the removal of up to 2km of overburden began during the Neogene (20-15Ma) and affected all parts of the SW UK. The driving mechanism for this episode has been revealed as compressional deformation based on evidence from seismic reflection data. Numerous workers have shown that the timing of the Neogene exhumation episode coincided with major compressional deformation all along the Atlantic margin as well as the development of Iceland. During this time a number of compressional domes formed and seismic and field data indicates that a widespread intra-Miocene (*c.* 16 Ma) unconformity was developed. Neogene inversion leading to exhumation of the SW UK was most likely caused by ridge-push forces enhanced by the emplacement of Iceland.

- All of the exhumation episodes show marked variability over short (50-100km) distances and illustrate the control of local faulting over the distribution of exhumation patterns. This study has confirmed the assertion of Ware & Turner (2002) that short wavelength variations in exhumation can occur as a result of basin compartmentalisation. This is further illustrated by the results from the onshore data which indicates marked variations associated with major normal and strike-slip faults such as the Sticklepath-Lustleigh and Watchet-Cothelstone faults.

- Palaeothermal data from the offshore wells in the NCSB, SCSB, BCB and SGCB show remarkably similar palaeogeothermal gradients for each of the thermal episodes recognised. These gradients are in excellent agreement with those derived for the NCSB by Corry & Brown (1998) suggesting that their use could be extended over the whole of the Celtic Sea-Western Approaches area.

- The data presented in this thesis suggests that for the western UKCS, Upper Triassic-Jurassic exhumation was driven by footwall uplift along major basin bounding faults; Lower Cretaceous exhumation was driven by compressional shortening caused by the Bay of Biscay spreading centre with an additional component of footwall uplift; early Paleogene exhumation was driven by compressional shortening caused by the Laramide episode of Alpine orogenesis with an additional component of thermal related uplift; Neogene exhumation was driven by the late Alpine compressional episode with additional components of uplift generated by ridge push supported by enhanced ridge push as a result of magmatism related to the Iceland hotspot.

- Compressional deformation has been shown to be the dominant process responsible for exhumation across the SW UK during Cenozoic times however there has also been

a component of regional uplift observed which cannot be accounted for by plate boundary processes. This observation has been repeated around the world both in passive margin and intra-plate settings (e.g. SW Africa, SE Australia and the Arabian Plate). The mechanism of regional dynamic uplift is proposed as the potential driving mechanism for those motions (see Chapter 8, Holford, 2006; Chapter 6 this study).

7.2: RECOMMENDATIONS FOR FURTHER WORK

1. The limited well database available for this study was insufficient to fully map the pattern of exhumation in the SW UK. A detailed exhumation study incorporating sonic velocity data, VR measurements and AFTA data from the entire Celtic Sea-Western Approaches region would help to further constrain the pattern of denudation on the UKCS. If possible, such a study should aim to produce maps of apparent exhumation covering the WAB, NCSB, SCSB, BCB and SGCB. Similar data for a larger suite of onshore boreholes would also be beneficial in deducing the extent of exhumation. Additional data should be sought from across Devon, Somerset, Dorset and South Wales. Extending the data coverage for the area by including wells in the WAB and more importantly onshore boreholes would allow the southern extent of exhumation to be determined and allow the assessment of onshore palaeogeothermal gradients. Equally there are a number of wells within the Celtic Sea area that were not available to this study (such as well 102/29-1 for example). Interpretation of data from these wells would help to further constrain the distribution of exhumation across the SW UK.

2. Equally further onshore collection of outcrop samples particularly in the Cornubian Peninsular, where data-points are scarce would enhance the interpretation of exhumation distribution. A further suite of samples collected from around Start Point, South Devon would also be useful, since previous samples collected from there did not contain sufficient uranium to carry out AFTA.

3. Acquisition of the full suite of geophysical-log data for all offshore wells would allow much more detailed analysis of exhumation. The approach of deriving an ITT transform from density derived porosities clearly has its merits (Chapter 4) and would greatly benefit from many more data points to constrain the necessary transform that would fit the SW UK. This technique is reliant on having access to the density and gamma logs, but additional data from the other geophysical logs could act as further filters to ensure spurious data does not affect the derivation of the transform. Having the density data for all of the wells would also give an independent estimate of exhumation to compare the various sonic techniques.

4. Exhumation during the Jurassic across the Irish landmass remains somewhat of a mystery and as such a detailed investigation into magnitude and distribution of this exhumation would be beneficial in determining the cause of this episode and its relation (if any) to thermal doming in the North Sea basin. In particular, it would be important to determine whether a thermal dome existed in the region of southern Ireland as postulated by Tate & Dobson (1989). Further investigation should be able to resolve the driving mechanism for Upper Triassic-Lower Jurassic exhumation as being solely due to footwall uplift or indeed if a thermal component contributed to the uplift.

5. This study has mainly used sparse 2D seismic lines to integrate offshore structural geology with the thermal and compactional data. Acquisition and interpretation of 3D seismic datasets could prove useful in determining the relative importance of horizontal compressional shortening versus vertical epeirogenic movements. Alternatively analysis of a denser higher quality 2D grid could provide the same benefits and might serve to elucidate the driving mechanism(s) of exhumation in the offshore basins.

6. As noted by Holford (2006), integration of the results from studies such as this along the Atlantic margin, should be incorporated in the latest models of upper mantle convection at rifted continental margins. This would establish any causative links between processes in the mantle and subsequent vertical motions in the crust across intra-plate and passive margin settings.

7. Clearly there is much work to be done in regards to calculating porosity-depth relationships for the SW UK. It is suggested that physical examination of core samples would be useful to physically calculate porosity rather than relying on a mathematical transform to derive it. Such a value could then be compared to those values calculated from sonic data transforms and velocity-depth trends to better constrain the absolute magnitude of exhumation and where a well has not been exhumed the normal velocity/porosity-depth trend.

8. As mentioned in Chapter 4, there has not been a study of the Celtic Sea-Western Approaches to calibrate a correction factor to the Wyllie and Raymer equations. Such a study is crucial in determining absolute magnitudes of exhumation as the correction factor can have a profound affect on the value of exhumation recorded for a particular

data point. Correct evaluation of the rock matrix velocity is equally critical. A detailed study of the rock mechanics of the Celtic Sea-Western Approaches should therefore be carried out to better constrain these values which would subsequently tighten the constraints of the range of exhumation values for a particular location. Such a study should also seek to develop a calibrated 'normal' porosity-depth curve for the SW UK which would also constrain the absolute magnitude of exhumation rather than relying on proxies such as the Sclater & Christie (1980) trend.

9. This study would benefit from more AFTA data in the offshore wells. Ideally samples should be collected in each well studied over a range of depths to better constrain the palaeogeothermal gradients in these wells. As mentioned in Chapter 5, a number of the offshore wells VR data is suggestive of geochemical suppression which has implications for the palaeogeothermal gradient derivation from VR data. Access to AFTA samples should be able to highlight this in a number of the wells as well as provide tighter constraints for the gradients and more importantly timing of the palaeothermal episodes which have affected the offshore wells.

10. As a compliment to the AFTA and VR data a detailed fluid inclusion study of the SW UK and offshore basins could help determine if fluid-related heating has affected the computed palaeogeothermal gradients and thus whether igneous intrusion caused this fluid flow. This could be useful in deducing if some of the anomalously high VR values have been affected by hydrothermal episodes particularly in wells such as 107/16-1.

11. This study could be expanded to include the more proximal basins to the Goban Spur (such as the Porcupine Basin) and Mid Atlantic Ridge (such as the Rockall Trough).

This would allow discrimination of the variously proposed driving mechanisms for intra-plate exhumation and provide a test for how far from the margins the stresses generated could travel. Indeed expansion and integration with studies across the whole of Northwest Europe from Iceland to the Alps would allow the variation in magnitude and style of exhumation to be fully analysed and should allow separation of the extent to which the different stresses affect exhumation at various distances from their sources.

REFERENCES

ABBOTT, L.D., SILVER, E.A., ANDERSON, R.S., SMITH, R., INGLE, J.C., KLING, S.A., HAIG, D., GALEWSKY, J. & SLITER, W. 1997. Measurement of tectonic surface uplift rate in a young collisional mountain belt. *Nature,* **385,** p. 501-507.

AINSWORTH, N.R., O'NEIL, M., RUTHERFORD, M.M., CLAYTON, G., HORTON, N.F. AND PENNY, R.A. 1987. Biostratigraphy of the Lower Cretaceous, Jurassic and Uppermost Triassic of the North Celtic Sea and Fastnet Basins. *In:* BROOKS, J. & GLENNIE, K.W. (eds.), *Petroleum Geology of Northwest Europe*. London: Graham & Trotman, **2**, p. 611-622.

ALBERTY, M., 1994. The influence of the borehole environment upon compressional sonic logs. *Paper S, presented at the SPWLA 35th Annual Logging Conference, Dallas.*

AL-KINDI, S., WHITE, N., SINHA, M., ENGLAND, R. & TILEY, R. 2003. Crustal trace of a hot convective sheet. *Geology,* **31,** p. 207-210.

ALLEN, P. 1959. The western Environment: Anglo-Paris Basin. *Philosophical Transactions of the Royal Society, London*, **B242**, p. 283-346.

ALLEN, P. 1976. Wealden of the Weald: a new model. *Proceedings of the Geologists Association*, **86**, p. 389-437.

ALLEN, P. 1981. Pursuit of Wealden models. *Journal of the Geological Society of London*, **138**, p. 375-405.

ALLEN, P.A., CORCORAN, D., CLAYTON, G. 1998. Forward models of heat flow and inversion of vitrinite reflectance data in investigating Tertiary inversion events. *In:* SIMMS, M. (ed.), *Ireland since the Carboniferous: a 300 Million Year Enigma*. Handbook,
Conference at Ulster Museum Belfast, 9–10 September 1998. Ulster Museum, Belfast.

ALLEN, P.A., BENNETT, S.D., CUNNINGHAM, M.J.M., CARTER, A., GALLAGHER, K., LAZZARETTI, E., GALEWSKY, J., DENSMORE, A.L., PHILLIPS, W.E.A., NAYLOR, D. & HACH, C.S. 2002. The post-Variscan thermal and denudational history of Ireland. *In:* DORÉ, A.G., CARTWRIGHT, J.A., STOKER, M.S., TURNER, J.P. & WHITE, N (eds.), *Exhumation of the North Atlantic Margin: Timing, Mechanisms and Implications for Petroleum Exploration.* Geological Society, London. Special Publications, **196**, p. 371-399.

ALLEN, P.A. & ALLEN, J.R., 2005. *Basin Analysis (2nd edition).* Oxford: Blackwell.

ANDERSEN, D.L. 2001. Top-Down Tectonics? *Science,* **293,** p. 2016-2018.

ANDERTON, R. 2000. Tertiary events: the North Atlantic plume and Alpine pulses. *In:* WOODCOCK, N.H. & STRACHAN, R.A. (eds.), *Geological History of Britain and Ireland.* Oxford: Blackwell Publishing, p. 374-391.

ANDRIESSEN, P.A.M. 1995. Fission-track analysis: principles, methodology and implications for tectono-thermal histories of sedimentary basins, orogenic belts, and continental margins. *Geologie en Mijnbouw*, **74**, p. 1– 12.

ANNEN, C. & SPARKS, R.S.J. 2002. Effects of repetitive emplacement of basaltic intrusions on thermal evolution and melt generation in the crust. *Earth and Planetary Science Letters,* **203,** p. 937-955.

ARCHER, A.A. 1968. *Geology of the South Wales Coalfield (Special Memoir), The Gwendraeth Valley and Adjoining areas*. Memoir of the Geological Survey of Great Britain.

ARGENT, J.D., STEWART, S.A., GREEN, P.F. & UNDERHILL, J.R., 2002. Heterogenous exhumation in the Inner Moray Firth, UK North Sea: constraints from new AFTA and seismic data. *Journal of the Geological Society of London*, **159**, p. 715-729.

ARKELL, W.J. 1933. *The Jurassic System in Great Britain.* Oxford: Clarendon Press.

ARTER, G. & FAGIN, S.W. 1993. The Fleetwood Dyke and the Tynwald fault zone, Block 113/27, East Irish Sea Basin. *In:* PARKER, J.R. (ed.), *Petroleum Geology of Northwest Europe: Proceedings of the 4th Conference.* Geological Society, London, p. 835-843.

ARTHUR, M.J. 1989. The Cenozoic evolution of the Lundy Pull-Apart Basin into the Lundy Rhomb Horst. *Geological Magazine,* **126,** p. 187-198.

ATHY, L.F., 1930. Density, porosity and compaction of sedimentary rocks. *AAPG Bulletin,* **14**, p. 1-24.

ATKINS, J.E. & MCBRIDE, E.F., 1992. Porosity and packing of Holocene river , dune, and beach sands. *AAPG Bulletin,* **76**, p. 339-355.

BADA, G., HORVATH, F., CLOETINGH, S., COBLENTZ, D.D. & TOTH, T. 2001. Role of topography induced gravitational stresses in basin inversion: the case study of the Pannonian basin. *Tectonics,* **20,** p. 343-363.

BADHAM, J.P.N. 1982. Strike-slip orogens -an explanation for the Hercynides. *Journal of the Geological Society of London*, **l39**, p. 493-504.

BADLEY, M.E., PRICE, J.D. & BLACKSHALL, L.C. 1989. Inversion, reactivated faults and related structures: seismic examples from the southern North Sea. *In:* COOPER, M.A. & WILLIAMS, G.D. (eds.), *Inversion Tectonics.* Geological Society, London, Special Publications, **44,** p. 201-219.

BALDWIN, B. & BUTLER, C.O., 1985. Compaction curves. *AAPG Bulletin,* **69**, p. 622-626

BALESTRIERI, M.L., STUART, F.M., PERSANO, C., ABBATE, E. & BIGAZZI, G. 2005. Geomorphic development of the escarpment of the Eritrean margin, southern Red Sea, from combined apatite fission track and (U-Th)/He thermochronometry. *Earth and Planetary Science Letters,* **231,** p. 97-110.

BALLY, A.W. 1982. Musing over sedimentary basin evolution. *In:* PETER-KENT, SIR., BOTT, M.H.P., MCKENZIE, D.P. & WILLIAMS, C.A. (eds.), *The Evolution of Sedimentary Basins.* Philosophical Transactions of the Royal Society, London, **305A**, p.325-338.

BARBARAND, J., HURFORD, A.J. & CARTER, A. 2003*a*. Variation in apatite fission-track length measurement: implications for thermal history modelling. *Chemical Geology,* **198,** p. 77-106.

BARBARAND, J., CARTER, A., WOOD, I. & HURFORD, A.J. 2003*b*. Compositional and structural control of fission-track annealing in apatite. *Chemical Geology,* **198,** p. 107-137.

BARCLAY, W.J. 1989. Geology of the South Wales Coalfield, Part II, the country around Abergavenny. *Memoir of the British Geological Survey*, Sheet **232** (England and Wales).

BARKER, C.E. 1988. Geothermics of petroleum systems: implications of the stabilisation of kerogen thermal maturation after a geologically brief heating duration at peak temperature. *In:* MAGOON, L.B. (ed.), Petroleum Systems of the United States. United States Geological Survey Bulletin, **1870**, p. 26– 29.

BARKER, C.E. & GOLDSTEIN, R.H. 1990. Fluid-inclusion technique for determining maximum temperature in calcite and its comparison to vitrinite reflectance. *Geology*, **18**, p. 1003– 1006.

BARKER, C.E. & PAWLEWICZ, M.J. 1986. The correlation of vitrinite reflectance with maximum heating in humic organic matter. *In:* BUNTEBARTH, G. & STEGENA, L. (eds.), *Palaeogeothermics.* New York: Springer, p. 79-93.

BARR, K.W., COLTER, V.S. & YOUNG, R., 1981. The Geology of the Cardigan Bay-St. George's Channel Basin. *In:* ILLING, L.V. & HOBSON, G.D. (eds), *Petroleum Geology of the Continental Shelf of North-West Europe.* London: Heyden, p. 432-444.

BEACH, A. 1987. A regional model for linked tectonics in north-west Europe. *In:* BROOKS, J. & GLENNIE, K. (eds.), *Petroleum Geology of North West Europe*. London: Graham & Trotman, p. 43–48.

BEARD, D.C. & WEYL, P.K., 1973. Influence of texture on porosity and permeability of unconsolidated sand. *AAPG Bulletin,* **57**, p. 345-369.

BEAMISH, D., & SMYTHE, D.K. 1986. Geophysical images of the deep crust: the Iapetus suture. *Journal of the Geological Society of London,* **143,** p. 489-497.

BEARDSMORE, G.R. & CULL, J.P. 2001. *Crustal Heat Flow.* Cambridge University Press.

BELOUSSOV, V.V. 1962. *Basic problems in geotectonics.* New York: McGraw-Hill.

BENNET, G., COPESTAKE, P. & HOOKER, N.P. 1985. Stratigraphy of the Britoil 72/10-1A well, Western Approaches. *Proceedings of the Geologists Association*, **96**, p. 255-261.

BERCOVICI, D. 2003. The generation of plate tectonics from mantle convection. *Earth and Planetary Science Letters,* **205,** p. 107-121.

BERRYMAN, J.G., 1980. Long-wavelength propagation in composite elastic media. *Journal of the Accoustic Society of America*, **68**, p.1809-1831.

BETHKE, C.M., 1985: A numerical model of compaction-driven groundwater flow and heat transfer and its application to the paleohydrology of intracratonic sedimentary basins. *Journal of Geophysical Research*, **90**, p. 6817–6828.

BIRPS & ECORS 1986. Deep seismic reflection profiling between England, France and Ireland. *Journal of the Geological Society of London,* **143,** p. 45-52.

BJØRLYKKE, K., AAGAARD, P., DYPVIK, H., HASTINGS, D.S. & HARPER, A.S. 1986. Diagenesis and reservoir properties of Jurassic sandstones from the Haltenbanken area, offshore mid Norway. Habitat of hydrocarbons on the Norwegian Continental Shelf. *Proceedings of the Norwegian Petroleum Society Symposium Stavanger,* p. 275-286.

BJØRLYKKE, K., RAMM, M. & SAIGAL, G.C. 1989. Sandstone diagenesis and porosity modification during basin evolution. *In:* POLECHAU, H.S. & MANN, U. (eds.), *Geologic modelling – aspects of integrated basin analysis and numerical simulation.* Geol Rundsch 78, p. 243-268.

BJØRLYKKE, K. & KØEG, K. 1997. Effects of burial diagenesis on stresses, compaction and fluid flow in sedimentary basins. *Marine and Petroleum Geology,* **14,** p. 267-276.

BLUCK, B.J., GIBBONS, W. & INGHAM, J.K. 1992. Terranes. *In:* COPE, J.C.W., INGHAM, J.K. & RAWSON, P.F. (eds.), *Atlas of Palaeogeography and Lithofacies.* Geological Society, London, Memoir, **13,** p. 1-4.

BLUNDELL, C.R.K. 1952. The succession and structure of the North-Eastern area of the South Wales Coalfield. *Quarterly Journal of the Geological Society of London*, **107**, p. 307-333.

BLUNDELL, D.J. 2002. Cenozoic inversion and uplift of southern Britain. *In*: DORÉ, A.G., CARTWRIGHT, J.A., STOKER, M.S., TURNER, J.P. & WHITE, N. (eds.), *Exhumation of the North Atlantic Margin: Timing, Mechanisms and Implications for Petroleum Exploration.* Geological Society, London, Special Publications, **196,** p. 85-101.

BLUNDELL, D.G., DAVEY, F.J. & GRAVES, L.J. 1971. Geophysical surveys over the South Irish Sea and Nymphe Bank. *Journal of the Geological Society of London*, **127**, p. 339–375.

BOIS, C., GARIEL, O. & PINET, B. 1990. ECORS deep seismic surveys across Paleozoic and Mesozoic basins in France and adjacent areas. *In:* PINET, B. & BOIS, C. (eds.), *The Potential of Deep Seismic Profiling for Hydrocarbon Exploration*. Paris: Technip, p. 138-401.

BOLDREEL, L.O. & ANDERSEN, M.S. 1993. Late Palaeocene to Miocene compression in the Faeroe-Rockall area. *In*: PARKER, J.R. (ed.), *Petroleum Geology of Northwest Europe: Proceedings of the 4th Conference.* Geological Society, London, p. 1025-1034.

BOLDREEL, L.O. & ANDERSEN, M.S. 1998. Tertiary compressional structures on the Faroe-Rockall Plateau in relation to northeast Atlantic ridge-push and Alpine foreland stresses. *Tectonophysics,* **300,** p. 13-28.

BOLES, J.R. 1982. Active albitisation of plagioclase, Gulf Coast Tertiary. *American Journal of Science*, **282**, p. 165-180.

BOTT, M.H.P. 1993. Modelling the plate-driving mechanism. *Journal of the Geological Society of London,* **150,** p. 941-951.

BOTT, M.H.P. & BOTT, J.D.J. 2004. The Cenozoic uplift and earthquake belt of mainland Britain as a response to an underlying hot, low-density upper mantle. *Journal of the Geological Society of London,* **161,** p. 19-29.

BOUTILIER, R.R. & KEEN, C.E. 1999. Small-scale convection and divergent plate boundaries. *Journal of Geophysical Research,* **104B,** p. 7389-7403.

BRAY, R., GREEN, P.F. & DUDDY, I.R. 1992. Thermal history reconstruction in sedimentary basins using apatite fission track analysis and vitrinite reflectance data: a case study from the east Midlands of England and the Southern North Sea. *In:* HARDMAN, R.F.P. (ed.), *Exploration Britain: Into the Next Decade.* Geological Society, London, Special Publications, **67,** p. 3-25.

BRAY, R.J., DUDDY, I.R. & GREEN, P.F. 1998. Multiple heating episodes in the Wessex basin: implications for geological evolution and hydrocarbon generation. *In*: UNDERHILL, J.R. (ed.), *Development, Evolution and Petroleum Geology of the Wessex Basin.* Geological Society, London, Special Publications, **133,** p. 199-213.

BRERETON, R. & MCCANN, D., 1990. A fresh look at predictive equations for compressional wave velocity-porosity. *In*: *European Core Analysis Symposium,* p. 270-298.

BROOKS, M., TRAYNER, P.M. & TRIMBLE, T.J., 1988. Mesozoic reactivation of Variscan thrusting in the Bristol Channel area, UK. *Journal of the Geological Society of London*, **145**, p. 439-444.

BRODIE, J., & WHITE, N. 1994. Sedimentary basin inversion caused by igneous underplating. *Geology,* **22,** p. 147-150.

BRODIE, J. & WHITE, N. 1995. The link between sedimentary basin inversion and igneous underplating. *In*: BUCHANAN, J.G. & BUCHANAN, P.G. (eds.), *Basin Inversion*. Geological Society, London, Special Publication, **88**, p. 21-38.

BROWN, R.W. 1991. Discussion on thermal and tectonic history of the East Midlands shelf (onshore UK) and surrounding regions assessed by apatite fission track analysis. *Journal of the Geological Society of London,* **148,** p. 785-786.

BROWN, R.W., GALLAGHER, K., GLEADOW A.J.W. & SUMMERFIELD, M.A. 1997. Morphotectonic evolution of the South Atlantic margins of Africa and South America. *In:* SUMMERFIELD, M.A. (ed.), *Geomorphology and Global Tectonics*. Chichester: Wiley & Sons.

BROWNE, B.C. & COOPER, R.I.B. 1950. The British submarine gravity surveys of 1938 and 1946. *Philosophical Transactions of the Royal Society, London*, **A242**, p. 243-310.

BUCHANAN, J.G. & BUCHANAN, P.G., 1995. *Basin inversion.* Geological Society, London. Special Publications, **88**. 596p

BUKOVICS, C. & ZIEGLER, P.A. 1985. Tectonic development of the Mid-Norway continental margin. *Marine and Petroleum Geology*, **2**, p. 2-22.

BULAT, J. & STOKER, S.J. 1987. Uplift determination from interval velocity studies, UK southern North Sea. *In:* Brooks, J. & Glennie, K. (eds.), *Petroleum Geology of North West Europe.* London: Graham & Trotman, p. 293-305.

BULLERWELL, W. & MCQUILLIN, R. 1969. Preliminary report on a seismic reflection survey in the southern Irish Sea, July 1968. *Report of the Institute of Geological Sciences*, No. **69/2**.

BULNES, M. & MCCLAY, K.R. 1998. Structural analysis and kinematic evolution of the inverted South Celtic Sea Basin. *Marine and Petroleum Geology,* **15,** p. 667-687.

BURGESS, P.M. & GAYER, R.A., 2000. Late Carnoniferous tectonic subsidence in South Wales: implications for Variscan basin evolution and tectonic history in SW Britain. *Journal of the Geological Society of London*, **157 (1)**, p. 93-104.

BURNHAM, A.K. & SWEENEY, J.J. 1989. A chemical kinetic model of vitrinite reflectance maturation. *Geochimica et Cosmochimica Acta,* **53,** p. 2649-2657.

BUROV, E.B., LOBKOVSKY, L.I., CLOETINGH, S. & NIKISHIN, A.M. 1993. Continental lithosphere folding in Central Asia (Part II): constraints from gravity and topography. *Tectonophysics*, **226**, p. 73-87.

BURST, J.F., 1969. Diagenesis of Gulf Coast clayey sediments and its possible relation to petroleum migration. *AAPG Bulletin,* **72**, p. 416-424.

BUSHELL, T.P. 1986. Reservoir Geology of the Morecambe Field. *In:* BROOKS, J., GOFF, G. & VAN HOORN, B. (eds.), *Habitat of Palaeozoic Gas in Europe.* Geological Society, London, Special Publications, **23,** p. 189-208.

CARLSON, W.D., 1990. Mechanisms and kinetics of apatite fission-track annealing. *American Mineralogist,* **75**, p. 1120-1139.

CARLSON, W.D., DONELICK, R.A. & KETCHAM, R.A. 1999. Variability of apatite fission-track annealing kinetics: I. Experimental results. *American Mineralogist,* **84,** p. 1213-1223.

CARR, A.D. 1999. A vitrinite reflectance kinetic model incorporating overpressure retardation. *Marine and Petroleum Geology,* **16,** p. 355-377.

CARR, A.D. 2000*a*. Suppression and retardation of vitrinite reflectance, part 1. Formation and significance for hydrocarbon generation. *Journal of Petroleum Geology,* **23,** p. 313-343.

CARR, A.D. 2000*b.* Suppression and retardation of vitrinite reflectance, part 2. Derivation and testing of a kinetic model for suppression. *Journal of Petroleum Geology,* **23,** p. 475-496.

CASEY, R. & RAWSON, P.F. 1973. A review of the boreal Lower Cretaceous. *In:* CASEY, R. & RAWSON, P.F. (eds.), *The Boreal Lower Cretaceous*. Geological Society, London, Special Publications, **5**, p.415-430.

CASTAGNA, J.P., BATZLE, M.L. & EASTWOOD, R.L. 1985. Relationships between compressional wave and shear wave velocities in clastic rocks. *Geophysics*, **50**, p. 571–581.

CASTON, V.N.D., DEARNLEY, R., HARRISON, R. K., RUNDLE, C.C. & STYLES, M.T. 1981. Olivine dolerite intrusions in the Fastnet Basin. *Journal of the Geological Society of London,* **138**, p. 31-46.

CARTWRIGHT, J.A. 1989. The kinematics of inversion in the Danish Central Graben. *In:* COOPER, M.A. & WILLIAMS, G.D. (eds.), *Inversion Tectonics*. Geological Society, London, Special Publications, **44**, p. 153-175.

CAZES, M. & TORREILLES, G. (eds.) 1988. *Ėtude de la croûte terrestre par sismique profonde. 1. Profil nord de la France*. Paris: Editions Technip [In French.].

CERAMICOLA, S., STOKER, M., PRAEG, D., SHANNON, P.M., DE SANTIS, L., HOULT, R., HJELSTUEN, B.O., LABERG, S. & MATHIESEN A. 2005. Anomalous Cenozoic subsidence along the 'passive' continental margin from Ireland to mid-Norway. *Marine and Petroleum Geology*, **22**, p. 1045-1067.

CHADWICK, R.A. 1985. Cretaceous sedimentation and subsidence (Cenomanian to Maastrichtian). In: WHITTAKER, A. (ed.), *Atlas of onshore sedimentary basins in England and Wales: Post Carboniferous tectonics and Stratigraphy*. Glasgow: Blackie, p. 59-60.

CHADWICK, R.A., 1986. Extension tectonics in the Wessex Basin, southern England. *Journal of the Geological Society of London*, **143 (3),** p. 465-488.

CHADWICK, R.A. 1993. Aspects of basin inversion in Southern Britain. *Journal of the Geological Society of London*, **150**, p. 311-322.

CHADWICK, R.A & EVANS, D.J. 1995. The timing and direction of Permo-Triassic extension in southern Britain. In: BOLDY, S.A.R. (ed.), Permian and Triassic rifting in Northwest Europe. Geological Society, London, Special Publications, **91**, p. 161-192.

CHADWICK, R.A. & PHAROAH, T.C. 1998. The seismic reflection Moho beneath the United Kingdom and adjacent areas. *Tectonophysics*, **299**, p. 255-279.

CHADWICK, R.A., KIRBY, G.A. & BAILY, H.E. 1994. The post-Triassic structural evolution of northwest England and adjacent parts of the East Irish Sea. *Proceedings of the Yorkshire Geological Society,* **50,** p. 91-102.

CHAMBERS, L.M., PRINGLE, M.S. & PARRISH, R.R. 2005. Rapid formation of the Small Isles Tertiary centre constrained by precise 40Ar/39Ar and U-Pb ages. *Lithos,* **79,** p. 367-384.

CHAPMAN, R.E., 1981. Geology and Water, Developments in applied Earth Sciences 1. The Hague: Nijhoff-Junk. 228p.

CHAPMAN, T.J., 1989. The Permian to Cretaceous structural evolution of the Western Approaches Basin (Melville sub-basin), UK. *In:* COOPER, M.A. & WILLIAMS, G.D. (eds.), *Inversion Tectonics.* Geological Society, London. Special Publications, **44**, p. 177-200.

CHEADLE, M.J., MCGEARY, S., WARNER, M.R. & MATTHEWS, D.H., 1987. Extensional structures on the western UK continental shelf: a review of evidence from deep seismic profiling. *In:* COWARD, M.P., DEWEY, J.F. & HANCOCK, P.L. (eds.), *Continental Extension Tectonics.* Geological Society, London. Special Publications, **28**, p. 445-465.

CHEN, Q. & NUR, A. 1994. Critical concentration models for porous materials. *In:* CORAPCIOGLU, M.Y. (ed.), *Advances in Porous Media*. Amsterdam: Elsevier, p. 169-308.

Y. CHEN, Y., ZENTILLI, M.A., CLARK, A.H., FARRAR, E., GRIST, A.M. & WILLIS-RICHARDS, J. 1996. Geochronological evidence for post-Variscan cooling and uplift of the Carnmenellis granite, SW England. *Journal of the Geological Society of London*, **153**, p. 191-195.

CHILLINGARIAN, G.V. 1983. Compactional diagenesis. *In:* PARKER, A. & SELLWOOD, B.W. (eds.), *Sediment Diagenesis*. Reidel, p. 57-168.

CLAYTON, K. & SHAMOON, N. 1998. A new approach to the relief of Great Britain I. The machine readable database. *Geomorphology,* **25,** p. 31-42.

CLAYTON, K. & SHAMOON, N. 1999. A new approach to the relief of Great Britain III. Derivation of the contribution of neotectonic movements and exceptional regional denudation to the present relief. *Geomorphology,* **27,** p. 173-189.

CLIFT, P.D. 1999. The thermal impact of Paleocene magmatic underplating in the Faeroe-Shetland-Rockall region. *In*: FLEET, A.J. & BOLDY, S.A.R. (eds.), *Petroleum Geology of Northwest Europe: Proceedings of the 5th Conference.* Geological Society, London, p. 583-593.

CLIFT, P.D. & TURNER, J. 1998. Paleogene igneous underplating and subsidence anomalies in the Rockall-Faeroe-Shetland area. *Marine and Petroleum Geology,* **15,** p. 223-243.

CLOETINGH, S. 1988. Intra-plate stresses: A new element in basin analysis. *In:* KLEINSPEHN, K. L. & PAOLA, C. (eds.), *New Perspectives in Basin Analysis*. New York: Springer-Verlag, p. 205–230.

CLOETINGH, S. & KOOI, H. 1992. Intra-plate stress and dynamical aspects of rift basins. *In:* ZIEGLER, P.A. (ed.), *Geodynamics of Rifting Volume III: Thematic discussions*. Tectonophysics, **215**, p. 167-185.

CLOETINGH, S., GRADSTEIN, F.M., KOOI, H., GRANT, A.C. & KAMINSKI, M., 1990. Plate reorganisation – a cause of rapid late Neogene subsidence and sedimentation around the North Atlantic? *Journal of the Geological Society of London*, **147**, p. 495-506.

COBBOLD, P.R., MEISLING, K.E. & MOUNT, V.S. 2001. Reactivation of an obliquely rifted margin, Campos and Santos basins, southeastern Brazil. *AAPG Bulletin*, **85**, p. 1925-1944.

COCKBURN, H.A.P., BROWN, R.W., SUMMERFIELD, M.A. & SEIDL, M.A. 2000. Quantifying passive margin denudation and landscape development using a combined fission-track thermochronology and cosmogenic isotope analysis approach. *Earth and Planetary Science Letters,* **179,** p. 429-435.

COLTER, V.S. 1978. Exploration for gas in the Irish Sea. *In:* VAN LOON, A.J. (ed.), *Key notes of the MEGS-II (Amsterdam 1978),* Geologie en Mijnbouw*,* **57,** p. 503-516.

CONNAN, J., 1974. Time-temperature relations in oil genesis. *AAPG Bulletin,* **58**, p. 2516-2521.

COOPER, M.A. & WILLIAMS, G.D., 1989. *Inversion Tectonics*. Geological Society, London. Special Publications, **44**. 375p

COPE, J.C.W. 1984. The Mesozoic history of Wales. *Proceedings of the Geologists Association,* **95,** p. 373-385.

COPE, M.J. 1986. An interpretation of vitrinite reflectance data from the Southern North Sea Basin. *In:* BRROKS, J., GOFF, J.C. & VAN HOORN, B. (eds.), *Habitat of Palaeozoic Gas in NW Europe.* Geological Society, London. Special Publications, **23**, p. 85-98.

COPE, J.C.W. 1994. A latest Cretaceous hotspot and the southeasterly tilt of Britain. *Journal of Geological Society of London,* **151,** p. 905-908.

COPE, J.C.W., GETTY, T.A., HOWARTH, M.K. & TORRENS, T.S. 1980*a*. *A correlation of Jurassic rocks in the British Isles: Part One: Introduction and Lower Jurassic*. Geological Society, London, Special Reports, **14**.

COPE, J.C.W., INGHAM, J.K. & RAWSON, P.F. (eds.) 1992. *Atlas of Palaeogeography and Lithofacies.* Geological Society, London, Memoirs, **13.**

CORCORAN, D.V. & CLAYTON, G. 1999. Interpretation of vitrinite reflectance profiles in the Central Irish Sea area: implications for the timing of organic maturation. *Journal of Petroleum Geology,* **22,** p. 261-286.

CORCORAN, D.V. & CLAYTON, G. 2001. Interpretation of vitrinite reflectance profiles in sedimentary basins, onshore and offshore Ireland. *In:* SHANNON, P.M., HAUGHTON, P.D.W. & CORCORAN, D.V. (eds.), *The Petroleum Exploration of Ireland's Offshore Basins*. Geological Society, London, Special Publications, **188**, p. 61-90.

CORCORAN, D.V. & DORÉ, A.G. 2002. Depressurization of hydrocarbon-bearing reservoirs in exhumed basin settings: evidence from Atlantic margin and borderland basins. *In*: DORÉ, A.G., CARTWRIGHT, J.A., STOKER, M.S., TURNER, J.P. & WHITE, N. (eds.) *Exhumation of the North Atlantic Margin: Timing, Mechanisms and Implications for Petroleum Exploration.* Geological Society, London, Special Publications, **196,** p. 457-483.

CORCORAN, D.V. & DORÉ, A.G. 2005. A review of techniques for the estimation of magnitude and timing of exhumation in offshore basins. *Earth-Science Reviews,* **72,** p. 129-168.

CORCORAN, D.V. & MECKLENBURGH, R. 2005. Exhumation of the Corrib Gas Field, Slyne Basin, offshore Ireland. *Petroleum Geoscience,* **11,** p. 239-256.

CORFIELD, S.M., GAWTHORPE, R.L., GAGE, M., FRASER, A.J. & BESLY, B.M. 1996. Inversion tectonics of the Variscan foreland of the British Isles. *Journal of the Geological Society of London,* **153,** p. 17-32.

CORNFORD, C. 1986. The Bristol Channel Graben: organic geochemical limits on subsidence and speculation on the origin of inversion (oil-implications). *Proceedings of the Ussher Society,* **6 (3),** p. 360-367.

CORNFORD, C., YARNELL, L. & MURCHISON, D.G. 1987. Initial vitrinite reflectance results from the Carboniferous of north Devon and north Cornwall. *Proceedings of the Ussher Society*, **6 (4),** p. 461-467.

CORRIGAN, J., 1992. Annealing models under the microscope. *On Track,* **2**, p. 9-11.

CORRY, D. & BROWN, C. 1998. Temperature and heat flow in the Celtic Sea basins. *Petroleum Geoscience,* **4,** p. 317-326.

COURTNEY, R.C. & WHITE, R.S. 1986. Anomalous heat flow and geoid across the Cape Verde rise: evidence for dynamic support from a thermal pulse in the mantle. *Geophysical Journal of the Royal Astronomical Society,* **87,** p. 815-867.

COWAN, G., BURLEY, S.D., HOEY, N., HOLLOWAY, P., BERMINGHAM, P., BEVERIDGE, N., HAMBORG, M. & SYLTA, Ø. 1999. Oil and gas migration in the Sherwood Sandstone of the East Irish Sea Basin. *In*: FLEET, A.J. & BOLDY, S.A.R. (eds.), *Petroleum Geology of Northwest Europe: Proceedings of the 5th Conference.* Geological Society, London, p. 1383-1398.

COWARD, M.P. 1990. The Precambrian, Caledonian and Variscan framework to NW Europe. *In:* HARDMAN, R.F.B. & BROOKS, J. (eds.), *Tectonic events responsible for Britain's Oil and Gas reserves*. Geological Society, London. Special Publications, **55**, p. 1-35.

COWARD, M.P. 1994. Inversion Tectonics. *In*: HANCOCK, P.L. (ed.), *Continental Deformation*. Pergamon Press, p. 280-304.

COWARD, M.P. 1995. Structural and tectonic setting of the Permo-Triassic basins of northwest Europe. *In:* BOLDY, S.A.R. (ed.), *Permian and Triassic Rifting in Northwest Europe.* Geological Society, London, Special Publications, **91,** p. 7-39.

COWARD, M.P. & SMALLWOOD, S. 1984. An interpretation of the Variscan of SW Britain. *In:* HUTTON, D.H.W. & SANDERSON, D.J. (eds.), *Variscan tectonics of the North Atlantic region*. Geological Society, London, Special Publications, **14**, p. 89-102.

COWARD, M.P. & TRUDGILL, B. 1989. Basin development and basement structure of the Celtic Sea basins (SW Britain). *Bulletin of the Geological Society of France,* **8,** p. 423-436.

COWARD, M.P., DEWEY, F.J., HEMPTON, M. & HOLROYD, J. 2003. Tectonic evolution. *In:* EVANS, D., GRAHAM., C., ARMOUR, A. & BATHHURST, P. (eds.) *The Millennium Atlas: Petroleum Geology of the Central and Northern North Sea.* Geological Society, London, p. 17-33.

COX, K.G. 1993. Continental magmatic underplating. *Philosophical Transactions of the Royal Society of London*, **342A,** p. 155-166.

CROWHURST, P.V., GREEN, P.F. & KAMP, P.J.J., 2002. Appraisal of (U-Th)/He apatite thermochronology as a thermal history tool for hydrocarbon exploration: an example from the Taranaki Basin, New Zealand. Bulletin of the *American Association of Petroleum Geologists*, **86**, p. 1801-1819.

CROWLEY, K.D., CAMERON, M., & SCHAEFER, R.L., 1991. Experimental studies of annealing of etched fission-tracks in apatite. *Geochemica et Cosmochimica Acta,* **55**, p. 1449-1465.

CUNNINGHAM, M.J.M., DENSMORE, A.L., ALLEN, P.A., PHILLIPS, W.E.A., BENNET, S.D., GALLAGHER, K. & CARTER, A. 2003. Evidence for post-early Eocene tectonic activity in southeastern Ireland. *Geological Magazine,* **140,** p. 101-118.

CUNNINGHAM, M.J.M., PHILLIPS, W.E.A. & DENSMORE, A.L. 2004. Evidence for Cenozoic tectonic deformation in SE Ireland and near offshore. *Tectonics,* **23,** 6002, doi:10.1029/2003TC001597.

CURRY, D. 1965. The Palaeogene beds of South-East England. *Proceedings of the Geologists Association*, **76**, p. 151-173.

CURRY, D. 1992. Tertiary. *In:* DUFF, P.MCL.D. & SMITH, A.J. (eds.), *Geology of England and Wales.* Geological Society, London, p. 389-411.

CURRY, D. & SMITH, A.J. 1975. New discoveries concerning the geology of the central and eastern parts of the English Channel. *Philosophical Transactions of the Royal Society, London,* **A279**, p.155-167.

CURRY, D., GRAY, F., HAMILTON, D. & SMITH, A.J. 1967. Upper Chalk from the sea bed, south of Cork, Eire. *Proceedings of the Geological Society of London*, **1640**, p. 134-136.

CURRY, D., ADAMS, C.G., BOULTER, M.C., DILLEY, F.C., EAMES, F.E., FUNNELL, B.M. & WELLS, M.K. 1978. *A Correlation of Tertiary Rocks in the British Isles.* Geological Society of London Special Report, **12**.

DANIELS, E.J., ALTANER, S.P., MARSHAK, S. & EGGLESTON, J.R. 1990. Hydrothermal alteration in anthracite from eastern Pennsylvania; implications for mechanisms of anthracite formation. *Geology*, **18**, p. 247-250.

DART, C. J., MCCLAY, K.R. &. HOLLINGS, P.N. 1995. 3D analysis of inverted extensional fault systems, southern Bristol Channel Basin, UK. *In:* BUCHANAN, J.G. & BUCHANAN, P.G. (eds.), *Basin Inversion.* Geological Society, London. Special Publications, **88**, p. 393-413.

DAVIES, G.A. 1995. *The relationship between deformation and thermal maturation of anthracite within the South Wales coalfield*. Unpublished PhD thesis, University of Wales Cardiff, UK.

DAVIES, R., CLOKE, I., CARTWRIGHT, J., ROBINSON, A. & FERRERO, C. 2004. Post-breakup compression of a passive margin and its impact on hydrocarbon prospectivity: An example from the Tertiary of the Faeroe-Shetland Basin, United Kingdom. *AAPG Bulletin,* **88,** p. 1-20.

DAVIES, R.J., TURNER, J.D. & UNDERHILL, J.R. 2001. Sequential dip-slip fault movement during rifting: a new model for the evolution of the Jurassic trilete North Sea rift system. *Petroleum Geoscience,* **7,** p. 371-388.

DAVIS, M. & KUSZNIR, N.J. 2004. Depth-dependent lithospheric stretching at rifted continental margins. *In:* KARNER, G.D. (ed.), *Proceedings of NSF Rifted Margins Theoretical Institute.* Columbia University Press, p. 92-136.
DAVIS, W.M. 1895. The development of certain English rivers. *The Geographical Journal,* **5,** p. 127-146.

DE GRACIANSKY, P.C., POAG, C.W., CUNNINGHAM, R., LOUBERE, P., MASSON, D.G., MAZULLO, J.M., MONTADERT, L., MÜLLER, C., OTSUKA, K., REYNOLDS, L.A., SIGAL, J., SNYDER, S.W., TOWNSEND, H.A., VAOS, S.P. & WAPLES, D. 1985. The Goban Spur transect: Geologic evolution of a sediment-starved passive continent margin. *Geological Society of America Bulletin,* **96,** p. 58-76.

DEMBICKI JR., H. 1984. An interlaboratory comparison of source rock data. *Geochimica et Cosmochimica Acta*, **48**, p. 2641–2649.

DERCOURT, J. ET AL. 1986. Geological evolution of the Tethys Belt from Atlantic to Pamir since Liassic. *Tectonophysics*, **123**, p. 241-315.

DERCOURT, J., RICOU, L.E. & VRIELYNCK, B. (eds.) 1993. *Atlas Tethys Palaeoenvironmental maps.* Paris: Gauthier-Villars. 307p.

DEWEY, J.F. 1982. Plate tectonics and the evolution of the British Isles. *Journal of the Geological Society of London,* **139,** p. 371-412.

DEWEY, J.F. 2000. Cenozoic tectonics of western Ireland. *Proceedings of the Geologists Association,* **111,** p. 291-306.

DEWEY, J.F. & WINDLEY, B.F. 1988. Paleocene-Oligocene tectonics of North West Europe. *In:* MORTON, A.C. & PARSON, L.M. (eds.), *Early Tertiary Volcanism and the opening of the North East Atlantic*. Geological Society, London, Special Publications, **39**, p. 25-31.

DEWEY, J.F., HELMAN, M.L., TURCO, E., HUTTON, D.H.W. & KNOTT, S.D. 1989. Kinematics of the Western Mediterranean. *In:* Coward, M.P., Dietrich, D. & Park, R.G. (eds.), *Alpine Tectonics.* Geological Society, London, Special Publications, **45,** p. 265-283.

DÉZES, P. & ZIEGLER, P.A. 2002. Moho depth map of Western and Central Europe. World Wide Web Address: http://www.unibas.ch/eucor-urgent

DICKINSON, G., 1953. Geological aspects of abnormal reservoir pressures in Gulf Coast, Louisiana. *AAPG Bulletin,* **37**, p. 410-432.

DIGBY, P.J., 1981. The effective elastic moduli of porous ghranular rocks. *Journal of Applied Mechanics*, **48**, p. 803-808.

DIMITROPOLOUS, K. & DONATO, J.A. 1983. The gravity anomaly of the St. George's Channel Basin, southern Irish Sea – a possible explanation in terms of salt migration. *Journal of the Geological Society of London,* **140,** p. 239-244.

DOBSON, M. R. & WHITTINGTON, R. J. 1987. The geology of Cardigan Bay. *Proceedings of the Geological Association,* **98(4)**, p. 331–353.

DONELICK, R.A. 1991. Crystallographic orientation dependence of mean etchable fission track length in apatite: An empirical model and experimental observations. *American Mineralogist,* **76,** p. 83-91.

DONELICK, R.A., KETCHAM, R.A. & CARLSON, W.D. 1999. Variability of apatite fission-track annealing kinetics: II. Crystallographic orientation effects. *American Mineralogist,* **84,** p. 1224-1234.

DONOVAN, D.T., SAVAGE, R.J.G., STRIDE, A.H. & STUBBS, A.R. 1961. Geology of the floor of the Bristol Channel. *Nature*, **189** p. 51-52.

DORÉ, A.G. 1976. Preliminary geological interpretation of the Bristol Channel Approaches. *Journal of the Geological Society of London*, **132**, p. 453-459.

DORÉ, A.G. & JENSEN, L.N., 1996. The impact of late Cenozoic uplift and erosion on hydrocarbon exploration: offshore Norway and some other uplifted basins. *Global and Planetary Change*, **12**, p. 415-436.

DORÉ, A.G. & LUNDIN, E.R. 1996. Cenozoic compressional structures on the NE Atlantic margin: nature, origin and potential significance for hydrocarbon exploration. *Petroleum Geoscience,* **2,** p. 299-311.

DORÉ, A.G., LUNDIN, E.R., FICHLER, C. & OLESEN, O. 1997. Patterns of basement structure and reactivation along the NE Atlantic margin. *Journal of the Geological Society of London,* **154,** p. 85-92.

DORÉ, A.G., LUNDIN, E.R., JENSEN, L.N., BIRKELAND, Ø., ELIASSEN, P.E. & FILCHER, C. 1999. Principal tectonic events in the evolution of the northwest European Atlantic margin. *In*: FLEET, A.J. & BOLDY, S.A.R. (eds.), *Petroleum Geology of Northwest Europe: Proceedings of the 5th Conference,* p. 41-61.

DORÉ, A.G., CARTWRIGHT, J.A., STOKER, M.S., TURNER, J.P. & WHITE, N.J., 2002*a*. Exhumation of the North Atlantic margin: introduction and background. *In:* DORÉ, A.G., CARTWRIGHT, J.A., STOKER, M.S., TURNER, J.P. & WHITE, N (eds), *Exhumation of the North Atlantic Margin: Timing, Mechanisms and Implications for Petroleum Exploration.* Geological Society, London. Special Publications, **196**, p. 1-12.

DORÉ, A.G., CORCORAN, D.V. & SCOTCHMAN, I.C., 2002*b*. Prediction of the hydrocarbon system in exhumed basins and application to the NW European margin. *In:* DORÉ, A.G., CARTWRIGHT, J.A., STOKER, M.S., TURNER, J.P. & WHITE, N (eds), *Exhumation of the North Atlantic Margin: Timing, Mechanisms and Implications for Petroleum Exploration.* Geological Society, London. Special Publications, **196**, p. 401-429.

DOW, W. 1977. Kerogen studies and geological interpretations. *Journal of Geochemical Exploration,* **7,** p. 79-99.

DROZDZEWSKI, G. 1988. Die wurzel der Osning-überschiebung und der mechanismus der herzynischer Inversionsstörungen in Mitteleuropa. *Geol Rundsch*, **77**, p. 127-141.

DUDDY, I.R., GREEN, P.F., & LASLETT, G.M., 1988. Thermal annealing of fission tracks in apatite III: Variable temperature behaviour. *Chemical Geology (Isotope Geoscience Section),* **73**, p. 25-38.

DUDDY, I.R., GREEN, P.F., HEGARTY, K.A., BRAY, R.J. & O'BRIEN, G.W. 1998. Dating and duration of hot fluid flow events determined using AFTA® and vitrinite reflectance-based thermal history reconstruction. *In*: PARNELL, J. (ed.), *Dating and Duration of Fluid Flow and Fluid-Rock Interaction.* Geological Society, London, Special Publications, **144,** p. 41-51.

DUDDY, I.R., GREEN, P.F., HEGARTY, K.A. & BRAY, R.J. 1991. Reconstruction of thermal history in basin modelling using apatite fission track analysis: what is really possible? *Proceedings of the First Offshore Australia Conference (Melbourne),* **III**, p. 49-61.

DUDDY, I.R., GREEN, P.F., BRAY, R.J. & HEGARTY, K.A. 1994. Recognition of the thermal effects of fluid flow in sedimentary basins. *In*: PARNELL, J. (ed.), *Geofluids: Origin, Migration and Evolution of Fluids in Sedimentary Basins.* Geological Society, London, Special Publications, **78,** p. 325-345.

DUDDY, I.R., GREEN, P.F., GIBSON, H.J. & HEGARTY, K.A. 2003. Regional palaeo-thermal episodes in northern Australia. *Timor Sea Petroleum Geoscience (Proceedings of the Timor Sea Symposium) 2003,* p. 567-591.

DUNCAN, W.I., GREEN, P.F. & DUDDY, I.R. 1998. Source rock burial history and seal effectiveness: key facets to understanding hydrocarbon exploration potential in the East and Central Irish Sea Basins. *AAPG Bulletin,* **82,** p. 1401-1415.

DUNFORD, G.M., DANCER, P.N. & LONG, K.D. 2001. Hydrocarbon potential of the Kish Bank Basin: integration within a regional model for the Greater Irish Sea Basin. *In*: Shannon, P.M., Haughton, P.D.W. & Corcoran, D.V. (eds.), *The Petroleum Exploration of Ireland's Offshore Basins*. Geological Society, London, Special Publications, **188,** p. 135-154.

DVORKIN, J., NUR, A. & YIN, H. 1994. Effective properties of cemented granular materials. *Mechanics of Materials*, **18**, p. 351-366.

DVORKIN, J. & NUR, A. 1998. Time-average equation revisited. *Geophysics*, **63 (2)**, p. 460-464.

DYMENT, J. 1989. SWAT and the Celtic Sea basins – relations with the Variscan crust and recent formation of the Moho. *Bulletin de la Societe Geologique de France*, **5**, p. 477-487.

DYMENT, J. & BANO, M. 1991. Deep crustal features of the Celtic Sea from complementary processing on the SWAT data. *Geophysics Journal International,* **105**, p. 71–83.

DYMENT, J., SIBUET, J.C. & B. PINET, B. 1990. Deep structure of the Celtic Sea: a discussion on the formation of basins. *Tectonophysics,* **173**, p. 435–444.

EARLE, M.M., JANKOWSKI, E.J. & VANN I.R. 1989. Structual and stratigraphic evolution of the Faroe-Shetland Channel and northern Rockall Trough. *In:* TANKARD, A.J. & BALKWILL, H.R. (eds.), *Extensional tectonics and Stratigraphy of the North Atlantic margins*. American Association of Petroleum Geologists Memoir, **46**, p. 461-469.

ELLIS, D.V., 1987. *Well-logging for Earth scientists.* Amsterdam: Elsevier. 532p.

ENGLAND, P. & MOLNAR, P. 1990. Surface uplift, uplift of rocks, and exhumation of rocks. *Geology,* **18,** p. 1173-1177.

ENGLAND, R.W. & SOPER, N.J. 1997. Lower crustal structure of the East Irish Sea from deep seismic reflection data. *In*: MEADOWS, N.S., TRUEBLOOD, S., HARDMAN, M. & COWAN, G. (eds.), *Petroleum Geology of the Irish Sea and Adjacent Areas*. Geological Society, London, Special Publications, **124**, p. 61-72.

ENOS, P. & SAWATSKY, L.H., 1981. Pore networks in Holocene carbonate sediments. *Journal of Sedimentary Petrology,* **51**, p. 961-985.

ERICKSON, S.N. & JARRARD, R.D. 1998. Velocity porosity relationships for water-saturated siliciclastic sediments. *Journal of Geophysical Research*, **103** (B12), p. 30385-30406.

ETNYRE, L.M. 1989. *Finding oil and gas from well logs.* New York: Van Nostrand Reinhold. 305p.

EVANS, C.D.R., 1990. *United Kingdom Offshore Regional Report: The geology of the western English Channel and its western approaches*. London: HMSO for the British Geological Survey. 93p

EVANS, C.D.R. & HUGHES, M.J. 1984. The Neogene succession of the South Western Approaches, Great Britain. *Journal of the Geological Society of London*, **141**, p. 315-326.

EVANS, A. & CLAYTON, G. 1998. The geological history of the Ballydeenlea Chalk Breccia, County Kerry, Ireland. *Marine and Petroleum Geology*, **16**, p. 299–307.

EYLES, N. 1996. Passive margin uplift around the North Atlantic region and its role in Northern Hemisphere late Cenozoic glaciation. *Geology,* **24,** p. 103-106.

EYNON, G. 1981. Basin development and sedimentation in the Middle Jurassic of the northern North Sea. *In*: ILLING, L.V. & HOBSON, G.D. (eds.), *Petroleum Geology of the Continental Shelf of North-West Europe*. London: Heyden, p. 236-244.

FALVEY, D.A. & MIDDLETON, M.F., 1981. Passive continental margins. Evidence for a pre-break up deep crustal metamorphic subsidence mechanism. *In: Proceedings 26th International Geological Congress, Geology of Continental Margins Symposium Colloquium,* p. 103-114

FALVEY, D.A. & DEIGHTON. 1982. Recent advances in burial and thermal geohistory analysis. *Journal of the Australian Exploration Society*, **22**, p. 65-81.

FISHER, M.J. & MUDGE, D.C. 1998. Triassic. *In:* GLENNIE, K.W. (ed.), *Petroleum Geology of the North Sea (4th edition).* Oxford: Blackwell Science, p. 212-244.

FITCH, F.J., MILLER, J.A. & MITCHELL, J.G. 1969. A new approach to radio-isotopic dating in orogenic belts. *In:* KENT, P.E., SATTERTHWAITE, G.E. & SPENCER, A.M. (eds.), *Time and Place in Orogeny*. Geological Society, London, Special Publications, **3**, p. 157-195.

FITCHES, W.R. & CAMPBELL, S.D.G. 1987. Tectonic evolution of the Bala Lineament in the Welsh Basin. *Geological Journal,* **22**, p. 131–153.

FLEISCHER, R.L., PRICE, P.B. & WALKER, R.M. 1965. Effects of temperature, pressure and ionization on the formation and stability of fission tracks in minerals and glasses. *Journal of Geophysical Research,* **70,** p. 1497-1502.

FLOODPAGE, J., NEWMAN, P. & WHITE, J. 2001. Hydrocarbon prospectivity in the Irish Sea area: insights from recent exploration of the Central Irish Sea, Peel and Solway basins. *In* SHANNON, P.M., HAUGHTON, P.D.W. & CORCORAN, D.V. (eds.), *The Petroleum Exploration of Ireland's Offshore Basins*. Geological Society, London, Special Publications, **188**, p. 107-134.

FORD, M., KLEMPERER, S.L. & RYAN, P.D. 1992. Deep structure of southern Ireland: a new geological synthesis using BIRPS deep seismic reflection profiling. *Journal of the Geological Society of London,* **149,** p. 915-922.

FORD, M., LICKORISH, W.H. & KUSZNIR, N.J. 1999. Tertiary foreland sedimentation in the Southern Subalpine Chains, SE France: a geodynamic appraisal. *Basin Research,* **11,** p. 315-336.

FOULGER, G.R. 2002. Plumes, or plate tectonic processes? *Astronomy & Geophysics,* **43,** 6.19-6.23.

FOULGER, G.R. 2006. Old crust underlies Iceland. *Geophysical Journal International.*

FOULGER, G.R. & ANDERSON, D.L. 2005. A cool model for the Iceland hotspot. *Journal of Volcanology and Geothermal Research,* **141,** p. 1-22.

FOULGER, G.R. & NATLAND, J.H. 2003. Is "Hotspot" Volcanism a Consequence of Plate Tectonics? *Science,* **300,** p. 921-922.

FRANKE, W. & ENGEL, W., 1982. Variscan sedimentary basins on the continent and relations with south west England. *Proceedings of the Ussher Society*, **5**, p. 256-269.

FRIEDMAN, G.M. 1975. The making and unmaking of limestones or the downs and ups of porosity. *Journal of Sedimentary Petrology*, **45** p. 379-398.

FRODSHAM, K. & GAYER, R.A., 1997. Variscan compressional structures within the main productive coal-bearing strata of South Wales. *Journal of the Geological Society of London*, **154**, p. 195-208.

FÜCHTBAUER, H. & MÜLLER, G. 1970. *Sedimente und Sedimentgesteine*. Schweizerbart'sche Verlagsbuchhandlung, Stuttgart.

FYFE, J.A., ABBOTTS, I. & CROSBY, A. 1981. The Subcrop of the Mid-Mesozoic Unconformity in the UK Area. *In*: ILLING, L.V. & HOBSON, G.D. (eds.), *Petroleum Geology of the Continental Shelf of North-West Europe*. London: Heyden, p. 236-244.

GALBRAITH, R.F. 1981. On statistical models for fission track counts. *Mathematical Geology,* **13,** p. 471-488.

GALBRAITH, R.F. 1990. The radial plot: graphical assessment of spread in ages. *Nuclear Tracks,* **17,** p. 207-214.

GALBRAITH, R.F. & LASLETT, G.M. 1993. Statistical methods for mixed fission track ages. *Nuclear Tracks*, **21**, p. 459-470.

GALE, A.S., JEFFREY, P.A., HUGGETT, J.M. & CONNOLLY, P. 1999. Eocene inversion history of the Sandown Pericline, Isle of Wight, southern England. *Journal of the Geological Society of London,* **156,** p. 327-339.

GALLAGHER, K. 1995. Evolving temperature histories from apatite fission-track data. *Earth and Planetary Science Letters,* **136,** p. 421-435.

GALLAGHER, K. & BROWN, R. 1997. The onshore record of passive margin evolution. *Journal of the Geological Society of London,* **154,** p. 451-457.

GALLAGHER, K. & BROWN, R. 1999. Denudation and uplift at passive margins: the record on the Atlantic Margin of southern Africa. *Philosophical Transactions of the Royal Society of London,* **A357,** p. 835-859.

GALLAGHER, K., BROWN, R. & JOHNSON, C. 1998. Fission track analysis and its applications to geological problems. *Annual Reviews of Earth and Planetary Sciences,* **26,** p. 519-572.

GALLAGHER, K., RAMSDALE, M., LONERGAN, L. & MORROW, D. 1997. The role of thermal conductivity measurements in modelling thermal histories in sedimentary basins. *Marine and Petroleum Geology,* **14,** p. 201-214.

GALLOWAY, W.E., 1974. Deposition and the diagenetic alteration of sandstone in northeast Pacific arc-related basins. Implications for greywacke genesis. *Bulletin of the Geological Society of America,* **85**, p. 379-390

GARDINER, P.R.R. & SHERIDAN, D.J.R. 1981. Tectonic framework of the Celtic Sea and adjacent areas with special reference to the location of the Variscan Front. *Journal of Structural Geology,* **3(3)**, p. 317–331.

GASSMANN, R. 1951. Elastic waves through a packing of spheres. *Geophysics*, **16**, p. 673-685.

GAYER, R.A. & JONES, J., 1989. The Variscan foreland in South Wales. *Proceedings of the Ussher Society*, **7**, p. 177-179.

GAYER, R.A., COLE, J.E., GREILING, R.O., HECHT, C. & JONES, J.A., 1993. Comparative evolution of coal bearing foreland basins along the Variscan northern margin in Europe. *In:* GAYER, R.A., GREILING, R.O. & VOGEL, A. (eds.), *The Rhenohercynian and Subvariscan Fold Belts.* Vieweg Braunschweig, p. 48-82.

GEARHEART INC, 1983. *Formation evaluation data handbook.* Gearheart Inc publication.

GEIKIE, A. 1901. *The Scenery of Scotland.* London.

GEORGE, R.P., DE MONTEYARD, B., HARDY, M.J., MURATOV, N.I., WILLAN, C.G., GRABOWSKI, G.J., MITCHELL, J.C., STEINHAUFF, D.M., KING, K.C., KING, J.K., BEEMAN, C.R., LOPEZ, J.A., SEMPERE, J-C. & KLEIST, R.J. 2005. Plate-scale tectonic events inferred from Mesozoic and Cenozoic stratigraphic of the southeastern portion of the Arabian plate. *American Association of Petroleum Geologists, Paris, Abstracts with Program.*

GEORGE, T.N. 1967. Landform and structure in Ulster. *Scottish Journal of Geology,* **3,** p. 413-448.

GIBBS, A.D. 1987. Basin development, examples from the United Kingdom and comments on hydrocarbon prospectivity. *Tectonophysics,* **133**, p. 189–198.

GIBSON, D., MCCORMICK, A.G., MEIGHAN, I.G. & HALLIDAY, A.N. 1987. The British Tertiary Igneous Province: Young Rb-Sr ages for the Mourne Mountains granites, *Scottish Journal of Geology,* **23**, p. 221 – 225.

GILES, M.R., 1996. *Diagenesis – a quantitative perspective.* Dordrecht: Kluwer Academic Publishers.

GILES, M.R. & DE BOER, R.B., 1990. Origin and significance of redistributional secondary porosity. *Marine and Petroleum Geology,* **7**, p. 378-397

GILES, M.R., INDRELID, S.L. & JAMES, D.M.D., 1998. Compaction – the great unknown in basin modelling. *In:* DÜPPENBECKER, S.J. & ILIFFE, J.E. (eds.) *Basin modelling: Practice and Progress.* Geological Society, London. Special Publications, **141**, p. 15-43.

GILLCRIST, R., COWARD, M. & MUGNIER, J-L. 1987. Structural inversion and its controls: examples from the Alpine foreland and the French Alps. *Geodinamica Acta*, **1**, p. 5– 34.

GLEADOW, A.J.W. & DUDDY, I.R., 1981. A natural long-term track annealing experiment for apatite. *Nuclear Tracks,* **5**, p.169-174.

GLEADOW, A.J.W., DUDDY, I.R. & LOVERING, J.F., 1983. Fission-track analysis: A new tool for the evaluation of thermal histories and hydrocarbon potential. *APEA Journal,* **23**, p.93-102.

GLEADOW, A.J.W., DUDDY, I.R., GREEN, P.F. & LOVERING, J.F., 1986. Confined fission track lengths in apatite – a diagnostic tool for thermal history analysis. *Contributions to Mineralogy and Petrology,* **94**, p.405-415.

GLEADOW, A.J.W., KOHN, B.P., BROWN, R.W., O'SULLIVAN, P.B. & RAZA, A. 2002. Fission track thermotectonic imaging of the Australian continent. *Tectonophysics,* **349,** p. 5-21.

GLENNIE, K.W. & BOEGNER, P.L.E. 1981. Sole Pit inversion tectonics. *In*: ILLING, L.V. & HOBSON, G.D. (eds.), *Petroleum Geology of the Continental Shelf of North-West Europe*. London: Heyden, p. 110-120.

GÖLKE, M. & COBLENTZ, D. 1996. Origins of the European regional stress field. *Tectonophysics*, **266**, p. 11-24.

GRADSTEIN, F.M., OGG, J.G. & SMITH, A.G. 2004. *A Geologic Time Scale 2004.* Cambridge: Cambridge University Press.

GREEN, C.P. 1985. Pre-Quaternary weathering residues, sediments and landform development: examples from southern Britain. *In:* RICHARDS, K.S. & ARNETT, R.R., ELLIS, S. (eds.), *Geomorphology and Soils*. London: George, Allen & Unwin, p. 58-77.

GREEN, P.F. 1981. A new look at statistics in fission-track dating. *Nuclear Tracks and Radiation Measurements,* **5,** p. 77-86.

GREEN, P.F. 1986. On the thermo-tectonic evolution of Northern England: evidence from fission track analysis. *Geological Magazine*, **123**, p. 493-506.

GREEN, P.F., 1988. The relationship between track shortening and fission-track age reduction in apatite: Combined influences of inherent instability, annealing anisotropy, length bias and system calibration. *Earth Planetary Science Letters,* **89**, p.335-352.

GREEN, P.F. 1989. Thermal and tectonic history of the East Midlands shelf (onshore UK) and surrounding regions assessed by apatite fission track analysis. *Journal of the Geological Society, London,* **146,** p. 755-773.

GREEN, P.F. 2002. Early Tertiary palaeo-thermal effects in Northern England: reconciling results from apatite fission track analysis with geological evidence. *Tectonophysics,* **349,** p. 131-144.

GREEN, P.F. 2004. The importance of validating annealing models. *10th International Fission Track Dating and Thermochronology Conference*, Abstract ANN-04-O.

GREEN, P.F. 2005. Burial and exhumation histories of Carboniferous rocks of the Southern North Sea and onshore UK, with particular emphasis on post-Carboniferous events. *In:* COLLINSON, J.D., EVANS, D.J., HOLLIDAY, D.W. & JONES, N.S. (eds.), *Carboniferous Hydrocarbon Resources: the Southern North Sea and Surrounding Areas.* Yorkshire Geological Society Occasional Publication Series, **7,** p. 25-34.

GREEN, P.F., DUDDY, I.R., GLEADOW, A.J.R., TINGATE, P.R. & LASLETT, G.M. 1985. Fission track annealing in apatite: track length measurements and the form of the Arrhenius plot. *Nuclear tracks,* **10,** p. 323-328.

GREEN, P.F., DUDDY, I.R., GLEADOW, A.J.W., TINGATE, P.R. & LASLETT, G.M., 1986. Thermal annealing of fission-tracks in apatite I: A qualitative description. *Chemical Geology (Isotope Geoscience Section),* **59**, p. 237-253.

GREEN, P.F., DUDDY, I.R., GLEADOW, A.J.W. & LOVERING, J.F., 1989*a*. Apatite Fission Track Analysis as a palaeotemperature indicator for hydrocarbon exploration. *In:* NAESER, N.D. & MCCULLOH, T. (eds.), *Thermal history of sedimentary basins – methods and case histories.* New York: Springer-Verlag.

GREEN, P.F., DUDDY, I.R., LASLETT, G.M., HEGARTY, K.A., GLEADOW, A.J.W. & LOVERING, J.F., 1989*b*. Thermal annealing of fission-tracks in apatite IV: Quantitative modelling techniques and extension to geological timescales. *Chemical Geology (Isotope Geoscience Section),* 79, p. 155-182.

GREEN, P.F., LASLETT, G.M. & DUDDY, I.R., 1993. Mechanisms and kinetics of apatite fission-track annealing: Discussion. *American Mineralogist,* 78, p. 441-445.

GREEN, P.F., DUDDY, I.R., BRAY, R.J. & LEWIS, C.L.E. 1993. Elevated palaeotemperatures prior to Early Tertiary cooling throughout the UK region: implications for hydrocarbon generation. *In*: PARKER, J.R. (ed.), *Petroleum Geology of Northwest Europe: Proceedings of the 4th Conference.* Geological Society, London, p. 1067-1074.

GREEN, P.F., DUDDY, I.R. & BRAY, R.J., 1995. Applications of thermal history reconstruction in inverted basins. *In:* BUCHANAN, J.G. & BUCHANAN, P.G. (eds.), *Basin Inversion.* Geological Society, London. Special Publications, **88**, p. 148-165.

GREEN, P.F., HEGARTY, K.A. & DUDDY, I.R. 1996. Compositional influences on fission track annealing in apatite and improvement in routine application of AFTA®. *American Association of Petroleum Geologists, San Diego, CA, Abstracts with Program,* A56.

GREEN, P.F., DUDDY, I.R. & BRAY, R.J. 1997. Variation in thermal history styles around the Irish Sea and adjacent areas: implications for hydrocarbon occurrence and tectonic evolution. *In*: MEADOWS, N.S., TRUEBLOOD, S.P., HARDMAN, M. & COWAN, G. (eds.), *Petroleum Geology of the Irish Sea and Adjacent Areas.* Geological Society, London, Special Publications, **124,** p. 73-93.

GREEN, P.F., DUDDY, I.R., HEGARTY, K.A. & BRAY, R.J. 1999. Early Tertiary heat flow along the UK Atlantic margin and adjacent areas. *In*: FLEET, A.J. & BOLDY, S.A.R. (eds.), *Petroleum Geology of Northwest Europe: Proceedings of the 5th Conference.* Geological Society, London, p. 348-357.

GREEN, P.F., DUDDY, I.R., HEGARTY, K.A., BRAY, R.J., SEVASTAPULO, G.D., CLAYTON, G. & JOHNSTON, D. 2000. The post-Carboniferous evolution of Ireland: Evidence from Thermal History Reconstruction. *Proceedings of the Geologists' Association*, **111**, p. 307-320.

GREEN, P.F., DUDDY, I.R., BRAY, R.J. DUNCAN, W.I & CORCORAN, D.V., 2001*a*. The influence of thermal history on hydrocarbon prospectivity in the Central Irish Sea Basin. *In:* SHANNON, P.M., HAUGHTON, P.D.W & CORCORAN, D.V. (eds.), *The Petroleum Exploration of Ireland's Offshore Basins.* Geological Society, London. Special Publications, **188**, p. 171-188.

GREEN, P.F., THOMSON, K. & HUDSON, J.D. 2001*b*. Recognising tectonic events in undeformed regions: contrasting results from the Midland Platform and East Midlands Shelf, Central England. *Journal of the Geological Society of London,* **158,** p. 59-73.

GREEN, P.F., DUDDY, I.R. & HEGARTY, K.A., 2002. Quantifying exhumation in sedimentary basins of the UK from apatite fission track analysis and vitrinite reflectance data: precision, accuracy and latest results. *In:* DORÉ, A.G., CARTWRIGHT, J.A., STOKER, M.S., TURNER, J.P. & WHITE, N (eds.), *Exhumation of the North Atlantic Margin: Timing, Mechanisms and Implications for Petroleum Exploration.* Geological Society, London. Special Publications, **196**, p. 331-354.

GREEN, P.F., CROWHURST, P.V. & DUDDY, I.R. 2004. Integration of AFTA and (U-Th)/He thermochronology to enhance the resolution and precision of thermal history reconstruction in the Anglesea-1 well, Otway Basin, SE Australia. *In:* BOULT, P.J., JOHNS, D.R. & LANG, S.C. (eds.), *Eastern Australian Basins Symposium II.* Petroleum Exploration Society of Australia, Special Publication, p. 117-131.

GREEN, P.F., DUDDY, I.R. & HEGARTY, K.A. 2005. Comment on compositional and structural control on fission track annealing in apatite. *Chemical Geology,* **214,** p. 351-358.

GREENSMITH, J. 1978. *The Petrology of the Sedimentary Rocks.* Hemel Hempstead: Allen & Unwin.

GRIFFITHS, D.H., KING, R.F. & WILSON, C.D.V. 1961. Geophysical investigations in Tremadoc Bay, North Wales. *Quarterly Journal of the Geological Society of London,* **117,** p. 171-191.

HAENEL, R. 1979. A critical review of heat flow measurements in sea and lake bottom sediments. *In:* CERMAK, V. & RYBACH, L. (eds.), *Terrestrial Heat Flow in Europe*. Berlin: Springer, p. 49-73.

HALL, B.D. & WHITE, N. 1994. Origin of anomalous Tertiary subsidence adjacent to North Atlantic continental margins. *Marine and Petroleum Geology,* **11,** p. 702-714.

HALLAM, A. 1959. The concept of Jurassic axes of uplift. *Science Progress,* **183**, p. 441-449.

HALLAM, A. 1963. Major epeirogenic and eustatic changes since the Cretaceous, and their possible relationships to crustal structure. *American Journal of Science,* **261,** p. 397-423.

HALLAM, A. 1978. Eustatic cycles in the Jurassic. *Palaeogeography, Palaeoclimate and Palaeoecology*, **23**, p. 1-32.

HALLAM, A. 1992. Jurassic. *In*: DUFF, P.MCL.D. & SMITH, A.J. (eds.), *Geology of England and Wales*. Geological Society, London, p. 325-354.

HALLAM. A. & SELWOOD, B.W. 1976. Middle Mesozoic sedimentation in relation to tectonics in the British area. *Journal of Geology,* **84,** p. 302-321.

HALLIDAY, A.N. & MITCHELL, J.G. 1976. Structural K-Ar and $^{40}Ar/^{39}Ar$ age studies of adularia K-feldspars from the Lizard Complex, England. *Earth and Planetary Science Letters*, **29**, p. 227-237.

HAMBLIN, R.J.O., CROSBY, A., BALSON, US., JONES, S.M., CHADWICK, R.A., PENN, I.E. & ARTHUR, M.J. 1992. *United Kingdom Offshore Regional Report: the Geology of the English Channel*. HMSO, London.

HAMILTON, E.L. 1976. Variations of density and porosity with depth in deep-sea sediments. *Journal of Sedimentary Petrology,* **146,** p. 280-300.

HAN, D., NUR, A. & MORGAN, D. 1986. The effects of porosity and clay content on wave velocities of sandstones. *Geophysics*, **51**, p. 2093–2097.

HANCOCK, J.M. & RAWSON, P.F. 1992. Cretaceous. *In:* Cope, J.C.W., Ingham, J.K. & Rawson, P.F. (eds.), *Atlas of Palaeogeography and Lithofacies.* Geological Society, London, Memoir, **13,** p. 131-139.

HAO, F. & CHEN, J. 1992. The cause and mechanism of vitrinite reflectance anomalies. *Journal of Petroleum Geology*, **15**, p. 419–434.

HAQ, B.U., HARDENBOL, J. & VAIL, P.R. 1987. Chronology of fluctuating sea levels since the Triassic. *Science,* **235,** p. 1156-1167.

HARDMAN, M., BUCHANAN, J., HERRINGTON, P. & CARR, A. 1993. Geochemical modelling of the East Irish Sea Basin: its influence on predicting hydrocarbon type and quality. *In*: PARKER, J.R. (ed.), *Petroleum Geology of Northwest Europe: Proceedings of the 4th Conference.* Geological Society, London, p. 809-821.

HARLAND, W.B., ARMSTRONG, R.L., COX, A.V., CRAIG, L.E., SMITH, A.G. & SMITH, D.G. 1989. *A Geologic Time Scale*. Cambridge: Cambridge University Press.

HARRISON, T.M., ARMSTRONG, R.L., NAESER, C.W. & HARAKAL, J.E. 1979. Geochronology and thermal history of the Coast Plutonic Complex, near Prince Rupert, British Columbia, Canada. *Journal of Earth Science*, **16**, p. 400-410.

HARTLEY, A.J., 1993*b*. A depositional model for the mid-Westphalian A to late Westphalian B Coal Measures of South Wales. *Journal of the Geological Society of London,* **150**, p. 1121-1136.

HARTLEY, A.J. & WARR, L.N. 1990. Upper Carboniferous foreland basin in SW Britain. *Proceedings of the Ussher Society*, **7**, p. 212-216.

HASEBE, N., BARBARABD, J., JARVIS, K., CARTER, A. & HURFORD, A.J. 2004. Apatite fission track chronometry using laser ablation ICP-MS. *Chemical Geology,* **207,** p. 135-145.

HAYWARD, A.B. & GRAHAM, R.G. 1989. Some geometrical characteristics of inversion. *In:* COOPER, M.A. & WILLIAMS, G.D. (eds.), *Inversion Tectonics.* Geological Society, London, Special Publications, **44,** p. 17-39.

HEASLER, H.P. & KHARITONOVA, N.P. 1996. Analysis of sonic well logs applied to erosion estimates in the Bighorn Basin, Wyoming. *AAPG Bulletin,* **80,** p. 630-646.

HEDBERG, H.D. 1936. Gravitational compaction of clays and shales. *American Journal of Science*, **31**, p. 241-278.

HERRING, E.A., 1973. Estimating abnormal pressures from log data in the North Sea. *Petroleum Engineer,* November, SPE4301.

HESSELBO, S.P. 2000. Late Triassic and Jurassic: disintegrating Pangaea. *In:* WOODCOCK, N.H. & STRACHAN, R.A. (eds.), *Geological History of Britain and Ireland.* Oxford: Blackwell Publishing, p. 314-338.

HIBSCH, C., JARRIGE, J.J., CUSHING, E.M. & MERCIER, J. 1995. Palaeostress analysis, a contribution to the understanding of basin tectonics and geodynamic evolution. Example of the Permian/Cenozoic tectonics of Great Britain and geodynamic implications in western Europe. *Tectonophysics,* **252,** p. 103-136.

HILLIS, R.R., 1988. *The Geology and Tectonic evolution of the Western Approaches Trough.* PhD. Thesis, University of Edinburgh, UK.

HILLIS, R.R. 1991. Chalk porosity and Tertiary uplift, Western Approaches Trough, SW UK and NW French continental shelves. *Journal of the Geological Society of London,* **148,** p. 669-679.

HILLIS, R.R. 1992. A two-layer lithospheric compressional model for the Tertiary uplift of the southern United Kingdom. *Geophysical Research Letters,* **19,** p. 573-576.

HILLIS, R.R. 1993. Tertiary erosion magnitudes in the East Midlands Shelf, onshore UK. *Journal of the Geological Society of London,* **150,** p. 1047-1050.

HILLIS, R.R. 1995*a*. Regional Tertiary exhumation in and around the United Kingdom. *In*: BUCHANAN, J.G. & BUCHANAN, P.G. (eds.), *Basin Inversion*. Geological Society, London, Special Publications, **88**, p. 167-190.

HILLIS, R.R. 1995*b*. Quantification of Tertiary exhumation in the United Kingdom southern North Sea using sonic velocity data. *AAPG Bulletin,* **79,** p. 130-152.

HILLIS, R.R. & CHAPMAN, T.J., 1992. Variscan structure and its influence on post-Carboniferous basin development, Western Approaches Basin, SW UK continental shelf. *Journal of the Geological Society of London*, **149 (3)**, p. 413-417.

HILLIS, R.R. & NELSON, E.J. 2005. *In situ* stresses in the North Sea and their applications: petroleum geomechanics from exploration to development. *In:* DORÉ, A.G. & VINING, B.A. (eds.), *Petroleum Geology: North-West Europe and Global Perspectives – Proceedings of the 6th Petroleum Geology Conference.* Geological Society, London, p. 551-564.

HILLIS, R.R., THOMSON, K. & UNDERHILL, J.R. 1994. Quantification of Tertiary erosion in the Inner Moray Firth using sonic velocity data from the Chalk and the Kimmeridge Clay. *Marine and Petroleum Geology,* **11,** p. 283-293.

HOLFORD, S.P. 2006. *The Mesozoic-Cenozoic Exhumation History of the Irish Sea Basin System, Western UK*. PhD Thesis, University of Birmingham, UK.

HOLFORD, S.P., GREEN, P.F. & TURNER, J.P., 2005*a*. Palaeothermal and compaction studies in the Mohcras borehole (NW Wales) reveal early Cretaceous and Neogene exhumation and argue against regional Paleogene uplift in the southern Irish Sea. *Journal of the Geological Society of London*, **162**, p. 829-840.

HOLFORD, S.P., TURNER, J.P. & GREEN, P.F. 2005*b*. Reconstructing the Mesozoic-Cenozoic exhumation history of the Irish Sea basin system using apatite fission-track analysis and vitrinite reflectance data. *In*: DORÉ, A.G. & VINING, B. (eds.), *North West Europe and Global Perspectives: Proceedings of the 6th Petroleum Geology Conference.* Geological Society, London, p. 1095-1108.

HOLLIDAY, D.W. 1993. Mesozoic cover over northern England: interpretation of apatite fission track data. *Journal of the Geological Society of London,* **150,** p. 657-660.

HOLLIDAY, D.W. 1999. Palaeotemperatures, thermal modelling and depth of burial studies in northern and eastern England. *Proceedings of the Yorkshire Geological Society,* **52,** p. 337-352.

HOLLOWAY, S. 1985*b*. Lower Jurassic: The Lias. *In:* WHITTAKER, A. (ed.), *Atlas of onshore sedimentary basins in England and Wales: Post-Carboniferous tectonics and Stratigraphy*. Glasgow: Blackie, p.37-40.

HOLLOWAY, S. & CHADWICK, R.A., 1986. The Sticklepath-Lustleigh fault zone: Tertiary sinistral reactivation of a Variscan strike-slip fault. *Journal of the Geological Society of London*, **143**, p. 447-452.

HOLTEDAHL, O. 1953. On the oblique uplift some northern lands. *Norsk. Geograph. Tidskr*., **14**, p. 132-139.

HORSTMAN, E.L. 1984. Evidence for post-Permian eperiogenic uplift in the Canning basin from vitrinite reflectance data. *In:* PURCELL, P.G. (ed.), *The Canning basin*. W.A. Geological Society of Australia/Petroleum Exploration Society of Australia Canning Basin Symposium Proceedings, p. 401–409.

HOTTMAN, C.E. & JOHNSON, R.K., 1965. Estimation of formation pressures from log derived shale properties. *Journal of Petroleum Technology,* June.

HOUSEKNECHT, D.W. 1987. Assessing the relative importance of compaction processes and cementation to reduction of porosity in sandstones. *AAPG Bulletin*, **71**, p. 633-642.

HUANG, Z. & GRADSTEIN, F.M. 1990. Depth-porosity relationship from deep sea sediments. *Scientific Drilling*, **1**, p. 157-162.

HUBBERT, M.K. & RUBEY, W.W. 1959. Role of fluid pressure in mechanics in overthrust faulting. I. Mechanics of fluid-filled porous solids and its application to overthrust faulting. *Bulletin of the Geological Society of America*, **70**, p.115-166.

HUDSON, J.A., 1990. Overall elastic properties of isotropic materials with arbitrary distribution of circular cracks. *Geophysical Journal International*, **102**, p. 465-469.

HURFORD, A.J. & GREEN, P.F. 1982. A user's guide to fission track dating calibration. *Earth and Planetary Science Letters,* **59,** p. 343-354.

HURFORD, A.J. & GREEN, P.F. 1983. The zeta age calibration of fission-track dating. *Chemical Geology,* **1,** p. 285-317.

HURFORD, A.J., BARBARAND, J. & CARTER, A. 2005. Reply to comment on compositional and structural control on fission-track annealing in apatite. *Chemical Geology,* **214,** p. 359-361.

ISSLER, D.R., 1992. A new approach to shale compaction and stratigraphic restoration, Beaufort-Mackenzie Basin and Mackenzie corridor, northern Canada. *Bulletin of the American Association of Petroleum Geologists,* **76** (8), pp.1170-1189.

IZATT, C., MAINGARM, S. & RACEY, A. 2001. Fault distribution and timing in the Central Irish Sea Basin. *In:* SHANNON, P.M., HAUGHTON, P.D.W. & CORCORAN, D. (eds.), *The Petroleum Exploration of Ireland's Offshore Basins*. Geological Society, London, Special Publications, **188**, p. 155-169.

JACKSON, J.A., WHITE, N.J., GARFUNKEL, Z. & ANDERSON, H. 1988. Relations between normal-fault geometry, tilting and vertical motions in extensional terrains: an example from the southern Gulf of Suez. *Journal of Structural Geology*, **10**, p. 155–170.

JACKSON, D.I., JACKSON, A.A., EVANS, D., WINGFIELD, R.T.R., BARNES, R.P. & ARTHUR, M.J. 1995. *United Kingdom offshore regional report: The geology of the Irish Sea*. London: HMSO for the British Geological Survey.

JACKSON, J.A. & MCKENZIE, D.P. 1983. The geometrical evolution of normal fault systems. *Journal of Structural Geology,* **5,** p. 471-482.

JANKOWSKY, W., 1962. Diagenese und ölinhalt als Hilfmittel für die strukturgeschichtliche Analyse des Nordwestdeutschen Beeckens. *Zeitschrift Deutsch Geologische Gesellschaft*, **114**, p. 452-460.

JAPSEN, P., 1993. Influence of lithology and Neogene uplift on seismic velocities in Denmark; implications for depth conversions of maps. *AAPG Bulletin*, **77**, p. 194-211.

JAPSEN, P. 1997. Regional Neogene exhumation of Britain and the Western North Sea. *Journal of the Geological Society of London,* **154,** p. 239-247.

JAPSEN, P. 1998. Regional velocity-depth anomalies, North Sea Chalk: a record of overpressure and Neogene uplift and erosion. *AAPG Bulletin,* **82,** p. 2031-2074.

JAPSEN, P. 2000. Investigation of multi-phase erosion using reconstructed shale trends based on sonic data, Sole Pit axis, North Sea. *Global and Planetary Change,* **24,** p. 189-210.

JAPSEN, P., BIDSTRUP, T. & LIDMAR-BERGSTRÖM, K. 2002. Neogene uplift and erosion of southern Scandinavia induced by the rise of the South Swedish Dome. *In*: DORÉ, A.G., CARTWRIGHT, J.A., STOKER, M.S., TURNER, J.P. & WHITE, N. (eds.), *Exhumation of the North Atlantic Margin: Timing, Mechanisms and Implications for Petroleum Exploration.* Geological Society, London, Special Publications, **196,** p. 183-207.

JAPSEN, P. & CHALMERS, J.A., 2000. Neogene uplift and tectonics around the North Atlantic: Overview. *Global and Planetary Change*, **24**, p. 189-210.

JAPSEN, P., WAGNER, H., GOMMESEN, L. & MAVKO, G. 2000. Rock physics of Chalk: modelling the sonic velocity of the Tor Formation, Danish North Sea. *Paper presented at the EAGE 62nd Annual Conference and Technical Exhibition*, Glasgow, Scotland, 4pp.

JAPSEN, P., GREEN, P.F. & CHALMERS, J.A. 2005. Separation of Palaeogene and Neogene uplift on Nuussuaq, West Greenland. *Journal of the Geological Society of London,* **162,** p. 299-314.

JAPSEN, P., MUKERJI, T. & MAVKO, G. 2007. Constraints on velocity-depth trends from rock physics models. *Geophysical Prospecting*, **55**, p. 135-154.

JAPSEN, P., GREEN, P.F., NIELSEN, L.H., RASMUSSEN, E.S. & BIDSTRUP, T. 2007. Mesozoic-Cenozoic exhumation events in the eastern North Sea basin: A multi-disciplinary study based on palaeothermal, palaeoburial, stratigraphic and seismic data. *Basin Research*, **19**, p. 451-490.

JARVIS, I. & WOODROFF, P. 1981. The phosphatic chalks and hardgrounds of Boxford and Winterbourne, Berkshire – two tectonically controlled facies in the late Coniacian to early Campanian (Cretaceous) of southern England. *Geological Magazine*, **118**, p. 175-187.

JEANS, C.V., MERRIMAN, R.J. & MITCHELL, J.G. 1977. Origin of Middle Jurassic and Lower Cretaceous Fullers Earth in England. *Clay Minerals*, **2**, p. 11-14.

JENNER, J.K. 1981. The Structure and Stratigraphy of the Kish Bank Basin. *In*: ILLING, L.V. & HOBSON, G.D. (eds.), *Petroleum Geology of the Continental Shelf of North-West Europe.* London: Heyden, p. 426-431.

JOHNSON, H., RITCHIE, J.D., HITCHEN, K., MCINROY, D.B. & KIMBELL, G.S. 2005. Aspects of the Cenozoic deformational history of the Northeast Faroe-Shetland Basin, Wyville-Thomson Ridge and Hatton Bank areas. *In:* DORÉ, A.G. & VINING, B.A. (eds.), *Petroleum Geology: North-West Europe and Global Perspectives – Proceedings of the 6th Petroleum Geology Conference.* Geological Society, London, p. 993-1007.

JOHNSTON, S., DORÉ, A.G. & SPENCER, A.M. 2001. The Mesozoic evolution of the southern North Atlantic region and its relationship to basin development in the south Porcupine Basin, offshore Ireland. *In:* SHANNON, P.M., HAUGHTON, P.D.W. & CORCORAN, D.V. (eds.), *The Petroleum Exploration of Ireland's Offshore Basins*. Geological Society, London, Special Publications, **188**, p. 237-263.

JONES, J.A. 1989. The influence of contemporaneous tectonic activity on Westphalian sedimentation in the South Wales Coalfield. *In:* ARTHURTON, R.S., GUTTERIDGE, P. & NOLAN, S. (eds.), *Devonian and Carboniferous Tectonics and Sedimentation*. Occasional Publications of the Yorkshire Geological Society, **6**, p. 243-253.

JONES, J.A., 1991. A mountain front model for the Variscan deformation of the South Wales coalfield. *Journal of the Geological Society of London,* **148 (5),** p. 881-891.

JONES, O.T. 1936. Some observations on recent geological movements of the British coastline. *Antiquity,* **31,** p. 303-309.

JONES, S.M., WHITE, N., CLARKE, B.J., ROWLEY, E. & GALLAGHER, K. 2002. Present and past influence of the Iceland Plume on sedimentation. *In*: DORÉ, A.G., CARTWRIGHT, J.A., STOKER, M.S., TURNER, J.P. & WHITE, N. (eds.), *Exhumation of the North Atlantic Margin: Timing, Mechanisms and Implications for Petroleum Exploration.* Geological Society, London, Special Publications, **196,** p. 13-25.

JONES, S.M., WHITE, N. & LOVELL, B. 2001. Cenozoic and Cretaceous transient uplift in the Porcupine Basin and its relationship to a mantle plume. *In:* SHANNON, P.M., HAUGHTON, P.D.W. & CORCORAN, D.V. (eds.), *The Petroleum Exploration of Ireland's Offshore Sedimentary Basins.* Geological Society, London, Special Publications, **188,** p. 345-360.

KAMB, W.B., 1961. The thermodynamic theory of non-hydrostatically stressed solids. *Journal of Geophysical Research,* **66**, pp. 259-271.

KAMERLING, P., 1979. The geology and hydrocarbon habitat of the Bristol Channel Basin. *Journal of Petroleum Geology*, **2**, p. 75-93.

KAMP, P.J.J. & GREEN, P.F. 1990. Thermal and tectonic history of selected Taranaki Basin (New Zealand) wells assessed by apatite fission track analysis. *AAPG Bulletin,* **74,** p. 1401-1419.

KARNER, G.D., LAKE, S.D. & DEWEY, J.F., 1987*a*. The thermal and mechanical development of the Wessex Basin, southern England. *In:* COWARD, M.P., DEWEY, J.F. & HANCOCK, P.L. (eds.), *Continental Extension Tectonics.* Geological Society, London. Special Publications, **28**, p. 517-537.

KATZ, B.J., PHEIFER, R.N. & SCHUNK, D.J. 1988. Interpretation of discontinuous vitrinite reflectance profiles. *AAPG Bulletin*, **72**, p. 926– 931.

KEELEY, M. L., LEWIS, C.L.E., SEVASTOPULO, G.D., CLAYTON, G. & BLACKMORE, R. 1993. Apatite fission track data from southeast Ireland: implications for post-Variscan burial history. *Geological Magazine,* **130 (2),** p. 171–176.

KELLEY, S.A. 2005. Comparison of Exhumation estimated from sonic log velocities in Cretaceous shale in the San Juan and Raton basins, New Mexico and Colorado. *Salt Lake City Annual Meeting October 16–19, Geological Society of America Abstracts with Programs*, **37** (7), p. 295.

KELLING, G. 1974. Upper Carboniferous sedimentation in South Wales. *In:* OWEN, T.R. (ed.), *The Upper Paleozoic and post-Paleozoic rocks of Wales*. Cardiff: University of Wales Press, p. 185-224.

KELLING, G., 1988. Silesian sedimentation and tectonics in the South Wales basin: a brief review. *In*: BESLY, B., KELLING, G. (eds), *Sedimentation in a Synorogenic Basin Complex, The Upper Carboniferous of Northern Europe*. London: Blackie, p. 38–42.

KEMP, S.J., MERRIMAN, R.J. & BOUCH, J.E. 2005. Clay mineral reaction progress – the maturity and burial history of the Lias Group of England and Wales. *Clay Minerals,* **40,** p. 43-61.

KENT, P.E. 1976. Major synchronous events in Continental Shelves. *Tectonophysics*, **36**, p. 87-91.

KETCHAM, R.A., DONELICK, R.A. & CARLSON, W.D. 1999. Variability of apatite fission-track annealing kinetics: III. Extrapolation to geological time scales. *American Mineralogist,* **84,** p. 1235-1255.

KETCHAM, R.A., DONELICK, R.A. & DONELICK, M.B. 2000. AFTSolve: A program for multi-kinetic modelling of apatite fission-track data. *Geological Materials Research,* **2,** 1.

KIMBELL, G.S., RITCHIE, J.D., JOHNSON, H. & GATLIFF, R.W. 2005. Controls on the structure and evolution of the NE Atlantic margin revealed by regional potential field imaging and 3D modelling. *In:* DORÉ, A.G. & VINING, B.A. (eds.), *Petroleum Geology: North-West Europe and Global Perspectives – Proceedings of the 6th Petroleum Geology Conference.* Geological Society, London, p. 933-945.

KING, C. 1981. The stratigraphy of the London Clay and associated deposits. *Tertiary Research Special Papers,* **6**.

KING, A.F. & MCMILLAN, N.J. 1985. A mid-Mesozoic breccia from the coast of Labrador. *Canadian Journal of Earth Sciences*, **12**, p. 44-51.

KING, S.D. & ANDERSEN, D.L. 1998. Edge-driven convection. *Earth and Planetary Science Letters,* **160,** p. 289-296.

KING, S.D., LOWMAN, J.P. & GABLE, C.W. 2002. Episodic tectonic plate reorganizations driven by mantle convection. *Earth and Planetary Science Letters,* **203,** p. 83-91.

KLEIN, R.J. & BARR, M.V. 1986. Regional state of stress in western Europe. *Proceedings of the International Symposium of Rock Stress and Rock Stress Measurements, Stockholm*, p. 33-44.

KLEMPERER, S.L. & HOBBS, R.W. 1991. *The BIRPS Atlas: Deep seismic reflection profiles around the British Isles.* Cambridge: Cambridge University Press.

KLUTH, C.F. 1986. Plate tectonics of the ancestral Rocky Mountains. *In:* PETERSEN, J.E. (ed.), *Palaeotectonics and sedimentation in the Rocky Mountains Region, United States.* American Association of Petroleum Geologists Memoir, **41**, p. 353-369.

KNIPE, R.J., COWAN, G. & BALENDRAN, V.S. 1993. The tectonic history of the East Irish Sea Basin with reference to the Morecambe fields. *In*: PARKER, J.R. (ed.), *Petroleum Geology of Northwest Europe: Proceedings of the 4th Conference.* Geological Society, London, p. 857-866.

KNOTT, S.D., BURCHELL, M.T., JOLLEY, E.J. & FRASER, A.J. 1993. Mesozoic to Cenozoic plate reconstructions of the North Atlantic and hydrocarbon plays of the Atlantic margins. *In:* PARKER, J. R. (ed.), *Petroleum Geology of Northwest Europe: Proceedings of the 4th Conference*. London: Geological Society, p. 953–974.

KNOTT, S.D. 2001. Gravity-driven crustal shortening in failed rifts. *Journal of the Geological Society of London,* **158**, p. 193–196.

KOHN, B.P., BELTON, D.X., BROWN, R.W., GLEADOW, A.J.W., GREEN, P.F. & LOVERING, J.F. 2003. Comment on experimental evidence for the pressure dependence of fission track annealing in apatite. *Earth and Planetary Science Letters,* **215,** p. 299-306.

KOHN, B.P., GLEADOW, A.J.W. & COX, S.J. 1999. Denudation history of the Snowy Mountains: constraints from apatite fission track thermochronology. *Australian Journal of Earth Sciences,* **46,** p. 181-198.

KORVIN, G. 1984. Shale compaction and statistical Physics. *Geophysical Journal International*, **78**, p.35-50.

KRUMBEIN, W.C. & MONK, G.D., 1942. Permeability as a function of the size parameters of unconsolidated sand. *Petroleum Technology, AIME Publication 1942*, **5**, p. 1-11.

KUSTER, G.T. & TOKSÕZ, M.N. 1974. Velocity and attenuation of seismic waves in two-phase media: Part I. Theoretical Formulations. *Geophysics*, **39**, p. 587-606.

KUSZNIR, N.J. & ZIEGLER, P.A. 1992. The mechanics of continental extension and sedimentary basin formation: a simple-shear/pure-shear flexural cantilever model. *Tectonophysics*, **215**, p. 117-131.

KUSZNIR, N.J., HUNSDALE, R. & ROBERTS, A.M. 2004. Timing of depth-dependent lithosphere stretching on the S. Lofoten rifted margin offshore mid-Norway: pre-breakup or post-breakup? *Basin Research,* **16,** p. 279-296.

KUSZNIR, N.J., HUNSDALE, R., ROBERTS, A.M. & ISIMM TEAM. 2005. Timing and magnitude of depth-dependent lithospheric stretching on the southern Lofoten and northern Vøring continental margins offshore mid-Norway: implications for subsidence and hydrocarbon maturation at volcanic rifted margins. *In:* DORÉ, A.G. & VINING, B.A. (eds.), *Petroleum Geology: North-West Europe and Global Perspectives – Proceedings of the 6th Petroleum Geology Conference.* Geological Society, London, p. 767-783.

KUSZNIR, N.J., MARSDEN, G. & EGAN, S.S. 1991. A flexural cantilever simple-shear/pure-shear model of continental extension. *In:* ROBERTS, A.M., YIELDING, G. & FREEMAN, B. (eds.), *The Geometry of Normal Faults.* Geological Society, London, Special Publications, **56,** p. 41-60.

KYRKJEBØ, R., GABRIELSEN, R.H. & FALEIDE, J.I. 2004. Unconformities related to the Jurassic-Cretaceous synrift-post-rift transition of the northern North Sea. *Journal of the Geological Society of London,* **161,** p. 1-17.

LAKE, S.D. & KARNER, G.D. 1987. The structure and evolution of the Wessex Basin, southern England: an example of inversion tectonics. *Tectonophysics,* **137**, p. 347–378.

LAMPE, C., PERSON, M., NÖTH, S. & RICKEN, W. 2001. Episodic fluid flow within continental rift basins: some insights from field data and mathematical models of the Rhine graben. *Geofluids,* **1,** p. 42-52.

LANG, W.H.J., 1978. The determination of prior depth of burial uplift and erosion using interval transit time. *SPWLA 19th Annual Log Symposium Transactions,* paper B, p.1-17.

LARSEN, G. & CHILLINGAR, G.V. 1979. *Diagenesis in sediments and sedimentary rocks. Developments in Sedimentology 25A*. Amsterdam: Elsevier.

LASLETT, G.M., KENDALL, W.S., GLEADOW, A.J.W. & DUDDY, I.R., 1982. Bias in measurement of fission-track length distributions. *Nuclear Tracks,* **6**, p.79-85.

LASLETT, G.M., GREEN, P.F., DUDDY, I.R. & GLEADOW, A.J.W., 1987. Thermal annealing of fission tracks in apatite II: A qualitative analysis. *Chemical Geology (Isotope Geoscience Section),* 65, p.1-13.

LAWVER, L.A. & MÜLLER, R.D. 1994. Iceland hotspot track. *Geology,* **22**, p. 311–314.

LEEDER, M.R. & MCMAHON, A., 1988. Upper Carboniferous (Silesian) basin subsidence in northern Britain. *In*: BESLY, B.M. & KELLING, G. (eds.), *Sedimentation in a synorogenic basin complex: the Upper Carboniferous of Northwest Europe*. Glasgow: Blackie, p. 43-52.

LEUTWEIN, F., SONET, J. & ZIMMERMAN, J.L. 1972. Dykes basiques du Massif Amoricain Septentrional. Contribution à leur étude géochronologique. *Cent. Rech. Habd. Séance Acad. Sci. Paris*, **D275**, p. 1327-1329.

LEWIS, C.L.E., GREEN, P.F., CARTER, A. & HURFORD, A.J. 1992. Elevated K/T palaeotemperatures throughout Northwest England: three kilometres of Tertiary erosion? *Earth and Planetary Science Letters*, **112**, p. 131-145.

LITHGOW-BERTOLLONI, C. & SILVER, P.G. 1998. Dynamic topography, plate driving forces and the African superswell. *Nature,* **395,** p. 269-272.

LIVERMORE, R.A. & SMITH, A.G. 1985. Some boundary conditions for the evolution of the Mediterranean Region. *In:* STANLEY, D.J. & WEZEL, F.C. (eds.), *Geological Evolution of the Mediterranean Basin*. Raimond Selli commemorative volume. Berlin: Springer-Verlag, p. 83-100.

LLOYD, A.J. 1963. Upper Jurassic rocks beneath the Bristol Channel. *Nature*, **198**, p. 375-376.

LOW, P.F. 1976. Viscosity of interlayer water in montmorillonite. *Proceedings of the American Soil Society*, **40**, p. 500-505.

LUNDIN, E.R. & DORÉ, A.G. 2002. Mid-Cenozoic post-breakup deformation in the 'passive' margins bordering the Norwegian-Greenland Sea. *Marine and Petroleum Geology,* **19,** p. 79-93.

LUNDIN, E.R. & DORÉ, A.G. 2005*a*. NE Atlantic break-up: a re-examination of the Iceland mantle plume model and the Atlantic – Arctic linkage. *In:* DORÉ, A.G. & VINING, B.A. (eds.), *Petroleum Geology: North-West Europe and Global Perspectives – Proceedings of the 6th Petroleum Geology Conference.* Geological Society, London, p. 739-754.

LUNDIN, E.R. & DORÉ, A.G. 2005*b*. Fixity of the Iceland "hotspot" on the Mid-Atlantic Ridge: Observational evidence, mechanisms, and implications for Atlantic volcanic margins. *In:* FOULGER, G.R., NATLAND, J.N., PRESNALL, D.C. & ANDERSON, D.L. (eds.), *Plates, Plumes and Paradigms.* GSA Special Paper **388,** p. 627-652.

LUO, X. & VASSEUR, G. 1995. Modelling of pore pressure evolution associated with sedimentation and uplift in sedimentary basins. *Basin Research,* **7,** p. 35-52.

MADDOX, S.J., BLOW, R. & HARDMAN, M. 1995. Hydrocarbon prospectivity of the Central Irish Sea Basin with reference to Block 42/12, offshore Ireland. *In:* CROKER, P.F. & SHANNON, P.M. (eds.), *The Petroleum Geology of Ireland's Offshore basins*. Geological Society, London. Special Publications, **93**, p. 59-77.

MACGREGOR, D.S., 1995. Hydrocarbon habitat and classification of inverted rift basins. *In:* BUCHANAN, J.G. & BUCHANAN, P.G. (eds), *Basin Inversion.* Geological Society, London. Special Publications, **88**, p. 83-93.

MACLENNAN, J. & LOVELL, B. 2002. Control of regional sea level by surface uplift and subsidence caused by magmatic underplating of Earth's crust. *Geology,* **30,** p. 675-678.

MACKAY, L.M., TURNER, J., JONES, S.M. & WHITE, N.J. 2005. Cenozoic vertical motions in the Moray Firth Basin associated with initiation of the Iceland Plume. *Tectonics,* **24,** 5004, doi:10.1029/2004TC001683.

MAGARA, K., 1968. Compaction and migration of fluids in Miocene mudstones, Nagaoka Plain, Japan. *AAPG Bulletin,* **52 (12),** p. 2466-2501.

MAGARA, K. 1976. Thickness of removed sedimentary rocks, palaeopore pressure and palaeotemperature, Southwestern Canada Basin. *AAPG Bulletin*, **60 (4),** p. 554-565.

MAGARA, K. 1977. Water expulsion from clastic sediments during compaction – directions and volumes. *AAPG Bulletin*, **60**, p. 543-553.

MAGARA, K. 1978. Compaction and Fluid Migration. *Developments in Petroleum Science,* **9.** Amsterdam: Elsevier.

MAGARA, K. 1979. Structured water and its significance in primary oil migration. *Bulletin of Canadian Petroleum Geology,* **27**, p. 87-92.

MAGARA, K. 1980. Comparison of porosity-depth relationships of shale and sandstone. *Journal of Petroleum Geology*, **3 (2),** p. 175-185.

MAINGARM, S., IZZAT, C., WHITTINGTON, R.J. & FITCHES, W.R. 1999. Tectonic evolution of the southern-Central Irish Sea Basin. *Journal of Petroleum Geology,* **22,** p. 287-304.

MARIE, J.P.P. 1975. Rotliegendes stratigraphy and diagenesis. *In:* WOODLAND, A.W. (ed.), *Petroleum and the Continental Shelf of North-west Europe, Volume 1, Geology,* Applied Science Publishers, p. 205-211.

MARION, D., NUR, A., YIN, H. & HAN, D. 1992. Compressional velocity and porosity in sand–clay mixtures. *Geophysics*, **57**, p. 554– 563.

MASEK, J.G., ISACKS, B.L., GUBBELS, T.L. & FIELDING, E.J. 1994. Erosion and tectonics at the margins of continental plateaus. *Journal of Geophysical Research,* **99B**, p. 13941-13956.

MASSON, D.G. & MILES, P.R. 1986. Development and hydrocarbon potential of Mesozoic sedimentary basins around margins of North Atlantic. *AAPG Bulletin*, **70**, p. 721-729.

MAVKO, G., MUKERJI, T. & DVORKIN, J. 1998. *The Rock Physics Handbook*. Cambridge: Cambridge University Press.

MAVROMATIDIS, A. & HILLIS, R.R. 2005. Quantification of exhumation in the Eromanga Basin and its implications for hydrocarbon exploration. *Petroleum Geoscience,* **11,** p. 79-92.

MAVROMATIDIS, A. 2007. Two layer model of lithospheric compression and uplift/exhumation in an intracratonic setting: an example from the Cooper–Eromanga Basins, Australia. *International Journal of Earth Science (Geol Rundsch),* **97**, p. 623–634.

MAXWELL, J.C., 1960. Experiments on the compaction and cementation of sand. In: GRIGGS, D.T. & HANDIN, J. (eds.), *Rock deformation,* Geological Society of America Memoir 79, Boulder, Colorado, p. 105-312.

MAYNARD, J.R., HOFMANN, W., DUNAY, R.E., BENTHAM, P.N., DEAN, K.P. & WATSON, I. 1997. The Carboniferous of western Europe: the development of a petroleum system. *Petroleum Geoscience*, **3**, p. 97-115.

MCBRIDE, E.F. 1984. Rules of sandstone diagenesis related to reservoir quality. *Trans Gulf Coast Association of Geologists Society 34th Annual Meeting, Shreveport, Louisiana*, p. 137-139.

MCCANN, T. & SHANNON, P.M. 1994. Late Mesozoic reactivation of Variscan faults in the North Celtic Sea Basin, Ireland. *Marine and Petroleum Geology,* **11(1)**, p. 94–103.

MCGEARY, S., CHEADLE, M.J., WARNER, M.R. & BLUNDELL, D.J. 1987. Crustal structure of the continental shelf around Britain derived from BIRPS deep seismic reflection profiling. *In:* BROOKS, J. & GLENNIE, K. (eds.), *Petroleum Geology of North West Europe.* London: Graham & Trotman, p. 33-41.

MCKENZIE, D. 1978. Some remarks on the development of sedimentary basins. *Earth and Planetary Sciences Letters,* **40,** p. 25-32.

MCKENZIE, D. 1984. A possible mechanism for epeirogenic uplift. *Nature,* **307,** p. 616-618.

MCMAHON, N.A. & TURNER, J. 1998. The documentation of a latest Jurassic-earliest Cretaceous uplift throughout southern England and adjacent offshore areas. *In*: UNDERHILL, J.R. (ed.), *Development, Evolution and Petroleum Geology of the Wessex Basin.* Geological Society, London, Special Publications, **133,** p. 215-240.

MCMAHON, N.A. & UNDERHILL, J.R. 1995. The regional stratigraphy of the southwest United Kingdom and adjacent offshore areas with particular reference to the major intra-Cretaceous unconformity. *In*: CROKER, P.F. & SHANNON, P.M. (eds.), *The Petroleum Geology of Ireland's Offshore Basins*. Geological Society, London, Special Publications, **93,** p. 323-325.

MCTAVISH, R.A. 1998. The role of overpressure in the retardation of organic matter maturation. *Journal of Petroleum Geology*, **21**, p. 153–185.

MEADOWS, N.S., TRUEBLOOD, S.P., HARDMAN, M. & COWAN, G. 1997. *Petroleum Geology of the Irish Sea and Adjacent Areas*. Geological Society, London, Special Publications, **124**.

MEIER, L. & EISBACHER, G.H. 1991. Crustal kinematics and deep structure of the Northern Rhine Graben. *Tectonics*, **10**, p. 621-630.

MEISSNER, F.F. 1978. Petroleum geology of the Bakken Formation, Williston Basin, North Dakota and Montana: Proceedings of 1978 Williston Basin Symposium, September 24-27. *Montana Geological Society Billings*, p. 207-227.

MENPES, R.J. & HILLIS, R.R. 1995. Quantification of Tertiary exhumation from sonic velocity data, Celtic Sea/South-Western Approaches. *In:* BUCHANAN, J.G. & BUCHANAN, P.G. (eds.), *Basin Inversion.* Geological Society, London, Special Publications, **88,** p. 191-207.

MIDDLETON, D.W.J., PARNELL, J., GREEN, P.F., XU, G. & MCSHERRY, M. 2001. Hot fluid flow events in Atlantic margin basins: an example from the Rathlin Basin. *In:* SHANNON, P.M., HAUGHTON, P.D.W. & CORCORAN, D.V. (eds.), *The Petroleum Exploration of Ireland's Offshore Sedimentary Basins.* Geological Society, London, Special Publications, **188,** p. 91-105.

MILIORIZOS, M., RUFFELL, A. & BROOKS, M., 2004. Variscan structure of the inner Bristol Channel, UK. *Journal of the Geological Society of London*, **161 (1),** p. 31-44.

MILLSON, J.A. 1987. The Jurassic evolution of the Celtic Sea basins. *In:* BRROKS, J. & GLENNIE, K.W. (eds.), *Petroleum Geology of Northwest Europe*. London: Graham & Trotman, **2**, p. 599-610.

MOLNAR, P. & ENGLAND, P. 1990. Late Cenozoic uplift of mountain ranges and global climate change: chicken or egg? *Nature,* **346,** p. 29-34.

MOORE, L.R. 1945. The geological sequence of the South Wales Coalfield: the south crop and Caerphilly basin and its correlation with the Taff Valley sequence. *Proceedings of the South Wales Institute of Engineers*, **60**, p. 141-227.

MOORE, L.R. 1947. The sequence and structure of the southern portion of the east crop of the South Wales Coalfield. *Quarterly Journal of the Geological Society of London*, **103**, p. 261-300.

MOORE, L.R. & COX, A.H. 1943. The Coal Measure sequence in the Taff Valley, Glamorgan and its correlation with the Rhondda Valley sequence. *Proceedings of the South Wales Institute of Engineers*, **59**, p. 189-224.

MORTON, A.C. & PARSON, L.M. 1988. *Early Tertiary volcanism and the opening of the NE Atlantic*. Geological Society, London, Special Publications, **39**. 477p.

MORTON, A.C., HALLSWORTH, C.R. & WILKINSON, G.C. 1993. Stratigraphic evolution of sand provenance during Palaeocene deposition in the Northern North Sea area. *In:* PARKER, J.R. (ed.), *Petroleum Geology of Northwest Europe: Proceedings of the 4th Conference.* Geological Society, London, p. 73-84.

MOSAR, J., LEWIS, G. & TORSVIK, T.H. 2002. North Atlantic sea-floor spreading rates: implications for the Tertiary development of inversion structures of the Norwegian-Greenland Sea. *Journal of the Geological Society of London,* **159,** p. 503-515.

MÜLLER, B., ZOBACK, M.L., FUCHS, K., MASTIN, L., GREGERSEN, S., STEPHANSSON, O. & LJUNGGREN, C. 1992. Regional patterns of tectonic stress in Europe. *Journal of Geophysical Research,* **97B,** p. 11783-11803.

MURDOCH, L.M., MUSGROVE, F.M. & PERRY, J.S. 1995. Tertiary uplift and inversion history in the North Celtic Sea Basin and its influence on source rock maturity. *In*: CROKER, P.F. & SHANNON, P.M. (eds.), *The Petroleum Geology of Ireland's Offshore Basins*. Geological Society, London, Special Publications, **93,** p. 297-319.

MURRAY, J.W. 1992. Palaeogene and Neogene. *In:* COPE, J.C.W., INGHAM, J.K. & RAWSON, P.F. (eds.), *Atlas of Palaeogeography and Lithofacies.* Geological Society, London, Memoir, **13,** p. 141-147.

MUSSETT, A.E., DAGLEY, P. & ECKFORD, M. 1976. The British Tertiary igneous province: palaeomagnetism and ages of dykes, Lundy Island, Bristol Channel. *Geophysical Journal of the Royal Astronomical Society,* **46,** p. 595-603.

MUSSETT, A.E., DAGLEY, P. & SKELHORN, R.R. 1988. Time and duration of activity in the British Tertiary Igneous Province. *In:* MORTON, A.C. & PARSON, L.M. (eds.), *Early Tertiary Volcanism and the Opening of the NE Atlantic.* Geological Society, London, Special Publications, **39,** p. 337-348.

NADIN, P.A. & KUSZNIR, N.J. 1995. Palaeocene uplift and Eocene subsidence in the northern North Sea Basin from 2D forward and reverse stratigraphic modelling. *Journal of the Geological Society of London,* **152,** p. 833-848.

NADIN, P.A., KUSZNIR, N.J. & TOTH, J. 1995. Transient regional uplift in the Early Tertiary of the northern North Sea and the development of the Iceland Plume. *Journal of the Geological Society of London,* **152,** p. 953-958.

NAESER, C.W. & FAUL, H. 1969. Fission track annealing in apatite and sphene. *Journal of Geophysical Research,* **74,** p. 705-710.

NAGTEGAAL, P.J.C., 1978. Sandstone instability as a function of burial diagenesis. *Journal of the Geological Society of London,* **135**, p. 101-105

NALPAS, T., LE DOUARAN, S., BRUN, J-P., UNTERNEHR, P. & RICHERT, J-P. 1995. Inversion of the Broad Fourteens Basin (offshore Netherlands), a small-scale model investigation. *Sedimentary Geology*, **95**, p. 237– 250.

NAYLOR, D. & MOUNTENEY, S.N. 1975. *Geology of the North West European Continental Shelf, Vol. 1: The West British Shelf*. London: Graham & Trotman.

NAYLOR, D. & SHANNON, P.M. 1982. *Geology of Offshore Ireland and West Britain*. London: Graham and Trotman.

NAYLOR, D., HAUGHEY, N., CLAYTON, G. & GRAHAM, J.R. 1993. The Kish Bank Basin, offshore Ireland. *In:* PARKER, J.R. (ed.), *Petroleum Geology of Northwest Europe: Proceedings of the 4th Conference.* Geological Society, London, p. 845-855.

NEMCOK, M., R. GAYER, & M. MILIORIZOS (1995). Structural analysis of the inverted Bristol Channel Basin: implications for the geometry and timing of fracture porosity. *In:* BUCHANAN, J.G. & BUCHANAN, P. G. (eds.), *Basin Inversion*. Geological Society, London. Special Publications, **88**, p. 355-392.

NIELESEN, S.B. & HANSEN, D.L. 2000. Physical explanation of the formation and evolution of inversion zones and marginal troughs. *Geology,* **28.** p. 875-878.

NIELSEN, S.B., THOMSEN, E., HANSEN, D.L. & CLAUSEN, O.R. 2005. Plate-wide stress relaxation explains European Palaeocene basin inversions. *Nature,* **435,** p. 195-198.

NIELSEN, S.B., STEPHENSON, R. & THOMSEN, E. 2007. Dynamics of Mid-Palaeocene North Atlantic rifting linked with European intra-plate deformations. *Nature*, **450**, p. 1071-1074.

NIKISHIN, A.M., CLOETINGH, S., LOBKOVSKY, L.I., BUROV, E.B. & LANKREIJER, A.C. 1993. Continental lithosphere folding in Central Asia (Part I): Constraints from geological observations. *Tectonophysics*, **226**, p. 59-72.

NUR, A. & SIMMONS, G. 1969. Stress-induced velocity anisotropy in rock: an experimental study. *Journal of Geophysical Research*, **74**, p. 6667-6674.

NUR, A., MARION, D. & YIN, H. 1991. Wave velocities in sediments. *In:* HOVEM, J.M. (ed.), *Shear waves in Marine Sediments*, Kluwer Academic Publishers, p. 131-140.

NUR, A., MAVKO, G., DVORKIN, J. & GALMUNDI, D. 1998. Critical porosity; a key relating physical properties to porosity in rocks. *The Leading Edge*, **17**, p. 357-362.

OLDOW, J.S., BALLY, A.W., AVE LALLEMENT, H.G. & LEEMAN, W.P. 1989. Phanerozoic evolution of the North American cordillera; United States and Canada. *In:* BALLY, A.W. & PALMER, A.R. (eds.), *The Geology of North America – An overview*. The Geology of North America, **A**. Washington D.C.: The Geological Society of America, p. 139-232.

OLIVET, J-L., BONNIN, J., BEUZART, P. & AUZENDE, J-M. 1984. *Cinématique de l'Atlantique Nord et Central*. Publ. Cent. Nat. Expl. Oceans. Rap. Sci. Tech, **54**. 108p.

OLLIER, G.D. 1982. The Great Escarpment of eastern Australia: tectonic and geomorphic significance. *Journal of the Geological Society of Australia,* **29,** p. 13-23.

OSBORNE, M.J. & SWARBRICK, R.E. 1997. Mechanisms for generating overpressure in sedimentary basins: a reevaluation. *AAPG Bulletin,* **81,** p. 1023-1041.

O'SULLIVAN, P.B., FOSTER, D.A., KOHN, B.P. & GLEADOW, A.J.W. 1996. Multiple postorogenic denudation events: An example from the eastern Lachlan fold belt, Australia. *Geology,* **24,** p. 563-566.

O'SULLIVAN, P.B., MITCHELL, M.M., O'SULLIVAN, A.J., KOHN, B.P. & GLEADOW, A.J.W. 2000. Thermotectonic history of the Bassian Rise, Australia: implications for the breakup of eastern Gondwana along Australia's southeastern margins. *Earth and Planetary Science Letters,* **182,** p. 31-47.

PARNELL, J., CAREY, P.F., GREEN, P. & DUNCAN, W. 1999. Hydrocarbon migration history, West of Shetland: integrated fluid inclusion and fission track studies. *In*: FLEET, A.J. & BOLDY, S.A.R. (eds.), *Petroleum Geology of Northwest Europe: Proceedings of the 5th Conference.* Geological Society, London, p. 613-625.

PARNELL, J., GREEN, P.F., WATT, G. & MIDDLETON, D. 2005*a.* Thermal history and oil charge on the UK Atlantic margin. *Petroleum Geoscience,* **11,** p. 99-112.

PARNELL, J., OSINSKI, G.R., LEE, P., GREEN, P.F. & BARON, M.J. 2005*b*. Thermal alteration of organic matter in an impact crater and the duration of post impact heating. *Geology,* **33,** p. 373-376.

PARRY, C. 1966. *The effects of differential subsidence on the principal coal seams of Ammanian age in the eastern part of the South Wales Coalfield and the factors controlling sedimentation*. Unpublished MSc thesis, Univeristy of Wales, Swansea, UK.

PATERSON, M.S., 1973. Non-hydrostatic thermodynamics and its geologic applications. *Reviews in Geophysics and Space Physics,* **11**, p. 355-359.

PAUL, T. & FITZGERALD, P.F. 1992. Transmission electron microscope investigation of fission tracks in apatite. *American Mineralogist,* **77,** p. 336-344.

PAZZAGLIA, F.J. & GARDNER, T.W. 1994. Late Cenozoic flexural deformation of the middle United-States Atlantic passive margin. *Journal of Geophysical Research, Solid Earth Section*, **99**, p. 12143–12157.

PEARSON, M.J. & RUSSELL, M.A. 2000. Subsidence and erosion in the Pennine Carboniferous Basin, England: lithological and thermal constraints on maturity modelling. *Journal of the Geological Society of London,* **157,** p. 471-482.

PENN, I.E. & EVANS, C.D.R. 1976. The Middle Jurassic (mainly Bathonian) of Cardigan Bay and its palaeogeographical significance. *Report of the Institute of Geological Sciences*, No. 76/6, HMSO.

PENN, I.E., CHADWICK, R.A., HOLLOWAY, S., ROBERTS, G., PHARAOH, T.C., ALLSOP, J.M., HULBERT, A.G. & BURNS, I.M. 1987. Prinicipal features of the hydrocarbon prospectivity of the Wessex-Channel Basin. *In:* BROOKS, J. & GLENNIE, K.W. (eds.), *Petroleum Geology of northwest Europe*. London: Graham & Trotman, p. 109–118.

PERSANO, C., STUART, F.M., BISHOP, P. & BARFOD, D.N. 2002. Apatite (U-Th)/He age constraints on the development of the Great Escarpment on the southeastern Australian passive margin. *Earth and Planetary Science Letters,* **200,** p. 79-90.

PETRIE, S.H., BROWN, J.R., GRANGER, P.J. & LOVELL, J.P.B. 1989. Mesozoic history of the Celtic Sea Basins. *American Association of Petroleum Geology Memoir*, **46**, p. 433-444.

PINET, B., MONTADERT, L., MASCLE, A., CAZES, M. & BOIS, C. 1987. New insight on the structure and the formation of sedimentary basins from deep seismic profiling in Western Europe. *In:* BROOKS, J. & GLENNIE, K.W. (eds.), *Petroleum Geology of Northwest Europe*. London: Graham & Trotman, **1**, p. 11-31.

PIRMEZ, C., FLOOD, R.D., BAPTISTE, J., HEZHU, Y. & MANLEY, R.L. 1997. Clay content, porosity and velocity of Amazon fan sediments determined from ODP Leg 155 cores and wireline logs. *Geophysical Research Letters*, **24** (3), p. 317-320.

PITTMAN, E.D. & LARESE, R.E. 1991. Compaction of lithic sands: experimental results and applications. *AAPG Bulletin*, **75**, p. 1279-1299.

PLINT, A.G. 1982. Eocene sedimentation and tectonics in the Hampshire Basin. *Journal of the Geological Society of London*, **139** (3), p. 249-254.

POELCHAU, H. S. & ZWACH, C. 1994. Basin simulation and diagenetic models: Albian Cadotte Sandstone, Alberta Deep Basin, Canada. *Berichte des Forschungszentrums Jülich-Jül*, **2882**, p. B1.1–142.

POELCHAU, H.S., BAKER, D.R., HANTSCHEL, T.H., HORSFIELD, B. & WYGRALA, B. 1997. Basin simulation and the design of the Conceptual Basin Model. *In:* WELTE, D.H., HORSFIELD, B. & BAKER, D.R. (eds.), *Petroleum and Basin Evolution: Insights from Petroleum Geochemistry, Geology and Basin Modelling*. Berlin: Springer Verlag. p. 5-70.

POWELL, D.W. 1956. Gravity and magnetic anomalies in North Wales. *Quarterly Journal of the Geological Society of London,* **111,** p. 375-397.

POWERS, M.C. 1967. Fluid release mechanisms in compacting marine mudrocks and their importance in oil exploration. *AAPG Bulletin*, **51**, p. 1240-1254.

PRAEG, D., STOKER, M.S., SHANNON, P.M., CERAMICOLA, S., HJELSTUN, B., LABERG, J.S. & MATHIESEN, A. 2005. Episodic Cenozoic tectonism and the development of the NW European 'passive' continental margin. *Marine and Petroleum Geology,* **22**, p. 1007-1030.

PRODEHL, C., MÜLLER, ST., GLAHN, A., GUTSCHER, M. & HAAK, V. 1992. Lithospheric cross sections of the European Cenozoic Rift System. *Tectonophysics*, **208**, p. 119-138.

PRODEHL, C., MÜLLER, ST. & HAAK, V. 1995. The European Cenozoic Rift System. *In:* OLSEN, K.H. (ed.), *Continental Rifts: Evolution, Structure, Tectonics. Developments in Geotectonics vol. 25*. Amsterdam: Elsevier, p. 133-212.

PRYOR, W.A., 1973. Permeability-porosity patterns and variations in some Holocene sand bodies. *AAPG Bulletin,* **57**, p. 162-189.

RAIGA-CLEMENCEAU, J., 1988. Taking into account the conductivity and contribution of shale laminations when evaluating closely interlaminated sand-shale hydrocarbon bearing reservoirs. *SPWLA 29th Annual Symposium Transactions,* paper DD, p. 1-14.

RAWSON, P.F. & RILEY, L.A. 1982. Latest Jurassic-Early Cretaceous events and the "late Cimmerian unconformity" in North Sea area. *AAPG Bulletin*, **66 (12)**, p. 2628-2648.

RAWSON, P.F., CURRY, D., DILLEY, F.C., HANCOCK, J.M., KENNEDY, W.J., NEALE, J.W., WOOD, C.J. & WORSSAM, B.C. 1978. *A correlation of Cretaceous rocks in the British Isles*. Geological Society, London, Special Report, **9**.

RAYMER, L.L., HUNT, E.R. & GARDNER, J.J., 1980. An improved sonic transit time to porosity transform. *SPWLA 21st Annual Symposium Transactions,* paper P, Tulsa, Oklahoma.

REED, J.S., ERIKSSON, K.A. & KOWALEWSKI, M. 2005. Climatic, depositional and burial controls on diagenesis of Appalachian Carboniferous sandstones: qualitative and quantitative methods. *Sedimentary Geology*, **176**, p. 225-246.

REIKE, H.H. & CHILLINGARIAN, G.V. 1974. *Compaction of Agrillaceous Sediments*. Amsterdam: Elsevier. 424p.

REINECKER, J., HEIDBACH, O. & MUELLER, B. 2003. The 2003 release of the World Stress Map (available online at http://www.world-stress-map.org).

RICHARDSON, L. 1911. The Rhaetic and contiguous deposits of west, mid and part of east Somerset. *Quarterly Journal of the Geological Society of London*, **67**, p. 1-74.

RICHARDSON, R.M. 1992. Ridge forces, absolute plate motions and the intraplate stress field. *Journal of Geophysical Research*, **97**, p. 11739-11748.

RIDER, M.H., 1996. *The Geological Interpretation of Well Logs (2nd Edition).* Caithness: Whittles Publishing.

RIIS, F. & FJELDSKAAR, W. 1992. On the magnitude of the late Tertiary and Quaternary erosion and its significance for the uplift of Scandinavia and the Barents Sea. *In:* LARSEN, R.M., BREKKE, H., LARSEN, B.T. & TELLERNAS, E. (eds.), *Structural and tectonic modelling and its application to petroleum geology.* NPF Special Publication, **1,** p. 163-185.

ROBERTS, A.M. & YIELDING, G. 1991. Deformation around basin-margin faults in the North Sea/mid-Norway rift. *In*: ROBERTS, A.M., YIELDING, G. & FREEMAN, B. (eds.), *The Geometry of Normal Faults*. Geological Society, London, Special Publications, **56**, p. 61-78.

ROBERTS, D.G. 1989. Basin inversion in and around the British Isles. *In*: COOPER, M.A. & WILLIAMS, G.D. (eds.), *Inversion Tectonics*. Geological Society, London, Special Publications, **44**, p. 131-150.

ROBERTS, D.G., THOMPSON, M., MITCHENER, B., HOSSACK, J., CARMICHAEL, S. & BJØRNSETH, H-M. 1999. Palaeozoic to Tertiary rift and basin dynamics: mid-Norway to the Bay of Biscay – a context for hydrocarbon prospectivity in the deep water frontier. *In*: FLEET, A.J. & BOLDY, S.A.R. (eds.), *Petroleum Geology of Northwest Europe: Proceedings of the 5th Conference,* p. 7-40.

ROBERTSON, T. 1933. The Geology of the South Wales Coalfield, Part 5. The country around Merthyr Tydfil, 2nd Edition. *Memoir of the Geological Survey of Great Britain*.

ROBINSON, K.W., SHANNON, P.M. & YOUNG, D. 1981. The Fastnet Basin: an integrated analysis. *In:* ILLING, L.V. & HOBSON, G.D. (eds.), *Petroleum Geology of the Continental Shelf of North-West Europe*. London: Heyden, p. 444-454.

ROHRMAN, M. & VAN DER BEEK, P. 1996. Cenozoic postrift domal uplift of North Atlantic margins: An asthenospheric diapirism model. *Geology,* **24,** p. 901-904.

ROHRMAN, M., VAN DER BEEK, P., VAN DER HILST, R.D. & REEMST, P. 2002. Timing and mechanisms of North Atlantic Cenozoic uplift: evidence for mantle upwelling. *In*: DORÉ, A.G., CARTWRIGHT, J., STOKER, M.S., TURNER, J.P. & WHITE, N. (eds.), *Exhumation of the North Atlantic Margin: Timing, Mechanisms and Implications for Petroleum Exploration.* Geological Society, London, Special Publications, **196**, p. 27-43.

ROHRMAN, M., VAN DER BEEK, P., ANDRIESSEN, P. & CLOETINGH, S. 1995. Meso-Cenozoic morphotectonic evolution of southern Norway: Neogene domal uplift inferred from apatite fission track thermochronology. *Tectonics,* **14,** p. 704-718.

ROSS, C.A. & ROSS, J.R.P. 1985. Paleozoic tectonics and sedimentation in West Texas, southern New Mexico and southern Arizona. *In:* DICKERSON, P.W. & MUEHLBERGER, W.R. (eds.), *West Texas Geological Society Field Conference*. Publication 85-81, p. 221-230.

ROSS, C.A. & ROSS, J.R.P. 1986. Paleozoic palaeotectonics and sedimentation in Arizona and New Mexico. *American Association of Petroleum Geologists Memoir,* **41**, p. 653-668.

ROWELL, P. 1995. Tectono-stratigraphy of the North Celtic Sea Basin. *In:* CROKER, P.F. & SHANNON, P.M. (eds.), *The Petroleum Geology of Ireland's Offshore basins*. Geological Society, London. Special Publications, **93**, p. 101-137.

ROWLEY, E. & WHITE, N. 1998. Inverse modelling of extension and denudation in the East Irish Sea and surrounding areas. *Earth and Planetary Science Letters*, **161**, p. 57-71.

RUBEY, W.W. & HUBBERT, M.K., 1959. Role of fluid pressure in mechanics of overthrust faulting II. *Bulletin of the Geological Society of America,* **70**, p. 167-206

RUFFELL, A.H. 1992. Early to mid-Cretaceous tectonics and unconformities of the Wessex Basin (southern England). *Journal of the Geological Society of London,* **149,** p. 443-454.

RUFFELL, A.H. & COWARD, M.P. 1992. Basement tectonics and their relationship to Mesozoic mega sequences in the Celtic Seas and Bristol Channel area. *In:* PARNELL, J. (ed.), *Basins on the Atlantic Seaboard: Petroleum Geology, Sedimentology and Basin Evolution.* Geological Society, London, Special Publications, **62,** p. 385-394.

SANDEMAN, H.A., CHEN, Y., CLARK, A.H. & FARRAR, E. 1995. Constraints on the P-T conditions and age of emplacement of the Lizard Ophiolite, Cornwall: plagioclase thermobarometry and $^{40}Ar/^{39}Ar$ geochronology of basal amphibolites. *Journal of Earth Sciences*, **32**, p. 261-272.

SARMIENTO, R., 1961. Geological factors influencing porosity estimates from velocity logs. *AAPG Bulletin,* **45** (5), p.633-644.

SAVOSTIN, L.A., SIBUET, J-C., ZONNENSCHAIN, L.P., LE PICHON, X. & ROULET, M-J. 1986. Kinematic evolution of the Tethys Belt from the Atlantic Ocean to the Pamirs since the Triassic, *Tectonophysics*, **123**, p. 1-35.

SCHENK, C.J., 1983. Textural and structural characteristics of some experimentally formed Aeolian strata. *Developments in Sedimentology,* **38**, p. 41-49.

SCHLUMBERGER, 1985. *Log interpretation charts.* Schlumberger publication.

SCHMERTMANN, J.H. 1955. The undisturbed consolidation behaviour of clay. *Transactions of the American Society of Civil Engineers*, **120**, p. 1201-1233.

SCHMIDT, G. W., 1973. Interstitial water composition and geochemistry of deep Gulf Coast shales and sandstones. *AAPG Bulletin,* **57** (2), p. 321-337.

SCHMOKER, J.W. & HALLEY, R.B. 1982. Carbonate porosity versus depth: a predictable relation for south Florida. *AAPG Bulletin*, **66**, p. 2561–2570.

SCHOLLE, P.A. 1977. Chalk diagenesis and its relation to petroleum exploration: oil from chalks, a modern miracle? *AAPG Bulletin,* **61,** p. 981-1009.

SCHOPPER, J.R. 1982. Porosity and Permeability. *In:* HELLWEGE, K.H. (ed.), *Landolt-Börnstein Numerical data and functional relationships in science and technology, vol 1. Physical Properties of Rocks*. Berlin: Springer, p. 184-303.

SCLATER, J.G. & CHRISTIE, P.A.F., 1980. Continental stretching: An explanation of the post Mid-Cretaceous subsidence of the Central North Sea Basin. *Journal of Geophysical Research,* **85** (B7), p.3711-3739

SCOTCHMAN, I.C. 2001. Petroleum geochemistry of the Lower and Middle Jurassic in Atlantic margin basins of Ireland and the UK. *In:* SHANNON, P.M., HAUGHTON, P.D.W. & CORCORAN, D.V. (eds.), *The Petroleum Exploration of Ireland's Offshore Basins.* Geological Society, London, Special Publications, **188,** p. 31-60.

SCRUTTON, R.A. & BENTLEY, P.A.D. 1988. Major Cretaceous volcanic province in the southern Rockall Trough. *Earth and Planetary Science Letters,* **91,** p. 198-204.

SELLEY, R.C. 1978. Porosity gradients in the North Sea oil-bearing sandstones. *Journal of the Geological Society of London*, **135**, p.119-132.

SELLEY, R.C. & STONELEY, R. 1987. Petroleum habitat in South Dorset. *In:* BROOKS, J. & GLENNIE, K.W. (eds.), *Petroleum Geology of Northwest Europe*. London: Graham & Trotman, **1**, p.139-148.

SELLWOOD, B.W., SCOTT, J. & LUNN, G. 1986. Mesozoic basin evolution in southern England. *Proceedings of the Geologists Association*, **97**, p. 259–289.

SERRA, O., 1979. Diagraphies différées. Bases d'interprétation tome l: Acquisition des données Diagraphiques. *Bulletin centre rech expl-prod Elf Aquitaine Mem 1.* Paris: Technip. 328p.

SERRA, O., 1984. *Fundamentals of well-log interpretation 1. Acquisition of logging data*. United Kingdom: Elsevier.

SHANNON, P.M. 1991. The development of Irish offshore sedimentary basins. *Journal of the Geological Society of London,* **148**, p. 181–190.

SHANNON, P.M. & NAYLOR, D. 1998. An Assessment of Irish Offshore Basins and Petroleum Plays. *Journal of Petroleum Geology,* **21(2)**, p. 125–152.

SHERRIF, R.E. & GELDART, L.P. 1995. *Exploration Seismology 2nd Edition*. Cambridge: Cambridge University Press. 592p.

SHUMWAY, G. 1958. Sound velocity vs. temperature in water saturated sediments. *Geophysics*, **23** (3), p. 494-505.

SIBSON, R.H. 1995. Selective fault reactivation during basin inversion: potential for fluid redistribution through fault-valve action. *In:* BUCHANAN, J.G. & BUCHANAN, P.G. (eds.), *Basin Inversion.* Geological Society, London, Special Publications, **88,** p. 3-21.

SIBSON, R.H. 2007. An episode of fault-valve behaviour during compressional inversion? - the 2004 MJ6.8 Mid-Niigata Prefecture, Japan, earthquake sequence. *Earth and Planetary Science Letters*, doi: 10.1016/j.epsl.2007.02.031.

SIBUET, J. C., DYMENT, J., BOIS, C. & PINET, B. 1990. Crustal Structure of the Celtic Sea and Western Approaches from Gravity Data and Deep Seismic Profiles: Constraints on the Formation of Continental basins. *Journal of Geophysical Research,* **95(B7),** p. 10999–11020.

SMALLWOOD, J.R. & WHITE, R.S. 2002. Ridge-plume interaction in the North Atlantic and its influence on continental breakup and seafloor spreading. *In*: JOLLEY, D.W. & BELL, B.R. (eds.), *The North Atlantic Igneous Province: Stratigraphy, Tectonic, Volcanic and Magmatic Processes*. Geological Society, London, Special Publications, **197,** p. 15-37.

SMITH, A.J. 1984. Structural evolution of the English Channel region. *Ann. Soc. géol. Nord*, **53**, p.253-264.

SMITH, K., GATLIFF, R.W. & SMITH, N.J.P. 1994. Discussion on the amount of Tertiary erosion in the UK estimated using sonic velocity analysis. *Journal of the Geological Society of London*, **151**, p. 1041– 1044.

SORENSON, A.B. 2006. Stratigraphy, structure and petroleum potential of the Lady Franklin and Maniitsoq Basins, offshore southern West Greenland. *Petroleum Geoscience*, **14**, p. 221-234.

SQUIRRELL, H.C. & DOWNING, R.A. 1969. Geology of the South Wales Coalfield, Part 1. The country around Newport (Mon.). *Memoirs of the Geological Survey of Great Britain*, Sheet **249** (England and Wales).

STEVENSON, G.M. & BARRS, D.L. 1986. The paradox: A pull-apart basin of Pensylvanian age. *In:* PETERSEN, J.E. (ed.), *Palaeotectonics and sedimentation in the Rocky Mountain region, United States*. American Association of Petroleum Geologists Memoir, **41**, p. 513-539.

STEWART, S.A. & BAILEY, H.W. 1996. The Flamborough Tertiary outlier, UK southern North Sea. *Journal of the Geological Society of London,* **153,** p. 163-173.

STEWART, S.A., RUFFELL, A.H. & HARVEY, M.J. 1997. Relationship between basement-linked and gravity-driven fault systems in the UKCS salt basins. *Marine & Petroleum Geology,* **14,** p. 581-604.

STILLE, H. 1924. *Grundfragen der vergleichenden Tektonik.* Borntraeger, Berlin.

STOKER, M.S. 2002. Late Neogene development of the UK Atlantic margin. *In*: DORÉ, A.G., CARTWRIGHT, J., STOKER, M.S., TURNER, J.P. & WHITE, N. (eds.), *Exhumation of the North Atlantic Margin: Timing, Mechanisms and Implications for Petroleum Exploration.* Geological Society, London, Special Publications, **196**, p. 313-329.

STOKER, M.S., NIELSEN, T., VAN WEERING, T.C.E. & KUIJPERS, A. 2002. Towards an understanding of the Neogene tectonostratigraphic framework of the NE Atlantic margin between Ireland and the Faroe Islands. *Marine Geology,* **188,** p. 233-248.

STOKER, M.S., HOULT, R.J., NIELSEN, T., HJELSTUN, B.O., LABERG, J.S., SHANNON, P.M., PRAEG, D., MATHIESEN, A., VAN WEERING, T.C.E. & MCDONNELL, A. 2005*a*. Sedimentary and oceanographic responses to early Neogene compression on the NW European margin. *Marine and Petroleum Geology*, **22**, p. 1031–1044.

STOKER, M.S., PRAEG, D., SHANNON, P.M., HJELSTUEN, B.O., LABERG, J.S., NIELSEN, T, VAN WEERING, T.C.E., SERJUP, H.P. & EVANS, D. 2005*b.* Neogene evolution of the Atlantic continental margin of NW Europe (Lofoten Islands to SW Ireland): anything but passive. *In:* DORÉ, A.G. & VINING, B.A. (eds.), *Petroleum Geology: North-West Europe and Global Perspectives – Proceedings of the 6th Petroleum Geology Conference.* Geological Society, London, p. 1057-1076.

SUMMERFIELD, M.A. 1991. *Global Geomorphology.* Longman.

SWEENEY, J.J. & BURNHAM, A.K. 1990. Evaluation of a simple model of vitrinite reflectance based on chemical kinetics. *AAPG Bulletin,* **74,** p. 1559-1570.

SWIFT, A. & MARTILL, D.M. 1999. *Fossils of the Rhaetian Penarth Group. The Palaeontological Association*. London: Blackie.

TAPPIN, D.R., CHADWICK, R.A., JACKSON, A.A., WINGFIELD, R.T.R. & SMITH, N.J.P., 1994. *United Kingdom offshore regional report: The geology of Cardigan Bay and the Bristol Channel.* London: HMSO for the British Geological Survey. 107p

TANNER, H.C. 1999. The petroleum geology of the St George's Channel Basin. *In:* CROKER, P.E & O'LOUGHLIN, O. (eds.), *The Petroleum Exploration of Ireland's Offshore Basins Conference, Dublin, 29-30 April 1999, Extended Abstracts*. Petroleum Affairs Division, Department of the Marine and Natural Resources, Dublin, p. 44-45.

TATE, M.P. & DOBSON, M.R. 1989. Late Permian to early Mesozoic rifting and sedimentation offshore NW Ireland. *Marine and Petroleum Geology,* **6**, p. 49-59.

THOMAS, L.P. 1967. *A sedimentary study of the sandstones between the horizons of the Four-Foot Coal and the Gorllwyn Coal of the middle Coal Measures of the South Wales Coalfield*. Unpublished PhD Thesis, University of Wales, Swansea, UK.

THOMAS, L.P. 1974. The Westphalian Coal Measures in South Wales. *In:* OWEN, T.R. (ed.), *The Upper Paleozoic and Post-Paleozoic rocks of Wales*. Cardiff: University of Wales Press, p. 133-160.

THOMPSON, R.N. 1974. Primary basalts and magma genesis, I: Skye, Northwest Scotland. *Contributions to Mineralogy and Petrology,* **45,** p. 317-341.

THOMSON, K. 1995. Discussion on a latest Cretaceous hotspot and the southeasterly tilt of Britain. *Journal of the Geological Society of London,* **152,** p. 729.

THOMSON, K. & UNDERHILL, J.R. 1993. Controls on the development and evolution of structural styles in the Inner Moray Firth Basin. *In*: PARKER, J.R. (ed.), *Petroleum Geology of Northwest Europe: Proceedings of the 4th Conference.* Geological Society, London, p. 1167-1178.

THOMSON, K. & HILLIS, R.R. 1995. Tertiary structuration and erosion of the Inner Moray Firth. *In:* SCRUTTON, R.A., SHIMMIELD, G.B., STOKER, M.S. & TUDHOLPE, A.W. (eds.), *The tectonics, sedimentation and palaeooceanography of the North Atlantic region.* Geological Society, London, Special Publications, **90,** p. 249-269.

THOMSON, K., GREEN, P.F., WHITHAM, A.G., PRICE, S.P. & UNDERHILL, J.R. 1999*a*. New constraints on the thermal history of North-East Greenland from apatite fission-track analysis. *Geological Society of America Bulletin,* **111,** p. 1054-1068.

THOMSON, K., HEGARTY, K.A., MARSHALLSEA, S.J. & GREEN, P.F. 2002. Thermal and tectonic evolution of the Falkland Islands: implications for hydrocarbon exploration in the adjacent offshore region. *Marine and Petroleum Geology,* **19,** p. 95-116.

THOMSON, K., UNDERHILL, J.R., GREEN, P.F., BRAY, R.J. & GIBSON, H.J. 1999*b*. Evidence from apatite fission-track analysis for the post-Devonian burial and exhumation history of the northern Highlands, Scotland. *Marine and Petroleum Geology,* **16,** p. 27-39.

TICKELL, F.G. & HIATT, W.N., 1938. Effect of angularity of grains on porosity and permeability of unconsolidated sands. *AAPG Bulletin,* **22**, p. 1272-1274.

TILEY, R., MCKENZIE, D. & WHITE, N. 2003. The elastic thickness of the British Isles. *Journal of the Geological Society of London,* **160,** p. 499-502.

TILLMAN, R.W. & ALMON, W.R. 1979. *Diagenesis of Frontier formation offshore bar sandstones, Spearhead Ranch Field, Wyoming*. SEPM Special Publications, **26**, p. 337-378.

TIMUR, A. 1977. Temperature dependence of compressional and shear wave velocities in rocks. *Geophysics*, **42 (5)**, p. 950-956.

TISSOT, B.P. & WELTE, D.H. 1984. *Petroleum Formation and Occurrence (2nd edition).* New York: Springer-Verlag.

TOLLMANN, A. 1980. Grossetektonische Ergebnisse aus den Ostalpen im Sinne der Plattentektonik. *Mitt. österr. geol. Ges*., **71/72**, p. 37-44.

TOSAYA, C., NUR, A. 1982. The effects of diagenesis and clays on compressional velocities in rocks. *Geophysical Research Letters*, **9**, p. 5–8.

TRÜMPY, R. 1960. Palaeotectonic evolution of the central and western Alps. *Bulletin of the Geological Society of America*, **71**, p. 843-908.

TRÜMPY, R. 1980. Geology of Switzerland, A guide Book, part A. An outline of the geology of Switzerland. Basel: Wepf Publishers. 104p.

TUCKER, R.M. & ARTER, G. 1987. The tectonic evolution of the North Celtic Sea and Cardigan Bay basins with specific reference to basin inversion. *Tectonophysics,* **137,** p. 291-307.

TURNER, J.P. 1996. Gravity-driven nappes and their relation to palaeobathymetry: examples from West Africa and Cardigan Bay, UK. *In:* BUCHANAN, P.G. & NIEUWLAND, D.A. (eds.), *Modern Developments in Structural Interpretation, Validation and Modelling.* Geological Society, London, Special Publications, **99,** p. 345-362.

TURNER, J.P. 1997. Strike-slip fault reactivation in the Cardigan Bay basin. *Journal of the Geological Society of London,* **154,** p. 5-8.

TURNER, J.P. & WILLIAMS, G.D., 2004. Sedimentary basin inversion and intra-plate shortening. *Earth Science Reviews*, **65**, p. 277-304.

UMBGROVE, J.H.F. 1947. *The Pulse of the Earth (2nd Edition).* The Hague: Martinus Nijhoff.

UNDERHILL, J.R. & PARTINGTON, M.A. 1993. Jurassic thermal doming and deflation in the North Sea: implications of the sequence stratigraphic evidence. *In:* PARKER, J.R. (ed.), *Petroleum Geology of Northwest Europe: Proceedings of the 4th Conference.* Geological Society, London, p. 337-345.

UNDERHILL, J.R. & PATERSON, S. 1998. Genesis of tectonic inversion structures: seismic evidence for the development of key structures along the Purbeck – Isle of Wight disturbance. *Journal of the Geological Society of London,* **155,** p. 975-992.

UNOMAH, G.I. & EKWEOZOR, C.M. 1993. Application of vitrinite reflectance in reconstruction of tectonic features in Anambra Basin, Nigeria: implication for petroleum potential. *AAPG Bulletin*, **77**, p. 436– 451.

VAGNES, E., GABRIELSEN, R.H. & HAREMO, P. 1998. Late Cretaceous-Cenozoic intra-plate contractional deformation at the Norwegian continental shelf: timing, magnitude and regional implications. *Tectonophysics,* **300**, p. 29–46.

VAIL, P.R. & TODD, R.G. 1981. Northern North Sea Jurassic unconformities, chronostratigraphy and sea-level changes from seismic stratigraphy. *In:* ILLING, L.V. & HOBSON, G.D. (eds.), *Petroleum Geology of the Continental Shelf of Northwest Europe*. Institute of Petroleum, London. London: Heyden & Son, p. 216-235.

VAIL, P.R., MITCHUM JR., R.M. & THOMPSON, S. 1977. Seismic Stratigraphy and Global Changes of Sea Level, Part 4: Global Cycles of Relative Changes of Sea Level. *In:* PAYTON, C.E. (ed.), *Seismic Stratigraphy – applications to global hydrocarbon exploration*. American Association of Petroleum Geologists Memoir, **26**, Tulsa, p. 83-97.

VAN HOORN, B., 1987*a*. The South Celtic Sea/Bristol Channel Basin: origin, deformation and inversion history. *Techtonophysics*, **137**, p. 309-334.

VAN HOORN, B. 1987*b*. Structural evolution, timing and tectonic style of Sole Pit inversion. *Tectonophysics,* **137,** p. 239-284.

VAN WEES, J.D. & CLOETINGH, S. 1996. 3D Flexure and intraplate compression in the North Sea Basin. *Tectonophysics*, **266**, p. 343-359.

VAN WEES, J.D. & BEEKMAN, F. 2000. Lithosphere rheology during intraplate basin extension and inversion: inferences from automated modelling of four basins in western Europe. *Tectonophysics,* **320,** p. 219-242.

VEEVERS, J.J. (ed.) 2000. *Billion-year earth history of Australia and neighbours in Gondwanaland.* Sydney: Gemoc Press.

VORREN, T.O., RICHARDSON, G. & KNUTSEN, S-M. 1991. Cenozoic erosion and sedimentation in the western Barents Sea. *Marine and Petroleum Geology,* **8** (3), p. 317-340.
WALTON, K., 1987. The effective elastic moduli of a random packing of spheres. *Journal of the Mechanics and Physics of Solids*, **35**, p. 213-226.

WANG, Z. & NUR, A. 1992. *Seismic and acoustic velocities in reservoir rocks, Volume 2*. SEG Geophysics Reprint Series 10.

WAPLES, D.W. & COUPLES, G.D. 1998. Some thoughts on porosity reduction – rock mechanics, overpressure and fluid flow. *In:* DÜPPENBECKER, S.J. & ILIFFE, J.E. (eds.) *Basin Modelling: Practice and Progress*. Geological Society, London, Special Publications, **141**, p. 73-81.

WARE, P.D. 1999. *Application of Sonic Velocity Analysis to Quantify Tertiary Exhumation, East Irish Sea & Kish Bank Basin*. MPhil Thesis, University of Birmingham, UK.

WARE, P.D. & TURNER, J.P. 2002. Sonic velocity analysis of the Tertiary denudation of the Irish Sea basin. *In*: DORÉ, A.G., CARTWRIGHT, J., STOKER, M.S., TURNER, J.P. & WHITE, N. (eds.), *Exhumation of the North Atlantic Margin: Timing, Mechanisms and Implications for Petroleum Exploration.* Geological Society, London, Special Publications, **196**, p. 355-370.

WARRINGTON, G. & IVIMEY-COOK, H.C. 1995. The late Triassic and early Jurassic of coastal sections in west Somerset and South and mid-Glamorgan. *In:* TAYLOR, P.D. (ed.), *Field Geology of the British Jurassic*. London: Geological Society, p. 9-30.

WARRINGTON, G. & SCRIVNER, R.C. 1988. Late Permian fossils from Devon: regional geological implications. *Proceedings of the Ussher Society*, **7**, p. 95-96.

WARRINGTON, G., AUDLEY-CHARLES, M.G., ELLIOT, R.E., EVANS, W.B., IRVIMEY-COOK, H.C., KENT, P.E., ROBINSON, P.L., SHORTON, F.W. & TAYLOR, F.M. 1980. *A correlation of Triassic rocks in the British Isles*. Geological Society, London, Special Report, **13**. 78p.

WATERS, R.A. & LAWRENCE, D.J.D. 1987. The Geology of the South Wales Coalfield, Part 3: The Country around Cardiff, 3rd edition. *Memoirs of the British Geological Survey*, Sheet 263 (England and Wales).

WATERS, C.N., GLOVER, B.W. & POWELL, J.H. 1994. Structural synthesis of S Staffordshire, UK: implications of the Variscan evolution of the Pennine Basin. *Journal of the Geological Society of London*, **151**, p. 697-713.

WATSON, J. 1985. Northern Scotland as an Atlantic-North Sea divide. *Journal of the Geological Society of London,* **142,** p. 221-243.

WATTS, A.B. 2001. *Isostasy and Flexure of the Lithosphere.* Cambridge University Press.

WATTS, A.B., MCKERROW, W.S. & FIELDING, E. 2000. Lithospheric flexure, uplift and landscape evolution in south-central England. *Journal of the Geological Society of London,* **157,** p. 1169-1177.

WATTS, A.B., MCKERROW, W.S. & RICHARDS, K. 2005. Localized Quaternary uplift of south-central England. *Journal of the Geological Society of London,* **162,** p. 13-24.

WELCH, M.J. & TURNER, J.P., 2000. Triassic-Jurassic development of the St. George's Channel Basin, offshore Wales, UK. *Marine and Petroleum Geology*, **17**, p. 723-750.

WELLS, R.E., 1990. Palaeomagnetic rotations and the Cenozoic tectonics of the Cascade Arc, Washington, Oregon, and California. *Journal of Geophysical Research*, **95**, p. 19409-19417.

WENDT, A.S., VIDAL, O. & CHADDERTON, L.T. 2002. Experimental evidence for the pressure dependence of fission track annealing in apatite. *Earth and Planetary Science Letters,* **201,** p. 593-607.

WEISSEL, J.K. & KARNER, G.D. 1989. Flexural Uplift of Rift Flanks Due to Mechanical Unloading of the Lithosphere During Extension. *Journal of Geophysical Research,* **94B,** p. 13919-13950.

WHEELER, P. & WHITE, N. 2000. Quest for dynamic topography: Observations from Southeast Asia. *Geology,* **28,** p. 963-966.

WHITE, J.E., MARTINEAU-NICOLETIS, L. & MONASH, C. 1983. Measured anisotropy in Pierre Shale. *Geophysical Prospecting*, **31 (5)**, p. 709-725.

WHITE, N. & LOVELL, B. 1997. Measuring the pulse of a plume with the sedimentary record. *Nature,* **387,** p. 888-891.

WHITE, R.S. 1988. A hot-spot model for early Tertiary volcanism in the N Atlantic. *In:* MORTON, A.C. & PARSON, L.M. (eds.), *Early Tertiary Volcanism and the Opening of the NE Atlantic.* Geological Society, London, Special Publications, **39,** p. 3-13.

WHITE, R.S. 1992. Crustal structure and magmatism of North Atlantic continental margins. *Journal of the Geological Society of London,* **149,** p. 841-854.

WHITE, R.S. & MCKENZIE, D.P. 1989. Magmatism at Rift Zones: The Generation of Volcanic Continental Margins and Flood Basalts. *Journal of Geophysical Research,* **94B,** p. 7685-7729.

WHITE, R.S., SPENCE, G.D., FOWLER, S.R., MCKENZIE, D.P., WESTBROOK, G.K. & BOWEN, A.N. 1987. Magmatism at rifted continental margins. *Nature,* **330,** p. 439-444.

WHITTAKER, A. (ed.) 1985. *Atlas of Onshore sedimentary basins in England and Wales: Post Carboniferous Tectonics and stratigraphy*. Glasgow: Blackie.

WHITTAKER, A. & GREEN, G.W. 1983. The Geology of the Country Around Weston-Super-Mare. *Memoirs of the Geological Survey of Great Britain*, Sheet **279**, with parts of **263** and **295**.

WHITTAKER, A., HOLLIDAY, D.W. & PENN, I.E., 1985. *Geophysical logs in British Stratigraphy.* Boston: Blackwell. 79p.

WILLIAMS, G.A., 2002. *The role of tectonic inversion in the uplift and erosion of the St. George's and Bristol Channel basins, Western UK*. PhD. Thesis, University of Birmingham, UK.

WILLIAMS, G.A., TURNER, J.P. & HOLFORD, S.P. 2005. Inversion and exhumation of the St. George's Channel Basin, offshore Wales, UK. *Journal of the Geological Society of London*, **162**, p. 97-110.

WILLIAMS, G.D., POWELL, C.M. & COOPER, M.A. 1989. Geometry and kinematics of inversion tectonics. *In:* COOPER, M.A. & WILLIAMS, G.D. (eds.), *Inversion Tectonics.* Geological Society, London, Special Publications, **44,** p. 3-15.

WILSON, D., DAVIES, J.R., FLETCHER, C.J.N. & SMITH, M. 1990. Geology of the South Wales Coalfield, part 6, the country around Bridgend. *Memoir of the British Geological Survey*, Sheets **261** and **262** (England and Wales).

WOOD, A. & WOODLAND, A.W. 1968. Borehole at Mochras, west of Llanbedr, Meirionethshire. *Nature,* **219,** p. 1352-1354.

WOODHALL, D. & KNOX, R.W.O'B. 1979. Mesozoic volcanism in the northern North Sea and adjacent areas. *Bulletin of the Geological Survey of Great Britain*, **70**, p. 34-56.

WOODLAND, A.W. (ed.), 1971. *The Llanbedr (Mochras Farm) borehole.* Report of the Institute of Geological Sciences, No. 71/18.

WOODLAND, A.W. & EVANS, W.B. 1964. The geology of the South Wales Coalfield, part 4. The country around Pontypridd and Maesteg. *Memoirs of the British Geological Survey*, Sheet **248** (England and Wales).

WOOLRIDGE, S.W. 1926. The structural evolution of the London Basin. *Proceedings of the Geological Association*, *London*, **37**, p. 162-196.

WORUM, G. & MICHON, L. 2005. Implications of continuous structural inversion in the West Netherlands Basin for understanding controls on Palaeogene deformation in NW Europe. *Journal of the Geological Society of London,* **162,** p. 73-85.

WYCHERLEY, H.L., PARNELL, J., CHEN, H. & BOYCE, A.J. 2003. Indicators of hot fluid migration in sedimentary basins: evidence from the UK Atlantic Margin. *Petroleum Geoscience*, **9**, p. 357–374.

WYLLIE, M.R.J., GREGORY, A.R. & GARDNER, L.W., 1956. Elastic wave velocities in heterogenous and porous media. *Geophysics,* **21**, p. 41-70.

WYLLIE, M. R. J., GREGORY, A.R. & GARDNER, G.H.F. 1958. An experimental investigation of factors affecting elastic wave velocities in porous media. *Geophysics,* **23**, p. 459-493.

YALÇIN, M.N., LITTKE, R. & SACHSENHOFER, R.F. 1997. Thermal history of sedimentary basins. *In:* WELTE, D.H., HORSFIELD, B. & BAKER, D.R. (eds.), *Petroleum and Basin Evolution,* Springer, p. 71-167.

YIELDING, G. 1990. Footwall uplift associated with Late Jurassic normal faulting in the northern North Sea. *Journal of the Geological Society of London,* **147,** p. 219-222.

ZIAGOS, J.P. & BLACKWELL, D.D. 1986. A model for the transient temperature effects of horizontal fluid flow in geothermal systems. *Journal of Volcanology and Geothermal Research,* **27,** p. 371-397.

ZIEGLER, A. 1982. *Geological Atlas of Western and Central Europe*. Amsterdam: Elsevier.

ZIEGLER, P.A. 1987*a*. Celtic Sea-Western Approaches area: an overview. *Tectonophysics*, **137**, p. 285-289.

ZIEGLER, P.A. 1987*b*. Evolution of the Western Approaches Trough. *Tectonophysics*, **137**, p. 341-346.

ZIEGLER, P.A. 1987*c*. Late Cretaceous and Cenozoic intra-plate compressional deformations in the Alpine foreland – a geodynamic model. *Tectonophysics*, **137**, p. 389-420.

ZIEGLER, P.A. 1989*a*. Geodynamic model for Alpine intra-plate compressional deformation in Western and Central Europe. *In:* COOPER, M.A. & WILLIAMS, G.D. (eds.), *Inversion Tectonics.* Geological Society, London, Special Publications, **44,** p. 63-85.

ZIEGLER, P.A. 1989*b*. Evolution of the North Atlantic – An Overview. *In:* TANKARD, A.J. & BALKWILL, H.R. (eds.), *Extensional Tectonics and Stratigraphy of the North Atlantic Margins.* AAPG Memoirs, **46,** p. 471-500.

ZIEGLER, P.A. 1990. *Geological Atlas of Western and Central Europe 2nd Edition.* The Hague: Shell.

ZIEGLER, P.A. 1992. Plate tectonics, plate moving mechanisms and rifting. *Tectonophysics*, **215**, p. 9-34.

ZIEGLER, P.A. 2004. Europe: Permian to Recent Evolution. *In:* SEELEY, R.C., COCKS, L.R., PLIMER, I.R. (eds.), *The Encyclopaedia of Geology*. Amsterdam: Elsevier, p. 102-125.

ZIEGLER, P.A. & CLOETINGH, S. 2004. Dynamic processes controlling evolution of rifted basins. *Earth Science Reviews*, **64**, p. 1-50.

ZIEGLER, P.A., CLOETINGH, S. & VAN WEES, J-D. 1995. Dynamics of intra-plate compressional deformation: the Alpine foreland and other examples. *Tectonophysics*, **252,** p. 7-59.

ZIEGLER, P.A., VAN WEES, J-D. & CLOETINGH, S. 1998. Mechanical controls on collision-related compressional intra-plate deformation. *Tectonophysics,* **300,** p. 103-129.

ZIMMERMAN, R.W. 1991. *Compressibility of Sandstones, Developments in Petroleum Science, 29*. Amsterdam: Elsevier.

ZOBACK, M.L. 1992. First- and second-order patterns of stress in the lithosphere: the World Stress Map Project. *Journal of Geophysical Research,* **97B,** p. 11703-11728.

APPENDIX A

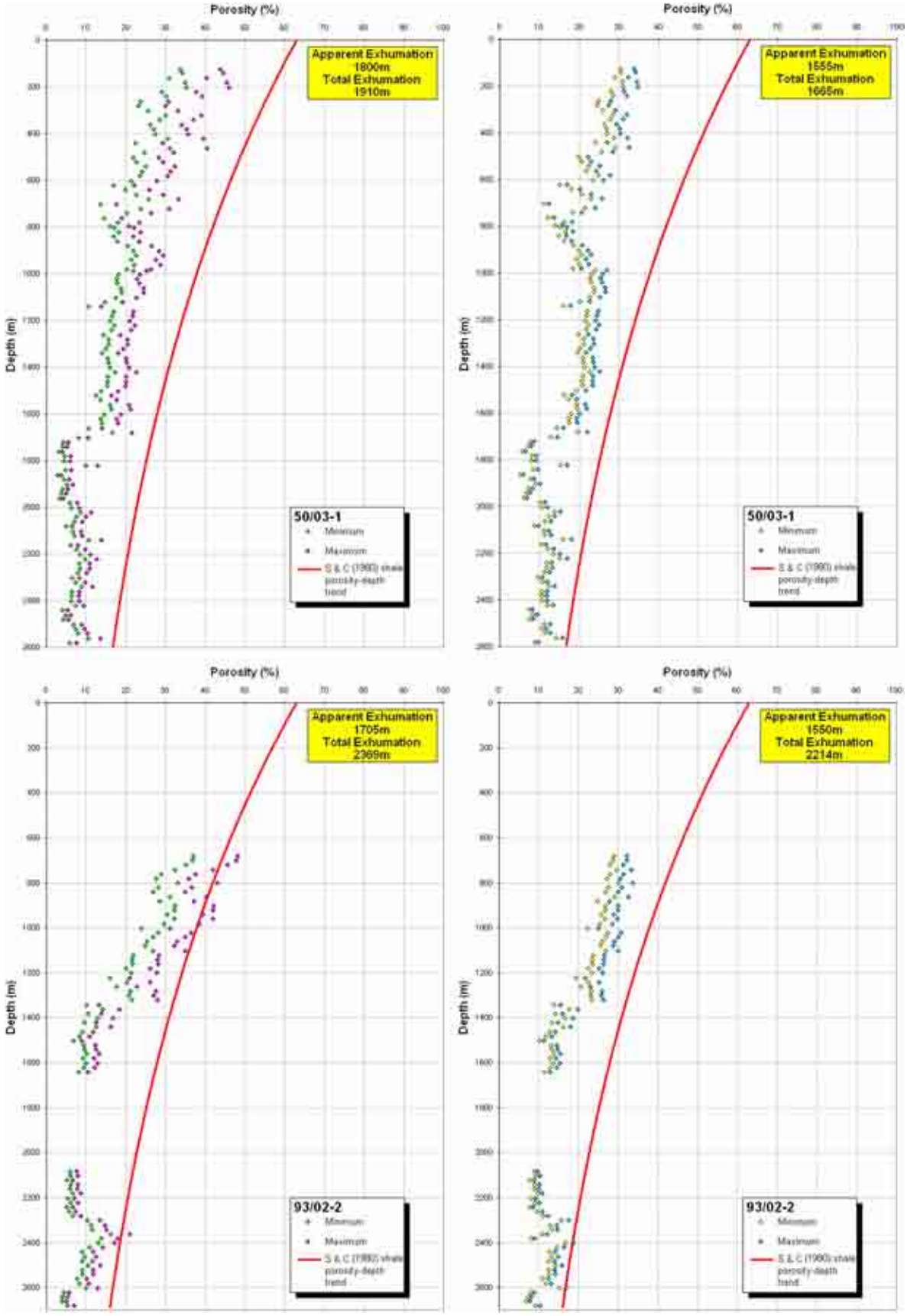

Figure A.1 – Porosity data for well 50/03-1 and 93/02-2 using the (left) Wyllie time-average equation and (right) Raymer-Hunt-Gardner transform. Red line is the Sclater & Christie (1980) shale porosity depth trend.

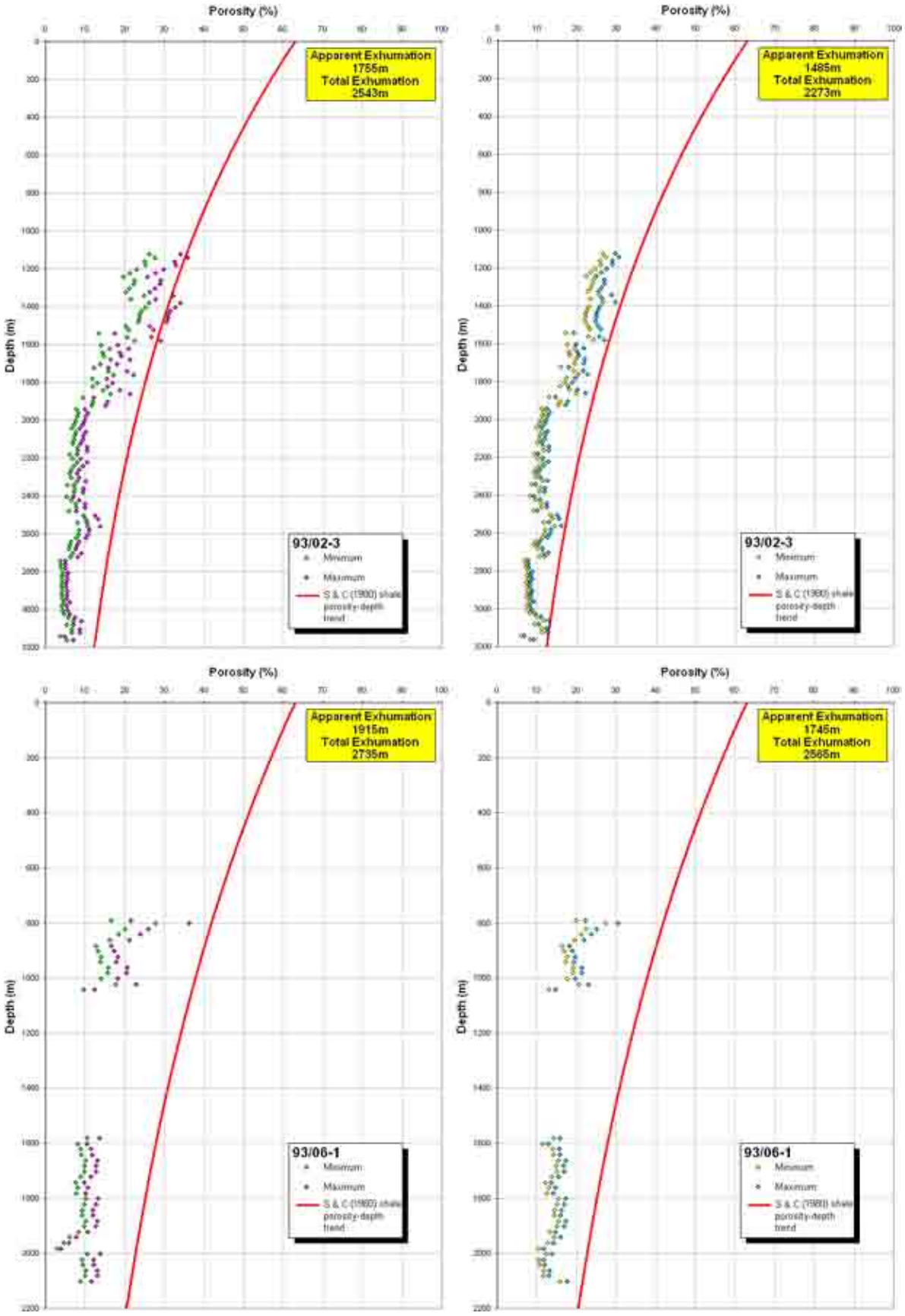

Figure A.2 – Porosity data for well 93/02-3 and 93/06-1 using the (left) Wyllie time-average equation and (right) Raymer-Hunt-Gardner transform. Red line is the Sclater & Christie (1980) shale porosity depth trend.

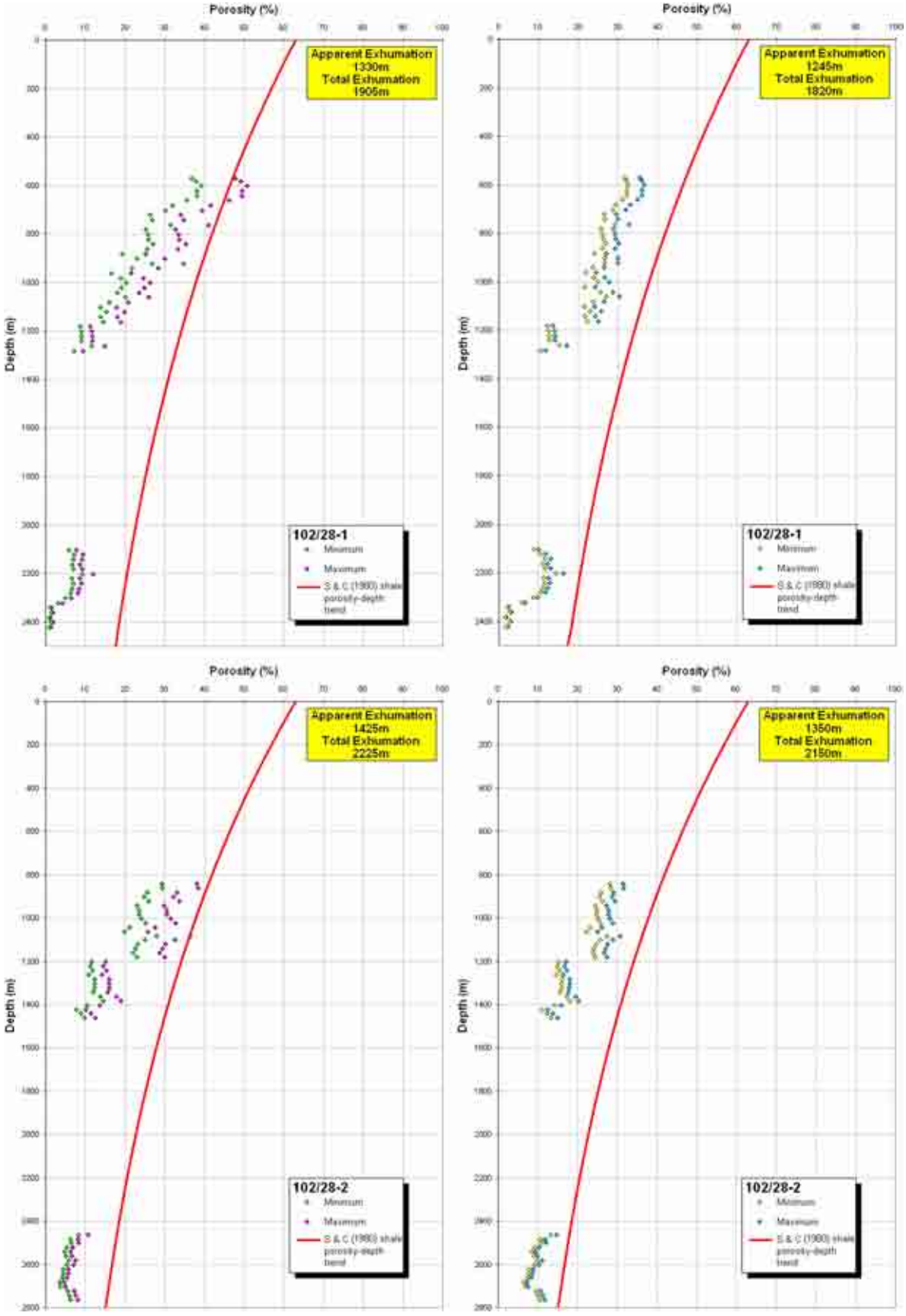

Figure A.3 – Porosity data for well 102/28-1 and 102/28-2 using the (left) Wyllie time-average equation and (right) Raymer-Hunt-Gardner transform. Red line is the Sclater & Christie (1980) shale porosity depth trend.

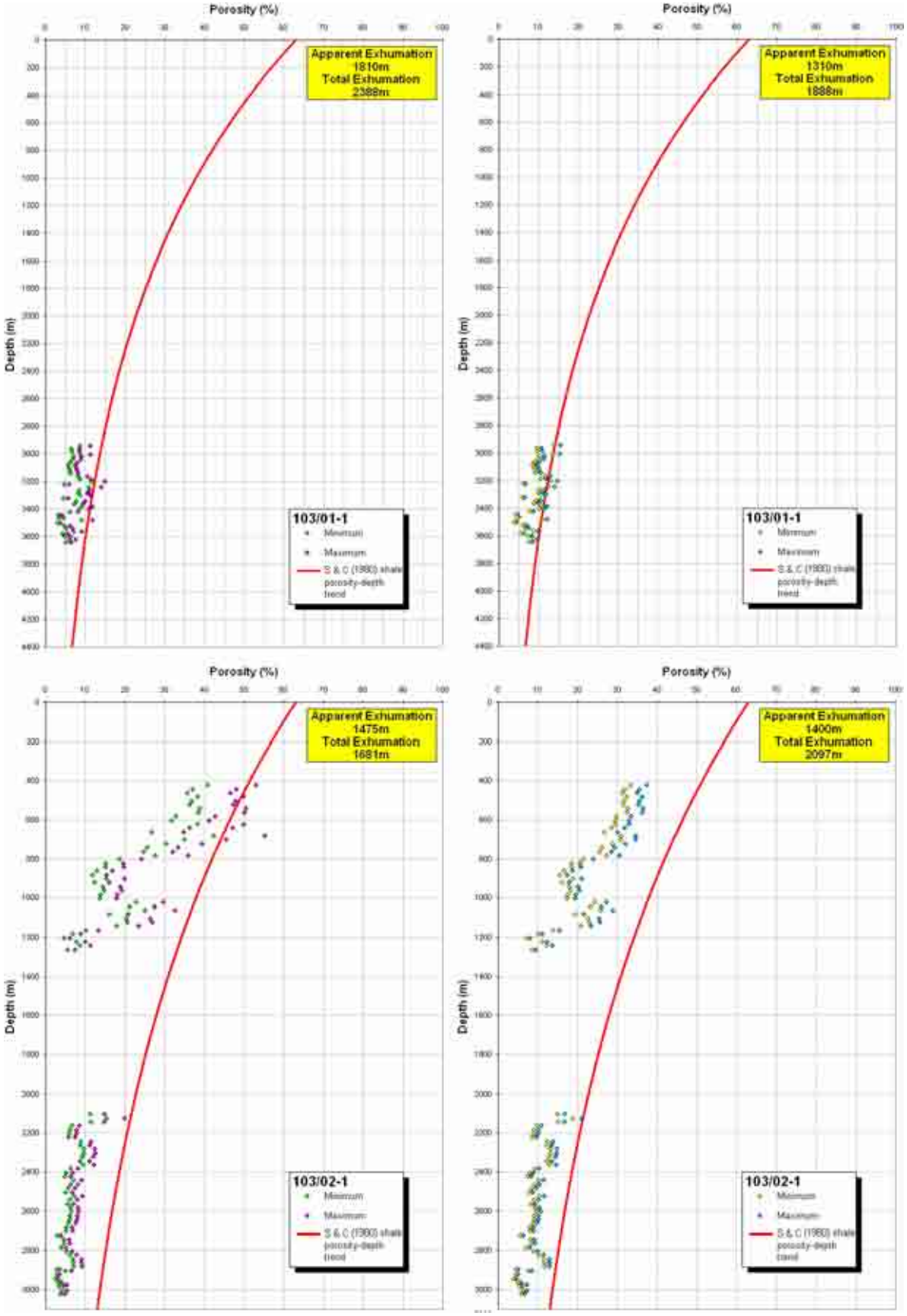

Figure A.4 – Porosity data for well 103/01-1 and 103/02-1 using the (left) Wyllie time-average equation and (right) Raymer-Hunt-Gardner transform. Red line is the Sclater & Christie (1980) shale porosity depth trend.

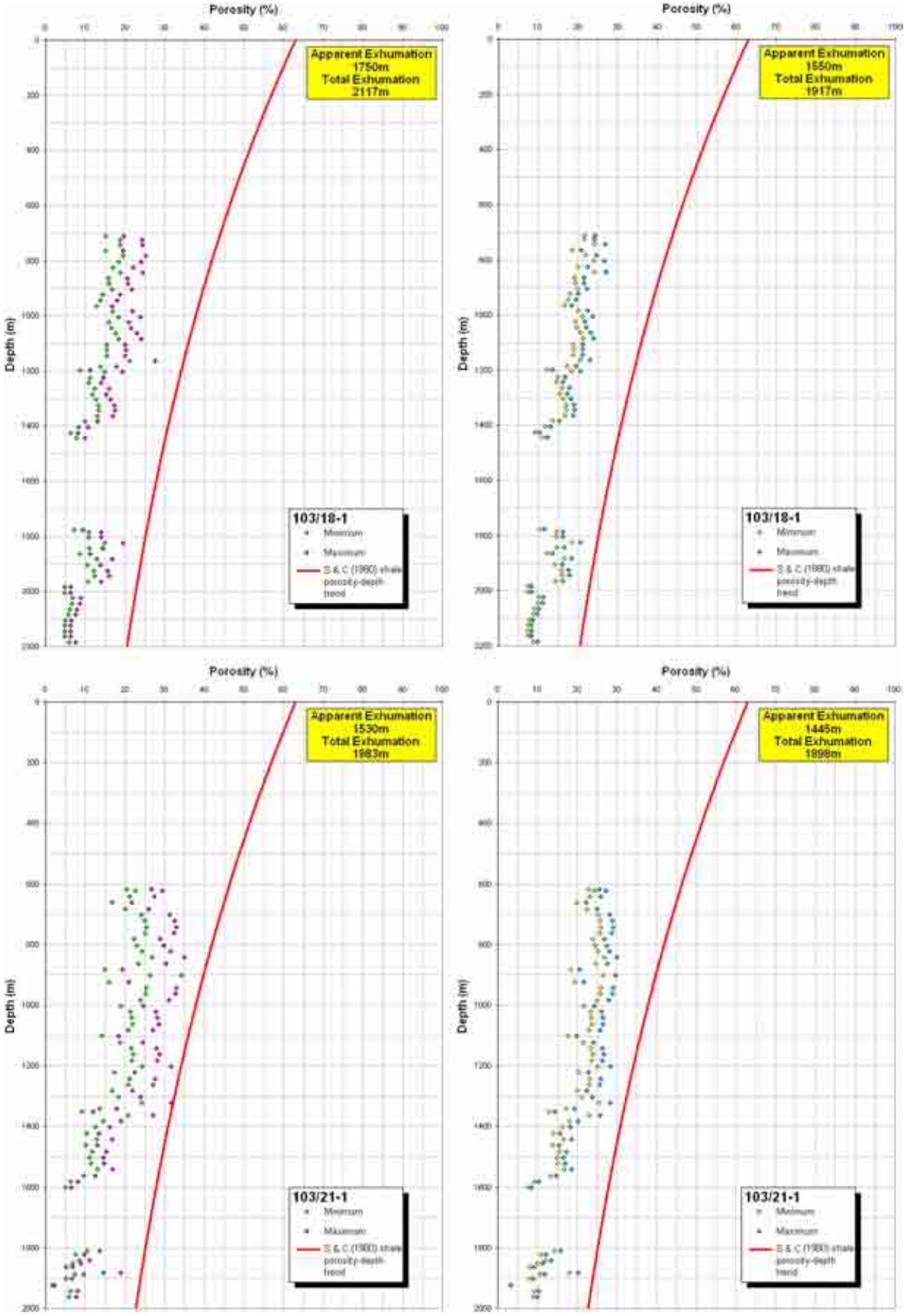

Figure A.5 – Porosity data for well 103/18-1 and 103/21-1 using the (left) Wyllie time-average equation and (right) Raymer-Hunt-Gardner transform. Red line is the Sclater & Christie (1980) shale porosity depth trend.

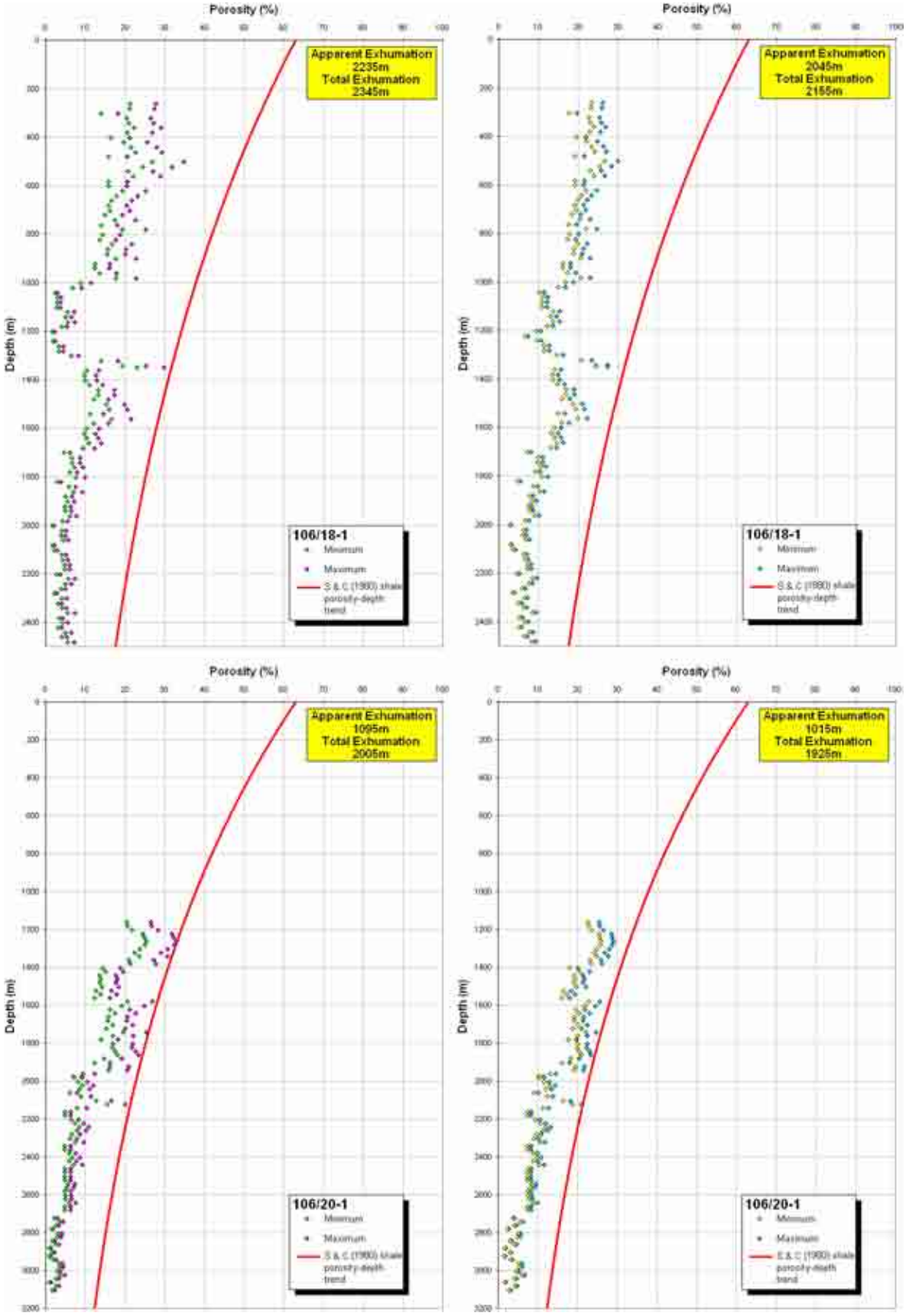

Figure A.6 – Porosity data for well 106/18-1 and 106/20-1 using the (left) Wyllie time-average equation and (right) Raymer-Hunt-Gardner transform. Red line is the Sclater & Christie (1980) shale porosity depth trend.

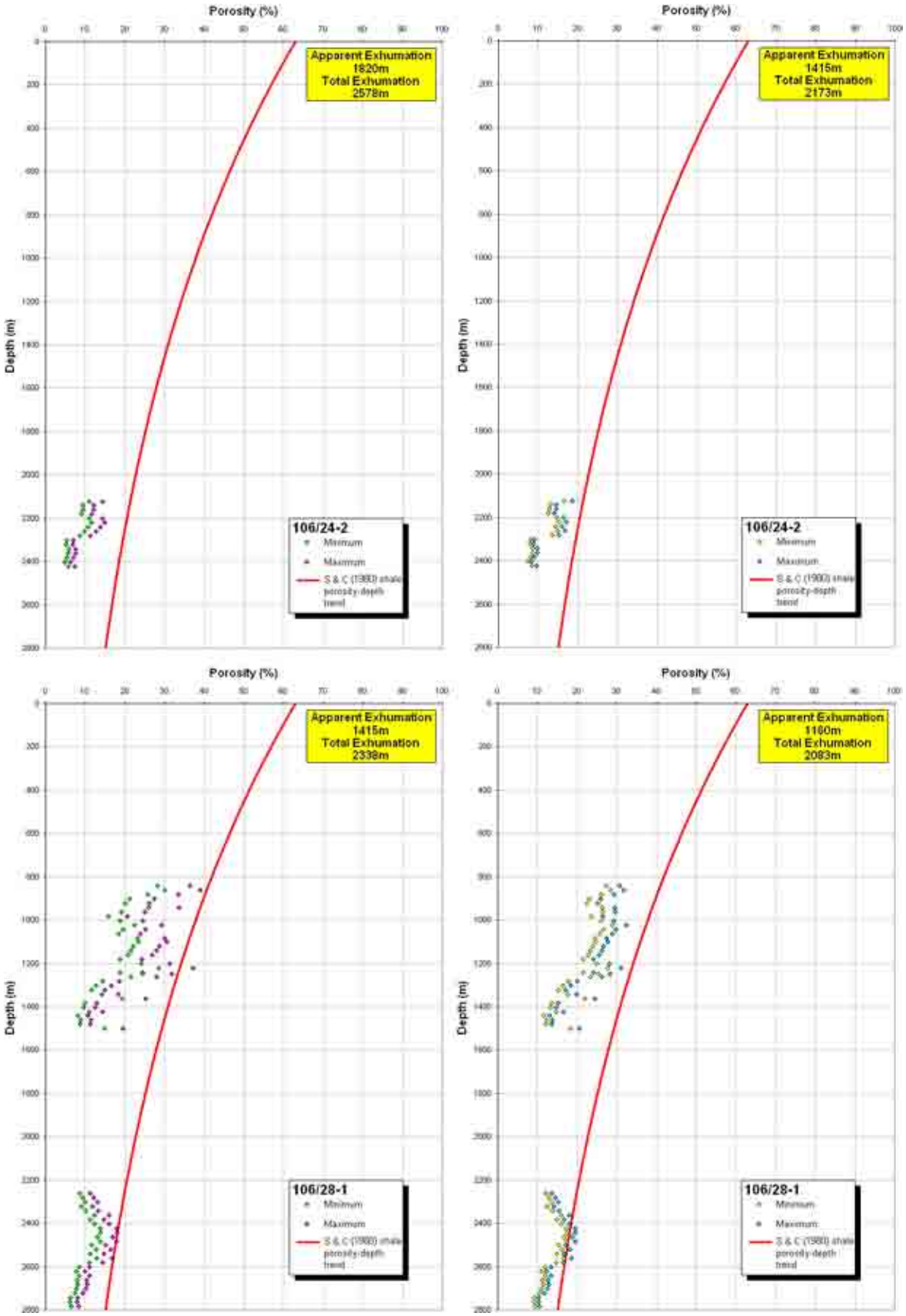

Figure A.7 – Porosity data for well 106/24-2 and 106/28-1 using the (left) Wyllie time-average equation and (right) Raymer-Hunt-Gardner transform. Red line is the Sclater & Christie (1980) shale porosity depth trend.

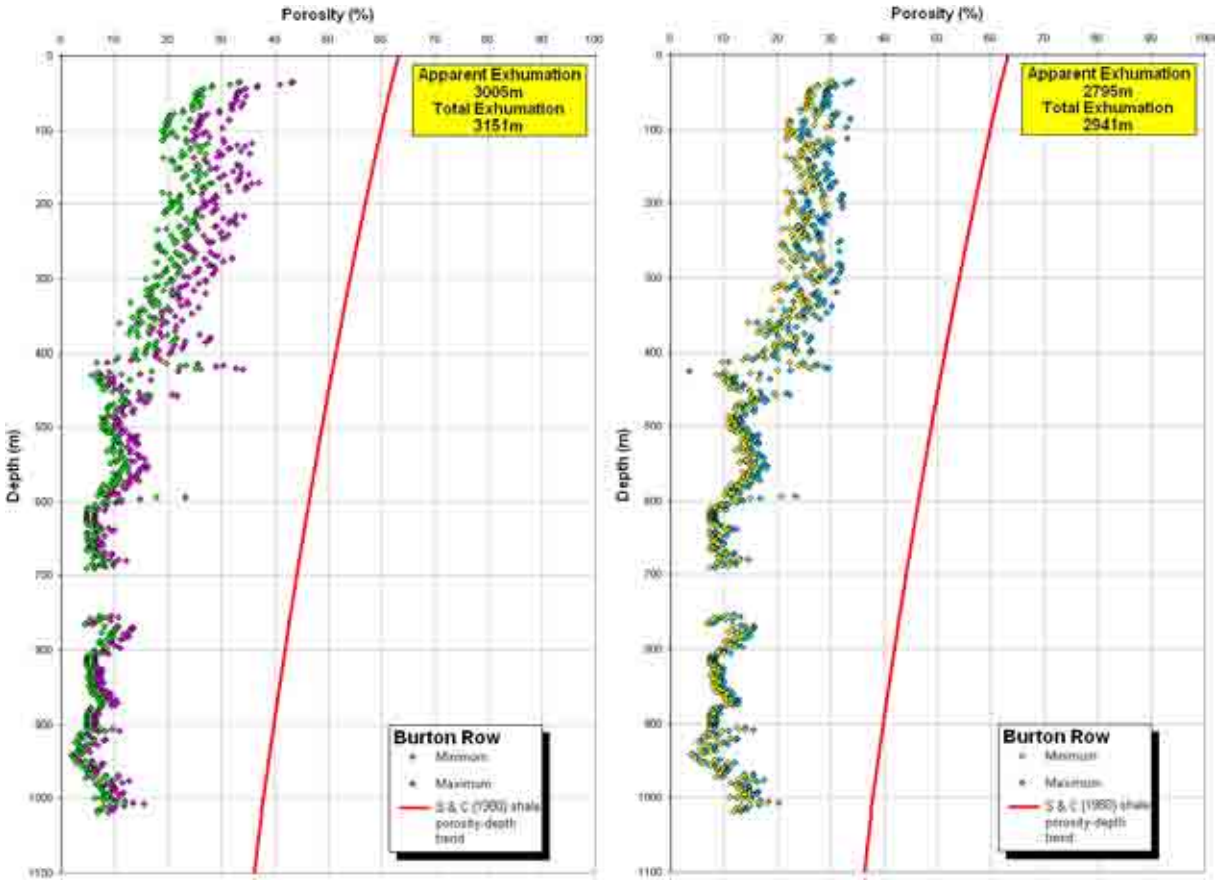

Figure A.8 – Porosity data for the Burton Row borehole using the (left) Wyllie time-average equation and (right) Raymer-Hunt-Gardner transform. Red line is the Sclater & Christie (1980) shale porosity depth trend.

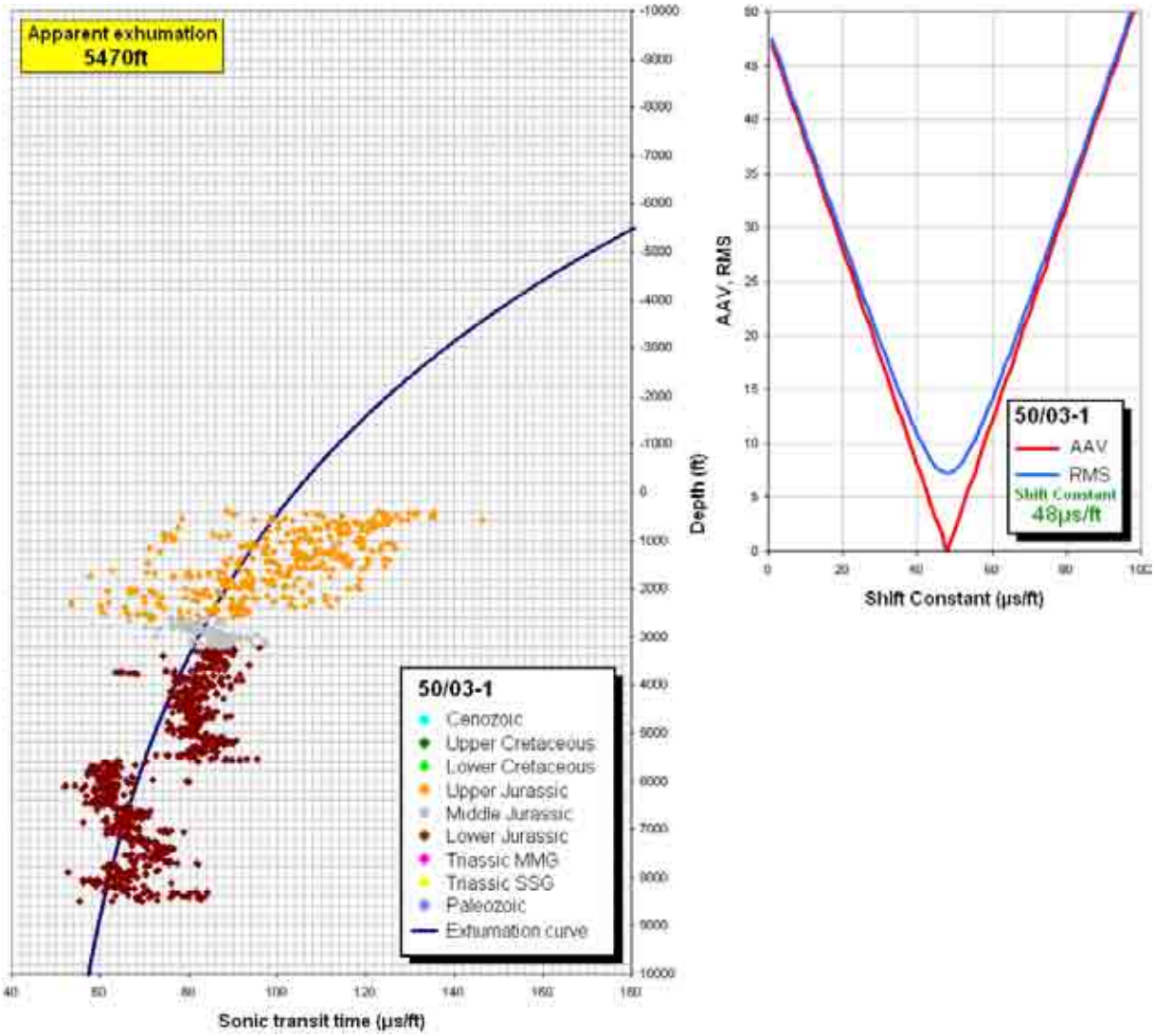

Figure A.9 – (Above) Graph showing the calculated compaction trend and erosion amount for well 50/03-1 revealing an apparent exhumation of 5470ft (1668m). (Above, right) Error assessment of statistical fit showing the optimum shift-constant of 48µs/ft.

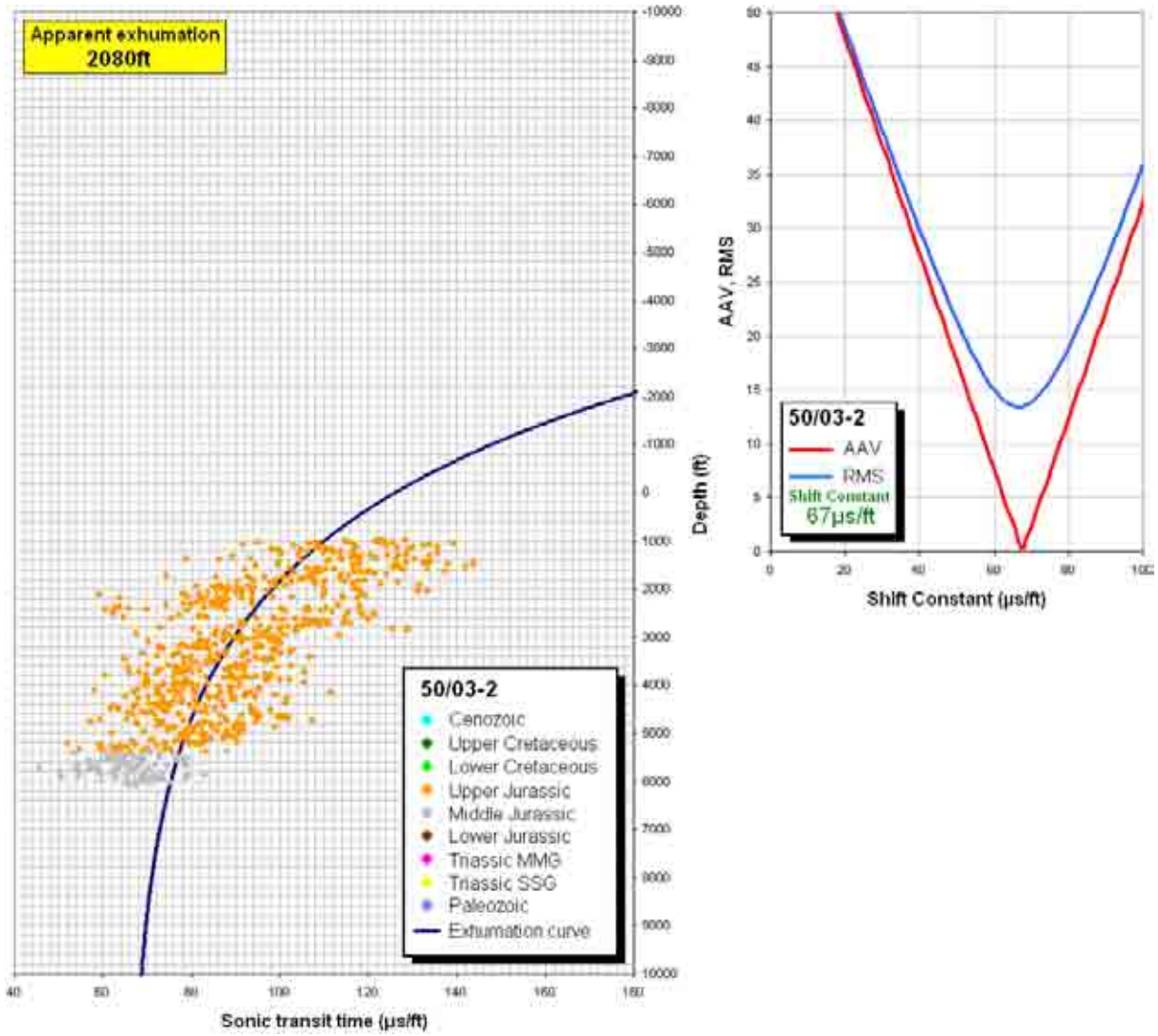

Figure A.10 – (Above) Graph showing the calculated compaction trend and erosion amount for well 50/03-2 revealing an apparent exhumation of 2080ft (634m). (Above, right) Error assessment of statistical fit showing the optimum shift-constant of 67µs/ft.

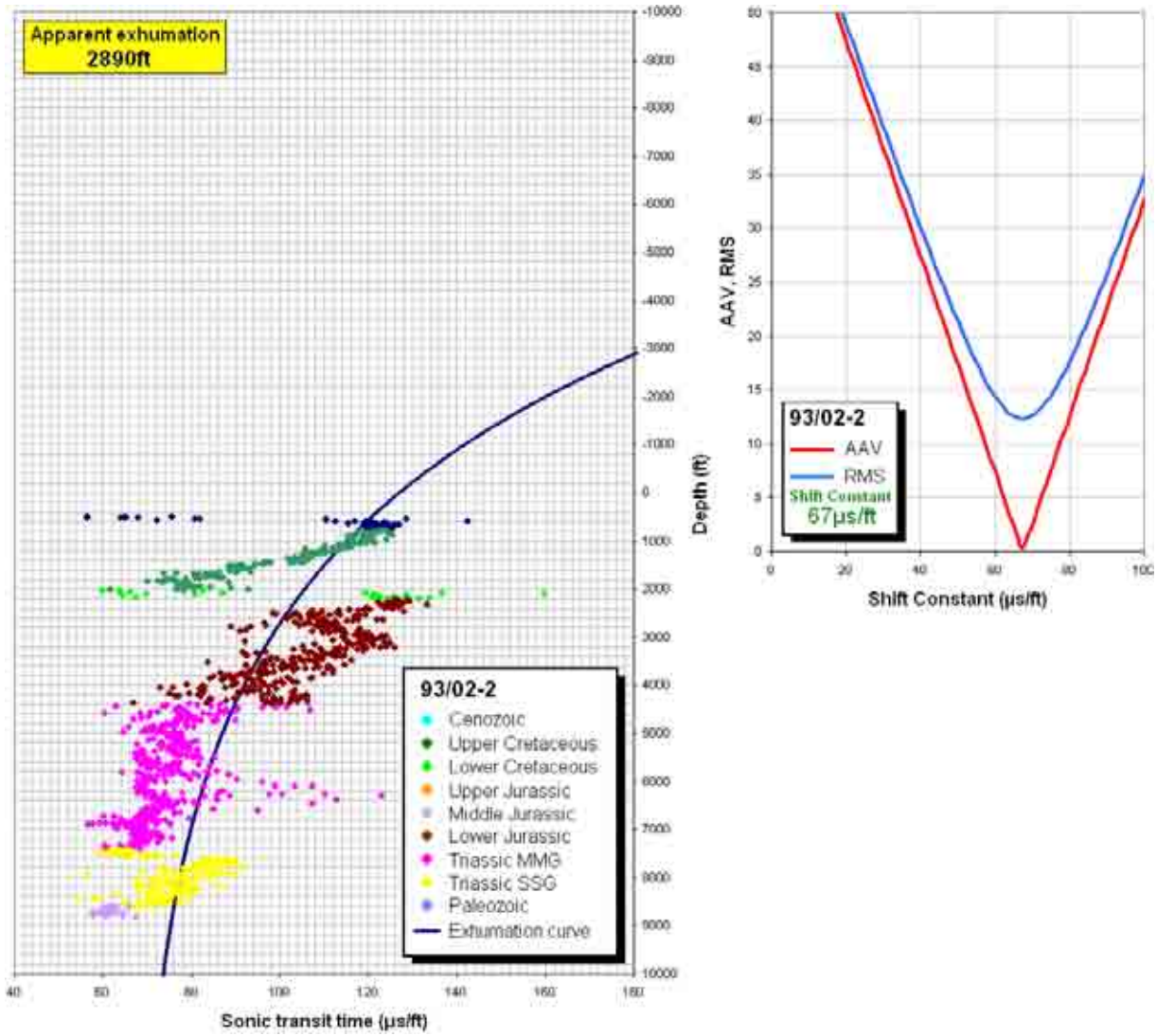

Figure A.11 – (Above) Graph showing the calculated compaction trend and erosion amount for well 93/02-2 revealing an apparent exhumation of 2890ft (881m). (Above, right) Error assessment of statistical fit showing the optimum shift-constant of 67µs/ft.

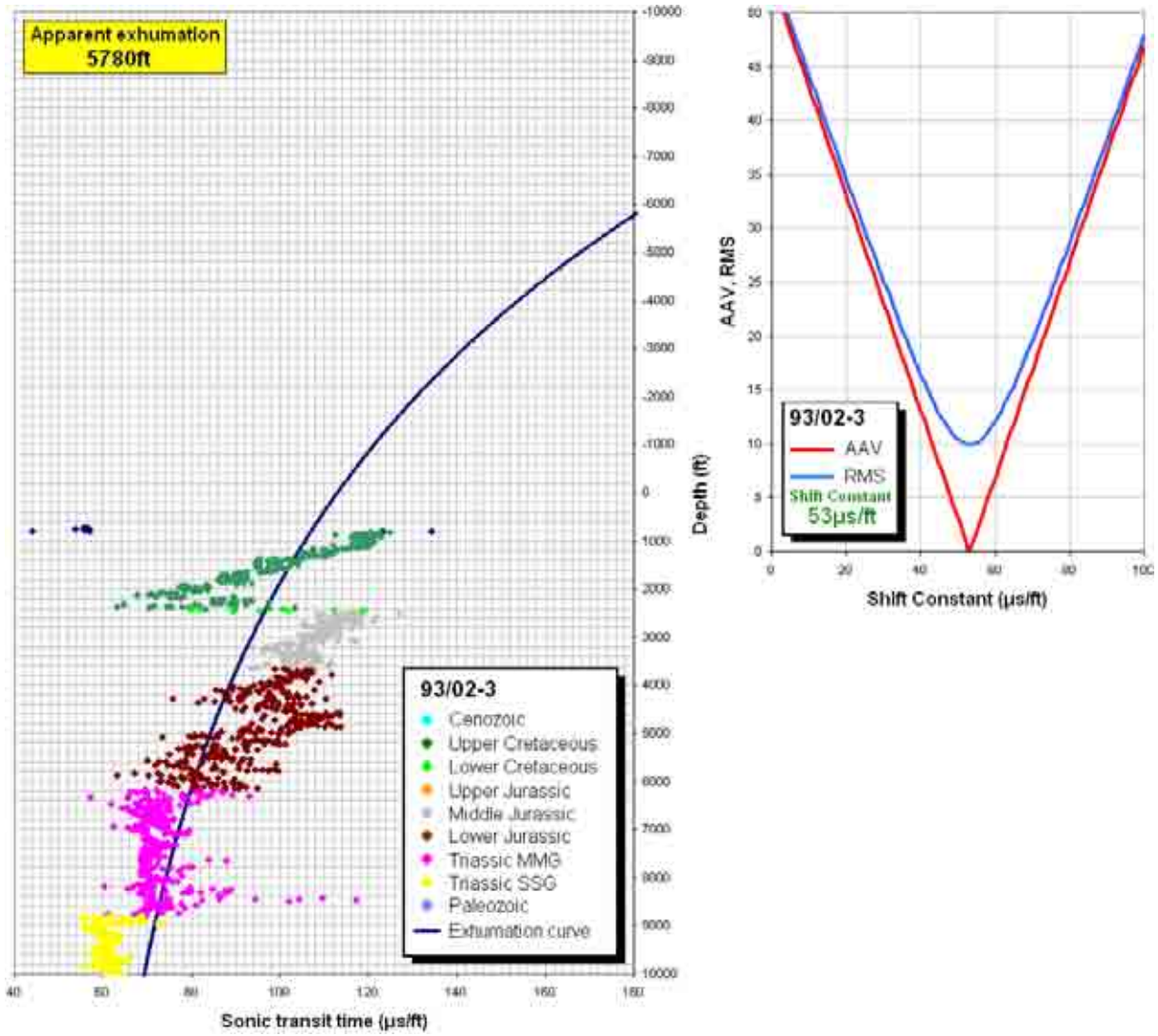

Figure A.12 – (Above) Graph showing the calculated compaction trend and erosion amount for well 93/02-3 revealing an apparent exhumation of 5780ft (1766m). (Above, right) Error assessment of statistical fit showing the optimum shift-constant of 53µs/ft.

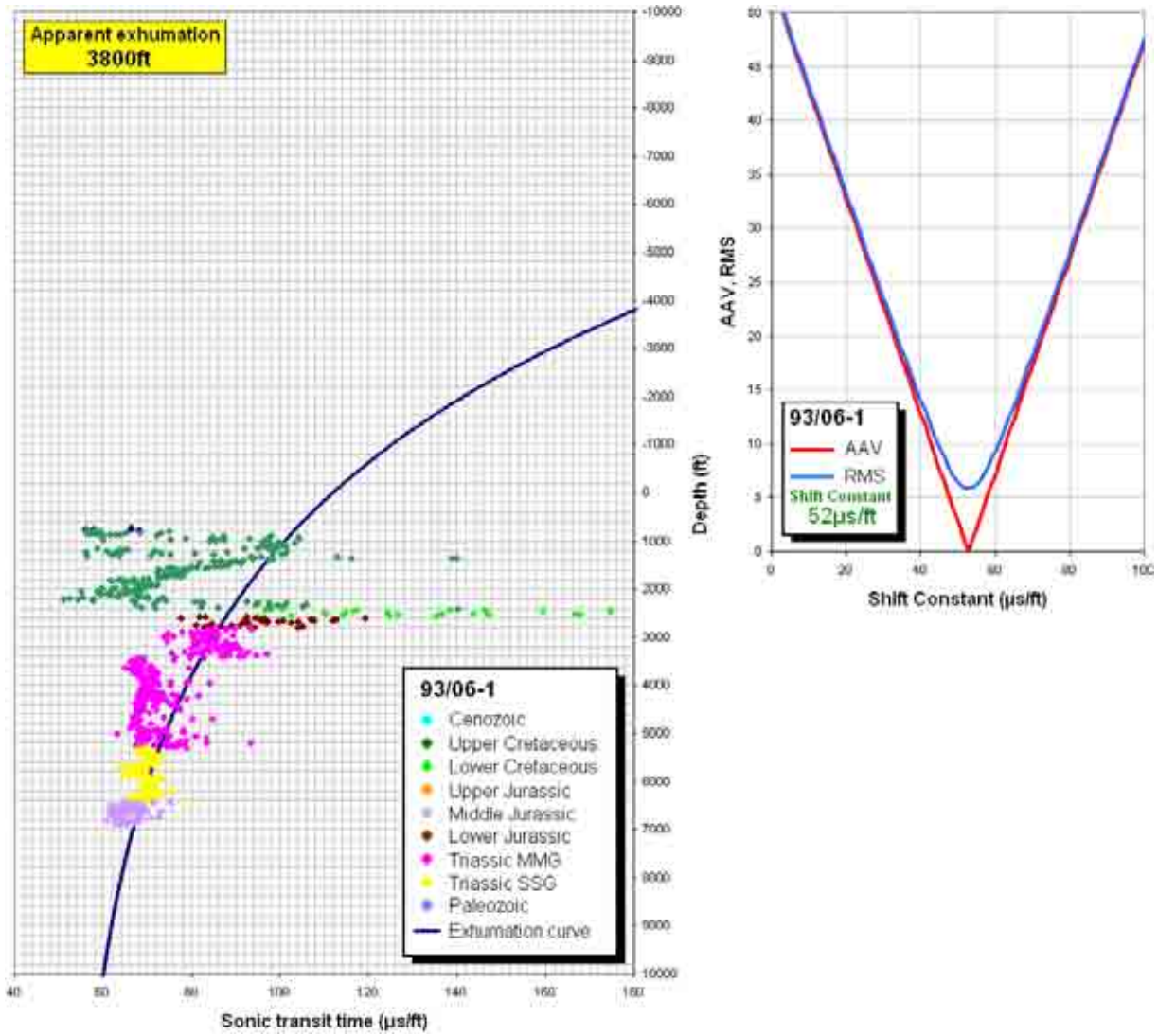

Figure A.13 – (Above) Graph showing the calculated compaction trend and erosion amount for well 93/06-1 revealing an apparent exhumation of 3800ft (1159m). (Above, right) Error assessment of statistical fit showing the optimum shift-constant of 52µs/ft.

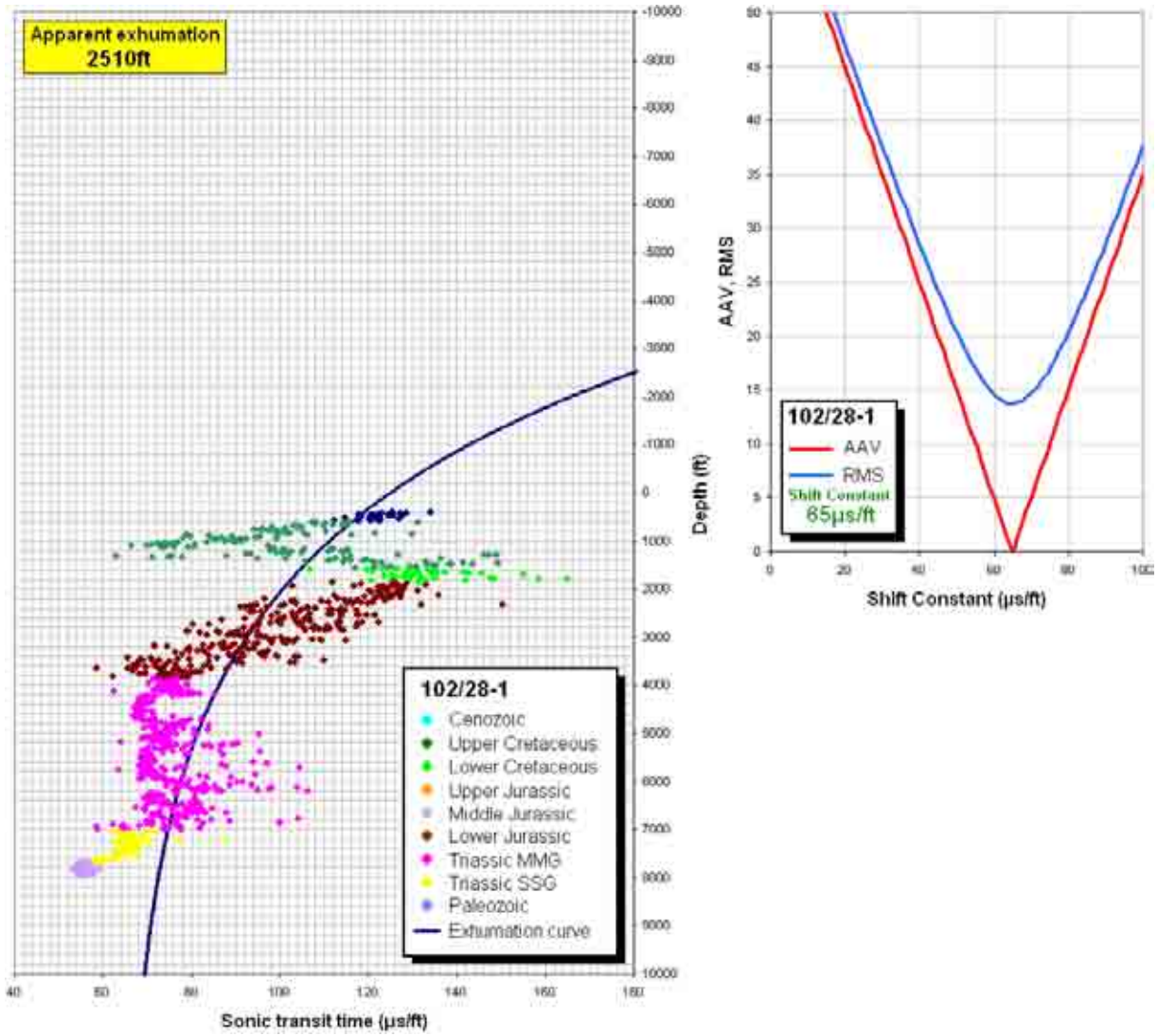

Figure A.14 – (Above) Graph showing the calculated compaction trend and erosion amount for well 102/28-1 revealing an apparent exhumation of 2510ft (766m). (Above, right) Error assessment of statistical fit showing the optimum shift-constant of 65µs/ft.

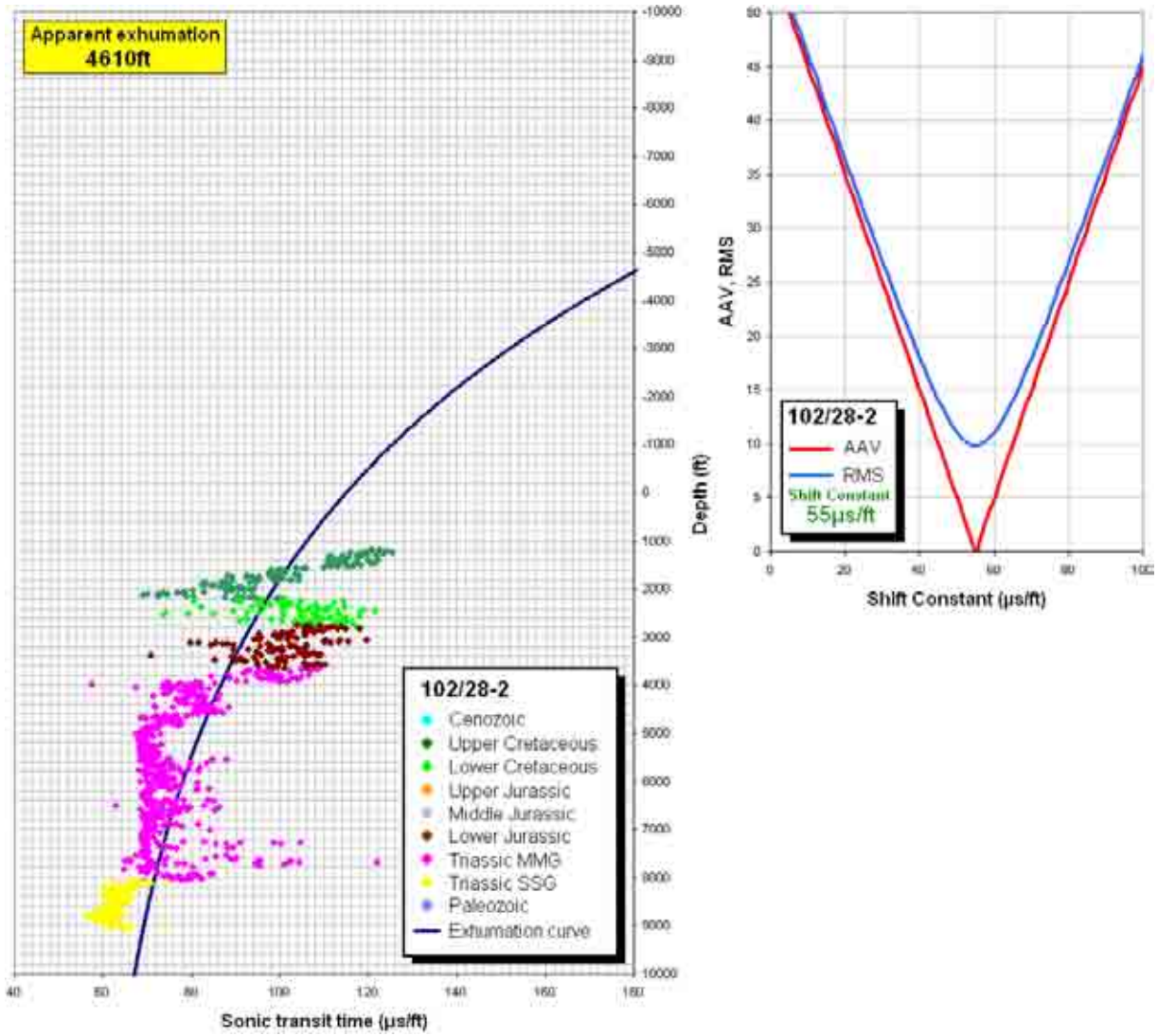

Figure A.15 – (Above) Graph showing the calculated compaction trend and erosion amount for well 102/28-2 revealing an apparent exhumation of 4610ft (1406m). (Above, right) Error assessment of statistical fit showing the optimum shift-constant of 55µs/ft.

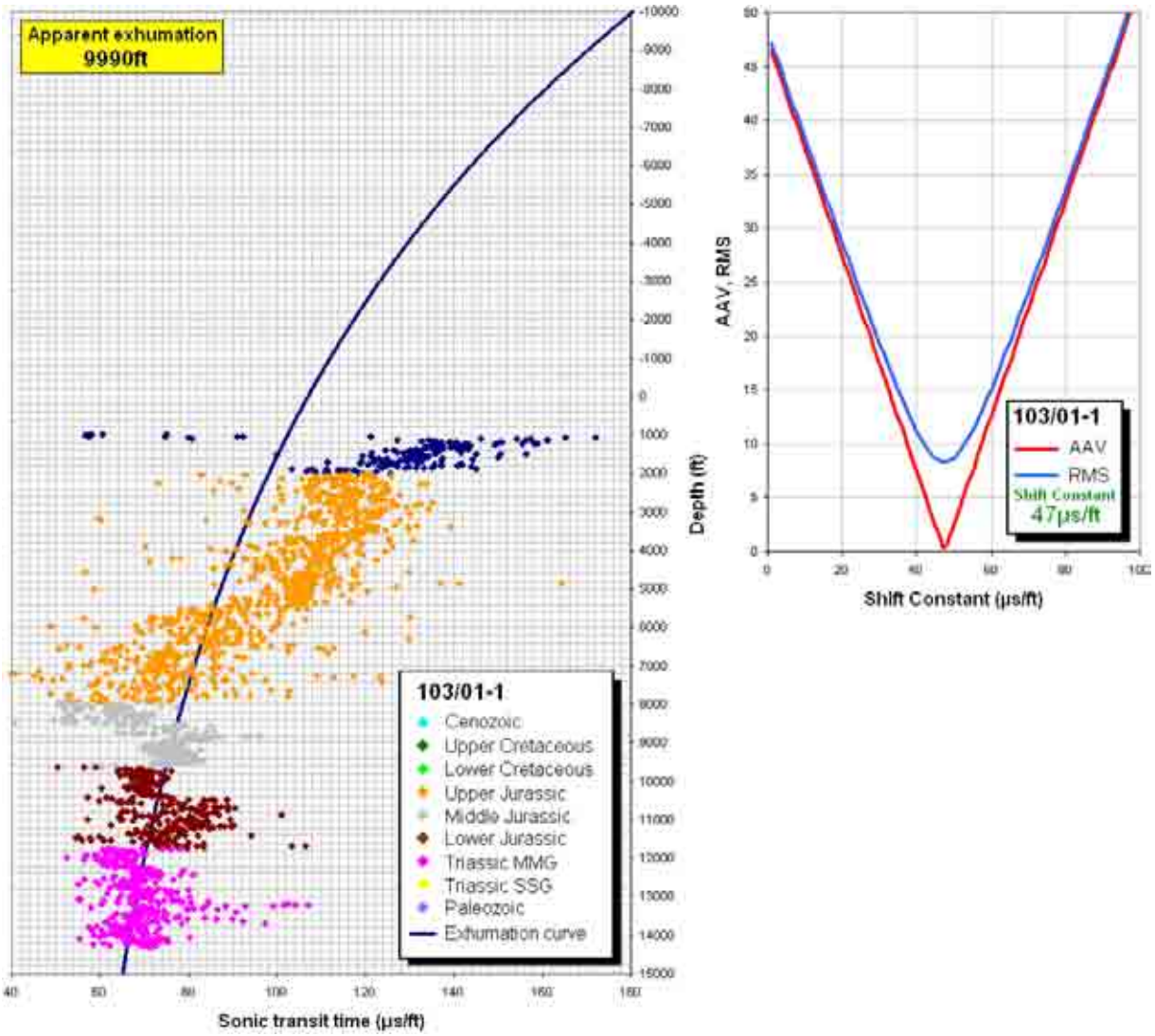

Figure A.16 – (Above) Graph showing the calculated compaction trend and erosion amount for well 103/01-1 revealing an apparent exhumation of 9900ft (3047m). (Above, right) Error assessment of statistical fit showing the optimum shift-constant of 47µs/ft.

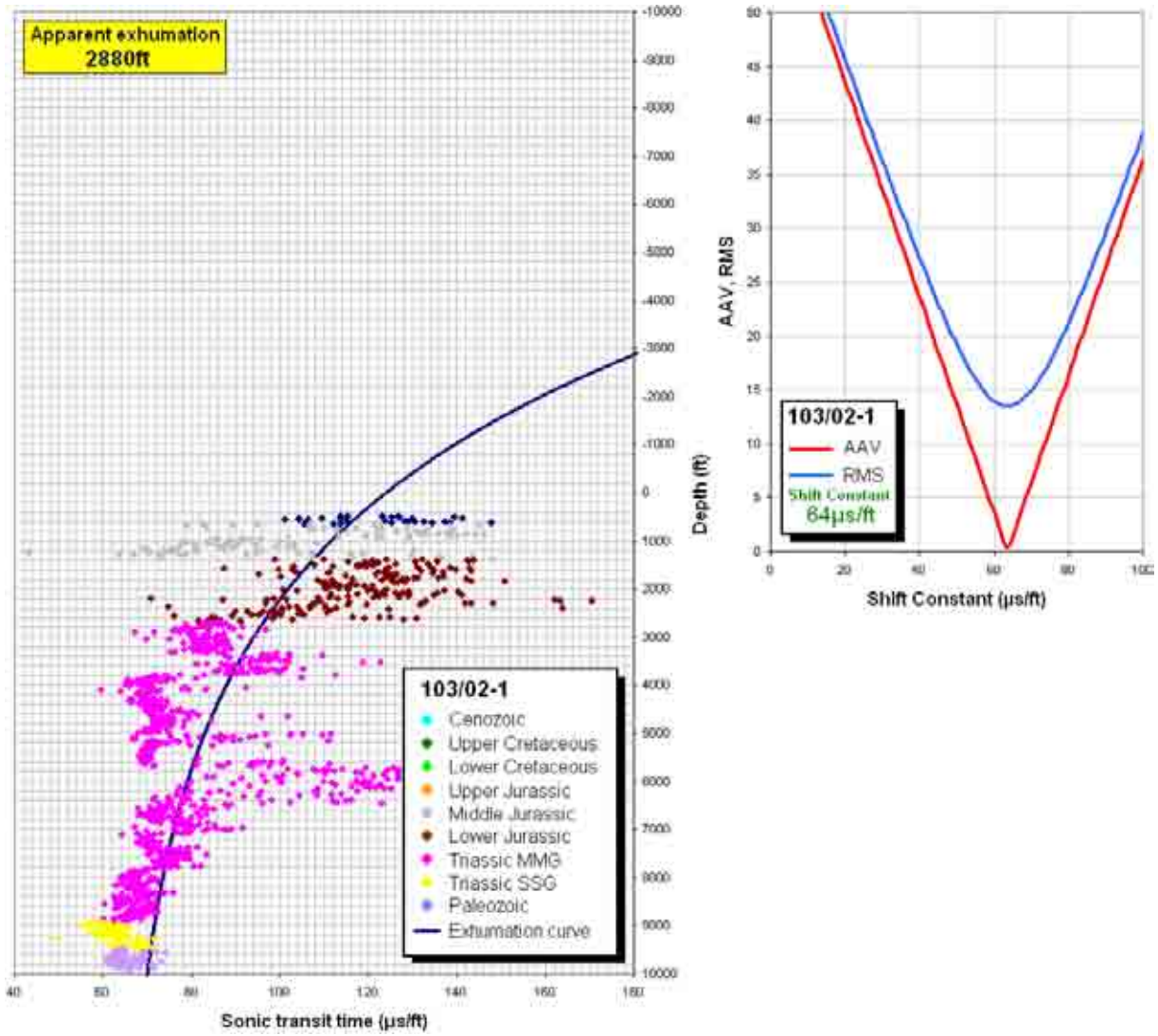

Figure A.17 – (Above) Graph showing the calculated compaction trend and erosion amount for well 103/02-1 revealing an apparent exhumation of 2880ft (878m). (Above, right) Error assessment of statistical fit showing the optimum shift-constant of 64µs/ft.

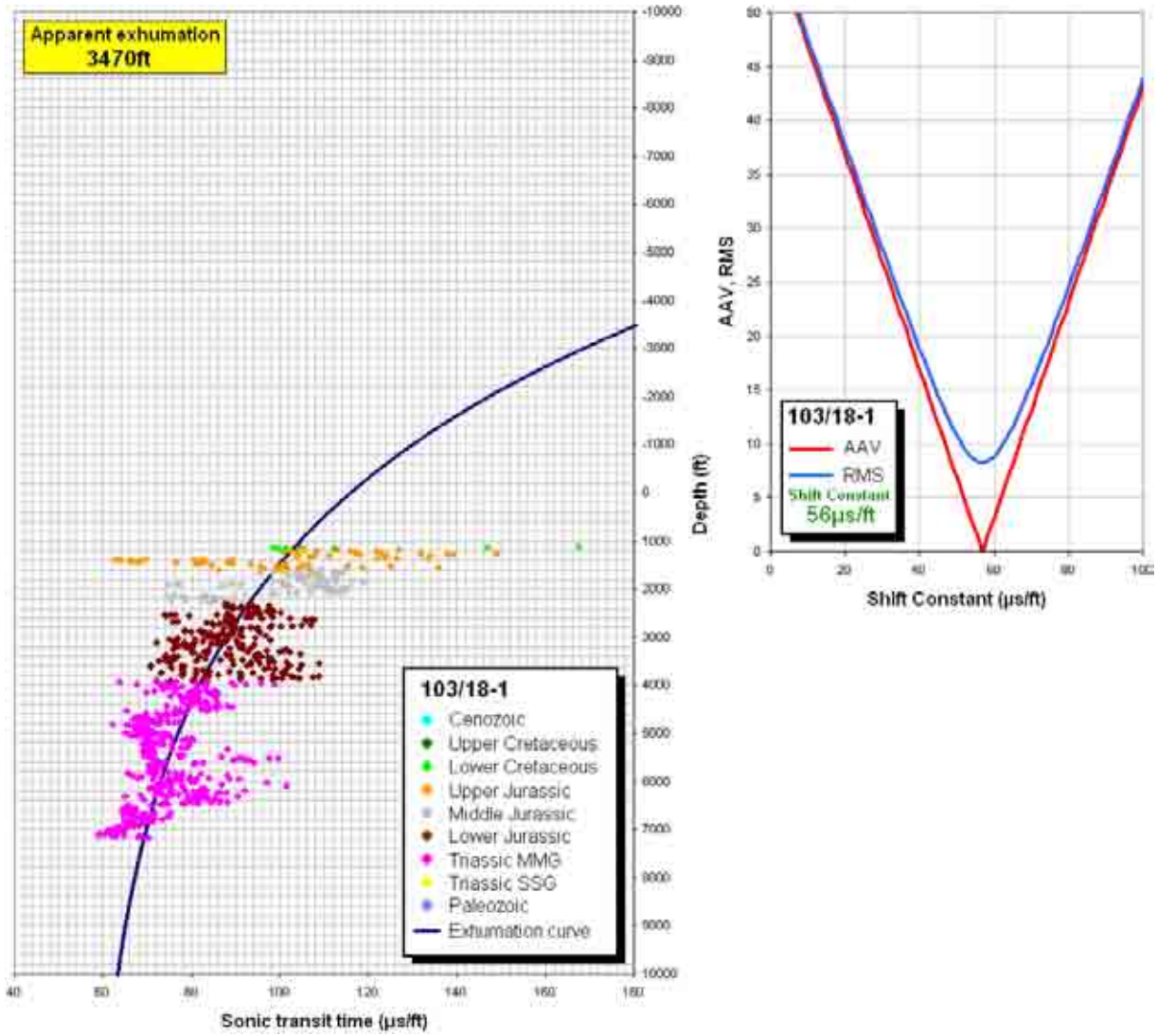

Figure A.18 – (Above) Graph showing the calculated compaction trend and erosion amount for well 103/18-1 revealing an apparent exhumation of 3470ft (1058m). (Above, right) Error assessment of statistical fit showing the optimum shift-constant of 56µs/ft.

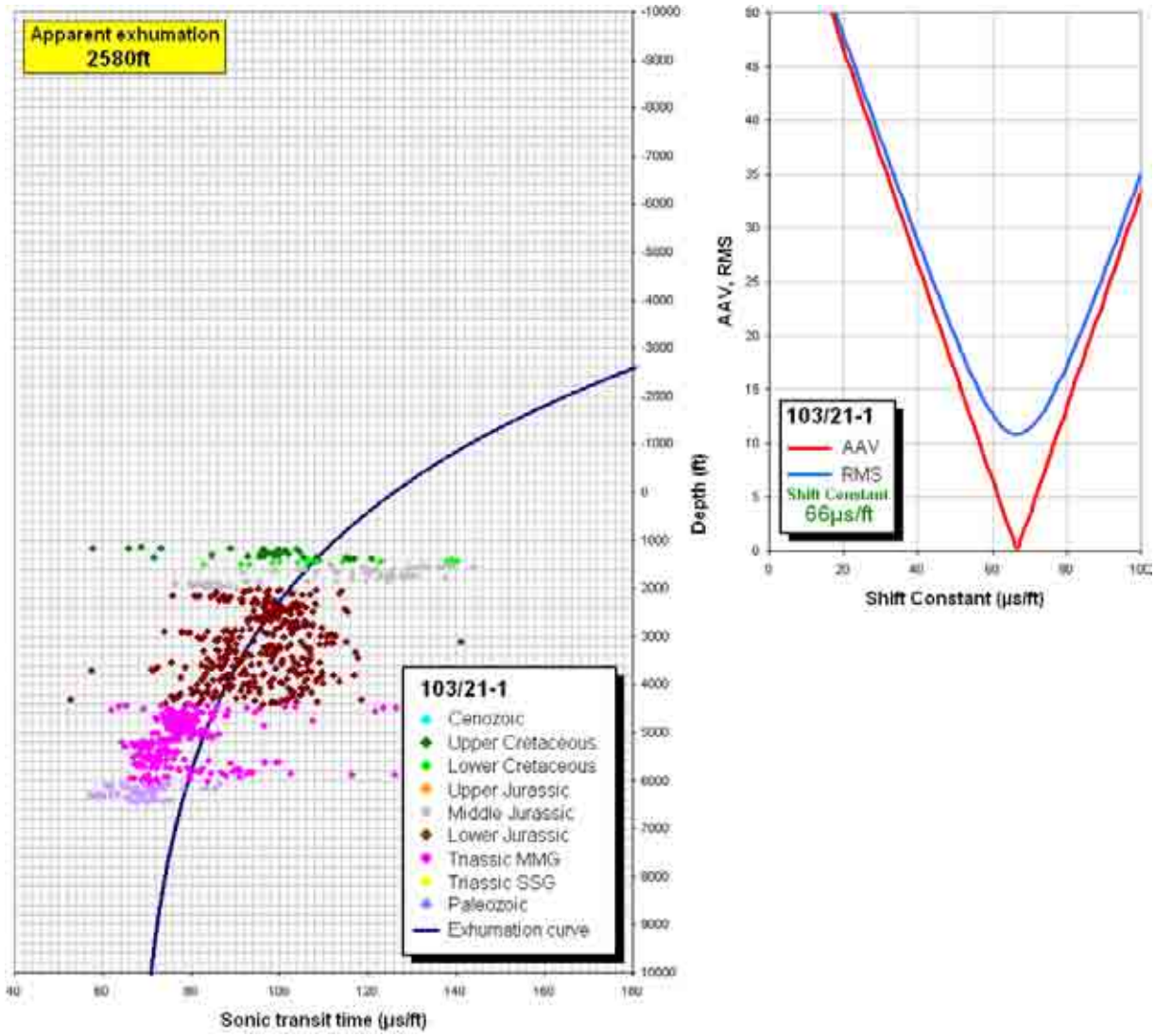

Figure A.19 – (Above) Graph showing the calculated compaction trend and erosion amount for well 103/21-1 revealing an apparent exhumation of 2580ft (787m). (Above, right) Error assessment of statistical fit showing the optimum shift-constant of 66µs/ft.

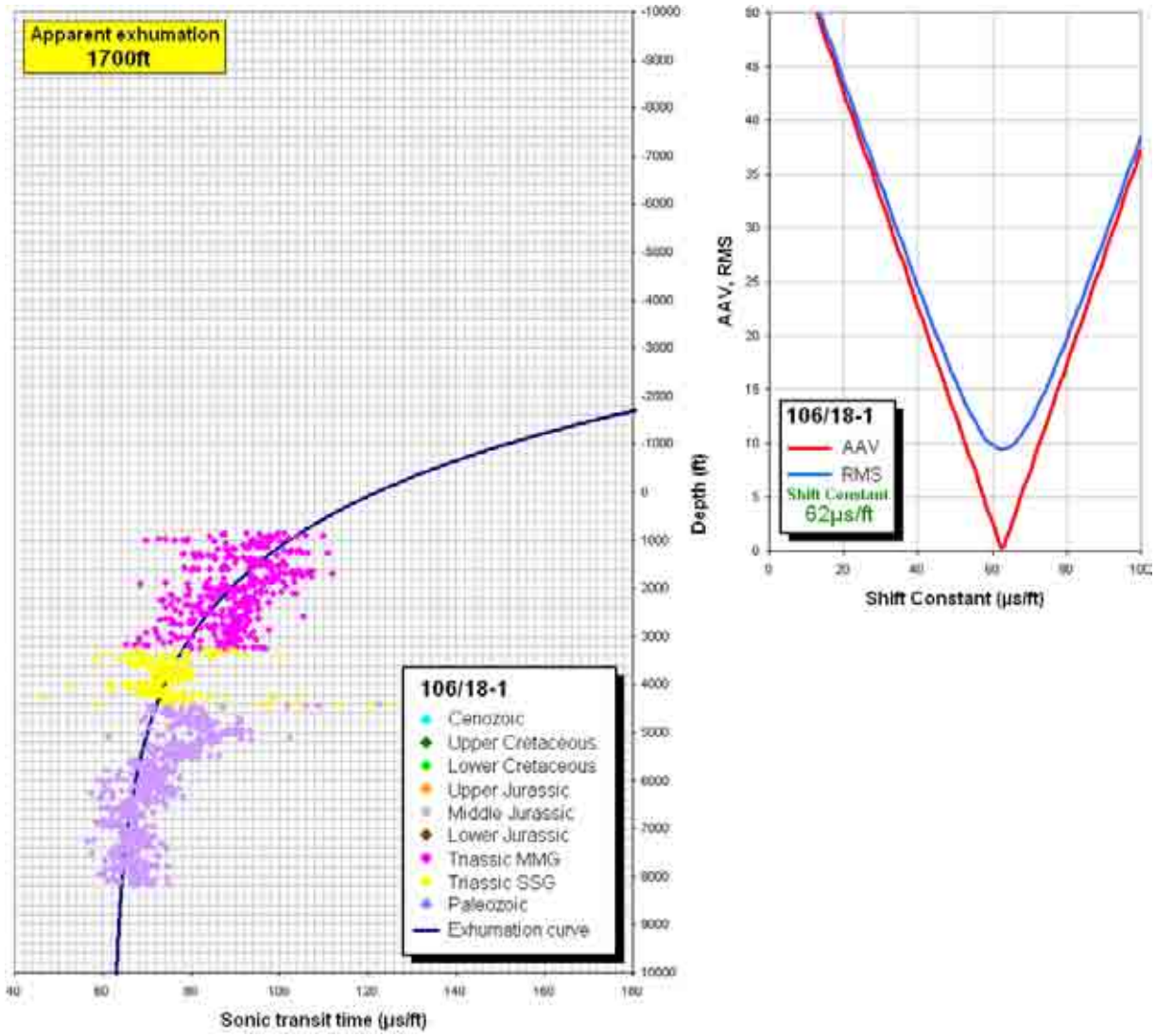

Figure A.20 – (Above) Graph showing the calculated compaction trend and erosion amount for well 106/18-1 revealing an apparent exhumation of 1700ft (519m). (Above, right) Error assessment of statistical fit showing the optimum shift-constant of 62µs/ft.

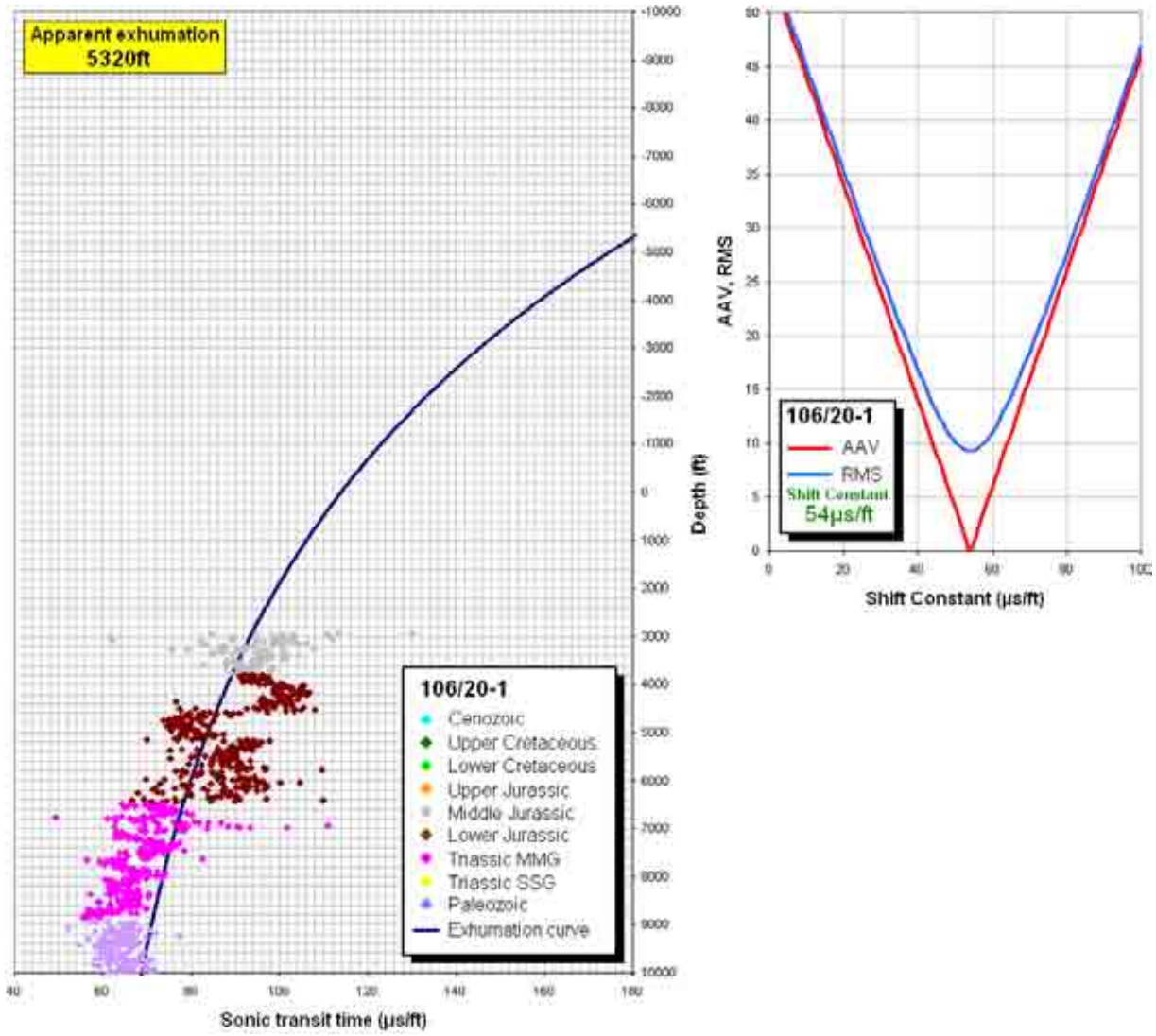

Figure A.21 – (Above) Graph showing the calculated compaction trend and erosion amount for well 106/20-1 revealing an apparent exhumation of 5320ft (1623m). (Above, right) Error assessment of statistical fit showing the optimum shift-constant of 54µs/ft.

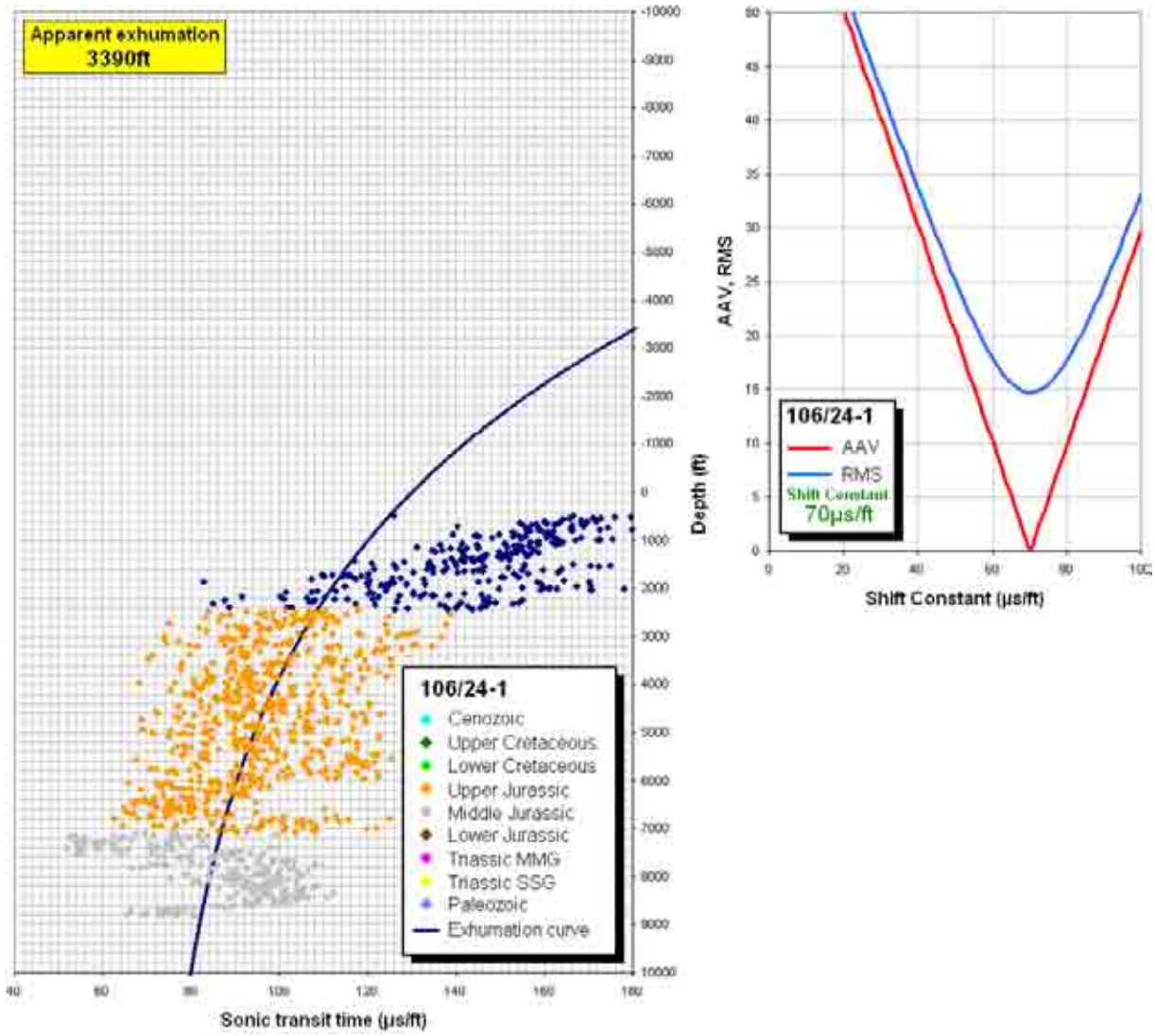

Figure A.22 – (Above) Graph showing the calculated compaction trend and erosion amount for well 106/24-1 revealing an apparent exhumation of 3390ft (1034m). (Above, right) Error assessment of statistical fit showing the optimum shift-constant of 70µs/ft.

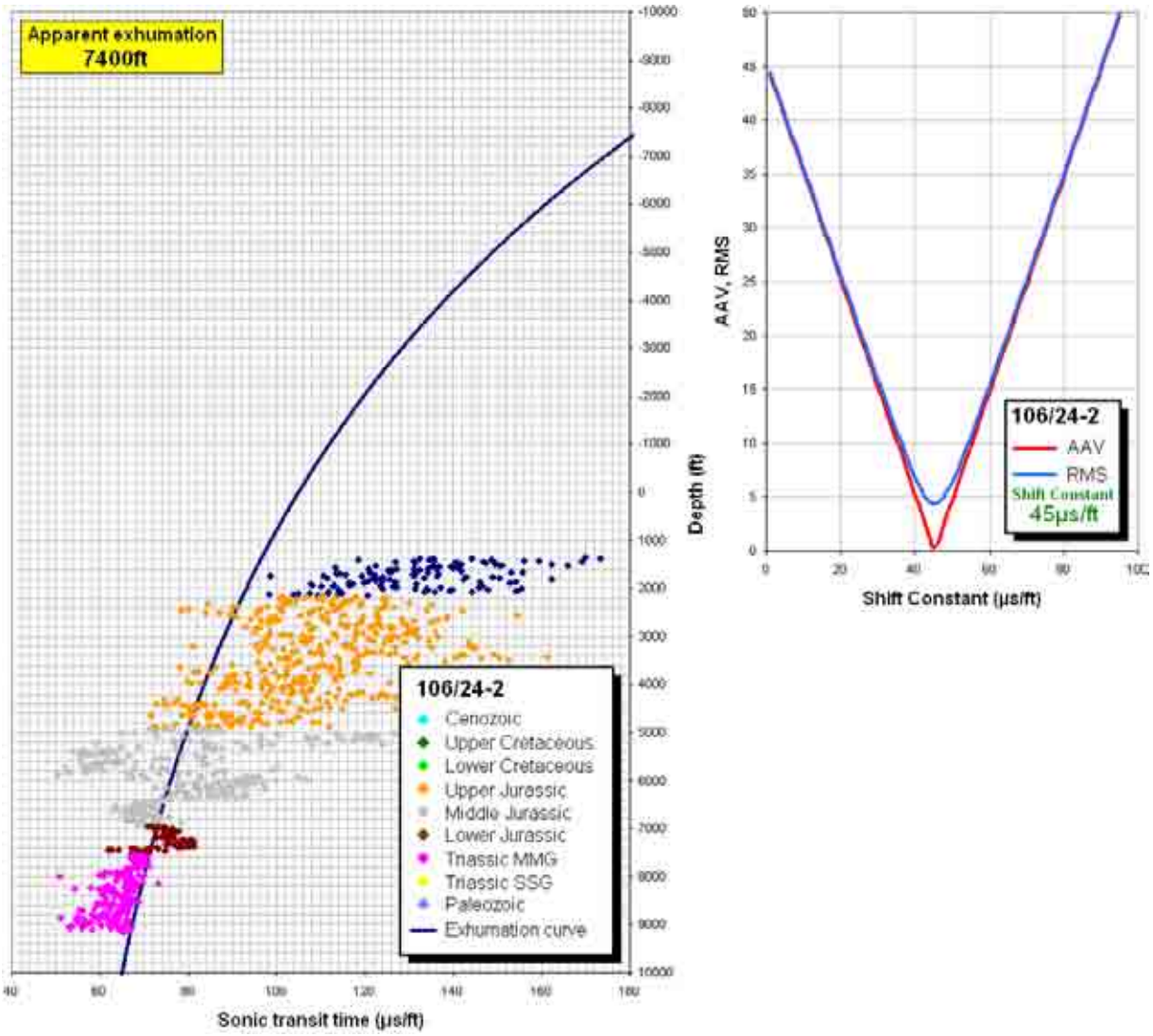

Figure A.23 – (Above) Graph showing the calculated compaction trend and erosion amount for well 106/24-2 revealing an apparent exhumation of 7400ft (2257m). (Above, right) Error assessment of statistical fit showing the optimum shift-constant of 45µs/ft.

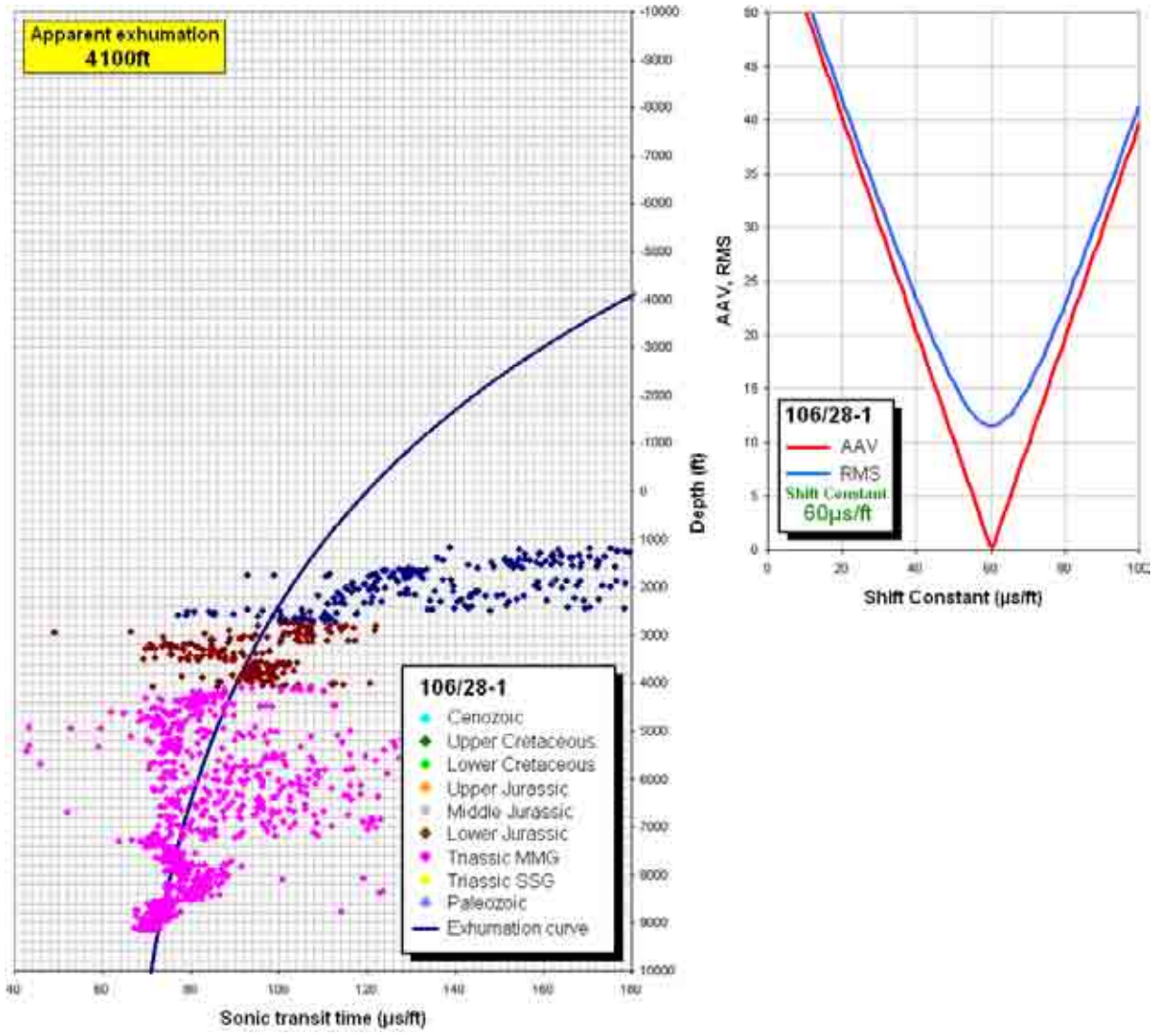

Figure A.24 – (Above) Graph showing the calculated compaction trend and erosion amount for well 106/28-1 revealing an apparent exhumation of 4100ft (1251m). (Above, right) Error assessment of statistical fit showing the optimum shift-constant of 60µs/ft.

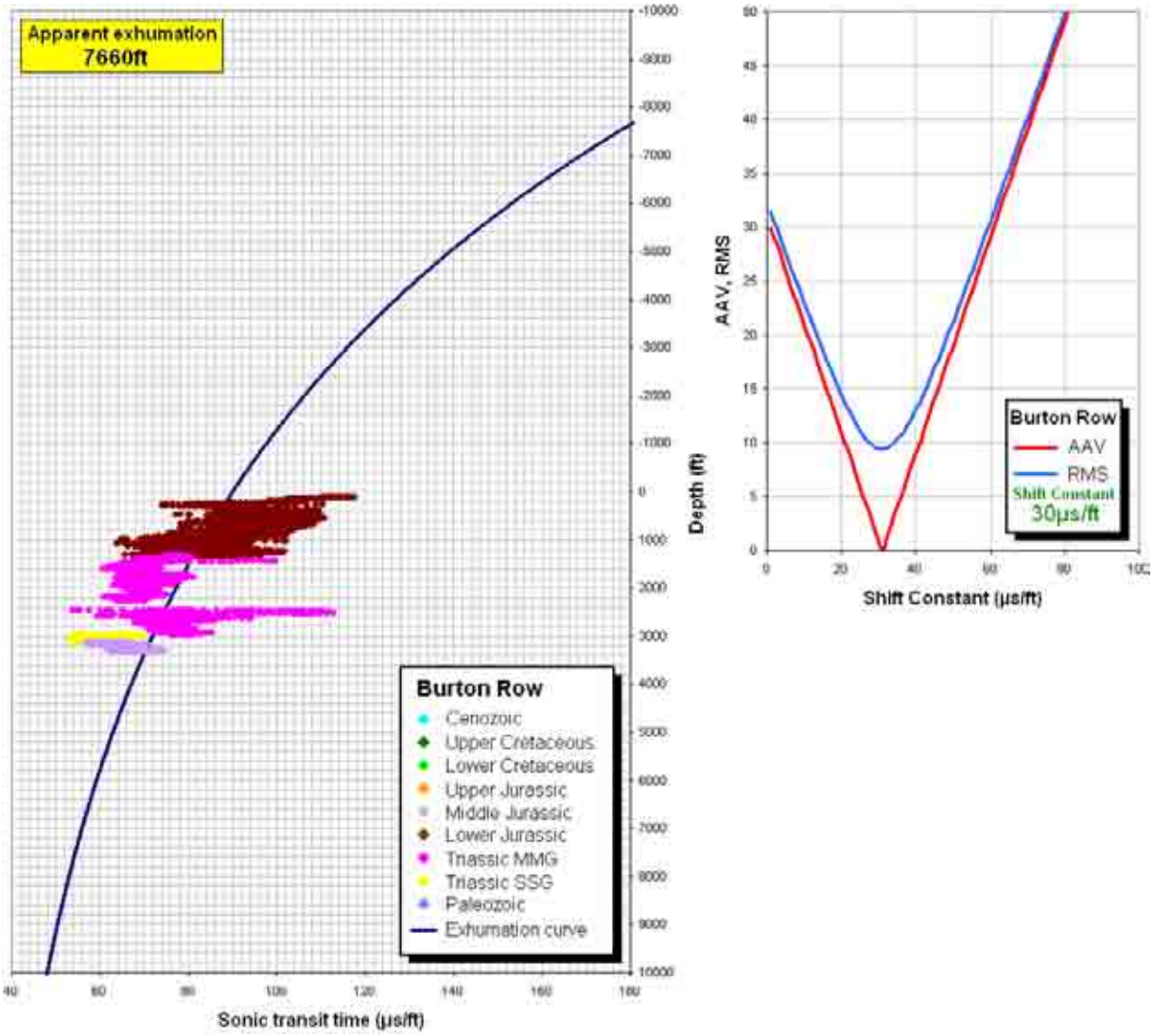

Figure A.25 – (Above) Graph showing the calculated compaction trend and erosion amount for the Burton Row borehole revealing an apparent exhumation of 7660ft (2336m). (Above, right) Error assessment of statistical fit showing the optimum shift-constant of 30µs/ft.

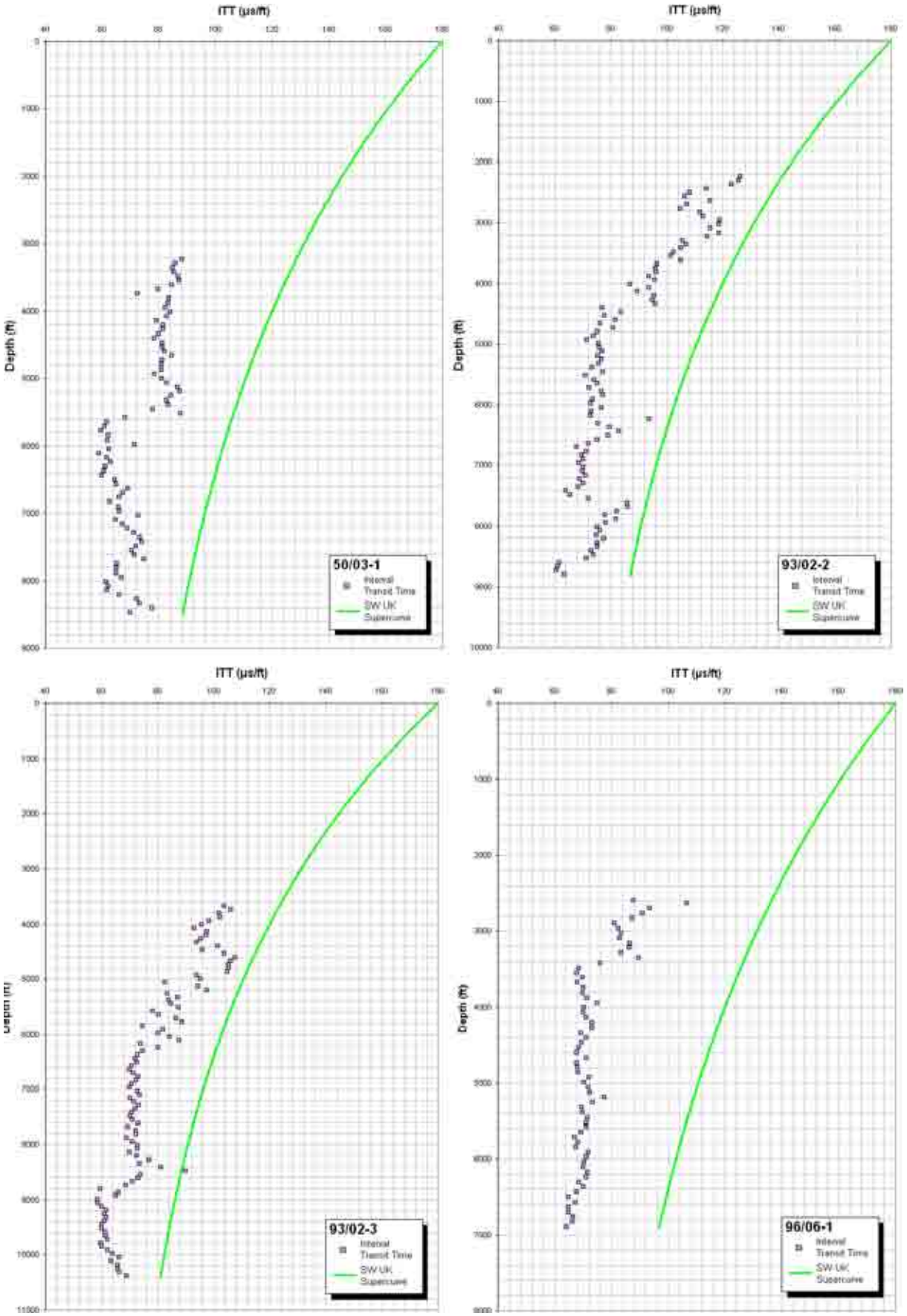

Figure A.26 – Comparison of ITT for the shale sequences of wells 50/03-1, 93/02-2, 93/02-3 and 93/06-1 with the supercurve derived for the SW UK.

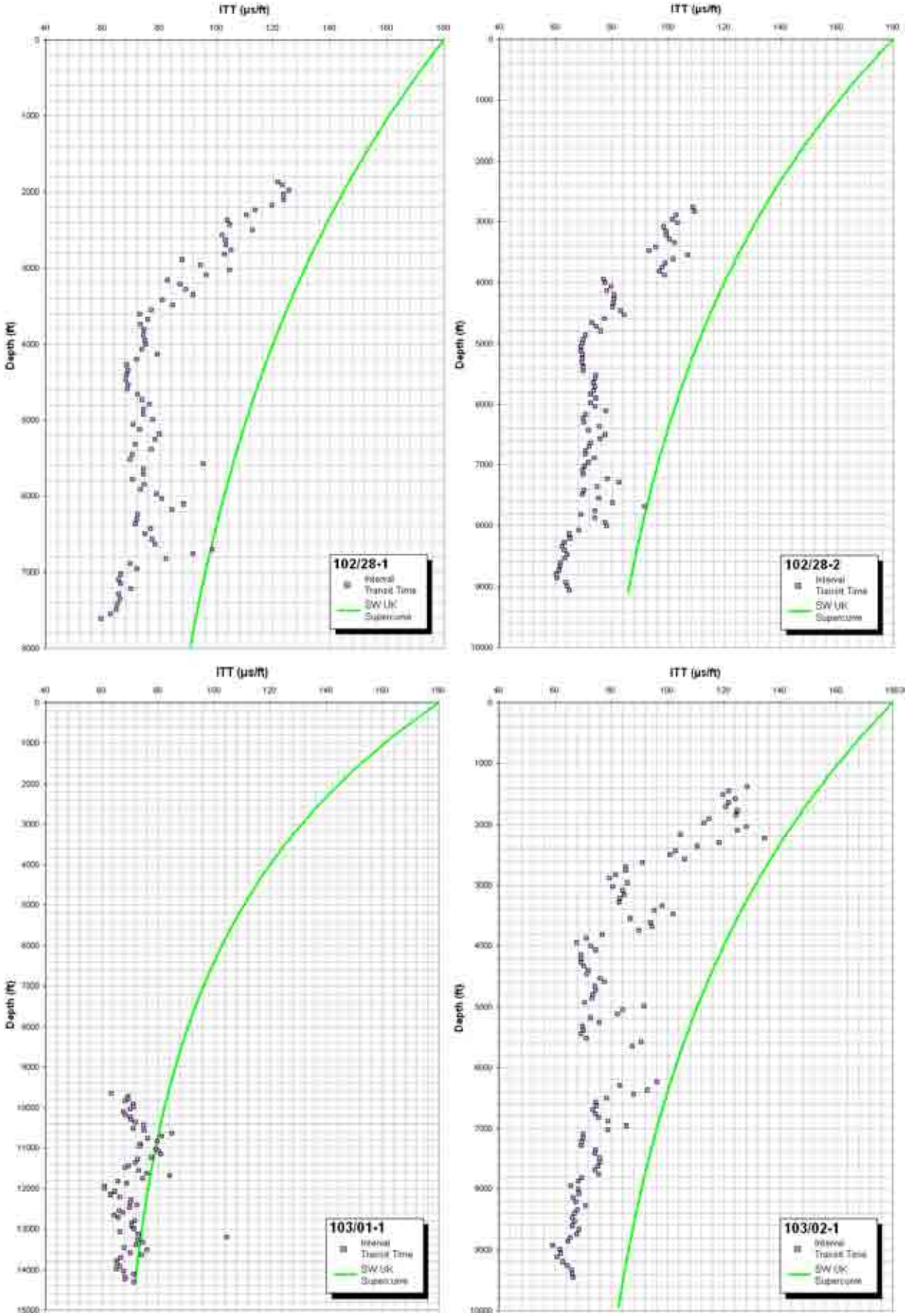

Figure A.27 – Comparison of ITT for the shale sequences of wells 102/28-1, 102/28-2, 103/01-1 and 103/02-1 with the supercurve derived for the SW UK.

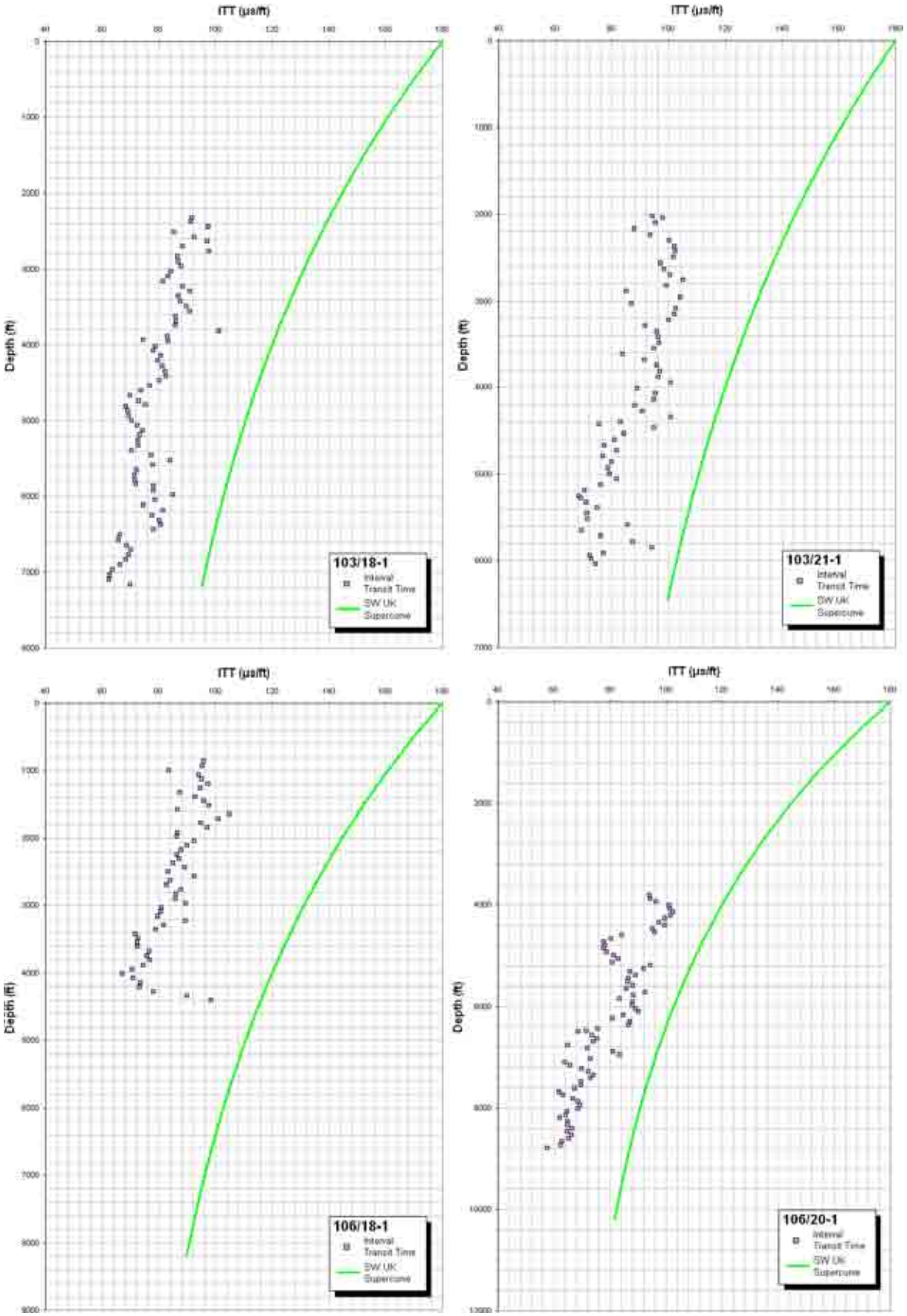

Figure A.28 – Comparison of ITT for the shale sequences of wells 103/18-1, 103/21-1, 106/18-1 and 106/20-1 with the supercurve derived for the SW UK.

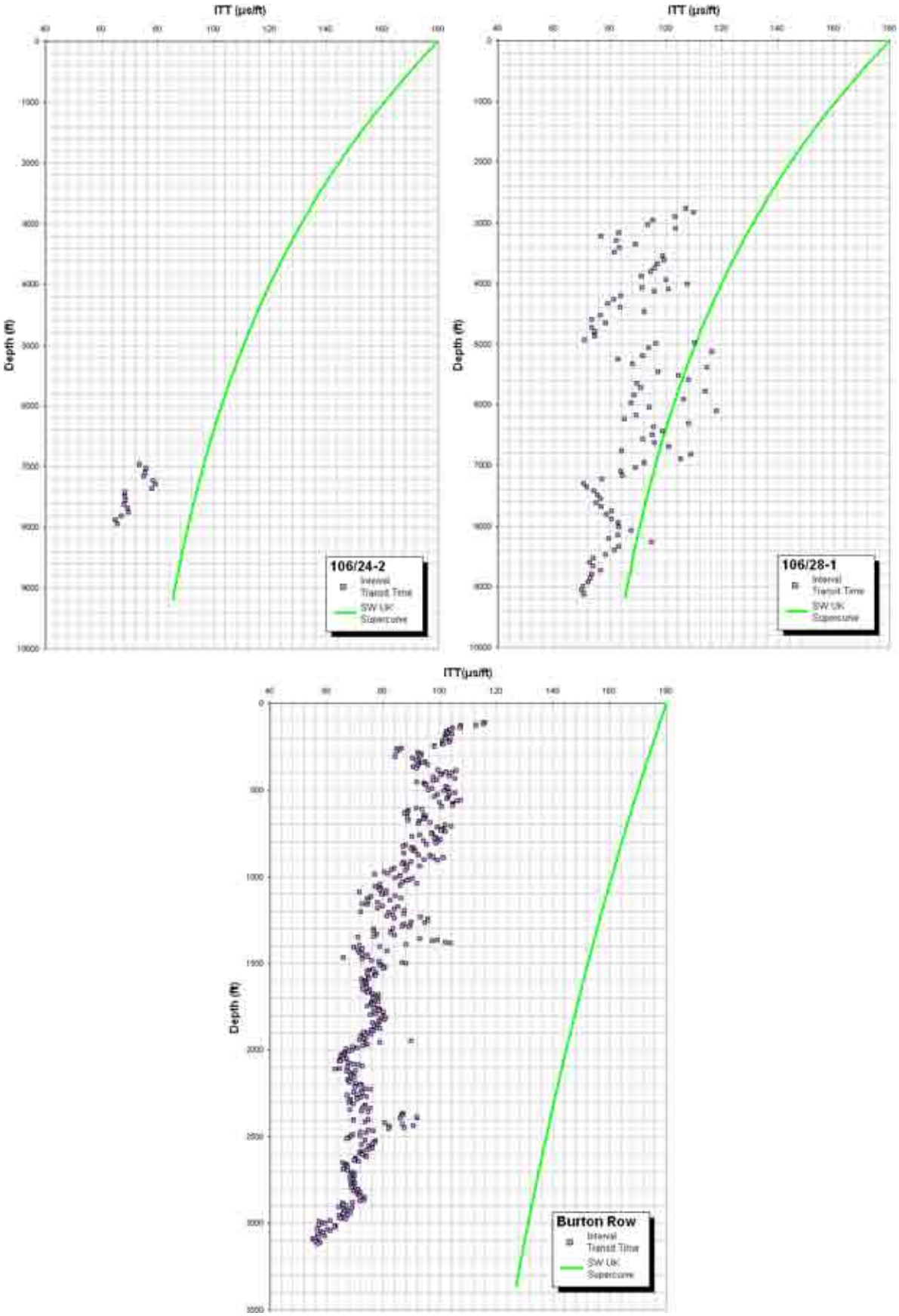

Figure A.29 – Comparison of ITT for the shale sequences of wells 106/24-2, 106/28-1 and the Burton Row borehole with the supercurve derived for the SW UK.

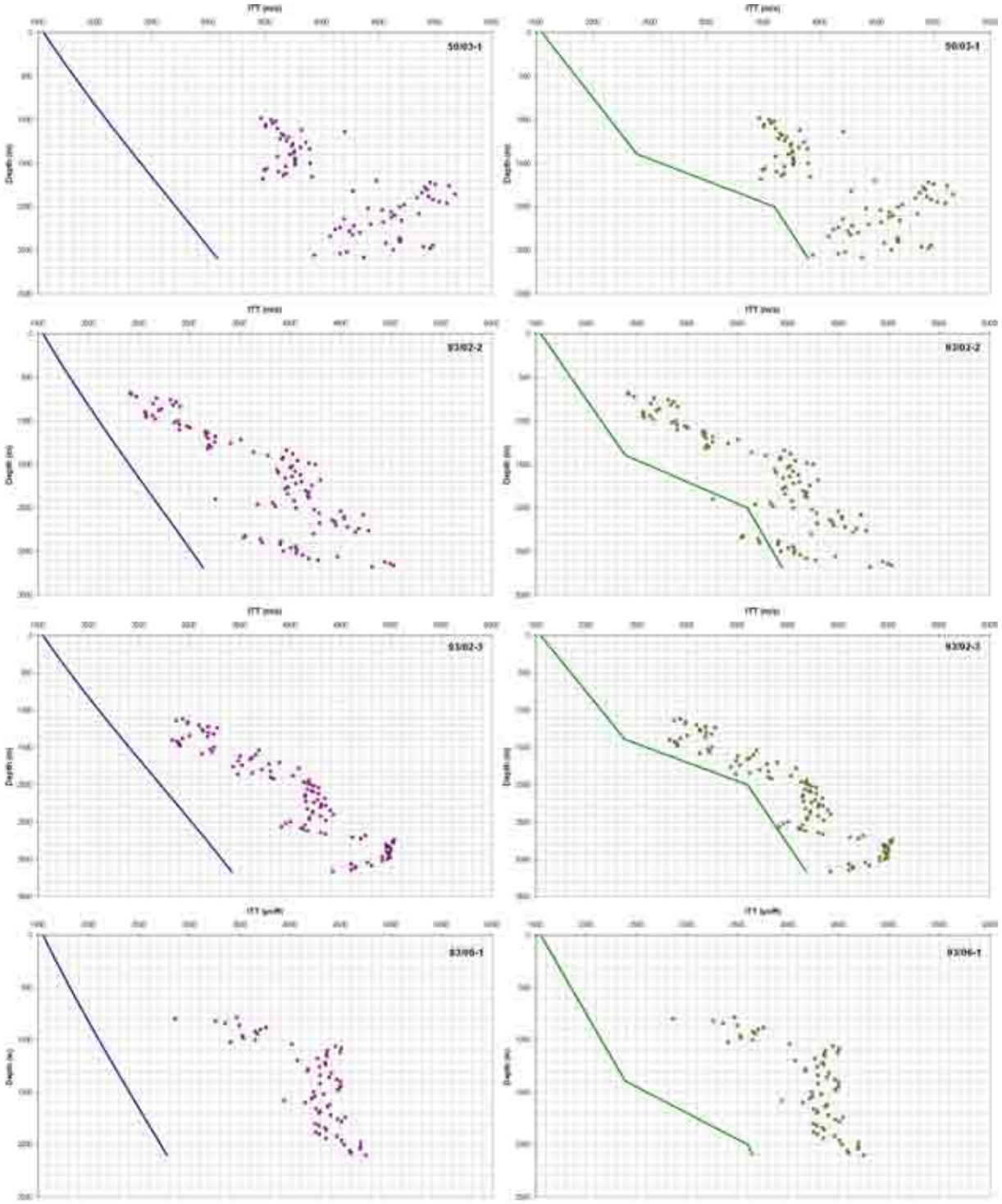

Figure A.30 – Comparison of interval transit time-depth values compared to the Lower Jurassic shale and Triassic Bunter shale trends of Japsen (2000) for wells 50/03-1, 93/02-2, 93/02-3 and 93/06-1.

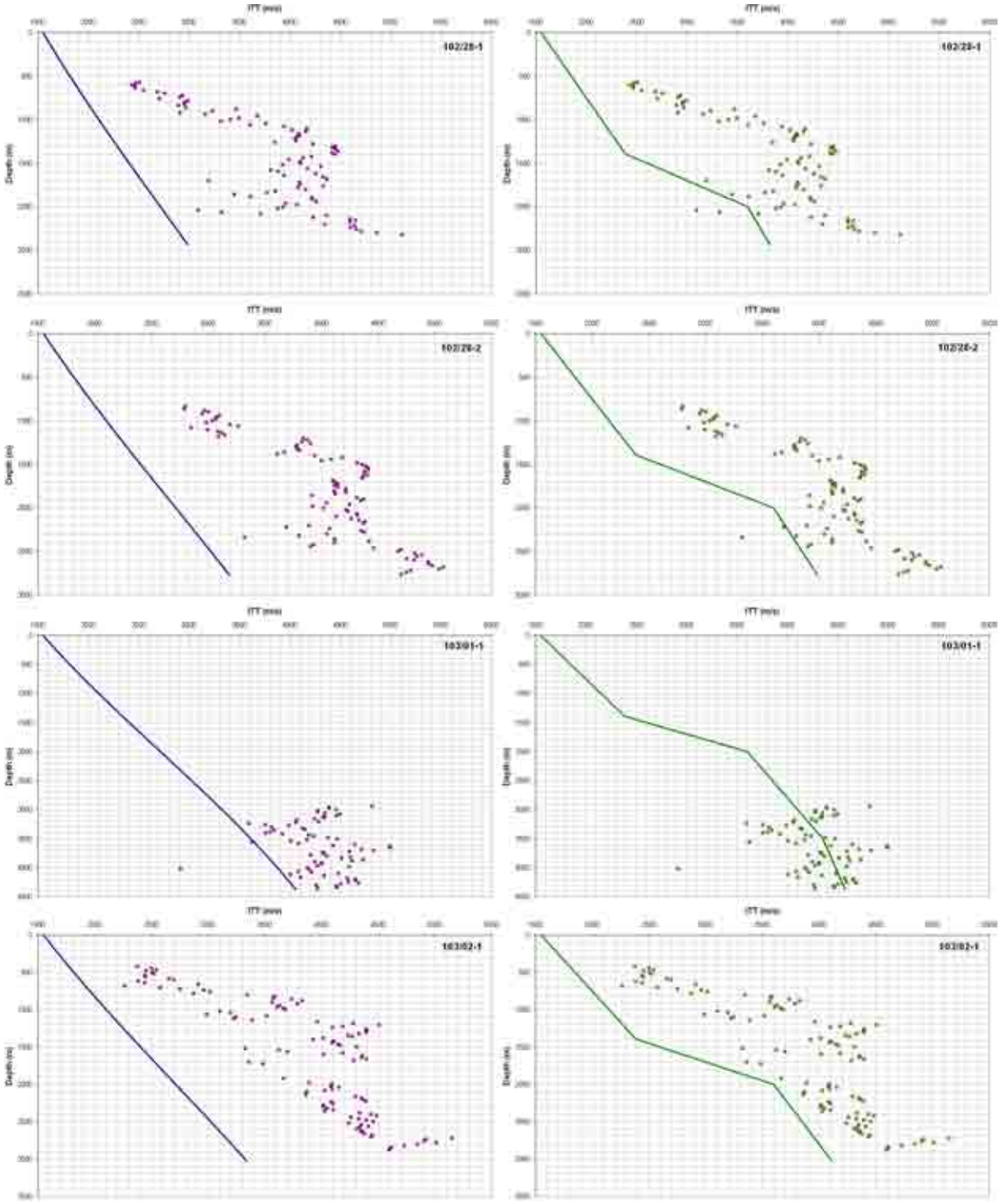

Figure A.31 – Comparison of interval transit time-depth values compared to the Lower Jurassic shale and Triassic Bunter shale trends of Japsen (2000) for wells 102/28-1, 102/28-2, 103/01-1 and 103/02-1.

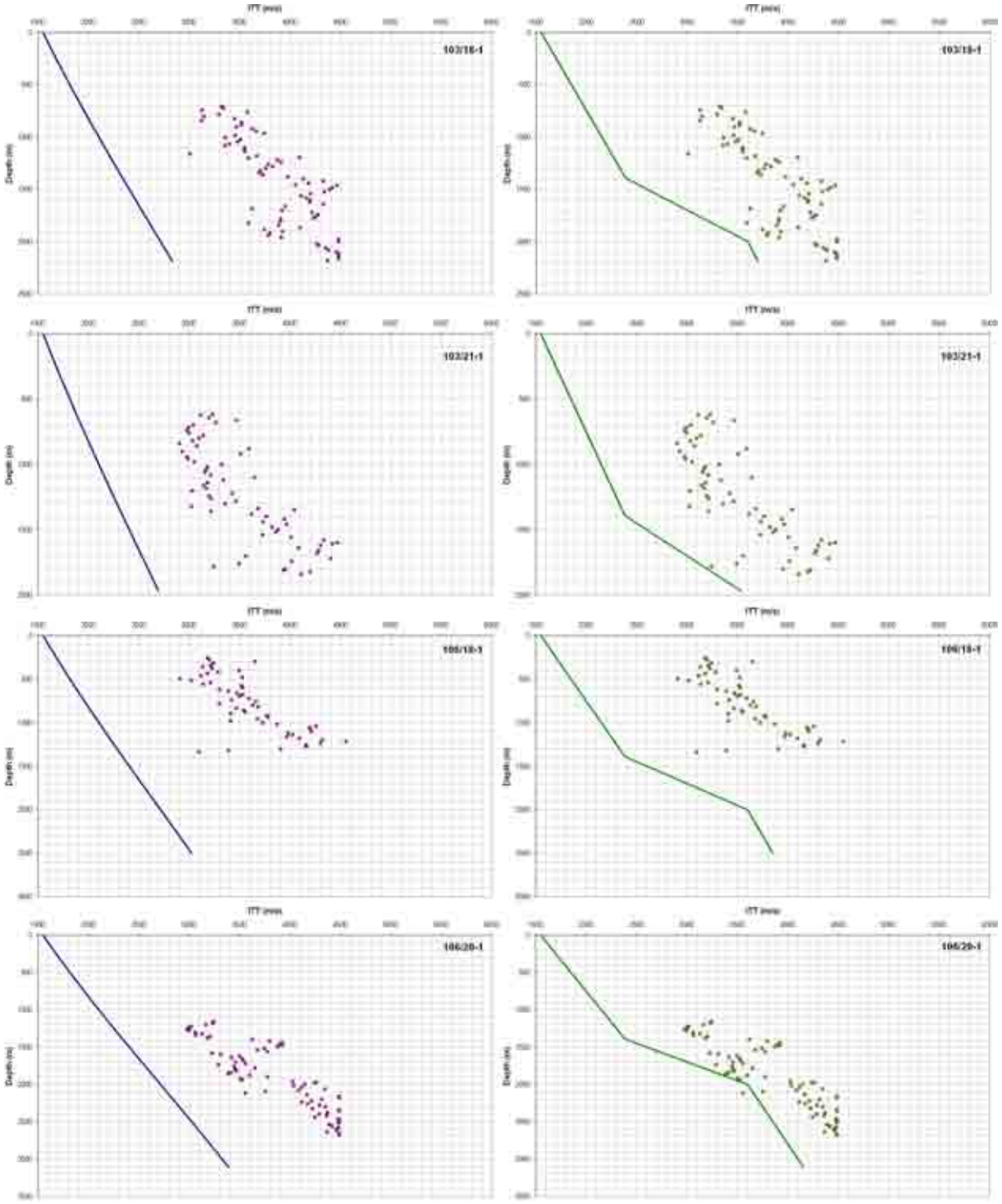

Figure A.32 – Comparison of interval transit time-depth values compared to the Lower Jurassic shale and Triassic Bunter shale trends of Japsen (2000) for wells 103/18-1, 103/21-1, 106/18-1 and 106/20-1.

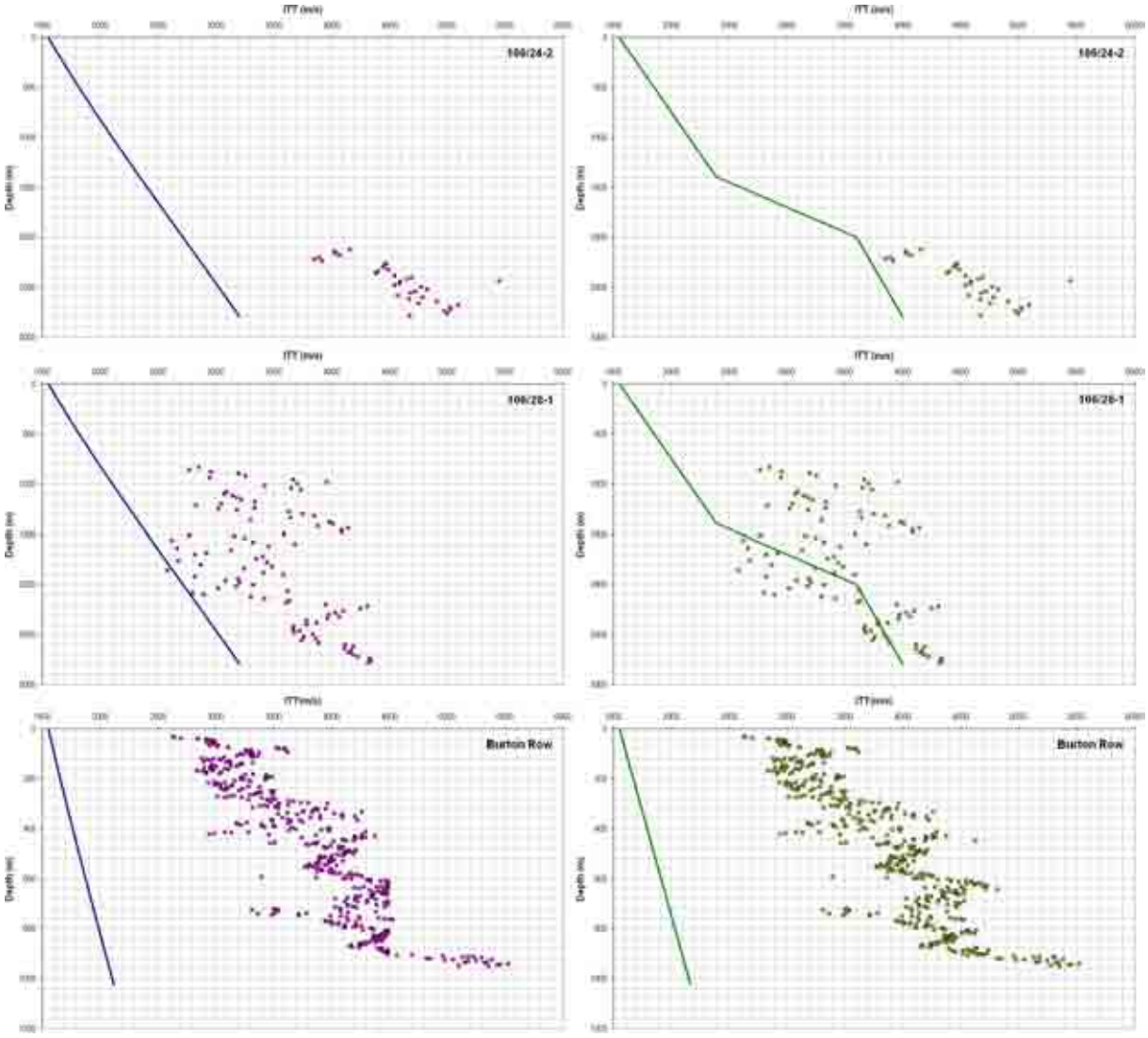

Figure A.33 – Comparison of interval transit time-depth values compared to the Lower Jurassic shale and Triassic Bunter shale trends of Japsen (2000) for wells 106/24-2, 106/28-1 and the Burton Row borehole.

		Depth to mid-point (m)					Average Chalk ITT	Average Greensand ITT	Average Lower Jurassic ITT	Average MMG ITT	Average SSG ITT
		Upper Cretaceous	Lower Cretaceous	Lower Jurassic	Mercia Mudstone	Sherwood Sandstone					
Wells	50/01-1			1700					73.62		
	50/03-2										
	93/02-2	491	651	1011	1621	2441	99.69	109.14	106.15	77.4	75.5
	93/02-3	497	751	1501	2391	2926	97.29	99.96	93.97	73.79	82.26
	93/06-1	491	766	826	961	1791	70.41	131.47	95.44	83.88	89.89
	98/28-1	333	526	876	1241	2241	103.59	132.34	81.24	75	66.91
	98/28-2	520	761	981	1301	2617	100.74	103.29	101.67	83.09	83.27
	99/01-1			3360	3621				73.7	84.89	
	99/02-1			621	1051	2837			116.02	83.79	83.23
	99/18-1				825	1176				89.93	
	99/20-1			1567	2336				98.04	85.27	
	99/23-1										
	99/24-2			2211	2888				74.66	87.88	
	99/28-1			1045	1360				94.68	81.08	
	Burton Row			225	561	930			90.63	74.77	99.14
Hillis Wells											
	47/29-1	602	664				86.14	96.71			
	48/19-1	386	708				94.23	93.69			
	49/05-1	423	628				101.89	107.54			
	49/09-2	285	594				106.67	112.88			
	49/09-3	330	690				106.09	99.76			
	49/14-3	379	764				99.81	96.54			
	50/06-1	107	536				109.03	123.07			
	50/12-2A	132	376				84.15	101.5			
	72/30-1A	1031			1662		87.17			82.92	
	73/01-1	1137			2064		93.16			82.99	
	73/02-1	799			1177		92.88			90.38	
	73/04-1	558	842		966		102.43	113.1		106.83	
	73/05-1	960	1221		1472		87.86	108.87		86.83	
	73/06-1	844	1029		1223		97.64	97.1		92.9	
	73/07-1	1028	1379		1883		87.36	92.04		79.62	
	73/08-1	878			1390		92.92			87.88	
	73/12-1A	1260			1659		86.88			86.76	
	73/13-1	1389			2207		83.44			72.56	
	73/18-1	1172			1694		84.44			80.99	
	74/01-1A	774	979		1145		92.64	121.26		92.02	
	83/24-1	472	667				104.46	112.25			
	85/28-1	686	862		1038		96.66	119.53		102.55	
	86/17-1	388	548		748		95.78	114		86.25	
	86/18-1	577	816				87.76	105.17			
	87/17-1A	192	260		469		76.47	111.38		89.13	
	87/21-1	368					89.15				
	87/26-1	398	670		786		93.02	110.09		96	
	88/02-1	76			700		100.13			94.52	
	92/29-1	347	431				90.83	102.09			
	93/18-1				1290					74.93	
	93/21-1	272	521		1410		98.66	112.16		76.65	
	Brezell	248					84.07				
	Gullveig	1224	1421				86.64	103.28			
	Glaeam	884	1398				97.92	73.5			
	Kettur	746					101.56				
	Kulreon	462			818		96.07			93.84	
	Lizann	438					79.05				
	Penma	1096	1398				94.05	94.36			
	Ste Gareon	1296	1642		2205		79.61	77.76		73.61	
	Tuvaak		229					122.23			
	Var Vas	287	340				86.26	104.12			

Table A.1 – Depth of formation mid-points below sea bed (m) and average interval transit times for formations and wells (μs/ft). Hillis wells refer to wells analysed by Menpes & Hillis (1995) whose values have been utilised to increase the coverage of the data.

APPENDIX B

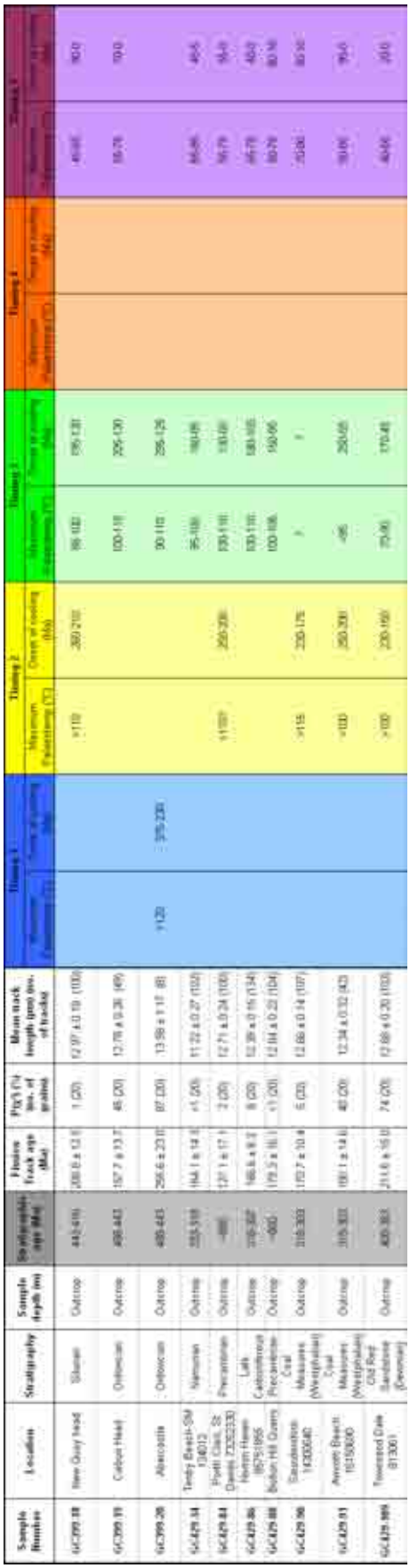

Table B.1 – AFTA sample details from Pembrokeshire and thermal history interpretation.

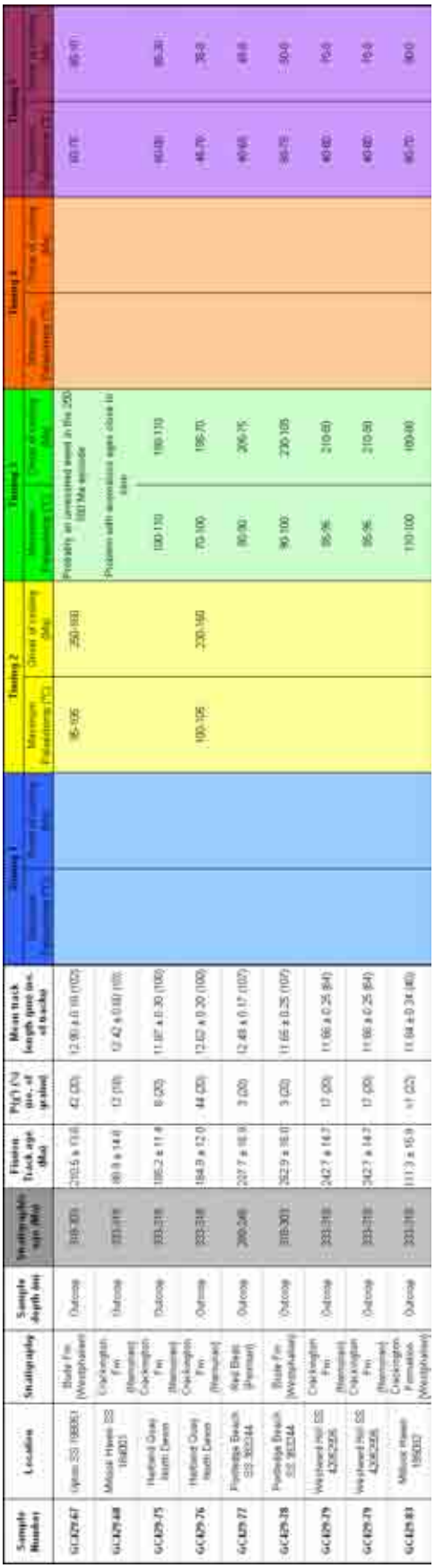

Table B.2 – AFTA sample details from North Devon and thermal history interpretation.

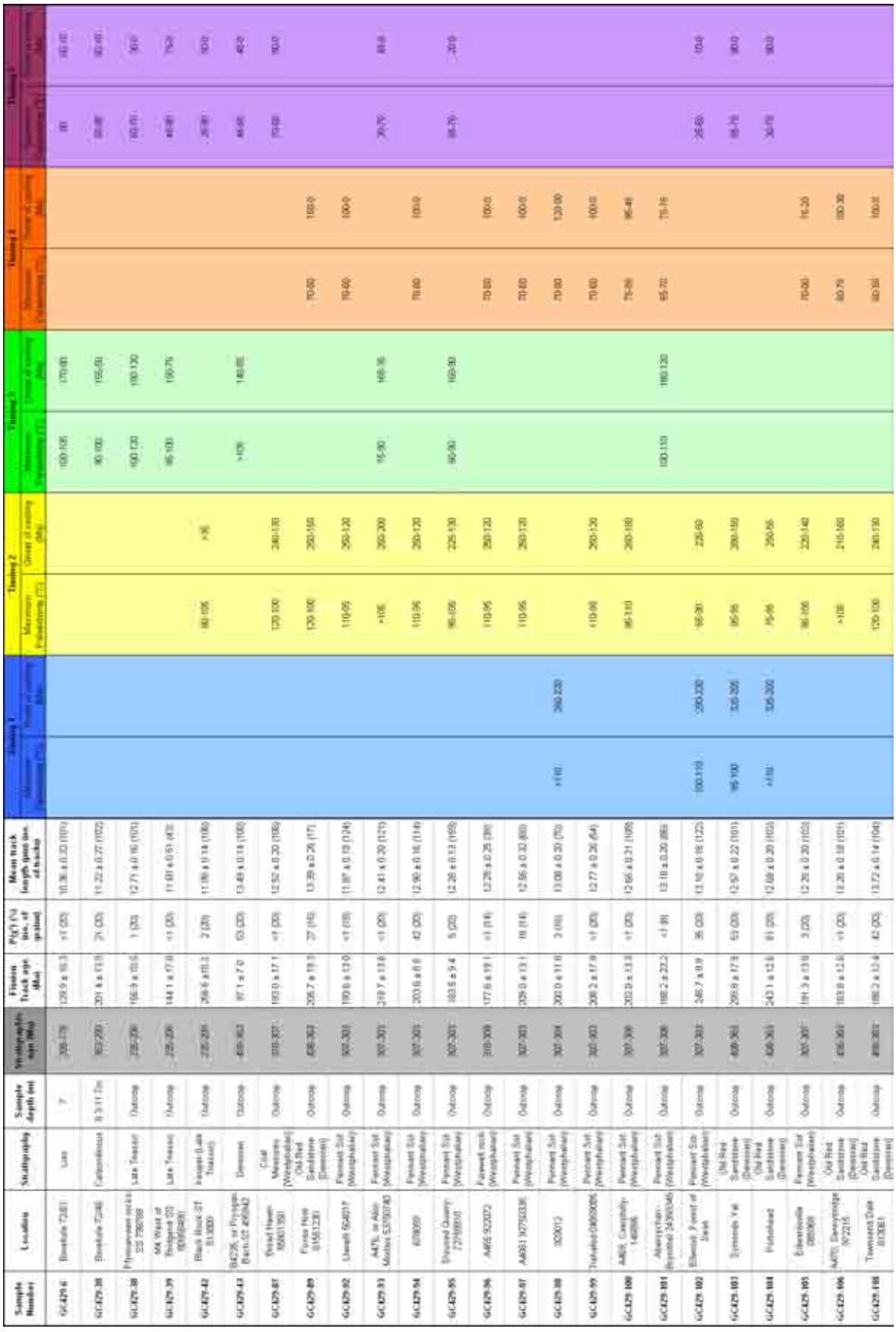

Table B.3 – AFTA sample details from South Wales and thermal history interpretation.

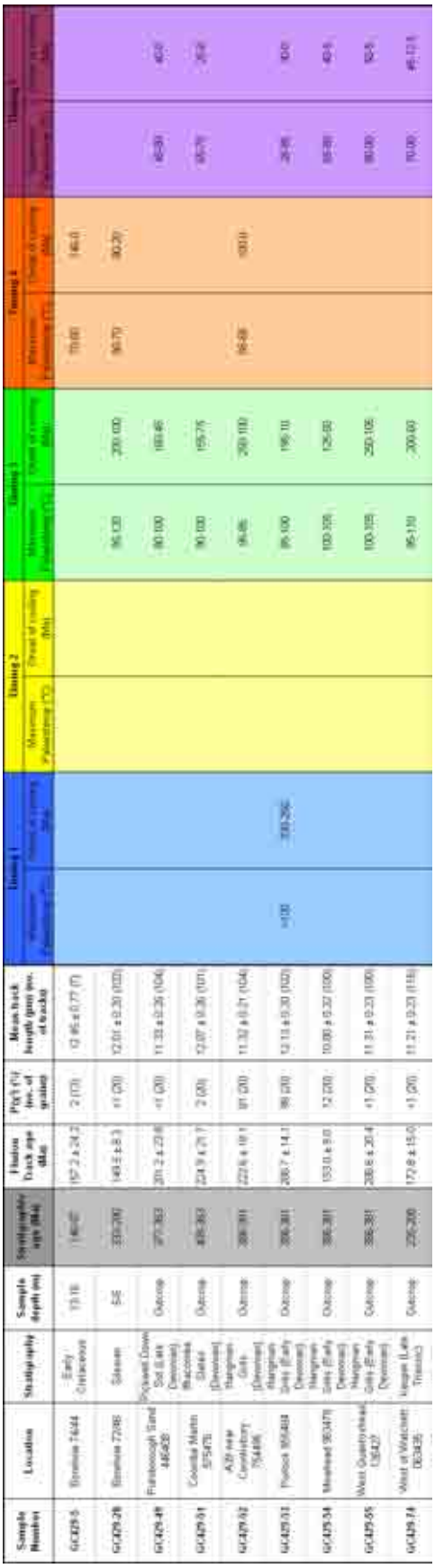

Table B.4 – AFTA sample details from North Somerset and thermal history interpretation.

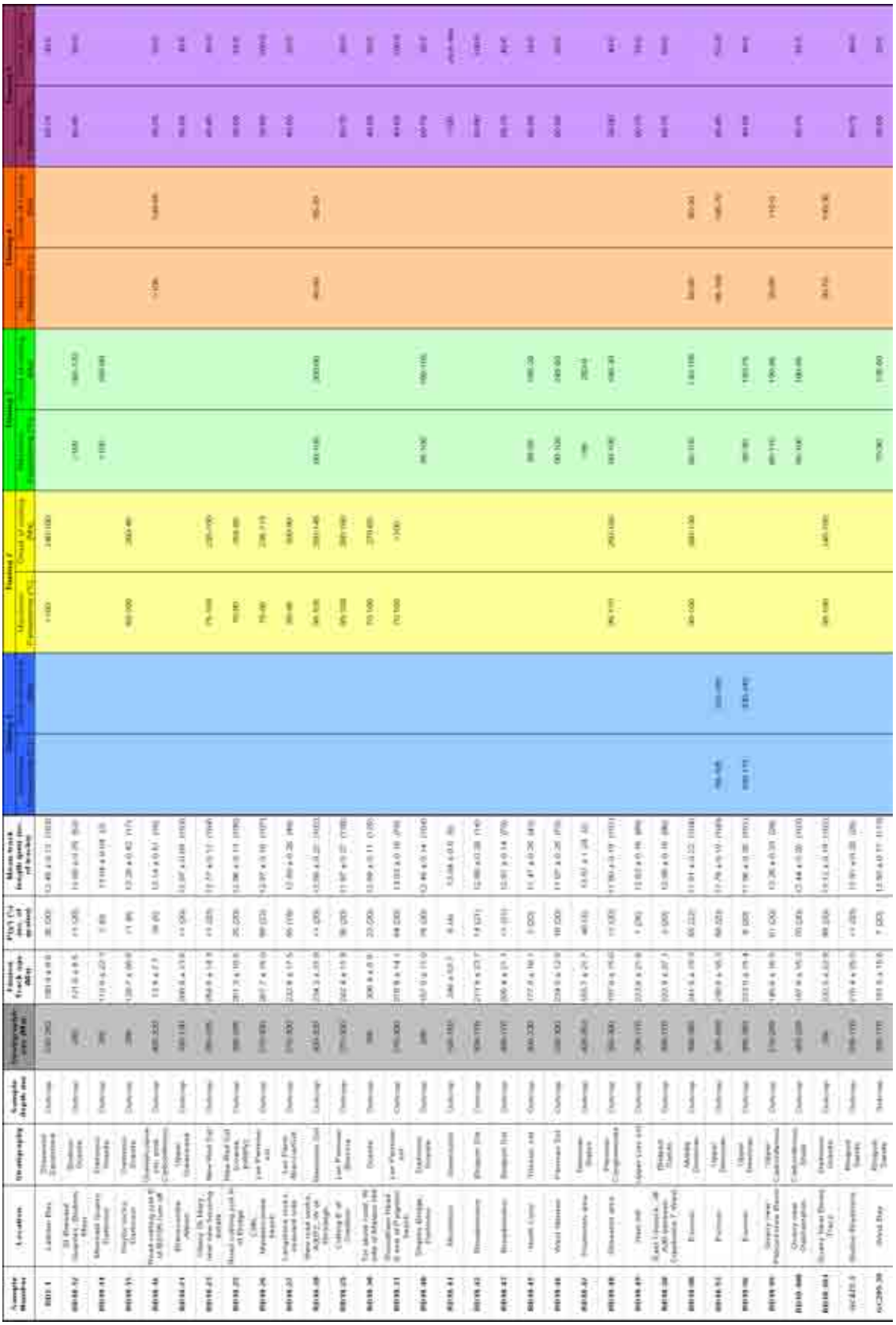

Table B.5 – AFTA sample details from South Devon, Somerset and Dorset and thermal history interpretation.

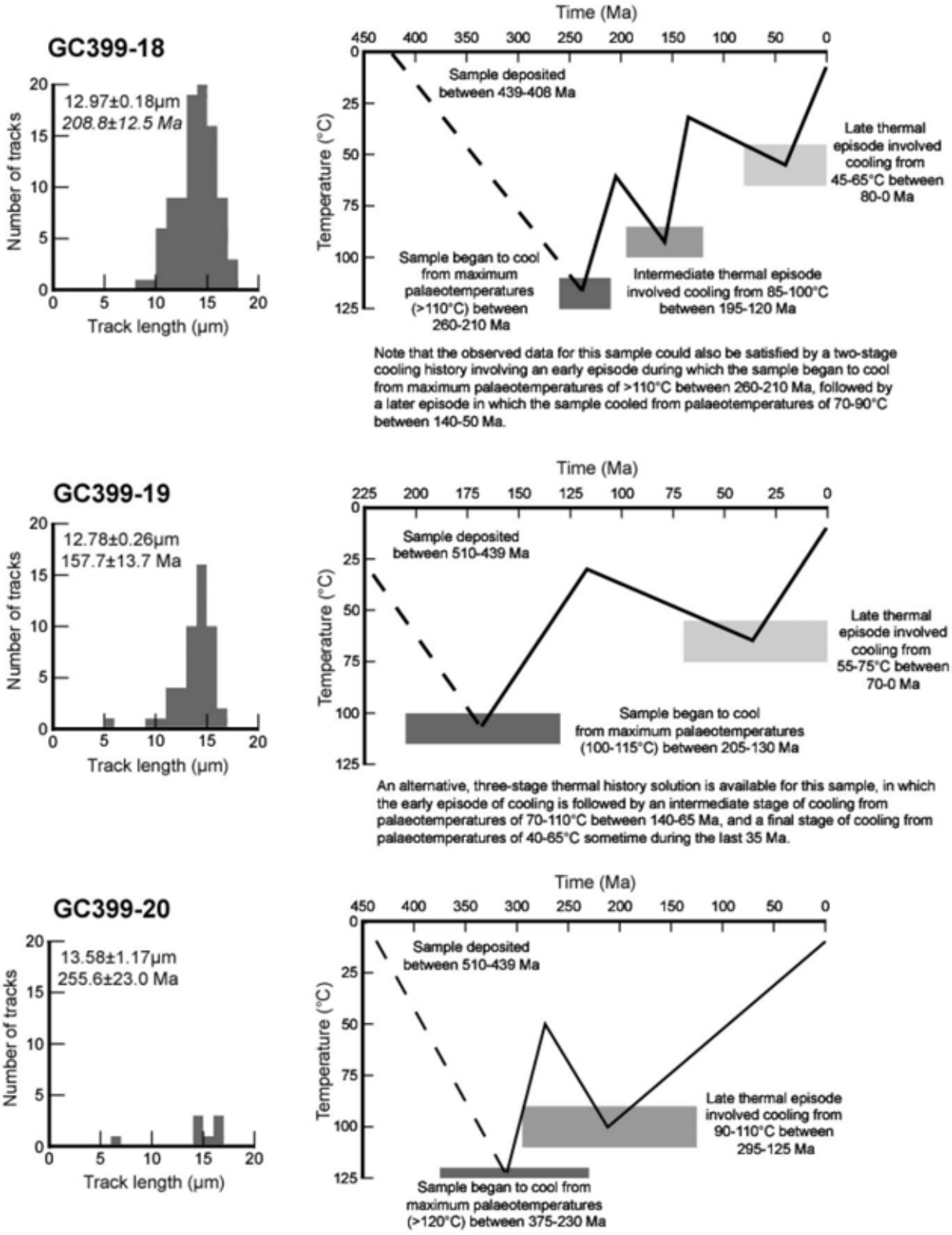

Figure B.1 – Fission track length distribution plots and modelled thermal history solutions for samples GC399-18, 19 and 20 (after Holford, 2006).

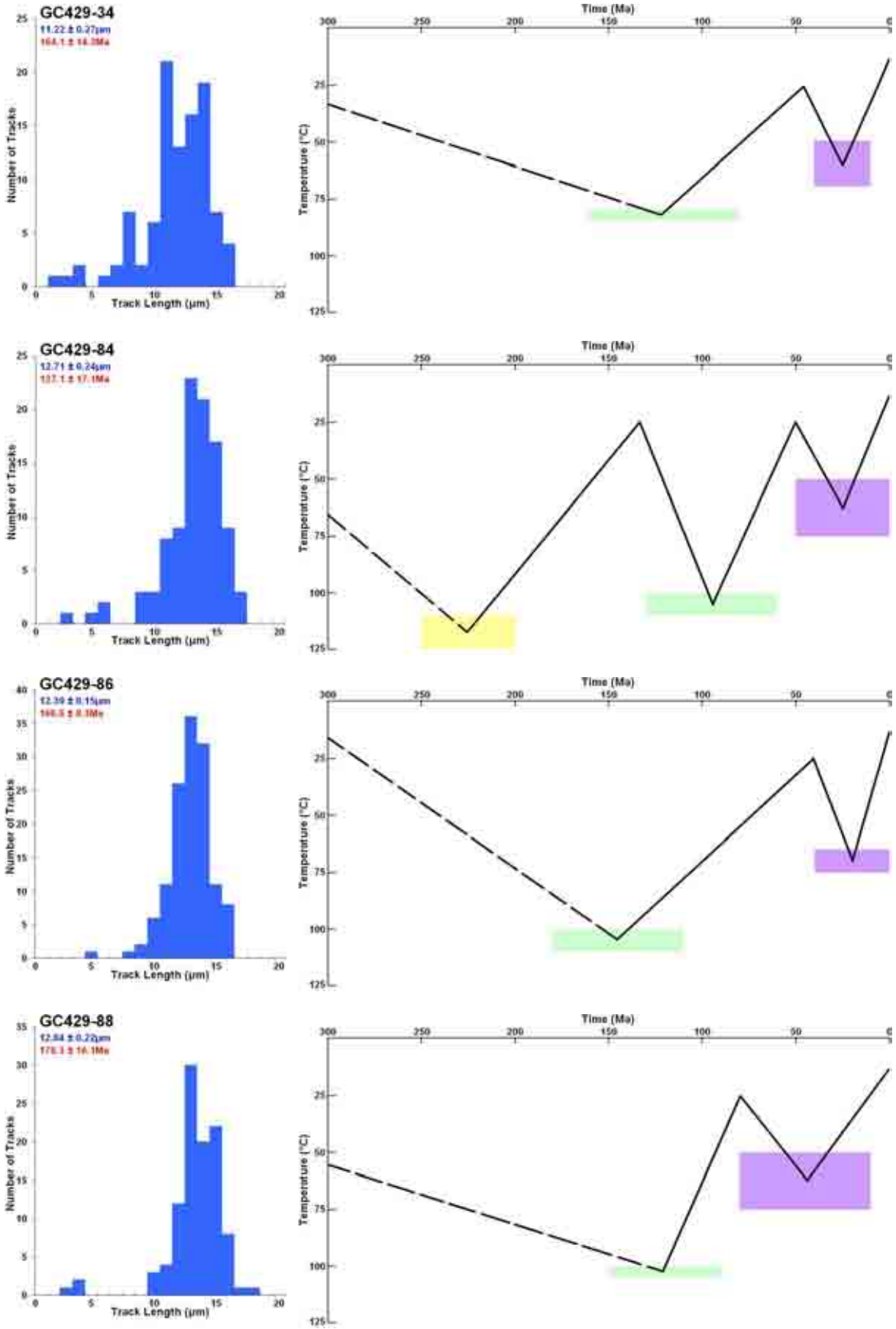

Figure B.2 - Fission track length distribution plots and modelled thermal history solutions for samples GC429-34, 84, 86 and 88.

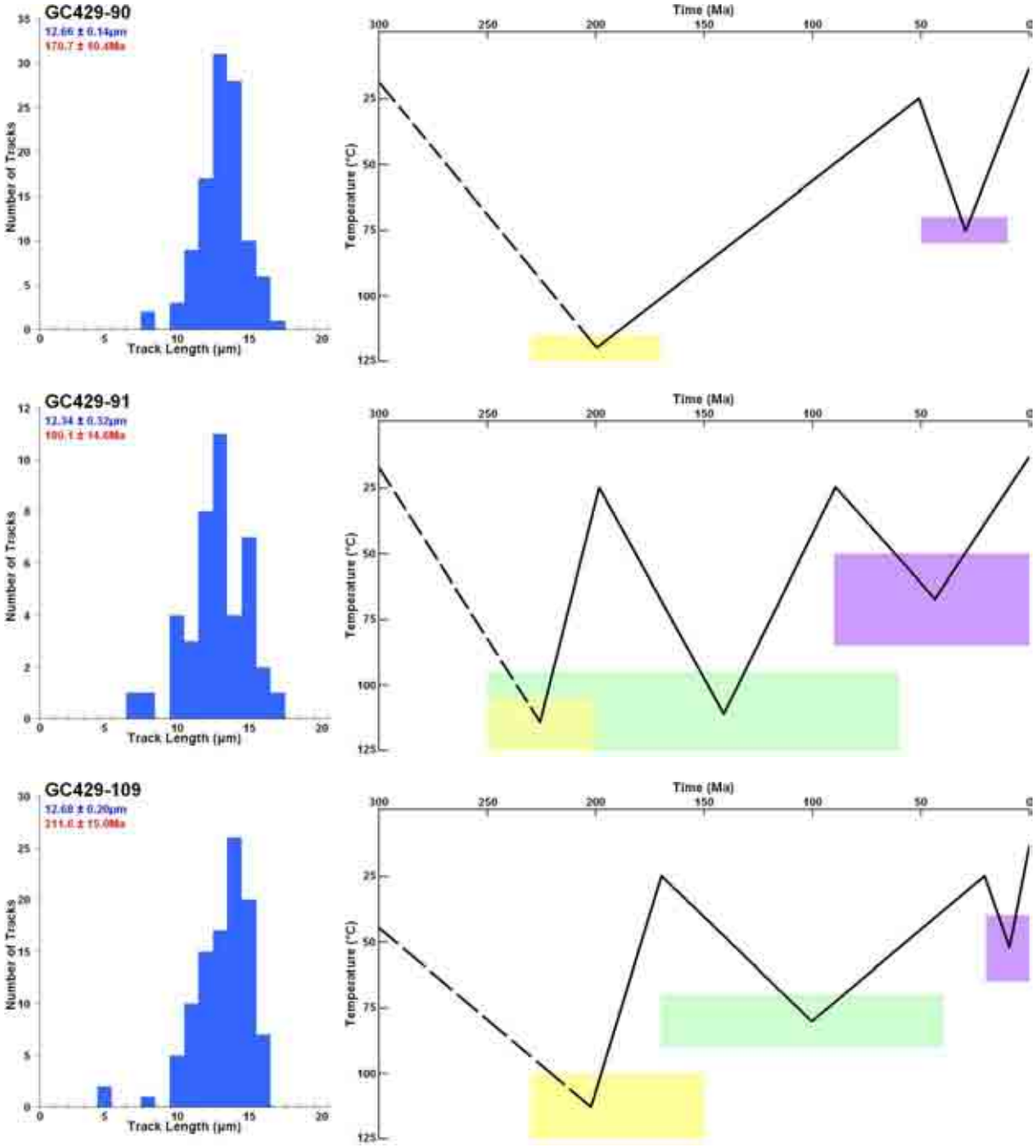

Figure B.3 - Fission track length distribution plots and modelled thermal history solutions for samples GC429-90, 91 and 109.

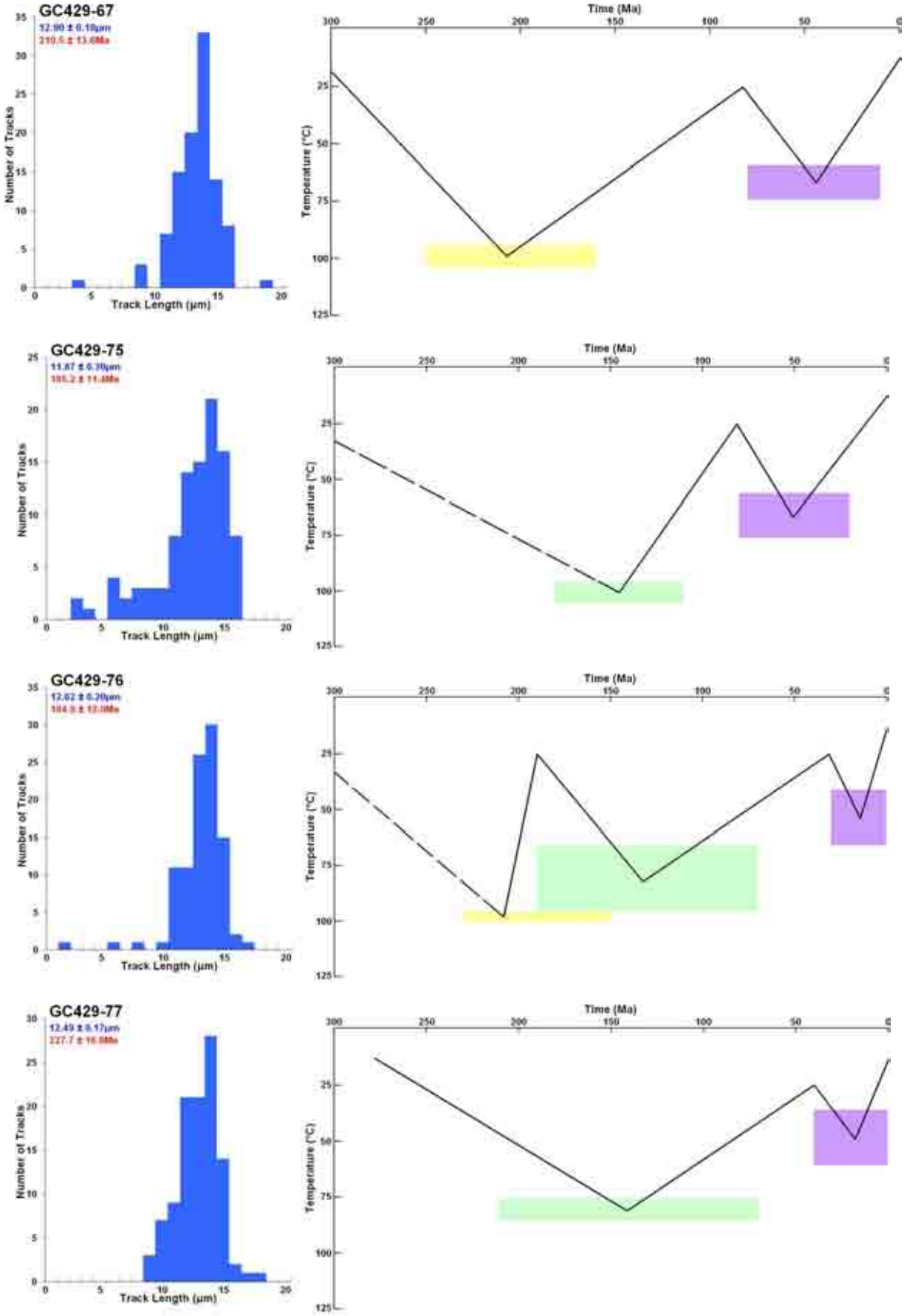

Figure B.4 - Fission track length distribution plots and modelled thermal history solutions for samples GC429-67, 75, 76 and 77.

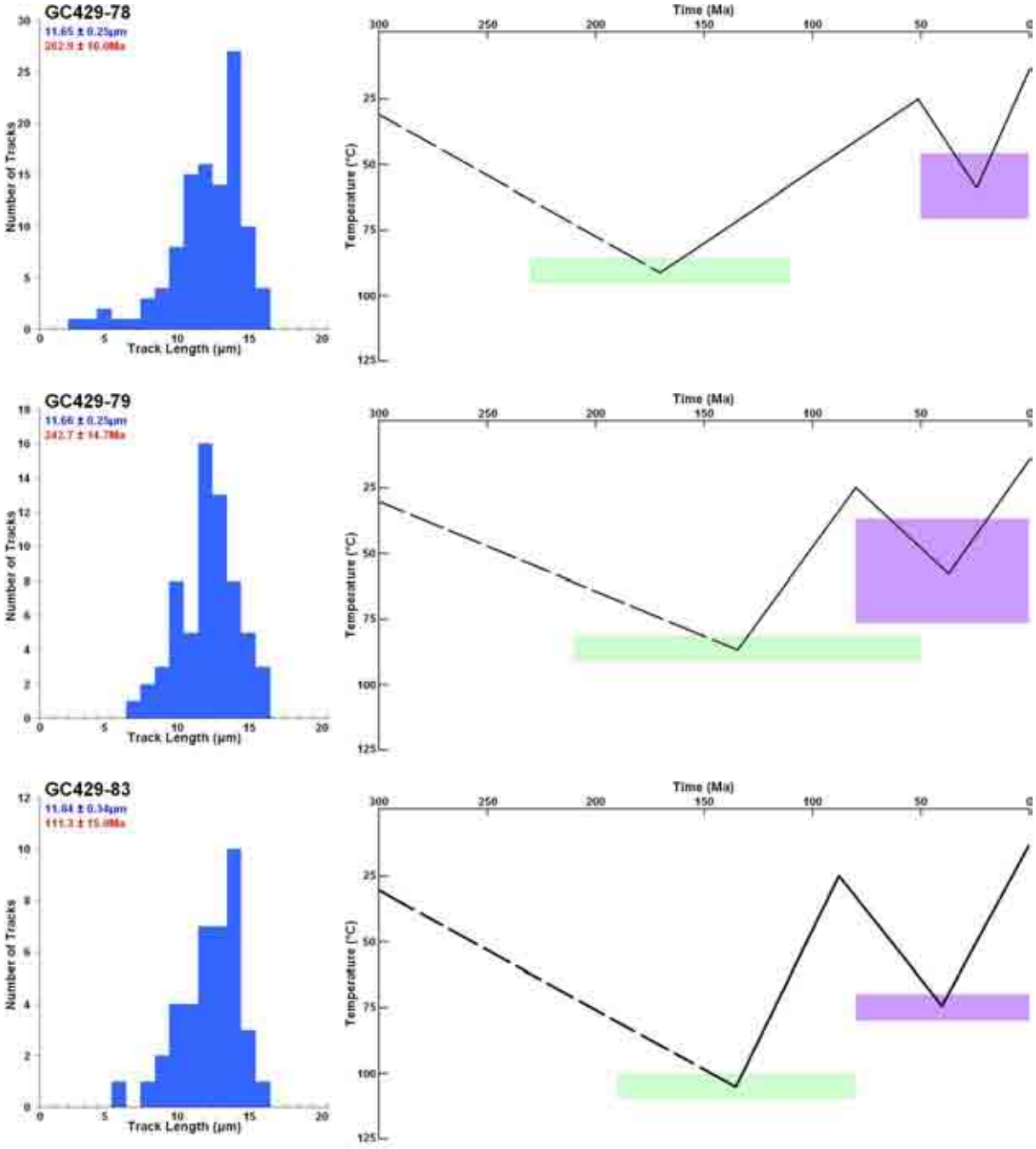

Figure B.5 - Fission track length distribution plots and modelled thermal history solutions for samples GC429-78, 79 and 83.

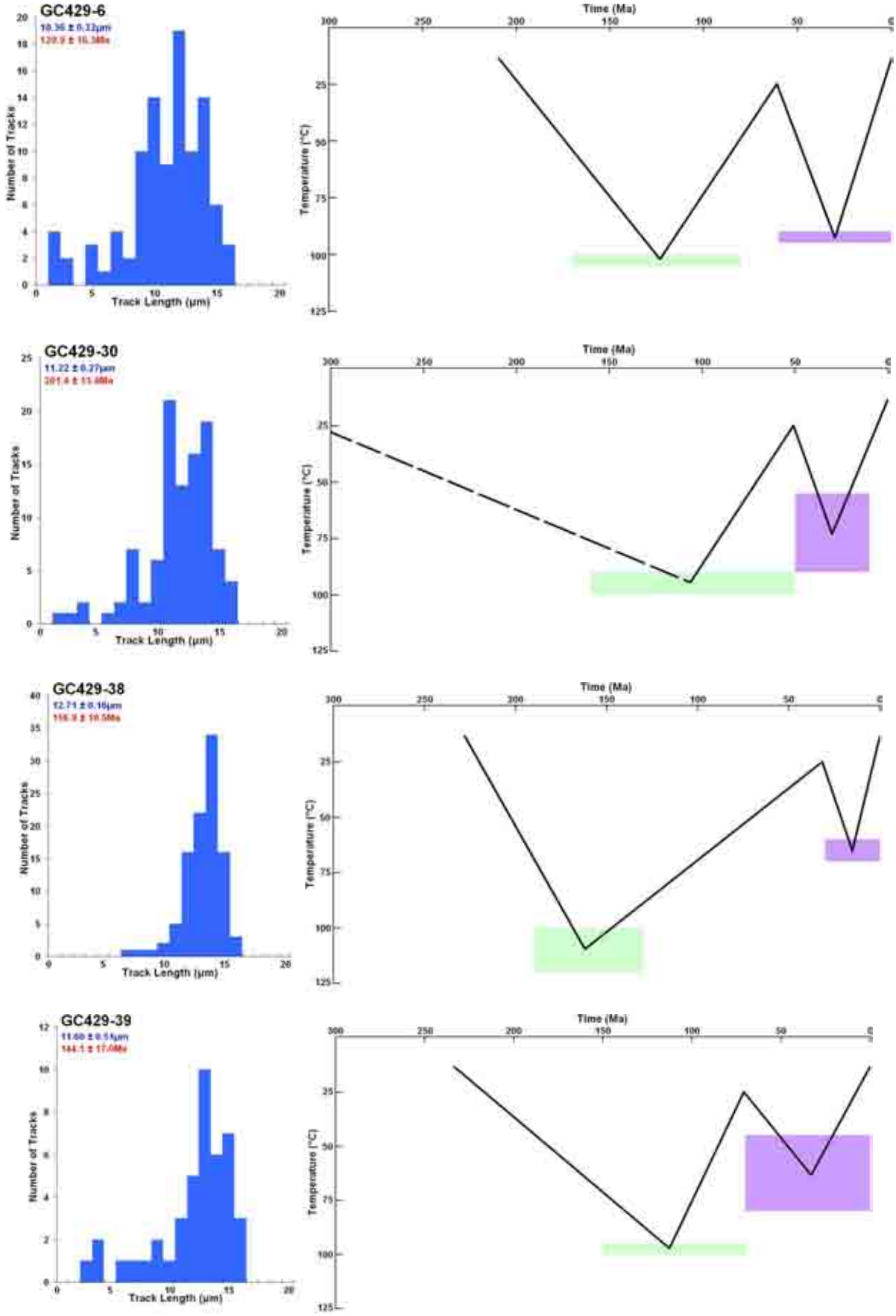

Figure B.6 - Fission track length distribution plots and modelled thermal history solutions for samples GC429-6, 30, 38 and 39.

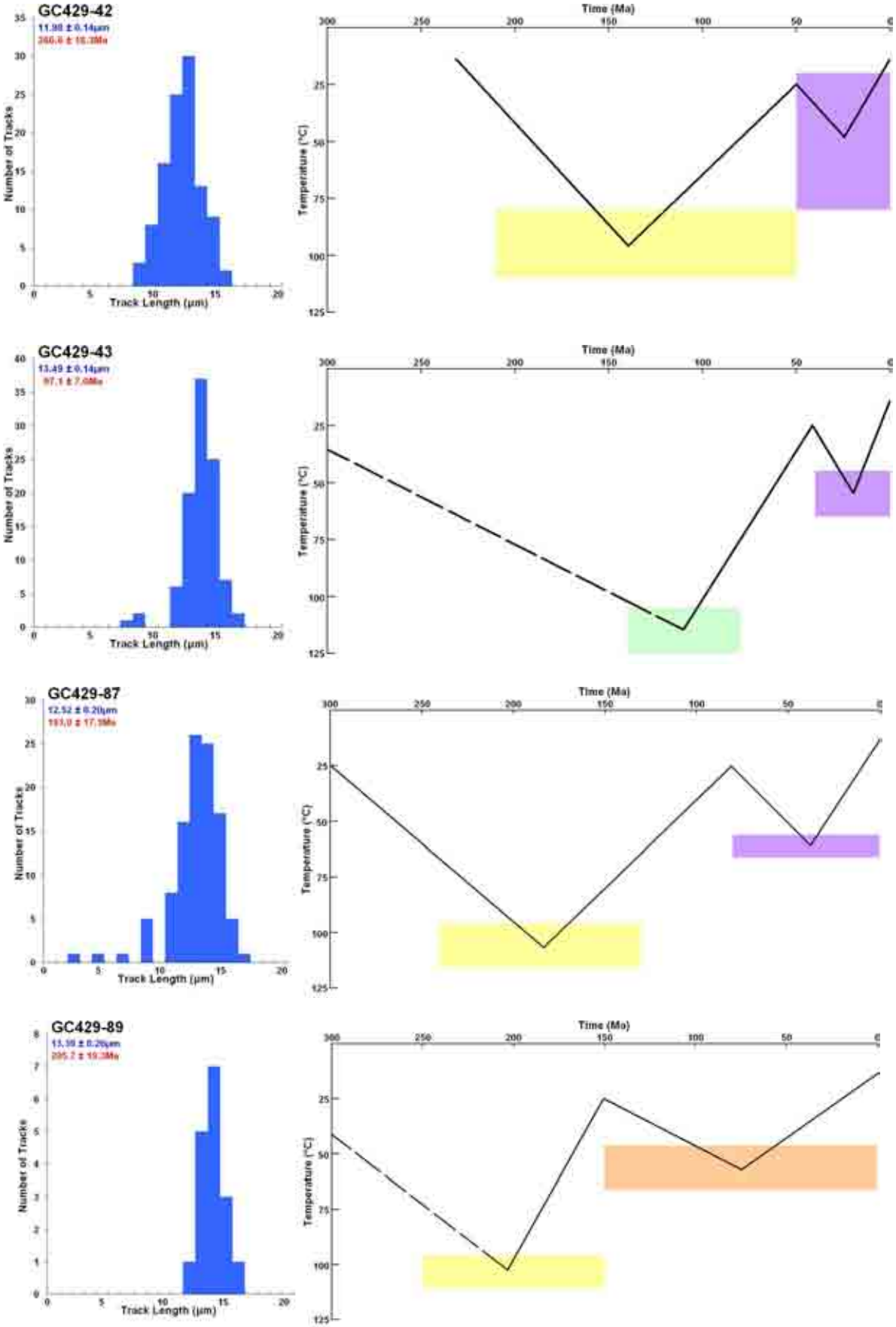

Figure B.7 - Fission track length distribution plots and modelled thermal history solutions for samples GC429-42, 43, 87 and 89.

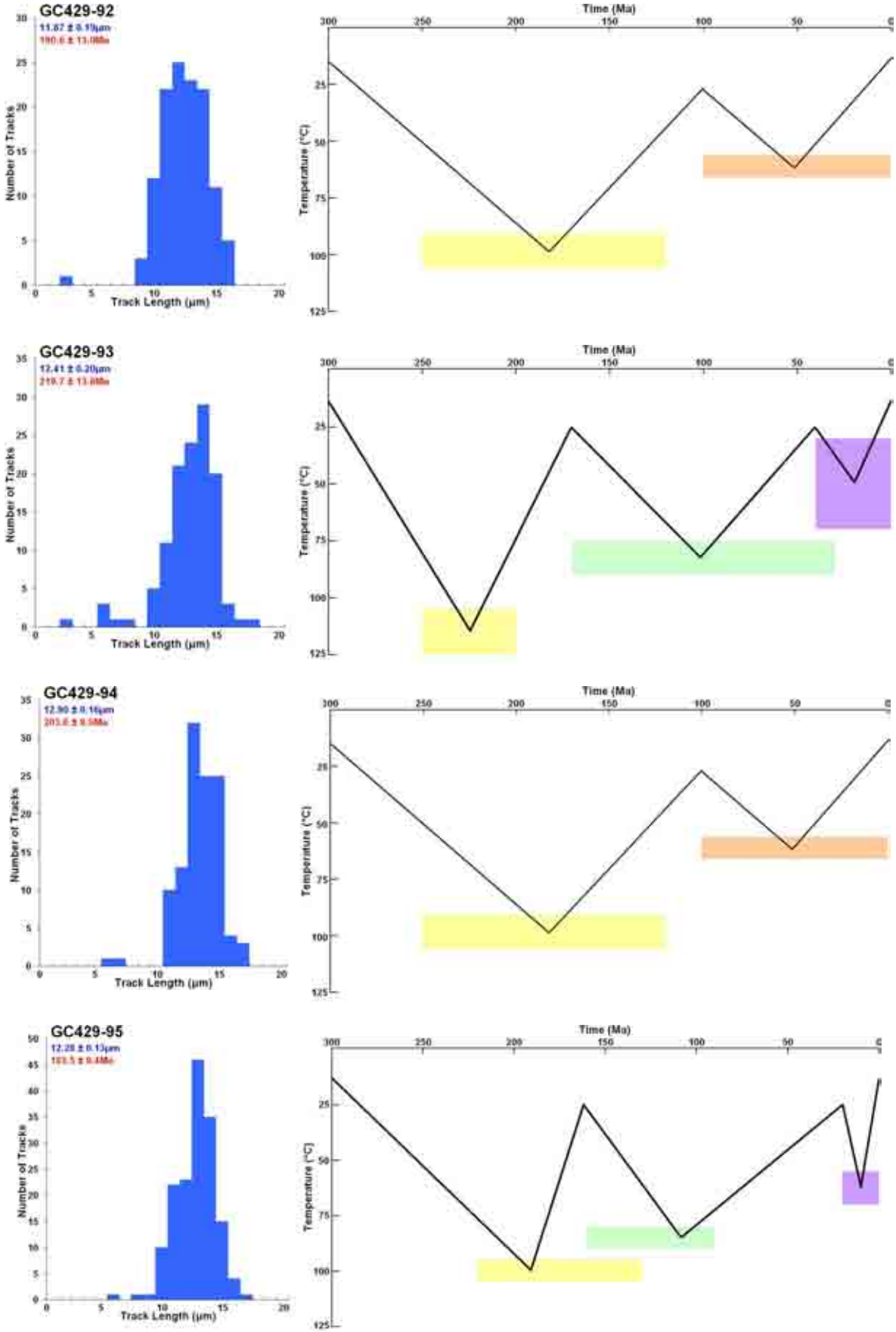

Figure B.8 - Fission track length distribution plots and modelled thermal history solutions for samples GC429-100, 101, 102 and 103.

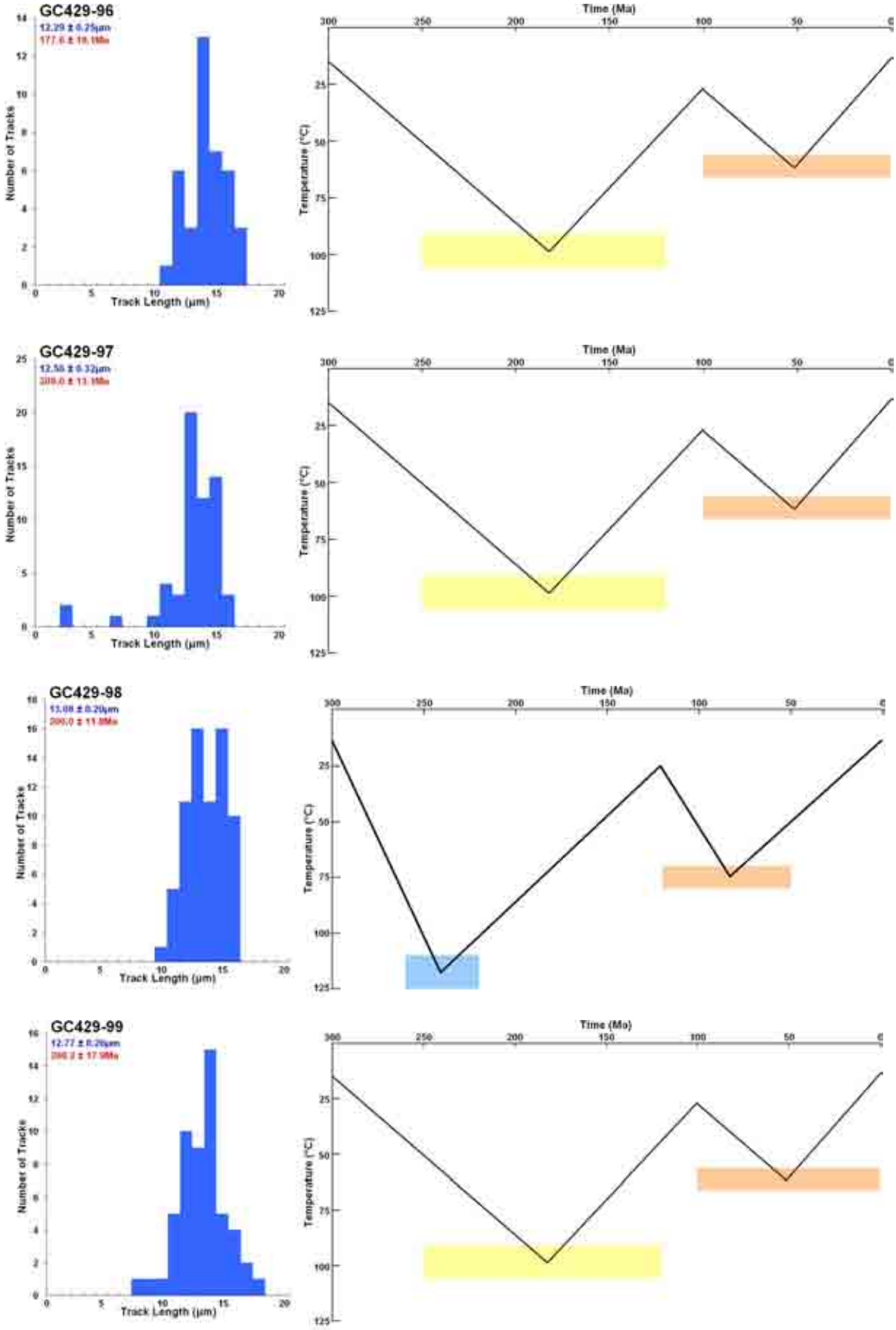

Figure B.9 - Fission track length distribution plots and modelled thermal history solutions for samples GC429-96, 97, 98 and 99.

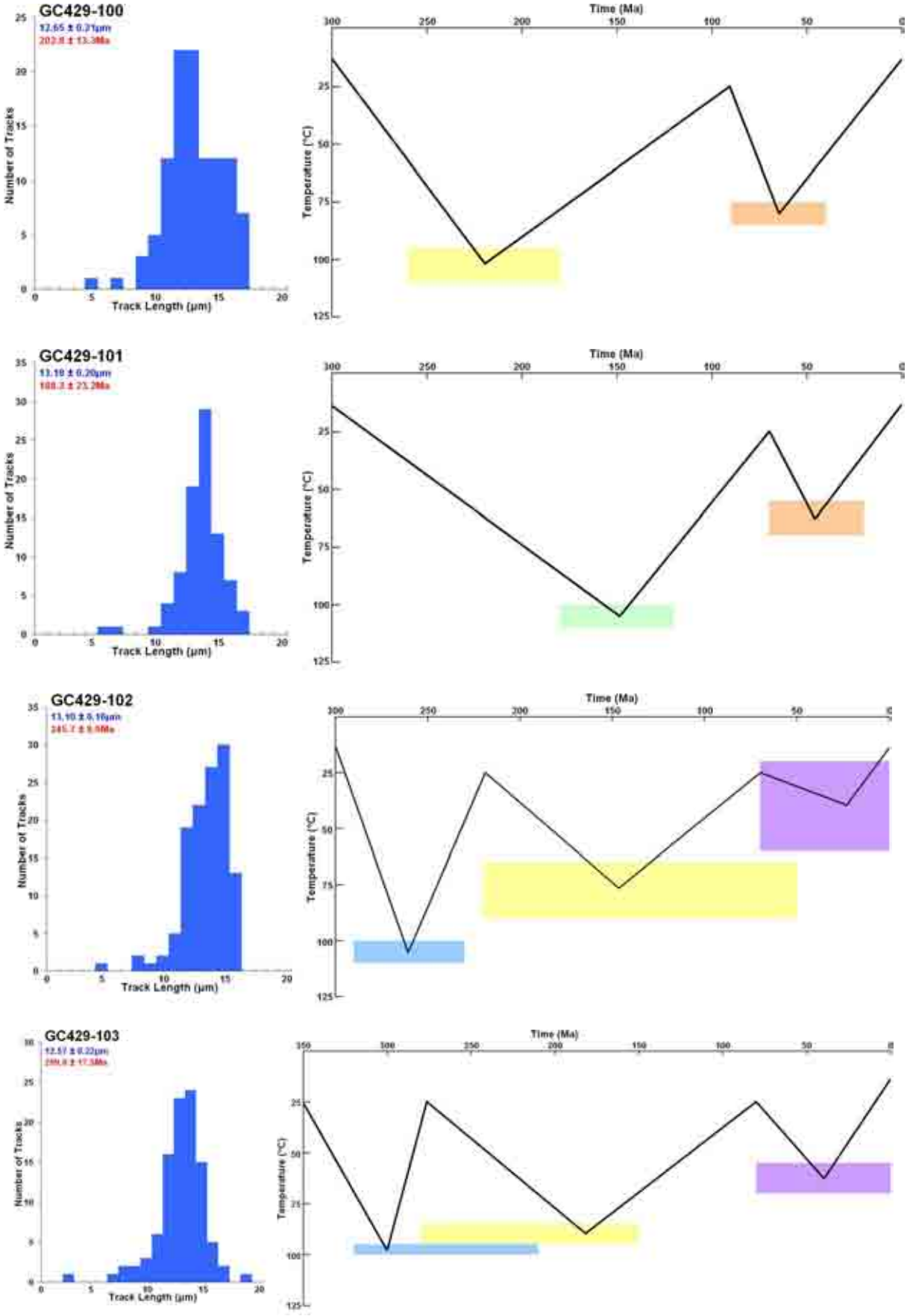

Figure B.10 - Fission track length distribution plots and modelled thermal history solutions for samples GC429-100, 101, 102 and 103.

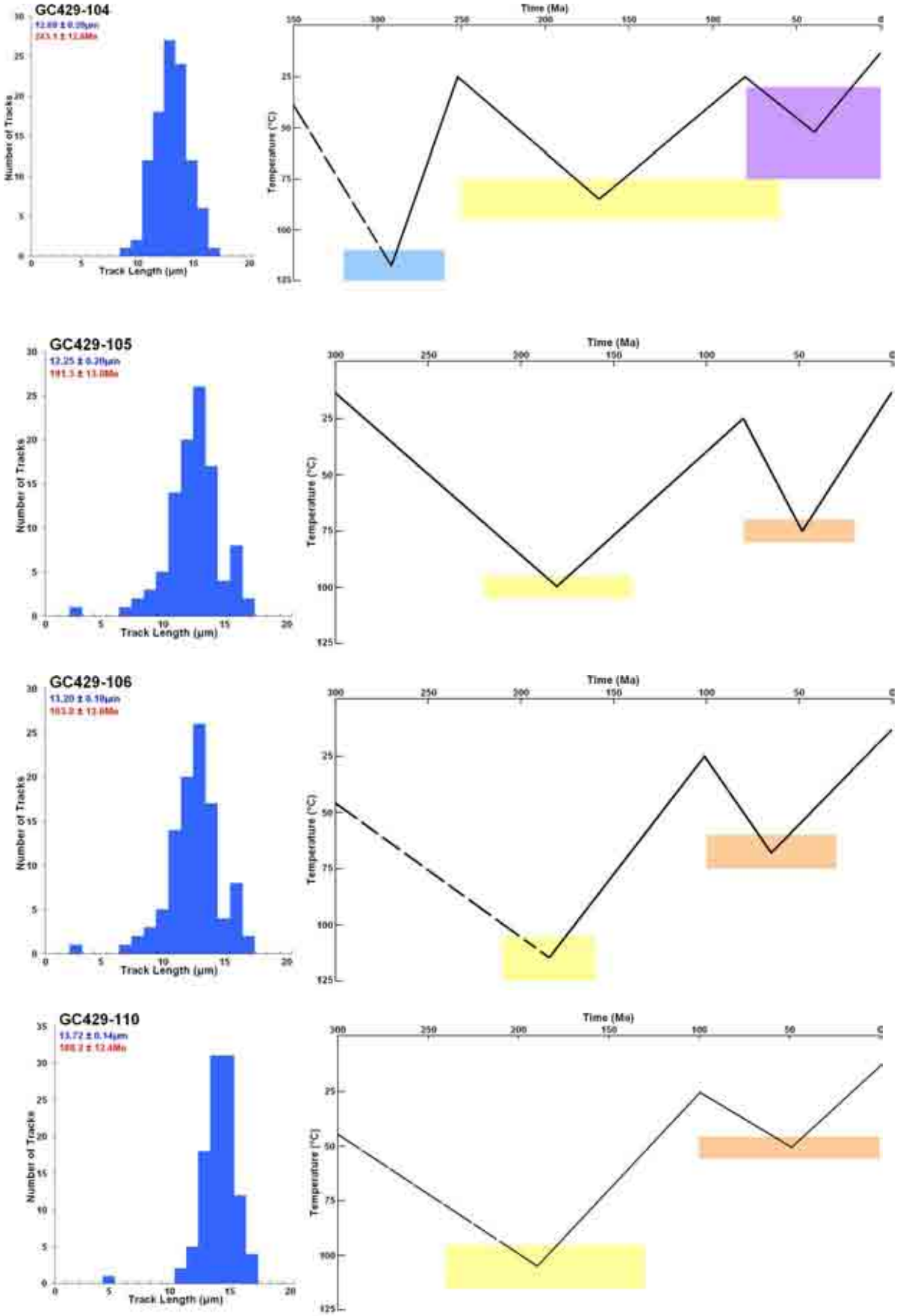

Figure B.11 - Fission track length distribution plots and modelled thermal history solutions for samples GC429-104, 105, 106 and 110.

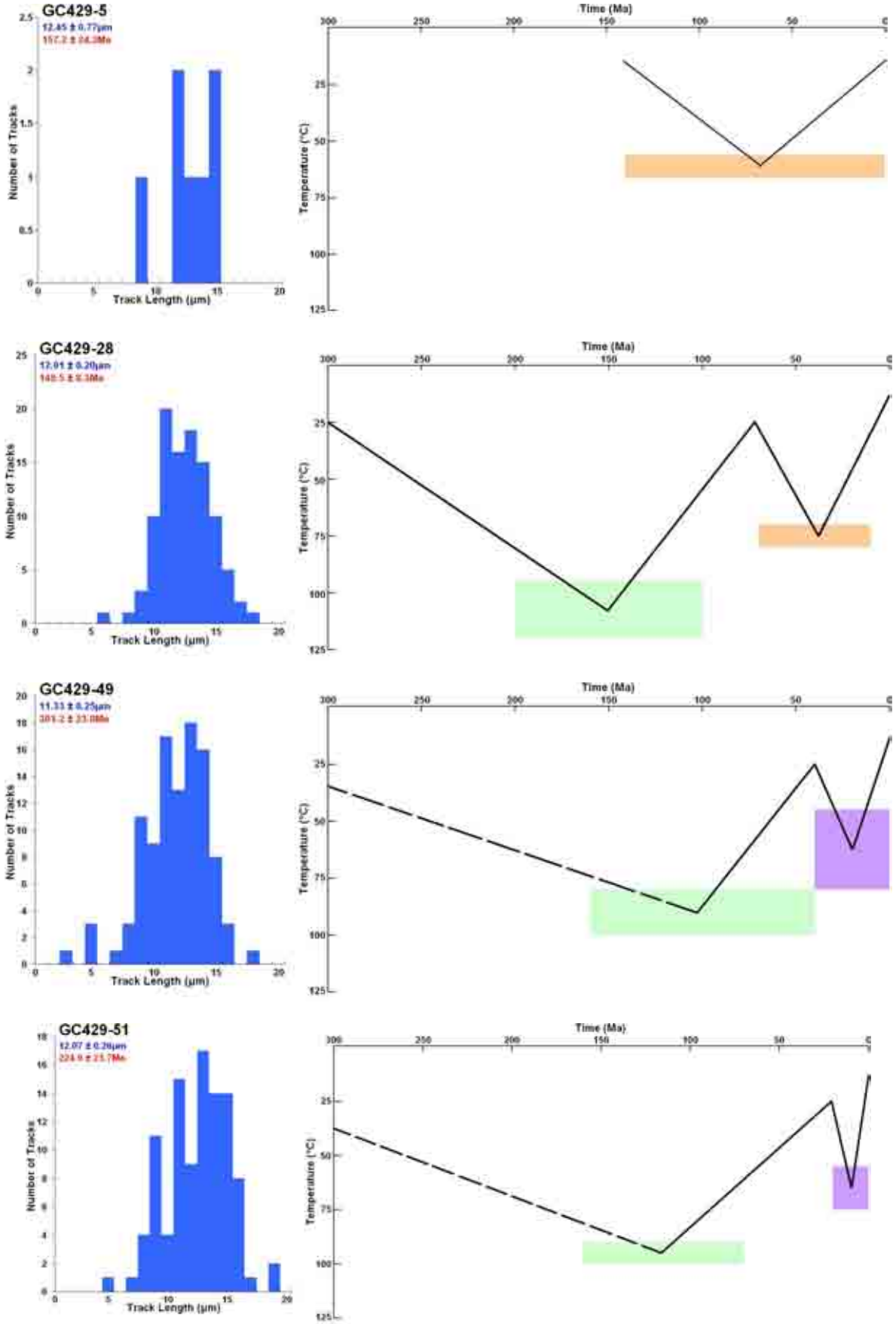

Figure B.12 - Fission track length distribution plots and modelled thermal history solutions for samples GC429-5, 28, 49 and 51.

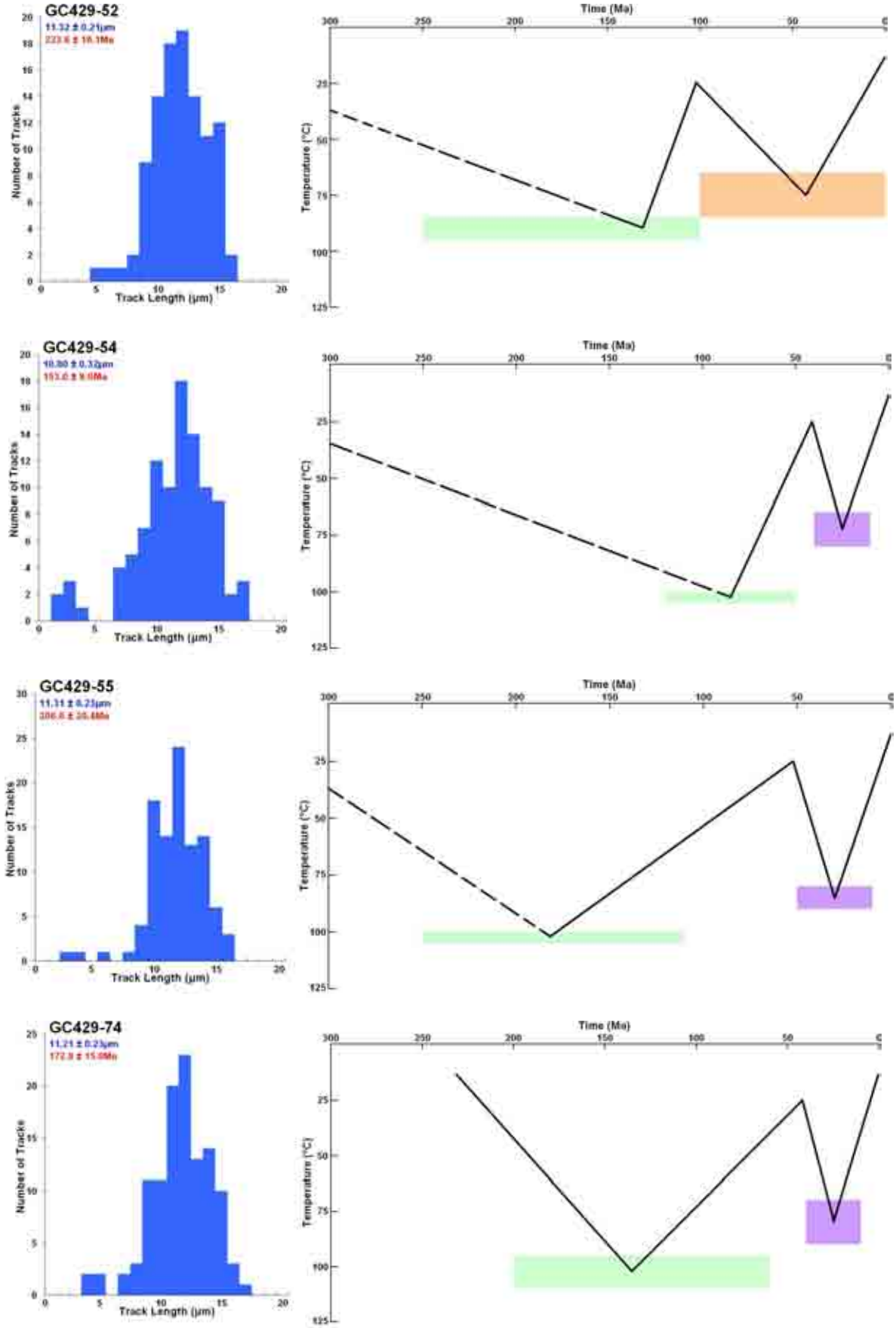

Figure B.13 - Fission track length distribution plots and modelled thermal history solutions for samples GC429-52, 54, 55 and 74.

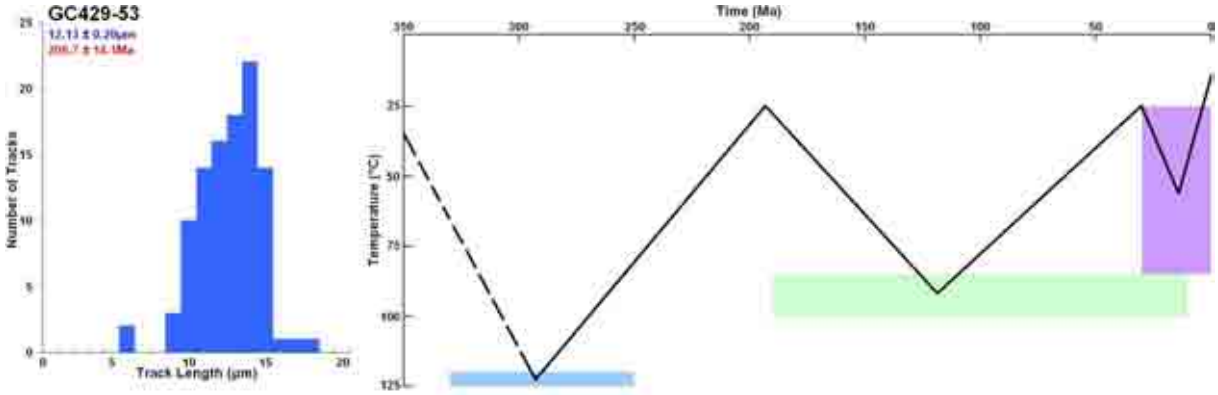

Figure B.14 - Fission track length distribution plot and modelled thermal history solution for sample GC429-53.

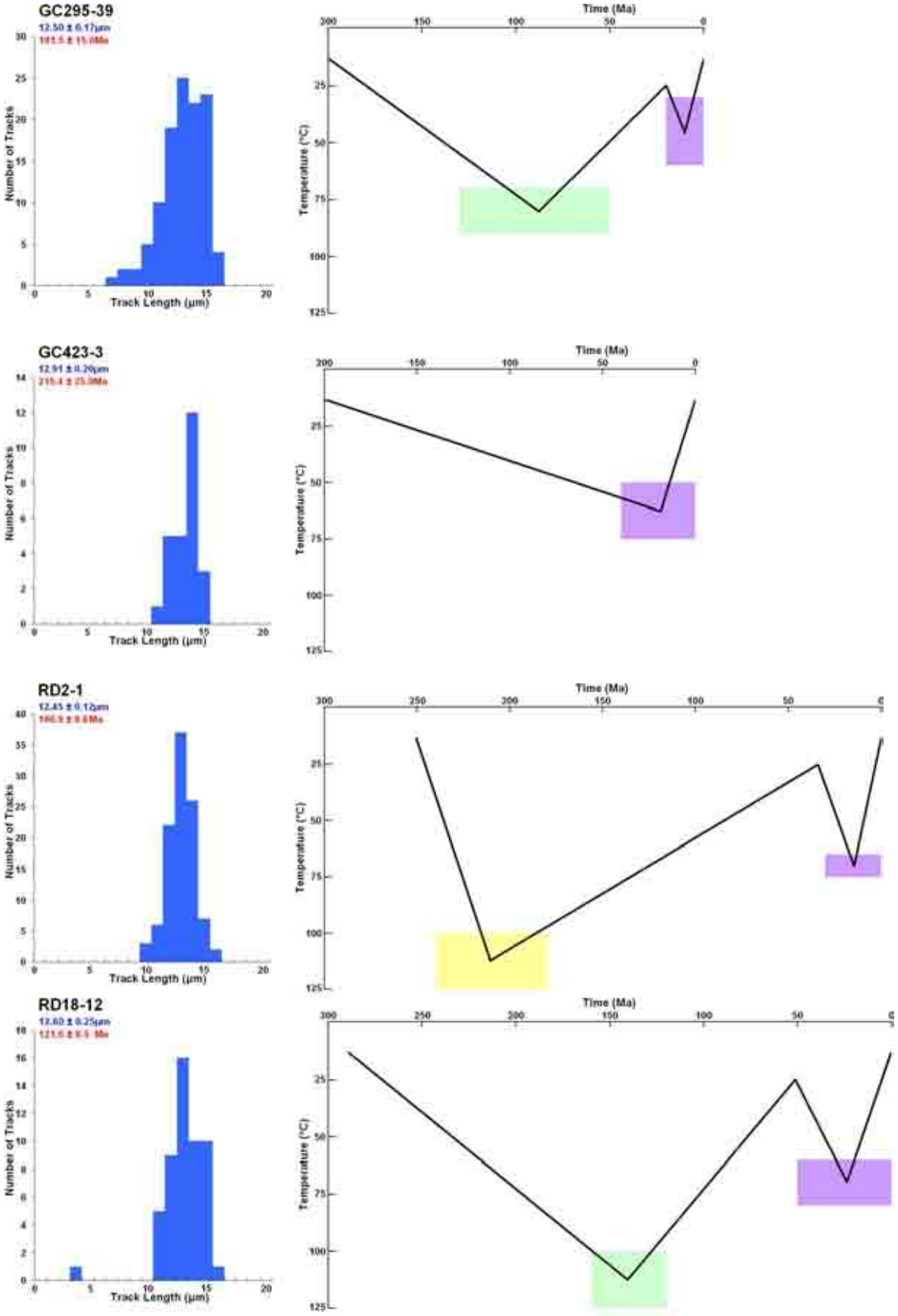

Figure B.15 - Fission track length distribution plots and modelled thermal history solutions for samples GC295-39, GC423-3, RD2-1 and RD18-12.

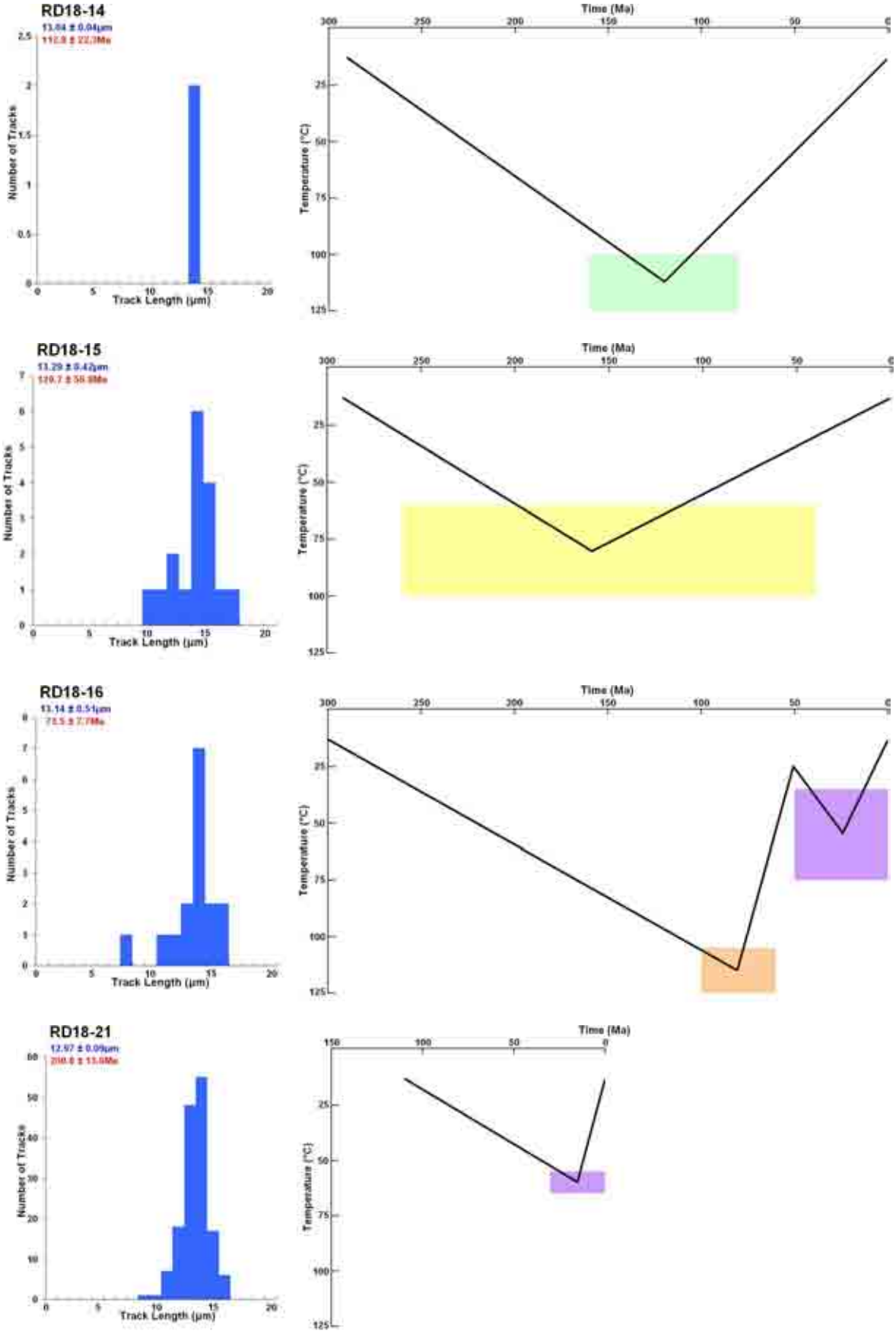

Figure B.16 - Fission track length distribution plots and modelled thermal history solutions for samples RD18-14, 15, 16 and 21.

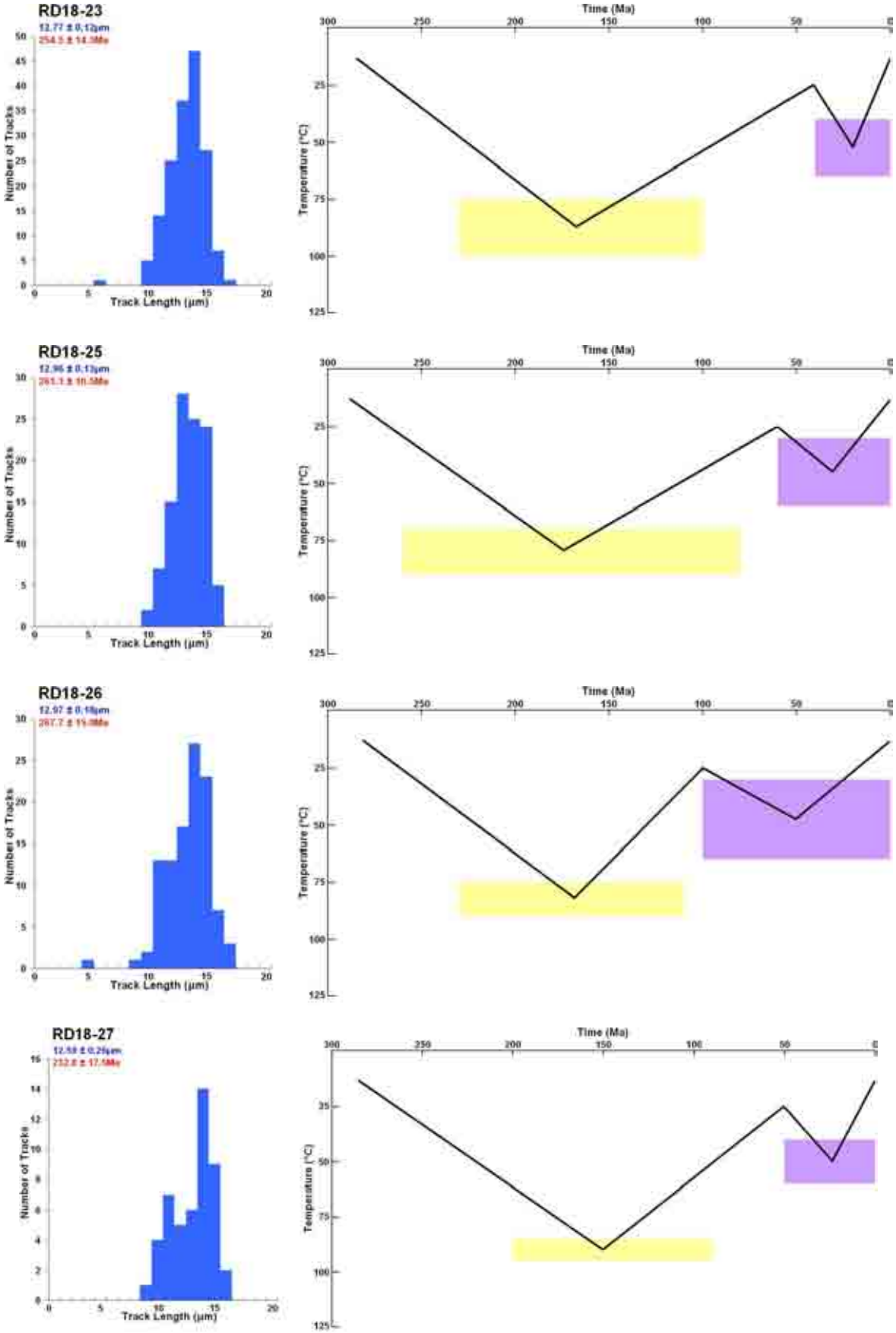

Figure B.17 - Fission track length distribution plots and modelled thermal history solutions for samples RD18-23, 25, 26 and 27.

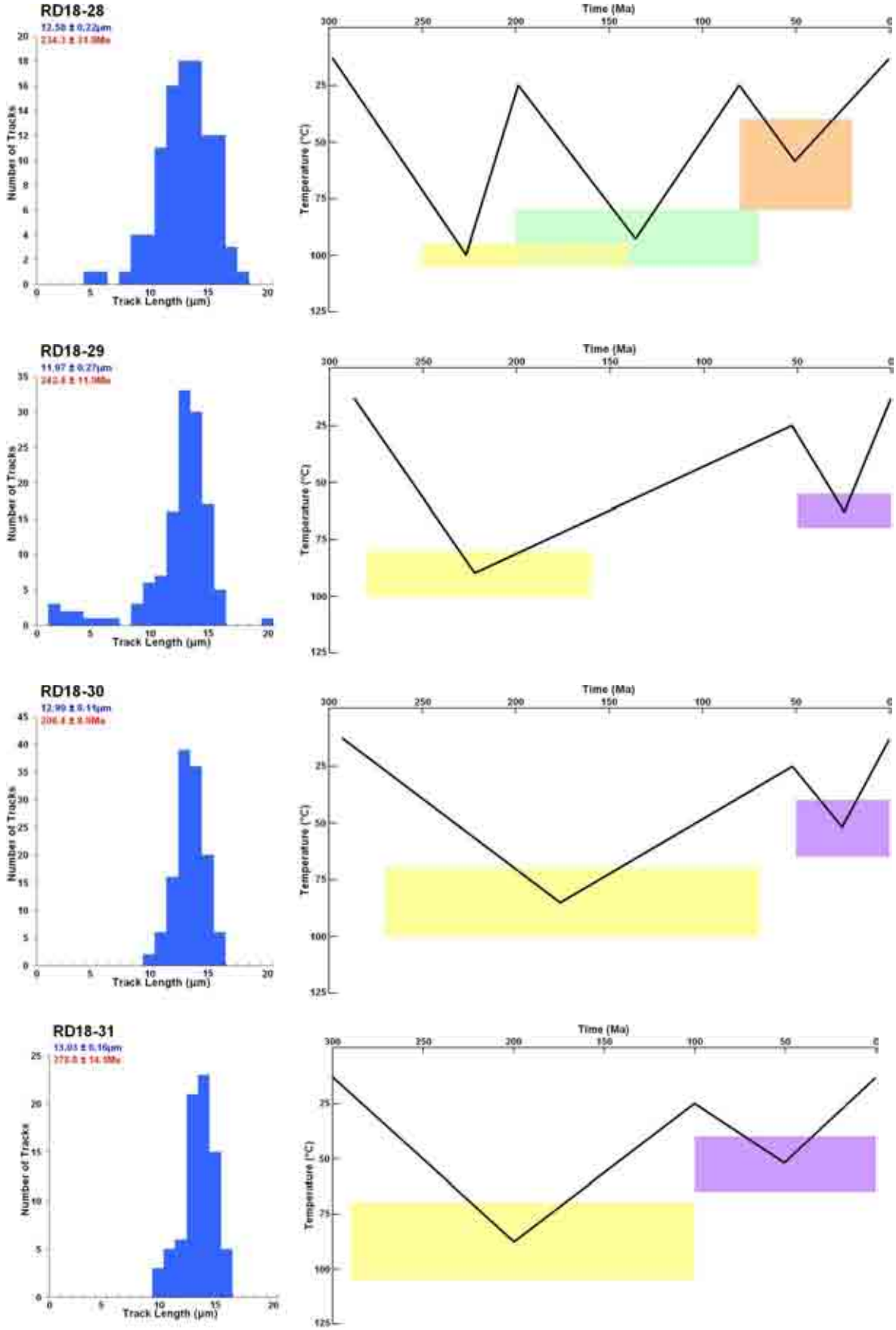

Figure B.18 - Fission track length distribution plots and modelled thermal history solutions for samples RD18-28, 29, 30 and 31.

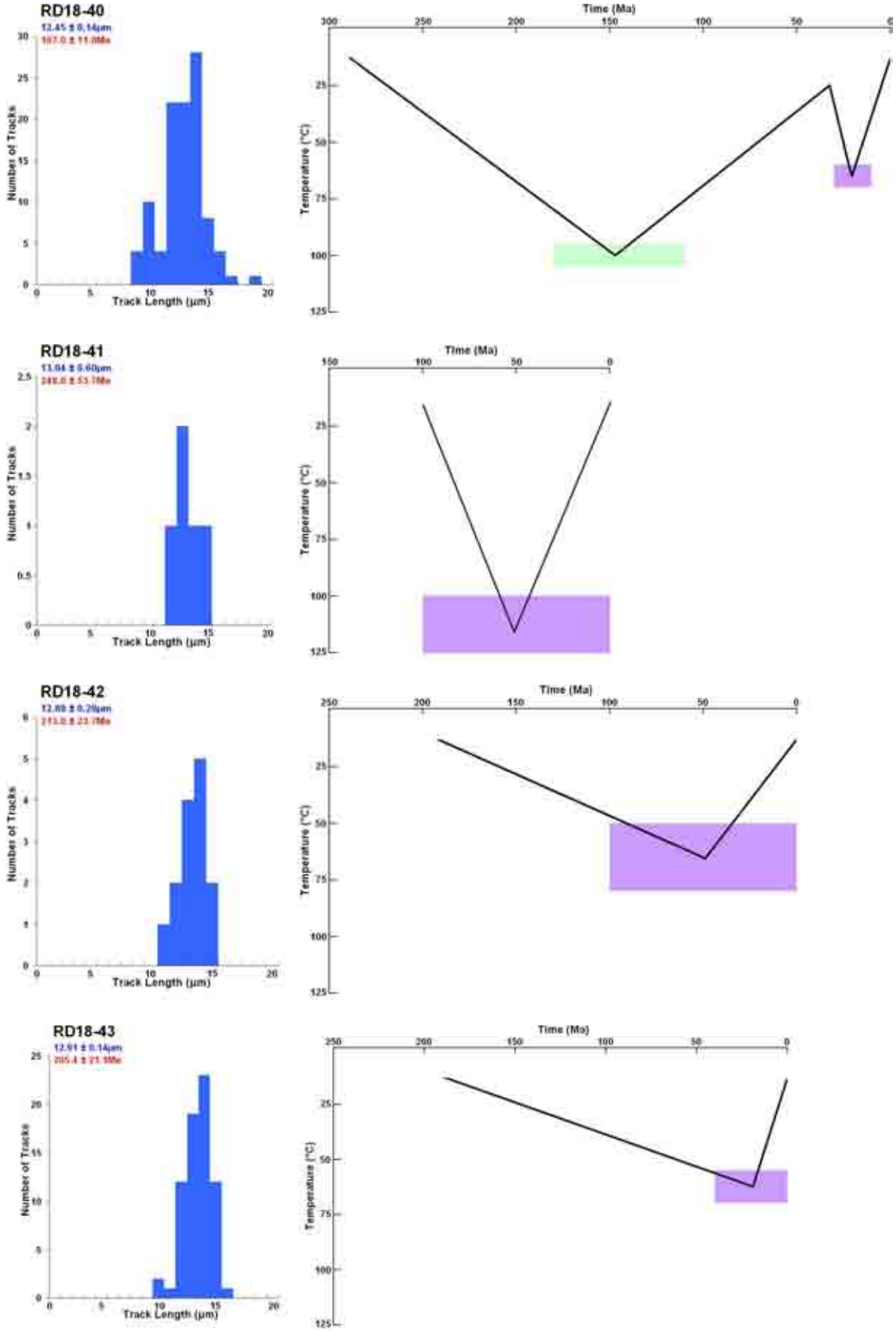

Figure B.19 - Fission track length distribution plots and modelled thermal history solutions for samples RD18-40, 41, 42 and 43.

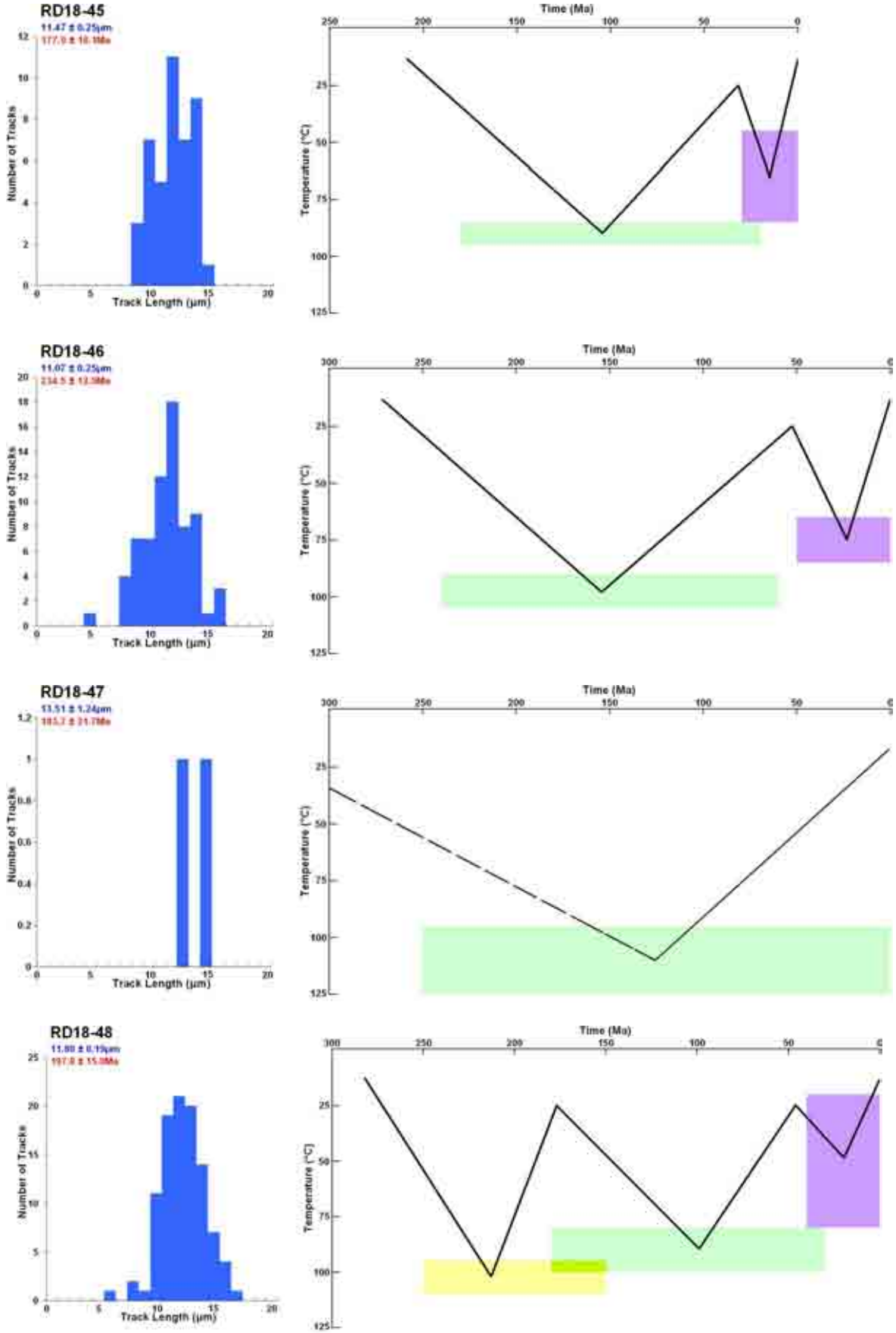

Figure B.20 - Fission track length distribution plots and modelled thermal history solutions for samples RD18-45, 46, 47 and 48.

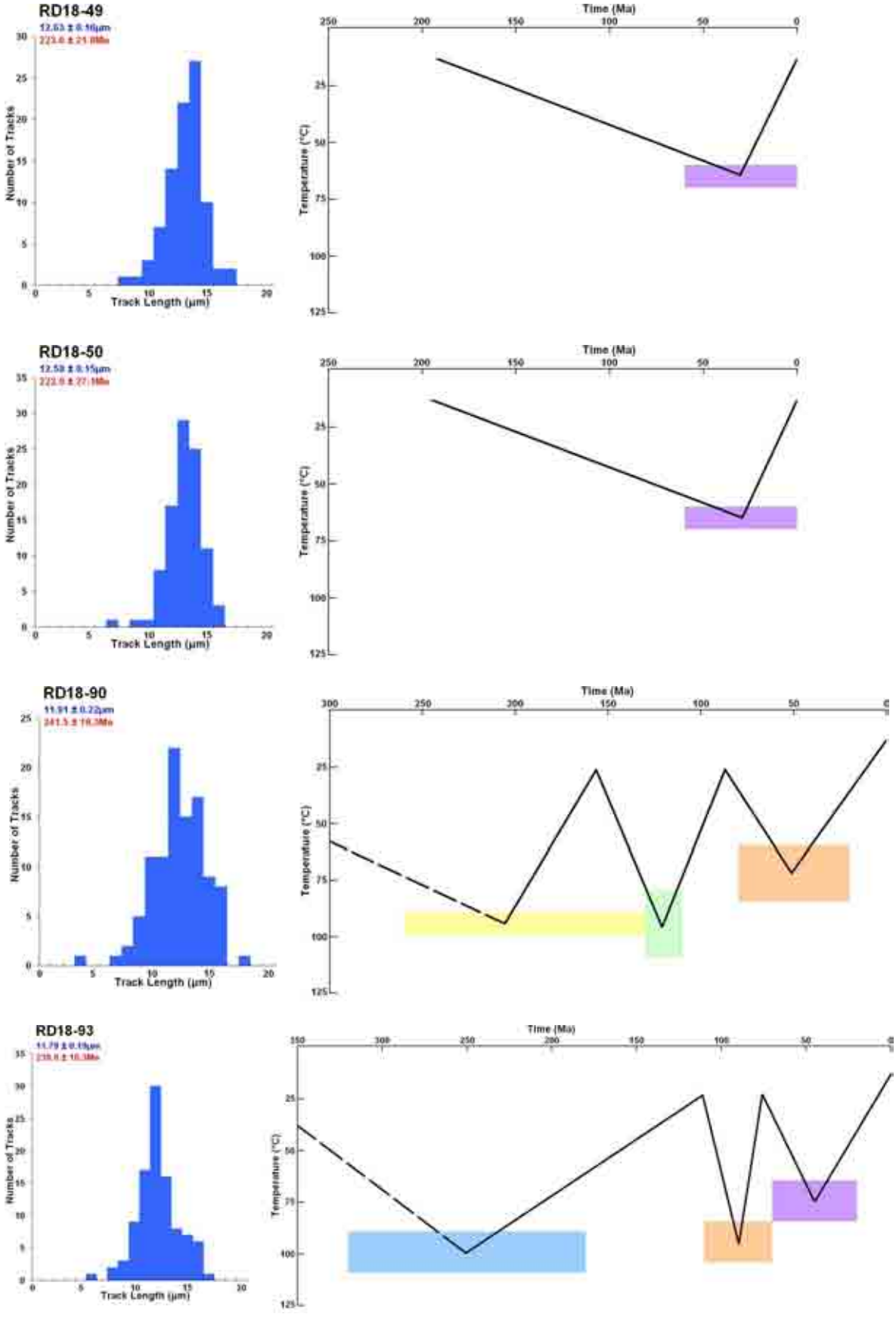

Figure B.21 - Fission track length distribution plots and modelled thermal history solutions for samples RD18-49, 50, 90 and 93.

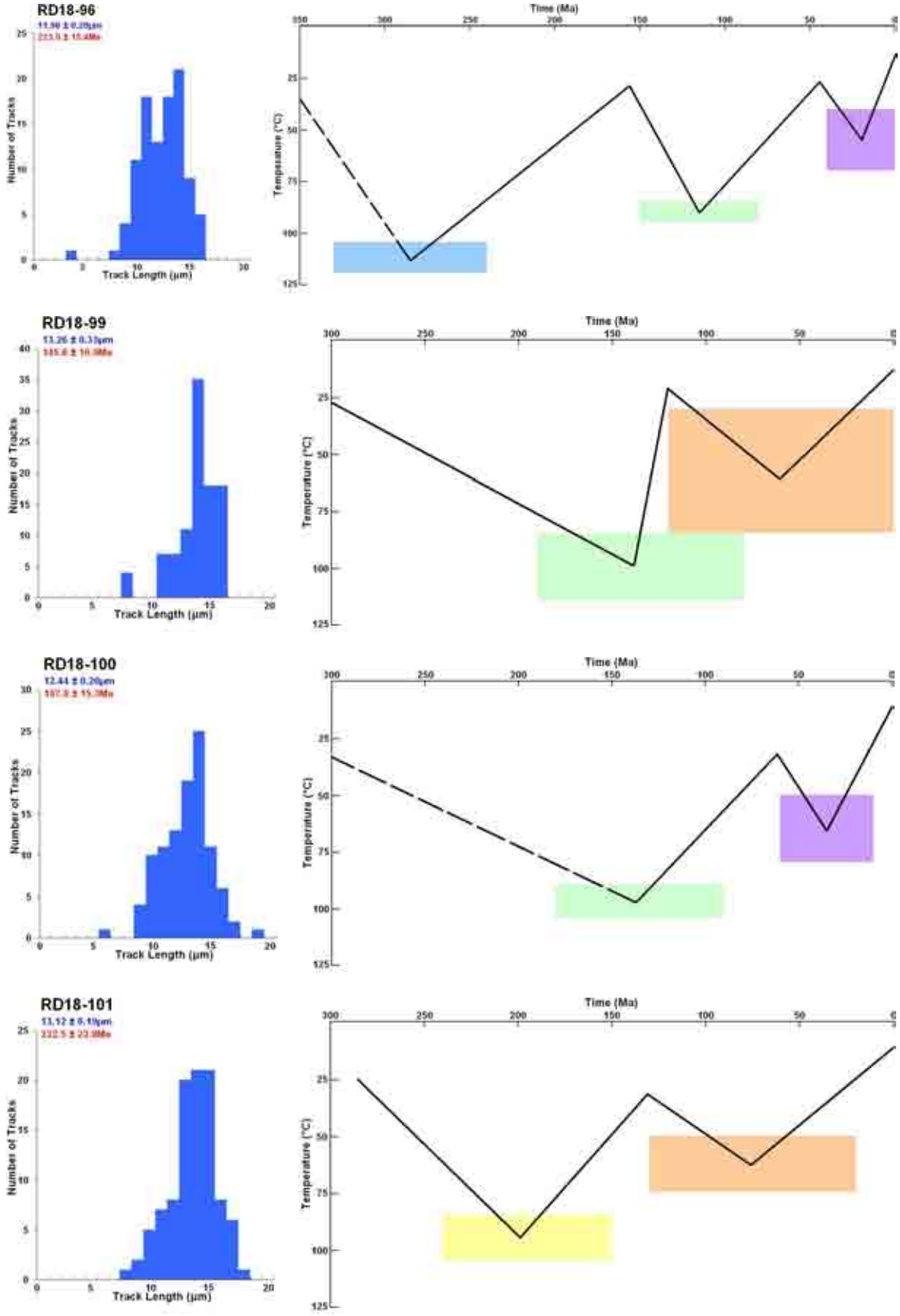

Figure B.22 - Fission track length distribution plots and modelled thermal history solutions for samples RD18-96, 99, 100 and 101.

Sample Number	Depth (m)	Stratigraphic details	Vitrinite Reflectance (R_0max) data			Palaeotemperature (°C)
			Mean	Range	N	
RD18-52	44	Lower Jurassic Lias Group (200-176Ma)	0.43	0.37-0.50	14	72
RD18-54	146	Lower Jurassic Lias Group (200-176Ma)	0.52	0.40-0.62	7	88
RD18-56	257	Lower Jurassic Lias Group (200-176Ma)	0.53	0.38-0.64	8	86
RD18-57	328	Lower Jurassic Lias Group (200-176Ma)	0.52	0.36-0.63	11	86
RD18-59	399	Lower Jurassic Lias Group (200-176Ma)	0.55	0.51-0.57	3	91
RD18-63	640	Upper Triassic Mercia Mudstone Group (245-228Ma)	0.61	0.61	1	100

Table B.6 – Vitrinite reflectance data from the Burton Row borehole. Estimates of maximum paleotemperature derived from mean VR or VR_{eq} using assumed heating and cooling rates of 1°C/Myr and 10°C/Myr, respectively.

Sample Number	Depth (m)	Stratigraphic details	Vitrinite Reflectance (R_0max) data			Palaeotemperature (°C)
			Mean	Range	N	
RD18-70	560	Carboniferous (318-303Ma)	1.35	1.24-1.50	25	160
RD18-71	710	Carboniferous (318-303Ma)	1.38	1.26-1.47	19	163
RD18-72	823	Carboniferous (318-303Ma)	1.42	1.32-1.54	4	166
RD18-74	1097	Carboniferous (318-303Ma)	1.69	1.68-1.71	2	173
RD18-75	1280	Devonian (416-360Ma)	2.12	2.07-2.17	2	189
RD18-76	1341	Devonian (416-360Ma)	2.01	2.01	1	185

Table B.7 – Vitrinite reflectance data from the Senghenydd borehole. Estimates of maximum paleotemperature derived from mean VR or VR_{eq} using assumed heating and cooling rates of 1°C/Myr and 10°C/Myr, respectively.

Sample Number	Depth (m)	Stratigraphic details	Vitrinite Reflectance (R_0max) data			Palaeotemperature (°C)
			Mean	Range	N	
RD18-81	97	Carboniferous (318-303Ma)	2.90	2.71-3.14	25	215
RD18-82	222	Carboniferous (318-303Ma)	3.00	2.83-3.18	25	220
RD18-83	394	Carboniferous (318-303Ma)	3.07	2.81-3.36	25	223
RD18-84	504	Carboniferous (318-303Ma)	3.13	2.94-3.32	25	225
RD18-85	695	Carboniferous (318-303Ma)	3.21	3.00-3.37	16	228
RD18-86	821	Devonian (416-360Ma)	3.37	3.11-3.55	18	236
RD18-87	864	Devonian (416-360Ma)	3.37	3.12-3.67	25	236
RD18-89	972	Devonian (416-360Ma)	3.44	3.40-3.47	2	238

Table B.8 – Vitrinite reflectance data from the Gwendraeth Valley 2 borehole. Estimates of maximum paleotemperature derived from mean VR or VR_{eq} using assumed heating and cooling rates of 1°C/Myr and 10°C/Myr, respectively.

Sample Number	Stratigraphic details	Vitrinite Reflectance (R_0max) data			Palaeotemperature (°C)
		Mean	Range	N	
GC429-34	Namurian (333-318Ma)	2.13	1.85-2.31	25	200
GC429-35	Westphalian (318-303Ma)	3.56	3.25-3.91	26	>250
GC429-36	Westphalian (318-303Ma)	4.47	3.90-4.85	27	>250
GC429-37	Westphalian (318-303Ma)	4.74	4.45-5.15	27	>250
GC429-46	Westphalian (318-303Ma)	3.21	2.89-3.64	29	230
GC429-57	Westphalian (318-303Ma)	2.77	2.41-3.11	26	220
GC429-58	Westphalian (318-303Ma)	2.50	2.18-2.78	26	210
GC429-59	Westphalian (318-303Ma)	2.77	2.08-3.07	27	220
GC429-60	Westphalian (318-303Ma)	2.77	2.54-3.13	26	220
GC429-61	Westphalian (318-303Ma)	2.72	2.47-3.16	26	220
GC429-62	Westphalian (318-303Ma)	4.89	4.58-5.12	28	>250
GC429-63	Westphalian (318-303Ma)	4.84	4.15-5.40	16	>250

Table B.9 - Vitrinite reflectance data from Pembrokeshire, South Wales. Estimates of maximum palaeotemperature derived from mean VR or VR_{eq} using assumed heating and cooling rates of 1°C/Myr and 10°C/Myr, respectively.

Sample Number	Stratigraphic details	Vitrinite Reflectance (R_0max) data			Palaeotemperature (°C)
		Mean	Range	N	
GC429-40	Lower Jurassic Lias Group (208-178Ma)	0.60	0.48-0.74	13	99
GC429-41	Penarth Group (210-208Ma)	1.15	1.15	1	150
GC429-44	Westphalian (307-303Ma)	0.74	0.63-0.87	27	121
GC429-45	Westbury Formation (210-208Ma)	0.49	0.42-0.54	4	81

Table B.10 - Vitrinite reflectance data from South Wales and the Severn Estuary. Estimates of maximum palaeotemperature derived from mean VR or VR_{eq} using assumed heating and cooling rates of 1°C/Myr and 10°C/Myr, respectively.

Sample Number	Stratigraphic details	Vitrinite Reflectance ($R_o$max) data			Palaeotemperature (°C)
		Mean	Range	N	
GC429-1	Cenozoic (65-2Ma)	0.29	0.20-0.40	26	40
GC429-2	Cenozoic (65-2Ma)	0.34	0.22-0.51	26	53
GC429-3	Cenozoic (65-2Ma)	0.30	0.24-0.35	25	43
GC429-4	Cenozoic (65-2Ma)	0.30	0.22-0.43	25	43
GC429-8	Jurassic (208-146Ma)	1.45	1.30-1.69	5	168
GC429-9	Portlandian (152-146Ma)	0.63	0.56-0.71	4	104
GC429-10	Portlandian (152-146Ma)	0.63	0.60-0.67	2	104
GC429-11	Portlandian (152-146Ma)	0.57	0.49-0.66	6	95
GC429-12	Kimmeridgian (154-152Ma)	0.59	0.54-0.64	2	97
GC429-13	Kimmeridgian (154-152Ma)	0.56	0.41-0.58	4	93
GC429-14	Bajocian (174-166Ma)	1.83	1.19-2.52	10	190
GC429-15	Bajocian (174-161Ma)	0.58	0.48-0.67	8	96
GC429-16	Bathonian (166-161Ma)	0.54	0.39-0.64	28	90
GC429-17	Lower Jurassic (208-178Ma)	0.48	0.48	1	80
GC429-18	Lower Jurassic (208-178Ma)	0.48	0.30-0.61	13	80
GC429-19	Toarcian (184-174Ma)	1.69	1.13-2.25	5	174
GC429-20	Pliensbachian (195-187Ma)	0.59	0.49-0.69	16	97
GC429-21	Pliensbachian (195-187Ma)	1.33	1.09-1.49	5	161
GC429-22	Pliensbachian (195-187Ma)	0.62	0.60-0.65	2	102
GC429-23	Sinemurian (204-195Ma)	0.48	0.34-0.63	26	80
GC429-24	Sinemurian (204-195Ma)	0.50	0.45-0.54	3	82
GC429-25	Carboniferous (363-290Ma)	1.75	1.57-1.95	8	180
GC429-26	Carboniferous (363-290Ma)	1.27	1.27	1	158
GC429-27	Carboniferous (363-290Ma)	6.24	6.10-6.35	4	>250
GC429-29	Carboniferous (363-290Ma)	5.78	5.45-6.00	7	>250
GC429-31	Carboniferous (363-290Ma)	1.68	1.41-2.01	7	174
GC429-32	Carboniferous (363-290Ma)	6.10	5.65-6.50	5	>250
GC429-33	Carboniferous (363-290Ma)	4.61	4.40-4.75	5	>250

Table B.11 - Vitrinite reflectance data from the Bristol Channel Basin. Estimates of maximum palaeotemperature derived from mean VR or VR_{eq} using assumed heating and cooling rates of 1°C/Myr and 10°C/Myr, respectively.

Sample Number	Stratigraphic details	Vitrinite Reflectance (R_0max) data			Palaeotemperature (°C)
		Mean	Range	N	
GC429-48	Tournaisian (363-333Ma)	4.94	4.10-6.15	25	>250
GC429-50	Late Devonian (377-367Ma)	2.83	2.58-3.23	4	220
GC429-64	Namurian (333-318Ma)	2.59	2.07-3.88	26	210
GC429-65	Westphalian (318-303Ma)	3.33	2.93-3.78	28	>250
GC429-66	Westphalian (318-303Ma)	5.80	5.07-6.79	18	>250

Table B.12 - Vitrinite reflectance data from North Devon. Estimates of maximum palaeotemperature derived from mean VR or VR_{eq} using assumed heating and cooling rates of 1°C/Myr and 10°C/Myr, respectively.

Sample Number	Stratigraphic details	Vitrinite Reflectance (R_0max) data			Palaeotemperature (°C)
		Mean	Range	N	
GC429-56	Lower Jurassic Lias Group (208-178Ma)	0.51	0.40-0.56	14	84
GC429-69	Rhaetian (209-208Ma)	0.66	0.56-0.78	9	109
GC429-70	Lower Jurassic Lias Group (208-178Ma)	0.67	0.51-0.81	12	111
GC429-71	Lower Jurassic Lias Group (208-178Ma)	1.76	1.15-2.59	11	180
GC429-72	Lower Jurassic Lias Group (208-178Ma)	0.43	0.25-0.53	16	72
GC429-73	Lower Jurassic Lias Group (208-178Ma)	0.43	0.32-0.63	26	72

Table B.13 - Vitrinite reflectance data from Somerset. Estimates of maximum palaeotemperature derived from mean VR or VR_{eq} using assumed heating and cooling rates of 1°C/Myr and 10°C/Myr, respectively.

APPENDIX C

WELLS IN WHICH VR DATA IS UNRELIABLE

The following wells were deemed to have inherent problems in their data so as not to provide a reliable result when estimating palaeogeothermal gradients and removed section. The results generated should therefore be treated with caution.

Exploration Well 42/16-1

This well penetrated the NW margin of the SGCB where Mercia Mudstone Group sediments subcrop a thin veneer (<50m) of Lower Jurassic and Quaternary deposits (Figure C.1). This well is considered to lie within the southern Central Irish Sea Basin by other workers (e.g. Corcoran & Clayton, 1999 and Green *et al.* 2001) however the surrounding region was arguably part of a much larger SGCB prior to Early Cretaceous uplift (which was confined to the basin margins). The sedimentary sequence encountered in this well is very similar to the SE margin of the SGCB (e.g. well 106/28-1), with the exception that Cenozoic sediments are entirely absent. The fact that Triassic rocks are buried at shallow depth beneath the sea-bed means that it is impossible to constrain the main phases of exhumation from the preserved stratigraphy alone. Green *et al. (*2001) reported that there was 3000m of Lower Cretaceous, 2000m of Late Cretaceous-Paleogene and 1500m of Neogene exhumation based on a lower geothermal gradient of 36.5°C/km and a palaeosurface temperature of 6°C.

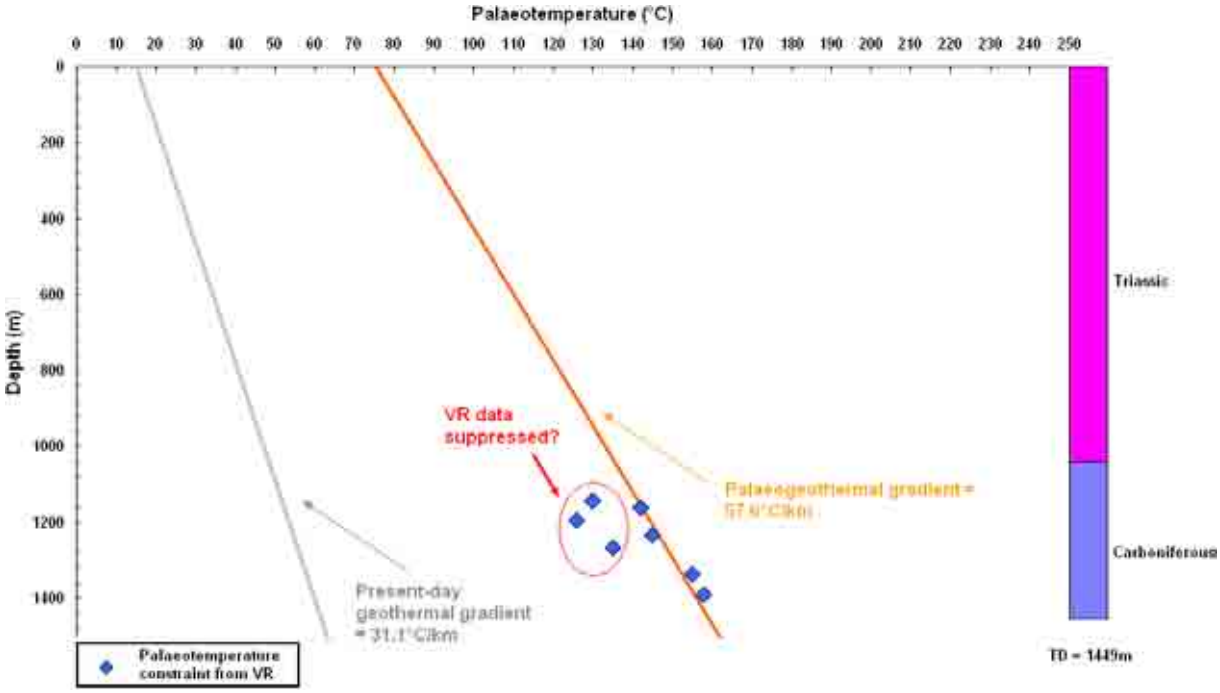

Figure C.1 – Palaeotemperature constraints from VR data from well 42/16-1 plotted against depth. These are used to infer palaeotemperature profiles prior to the cooling episode. A simplified stratigraphic column is also shown. On what basis do you ring a selection of your data as being suppressed – is it just that they don't fit the gradient you have chosen?

The well data comprises too few points to confidently place a palaeogeothermal gradient in the absence of further information (such as possible VR suppression) as there are a number of possibilities which could fit the data. Assuming the VR points to the left of the plotted palaeogeothermal gradient are suppressed gives a maximum likelihood estimate of

palaeogeothermal gradient prior to exhumation of 57.6°C/km (40.3-74.6°C/km at 95% confidence limits). Extrapolating this gradient to the surface indicates that the preserved Paleozoic-Mesozoic succession was more deeply buried by 1050m ±200m (540-1990 ±200m at 95% confidence limits) prior to exhumation. Green *et al.* (2001) also produced results from this well however the VR data was supported by a suite of AFTA samples (Figure C.2) thus their results should be considered more accurate. As reported by Green *et al.* (2001) in well 42/16-1 an additional 3475m of post-late Triassic sediment was deposited between 208-125Ma, 2975m of which were removed by uplift and erosion between 120-110Ma. Deposition of 2050m of sediment followed this exhumation episode between 110-65Ma with 2250m removed by uplift and erosion in the Paleogene (65-60Ma). A further 1000m were deposited between 60-15Ma with 1300m removed during a Neogene exhumation event (15-2Ma).

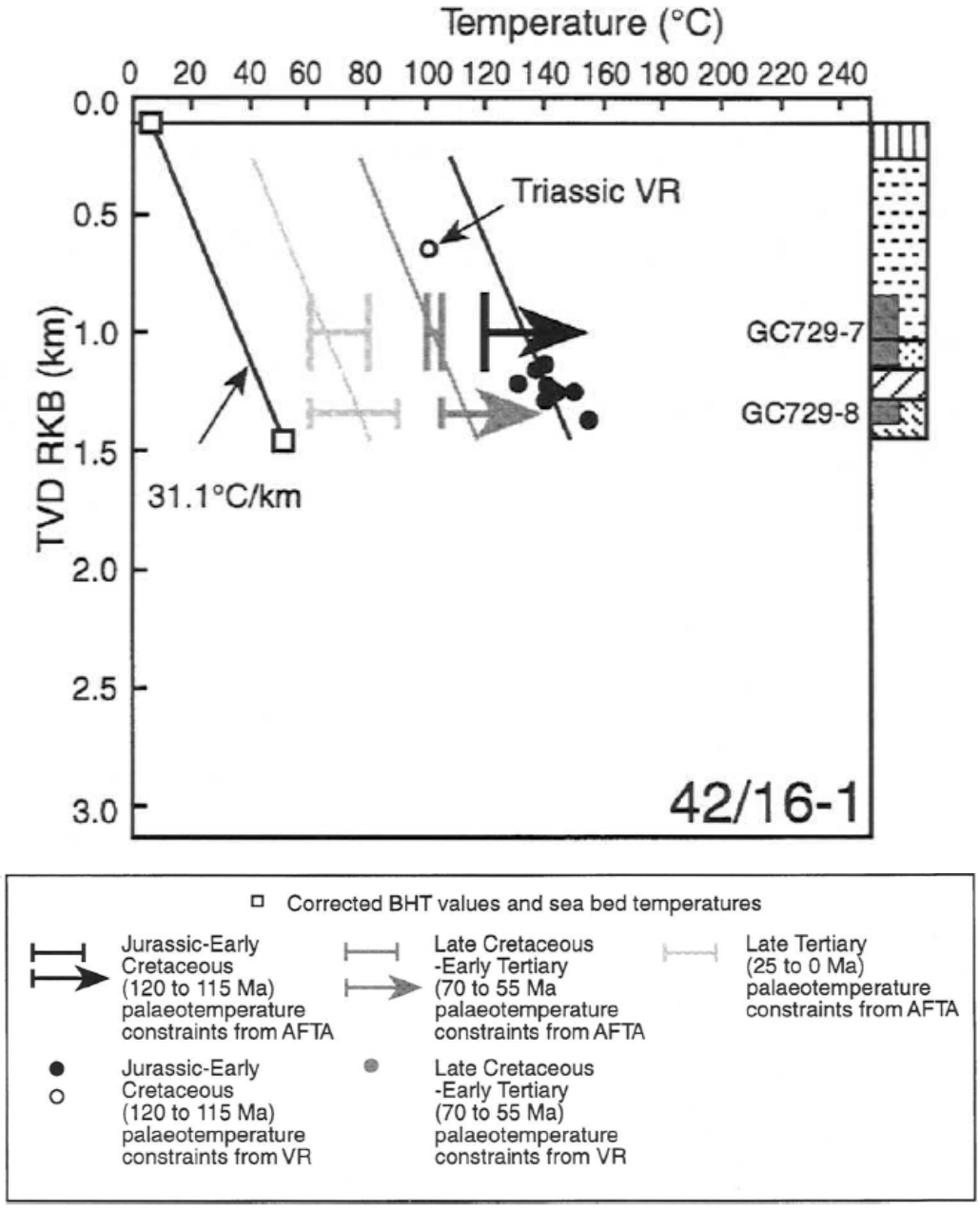

Figure C.2 - Palaeotemperature constraints derived from AFTA and VR data in individual samples from well 42/16-1 plotted against depth (after Green *at al.* (2001)).

Exploration Well 48/19-1

Well 48/19-1 was drilled in the NCSB and encountered a thick Cretaceous and Upper Jurassic sequence (Figure C.3). The large degree of scatter in the VR data suggests that some of the samples may be affected by suppression but no detailed maceral analysis is available to confirm this suspicion, nor are there any independent palaeotemperature measurements to indicate the range of palaeogeothermal gradients. For this reason it is not possible to confidently fit a palaeogeothermal gradient to the data in the absence of further information especially since no BHT data exists to constrain the present day geothermal gradient (using the assumption of 32°C/km gives a number of points below the curve).

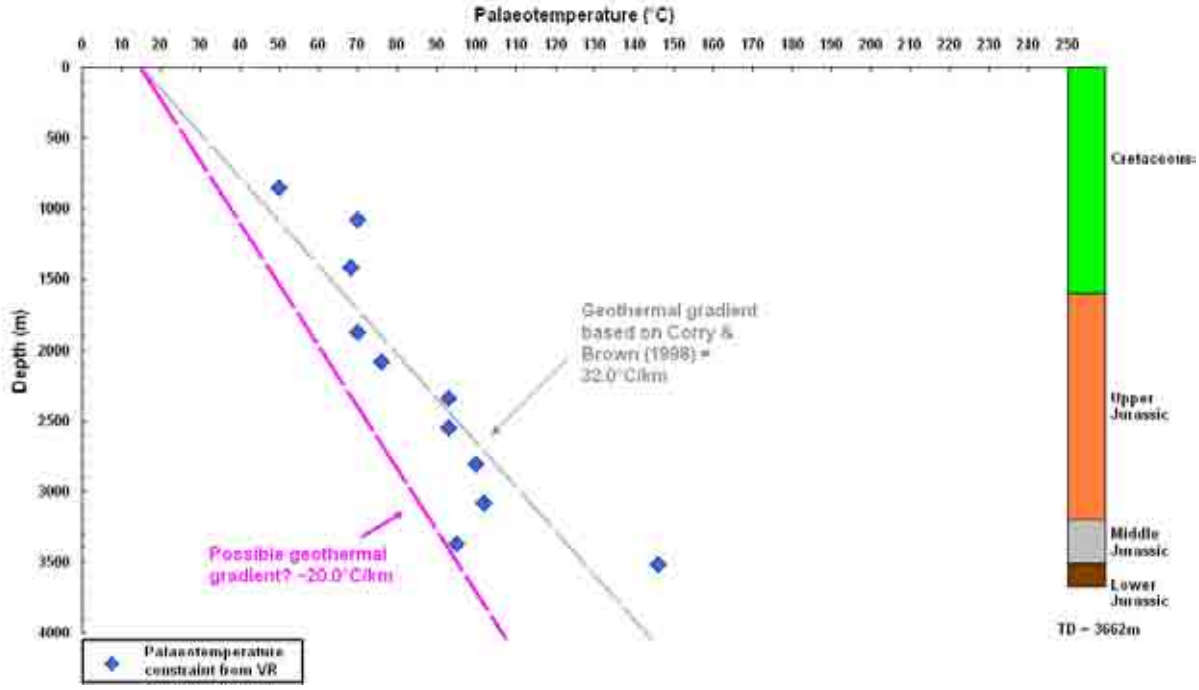

Figure C.3 – Palaeotemperature constraints from VR data from well 48/19-1 plotted against depth. The large degree of scatter in the data does not allow confident interpretation of the data. The present-day geothermal gradient clearly has to be steeper than the indicated gradient based on Corry & Brown (1998). A simplified stratigraphic column is also shown.

Exploration Well 50/03-1

Well 50/03-1 was drilled near the northern margin of the NCSB in the hangingwall of a fault and encountered a thick Jurassic succession. The distribution of VR values is highly suggestive of suppression given the almost vertical profile that some of the data points define. This makes assessment of an appropriate palaeogeothermal gradient for this well extremely difficult and for this reason the results were deemed to be completely unreliable. Basing the analysis only on the data points which lie on a sub-parallel gradient to the present day (Figure C.4) indicates the maximum likelihood estimate of palaeogeothermal gradient prior to exhumation is 38.1°C/km (25.1-50.0°C/km at 95% confidence limits) (Figure C.5) and extrapolation of this gradient to the surface indicates that the preserved Jurassic succession was more deeply buried by 850m ±200m (400-1790 ±200m at 95% confidence limits) prior to exhumation (Figure C.5). This is consistent with data presented by Murdoch *et al.* (1995) which suggested an additional section value of 1300m based on a geothermal gradient of 32.0°C.

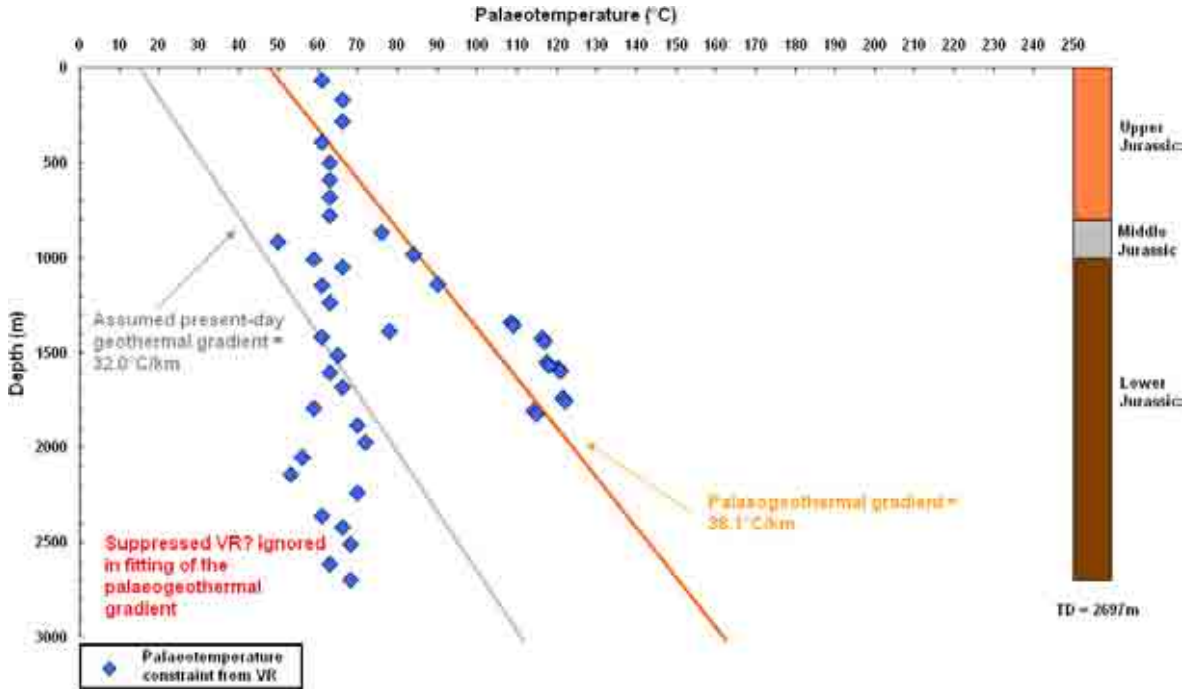

Figure C.4 – Palaeotemperature constraints from VR data from well 50/03-1 plotted against depth. These are used to infer palaeotemperature profiles prior to the Paleogene cooling episode. A simplified stratigraphic column is also shown. are these data useful?

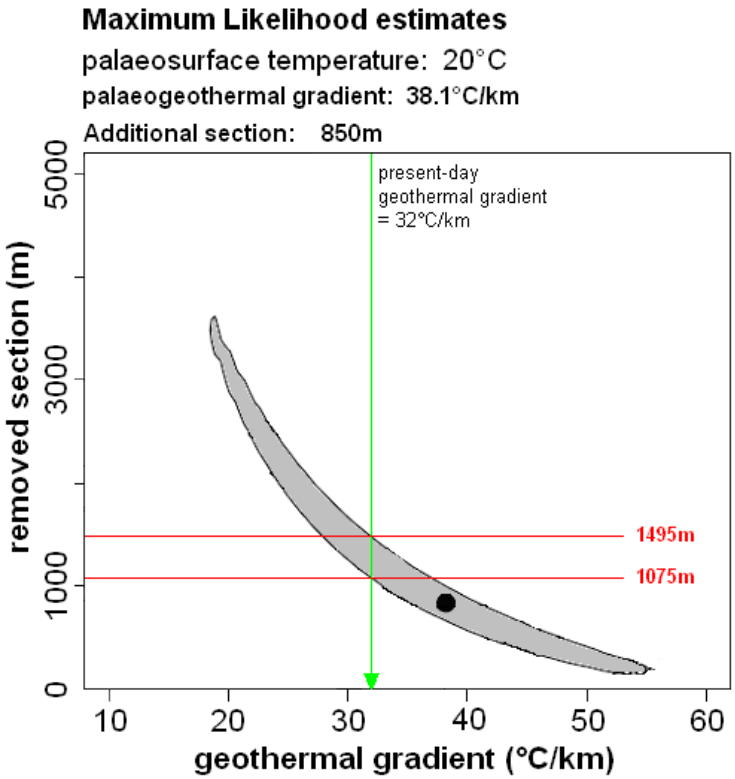

Figure C.5 – Amount of additional section and palaeogeothermal gradients required to explain the Paleogene palaeothermal episode. The shaded region defines the allowed range of values for each parameter that are consistent with the measured palaeotemperature constraints within 95% confidence limits. Black dots represent

the maximum likelihood estimates. Red horizontal bars indicate the range of exhumation estimates assuming no change in the present-day geothermal gradient.

Exploration Well 103/01-1

Well 103/01-1 was drilled in the southern SGCB in the footwall of the St. George's Fault, where it penetrated a thick Upper Jurassic sequence overlain by a thin Cenozoic and Quaternary cover. Given the small number of points from a limited vertical section it is not possible to reasonably fit a curve to the data (Figure C.6).

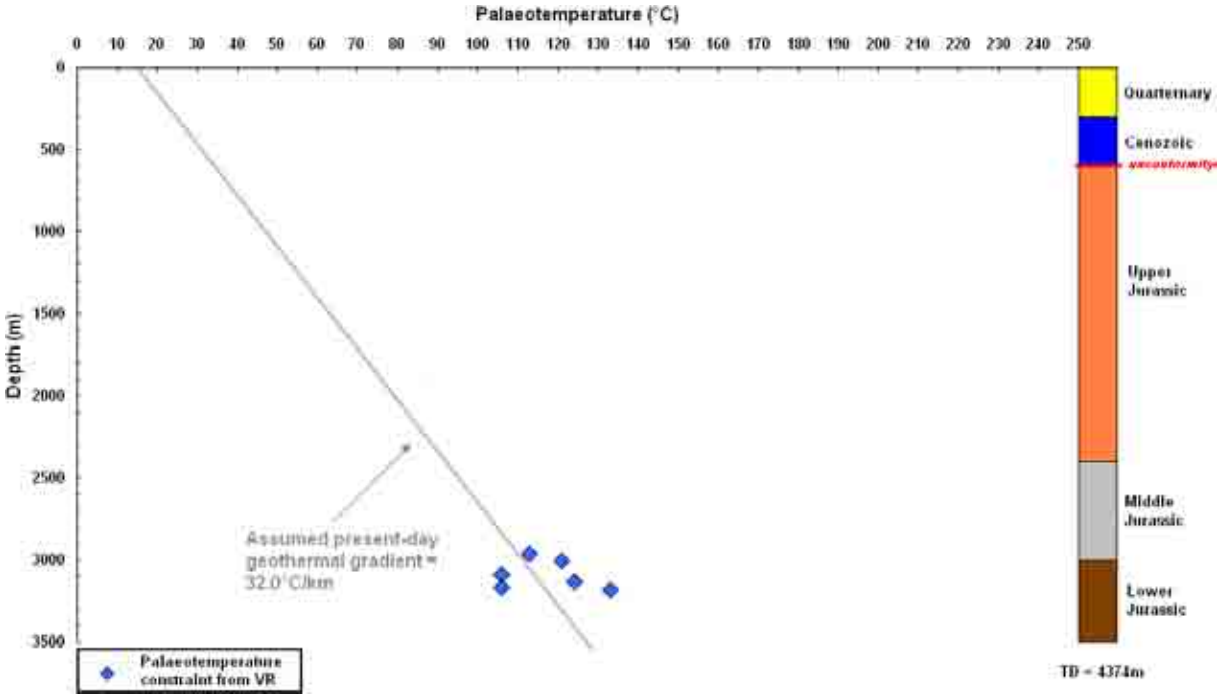

Figure C.6 – Palaeotemperature constraints from VR data from well 103/01-1 plotted against depth. These are too few points to reasonably fit a palaeogeothermal gradient to the data.. A simplified stratigraphic column is also shown.